

Peter Ring
Peter Schuck

The Nuclear Many-Body Problem

With 171 Illustrations



Springer-Verlag
New York Heidelberg Berlin

Peter Ring
Peter Schuck
Physik-Department
der TU München
Fachbereich Physik
James-Franck-Strasse
8046 Garching b. München
Federal Republic of Germany

Editors:

Wolf Beiglböck
Institut für Angewandte Mathematik
Universität Heidelberg
Im Neuenheimer Feld 5
D-6900 Heidelberg 1
Federal Republic of Germany

Maurice Goldhaber
Department of Physics
Brookhaven National Laboratory
Associated Universities, Inc.
Upton, NY 11973
USA

Elliott H. Lieb
Department of Physics
Joseph Henry Laboratories
Princeton University
P.O. Box 708
Princeton, NJ 08540
USA

Walter Thirring
Institut für Theoretische Physik
der Universität Wien
Boltzmanngasse 5
A-1090 Wien
Austria

ISBN 0-387-09820-8 Springer-Verlag New York
ISBN 3-540-09820-8 Springer-Verlag Berlin Heidelberg

Library of Congress Cataloging in Publication Data

Ring, Peter, 1941-
The nuclear many-body problem.

(Texts and monographs in physics)
Bibliography: p.
Includes indexes.
I. Problem of many bodies. 2. Nuclear physics.
I. Schuck, Peter, joint author. II. Title.
QC174.17.P7R56 530.1'44 79-25447

All rights reserved.

No part of this book may be translated or reproduced in any form without written permission from Springer-Verlag.

© 1980 by Springer-Verlag New York Inc.
Printed in the United States of America.

Preface

It is the aim of this book to describe in concise form our present theoretical understanding of the nuclear many-body problem. The presentation of the enormous amount of material that has accumulated in this field over the last few decades may be divided into two broad categories: One can either concentrate on the physical phenomena, such as the single-particle excitations, rotations, vibrations, or large-amplitude collective motion, and treat each of them using a variety of theoretical methods; or one may stress the methodology and technical aspects of the different theories that have been used to describe the nucleus. We have chosen the second avenue. The structure of this book is thus dictated by the different methods used—Hartree-Fock theory, time-dependent Hartree-Fock theory, generator coordinates, boson expansions, etc.—rather than by the physical subjects.

Many of the present theories have, of course, already been presented in other textbooks. In order to be able to give a more rounded picture, we shall either briefly review such topics (as in the case of the liquid drop or the shell model) or try to give more updated versions (as in the cases of rotations or the random phase approximation). Our essential aim, however, is to present the more modern theories—such as boson expansions, generator coordinates, time-dependent Hartree-Fock, semiclassical theories, etc.—which have either never been seen, or at best had little detailed treatment in, book form.

The book is essentially directed towards students who have had a conventional course in quantum mechanics and have some basic under-

standing of nuclear phenomena. Our intention has been to close the gap between the usual graduate lecture course and the literature presented in scientific journals. We have therefore put as much emphasis as possible on clarity, and to this end often go into quite extensive mathematical detail. We hope that the reader will thus be able to rederive many of the formulas presented without too much difficulty.

Originally our idea was to make an updated translation of an existing book on Nuclear Models by G. Baumgärtner and P. Schuck [BS 68a]. However, we soon found that theoretical nuclear physics had evolved so rapidly over the last decade that a completely new book was called for. Nevertheless, the reader will find some remnants of the original book, for example, in Chapters 2 and 6. The editing of the present work has been undertaken by Springer-Verlag, to whom we are grateful for their very constructive collaboration.

We are indebted to many of our colleagues for innumerable discussions and helpful remarks. In the first place, we wish to express our thanks to R. R. Hilton for his most careful reading of the entire manuscript, and for pointing out along the way many conceptual and countless linguistic errors.

Specifically, we are particularly grateful to the following people for clarifying discussions on a number of topics: for the rotational problem in nuclear physics—R. Arvieu, L. Egido, R. M. Lieder, H. J. Mang, E. Marshalek, J. Meyer-ter-Vehn, J. O. Rasmussen, and F. S. Stephens; for the theory of finite Fermi liquids and its applications to collective nuclear excitations—V. Klemt, J. Speth, E. Werner, and W. Wild; for the description of anharmonicities in nuclear spectra using boson expansion techniques—S. T. Belyaev, G. Holzwarth, S. Iwasaki, E. Marshalek, T. Marumori, K. Matsuyanagi, R. Piepenbring, F. Sakata, M. Yamamura, and V. G. Zelevinskii; for the generator coordinate method—T. Fliessbach, K. Goeke, G. Holzwarth and P. G. Reinhard; for the time-dependent Hartree-Fock approach—K. Dietrich, J. J. Griffin, S. E. Koonin; and for semiclassical methods in nuclear physics—J. Bartel, R. Bengtsson, R. K. Bhaduri, M. Brack, M. Durand, H. Gräf, G. Holzwarth, and B. Jennings.

Thanks are also due to L. Egido for a careful reading of several chapters, to S. Iwasaki for a reading of the chapter on boson expansions, and to R. K. Bhaduri, M. Brack, M. Durand, and G. Holzwarth for a careful reading of the chapter on semiclassical methods.

Our nuclear physics education has taken place within the Munich group, and we are happy to be able to take this opportunity to thank W. Brenig, K. Dietrich, H. J. Mang, H. Schmidt, and W. Wild for the patience and understanding they have shown in the numerous discussions we have had over the years.

Many aspects of the book were clarified during several stays by one of us (P. R.) at the Institute Laue-Langevin in Grenoble, for whose support

we are most thankful. Both of us have also had occasion to discuss many subjects with our French colleagues at the Institut de Sciences Nucléaires, Grenoble; the Institut de Physique Nucléaire, Orsay; and the Centre d'Etudes Nucléaires, Saclay. We hope they will not mind if we thank them here in such a "pauschal" fashion.

In spite of all this help and collaboration it is almost inevitable in a book of this kind that some misconceptions will still remain; naturally, they are our own responsibility. However, suggestions and criticisms from our readers would be welcomed for some possible future edition.

Various hands have assisted in the task of typing the manuscript and we should like finally to thank our many secretaries for their valuable contribution.

*Munich
Grenoble
February 1980*

P. Ring
P. Schuck

Contents

1	The Liquid Drop Model	1
1.1	Introduction	1
1.2	The Semi-empirical Mass Formula	2
1.3	Deformation Parameters	5
1.4	Surface Oscillations About a Spherical Shape	9
1.5	Rotations and Vibrations for Deformed Shapes	17
1.5.1	The Bohr Hamiltonian	17
1.5.2	The Axially Symmetric Case	22
1.5.3	The Asymmetric Rotor	26
1.6	Nuclear Fission	28
1.7	Stability of Rotating Liquid Drops	32
2	The Shell Model	36
2.1	Introduction and General Considerations	36
2.2	Experimental Evidence for Shell Effects	37
2.3	The Average Potential of the Nucleus	38
2.4	Spin Orbit Coupling	42
2.5	The Shell Model Approach to the Many-Body Problem	45
2.6	Symmetry Properties	50
2.6.1	Translational Symmetry	50

2.6.2 Rotational Symmetry	51
2.6.3 The Isotopic Spin	53
2.7 Comparison with Experiment	56
2.7.1 Experimental Evidence for Single-Particle (Hole) States	56
2.7.2 Electromagnetic Moments and Transitions	60
2.8 Deformed Shell Model	65
2.8.1 Experimental Evidence	65
2.8.2 General Deformed Potential	67
2.8.3 The Anisotropic Harmonic Oscillator	68
2.8.4 Nilsson Hamiltonian	70
2.8.5 Quantum Numbers of the Ground State in Odd Nuclei	78
2.8.6 Calculation of Deformation Energies	79
2.9 Shell Corrections to the Liquid Drop Model and the Strutinski Method	83
2.9.1 Introduction	83
2.9.2 Basic Ideas of the Strutinski Averaging Method	84
2.9.3 Determination of the Average Level Density	86
2.9.4 Strutinski's Shell Correction Energy	89
2.9.5 Shell Corrections and the Hartree-Fock Method	92
2.9.6 Some Applications	95

3 Rotation and Single-Particle Motion	96
---------------------------------------	----

3.1 Introduction	96
3.2 General Survey	97
3.2.1 Experimental Observation of High Spin States	97
3.2.2 The Structure of the Yrast Line	99
3.2.3 Phenomenological Classification of the Yrast Band	103
3.2.4 The Backbending Phenomenon	104
3.3 The Particle-plus-Rotor Model	107
3.3.1 The Case of Axial Symmetry	109
3.3.2 Some Applications of the Particle-plus-Rotor Model	119
3.3.3 The triaxial Particle-plus-Rotor Model	122
3.3.4 Electromagnetic Properties	125
3.4 The Cranking Model	126
3.4.1 Semiclassical Derivation of the Cranking Model	127
3.4.2 The Cranking Formula	130
3.4.3 The Rotating Anisotropic Harmonic Oscillator	133
3.4.4 The Rotating Nilsson Scheme	137
3.4.5 The Deformation Energy Surface at High Angular Momenta	139

3.4.6 Rotation about a Symmetry Axis	142
3.4.7 Yrast Traps	143
4 Nuclear Forces	147
4.1 Introduction	147
4.2 The Bare Nucleon–Nucleon Force	149
4.2.1 General Properties of a Two-Body Force	149
4.2.2 The Structure of the Nucleon–Nucleon Interaction	153
4.3 Microscopic Effective Interactions	156
4.3.1 Brückner's <i>G</i> -Matrix and Bethe Goldstone Equation	156
4.3.2 Effective Interactions between Valence Nucleons	164
4.3.3 Effective Interactions between Particles and Holes	170
4.4 Phenomenological Effective Interactions	172
4.4.1 General Remarks	172
4.4.2 Simple Central Forces	174
4.4.3 The Skyrme Interaction	175
4.4.4 The Gogny Interaction	176
4.4.5 The Migdal Force	177
4.4.6 The Surface-Delta Interaction (SDI)	179
4.4.7 Separable Forces and Multipole Expansions	180
4.4.8 Experimentally Determined Effective Interactions	185
4.5 Concluding Remarks	187
5 The Hartree–Fock Method	189
5.1 Introduction	189
5.2 The General Variational Principle	190
5.3 The Derivation of the Hartree–Fock Equation	192
5.3.1 The Choice of the Set of Trial Wave Functions	192
5.3.2 The Hartree–Fock Energy	194
5.3.3 Variation of the Energy	194
5.3.4 The Hartree–Fock Equations in Coordinate Space	196
5.4 The Hartree–Fock Method in a Simple Solvable Model	197
5.5 The Hartree–Fock Method and Symmetries	201
5.6 Hartree–Fock with Density Dependent Forces	203
5.6.1 Approach with Microscopic Effective Interactions	203
5.6.2 Hartree–Fock Calculations with the Skyrme Force	208
5.7 Concluding Remarks	215

6	Pairing Correlations and Superfluid Nuclei	217
6.1	Introduction and Experimental Survey	217
6.2	The Seniority Scheme	221
6.3	The BCS Model	228
6.3.1	The Wave Function	228
6.3.2	The BCS Equations	230
6.3.3	The Special Case of a Pure Pairing Force	232
6.3.4	Bogoliubov Quasi-particles—Excited States and Blocking	234
6.3.5	Discussion of the Gap Equation	238
6.3.6	Schematic Solution of the Gap Equation	240
7	The Generalized Single-Particle Model (HFB Theory)	244
7.1	Introduction	244
7.2	The General Bogoliubov Transformation	245
7.2.1	Quasi-particle Operators	245
7.2.2	The Quasi-particle Vacuum	249
7.2.3	The Density Matrix and the Pairing Tensor	251
7.3	The Hartree–Fock–Bogoliubov Equations	252
7.3.1	Derivation of the HFB Equation	252
7.3.2	Properties of the HFB Equations	255
7.3.3	The Gradient Method	258
7.4	The Pairing-plus-Quadrupole Model	259
7.5	Applications of the HFB Theory for Ground State Properties	262
7.6	Constrained Hartree–Fock Theory (CHF)	266
7.7	HFB Theory in the Rotating Frame (SCC)	271
8	Harmonic Vibrations	280
8.1	Introduction	280
8.2	Tamm–Dancoff Method	282
8.2.1	Tamm–Dancoff Secular Equation	282
8.2.2	The Schematic Model	285
8.2.3	Particle–Particle (Hole–Hole) Tamm–Dancoff Method	288
8.3	General Considerations for Collective Modes	289
8.3.1	Vibrations in Quantum Mechanics	289
8.3.2	Classification of Collective Modes	290
8.3.3	Discussion of Some Collective <i>ph</i> -Vibrations	293
8.3.4	Analog Resonances	297
8.3.5	Pairing Vibrations	299
8.4	Particle–Hole Theory with Ground State Correlations (RPA)	301

8.4.1 Derivation of the RPA Equations	301
8.4.2 Stability of the RPA	305
8.4.3 Normalization and Closure Relations	305
8.4.4 Numerical Solution of the RPA Equations	306
8.4.5 Representation by Boson Operators	307
8.4.6 Construction of the RPA Ground State	310
8.4.7 Invariances and Spurious Solutions	311
8.5 Linear Response Theory	314
8.5.1 Derivation of the Linear Response Equations	
	315
8.5.2 Calculation of Excitation Probabilities and Schematic Model	319
8.5.3 The Static Polarizability and the Moment of Inertia	321
8.5.4 RPA Equations in the Continuum	322
8.6 Applications and Comparison with Experiment	
	325
8.6.1 Particle-Hole Calculations in a Phenomenological Basis	325
8.6.2 Particle-Hole Calculations in a Self-Consistent Basis	328
8.7 Sum Rules	330
8.7.1 Sum Rules as Energy Weighted Moments of the Strength Functions	330
8.7.2 The S_1 -Sum Rule and the RPA Approach	331
8.7.3 Evaluation of the Sum Rules S_1 , S_{-1} , and S_3	332
8.7.4 Sum Rules and Polarizabilities	335
8.7.5 Calculation of Transition Currents and Densities	
	335
8.8 Particle-Particle RPA	339
8.8.1 The Formalism	339
8.8.2 Ground State Correlations Induced by Pairing Vibrations	341
8.9 Quasi-particle RPA	343
9 Boson Expansion Methods	346
9.1 Introduction	346
9.2 Boson Representations in Even-Even Nuclei	348
9.2.1 Boson Representations of the Angular Momentum Operators	348
9.2.2 Concepts for Boson Expansions	351
9.2.3 The Boson Expansion of Belyaev and Zelevinski	
	354
9.2.4 The Boson Expansion of Marumori	362
9.2.5 The Boson Expansion of Dyson	367
9.2.6 The Mathematical Background	368
9.2.7 Methods Based on pp -Bosons	372

9.2.8 Applications	375
9.3 Odd Mass Nuclei and Particle Vibration Coupling	381
9.3.1 Boson Expansion for Odd Mass Systems	382
9.3.2 Derivation of the Particle Vibration Coupling (Bohr) Hamiltonian	383
9.3.3 Particle Vibration Coupling (Perturbation Theory)	385
9.3.4 The Nature of the Particle Vibration Coupling Vertex	387
9.3.5 Effective Charges	389
9.3.6 Intermediate Coupling and Dyson's Boson Expansion	390
9.3.7 Other Particle Vibration Coupling Calculations	395
9.3.8 Weak Coupling in Even Systems	397

10	The Generator Coordinate Method	398
-----------	--	------------

10.1 Introduction	398
10.2 The General Concept	399
10.2.1 The GCM Ansatz for the Wave Function	399
10.2.2 The Determination of the Weight Function $f(\alpha)$	401
10.2.3 Methods of Numerical Solution of the HW Equation	404
10.3 The Lipkin Model as an Example	405
10.4 The Generator Coordinate Method and Boson Expansions	406
10.5 The One-Dimensional Harmonic Oscillator	409
10.6 Complex Generator Coordinates	411
10.6.1 The Bargman Space	411
10.6.2 The Schrödinger Equation	413
10.6.3 Gaussian Wave Packets in the Harmonic Oscillator	414
10.6.4 Double Projection	418
10.7 Derivation of a Collective Hamiltonian	419
10.7.1 General Considerations	419
10.7.2 The Symmetric Moment Expansion (SME)	420
10.7.3 The Local Approximation (LA)	423
10.7.4 The Gaussian Overlap Approximation (GOAL)	424
10.7.5 The Lipkin Model	428
10.7.6 The Multidimensional Case	430
10.8 The Choice of the Collective Coordinate	430
10.9 Application of the Generator Coordinate Method for Bound States	433
10.9.1 Giant Resonances	433
10.9.2 Pairing Vibrations	435

11	Restoration of Broken Symmetries	438
11.1	Introduction 438	
11.2	Symmetry Violation in the Mean Field Theory 441	
11.3	Transformation to an Intrinsic System 451	
11.3.1	General Concepts 451	
11.3.2	Translational Motion 454	
11.3.3	Rotational Motion 457	
11.4	Projection Methods 458	
11.4.1	Projection Operators 458	
11.4.2	Projection Before and After the Variation 460	
11.4.3	Particle Number Projection 463	
11.4.4	Approximate Projection for Large Deformations 466	
11.4.5	The Inertial Parameters 470	
11.4.6	Angular Momentum Projection 473	
11.4.7	The Structure of the Intrinsic Wave Functions 482	
12	The Time Dependent Hartree–Fock Method (TDHF)	485
12.1	Introduction 485	
12.2	The Full Time-Dependent Hartree–Fock Theory 486	
12.2.1	Derivation of the TDHF Equation 486	
12.2.2	Properties of the TDHF Equation 489	
12.2.3	Quasi-static Solutions 492	
12.2.4	General Discussion of the TDHF Method 493	
12.2.5	An Exactly Soluble Model 499	
12.2.6	Applications of the TDHF Theory 500	
12.3	Adiabatic Time-Dependent Hartree–Fock Theory (ATDHF) 505	
12.3.1	The ATDHF Equations 505	
12.3.2	The Collective Hamiltonian 510	
12.3.3	Reduction to a Few Collective Coordinates 513	
12.3.4	The Choice of the Collective Coordinates 516	
12.3.5	General Discussion of the Atdhf Methods 519	
12.3.6	Applications of the ATDHF Method 521	
12.3.7	Adiabatic Perturbation Theory and the Cranking Formula 523	
13	Semiclassical Methods in Nuclear Physics	527
13.1	Introduction 527	
13.2	The Static Case 528	
13.2.1	The Thomas–Fermi Theory 528	
13.2.2	Wigner–Kirkwood λ -Expansion 534	

13.2.3 Partial Resummation of the \hbar -Expansion	545
13.2.4 The Saddle Point Method	547
13.2.5 Application to a Spherical Woods-Saxon Potential	
549	
13.2.6 Semiclassical Treatment of Pairing Properties	
550	
13.3 The Dynamic Case	552
13.3.1 The Boltzmann Equation	553
13.3.2 Fluid Dynamic Equations from the	
Boltzmann Equation	555
13.3.3 Application of Ordinary Fluid Dynamics	
to Nuclei	558
13.3.4 Variational Derivation of Fluid Dynamics	562
13.3.5 Momentum Distribution of the Density ρ_0	564
13.3.6 Imposed Fluid Dynamic Motion	568
13.3.7 An Illustrative Example	573

APPENDICES

A Angular Momentum Algebra in the Laboratory and the Body-Fixed System	575
B Electromagnetic Moments and Transitions	580
B.1 The General Form of the Hamiltonian	580
B.2 Static Multipole Moments	581
B.3 The Multipole Expansion of the Radiation Field	584
B.4 Multipole Transitions	587
B.5 Single-Particle Matrix Elements in a Spherical Basis	591
B.6 Translational Invariance and Electromagnetic Transitions	592
B.7 The Cross Section for the Absorption of Dipole Radiation	593
C Second Quantization	595
C.1 Creation and Annihilation Operators	595
C.2 Field Operators in the Coordinate Space	598
C.3 Representation of Operators	599
C.4 Wick's Theorem	601

D Density Matrices	603
D.1 Normal Densities	603
D.2 Densities of Slater Determinants	605
D.3 Densities of BCS and HFB States	608
D.4 The Wigner Transformation of the Density Matrix	
609	
E Theorems Concerning Product Wave Functions	611
E.1 The Bloch–Messiah Theorem (BM 62)	611
E.2 Operators in the Quasi-particle Space	613
E.3 Thouless' Theorem	615
E.4 The Onishi Formula	618
E.5 Bogoliubov Transformations for Bosons	620
F Many-Body Green's Functions	623
F.1 Single-Particle Green's Function and Dyson's Equation	623
F.2 Perturbation Theory	628
F.3 Skeleton Expansion	631
F.4 Factorization and Brückner–Hartree–Fock	632
F.5 Hartree–Fock–Bogoliubov Equations	634
F.6 The Bethe–Salpeter Equation and Effective Forces	
640	
Bibliography	643
Author Index	681
Subject Index	699

100. - *Opisthonema* *leucostigma* (Günther)
= *Muraena* *leucostigma* (Günther)

Fig. 2

THE MURANE CROWN FISHES (MURAENIDÆ).

200. - *Muraena* *leucostigma* (Günther)
= *Opisthonema* *leucostigma* (Günther)
= *Muraena* *leucostigma* (Günther)

Fig. 2.

Fig. 2.



CHAPTER 1

The Liquid Drop Model

1.1 Introduction

The liquid drop model (LDM) of the nucleus was historically the first model to be proposed as an explanation of the different properties of the nucleus. Since it has regained interest in recent times, we begin with a short outline of this phenomenological model. Some aspects of this model will be taken up in the course of the book and explained from a more microscopic point of view. In this chapter we follow to a large extent the standard representation as given in the texts of, for example, J. A. Eisenberg and W. Greiner [EG 70], A. de Shalit and H. Feshbach [SF 74], and A. Bohr and B. R. Mottelson [BM 75].

The idea of considering the nucleus as a liquid drop originally came from considerations about its saturation properties (see below) and from the fact that the nucleus has a very low compressibility and a well defined surface. However, as we shall see, it is misleading to take this point of view too seriously, since in other respects a nucleus does not bear very much resemblance to an ordinary liquid. For instance, the mean distance of two particles in a liquid is roughly given by the value at which the interparticle force has its minimum value, which for nuclei would be ~ 0.7 fm. However, nucleons in nuclei are, on the average, ~ 2.4 fm apart. One reason for this big difference as compared with an ordinary liquid is that the nucleons obey Fermi statistics and a nucleus is thus a quantum fluid. The Pauli principle prevents the nucleons from coming too close to one another. Thus scattering events are very scarce in a quantum fluid, whereas in an ordinary fluid they are predominant.

Consequently, the mean free path of the nucleons inside a ground-state (or moderately excited state) nucleus is of the order of the nuclear dimension and resembles, therefore, apart from the statistics, a non-interacting gas. This fact has some drastic consequences that are absent in droplets of ordinary fluids. For instance, we want to mention that in a vibrating nuclear drop [e.g., (dynamical) quadrupole deformations] the momentum distribution of the nucleons may be influenced by the deformations; i.e., it can be anisotropic, whereas the velocity distribution in an ordinary fluid drop is always isotropic. These peculiarities of a quantum drop will be treated in more detail in Chapter 13. Here, instead, we shall follow the historical development of the LDM idea, since it is very useful in describing overall properties of the nucleus and in introducing many concepts of collective phenomena in nuclear physics in a simple way. This is the main purpose of the first chapter, where we will not bother about the specific differences between an ordinary liquid drop and a quantum drop.

1.2 The Semi-empirical Mass Formula

One quantity that should, according to the discussions above, vary only smoothly with mass number is the binding energy per particle. In fact, the total binding energy $B(Z, N)$, where N and Z are the number of neutrons and protons, respectively, grows with the number of nucleons, A , in such a way that the binding energy per particle $B(N, Z)/A$ stays fairly constant for nuclei with more than twelve nucleons:

$$\left. \frac{B(N, Z)}{A} \right|_{A > 12} \simeq -8.5 \text{ [MeV/nucleon].} \quad (1.1)$$

The explanation for the binding energy per nucleon being approximately constant can be given in the following qualitative way: If the binding of a system of A particles comes from the interaction energy of all possible two-particle pair combinations, then the total binding energy should grow roughly like the number of all possible pairs, namely as $\frac{1}{2} \cdot A \cdot (A - 1)$. The binding energy per particle should then be proportional to A . This is the case, for example, for the binding energies of the electrons in an atom.

The completely different behavior of the nuclear binding energy can be attributed to the saturation property of the nuclear forces: one nucleon in the nucleus interacts with only a limited number of nucleons. This has its origin in the short-range nuclear force and the combined effect of the Pauli and uncertainty principles: The total binding energy is a subtle difference effect between the total kinetic energy and the total potential energy; whereas due to the Pauli and uncertainty principles and the hard core [Br 65a], the kinetic energy rises steeply to positive values at decreasing nucleon distances [BM 69, p. 252] (see Fig. 1.1), and the potential energy is lowered to more and more negative energies. For small enough ($d \lesssim 2$ fm) internucleon distances the kinetic energy takes over so that the total

binding energy becomes positive, whereas for large distances ($d \lesssim 3$ fm), there is hardly any potential energy because of the short-range nucleon-nucleon force. Finally, a shallow minimum develops at around 2.4 fm, which is, compared to the strength of the nuclear forces, quite small. From these considerations it becomes clear why there can be only a limited number of nucleons within the interaction range of one nucleon. In this argument we have not taken into account surface effects and the Coulomb force. They have to be treated separately, as we shall see. Neglecting these effects, we expect that the total binding energy rises linearly with A , as in Eq. (1.1).

The saturation property also explains qualitatively the features found experimentally (by, for instance, electron scattering, μ -mesonic x-rays, etc. [FN 76]), that is, the roughly constant density of nucleons inside the nucleus and the nucleus's relatively sharp surface. Describing the nucleus as a sphere with a constant density and a *sharp* surface, we get for its radius

$$R = r_0 A^{1/3}, \quad (1.2)$$

where the parameter r_0 has empirically the value

$$r_0 = 1.2 \text{ [fm]}. \quad (1.3)$$

In Fig. 1.2, we see the dependence of the binding energy per nucleon on the mass number A in more detail.

Up to about $A = 12$, we get a steep rise until $B/A \approx 8$ MeV; at $A \approx 60$, we obtain the maximum of a little less than 9 MeV. The binding energy per

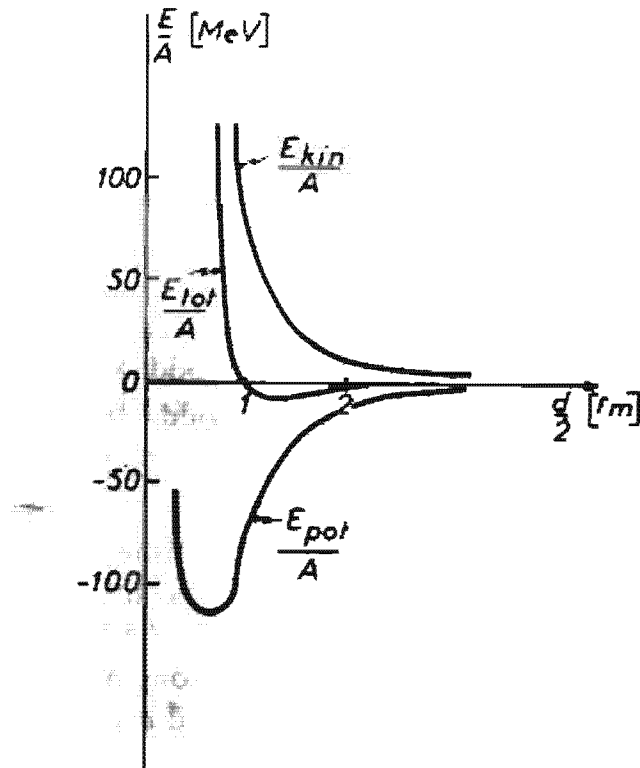


Figure 1.1. Qualitative explanation of nuclear saturation as a subtle difference effect of E_{kin} and E_{pot} .

4 The Liquid Drop Model

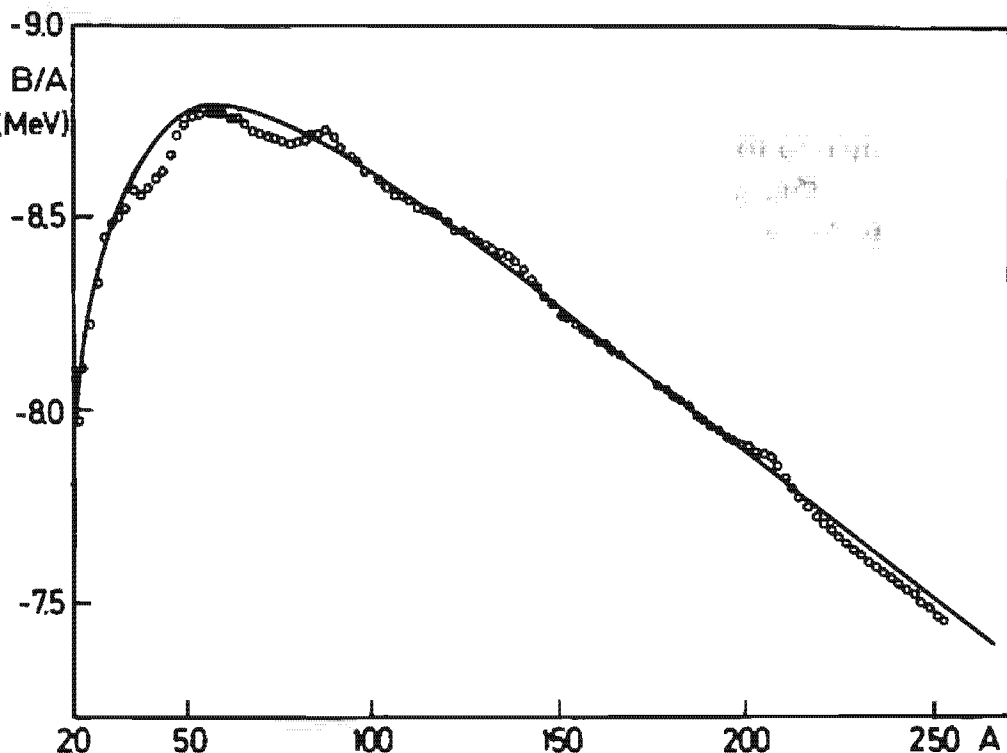


Figure 1.2. Experimental values of B/A for β -stable odd- A (\circ) nuclei and the calculated curve using a mass formula similar to Eq. (1.4). (From [Ho 75].)

nucleon then drops slightly until at $A = 250$ it is about 7.5 [MeV]. This is due to the increasing influence of the Coulomb repulsion of the protons.

There have been many attempts to reproduce the behavior of B/A as a function of N and Z . The best known formula of this kind is the semi-empirical mass formula of Bethe and Weizsäcker [We 35, BB 36]

$$B(N, Z) = a_V A + a_S A^{2/3} + a_C \frac{Z^2}{A^{1/3}} + a_I \frac{(N-Z)^2}{A} - \delta(A), \quad (1.4)$$

where one obtains by a fit (see also [MS 66, My 69, MS 69]):

$$a_V = -15.68; \quad a_S = 18.56; \quad a_C = 0.717; \quad a_I = 28.1 \quad [\text{MeV}]$$

$$\delta(A) = \begin{cases} 34 \cdot A^{-3/4} & \text{for even-even} \\ 0 & \text{for even-odd} \\ -34 \cdot A^{-3/4} & \text{for odd-odd} \end{cases} \text{ nuclei.} \quad (1.5)$$

In Fig. 1.2 we see that one obtains quite good overall agreement with the experimental curve with these kinds of semi-empirical mass formulae.

The physical meaning of formula (1.4) is the following. The first term is usually called the *volume term*, because it is proportional to A [$\propto R^3$ with Eq. (1.2)]. The reason that the value of a_V is not -8.5 [MeV] as in Eq. (1.1) is the following. In order to get the value -8.5 , one has to average over a wide range of A , and the other terms (a_S , a_C , and a_I) are positive and not negligible.

The second term is proportional to $A^{2/3}$ ($\propto R^2$), and is therefore called the *surface term*. It results from the fact that the nucleons close to the surface contribute less to the total binding energy. One can calculate from

the parameter a_S , a surface tension coefficient σ defined as the surface energy per unit area, and get with Eq. (1.3):

$$\sigma = \frac{a_S}{4\pi r_0^2} = 1.03 \text{ [MeV} \cdot \text{fm}^{-2}\text{]}. \quad (1.6)$$

The third term takes into account the Coulomb repulsion of the protons. It can be calculated approximately by assuming the charges to be uniformly distributed over a sphere. The *Coulomb energy* of such a system is proportional to the number of proton pairs ($\propto Z^2$) and inversely proportional to the radius.

Since the protons repel one another, it would be energetically more favorable for a nucleus to have only neutrons—if there were no Pauli principle. A proton decaying into a neutron must enter a state above the neutron Fermi level (see Chap. 2), which is energetically unfavored. The energy balance of the neutron excess $N - Z$ is taken care of in the fourth term of Eq. (1.4), the so-called *symmetry energy*. It cannot depend on the sign of $N - Z$. In the Fermi gas model [SF 74, p. 127 f], one can show that it is proportional to $(N - Z)^2/A$. The quadratic dependence of the binding energy on the proton–neutron mass difference is experimentally very well confirmed. Only the base of the experimental parabola is different according to whether we are considering an even–even, even–odd or odd–odd nucleus. This is due to the so-called *pairing effect*, as we shall see in Chapter 6, and is taken care of by the last term in Eq. (1.4).

Some aspects of the semi-empirical mass formula will be discussed again in Chapter 13 in the context of the Thomas–Fermi approach to nuclear physics.

It should be noted that Eq. (1.4) gives only an overall smooth fit to the binding energy as a function of A , and that locally there are strong deviations from it (see Fig. 2.2), mostly due to shell effects, which will be discussed in Section 2.9.

1.3 Deformation Parameters

Up to now, we have only studied static properties of the liquid drop model. In the following, we will assume that the nucleus has a sharp surface* which must not necessarily be spherical, and we imagine it to undergo dynamical shape or surface oscillations.

Before we can investigate these oscillations, we have to parametrize the surface in some way. One possibility is to describe it by the length of the radius vector pointing from the origin to the surface

$$R = R(\theta, \phi) = R_0 \left(1 + \alpha_{00} + \sum_{\lambda=1}^{\infty} \sum_{\mu=-\lambda}^{\lambda} \alpha_{\lambda\mu}^* Y_{\lambda\mu}(\theta, \phi) \right) \quad (1.7)$$

where R_0 is the radius of the sphere with the same volume. Such a surface

* Myers and Swiatecki [MS 69, 73] have given up this assumption and introduced a refined liquid drop model with a diffuse surface, the so-called "droplet model" [Ni 72].

6 The Liquid Drop Model

is certainly not the most general one* but it is widely used and extremely useful for problems of nuclear structure.

The constant α_{00} describes changes of the nuclear volume. Since we know that the incompressibility of the nuclear fluid is rather high, we require that the volume be kept fixed for all deformations as

$$V = \frac{4}{3} \pi R_0^3. \quad (1.8)$$

This defines the constant α_{00} . Up to second order, we get [EG 70]

$$\alpha_{00} = -\frac{1}{4\pi} \sum_{\lambda > 1, \mu} |\alpha_{\lambda\mu}|^2. \quad (1.9)$$

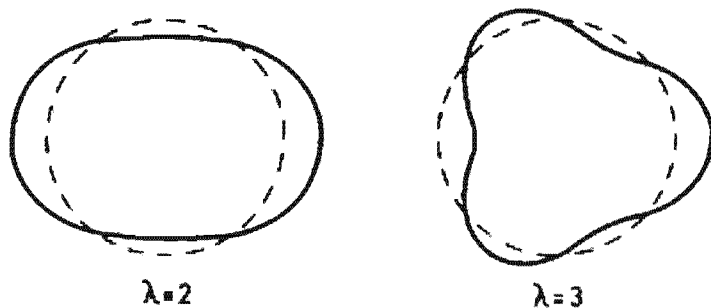
The term $\lambda = 1$ describes mainly (at least for small deformations) a translation of the whole system. The three parameters $\alpha_{1\mu}$ can be fixed by the condition that the origin coincides with the center of mass

$$\int_V \mathbf{r} d^3r = 0. \quad (1.10)$$

If the expansion (1.7) contains only even values of λ , this is fulfilled automatically. Otherwise $\alpha_{1\mu}$ starts with second order in the $\alpha_{\lambda\mu}$ ($\lambda > 2$). Therefore, in the following we omit both α_{00} and $\alpha_{1\mu}$, since we shall restrict our discussion to small deformations.

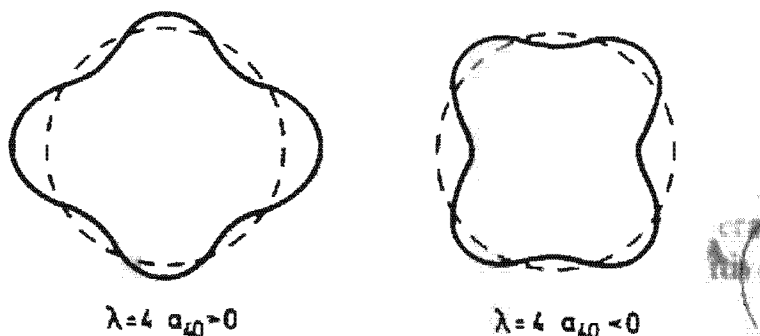
It is instructive to look at the shapes of lowest multipolarity in the expansion (1.7), as displayed in Fig. (1.3). The deformations corresponding

* For instance, shapes of two separated fragments in the fission process cannot be represented by (1.7), since R is then multivalued.



$\lambda=2$

$\lambda=3$



$\lambda=4 \ a_{40} > 0$

$\lambda=4 \ a_{40} < 0$

Figure 1.3. Nuclear shapes with quadrupole ($\lambda = 2$), octupole ($\lambda = 3$), and hexadecapole ($\lambda = 4$) deformations.

to $\lambda = 2$ look like ellipsoidal deformations. It should be noticed, however, that this is true only up to first order. A pure ellipsoid has non-vanishing $a_{\lambda\mu}$ for all $\lambda \geq 2$.

Another condition on R , and therefore on the parameters $a_{\lambda\mu}$, is the fact that R should be invariant under a reflection of the coordinate system and under a rotation of the coordinate system. In order for this to be the case, the $a_{\lambda\mu}$ must be multiplied by a factor $(-)^{\lambda}$ under a parity transformation, and must behave like $Y_{\lambda\mu}(\theta, \phi)$ under a rotation of the coordinate system (characterized by the Euler angles $\Omega = (\alpha, \beta, \gamma)$ [Eq. 57, Eq. (5.2.1.)]), i.e.,

$$(Y_{\lambda\mu})_{\text{new}} = \sum_{\mu'} D_{\mu'\mu}^{\lambda}(\Omega) (Y_{\lambda\mu'})_{\text{old}}, \quad (1.11)$$

$$a_{\lambda\mu} = \sum_{\mu'} D_{\mu'\mu}^{\lambda}(\Omega) a_{\lambda\mu'},$$

where $D_{\mu'\mu}^{\lambda}(\Omega)$ are the Wigner functions of the rotation and $a_{\lambda\mu}$ are the deformation parameters in the new system.

To make sure that the radius R in Eq. (1.7) is real, we have to use the property $Y_{\lambda\mu}^* = (-)^{\mu} \cdot Y_{\lambda-\mu}$, and get

$$a_{\lambda\mu}^* = (-)^{\mu} a_{\lambda-\mu}. \quad (1.12)$$

This will turn out to be the time reversal behavior of the $a_{\lambda\mu}$'s.

Before discussing the surface oscillations of general multipolarity, we mention two special cases:

- (i) First are the axially symmetric deformations. Choosing the z-axis as symmetry axis, we find that $a_{\lambda\mu}$ vanishes except when $\mu = 0$. The deformation parameters $a_{\lambda 0}$ are usually called β_{λ} .
- (ii) In the case of quadrupole deformations ($\lambda = 2$), we have five parameters $a_{\lambda\mu}$. Not all of them describe the shape of the drop. Three determine only the orientation of the drop in space, and correspond to the three Euler angles. By a suitable rotation, we can transform to the body-fixed system characterized by three axes 1, 2, 3, which coincide with the principal axes of the mass distribution of the drop. The five coefficients $a_{2\mu}$ reduce to two real independent variables a_{20} and $a_{22} = a_{2-2}$ ($a_{21} = a_{2-1} = 0$), which, together with the three Euler angles, give a complete description of the system. It is convenient to introduce instead of a_{20} and a_{22} the so-called Hill-Wheeler [HW 53] coordinates β, γ ($\beta > 0$) through the relation

$$a_{20} = \beta \cdot \cos \gamma, \\ a_{22} = \frac{1}{\sqrt{2}} \cdot \beta \cdot \sin \gamma, \quad (1.13)$$

from which we have

$$\sum_{\mu} |a_{2\mu}|^2 = a_{20}^2 + 2a_{22}^2 = \beta^2 \quad (1.14)$$

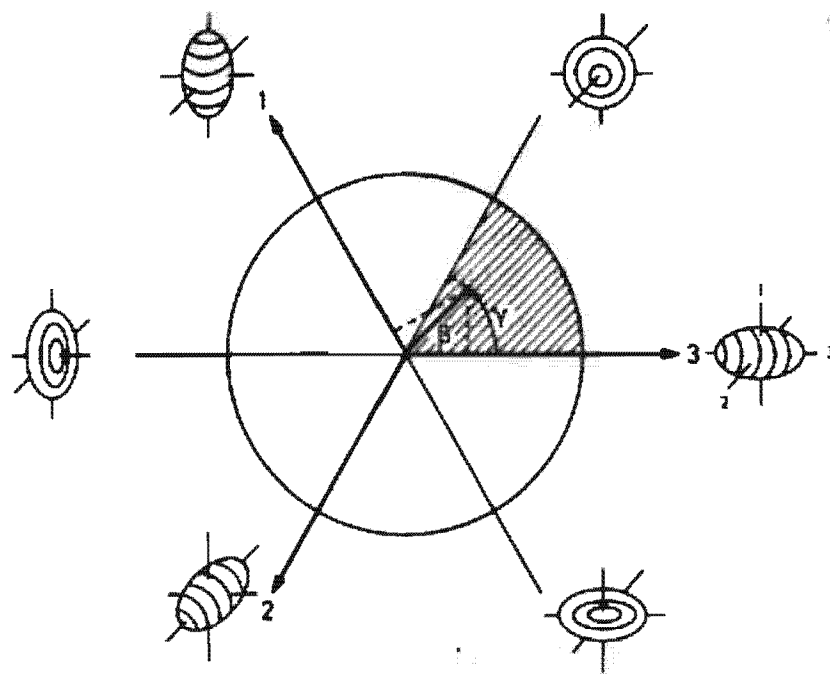


Figure 1.4. Nuclear shapes in the β, γ plane. The projections onto the three axes are proportional to the increments of δR_x (1.16).

and

$$R(\theta, \phi) = R_0 \left\{ 1 + \beta \sqrt{\frac{5}{16\pi}} (\cos \gamma (3\cos^2 \theta - 1) + \sqrt{3} \sin \gamma \sin^2 \theta \cos 2\phi) \right\}. \quad (1.15)$$

In Fig. (1.4) the $\lambda=2$ shapes are represented in the polar coordinates β, γ . We see that

- (i) γ values of $0^\circ, 120^\circ$, and 240° yield prolate spheroids with the 3, 1 and 2 axes as axes of symmetry;
- (ii) $\gamma = 180^\circ, 300^\circ$, and 60° lead to the corresponding oblate shapes
- (iii) when γ is not a multiple of 60° it corresponds to a triaxial shape;
- (iv) there are discrete symmetries, namely, one can interchange all three axes without changing the shape, which means an invariance under the point group D_2 . The interval $0 < \gamma < 60^\circ$ is sufficient to describe all the $\lambda=2$ shapes. All other points in Fig. 1.4 are obtained by suitable exchanges of the different axes.
- (v) We can calculate the increments of the three semi-axes in the body-fixed frame as functions of β and γ :

$$\delta R_1 = R\left(\frac{\pi}{2}, 0\right) - R_0 = R_0 \sqrt{\frac{5}{4\pi}} \beta \cos\left(\gamma - \frac{2\pi}{3}\right),$$

$$\delta R_2 = R\left(\frac{\pi}{2}, \frac{\pi}{2}\right) - R_0 = R_0 \sqrt{\frac{5}{4\pi}} \beta \cos\left(\gamma + \frac{2\pi}{3}\right),$$

$$\delta R_3 = R(0, 0) - R_0 = R_0 \sqrt{\frac{5}{4\pi}} \beta \cos \gamma,$$

or

$$\delta R_\kappa = R_0 \sqrt{\frac{5}{4\pi}} \beta \cos\left(\gamma - \frac{2\pi}{3}\kappa\right), \quad \kappa = 1, 2, 3. \quad (1.16)$$

We have to remember, however, that the parameters β and γ (with (1.7)) only describe exactly ellipsoidal shapes in the limit of small β -values (see also Eq. 1.88).

1.4 Surface Oscillations About a Spherical Shape

The first kind of excitations are dynamical shape, or surface, oscillations. The dynamical variables are in this case the parameters which describe the surface, i.e., the surface coordinates $a_{\lambda\mu}$ ($\lambda > 2$) of Eq. (1.7). They are considered to be functions of time: $a_{\lambda\mu}(t)$. For the low-lying excitations one can expect that they produce small oscillations around the spherical equilibrium shape with $a_{\lambda\mu} = 0$, and that the classical Hamilton function H_{coll} that describes this process is of a harmonic oscillator form [Bo 52]:

$$H_{\text{coll}} = T + V = \frac{1}{2} \sum_{\lambda, \mu} \left(B_\lambda |\dot{a}_{\lambda\mu}|^2 + C_\lambda |a_{\lambda\mu}|^2 \right), \quad (1.17)$$

Here the parameters of inertia B_λ and of stiffness C_λ are real constants. This is, in fact, the only quadratic form which is invariant under rotation and time reversal.*

Following the usual rules of canonical quantization (see for instance, [EG 70, p. 40]), we obtain the quantized form† (see also Appendix C)

$$\hat{H}_{\text{coll}} = \sum_{\lambda\mu} \hbar \Omega_\lambda \left(B_{\lambda\mu}^+ B_{\lambda\mu} + \frac{1}{2} \right) \quad (1.18)$$

with the frequencies

$$\Omega_\lambda = \left(\frac{C_\lambda}{B_\lambda} \right)^{1/2}. \quad (1.19)$$

The operators $B_{\lambda\mu}$ obey Bose commutation rules

$$[B_{\lambda\mu}, B_{\lambda'\mu'}] = 0; \quad [B_{\lambda\mu}, B_{\lambda'\mu'}^+] = \delta_{\lambda\lambda'} \delta_{\mu\mu'}. \quad (1.20)$$

and have a corresponding Bose vacuum $|0\rangle$ such that $B_{\lambda\mu}|0\rangle = 0$. The Boson operators $B_{\lambda\mu}$ are related to the coordinates $\hat{a}_{\lambda\mu}$ and corresponding momenta $\hat{p}_{\lambda\mu}$ by

$$\hat{a}_{\lambda\mu} = \left(\frac{\hbar}{2B_\lambda \Omega_\lambda} \right)^{1/2} (B_{\lambda\mu}^+ + (-)^\mu B_{\lambda-\mu}), \quad (1.21)$$

$$\hat{p}_{\lambda\mu} = i \left(\frac{\hbar}{2} B_\lambda \Omega_\lambda \right)^{1/2} ((-)^{\mu} B_{\lambda-\mu}^+ - B_{\lambda\mu}).$$

* The time reversal operation is discussed in great detail by Messiah [Me 61] and it is shown that in a system without spin, as we have here, time reversal corresponds to complex conjugation.

† One should not mix up the boson operators $B_{\lambda\mu}$ with the inertia parameters B_λ .

10 The Liquid Drop Model

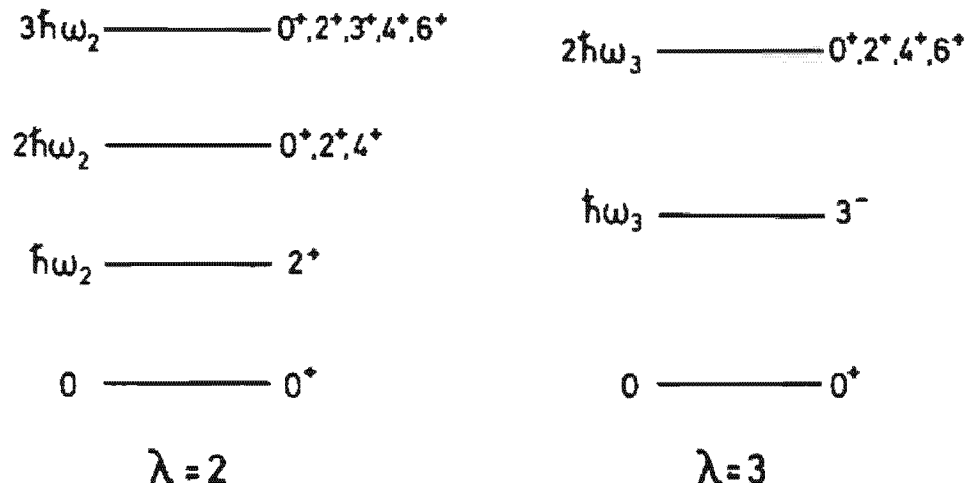


Figure 1.5. Harmonic energy spectra for the quadrupole ($\lambda = 2$) and octupole ($\lambda = 3$) surface oscillations.

From the above considerations, it follows that for each λ we have a harmonic spectrum of surface vibrations as illustrated in Fig. 1.5.

From the fact that $a_{\lambda\mu}$ and $B_{\lambda\mu}^+$ behave like spherical tensors under rotations of the coordinate system (Eq. (1.11), [Ed 57, Eq. (5.2.1)]) we know the commutation relations of the angular momentum operators with $B_{\lambda\mu}^+$ and find that the one-boson states

$$|\lambda\mu\rangle = B_{\lambda\mu}^+ |0\rangle \quad (1.22)$$

have angular momentum $I = \lambda$ and z -component $M = \mu$ with parity $(-)^{\lambda}$.

To construct multi-boson states we have to use the rules of angular momentum coupling [Ed 57] and also have to take into account that states with more than two bosons are symmetric under the exchange of any two of them. For instance, we get, for the superposition of two quadrupole bosons ($\lambda = 2$), the three combinations $I'' = 0^+, 2^+, 4^+$

$$|IM\rangle = \frac{1}{\sqrt{2}} \sum_{\mu_1\mu_2} C_{\mu_1\mu_2 M}^{2\ 2\ I} B_{2\mu_1}^+ B_{2\mu_2}^+ |0\rangle. \quad (1.23)$$

The states with $I = 1, 3$ vanish identically because of the behavior of the Clebsch-Gordan coefficients* [Ed 57, Eq. (3.5.14)]

$$C_{\mu_1\mu_2 M}^{2\ 2\ I} = (-)^I C_{\mu_2\mu_1 M}^{2\ 2\ I}.$$

under an exchange of μ_1 and μ_2 .

Indeed, many spherical nuclei show in their spectrum a low-lying 2^+ state and, at roughly double the excitation energy, a so-called two-boson triplet $(0^+, 2^+, 4^+)$ which is, however, usually split up a little (see Fig. 9.4).

The constants B_λ and C_λ can be calculated within the fluid picture; they depend on the flow associated with the surface oscillations. Therefore, it is necessary to postulate the nature of the fluid motion within the drop. At this point we should again discuss what the concept of a nuclear fluid

* We use the symbol $C_{m_1 m_2 m_3}^{j_1 j_2 j_3}$ which is the same as $(j_1 m_1 j_2 m_2 | j_1 j_2 j_3 m_3)$.

implies. In Chapter 13 we will investigate this point in detail and show that the fact that the nucleus is a Fermi liquid and not an ordinary liquid plays an important role. The simplest assumption about the flow pattern of the fluid we can make is that it is irrotational, i.e., $\text{rot } \mathbf{v}(\mathbf{r}) = 0$, where \mathbf{v} is the velocity field. We shall also study the justification of this point in Chapter 13, but for the moment let us take it for granted and thus have:

$$\mathbf{v}(t) = -\nabla\Phi(\mathbf{r}). \quad (1.24)$$

The next assumption is that of *incompressibility*, which is quite well justified for nuclei. It means that the density inside the nucleus is constant ($\dot{\rho} = 0$), and we get from the equation of continuity

$$\nabla \cdot \mathbf{v} = 0 \quad (1.25)$$

and, from (1.24),

$$\Delta\Phi = 0. \quad (1.26)$$

The most general solution of Eq. (1.26) regular at the origin can be written in the form

$$\Phi(\mathbf{r}) = \sum_{\lambda\mu} d_{\lambda\mu}^* r^\lambda Y_{\lambda\mu}(\theta, \phi). \quad (1.27)$$

For small deformations we have the boundary condition that the radial component of the velocity is, in lowest order, given by:

$$v_r = -\frac{\partial}{\partial r}\Phi = \dot{R} \quad \text{at } r = R_0,$$

which, with Eq. (1.7), yields the following relation between the coefficients $d_{\lambda\mu}$ and $\alpha_{\lambda\mu}$:

$$d_{\lambda\mu} = -\frac{1}{\lambda} R_0^{2-\lambda} \dot{\alpha}_{\lambda\mu}. \quad (1.28)$$

The kinetic energy of the surface vibrations is given by

$$T = \frac{m}{2} \rho \int_V v^2(\mathbf{r}) d^3r = \frac{m}{2} \rho \int_V |\nabla\Phi|^2 d^3r = \frac{m}{2} \rho \oint_S \Phi^* \nabla\Phi ds,$$

where ρ is the constant density of nucleons with the mass m . Using the gradient formula for spherical harmonics [Ed 57, Eq. (5.9.17)] and [Ed 57, Eqs. (5.9.13) and (5.9.16)] we arrive in the approximation of small deformations (integrating over a sphere), in the following expression for the kinetic energy.

$$T = \frac{R_0^5 m \rho}{2} \sum_{\lambda\mu} \frac{|\dot{\alpha}_{\lambda\mu}|^2}{\lambda}. \quad (1.29)$$

Comparison with (1.17) yields the mass parameter

$$B_\lambda = \frac{\rho m R_0^5}{\lambda} = \frac{3}{4\pi\lambda} A \cdot m R_0^2. \quad (1.30)$$

For oscillations about a spherical equilibrium shape the mass parameter is not a function of μ ; this would not be so for a deformed nuclear drop.

The potential energy of a liquid drop with a surface deformation characterized by the parameters $\alpha_{\lambda\mu}$ can be obtained from the coefficients of the Bethe-Weizsäcker formula (1.4) if we neglect changes of the symmetry and pairing energy with deformation.

Because of the assumption of incompressibility, it is tempting to say that the volume term does not depend on the deformation. This is, however, only true for ordinary fluids, and we will see in Chapter 13 how in quantum fluids the volume term can depend on α in a quite subtle fashion. In the usual treatment of the liquid drop model [BM 53, EG 70], however, the volume term is not taken into account, and therefore the deformation energy has only two parts, resulting from the surface and Coulomb terms in Eq. (1.4). As we will discuss in more detail in Chapter 13 this will be sufficient for the monopole and the dipole resonance but not for resonances of other multipolarities.

The deformation energy is defined as the difference between the energy of the deformed and spherical drop:

$$V(\alpha) = E_S(\alpha) - E_S(0) + E_C(\alpha) - E_C(0). \quad (1.31)$$

The surface energy is given by the product of the surface with the surface tension σ [Eq. (1.6)]. With techniques similar to those used in the derivation of Eq. (1.29), we find up to second order in $\alpha_{\lambda\mu}$ [Wi 64, Chap. 2]:

$$E_S(\alpha) = \sigma \oint_S ds = E_S(0) + \frac{1}{2} \sum_{\lambda\mu} (\lambda - 1)(\lambda + 2) R_0^2 \sigma |\alpha_{\lambda\mu}|^2. \quad (1.32)$$

The Coulomb energy E_C is the sum of interactions between pairs of volume elements d^3r_1 and d^3r_2 [Wi 64]

$$E_C(\alpha) = (Ze)^2 \int_V \int_V \frac{d^3r_1 d^3r_2}{|\mathbf{r}_1 - \mathbf{r}_2|} = E_C(0) - \frac{1}{2} \sum_{\lambda\mu} \frac{3(\lambda - 1)(Ze)^2}{2\pi(2\lambda + 1)R_0} |\alpha_{\lambda\mu}|^2. \quad (1.33)$$

From (1.32), (1.33), and (1.17), we thus get the stiffness coefficients ($\lambda > 2$):

$$C_\lambda = (\lambda - 1)(\lambda + 2) R_0^2 \sigma - \frac{3(\lambda - 1)}{2\pi(2\lambda + 1)} \frac{(Ze)^2}{R_0}. \quad (1.34)$$

In principle, we are now able to calculate nuclear spectra from Eq. (1.19) and the coefficients B_λ and C_λ . It turns out, however, that the reproduction of spectra is not the most sensitive test for a nuclear model. A quantum mechanical state is represented by a wave function. Electromagnetic moments and transition probabilities depend strongly on the wave functions and provide a much better test. We therefore first discuss such quantities before comparing the theory with experimental data.

In Appendix B the calculation of the electromagnetic properties of a nucleus is shown. The essential quantities are the electric and magnetic multipole operators.

The electric multipole operators are in the limit of long wavelengths (low transition energies) given by [Eq. (B.18)]

$$\hat{Q}_{\lambda\mu} = e \int_V \rho_p(\mathbf{r}) r^\lambda Y_{\lambda\mu}(\theta, \phi) d^3r.$$

We can express them by the coordinates $\alpha_{\lambda\mu}$, taking in the integral a constant proton density ρ_p for a shape defined by Eq (1.7) and get

$$\hat{Q}_{\lambda\mu} = \rho_p \cdot e \cdot \int_{4\pi} d\cos\theta d\phi Y_{\lambda\mu}(\theta, \phi) \frac{1}{\lambda+3} R^{\lambda+3}(\theta, \phi),$$

which is up to second order in $\alpha_{\lambda\mu}$ (with [Eq 57, Eq. (4.6.3)])

$$\hat{Q}_{\lambda\mu} = \frac{3e}{4\pi} ZR_0^\lambda \left[\hat{\alpha}_{\lambda\mu} + \frac{1}{2}(\lambda+2) \sum_{\lambda_1\mu_1} \sum_{\lambda_2\mu_2} \hat{\alpha}_{\lambda_1\mu_1} \hat{\alpha}_{\lambda_2\mu_2} (-)^{\mu_1+\mu_2} \cdot \sqrt{\frac{(2\lambda_1+1)(2\lambda_2+1)(2\lambda+1)}{4\pi}} \begin{pmatrix} \lambda_1 & \lambda_2 & \lambda \\ 0 & 0 & 0 \end{pmatrix} \begin{pmatrix} -\lambda_1 & -\lambda_2 & \lambda \\ -\mu_1 & -\mu_2 & \mu \end{pmatrix} \right]. \quad (1.35)$$

The magnetic multipole operators are given by [Eq. (B. 22)]

$$\hat{M}_{\lambda\mu} = \frac{1}{c(\lambda+1)} \int_V (\mathbf{r} \times \mathbf{j}(\mathbf{r})) (\nabla r^\lambda Y_{\lambda\mu}) d^3r.$$

As in the case of the mass parameters, we could again use the assumption of irrotational flow to define the current density \mathbf{j} and express $\hat{M}_{\lambda\mu}$ by $\alpha_{\lambda\mu}$ and $\dot{\alpha}_{\lambda\mu}$ (see [Da 68, Chap. 6]). However, we will restrict ourselves to the case of $M1$ operators, which form a vector

$$\hat{\mathbf{M}}1 = \sqrt{\frac{3}{4\pi}} \hat{\mu}.$$

Since we have no spins in the system, we get for the magnetic dipole moment

$$\hat{\mu} = \frac{1}{2c} \int_V (\mathbf{r} \times \mathbf{j}) d^3r = \frac{Z}{A} \frac{e}{2mc} \int_V (\mathbf{r} \times m\mathbf{v}) d^3r = \frac{Z}{A} \frac{e\hbar}{2mc} \hat{\mathbf{l}} = g_R \hat{\mathbf{l}} \mu_N \quad (1.36)$$

with the gyromagnetic ratio of the rotor

$$g_R = \frac{Z}{A}. \quad (1.37)$$

The calculation of lifetimes and transition probabilities requires the knowledge of $BE\lambda$ - and $BM\lambda$ -values [see Eq. (B. 73)] defined by

$$B\left(\left(\frac{E}{M}\right)\lambda, I_i \rightarrow I_f\right) = \frac{1}{2I_i+1} \left| \langle I_f | \left\{ \frac{\hat{Q}_\lambda}{\hat{M}_\lambda} \right\} | I_i \rangle \right|^2. \quad (1.38)$$

Since the $M1$ -operator (1.36) conserves angular momentum, $M1$ -transitions are forbidden in this model. The most important transitions are $E2$ -transitions.

As an example, we calculate the $BE2$ -value for the transition from the one-boson state $B_{2\mu}^+|0\rangle$ to the ground state $|0\rangle$. Expressing $\hat{\alpha}_{2\mu}$ by the operators $B_{2\mu}$ and $B_{2\mu}^+$ (1.21), and using the wave function (1.22), we get to first order in the $\alpha_{2\mu}$'s

$$B(E2, 2_1^+ \rightarrow 0^+) = \left(\frac{3}{4\pi} ZeR_0^2 \right)^2 \frac{\hbar}{2B_{2\mu}\Omega_2}. \quad (1.39)$$

Before we compare these theoretical results of our model with experimental data, we must discuss which levels in the excitation spectra of nuclei would be appropriate candidates for such surface vibrations. We restrict the following discussion to 2^+ states. For other angular momenta similar considerations apply.

Figure 1.6 shows schematically the structure of the 2^+ spectra. They have a discrete part and a continuum with resonances. Among the discrete lines one 2^+ level is usually very low in energy. With a few exceptions it is the lowest excited state in each nucleus and, as shown in Fig. 1.6, it carries a large $BE2$ value, i.e., it has a high transition probability to the ground state (see Appendix B). The measured $BE2$ values are for spherical nuclei roughly ten to twenty times larger than one would expect from a pure single-particle transition [Weisskopf unit, see Eq. (B. 85)].

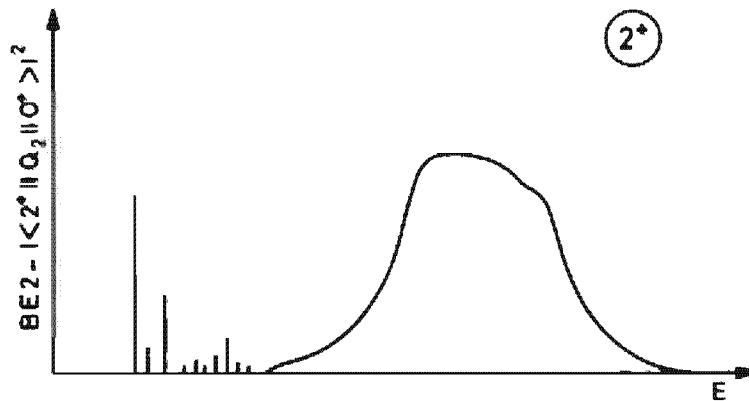


Figure 1.6. Schematic representation of the 2^+ spectra in nuclei. The ordinate gives the $BE2$ values for the discrete levels and the density of the $BE2$ strength in the resonance region. These quantities measure the transition probability to the ground state. The units are arbitrary.

The low-lying 2^+ states therefore have collective character, i.e., many particles contribute and they have very often been interpreted as surface quadrupole vibrations. Figure (1.7) shows the energy E_{2+} for the lowest 2^+ state in even-even nuclei. One observes large shell effects (see Chap. 2). Only the average trend is given by the liquid drop model with irrotational flow [Eqs. (1.19) (1.30) and (1.34)]. The absolute value is off by a factor of five. The reason for this failure will become clear below.

Experimentally, it has been found that there is a strong correlation between the $BE2$ value of the first 2^+ state and its energy $E_{2+} = \Omega_2$ [Gr 62]:

$$E_{2+} B(E2, 2^+ \rightarrow 0^+) \simeq (25 \pm 8) \frac{Z^2}{A} [\text{MeV } e^2 \text{ fm}^4]. \quad (1.40)$$

This empirical relation holds for all the nuclei throughout the nuclear table. Equation (1.39) shows the same energy dependence, but the A dependence is different. The strong shell effects in the low-lying 2^+ states indicate that they cannot be pure quadrupole surface oscillations and that there are other states which also have the character of such collective vibrations. From Eqs. (1.22), (1.21), and (1.35) we see that the quadrupole

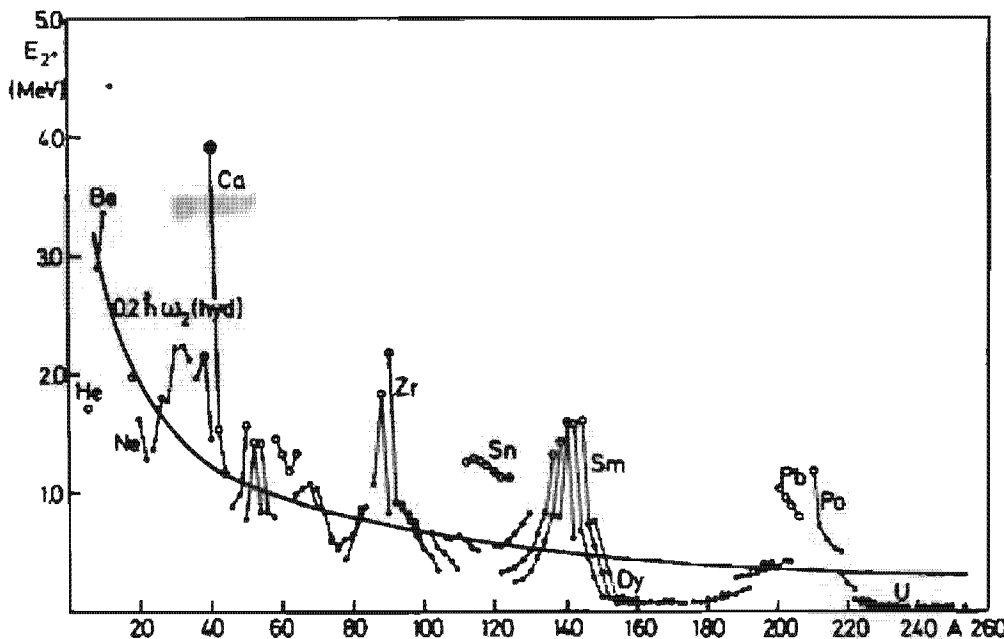


Figure 1.7. The energy of the first 2^+ state in even-even nuclei. The nuclei with closed neutron or proton shells are marked by open circles. (From [NN 65].)

surface vibration can be represented in linear order in α as:

$$|2\mu\rangle = B_{2\mu}^+ |0\rangle \propto \hat{\alpha}_{2\mu} |0\rangle \propto \hat{Q}_{2\mu} |0\rangle. \quad (1.41)$$

The overlap of an arbitrary state $|\nu\rangle$ with the quadrupole surface vibration is therefore proportional to its $BE2$ value:

$$|\langle \nu | 2\mu \rangle|^2 \propto |\langle \nu | \hat{Q}_{2\mu} |0\rangle|^2 \propto B(E2, \nu \rightarrow 0). \quad (1.42)$$

and the probability that it can be interpreted as such a vibration is given by the percentage to which it exhausts the sum rule

$$S_{2\mu}^0 = \sum_{\nu \neq 0} |\langle \nu | \hat{Q}_{2\mu} |0\rangle|^2. \quad (1.43)$$

Only if one state exhausts this sum rule to a large extent is it meaningful to call it a quadrupole surface vibration.

In Section 8.7 we will discuss in great detail the sum rules and how they can be evaluated. It is evident that in a model where the state $\hat{Q}_{2\mu} |0\rangle$ is an eigenstate of the system, like the model we are now investigating, this state exhausts the sum rules completely, because all the other states are orthogonal to it.

Experimentally, it has been found that the low-lying 2^+ state usually exhausts about 10–20% of the sum rule. The major part is exhausted by the resonances in the continuum [see Fig. (1.6)], the so-called giant resonances.

Such giant resonances for different I values have been observed. The most famous is the giant dipole resonance (1^-) which has been well known since more than 30 years and lies at an energy (see Fig. 1.8) (for more details see Chap. 13):

$$\Omega_{1^-}^{GR} \approx 77 \cdot A^{-1/3 + -1/6} [\text{MeV}]. \quad (1.44)$$

As we shall see in Chapters 8 and 13, it corresponds to a vibration of the neutron and proton sphere against one another and cannot be described in the present simple model.

In the last ten years, further giant resonances have been observed. The most important example is the isoscalar giant quadrupole resonance. It lies at (see Fig. 1.8)

$$\Omega_2^{\text{GR}} \approx 62 \cdot A^{-1/3} [\text{MeV}] \quad (1.45)$$

and exhausts in most cases a major part of the S_{2+} sum rule.

It seems, therefore, to be more reasonable to interpret this resonance as the quadrupole surface vibration mode discussed so far. The liquid drop model in this form is, however, not able to give the proper A -dependence. From Eqs. (1.19), (1.30), and (1.34) we get

$$\Omega_2 \propto A^{-1/2},$$

which does not agree with the experimental value (1.45). In Chapter 13 we will see that the reason for this deviation comes from the fact that the potential energy coefficients C_λ correspond to the total binding energy of the liquid drop [(1.31), (1.34)]. This total binding energy is, however, a sum of intrinsic kinetic and potential energy. The fact that (at least, for small deformations) the intrinsic kinetic energy depends on the deformation has been neglected in (1.34). This can be understood simply as an effect of the long mean free path of the nucleons and the uncertainty principle, which states that in an ellipsoidal shape the nucleons along the short axis have higher momenta than those along the long axis. An ellipsoidal momentum distribution, however, yields a larger kinetic energy than a spherical one. Since all particles are affected, it is a volume effect which dominates in general over the surface dependence given in (1.34). In Chapter 13 we will give a detailed discussion of this point.

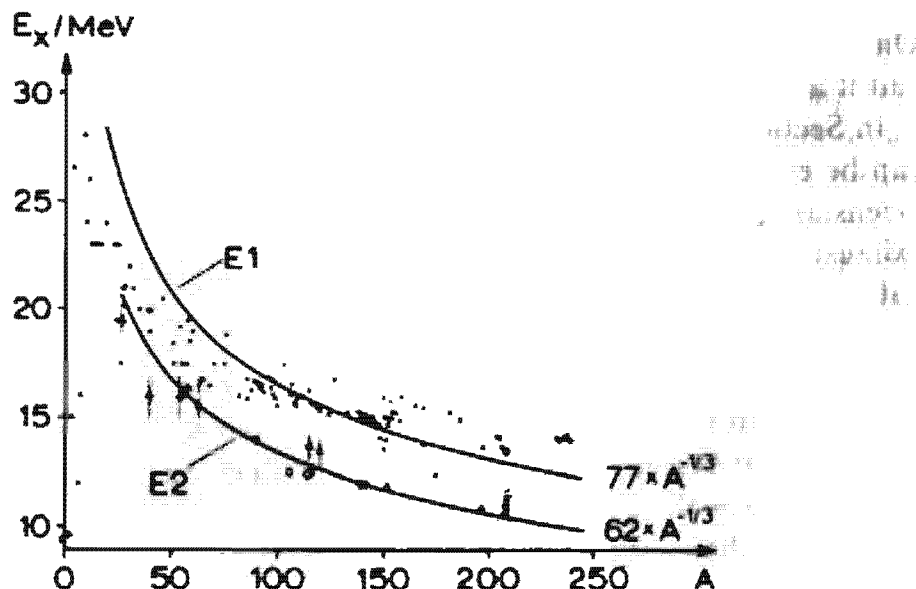


Figure 1.8. The energy of the giant dipole and the isoscalar giant quadrupole resonance as a function of mass number [Wa 73].

In spite of these deficiencies, the boson model presented so far has been extensively used over the years and has proved quite successful in explaining many features of the nuclear spectra [EG 70]. The reason for this is that many low-lying nuclear excitations have a rather collective character and can be represented to a good approximation as bosons. The parameters B_λ and C_λ may not be given very well in the liquid drop model, but, as we will show in Chapters 8 and 9, there are microscopic theories for fermions which allow more reliable calculations of B_λ and C_λ ; therefore, we should consider B_λ and C_λ more as open adjustable parameters than as determined by the LDM.

The microscopic theories also will show that the harmonic approximations (1.17) have only a very rough validity in the limit of very small vibrations. For collective motions with larger amplitudes, one has to take into account anharmonic terms such as

$$\alpha^4, \alpha^2 \cdot \dot{\alpha}^2, \dot{\alpha}^4, \dots$$

Again the corresponding parameters can be adjusted to experiment or calculated from a microscopic many-body theory (see Chap. 9).

1.5 Rotations and Vibrations for Deformed Shapes

1.5.1 The Bohr Hamiltonian

The pure liquid drop model has a stable equilibrium only for spherical surfaces. As we shall see later (Sec. 2.8) it can happen as a consequence of quantum mechanics—i.e., shell effects—that the potential $V(\alpha)$ in the collective Hamiltonian has minima at finite non-vanishing values of $\alpha = \alpha_0$. In such cases the nucleus can have a stable ground state deformation.

In this case, the nucleus can exhibit *rotations* which can be described by time-dependent surface parameters $\alpha_{\lambda\mu}$ in the laboratory frame. We shall call these rotations collective ones: This kind of rotation will not be possible around an axis of symmetry, because we cannot distinguish the rotated system from the original one in our variables $\alpha_{\lambda\mu}$.

In a quantum mechanical description, a system with an axis of symmetry (for example, the z -axis) is given by a wave function which is an eigenfunction of the angular momentum operator J_z , and any rotation about this axis produces only a phase. The rotating system has, therefore, the same wave function as the ground state, and the same energy.

This does not mean that there are no other degrees of freedom in the system that can be excited (for instance, single-particle degrees of freedom) and carry angular momentum parallel to the symmetry axis. Such a “rotation,” however, we do not call collective rotation.

Since in almost all nuclei the quadrupole degree of freedom plays a fundamental role, we will restrict the following considerations to the case $\lambda = 2$.

Assuming that the nucleus has a stable ground state deformation, it is preferable to transform to the body-fixed system, defined by the principal axes of the mass distribution (as discussed in Sec. 1.3).

After this transformation, we have five dynamical variables Ω , β , γ^* instead of the variables $a_{2\mu}$ ($\mu = -2, -1, 0, +1, +2$). We start again from the Hamiltonian (1.17). Only the potential in (1.17) is changed. It now has the form:

$$V(\beta, \gamma) = \frac{1}{2} C_{20}(a_{20}(\beta, \gamma) - a_{20}^0)^2 + C_{22}(a_{22}(\beta, \gamma) - a_{22}^0)^2. \quad (1.46)$$

This corresponds to a quadratic approximation in the vicinity of a deformed minimum β_0, γ_0 . The idea is that the nucleus has this deformation in its ground state, and the excitations are rotations and small oscillations around this equilibrium deformation.

Microscopic calculations of potential landscapes show, for certain nuclei, well pronounced minima of V for finite values $\beta_0 \approx 0.2 - 0.3$ and $\gamma_0 = 0$. These axially symmetric shapes are, therefore, the most important ones, and we will restrict a large part of our discussion to them.

The next step is the transformation of the kinetic energy in Eq. (1.17) to the body-fixed system. Applying Eq. (1.11), we have to differentiate the variables a_{20} , a_{22} , and Ω with respect to the time. Since the derivation is quite lengthy, and the intention in this chapter is not to be complete, we simply give the result (for the derivation, see, for example, [EG 70 Vol. I, Chap. 5]) for the so-called Bohr Hamiltonian [Bo 52]:

$$T = T_{\text{rot}} + \frac{1}{2} B_2 (\dot{\beta}^2 + \beta^2 \dot{\gamma}^2) \quad (1.47)$$

with

$$T_{\text{rot}} = \frac{1}{2} \sum_{\kappa=1}^3 \mathfrak{J}_\kappa \omega_\kappa^2,$$

where ω_κ is the angular velocity around the body-fixed κ -axis and \mathfrak{J}_κ are functions of β and γ given by

$$\mathfrak{J}_\kappa = 4B_2 \beta^2 \sin^2 \left(\gamma - \frac{2\pi}{3} \kappa \right), \quad \kappa = 1, 2, 3. \quad (1.48)$$

In case we have fixed deformations β, γ , T_{rot} is the kinetic energy of a rotor with the moment of inertia \mathfrak{J}_κ . As soon as we allow for changes of β and γ , the rotational and vibrational degrees of freedom are coupled by the deformation dependence of the moments of inertia. In this case, we no longer have a pure rotor. In fact, we see that in the case of $\beta_0 = 0$ the system can be transformed back to a harmonic vibrator (1.17) which has a harmonic spectrum.

However, even in the well deformed case with large stiffness parameters C and finite β_0 (where a constant $\beta = \beta_0$ is a rather good approximation),

* Unfortunately, the set of Euler angles $\Omega = (\alpha, \beta, \gamma)$ also contains the letters β and γ . However, we do not want to change this nomenclature [Ed 57] and we, as far as possible, use the abbreviation Ω .

\mathfrak{g}_κ are not the moments of inertia of a rigid rotor. Using (1.30), we get from Eq. (1.48) the so-called irrotational moment of inertia:

$$\mathfrak{g}_\kappa^{\text{irr}} = \frac{3}{2\pi} m A R_0^2 \beta^2 \sin^2 \left(\gamma - \frac{2\pi}{3} \kappa \right), \quad \kappa = 1, 2, 3.$$

It differs from the moment of inertia of a rigid body with the same deformation

$$\mathfrak{g}_\kappa^{\text{rig}} = \frac{2}{5} m A R_0^2 \left(1 - \sqrt{\frac{5}{4\pi}} \beta \cos \left(\gamma - \frac{2\pi}{3} \kappa \right) \right) \quad (1.49)$$

in the following ways.

- (i) In the γ -dependence (Fig. 1.9), $\mathfrak{g}^{\text{irr}}$ vanishes about the symmetry axes.
- (ii) $\mathfrak{g}^{\text{irr}}$ shows a strong dependence on the deformation ($\sim \beta^2$), whereas $\mathfrak{g}^{\text{rig}}$ changes much less with β (its main part is the moment of inertia of a rigid sphere).
- (iii) The experimental moment of inertia $\mathfrak{g}^{\text{exp}}$ can be found from the energy of the first 2^+ state of a rotational band [see Eq. (1.64)] $\mathfrak{g}^{\text{exp}} = 3/E_{2+}$ [MeV $^{-1}$]. Applying the empirical rule (1.40) and the formula (1.74) for the $BE2$ value, we get a connection between the deformation parameter β and the moment of inertia

$$\begin{aligned} \mathfrak{g}^{\text{exp}} &= \frac{27}{80\pi^2} r_0^4 \frac{A^{4/3} \cdot \beta^2 \cdot Z^2 e^2}{E_{2+} \cdot BE2} \approx \frac{27(1.2)^4 \cdot \beta^2 A^{7/3}}{80\pi^2 25} \\ &\approx \frac{\beta^2 A^{7/3}}{400} [\text{MeV}^{-1}]. \end{aligned} \quad (1.50)$$

In the case of well deformed nuclei ($\beta \sim 0.2 - 0.4$), $\mathfrak{g}^{\text{irr}}$ is usually smaller by a factor of 2–3 than the experimental values. On the other side, the values of $\mathfrak{g}^{\text{rig}}$ are a factor of 2 too large:

$$\mathfrak{g}^{\text{irr}} < \mathfrak{g}^{\text{exp}} < \mathfrak{g}^{\text{rig}}. \quad (1.51)$$

This shows that the flow structure within the nuclei is certainly not irrotational. On the other hand, it is not a rigid rotor, either.

The next step is again a quantization of the classical Hamiltonian (1.47). It is well known that there is no unique prescription for the quantization of a classical Hamiltonian in the general case [Me 61]. The ambiguity comes from the freedom in ordering noncommutable operators.* Commonly one adopts the Pauli prescription [Pa 33], which calculates the Laplace operator in curvilinear coordinates. If the classical kinetic energy has the form

$$T = \frac{1}{2} \sum_{ij} f g_{ij}(\xi) \dot{\xi}_i \dot{\xi}_j, \quad (1.52)$$

* A discussion with a list of references on the quantization problem is found in [MD 73].

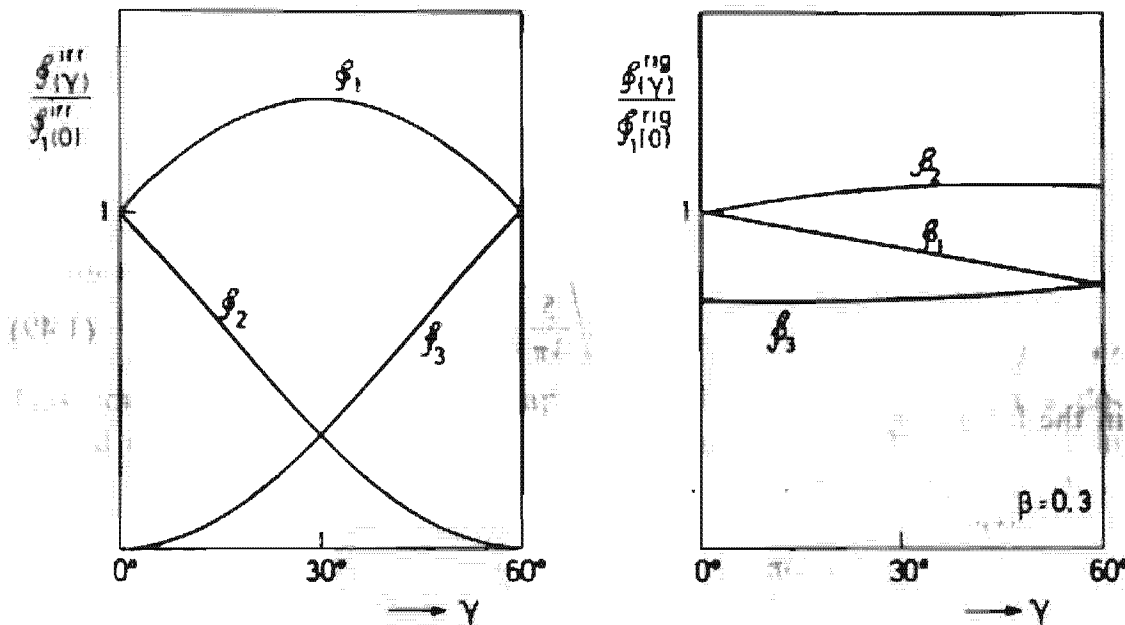


Figure 1.9. The γ -dependence of the irrotational (g_i^{irr}) and the rigid (g_i^{rig}) moments of inertia for fixed values of β .

then the corresponding quantized form is*

$$\hat{H}_{\text{kin}} = -\frac{\hbar^2}{2} \sum_{ij} g^{-1/2} \frac{\partial}{\partial \xi_i} g^{1/2} (g^{-1})_{ij} \frac{\partial}{\partial \xi_j}, \quad (1.53)$$

where g is the determinant and g^{-1} is the inverse of the matrix g_{ij} .

Applying this prescription to the Bohr Hamiltonians (1.46) and (1.47), we obtain:

$$\begin{aligned} \hat{H}_{\text{coll}} = & \frac{-\hbar^2}{2B_2} \left[\beta^{-4} \frac{\partial}{\partial \beta} \left(\beta^4 \frac{\partial}{\partial \beta} \right) + \frac{1}{\beta^2 \sin 3\gamma} \frac{\partial}{\partial \gamma} \left(\sin 3\gamma \frac{\partial}{\partial \gamma} \right) \right] \\ & + \hat{T}_{\text{rot}} + V(\beta, \gamma), \end{aligned} \quad (1.54)$$

where the rotational energy is found to be

$$\hat{T}_{\text{rot}} = \frac{\hat{I}_1^2}{2g_1} + \frac{\hat{I}_2^2}{2g_2} + \frac{\hat{I}_3^2}{2g_3}. \quad (1.55)$$

The operators \hat{I}_i are the projections of the total angular momentum $\hat{\mathbf{I}}$ represented in the Euler angles onto the body-fixed axes (for details, see Appendix A). Figure (1.10) shows the total angular momentum and its components $\hat{I}_z = M$ and $\hat{I}_3 = K$. The eigenfunctions of $\hat{\mathbf{I}}^2, \hat{I}_z, \hat{I}_3$ are given by

$$|IMK\rangle = \sqrt{\frac{2I+1}{8\pi^2}} D_{MK}^{I*}(\Omega). \quad (1.56)$$

Since $H_{\text{coll}}, \hat{\mathbf{I}}^2$ and \hat{I}_z commute, the eigenfunctions of the collective Hamil-

* To see that the Hamiltonian (1.53) is Hermitian, one has to take into account the volume element $\sqrt{g} d\xi_1 \dots d\xi_3$.

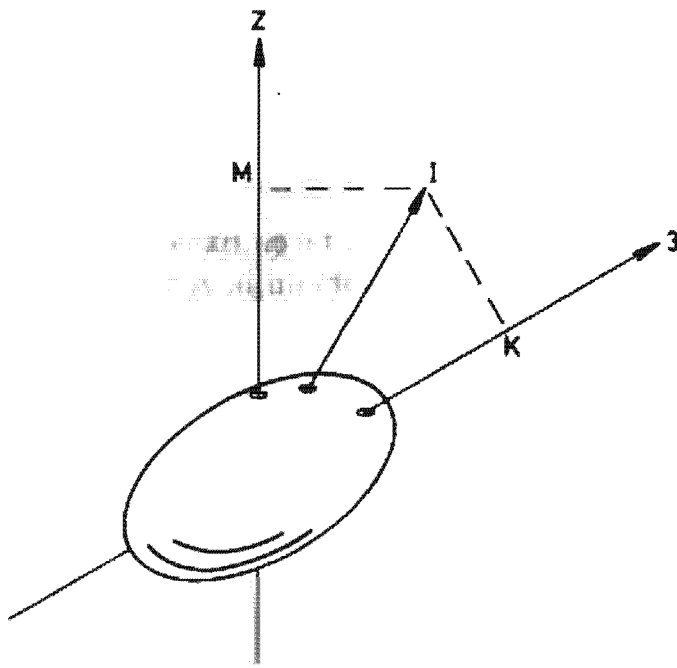


Figure 1.10. The relation between the total angular momentum \mathbf{I} and its projection M onto the laboratory z axis and its projection K onto the body-fixed 3 -axis.

tonian (1.54) have the general form

$$|\Psi_M^I\rangle = \sum_K g_K(\beta, \gamma) |IMK\rangle.$$

The triaxial rotor has certain discrete symmetries. \hat{H}_{coll} is invariant under the point group D_2 [Bo 52]. Therefore, one classifies the eigenstates according to the irreducible representations of this group, and one can derive from this some properties of the spectra [Da 68].

One example is the rotation of 180° around the 1-axis,

$$\mathcal{R}_1 = e^{i\pi \hat{J}_1}, \quad (1.57)$$

which is equivalent to a reflection with respect to the 2, 3-plane together with a parity transformation. It commutes with \hat{H}_{coll} and we require our eigenfunctions to have eigenvalue $+1^*$:

$$\mathcal{R}_1 |\Psi_M^I\rangle = |\Psi_M^I\rangle. \quad (1.58)$$

Using relation (A.24) of Appendix A, we find that this is only possible with

$$g_K(\beta, \gamma) = (-)^I g_{-K}(\beta, \gamma). \quad (1.59)$$

If we require, in the same way, symmetry with respect to

$$\mathcal{R}_2 = e^{i\pi \hat{J}_2}, \quad (1.60)$$

we get

$$g_K(\beta, \gamma) = (-)^{I+K} g_{-K}(\beta, \gamma). \quad (1.61)$$

* As we shall see in Eq. (11.123), the microscopic intrinsic wave function of the system is an eigenstate of this operation with eigenvalue +1 (see also [Bo 76 b]).

1.5.2 The Axially Symmetric Case

The Hamiltonian \hat{H}_{coll} (1.54) is still very general. We shall restrict ourselves to cases of very pronounced minima in the potential surface at axially symmetric deformations $\beta = \beta_0$ and $\gamma = 0$. We expect rotations and small vibrations of the nuclear surface. Expanding $T_{\text{rot}} = \hat{I}_3^2/2g_3$ (1.55) around the point $\beta = \beta_0$, $\gamma = 0$, we obtain in zeroth order the Hamiltonian of an axially symmetric rotor with the moment of inertia $g_0 = g_1(\beta_0, 0) = g_2(\beta_0, 0)$,

$$T'_{\text{rot}} = \frac{\hat{I}^2 - \hat{I}_3^2}{2g_0}. \quad (1.62)$$

First-order terms are proportional to the deviations ($\beta - \beta_0$) and γ . They mix rotational and vibrational degrees of freedom (rotational-vibrational coupling terms) and will be neglected here. The only remaining term in H_{coll} that still couples rotations and vibrations is $\hat{I}_3^2/2g_3$. It cannot be expanded, since g_3 vanishes for $\gamma = 0$. However (as T'_{rot}), it commutes with \hat{I}_3 and K is therefore a good quantum number.

We now have to distinguish

(I) $K = 0$ bands ($I_3 = 0$). In this case, the rotational and vibrational motions decouple. The wave function is of the type

$$|\Psi'_{M0}\rangle = g_0(\beta, \gamma)|IM0\rangle. \quad (1.63)$$

They are eigenfunctions of the rotational part of the Hamiltonian (1.54). \mathfrak{A}_1 -symmetry (1.59) requires the spin sequence $I = 0, 2, 4, \dots$. A detailed investigation of the vibrational part of H_{coll} [EG 70, Vol. I, Chap. 6] shows that it is easier to handle in the variables a_{20} and a_{22} (1.13). In the first step one neglects terms in the potential $V(a_{20}, a_{22})$, which couple these two degrees of freedom. In this case, the motion in the coordinate a_{20} (usually called β -vibration) decouples from the motion in the coordinate a_{22} (usually called γ -vibration). Axial symmetry with respect to the 3-axis is preserved by the β -vibration (quantum number n_β), but violated by the γ -vibration (quantum number n_γ). Both types of motion are shown qualitatively in Fig. 1.11.

Superimposed on each vibrational state (n_β, n_γ) is a rotational band. The spectrum is given by (see [EG 70, Vol. I, Chap. 6])

$$E_{n_\beta n_\gamma}(I) = E_{n_\beta n_\gamma}(0) + \frac{\hbar^2}{2g_0} I \cdot (I+1) \quad (1.64)$$

with the band head

$$\begin{aligned} E_{n_\beta n_\gamma}(0) &= \hbar\omega_\beta(n_\beta + 1/2) + \hbar\omega_\gamma(2n_\gamma + 1), \\ n_\beta &= 0, 1, 2, \dots, \quad n_\gamma = 0, 1, 2, \dots, \end{aligned} \quad (1.65)$$

where ω_β and ω_γ are the frequencies of β - and γ -vibrations.

$$\omega_\beta = (C_{20}/B_2)^{1/2} \quad \omega_\gamma = (C_{22}/B_2)^{1/2}$$

In fact, such bands have been observed in many even-even nuclei, in particular the ground state band ($n_\beta = n_\gamma = 0$) and the "β-band" ($n_\beta = 1$, $n_\gamma = 0$). However, as we have already discussed, the constants \mathfrak{g}_0 and ω_β , ω_γ of the hydrodynamical model do not agree with the experimental data.

(II) $K \neq 0$ bands. Together with \mathfrak{A}_1 -symmetry [Eq. (1.58)], we see that the wave function now has the form

$$|\Psi'_{MK}\rangle = g_K(\beta, \gamma) \frac{1}{\sqrt{2}} (|IMK\rangle + (-)^I |IM-K\rangle). \quad (1.66)$$

The \mathfrak{A}_1 and \mathfrak{A}_2 symmetries ((1.59) and (1.61)) give the selection rule: K must be even. Such $K \neq 0$ bands have, therefore, the spin sequence $I = |K|$, $|K|+1$, $|K|+2, \dots$. The motion in a_{20} (β -vibration) can again be separated from the rest. However, the term $\hat{I}_3/2\mathfrak{g}_3 = K^2/16B_2a_{22}^2$ couples the γ -vibration with the rotation around the 3-axis. We can easily understand this fact if we realize that a γ -vibration can be represented as a superposition of two rotations of a triaxial nucleus around the 3-axis, but with opposite K -values [BM 75, p. 656].

The following spectrum is obtained [EG 70, Vol. I, Chap. 6]

$$E_{K, n_\beta, n_\gamma}(I) = E_{K, n_\beta, n_\gamma}(0) + \frac{\hbar^2}{2\mathfrak{g}_0} (I(I+1) - K^2) \quad (1.67)$$

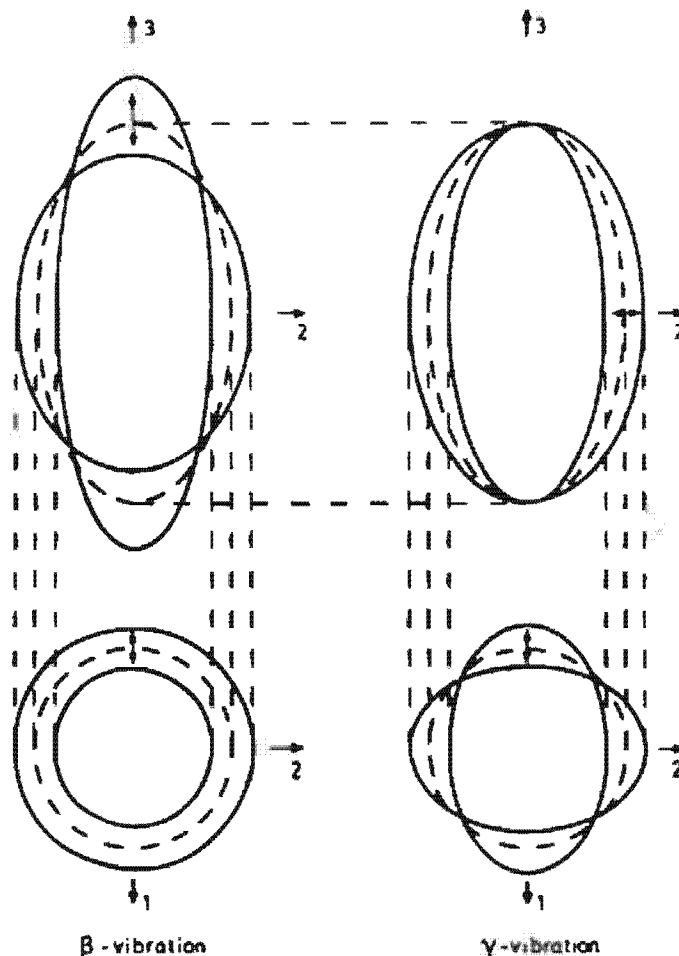


Figure 1.11. Schematic representation of β - and γ -vibrations by a cut along the (1,3) and (1,2) planes.

with the bandheads

$$E_{K, n_\beta, n_\gamma}(0) = \hbar\omega_\beta \left(n_\beta + \frac{1}{2} \right) + \hbar\omega_\gamma \left(2n_\gamma + 1 + \frac{|K|}{2} \right). \quad (1.68)$$

In fact, such bands have also been observed, especially the so-called “ γ -band” in many deformed nuclei, which has the quantum numbers $K=2$, $n_\beta=0$, $n_\gamma=0$. This γ -band has the vibrational quantum number $n_\gamma=0$, however, one is not allowed to apply the classical picture of no vibration in this case. It would correspond to $\gamma=0$ and imply $\Omega_3=0$, which would forbid a rotation with $K \neq 0$. Only the quantum mechanical zero point vibration in the γ -direction makes this possible.

Figure 1.12 shows the qualitative structure of the collective ($\lambda=2$) excitation in deformed and spherical nuclei.

The spherical nuclei have a harmonic spectrum. In the deformed nuclei we observe several rotational bands built on the ground state, on the β -vibrational state $K=0$, $n_\beta=1$, $n_\gamma=0$, and on the γ -vibrational state $K=2$, $n_\beta=n_\gamma=0$. However, these pure cases are not exactly realized in nature. In fact, we already observe in spherical nuclei a splitting of the two-boson triplet ($0^+, 2^+, 4^+$) and in the deformed nuclei deviations from the $I(I+1)$ law. There is also a wide range of transitional nuclei in between these two limits. Going from isotope to isotope, one can sometimes observe a gradual transition from a vibrational to a rotational spectrum (for instance, in the Os region [SDG 76]). This is indicated by dashed lines in Fig. 1.12.

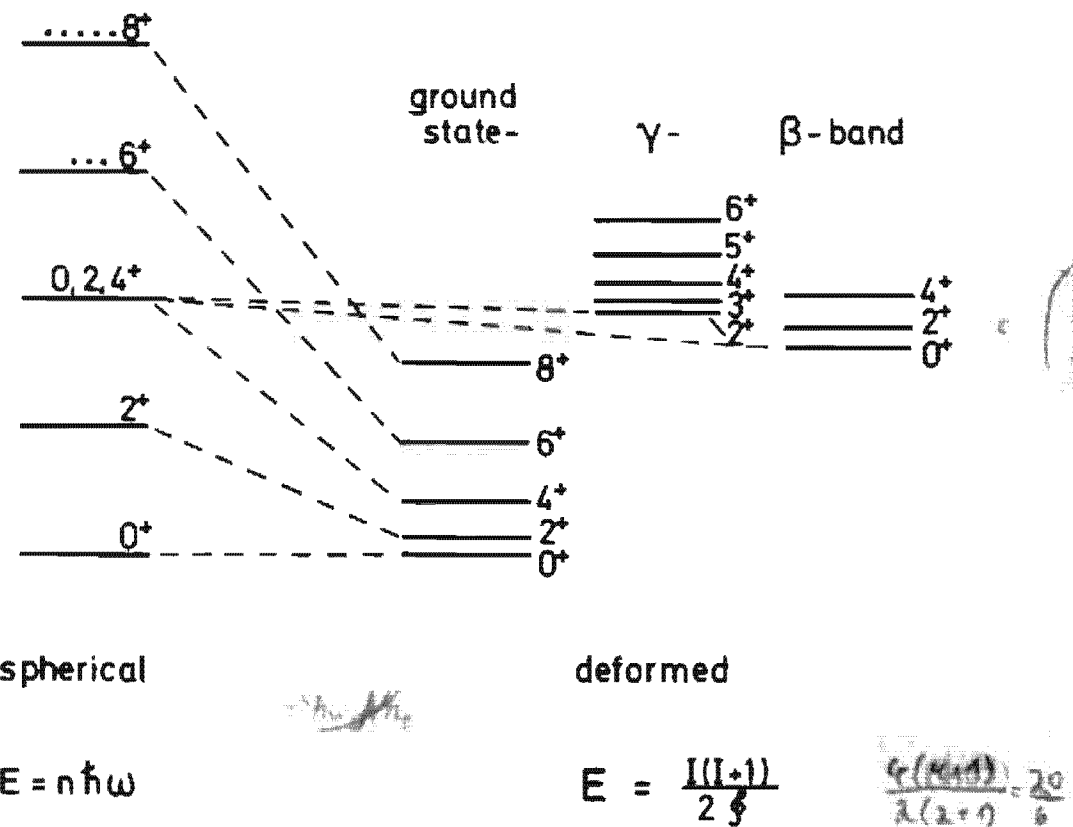


Figure 1.12. Schematic level schemes of spherical and deformed nuclei. (From [SDG 76].)

For a theoretical description of deviations from the $I \cdot (I+1)$ law, one has taken into account the rotational-vibrational coupling terms in \hat{H}_{coll} which one gets by expanding \mathfrak{g}_x in powers of the deviations $(\beta - \beta_0)$ and γ [FG 62, FG 64, FGS 65, 66, ABP 68]. This rotation-vibration interaction causes changes in the moment of inertia of a band and corresponds to a change of the nuclear shape under the influence of the rotation (stretching effect). However, there also exist quite different excitations of nuclei in this energy region, for instance, two quasi-particle states and pairing vibrations (see Chap. 8), which have a much stronger influence on the rotational bands, and which are not taken into account in this simple model of a liquid drop with surface oscillations.

Before we leave this section, we want to discuss very briefly how to calculate electromagnetic moments and transition probabilities. In Eqs. (1.35) and (1.36) we defined the electric multipole and the magnetic moment operator in the coordinates $\alpha_{\lambda\mu}$. They are obviously written down in the laboratory system. In a deformed nucleus it is usually very easy to calculate the moments in the intrinsic system. To get the moments in the laboratory frame—the experimental values—one has to apply the transformation (1.11) of spherical tensors:

$$\hat{Q}_{\lambda\mu}^{\text{intr}} = \sum_{\mu'} D_{\mu'\mu}^{\lambda} \hat{Q}_{\lambda\mu'}^{\text{lab}}. \quad (1.69)$$

Since Q^{intr} does not depend on the Euler angles, we get from [Ed 57, Eqs. 4.6.2 and 5.4.1] the reduced matrix elements with respect to $|IMK\rangle$:

$$\langle I_1 K_1 | \hat{Q}_{\lambda}^{\text{lab}} | I_2 K_2 \rangle = \sum_{\mu'} Q_{\lambda\mu'}^{\text{intr}} (-)^{I_1 - K_1} ((2I_1 + 1)(2I_2 + 1))^{1/2} \begin{pmatrix} I_1 & \lambda & I_2 \\ -K_1 & \mu' & K_2 \end{pmatrix}. \quad (1.70)$$

We restrict ourselves now to pure K -bands and calculate only intraband $E2$ -transitions ($n_{\gamma_1} = n_{\gamma_2}, n_{\beta_1} = n_{\beta_2}$). For the reduced matrix element we find

$$\begin{aligned} & \langle n_{\beta} n_{\gamma} I_1 K | \hat{Q}_2^{\text{lab}} | n_{\beta} n_{\gamma} I_2 K \rangle \\ &= \sqrt{\frac{5}{16\pi}} Q_0(n_{\beta}, n_{\gamma}) \sqrt{(2I_1 + 1)(2I_2 + 1)} (-)^{I_1 - K} \begin{pmatrix} I_1 & 2 & I_2 \\ -K & 0 & K \end{pmatrix}, \end{aligned} \quad (1.71)$$

where $Q_0(n_{\beta}, n_{\gamma})$ is the intrinsic quadrupole moment of this band. In the ground state band with fixed β -value, and $\gamma = 0$ we have [Eqs. (1.13) and (1.35)]

$$Q_0 = \sqrt{\frac{16\pi}{5}} \frac{3}{4\pi} Ze \cdot R_0^2 \cdot \beta. \quad (1.72)$$

From (B.73) and (1.71) we obtain, for example, for the so-called stretched $BE2$ -values in a rotational band,

$$B(E2, I+2 \rightarrow I) = Q_0^2 \frac{5}{16\pi} |C_K^{I+2 \rightarrow 0K}|^2, \quad (1.73)$$

which, for $K=0$ bands, gives

$$B(E2, I+2 \rightarrow I) = Q_0^2 \frac{5}{16\pi} \frac{3}{2} \frac{(I+1)(I+2)}{(2I+3)(2I+5)}. \quad (1.74)$$

For the spectroscopic quadrupole moments $Q = \sqrt{16\pi/5} \langle IIK | \hat{Q}_{20}^{\text{lab}} | IIK \rangle$ [Eq. (B.32)], we get

$$Q = Q_0 \frac{3K^2 - I \cdot (I+1)}{(2I+3)(I+1)}. \quad (1.75)$$

The quotient of $Q : Q_0$ is the expectation value of $D_{00}^2 = P_2(\cos \beta)$ in the state $M=I$. This means that one cannot measure the internal quadrupole moment Q_0 , but only the value averaged over the rotational motion. In fact, Q_0 is not a physical observable. Its definition depends on the introduction of a body-fixed system which moves with the nucleus and has a model character. For the band head we usually have $I=K$. That means the spectroscopic quadrupole moment Q of ground states with $I=0$ vanishes and we can get information about Q_0 only for the excited states (for instance, by the reorientation effect in Coulomb excitation [BE 68], which gives the sign and the absolute value of Q_0). Another way to determine the absolute value of Q_0 is the measurement of the $B(E2)$ -values (1.73) in the transitions within a band. Recent measurements up to high spin states [WCL 76, HJE 78] have shown that in many deformed nuclei the value of Q_0 stays fairly constant within these bands, even in cases where the spectrum shows deviations from the $I(I+1)$ character. This is a hint that these deviations are not caused by the change of deformation (stretching effect).

1.5.3 The Asymmetric Rotor

The rotational-vibrational interaction model discussed so far has been on the basis of a symmetric rotor. Further attempts to explain the deviations from the $I(I+1)$ law and the low-lying second 2^+ states in many nuclei have been undertaken by Davydov et al. using the picture of a pure triaxial rotor [DF 58, DR 59, Da 59, Da 65b]. As a first step they do not consider the vibrational excitations and diagonalize only the rotational energy (1.55). With the moments of inertia (1.48), this operator is proportional to β^{-2} and one can diagonalize it for all values of γ . The constant factor can afterwards be adjusted so as to reproduce the first 2^+ state. Using the symmetries \mathfrak{A}_1 and \mathfrak{A}_2 (1.59 and 1.61), the wave functions have the form

$$|\Psi'_M\rangle = \sum_{K=0,2,\dots} g_K \{ |IMK\rangle + (-)^I |IM-K\rangle \}. \quad (1.76)$$

Figure (1.13) shows the corresponding energy eigenvalues. For $\gamma=0^\circ$ and $\gamma=60^\circ$ one gets the $I(I+1)$ spectrum. Even for strong triaxial deformations one gets only slight deviations of this form. However, additional $2^+, 3^+, 4^+$ levels come down in energy. It is a characteristic of this structure to have a low-lying second 2^+ state. Although one can, with such a model, reproduce quite reasonably the experimental

data in some regions of the periodic table (for instance, for the Os-isotopes), strong objections can be raised to it:

- (i) It is impossible to describe β -vibrations. In this case, one has to include additional vibrational degrees of freedom [DC 60]
- (ii) Well pronounced minima in the energy surface that could justify a stable γ -deformation have not been found. Microscopic calculations for such transitional nuclei usually show only very shallow valleys in the γ direction [KB 68, ASS 69, GPA 72, GG 78].*

In recent years, stable γ -deformations have found new interest, because:

- (i) Experimental data in odd-even transitional nuclei can be very well reproduced by a model of a particle coupled to an asymmetric rotor (see Chap. 5 and [MSD 74, Me 75, TF 75]).
- (ii) Theoretical calculations for very high spin states (see Sec. 1.7 and [ALL 76]) show that nuclei can become triaxial in certain spin regions.

One can get a rough estimate of the level structure of triaxial nuclei by assuming a maximal triaxiality ($\gamma = 30^\circ$). In this case, $\mathfrak{g}_2 = \mathfrak{g}_3 = \frac{1}{4}\mathfrak{g}_1 = \frac{1}{2}\mathfrak{g}_0$ (\mathfrak{g}_0 is the moment of inertia at $\gamma = 0$), and we have symmetry about the 1-axis (in the kinetic energy). The projection α of I on to this axis is a good quantum number and one finds

$$E_\alpha(I) = \frac{3A^2}{8\mathfrak{g}_0} (4I \cdot (I+1) - 3\alpha^2). \quad (1.77)$$

* Willets and Jean [WJ 56] proposed a model which is completely γ -soft, i.e., $C_{22} = 0$ in Eq. (1.46).

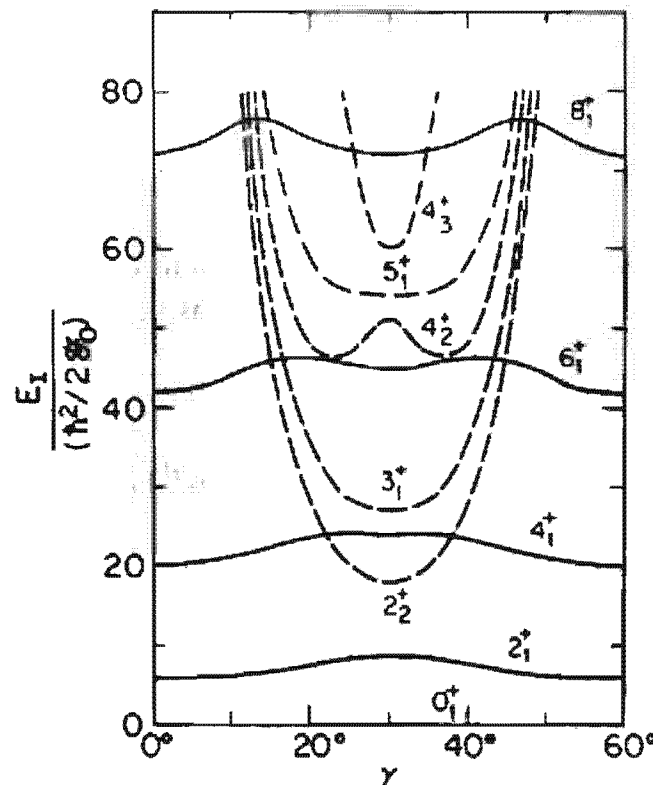


Figure 1.13. The energy eigenvalues of a deformed, asymmetric rotor with the hydrodynamic moments of inertia. (From [Me 75].)

Ω_1 and Ω_2 symmetry requires I and α to be even. For each I the level with the lowest energy (the so-called "yrast" level) has $\alpha = I$. Next in energy comes the band with $\alpha = I - 2$, then $\alpha = I - 4$, and so on. Therefore, we have a sequence of bands characterized by the "wobbling" quantum number $n = I - \alpha$ [BM 75]. One can calculate that the states with the same n are connected by large $E2$ -transition probabilities. We get their spectrum from (1.77):

$$E_n(I) = \frac{3\hbar^2}{8g_0}(I(I+4) + 3n(2I-n)). \quad (1.78)$$

However, one has to keep in mind that the structure of the spectrum (Fig. 1.13) depends drastically on the γ -dependence of the moments of inertia. There the hydrodynamical values have been used. For the rigid body values the spectrum would certainly look quite different.

1.6 Nuclear Fission

Up to now we have studied only small vibrations around the equilibrium shape in the liquid drop model. Shortly after the discovery of nuclear fission, attempts were made to understand this phenomenon using the concept of the nuclear drop [MF 39, Fr 39, BW 39].

In fact, a uniformly charged classical drop is only stable against fission (and spherical) if the Coulomb energy does not exceed a certain critical value. The Coulomb repulsion wants to deform the drop, the particles then being, on the average, further apart. The surface energy, on the contrary, being proportional to the surface of the drop, wants to keep it spherical. It is thus a subtle process of balance between these two effects (each being several hundred MeV in magnitude), which tells us whether there will be fission or not, according to a classical calculation. Of course, for such fission process, involving large deformations, one must go beyond the harmonic approximation discussed in the foregoing sections [BW 39].

The first step in describing the fission process [HW 53] is the choice of a suitable set of deformation parameters, which we call α . It has to be general enough to describe all the deformations that can occur. Cohen and Swiatecki [CS 62, 63], for instance, took as many as 18 multipolarities into account for the calculation of symmetric shapes of the form

$$R = R_0 \left(1 + \sum_{i=1}^{18} \alpha_i P_i(\cos \theta) \right). \quad (1.79)$$

This allows one to describe very general shapes. On the other hand, if one knows qualitatively the behavior of the droplet in the fission process, one is interested in introducing as few parameters as possible. Since one also wants to describe separated fragments, the set (1.79) is certainly not the most suitable one. For a realistic description of the fission process one needs at least three parameters [NS 65, Ni 72]:

- (i) a parameter c , which describes in some way the length of the major semi-axis at the beginning of the fission process, and goes over into

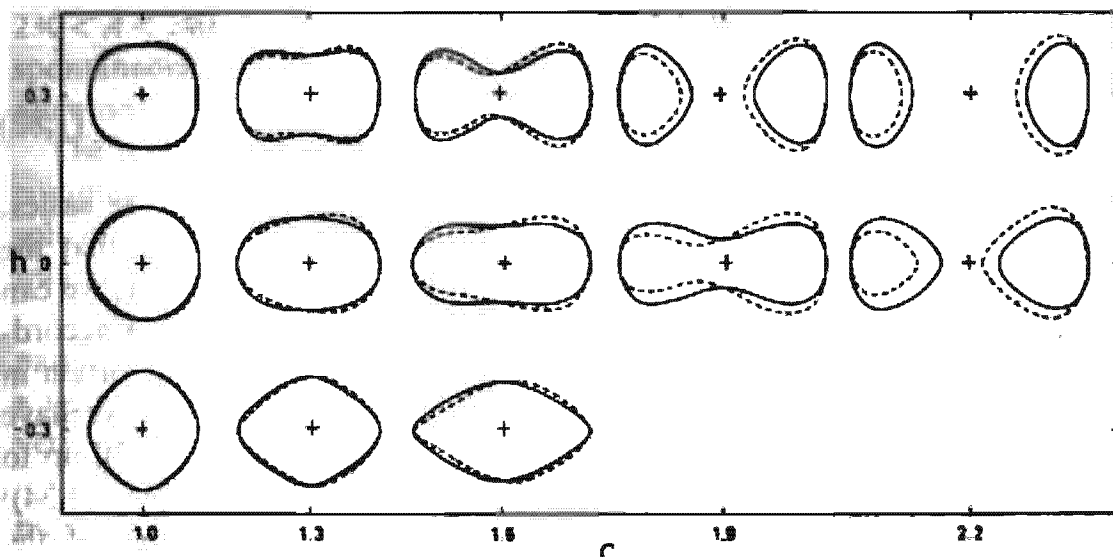


Figure 1.14. Some shapes in a suitable parameterization (c, h). Solid lines show symmetric shapes. Dotted lines have a non-vanishing asymmetry parameter α . (Taken from [BDJ 72].)

the distance between the separated fragments (*elongation coordinate*);

- (ii) a parameter h which characterizes the thickness of the neck between the fragments in formation (*neck coordinate*);
- (iii) an asymmetry parameter α , which measures the deviation from symmetry in the mass distribution of the separating fragments (in the case of asymmetric fission) (*fragmentation coordinate*).

Figure 1.14 shows an example for such a parameterization [BDJ 72].

In the next step, one has to calculate the *Hamiltonian* in the parameters α . The first part is the *potential energy* $V(\alpha)$. One usually measures it in units of the surface energy* of the corresponding sphere and gets

$$V(\alpha) = (B_S(\alpha) - 1) + 2x \cdot (B_C(\alpha) - 1), \quad (1.80)$$

where B_S and B_C are the surface energy [in units of $E_S(0)$] and Coulomb energy [in units of $E_C(0) = \frac{2}{3}(eZ)^2/R_0$]. They are calculated as in Eqs. (1.32) and (1.33). However, now one can no longer suppose small deformations and must carry out the integrals explicitly. B_S and B_C depend only on the geometry. The only parameter that characterizes the nucleus is the so-called fissibility parameter x . We find

$$x = \frac{E_C(0)}{2E_S(0)} = \frac{Z^2/A}{(Z^2/A)_{\text{crit}}}, \quad (1.81)$$

*As we have discussed earlier, the potential energy can have a volume dependence corresponding to the intrinsic kinetic energy. For the large deformations implied in the fission process the dynamics can, however, have an important effect on $V(\alpha)$: Usually one assumes that the process of spontaneous fission is so slow that the nucleons have time to adjust their momentum distribution in such a way that it gives minimal total energy at each deformation. This momentum distribution is, of course, the spherical one. (For a more detailed discussion of this point, see Chap. 13.)

where

$$\left(\frac{Z^2}{A} \right)_{\text{crit}} = \frac{40\pi}{3} \frac{r_0^3 \sigma}{e^2} \approx 50. \quad (1.82)$$

The calculations of Cohen and Swiatecki [CS 62, 63] show that the easiest way to deform the nucleus is the quadrupole deformation, and that the nuclear drop in general either stays spherical or fissions. Therefore, we can already decide, at zero deformation, whether or not fission occurs according to whether the curvature of the potential surface $V(\alpha)$ at the origin in the quadrupole direction is positive or negative. This, however, we have already calculated in considering the Bohr Hamiltonian [Eq. (1.17)] up to quadratic terms. Indeed, we see that the stiffness coefficient C_2 [Eq. (1.34)] is given by the difference of the surface and the Coulomb part of the deformation energy and C_2 starts to go negative for [Wi 64]

$$\frac{Z^2}{A} = \left(\frac{Z^2}{A} \right)_{\text{crit}} \quad \text{or} \quad x = 1. \quad (1.83)$$

This means that the classical droplet stays stable and spherical for $Z^2/A \lesssim 50$ or $x < 1$. For $x > 1$, it fissions immediately. This can be verified experimentally in giving increasing charge on a mercury drop.

For ^{238}U the mass formula (1.4) gives a Coulomb energy $E_C(0) = 830$ MeV and a surface energy $E_S(0) = 520$ MeV; for the fissibility parameter, we therefore obtain $x \approx 0.8$, which is a typical value for the mass region

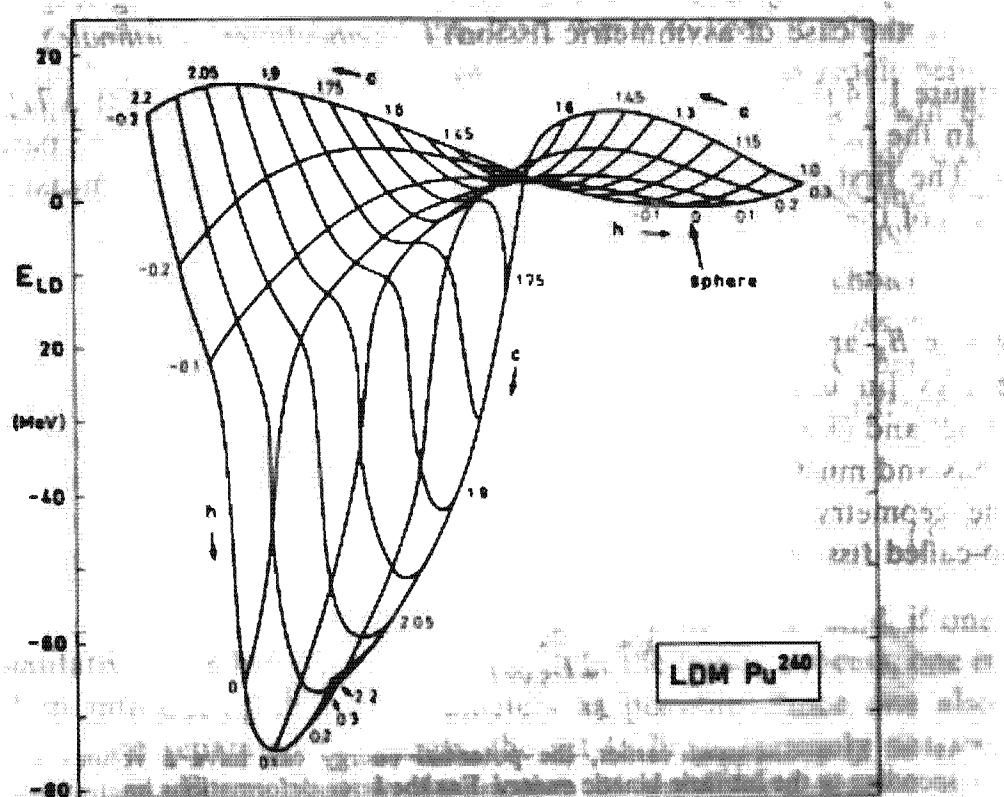


Figure 1.15. Perspective plot of the liquid drop model energy surface of ^{240}Pu . h describes the elongation and c the necking degree of freedom. (From [BDJ 72].)

$230 < A < 240$. Therefore, the classical liquid drop model cannot describe spontaneous fission. Observed spontaneous fission is thus due to the quantum mechanical tunnelling effect.

The potential energy surface (1.80) of the liquid drop has, in general, a complicated structure. For $x < 1$, we expect a minimum corresponding to a sphere, and for large distances outgoing valleys corresponding to different fragmentations [NS 65, Ni 69, MN 76].

Considering, for instance, only symmetric fission, we get for the two parameters c and h a surface as shown in Fig. 1.15. We see that it develops a well-defined saddle. Outside the saddle, the deformation energy falls off very steeply.

Cohen and Swiatecki [CS 63] have calculated the saddle-point shapes for many x -values with the ansatz (1.79). Some of them are shown in Fig. 1.16.

The meaning of these saddle-point shapes is that for a given x the drop would inevitably undergo fission if one, roughly speaking, elongates it a little bit more; conversely, it would fall back into its spherical shape if it was shortened a little bit. Going over the saddle along a line of steepest descent, the "bottom" of the fission valley defines a one-dimensional path. The length along this path is usually called the fission coordinate s . Figure 1.17 shows schematically the potential energy along this coordinate.

The fission barrier E_b is typically only a few, say, 5–7 MeV high. (This should be compared to several thousand MeV of total binding energy). Far out, the slope of the curve is due purely to Coulomb repulsion of the two droplets and thus falls off quite steeply for large Z .

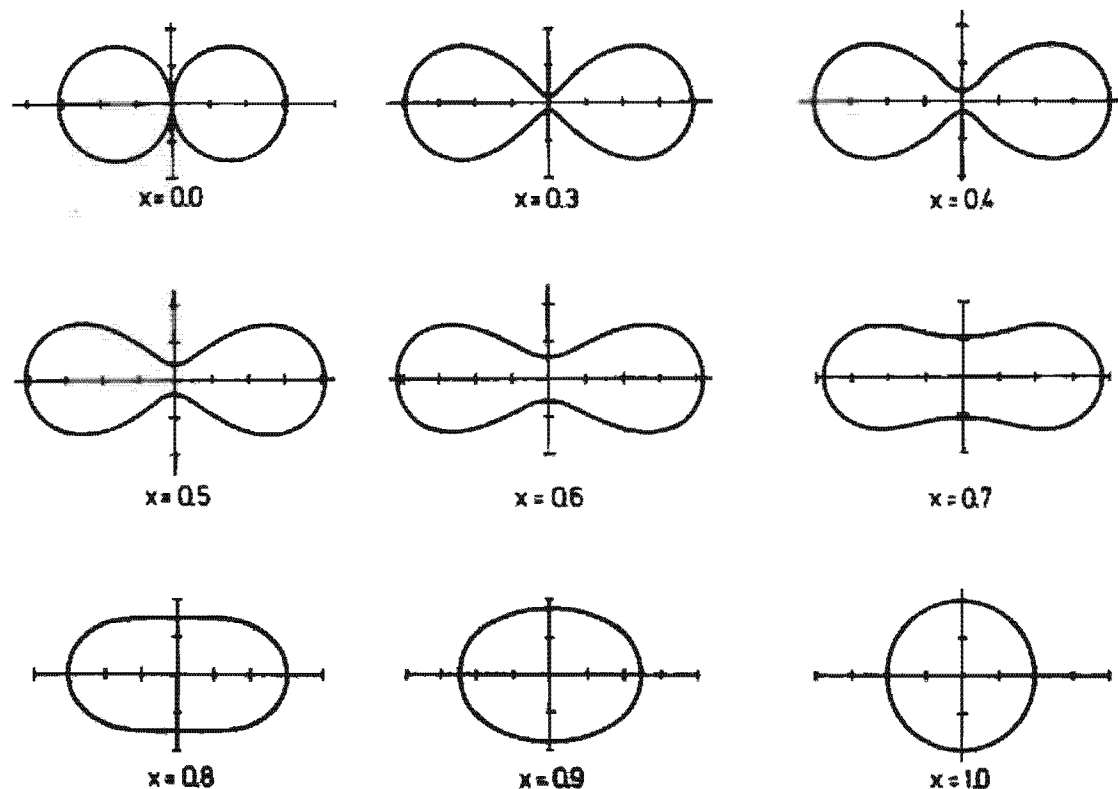


Figure 1.16. Saddle-point shapes for various values of the fissibility parameter x . (From [CS 63].)

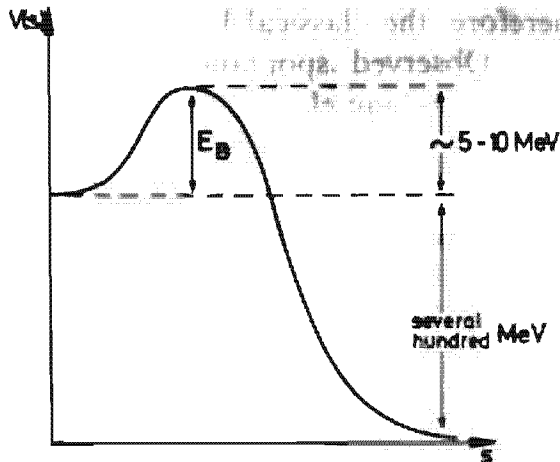


Figure 1.17. Schematic representation of the liquid drop fission barrier.

The next step in a dynamical description of fission would be the calculation of the *kinetic energy* (i.e., of mass parameters, which certainly depend on the deformation [HD 71, Gr 71]. Since the hydrodynamic model has not given good mass parameters for small oscillations, we cannot expect that it would work here either. We shall see in Section 12.3.7 how one usually calculates such quantities.

The final step would be a proper *quantization* and *solution* of the resulting Schrödinger equation. It goes far beyond the scope of this chapter to discuss such problems in detail. We only wish to mention that one usually calculates the lifetime for spontaneous fission from a WKB formula for a one-dimensional barrier penetration [Wi 64]. An essential ingredient of this formula is the shape of the potential $V(s)$, as shown in Fig. 1.17.

Unfortunately, the liquid drop model can in no way quantitatively describe fission, one of the major deficiencies being that the drop always fissions into two equally heavy fragments, whereas in fact nuclei quite often fission into unequal masses (asymmetric fission). From the fact that the fission barrier is a small number obtained from the difference of two huge numbers, we see that nuclear fission is an extremely subtle process, and we can easily imagine that, for example, quantum effects, like shell effects in the single particle motion (see Sec. 2.9), may very much affect it.

1.7 Stability of Rotating Liquid Drops

We have seen in Section 1.5 that among the vibrations of a liquid drop about a spherical surface there are rotation-like motions. In order to decouple them from the vibrations, however, we required stable finite deformations, which can only be explained by quantum mechanical shell effects. In fact, one finds rotational spectra in the experiment that justify such an assumption.

Heavy ion experiments allow the transfer of very large amounts of angular momentum (up to $80-100\hbar$) to a nucleus. At such high excitations, one should expect that quantum effects no longer play any role, and one can then ask how a classical liquid drop having such angular velocities behaves.

In this section, we are therefore only interested in the purely classical problem of how a charged and incompressible liquid drop with a sharp surface and a certain surface energy behaves under rotation around a fixed axis in space. We are not interested in surface vibrations and therefore look for the stable shapes in this system.

Again we have to say something about the flow structure in this drop, and we shall assume rigid rotation; i.e., the moment of inertia is given by

$$I = I^{\text{rig}} = \int_V r_\perp^2 \rho_0 d^3r, \quad (1.84)$$

where r_\perp is the distance of the volume d^3r from the rotational axis. As we shall see in Section 3.4, this assumption is very reasonable, because one expects the nuclear moment of inertia to approach the rigid value for high angular momenta.

The problem is very similar to the old astronomical problem of gravitating and incompressible homogeneous rotating masses. There the attractive force is the gravitation, which has the same structure (but the opposite sign) as the Coulomb force, and a surface force is neglected. Beginning with Newton, this problem has been studied by many famous mathematicians (for a historical review, see [Ch 69, Chap. 1]).

One of the results is that a gravitating droplet without surface tension has, for vanishing angular velocity ω , a spherical shape. With $\omega > 0$, it assumes first exact oblate spheroidal shapes where the rotational axis is an axis of symmetry (*Maclaurin shapes*). For increasing ω it flattens more and more, up to a certain angular velocity ω_* . For ω -values larger than ω_* , a new type of stable shape develops*—triaxial ellipsoids (*Jacobi shapes*)—and the drop rotates around the shortest principal axis. This point, ω_* , is called a bifurcation point, because for $\omega > \omega_*$ the Maclaurin shapes are still stationary, but they are no longer minima in all degrees of freedom [Ro 67]. One calls this *secularly unstable*. However, in uniformly rotating systems (gyrostatic systems) without friction forces, they can represent a stable motion (*ordinary stability*) [Ly 58]. Following the Jacobi shapes for higher ω -values, one reaches further bifurcation points. New shapes of stability develop and finally the droplet disintegrates.

Cohen, Plasil, and Swiatecki [CPS 74] investigated the problem of stability for the rotating nuclear liquid drop. They looked for the stationary surfaces of the energy

$$\begin{aligned} E(\alpha) &= E_S(\alpha) + E_C(\alpha) + E_R(\alpha) \\ &= E_S(0)(B_S(\alpha) + 2x \cdot B_C(\alpha) + yB_R(\alpha)). \end{aligned} \quad (1.85)$$

In addition to the surface (E_S) and the Coulomb (E_C) energies (see Eq. (1.32) f.), we now have the rotational energy at an angular momentum I :

$$E_R(\alpha) = \frac{\hbar^2 I^2}{2g(\alpha)} = y E_S(0) B_R(\alpha). \quad (1.86)$$

The moment of inertia is given by Eq. (1.84): $I(0) = \frac{1}{3}MR_0^2$. In addition to the fissibility parameter x , which measures the relation of Coulomb and surface energy, there is now the parameter

$$y = \frac{E_R(0)}{E_S(0)} = \frac{5}{16\pi} \frac{\hbar^2 I^2}{\sigma m r_0^4} \frac{1}{A^{7/3}} \approx 2I^2 A^{-7/3}, \quad (1.87)$$

* This corresponds to a second-order phase transition [BR 76].

which measures the relation of rotation and surface energy. The parameters x and y are determined by the properties of the nucleus and by the angular momentum one is interested in; again, the rest is pure geometry.

The result of these investigations [CPS 74] is that the nucleus behaves similarly to the gravitating droplet. At low angular momenta (low y -values), one gets flattened shapes with axial symmetry around the rotational axis. They are called *Hiskes shapes* and look similar to exact spheroids (Maclaurin shapes). They remain stable up to a critical value y_J , which corresponds to the *Jacobi point*. The value of y_J depends on x . For very heavy nuclei $x > 0.81$ the system fissions for $y > y_J$. For the rest of the nuclei a new kind of stable shape develops. These are called *Berenger-Knox shapes* [BK 61] and are similar to the Jacobi shapes. For very large angular momenta, these shapes get nearly axially symmetric around an axis perpendicular to the symmetry axis and finally become unstable against fission (y_{II}).

These calculations involve a large number of deformation parameters. One can describe the same features under the restriction of pure ellipsoidal shapes, whose half-axes a_1, a_2, a_3 are given by the two parameters β and γ^* :

$$a_\kappa = R_0 \exp \left\{ \sqrt{\frac{5}{4\pi}} \beta \cos \left(\gamma - \frac{2\pi}{3} \kappa \right) \right\} \quad (\kappa = 1, 2, 3). \quad (1.88)$$

This definition guarantees volume conservation.

* We have used the Hill-Wheeler coordinates β and γ already for the description of small quadrupole deformations [Eq. (1.13)] of the nuclear surface. Here we define the nuclear surface as an exact ellipsoid by its half axis. This was the original definition of Hill and Wheeler [HW 53]. It agrees with Eq. (1.7) only for small β -values.

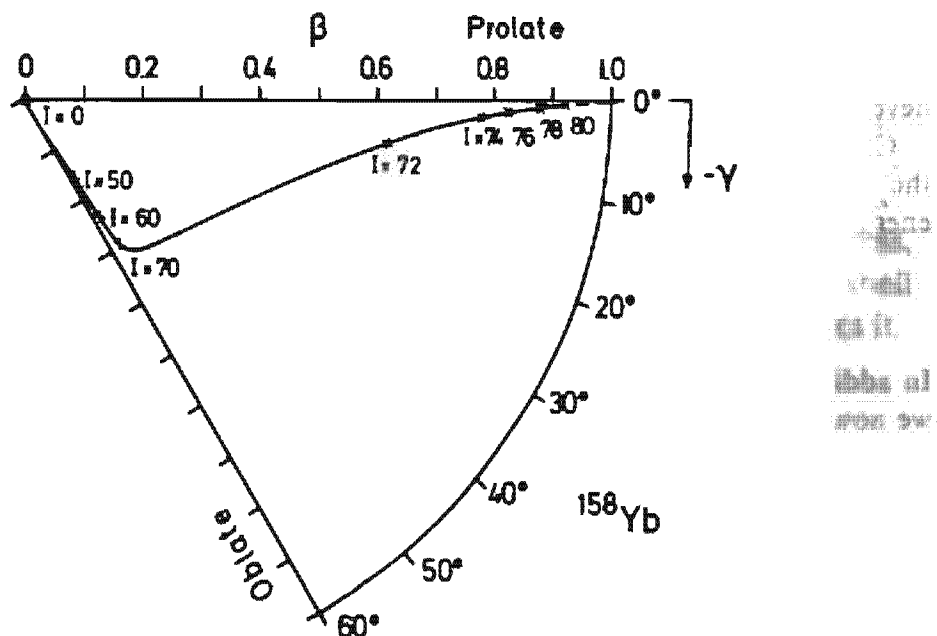


Figure 1.18. The equilibrium shapes (in terms of β and γ) of a rotating liquid drop as a function of angular momentum I . Since the I -axis is the axis of rotation, we need negative γ -values, in contrast to the usual case where the three axes are equivalent. The nucleus ^{158}Yb has a value of $x = 0.618$. (From [ALL 76].)

It is relatively easy to calculate the rigid moment of inertia, and the surface and the Coulomb energies for these ellipsoids* as a function of β and γ and to look for the minimum of the energy surface for each value of I . Connecting these stable shapes, one gets a trajectory in the $\beta-\gamma$ plane, as in Fig. 1.18.

For each I , we have an energy surface whose local minima are investigated. As in the case of $I=0$ (Sec. 1.6), there also exists, besides the minimum, a fission valley with a saddle point. Because of the centrifugal force, the barrier height gets smaller for increasing angular momentum and a family of shapes becomes unstable against fission if the barrier disappears. As an example, we take the nucleus ^{127}La [CPS 74]. At angular momentum $I=0$ its LDM fission barrier is 40.0 MeV high. Its Jacobi point (γ_J) corresponds to $I=67.8\hbar$. At this angular momentum it has an excitation energy of 44.31 MeV [$E_S(0)=49.5$ MeV] and the barrier height is only 7.8 MeV.

From this consideration it becomes clear that no nucleus can support more than a limiting angular momentum, otherwise it becomes unstable against fission. Figure 1.19 shows the angular momenta I_{II} at which the fission barrier vanishes as a function of the mass number A in the valley of beta stability [approximated by $N=A/2+0.2 \cdot A^2/(200+A)$]. Light nuclei cannot support many units of angular momentum, because of their small size. Heavy nuclei have a reduced stability caused by the Coulomb energy. Nuclei with $A \approx 130$ can reach the highest angular momenta of $\sim 100\hbar$. Experiments with heavy ions [BES 76] seem to be consistent with these limiting values of the liquid drop model.

* See, for instance, [Ca 61, CM 63].

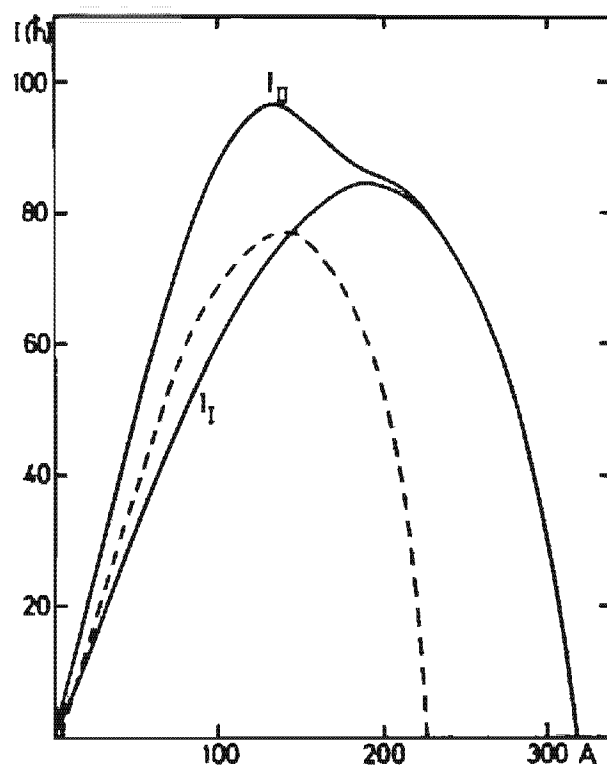


Figure 1.19. Maximal angular momentum I_{II} that a β -stable nucleus with mass number A can support, and the critical angular momentum I_1 (Jacobi-bifurcation point). The dashed line corresponds to fission barrier heights of 8 MeV, which guarantees a reasonable lifetime against fission. (From [CPS 74].)

CHAPTER 2

The Shell Model

2.1 Introduction and General Considerations

In the last chapter we considered the bulk properties of the nucleus, that is, we discussed (static or dynamic) properties for which at least a good fraction of all the nucleons in a nucleus participate. In this chapter we are going to talk about a completely different aspect of the nucleus. Indeed, many nuclear properties seem to be describable in terms of the idea that the nucleons in a nucleus are to be considered as independent particles moving on almost unperturbed single particle orbits. The reasons for this, as we stated at the beginning of the first chapter, is the fact that, mostly due to the action of the Pauli and uncertainty principles, the nucleus is not a very dense system. It is now quite well established that the nucleon-nucleon force has an almost infinitely repulsive core (see [Vi 78]) at a radius c of about $c = 0.4$ fm. Therefore, the ratio of the closest packed volume V_c to the actual volume V of a nucleus is [BM 69, Sec. 2.5]

$$\frac{V_c}{V} = \left(\frac{c}{2r_0} \right)^3 \approx \frac{1}{100}.$$

Thus the known “strong” character of the nucleon-nucleon forces is considerably reduced by the fact that the nucleons are, on the average, quite far apart, and therefore “feel” only the tail of the attractive part of the nuclear force. In other words, the violent interactions due to the singular force occur only quite seldom and the system can be described, at least in a first approximation, in terms of independent particle motion. The

fact that despite these considerations the nucleus develops a very well-defined surface, contrary to a gas, is due to a very subtle interplay of the nuclear forces and the Pauli principle [BP 77a]. For a further, more elaborate discussion of these considerations, see also [BM 69, Sec. 2.5]. The mean free path of the nucleons in a nucleus, as can be estimated from scattering experiments, seems to be at least of the order of the dimension of the nucleus [BM 69, Sec. 2.1; KK 68] and is mentioned as the first piece of experimental evidence for the unperturbed particle motion in a nucleus.

The idea of independent particles accepted, it is quite natural to envisage that this single particle motion is governed by some average potential created by all the nucleons in the nucleus. Of course, the motion of the nucleons will be considerably different in the interior of the nucleus, where it is more or less force free, from the one at the surface where the Pauli principle ceases to act and the particles feel a force confining them to the interior of the nucleus.

In this chapter we will briefly describe further experimental evidence for, and the phenomenological description and consequences of, such an average potential.

2.2 Experimental Evidence for Shell Effects

If the validity of an average potential in which the nucleons can move independently can be assumed, this immediately has some obvious consequences similar to those with which we are familiar from atomic physics.

The occurrence of the so-called magic numbers 2, 8, 20, 28, 50, 82, and 126 has, from the experimental point of view, been one of the strongest motivations for the formulation of a nuclear shell model. At these proton or neutron numbers, effects analogous to shell closure of electron shells in atoms are observed. Here we will mention just a few of them.

The single-particle separation energy is defined as the energy required to remove the least bound particle from the nucleus. In Fig. 2.1 the observed separation energies for protons and neutrons are shown.

For most nuclei the separation energy is about 8 MeV, although there are quite prominent exceptions at the magic numbers. The separation energy is largest for doubly magic nuclei. Similar exceptions for the separation energy are found for the electrons in noble gases.

The magic numbers can be seen in Fig. 2.2, which shows that the magic and doubly magic nuclei are exceptionally strongly bound. Strong binding means that the nucleus is very stable against excitations, and in Fig. 1.7 we have already shown the variation of the first 2^+ state in nuclei as a function of nucleon number. We can see especially pronounced shell effects at the magic numbers, the excitation energy rising sharply in the neighborhood of shell closures. Other collective excitations show the same variation. These examples should be sufficient as a demonstration of the occurrence of magic numbers in nuclei and of the shells corresponding to

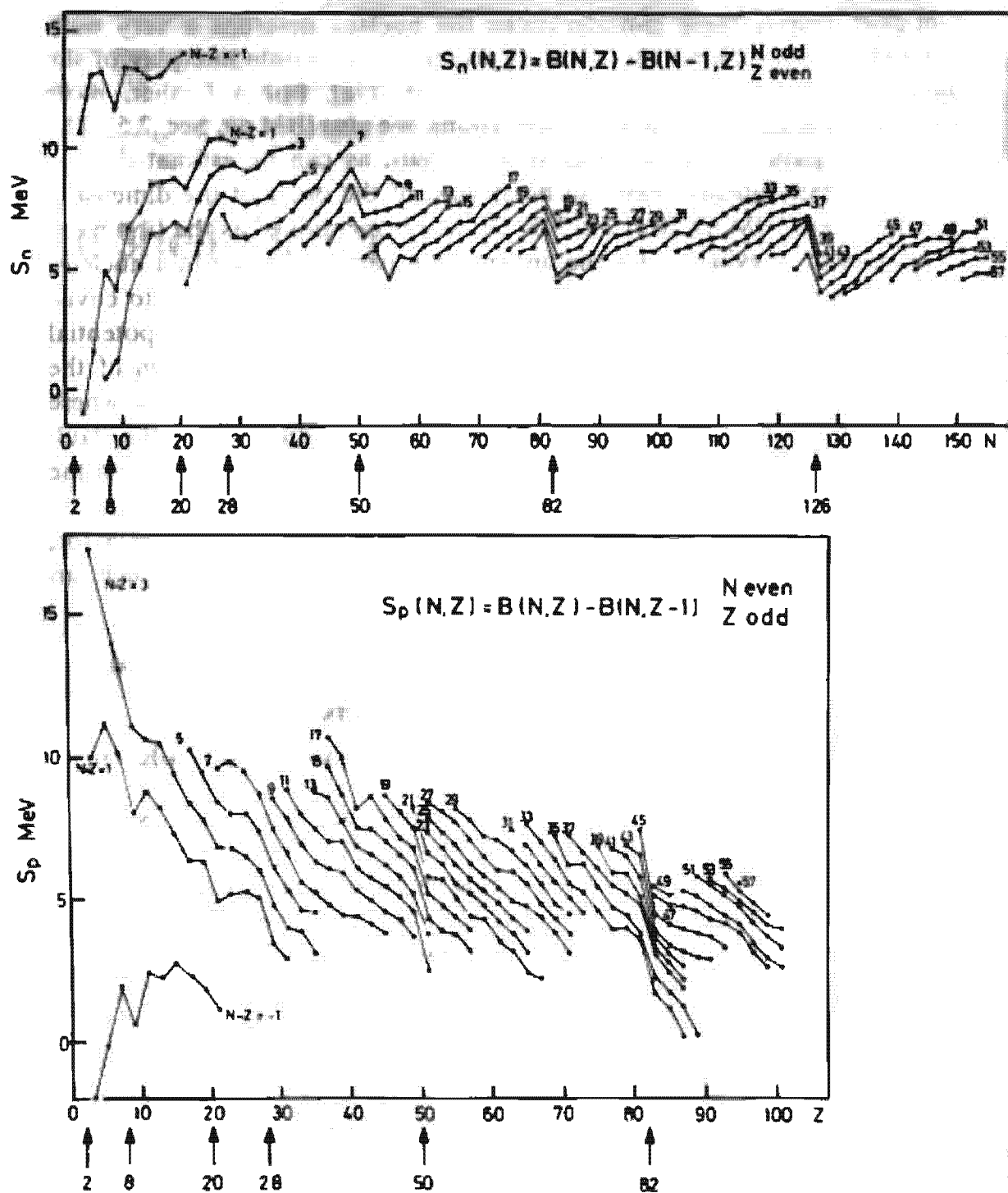


Figure 2.1. Neutron and proton separation energies as a function of neutron and proton number, respectively. (From [Ir 72].)

an average potential analogous to the ones observed in atoms. (More details may be found in [MJ 55].)

2.3 The Average Potential of the Nucleus

As mentioned above, the exceptional role of the magic numbers reveals a strong analogy to the situation of the electrons in an atom. There the strong central Coulomb potential of the nucleus imposes sphericity. As a consequence, there exist groups of degenerate levels with quite large energy differences in between the electron shells.

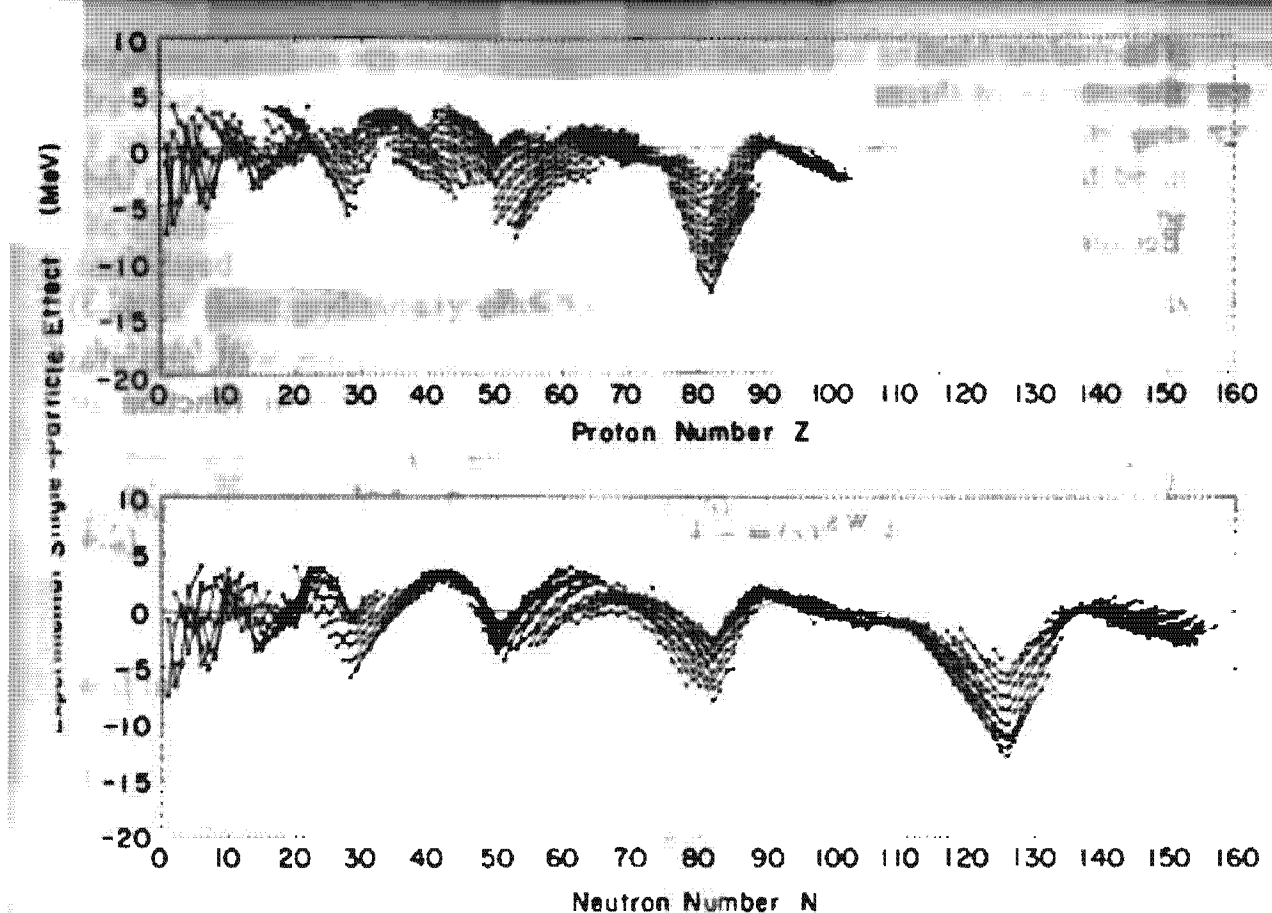


Figure 2.2. Deviations of nuclear masses from their mean values plotted as a function of neutron and proton number. (From [MS 66].)

For the nucleons of a nucleus, there exists a priori no such central field. As we have already discussed in the introduction, however, we can imagine such a potential as being built up by the action of all the nucleons. (Such an average potential also exists in the case of the electrons in an atom; there it makes an extra contribution and has to be added to the nuclear Coulomb potential. The whole is then well known as the Hartree or Hartree-Fock potential of the atom.) A model which describes the dynamics of the nucleons only with such an average potential treats the nucleons as completely independent of one another (the nucleon-nucleon interaction nevertheless comes into it in an indirect way, since it gives rise to the average potential in the first place). In the following, we will call such a model the shell model or independent particle model.

In Chapter 5 we will discuss, in great detail, how one can derive the form of this average field from a microscopic two-body force. In this chapter, we will assume that we have such a one-body potential which describes, to a good approximation, the effects of the mutual interaction between the nucleons, and investigate their consequences.

For further consideration, we have to discuss first the shape of the ad hoc introduced shell model potential. A nucleon close to the center of the nucleus will feel the nuclear forces uniformly, that is, there will be no net force

$$\left(\frac{\partial V(r)}{\partial r} \right)_{r=0} = 0. \quad (2.1)$$

The nuclear binding forces get stronger going from the surface ($r = R_0$) to the interior of the nucleus:

$$\left(\frac{\partial V}{\partial r} \right)_{r < R_0} > 0. \quad (2.2)$$

Because of the finite range of the nuclear forces, we have:

$$V(r) \approx 0, \quad r > R_0. \quad (2.3)$$

An analytic ansatz which represents these conditions quite well, and also yields quite reasonable density distributions, is the Fermi function or *Woods-Saxon potential* [WS 54] (Fig. 2.3):

$$V^{WS}(r) = -V_0 \left[1 + \exp\left(\frac{r - R_0}{a}\right) \right]^{-1} \quad (2.4)$$

with

$$R_0 = r_0 A^{1/3}; \quad V_0 \approx 50 \text{ [MeV]}; \quad a \approx 0.5 \text{ [fm]}; \quad r_0 \approx 1.2 \text{ [fm]}.$$

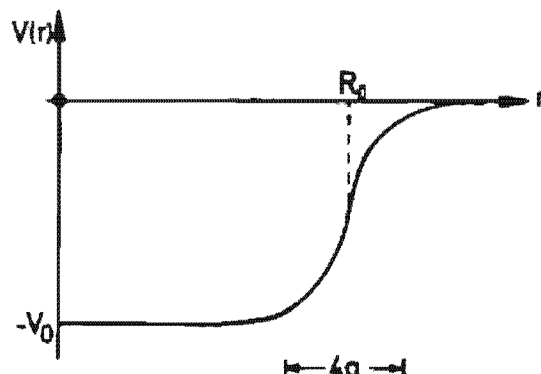


Figure 2.3. Shape of the Woods-Saxon potential.

(The Woods-Saxon potential actually has a finite but negligible slope at $r=0$.) Since the eigenfunctions for this potential cannot be given in closed form, one often uses the following two approximations for qualitative considerations, and also for calculations:

(i) harmonic oscillator

$$V(r) = -V_0 \left[1 - \left(\frac{r}{R_0} \right)^2 \right] = \frac{m}{2} \omega_0^2 (r^2 - R_0^2) \quad (2.5)$$

(ii) square well

$$V(r) = \begin{cases} -V_0 & \text{for } r < R_0, \\ +\infty & \text{for } r > R_0. \end{cases} \quad (2.6)$$

Before we discuss the solutions of Eqs. (2.4), (2.5), and (2.6) in more detail, we should perhaps note that all three potentials are spherically symmetric. For the moment, we will restrict our considerations to this case; the discussion of deformed potentials will be taken up in Section 2.8. Furthermore, it should be pointed out that (2.5) and (2.6) represent somewhat unphysical potentials, since they are infinite. However as long as we are

only interested in bound single-particle states, this is not too serious a drawback, as only the exponential tails of the wave functions are affected. If one considers excitations in these potentials, however, one easily gets into regions in which the states in the realistic potential (2.4) would be in the continuum. The use of infinite potentials in such cases is then to be considered with extreme care.

After these preliminary remarks, we want to discuss the energy levels obtained from the solution of the eigenvalue problem

$$\left\{ -\frac{\hbar^2}{2m} \Delta + V(r) \right\} \phi_i(r) = \epsilon_i \phi_i(r) \quad (2.7)$$

for the case of the potentials (2.5) and (2.6).

As is well known, the harmonic oscillator gives equidistant energy levels

$$\epsilon_N = \hbar \omega_0 \left(N + \frac{3}{2} \right) - V_0 \quad (2.8)$$

with

$$N = 2(n - 1) + l, \quad \text{where } n = 1, 2, \dots, \text{ and } l = 0, 1, 2, \dots \quad (2.9)$$

These levels are $D(N)$ -fold degenerate:

$$D(N) = \frac{1}{2}(N+1)(N+2), \quad (2.10)$$

where N is the number of quanta in the oscillator, n is the radial quantum number, l is the angular momentum, and ω_0 is the oscillator frequency. The oscillator constant ω_0 is usually determined from the mean square radius of a sphere

$$\langle R^2 \rangle = \frac{1}{A} \sum_{i=1}^A \langle r^2 \rangle_i \approx \frac{3}{5} (1.2 A^{1/3})^2 [\text{fm}^2]. \quad (2.11)$$

For oscillator states we can calculate $\langle r^2 \rangle_i$ and get

$$\frac{m}{2} \omega_0^2 \langle r^2 \rangle_i = \frac{\hbar \omega_0}{2} \left(N_i + \frac{3}{2} \right).$$

Together with Eq. (2.10), we find [Mo 57, p. 469]

$$\hbar \omega_0 \approx \frac{5}{4} \left(\frac{3}{2} \right)^{1/3} \frac{\hbar^2}{mr_0^2} A^{-1/3} = 41 \cdot A^{-1/3} [\text{MeV}] \quad (2.12)$$

and for the oscillator length

$$b = \sqrt{\frac{\hbar}{m \omega_0}} = 1.010 \cdot A^{1/6} [\text{fm}]. \quad (2.13)$$

The levels with a definite N we call an oscillator shell. Because of Eq. (2.9), the oscillator shells only contain either even or odd l -values, that is one oscillator shell contains only states with the same parity. It also follows from (2.9) that levels with the same N and with different n and l are degenerate. This accidental degeneracy of the harmonic oscillator is removed in the square-well potential (Fig. 2.4). The true energies lie between the two limits given by the potentials of Eqs. (2.5) and (2.6).

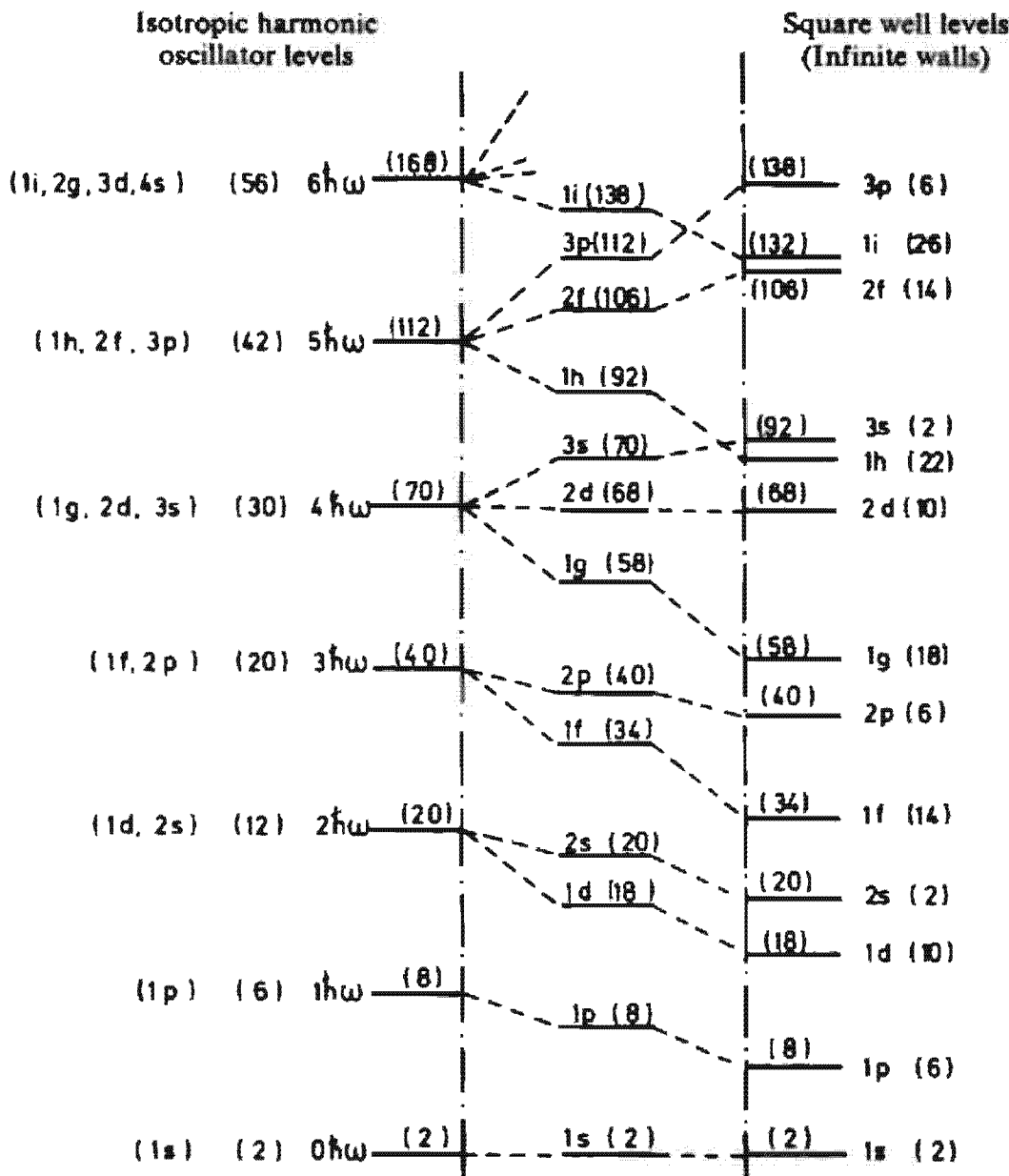


Figure 2.4. Level scheme of the isotropic harmonic oscillator (l.h.s.) and of the infinite square well (r.h.s.). (From [MJ 55]).

Filling up the level scheme with nucleons (by analogy with the periodic system of the atoms), we see that according to the Pauli principle, $D(N)$ protons and $D(N)$ neutrons can be put into each oscillator shell. This means that both potentials reproduce the magic numbers 2, 8, and 20. This model can therefore account for the unusual stability of ${}^4_2\text{He}_2$, ${}^{16}_8\text{O}_8$, and ${}^{40}_{20}\text{Ca}_{20}$. On the other hand, Fig. 2.4 contains no indications for the higher magic numbers. We will see in the next section how this deficiency of this simple model can be removed. Later, we will also discuss how the Coulomb interaction of the protons influences the average potential (Sec. 2.5).

2.4 Spin Orbit Coupling

Up to now, we have not taken into account the spin of the nucleons (apart from a factor of 2 in determining the magic numbers), that is, we considered the nuclear forces as spin independent. Treating the electrons in

atoms relativistically yields a spin dependent force in the form of a spin orbit coupling

$$f(r)ls. \quad (2.14)$$

This gives a splitting of the otherwise degenerate levels with $j = l \pm \frac{1}{2}$. In the nucleus such a splitting has also been found experimentally. Scattering of protons or neutrons on α particles yields for the lowest resonance the (unbound) ground state of ^5Li or ^5He . According to Fig. 2.4 these lowest resonances should have the quantum numbers $l = 1, j = \frac{1}{2}, \frac{3}{2}$, as the 1s-shell in ^4He is closed. One observes resonances at 1.25 and 2.4 MeV for the scattering of neutrons and protons, respectively. At these energies the angular distributions show that the resonances are predominantly $j = \frac{3}{2}$, whereas the $j = \frac{1}{2}$ resonances lie a few MeV higher in energy.

It was a decisive idea (Haxel, Jensen, and Suess [HJS 49]; Goeppert-Mayer [Ma 49]) to incorporate a strong spin orbit term into the single-particle Hamilton operator of Eq. (2.7). It was only then that the success of the shell model was confirmed. Mathematically this yields a jj -coupling scheme, since $\mathbf{l} \cdot \mathbf{s}$ commutes with $s^2, \mathbf{l}^2, \mathbf{j}^2, j_z$ but not with l_z and s_z . The levels are characterized in this coupling scheme by the quantum numbers n, l, j (e.g., $(2d\frac{5}{2}) \hat{=} (n=2, l=2, j=2 + \frac{1}{2})$), and a single particle wave function takes the following form*:

$$\phi(\mathbf{r})_{nljm} = \langle \mathbf{r} | nslijm \rangle = \phi_{nl}(r) \sum_{m_l m_s} C_{m_l m_s}^{\frac{1}{2}} Y_{lm}(θ, φ) |\frac{1}{2} m_s \rangle. \quad (2.15)$$

With the relations

$$\begin{aligned} 2ls|sljm\rangle &= (j^2 - l^2 - s^2)|sljm\rangle \\ &= [j(j+1) - l(l+1) - \frac{1}{4}]|sljm\rangle \end{aligned} \quad (2.16)$$

we are able to give the spin orbit splitting of the doubly degenerate levels $|slj = l \pm \frac{1}{2}\rangle$ for $f(r) = \text{const.}$:

$$\Delta E(l) \sim [l - (-l - 1)] = 2l + 1. \quad (2.17)$$

An attractive spin orbit potential will assure the experimentally observed fact that the $l + \frac{1}{2}$ levels are energetically always below the $l - \frac{1}{2}$ levels. Equation (2.17) shows furthermore that the splitting increases with growing values of l .

Inclusion of the spin orbit interaction to the interpolated level scheme of Fig. 2.4 yields the modified level scheme of Fig. 2.5. The model now reproduces all magic numbers correctly. The sequence of the levels within the different shells depends on the choice of $f(r)$.

The value of $f(r)$ which one could derive by analogy with the theory of electrons in an atom using a Lorentz invariant treatment of the electromagnetic interactions of the nucleons (Thomas term: cf. [MJ 55, p. 60] and [EG 70, Chap. 8]) turns out to be about an order of magnitude too small.

* For calculations one has to pay particular attention to the coupling order of the angular momenta, since a different order introduces a phase which is the source of frequent errors.

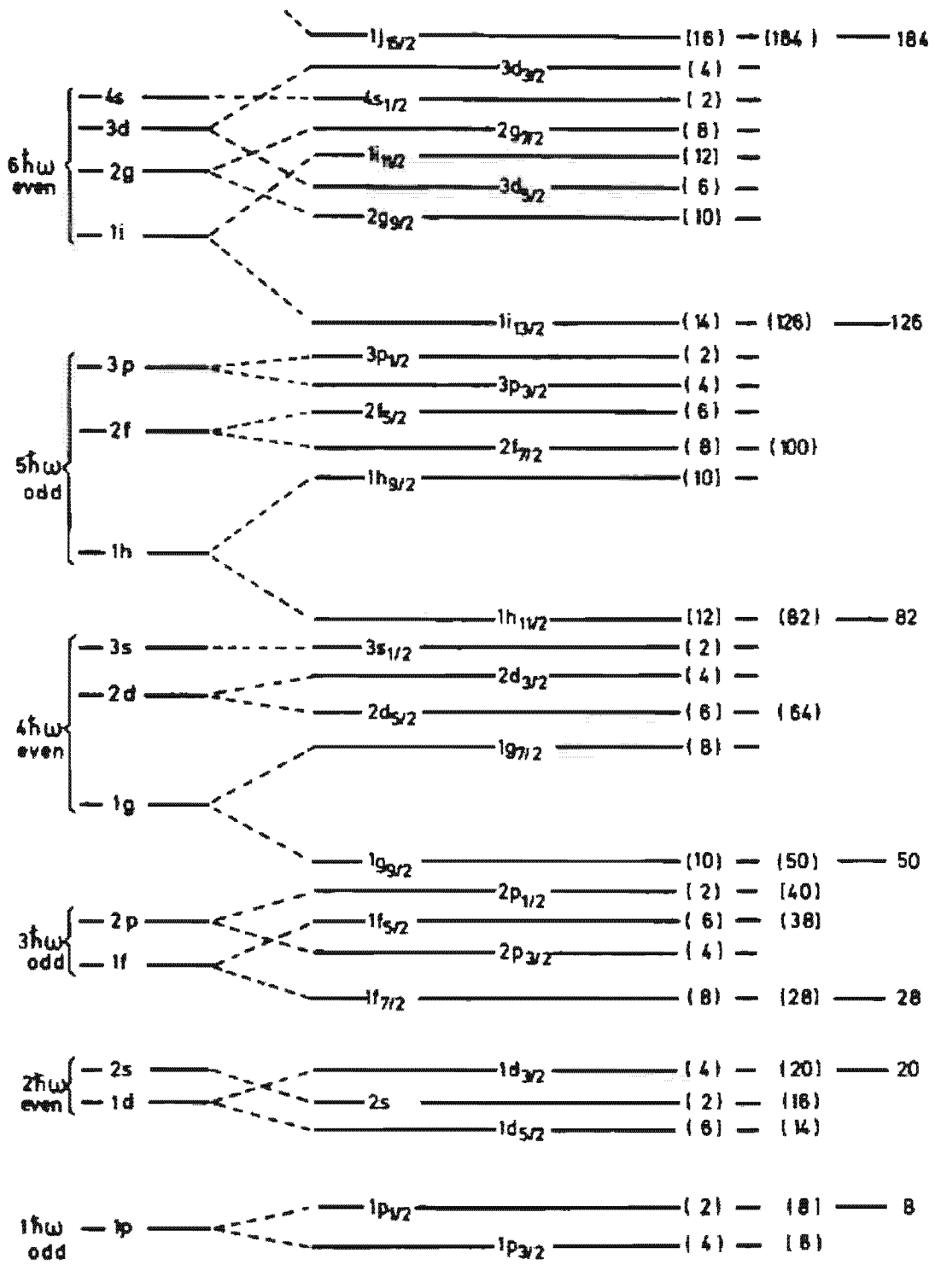


Figure 2.5. Schematic nuclear levels of the shell model with spin-orbit term. (From [MJ 55].)

As we will discuss in Chapter 4, the nucleon-nucleon forces exhibit strong spin orbit parts, and it is thus not very surprising that the average single particle potential also has a spin orbit part with a strength compatible with the strong nuclear forces.*

* Recent investigations have shown that one obtains the proper spin orbit term in the single-particle potential by a relativistic Hartree-Fock treatment of one-boson-exchange-potentials (Br 78).

One can show [Ho 75] that $f(r)$ is peaked at the nuclear surface. By analogy with the electronic case, one quite often chooses $f(r)$ related to the spin independent part of the average potential in the following way—

$$f(r) = \lambda \frac{1}{r} \frac{dV}{dr}; \quad \lambda \approx -0.5 [\text{fm}^2] \quad (2.18)$$

—but also other surface-peaked radial dependences of $f(r)$ can be envisaged. It is interesting to note that the use of the Skyrme force (see Chap. 5) yields a spin orbit dependence for the average potential with $f(r) \sim (1/r) \cdot (dp/dr)$, where ρ is the single particle density. Since $V(r)$ roughly follows the form of ρ , this is consistent with Eq. (2.18).

2.5 The Shell Model Approach to the Many-Body Problem

The single-particle model takes into account the individual nucleons. It therefore provides a microscopic description of the nucleus. This is certainly only an approximation of the exact many-body problem. We will see, however, in the following, that the shell model can be used as a basis for more elaborate many-body theories, so before we talk about further details of the model, we want to discuss some general properties of the single particle model.

The microscopic theory of the nucleus is usually based on the following three properties.

- (i) The nucleus is a quantum mechanical many-body system.
- (ii) The velocities in the nucleus are small enough so that one can neglect relativistic effects [$(v/c)^2 \sim 1/10$].
- (iii) The interaction between the nucleons has a two-body character.

A full microscopic theory of the nucleus would then be given by the solution of the many-body Schrödinger equation

$$H\Psi = \left\{ \sum_{i=1}^A -\frac{\hbar^2}{2m} \Delta_i + \sum_{i < j} v(i, j) \right\} \Psi(1, \dots, A) = E\Psi(1, \dots, A), \quad (2.19)$$

where i represents all coordinates of the i th nucleon, for instance,

$$(i) = (\mathbf{r}_i, s_i, \ell_i), \quad (2.20)$$

where ℓ_i will be $\frac{1}{2}$ for neutrons and $-\frac{1}{2}$ for protons. With the assumption of the nuclear shell model, the above equation reduces to the much simpler equation

$$H_0\Psi = \left\{ \sum_{i=1}^A h_i \right\} \Psi = \sum_{i=1}^A \left\{ -\frac{\hbar^2}{2m} \Delta_i + V(i) \right\} \Psi = E\Psi. \quad (2.21)$$

The solutions Ψ of Eq. (2.21) are anti-symmetrized products of single-particle functions, which are eigenfunctions to the single-particle Hamil-

nian \hbar :

$$h_i \phi_k(i) = \epsilon_k \phi_k(i). \quad (2.22)$$

The functions ϕ_k provide an orthogonal basis for an occupation number representation within the framework of second quantization (see Appendix C). To each level k corresponds a pair of creation and annihilation operators a_k^+ , a_k which create or annihilate particles with wave function ϕ_k . Since nucleons are Fermions, each level can be occupied only once, and the operators a_k , a_k^+ obey Fermi commutation relations (C. 23).

The shell model Hamiltonian H_0 has the form

$$H_0 = \sum \epsilon_k a_k^+ a_k.$$

Using the bare vacuum $|-\rangle$ its eigenfunctions can be represented as

$$|\Phi_{k_1 \dots k_A}\rangle = a_{k_1}^+ \dots a_{k_A}^+ |-\rangle.$$

They are Slater determinants

$$\Phi_{k_1 \dots k_A}(1, \dots, A) = \begin{vmatrix} \phi_{k_1}(1) & \dots & \phi_{k_1}(A) \\ \vdots & & \vdots \\ \phi_{k_A}(1) & & \phi_{k_A}(A) \end{vmatrix} \quad (2.23)$$

with eigenvalues

$$E_{k_1 \dots k_A} = \epsilon_{k_1} + \dots + \epsilon_{k_A}. \quad (2.24)$$

In the ground state the levels are filled successively according to their energy (see Fig. 2.6)

$$|\Phi_0\rangle = a_1^+ \dots a_A^+ |-\rangle. \quad (2.25)$$

Thus we have for closed shells the following unique prescription for the construction of the A particle ground state as well as for the A particle excitation spectrum: Starting with the $(1s_{1/2})$ level, one has to occupy each level $|nsljm\rangle$ with just one particle until all A particles are used up. We thus obtain an A nucleon ground state where all different quantum states are occupied with just one particle up to the Fermi level (the highest occupied level); above the Fermi level all levels are unoccupied.

The independent particle picture of the nucleus is different from that in an atom in the sense that in a nucleus there are two different kinds of particles, the proton and the neutron, whereas in an atom there is only the

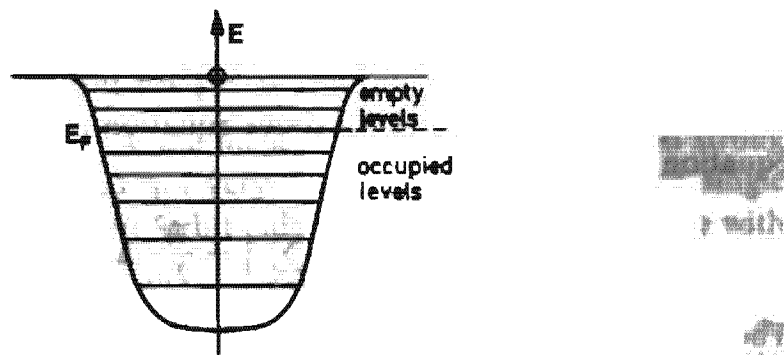


Figure 2.6. Shell model potential and Fermi level.

electron. Protons and neutrons feel different average potentials for two reasons:

- (i) Protons also interact via the *Coulomb force*. One therefore usually adds the potential of a homogeneously charged sphere

$$V_C(r) = \begin{cases} \frac{Ze^2}{R} \frac{1}{2} \left(3 - \left(\frac{r}{R} \right)^2 \right) & r < R, \\ \frac{Ze^2}{r} & r > R. \end{cases} \quad (2.26)$$

Sometimes (see Sec. 2.8), this feature is approximated by using different potential parameters for protons and neutrons.

- (ii) The *symmetry energy* [see Eq. (1.4)] favors a configuration with an equal number of protons and neutrons. Because of the Coulomb repulsion for heavier nuclei, one has a neutron excess: If, in the nucleus, we replace a neutron by a proton, we gain symmetry energy and lose Coulomb energy. Since the Coulomb energy is already taken into account by Eq. (2.26), there must be an additional difference between the single-particle potential for protons and neutrons, which is caused by the symmetry energy. The *nuclear* part of the proton potential is therefore deeper (see Fig. 2.7, dashed line).

These two effects go in opposite directions, but they do not cancel. In the end, the Fermi surfaces for protons and neutrons must be equal, otherwise protons would turn into neutrons by β -decay or vice versa, whichever is energetically favored.

In $N \neq Z$ nuclei, energy levels with the same quantum numbers for protons and neutrons are therefore shifted with respect to one another by an amount Δ_e , resulting from a positive contribution Δ_C from the Coulomb force and a negative contribution $-\Delta_S$ from the symmetry energy

$$\epsilon_{n\ell}^{(p)} - \epsilon_{n\ell}^{(n)} = \Delta_e = \Delta_C - \Delta_S. \quad (2.27)$$

In heavy nuclei, this difference is such that the protons and neutrons at the Fermi surface belong to different major shells.

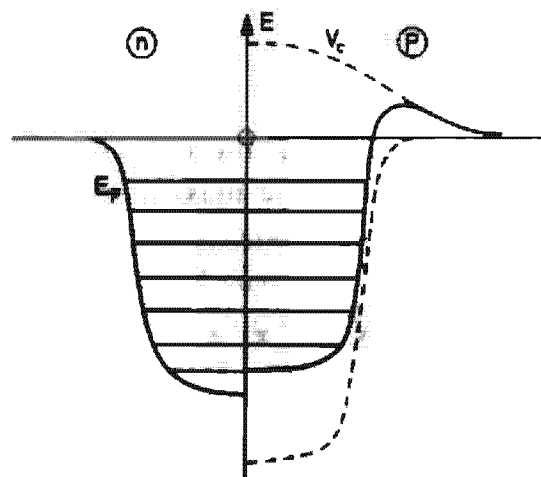


Figure 2.7. Comparison of the shell model potential for neutrons and protons in a nucleus with neutron excess.

Strong support of the independent particle idea comes from the experimental fact that magic numbers are the same for protons and neutrons (see Fig. 2.2; the magic number 126 exists only for neutrons, since for the heaviest nucleus known so far we only have $Z = 103$). If correlations played a major role, then, for example, the neutron excess in heavier nuclei would eventually influence the proton magic numbers in these nuclei (the nuclear force is almost charge independent; see Chap. 4) to be different from the corresponding neutron numbers. However, as we have said, this is not the case. The subshells of a major shell have, in some cases, a different order.

In the shell model, the *excitations of the system* are given by analogy with the free Fermi gas by a transfer of nucleons from below the Fermi level to levels above it. In the case of only a single nucleon transfer, we talk of an $1p - 1h$ state with excitation energy of $\sim \hbar\omega_0$. For $^{40}\text{Ca}_{20}$ such a state is, for example, given by

$$(2s_{\frac{1}{2}})^{-1}(1f_{\frac{5}{2}}).$$

The Fermi level coincides in this case with the $1d_{3/2}$ level (see Fig. 2.5).

If we use the indices i, j for the levels below the Fermi surface ($\epsilon_i < \epsilon_F$), and the indices m, n for the levels above the Fermi surface ($\epsilon_m > \epsilon_F$), the lowest excitations in the shell model are then ph excitations of the form

$$|\Phi_{mn}\rangle := a_m^+ a_i |\Phi_0\rangle = \pm a_m^+ a_i^+ \dots a_{i-1}^+ a_{i+1}^+ \dots a_n^+ |-\rangle \quad (2.28)$$

with excitation energy $\epsilon_{mn} = \epsilon_m - \epsilon_i$.

In fact one has observed such states in magic nuclei. They are, however, not the lowest states. As we have already seen in Chapter 1, there are low-lying collective states which cannot be explained in the independent particle model.

The Slater determinants (2.23) form a *complete set* of states for the A nucleon system [Lö 55]. Each state of the system is characterized by the distribution of the nucleons among the levels of the single particle potential, that is, by the "occupation numbers" of the levels. It is usual to classify all excited states by taking the ground state as a reference state. The nucleons that are missing in the ground state are denoted by holes, those above the Fermi levels by particles. A typical multiparticle–multihole configuration is shown in Fig. 2.8

Starting from a magic nucleus with the mass number A , we can add a particle and obtain a nucleus with the mass number $A + 1$. If we put the

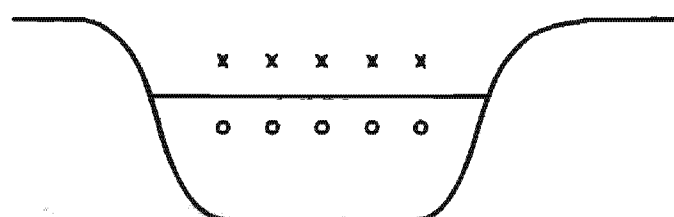


Figure 2.8. Schematic representation of a typical five-particle (crosses), five-hole (open circles) state.

particle into the level m , the wavefunction is

$$|\Phi_m\rangle = a_m^+ |\Phi_0\rangle \quad (2.29)$$

and we get the energy difference

$$\epsilon_m = E_m(A+1) - E_0(A). \quad (2.30)$$

In this way one is able to measure the single-particle energies (see Sec. 2.7). These are the simplest states in $A+1$ nuclei. More complicated states have a $2p-1h$ structure, and so on. In complete analogy, there are $1h, 1p-2h$, etc., states in $A-1$ nuclei.

It often turns out to be very convenient to define quasiparticles by the operators

$$\begin{aligned} a_m^+ &= a_m^+, & a_m &= a_m, & \text{for } \epsilon_m > \epsilon_F; \\ a_i^+ &= a_i, & a_i &= a_i^+, & \text{for } \epsilon_i < \epsilon_F. \end{aligned} \quad (2.31)$$

These quasiparticles are again fermions. They are particles for states above, and holes for states below, the Fermi surface, so that we have

$$a_k |\Phi_0\rangle = 0, \quad (2.32)$$

that is, the ground state of the magic nucleus is a "vacuum" with respect to these quasi-particles; ph states are two-quasi-particle states, and so on. The multi-quasi-particle states

$$|\Phi_{k_1 \dots k_n}\rangle = a_{k_1}^+ \dots a_{k_n}^+ |\Phi_0\rangle \quad (2.33)$$

form a complete orthogonal set in the many-body Hilbert space.

This basis is often used for further investigation of the many-body Hamiltonian H (2.19). In the shell model, one decomposes H ,

$$H = T + \sum_{i < j} v(i, j) = H_0 + V_R, \quad (2.34)$$

with the residual interaction

$$V_R = \sum_{i < j} v(i, j) - \sum_i V(i) \quad (2.35)$$

in such a way that V_R is as small as possible and can be neglected. More elaborate theories investigate V_R in the basis in which H_0 is diagonal, the shell model basis (see Chap. 8).

The exact ground state wave function of a magic nucleus has the form

$$|\Psi_0\rangle = C_0 |\Phi_0\rangle + \sum_{mi} C_{mi} a_m^+ a_i^+ |\Phi_0\rangle + \frac{1}{4} \sum_{\substack{mi \\ m'i'}} C_{mim'i'} a_m^+ a_m^+ a_i^+ a_{i'}^+ |\Phi_0\rangle + \dots \quad (2.36)$$

If the shell model is a good approximation to the nucleus, the coefficients C_{mi} , $C_{mim'i'}$, etc. should be small (see Fig. 10.3).

At this point we would like to again stress the fact that we have always been talking about a *spherical shell model* potential. Since, as we shall see, spherical nuclei exist only in the neighborhood of magic nuclei, by the same token this means that we have restricted our discussion to such nuclei. As this spherical average potential is created by the nucleons themselves, it may depend (though not abruptly) on the nucleon number A in quite a subtle way, in contrast to the atomic case. It is such that we

cannot take a once-and-for-all fixed single-particle potential and hope to find the corresponding single-particle states realized very accurately, be it even over a very limited range of neighboring nuclei.

We should keep these precautions in mind when talking about the shell model. As we said, the filling of the shells is without ambiguity, if we have closed shells. When we start filling neutrons and protons in *unfilled shells* these states will be degenerate, because the j -shells have a $(2j+1)$ -fold degeneracy. The configuration of the nucleus can then be characterized by two numbers, κ and λ , which stand for the proton and neutron numbers, respectively, in the partially filled j -shell. Let the partially filled neutron shell be characterized by the quantum numbers $(n \ l \ j)$, and the partially filled proton shell by $(n' \ l' \ j')$. One then denotes the configuration by

$$(vnlj)^\kappa (\pi n'l'j')^\lambda.$$

Because of the $2j+1$ -fold degeneracy of each j -shell, all possible shell model states corresponding to this configuration are also degenerate. The number of antisymmetric, linearly independent products is given by the product of the binomial coefficients

$$\binom{2j+1}{\kappa} \binom{2j'+1}{\lambda}. \quad (2.37)$$

The degeneracy of all these states will, of course, be removed in reality due to the action of the residual interaction V_R (2.35), which is neglected in the shell model. Taking one of the phenomenological nucleon-nucleon forces, as discussed in Chapter 4, one can diagonalize V_R in the subspace (2.37). Usually one takes not only this subspace into account, but also the one which corresponds to the nearly degenerate levels of a whole major shell. The $s_{1/2}$, $d_{5/2}$, $d_{3/2}$ levels of the $s-d$ shell is such a case, covering nuclei from ^{16}O up to ^{40}Ca . One can easily be convinced that the dimension of the matrices to be diagonalized becomes exceedingly large for more than two particles in open shells. Special procedures have been developed to diagonalize such huge matrices [Wh 72, SZ 72, WWC 77].

To reduce the size of these matrices, symmetries such as isospin or angular momentum (see Sec. 2.6) can be of great help (see, for instance, [FHM 69, WMH 71, HMW 71, GED 71, VGB 72, Wi 76]).

2.6 Symmetry Properties

2.6.1 Translational Symmetry

For any solution of the eigenvalue problem (2.19) we must require that a series of symmetry or invariance properties are fulfilled. Among these are, for example, translational and rotational invariance.* In the shell model

* Besides these exact symmetries, in some regions of the periodic table one often also has approximate symmetries, as, for instance, the isospin (see Sec. 2.6.3), which can be used for a classification of spectra (see [He 73a]).

one of these invariances is always violated: the *translational invariance*. This comes from the fact that we have to fix the potential in space in contradiction to the homogeneity of space. The most serious consequence of this violation is the appearance of spurious states in the excitation spectrum of the system. This occurs because we have introduced redundant degrees of freedom. If we fix the nucleus in space, it has only $3A - 3$ spatial degrees of freedom left. The shell model, however, contains $3A$ variables. These spurious states are therefore not true excitations of the system, but correspond to motions of the nucleus as a whole. Almost all approximation schemes in nuclear physics have inherent symmetry violations. In Chapter 11 we will, therefore, show in fair detail how such violations can be removed.

2.6.2 Rotational Symmetry

The spherical shell model Hamiltonian H_0 (is term included) conserves rotational symmetry. Therefore, it is possible to construct eigenstates of the total angular momentum

$$\mathbf{J} = \sum_{i=1}^A \mathbf{j}_i^{(i)} \quad \text{and} \quad J_z = \sum_{i=1}^A j_i^{(i)} \quad (2.38)$$

by a linear combination of the Slater determinants (2.23). The closed shell ground state is not degenerate; the only nondegenerate angular momentum eigenstate has $J=0$, which is therefore identified with the ground state. This consequence is experimentally confirmed with no exception. It is then clear that, having only one nucleon outside closed shells, the ground state angular momentum of such even-odd nuclei will correspond to the j -value of the odd nucleon. The same, of course, is true if there is one nucleon missing (a hole) in a filled shell. This rule is also experimentally confirmed with only very few exceptions.

If we fill (remove) more than one particle into (from) an unfilled (filled) j -level, the situation gets more complicated, because different J -values will be degenerate. Again, we can remove this degeneracy by diagonalizing the residual interaction. The matrices are now much smaller as we get one for each J value.

The construction of eigenfunctions of \mathbf{J}^2 will be shown explicitly for a very simple example (for more complicated situations, see [ST 63]). Suppose that in a j -shell there are only two protons, the configuration of which is then $(\pi j)^2$. Out of the degenerate two-particle states (which we want to denote by $|m_1 m_2\rangle$, m being the magnetic quantum number), we construct, according to the rules of angular momentum coupling, an eigenstate $|JM\rangle$ of \mathbf{J}^2 and J_z with

$$\mathbf{J}^2 = (\mathbf{j}_1 + \mathbf{j}_2)^2. \quad (2.39)$$

We obtain

$$|JM\rangle = \frac{1}{\sqrt{2}} \sum_{m_1 m_2} C_{m_1 m_2}^j |m_1 m_2\rangle. \quad (2.40)$$

Using the symmetry properties of the Clebsch-Gordan coefficients, (see [Ed 57, Eq. (3.5.14)]), we have with proper normalization

$$|IM\rangle = \frac{1}{\sqrt{2}} \sum_{m_1 m_2} (C_{m_1 m_2 M}^j + (-)^{J-I} C_{m_2 m_1 M}^j) |m_1 m_2\rangle \quad (2.41)$$

which, upon noting the antisymmetry $|m_2 m_1\rangle = -|m_1 m_2\rangle$ yields

$$|IM\rangle = \frac{1}{\sqrt{2}} \sum_{m_1 m_2} C_{m_1 m_2 M}^j (1 + (-)^{J-I+1}) |m_1 m_2\rangle. \quad (2.42)$$

We see from Eq. (2.42) that $|IM\rangle$ is only different from zero for

$$2j - I + 1 = 2n \quad \text{or} \quad I = 2n; \quad n = 0, 1, 2, \dots, \quad (2.43)$$

that is, for even angular momenta. Taking as a definite example $j = 3/2$, we see that the six independent components

$$|m_1 m_2\rangle : |\frac{3}{2} \frac{1}{2}\rangle, |\frac{3}{2} - \frac{1}{2}\rangle, |\frac{3}{2} - \frac{3}{2}\rangle, |\frac{1}{2} - \frac{1}{2}\rangle, |\frac{1}{2} - \frac{3}{2}\rangle, |-\frac{1}{2} - \frac{3}{2}\rangle$$

have been transformed by a unitary transformation to the six angular momentum coupled components, which are degenerate among themselves:

$$|IM\rangle : |00\rangle, |22\rangle, |21\rangle, |20\rangle, |2-1\rangle, |2-2\rangle.$$

In the general case these considerations are a little tedious. In Table 2.1 the possible total angular momenta for a pure proton configuration are presented.

The factor $1/\sqrt{2}$ in Eq. (2.40) is a normalization in the case in which both particles are in the same shell. In general, we have for the coupling of two particles:

$$(a_{njf}^+ a_{n'f'}^+)_{JM} = \frac{1}{\sqrt{1 + \delta_{jj'} \delta_{ff'} \delta_{nn'}}} \sum_{mm'} C_{m m' M}^j C_{m' m M}^{j'} a_{njm}^+ a_{n'f'm'}^+. \quad (2.44)$$

Special care has to be applied in coupling hole states. The operator a_{njm}^+ transforms like the eigenfunction ϕ_{njm} , that is cogredient, under a rotation of the coordinate system and therefore like a spherical tensor of rank j (i.e., with $D_{mm'}^j$; see Appendix A). On the other hand, the annihilation operator a_{njm} transforms with $D_{mm'}^{j''}$, that is, contragredient. The normal coupling rules (2.44) apply only for tensors, which are both cogredient or both contragredient. We can therefore only couple a_{njm}^+ with the time reversed operator (see [Me 61]),

$$a_{njm}^- = T a_{njm}^+ T^+ = (-)^{I+j-m} a_{nj-m}^+, \quad (2.45)$$

which is, of course, cogredient. The ph coupling rule is therefore

$$(a_{njf}^+ a_{n'f'}^+)_{JM} = \sum_{mm'} (-)^{J-m'} C_{m m' M}^j C_{m' m M}^{j'} a_{njm}^+ a_{n'f'm'}^+, \quad (2.46)$$

where we have left out the unimportant phase $(-)^{J+1}$.

From pure angular momentum coupling one cannot as yet decide which of the degenerate states corresponds to the ground state. For that we have, as we have said, to diagonalize V_R in a certain subspace. This confirms, in general, the experimentally observed rule that even-even groundstates have $I = 0$.

Another experimentally found coupling rule which the pure shell model cannot explain without configuration mixing is the fact that even odd nuclei far from closed shells have ground state spins equal to the j -value of the odd particle. We will see in Chapter 6 how this finds a natural explanation by taking correlations of the nucleons into account.

Table 2.1 List of possible total angular momenta J for the configuration $(j)^k$ ([MJ 55, p. 64])

j	k	possible J
$j = \frac{1}{2}$	1	$\frac{1}{2}$
$j = \frac{1}{2}$	2	0, 2
$j = \frac{1}{2}$	3	$\frac{1}{2}, \frac{3}{2}, \frac{5}{2}$
$j = \frac{1}{2}$	4	0, 2 (twice), 4 (twice), 5, 6, 8
$j = \frac{1}{2}$	5	$\frac{1}{2}, \frac{3}{2}, \frac{5}{2}, \frac{7}{2}, \frac{9}{2}, \frac{11}{2}, \frac{13}{2}$
$j = \frac{11}{2}$	1	$\frac{11}{2}$
$j = \frac{11}{2}$	2	0, 2, 4, 6, 8
$j = \frac{11}{2}$	3	$\frac{1}{2}, \frac{3}{2}, \frac{5}{2}, \frac{7}{2}, (\text{twice}), \frac{11}{2}, \frac{13}{2}, \frac{15}{2}, \frac{17}{2}$
$j = \frac{11}{2}$	4	0 (twice), 2 (twice), 3, 4 (3 times), 5, 6 (3 times), 7, 8 (twice), 9, 10, 12
$j = \frac{11}{2}$	5	$\frac{1}{2}, \frac{3}{2}, \frac{5}{2} (\text{twice}), \frac{7}{2} (\text{twice}), \frac{9}{2} (\text{3 times}), \frac{11}{2} (\text{twice}), \frac{13}{2} (\text{twice}), \frac{15}{2} (\text{twice}), \frac{17}{2} (\text{twice}), \frac{19}{2}, \frac{21}{2}, \frac{23}{2}$
$j = \frac{11}{2}$	6	0 (3 times), 2 (4 times), 3 (3 times), 4 (6 times), 5 (3 times), 6 (7 times), 7 (4 times), 8 (6 times), 9 (4 times), 10 (5 times), 11 (twice), 12 (4 times), 13 (twice), 14 (twice), 15, 16, 18

2.6.3 The Isotopic Spin

Up to now we have always considered the neutrons and protons separately. As a consequence we have, for example, in Eq. (2.23), a product of two Slater determinants—one for protons and one for neutrons. Apart from their electromagnetic interactions, protons and neutrons have practically the same physical properties. We will see, for instance, in Chapter 4, that nuclear forces are to a large extent independent of whether we consider protons or neutrons—that is, they are charge independent. As long as the influence of the Coulomb force on the nuclear properties can be neglected, we can consider the proton and the neutron as just two

different manifestations of the same particle: the nucleon. Mathematically we say that the nucleon can be in two different states, the basis vectors of which may be written as $\pi = \begin{pmatrix} 1 \\ 0 \end{pmatrix}$ and $\nu = \begin{pmatrix} 0 \\ 1 \end{pmatrix}$, thus forming a two-dimensional space. This then is very similar to what we have in the spin case. Instead of a quantum number indicating whether the nucleon spin is up or down, we now have an additional quantum number, indicating whether the nucleon is a proton or a neutron, called the isotopic spin because of its formal analogy to ordinary spin.* With this additional quantum number we can write the nuclear shell model wave function as a single determinant. However one should realize that, contrary to the ordinary spin, the isospin has nothing to do with rotations in the coordinate space. Therefore, the treatment of isospin is much simpler than that of ordinary spin which, unlike the isospin, has to be coupled to the orbital angular momentum.

As in the case of ordinary spin, one can set up the usual spin algebra:

$$t_3 \nu = \frac{1}{2} \nu, \quad (2.47)$$

$$t_3 \pi = -\frac{1}{2} \pi,$$

with

$$t_3 = \frac{1}{2} \begin{pmatrix} 1 & 0 \\ 0 & -1 \end{pmatrix}. \quad (2.48)$$

The lowering and raising operators t_- and t_+ change the neutron into a proton and vice versa, respectively,

$$\begin{aligned} t_- \nu &= \pi, & t_+ \nu &= 0, \\ t_- \pi &= 0, & t_+ \pi &= \nu, \end{aligned} \quad (2.49)$$

with

$$t_+ = \begin{pmatrix} 0 & 1 \\ 0 & 0 \end{pmatrix}; \quad t_- = \begin{pmatrix} 0 & 0 \\ 1 & 0 \end{pmatrix}. \quad (2.50)$$

Like ordinary spin, the isospin vector operator is formed out of its three cartesian components

$$\mathbf{t} = \{t_1, t_2, t_3\}. \quad (2.51)$$

We can therefore define the total isospin of a system of A nucleons

$$\mathbf{T} = \sum_{i=1}^A \mathbf{t}^{(i)} \quad (2.52)$$

and its 3-component

$$T_3 = \sum_{i=1}^A t_3^{(i)}. \quad (2.53)$$

Since we have the same algebra for isotopic spin as for ordinary spin, the same coupling rules can be applied.

The 3-component of the total isospin is a measure of the total neutron

* The concept of isospin was introduced originally by Heisenberg [He 32]. Later on it was much developed by Wigner [Wi 37].

excess of the nucleus:

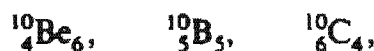
$$\begin{aligned} T_3 \Psi(1 \dots A) &= \left\{ -\frac{1}{2} - \frac{1}{2} \cdots - \frac{1}{2} + \frac{1}{2} + \frac{1}{2} \cdots + \frac{1}{2} \right\} \Psi(1 \dots A) \\ &= \frac{1}{2}(N - Z) \Psi(1 \dots A). \end{aligned} \quad (2.54)$$

The eigenvalue is therefore equal to half the neutron excess. For systems where T^2 commutes with the nuclear Hamiltonian, the eigenvalue T corresponding to T^2 can take on the values

$$|T_3| \leq T \leq \frac{A}{2}. \quad (2.55)$$

Each nuclear state then has a good total isospin quantum number T as long as Coulomb forces, which do not commute with T^2 , can be neglected.

As a simple example, we will show how to attribute total isotopic spin to certain nuclear states. For the three isobar nuclei



the 3-component of the total isospin is, according to Eq. (2.54),

$$T_3^{(\text{Be})} = -1, \quad T_3^{(\text{B})} = 0, \quad T_3^{(\text{C})} = 1. \quad (2.56)$$

The total isospin can therefore be either $T = 1$ or $T = 0$ [Eq. (2.55)].

In the first case we speak of an isospin triplet, states of which should be found in all three nuclei at the same energy (slight differences will nevertheless occur because of the Coulomb energy); the second case is an isospin singlet, which can only be attributed to boron. In Fig. 2.9 we show the low-lying states of the three isobars and their identification with isospin quantum numbers.

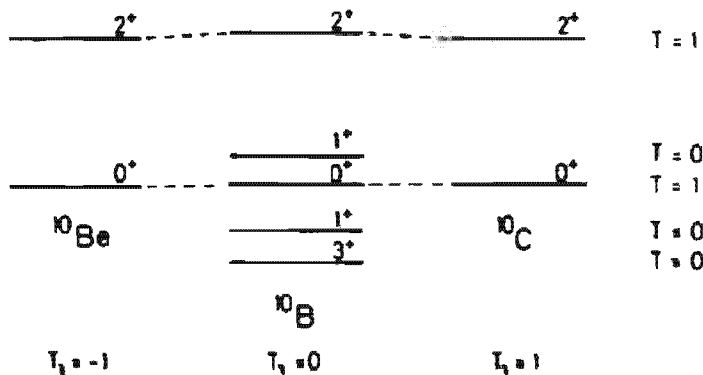


Figure 2.9. Isospin triplets and singlets in the excitation spectrum of isobars.

From these considerations it may seem that the concept of isospin can only be applied to light nuclei, where the Coulomb energy is negligible. However it turns out in *heavy nuclei* also, that the low-lying states have almost good isospin. This can be understood qualitatively using the following arguments.

We first consider a pure shell model and assume that the wave functions for protons and neutrons with the same quantum numbers are identical, that is that the proton and the neutron wells are identical to within a constant shift Δ_c (2.27). This is a rather good approximation for the bound states.

In Fig. 2.10 we have side by side the levels with the same quantum numbers. This is a bit misleading for energy arguments, but useful in the following discussion.

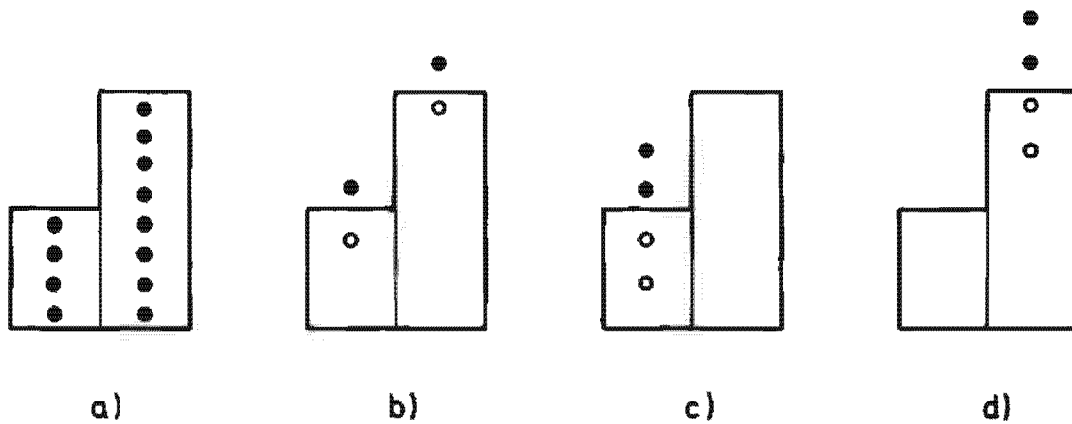


Figure 2.10. Schematic representation of shell model configurations.

From Fig. 2.10a we see that a shell model state where all occupied proton levels are also occupied by neutrons has $T = T_3$, because operating with $T_+ = \sum_i t_+^{(i)}$ onto this state gives 0, that is, this state has the maximal value of T_3 for a fixed value of T . This shows in particular that the shell model ground state for $N = Z$ nuclei has $T = 0$.

For non-magic heavy nuclei the shell model ground state is certainly not a good approximation to the exact ground state. There are admixtures of $1p\text{-}1h$, $2p\text{-}2h$ states. As we will show in Chapter 5, the construction of a self-consistent, one-particle potential assures that there are no $1p\text{-}1h$ admixtures. Since the shell model potential is a good approximation to such a potential, we neglect these contributions here and argue about $2p\text{-}2h$ admixtures. Furthermore, we assume that $\Delta_r \approx \hbar\omega_0$, which is the case for heavy nuclei like ^{208}Pb , and neglect $2p\text{-}2h$ configurations with an unperturbed energy larger than $2\hbar\omega_0$. As we see from Fig. 2.10b, c, d there are three types of configurations. Only type b contains configurations which violate the isospin, namely, those where the proton particle sits in the same level as the neutron hole. The ratio of the number of these configurations to the number of all configurations of type b is $1/(N - Z)$, where $(N - Z)$ is the neutron excess. If we make the statistical assumption that all these configurations are admixed with the same weight, we find that the isospin impurity in the ground state of heavy nuclei is roughly $1/(N - Z)$. Similar considerations apply for excited states, and we find that heavy nuclei with large neutron excesses have rather pure isospin. This result has also been found in more detailed investigations [LS 62, SK 65, KW 69, So 69, LM 74].

2.7 Comparison with Experiment

2.7.1 Experimental Evidence for Single-Particle (Hole) States

Besides the success of the shell model as an explanation of the magic numbers and angular momenta of the ground state, one would like to have direct experimental evidence for the nuclear shells. It turns out that direct stripping [e.g., (d, p)] and pickup (p, d) reactions, as well as direct $(p, 2p)$ and $(e, e'p)$ reactions, are well suited for this purpose. For example, a direct $(p, 2p)$ process is ideally one where the energy of the incoming proton is so high that it interacts only once with another proton in the

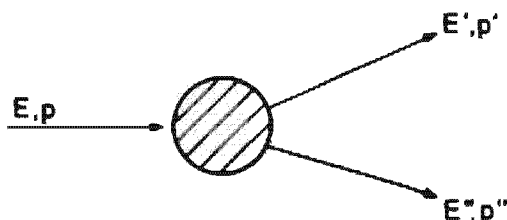


Figure 2.11. Schematic representation of the $(p, 2p)$ reaction.

nucleus, both protons leaving the nucleus without further interactions (Fig. 2.11).

Suppose that the knocked-out nucleon has been in a shell model state (Fig. 2.12). For its binding energy we have

$$E_B = E - E' - E''.$$

The cross section according to the shell model should have, as a function of the energy, resonances only at discrete values of E_B .

In reality, these resonances are broadened because of the influence of the residual interaction, as shown in Fig. 2.13 for the experimental cross section of ^{16}O ($p, 2p$) ^{15}N . Nevertheless, one can clearly identify the

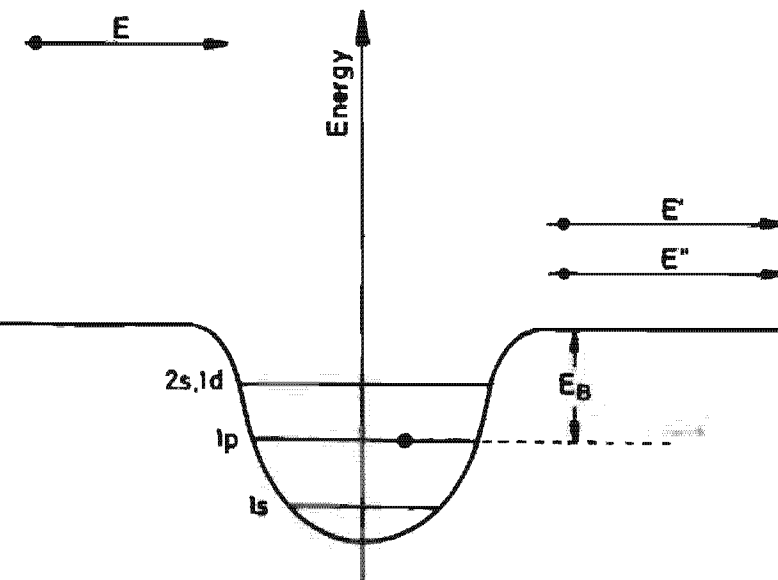


Figure 2.12. $(p, 2p)$ reaction in the shell model.

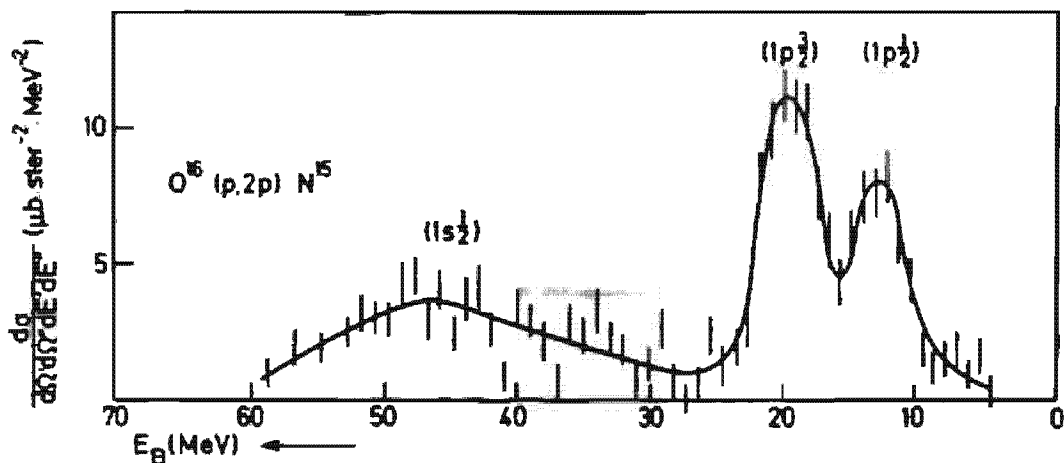


Figure 2.13. Experimental ^{16}O ($p, 2p$) ^{15}N cross section [MHT 58].

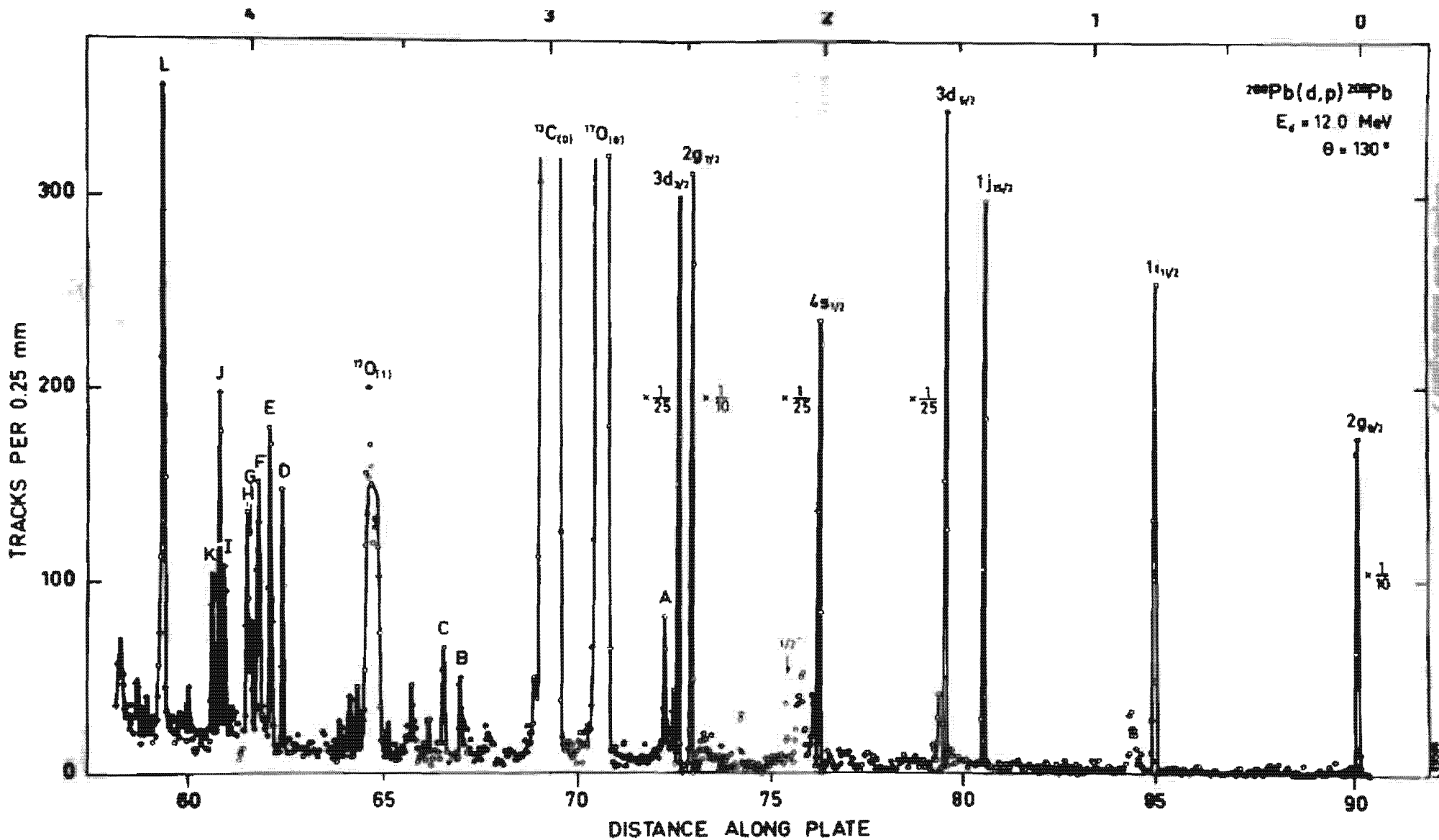


Figure 2.14. Neutron spectrum from the $^{208}\text{Pb} (d, p) ^{209}\text{Pb}$ reaction. The intensity peaks are labelled by their shell model assignment. (From EKV 69)

$(\pi 1s_{1/2})$ level and the spin orbit split levels $(\pi 1p_{3/2})$ and $(\pi 1p_{1/2})$. Theoretical calculations for these reactions have been done by R. Lipperheide et al. [FLW 75].

In a similar manner, one can use stripping or pickup reactions like (d, p) and (p, d) to create neutron particle or neutron hole states, but the kinematical analysis has to be corrected for the binding of the deuteron. A nice example for neutron particle states in ^{209}Pb obtained with a (d, p) stripping reaction is presented in Fig. 2.14. It should be compared with Fig. 2.15, where experimentally determined proton and neutron single-particle energies for ^{208}Pb are shown in comparison with calculated levels, using a Woods-Saxon potential [BW 60].

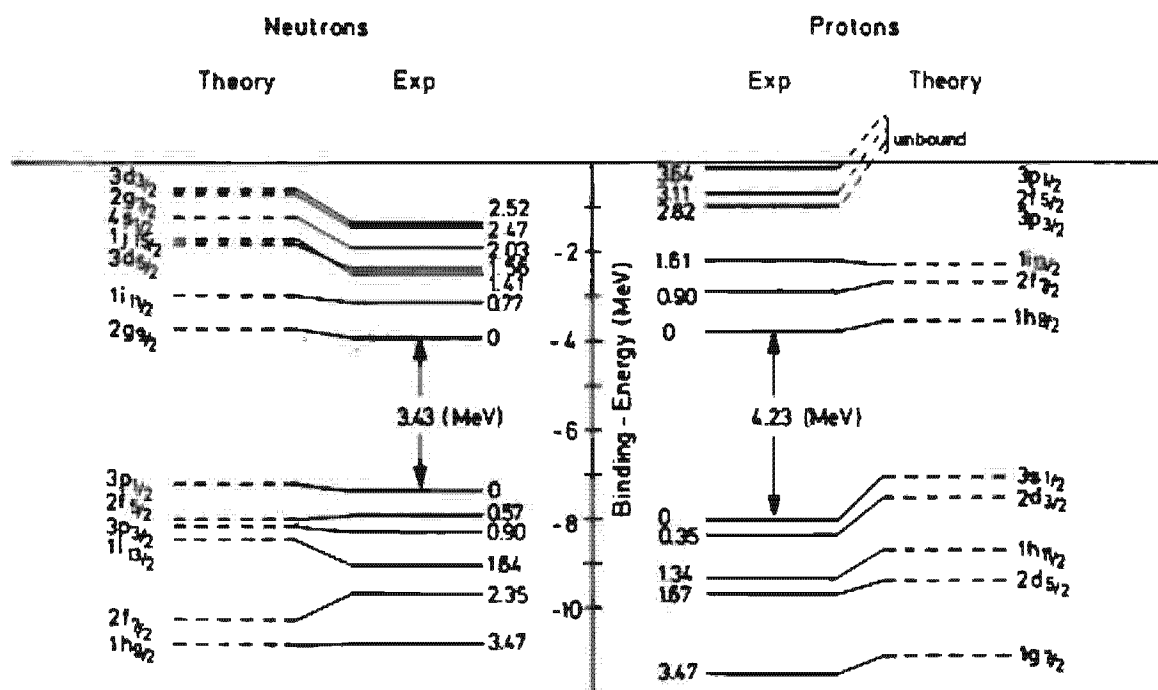


Figure 2.15. Comparison of experimental and calculated single-particle levels in ^{208}Pb .

One can show (see, for instance, [GL 70, Au 70, Ho 71b, EW 72]) that the absolute values of the cross sections of these reactions are proportional to the so-called spectroscopic factor

$$S_k = |\langle \Psi_{A+1} | a_k^+ | \Psi_A \rangle|^2, \quad (2.57)$$

where $|\Psi_A\rangle$, $|\Psi_{A+1}\rangle$ are the exact wave functions of the initial and final nucleus, and k stands for the quantum numbers of the observed single-particle state. If for the wave functions we use the pure shell model approximation, the spectroscopic factor is clearly equal to one.* However, if the wave functions contain admixtures of more complicated particle and hole configurations, which are introduced by the diagonalization of the residual interaction (2.35), the spectroscopic factor differs from one. Therefore, it is a measure of the purity of the single-particle states. The spectroscopic factors of the levels shown in Fig. 2.14 are in the range 0.8–0.9 (see, for instance, [RW 73]).

* This statement applies only for pure product states without angular momentum coupling. With angular momentum coupling, the different levels with different m values are partially filled and one has to take into account the Pauli principle.

2.7.2 Electromagnetic Moments and Transitions

Other important quantities ready for comparison with experiments are the electromagnetic moments and transition probabilities in odd mass nuclei. In a first approximation, one assumes that they are described by one external particle sitting on an inert core with even mass:

$$|\Phi_m\rangle = a_m^+ |\Phi_0\rangle, \quad (2.58)$$

where a_m^+ creates a particle in the level m and $|\Phi_0\rangle$ represents the wave function of the core (2.25).

The electromagnetic multipole operators $\hat{Q}_{\lambda\mu}$ and $\hat{M}_{\lambda\mu}$ (as defined in Appendix B), are one-particle operators. As shown in Appendix C, they can be represented as

$$\hat{Q} = \sum_{k_1 k_2} Q_{k_1 k_2} a_{k_1}^+ a_{k_2}, \quad (2.59)$$

in the shell model basis. Using the Fermi commutation relations (C.23) for the operators a_k, a_k^+ and the fact that the levels m, m' are empty in the core ($a_m |\Phi_0\rangle = a_{m'} |\Phi_0\rangle = 0$), we get

$$\langle \Phi_m | \hat{Q} | \Phi_m \rangle = \langle \Phi_0 | \hat{Q} | \Phi_0 \rangle \delta_{mm'} + Q_{mm'}. \quad (2.60)$$

The picture becomes especially simple if we assume that the core is a closed shell nucleus. In this case, all the electromagnetic matrix elements of the core ($I=0$) vanish. The single-particle states are characterized by the quantum numbers $|k\rangle = |nljm\rangle$ and the electromagnetic properties can be calculated from the matrix elements

$$Q_{kk'} = \langle nljm | \hat{Q} | n'l'j'm' \rangle, \quad (2.61)$$

which are given in Eqs. (B.81) and (B.82) of Appendix B.

For instance, we get the electromagnetic moments [(B.31) and (B.32)] as expectation values in the states $|nljm=j\rangle$ and the electromagnetic transition probabilities (B.72) from the reduced matrix elements of these operators.

Special care has to be taken in the case of single hole states (one particle less than a closed shell). As we have seen, they can be described in the same simple way as the single-particle states. Their wave function can be expressed by analogy with Eq. (2.58):

$$|\Phi_i\rangle = a_i |\Phi_0\rangle, \quad (2.62)$$

where $|\Phi_0\rangle$ is again the wave function of the core and a_i annihilates a particle in a level i occupied in $|\Phi_0\rangle$. By analogy with (2.60), we get

$$\langle \Phi_i | \hat{Q} | \Phi_i \rangle = \langle \Phi_0 | \hat{Q} | \Phi_0 \rangle \delta_{ii} - Q_{ii}. \quad (2.63)$$

Since the electromagnetic multipole operators are self-adjoint in the sense of [Ed 57, Eq. (5.5.2)], the difference between (2.63) and (2.60) does not enter into the electromagnetic transition probabilities. However, in the case of electromagnetic moments, one has to take care of the sign in (2.63) and an additional phase. Since one is interested in the expectation value of a

state with angular momentum quantum numbers $j, m = j$, one has to create a hole in the level $|jm = -j\rangle$, which is proportional to the time-reversed level $T|jm = j\rangle$ [Eq. (2.45)]. Together with the minus sign in Eq. (2.63), one finds that hole states have the same magnetic moments as the corresponding particle states (the magnetic multipole operators are time odd), whereas the electric multipole moments of particle and hole states have different signs (the electric multipole operators are time even).

One example is the magnetic dipole moment (B.31)

$$\mu = \langle nljj | \mu_z | nljj \rangle = \sqrt{\frac{4\pi}{3}} \langle nljj | \hat{M}_{10} | nljj \rangle, \quad (2.64)$$

where the magnetic vector μ is given by

$$\mu = \mu_N (g' \mathbf{l} + g^* \mathbf{s}), \quad (2.65)$$

where $\mu_N = e\hbar/2mc$ is the nuclear magneton and g' and g^* are the gyro-magnetic ratios for orbital angular momentum and spin ($g' = 1, g^* = 5.586$ for protons and $g' = 0, g^* = -3.826$ for neutrons).

The magnetic moment μ can easily be calculated with the projection theorem for vector operators \mathbf{A} ,

$$\langle jm | \mathbf{A} | jm' \rangle = \langle jm | \mathbf{j} | jm' \rangle \frac{\langle jj | \mathbf{A} j | jj \rangle}{j(j+1)}. \quad (2.66)$$

which can be derived from the Wigner-Eckart theorem [Ed 57, Eq. (5.4.1)]. Applying it to the vector μ , we get

$$\begin{aligned} \mu &= \mu_N \frac{1}{j+1} \langle jj | g' \mathbf{l} j + g^* \mathbf{s} j | jj \rangle \\ &= \mu_N \frac{1}{2(j+1)} \left[g'(j(j+1) + l(l+1) - \frac{3}{4}) + g^*(j(j+1) + \frac{3}{4} - l(l+1)) \right]. \end{aligned} \quad (2.67)$$

For $j = l \pm \frac{1}{2}$ we get

$$\mu = \mu_N \left\{ \begin{array}{l} g'(j - \frac{1}{2}) + \frac{1}{2} g^* \\ \left[g'(j + \frac{1}{2}) - \frac{1}{2} g^* \right] \frac{j}{j+1} \end{array} \right\} \text{ for } \begin{cases} j = l + \frac{1}{2} \\ j = l - \frac{1}{2} \end{cases}. \quad (2.68)$$

The functions $\mu(j)/\mu_N$ for $j = l \pm 1/2$ are called Schmidt lines (Figs. 2.16 and 2.17) (j can only take on discrete values $\mu(j)/\mu_N$, though it is shown here as a continuous function of j). The experimental values are given for comparison.

If the theory were exact, all μ -values would lie on the Schmidt lines and all orbital angular momenta $l = j \pm \frac{1}{2}$ would be determined. The experimental values, almost without exception, lie in between the two lines, most of them being grouped closer to one of the two lines. The l -values determined in this way almost always agree with those predicted by the shell model. The shell model should work best near magic numbers. Indeed, one finds close agreement, for example, for ^{15}N , ^{17}O , ^{39}K , ^{41}K , and ^{207}Pb . The

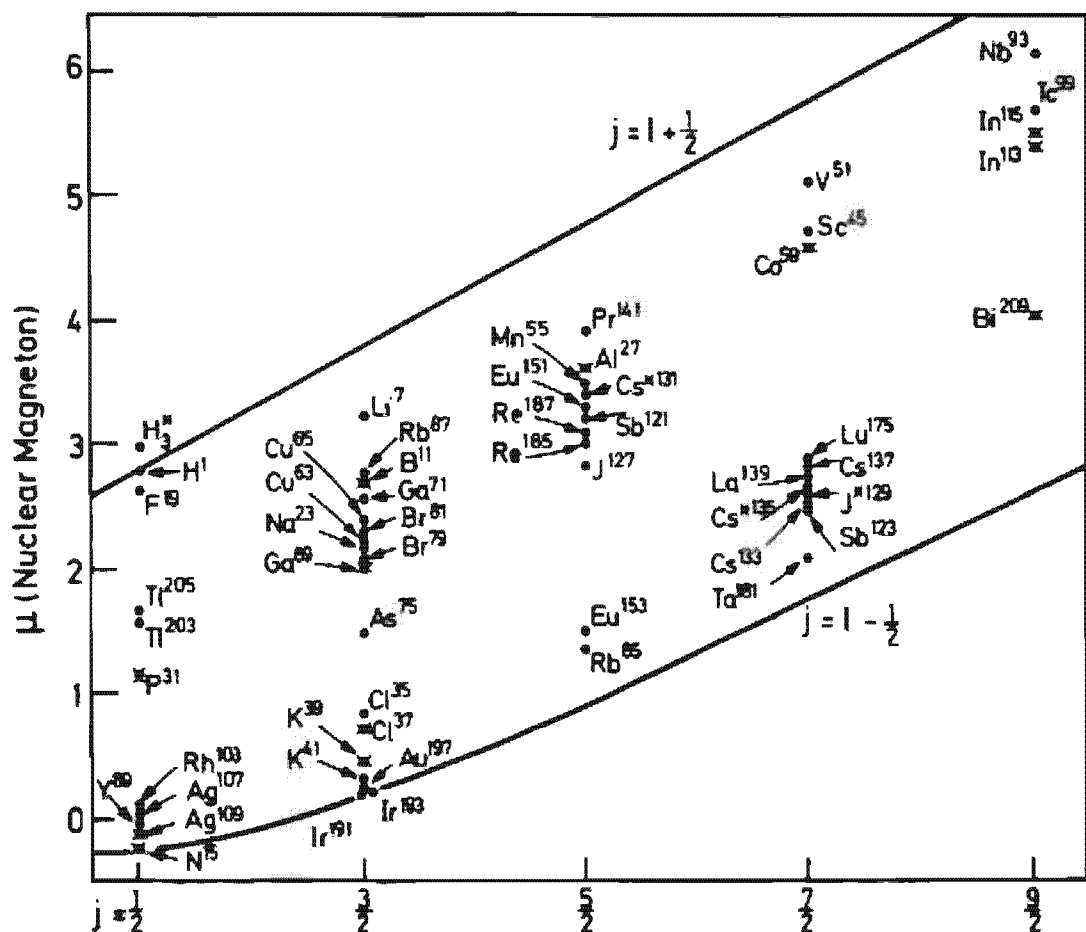


Figure 2.16. Magnetic moments for Z -odd nuclei as a function of angular momentum. (From [MJ 55].)

agreement is also not too bad for many nuclei far from closed shells. One can qualitatively understand this, because the magnetic moment in time-reversed levels is always of opposite sign. Since, as we shall see in Chapter 6, time-reversed levels are always occupied pair-wise, the most important contribution comes from the last odd particle. This is, however, only a

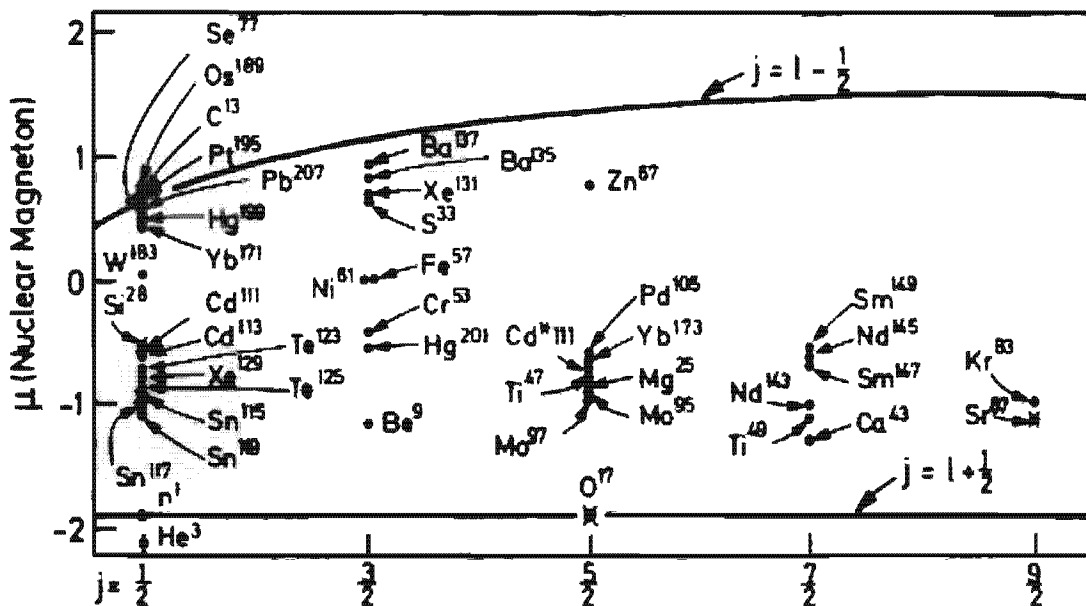


Figure 2.17. Magnetic moments of N -odd nuclei as a function of angular momentum. (From [MJ 55].)

qualitative argument and one also finds many deviations, especially for heavier nuclei, even in cases of rather pure one-particle or one-hole configurations.

There are two main reasons for these deviations:

- (i) As we see in Appendix B, we have used the g -factors of bare nucleons in the calculation of the magnetic multipole operators. Within the nucleus however, there exist pionic currents between the nucleons that change these values, and effective g -factors, \tilde{g} , should be used.
- (ii) The core usually does not stay inert in an external electromagnetic field. This can excite virtual vibrations which interact with the external particle. This effect is called a polarization of the core. To a large extent, it can be taken into account again by effective g -values. We will see in Section 9.3 how this polarization effect can be calculated microscopically.

The most important magnetic transitions are M1-transitions. In the pure single-particle model, the M1-operator (2.65) commutes with I^2 . This means that M1-transitions between levels with different I -quantum numbers are forbidden (I -forbidden transitions). In fact, such transitions are observed experimentally, but with a very small BM1-value. They cannot be understood by using only effective g -values, because one does not change the selection rules in this case. This clearly shows that mesonic effects (i) and polarizations (ii) produce not only vector components $\sim I$ and $\sim s$, but also more complicated effects. The simplest one is a "tensor component"

$$\delta\mu = \kappa r^2 [Y_2 s]_{1/3}. \quad (2.69)$$

By adjusting the constant κ in a reasonable way, one is able to describe these I -forbidden transitions quantitatively (see [BM 69, WB 69, and BSK 73]).

Let us come now to the electric properties. There are two important differences to the magnetic case:

- (i) The electric operators are time-even. There are no cancellations of the contributions of time-reversed levels, but on the contrary they add up. This means that one cannot expect that the spherical single-particle model works outside the region of closed shells.
- (ii) Since one can, in the long wavelength limit, (see Appendix B) neglect the contributions of currents to the electric multipole operators, we can use the conservation law for the electric charge and show that exchange effects do not play any role in the electric multipole operators. This means that apart from polarization effects, we can use the bare electric charge (Siegert theorem [Si 37]).

By analogy with the magnetic moment, one obtains for the electric quadrupole moment (B.81) of a single-particle state [EL 57, p. 255]

$$Q = e \sqrt{\frac{16\pi}{5}} \langle nljj | r^2 Y_{20} | nljj \rangle = -e \langle r^2 \rangle \frac{2j-1}{2j+2}, \quad (2.70)$$

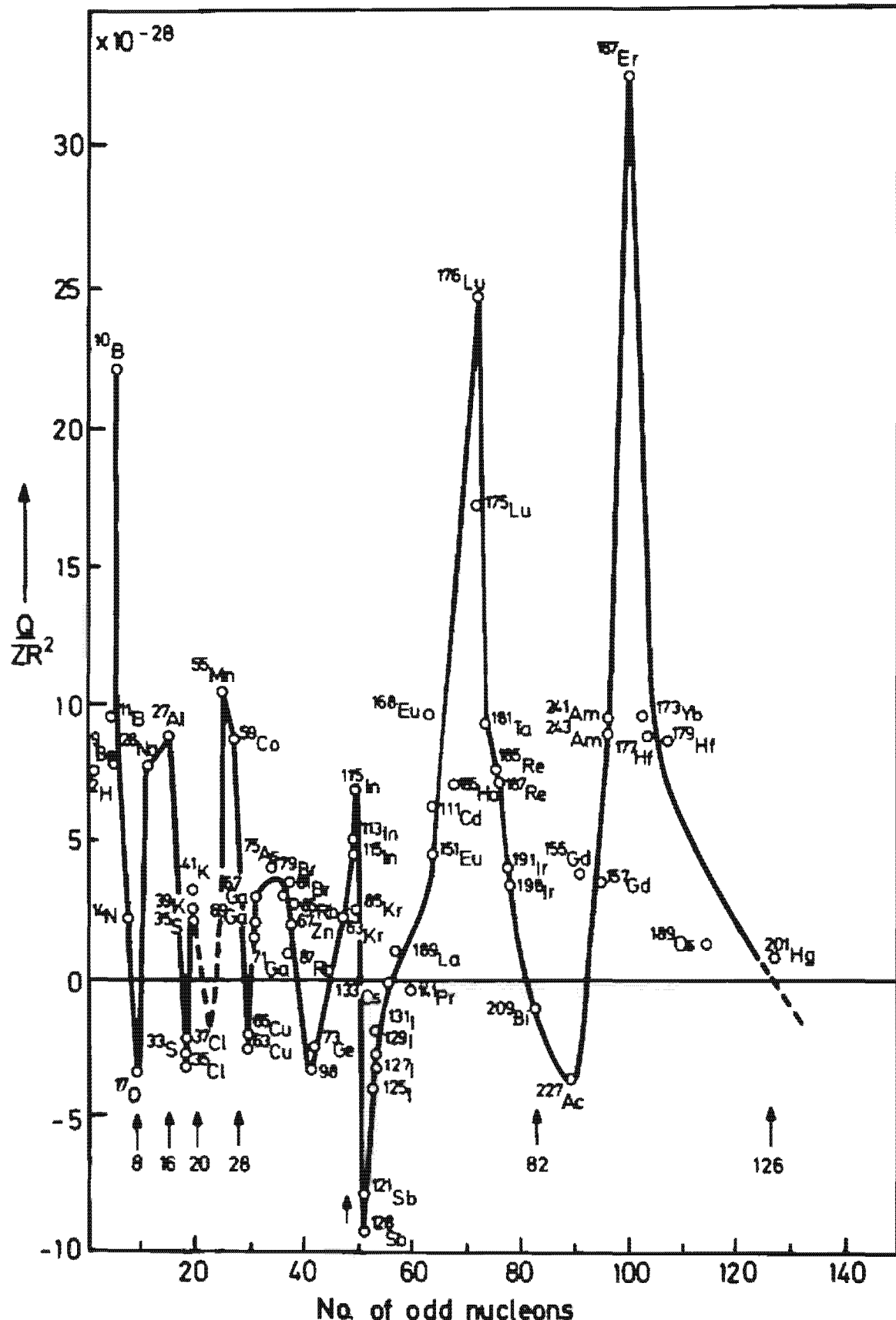


Figure 2.18. Quadrupole moments for odd- A nuclei against the number of odd nucleons. Arrows indicate closed shells. (From [Se 64].)

where $\langle r^2 \rangle$ is the average square radius of a particle in the state $|nljm\rangle$. For $j > 1/2$, the quadrupole moments turn out to be negative, that is, the probability distribution looks like a pancake in the plane perpendicular to the z -axis. For holes we have the opposite (i.e., prolate probability distributions). In Fig. 2.18, we see that this picture is qualitatively right in the neighborhood of magic numbers. However, as one fills the next shell with more and more nucleons, we soon find experimentally a transition to positive quadrupole moments with very large values. We shall see in the next chapter that in this case the average field of the nucleons is no longer spherical and we obtain a deformed density distribution. Only at the end of the shell, when nearly all levels are occupied, does one again get the picture of one or a few holes in a spherical core.

Even for one-particle or one-hole states with a magic core, this picture only gives qualitative agreement. Quantitatively, the measured quadrupole moments for proton states are roughly a factor of two larger than one would expect from (2.70) and values for neutron states do not vanish as they should according to Eq. (2.70), but behave as if the neutron had a charge. One usually expresses this fact by an effective charge e^{eff} . These effective charges can be explained by the polarization effect (see Sec. 9.3). Experimentally, it is observed that $e^{eff} \approx 1$ for neutrons and $e^{eff} \approx 2$ for protons.

The electric transitions behave very much like the corresponding moments. Only for the single-particle and single-hole nuclei near closed shells do they have values predicted by the single-particle shell model, with roughly the same effective charge as determined from the quadrupole moments.

Levels with *high angular momenta near closed shell nuclei* are often a mixture of only very few configurations (often there is only one configuration possible in a wide energy range). Sometimes—because of the selection rules of spin and parity—they can decay only by radiation with a high multipolarity. From Appendix B we learn that such transitions are highly suppressed because of kinematical factors. We therefore expect a very long lifetime for such nuclei. In fact, quite a few such “isomeric” states have been found in spherical nuclei (islands of isomers; see also Sec. 3.4.7).

2.8 Deformed Shell Model

2.8.1 Experimental Evidence

The assumption of approximately independent motion of nucleons in an average field is the basis of the shell model and of all microscopic theories of finite nuclei. This container potential is produced by the nucleons themselves and their mutual interaction. In Chapter 5 we shall see how to calculate this average potential. In its most simple form the potential well is spherical. This is true for nuclei with closed or nearly closed shells and, as we have seen in the last section, for such nuclei the spherical shell model

is very successful. Far from closed shells—that is, for mass numbers $A \approx 25$ (Al, Mg), $150 < A < 190$ (nuclei of the rare earths) and for $A > 220$ (the actinides)—the independent particle picture again works quite well. However, in these regions one has to assume a deformed single particle potential. [Ra 50, 76, Bo 51].

The assumption of a deformation is able to explain many experimental facts, of which the most important are:

- (I) **The existence of rotational bands.** In the mass regions mentioned above, the nuclear excitation spectra show pronounced rotational bands with an $I(I+1)$ spectrum, as in Eq. (1.64) (see, for instance, [BM 75]). As discussed in Chapter 1.5, such collective rotational bands are closely related to stable nuclear deformations.
- (II) **Very large quadrupole moments.** We have already seen in Section 2.7 that the spherical single-particle model with an inert core is by no means able to explain the large quadrupole moments in the regions far from closed shells (Fig. 2.18). This experimental fact is a hint about stable nuclear deformations, where the core also contributes to the quadrupole moment. Using the Bohr model [Eq. (1.75)] we can determine from the experimental (spectroscopic) quadrupole moment Q an intrinsic value Q_0 , and derive a deformation parameter β [Eqs. (1.13) and (1.72)]. The “experimental” values of β , determined in this way, are for axial symmetric nuclei ($\gamma=0$) in the rare earth region around

$$\beta \approx 0.2-0.3. \quad (2.71)$$

The sign is positive. This means that we have cigar-shaped or prolate deformations. In other regions (for instance, $A \approx 25$, $A \approx 150$ or $A \approx 185-190$) there also exist pancake-shaped or oblate nuclei. Whether there also exist triaxial nuclei is still open to question (see Secs. 1.5.3 and 3.3.3).

- (III) **Strongly enhanced quadrupole transition probabilities.** In the rotational model, the quadrupole transition probabilities are directly connected to the intrinsic quadrupole moment Q_0 [see Eq. (1.73)]. The strongly enhanced BE2-values within the rotational bands are, therefore, another indication of stable quadrupole deformations.
- (IV) **Hexadecupole matrix elements.** In (α, α') scattering [HGH 68] and Coulomb excitation, extremely large hexadecupole matrix elements have been found. This is a hint about stable hexadecupole deformations β_4 . They are positive (diamond shaped figures; see Fig. 1.3) at the beginning, go to zero in the middle, and turn slightly negative at the end of the rare earth region.
- (V) **Single particle structure.** A very sensitive experimental test for the deformation comes about from the experimentally observed single-particle energies, which depend very much on the details of the deformation (see Fig. 2.21).
- (VI) **Fission isomers.** In some of the heaviest nuclei are found long

lived states (shape isomers $\tau \lesssim 1$ msec) that have extremely large deformations ($\beta \sim 0.6$) [PDK 62, St 66, Va 77]. The corresponding rotational spectra have been measured [SWK 72, Sp 74] and we can deduce the corresponding moments of inertia. It is clear that such large deformations play an important role in nuclear fission, and the deformed shell model will therefore also be of importance for this process.

Microscopic Hartree-Fock calculations in this region result in a deformed average potential and are indeed able to explain quantitatively the experimental findings (see Chap. 7). Conceptually, the deformed shell model is more involved than the spherical one, since in the formulation of the former we have to accept another symmetry violation—that of rotational invariance.

2.8.2 General Deformed Potential

If we accept the arguments given in Section 2.8.1 about stable nuclear deformation, we are naturally led to the assumption that the average nuclear potential is also deformed. Since the nuclear forces have a small range (~ 1 fm) compared to the nuclear diameter, one expects that the shape of this potential will be similar to the shape of the nuclear density distribution (which can be determined at least in principle from experimental data, e.g., the quadrupole or higher multipole moments). As we have already seen in the case of the spherical shell model, the Woods-Saxon potential (Eq. (2.4)) represents quite a good average potential. It is thus natural to generalize it to the deformed case* [FS 66, DPP 69, GPA 71]

$$V(r, \theta, \phi) = -V_0 \left[1 + \exp\left(\frac{r - R(\theta, \phi)}{a(\theta, \phi)}\right) \right]^{-1}. \quad (2.72)$$

- In the spherical case, the parameter a describes the surface diffuseness and is approximately constant over all spherical nuclei, and therefore does not depend on the curvature of the surface. To get such a constant surface diffuseness for deformed nuclei also, one has to allow for a small dependence of $a(\theta, \phi)$ on the angles θ, ϕ (for more details, see [BM 75] and [BDJ 72]).

As we have seen in Section 2.4, the spin orbit term plays a very important role for the explanation of the level structure of spherical nuclei. In the deformed region, we also have to take it into account and a straightforward generalization of Eq. (2.18) is given by

$$V_{LS} = \lambda (\nabla V(r, \theta, \phi) \wedge \mathbf{p}) \cdot \mathbf{s}. \quad (2.73)$$

This definition coincides with the one for the spherical case.

* For single-particle energies and wave functions of rare earth nuclei in a deformed Woods-Saxon potential, see [GIS 73].

As in the case of the spherical Woods-Saxon potential, another useful approximation to the general potential (2.72) and (2.73) is the harmonic oscillator, which has then, of course, to be deformed. This study, which we shall discuss now, was originally carried out by S. G. Nilsson [Ni 55].

2.8.3 The Anisotropic Harmonic Oscillator

If we suppose for the moment that the density of a deformed nucleus can be ideally represented by an ellipsoidal distribution, then it follows from what has been said above that the average potential should also be ellipsoidal. In the harmonic oscillator approximation to the potential (2.72), this is most easily achieved by using the anisotropic harmonic oscillator as average field:

$$h_0 = -\frac{\hbar^2}{2m} \Delta + \frac{m}{2} (\omega_x^2 x^2 + \omega_y^2 y^2 + \omega_z^2 z^2). \quad (2.74)$$

The three frequencies $\omega_x, \omega_y, \omega_z$ have to be chosen proportional to the inverse of the half axes a_x, a_y, a_z of the ellipsoid:

$$\omega_\nu = \omega_0 \frac{R_0}{a_\nu}, \quad (\nu = x, y, z). \quad (2.75)$$

The condition for volume conservation is, therefore,

$$\omega_x \omega_y \omega_z = \text{const.} = \omega_0^3. \quad (2.76)$$

The Hamiltonian (2.74) is separable in x, y, z . The eigenstates are characterized by the quantum numbers n_x, n_y, n_z , and the eigenvalues are:

$$\epsilon_0(n_x, n_y, n_z) = \hbar \omega_x (n_x + \frac{1}{2}) + \hbar \omega_y (n_y + \frac{1}{2}) + \hbar \omega_z (n_z + \frac{1}{2}). \quad (2.77)$$

In the case of *axially symmetric shapes*, one usually chooses the z -axis as symmetry axis and introduces a deformation parameter δ by the following definition:

$$\begin{aligned} \omega_\perp^2 &= \omega_x^2 = \omega_y^2 = : \omega_0^2(\delta) (1 + \frac{2}{3}\delta), \\ \omega_z^2 &=: \omega_0^2(\delta) (1 - \frac{1}{3}\delta), \end{aligned} \quad (2.78)$$

where δ is the only deformation parameter in this case, since $\omega_0(\delta)$ is determined in such a way that volume conservation is guaranteed. Up to quadratic terms in δ , we get from Eq. (2.76),

$$\omega_0(\delta) = \omega_0(1 + \frac{2}{3}\delta^2). \quad (2.79)$$

Nilsson therefore introduced a deformation-dependent oscillator length $b(\delta) = (\hbar/m\omega_0(\delta))^{1/2}$ and dimensionless coordinates $r' = r/b$. In these coordinates the Hamiltonian (2.74) has the form

$$h_0(\delta) = \hbar \omega_0(\delta) \left(-\frac{1}{2} \Delta' + \frac{1}{2} r'^2 - \frac{1}{3} \sqrt{\frac{16\pi}{5}} \delta r'^2 Y_{20}(\theta', \phi') \right). \quad (2.80)$$

The equipotential surfaces are ellipsoids. In first order in the deformation δ they can be represented by Eq. (1.7).

$$r' \sim (1 + \beta Y_{20}(\theta', \phi')), \quad (2.81)$$

with

$$\beta = \frac{1}{3} \sqrt{\frac{16\pi}{5}} \delta + \dots = 1.057\delta + \dots \quad (2.82)$$

The deformation parameter δ of Eq. (2.78) is therefore roughly equal to β [Eq. (1.13)].

In the case of axial symmetry, it is convenient to use cylinder coordinates [Fl 71]. The eigenstates are characterized by quantum numbers n_z , n_ρ , m_l , where m_l is the projection of the orbital angular momentum on to the symmetry axis. With

$$N = n_z + 2n_\rho + m_l = n_x + n_y + n_z, \quad (2.83)$$

we get from Eq. (2.77)

$$\epsilon_0(n_z, n_\rho, m_l) = \hbar\omega_z(n_z + \frac{1}{2}) + \hbar\omega_\perp(2n_\rho + m_l + 1) \quad (2.84)$$

$$\simeq \hbar\dot{\omega}_0 \left[\left(N + \frac{3}{2} \right) + \delta \left(\frac{N}{3} - n_z \right) \right]. \quad (2.85)$$

The axial symmetry causes m_l to be a good quantum number. The same is true for the spin component s_z and the z -component j_z of the total angular momentum, which has the eigenvalue

$$\Omega = m_l + m_s = m_l \pm \frac{1}{2}. \quad (2.86)$$

It is usual to characterize the eigenstates of h_0 in the cylindrical basis by the set of "Nilsson" quantum numbers

$$\Omega \pi [N n_z m_l], \quad (2.87)$$

where π is the parity of the states [$\pi = (-1)^l = (-1)^N$; see Eq. (2.9)].

To discuss the level structure for a definite example, we use $N = 3$. From Eq. (2.85), we obtain in this case

$$\epsilon_0^{N=3}(n_z n_\rho m_l) \simeq \frac{9}{2} \hbar\dot{\omega}_0 + \hbar\dot{\omega}_0 \delta(1 - n_z). \quad (2.88)$$

Table 2.2 Construction of the Nilsson quantum numbers for $N = 3$

n_z	m_l	n_ρ	Ω	degeneracy
0	1	1	1/2 3/2	4-fold
	3	0	5/2 7/2	
1	0	1	1/2	3-fold
	2	0	3/2 5/2	
2	1	0	1/2 3/2	2-fold
3	0	0	1/2	1-fold

Using Eqs. (2.83) and (2.86), we get the following possibilities for the different quantum numbers, which are displayed in Table 2.2.

According to Eqs. (2.85) and (2.88), the levels with different values of n_z are split for small deformations proportionally to δ . This is shown in Fig. 2.19.

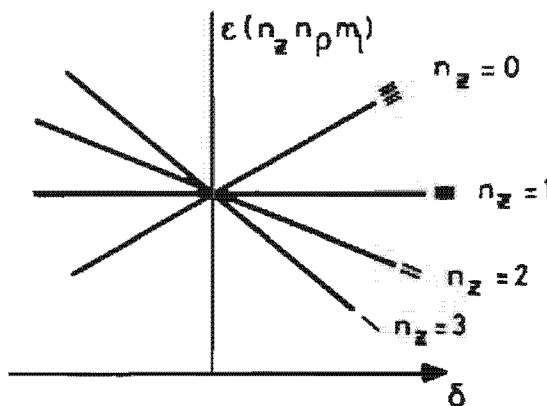


Figure 2.19. Levels of the anisotropic harmonic oscillator as a function of δ .

2.8.4 Nilsson Hamiltonian

As we have seen in Sec. 2.3, the pure harmonic oscillator has two essential drawbacks concerning the agreement with experimental single-particle spectra:

- (i) A strong spin orbit term must be added in order to reproduce the right magic numbers
- (ii) For heavy nuclei, the realistic average potential is rather flat in the interior of the nucleus. Compared to the harmonic oscillator, nucleons at the surface (i.e., nucleons with higher l -values) feel a deeper potential in the realistic case.

In order to include these effects, Nilsson [Ni 55] added two terms to the deformed harmonic oscillator (2.74) and (2.80) and used the Hamiltonian:

$$h = -\frac{\hbar^2}{2m}\Delta + \frac{m}{2}\omega_x^2(x^2 + y^2) + \frac{m}{2}\omega_z^2z^2 + C\text{ls} + Dl^2 \quad (2.89)$$

$$= \hbar\omega_0(\delta)\left(-\frac{1}{2}\Delta' + \frac{1}{2}r'^2 - \beta r'^2 Y_{20}\right) - \kappa\hbar\dot{\omega}_0(2\text{ls} + \mu l^2). \quad (2.90)$$

The constants C and D are given in the form:

$$C = -2\hbar\dot{\omega}_0\kappa, \quad D = -\hbar\dot{\omega}_0\kappa\mu, \quad (2.91)$$

where C gives the strength of the spin orbit force and $D \cdot l^2$ shifts the levels with higher l -values downward (Fig. 2.20; notice that different μ -values are taken for different shells, as explained below).

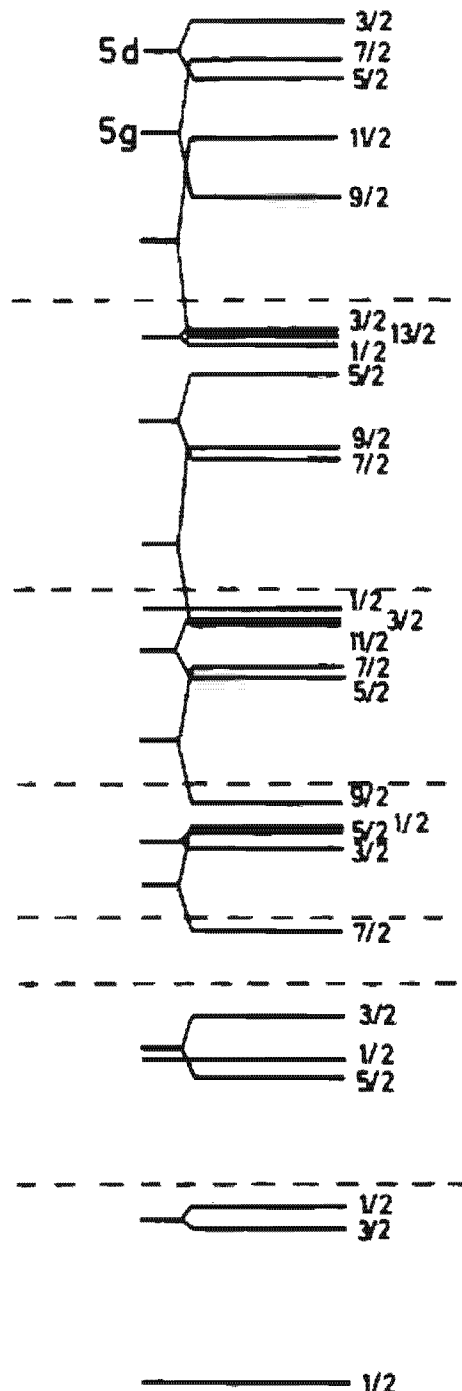
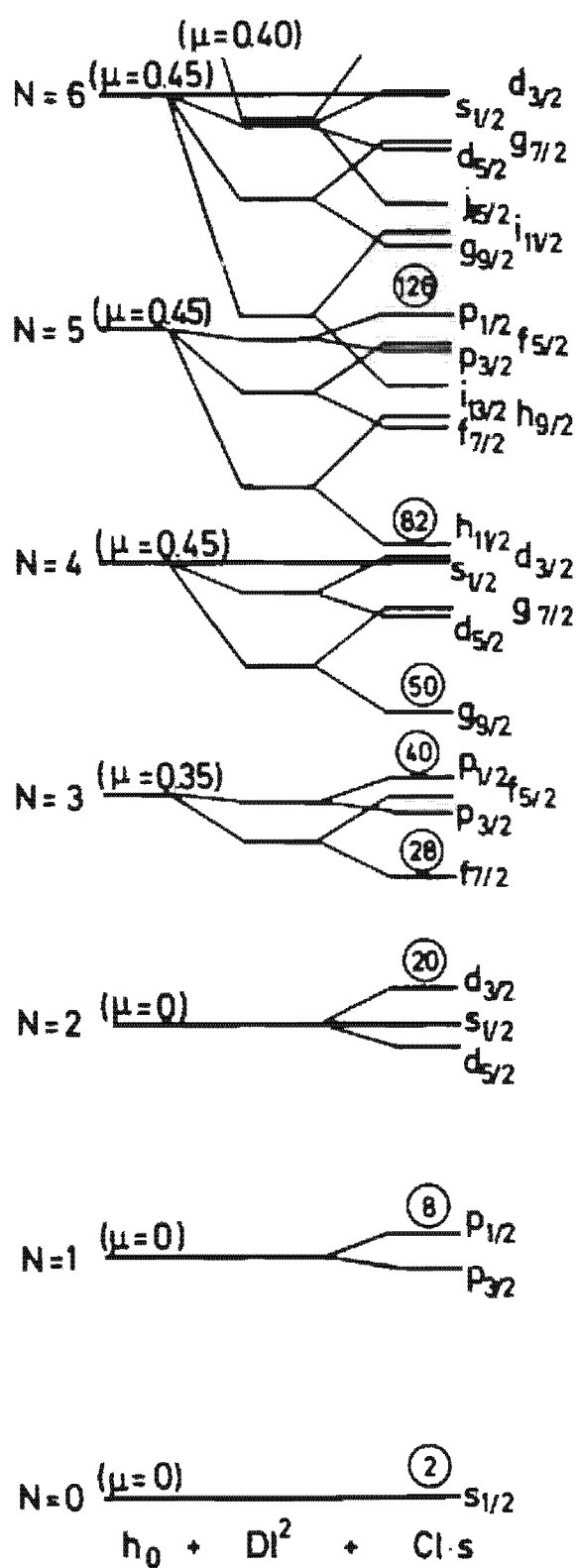


Figure 2.20. Comparison of experimentally determined level scheme [Kl 52] with calculations [Ni 55] using the Nilsson Hamiltonian for zero deformation.

In the original version, Nilsson used the term $D \cdot \mathbf{l}^2$. Later on one observed that for states with large N quantum numbers, the corresponding shift is too strong and the following replacement was made [GLN 67]

$$D \cdot (\mathbf{l}^2 - \langle \mathbf{l}^2 \rangle_N), \quad (2.92)$$

where $\langle \mathbf{l}^2 \rangle_N = \frac{1}{2} \cdot N(N+3)$ is the expectation value of \mathbf{l}^2 averaged over one major shell with quantum number N . In this case, only the states within the shells are shifted. The center of gravity between different major shells remains unaffected.

Of course, the \mathbf{l} -s and the \mathbf{l}^2 term are no longer diagonal in the representation $n_z n_p m_l$, nor in the representation n_x, n_y, n_z . The only quantum numbers that remain conserved are the parity π and the eigenvalue Ω of j_z . In fact, it is easily shown that h of Eq. (2.90) does not commute with \mathbf{j}^2 ; therefore the Slater determinant for a deformed shell model has no good quantum number for the total angular momentum. This means that the picture of a deformed nucleus, that is, a deformed shell model, is inevitably linked to the abandonment of rotational invariance. In nature, however, rotational invariance is never violated and one should therefore, at least in principle, re-establish this invariance before drawing any conclusions. How this can be done will be shown in Sec. 11.4. Approximate treatments of these so-called projection methods show that the main features of the deformed shell model are correct.

For large deformations, the \mathbf{l} s and \mathbf{l}^2 terms in Eq. (2.90) can be neglected in comparison with βY_{20} . In this limit, the quantum numbers (2.87) of the anisotropic harmonic oscillator become good quantum numbers. They are then also termed *asymptotic quantum numbers*.

In order to obtain the eigenvalues of the Nilsson Hamiltonian as a function of δ , it must be diagonalized in a suitable basis. The isotropic or anisotropic harmonic oscillator [BP 71] can be used as a basis set. In his original paper, Nilsson [Ni 55] worked in a spherical basis. In this case, the \mathbf{l}^2 and \mathbf{l} s terms are diagonal and only the term βY_{20} mixes states with the same principal quantum number N ($\Delta N = 0$) with those with $\Delta N = 2$. By using stretched coordinates Nilsson could show [Ni 55] that the $\Delta N = 2$ admixtures are only of higher order in the deformation parameter and can therefore be neglected to a good approximation. The deformation parameters in the stretched coordinates are usually called ϵ . Because of the \mathbf{l} s and \mathbf{l}^2 terms, the levels with the same n_z in Fig. 2.19 split up and only the degeneracy $\pm \Omega$ is conserved. Nevertheless, the levels with the same n_z are, in the asymptotic region, nearly parallel. This effect can be seen in the so-called Nilsson diagram of Fig. 2.21a, for instance, for the levels with $N = 3$. In Figs. 2.21b and 2.21c the Nilsson diagrams for higher shells are given for neutrons and protons, respectively. Again, we can see that levels with the same n_z are parallel in the asymptotic region. For the correct attribution of the n_z quantum number, one should also notice that according to Eq. (2.85), levels with higher (lower) n_z values are lower than those

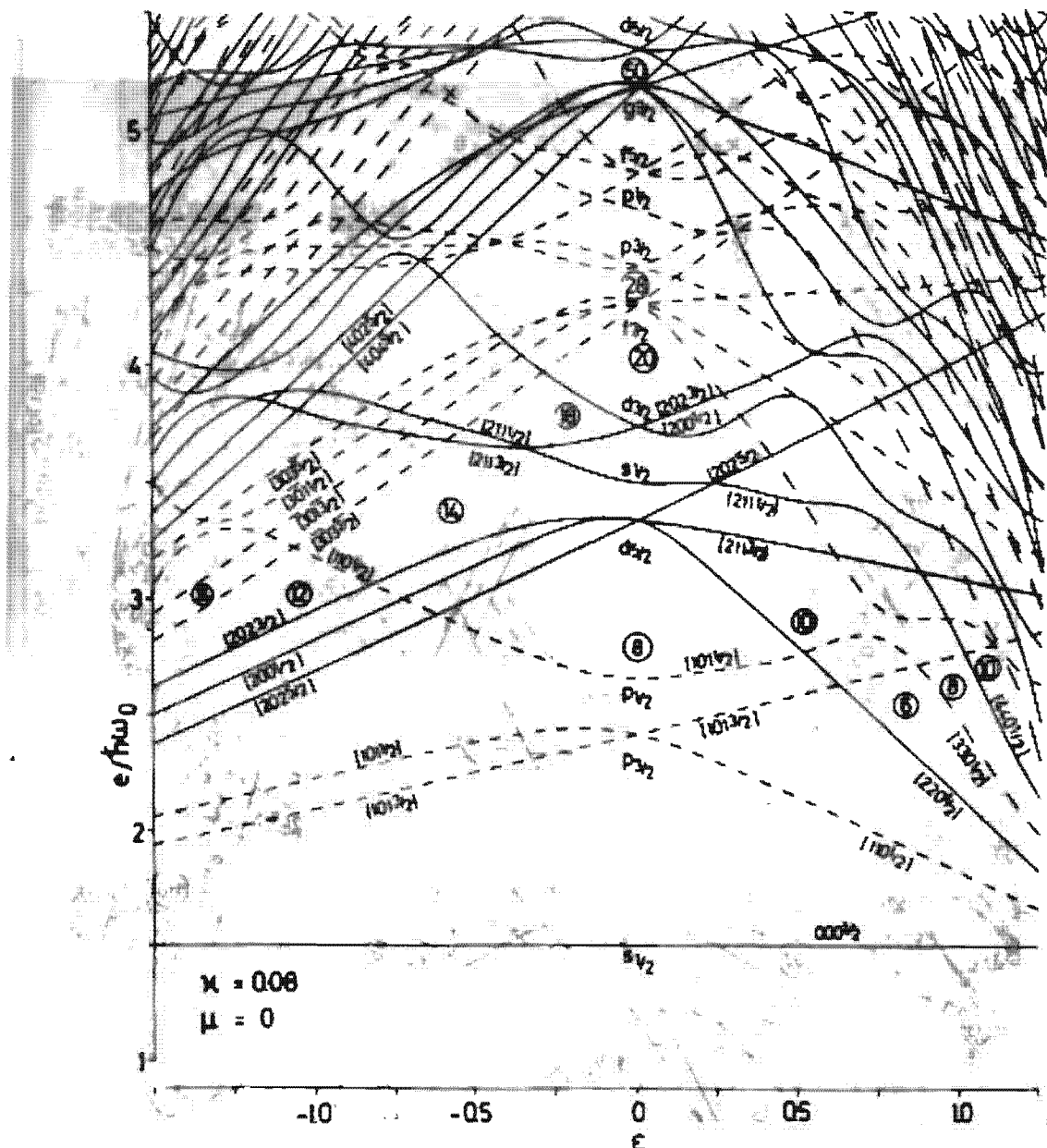


Figure 2.21a. Level scheme of the Nilsson Model for light nuclei. The figure shows the single-particle energies e [the eigenvalues of the Nilsson Hamiltonian (2.90)] in units of the oscillator energy $\hbar\omega_0(\epsilon)$ at the corresponding deformations $\epsilon = \epsilon_2$ (stretched coordinate; see text). The full lines correspond to levels with positive parity, the dashed lines to those with negative parity. The numbers on the lines correspond to the quantum numbers N, n_z, m_z, Ω . Also indicated are the magic numbers in the spherical case and for finite deformations. (We are grateful to Dr. S. Åberg for the preparation of the figure.)

with lower (higher) n_z -values for positive (negative) δ . Knowing N , n_z , and Ω one can also determine the m_z value, and hence the complete set of asymptotic quantum numbers, from tables analogous to Table 2.2.

The Nilsson Hamiltonian (2.90) contains no Coulomb term. The effect of that term is incorporated into an appropriate choice of the constants κ and μ . They are actually fitted such that the observed levels in deformed nuclei are reproduced. The spherical single-particle energies that one obtains with these parameters agree qualitatively with the single-particle or

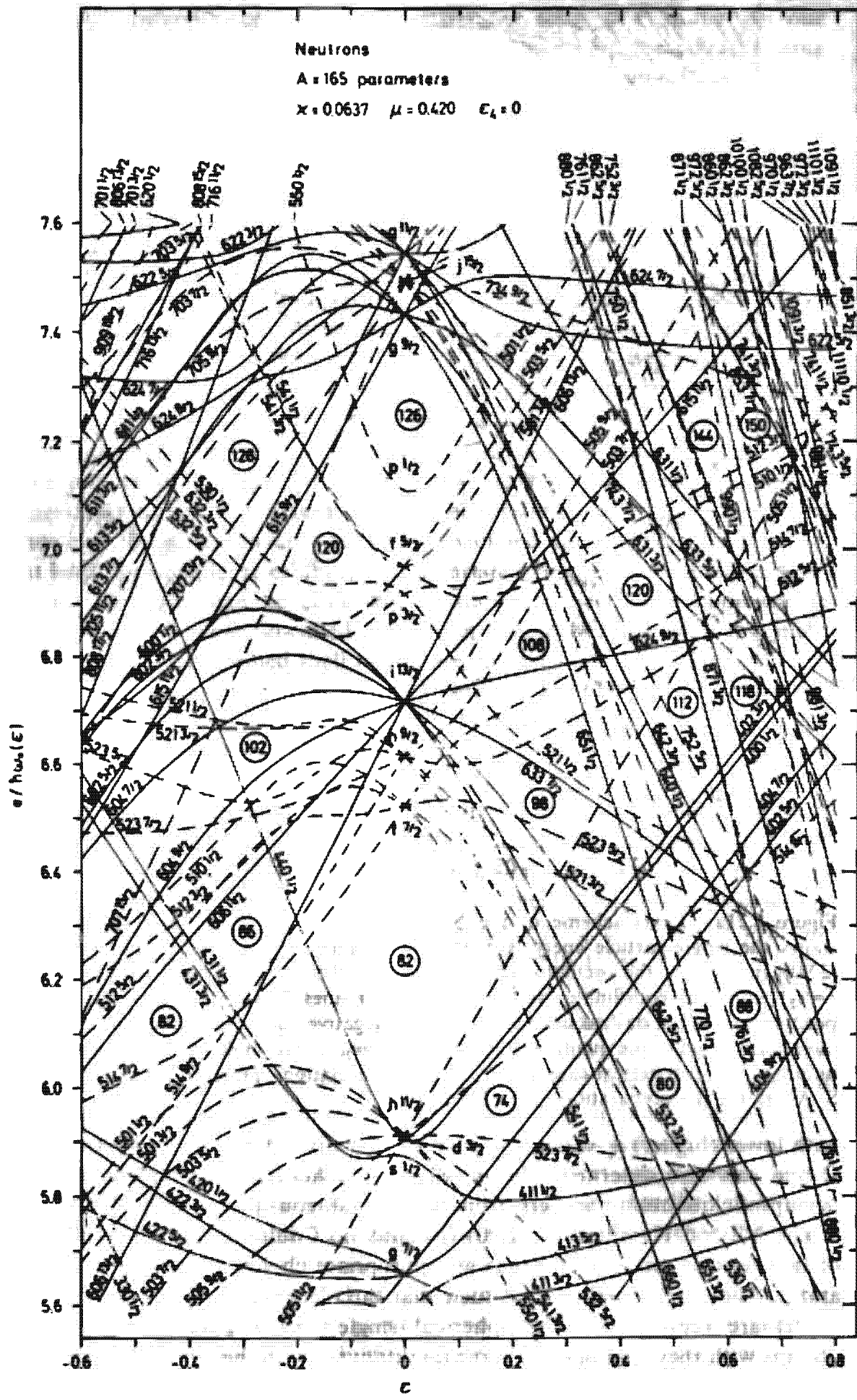


Figure 2.21b. Same as Fig. 2.21a for neutrons in heavy nuclei.

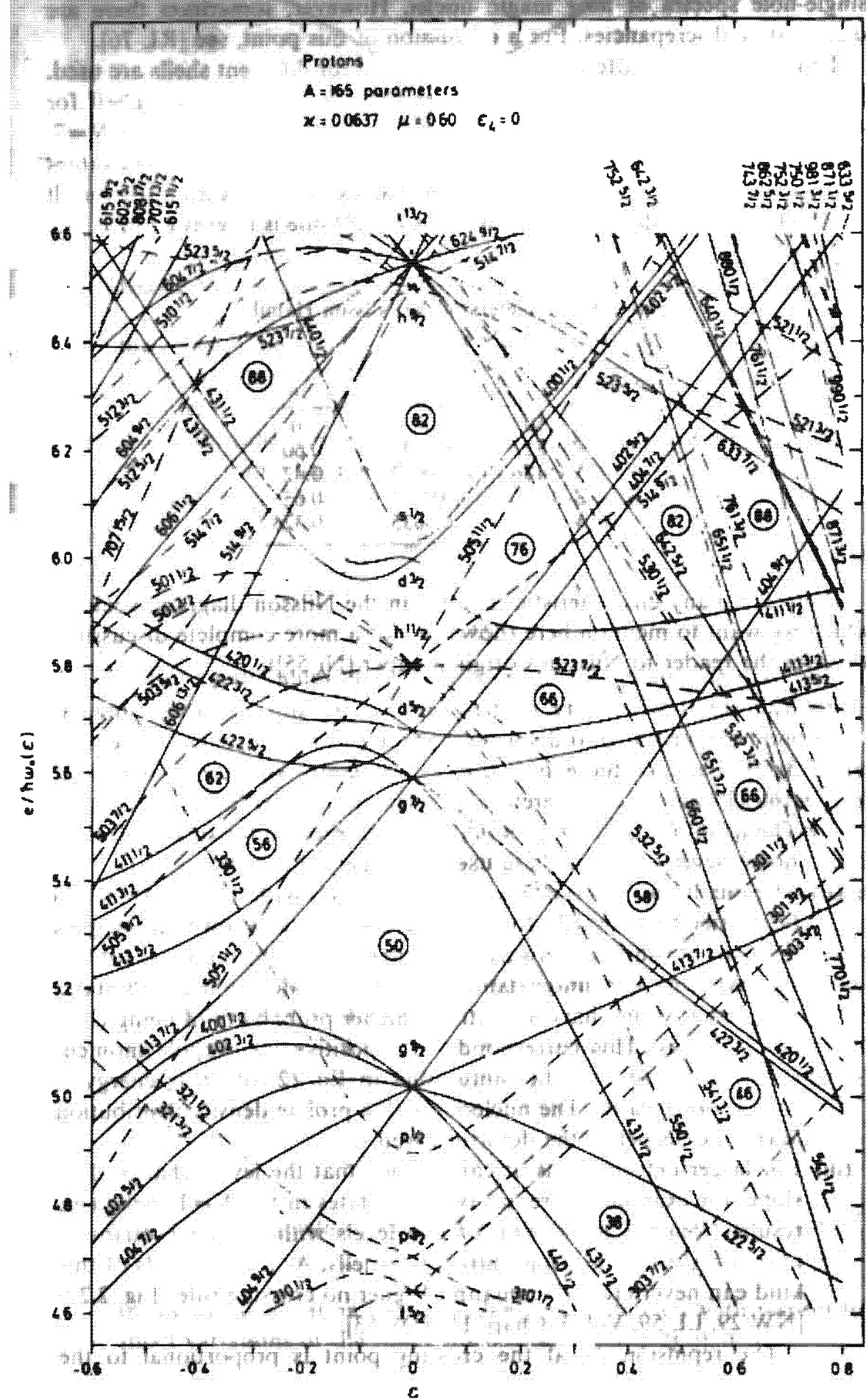


Figure 2.21c. Same as Fig. 2.21a for protons in heavy nuclei.

single-hole spectra of near magic nuclei. However, sometimes there are quantitative discrepancies. For a discussion of this point, see [RL 76].

To get a good fit, different values of κ and μ for different shells are used. In his original paper, Nilsson used $\kappa = 0.05$ for all shells and $\mu = 0$ for $N = 0, 1, 2$; $\mu = 0.35$ for $N = 3$; $\mu = 0.45$ for $n = 4, 5, 6$; and $\mu = 0.4$ for $N = 7$. Later these parameters were more carefully adjusted. Table 2.3 gives values that are now widely used. There the same values of μ and κ are used for all the shells, but they depend on the nucleus (N, Z) one is interested in.

Table 2.3 Parameters of the Nilsson Hamiltonian (from [GLN 67])

Region	κ	μ
$N, Z < 50$	0.08	0
$50 < Z < 82$	0.0637	0.60
$82 < N < 126$	0.0637	0.42
$82 < Z$	0.0577	0.65
$126 < N$	0.0635	0.325

There are many characteristic features in the Nilsson diagram, some of which we want to mention here (however, for a more complete discussion, we refer the reader to Nilsson's original paper [Ni 55]):

- (i) The shells which are determined by the single particle angular momentum j at zero deformation, split up into $(2j+1)/2$ levels for $\delta \neq 0$. Each of these is twofold degenerate with eigenvalues $\pm \Omega$ ($[h, j_z] = 0$) and can therefore be characterized by $|\Omega|$ and its parity. The quantum numbers $[Nn, m_j]$ are not conserved for small deformations, nevertheless they are used to classify the levels.
- (ii) The quadrupole field $r^2 Y_{20}$ causes the levels with lower Ω values to be shifted downwards for positive deformations (prolate shapes) and to be shifted upwards for negative deformations (oblate shapes). One can understand this effect, realizing that the states with low Ω -values have a relatively higher probability of being close to the z -axis. This corresponds to a positive quadrupole moment $\langle r^2 Y_{20} \rangle$. Because of the minus sign in Eq. (2.90), their energy is shifted downwards. The nucleons with a prolate density distribution $|\phi_r(r)|^2$ lie deeper in the deformed well.
- (iii) For larger deformations, it can happen that the levels change their slope, for example, there are two $1/2$ -states in the $N=1$ shell. This results from the interaction of two levels with the same quantum numbers $\Omega\pi$ coming from different j -shells. As a rule, levels of this kind can never cross (Neumann-Wigner no crossing rule; Fig. 2.22) [NW 29, LL 59, Vol. 3, Chap. 11; HW 53].

The repulsion $\Delta\epsilon$ at the crossing point is proportional to the interaction strength. Properties of the levels become interchanged at

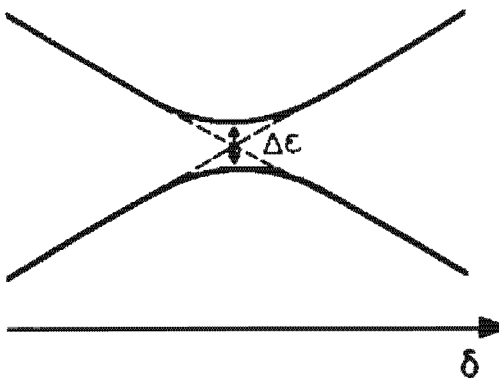


Figure 2.22. No crossing rule for two levels with the same symmetry.

the crossing point and the wave functions corresponding to the two levels far from the crossing point are the same as if there had been no interaction at all.

- (iv) If one diagonalizes the Nilsson Hamiltonian using the basis $|Nlj\Omega\rangle$ of the isotropic harmonic oscillator, the Nilsson wave functions are given by a superposition of spherical harmonic oscillator functions:

$$|k\rangle = \sum_{\alpha} D_{ak} |\alpha\rangle, \quad (2.93)$$

where

$$\alpha = \{Nlj\Omega\}.$$

For small values of δ , there is only small mixing, that is, one of the coefficients D_{ak} is nearly equal to one, and the others are close to zero. For larger deformations, the situation depends very much on the specific levels. For example, the $1g_{9/2}$ state in Fig. 2.21c splits up into five levels $\Omega = 1/2, \dots, 9/2$. Since for $\delta = 0$ the $g_{9/2}$ is rather far away from the other levels with the same N (it is lowered by the spin orbit term), there is only a small amount of mixing, and the corresponding levels are almost eigenstates of j^2 , even for quite large values of δ . The same effect is even more pronounced for heavier nuclei. For instance, the $i_{13/2}$ state is of this type and plays an important role in the rare earth region and contains almost no mixing for relevant deformation values.

- (v) The slope of the Nilsson levels ϵ_k [measured in units of $\hbar\omega_0(\epsilon)$] is given by the single-particle matrix element of the quadrupole operator $q = r'^2 Y_{20}$ in the corresponding single-particle state $|k\rangle$

$$\frac{d\epsilon_k}{d\beta} = -\langle k | r'^2 Y_{20} | k \rangle.$$

To prove this relation, we use the fact that the eigenvalues

$$\epsilon_k = \langle k | h(\beta=0) - \beta q | k \rangle$$

of the diagonalization problem (2.90) are stationary with respect to small variations of the functions $|k\rangle$ (see Sect. 5.2), that is,

$$\delta \langle k | h(\beta=0) | k \rangle - \beta \delta \langle k | q | k \rangle = 0.$$

We thus obtain

$$\frac{d\epsilon_k}{d\beta} = \frac{d}{d\beta} \langle k | h(\beta=0) | k \rangle - \beta \frac{d}{d\beta} \langle k | q | k \rangle - \langle k | q | k \rangle = 0 - \langle k | q | k \rangle.$$

2.8.5 Quantum Numbers of the Ground State in Odd Nuclei

The spherical shell model fails in its prediction for the angular momenta and parities of the ground state for nuclei in the deformed region. However, the Nilsson model is able to explain the experimental data in the following way [MN 59].

For a specific nucleus, one determines the deformation parameter δ from the measured quadrupole moment Q_0 , as discussed in Section 2.8.1. For this value of δ one successively fills two protons and two neutrons in each level starting from the bottom. Because of the degeneracy of each Nilsson level ($\pm \Omega$), every nucleon pair has, qualitatively speaking, spin zero. Therefore spin and parity of odd nucleons are determined by the last odd nucleon. Since Ω is not a directly measurable quantity, we must determine it indirectly by using a model. We will see in Section 3.3.1.1 that the appropriate concept here is the particle-plus-rotor model. There it will turn out that the angular momentum I_0 of the band head of a rotational band coincides with Ω ($I_0 = \Omega$). The lowest band head is, therefore, the ground state spin of the odd nucleus. Often in the region of the experimentally determined value of δ several possibilities for the Ω of the last particle exist. In fact, the observed value of the ground state spin for many deformed nuclei is among the possible Ω values indicated in Table 2.4. In Fig. 2.23 this method is explained for $^{183}_{74}\text{W}_{109}$. The other possible Ω values

Table 2.4 Comparison of theoretically and experimentally determined ground state spins [He 61, p. 648]

	δ	I_0 theo	I_0 exp		δ	I_0 theo	I_0 exp
$^{63}\text{Eu}^{151}$	0.16	$3/2^\pm, 5/2^\pm,$ $1/2^-$	$5/2$	Gd^{155}_{91}	0.31	$5/2^+, 3/2^-$	$3/2$
$^{63}\text{Eu}^{153}$	0.30	$5/2^+, 3/2^+$	$5/2$	Gd^{157}_{93}	0.31	$3/2^-, 5/2^+$	$3/2$
$^{65}\text{Tb}^{159}$	0.31	$3/2^+, 5/2^+$	$3/2$	Dy^{161}_{95}	0.31	$5/2^-$	
$^{67}\text{Ho}^{165}$	0.30	$7/2^-, 1/2^+$	$7/2$	Er^{167}_{99}	0.29	$1/2^-, 7/2^+, 11/2^-$	$7/2$
$^{69}\text{Tm}^{169}$	0.28	$1/2^+, 7/2^-$	$1/2$	Yb^{171}_{101}	0.29	$7/2^+, 1/2^-, 11/2^-$	$1/2$
$^{71}\text{Lu}^{175}$	0.28	$7/2^+, 5/2^+$	$7/2$	Yb^{173}_{103}	0.29	$5/2^-$	$5/2$
$^{73}\text{Ta}^{181}$	0.23	$5/2^+, 7/2^+$	$7/2$	Hf^{177}_{105}	0.26	$7/2^-$	$7/2$
$^{75}\text{Re}^{183}$	0.19	$9/2^-, (5/2^+)$	$5/2$	Hf^{179}_{107}	0.27	$9/2^+$	$9/2$
$^{75}\text{Re}^{187}$	0.19	$9/2^-, (5/2^+)$	$5/2$	W^{183}_{109}	0.21	$1/2^-, 7/2^-, 3/2^-$	$1/2$
$^{77}\text{Ir}^{191}$	0.14	$3/2^+, 1/2^+,$ $11/2^-$	$3/2$	Os^{187}_{111}	0.18	$1/2^-, 3/2^-, 9/2^-$	$1/2$
$^{77}\text{Ir}^{193}$	0.12	$3/2^+, 1/2^+,$ $11/2^-$	$3/2$	Os^{189}_{113}	0.15	$1/2^-, 3/2^-, 11/2^+,$ $(9/2^-)$	$3/2$

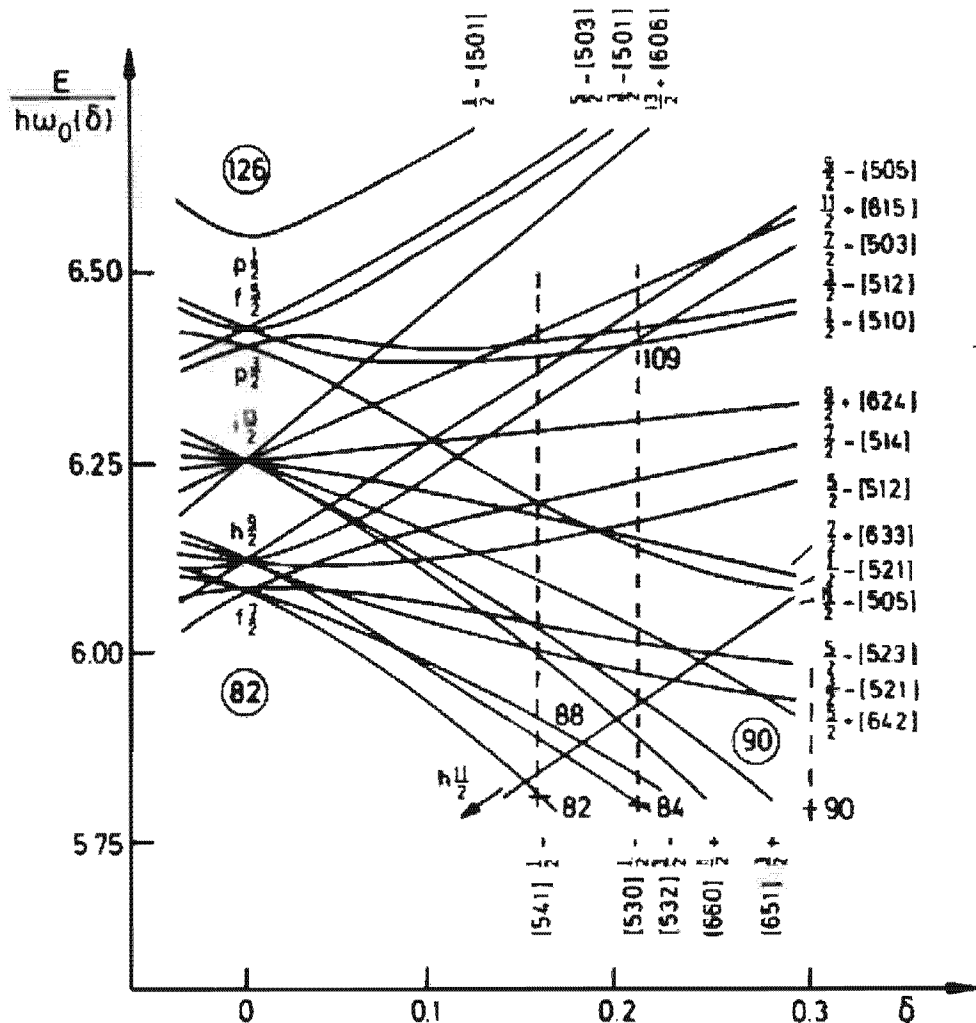


Figure 2.23. Determination of the ground state spin in the Nilsson model. (From [He 61, p. 647].)

are usually seen in the spectra as band heads of excited rotational bands, which is a nice success of the Nilsson model. Single-particle energies in this scheme can be found in [Ch 66, BR 71a, OWP 71, GIS 73, GSK 75, CAF 77].

2.8.6 Calculation of Deformation Energies

In order to obtain the ground state energy of the nucleus in the (spherical or deformed) shell model, we cannot simply sum the single-particle energies from the bottom of the potential up to the Fermi level, because the effect of the nucleon–nucleon interaction would be counted twice (see also Sec. 5.3). To account for this, we proceed with the following qualitative considerations.

We assume that the average potential which is felt by the i th nucleon is given by the sum of all two-body potentials acting on this particle:

$$V_i = \sum_{j \neq i} v_{ij}. \quad (2.94)$$

The Hamilton operator

$$H = \sum_{i=1}^A t_i + \frac{1}{2} \sum_{\substack{i, j \\ i \neq j}} o_{ij} \quad (2.95)$$

is then given by

$$H = \frac{1}{2} \sum_{i=1}^A h_i + \frac{1}{2} \sum_{i=1}^A t_i; \quad h_i = t_i + V_i. \quad (2.96)$$

If V_i has the form of a harmonic oscillator, we have, because of the virial theorem [Da 65a, Chap. II],

$$\langle t_i \rangle = \langle V_i \rangle = \frac{1}{2} \langle h_i \rangle \quad (2.97)$$

and we get as the ground state energy

$$E_0(\delta) = \langle H \rangle = \frac{1}{4} \sum_{i=1}^A \langle h_i \rangle = \frac{1}{4} \sum_{i=1}^A \epsilon_i(\delta). \quad (2.98)$$

In practice we determine the equilibrium deformation δ_{eq} in calculating E_0 as a function of δ ; the absolute minimum then determines δ_{eq} . This procedure does not, of course, include any residual interaction and, in fact, fails to reproduce the absolute value of the binding energies. Only the resulting equilibrium deformations are approximately right (see Fig. 2.24). Further investigations on these lines [BS 61, Sz 61, So 67, and GLN 67] have taken into account the following additional points.

- (i) A *residual interaction* of the pairing type (see Chap. 6)
- (ii) The expectation value of the *Coulomb force*

$$E_{Coul} = \left\langle \sum_{\text{prot}} \frac{e^2}{|\mathbf{r}_i - \mathbf{r}_j|} - \kappa \hbar \dot{\omega}_0 \Delta \mu \sum_{\text{prot}} (\mathbf{l}^2 - \langle \mathbf{l}^2 \rangle_N) \right\rangle, \quad (2.99)$$

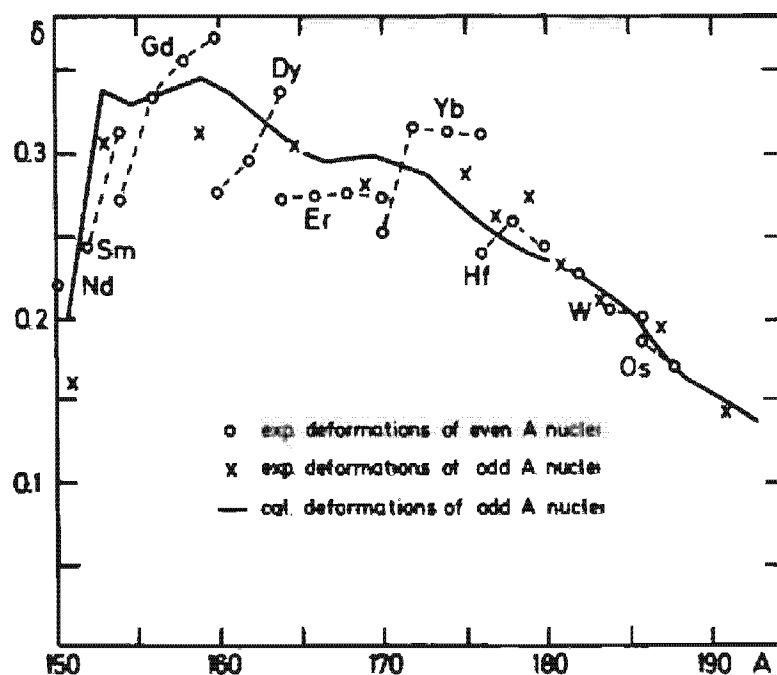


Figure 2.24. Comparison of theoretically and experimentally determined deformations. (From [MN 55].)

where $\Delta\mu = \mu_{\text{prot}} - \mu_{\text{neut}}$ corrects for the Coulomb effect already taken into account by the difference between the proton and neutron parameters μ . It turns out that the effect of the Coulomb repulsion favors larger deformations, whereas the effect of the pairing correlations is the converse. On the whole, the results of the old Nilsson model are reproduced, because Coulomb and pairing forces counteract one another at the equilibrium point.

- (iii) *Higher shapes.* It is evident that quadrupole deformations alone are not able to describe for instance the fission process. On the other hand, there exists evidence for hexadecupole deformations in the ground state of some nuclei [HGH 68]. It is possible to describe such effects within the Nilsson model by including, besides Y_{20} , higher terms such as Y_{40} and Y_{60} [NTS 69, Mö 72, MN 73, RNS 78].

For the fission process it is often useful to introduce deformed potentials that allow us to describe two separated fragments at large distances. In contrast to the Nilsson model, such potentials have the right asymptotic behavior. Several versions of such potentials have been used:

- (i) *Two-center models* [DR 66, HMG 69, ADD 70, GMG 71, SGM 71, MG 72, MMS 73], which are based on two oscillators with separated centers.
- (ii) The *Folded Yukawa Potential* [Ni 69, BFN 72, Ni 72, MN 73] which starts with a density of sharp surface but arbitrary shape. To get the corresponding potential, it is folded with a short-range Yukawa force.
- (iii) *Generalized Wood-Saxon* potentials with a deformation-dependent surface thickness [DPP 69, BDJ 72, Pa 73, BLP 74, JH 77].

The method of simply summing up the single-particle energies fails to reproduce the absolute binding energies and to describe the energy surface at very large distortions. The reason for this is that the binding energy is a bulk property. In fact, rather small shifts in the single-particle energies produce large errors in the binding energy. To get the proper values for the binding energy together with shell effects, we must use a combination of the liquid drop and the shell model, as proposed by Strutinski (see Sec. 2.9). Calculations within this method show that the pure shell model as described in this chapter allows us to determine only ground state deformations.

The fact that the absolute energy minimum occurs at finite values of δ for nuclei between closed shells, can be understood qualitatively by considering the level density as a function of deformation. It turns out that for quite general average potentials the level density develops shell effects for certain definite values of the deformation; that is, at these deformations the levels are not randomly distributed as a first glance on the Nilsson

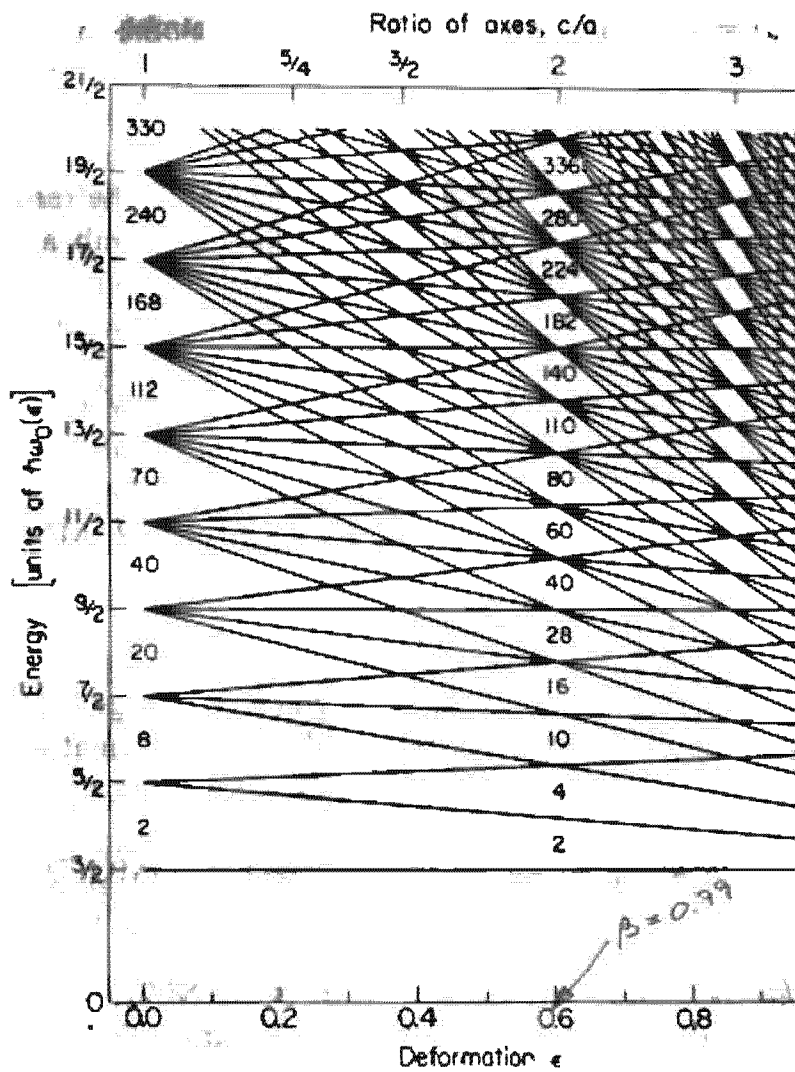


Figure 2.25. Energy levels of an harmonic-oscillator potential for prolate spheroidal deformations ϵ . (From [MN 73].)

diagram would indicate, but are, for instance, grouped in bunches at larger deformations.* This is shown in Fig. (2.25) for the harmonic oscillator.

If one plots the energy as a function of the deformation, one finds that whenever the Fermi level is situated in a low density region, the nucleus is more bound, whereas it is less bound when the Fermi level is in a high density region. This, in turn, means that the occupied levels are, on the average, more bound if the Fermi level is in a low density region than if it is in a high density region. Since for nuclei between closed shells the Fermi level for $\delta=0$ is in a region of high level density, it becomes qualitatively understandable that these nuclei want to deform into a region where the Fermi energy is in a lower level density region. From this it also becomes clear that in any nucleus more than one minimum, as a function of deformation, can eventually develop. As we discussed in Section 2.8.2, in very heavy nuclei we find second minima at about $\delta \approx 0.6$, somewhat

* One can understand from semiclassical arguments, at which deformations such shell closures have to occur [BM 75, St 75b, SM 76, SMO 77].

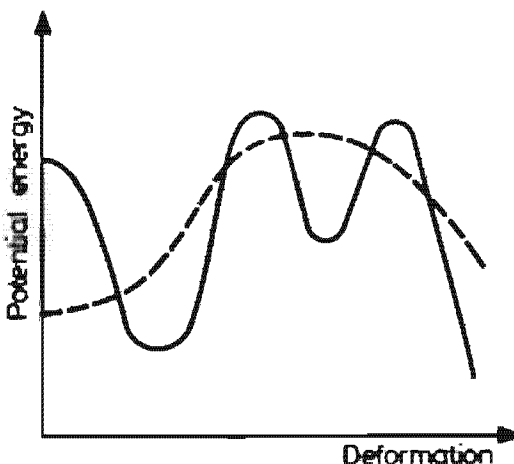


Figure 2.26. Schematic variation of the energy with deformation for a nucleus with a second minimum. The dashed line corresponds to the liquid drop barrier.

higher than the first minimum, which gives rise to the so-called shape isomeric states [St 66]. Qualitatively, the energy as a function of deformation is shown in Fig. 2.26.

2.9 Shell Corrections to the Liquid Drop Model and the Strutinski Method

2.9.1 Introduction

Up to now we have studied two quite different descriptions of the atomic nucleus. The *liquid drop model* (LDM) assumes that the nucleons produce a spatially uniform density distribution in the nucleus with a sharp edge at the surface. It is able to reproduce the overall features of the nucleus, that is, most properties that depend only in a smooth way on the nucleon number, as, for example, in Chapter 1, the A dependence of the nuclear binding energy (Fig. 1.2). On the other hand, there is the *shell model*. It assumes a quantized independent particle motion in an average potential to be valid, and we have seen in Section 2.3 and 2.8 that this model reproduces nicely those particular nuclear properties in which only the nucleons in the vicinity of the Fermi surface are involved.

Phenomenological shell models (in contrast to Hartree-Fock calculations; see Chap. 5), however, fail to correctly reproduce properties of the nucleus in which *all* nucleons contribute (the so-called bulk properties), like, for instance, the total binding energy. Strutinski [St 67, 68] invented a very elegant method* to reconcile both phenomenological descriptions of the nucleus which eliminates their defects but keeps their qualities. This is the *Strutinski shell correction procedure*. It is able to reproduce not only the

* Investigations on a similar line have been carried out by Myers and Swiatecki [MS 66].

experimental ground state energies of nuclei, but also their dependence on deformation parameters. This method was used extensively for the calculation of energy surfaces in the fission process.

2.9.2 Basic Ideas of the Strutinski Averaging Method

As we discussed in Chapter 1, the nuclear binding energies E as a function of A have a smooth part E_{LDM} well represented by the Bethe–Weizäcker mass formula (1.4) (Fig. 1.2) and, in addition, an oscillatory part E_{osc} defined by

$$E = E_{\text{osc}} + E_{\text{LDM}}. \quad (2.100)$$

Similar oscillations would occur if we could calculate the exact energy of the many-body system as a function of the deformation and compare it with the corresponding LDM value. These oscillations are due to the occurrence of shell closures, that is, they have maxima at the magic numbers, as we mentioned at the beginning of Section 2.2 (Fig. 2.2). Therefore, their origin is entirely of a quantum mechanical nature. As a matter of fact, if we calculate the binding energies in the shell model [for example, in the Nilsson model; see Eq. (2.90)], one finds such oscillations. Only the corresponding average part is wrong. Furthermore, as we explained at the end of the last chapter, these oscillations are due to a grouping of levels into bunches—the shells. In fact, it is clear that for a smooth distribution of levels, the binding energy per particle depends in a smooth way on the position of the Fermi level, whereas for a shell-like distribution of the levels there is also an oscillatory behavior superimposed on top of it. We demonstrate this in Fig. 2.27, where we compare two such level densities whose average densities are equal.

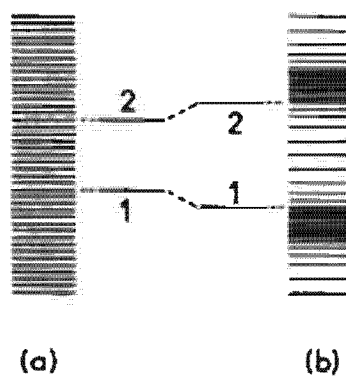


Figure 2.27. Comparison of an equally spaced level density to a schematic shell model level density. For the Fermi level (1), the binding in (b) is stronger than in (a), whereas for (2) the opposite is true.

We see that if the Fermi level is situated just above a shell we get more binding than on the average, whereas if it is placed just below we get less

binding than on the average. This picture is certainly very schematic, since, for example, the real average level density is not a constant; this however, is a smooth effect and should not influence the previous conclusions. The binding energies corresponding to the shell distribution (b) oscillate around the ones given by the "average" level density (a). Therefore, the average level density is responsible for the average behavior of the binding energies. It is this average part which has the wrong value in the phenomenological shell model. It was the decisive idea of Strutinski to calculate only the fluctuating part E_{osc} of the total energy E in Eq. (2.100) within the shell model and to take the rest, E_{LDM} , from the liquid drop model. This procedure contains the assumption that the fluctuating part E_{osc} is well approximated by the fluctuating part of the shell model energy. At the end of this chapter we will discuss the way we can justify this assumption. There then remains only the problem of how to divide up the shell model energy into an oscillating part, E_{osc} , and a smoothly varying part, \tilde{E}_{sh} .

$$E_{\text{sh}} = \sum_{i=1}^A \epsilon_i = E_{\text{osc}} + \tilde{E}_{\text{sh}}. \quad (2.101)$$

[Expression (2.101) does not take into account any effect coming from the two-body interaction as, for example, in Eq. (2.98). We will see that in the end this is of no importance.]

The decomposition (2.101) is a problem which has to be solved completely within the shell model. Therefore, it is useful to introduce the concept of the level density $g(\epsilon)$ by defining $g(\epsilon) \cdot d\epsilon$ as the number of levels in the energy interval between ϵ and $\epsilon + d\epsilon$. In the shell model the level density is given by

$$g(\epsilon) = \sum_i \delta(\epsilon - \epsilon_i). \quad (2.102)$$

If we know $g(\epsilon)$, we can calculate the particle number

$$A = \int_{-\infty}^{\lambda} g(\epsilon) d\epsilon \quad (2.103)$$

with a properly chosen Fermi energy λ .

In the shell model, λ is not defined uniquely by Eq. (2.103). It can be arbitrarily chosen to be between the last filled and the first unfilled level. For the shell model energy, we get

$$E_{\text{sh}} = \int_{-\infty}^{\lambda} \epsilon g(\epsilon) d\epsilon. \quad (2.104)$$

The shell model levels are grouped into bunches with an average distance of $\hbar\omega_0 \approx 41 A^{-1/3}$ (MeV) [see Eq. (2.12)]. Therefore, the level density g shows oscillations with roughly this frequency.

Since, as we have seen in Fig. 2.27, the fluctuations in the shell model energy E_{sh} are due to these oscillations, it is obvious that we can calculate the smooth part \tilde{E}_{sh} in Eq. (2.101) by introducing a continuous function $\tilde{g}(\epsilon)$, which represents the smooth part of the level density $g(\epsilon)$. It should

have the mean functional behavior of g , but must not contain oscillations with a frequency $\approx \hbar\omega_0$. In a real nucleus the level density is by far more complex than in our simple picture of Fig. 2.27. Its increase, for instance, with increasing energy is in general nonlinear and certainly far from being a constant. Therefore, one has to give a well-defined mathematical prescription of how one can extract from a given level density its mean part. This will be explained in the next section. For the moment, we shall assume that we are given the average part $\tilde{g}(\epsilon)$ of the shell model level density $g(\epsilon)$. Then we can again calculate a corresponding Fermi energy $\tilde{\lambda}$ by the condition

$$A = \int_{-\infty}^{\tilde{\lambda}} \tilde{g}(\epsilon) d\epsilon. \quad (2.105)$$

Since \tilde{g} is continuous, $\tilde{\lambda}$ is well defined by this implicit equation and is usually different from λ . For the smooth part of the energy we finally get

$$\tilde{E}_{sh} = \int_{-\infty}^{\tilde{\lambda}} \epsilon \tilde{g}(\epsilon) d\epsilon. \quad (2.106)$$

The total energy E of the system is therefore given by

$$E = E_{LDM} + E_{osc} = E_{LDM} + E_{sh} - \tilde{E}_{sh}. \quad (2.107)$$

As we have seen in Chapter 1, stable liquid drops are always spherical. Because of the additional term E_{osc} , it can happen that in some region of the periodic table the "Strutinski averaged energy" (2.107) has its minimum at finite values of the deformation. However, before we go on to the general discussion of the Strutinski method, let us show how one can define appropriately the average part of the level density.

2.9.3 Determination of the Average Level Density

In this section we have to deal with the problem of how to define in an appropriate mathematical way an average level density, if we are given a shell model density in an infinite three-dimensional well (the restriction to infinite potentials is not essential and the following considerations can be generalized for finite potentials [SI 75]).

$$g(\epsilon) = \sum_{i=1}^{\infty} \delta(\epsilon - \epsilon_i). \quad (2.108)$$

The difficulty comes from the fact that for a three-dimensional potential the level density increases with energy in a nonlinear way. This rise, however, does not go smoothly, but the levels are grouped in bunches roughly $\hbar\omega_0$ apart. If we imagine, for convenience of presentation, the level density smeared out with a Gaussian of width $\ll \hbar\omega_0$, then we get, schematically, the picture in Fig. 2.28. In which way, then, can the average part, and the oscillating part of such a density distribution, be separated?

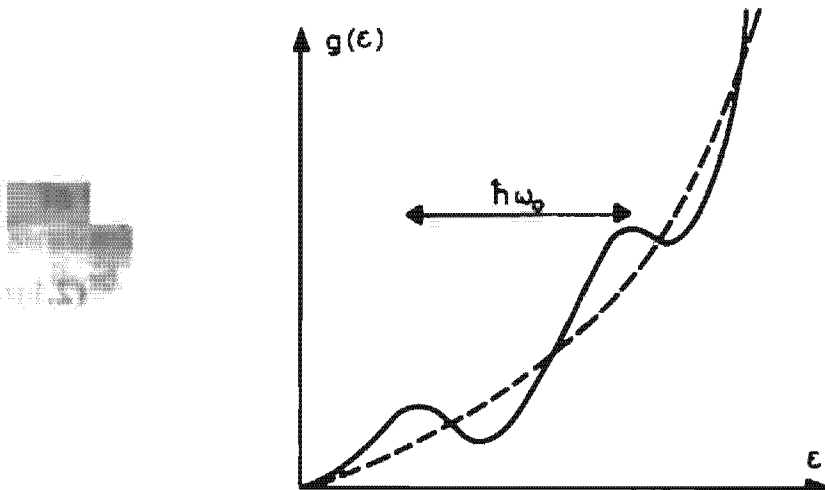


Figure 2.28. Schematic representation of the level density in an infinite three-dimensional potential.

As usual, we will think of the average density as given by a folding procedure

$$\tilde{g}(\epsilon) = \frac{1}{\gamma} \int_{-\infty}^{+\infty} g(\epsilon') f\left(\frac{\epsilon' - \epsilon}{\gamma}\right) d\epsilon', \quad (2.109)$$

and as a straightforward possibility we could think of f as being a Gaussian with $\gamma \approx \hbar\omega_0$. However, this is not sufficient, because an appropriate averaging procedure should leave the averaged level density $\tilde{g}(\epsilon)$ unchanged if averaged again with the same procedure, that is,

$$\tilde{g}(\epsilon) = \frac{1}{\gamma} \int_{-\infty}^{+\infty} \tilde{g}(\epsilon') f\left(\frac{\epsilon' - \epsilon}{\gamma}\right) d\epsilon'. \quad (2.110)$$

For f a Gaussian and g not a constant, condition (2.110) is clearly not fulfilled. In general, it will be difficult to do this for a given \tilde{g} exactly, and it is not our intention to fulfill Eq. (2.110) for an arbitrary \tilde{g} , since then f would have to be a δ -function. Equation (2.110) will only be required to be fulfilled for smooth functions \tilde{g} . Since the essential contributions to the integral (2.110) come from the vicinity of the point $\epsilon' = \epsilon$, we suppose that $\tilde{g}(\epsilon)$ can be represented locally by a polynomial of degree $2M$ (usually $2M = 2, 4$, or 6). The condition (2.110) can then be fulfilled if one constructs f in the following way:

$$f(x) = P(x)w(x), \quad (2.111)$$

where $P(x)$ is an even polynomial of degree $2M$ and $w(x)$ is a weighting function like a Gaussian or a Lorentzian, for example.

We can check that Eq. (2.110) is satisfied in this approximation by [AS 65]

$$P(x) = \sum_{n=0}^M Q_{2n}(x)Q_{2n}(0), \quad (2.112)$$

where the set of orthogonal polynomials $Q_m(x)$ is determined by the condition

$$\int_{-\infty}^{\infty} w(x) Q_m(x) Q_n(x) dx = \delta_{mn}. \quad (2.113)$$

If we take for w a Gaussian

$$w(x) = \frac{1}{\sqrt{\pi}} e^{-x^2}, \quad (2.114)$$

then $P(x)$ is given by a generalized Laguerre Polynomial [AS 65, Chap. 22]

$$P(x) = \sum_{n=0}^{M} (2^{2n} \cdot (2n)!)^{-1} \cdot H_{2n}(x) H_{2n}(0) = L_M^{1/2}(x^2), \quad (2.115)$$

where $H_{2n}(x)$ are the Hermite Polynomials. Thus we have explicitly constructed an averaging function f satisfying condition (2.110) for $\tilde{g}(\epsilon)$ which is locally approximated by a polynomial of degree $2M$. For practical applications, we give the coefficients of the polynomials $L_M^{1/2}(x^2)$ for $M=0, 2, 4, 6$ (Table 2.5):

$$L_M^{1/2}(x^2) = \sum_{n=0}^{M} a_{2n} x^{2n}. \quad (2.116)$$

Table 2.5 Coefficients of the four lowest Laguerre Polynomials

M	a_0	a_2	a_4	a_6
0	1	—	—	—
1	3/2	-1	—	—
2	15/8	-5/2	1/2	—
3	35/16	-35/8	7/4	-1/6

There remains now the question of how to determine the precise values of γ and M . In general, the results will depend on these parameters. Since we want to take out of $g(\epsilon)$ the oscillation with the approximate frequency $\hbar\omega_0$, our method will only be meaningful if we can find a certain interval of reasonable γ -values ($\gamma \approx 1 - 1.5 \hbar\omega_0$) and corresponding M -values within which this dependence is practically negligible. We can say, then, that our results are independent of the averaging procedure (as should of course be the case). More precisely, this means that the averaged energy must show a "plateau" as a function of γ for fixed M within which the "plateau condition" [BP 73]

$$\frac{\partial \tilde{E}_{ph}}{\partial \gamma} = 0 \quad (2.117)$$

is valid. Certainly for an arbitrary distribution of single-particle levels there will be no such plateau. But for the physically interesting distributions there always exists a certain bunching of levels with a frequency of roughly

$\hbar\omega_0$, so that we can expect that there is a plateau. (In practical calculations with finite potentials of the Woods-Saxon type, there are sometimes difficulties in finding a plateau. However, special methods have been developed to deal with such problems [BP 73, SI 75].)

In Chapter 13, we will show that there is a close connection between the Strutinski smoothing procedure and the semiclassical (Thomas-Fermi) method. This is not surprising, since it is known from the Thomas-Fermi theory of atoms that this method gives the relevant average quantities. We therefore urge the reader to consult Chapter 13 for a deeper understanding of this subject.

2.9.4 Strutinski's Shell Correction Energy

Having defined γ and the averaging function $f(x)$, we get the smooth level density from Eqs. (2.108) and (2.109).

$$\tilde{g}(\epsilon) = \sum_i \frac{1}{\gamma} f\left(\frac{\epsilon' - \epsilon_i}{\gamma}\right) \quad (2.118)$$

and the smooth part of the ground state energy in the shell model:

$$\tilde{E}_{sh} = \int_{-\infty}^{\tilde{\lambda}} \tilde{g}(\epsilon) \epsilon d\epsilon. \quad (2.119)$$

The chemical potential $\tilde{\lambda}$ is determined by the condition (2.105)

$$A = \sum_i \tilde{n}_i = \sum_i \int_{-\infty}^{t_i} f(x) dx; \quad t_i = \frac{\tilde{\lambda} - \epsilon_i}{\gamma}. \quad (2.120)$$

The \tilde{n}_i can be considered as generalized occupation numbers. Therefore, for fixed A , Eq. (2.120) allows the determination of $\tilde{\lambda}$ through an iteration procedure. It is convenient to rearrange Eq. (2.119) a little:

$$\tilde{E}_{sh} = \sum_i \epsilon_i \tilde{n}_i + F, \quad (2.121)$$

where F is then given by

$$F = \sum_i \int_{-\infty}^{\tilde{\lambda}} (\epsilon - \epsilon_i) \frac{1}{\gamma} f\left(\frac{\epsilon - \epsilon_i}{\gamma}\right) d\epsilon = \gamma \sum_i \int_{-\infty}^{t_i} x f(x) dx. \quad (2.122)$$

With this equation and Eq. (2.121), we get for the plateau condition (2.117)

$$\begin{aligned} \frac{\partial \tilde{E}_{sh}}{\partial \gamma} &= \frac{\partial}{\partial \gamma} \sum_i \epsilon_i \tilde{n}_i + \frac{1}{\gamma} F + \gamma \sum_i \frac{\partial t_i}{\partial \gamma} t_i f(t_i) \\ &= \frac{1}{\gamma} F + \tilde{\lambda} \frac{\partial}{\partial \gamma} \sum_i \tilde{n}_i \\ &= \frac{1}{\gamma} F + \tilde{\lambda} \frac{\partial}{\partial \gamma} A = \frac{1}{\gamma} F. \end{aligned} \quad (2.123)$$

The last equality follows because the particle number A is a constant. Therefore, we find that the plateau condition (2.117) is equivalent to the vanishing of F .

Introducing the shell model occupation numbers

$$\begin{aligned} n_i &= 0 \quad \text{for } \epsilon_i > \epsilon_F, \\ n_i &= 1 \quad \text{for } \epsilon_i < \epsilon_F, \end{aligned} \quad (2.124)$$

we find for the total shell correction:

$$E_{\text{osc}} = \sum_i \epsilon_i (n_i - \tilde{n}_i) = \sum_i \epsilon_i \delta n_i. \quad (2.125)$$

Figure 2.29 shows the quantities δn_i for the actual case of a deformed Woods-Saxon potential and a Gaussian average with $M=2$ and a width of $\gamma = 6.6$ MeV.

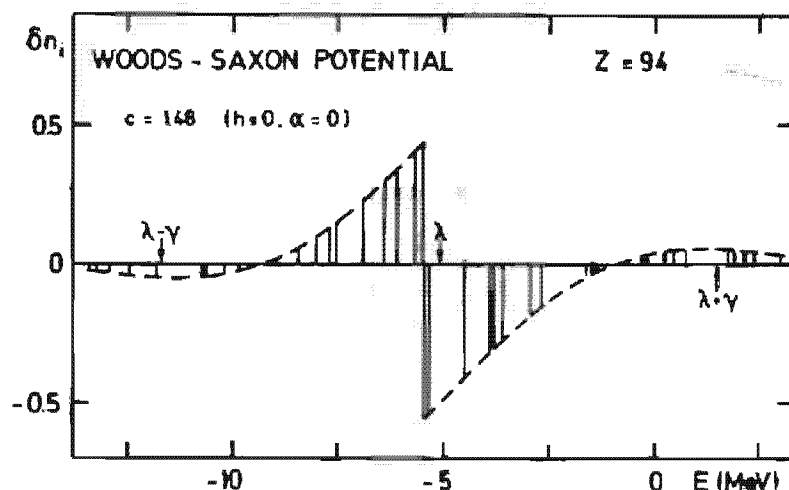


Figure 2.29. Deviations from the shell model occupation numbers resulting from a Strutinski averaging procedure for a Woods-Saxon potential. (From [BP 73].)

It is important to notice that the quantities \tilde{n}_i are not actually occupation probabilities, as they can in fact have negative values. On the other hand, the \tilde{n}_i behave like real occupation numbers and they indicate, for instance, how far we have to smear out the sharp Fermi surface of the shell model to get the smooth part of the ground state energy.

Having calculated the values δn_i , we are able to calculate the shell corrections to the density in configuration space [Di 71]:

$$\delta \rho_{\text{osc}}(\mathbf{r}, \mathbf{r}') = \sum_i^A \phi_i(\mathbf{r}) \phi_i^*(\mathbf{r}') \delta n_i. \quad (2.126)$$

This expression allows the calculation of averaged expectation values for all single-particle operators.

To give a definite example we will present the results of such a Strutinski calculation for the harmonic oscillator, which is naturally an over-idealized

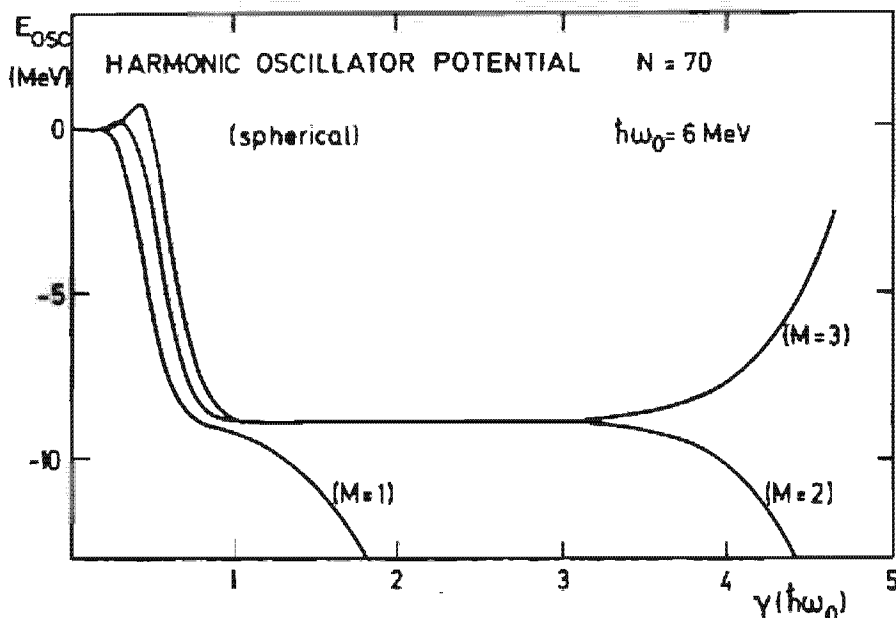


Figure 2.30. Shell correction energy for the harmonic oscillator as a function of γ and M . (From [BP 73].)

system, but which has the advantage of being rather instructive. In Fig. 2.30, the shell correction E_{osc} is shown calculated with a Gaussian weighting as a function of γ and M . We see that for $M > 2$ a well pronounced plateau develops at $E_{\text{sh}} = -8.91 \text{ MeV}$.

It can also be shown that a plateau develops at precisely the same energy if we had taken $w = 1/2 \cosh^2 x$ instead of a Gaussian for the weight function.

From the behavior of the values δn_i shown in Fig. 2.29 we conclude that only the shells in the neighborhood of the Fermi surface are important for the calculation of the shell correction. It is therefore usually sufficient to include three major shells in the averaging procedure. Only energies in the neighborhood of the Fermi surface are described well by the shell model, and it is exactly these which go into the shell corrected liquid drop energy. This is quite gratifying, since the phenomenological models are adjusted so as to reproduce the single-particle levels close to the Fermi level.

For the sake of completeness we have to mention that pairing correlations play an important role in heavy nuclei. They are usually treated in the BCS-model (see Chaps. 6 and 7). Since they are closely connected with the level density at the Fermi surface, one also observes oscillations in the pairing energy P . The liquid drop energy is adjusted to experimental masses. Therefore, it already contains the smooth part of the exact pairing energy, and we have to add only the oscillating part P_{osc} . It is obtained using the same philosophy as the difference between the pairing energy P_{BCS} in the BSC-model and its smooth part \tilde{P}_{BCS} . The total energy then has the form

$$E = E_{\text{LDM}} + E_{\text{sh}} - \tilde{E}_{\text{sh}} + P_{\text{BCS}} - \tilde{P}_{\text{BCS}}. \quad (2.127)$$

The smooth part of the pairing energy \tilde{P}_{BCS} can be calculated with similar methods as presented here. For details the reader is referred to the literature [BDJ 72]. Another way to obtain the average properties for pairing correlations would be the extension of the Thomas-Fermi method to superfluid systems (see Sec. 13.2.6)

2.9.5 Shell Corrections and the Hartree-Fock Method

As we will explain in Chapter 5, there exists a theory which allows one to calculate the shell model potential microscopically. This theory is the Hartree-Fock method and its generalizations [HFB; see Chapter 7]. Modern calculations of this type give quite good and detailed agreement of the binding energies over the whole mass region, indicating that in those calculations the bulk properties are also well described. Nevertheless, one can still try to separate the smooth part and the oscillating part of the quantities calculated in this theory. The smooth part should correspond exactly to the liquid drop results, and it has been shown that this is in fact the case [BQ 75a, b]. As an example, Fig. 2.31 shows the deformation energy of the nucleus ^{168}Yb as a function of the quadrupole moment Q_2 .

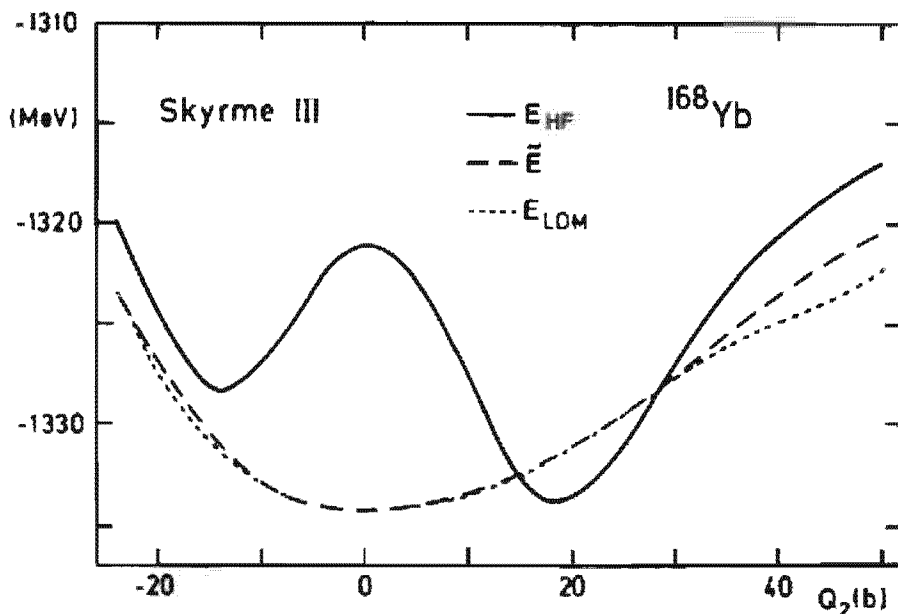


Figure 2.31. Deformation energies of the nucleus ^{168}Yb calculated with the force Skyrme III (see Chap. 4). E_{HF} is the exact HF-energy, \tilde{E} the corresponding averaged part [Eq. (2.132)] and E_{LDM} is the liquid drop energy on the same path in the deformation coordinates Q_2 (quadrupole moment) and Q_4 (hexadecupole moment). (From [BQ 75b].)

To show that the Strutinski procedure based on a shell model potential gives, to a high degree of accuracy, the same results as a complicated Hartree-Fock

calculation, we now have only to prove that the oscillating part of the ground state energy in the Hartree-Fock theory is actually the same as the one derived in Eq. (2.125) from a shell model calculation. This we will do in the following, and we advise the reader who is not familiar with Hartree-Fock theory to return to the following somewhat subtle considerations after having progressed to the microscopic theories and, in particular, after having studied Chapter 5.

The Hartree-Fock ground state energy is, in a representation-independent way, given by* [see Eq. (5.28)]:

$$E_0^{\text{HF}} = \text{Tr}(\iota\rho) + \frac{1}{2}\text{Tr}_1\text{Tr}_1\rho\bar{\epsilon}\rho. \quad (2.128)$$

where ρ is the self-consistent single-particle density and $H = \iota + V$ is the total Hamiltonian of the system with ι and V the kinetic and potential energies, respectively. The Hartree-Fock part \hbar^{HF} of the Hamiltonian is a one-particle operator, and is defined by

$$\hbar^{\text{HF}} = \iota + \text{Tr}_1\bar{\epsilon}\rho. \quad (2.129)$$

Now we can divide the density of ρ in the sense of Strutinski (Sec. 2.9.3) into a smooth and an oscillating part:

$$\rho = \tilde{\rho} + \delta\rho, \quad (2.130)$$

where $\delta\rho$ is defined by analogy with Eq. (2.126) for HF-single-particle energies.

Inserting this into Eq. (2.128) and collecting terms of different order in $\delta\rho$, we get

$$E_0^{\text{HF}} = \tilde{E} + \text{Tr} \tilde{\hbar}^{\text{HF}} \delta\rho + O(\delta\rho^2), \quad (2.131)$$

where

$$\tilde{E} = \text{Tr}(\iota\tilde{\rho}) + \frac{1}{2}\text{Tr}_1\text{Tr}_1\tilde{\rho}\bar{\epsilon}\tilde{\rho} \quad (2.132)$$

and

$$\tilde{\hbar}^{\text{HF}} = \iota + \text{Tr}_1\bar{\epsilon}\tilde{\rho}. \quad (2.133)$$

Therefore, if the phenomenological shell model potential gives the same single-particle spectrum in the vicinity of the Fermi surface as the averaged Hartree-Fock potential, $\tilde{\hbar}^{\text{HF}}$, then the definitions of the oscillating part of the ground state energy, as given by the second term on the r.h.s. of Eq. (2.131) and by Eq. (2.125), agree if second-order terms in $\delta\rho$ can be neglected. These have been checked numerically and indeed turn out to be small corrections [BKS 72, BDJ 72, BQ 75a].

If the phenomenological single-particle spectrum does not give exactly the same single-particle spectrum as the operator $\tilde{\hbar}^{\text{HF}}$, the above statement nevertheless stays true, because small deviations again give contributions of second order in Eq. (2.131). Equation (2.131) is also called the *Strutinski energy theorem* [St 68, St 74]. It states that all shell effects of first order in $\delta\rho$ are taken into account by summing up single-particle energies of an averaged single-particle Hamiltonian.

In this sense, the Strutinski procedure provides a method which reproduces microscopic results in an optimal way using phenomenological models. Needless to say, the latter are much easier to handle for realistic calculations.

* The definition of Tr_1 is given in Eq. (E.19).

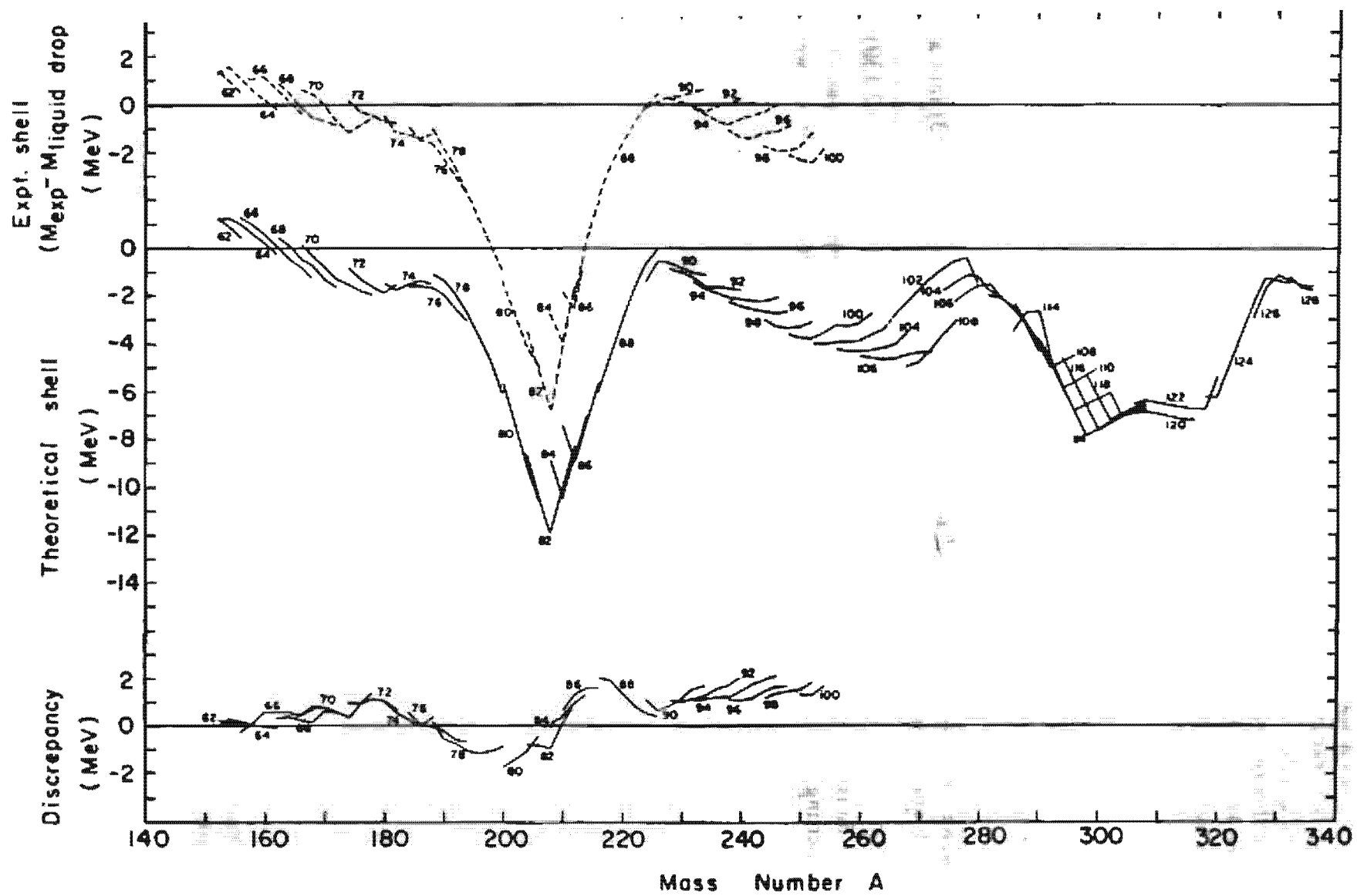


Figure 2.32. Comparison of theoretical mass corrections with experimental values. (From [NTT 69].)

2.9.6 Some Applications

The combination of the shell model with the liquid drop model as provided by Strutinski's theory has, for instance, been applied to the calculation of nuclear masses [NTT 69]. Figure 2.32 shows the theoretical mass corrections to the liquid drop model and compares them with the experimental data. The overall agreement is very good; the oscillating structure in the vicinity of the double magic nucleus ^{208}Pb is especially well reproduced. However, we must realize that these shell corrections were calculated with Nilsson's single-particle energies, which do not reproduce the experimental single-particle level scheme of ^{208}Pb (see Fig. 2.15) very well. In fact, the shell correction calculated with these experimental levels is 5 MeV off in ^{208}Pb . For a discussion of this discrepancy, see [BDJ 72].

Another application of the Strutinski method is the calculation of energy versus deformation curves. As we mentioned briefly at the end of Section 2.8, the calculation of the energy as a function of not only the quadrupole deformations but also octupole, hexadecupole, and higher deformations gives rise to multidimensional energy surfaces. As in the shell model, we find deformed minima in the rare earth nuclei as well as in the actinides, and sometimes second minima for very large deformations (fission isomers). It turns out that the ground state minima are reproduced roughly at the same deformations as in the pure Nilsson model. However, at large deformations, the deformation surfaces look different (for a detailed investigation, see [BDJ 72]). In these surfaces one looks for the path which goes from the equilibrium deformation past the lowest barrier and out to the region of deformation in which fission occurs. The knowledge of this path and its actual shape for a nucleus then allows an estimate of its fission lifetimes [ADD 70, JNS 70, BFN 72, Ni 72, BDJ 72, Pa 73, LP 73, MN 73, RNS 78]. In particular the stabilities of superheavy nuclei have also been investigated in this way (see [Ni 72, NN 74, BN 77] and references given there).

CHAPTER 3

Rotation and Single-Particle Motion

3.1 Introduction

The experimental level schemes of nuclei show an enormous complexity. On the way to understanding at least the basic features of their structure, we have introduced in the first part of this book two rather contrasting models: On the one hand the liquid drop model describes collective phenomena, such as vibrations and rotations, where many nucleons are involved. On the other hand the shell model treats the individual nucleons as independent particles and provides an understanding of single-particle excitations. However, these two models are only limiting cases that are never realized exactly in nature. We always have some deviations and we usually find all kinds of transitions between these extreme models.

For a deeper understanding of the underlying structures, we have to solve, in principle, the nuclear many-body problem and investigate in which limits solutions are provided corresponding to the above simple phenomenological pictures, and in which cases new models must be introduced to obtain a simple description. In the following chapters of this book, we will treat such microscopic methods in much detail, and will reproduce many of the results of the phenomenological models. Although such theories are extremely useful for an understanding of principal questions, they usually involve a terrible amount of numerical effort and are not very useful for a fast and qualitative interpretation of experimental data.

Therefore, it seems to be worthwhile going further on the phenomenological path in this chapter and trying to describe more complicated spectra by a combination of the collective model and the single-particle model. In the last chapter, we saw that such a combination is very useful in describing bulk properties such as nuclear binding energies and deformations. In that case, we had to deal with fluctuations of the level density, and we did not have to take into account the individual degrees of freedom in detail. Now we want to describe individual spectra. For this we have to again try a combination of the single-particle and collective models. We can, for instance, couple one or a few particles to a collective rotor or vibrator. This so-called "*unified model*" was introduced by Bohr and Mottelson [Bo 52, BM 53], and has been described in great detail in many textbooks (see, for instance, [Da 68, EG 70, Ro 70, SF 74, or BM 75]). In the case of collective vibrations, we will deduce the corresponding Hamiltonian and discuss the model of a particle coupled to a vibrator in Chapter 9. In the case of rotations, such a derivation from first principles has been missing till now. Methods have been developed to describe rotations microscopically (see Chap. 11), but they turn out to be extremely complicated. Only in the limit of strong deformations is it possible to deduce a simple rotational model, the cranking model.

In the last few years considerable experimental effort has been made to investigate rotations, and a great variety of new phenomena has been observed. Since these phenomena can be understood to a large extent by the interplay between single-particle motion and collective rotational motion, we think it is necessary to introduce in this chapter two theoretical but phenomenological models which deal with these effects.

In Section 3.2 we give a general survey of the features one expects in rotating nuclei. In Section 3.3 we discuss the rotational part of the unified model, the so-called particle-plus-rotor model (PRM), and in Section 3.4 we present the microscopic cranking model.

We want to emphasize, however, that we do not give a complete description of nuclear rotation in this chapter. The residual interactions in the form of pairing correlations play an important role in this context. They will be treated in Chapter 7.

3.2 General Survey

3.2.1 Experimental Observation of High Spin States

New experimental techniques, namely, heavy ion fusion reactions [MG 63, SLD 65], Coulomb excitation with heavy projectiles [HZ 53, AW 66, 74, WCL 76], and pion capture reactions [EAD 75] have made it possible to excite nuclear states with angular momenta large enough to generate major modifications in the nuclear structure (for a review, see [JS 73, St 76, LR 78]).

The most important such reactions are of the ($H1, xn$) type, where one bombards the target with heavy ions (α , Ne, Ar, etc.) carrying a large amount of orbital angular momentum. After fusion, the combined system evaporates some neutrons and ends up in highly excited states with very large spin (depending on the projectile and the incoming energy up to $\sim 100 \text{ h}$). This highly excited final nucleus then de-excites in a cascade of γ -radiation. The fastest transitions are *statistical E1-transitions*. They carry away much energy, but only a few units of angular momentum. In a plot of the energy versus the angular momentum (Fig. 3.1), these statistical cascades correspond to nearly vertical lines. They end up at the so-called *yrast line*, * the line which connects the levels of lowest energy to each angular momentum (or the levels with highest angular momentum at a given energy). The rest of the cascade has to follow this line. For deformed nuclei these are *collective E2-transitions* ($\Delta I = 2$), which finally go over into the well-known ground state rotational band (see Sec. 1.5).

Until now, only the last part of these cascades could be resolved into discrete lines (see Fig. 3.5). The highest angular momenta observed in this way lie between 30 and 40 h . The rest of the cascade is measured as a γ -continuum, and one can draw only indirect conclusions from these data [GG 67, BSC 75, SBC 76, Di 76, HLM 78, ABH 78, WF 78b]. There are, however, indications that collective transitions along lines parallel to the yrast line (see Fig. 3.1) play an important role, and that there is a

* The Swedish word *yrast* means "fastest rotating" [Gr 67]. One also uses the name *yrare* for the level with the second lowest energy at each I -value.

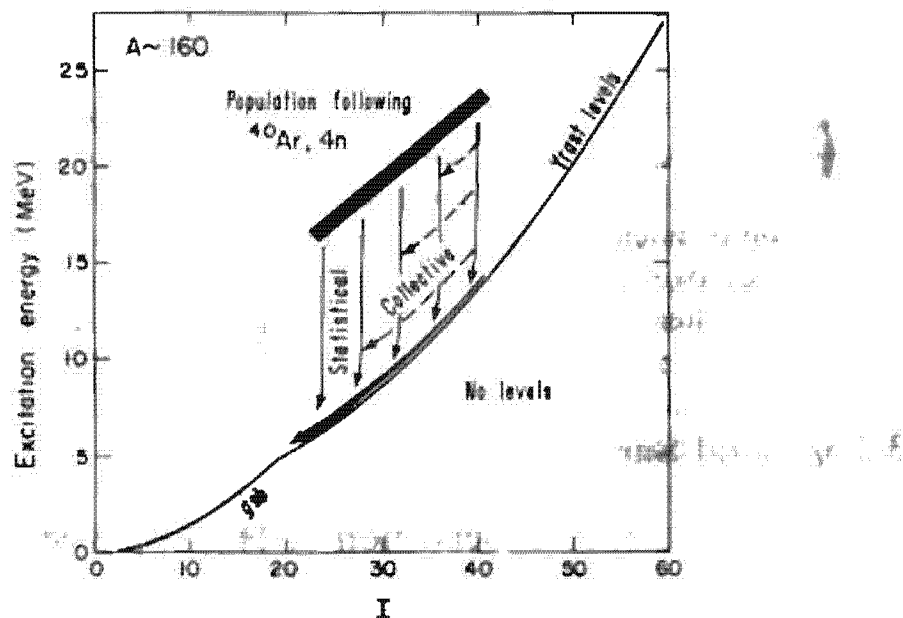


Figure 3.1. Excitation energy as a function of angular momentum I for the reaction ($^{40}\text{Ar}, 4n$). After the evaporation of four neutrons, the nucleus decays by a γ -cascade of statistical $E1$ - and collective $E2$ -transitions down to the *yrast line*, and then to the ground state by a series of $E2$ -transitions along this line. The *yrast band* shows an increasing intensity, because it collects all the statistical transitions ("side feeding"). (From [SBD 77].)

competition between collective and statistical effects in the region of a few MeV above the yrast line [SBD 77].

3.2.2 The Structure of the Yrast Line

In Section 1.7 we saw that a *classical liquid drop* [CPS 74] rotates at low angular frequencies around the symmetry axis of its oblate shape (Hiskes regime, Fig. 3.2a). Only for very high angular velocities does it undergo a phase transition to the Beringer-Knox regime, where it has a triaxial, but nearly prolate, shape and the rotational axis is perpendicular to the approximate symmetry axis (Fig. 3.2b). For still higher frequencies it finally fissions (Fig. 3.2c).

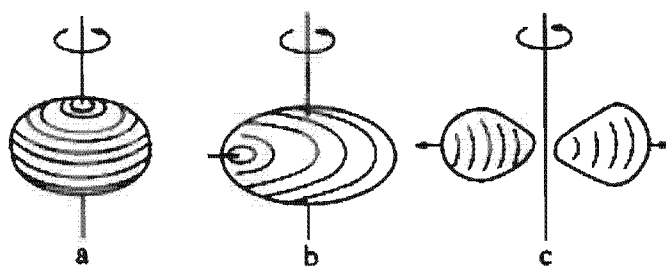


Figure 3.2. The behavior of a classical liquid drop for increasing angular velocity.

The *real nucleus*, however, is a quantum mechanical system. It shows shell effects (see Chap. 2.9), which cause stable deformations already in the ground state for some regions of the periodic table. The yrast line corresponds to the lowest energy for each angular momentum; all the excitation energy of several tens of MeV with respect to the ground state is rotational energy and used to generate angular momentum. Consequently, the level density along this line is low, much lower than the level density of the $I = 0$ states at the corresponding energy. It resembles that of the ground state, though we will see that there are characteristic deviations from it. Since the nucleus is cold in the yrast region, we can expect a high degree of order. Shell effects play an important role.

The prolate deformations caused by the shell effects are of the same order of magnitude as the oblate deformations of a classical drop at high angular velocities (see Sec. 1.7). We therefore expect a delicate interplay between macroscopic centrifugal effects and microscopic shell structure when we study the nuclear shapes as a function of the angular momentum.

Let us first study the case of well-deformed heavy nuclei (for instance, in the rare earth region). In the ground state they show a prolate axial symmetric quadrupole deformation caused by shell effects. The levels in the corresponding deformed potential are occupied pairwise by nucleons with the opposite single-particle angular momentum ($\pm \Omega$). We will see in Chapter 6 that the two nucleons in such a pair do not move independently, as was assumed in the last chapter, but are coupled by a pairing force to the so-called Cooper pairs with spin zero; that is, these deformed nuclei

show a *superfluid behavior* and their ground state energy is lowered by a few MeV.

With increasing angular momentum, we can distinguish several regimes where the yrast states show quite a different structure [BM 74]:

- (a) For low angular momenta $I = 0, 2, 4, \dots$, the yrast line follows the *ground state rotational band*, as discussed in Section 1.5. The rotation is collective, that is, it has to be perpendicular to the symmetry axis (see Fig. 3.3a, where we have indicated the coupled pairs of nucleons oriented along the symmetry axis).

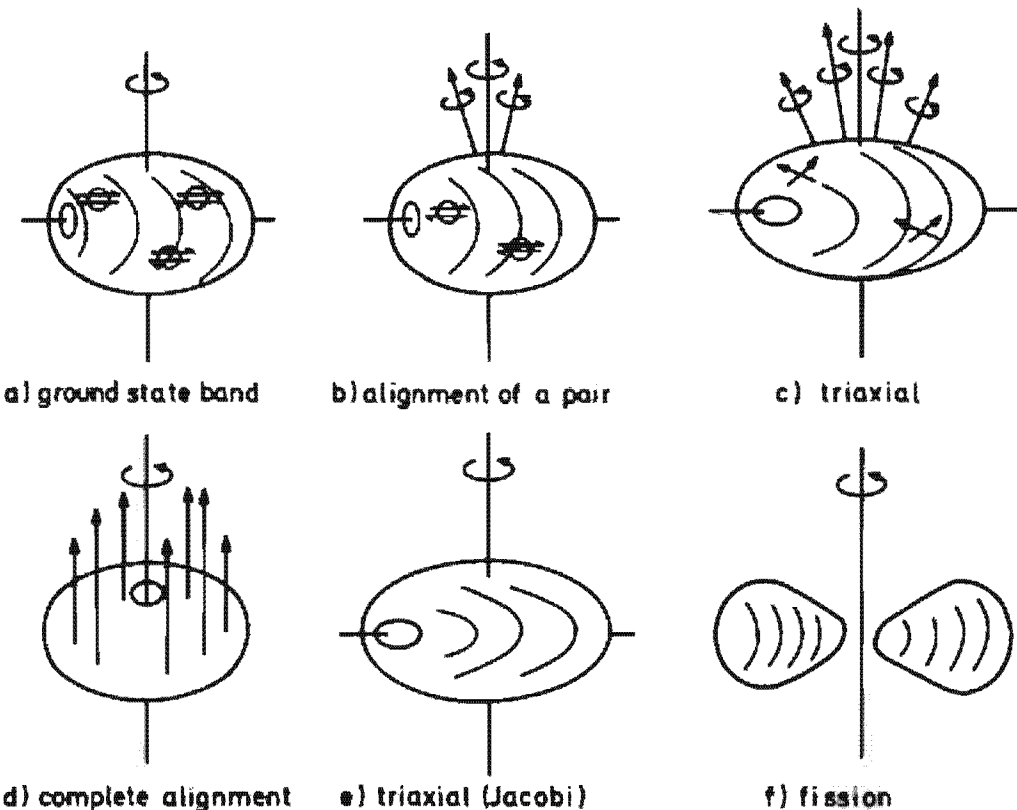


Figure 3.3. Possible structures along the yrast line of a deformed nucleus.

The nucleus feels a slowly rotating deformed potential (for a more detailed discussion, see Sec. 3.4). The Coriolis forces act on both spins of a pair with opposite angular momenta $\pm \Omega$ in opposite directions and try to align them parallel to the rotational axis, that is, they try to break the Cooper pairs [*Coriolis anti-pairing (CAP) effect*]. However, for low angular momenta the Coriolis forces are weak and unable to break pairs: The nucleus rotates more or less with the same structure as the ground state.

We have to emphasize, however, that in a microscopic picture the total angular momentum has to be generated by the angular momenta of single nucleons. In a collective rotation this is achieved by aligning all the particles a little bit in the direction of the rotational axis. For each pair this effect is very small; the spins of the pairs are still oriented nearly anti-parallel along the symmetry axis of the potential. By summing up all the small contributions we obtain the total angular momentum $I = 2, 4, \dots$.

(b) Going to higher and higher angular momenta, the Coriolis force, increases more and more and at a certain angular momentum it will be able to break pairs. Therefore, at some critical angular momentum I_c , we expect that all pairs are broken. The pairing correlations break down completely and a *phase transition* from the superfluid phase to the normal phase is observed. This effect was predicted by Mottelson and Valatin in 1960 [MV 60]. More detailed investigations, however, have shown that the Coriolis force is proportional to the size of the single-particle angular momentum j of the nucleon under consideration. We have seen in Section 2.8 that the nucleons in the vicinity of the Fermi surface belong to subshells with rather different j -values, and we expect those nucleons with large j -values to align first along the rotational axis. These are usually the levels with high spin and opposite parity, shifted downwards by the spin orbit term, as for instance the $i_{13/2}$ shell for neutrons in the rare earth region (Stephens-Simon effect [SS 72a]).

In the second regime of the yrast line (Fig. 3.3b), we therefore expect *alignment processes* of one or the other broken pairs, whereas the rest of the nucleus stays more or less unchanged. The yrast band can then no longer be identified with the ground state band, but rather with a band of two aligning particles sitting on the rotating core. Two $i_{13/2}$ particles can contribute 12 units of angular momentum to the rotation. Such an alignment is therefore connected with a rapid increase of the angular momentum I as a function of the collective angular velocity and leads to a series of anomalies in the spectra [JRS 71, JRH 72], for example, the "back-bending phenomenon" (see below).

(c) Each alignment process is connected with a certain change in the collective properties by its influence on the mean field: Broken pairs no longer contribute to the pairing correlations; because of the blocking effect (see Sec. 6.3.4.) these correlations will disappear completely after a few alignments. Particles aligned to the rotational axis have an oblate density distribution, with the rotational axis as the symmetry axis. We therefore get triaxial admixtures to the prolate density distribution of the core.

In a third regime (Fig. 3.3c) which should correspond roughly to angular momenta $30 \lesssim I \lesssim 50$, we expect the Coriolis and centrifugal forces to produce effects comparable in strength to the shell structure effects, namely, changes in the shapes to *triaxial deformations*. Such a system without a symmetry axis shows more collective states than the axial symmetric rotor (see Sec. 1.5.3): We expect a sequence of rotational states parallel to the yrast line corresponding to a *wobbling motion*.

(d) If an essential part of the nucleons are aligned parallel to the rotational axis, we finally expect an *axially symmetric oblate shape*.

The nuclear wave function is symmetric with respect to rotations around this axis. The rotation is no longer collective. Instead, the total angular momentum is made up by reoccupation of distinct particles in the deformed well.

This kind of motion is called “*single-particle*” rotation. The energy of the states along the yrast line in this region is determined by the single-particle energies in the rotating oblate well. The energy differences between adjacent states vary statistically. Only on the average do they follow an $J \cdot (J + 1)$ law with the moment of inertia of a rigid rotor (see Sec. 3.4.6.). The transition from one state to the next corresponds to a reoccupation, and the matrix elements should adopt single-particle values, that is, the transition probability should be drastically reduced.

Because of the statistical nature of the levels in that region of the yrast line, one also expects long lived *high spin isomeric states*, so-called *yrast traps* [BM 74] which could eventually produce a delayed decay such that we could observe the whole yrast cascade of discrete lines without the background of all statistical transitions.

- (e) For very large angular momenta we finally expect only the macroscopic properties to be essential, that is, the nucleus should again undergo a transition from oblate to triaxial and prolate shapes before it fissions (Fig. 3.3e, f).

So far, only discrete levels in the regimes (a) and (b) have been observed; the rest of these considerations is to a large extent speculation. We will see in Sec. 3.4.5 the kind of models one has used to obtain theoretical predictions. In fact, in the calculations one has found all the different regimes discussed above.

It seems to be possible, however, that many nuclei do not pass through all these stages. In particular, weakly deformed or spherical nuclei adopt from the beginning the regime (d), namely, a rotation of an oblate shape around the symmetry axis before going triaxial and fissioning. On the other hand, in many well-deformed nuclei the change in deformation produced by the alignment processes is not strong enough to compensate the shell effect of a prolate deformation. They only become triaxial (Fig. 3.3c, d), not oblate, before fissioning. Experimentally, one has observed longliving high spin isomers (*yrast traps*) only for weakly deformed nuclei (see Sec. 3.4.6). This seems to be in agreement with theoretical calculations.

Besides the yrast band, one has observed many other rotational bands in the low and *medium spin region*. They are based on more complex configurations, such as quasi-particle excitations or vibrational states.

Depending on the size of the j shell orbitals, which are involved in such configurations, one can imagine a large variety of alignment processes. For example, in an odd mass nucleus the alignment of the odd neutron in the $i_{13/2}$ shell, which leads to so-called *decoupled bands*. Another example is the rotational band in an odd-odd nucleus, where only the neutron in the $i_{13/2}$

shell aligns, whereas the proton stays oriented along the symmetry axis. Such a band has a *semidecoupled* structure [NVR 75].

The particle-plus-rotor model discussed in Section 3.3 provides a phenomenological method to describe such processes. In that section we will come back to some examples of this type in more detail.

3.2.3 Phenomenological Classification of the Yrast Band

Over the years some phenomenological models have been introduced to characterize the properties of rotational bands. In the low spin region (Fig. 3.3a), the spectra often follow exactly the $I \cdot (I+1)$ law, but for higher I -values there occur deviations to a greater or lesser extent*. In order to describe the deviations from the ideal rotational spectrum, one often applies the following parametrization:

$$E(I) = A \cdot I \cdot (I+1) + B \cdot (I(I+1))^2 + C \cdot (I(I+1))^3 + \dots \quad (3.1)$$

It turns out that in many cases the convergence of this expansion is rather poor and an expansion in the *angular frequency* ω is more appropriate.

In principle, ω is not a measurable quantity. We can define it, however, semiclassically as

$$\omega = \frac{dE}{dJ}, \quad \text{with} \quad J = \sqrt{I(I+1)}. \quad (3.2)$$

Replacing the differential quotient by a quotient of finite differences,[†] we obtain a definition of an "experimental" value for the *angular velocity*[‡]

$$\omega_{\text{exp}} \simeq \left. \frac{\Delta E}{\Delta \sqrt{I(I+1)}} \right|_{I, I-2} \simeq \frac{E(I) - E(I-2)}{\sqrt{I(I+1)} - \sqrt{(I-2)(I-1)}}. \quad (3.3)$$

The *moment of inertia* is defined by

$$J = \frac{I}{\omega} = \frac{1}{2} \left(\frac{dE}{dJ^2} \right)^{-1} \simeq \frac{2I-1}{\Delta E_{I, I-2}}. \quad (3.4)$$

With these definitions, we can calculate values of ω and J for each level of the yrast band.

Harris [Ha 65a] proposed the following parametrization of the spectrum:

$$E(I) = \alpha \omega^2 + \beta \omega^4 + \gamma \omega^6 + \dots \quad (3.5)$$

Odd powers in ω do not occur, since E cannot change by reversing the angular velocity. For ω as a function of I we can either choose the experimental value (3.3) or avoid the ambiguity of its definition by using a similar expansion of J . From

$$\frac{dE}{d\omega} = \frac{dE}{dJ} \frac{dJ}{d\omega} = \omega \frac{dJ}{d\omega} \quad (3.6)$$

we obtain

$$J(I) = \sqrt{I(I+1)} = 2\alpha\omega + \frac{4}{3}\beta\omega^3 + \frac{6}{5}\gamma\omega^5 + \dots$$

* For a compilation of such data, see [SHJ 73, SSM 75].

[†]This replacement is not unique, however, and some groups use different prescriptions (see [JS 73, So 73, LR 78]).

[‡]Within this chapter we always use the units $\hbar = 1$.

Of course, this expansion is valid only as long as J is not a multivalued function of ω , that is, it is of no use in the backbending region (see Sec. 3.2.4.).

Another model which is widely used for the classification of rotational and even transitional nuclei is the *variable moment of inertia* (VMI) model [MSB 69, SDG 76]. The moment of inertia \mathfrak{J} is considered as a variable on which the intrinsic energy V depends:

$$E(I, \mathfrak{J}) = \frac{1}{2\mathfrak{J}} I(I+1) + V(\mathfrak{J}). \quad (3.7)$$

According to the variation principle (discussed in Sec. 5.2), the total energy E has to be minimized for a fixed value of I with respect to \mathfrak{J} . This determines the functional dependence $\mathfrak{J}(I)$. Assuming we know $V(\mathfrak{J})$, $\mathfrak{J}(I)$ is implicitly given by

$$\left. \frac{dE}{d\mathfrak{J}} \right|_I = -\frac{1}{\mathfrak{J}} \frac{I(I+1)}{2\mathfrak{J}} + \frac{dV}{d\mathfrak{J}} = 0.$$

Usually one expands on $V = \frac{1}{2} C(\mathfrak{J} - \mathfrak{J}_0)^2$, where \mathfrak{J}_0 is the value of \mathfrak{J} at $I=0$. The coefficients C and \mathfrak{J}_0 are adjusted to the experimental spectrum $E(I)$. With the identification $J = \omega \cdot \mathfrak{J}$ this corresponds to the Harris model to order ω^4 , but the ansatz (3.7) is certainly more general [DB 73, SDG 76].

3.2.4 The Backbending Phenomenon

In the region between 10 and 20 units of angular momentum, an anomaly is observed in the yrast band of many nuclei. It can be most easily demonstrated if one plots the moment of inertia \mathfrak{J} as a function of ω^2 . In lowest order in the VMI model ($\mathfrak{J} = \mathfrak{J}_0 + b\omega^2 + \dots$) this should give a straight line. The deviation from a constant is then a measure of the validity of the $I \cdot (I+1)$ law. Figure 3.4 gives two examples for such curves, measured by the Jülich group [LR 78].

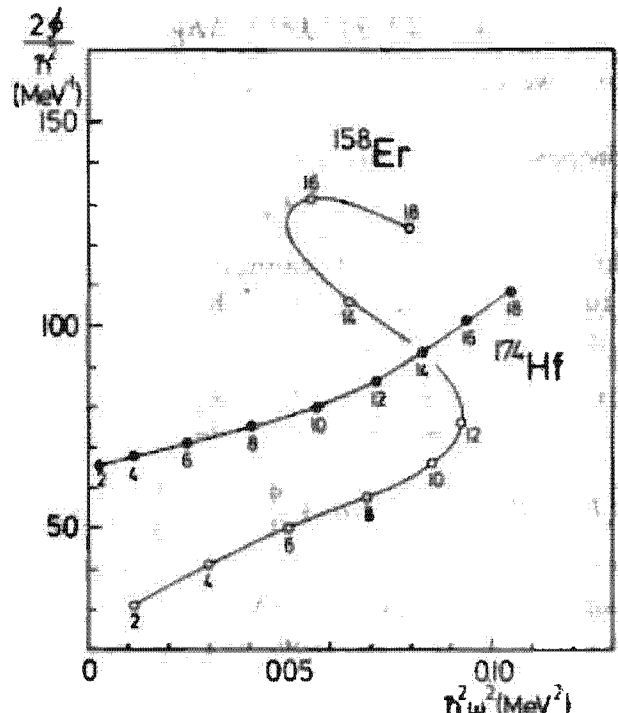


Figure 3.4. Moment of inertia \mathfrak{J} as a function of the rotational frequency squared for ^{158}Er and ^{174}Hf .

For low spin values one indeed finds straight lines. In the nucleus ^{174}Hf the deviations are, in fact, smooth. In ^{158}Er , however, a very steep increase occurs for certain I values, the curve even bending backwards, ("backbending" phenomenon [JRH 72]). This means experimentally that the transition energy $\Delta E_{I, I-2}$, which should increase linearly with I for the constant rotor as

$$\Delta E_{I, I-2} = \frac{1}{2g}(4I - 2), \quad (3.8)$$

does not increase, but decreases for certain I values. Figure 3.5 shows the experimental data that correspond to Figure 3.4.

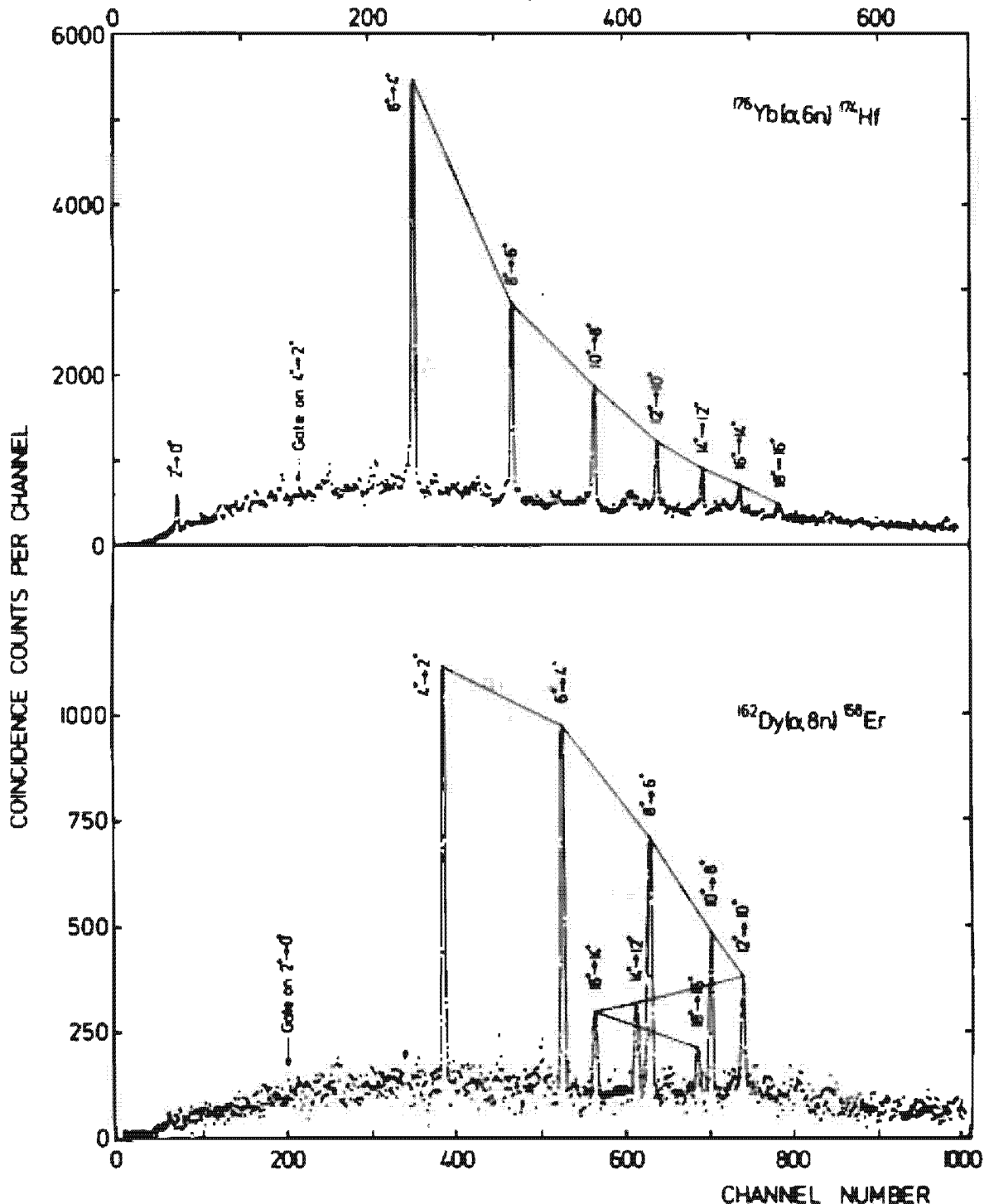


Figure 3.5. The reactions $^{176}\text{Yb}(\alpha, 6n)^{174}\text{Hf}$ and $^{162}\text{Dy}(\alpha, 8n)^{158}\text{Er}$. The last reaction shows the anomaly called backbending in the I region $10^+ - 14^+$. This is revealed in combining dependent peak heights by straight lines. (From [LP 78].)

Such a phenomenon can easily be reproduced as an effect due to the crossing of two bands (in some cases one has even observed the second band experimentally, see Fig. 7.6 and [KSM 78]). To see this, let us assume that the two bands have different moments of inertia (Fig. 3.6) corresponding to two parabolas in an E versus I plot. If $\mathfrak{g}_2 > \mathfrak{g}_1$, the bands cross in a certain region of I . Because of the residual interaction, such a crossing does not take place (the no-crossing rule; see Sec. 2.8.4), and we can get a region in which the second derivative is negative:

$$0 > \frac{d^2E}{dI^2} = \frac{d\omega}{dJ}. \quad (3.9)$$

This means we have an increasing J with decreasing ω , while at the same time the properties of the bands are exchanged. In fact, it is easy to fit such backbending curves by a band mixing calculation with few parameters, one of which is the interaction V between the bands. For small values of V , one obtains a sudden transition which produces backbending, whereas for large values of V the transition region is very broad and no backbending occurs [MR 72, GG 74b].

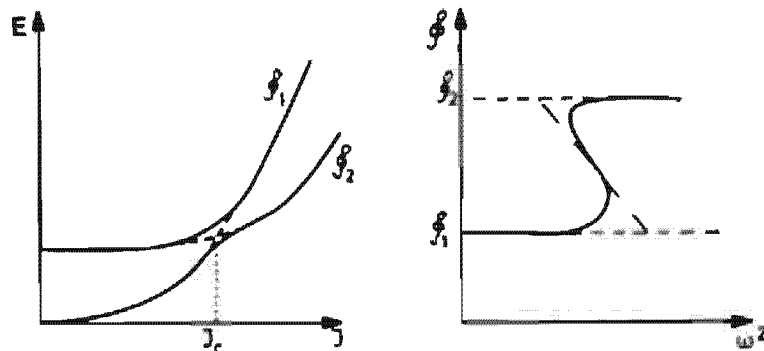


Figure 3.6. Schematic picture of two intersecting bands with different moments of inertia \mathfrak{g}_1 and \mathfrak{g}_2 , and the corresponding backbending plot. (From [LR 78].)

On the other hand, it is also clear that the strange backbending behavior in the plot of the moment of inertia \mathfrak{g} against ω^2 has its origin in the fact that we follow the yrast line in the critical region, that is, we switch over to the crossing band with a different internal structure. If we would stay in the ground state band, which is no longer the yrast band for the large I -values, we would obtain a very smooth behavior for the ω -dependence of the moment of inertia (dashed-line in Fig. 3.6). The reason that one usually follows the yrast band is that these levels are experimentally the most easily accessible.

In all of these considerations, one should, however, keep in mind that these kinds of phenomenological descriptions only give a classification of the spectra and do not say anything about their physical origin. In the case of backbending there is, for instance, the question concerning the nature of the second band. Three types of theoretical interpretations have been given:

- (i) In the second band the nucleus has a different deformation, for

instance, a triaxial one. This means that backbending is caused by a sudden change of deformation [Th 73, SV 73].

- (ii) The second band is not superfluid, as in the ground state band. This would interpret backbending as a phase transition from a superfluid to a normal-fluid state (Mottelson–Valatin effect [MV 60]).
- (iii) The second band is a two quasi-particle band of particles which are rotationally aligned along the axis of rotation (see Sec. 3.3). Then backbending would correspond to a sudden alignment of a pair of nucleons (as proposed by Stephens and Simon [SS 72a]).

The general result of theoretical investigations, which include all these degrees of freedom (see Sec. 7.7), is that for the well deformed nuclei (the classical rotors) the reduction of the pairing correlations is only responsible for the slow change of the moment of inertia at low spin values, but that sudden effects such as backbending are due to alignment of a single high j pair of nucleons. There is also a large number of experimental indications [GSD 73, RSS 74, WBB 75, NLM 76, St 76] for this interpretation of the backbending phenomenon.

In the rare earth nuclei, the $i_{13/2}$ neutrons play an essential role. There is, however, experimental evidence for a second irregularity at spins of $\sim 26\text{--}30 \ h$ [LAD 77, BBB 79a] a so-called *second backbending*, which has been interpreted as the alignment of an $h_{11/2}$ proton pair [FP 78]. Other high j -orbitals may play similar roles in different regions of the periodic table.

3.3 The Particle-plus-Rotor Model

To describe the interplay between the motion of particles and the collective rotation, Bohr and Mottelson [BM 53] proposed to take into account only a few so-called valence particles, which move more or less independently in the deformed well of the core, and to couple them to a collective rotor which stands for the rest of the particles. The division into core and valence particles is not always unique. It is, however, reasonable to use the unpaired nucleon in an odd mass nucleus as a valence nucleon on an even–even core. One also can attribute the particle and the hole of a particle–hole excitation to the valence particles. More generally, one divides the Hamiltonian into two parts: an intrinsic part H_{intr} , which describes microscopically a valence particle or a whole subgroup of particles near the Fermi level; and a phenomenological part H_{coll} which describes the inert core:

$$H = H_{\text{intr}} + H_{\text{coll}}. \quad (3.10)$$

The *intrinsic part* has the form

$$H_{\text{intr}} = \sum_k \epsilon_k a_k^+ a_k + \frac{1}{4} \sum_{klmn} \bar{v}_{klmn} a_k^+ a_l^+ a_n a_m, \quad (3.11)$$

where ϵ_k are single-particle energies in the deformed potential (e.g., Nilsson energies) and \tilde{v} is the interaction between the valence particles which is, or can be, neglected in many cases.*

The *collective part* describes the rotations of the inert core:

$$H_{\text{coll}} = \frac{R_1^2}{2g_1} + \frac{R_2^2}{2g_2} + \frac{R_3^2}{2g_3}, \quad (3.12)$$

where the R_i are the body-fixed components of the collective angular momentum of the core. Together with the angular momentum of the valence particles J (which is the sum over the single-particle angular momenta) it forms the total angular momentum I (see Appendix A):

$$I = R + J. \quad (3.13)$$

Eliminating R , H_{coll} can be decomposed into three parts:

$$H_{\text{coll}} = H_{\text{rot}} + H_{\text{rec}} + H_{\text{cor}}, \quad (3.14)$$

where

$$H_{\text{rot}} = \frac{I_1^2}{2g_1} + \frac{I_2^2}{2g_2} + \frac{I_3^2}{2g_3} \quad (3.15)$$

is the pure rotational operator of the rotor [Eq. (1.55)], which acts only on the degrees of freedom of the rotor, that is, the Euler angles. The term

$$H_{\text{rec}} = \sum_{i=1}^3 \frac{j_i^2}{2g_i} \quad (3.16)$$

is usually called the recoil term. It represents a recoil energy of the rotor. This operator acts in the coordinates of the valence particles only. For more than one valence particle, it contains a two-body interaction.

Finally, the coriolis interaction

$$H_{\text{cor}} = - \sum_{i=1}^3 \frac{I_i j_i}{g_i} \quad (3.17)$$

couples the degrees of freedom of the valence particles to the degrees of freedom of the rotor. This purely kinematic coupling is the only coupling in the model.

It should be noticed that the total angular momentum operators in the laboratory system I_x, I_y, I_z commute with the Hamiltonian (3.10). Although the rotational symmetry is violated in the intrinsic frame (e.g., in the Nilsson Hamiltonian), the model conserves angular momentum for the total system, because the operators I_x, I_y and I_z act only on the Euler angles and commute with the intrinsic components I_1, I_2 and I_3 (see Appendix A). However, it must be emphasized that this rotational invariance is achieved only through the introduction of a phenomenological

*We will see in Chapter 6 that pairing correlations play an important role in deformed nuclei and we should therefore talk about quasi-particles rather than particles. This only yields simple occupation factors to the formulae shown below, which we give sometimes for the sake of completeness, however. For a deeper understanding, the reader is referred to Chapter 6.

core. If one wants to treat all particles microscopically (the limit of vanishing core), the Euler angles are redundant variables (see Sec. 11.3).

The wave function of the system may be written as

$$|\Psi_M\rangle = \sum_K \Phi_K |IMK\rangle, \quad (3.18)$$

where Φ_K depends on the coordinates of the valence particles and the $|IMK\rangle$ depend on the Euler angles and are defined in Eq. (A.21). In the simplest case, there is only one valence particle and an axially symmetric rotor. Using this model a large number of the experimental spectra of odd nuclei has been reproduced very accurately, and from this point of view it is certainly one of the most powerful models in nuclear physics. However, until now a clear-cut microscopic derivation has been missing. Such a derivation should start from a many-body Hamiltonian (2.19). The set of $3A$ particle coordinates should be transformed in a proper way into a set of $3A - 3$ internal coordinates and 3 Euler angles which describe the collective motion. To this transformation should correspond a decomposition of the Hamiltonian into an internal and a collective part, as in Eq. (3.10). Finally, one could hope to describe the internal motion by a deformed shell model.

Many attempts have been made in this direction and we give a short discussion of them in Section 11.3, but up to the present time the problem has still not been completely solved. In the case of well deformed nuclei the model can be backed by the following arguments.

- (i) Microscopic Hartree-Fock calculations show very pronounced minima in the energy surface at axial symmetric deformations, which justifies the notion of a rotating core.
- (ii) The model is to some extent equivalent to the cranking model (see Sec. 3.4), which is microscopically founded at least in the limit of strong nearly axial symmetric deformations.
- (iii) Villars and Cooper [VC 70] have shown that, in introducing redundant coordinates, a Hamiltonian of a form similar to that in Eq. (3.10) can be found with, however, additional coupling terms. In the limit of strong deformation and with further assumptions, they obtained the correct expression for the moment of inertia.

The particle-plus-rotor model has, however, also been applied with great success to nuclei in the region of small deformations and to transitional nuclei. It is not clear at the present time how this can be explained microscopically.

3.3.1 The Case of Axial Symmetry

Assuming that the rotor has the 3-axis as axis of symmetry, that is, $\mathfrak{g}_1 = \mathfrak{g}_2 = 4$, there can be no collective rotation around this axis and the 3-component of \mathbf{R} has to vanish (see Sec. 1.5). From Eq. (3.13) it follows

immediately that K , the 3-component of the total angular momentum \mathbf{L} , has to be equal to Ω , the 3-component of \mathbf{j} :

$$K = \Omega. \quad (3.19)$$

For the different terms of the Hamiltonian (3.10), (3.14), we obtain in this case

$$H_{\text{intr}} = \sum_{i, \Omega} \epsilon'_{\Omega} a_{i\Omega}^+ a_{i\Omega}, \quad (3.20)$$

$$H_{\text{rot}} = \frac{\mathbf{I}^2 - I_3^2}{2g}, \quad (3.21)$$

$$H_{\text{rec}} = \frac{1}{2g} (j_1^2 + j_2^2), \quad (3.22)$$

$$H_{\text{cor}} = -\frac{1}{g} (I_1 j_1 + I_2 j_2) = -\frac{1}{2g} (I_+ j_- + I_- j_+). \quad (3.23)$$

In (3.20) we have neglected the residual interaction. The single-particle levels in the axially symmetric well are labeled by $k = (i, \Omega)$ and the corresponding eigenfunctions will be denoted by Φ'_{Ω} .

The recoil term acts only in the intrinsic coordinates. It is often neglected, because the intrinsic single-particle energies ϵ'_{Ω} are adjusted to experimental data. We follow this argument in the following discussion and omit H_{rec} for the moment. Only in Section 3.3.2.1 will we take it up again. The Hamiltonian (3.20–3.23) has eigenfunctions of the type (3.18), which can be found by a numerical diagonalization of the Hamiltonian (3.10). However, the different terms in (3.20–3.23) are of different importance, depending on the physical situation. Therefore, it is useful to consider three limits in which one of the terms becomes predominant and which as a consequence can be solved analytically (for a review, see [St 75a]):

In the *strong coupling limit*, the odd particle adiabatically follows the rotations of the even mass core. It is realized if the coupling to the deformation is much stronger than the perturbation of the single particle motion by the Coriolis interaction.

In the *weak coupling limit*, which is realized for very small deformations, the odd particle essentially moves on spherical shell model levels only slightly disturbed by, for example, the quadrupole vibrations (see Sec. 9.3.3).

In the *decoupling limit*, the Coriolis force is so strong that the coupling to the deformation of the core may be neglected. The total angular momentum and the single-particle angular momentum are then parallel to one another.

3.3.1.1 The Strong Coupling Limit (Deformation Alignment). The strong coupling limit is realized when the Coriolis interaction matrix elements are small compared with the level splitting of the single-particle energies in the deformed shell model for different values of Ω . We should expect that this

is the case

- (i) for large deformations β , because the level splitting in the Nilsson Hamiltonian is $\propto \beta$, whereas the rotational constant $\hbar^2/2\beta$ is, according to a simple empirical rule (Eq. (1.50), $\propto \beta^{-2}$; and
- (ii) for small Coriolis matrix-elements. As we shall see in Eq. (3.33), they are $\propto [(I(I+1) - K^2)(j(j+1) - \Omega^2)]^{1/2}$, that is, they are small either for low spins I or for nucleons in orbitals with small particle angular momenta j . For large j -values they can only be neglected for high Ω values.

It is called the *strong coupling* or *deformation aligned* limit because in this case K is a good quantum number. The angular momentum J of the valence particles is strongly coupled to the motion of the core. In a semiclassical picture, j precesses around the 3-axis, which is shown in the coupling scheme of Fig. 3.7a. Since H_{cor} is the only term in the Hamiltonian which couples the particle and rotor degrees of freedom, the eigenfunctions are in this limit products of the functions Φ'_K (eigenfunctions of H_{intr} , e.g., the single-particle Nilsson functions) and the eigenfunctions of the symmetric rotor $|IMK\rangle$ (see Appendix A).

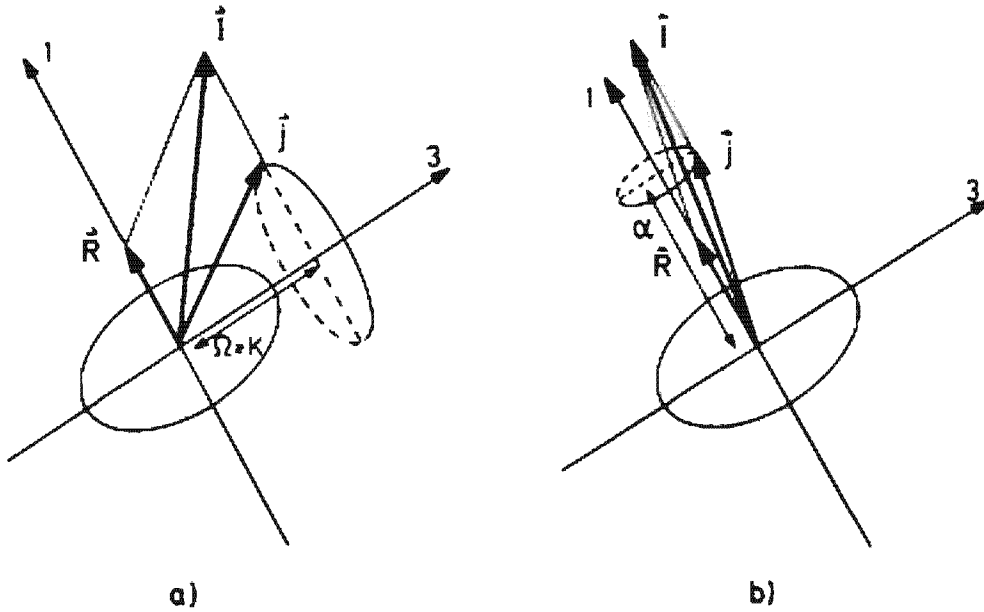


Figure 3.7. Coupling schemes in the particle-plus-rotor model: (a) strong coupling; (b) rotational alignment.

We have seen in Section 1.5.1 that the Hamiltonian (3.10) has an additional symmetry, \mathcal{R}_1 , which describes a rotation of the core by 180° around the 1-axis of the body-fixed system

$$\mathcal{R}_1 = e^{i\pi R_1} = e^{i\pi I} e^{-i\pi j_1}. \quad (3.24)$$

We therefore have to symmetrize the wave function (3.18) and get together with Eq. (A.24) the following set of eigenfunctions [Ke 56]

$$|\Psi'_{MK}\rangle = \frac{1}{\sqrt{2(1 + \delta_{K0})}} \{ \Phi'_K |IMK\rangle + (-)^I e^{-i\pi j_1} \Phi'_K |IM-K\rangle \}. \quad (3.25)$$

If we know the decomposition of Φ_K^i into eigenstates of j^2

$$|\Phi_{K=0}^i\rangle = \sum_{nj} C_{nj}^i |nj\Omega\rangle, \quad (3.26)$$

we find

$$e^{-i\theta j} |\Phi_{K=0}^i\rangle = \sum_{nj} C_{nj}^i (-)^{-j} |nj-\Omega\rangle. \quad (3.27)$$

The energy spectrum which corresponds to (3.25) is given by

$$E_K^i(I) = \epsilon_K^i + \frac{1}{2g} (I \cdot (I+1) - K^2) \quad (3.28)$$

[usually, instead of ϵ_K^i in (3.28), we have quasi-particle energies E_K^i as they are defined in Eq. (6.72)]. This is the spectrum of a rotational band. The lowest possible spin is $I_0 = K$. The bandhead $E_K^i(I_0)$ is not precisely ϵ_K^i , but shifted a little, especially if we take into account the recoil term and the residual interaction. The spectrum has a spacing $\Delta I = 1$ and its moment of inertia is that of the rotor.

In this strong coupling limit we have neglected the Coriolis interaction completely. Taking it into account at least in first order perturbation theory, we get a contribution only for $K = 1/2$ bands

$$E_{K=1/2}^i(I) = \epsilon_{K=1/2}^i + \frac{1}{2g} \left\{ I(I+1) - \frac{1}{4} + a' \left(I + \frac{1}{2} \right) (-)^{I+1/2} \right\}, \quad (3.29)$$

where the so-called *decoupling factor* is given by

$$a' = i \langle \Phi_{1/2}^i | j_+ e^{-i\theta j} | \Phi_{1/2}^i \rangle \quad (3.30)$$

or if Φ_K^i is of the form (3.26),

$$a' = - \sum_{nj} |C_{nj}^i|^2 (-)^{j+1/2} (j + \frac{1}{2}). \quad (3.31)$$

This means, for example, that for a positive decoupling factor (major components with $j + \frac{1}{2}$ odd) the levels with odd values of $I + \frac{1}{2}$ ($I = \frac{1}{2}, \frac{3}{2}, \frac{5}{2}, \dots$) are shifted downwards. This explains very nicely the rather distorted bands for $K = \frac{1}{2}$ in many nuclei [ABH 56] where there are, in fact, two bands having $\Delta I = 2$ each (even and odd values of $I + \frac{1}{2}$) shifted against one another. The reason for this decoupling comes from the symmetrization Eq. (3.25) with respect to \mathcal{R}_1 mixing states with $K = \frac{1}{2}$ and $K = -\frac{1}{2}$ via the Coriolis matrix elements. The strength of the decoupling factor a' depends on the j -components which contribute to the single-particle wave function $\Phi_{1/2}^i$. If levels with large single-particle angular momenta are involved, it is very strong. However, perturbation theory is no longer valid in such cases, and also other matrix elements of the Coriolis operator come into play. Therefore, the strong coupling limit is no longer realized and we have to consider a different limit.

3.3.1.2 The Weak Coupling Limit (No Alignment). As we have said, the strong coupling approximation breaks down if the Coriolis matrix elements are no longer negligible compared to the energy splitting of the single-

particle levels belonging to different K values. Let us therefore study the Coriolis matrix elements in more detail.

$$\langle \Psi'_{MK+1} | H_{\text{cor}} | \Psi'_{MK} \rangle = -\frac{1}{g} \sqrt{I(I+1) - K(K+1)} \langle \Phi_{0+1} | j_z | \Phi_0 \rangle. \quad (3.32)$$

If Φ_0 is of the form shown in Eq. (3.26), we obtain

$$\begin{aligned} & \langle \Psi'_{MK+1} | H_{\text{cor}} | \Psi'_{MK} \rangle \\ &= -\frac{1}{2g} \sum_{nj} |C_{nj}|^2 \sqrt{I(I+1) - K(K+1)} \sqrt{j(j+1) - \Omega(\Omega+1)}. \end{aligned} \quad (3.33)$$

We see that these matrix elements are large for large values of I/K and j/Ω . That is, if, for example, levels with large j and small Ω values are involved. Particles in such levels have high angular momentum and a density distribution close to the 3-axis. Therefore, it is clear that a rotation of the core perpendicular to this axis has a great influence on the motion of these particles.

A well known example is the neutron $1i_{13/2}$ level, which lies in the vicinity of the Fermi level for light rare earth nuclei such as Dy and Er. One can estimate the Coriolis matrix element for the $\Omega = \frac{1}{2}$ case to be $0.1 \times I$ [MeV], which is in fact quite large compared with the level spacing of H_{intr} . Since such levels with high j -values are drastically shifted downwards by the spin orbit term of the shell model (see Sec. 2.4) into a shell with a different N -quantum number, these levels are rather pure configurations, that is, $C_{nj} \approx 1$ (intruder state). It is therefore sufficient in the following to consider *only one such single j -shell*. The $1i_{13/2}$ shell is not the only such case. The energy of the largest j -value in each major shell is lowered drastically and has an important role in many rotational spectra.

Vogel [Vo 70] proposed a limit (usually called weak coupling or no alignment limit) in which the K -splitting of H_{intr} is totally neglected. (This, of course, can only be a valid approximation for small deformation.) Now J^2 and \mathbf{R}^2 commute with H_{intr} and we can construct eigenfunctions of \mathbf{R}^2 and R_3 (the eigenvalue of the latter is, of course, zero). A proper angular momentum coupling gives*

$$|\Psi_M^{IR}\rangle = \sum_K (-)^{j-K} C_K^I |j_K^R \Phi_K |IMK\rangle. \quad (3.34)$$

These wave functions diagonalize \mathbf{R}^2 , and the corresponding spectrum is of the form

$$E(I) = E_{\text{intr}} + \frac{1}{2g} R(R+1), \quad (3.35)$$

with

$$|j-R| \leq I \leq j+R; R=0, 2, 4, \dots (\text{R}_1 \text{ symmetry}). \quad (3.36)$$

This means that for each rotational quantum number R , J can have $2j+1$ orientations without changing the energy of the system (zero cou-

*Since we couple the angular momenta I and $-J$ to $R=I-J$, we have to apply a coupling rule as in the $p\bar{n}$ -case of Eq. (2.46).

pling). The splitting of the $2j+1$ levels can be taken into account in first-order perturbation theory (we will take a Nilsson term $\sim \beta r^2 Y_{20}$ as perturbation).

$$E(I) = E_0 + \frac{1}{2g} R(R+1) - \beta \hbar \omega_0 \langle \Psi_M^{IR} | r^2 Y_{20} | \Psi_M^{IR} \rangle. \quad (3.37)$$

To each orientation of J there is a whole rotational band of the core with $\Delta R=2$. The levels with the highest I values $I=R+j$ for a given energy (i.e., for a given R) correspond to the yrast levels. These levels are connected by strong $E2$ transitions [Re 75a] and are experimentally the most easily accessible. They are called *favored states** [St 75a] and their energy is given by

$$E(I) = E_{\text{intr}} + \frac{1}{2g} (I-j)(I-j+1). \quad (3.38)$$

This means that these states lie on a parabola with a minimum at $I \approx j$, which is experimentally widely confirmed, an example of which is shown in Fig. 3.8.

* Levels with a lesser degree of alignment (e.g. $I=j+R-1$) are called *unfavored states*.

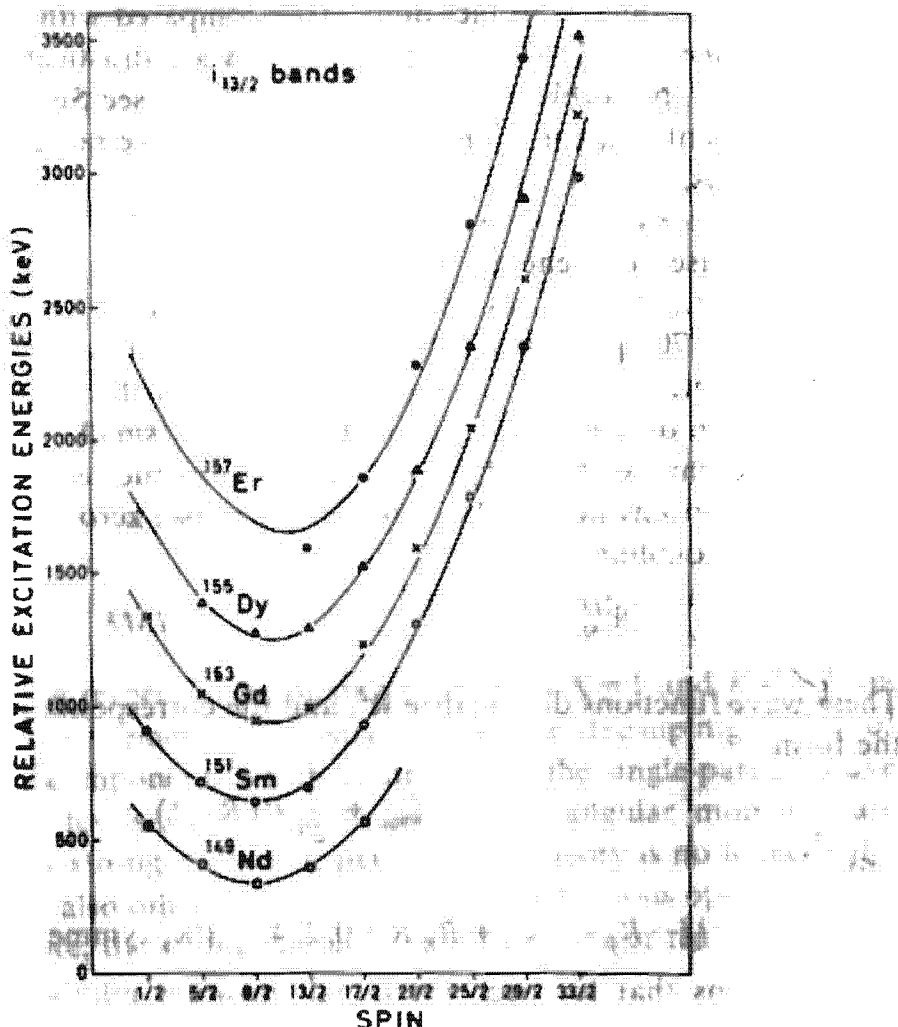


Figure 3.8. Relative excitation energies as a function of spin for the $13/2^+$ bands in some $N=89$ nuclei. (The experimentally observed band members are plotted such that the $13/2^+$ states are equally spaced (300 keV).) (From [LR 76].)

On the right branch of this parabola J and R are aligned ($J \parallel R$),

$$I = j + R = j, j + 2, j + 4, \dots,$$

and on the left branch J and R are anti-aligned ($J \parallel -R$); the core rotates in the opposite direction as J^* :

$$I = j - R = j - 2, j - 4, \dots, \frac{1}{2} (\text{or } \frac{1}{2}).$$

As an empirical rule one can say that the weak coupling limit is strictly valid only for very small deformations $|\beta A^{2/3}| < 4$. We shall see in the next section, however, that the states with $I \parallel J$ are energetically favoured even in the case of stronger deformations, where neglecting the Ω -dependence of H_{intr} is no longer justified. Therefore, the formula (3.38) is also valid for many levels in more deformed nuclei (see for instance Fig. 3.8) in the so-called rotation aligned coupling scheme.

3.3.1.3 The Decoupling Limit (Rotational Alignment). In the case of intermediate deformations, the energy splitting in the intrinsic part of the Hamiltonian can no longer be neglected. In this case, the orientation of the external large j -particle is no longer independent of the motion of the core. Stephens et al. [SDN 73] realized that the requirement of maximal overlap of the single-particle density distribution (which is concentrated mostly in a plane perpendicular to j) with the core can be fulfilled if the external particle is aligned along the rotational axis of a prolate nucleus (see also Sec. 2.8.4).

Mathematically, we can understand this in the model of a single j -shell ($C_j \approx 1$, like, for example, in the $i_{13/2}$ case). Neglecting I^2 and $I\sigma$ -term, the Nilsson energies are simply given by the diagonal matrix element

$$\begin{aligned} \epsilon_{\Omega} &= \epsilon_0 - \beta \cdot \hbar \omega_0 \langle nlj\Omega | r^2 Y_{20} | nlj\Omega \rangle \\ &= \epsilon_0 + \beta k \frac{3\Omega^2 - j(j+1)}{4j(j+1)} = \epsilon_0 - \frac{1}{4} \beta k + C\Omega^2, \end{aligned} \quad (3.39)$$

where k and C do not depend on Ω . Also, the recoil term (3.22) can be calculated as a diagonal matrix element and yields

$$H_{\text{rec}} = \frac{1}{2g} \{ j(j+1) - \Omega^2 \}. \quad (3.40)$$

Therefore, the Hamiltonian (3.10) in this approximation is:

$$H = \epsilon_0 - \frac{1}{4} \beta k + \frac{1}{2g} (I(I+1) + j(j+1)) + \left(C - \frac{1}{g} \right) I_3^2 + H_{\text{cor}}. \quad (3.41)$$

In a certain region of deformation, where $C \approx 1/g$, there is thus a cancellation of the K dependence coming from the intrinsic and rotational parts of the Hamiltonian. This turns out to apply for a rather broad domain of intermediate deformations. Unfortunately, the eigenfunctions of H_{cor} which we needed to solve (3.41) cannot be given analytically in the general case. Thus, we wish to give a qualitative discussion. Writing the

* In principle, there are also anti-aligned states with $R > j$ [PO 78].

Coriolis term in the form*

$$H_{\text{cor}} = -\frac{1}{2} \mathbf{I}_{\perp} \cdot \mathbf{j}_{\perp}, \quad (3.42)$$

we see that it has its lowest expectation value for the wave functions with $\langle \mathbf{I} \rangle \parallel \langle \mathbf{j} \rangle$. Since \mathbf{R} is perpendicular to the 3-axis, one gets the lowest eigenvalue for wave functions with a single-particle angular momentum aligned along a rotational axis perpendicular to the symmetry axis. For this purpose, we choose the 1-axis and accordingly construct eigenfunctions $|\tilde{\Phi}_\alpha\rangle$ of j_1 with eigenvalues α by rotating the eigenfunctions $|\Phi_K\rangle$ of j_3 through 90° about the 2-axis:

$$|\tilde{\Phi}_\alpha\rangle = \sum_K d_{K\alpha}^l \left(-\frac{\pi}{2}\right) |\Phi_K\rangle, \quad (3.43)$$

where $d_{K\alpha}^l$ is the Wigner function of this rotation [Ed 57].

For the total wave function it is, however, not so easy to make such a construction in which α is a good quantum number. The ansatz

$$|\Psi_M^{I,j}\rangle = \sum_K d_{K\alpha}^l \left(-\frac{\pi}{2}\right) \Phi_K |IMK\rangle \quad (3.44)$$

is an eigenfunction of H_{cor} at least for $I \gg K$. With

$$I_- |IMK\rangle = \sqrt{I(I+1) - K(K+1)} |IMK+1\rangle \approx I |IMK+1\rangle \quad (3.45)$$

we then easily get

$$H_{\text{cor}} |\Psi_M^{I,j}\rangle = -\frac{1}{2} I \cdot \alpha |\Psi_M^{I,j}\rangle \quad (I \gg K), \quad (3.46)$$

which shows that α is the projection of \mathbf{j} onto \mathbf{I} .

From Eq. (A24) and [Ed 57, Eq. (4.2.4)] we obtain

$$\mathcal{R}_1 |\Psi_M^{I,j}\rangle = (-)^{I-\alpha} |\Psi_M^{I,j}\rangle, \quad (3.47)$$

which means that $I - \alpha$ has to be even in order to fulfill the symmetry condition $\mathcal{R}_1 = 1$.

In the case of $C \approx 1/2$, we find for the spectrum of the Hamiltonian (3.41):

$$\begin{aligned} E(I, \alpha) &= \text{const.} + \frac{1}{2g} (I(I+1) + j(j+1) - 2I\alpha) \\ &= \text{const.} + \frac{1}{2g} (I - \alpha)(I - \alpha + 1) \end{aligned} \quad (3.48)$$

$$= \text{const.} + \frac{1}{2g} R(R+1) \quad (3.49)$$

where $R = I - \alpha = 0, 2, 4, \dots$ has to be even because of the symmetry condition (3.47).

The lowest lying states are therefore the ones which are maximally aligned ($\alpha = j$, *favored states*). This corresponds exactly to the picture of a valence particle whose spin is oriented perpendicular to the 3-axis while

* \mathbf{I}_{\perp} and \mathbf{j}_{\perp} are the components of \mathbf{I} and \mathbf{j} perpendicular to the symmetry axis.

the core is completely decoupled and rotates with $R = I - \alpha$, giving rise to a spectrum $\Delta I = 2$, but which is otherwise equivalent to that of the neighboring even nucleus. Such bands have been seen, for example, in weakly deformed nuclei (see Figs. 3.8 and 3.9).

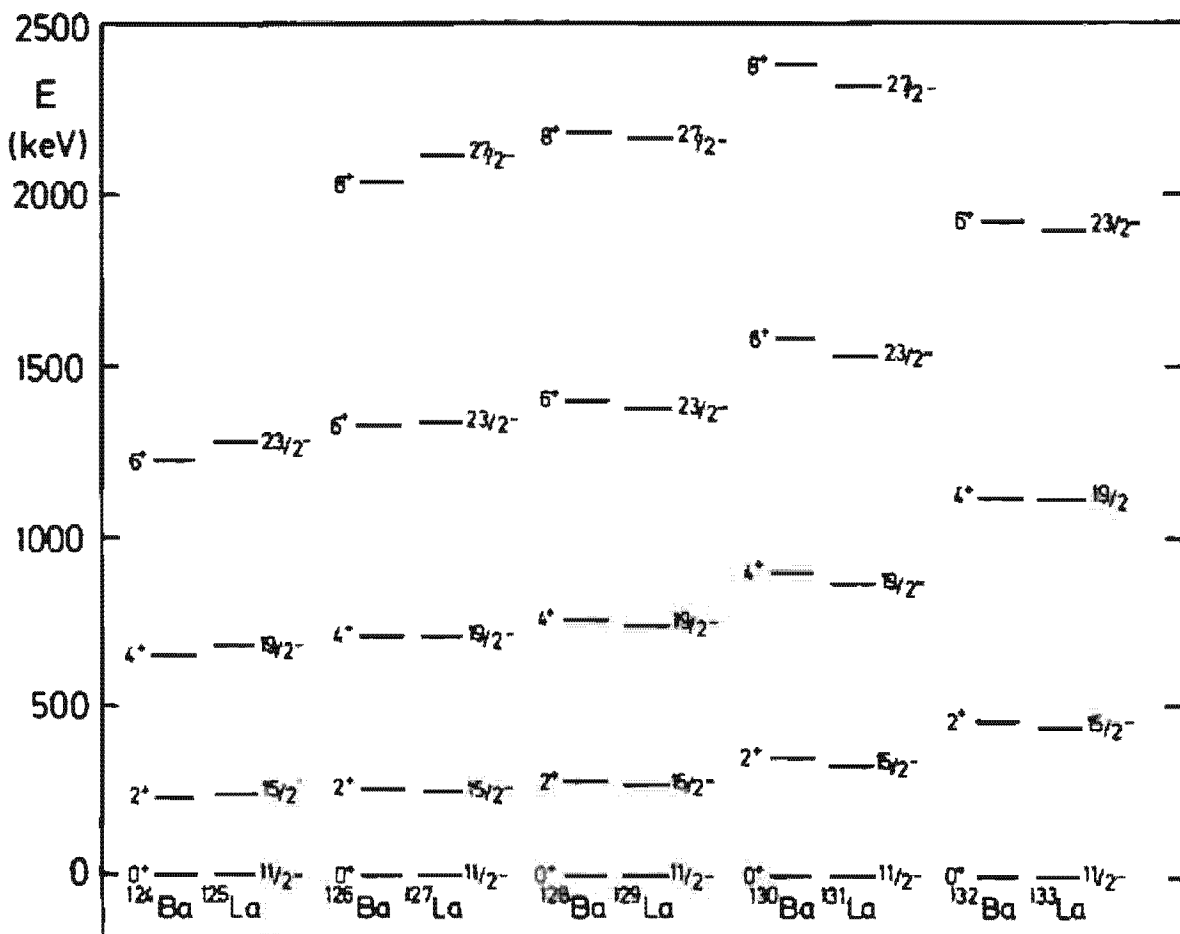


Figure 3.9. Comparison of ground band levels in some Ba isotopes with negative parity bands in the neighboring La nuclei. In most cases the La $11/2$ level is not the ground state, and its energy has been subtracted from all levels shown for that isotope. (From [SDL 72].)

Lesser aligned states (*unfavored states*) have $\alpha = j - 1$. They often lie at higher energies and are then not populated in (Hd, xn) reactions.

Figure 3.10 shows the exact solution of the axially symmetric particle-plus-rotor model for one valence nucleon in a $1h_{11/2}$ shell as a function of the deformation β . For very small β -values, one has the weak coupling scheme of several nearly degenerate multiplets. On the oblate side ($\beta < 0$) the strong coupling is realized. In this case, the lowest level in the Nilsson scheme (see Fig. 2.21.) is the $\Omega = 11/2$ level. Its Coriolis matrix element is very small and a strongly coupled band with $\Delta I = 1$ is observed. On the prolate side the opposite is true: The lowest level has $\Omega = \frac{1}{2}$ and a very large Coriolis matrix element. The yrast band (the levels with the highest I -values) is now formed by a decoupled band $I = 11/2, 15/2, 19/2, \dots$ with $\Delta I = 2$ and a level spacing, which is more or less that of the rotor (as seen at $\beta = 0$). We see also that for these completely aligned yrast levels the rotation aligned coupling scheme is very well realized over a wide range of

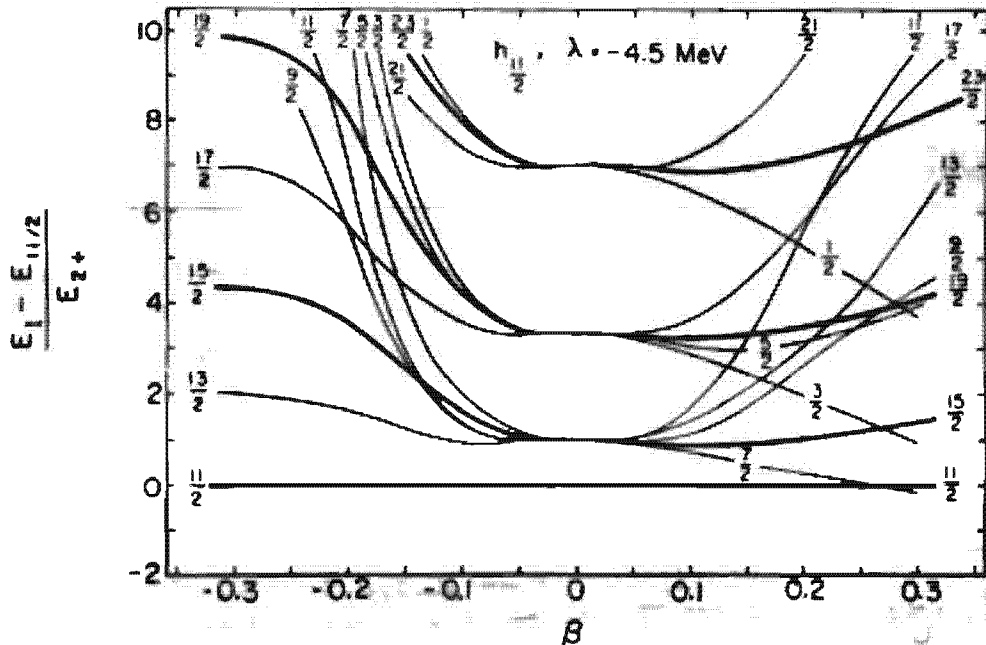


Figure 3.10. The eigenvalues of an axially symmetric particle-plus-rotor model, with one particle sitting in the $1h_{11/2}$ shell, as a function of the deformation β . Plotted are the excitation energies over the $I = 11/2$ level. The Fermi surface λ is below the entire $h_{11/2}$ orbital. (From [St 75a].)

intermediate β -values: $0.13 \sim \beta < 0.23$. Only at very large deformations does one find deviations.

The structure of the bands also depends, of course, on the position of the Fermi level. We had here the simplest case of only one particle in the shell. The complete analogue is one hole in the high j -shell. There the situation is reversed: On the prolate side are the levels with large Ω -values—that is, one observes a strongly coupled scheme—and on the oblate side are the levels with small Ω -values and a decoupled scheme.

These considerations show that the structure of the rotational bands built on such high j levels provides an excellent tool to distinguish experimentally between prolate and oblate deformations in the transition region.

Summarizing the results of this section, we can say that

- (i) In many cases, the Coriolis interaction can be neglected. Then the valence nucleons rotate around the symmetry axis of the core and change their orientation with it (strong coupling $\Delta I = 1$).
- (ii) In cases of small deformation and strong Coriolis interaction, the valence nucleons orient their angular momentum more or less independently of the orientation of the core. The core rotates with $\Delta I = 2$ (weak coupling).
- (iii) For intermediate deformations it can happen by a cancellation effect that a rotational alignment takes place. The valence particles orient their angular momentum parallel to the collective angular momentum (perpendicular to the symmetry axis of the core) and again we have $\Delta I = 2$.

3.3.2 Some Applications of the Particle-plus-Rotor Model

The model of a few valence particles coupled to a symmetric rotor has been used in a very large number of cases to fit the experimental rotational bands. In general, it has been very successful. We do not want here to go into the many different versions which have been used but wish to discuss a few characteristic examples.

3.3.2.1 Strongly Mixed Bands in Well-Deformed Odd Mass Nuclei. The spectra of odd mass nuclei in the deformed region show many rotational bands which reveal very nicely the strong coupling picture. Only in cases where the particle sits in a single-particle shell with a high j -value (e.g., the $1i_{13/2}$ shell in the Er region), one also observes very distorted bands.* For small I values they start out like strongly coupled bands with $\Delta I = 1$, but soon we observe staggering: The levels with $I + 1/2$ even are shifted more and more against the levels with $I + 1/2$ odd, so that in the end we have two separate bands with $\Delta I = 2$ (see the positive parity band in Fig. 3.11 and [BDL 75]).

*For a comparison of these distorted bands with the backbending behavior in neighboring even nuclei, see [SKS 74].

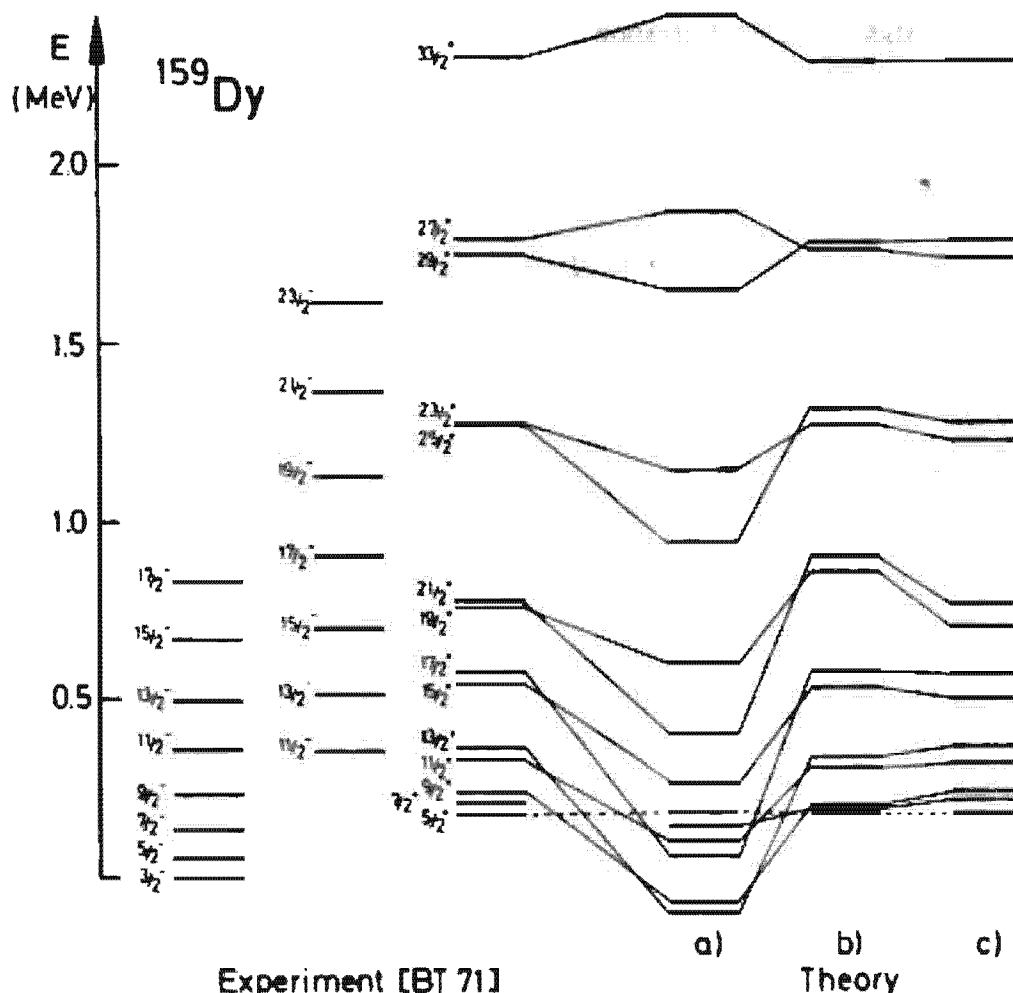


Figure 3.11. Three rotational bands in the nucleus ^{159}Dy . The $3/2^+$ and the $11/2^-$ bands are strongly coupled ($\Delta I = 1$). The positive parity band with the band head $I = 5/2$ is strongly perturbed, as discussed in the text. It is compared with three calculations: (a) a particle-plus-rotor fit without attenuation ρ , (b) a particle-plus-rotor fit with attenuation $\rho = 0.5$, and (c) a self-consistently determined attenuation according to Eq. (3.56). (From [Ri 77].)

To describe these bands one usually diagonalizes the Hamiltonian (3.10) in the strong coupling basis (3.25). The single (quasi-) particle energies are taken from a Nilsson model and the parameters like the deformation β (and the gap Δ , see Chap. 6) are used to fit the spectrum. It thereby turns out that one can only reproduce the experimental spectrum if one introduces an additional parameter ρ —the *attenuation factor*—which weakens the Coriolis interactions, that is, if we use $\rho \cdot H_{\text{cor}}$ instead of H_{cor} [HRH 70, LRB 72, HK 77]. The original Coriolis force turns out to be much too strong and it has to be reduced by a factor $\rho \sim 0.4 - 0.8$. With this ad hoc attenuation and the other parameters of the model reasonably chosen, we are able to reproduce the distorted bands and find that for low I -values, that is, for small Coriolis interaction, one is in the strong coupling limit with $\Delta I = 1$. For higher I -values, however, the Coriolis force gets stronger and aligns the odd particle with the large j -value parallel to the rotational axis. For I -values $I \gtrsim j$, we have a rotational aligned motion, that is, large K -mixing and a splitting of the band in favored states with maximal alignment $\alpha = j$ for $(I-j)$ even, and unfavored states with lesser alignment $\alpha = j-1$ for $(I-j)$ odd. For the same value of angular momentum R of the core, which is given by $R = I - \alpha$, these two bands are almost degenerate (see Fig. 3.11).

Several attempts have been made to explain the *attenuation factors* as a kind of effective charge in the linear response approach [BPC 72, HK 75]. It turns out that this problem is closely connected with a proper treatment of the recoil term (3.22). The argument, that it is already taken into account in the fit of the band head energies, does not apply because in the one-particle case it is proportional to $j^2 - K^2$ and therefore has a strong K -dependence which shifts the band heads [ORG 75].

To understand qualitatively the effect of the recoil term we restrict ourselves to the case of only one particle and rewrite the particle-plus-rotor Hamiltonian (3.20ff) in the following way [Kr 79].

$$H = H_{\text{intr}} + \frac{1}{2g} (I(I+1) - J^2) + H'_{\text{cor}} \quad (3.50)$$

with the new Coriolis term

$$H'_{\text{cor}} = -\frac{1}{q} (I-J) J_{\perp} = -\frac{1}{q} \mathbf{R} \mathbf{j} = -\omega \mathbf{j}, \quad (3.51)$$

where the collective angular velocity is given by

$$\omega = -\mathbf{R}/\mathfrak{J}. \quad (3.52)$$

The Coriolis term H'_{cor} in Eq. (3.51) is attenuated compared to H_{cor} (3.23). To see this we go into the limit, where the odd particle is nearly aligned to the collective rotation \mathbf{R} . We then have

$$\mathbf{R} \approx \mathbf{I}_{\perp} \left(1 - \frac{\alpha}{I}\right) \quad (3.53)$$

and find that H'_{cor} is in this case proportional to H_{cor} :

$$H'_{\text{cor}} = \left(1 - \frac{\alpha}{I}\right) H_{\text{cor}} = \rho \cdot H_{\text{cor}} \quad (3.54)$$

with an I -dependent attenuation factor

$$\rho = 1 - \frac{\alpha}{I}. \quad (3.55)$$

Only for very high I -values does the attenuation disappear.

So far, the discussion of the influence of the recoil term has been restricted to the pure single-particle part of this operator. In fact, it also contains a two-body

term $\mathbf{j}_{ik} \cdot \mathbf{j}_{lm} a_i^+ a_l^+ a_m a_k$, which produces an interaction with the particles of the core. We can treat it in the mean field approximation [Ri 77] and end up with a self-consistent attenuation factor

$$\rho = 1 - \frac{\langle j_i \rangle}{\sqrt{I(I+1) - \langle j_i^2 \rangle}}. \quad (3.56)$$

At the limit of alignment it goes over into the form (3.55). We can also show that this approximation is equivalent to the cranking model (see Sec. 3.4). In a microscopic treatment of rotational bands in odd mass nuclei within the self-consistent cranking model (see Sec. 7.7), the attenuation of the Coriolis interaction is automatically incorporated [RMB 74, RM 74].

3.3.2.2 Backbending in Even Nuclei. The backbending phenomenon (see Sec. 3.2.4.) has been explained by Stephens and Simon [SS 72a] as an alignment of two neutrons in the $1i_{13/2}$ shell. If these two neutrons, instead of rotating around the 3-axis, align along the rotation axis of the nucleus, this adds an additional $13/2 + 11/2 = 12$ units of angular momentum. Therefore, the nucleus can decrease its collective rotation while increasing its total angular momentum through the addition of single-particle angular momentum.

To describe this idea mathematically, Stephens and Simon diagonalized the Hamiltonian (3.10) (with attenuation of the Coriolis term) taking as the basis the Slater determinant of the unperturbed core

$$|\Phi_0\rangle = |IMK=0\rangle$$

and two quasi-particle excitations (see Chap. 7)

$$|\Phi_K\rangle = \beta_{K_1}^+ \beta_{K_2}^+ |IMK=K_1+K_2\rangle, \quad (3.57)$$

where β_K^+ is a creation operator for a quasi-particle in the state $\Omega = K$ of the $1i_{13/2}$ shell.

For low I values, the yrast states are given mainly in the zero quasi-particle state $|\Phi_0\rangle$ of the pure rotor. The excited bands are two quasi-particle bands. For higher I -values, the particles align their angular momenta along the axis of rotation, one of them to $\alpha = j = 13/2$, the second to $\alpha = j - 1 = 11/2$. Thus, we find a mixing of the states Φ_0 and Φ_K ($K = 0, 1, \dots$) and arrive, at the limit of full alignment, at a two-quasi-particle state of the form [see Eq. (3.44)]:

$$|\Phi\rangle_{\text{eff}} = \sum_{K_1 K_2} d_{K_1 J} \left(-\frac{\pi}{2} \right) d_{K_2 J-1} \left(-\frac{\pi}{2} \right) \beta_{K_1}^+ \beta_{K_2}^+ |IMK_1+K_2\rangle. \quad (3.58)$$

It can be written schematically as $\tilde{\beta}_j^+ \cdot \tilde{\beta}_{j-1}^+ |\Phi_0\rangle$, where the $\tilde{\beta}_\alpha^+$ are the quasi-particle operators quantized along the 1-axis.

Stephens and Simon [SS 72a] were able to reproduce the experimental backbending spectra reasonably well with this method. Since they did not take into account, however, the gradual change in the pairing correlations caused by the Coriolis-anti-pairing effect, they could not obtain the deviations from the $I \cdot (I+1)$ law at low spin values.

In spite of the fact that this model describes the important effect of two aligning particles properly, it does not allow us to decide whether there is any other mechanism which could be the origin of the observed backbending phenomenon. To decide whether it is caused by a change in shape, by a phase transition to a normal fluid state, or by an alignment process, one has to carry out a microscopic calculation which allows for all these degrees of freedom. Such investigations have been done (see Sec. 7.7). They show that the rotational alignment of two particles is

the most important effect. These processes are found in all nuclei in which a high j -shell exists in the vicinity of the Fermi surface. However, it is another question as to whether they produce backbending. This depends finally on the strength of the interaction between the two crossing bands: Only for rather small coupling matrix elements do we observe a sudden transition, that is backbending.*

3.3.3 The Triaxial Particle-plus-Rotor Model

We have already seen in Section 1.5.3 that Davydov et al. [DF 58] used a triaxial rotor to explain the low lying 2^+ states in some transitional nuclei. The model can also be extended to odd mass nuclei by the coupling of an external particle to a triaxial rotor [Pa 61, HS 62, PR 62, PS 65, MSD 74, Me 75, FT 75, TF 75, Le 76, DF 77, LLR 78]. It has been applied to cases where the external particle sits in a high j -shell, and has turned out to be very powerful as a description of energy levels and decay schemes of many transitional nuclei.[†] However, at present the microscopic foundation is missing. Using microscopic theories, the calculations of static energy surfaces in these mass regions show no pronounced minima at triaxial deformations, which would justify this simple picture. In fact, there exist other models based on a *vibrational picture* [AP 76, PVD 77, YNN 76] that are also able to reproduce such spectra. It is not clear at present whether there is any connection between these two pictures of transitional nuclei.

We restrict ourselves in the following discussion to one external particle in a high j -shell (e.g., $h\ 11/2$) and couple it to a triaxial rotor. In this case, the Hamiltonian has the form [MSD 74]:

$$h = \sum_{i=1}^3 \frac{R_i^2}{2\beta_i} + h_0 + kr^2\beta \left\{ \cos\gamma Y_{20} + \sin\gamma \frac{1}{\sqrt{2}} (Y_{22} + Y_{2-2}) \right\}. \quad (3.59)$$

The β, γ -dependence of the moment of inertia β_i is that for irrotational flow [eq. (1.48)] and only the overall constant is adjusted. The constant k is given by the splitting of the j -shell in the Nilsson scheme. h_0 is the spherical harmonic oscillator. Usually a single-particle pairing field with constant gap Δ is also taken into account.

Figure 3.12 shows the spectrum of the Hamiltonian (3.59) as a function of γ at a typical deformation $\beta = 5A^{-2/3}$. On the prolate side ($\gamma = 0$) and on the oblate side ($\gamma = 60^\circ$) we see again the same spectra as in Fig. 3.10. However, these two limits are now connected through a circle in the β, γ plane (Fig. 1.4) with constant deformation β . We no longer pass through the weak coupling limit at $\beta = 0$. On both sides the spectra do not depend very drastically on the triaxiality γ . The essential transition from the strongly coupled to the decoupled scheme takes place in a relatively small γ region around $\gamma = 30^\circ$. There are many spectra in weakly deformed transitional nuclei that can be nicely reproduced with γ -values between 20° and 40° . This agreement can be improved even more by incorporating the change of the moment of inertia in a VMI-model type calculation [FT 75].

* Recently, Bengtsson et al. [BHM 78] have found an oscillating behavior of this interaction as a function of the chemical potential λ . For an interpretation of this fact see [FPS 80] and the references given there.

[†] For extension of the triaxial rotor model to multiparticle configurations, see [TNV 77, YTF 77, TYF 77, YTF 78].

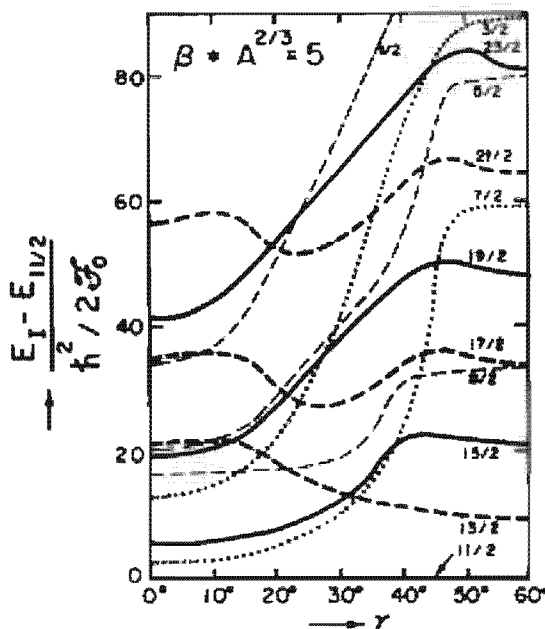


Figure 3.12. Spectrum of a $j = 11/2$ particle coupled to an asymmetric rotor with all yrast levels $I < 23/2$ as function of γ . (From [MSD 74].)

The *dynamical behavior* of a system of an odd high- j particle coupled to a rotating triaxial core is determined by three physical effects (see [Me 75]):

- (i) The core prefers to rotate around the axis with the maximal moment of inertia in order to minimize the rotational energy.
- (ii) The particle moving in the deformed well prefers maximal mass overlap with the core, because in this case its potential energy is minimal.
- (iii) The Coriolis interaction tries to align the angular momenta of the particle J and the core R .

For high j -values the alignment dominates as long as we have only one particle in the j -shell. Since the density distribution of an aligned particle is oblate with j as symmetry axis, condition (ii) is optimally satisfied if the core is oblate ($\gamma = 60^\circ$), which corresponds to the 2-axis as the symmetry axis. However, in this case $\mathfrak{J}_2 = 0$ and condition (i) is violated. Therefore, R will be perpendicular to the 2-axis and we no longer have alignment. In the triaxial case, \mathfrak{J}_2 no longer vanishes and conditions (i), (ii), and (iii) can all be satisfied together. There is an alignment of J and I along the 2-axis. In fact, the calculations show that the odd particle tends to align along the 2-axis of the core. This axis serves as an approximate symmetry axis in the sense that the approximate quantum numbers \bar{K} and $\bar{\Omega}$ (representing the projections of I and J onto the 2-axis) are meaningful for a classification. The result is a new level scheme characteristic for a triaxial rotor.

The yrast levels are given by $\bar{\Omega} = j$ and $\bar{K} = j, j \pm 2, j \pm 4$, as in the rotation aligned coupling scheme of Stephens. For these levels, I , J , R , and the 2-axis are parallel. They lie on the usual parabola with $\Delta I = 2$ (see Fig. 3.13). Contrary to the axial symmetric case, where the direction of the alignment was arbitrary in the 1, 2 plane (usually one chooses the 1-axis), we have the asymmetric case with no such symmetry. Alignment favors the 2-axis. This has the consequence that on each yrast level there exists a rotational band with the spin order $\Delta I = 1$. In fact, such levels have been experimentally observed [ABR 75].

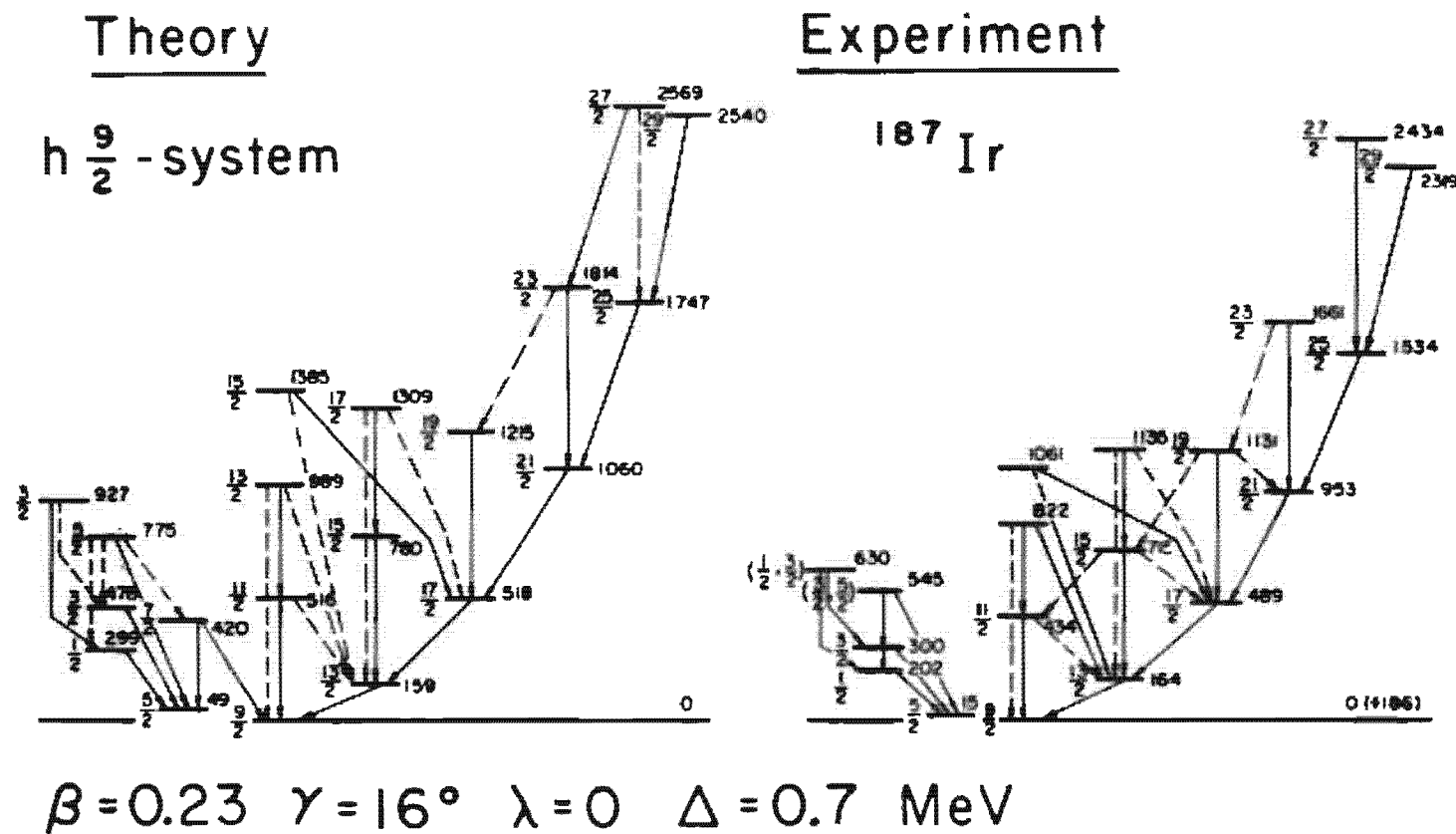


Figure 3.13. The $h\frac{9}{2}$ family of negative parity states in ^{187}Ir . (From [Me 75].)

3.3.4 Electromagnetic Properties

According to the separation of the system into valence particles and a core, we also have two contributions for the electromagnetic multipole operators:

$$Q_{\lambda\mu} = Q_{\lambda\mu}^{(c)} + Q_{\lambda\mu}^{(p)}. \quad (3.60)$$

The core part is given by Eq. (1.35) and $Q^{(p)}$ is defined in Eqs. (B.23, B.24) where the sum over i however is restricted to the number of valence particles.

In the following we shall restrict ourselves to the axially symmetric case without pairing. It is then relatively simple to generalize the formulae to more complicated cases.

The *magnetic dipole moment* of the rotor is given by Eq. (1.36) as $\mu = \mu_N \cdot g_R \mathbf{R}$. We therefore gain for the $M1$ operator:

$$M_1 = \sqrt{\frac{3}{4\pi}} \mu_N \cdot g_R (\mathbf{I} - \mathbf{J}) + M_1^{(p)}. \quad (3.61)$$

The magnetic dipole moment is defined in Eq. (B.31). With the wave function of Eq. (3.25) we obtain for $K \neq 1/2$, using the projection theorem (2.66),

$$\mu = \sqrt{\frac{4\pi}{3}} \langle \Psi'_{IK} | M_{1z} | \Psi'_{IK} \rangle = \mu_N \left\{ g_K \frac{I(I+1)-K^2}{I+1} + g_K \frac{K^2}{I+1} \right\} \quad (3.62)$$

where we have introduced the gyromagnetic ratio g_K in the following way.

$$\begin{aligned} g_K \cdot K &= \frac{1}{\mu_N} \sqrt{\frac{4\pi}{3}} \langle \Phi_K | M_{1z}^{(p)} | \Phi_K \rangle \\ &= \langle \Phi_K | g \cdot s_3 + g_I l_3 | \Phi_K \rangle \\ &= g_I K + (g_s - g_I) \cdot \langle \Phi_K | s_3 | \Phi_K \rangle. \end{aligned} \quad (3.63)$$

The matrix element $\langle \Phi_K | s_3 | \Phi_K \rangle$ can be calculated with a Nilsson wave function. For $K = 1/2$ one gets an additional contribution to the magnetic moment which contains the decoupling factor a of Eq. (3.30).

The magnetic moments obtained from Eq. (3.62) have been calculated for a large range of nuclei [MN 59, NN 65 p. 653] and one has found that agreement with experimental data is usually better for protons than for neutrons. A detailed investigation shows, however, that one again needs polarization charges for g_s : $g_s^{\text{eff}} \approx 0.7 g_s^{\text{rec}}$ (see [BM 75 p. 302ff]).

Similarly, we can calculate the reduced matrix elements for $M1$ -transitions. The operator I does not cause any transitions. For the rest we use Eq. (1.70) and get for $K \neq 1/2$ and $I_i \neq I_f$:

$$B(M1, I_i \rightarrow I_f) = \frac{1}{2I_i + 1} |\langle \Psi'_K | M_1 | \Psi'_K \rangle|^2 = \frac{3}{4\pi} \mu_N^2 (g_K - g_K)^2 K^2 |C_{K0K}^{I_i+1/2}|^2. \quad (3.64)$$

These $M1$ -transitions are only possible for rotational bands in odd nuclei. Also, reasonable agreement with experiment has been found [SBP 67].

Again using Eq. (1.70) we can also derive the $B(E2)$ values for *electric quadrupole transitions*. For transitions between states with the same K value the core contribution is much larger than the particle contribution because of the large Q_0 values. Therefore, the latter can be neglected, and we obtain

$$B(E2, I_i \rightarrow I_f) = Q_0^2 \frac{5}{16\pi} |C_{K0K}^{I_i+2 I_f}|^2. \quad (3.65)$$

This equation is used to determine the experimental values for the deformations appearing in Q_0 . In Sec. 2.8.6 we saw that they agree with the theoretically determined deformations. Therefore, the particle-plus-rotor model gives the proper $E2$ transition probabilities for transitions with the same K -value.

For transitions with different K -values, the collective part vanishes. Such transitions are, in fact, very weak (K -*forbidden*) because the single-particle part contains only the single-particle matrix element of $r^2 Y_{20}$ in the intrinsic frame. We have already seen in Section 2.7.2 that they are small compared to the collective values. On the other hand, a pure single-particle model cannot explain the effective charges in spherical nuclei (see Sec. 2.7.2). The same difficulties occur here again. For a detailed discussion, see the paper of Löbner and Malinskog [LM 66], which contains much experimental data together with possible ways to improve the simple Nilsson estimate.

Finally, we have to mention that the above considerations apply only to pure K -bands. For transition probabilities and electromagnetic moments in K -mixed bands, like rotational aligned bands or bands in an asymmetric rotor, we have to take into account the mixing coefficients.

3.4 The Cranking Model*

We have seen in the last section how the motion of particles in a deformed well can be connected with the idea of a rigid rotor. This model is very successful in the description of the level structure of rotational and even transitional nuclei. However there exists no straightforward microscopic derivation; in particular, one cannot calculate the inertial parameters in this model.

On the other hand, nearly all fully microscopic theories of nuclear rotation are based on or related in some way to the cranking model, which was introduced by Inglis [In 54, 56] in a semiclassical way, but as we shall see in Section 11.4, it can be derived fully quantum mechanically, at least in the limit of large deformations, and not too strong K -admixtures ($K \ll I$).

The cranking model has the following advantages.

- (i) In principle, it provides a fully microscopic description of the rotating nucleus. There is no introduction of redundant variables, therefore, we are able to calculate the rotational inertial parameters microscopically within this model and get a deeper insight into the dynamics of rotational motion.
- (ii) It describes the collective angular momentum as a sum of single-particle angular momenta. Therefore, collective rotation as well as single-particle rotation, and all transitions in between such as decoupling processes, are handled on the same footing.
- (iii) It is correct for very large angular momenta, where classical arguments apply (even if the quantum mechanical derivation does not work in this limit [BMR 70]).

* In this chapter, we treat only cranking theory for rotations. We can, however, also apply a similar theory for general collective motions, as discussed in Section 12.3.7.

The shortcomings of the model are:

- (i) As we shall see, it is basically a nonlinear theory. Only in the limit of small angular momenta can one linearize it using perturbation theory (cranking formula for the moment of inertia). In general, the calculations are therefore complicated, especially in cases where one has several solutions.
- (ii) The resulting wave functions are not eigenstates of the angular momentum operators. It is therefore not clear a priori how one has to calculate, for example, electromagnetic transition probabilities. In fact, we shall see in Section 11.4 that cranking model wave functions are in a sense only *internal wave functions* and that one has to use projection techniques to get the wave functions in the laboratory system.

In the following we shall give the usual semiclassical derivation (see, for instance, [Vi 57b, So 73]) and discuss the cranking model in connection with a pure single-particle Hamiltonian. Many of the arguments in the next sections can, however, also be applied to a general two-body Hamiltonian (see Sec. 7.7).

3.4.1 Semiclassical Derivation of the Cranking Model

The basic idea of the cranking model is the following classical assumption: If one introduces a coordinate system which rotates with constant angular velocity ω around a fixed axis in space, the motion of the nucleons in the rotating frame is rather simple if the angular frequency is properly chosen; in particular, the nucleons can be thought of as independent particles moving in an average potential well which is rotating with the coordinate frame.

In Section 11.4, we will see how the consequences of this picture can also be derived from quantum mechanics using projection techniques. For the moment, however, we want to stay with the classical description because of its intuitive character. Also, we do not want to take into account any residual interaction. Therefore, we assume a single-particle potential V of fixed shape, which rotates in space, and accordingly we must consider the time-dependent single-particle Hamiltonian

$$h(t) = \frac{\mathbf{p}^2}{2m} + V(\mathbf{r}, t) \quad (3.66)$$

and the corresponding Schrödinger equation

$$h(t)\psi(t) = i\hbar \frac{\partial}{\partial t} \psi(t). \quad (3.67)$$

Introducing spherical coordinates r, θ, ϕ with respect to the axis ω , we can represent the time-dependence of $V(t)$ in the following way. If $V(\mathbf{r}, 0)$ is the

potential at time $t = 0$, then we have at time t :

$$V(\mathbf{r}, t) = V(r, \theta, \varphi - \omega t, 0). \quad (3.68)$$

Again we realize that V is only time dependent if it depends on φ . In other words, V should not have axial symmetry around the rotational axis, because then there can be no collective rotation possible around an axis of symmetry for a quantum mechanical system (see Sec. 1.5.1). Because of the very simple time dependence of $V(t)$ in Eq. (3.68), a unitary transformation exists which eliminates this time dependence. It is

$$U = e^{i\omega t} \quad (3.69)$$

with $\omega \cdot \mathbf{l} = (\hbar/i)\omega \cdot \partial/\partial\varphi$. U produces a rotation of an angle ωt around the rotational axis ω .

We find the time-dependent operator

$$Uh(t)U^{-1} = h(0) \quad (3.70)$$

and define

$$\tilde{\psi} = U\psi, \quad (3.71)$$

with

$$i\hbar\dot{\tilde{\psi}} = i\hbar U\dot{\psi} + i\hbar\dot{U}\psi = (h(0) - \omega l)\tilde{\psi}. \quad (3.72)$$

Equation (3.72) is a time-dependent Schrödinger equation with an explicitly time-independent effective Hamiltonian h_ω . It thus can be solved as an eigenvalue problem in the standard way:

$$h_\omega\tilde{\psi} = (h(0) - \omega l)\tilde{\psi} = \epsilon'_\omega\tilde{\psi}, \quad (3.73)$$

where ϵ'_ω are eigenvalues of the effective Hamiltonian. To get the energies of the original Hamiltonian, we have to calculate

$$\epsilon_\omega = \langle \psi | h(t) | \psi \rangle = \langle \tilde{\psi} | h(0) | \tilde{\psi} \rangle = \epsilon'_\omega + \omega \langle \tilde{\psi} | \mathbf{l} | \tilde{\psi} \rangle. \quad (3.74)$$

The term ωl is usually called the Coriolis term.

We have now solved the time-dependent Schrödinger equation in a rotating potential and found that we must diagonalize an effective time-independent Hamiltonian. We want to emphasize that we have not derived a priori the Hamiltonian as it is seen from the rotating coordinate system, since we transformed only the coordinates and not the momenta. In fact, in the case of pure translational motion, we would get a similar result [$h_\omega = h(0) - \mathbf{v} \cdot \mathbf{p}$], but from Galilean invariance we require that the Hamiltonian seen from the moving coordinate system is the same as in the rest frame. Nevertheless, it turns out that in the special case of rotations, h_ω in Eq. (3.73) is identical with the Hamiltonian as seen from the rotating system [Va 56; Br 64, p. 69]. From the term ωl , we can derive the Coriolis force as well as the centrifugal force.

For systems with spin the operator which generates rotations is $\mathbf{j} = \mathbf{l} + \mathbf{s}$. The orientation of the rotational axis is usually chosen as parallel to the x -axis because it is understood to be perpendicular to the axis of symme-

try, which for $\omega=0$ is the z -axis. For higher angular momenta, one also investigates nonsymmetric single-particle potentials. Nevertheless, we require that ω is parallel to a principal axis of the potential. Therefore, the many-body Hamiltonian of the cranking model is given by ($J_x = \sum_{i=1}^A j_x^{(i)}$):

$$H_\omega = H - \omega J_x = \sum_{i=1}^A h_\omega^{(i)}, \quad (3.75)$$

where H is a sum of deformed single-particle Hamiltonians.

Within the cranking model we must now diagonalize H_ω , and the resulting ground state wave function Φ_ω is a Slater determinant. As in the normal shell model (with $\omega=0$) the question arises how the levels in the single-particle potential should be filled to obtain the lowest energy state for any given angular momentum (the yrast level). The answer to this question (given in Sec. 11.4) is that we have to minimize the energy $E' = \langle \Phi | H - \omega J_x | \Phi \rangle$, that is, we have to fill up the potential in the usual way *in the rotating frame*.

For the energy in the laboratory system, from Eq. (3.74) we get

$$E(\omega) = \langle \Phi_\omega | H | \Phi_\omega \rangle = \langle \Phi_\omega | H_\omega | \Phi_\omega \rangle + \omega \langle \Phi_\omega | J_x | \Phi_\omega \rangle. \quad (3.76)$$

Since $E(\omega)$ cannot depend on the sign of ω , one finds

$$E(\omega) = E(0) + \frac{1}{2} g_1 \omega^2 + \dots \quad (3.77)$$

and, since for $\omega=0 \langle \Phi_0 | J_x | \Phi_0 \rangle = 0$,

$$J(\omega) = \langle \Phi_\omega | J_x | \Phi_\omega \rangle = g_2 \omega + \dots \quad (3.78)$$

We can show that the constants g_1 and g_2 are equal [Sch 61],

$$g_1 = g_2, \quad (3.79)$$

using the fact that $E(\omega)$ is the lowest eigenvalue of H_ω . According to the variation principle of Ritz, we get Φ_ω as a solution of the equation

$$\delta \langle \Phi | H - \omega J_x | \Phi \rangle = 0, \quad (3.80)$$

where $|\Phi\rangle$ is any one from the family of all possible Slater determinants. The condition is also fulfilled if we take $|\Phi\rangle$ to be taken out of the set $\{\Phi_\omega\}$, where Φ_ω is an eigenfunction of $H - \omega' J_x$, and ω' runs through all real numbers. Then we find from Eq. (3.80):

$$\frac{d}{d\omega'} \langle \Phi_\omega | H | \Phi_\omega \rangle - \omega \frac{d}{d\omega'} \langle \Phi_\omega | J_x | \Phi_\omega \rangle = 0 \quad (3.81)$$

or

$$g_1 = \frac{1}{\omega} \frac{d}{d\omega} E(\omega) \Big|_{\omega=0} = \frac{d}{d\omega} J(\omega) \Big|_{\omega=0} = g_2.$$

We also derive from Eq. (3.80):

$$\omega = \frac{dE}{dJ}. \quad (3.82)$$

To have a comparison with experiment, we have to determine the value of

the angular velocity. Inglis [In 54] proposed to include the zero-point oscillations at least semiclassically by requiring

$$J = \langle \Phi_\omega | J_x | \Phi_\omega \rangle = \sqrt{I(I+1)}. \quad (3.83)$$

In first order we get

$$\omega = \frac{\sqrt{I(I+1)}}{g_1} \quad (3.84)$$

and, from (3.77),

$$E(I) = E(0) + \frac{1}{2g_1} I \cdot (I+1). \quad (3.85)$$

For higher ω -values there are deviations from this $I(I+1)$ law. In general, the moment of inertia is defined as

$$g = \frac{J}{\omega}. \quad (3.86)$$

Up to now we have investigated only completely independent particle motion, by which we mean that we have even neglected the influence of the rotation on the average field. In Section 7.7 we will show how this can be taken into account.

3.4.2 The Cranking Formula

In the case of a pure $I(I+1)$ spectrum, we need calculate only one constant, the *moment of inertia*. It is already determined by the 2^+ state and therefore it seems meaningful to apply perturbation theory for such small I -values.

We start with the unperturbed system of a deformed potential, which is filled up to the Fermi level. Levels below will be called holes (indices i, i', \dots); levels above will be called particles (indices m, m', \dots). The shell model basis consists of the ground state $|\Phi_0\rangle$, ph -states $|mi\rangle = a_m^+ a_i |\Phi_0\rangle$, $2p-2h$ states, and so on. The perturbation $\omega \cdot J_x$ is a one-particle operator and can therefore excite only one ph pair at a time. Therefore, we get for the perturbed wave function up to first order

$$|\Phi\rangle = |\Phi_0\rangle + \omega \sum_{im} \frac{\langle mi | J_x | \Phi_0 \rangle}{\epsilon_m - \epsilon_i} a_m^+ a_i |\Phi_0\rangle, \quad (3.87)$$

where ϵ_i and ϵ_m are the single-particle energies of the Hamiltonian H . The expectation value of J_x up to first order in ω is then

$$J = \langle \Phi | J_x | \Phi \rangle = 2\omega \sum_{im} \frac{|\langle mi | J_x | \Phi_0 \rangle|^2}{\epsilon_m - \epsilon_i}, \quad (3.88)$$

which, together with (3.78) gives for the moment of inertia*

$$g_{\text{Inglis}} = 2 \cdot \sum_{mi} \frac{|\langle mi | J_x | i \rangle|^2}{\epsilon_m - \epsilon_i}. \quad (3.89)$$

* In molecular physics a similar formula has been derived by Wick [Wi 48].

This is the well known *Inglis formula* for the moment of inertia [In 54, BM 55].

The moments of inertia that result from this formula are usually very close to the rigid body value of the moment of inertia [Eq. (1.49)]. In fact, we shall see in Section 3.4.3 that, in the case of a pure anisotropic oscillator, this will be an exact result. Lüders [Lü 60] showed that this is the result for any independent particle model in the limit of large particle numbers (see also [AB 59, Ro 59, SB 64, Da 75, KG 78]).

We can understand this result qualitatively, if we realize that the velocity distribution of the ground state in a deformed static potential is nearly isotropic (see Sec. 13.3), and that this fact is not changed in the rotating system by Coriolis or centrifugal forces (see [BJ 76b]). Then there is no net flow in the intrinsic system and from the laboratory frame we observe a rigid-rotation velocity distribution.

As we have seen in Section 1.5.1, the experimental moments of inertia are a factor of 2 to 3 smaller than their rigid body values. Bohr and Mottelson [BM 55, Mo 56] already indicated that residual two-body interactions would lower these values. The most important influences in this respect are the correlations of the pairing type. Since they can be included very easily within the BCS-formalism (see Chap. 6) in a single-particle description, we give here the derivation of the so-called Belyaev formula [Be 59, 61], which is the extension of the Inglis formula (3.89) that includes pairing correlations. (Readers not familiar with this formalism are referred to Chapter 6.)

In this case, $|BCS\rangle$ represents the BCS-ground state (6.31) and excitations are given by the two-quasi-particle states $\alpha_k^+ \alpha_{k'}^- |BCS\rangle$, four-quasi-particle states, etc. By analogy with Eq. (3.87), we obtain the perturbed wave function

$$|\Phi\rangle = |BCS\rangle + \omega \sum_{k < k'} \frac{\langle BCS | \alpha_k^- \alpha_{k'}^+ J_x | BCS \rangle}{E_k + E_{k'}} \alpha_k^+ \alpha_{k'}^- |BCS\rangle, \quad (3.90)$$

where $E_k + E_{k'}$ is the excitation energy of the quasi-particle pair k, k' . The quasi-particle energies are given by

$$E_k = \sqrt{(\epsilon_k - \lambda)^2 + \Delta_k^2}. \quad (3.91)$$

Proceeding as in Eqs. (3.88) and (3.89), we find for the moment of inertia

$$\mathfrak{J}_{\text{Belyaev}} = 2 \sum_{k < k'} \frac{|J_{x_{kk'}}^{(2)}|^2}{E_k + E_{k'}}. \quad (3.92)$$

From Eq. (E.16), we find $J_x^{(2)}$ and get

$$\mathfrak{J}_{\text{Belyaev}} = 2 \sum_{k, k' > 0} \frac{|\langle k | J_x | k' \rangle|^2}{E_k + E_{k'}} (u_k v_{k'} - u_{k'} v_k)^2. \quad (3.93)$$

This formula for the moment of inertia indeed yields lower values as compared to expression (3.89). Two effects are responsible for this:

- (i) The energy denominator is much larger than the particle-hole energies in Eq. (3.89). The parameter Δ [Eq. (3.91)] produces a gap of at least $2\Delta \approx 2$ MeV for the important levels in the neighborhood of the Fermi surface
- (ii) The factor $(u_k v_{k'} - u_{k'} v_k)^2$ is usually somewhat smaller than unity.

The lowering of the moment of inertia in the BCS-theory, as compared to the rigid body value, corresponds to a superfluid slippage of some nucleons as the nucleus rotates [Mi 59, 60].

Extended numerical calculations [GR 60, NP 61, MT 75] for realistic nuclei show a remarkable agreement with the experimental values. As we shall see in the next section, it is very important to apply the Inglis or the Belyaev formula to self-consistent wave functions, that is, those calculated at deformations that correspond to the energy minimum. In most of these calculations, this is achieved by using Nilsson wave functions and energies at the experimentally observed deformations as well as the experimentally determined values of the gap Δ (see also [MN 59]).

The success of these calculations, which produce roughly correct moments of inertia lying between the (too small) irrotational values and the (too large) rigid body value gives us great confidence that the picture of rotational nuclei as a deformed superfluid many-body system is correct.

Of course, we can investigate the influence of the *residual interaction* on the moment of inertia. This can be done within the framework of linear response theory (see Sec. 8.5.3 and [MSV 72]). In this kind of theory, the external field represented by the Coriolis operator J_x can excite virtual vibrations of the core which, in turn, have an influence on the moment of inertia. There are two types of such vibrations: surface oscillations (*ph* vibrations), which correspond to the stretching effect, and oscillations in the pairing correlations (*pp*-vibrations; see Sec. 8.3.5). The net result of such calculations is that both effects more or less cancel, and we get roughly the same values for the moments of inertia (Fig. 3.14) as given by the BCS theory.

We have now discussed the application of perturbation theory to the calculation of the expectation value of J_x , that is, the moment of inertia. In a similar fashion, we can calculate other properties of the rotating nucleus, for example, the *gyromagnetic ratio* g_R or the magnetic moment of the first 2^+ state. Since the magnetic moment μ is defined as the expectation value of μ_z in the state $|I, M=I\rangle$ [Eq. (B.31)] and the cranking model wave functions are not eigenfunctions of angular momentum, it is not clear at this point how to calculate μ . In Sec. 11.4, we will see that a projection technique has to be applied. In lowest order, we get a very simple result, which can be understood easily within the semiclassical picture of the cranking model:

$$\mu = \langle \Phi_\omega | \mu_x | \Phi_\omega \rangle. \quad (3.94)$$

We can therefore define the gyromagnetic ratio (1.37) by

$$\mu = g_R \cdot J = g_R \cdot \langle \Phi_\omega | J_x | \Phi_\omega \rangle. \quad (3.95)$$

From (3.90), in first order perturbation theory, we get

$$g_R = \frac{1}{\beta} \sum_{k, k' > 0} \frac{\langle \langle k | J_x | k' \rangle \langle k' | \mu_x | k \rangle + c.c.)}{E_k + E_{k'}} (u_k v_{k'} - u_{k'} v_k)^2. \quad (3.96)$$

The values calculated with these formulae are smaller than the liquid drop value $g_R = Z/A$ [Eq. (1.37)] and agree quite well with the experimental data [MSV 72].

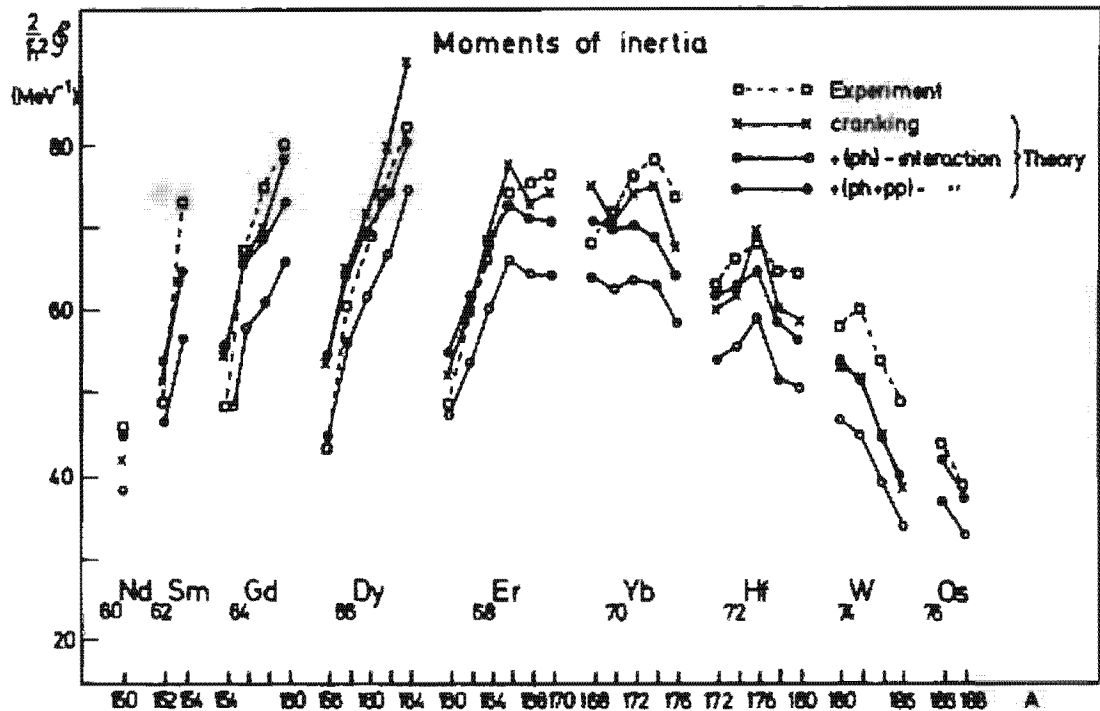


Figure 3.14. Moments of inertia in rare earth nuclei. The squares indicate experimental values [NP 61]; the crosses are obtained from the Belyaev formula (3.93). The open circles take into account only the stretching effect (ph interaction); in addition to that, the closed circles also take into account the antipairing effect (pp -interaction). (From [MSV 72].)

As we have seen in Section 3.2, deviations from the $I(I+1)$ law occur as we go to higher angular momenta. To calculate the B and C coefficients [Eq. (3.1)] connected with these deviations, one has used perturbation theory in higher order, including the effects of a residual interaction [Ma 65, Ma 67a, MR 70], so that the most important effect is the so-called Coriolis-antipairing effect, which we will discuss in Section 7.7. As we shall see, it is only at the very high spin states with $I > 30$ or 40 that one can expect the pairing correlations to vanish.

3.4.3 The Rotating Anisotropic Harmonic Oscillator

We have seen in Section 2.8.3 that the anisotropic harmonic oscillator can be solved analytically and that it provides at least a qualitative model for a deformed nucleus. It turns out that it can also be solved analytically in the rotating frame (see [Va 56, Ze 75, RBK 75, GMZ 78]), because $I_x = yp_z - zp_y$ is a quadratic form in the coordinates x, y, z and momenta p_x, p_y, p_z .

We can forget about the spin, since the potential does not depend on it (the term $-\omega s_x$ in the Coriolis operator can be diagonalized separately in the spin space and gives only a diagonal contribution). The Hamiltonian then has the form

$$h_\omega = -\frac{\hbar^2}{2m}\Delta + \frac{1}{2}m(\omega_x^2x^2 + \omega_y^2y^2 + \omega_z^2z^2) - \omega(yp_z - zp_y). \quad (3.97)$$

We introduce the creation and annihilation operators for the harmonic oscillator

bosons in x , y , and z directions a_x , a_y , and a_z :

$$\begin{aligned} x &= \left(\frac{\hbar}{2m\omega_x} \right)^{\frac{1}{2}} (a_x + a_x^+) \quad p_x = \frac{\hbar}{i} \left(\frac{m\omega_x}{2\hbar} \right)^{\frac{1}{2}} (a_x - a_x^+), \\ y &= i \left(\frac{\hbar}{2m\omega_y} \right)^{\frac{1}{2}} (a_y - a_y^+) \quad p_y = \hbar \left(\frac{m\omega_y}{2\hbar} \right)^{\frac{1}{2}} (a_y + a_y^+), \\ z &= \left(\frac{\hbar}{2m\omega_z} \right)^{\frac{1}{2}} (a_z + a_z^+) \quad p_z = \frac{\hbar}{i} \left(\frac{m\omega_z}{2\hbar} \right)^{\frac{1}{2}} (a_z - a_z^+). \end{aligned} \quad (3.98)$$

In these operators, $\hbar\omega$ is of the form

$$\begin{aligned} \hbar\omega &= \hbar\omega_x \left(a_x^+ a_x + \frac{1}{2} \right) + \hbar\omega_y \left(a_y^+ a_y + \frac{1}{2} \right) + \hbar\omega_z \left(a_z^+ a_z + \frac{1}{2} \right) \\ &\quad + \frac{\hbar\omega}{2\sqrt{\omega_x\omega_y}} \{ (\omega_y - \omega_z)(a_y^+ a_z^+ + a_y a_z) + (\omega_y + \omega_z)(a_y^+ a_z + a_z^+ a_y) \}. \end{aligned} \quad (3.99)$$

The Coriolis operator in (3.99) has two contributions. The first one creates or annihilates two oscillator quanta. Therefore, it couples shells with major quantum numbers N and $N \mp 2$.* The second part conserves the total number of quanta, but shifts quanta from the y -direction into the z -direction and vice versa.

3.4.3.1 The Inglis Formula. First we want to treat the Coriolis term in perturbation theory. In the Inglis formula (3.89), the $\Delta N = \pm 2$ part has the energy denominator $\pm \hbar(\omega_y + \omega_z)$ and the $\Delta N = 0$ part has the denominator $\pm \hbar(\omega_y - \omega_z)$. The matrix elements of a, a^+ are given in Eq. (C. 12f),

$$\langle n - l | a | n \rangle = \sqrt{n}, \quad \langle n + l | a^+ | n \rangle = \sqrt{n+1},$$

and we get, from (3.89)

$$g_{\text{Inglis}} = \frac{\hbar}{2\omega_y\omega_z} \left\{ \frac{(\omega_y - \omega_z)^2}{\omega_y + \omega_z} (N_y + N_z) + \frac{(\omega_y + \omega_z)^2}{\omega_y - \omega_z} (N_z - N_y) \right\}, \quad (3.100)$$

where the

$$N_{x, y, z} = \sum_{i=1}^A \left(a_{x, y, z}^+ + \frac{1}{2} \right), \quad (3.101)$$

satisfy the relations

$$\bar{x}^2 = \frac{1}{A} \sum_{i=1}^A \langle x^2 \rangle_i = \frac{1}{A} \frac{\hbar}{m\omega_x} \sum_{i=1}^A \left(n_x + \frac{1}{2} \right)_i = \frac{\hbar}{Am\omega_x} \cdot N_x. \quad (3.102)$$

Very important for the following discussion is the *self-consistency condition*, [BM 75], namely, that the potential (given by $\omega_x, \omega_y, \omega_z$) has the same shape as the density distribution (given by \bar{x}^2, \bar{y}^2 and \bar{z}^2):

$$\sqrt{\bar{x}^2} : \sqrt{\bar{y}^2} : \sqrt{\bar{z}^2} = \frac{1}{\omega_x} : \frac{1}{\omega_y} : \frac{1}{\omega_z}. \quad (3.103)$$

Together with Eq. (3.102), we find

$$\omega_x N_x = \omega_y N_y = \omega_z N_z = C. \quad (3.104)$$

* It vanishes for small deformations ($\omega_y \approx \omega_z$) and is therefore often neglected [ALL 76].

With this condition we can rewrite Eq. (3.100):

$$g_{\text{ring}} = \hbar \left(\frac{N_y}{\omega_y} + \frac{N_z}{\omega_z} \right). \quad (3.105)$$

The value of the moment of inertia so obtained is identical to the rigid body value. From Eq. (3.102) we get

$$g^{\text{rig}} = m \sum_{i=1}^A (\langle y^2 \rangle_i + \langle z^2 \rangle_i) = \hbar \left(\frac{N_y}{\omega_y} + \frac{N_z}{\omega_z} \right). \quad (3.106)$$

Once again, we would like to stress the point that the self-consistency condition (3.104) is crucial for this result. If we occupied the y - and z -direction with the same number of oscillator quanta ($N_y = N_z$), we would get from Eqs. (3.100) and (3.102) a value

$$g = \hbar \frac{(N_y/\omega_y - N_z/\omega_z)^2}{(N_y/\omega_y + N_z/\omega_z)} = Am \frac{(\bar{y}^2 - \bar{z}^2)^2}{\bar{y}^2 + \bar{z}^2}, \quad (3.107)$$

which is proportional to the irrotational flow value [BM 75].

3.4.3.2 Exact Solution. In the next step, we go beyond perturbation theory and diagonalize the single-particle Hamiltonian (3.99) exactly.* It is a quadratic form in the boson operators a, a^* and can therefore be diagonalized [RBK 75] in the same way as one diagonalizes quadratic forms of the RPA-type (see Chap. 8).

To diagonalize the single-particle Hamiltonian, we introduce a canonical transformation among the momenta p_y, p_z and the coordinates y, z [Va 56]:

$$\begin{aligned} Q_2 &= \alpha_2(y + \beta p_z), \\ Q_3 &= \alpha_3(z + \beta p_y), \\ P_2 &= \alpha_2^{-1}(1 - \delta\beta)^{-1}(p_y + \delta z), \\ P_3 &= \alpha_3^{-1}(1 - \delta\beta)^{-1}(p_z + \delta y), \end{aligned} \quad (3.108)$$

which guarantees that the Q_i, P_i fulfill the commutation relations of momenta and coordinates. The constants β and δ are determined by the requirement that the Hamiltonian (3.97) contains no mixed terms $P_2 Q_3$ or $P_3 Q_2$ in the new representation. The constants α_2 and α_3 normalize the new coordinates in such a way that the mass parameter is again m . In the new variables, the Hamiltonian has the form [Va 56]

$$h_\omega = \left(-\frac{P_x^2}{2m} + \frac{1}{2}m\omega_x^2 x^2 \right) + \left(-\frac{P_2^2}{2m} + \frac{1}{2}m\Omega_2^2 Q_2^2 \right) + \left(-\frac{P_3^2}{2m} + \frac{1}{2}m\Omega_3^2 Q_3^2 \right). \quad (3.109)$$

The coordinates x, Q_2, Q_3 are the normal coordinates of the problem, and the frequencies Ω_i are given by

$$\Omega_{2,3}^2 = \omega^2 + \omega_\pm^2 \pm \sqrt{\omega_-^4 + 4\omega^2\omega_+^2}, \quad (3.110)$$

with

$$\omega_\pm^2 = \frac{1}{2}(\omega_y^2 \pm \omega_z^2). \quad (3.111)$$

* For the calculation of matrix elements in this rotating oscillator basis, see [LR 77].

We can now define rotating bosons B_2^+ , B_3^+ in analogy to Eq. (3.98):

$$B_2^+ = (2\hbar m\Omega_2)^{-\frac{1}{2}}(P_2 + im\Omega_2 Q_2), \quad (3.112)$$

$$B_3^+ = -i(2\hbar m\Omega_3)^{-\frac{1}{2}}(P_3 + im\Omega_3 Q_3),$$

and obtain for the Hamiltonian

$$h_\omega = \hbar\omega_x \left(a_x^+ a_x + \frac{1}{2} \right) + \hbar\Omega_2 \left(B_2^+ B_2 + \frac{1}{2} \right) + \hbar\Omega_3 \left(B_3^+ B_3 + \frac{1}{2} \right). \quad (3.113)$$

The corresponding eigenstates

$$|n_x, n_2, n_3\rangle \propto (a_x^+)^{n_x} (B_2^+)^{n_2} (B_3^+)^{n_3} |-\rangle \quad (3.114)$$

are characterized by the numbers of rotating bosons.

Their single-particle energies are

$$\epsilon_{n_x, n_2, n_3} = \hbar\omega_x \left(n_x + \frac{1}{2} \right) + \hbar\Omega_2 \left(n_2 + \frac{1}{2} \right) + \hbar\Omega_3 \left(n_3 + \frac{1}{2} \right). \quad (3.115)$$

Assuming again a fixed occupation in a Slater determinant $|-\rangle$, that is, a fixed set of numbers N_x, N_2, N_3 defined in analogy to Eq. (3.101) for rotating bosons, we find for the total energy in the rotating frame,

$$E'(\omega) = \langle H_\omega \rangle = N_x \hbar\omega_x + N_2 \hbar\Omega_2 + N_3 \hbar\Omega_3. \quad (3.116)$$

Remembering that $\langle H_\omega \rangle$ is stationary with respect to variations of the eigenfunctions, we can calculate the expectation value of the angular momentum [RBK 75].

$$\langle L_x \rangle = -\langle \frac{\partial H_\omega}{\partial \omega} \rangle = -\frac{\partial}{\partial \omega} E' = \omega \left\{ \frac{4\omega_x^2}{\Omega_2^2 - \Omega_3^2} \left(\frac{N_3}{\Omega_3} - \frac{N_2}{\Omega_2} \right) - \left(\frac{N_2}{\Omega_2} + \frac{N_3}{\Omega_3} \right) \right\} \quad (3.117)$$

and the shape parameters x^2, y^2, z^2 ,

$$x^2 = \langle x^2 \rangle = \frac{1}{m\omega_x} \langle \frac{\partial H_\omega}{\partial \omega_x} \rangle = \frac{1}{m\omega_x} \frac{\partial E'}{\partial \omega_x}, \quad y^2 = \dots, \quad (3.118)$$

and so on. The moment of inertia is given by

$$I = \frac{\langle L_x \rangle}{\omega} = m \langle y^2 + z^2 \rangle + \frac{4\hbar}{\Omega_2^2 - \Omega_3^2} (N_3 \Omega_3 - N_2 \Omega_2). \quad (3.119)$$

For the final construction of the many-body Slater determinant, however, we have to fix the occupation numbers N_x, N_2, N_3 .

In the nonrotating case, the numbers N_x, N_y, N_z were determined by the self-consistency condition (3.104). It can be motivated by different arguments, which all give the same results at $\omega=0$. For $\omega \neq 0$ this is no longer the case. Several methods have been proposed:

(i) *Minimizing the expectation value $E'(\omega)$ in Eq. (3.116) for fixed occupation as a function of the deformation parameters ω_x, ω_y and ω_z , and the frequency ω under the constraint of constant volume ($x^2, y^2, z^2 = \text{const.}$) and fixed angular momentum $\langle L_x \rangle$ [St 78, TA 79].*

(ii) *Requiring an isotropic velocity distribution in the rotating frame [RBK 75]. This is reasonable for heavy nuclei, where there are many level crossings and one has always filled up the lowest levels in the potential (see Sec. 13.3). We then get the modified self-consistency condition*

$$N_x \omega_x = N_2 \Omega_2 = N_3 \Omega_3. \quad (3.120)$$

It can be shown that under this condition the shape of the mass distribution (given by $\bar{x}^2, \bar{y}^2, \bar{z}^2$) is proportional to the shape of the potential if one includes the centrifugal potential $\frac{1}{2}m(\omega \times r)^2$.

From Eq. (3.119) we see that the self-consistency condition (3.120) yields the rigid-body value for the moment of inertia* at the actual deformation, which may change for large I -values.

3.4.4 The Rotating Nilsson Scheme

For realistic heavy nuclei, the pure harmonic oscillator is only of a limited importance, because it does not contain the drastic energy shift of high j shell orbitals due to the $I \cdot s$ term. As we have seen in Section 3.3, they play a crucial role in the interpretation of rotational spectra in all heavy nuclei.

One therefore has extended the Nilsson model and added a Coriolis term $-\omega j_x$ to the single-particle Hamiltonian (2.89) [ALL 76, RNS 78]:

$$h'(\omega) = h - \omega j_x \quad (3.121)$$

Figure 3.15 shows the qualitative behavior of some of the single-particle levels thus obtained as a function of ω . It shows the following features.

- (i) At $\omega=0$ are the usual Nilsson levels. They are twofold degenerate with respect to time reversal symmetry ($\pm \Omega$). For $\omega \neq 0$, this symmetry is broken by the Coriolis term, and a split into two single levels is observed.
- (ii) The cranked Nilsson Hamiltonian is still invariant under a rotation of 180° around the x -axis, that is, the two levels belong to eigenstates of the operator

$$\mathcal{R}_x = e^{i\pi j_x} \quad (3.122)$$

with the eigenvalues $r_x = \pm i$ ("signature" [Bo 76a, b]).

- (iii) Some levels show an extremely strong level splitting with increasing ω . They belong to orbits with large j - and small Ω -values (e.g., $1i_{13/2}, 660\frac{1}{2}, 651\frac{1}{2}, 642\frac{1}{2}$). They show strong Ω -mixing and alignment along the x -axis (decoupled bands).
- (iv) For even nuclei at moderate angular velocities, however, pairing correlations, as discussed in Section 3.2.2. and 7.7, should be taken into account. They counteract the rotational alignment and try to keep the particles in pairwise occupied orbits. In a full microscopic description of the backbending effect, the pair correlations must be taken into account self-consistently (see Sec. 7.7).
- (v) For large frequencies, the alignment effect brings levels from higher major shells down into the neighborhood of the Fermi surface.

* It has recently been shown [FR 76b] that electrons confined by a harmonic potential and submitted to a constant magnetic field are rotating uniformly around the axis formed by the field; this is the analogous effect to the rigid body value of the moment of inertia discussed here.

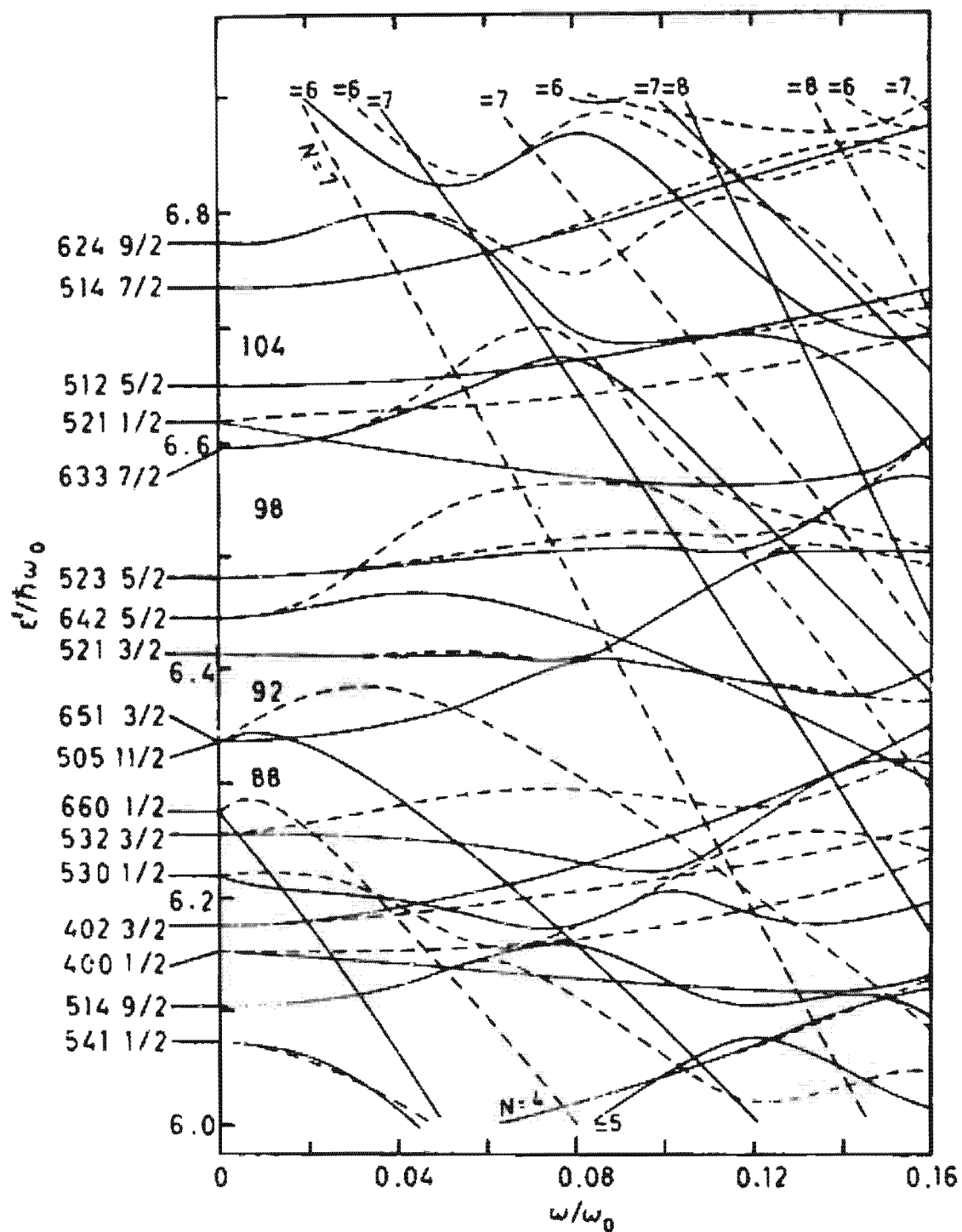


Figure 3.15. Qualitative behavior of the single-particle levels in a cranked Nilsson model at a prolate deformation ($\delta = 0.25$) as a function of the cranking frequency ω in units of $\hbar\omega_0$. Dashed lines correspond to levels with different r_x -quantum numbers. (We are grateful to Dr. R. Bengtsson for the preparation of this figure.)

- (vi) Eventually, new shell closures with new magic numbers develop at high angular momenta, which can influence the energy surface for the fission process (see Sec. 3.4.5).

3.4.5 The Deformation Energy Surface at High Angular Momenta

As we already discussed in Section 2.9, the pure Nilsson model cannot be used for the calculation of total energies nor for the calculation of the shape of the energy surfaces at large deformations, because the average part of the energy is not reproduced in a proper way within this model. Therefore, we calculate only the oscillating part of the deformation energy within this model and replace the smooth part by the liquid drop energy at the same deformation.

In the same way, we can calculate energy surfaces at a fixed angular momentum I as a function of the deformation. For an ellipsoidal shape [characterized by the parameters β and γ (Eq. 1.88)], the total energy is then given by

$$E(\beta, \gamma, I) = E_{\text{LDM}}(\beta, \gamma, I) + E_{\text{sh}}(\beta, \gamma, I) - \tilde{E}_{\text{sh}}(\beta, \gamma, I). \quad (3.123)$$

Here E_{LDM} is the deformation energy at a rotating ellipsoid with the rigid-body moment of inertia $I_{\text{rig}}(\beta, \gamma)$, because one assumes that at high angular momenta pairing correlations can be neglected.* E_{sh} is the shell model energy and is obtained by summing up the single-particle energies. \tilde{E}_{sh} is the averaged part of it, and is calculated by an appropriate smoothing procedure (see Sec. 2.9).

There are two ways to derive these quantities from the diagonalization of a deformed single-particle potential in the rotating frame: Work either at constant frequency ω [NPF 76] or at constant angular momentum I [ALL 76]. Both methods agree, if one uses a deformed Wood-Saxon potential, where the averaged moment of inertia is very close to the rigid-body value† [BJ 76b, NTP 77].

Several groups have carried out investigations along this line [BLL 75, NP 75, NPF 76, ALL 76, FDG 76, NTP 77] in many regions of the periodic table. Qualitatively they have found similar results:

- (i) For spherical or *weakly deformed nuclei* at the beginning of the rare earth region, the nuclei behave similarly to the classical liquid drop (Fig. 1.18): Up to angular momentum $I = 50-70\hbar$ they are oblate and rotate around the symmetry axis. In this region, the rotation is

* In fact, multiplicity measurement of the γ -cascade indicates the nucleus reaches the rigid-body moment of inertia at high spin values [SBC 76].

† The I^2 term in the Nilsson potential (2.89) is non-local and gives contribution to the effective mass. It produces an averaged moment of inertia which is $\sim 30-40\%$ larger than the rigid body value [Ty 70, 71, BR 71b, Je 73]. One has used scaling procedures to compensate for this effect [NTP 77].

not collective and one expects yrast traps (see Sec. 3.4.7). For higher I -values they rapidly change the shape to triaxial and prolate deformations (Jacobi-shapes; see Sec. 1.7). This transition corresponds to a drastic increase of the angular momentum ("giant backbending") as shown in Fig. 3.16. Finally, the nucleus fissions.

- (ii) Nuclei in the *middle of the rare earth region* start at low I -values at prolate shapes and rotate around an axis perpendicular to the symmetry axis. With increasing rotation the Coriolis force aligns more and more particles parallel to this axis, and at $I \sim 40-50$ we find a transition to triaxial and sometimes even oblate shapes,* as in Fig. 3.17. At very high angular momenta the nucleus again becomes triaxial and finally fission takes place.

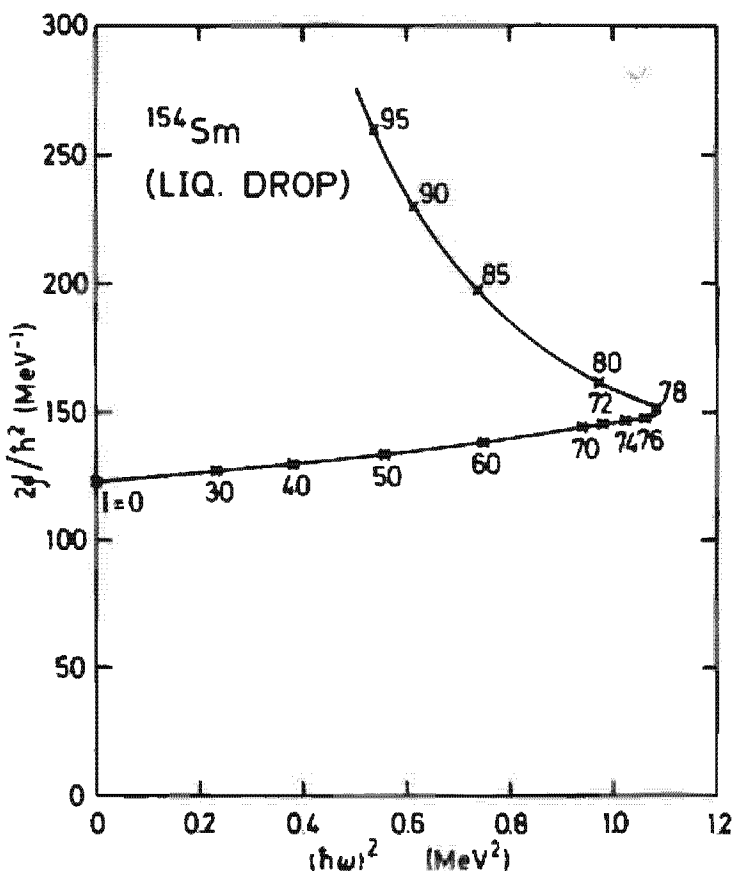


Figure 3.16. Backbending plot for the yrast spectrum of ^{154}Sm in terms of the rotating liquid drop model. (From [ALL 76].)

We want to conclude this section with the remark that such calculations can only give a qualitative impression of the behavior of the nuclear many-body system at such high angular momenta. Only for very low excitations and for energy surfaces with deep minima can we expect the nucleus to have a fixed deformation. In general, it will carry out quantum mechanical zeropoint fluctuations around these minima which ought to be described by a dynamical theory (see, for instance, Chap. 10).

* In calculations based on a Wood-Saxon potential [NTP 77], the nucleus does not reach such drastic γ -deformations, and fissions without having obtained an oblate shape.

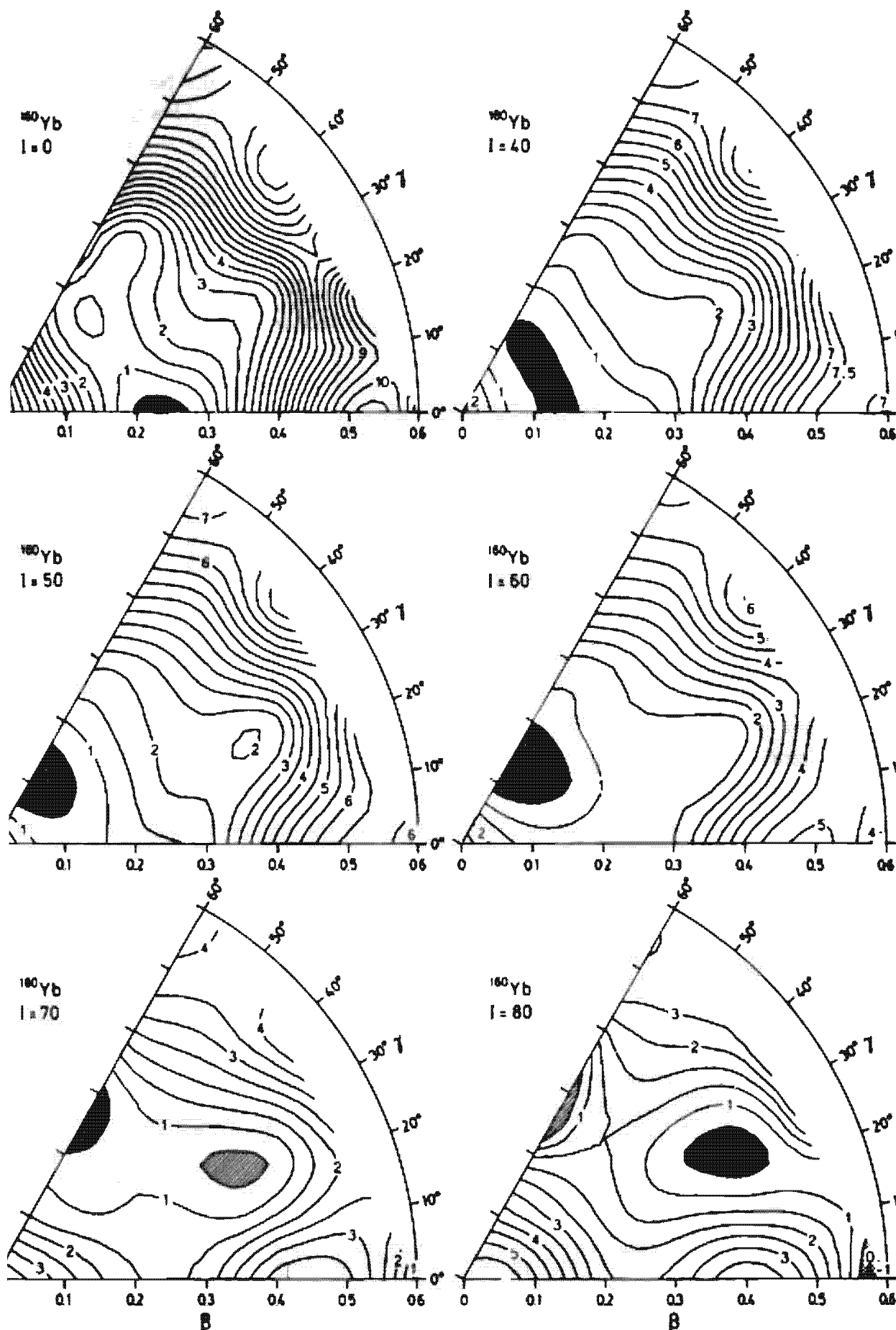


Figure 3.17. Potential energy surfaces in the (β, γ) plane with inclusion of shell corrections for ^{160}Yb as a function of angular momentum. (From [All 76]. Notice that these authors replace the Hill-Wheeler coordinate γ by $-\gamma$.)

3.4.6 Rotation about a Symmetry Axis

As we have seen in the last sections, there are regions in the periodic table where we find nuclei "rotating" around the symmetry axis. This happens in particular at the beginning and end of each major shell. At the beginning of each shell are a few particles sitting on a more or less spherical core. To create a large amount of angular momentum they all must align along the rotational axis (the x -axis), that is, classically speaking these particles have to run in the equatorial plane around the nucleus and produce an oblate density distribution.*

Such a configuration is certainly not collective rotation, since there are only a few particles involved. Each single particle wavefunction is an eigenfunction of j_x with the eigenvalue α_i . The component of the total angular momentum in the direction of the symmetry axis is given by

$$\langle J_x \rangle = \sum_{i=1}^A \alpha_i \quad (3.124)$$

To increase the angular momentum we have to change the occupation in the deformed well and to put particles from levels with lower (for instance negative) α -values into those with higher (positive) α -values.

Formally, this can be done again by a cranking procedure around the symmetry axis. Since the operator j_x commutes with h , we get the *single-particle energies in the "rotating frame."*

$$\epsilon'_i = \epsilon_i - \omega \alpha_i, \quad (3.125)$$

where ϵ_i are the eigenvalues of h in the nonrotating frame. These are straight lines as a function of ω (Fig. 3.18a) whose slope is given by

$$\frac{d\epsilon'_i}{d\omega} = -\alpha_i. \quad (3.126)$$

The condition to minimize the energy in the rotating frame

$$E' = \sum_{i=1}^A (\epsilon'_i - \omega \alpha_i) \quad (3.127)$$

guarantees that one always occupies the lowest levels ϵ'_i . With increasing frequency ω we thus obtain a stepwise increasing of the angular momentum (Fig. 3.18b). The distance between two steps and the size of the steps is given by the distances of the levels ϵ_i and the angular momentum values α_i . Therefore there is a statistical increase of the angular momentum with the frequency ω . The *moment of inertia* \mathfrak{g} is defined only on the average (dashed line in Fig. 3.18b).

To get an estimate for the size of this moment of inertia [Bo 76b], we realize that each line in Fig. 3.18a has the slope $-\alpha_i$ (increasing or

* At the end of a major shell similar arguments can be applied for holes. We then end up with a rotation about the symmetry axis of a prolate density distribution. In the middle of a shell there are many valence particles forming a prolate deformed shape. It is easy to generate large angular momentum from a few alignment processes, without too drastic changes in deformation.

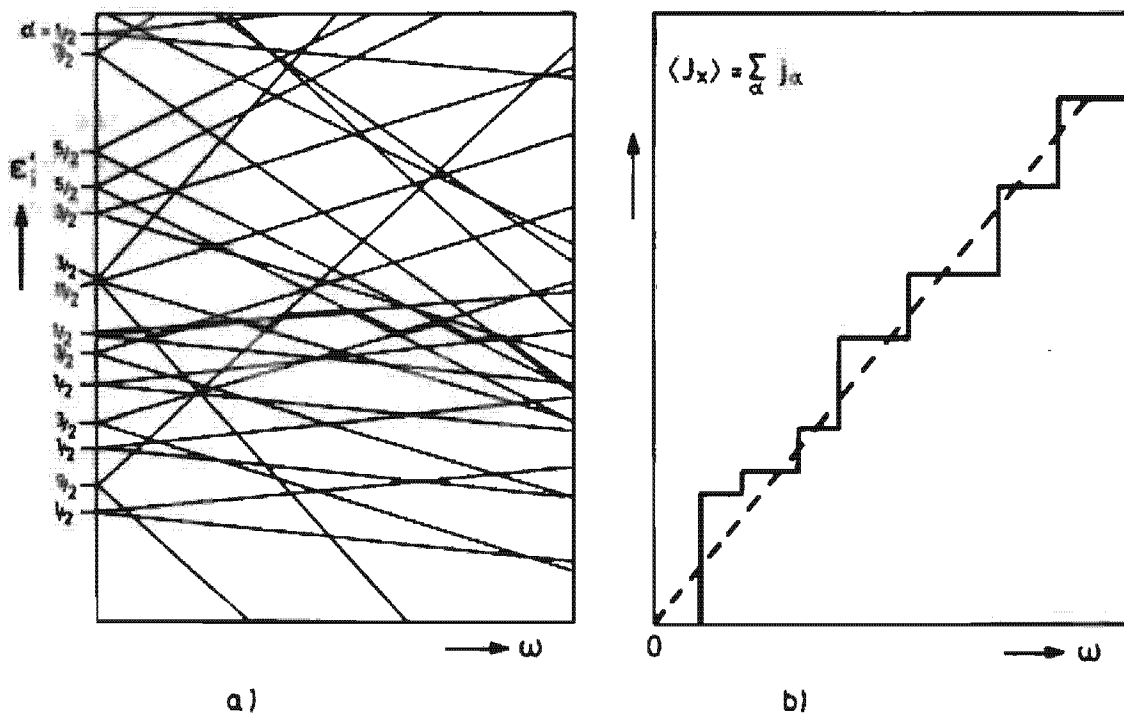


Figure 3.18. (a) Schematic representation of the eigenvalues ϵ' in Eq. (3.125) as a function of the cranking frequency. (b) The angular momentum $\langle J_x \rangle$ obtained by increasing values of ω and by always occupying the lowest levels in (a).

decreasing, depending on the sign of α). For $\omega=0$ the levels $\pm\alpha$, are all occupied pairwise. The resultant angular momentum vanishes. For finite ω some of these levels with negative α are no longer occupied, but other downward-coming levels with positive α -values are occupied anew. For a fixed value of α (for instance $\alpha = \frac{1}{2}$) the number of newly occupied levels is on the average $\omega g(\alpha)$, where $g(\alpha)$ is the density of levels with the quantum number α . Therefore, we obtain for the angular momentum on the average

$$\langle J_x \rangle_{av} = \sum_{i \leq \epsilon_s} \alpha_i = \sum_{\alpha} \alpha \cdot \omega \cdot \alpha \cdot g(\alpha) = \omega \sum_{\alpha} \alpha^2 \cdot g(\alpha), \quad (3.128)$$

and for the average moment of inertia

$$g_{av} = \sum_{\alpha} \alpha^2 g(\alpha). \quad (3.129)$$

An evaluation of this quantity within the Thomas-Fermi approximation gives exactly the rigid-body value for the moment of inertia [Bo 76b]. On the average, "single-particle" rotation around the symmetry axis therefore shows quite a similar behavior to collective rotation, although the internal structure is completely different.

3.4.7 Yrast Traps

Since the level spacing in the case of a rotation around the symmetry axis has a statistical character, one expects *yrast traps* (high spin isomeric states). They are defined as yrast states which cannot undergo a rapid γ -transition and have been predicted by Bohr and Mottelson [IBM 74].

Filling the levels in the rotating well always from the bottom, we eventually obtain, with increasing angular velocity, jumps in the angular momentum by several units (see Fig. 3.18b). This can be visualized most easily in a representation of the eigenvalues ϵ_i in the nonrotating oblate deformed Nilsson well as a function of the components α of the angular momentum along the symmetry axis (Fig. 3.19). For small deformations we have rather pure j -configurations. The eigenvalues ϵ_i for levels in the same j -shell lie on approximate parabolas [see Eq. (3.39); we have only to replace Ω by α]. At oblate deformations ($\beta < 0$) the highest α -values, that is, the most aligned states, have the deepest energy, because their oblate density distribution in the equatorial plane has the maximal overlap with the oblate density of the core.

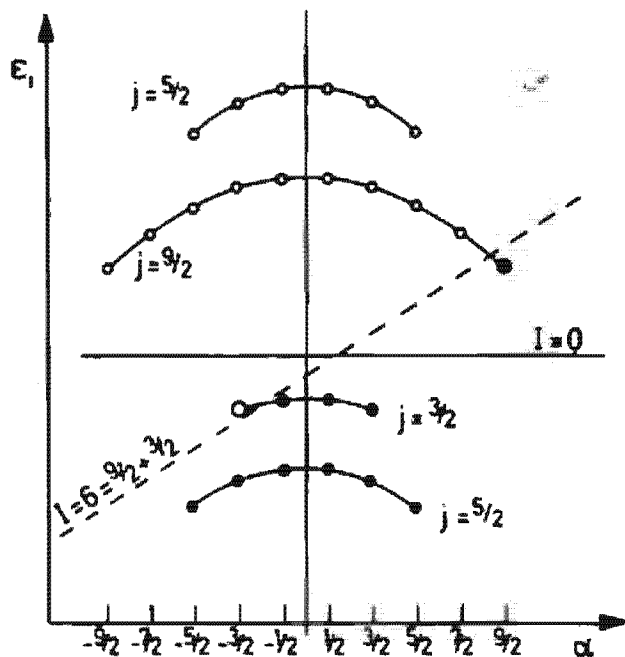


Figure 3.19. Schematic representation of the single-particle energies ϵ_i in an oblate deformed Nilsson well as a function of α (the eigenvalue of j_x) with the Fermi surface at $I = 0$ (full line) and at $I = 6$ (dashed line).

At $\omega = 0$, the Fermi surface is a horizontal line and all levels below it are occupied. At finite ω -values, according to Eq. (3.125), the Fermi level in the rotational frame has a slope ω . As the value of ω increases, levels with negative α -values are vacated and those with positive α -values are newly occupied. In Fig. 3.19 we show a situation where a jump of 6 units of angular momentum occurs. The remaining I -values on the yrast line can be obtained by constructing ph -configurations with respect to the rotated energy surface. This is usually connected with an increase in energy.

Therefore, it may happen that the yrast line is no longer a monotonically increasing function of I , and a certain level with $I = I_0$ can have a deeper energy than the neighboring levels with $I = I_0 - 1, I_0 - 2, \dots$. A fast γ transition of $E1$ -, $E2$ -, $M1$ - or $M2$ -character (i.e., with low multipolarity; see Appendix B) is then not allowed (so-called *energy spin traps*).

Even if this is not the case, the internal structure of the states with $I_0 - 1, I_0 - 2$ might be rather different from the structure of the state I_0 . Then the transition matrix elements can be very small and the lifetime of the state I_0 is very large (*structure spin traps*). Examples are cases where the states with $I_0 - 1$ or $I_0 - 2$ can only be reached from the state I_0 by a $2p-2h$ excitation, or cases where the γ -transition matrix element is hindered by the intrinsic selection rules of the single-particle wave functions (for instance, I -forbidden $M1$ -transitions; see Sec. 2.7.2.).

Several groups have investigated the theoretical possibility of yrast traps by searching for cases of rotation around the symmetry axis in the energy surfaces at high angular momenta and by investigating the detailed single-particle structure in these cases [ALL 76, CDS 77, AK 77, DNM 77, PFL 78, PTF 78, AHL 78, Ab 78, MDN 78]. Some regions in the periodic table have been found in which they should be expected. These are mostly weakly deformed nuclei such as Te, Ba, Ce, Sm, neutron deficient rare earth isotopes, and nuclei in the Pb-region.

On the *experimental side* we have known for a long time about states with large angular momenta and very long lifetimes for spherical nuclei. These are states with rather pure high j -shell configurations, which have no allowed γ -transition matrix elements of low multipolarity to other states at deeper energy. The most famous example [PAG 62] is the 18^+ isomer in ^{212}Po with a lifetime of 45 sec, which consists of an aligned $(\pi h_{9/2})^2(\nu i_{11/2})^2$ configuration.

Another group of high spin isomers, usually called *K-isomers*, were observed in well deformed nuclei, such as the $4s$ and the $3ly$ isomers in ^{178}Hf , which can be interpreted as a $K'' = 8^-$ and a $K'' = 16^+$ band head, whose γ -decay is *K*-forbidden [HR 68, KL 77].

Finally, in recent years an island of about 20 adjacent nuclei in the light rare earth region with long lived isomers has been found [PBB 77]. They are probably associated with oblate deformation and "single-particle" rotation [AHL 78].

The properties of nuclei in the vicinity of ^{208}Pb have usually been studied in terms of the spherical shell model with residual interaction and a proper angular momentum coupling. Since these configurations are rather pure, some calculations of this type could explain measured excitation energies with extraordinary accuracy [BBH 77].

The physical reason for the aligned high spin configurations having such a long lifetime is the same in this picture as we have explained in the model of rotations around a symmetry axis: Two nucleons with aligned spins gain energy because their residual interaction is largest for wave functions with a large spacial overlap* (see Sec. 4.4.8.). Therefore, these high spin levels are lower in energy than the neighboring states with smaller I -values, and fast γ -transitions are forbidden. In the description of

* This effect has been called the MONA-effect (Maximal Overlap of the Nuclear wave function by Alignment [FPD 76]).

these nuclei by the mean field approach in a rotation about a symmetry axis, the same effect shows up in the fact that (as discussed in Fig. 3.18) aligned levels with maximal α -values and oblate density distribution are shifted downwards in energy because of their large overlap with the oblate core.

Both methods—shell model calculations in a spherical basis based on angular momentum coupling techniques and cranking calculations in a slightly deformed well—are certainly hard to compare. The spherical shell model is certainly much better (though it takes more effort) as long as one can assume the spherical core to be inert, otherwise one has to take into account multiparticle-multipole configurations. It is therefore limited to the very close vicinity of magic nuclei. On the other side, the cranking model treats the residual interaction by a deformed well and is therefore much easier to handle over a wide range of nuclei. It allows, however, only very qualitative predictions, since it violates conservation of angular momentum and is microscopically derived only in the regions of well deformed nuclei with rotations perpendicular to the symmetry axis (see Sec. 11.4).

CHAPTER 4

Nuclear Forces

4.1 Introduction

Up to now we have only taken into account the forces acting between nucleons in a very qualitative way. We have used some of their properties—such as their short range and saturation character—to explain the volume and surface terms in the liquid drop model. We have also assumed that they give rise to an average single-particle potential. By adjusting a few parameters, we are able to reproduce a large quantity of experimental data. The success of these phenomenological models gives us the confidence to go a step further and investigate the nuclear many-body problem from a more microscopic point of view. In particular, we wish to apply the techniques of modern many-body theory.

The starting point for all these considerations is obviously the two-body interaction between nucleons. There are three basic assumptions in this concept:

- (i) Dynamical mesonic degrees of freedom can be neglected and the nucleus can be described as a system of A nucleons whose interaction can be represented by a potential.
- (ii) Relativistic effects are negligible.
- (iii) Only two-body forces are important.

Even with these rather drastic assumptions, we immediately run into two difficulties when we try to proceed in the way we have discussed:

these nuclei by the mean field approach in a rotation about a symmetry axis, the same effect shows up in the fact that (as discussed in Fig. 3.18) aligned levels with maximal α -values and oblate density distribution are shifted downwards in energy because of their large overlap with the oblate core.

Both methods—shell model calculations in a spherical basis based on angular momentum coupling techniques and cranking calculations in a slightly deformed well—are certainly hard to compare. The spherical shell model is certainly much better (though it takes more effort) as long as one can assume the spherical core to be inert, otherwise one has to take into account multiparticle-multipole configurations. It is therefore limited to the very close vicinity of magic nuclei. On the other side, the cranking model treats the residual interaction by a deformed well and is therefore much easier to handle over a wide range of nuclei. It allows, however, only very qualitative predictions, since it violates conservation of angular momentum and is microscopically derived only in the regions of well deformed nuclei with rotations perpendicular to the symmetry axis (see Sec. 11.4).

CHAPTER 4

Nuclear Forces

4.1 Introduction

Up to now we have only taken into account the forces acting between nucleons in a very qualitative way. We have used some of their properties—such as their short range and saturation character—to explain the volume and surface terms in the liquid drop model. We have also assumed that they give rise to an average single-particle potential. By adjusting a few parameters, we are able to reproduce a large quantity of experimental data. The success of these phenomenological models gives us the confidence to go a step further and investigate the nuclear many-body problem from a more microscopic point of view. In particular, we wish to apply the techniques of modern many-body theory.

The starting point for all these considerations is obviously the two-body interaction between nucleons. There are three basic assumptions in this concept:

- (i) Dynamical mesonic degrees of freedom can be neglected and the nucleus can be described as a system of A nucleons whose interaction can be represented by a potential.
- (ii) Relativistic effects are negligible.
- (iii) Only two-body forces are important.

Even with these rather drastic assumptions, we immediately run into two difficulties when we try to proceed in the way we have discussed:

(I). There exists no derivation of the *nucleon–nucleon force* from first principles. Though this should be possible in principle with the modern theory of gauge fields for quarks and gluons, attempts in this direction are only in their infancy [De 78]. On the other hand, theories that start out from an effective Lagrangian for interacting mesons and nucleons have recently proved quite successful (see, for example, [CLL 73, LLR 75, DSB 77, Vi 78, Ho 80]). The basic ingredient is the pion–nucleon coupling constant, which is known from experiment. The nucleon–nucleon force is obtained without a free parameter for particle distances greater than 0.8 fm. The part from 0 to 0.8 fm is represented by a phenomenological potential containing six parameters in each isospin channel. Excellent fits to the measured nucleon–nucleon phase shifts are achieved.

The potentials used until now have been almost entirely phenomenological (besides the Yukawa part resulting from the one-pion exchange; see below) and contain up to about 50 parameters. The experimental phase shifts are also very well reproduced with these potentials. On the basis of these forces, which we shall discuss very briefly in Section 4.2.2, we should be able to apply the method of many-body theory and to derive the phenomenological properties discussed in the preceding chapters in a quantitative way.

(II). There is, however, a second difficulty in nuclear theory. These bare nuclear forces are, from a numerical point of view, very ill behaved. They show strong repulsion at short distances (hard core) and cannot be treated straightforwardly by the usual many-body techniques. For instance, they are too strong to be treated by perturbation theory and the hard core makes a direct self-consistent field approach (see Chap. 5), for example, impossible. In fact, the nucleons within a nucleus do not feel the bare nucleon–nucleon interaction. Taking into account that they interact with one another in the presence of many other nucleons permits one to introduce an *effective nucleon–nucleon interaction*, which is rather well behaved and allows application of the usual many-body methods, such as Hartree–Fock theory (Chap. 5). Much work has been done to derive this effective interaction from the bare nucleon–nucleon force. We will in Sec. 4.3 discuss the basic ideas that have been used to achieve this goal. As a result, a great deal has been learned about the properties and the structure of these effective forces. However, in order to reproduce experimental data quantitatively one still needs phenomenological renormalization parameters, and from this point of view the theory is not yet very satisfying.

In most of the so-called microscopic descriptions of the nucleus one uses *phenomenological effective forces*, which are constructed on the basis of these considerations, but depend on some parameters that are adjusted to fit experimental data.

In this chapter we do not want to go into such attempts to derive the bare nucleon–nucleon force [BJ 76a]. In the second section we will discuss

some invariance principles that should be obeyed by the bare forces and which already allow one to draw some conclusions about their analytical structure. In the third section, we briefly present the microscopic description of effective interactions and discuss their properties and their field of application. The fourth section presents a number of phenomenological potentials that have been used to represent the residual interaction between the nucleons moving in a given average potential.

We wish to emphasize that in this chapter we are only dealing with the nuclear interaction. The *Coulomb interaction* has to be treated separately. When a comparison with experimental data is required one has always to subtract Coulomb effects first.

4.2 The Bare Nucleon–Nucleon Force

4.2.1 General Properties of a Two-Body Force

The most general quantum mechanical two-body potential V is completely specified by its matrix elements between two-body states (in a coordinate representation $|\mathbf{r}_1, s_1, t_1; \mathbf{r}_2, s_2, t_2\rangle$; where $s_i = \pm \frac{1}{2}$ and $t_i = \pm \frac{1}{2}$ are spin and isospin coordinates) as:

$$\langle \mathbf{r}'_1 s'_1 t'_1 | \mathbf{r}'_2 s'_2 t'_2 | V | \mathbf{r}_1 s_1 t_1 | \mathbf{r}_2 s_2 t_2 \rangle. \quad (4.1)$$

The space of two-particle states $|\mathbf{r}_1, s_1, t_1; \mathbf{r}_2, s_2, t_2\rangle$ is a product space of the coordinate wave functions $|\mathbf{r}_1\rangle$ and $|\mathbf{r}_2\rangle$ and the spin and isospin vectors $|s_1\rangle, |s_2\rangle$ and $|t_1\rangle, |t_2\rangle$. Since any operator in the spin space of one particle can be represented as a linear combination of the spin matrices $\sigma_1, \sigma_2, \sigma_3$ and the unity matrix $\sigma_0 = 1$, the most general form of the operator V is

$$V = \sum_{i, k=0}^3 V_{ik} \sigma_i^{(1)} \sigma_k^{(2)}. \quad (4.2)$$

The function V_{ik} also depends analogously on the isospin operators $\tau^{(1)}$ and $\tau^{(2)}$. In addition to this isospin dependence, the V_{ik} are, in general, integral operators in coordinate space

$$V |\mathbf{r}_1 \mathbf{r}_2\rangle = \int V(\mathbf{r}'_1, \mathbf{r}'_2, \mathbf{r}_1, \mathbf{r}_2) |\mathbf{r}'_1 \mathbf{r}'_2\rangle d^3 r'_1 d^3 r'_2. \quad (4.3)$$

In the special case in which $V(\mathbf{r}'_1, \mathbf{r}'_2, \mathbf{r}_1, \mathbf{r}_2)$ has the form

$$V(\mathbf{r}_1, \mathbf{r}_2, \mathbf{r}'_1, \mathbf{r}'_2) = \delta(\mathbf{r}_1 - \mathbf{r}'_1) \delta(\mathbf{r}_2 - \mathbf{r}'_2) V(\mathbf{r}_1, \mathbf{r}_2) \quad (4.4)$$

V is called a *local potential*, and we have

$$V |\mathbf{r}_1 \mathbf{r}_2\rangle = V(\mathbf{r}_1, \mathbf{r}_2) |\mathbf{r}_1 \mathbf{r}_2\rangle. \quad (4.5)$$

In this case the interaction between the two particles depends only on the points \mathbf{r}_1 and \mathbf{r}_2 (and eventually on the spin and isospin). It does not, for instance, depend on the velocity of the particles.

We shall show that, in general, nonlocal potentials correspond to a velocity dependence. We therefore expand*

$$\begin{aligned} |\mathbf{r}'_1, \mathbf{r}'_2\rangle &= |\mathbf{r}_1 \mathbf{r}_2\rangle + (\mathbf{r}'_1 - \mathbf{r}_1) \frac{\partial}{\partial \mathbf{r}_1} |\mathbf{r}_1 \mathbf{r}_2\rangle + (\mathbf{r}'_2 - \mathbf{r}_2) \frac{\partial}{\partial \mathbf{r}_2} |\mathbf{r}_1 \mathbf{r}_2\rangle + \dots \\ &=: \exp \left\{ (\mathbf{r}'_1 - \mathbf{r}_1) \frac{\partial}{\partial \mathbf{r}_1} + (\mathbf{r}'_2 - \mathbf{r}_2) \frac{\partial}{\partial \mathbf{r}_2} \right\} : |\mathbf{r}_1 \mathbf{r}_2\rangle \end{aligned} \quad (4.6)$$

and get, from (4.3),

$$\begin{aligned} V|\mathbf{r}_1 \mathbf{r}_2\rangle &= \int V(\mathbf{r}'_1, \mathbf{r}'_2, \mathbf{r}_1, \mathbf{r}_2) \exp \left\{ \frac{i}{\hbar} (\mathbf{r}'_1 - \mathbf{r}_1) \mathbf{p}_1 + \frac{i}{\hbar} (\mathbf{r}'_2 - \mathbf{r}_2) \mathbf{p}_2 \right\} |\mathbf{r}_1 \mathbf{r}_2\rangle d^3 r'_1 d^3 r'_2 \\ &= \tilde{V}(\mathbf{r}_1, \mathbf{p}_1, \mathbf{r}_2, \mathbf{p}_2) |\mathbf{r}_1 \mathbf{r}_2\rangle. \end{aligned} \quad (4.7)$$

This means that the most general potential can be represented by Eq. (4.2) where the V_{ik} are operators in coordinate space of the form (4.7) (for reasons of simplicity we neglected the isospin dependence).

In the following we investigate the symmetry properties of such potentials $V(1, 2) = V(\mathbf{r}_1, \mathbf{p}_1, \sigma^{(1)}, \tau^{(1)}, \mathbf{r}_2, \mathbf{p}_2, \sigma^{(2)}, \tau^{(2)})$. The form of this general function can, however, be restricted by requiring the imposition of a number of symmetries.

In particular, we require the following eight symmetries:

(I) Hermiticity

(II) Invariance under an exchange of the coordinates

$$V(1, 2) = V(2, 1). \quad (4.8)$$

This property is strongly connected with the symmetry of the two-particle wave function $|12\rangle$. Since nucleons are fermions, they have to be totally antisymmetric. For example, if we take a product wave function built out of ordinary space, a spin and an isospin part

$$\langle \mathbf{r}_1 s_1 t_1, \mathbf{r}_2 s_2 t_2 | 12 \rangle = \varphi(\mathbf{r}_1, \mathbf{r}_2) \chi(s_1, s_2) \zeta(t_1, t_2) \quad (4.9)$$

we have four combinations compatible with the Pauli principle, which are characterized by the symmetry of the coordinate space and spin part (Table 4.1). The isospin component is determined in each case by requiring the antisymmetry of the total wave function (4.9).

* :: means *normal ordering*, i.e., the derivatives $\partial/\partial \mathbf{r}_i$ should not act on the coordinates \mathbf{r}_i in the expansion of the exponent.

Table 4.1 Characterization of the symmetries of the two-particle state (4.9)

Ψ	χ	abbreviation	ζ
even	singlet	es	+
even	triplet	et	-
odd	singlet	os	-
odd	triplet	ot	+

(iii) **Translational invariance.** The potential depends on the relative coordinate $\mathbf{r} = \mathbf{r}_1 - \mathbf{r}_2$ only

$$V(1, 2) = V(\mathbf{r}, \mathbf{p}_1, \sigma^{(1)}, \tau^{(1)}, \mathbf{p}_2, \sigma^{(2)}, \tau^{(2)}). \quad (4.10)$$

(iv) **Galilean invariance.** The potential is not changed by a transformation to a system which moves with constant velocity, that is, it depends only on the relative momentum $\mathbf{p} = \frac{1}{2}(\mathbf{p}_1 - \mathbf{p}_2)$:

$$V(1, 2) = V(\mathbf{r}, \mathbf{p}, \sigma^{(1)}, \tau^{(1)}, \sigma^{(2)}, \tau^{(2)}). \quad (4.11)$$

(v) **Invariance under space reflection.** Contrary to the weak interaction, there is no parity violation for strong interactions:

$$V(\mathbf{r}, \mathbf{p}, \sigma^{(1)}, \tau^{(1)}, \sigma^{(2)}, \tau^{(2)}) = V(-\mathbf{r}, -\mathbf{p}, \sigma^{(1)}, \tau^{(1)}, \sigma^{(2)}, \tau^{(2)}). \quad (4.12)$$

(vi) **Time reversal invariance** guarantees that the equations of motion do not depend on the direction in which the time evolves (for details, see [Me 61])

$$V(\mathbf{r}, \mathbf{p}, \sigma^{(1)}, \tau^{(1)}, \sigma^{(2)}, \tau^{(2)}) = V(\mathbf{r}, -\mathbf{p}, -\sigma^{(1)}, \tau^{(1)}, -\sigma^{(2)}, \tau^{(2)}). \quad (4.13)$$

(vii) **Rotational invariance in coordinate space.** Rotations in three-dimensional coordinate space act not only on the vectors \mathbf{r} and \mathbf{p} but also on the spin matrices $\sigma = 2 \cdot \mathbf{s}$. With respect to spin, the operator V has the form (4.2). It has to be a scalar under a rotation in coordinate space, which means in particular that V_{00} has to be a scalar. There exist three independent scalars which we can construct from the two vectors \mathbf{r} and \mathbf{p} , namely $\mathbf{r}^2, \mathbf{p}^2$ and $\mathbf{r} \cdot \mathbf{p} + \mathbf{p} \cdot \mathbf{r}$. However, the latter expression can only appear quadratically because of time reversal invariance (vi). It is more convenient to express $(\mathbf{r} \cdot \mathbf{p} + \mathbf{p} \cdot \mathbf{r})^2$ through $\mathbf{r}^2, \mathbf{p}^2$ and $\mathbf{L}^2 = (\mathbf{r} \times \mathbf{p})^2$. V_{00} can then be written as a function of $\mathbf{r}^2, \mathbf{p}^2$ and \mathbf{L}^2 . Because of invariance (ii) and (v) we find

$$V(\mathbf{r}, \mathbf{p}, \sigma^{(1)}, \sigma^{(2)}) = V(\mathbf{r}, \mathbf{p}, \sigma^{(2)}, \sigma^{(1)}). \quad (4.14)$$

The terms in (4.2) that are linear in $\sigma^{(1)}$ therefore depend only on

$$\mathbf{S} = \frac{1}{2}(\sigma^{(1)} + \sigma^{(2)}). \quad (4.15)$$

To form a scalar, \mathbf{S} has to be multiplied by a vector, which is invariant under space reflection. Only \mathbf{L} fulfills this requirement

$$\mathbf{L} \cdot \mathbf{S} = \frac{1}{2}\mathbf{L}(\sigma^{(1)} + \sigma^{(2)}) \quad (4.16)$$

The quadratic terms in σ in Eq. (4.2) form a tensor. It can be decomposed into a scalar $\sigma^{(1)} \cdot \sigma^{(2)}$, a vector $\sigma^{(1)} \times \sigma^{(2)}$, and a symmetric tensor with vanishing trace $(\sigma_i^{(1)}\sigma_k^{(2)} + \sigma_k^{(1)}\sigma_i^{(2)})/2 - \frac{1}{3}\delta_{ik}$. Because of (4.14), $\sigma^{(1)} \times \sigma^{(2)}$ cannot appear. As shown by Okubo and Marshak [OM 58], the only possible independent combinations are

$$\begin{aligned} & \sigma^{(1)}\sigma^{(2)}, (\mathbf{r}\sigma^{(1)})(\mathbf{r}\sigma^{(2)}), (\mathbf{p}\sigma^{(1)})(\mathbf{p}\sigma^{(2)}), \\ & (\mathbf{L}\sigma^{(1)})(\mathbf{L}\sigma^{(2)}) + (\mathbf{L}\sigma^{(2)})(\mathbf{L}\sigma^{(1)}). \end{aligned} \quad (4.17)$$

Each of these terms can be multiplied by an arbitrary function of $\mathbf{r}^2, \mathbf{p}^2$ and \mathbf{L}^2 .

(viii) **Rotational invariance in isospin space.** Within the isospin formalism, protons and neutrons are considered as quantum states of one elementary particle that

form a doublet (see Sec. 2.6.3) with isospin $\frac{1}{2}$. The two-dimensional representation of the rotational group reproduces all their transformation properties. Rotations within the isospin space (as long as they are not around the 3-axis) produce mixtures of protons and neutrons. Rotational invariance of the nuclear force therefore means the same as charge independence, that is, the proton-proton interaction has the same strength as the neutron-neutron interaction. This has been confirmed by nucleon-nucleon scattering experiments as well as by the symmetry properties of mirror nuclei (e.g., He^3 and H^3). Mathematically speaking, this means that the nucleon-nucleon interaction $V(1, 2)$ commutes with the operators of the total isospin

$$\mathbf{T} = \mathbf{t}_1 + \mathbf{t}_2. \quad (4.18)$$

Eigenstates can then be constructed of \mathbf{T}^2, T_3 with eigenvalues $T=0, T_3=0$ and $T=1, T_3=-1, 0, +1$ (isospin singlet and isospin triplet). Charge invariance means that \mathbf{T}^2 commutes with the operator of the nuclear force. Therefore, the interactions in $T=1$ states have to be the same (pp , nn , or symmetric $p\bar{n}$ states). However, they may be different in the $T=0$ state (antisymmetric $p\bar{n}$ system).

The formalism of isospin matrices $\tau = (\tau_1, \tau_2, \tau_3)$ is identical to that of regular spin. Since there is no other vector in isospin space, the only isospin invariant combination of the isospin matrices corresponding to particle 1 and 2 is

$$V_0 + V_\tau \tau^{(1)} \tau^{(2)}. \quad (4.19)$$

The functions V_0 and V_τ depend on the remaining coordinates such as $\mathbf{r}, \mathbf{p}, \sigma_1, \sigma_2$, as we have already discussed.

Not all of the combinations possible from the symmetric point of view have been used to describe the nuclear force. We will mention here only the most important terms:

(i). Among the local forces, which do not depend on the velocity, the *central force* is the most important. It depends only on the distance r between the nucleons:

$$V_C(1, 2) = V_0(r) + V_\sigma(r) \sigma^{(1)} \sigma^{(2)} + V_\tau(r) \tau^{(1)} \tau^{(2)} + V_{\sigma\tau}(r) \sigma^{(1)} \sigma^{(2)} \tau^{(1)} \tau^{(2)}. \quad (4.20)$$

(ii). The only remaining local part is the *Tensor force*

$$V_T(1, 2) = [V_{T_0}(r) + V_{T_\tau}(r) \tau^{(1)} \tau^{(2)}] \cdot S_{12} \quad (4.21)$$

with

$$S_{12} = \frac{3}{r^2} (\sigma^{(1)} \mathbf{r}) (\sigma^{(2)} \mathbf{r}) - \sigma^{(1)} \sigma^{(2)}.$$

The term $-\sigma^{(1)} \sigma^{(2)}$ is added to make sure that an average of $V_T(1, 2)$ taken over all directions of \mathbf{r} vanishes:

$$\int V_T(1, 2) d\Omega = 0 \quad \text{where} \quad \mathbf{r} = (r, \Omega). \quad (4.22)$$

An experimental hint of the existence of a tensor component in the

nucleon-nucleon potential is given by the quadrupole moment of the deuteron, which cannot be explained by pure central forces.

(iii). The most important nonlocal term is the *two-body spin orbit interaction*

$$V_{LS} = V_{LS}(r) \mathbf{L} \cdot \mathbf{S}. \quad (4.23)$$

As we shall see in Chap. 5, such a two-body spin orbit potential causes the one-body spin orbit term in the average single-particle nuclear potential, used to explain the magic numbers in nuclei.

(iv). One sometimes also uses a *second-order spin orbit interaction*:

$$V_{LL} = V_{LL}(r) \left\{ (\sigma^{(1)} \sigma^{(2)}) \mathbf{L}^2 - \frac{1}{2} [(\sigma^{(1)} \mathbf{L}) (\sigma^{(2)} \mathbf{L}) + (\sigma^{(2)} \mathbf{L}) (\sigma^{(1)} \mathbf{L})] \right\}. \quad (4.24)$$

4.2.2 The Structure of the Nucleon-Nucleon Interaction

The central force (4.20) is the most important part of the nucleon-nucleon interaction. It can also be represented in terms of exchange or projection operators.

The operators

$$P^\sigma = \frac{1}{2} (1 + \sigma^{(1)} \sigma^{(2)}), \quad P^\tau = \frac{1}{2} (1 + \tau^{(1)} \tau^{(2)}) \quad (4.25)$$

exchange the spin and isospin coordinates, respectively, in a wave function. For instance, we can apply P^σ to the wave function (4.9) and obtain

$$P^\sigma \varphi(\mathbf{r}_1, \mathbf{r}_2) \chi(s_1, s_2) \zeta(t_1, t_2) = \varphi(\mathbf{r}_1, \mathbf{r}_2) \chi(s_2, s_1) \zeta(t_1, t_2). \quad (4.26)$$

This is easy to understand by using the operator of the total spin \mathbf{S} (4.15). The eigenstates of \mathbf{S}^2 are singlet and triplet states and we find:

$$P^\sigma = \frac{1}{2} (1 + 2(\mathbf{S}^2 - \mathbf{s}^{(1)^2} - \mathbf{s}^{(2)^2})) = S(S+1) - 1 = \begin{cases} 1 & \text{for triplet} \\ -1 & \text{for singlet.} \end{cases} \quad (4.27)$$

We can also define an operator P' which exchanges the spacial coordinates \mathbf{r}_1 and \mathbf{r}_2 of the particles.* Since the wave function has to be antisymmetric under the exchange of all coordinates of the particles 1 and 2, the Pauli principle may be written in the form

$$P' P^\sigma P' = -1. \quad (4.28)$$

We can therefore express the operator $P' = -P' P^\sigma$ and eliminate the products $\sigma^{(1)} \sigma^{(2)}$ and $\tau^{(1)} \tau^{(2)}$ in Eq. (4.20).

* The operator P' can be represented by a nonlocal operator in coordinate space, viz:

$$V(r) P' \psi(r_1, r_2) = \int V(r_1 - r_2) \delta(r'_1 - r_2) \delta(r'_2 - r_1) \psi(r'_1, r'_2) d^3 r'_1 d^3 r'_2.$$

In this sense only Wigner forces (4.30) are local.

Finally, we obtain

$$V_C = V_w(r) + V_M(r)P' + V_B(r)P^o + V_H(r)P'P^o \quad (4.29)$$

with the following relations

$$\begin{aligned} V_w &= V_0 - V_o - V_r + V_{\sigma\sigma} && \text{(Wigner force)} \\ V_M &= -4V_{\sigma\sigma} && \text{(Majorana force)} \\ V_B &= 2V_o - 2V_{\sigma\sigma} && \text{(Bartlett force)} \\ V_H &= -2V_r + 2V_{\sigma\sigma} && \text{(Heisenberg force).} \end{aligned} \quad (4.30)$$

The names of these different components of the nuclear force go back to the years following 1930, when the first models of the nucleus were introduced and the saturation property of nuclear forces was explained by exchange terms without introducing a hard core (for a historical review of this work see [Br 65a]).

A third way of representing the central force uses projection operators

$$\begin{aligned} \Pi_s^o &= \frac{1}{2}(1 - P^o), & \Pi_t^o &= \frac{1}{2}(1 + P^o), \\ \Pi_s^r &= \frac{1}{2}(1 - P'), & \Pi_t^r &= \frac{1}{2}(1 + P'), \\ \Pi_o^r &= \frac{1}{2}(1 - P'), & \Pi_e^r &= \frac{1}{2}(1 + P'). \end{aligned} \quad (4.31)$$

These are projection operators ($P^2 = P$, $P^+ = P$), which project onto the singlet (s) and triplet (t), and onto the even (e) and odd (o) part of the nuclear two-body wave function (4.9) in the sense of Table 4.1. We can express the exchange operators P^o, P' by these projection operators and obtain

$$V(1, 2) = V_{et}(r)\Pi_e^r\Pi_t^o + V_{es}(r)\Pi_e^r\Pi_s^o + V_{ot}(r)\Pi_o^r\Pi_t^o + V_{os}(r)\Pi_o^r\Pi_s^o. \quad (4.32)$$

This representation is especially useful in practical applications; for instance, in $p-p$ scattering experiments we have only isospin triplet states, (i.e., only es and ot are important). Table 4.2 shows those functions obtained if one operates with the different representations on wave functions with different symmetry.

Table 4.2 Connections between the different representations of a central force

$\sigma^{(1)}\sigma^{(2)}$	$\tau^{(1)}\tau^{(2)}$	$V(\sigma^{(1)}\sigma^{(2)}, \tau^{(1)}\tau^{(2)})$	$V(P', P^o)$	$V(\Pi', \Pi^o)$	$ 12\rangle$
1	-3	$V_{00} + V_{0o} - 3V_{0r} - 3V_{0rr}$	$V_w + V_M + V_B + V_H$	V_{et}	$ jet\rangle$
-3	1	$V_{00} - 3V_{0o} + V_{0r} - 3V_{0rr}$	$V_w + V_M - V_B - V_H$	V_{es}	$ es\rangle$
1	1	$V_{00} + V_{0o} + V_{0r} + V_{0rr}$	$V_w - V_M + V_B - V_H$	V_{ot}	$ ot\rangle$
-3	-3	$V_{00} - 3V_{0o} - 3V_{0r} + 9V_{0rr}$	$V_w - V_M - V_B + V_H$	V_{os}	$ os\rangle$

The *radial dependence* of the functions V cannot be deduced from invariance principles. In 1937, Yukawa proposed an explanation of the nuclear force using a meson field theory. The nucleons influence each other by the exchange of one or several mesons. The simplest form is the one-pion exchange potential (OPEP). It has the radial dependence of the

Yukawa potential [Yu 35]

$$V_Y(r) = \frac{e^{-\mu r}}{\mu r}, \quad (4.33)$$

where $1/\mu = \hbar/m_\pi c$ is the Compton wavelength of the pion. The asymptotic form of this potential is uniquely determined by the properties of the pion and its coupling strength to the nucleonic field $g^2/\hbar c \approx 0.081$:

$$V^{\text{OPEP}} = \frac{g^2}{3\hbar c} m_\pi c^2 \frac{e^{-\mu r}}{\mu r} (\tau^{(1)} \tau^{(2)}) \left\{ \sigma^{(1)} \sigma^{(2)} + \left(1 + 3 \frac{1}{\mu r} + 3 \left(\frac{1}{\mu r} \right)^2 \right) S_{12} \right\}. \quad (4.34)$$

A phase shift analysis of the nucleon-nucleon scattering data shows that the OPEP-potential (4.34) is well able to reproduce the phase shifts for large orbital angular momenta $L > 6$ [Br 67b]. Since these high partial waves only feel the tail of the nuclear force at large distances ($r > 2$ fm), we can assume that the OPEP potential describes the nuclear force properly at such large distances. For smaller distances we must, in addition, also introduce the two-pion exchange and the ρ - and ω -meson exchange in order to obtain the medium-range part of the force. This has been achieved very successfully [BJ 76a, CLL 73, LLR 75, DSB 77, Vi 78, Ho 80], so that only the short-range part of the force still has to be fitted by a phenomenological ansatz. Only six parameters are needed for each isospin state. As we mentioned in the introduction, this potential is not used very much as yet, therefore phenomenological counterparts have been employed until now. These phenomenological parametrizations consist of combinations of central, tensor, spin orbit, and higher terms, and more or less arbitrary radial functions containing up to 50 parameters, which are fitted to the experimental scattering phase shifts and to the deuteron data. There are attractive and repulsive components. At large distances they go over into the OPEP-potential, whereas at short distances they have an extremely repulsive core. Several authors have therefore used a *hard core* [$V(r) = \infty$ for $r < r_c \approx 0.4$ fm]. Others use a very repulsive core which goes to infinity only for $r \rightarrow 0$. Such potentials are called *soft core* potentials.

Examples of such realistic nucleon-nucleon potentials using a hard core are the Hamada Johnston potential [HJ 62] and the Yale potential [LHR 62]. The Tabakin potential [Ta 64] is a nonlocal potential, separable in momentum space.

The Reid soft core potential [Re 68] is also widely used. It has the structure

$$V = V_C(\mu r) + V_T(\mu r)S_{12} + V_{LS}(\mu r)LS. \quad (4.35)$$

$V_C(x)$ and $V_{LS}(x)$ have the simple form

$$V_C(x) = \sum_{n=1}^{\infty} a_n \frac{e^{-nx}}{x}, \quad V_{LS} = \sum_{n=1}^{\infty} c_n \frac{e^{-nx}}{x}, \quad (4.36)$$

and $V_T(x)$ is given by

$$V_T(x) = \frac{b_1}{x} \left\{ \left(\frac{1}{3} + \frac{1}{x} + \frac{1}{x^2} \right) e^{-x} - \left(\frac{k}{x} + \frac{1}{x^2} \right) e^{-kx} \right\} + \sum_{n=2}^{\infty} b_n \frac{e^{-nx}}{x}. \quad (4.37)$$

The constants are different for all values of T , S and $I < 2$. Only a_1 , b_1 , and c_1 are fixed in such a way that we obtain the OPEP-potential for large distances. For $I > 2$, Reid uses the OPEP-potential.

4.3 Microscopic Effective Interactions

The bare nucleon-nucleon force has—as we have already seen in the preceding section—certain features that are rather difficult to handle in practice.

There is, for instance, the hard core (or at least the very repulsive core), which would make some of the usual concepts of nuclear many-body physics extremely complicated if not inapplicable (as in the Hartree-Fock case; see Chap. 5).^{*} This comes from the infiniteness of the matrix elements of a force with a hard core. In these theories, a way out of this situation is to use, in place of the bare interaction, a so-called effective interaction, which is itself an infinite sum of scattering processes of two nucleons in the nuclear medium. The bare interaction is then simply the Born term of this series. The object of this procedure is twofold: First, in re-summing the series one gets rid of the hard core problem, since the new interaction is well-behaved at short distances. Second, we can show that in replacing the bare interaction by its effective counterpart we have at the same time consistently summed up more of the many-body effects than if one had taken just the bare interaction.

The main fields of application are: (i) the ground state properties of nuclei, where the scattering of two nucleons within the nuclear medium has to be considered; (ii) the forces between the so-called valence nucleons; and (iii) effective forces between “particles” and “holes.” There are also effective three-body forces which we will ignore in this section.

4.3.1 Brückner's *G*-Matrix and Bethe Goldstone Equation[†]

One of the most important effective interactions in nuclear physics is the so-called Brückner *G*-matrix [Br 55, Da 67, and references therein]. It is, for two nucleons in the nuclear medium—in a sense yet to be specified—the analogue of the scattering matrix for two nucleons in free space.

We therefore start our considerations with the Lippmann-Schwinger equation for the scattering matrix (*T*-matrix; see Fig. 4.1) of two particles

* In this section, we must quite often anticipate theories and methods which are only treated later in this book. This is contrary to our usual strategy, which is to avoid this situation as much as possible. As the reader will notice, however, the microscopic theory of effective interactions is not in a very satisfactory state, so we prefer to give a short survey here together with the description of phenomenological forces, rather than devote an extra chapter to it later. (See also Appendix F.)

[†] The discussion in this section is partially based on Gomes, Walecka, and Weisskopf [GWW 58] and the textbook of Fetter and Walecka [FW 71].

(Messiah [Me 61] Chap. XIX, Sec. 14):

$$T_{\mathbf{k}_1 \mathbf{k}_2, \mathbf{k}'_1 \mathbf{k}'_2}^E = \bar{v}_{\mathbf{k}_1 \mathbf{k}_2, \mathbf{k}'_1 \mathbf{k}'_2} + \frac{1}{2} \sum_{\mathbf{p}_1 \mathbf{p}_2} \bar{v}_{\mathbf{k}_1 \mathbf{k}_2, \mathbf{p}_1 \mathbf{p}_2} \frac{1}{E - (\mathbf{p}_1^2/2m) - (\mathbf{p}_2^2/2m) + i\eta} T_{\mathbf{p}_1 \mathbf{p}_2, \mathbf{k}'_1 \mathbf{k}'_2}^E, \quad (4.38)$$

where $\mathbf{k}_1, \mathbf{k}_2$ and $\mathbf{k}'_1, \mathbf{k}'_2$ are the momenta of the incoming and outgoing particles, respectively, and E is the total scattering energy.

If we consider the scattering of two nucleons within a nuclear medium we can show (this is derived in Sec. F.4) that it makes sense to define a scattering matrix G^E analogous to that for free particles. The changes to be made for nucleons in a nucleus are almost obvious: the plane wave indices have to be changed to shell model indices, the kinetic single-particle energies figuring in the denominator of the r.h.s. of Eq. (4.38) have to be replaced by the corresponding shell model energies, and the sum over the intermediate states has to be restricted so that it does not include states below the Fermi surface. This latter feature comes from the fact that two nucleons below the Fermi surface can only scatter into states above the Fermi surface, because all other levels are occupied and are thus excluded by the Pauli principle. Therefore, we get the following equation for the G -matrix, which is usually known under the name Bethe–Goldstone equation [BG 57] (for its mathematical derivation, see Sec. F.4).

$$G_{ab, cd}^E = \bar{v}_{ab, cd} + \frac{1}{2} \sum_{m, n > \epsilon_F} \bar{v}_{ab, mn} \frac{1}{E - \epsilon_m - \epsilon_n + i\eta} G_{mn, cd}^E, \quad (4.39)$$

where ab, \dots, mn are shell-model indices and ϵ_F is the Fermi energy. This equation is usually represented graphically in an obvious way, as shown in Fig. 4.2. Two lines connecting two interactions represent the “propagator” $1/(E - \epsilon_n - \epsilon_m)$. (More will be explained about graphs in Chap. 8 and Appendix F.) For $E < \epsilon_F$, we can ignore the $i\eta$ in the denominator of (4.39), and in this case the G -matrix is obviously Hermitian as can be checked immediately by iterating Eq. (4.39). Equation (4.39) is also often

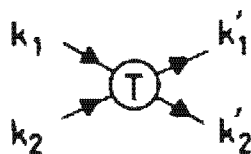


Figure 4.1. Graphical representation of the T -matrix.

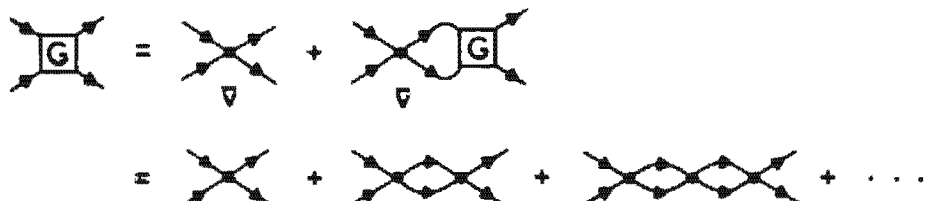


Figure 4.2. Graphical representation of the Bethe–Goldstone equation.

written in the operator form:

$$G = \bar{v} + \bar{v} \frac{Q_F}{E - H_0} G, \quad (4.40)$$

where H_0 is the shell model Hamiltonian and

$$Q_F = \sum_{\substack{m < n \\ > \epsilon_F}} |mn\rangle \langle mn| \quad (4.41)$$

is a projection operator excluding all occupied states.

In a very qualitative way, we can see from Eq. (4.40) how it can happen that G stays finite for points where \bar{v} is infinite. Solving Eq. (4.40) formally yields

$$G = \frac{\bar{v}}{1 - \bar{v} Q_F / (E - H_0)}. \quad (4.42)$$

If \bar{v} tends to infinity, G may stay finite. This is, of course, only a very crude argument and we shall in a definite example show in detail how this occurs. Before this, we have to discuss, however, some general features of Eq. (4.39). Despite the fact that Eq. (4.39) is formally very similar to Eq. (4.38), there are certain essential differences concerning, for instance, the boundary condition in the case of $E < \epsilon_F$ of the wave function defined in analogy to the scattered wave of two free particles by [Me 61, Chap. XIX 10]:

$$\begin{aligned} |\psi_{ab}\rangle &\equiv \bar{v}^{-1} G |ab\rangle = \left(1 + \frac{Q_F}{E - H_0} G \right) |ab\rangle \\ &= |ab\rangle + \frac{Q_F}{E - H_0} \bar{v} |\psi_{ab}\rangle, \end{aligned} \quad (4.43)$$

with

$$\langle r_1 r_2 | ab \rangle = \frac{1}{\sqrt{2}} (\varphi_a(r_1) \varphi_b(r_2) - \varphi_a(r_2) \varphi_b(r_1)) \quad (4.44)$$

and

$$H_0 |ab\rangle = (\epsilon_a + \epsilon_b) |ab\rangle. \quad (4.45)$$

The wave equation (4.43) formally resembles an equation for a scattered wave. However, contrary to the real scattering case, where the second term on the r.h.s. of (4.43) gives the outgoing scattered part of the wave function and thus does not vanish as the relative distance of the two particles $|r_1 - r_2|$ goes to infinity, in the present case of $E < \epsilon_F$, this term vanishes as $|r_1 - r_2|$ goes to infinity. This comes from the fact that for a real scattering process the T matrix of Eq. (4.38) enters Eq. (4.43) "on the energy shell," that is, the absolute value of the relative momenta of the two particles before and after the scattering process have to be the same; also, E must correspond to this value of the relative momentum. As a consequence, the corresponding energy denominator of Eq. (4.43) for a real scattering

process can be zero and introduce a singularity. In the present case this can never happen, since we suppose $E < \epsilon_F$ and therefore the second expression on the r.h.s. of Eq. (4.39) is never "on the energy shell," which is why it vanishes for large values of $|\mathbf{r}_1 - \mathbf{r}_2|$. A derivation is presented in a review article by Day [Da 67] which, however, would be too much of a digression to be repeated here. We have thus:

$$|\psi_{ab}^E\rangle \xrightarrow{|\mathbf{r}_1 - \mathbf{r}_2| \rightarrow \infty} |ab\rangle. \quad (4.46)$$

From Eqs. (4.43) and (4.41) we also immediately get the normalization condition for $a, b < \epsilon_F$:

$$\langle ij | \psi_{ij} \rangle = 1, \quad i, j < \epsilon_F. \quad (4.47)$$

It is also instructive to expand the correlated pair function $|\psi_{ij}\rangle$ in an uncorrelated basis. From (4.43) we have:

$$|\psi_{ij}\rangle = |ij\rangle + \frac{1}{2} \sum_{mn} C_{mn}^{ij} |mn\rangle, \quad (4.48)$$

that is, the correlated function contains, in addition to $|ij\rangle$, components above the Fermi level. It turns out that in the most important applications of the G -matrix E lies below the Fermi level. For instance, in the Brückner Hartree-Fock theory (see Chap. 5) we must calculate $G_{ab,ij}^{E=\epsilon_i+\epsilon_j}$ with $i, j < \epsilon_F$. We will therefore treat the hard core for this case in a very simplified but explicitly solvable model which, however, shows the essential features.

Let us consider a large nucleus, the interior of which will be presumed to be not very much different from the situation where we consider an infinitely large nucleus, usually termed nuclear matter. In addition, we will make a further crude assumption, namely, that the interaction consists of a hard core only:

$$V(r) = 0 \text{ for } r > c \quad \text{and} \quad V(r) = \infty \text{ for } r < c.$$

Furthermore, we assume that we have two distinguishable particles, for example, a proton and a neutron, which will be sufficient as a demonstration of the principle. Let us now write Eq. (4.43) in the form:

$$(E - H_0)|\psi_{ab}\rangle = (E - H_0 + Q_F G)|ab\rangle, \quad (4.49)$$

which in our case ($E = \epsilon_i + \epsilon_j$) specializes to

$$(\epsilon_i + \epsilon_j - H_0)|\psi_{ij}\rangle = Q_F G |ij\rangle = Q_F \mathbf{v} |\psi_{ij}\rangle, \quad (4.50)$$

where for the last equality use has been made of (4.43). The general solution of (4.50) is much harder than the solution of an ordinary Schrödinger equation because of the operator Q_F , which is a nonlocal integral operator. This is best seen in the \mathbf{r} -representation

$$\langle \mathbf{r}_1 \mathbf{r}_2 | Q_F | \mathbf{r}'_1 \mathbf{r}'_2 \rangle = \sum_{\substack{m < n \\ > \epsilon_F}} \langle \mathbf{r}_1 \mathbf{r}_2 | mn \rangle \langle mn | \mathbf{r}'_1 \mathbf{r}'_2 \rangle. \quad (4.51)$$

In nuclear matter it is clear that the single-particle wave functions that appear in (4.50) are plane waves. For simplicity we will also assume that the single-particle energies are purely kinetic energies (in a surrounding medium this will not gener-

ally be the case). Because of translational invariance, for nuclear matter the center of mass motion is trivial, and we have:

$$\langle \mathbf{r}_1 \mathbf{r}_2 | \psi_g \rangle \rightarrow \psi_{\mathbf{p}_1 \mathbf{p}_2}(\mathbf{r}_1 \mathbf{r}_2) = \frac{1}{(2\pi)^{3/2}} e^{i\mathbf{P}\mathbf{R}} \psi_{\mathbf{p}_k}(\mathbf{r}). \quad (4.52)$$

Here the following transformations to relative and center of mass coordinates have been made:

$$\begin{aligned} \mathbf{P} &= \mathbf{p}_1 + \mathbf{p}_2, & \mathbf{k} &= \frac{1}{2}(\mathbf{p}_1 - \mathbf{p}_2), \\ \mathbf{R} &= \frac{1}{2}(\mathbf{r}_1 + \mathbf{r}_2), & \mathbf{r} &= \mathbf{r}_1 - \mathbf{r}_2. \end{aligned} \quad (4.53)$$

With all these assumptions, Eq. (4.50) acquires the form

$$\begin{aligned} \frac{\hbar^2}{2m} \{ p_1^2 + p_2^2 + \Delta_1 + \Delta_2 \} \psi_{\mathbf{p}_1 \mathbf{p}_2}(\mathbf{r}_1 \mathbf{r}_2) \\ = \frac{1}{(2\pi)^6} \int_{|\mathbf{p}, \mathbf{p}'| > k_F} d^3 p d^3 p' \int d^3 r'_1 d^3 r'_2 e^{i(\mathbf{p}r_1 + \mathbf{p}'r_2 - \mathbf{p}'r'_1 - \mathbf{p}'r'_2)} v(|\mathbf{r}'_1 - \mathbf{r}'_2|) \psi_{\mathbf{p}_1 \mathbf{p}_2}(\mathbf{r}'_1 \mathbf{r}'_2). \end{aligned} \quad (4.54)$$

Transforming this equation to relative and center of mass coordinates according to (4.53) we obtain

$$\begin{aligned} \frac{\hbar^2}{m} \{ k^2 + \Delta_r \} e^{i\mathbf{P}\mathbf{R}} \psi_{\mathbf{p}_k}(\mathbf{r}) \\ = \frac{1}{(2\pi)^6} \int \int_{\left| \frac{\mathbf{P}}{2} \pm \mathbf{p} \right| > k_F} d^3 p d^3 p' \int \int d^3 R' d^3 r' e^{i(\mathbf{P}\mathbf{R} + \mathbf{p}(r - r'))} e^{-i\mathbf{p}\mathbf{R}'} v(r') e^{i\mathbf{P}\mathbf{R}'} \psi_{\mathbf{p}_k}(\mathbf{r}'). \end{aligned} \quad (4.55)$$

Since $\Phi^2 = p^2 + 2pp' \cos \theta + p'^2$, we see that even under the restriction $p, p' > k_F$, Φ can take on all values from 0 to ∞ . The integration over \mathbf{R}' gives $\delta(\mathbf{P} - \Phi)$ and we can therefore also perform the Φ integral. We are thus left with the following equation.

$$\frac{\hbar^2}{m} \{ k^2 + \Delta_r \} \psi_{\mathbf{p}_k}(\mathbf{r}) = \frac{1}{(2\pi)^3} \int_{\left| \frac{\mathbf{P}}{2} \pm \mathbf{p} \right| > k_F} d^3 p e^{i\mathbf{P}\mathbf{r}} \int d^3 r' e^{-i\mathbf{p}\mathbf{r}'} v(r') \psi_{\mathbf{p}_k}(\mathbf{r}'). \quad (4.56)$$

This equation is not only more complicated than a usual two-particle equation because of its integrodifferential structure, but also because the wave function has a nontrivial dependence on the center of mass momentum \mathbf{P} . For our purpose, it will be sufficient to evaluate it at $\mathbf{P} = 0$. Furthermore, we can decompose Eq. (4.56) into partial waves [Me 61 Chap. X, Sec. 8]:

$$\psi_{\mathbf{k}}(\mathbf{r}) = \sum_m \psi_{\mathbf{k}l}(r) Y_{lm}(\theta, \varphi). \quad (4.57)$$

Considering the equation for the s -wave and splitting the integral in (4.56) into two parts, $\int_{k_F}^{\infty} = \int_0^{\infty} - \int_0^{k_F}$, we obtain:

$$\begin{aligned} \frac{\hbar^2}{m} \left(k^2 + \frac{\partial^2}{\partial r^2} + \frac{2}{r} \frac{\partial}{\partial r} \right) \psi_{\mathbf{k}}(r) \\ = v(r) \psi_{\mathbf{k}}(r) - (4\pi)^2 \int_0^{k_F} \frac{dp p^2}{(2\pi)^3} j_0(pr) \int_0^{\infty} dr' r'^2 j_0(pr') v(r') \psi_{\mathbf{k}}(r'), \end{aligned} \quad (4.58)$$

where j_0 is the lowest-order spherical Bessel function. With $\psi_k(r) = (1/r)u_k(r)$, we finally get:

$$\frac{\hbar^2}{m} \left(k^2 + \frac{\partial^2}{\partial r^2} \right) u_k(r) = v(r)u_k(r) - k_F \int_0^\infty dr' \chi(r', r)v(r')u_k(r'), \quad (4.59)$$

with

$$\chi(r, r') = \frac{2rr'}{\pi k_F} \int_0^{k_F} dp p^2 j_0(pr)j_0(pr') = \frac{1}{\pi k_F} \left\{ \frac{\sin k_F(r-r')}{r-r'} - \frac{\sin k_F(r+r')}{r+r'} \right\}. \quad (4.60)$$

It is now convenient to introduce the following dimensionless quantities:

$$x = k_F \cdot r; \quad x' = k_F \cdot r'; \quad K = \frac{k}{k_F}; \quad \frac{mc}{k_F^2 \hbar^2} = w. \quad (4.61)$$

This leads to

$$\left(\frac{d^2}{dx^2} + K^2 \right) u_K(x) = w(x)u_K(x) - \int_0^\infty dx' \chi(x, x')w(x')u_K(x'). \quad (4.62)$$

For a square well barrier of finite height, the wave function and its first derivative are continuous at the edge of the barrier. We can be easily convinced that the first derivative of the wave function becomes discontinuous at the edge as the barrier height goes to infinity, that is:

$$u'_K(c + \epsilon) = A, \quad (4.63)$$

where A is a constant, $r = c$ is the radius of the hard core, and ϵ is an infinitesimally small positive quantity. In order to produce such a discontinuity for u of Eq. (4.62), the product $w \cdot u$ must be proportional to a δ function for $r = c$. Since for $r > c$ the potential w is zero and u finite, the product $w \cdot u$ vanishes outside the hard core radius. The wave function u cannot penetrate inside the infinite hard core ($u = 0$); since there $w = \infty$, the product $w \cdot u$ may be finite and we can write, with $c' = ck_F$:

$$w(x)u_K(x) = A\delta(x - c') + l(x)\theta(c' - x). \quad (4.64)$$

The function $l(x)$ can be determined from the requirement that for $x < c'$ the left hand side of Eq. (4.62) must be zero, since $u \equiv 0$ for $x < c'$. We therefore have from Eq. (4.62) with Eq. (4.64)

$$l(x) = A\chi(x, c') + \int_0^{c'} dx' \chi(x, x')l(x') \quad \text{for } x < c'. \quad (4.65)$$

Since the hard core is usually rather small ($c' = 0.57$ at the nuclear matter density for $c = 0.4$ fm), we can develop the kernel in Eq. (4.65) and obtain from Eq. (4.60)

$$\chi(x, x') \rightarrow \frac{2xx'}{3\pi} \quad x < c'; \quad x' < c'. \quad (4.66)$$

With Eqs. (4.66) and (4.65), we see that $l(x)$ is of order c'^2 , whereas any integral over $l(x)$ will be of order c'^3 . In (4.62) we can therefore neglect the second term in (4.64) to obtain a result which is correct to first order in c' . We obtain

$$\begin{aligned} \left(\frac{d^2}{dx^2} + K^2 \right) u_K(x) &\approx A[\delta(x - c') - \chi(x, c')] + A\chi(x, c')\theta(c' - x) \\ &= A \frac{2xc'}{\pi} \int_1^\infty dp p^2 j_0(px)j_0(pc') + A\chi(x, c')\theta(c' - x) \\ &= F(x). \end{aligned} \quad (4.67)$$

where we have made use of the identity

$$\int_0^\infty dp p^2 j_l(pr) j_l(pr') = \frac{\pi}{2r^2} \delta(r - r'). \quad (4.68)$$

We remark that since the r.h.s. of Eq. (4.67) is only correct to first order in c' , it is somewhat arbitrary whether to include the second term of the r.h.s. of Eq. (4.67), which is of second order. The general solution of Eq. (4.67),

$$u_K(x) = \frac{\sin Kx}{K} \int_{c'}^x dy F(y) \cos Ky - \frac{\cos Kx}{K} \int_{c'}^x dy F(y) \sin Ky, \quad (4.69)$$

is obviously zero for $x = c'$. Equation (4.69) is the solution to Eq. (4.67), as can be easily verified by direct insertion.

The only unknown in the solution (4.67, 4.69) is the constant A , which we are going to determine by the requirement (4.46) that u_K has to approach asymptotically the unperturbed value. To this end we will first show that the second integral on the r.h.s. of Eq. (4.69) is zero in the limit $x \rightarrow \infty$. Since we considered our solution in the limit of very small c' , we can take the integral from 0 to ∞ instead of from c' to ∞ , and thus have

$$\begin{aligned} \frac{1}{K} \int_0^\infty dy F(y) \sin Ky &= \frac{2Ac'}{\pi} \int_1^\infty dp p^2 j_0(p c') \int_0^\infty dy y^2 j_0(Ky) j_0(py) \\ &= \frac{2Ac'}{\pi} \int_1^\infty dp p^2 j_0(p c') \frac{\pi}{2Kp} \delta(K - p) \\ &= 0. \end{aligned} \quad (4.70)$$

The last integral vanishes because p is outside the Fermi sphere, whereas K is inside. For $r \rightarrow \infty$ we therefore find the result that the wave function approaches the unperturbed result ($\psi \rightarrow j_0$) [see Eq. (4.46)] only if

$$\int_0^\infty dy F(y) \cos Ky = 1, \quad (4.71)$$

and we therefore get, using Eq. (4.67):

$$A = \left\{ \cos Kc' - \int_0^\infty dy \cos(Ky) \chi(y, c') \right\}^{-1}, \quad (4.72)$$

which completes the determination of the wave function $u_K(x)$ of Eqs. (4.67) and (4.69) for a hard sphere potential.

In Fig. 4.3 we show the solution $\psi_k(r)$ for $k = 0$, which reveals several interesting features. The wave function vanishes inside the hard core. With (4.69) and (4.72) it can easily be seen that it approaches rapidly (by

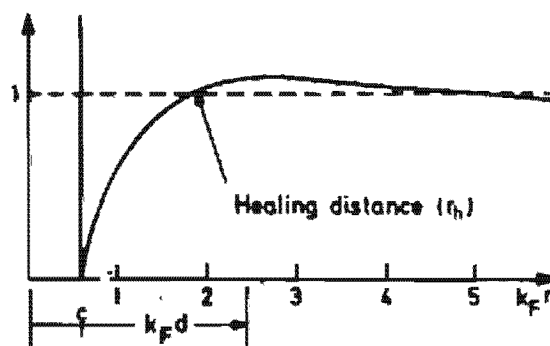


Figure 4.3. S-wave solution of the Bethe-Goldstone equation for a pure hard core potential in nuclear matter. For details of the figure, see text. (From [FW 71].)

damped oscillations) the value of the wave function for the noninteracting pair (which is itself equal to 1 for $k = 0$ and all values of r). The r value at which the wave function first attains the unperturbed value is called the *healing distance* r_h , because it is only for distances smaller than this value that the hard core wave function differs appreciably from the unperturbed wave function. For the values chosen in our example, the healing distance is:

$$k_F r_h \approx 1.9. \quad (4.73)$$

(This value is more or less independent of P and k , as a more general study of Eq. (4.59) shows [WG 67a]. It is important to note that this value is appreciably smaller than the average interparticle distance d in nuclear matter defined by the expression $1/d^3 \equiv N/V = (4 \int_{p < \Lambda k_F} dp \int dr)/V(2\pi\hbar)^3 = 2k_F^3/3\pi^2$, which would yield for the interparticle distance:

$$k_F d = \left(\frac{3\pi^2}{2} \right)^{1/3} = 2.46. \quad (4.74)$$

On the average, therefore, the nucleons return after a collision to their independent particle wave function *before* the next collision takes place. A great portion of the nuclear wave function therefore consists of a determinant built out of independent particle wave functions. This can be considered as a justification of the independent particle model—the Pauli principle suppressing the low momentum components of the scattering process, that is, suppressing the long range correlations. The nucleons thus move through the nucleus most of the time as independent particles because of the exclusion principle. That this can happen in a strongly interacting but dilute Fermi gas was first pointed out by Weisskopf [We 50].

We have seen that the solution of the Bethe–Goldstone Equation (4.39) is far from trivial, and one can easily imagine that the task can become tremendously difficult for finite nuclei, where the wave functions are no longer plane waves and translational invariance is also lost. Several approximation schemes have therefore been currently applied. As we have seen in our example, it is the projection operator Q_F which makes things so difficult. It has been proposed, that the Pauli principle should be treated only perturbatively in the *separation method* of Moszkowski and Scott [MS 60] and in the *reference spectrum method* of Bethe, Brandow, and Petschek [BBP 63]. We do not wish to go into details of these approximation methods and refer the reader to the text books of Brown [Br 64], de Shalit and Feshbach [SF 74], and the review article by Bethe [Be 71], in which these and further methods, like the use of the oscillator basis for the solution of the Bethe–Goldstone equation in finite nuclei, are explained in detail. Here we want to mention only one other approximation scheme which has recently become very successful in connection with the Brückner–Hartree–Fock theory (see Chap. 5). This is the *local density approximation* by Negele [Ne 70, 75], originally introduced by Brückner, Gammel, and Weitzner [BGW 58] and Brückner, Lockett, and Rotenberg [BLR 61]. The assumption is that the G -matrix at any place in a finite nucleus is the same as that for nuclear matter at the same density, so that locally one can

calculate the G -matrix as in a nuclear matter calculation [Be 71, Ne 75]. We shall come back to this approximation in Chapter 5.

4.3.2 Effective Interactions between Valence Nucleons

Another field to which the Brückner G -matrix has important applications is the effective forces between the so-called valence nucleons (for a review, see [Ku 74b] and references therein). As a definite example, let us take ^{18}O or ^{18}F , where we have two nucleons (the "valence nucleons") on top of a doubly magic nucleus ^{16}O . In the pure shell model approximation the two nucleons will be in the $1d5/2$ level. We may hope to get a good description of the low-lying states of ^{18}O by making a configuration mixing calculation using the states $1d5/2, 2s1/2, 1d3/2$ which just form the first shell above the ^{16}O core. Such shell model calculations have been described to some extent in Chapter 2 and will be treated in greater detail in Chapter 8, where we will show, for instance, that such two-valence nucleons may be well described by the particle-particle Tamm-Dancoff secular equation [see Chap. 8, Eq. (8.10)]:

$$(E_p^{\text{TD}} - \epsilon_m - \epsilon_n) R_{mn}^p = \frac{1}{2} \sum_{m'n'} \bar{v}_{mn, m'n'} R_{m'n'}^p. \quad (4.75)$$

Here the ϵ_m 's are the single-particle energies of the phenomenological or self-consistent (see Chap. 5) single-particle Hamiltonian H_0 and all the indices in Eq. (4.75) are in the *model space* above the Fermi level of the core (e.g., the $d5/2, 2s1/2$, and $d3/2$ states in our example). For the two-particle interaction in Eq. (4.75), we cannot take the bare interaction, since this force has to simulate and correct at least approximately the omission of (a) the rest of the two-particle configuration above the Fermi level, and (b) contributions from higher configurations of the shell model basis like $3p-1h, 4p-2h$, etc.

In the following we will derive an exact equation, formally almost identical to Eq. (4.75), with, however, \bar{v} replaced by an effective (energy dependent) interaction, calculable at least in principle, from the bare interaction (such as, e.g., the Hamada-Johnston potential). We start out with the observation of Chapter 2 that the shell model provides a complete set of states; therefore, any exact wave function can be expanded in this basis. A convenient way to do this is given by the formalism of second quantization, in which the expansion of, for example, an $A+2$ nucleon state can be written in the following way (see also Chap. 8). (In the following, the indices m, n, r, p , and i, j shall be states above and below the Fermi level, respectively.)

$$\begin{aligned} |A+2, \tau\rangle = & \sum_{m < n} R_{mn}^r a_m^+ a_n^+ |HF\rangle + \sum_{m < n < r, i} R_{mnr, i}^r a_m^+ a_n^+ a_r^+ a_i |HF\rangle \\ & + \sum_{\substack{m < n < r < p \\ i < j}} R_{mnrp, ij}^r a_m^+ a_n^+ a_r^+ a_p^+ a_i a_j |HF\rangle. \end{aligned} \quad (4.76)$$

Here we assume that the ground state $|HF\rangle$ of the A nucleus in the shell model is ideally given by a Hartree-Fock calculation (see Chap. 5), but our considerations hold equally for any phenomenological shell model. The indices m, n, r, p and i, j in Eq. (4.76), of course, correspond to the shell model potential in question. The expansion consists of multiparticle-multiparticle components ranging from $2p-0h$ up to, in principle, $(A+2)p-Ah$ components. We now introduce two projectors P and Q . The projector P projects on those $2p-0h$ states which lie within the given model space and Q projects onto the rest, that is, on those $2p-0h$ components which do not lie in the model space and on all $3p-1h, 4p-2h$, etc. components. Therefore, $I = P + Q$ and

$$P = \sum'_{m < n} a_m^+ a_n^+ |HF\rangle \langle HF| a_n a_m, \quad (4.77)$$

where the prime on the sum indicates that it goes over the model space only. We also have the usual relations for projectors, viz:

$$Q^2 = Q; \quad P^2 = P; \quad P^+ = P; \quad Q^+ = Q; \quad PQ = QP = 0. \quad (4.78)$$

With the aid of these projectors we can write for Eq. (4.76):

$$|\tau\rangle = P|\tau\rangle + Q|\tau\rangle = PR|HF\rangle + QS|HF\rangle, \quad (4.79)$$

where $R = \sum'_{m < n} R_{mn}^+ a_m^+ a_n^+$, the prime having the same meaning as in Eq. (4.77); the operator S is then defined in an obvious way by Eqs. (4.76) and (4.79). The Schrödinger equation $(H_0 + V)|\tau\rangle = E_\tau|\tau\rangle$, where H_0 is the shell model Hamiltonian and V the residual interaction (see Chaps. 2 and 8) can now be written in the following form [Fe 62].

$$(-E_\tau + H_0 + PVQ)P|\tau\rangle = -PVQ|\tau\rangle, \quad (4.80)$$

$$(-E_\tau + H_0 + QVQ)Q|\tau\rangle = -QVP|\tau\rangle. \quad (4.81)$$

Here we have multiplied the Schrödinger equation from the left once with P and once with Q and observed that P and Q commute with H_0 . Solving Eq. (4.81) for $Q|\tau\rangle$ and substituting into Eq. (4.80) yields

$$(H_0 + PV_{\text{eff}}^E P)P|\tau\rangle = E_\tau P|\tau\rangle \quad (4.82)$$

with

$$V_{\text{eff}}^E = V + VQ \frac{1}{E_\tau - H_0 - QVQ} QV. \quad (4.83)$$

Multiplying Eq. (4.82) from the left with $\langle HF|a_n a_m$, where n, m are in the model space, we can write:

$$\begin{aligned} (\langle HF|[a_n a_m, H_0] + \langle HF|a_n a_m PV_{\text{eff}}^E P) \sum'_{m' < n'} a_{n'}^+ a_{m'}^+ |HF\rangle R_{mn'}^+ \\ = (E_\tau - E_0^{HF}) R_{mn}^+ \end{aligned} \quad (4.84)$$

with

$$H_0|HF\rangle = E_0^{HF}|HF\rangle.$$

The commutator in Eq. (4.84) is easily evaluated, and we finally obtain an

equation which is formally very similar to the two-particle Tamm-Dancoff Eq. (4.75) but is, in fact, rigorously exact:

$$[(E_r - E_0^{HF}) - \epsilon_m - \epsilon_n] R_{mn}^r = \sum'_{m' < n'} \langle mn | V_{\text{eff}}^r | m' n' \rangle R_{m'n'}^r. \quad (4.85)$$

We see that the difference between Eqs. (4.85) and (4.75) is simply that the matrix elements of the phenomenological two-body interaction have been replaced by those of an effective energy dependent interaction which (at least in principle) can be calculated from the bare interaction.* The expression (4.83) can be rewritten as an integral equation for V_{eff} :

$$V_{\text{eff}} = V + VQ \frac{1}{E - H_0} QV_{\text{eff}}. \quad (4.86)$$

This can be verified either by expanding both (4.86) and (4.83) in powers of V , or by direct substitution of (4.83) in (4.86) and using decomposition into partial fractions. In order to investigate the simplest contributions to V_{eff} , we have to look at the structure of the projection operator Q . We can distinguish three different contributions: (i) $2p-0h$ excited states, where only one particle is outside the model space; (ii) two-particle excited states, where both particles of the $2p-0h$ components are outside the model space; (iii) those components which involve holes ($3p-1h$, etc.) The excited states of type (i) probably do not contribute very much, since it has been shown that their contribution vanishes exactly in nuclear matter [Ma 69], and are thus expected to be small in finite (but heavy) nuclei. Their contribution is thus omitted in practical calculations. The two-particle excited states give the most important contribution, as practical calculations have shown, therefore we want to study how they can be treated and what their relation to the Brückner G -matrix will be.

We shall call that part of Q which corresponds to the two-particle excited states (ii) Q_{2p} . Retaining in (4.86) only the Q_{2p} part and expanding in powers of V , we obtain up to second order

$$\langle mn | V_{\text{eff}} | m' n' \rangle = \bar{v}_{mn, m'n'} + \sum_{\substack{p < q \\ > \epsilon_{\text{max}}}} \frac{\bar{v}_{mn, pq}}{\Omega_r - \epsilon_p - \epsilon_q} \bar{v}_{pq, m'n'} + \dots, \quad (4.87)$$

where ϵ_{max} is the upper limit of the model space and $\Omega_r = E_r^{A+2} - E_0^A$ in accordance with the footnote on this page (no problems with linked or unlinked terms appear at this level). This shows that this part of the

* The effective interaction defined by Eqs. (4.83) and (4.85) contains so-called unlinked contributions [Ma 69]. By reordering these terms in Eq. (4.85) we can show that one obtains an equation structurally equal to Eq. (4.85), where, however, E_0^{HF} is replaced by the exact ground state energy E_0^A of the core. The argument $E_r^{A+2} - H_0$ in the denominator of Eq. (4.83) is changed to $E_r^{A+2} - E_0^A - (H_0 - E_0^{HF})$ and only the linked contributions of Eq. (4.83) have to be taken into account. However, no integral equation for this quantity is known [compare Eq. (4.86)]. More details of this procedure can be found in the review articles by MacFarlane [Ma 69] and Barrett and Kirson [BK 73]. Brandow [Br 67a] has shown that we can also get rid of the energy dependence of the effective interaction by introducing the so-called "folded diagram" (see also [JB 71, EO 77]). The discussion of these rather involved techniques would go beyond the scope of this book, thus we refer the interested reader to the original literature.

effective interaction is equal to the Brückner G -matrix (4.39) with ϵ_F replaced by ϵ_{\max} , that is,

$$(V_{\text{eff}}^{(2p)})_{mn, m'n'} = G_{mn, m'n'}^{E_4^{\alpha+1} - E_0^{\alpha}} (\epsilon_F \rightarrow \epsilon_{\max}). \quad (4.88)$$

The whole intention and philosophy of rewriting the exact Schrödinger equation in the form (4.85) is based on the hope that V_{eff} is an operator which for the physical problem of two valence nucleons can be calculated to a good approximation in some perturbative way. One must therefore assume that V_{eff} is well behaved in the sense that it has, for instance, no strong energy dependence. The energy dependence of G in Eq. (4.88) is thus usually neglected and replaced by

$$\Omega_r \approx \frac{1}{2} (\epsilon_m + \epsilon_n + \epsilon_{m'} + \epsilon_{n'}). \quad (4.89)$$

Also, all the other approximations commonly applied to solve the Bethe-Goldstone equation should not influence the result too much (see, for example, [Ma 69] and [SF 74]). Kuo and Brown [KB 66] have solved the Bethe-Goldstone equation in the harmonic oscillator approximation [SF 74] for ^{18}O and ^{18}F using as bare interaction the Hamada-Johnston force. This force was subsequently used in Eq. (4.85) for a diagonalization in the model space where the experimental values found in ^{17}O have been used for the single particle energies. In Fig. 4.4 we show a comparison of the

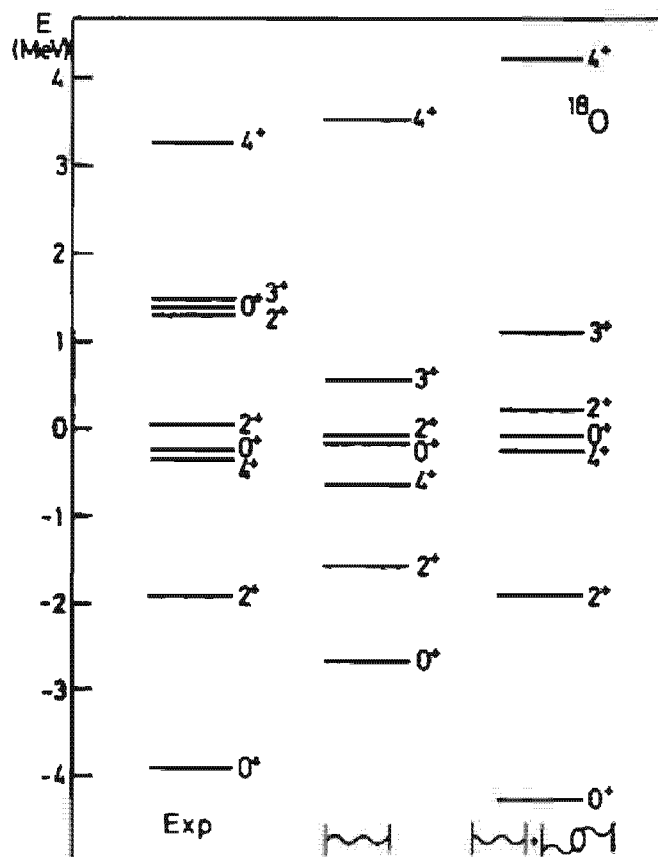


Figure 4.4. The spectrum of ^{18}O . The first column shows the experimental values. The second one was calculated with the pure G -matrix. The third also includes the polarization term (4.90). (From [HK 72].)

low-lying spectrum of ^{18}O as calculated by these authors, with the spectrum of the experiment; in Fig. 4.5 we show the same for the case of ^{210}Pb . The latter calculations were performed by Herling and Kuo [HK 72] using in principle the same method as Kuo and Brown. Their model space consisted of the following single-particle states:

neutrons: $2g9/2$ $1i11/2$ $1j15/2$ $3d5/2$ $4s1/2$ $2g7/2$ $3d3/2$

protons: $1h9/2$ $2f7/2$ $1i13/2$ $2f5/2$ $3p3/2$ $3p1/2$

As can be seen from Fig. 4.4 and Fig. 4.5, the comparison of these two calculations with experiment is not very satisfying and the agreement can be considered as qualitative only. The disagreement is probably not due to the various approximations which entered the solution of the Bethe-Goldstone equation, but rather to the omission of other configurations like $3p-1h$, etc. In both of the calculations mentioned it has been shown that at least perturbative inclusion of $3p-1h$ configurations improves agreement with experiment very much. The procedure was to calculate the contribution to V_{eff} from Q_{3p-1h} in Eqs. (4.83) and (4.85) in second order perturbation theory (omitting the unlinked terms, see footnote on page 166). This is

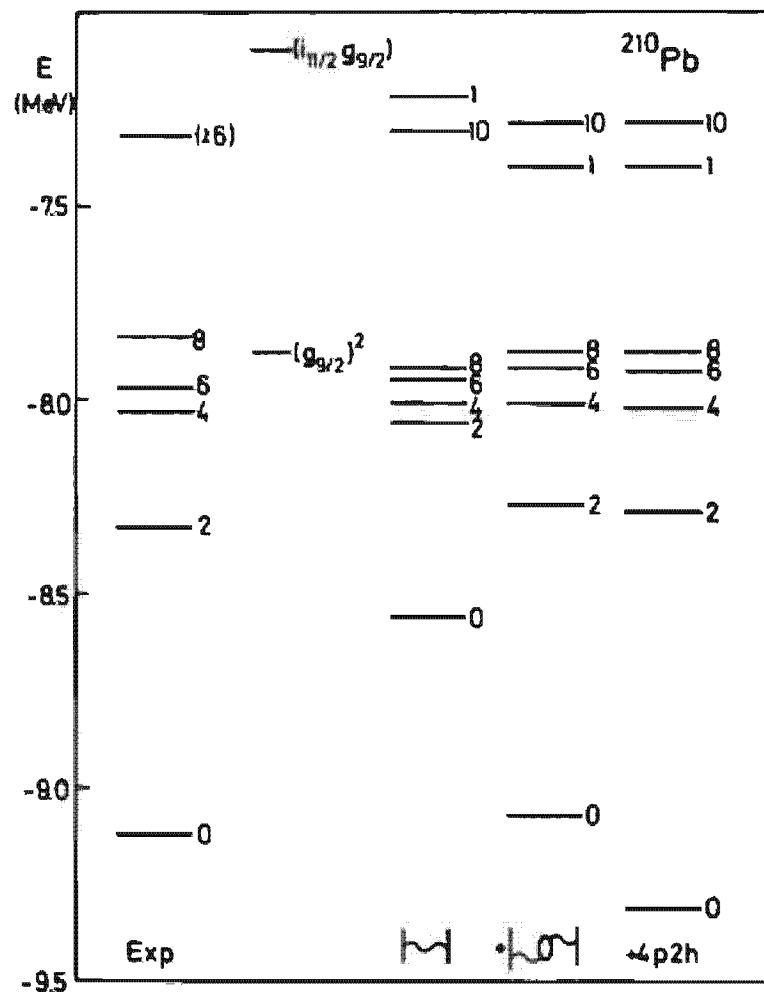


Figure 4.5. The spectrum of ^{210}Pb . The first three spectra have the same meaning as those of Fig. 4.4. In the fourth spectrum also, $4p-2h$ polarization terms were taken into account. Also indicated is the free two-particle energy. (From [HK 72].)

not too hard to carry out using our definition [(4.83) and (4.85)] and the result is:

$$(V_{\text{eff}}^{3p-1h})_{mn, m'n'} = \left\{ \sum_{pi} \frac{\bar{v}_{mi, m'p} \bar{v}_{pn, in'}}{\Omega_i - \epsilon_{m'} - \epsilon_n - \epsilon_p + \epsilon_i} - (n' \leftrightarrow m') \right\} - (m \leftrightarrow n). \quad (4.90)$$

In this expression we neglected all terms which give a renormalization of the single-particle energies, that is, terms of the structure $(V_{\text{eff}})_{mn, m'n'} = A_{mn} B_{m'n'} - (m' \leftrightarrow n')$, because it is believed that these terms are already included in the experimental single-particle energies used in the specific calculations. Usually one represents the term (4.90) graphically, as displayed in Fig. 4.6 (more about graphs is explained in Chap. 8 and Appendix F). The second order part however cannot be used as it stands because of the hard core potential. It can be shown [BK 67a] that it is a consistent re-summation of higher order terms to replace the bare interactions by their corresponding G -matrices in the second order contribution of the $3p-1h$ states to V_{eff} (e.g., (4.90)). We do not wish to go into the details of such arguments here because they would lead us outside the scope of this book. In Figs. 4.4 and 4.5 are also shown results with the inclusion of these "renormalized" second order $3p-1h$ contributions (the "core polarization") and, as can be seen, the agreement with experiment proves in both cases almost perfect. If this were the whole story, the results would be very satisfying, since we would have explained the low-lying part of the spectrum of these nuclei using essentially no free parameter. Unfortunately, things are far from being settled, since further studies have shown that inclusion of higher order terms will again worsen the results. This effect is shown in Fig. 4.5, where not only $3p-1h$ but also $4p-2h$ terms are included. More systematic but complicated studies in this direction have been performed by Barrett and Kirson [BK 73] and Kirson and Zamick [KZ 70], which show that great fluctuations of the results as a function of different higher order terms are observed and, therefore, no definite conclusions can be drawn; in particular, it remains unexplained why the second order $3p-1h$ inclusion gives such good agreement with experiment. One may, therefore, draw the conclusion that the microscopic theory of effective interactions is still not at a very satisfying stage.

Nevertheless, we want to come back to two formal points in the theory. The first concerns the energy dependence of the effective interaction V_{eff}^E . In all calculations this energy dependence has been more or less neglected. As we have already stated, this is, of course, only true as long as the energy

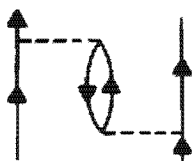


Figure 4.6. Graphical representation of a core polarization term.

dependence is really weak. However, it can happen that V_{eff}^E has poles, as a function of E , which lie close or even in the region of the low-lying states of interest; for example, this is the case for ^{16}O , where a collective $4p-2h$ pole comes very low in energy [Sch 75]. In this case, such a pole has to be treated separately, since it gives rise to a strong energy dependence in the region of interest. The states also cause difficulties in the case of the folded diagram formalism (see footnote on page 166), where they have been called *intruder states* [SW 72, 73]. There, it turns out that the perturbation series of the corresponding effective interaction in powers of the G -matrix very likely diverge in such cases. Special techniques have been developed to handle this problem [SW 72, 73, HLR 74].

Up to now we have considered only two-particle systems, however, the same considerations can be made for the case of more than two valence nucleons [Ma 69], although we do not want to go into these details.

4.3.3 Effective Interactions between Particles and Holes

The problem of effective interactions between particles and holes arises mainly in the study of vibrational states of closed shell nuclei (see Chap. 8). However, from a microscopic point of view this case has been much less investigated than the interaction between valence nucleons (see, for example, [BK 69, KBB 70]). One can argue that it would be desirable to express also the effective ph force by a microscopic G -matrix with perhaps some higher order corrections, like the polarization diagrams for the valence nucleons. This can, in fact, be achieved. The discussion is complicated by the fact that, for the most part, the random phase approximation, (see Chap. 8) is considered the appropriate theory and not the Tamm-Dancoff approximation, for the ph case. However, in order not to complicate things too much we shall restrict ourselves to the Tamm-Dancoff case.

The Tamm-Dancoff equation (see Chap. 8) has the following form.

$$(E_p^{\text{TDA}} - \epsilon_m + \epsilon_i) C_{mi}^\mu = \sum_{nj} \bar{v}_{mj, in} C_{nj}^\mu. \quad (4.91)$$

This equation, where m, n (i, j) are indices above (below) the Fermi level, is usually solved in a model space with, say, one shell below and one above the Fermi level. In analogy to the case of two valence nucleons, the phenomenological interaction entering Eq. (4.91) has to simulate the effect of the $1p-1h$ states not included in the model space, and also $2p-2h$, $3p-3h$, etc. effects.

In general, for a closed shell nucleus we can make the following expansion of such a vibrational state (see Chap. 8):

$$|\mu\rangle = \sum_{mi} C_{mi}^\mu a_m^+ a_i |\text{HF}\rangle + \sum_{\substack{m < n \\ i < j}} C_{mn, ij}^\mu a_m^+ a_n^+ a_i a_j |\text{HF}\rangle + \dots. \quad (4.92)$$

However, the procedure for arriving at an effective interaction starting from Eq. (4.92) has to be somewhat different from the valence nucleon case. First we introduce the projector P which projects onto the whole $1p-1h$ subspace, that is:

$$P = \sum_{mi} a_m^+ a_i |\text{HF}\rangle \langle \text{HF}| a_i^+ a_m, \quad (4.93)$$

$$Q = 1 - P,$$

with no restriction on the sum. Using the same formalism as for arriving at Eq. (4.85), we obtain in the *ph* case

$$[E_\mu - E_0^{\text{HF}} - \epsilon_m + \epsilon_i] C_{mj}^\mu = \sum_{nj} \langle mi | V_{\text{eff}}^{E_\mu} | nj \rangle C_{nj}^\mu, \quad (4.94)$$

where V_{eff} is formally given by the same expression as in Eq. (4.83) with, however, the projection operators P and Q given by Eq. (4.93). The first contribution to Q comes from the $2p-2h$ components, that is, from Q_{2p-2h} . Calculating the contribution of this term to second order perturbation theory in V , we obtain:

$$\begin{aligned} (V_{\text{eff}}^{(2p-2h)}) &= \sum_{m' < n'} \bar{v}_{mj, m'n'} \frac{1}{\Omega_\mu + \epsilon_i + \epsilon_j - \epsilon_{n'} - \epsilon_{m'}} \bar{v}_{n'm', in} \\ &- \sum_{i' < j'} \bar{v}_{j'i, ni} \frac{1}{\Omega_\mu - \epsilon_m - \epsilon_n + \epsilon_i + \epsilon_{j'}} \bar{v}_{jn, i'j} \\ &- \sum_{n'j'} \bar{v}_{mj, nn'} \frac{1}{\Omega_\mu - \epsilon_n + \epsilon_i - \epsilon_{n'} + \epsilon_{j'}} \bar{v}_{jn', ij'} \\ &- \sum_{m'i'} \bar{v}_{ji, mi} \frac{1}{\Omega_\mu - \epsilon_m + \epsilon_j - \epsilon_{m'} + \epsilon_{i'}} \bar{v}_{mm', i'n}, \end{aligned} \quad (4.95)$$

where $\Omega_\mu = E_\mu^A - E_0^{\text{HF}}$ and terms which renormalize single-particle energies are not included. The first term on the r.h.s. of Eq. (4.95) together with the first order term of V_{eff} just gives the first two terms of the G -matrix:

$$G_{mj, in}^{\Omega_\mu + \epsilon_i + \epsilon_j}. \quad (4.96)$$

Indeed, we can verify that to each order in V there exists in V_{eff} a term which corresponds to the corresponding order in Eq. (4.96). Therefore, V_{eff} consists of a first term which is the G -matrix (4.96). The second term on the r.h.s. of Eq. (4.95) represents hole-hole correlations which numerically are found to be small and therefore may be neglected. The third and fourth term are analogous to the polarization diagram (Fig. 4.6) for the case of two valence nucleons. Again, these terms cannot be used as they stand, but we can show that it is a consistent re-summation of higher order terms to replace the bare matrix elements by their corresponding G -matrix elements. The polarization diagram in the *ph* case is displayed in Fig. 4.7. The fact that we already have a G -matrix in the full *ph* space to lowest order is the essential difference between the *ph* and *pp* cases. In recognizing this, we may now convert Eq. (4.94) to one in a model *ph* space. For this purpose we split the projector P into a part P_M which projects onto the model *ph* space and into a part P_R which projects onto the rest of the *ph* space:

$$P = P_M + P_R.$$

Eliminating the components in Eq. (4.94) that are outside the model space with the aid of the Feshbach projection operator formalism [Fe 62], which we have already used [see, for example, Eqs. (4.80) and (4.81)], leads to a TDA equation in the model space. The effective interaction appearing there can be expanded up to

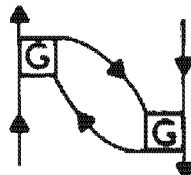


Figure 4.7. Polarization diagram in the particle-hole case.

second order in the G -matrix. The term which comes from Eq. (4.96) is shown in Fig. 4.8, where it should be appreciated that the summation over the intermediate lines goes only over states that are *not* in the modelspace. Realistic calculations [BK 69, KBB 70] show that the inclusion of the polarization diagram Fig. 4.7 has an important effect: Whereas RPA calculations (see Chap. 8) without it give imaginary solutions, the polarization contribution stabilizes the solutions. The reason for this—as discussed in more detail in Chap. 8—is that the RPA overestimates ground state correlations and polarization or screening terms have to be introduced to reduce them.



Figure 4.8. Second order contribution to V_{eff} in the model $p\hbar$ space. The broken intermediate lines shall indicate that one has to sum only over states not contained in the model space.

With these remarks we wish to finish our consideration of the microscopic effective interaction and, in the next section, turn to their phenomenological counterparts.

4.4 Phenomenological Effective Interactions

4.4.1 General Remarks

In Section 4.3 we saw how effective forces can be defined microscopically and how difficult it is in practice to calculate them and get quantitative agreement with experiment. Consequently, from the early days of nuclear physics the use of phenomenological forces, which contain a certain number of *fit parameters* adjusted to reproduce the experimental data has been adopted. In many cases this procedure has turned out to be extremely successful and, using only a few parameters chosen once and for all, much experimental data covering quite a large range of nuclear masses can be explained. Therefore, it is all the more disconcerting that a really satisfying microscopic theory able to explain the success of these phenomenological forces is somehow still missing.

There exists, of course, an enormous number of different phenomenological interactions that have been applied to problems in nuclear physics. Each of them has been used for a specific problem and their range of

validity and success varies very much. It lies outside the scope of this book to give a complete picture, and we will restrict our discussion to certain essential properties and the presentation of only the most successful examples. Most of them are only constructed for a special purpose, as, for example, for Hartree-Fock calculations (see Chap. 5), which calculate the nuclear self-consistent field, and bulk properties of nuclei such as binding energies and saturation densities. Others serve as effective forces between valence nucleons or between particles and holes (see Sec. 4.3). Therefore, we must be very careful in comparing these different types of interaction, even if, as we shall see, they look very similar in mathematical structure.

As we discussed in the last section, the effective interactions are used in a certain shell model configuration space: *the model space*. We therefore have to expect a certain dependence of the effective interaction on the space, that is, different interactions have to be taken for different sizes of the model space. As we have seen, the microscopically defined effective interaction is always energy dependent, while most of the time there is no explicit energy dependence in the phenomenological forces. It is usually sufficient to put all these dependences in a varying strength parameter.

It is evident that we prefer to choose the analytical form of the effective interaction to be as simple as possible. For example, it is often assumed that the effective interaction obeys the same *invariance principles* as the bare nucleon-nucleon interaction (see Sec. 4.2). This is certainly not always true. For instance, we should expect the renormalization procedure which describes the transition from the bare nucleon-nucleon interaction to the effective one to depend on the actual density of the system, that is, we get a different force in the interior of the system than in the surface and outer regions. For a shell model calculation in a fixed well, we should therefore not expect a translationally invariant residual interaction.

We know that the *range of the nuclear force* is rather short. We have seen in Section 4.3 that this is true even for the range of the effective *G*-matrix. The simplest ansatz therefore consists in using a *zero range* force whose radial dependence is described by a δ -function. In fact, such forces turn out to be rather useful because they are simple to handle and they describe many nuclear properties quite well. More realistic forces, however, need to have a finite non-vanishing range (see [AS 71, Sch 72b]). A *finite range* can be simulated by a *momentum dependence*. To show this we transform a function $V(r)$ of the relative distance $r = r_1 - r_2$ into momentum space

$$\langle \mathbf{p} | V | \mathbf{p}' \rangle = \frac{1}{(2\pi\hbar)^3} \int e^{-\frac{i}{\hbar}(\mathbf{p}-\mathbf{p}')\cdot \mathbf{r}} V(\mathbf{r}) d^3r. \quad (4.97)$$

We see that a δ -force is a constant and that any range represents a p -dependence in momentum space. The simplest rotationally invariant one is of the form

$$(2\pi\hbar)^3 \langle \mathbf{p} | V | \mathbf{p}' \rangle = V_0 + V_1 p'^2 + V_2 p^2 + V_3 \mathbf{p} \cdot \mathbf{p}', \quad (4.98)$$

which in coordinate space corresponds to the momentum dependent operator

$$V(\mathbf{r}) = V_0 \delta(\mathbf{r}) + V_1 (\hat{\mathbf{p}}^2 \delta(\mathbf{r}) + \delta(\mathbf{r}) \hat{\mathbf{p}}^2) + V_2 \hat{\mathbf{p}} \delta(\mathbf{r}) \hat{\mathbf{p}}. \quad (4.99)$$

Effective forces usually depend on the density $\rho(\mathbf{r})$. Such *density dependence* is easy to understand if, for example, we consider expression (4.39) for the G -matrix: The range of the summation depends on the Fermi energy, which is itself a function of the density. It is also quite easy to see that the different projection operators Q entering the definition of the effective interactions [see Eqs. (4.40) and (4.77)] can be expressed as a nonlocal density which is therefore another source of density dependence.

Other simple forms that work surprisingly well are separable two-body forces, that is, forces which can be represented as products (or as a sum of products), in which each factor acts on only one of the two particles.

4.4.2 Simple Central Forces

There exists a large number of forces which use only the central part (4.20), but differ in their radial dependence $V(r)$. Some simple potentials that have been used are, for example, the Yukawa potential (4.33) or

$$V(r) = -V_0 e^{-r^2/r_0^2} \quad (\text{Gauss potential}), \quad (4.100)$$

$$V(r) = -V_0 \frac{e^{-r/r_0}}{1 - e^{-r/r_0}} \quad (\text{Hulthen potential}), \quad (4.101)$$

$$V(r) = -V_0 \delta\left(\frac{r}{r_0}\right) \quad (\text{contact potential}). \quad (4.102)$$

The potential depth V_0 and the range r_0 are adjusted to fit experimental data. One finds $V_0 \approx 50$ MeV and $r_0 \approx 1 - 2$ fm (the Compton wavelength of the pion is 1.4 fm).

For the r -dependent coefficients $V(r)$ in Eq. (4.20) the same radial dependence is usually assumed; only their strength and sign are adjusted to fit empirical data. Here we do not wish to discuss which one of the

Table 4.3 Coefficients for the exchange mixtures

Mixture	a_{tt}	a_{ts}	a_{st}	a_{ss}
Wigner	1	1	1	1
Kurath [Ku 56, SW 66]	1	0.6	-0.6	-1
Serber [HS 57]	1	1	0	0
Rosenfeld [EF 57]	1	0.6	-0.34	-1.78
Ferrel-Visscher [VF 57]	1	0.634	-0.366	0
Soper [So 57]	1	0.46	0.14	-0.4
Gillet [GGS 66] I	1	0.6	-0.6	0.6
II	1	0.4	-0.2	0.2

different exchange mixtures is to be preferred; we wish only to give some of the most commonly used values of the coefficients (Table 4.3).

$$V(1,2) = V_0 f\left(\frac{r}{r_0}\right) (a_{ee} \Pi'_e \Pi'_e + a_{es} \Pi'_e \Pi'_s + a_{se} \Pi'_s \Pi'_e + a_{ss} \Pi'_s \Pi'_s). \quad (4.103)$$

Other forces of a similar type have been used by Kallio and Koltveit [KK 64] and by Elliott and Clark [CE 65]. The latter authors also include a tensor term and a two-body spin orbit force.

4.4.3 The Skyrme Interaction

In 1956 Skyrme [Sk 56, 59] proposed an effective interaction with a three-body term viz:

$$V = \sum_{i < j} V(i,j) + \sum_{i < j < k} V(i,j,k). \quad (4.104)$$

To simplify the calculations, he used a short-range expansion in the form of Eq. (4.99) for the two-body part:

$$\begin{aligned} V(1,2) = & t_0 (1 + x_0 P^0) \delta(\mathbf{r}_1 - \mathbf{r}_2) \\ & + \frac{1}{2} t_1 [\delta(\mathbf{r}_1 - \mathbf{r}_2) \mathbf{k}^2 + \mathbf{k}^2 \delta(\mathbf{r}_1 - \mathbf{r}_2)] + t_2 \mathbf{k} \delta(\mathbf{r}_1 - \mathbf{r}_2) \mathbf{k} \\ & + i W_0 (\sigma^{(1)} + \sigma^{(2)}) \mathbf{k} \times \delta(\mathbf{r}_1 - \mathbf{r}_2) \mathbf{k}, \end{aligned} \quad (4.105)$$

where $\mathbf{k} = (1/\hbar)\mathbf{p}$ is the operator of the relative momentum

$$\mathbf{k} = \frac{1}{2i} (\nabla_1 - \nabla_2). \quad (4.106)$$

For the three-body force Skyrme also assumed a zero range force of the form

$$V(1,2,3) = t_3 \delta(\mathbf{r}_1 - \mathbf{r}_2) \delta(\mathbf{r}_2 - \mathbf{r}_3). \quad (4.107)$$

The five constants— t_0 , t_1 , t_2 , t_3 , x_0 —and W_0 were adjusted to the experimental binding energies and radii. There are several sets of parameters called Skyrme I, II, etc. (see Sec. 5.6) resulting from different fits. We present here Skyrme III [BFG 75]:

$$\begin{aligned} t_0 &= -1128.75 \text{ MeV fm}^3; & t_1 &= 395.0 \text{ MeV fm}^5; \\ t_2 &= -95.0 \text{ MeV fm}^5; & t_3 &= 14000.0 \text{ MeV fm}^6; \\ W_0 &= 120 \text{ MeV fm}^5; & x_0 &= 0.45. \end{aligned} \quad (4.108)$$

The parameter t_0 describes a pure δ -force with a spin-exchange; t_1 and t_2 simulate an effective range, as in Eq. (4.99). The fourth term in Eq. (4.105) represents a two-body spin orbit interaction. It can be obtained [BS 56] from a normal spin orbit term [see Eq. (4.23)] in the short range limit.

In Chapter 5, we shall see that this force has been used extensively in

Hartree-Fock calculations. For spin saturated even-even nuclei, the three-body term (4.104) turns out to be equivalent to a density dependent two-body interaction*:

$$V_\rho(1, 2) = \frac{1}{6} t_3 (1 + P^\sigma) \delta(\mathbf{r}_1 - \mathbf{r}_2) \rho(\frac{1}{2}(\mathbf{r}_1 + \mathbf{r}_2)). \quad (4.109)$$

Such a density dependent term can also be regarded as the phenomenological representation of the ρ -dependence of the microscopic effective interaction. This interpretation is preferable to the view that the Skyrme force contains a three-body interaction, since we know that three-body interactions are rather weak in nuclei.

There are essentially three reasons why this force has gained so much importance over the last ten years:

- (i) Vautherin and Brink [VB 72] (see Chap. 5) were able to reproduce the nuclear binding energies over the whole periodic table with a reasonable set of parameters and, at the same time, the nuclear radii. This had not been possible with the usual non-density dependent forces.
- (ii) Negele and Vautherin [NV 72] gave the connection between this force and the more fundamental G -matrix discussed in the last sections.
- (iii) The mathematical form of the force is extremely simple. The δ -functions simplify all types of calculations enormously.

There are similar types of interactions originally proposed by Moszkowski [Mo 70], the so-called *modified δ -interactions* (MDI). They differ from the Skyrme interaction by the absence of the t_2 -term and the spin orbit force and also by a different ρ -dependence ($\sim \rho^\sigma$ with $\sigma < 1$).†

4.4.4 The Gogny Interaction

Despite the great success of the Skyrme interaction, it has been argued that zero range forces might not be able to simulate the long range or even the intermediate range parts of the realistic effective interaction. In particular, the present versions of the Skyrme force are not able to properly describe pairing correlations in nuclei (see Chap. 6), therefore Gogny [Go 75b] replaced the t_0 , t_1 and t_2 parts of the Skyrme force by a sum of two

*This is no longer true for systems without spin saturation. In such cases, the three-body term (4.107) in the Skyrme force, which is purely local and repulsive, favors parallel spin alignment, that is, nuclear ferromagnetism. This contradicts the observed spin saturation and the pairing properties in nuclei. This difficulty can be avoided by using either a density dependent two-body interaction [BJS 75] of the form (4.109) or a nonlocality in the three-body term [ON 78].

†There is a strong correlation between the nuclear compressibility and the exponent σ in the density dependence [CS 72].

Gaussians* with spin-isospin exchange mixtures (a force which was originally used by Brink and Booker [BB 67]) and got

$$\begin{aligned} V(1,2) = & \sum_{i=1}^2 e^{-(r_1-r_2)^2/\mu_i^2} (W_i + B_i P^0 - H_i P^r - M_i P^0 P^r) \\ & + i W_0 (\sigma_1 + \sigma_2) \mathbf{k} \times \delta(\mathbf{r}_1 - \mathbf{r}_2) \mathbf{k} \\ & + t_3 (1 + P^0) \delta(\mathbf{r}_1 - \mathbf{r}_2) \rho^{1/3} \left(\frac{1}{2} (\mathbf{r}_1 + \mathbf{r}_2) \right). \end{aligned} \quad (4.110)$$

The parameters were adjusted to the properties of finite nuclei, and for nuclear matter (Table 4.4).

Table 4.4 Force parameters of the Gogny force (D1)

i	μ_i [fm]	W_i	B_i	H_i	M_i [MeV]	$W_0 = +115$ [MeV fm ³]
1	0.7	-402.4	-100.	-496.2	-23.56	$t_3 = 1350$ [MeV fm ⁴]
2	1.2	-21.30	-11.77	37.27	-68.81	

4.4.5 The Migdal Force

This force was proposed by Migdal [Mi 67] in his theory of finite Fermi systems. Based on the interacting quasi-particle concept of Landau's theory of a Fermi liquid [La 59], Migdal introduces this force to describe the collective excitations in nuclei.*

Starting from the ground state of an even-even system, the quasi-particles are defined as the low-lying excitations in the neighboring odd mass nuclei. The ground state of the even system contains no quasi-particles, and excited states are characterized by the quasi-particle occupation numbers n_λ . A change of these occupation numbers by the amount δn_λ causes a change in the total energy E_0 of the system by the amount

$$\delta E_0 = \sum_\lambda \epsilon_\lambda^0 \delta n_\lambda + \frac{1}{2} \sum_{\lambda\lambda'} F_{\lambda\lambda'} \delta n_\lambda \delta n_{\lambda'},$$

where ϵ_λ^0 are the energies of a quasi-particle λ in the absence of any other quasiparticle and $F_{\lambda\lambda'}$ is the so-called quasi-particle interaction. Migdal introduces an effective particle-hole interaction F^w and an effective particle-particle (or hole-hole) interaction F^t .

In an infinite system with translational invariance, the quasi-particles are characterized by the momentum \mathbf{k} , and Landau could show that the ph -interaction $F(\mathbf{k}, \mathbf{k}')$ is given by the second derivative of the total energy

* Similar density dependent effective interactions have been used in [Kr 70, ZR 71, RPS 72, LMV 73, RBP 77].

[†] It would be beyond the scope of this book to go into the details of this theory. The reader may, however, find some basic ingredients in Section F.7.

E_0 with respect to the quasi-particle densities $n(\mathbf{k})$:

$$F^{ph}(\mathbf{k}, \mathbf{k}') = \frac{\delta^2 E_0}{\delta n(\mathbf{k}) \delta n(\mathbf{k}')} . \quad (4.111)$$

At the Fermi surface this is an exact relation.

In a finite system the quasi-particle density $\bar{\rho}_{\lambda\lambda'}$ is no longer completely determined by its diagonal elements (the occupation numbers n_λ), but it also contains information about the form of the single-particle wave functions φ_λ . The effective interaction then depends on four indices, and it has been proposed to derive this quantity, in analogy to Eq. (4.111), from the exact ground state energy [Br 71]

$$F_{psqr}^{ph} = \frac{\delta E_0}{\delta \bar{\rho}_q \delta \bar{\rho}_r} . \quad (4.112)$$

So far it has not been shown that this is an exact relation. However, a very similar expression is obtained in a quite different (*approximate*) theory: the time dependent Hartree–Fock theory in the limit of a motion with small amplitudes (see Sec. 8.5). Starting from the assumption that the wave function is a Slater determinant (i.e., $\rho^2 = \rho$; see Sec. 5.3.3) and that the total energy can be expressed by a functional $E_0[\rho]$, we obtain in this case the effective *ph*-interaction as the second derivative of $E_0[\rho]$ with respect to ρ [Eq. (8.124)], just as in Eq. (4.112).

It is clear from the above that, for instance, the Skyrme force (Sec. 4.4.3) cannot be compared with the Migdal force directly, even though, as we shall see, it looks very similar. Within the approximation $\rho^2 \approx \rho$, however, an indirect relation may be established by differentiating the ground state energy calculated with the Skyrme interaction twice with respect to the density.

Like the Skyrme force, the Migdal force is an expansion in momentum space. However, contrary to potentials suitable for Hartree–Fock calculations (such as the Skyrme force), the p^2 -terms do not play an essential role, as the Migdal forces do not have to guarantee saturation (they are constructed to describe different physical situations anyway). In most calculations it is therefore sufficient to take into account only the constant in momentum space which gives a pure δ -force in coordinate space. On the other hand, spin and isospin exchange mixtures are now very important. They are different for the particle–particle and particle–hole forces:

$$V(1, 2) = V_0 \delta(\mathbf{r}_1 - \mathbf{r}_2) (f + f' \tau^{(1)} \tau^{(2)} + g \sigma^{(1)} \sigma^{(2)} + g' \sigma^{(1)} \sigma^{(2)} \tau^{(1)} \tau^{(2)}) . \quad (4.113)$$

V_0 is a strength parameter which has to be adjusted to the configuration space (e.g., in the ^{208}Pb region $V_0 = 380 \text{ MeV fm}^3$). Guman and Birbrair [GB 65] proposed to take into account the different interaction strengths inside and outside the nucleus and the diffuseness of the nuclear surface by a linear density dependence of the constants f, f' ,

$$f = f^{\text{ex}} + (f^{\text{in}} - f^{\text{ex}}) \rho(r) , \quad (4.114)$$

where $\rho(r)$ has the form of a Fermi distribution

$$\rho(r) = \frac{1}{1 + \exp[(r - R)/a]} . \quad (4.115)$$

The additional parameters R and a represent the radius and the diffuseness, respectively, of the nucleus. Contrary to a Hartree-Fock calculation with a density dependent interaction (see Chap. 5), the density (4.114) is not adjusted self-consistently. Therefore, the Migdal force violates translational invariance. Of course, this is no drawback, since the renormalization procedure is closely connected with the underlying single-particle potential, which also violates translational invariance. In fact, a proper choice of the effective residual interaction should restore this invariance (see Mikeska and Brenig [MB 69]). From this condition one can deduce additional relations among the parameters f, f', g, g' [NW 72, 74].

The Migdal force has been widely used to calculate low-lying collective vibrations in nuclei within the framework of the random phase approximation (see Chap. 8). The effective charges caused by such vibrations (see Chap. 9) provide an enormous amount of experimental data with which to adjust the six parameters $f^{\text{in}}, f'^{\text{in}}, f'^{\text{ex}}, f'^{\text{ex}}$, and g, g' for the particle-hole and particle-particle forces (for details, see [RBS 73, BSK 73, BER 75]). For the particle-hole force Ring and Speth [RS 74a] found:

$$\begin{aligned} f^{\text{in}} &= 0.0685; & f'^{\text{in}} &= 0.3315; & f'^{\text{ex}} &= -2.165; \\ f'^{\text{ex}} &= 0.465; & g &= 0.575; & g' &= 0.725. \end{aligned} \quad (4.116)$$

It is important to note that this is an effective ph -force which does not have to be antisymmetrized [KMS 76]. It shows strong attraction outside the nucleus and is close to zero inside the nucleus.

4.4.6 The Surface-Delta Interaction (SDI)

Like the Migdal interaction, this force is thought of as an effective residual interaction among the particles near the Fermi surface. The main physical idea is that the nucleons move almost independently in the nuclear interior. In fact, the residual interaction of Migdal is rather weak inside the nucleus. Most of the collisions occur at the nuclear surface where the Pauli principle loses its importance and the nucleons feel the strong attractive interaction [GM 65]. The behavior of the force outside the surface is again not very important because there the wave functions have exponentially decaying tails, that is, the probability of finding a nucleon there goes rapidly to zero. Therefore, it is a meaningful approximation to restrict the whole interaction to the nuclear surface and to define the so-called surface delta interaction:

$$V(1, 2) = -V_0 \delta(\mathbf{r}_1 - \mathbf{r}_2) \delta(|\mathbf{r}_1| - R_0). \quad (4.117)$$

V_0 can still depend on the spin and isospin coordinates in the usual way

(4.20). This force has very simple geometrical properties. Using the expansion of the δ -function in Legendre polynomials—

$$\delta(\mathbf{r}_1 - \mathbf{r}_2) = \frac{\delta(r_1 - r_2)}{r_1 r_2} \sum_l \frac{2l+1}{4\pi} P_l(\cos \theta_{12}), \quad (4.118)$$

where θ_{12} is the angle between the vectors \mathbf{r}_1 and \mathbf{r}_2 —and the addition theorem of the spherical harmonics [Ed 57, Eq. 4.6.6], we get:

$$V(1, 2) = -V_0 \sum_{lm} \frac{\delta(r_1 - R_0)}{r_1} Y_{lm}^*(\theta_1 \varphi_1) \frac{\delta(r_2 - R_0)}{r_2} Y_{lm}(\theta_2 \varphi_2). \quad (4.119)$$

This is an infinite sum over separable terms. In a spherical basis, the matrix elements coupled to a good angular momentum become extremely simple because only one term of the sum in (4.119) survives. This model force has been applied [KS 63, PAM 66, FP 67, Fä 68, VPK 69] in many calculations. It has been used—like the Migdal force—as an effective force among the valence particles. It is, however, not meaningful to extend the underlying configuration space over more than two major shells, because in that case we have levels with the same angular momentum quantum numbers. Since the radial integrals are approximated by the value of the wave function at $r = R_0$, there is no cancellation for wave functions with different numbers of radial nodes. Consequently, the particles in such levels feel an unphysical strong interaction.

4.4.7 Separable Forces and Multipole Expansions

In the last section we saw that the surface-delta interaction is extremely simple to handle because of its separability in a shell model basis.

We call a force *separable in particle hole direction* if it can be written in second quantization in the form [: : means normal ordering in the sense of Eq. (C.50)]

$$V = :Q^+ \cdot Q:, \quad (4.120)$$

where

$$Q = \sum_{k_1 k_2} q_{k_1 k_2} a_{k_1}^+ a_{k_2} \quad (4.121)$$

is a one-particle operator. Acting on a Slater determinant, it creates a superposition of *ph*-pairs. A force is called *separable in pp-direction* if it has the form

$$V = P^+ \cdot P, \quad (4.122)$$

where

$$P^+ = \frac{1}{2} \sum_{k_1 k_2} p_{k_1 k_2} a_{k_1}^+ a_{k_2}^+ \quad (4.123)$$

is a pair creation operator. Acting on a Slater determinant, it creates a

superposition of pp -pairs. It seems very unlikely that a realistic force can be represented by so simple an ansatz as Eqs. (4.120) and (4.122), however, it has been shown that the matrix elements of these schematic forces with a suitably chosen strength are of the same magnitude as those calculated from a microscopic G -matrix with polarization terms (see Sec. 4.3 and F.5) [BK 67b].

We wish here to study the question of *separability* somewhat further and investigate a general *phenomenological effective force* without spin and isospin dependence. The force shall depend only on the relative distance between the nucleons, therefore we can expand in the following way [La 64].

$$V(|\mathbf{r}_1 - \mathbf{r}_2|) = \sum_l V_l(r_1, r_2) \sum_m Y_{lm}^*(\theta_1 \varphi_1) Y_{lm}(\theta_2 \varphi_2), \quad (4.124)$$

with

$$V_l(r_1, r_2) = 2\pi \int_{-1}^1 V(|\mathbf{r}_1 - \mathbf{r}_2|) P_l(\cos \theta_{12}) d \cos \theta_{12}. \quad (4.125)$$

For a δ -force, $V = -V_0 \delta(r)$, we find that V_l does not depend on l :

$$V_l(r_1, r_2) = -V_0 \frac{\delta(r_1 - r_2)}{r_1 r_2}. \quad (4.126)$$

In Eq. (4.124) we have written a general force as an infinite sum of terms, each of which are separable in the angular coordinates. As we see from the δ -force, we cannot expect this expansion to converge rapidly for a short range force. In fact, we obtain an estimate for the effective range of each component in the expansion (4.124) if we restrict ourselves to a small region in space where $r_1 \approx r_2 \approx r$. The function $P_l(\cos \theta_{12})$ has its major contributions only in the region $0 < \theta_{12} \lesssim 1/l$ (Fig. 4.9), that is, V_l (4.125) is small, if the range of the potential $V(r_{12})$ is large compared to r/l , that is,

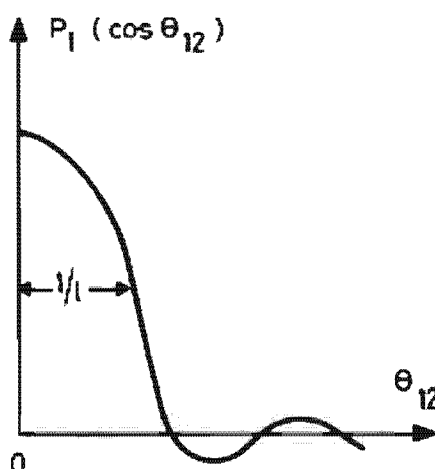


Figure 4.9. Legendre polynomial of degree l as a function of the angle θ_{12} between \mathbf{r}_1 and \mathbf{r}_2 .

the larger the strength of the high l -components V_l , the shorter the range of the force. In a force with zero range (δ -force), all l -components have the same relative weight.

We now come back to the question of separability. The general force (4.124) and the δ -force (4.126) are not separable because of the radial dependence in $V_l(r_1, r_2)$. On the other hand, if one assumes that the interaction is surface peaked as the SDI-interaction (4.117), it then becomes a sum of separable terms because of the additional factor $\delta(r - R_0)$.

$$V_l^{\text{SDI}}(r_1, r_2) = \frac{-V_0}{r_1} \delta(r_1 - R_0) \frac{1}{r_2} \delta(r_2 - R_0). \quad (4.127)$$

A more general separable ansatz of this kind is

$$V_l(r_1, r_2) = f_l(r_1) \cdot f_l(r_2). \quad (4.128)$$

One often chooses $f_l \sim r^l$ and obtains the multipole-multipole forces

$$V = -\frac{1}{2} \sum_{lm} \chi_l : Q_{lm}^+ Q_{lm} := -\frac{1}{2} \sum_l \chi_l : Q_l^+ \cdot Q_l :, \quad (4.129)$$

where χ_l are constants and Q_{lm} is the multipole operator

$$Q_{lm} = \sum_{k_1 k_2} \langle k_1 | r^l Y_{lm}(\theta, \varphi) | k_2 \rangle a_{k_1}^+ a_{k_2}. \quad (4.130)$$

If we take into account only the components with small l -values, we obtain long range forces. The most well known is the quadrupole-quadrupole force [El 58, KS 63]. We shall see in Chapter 7 that it can be used to describe the quadrupole deformations of nuclei self-consistently.

Again we must emphasize that these multipole forces are only to be considered as an effective force between valence particles within a restricted configuration space. If there are many such valence particles we can apply a Hartree-Fock approximation for them* (see Chap. 5). However, such HF-calculations with multipole forces for valence nucleons should not be mixed up with the basic HF-calculations for the binding energies.

The expansion (4.124) turns out to be very useful for the *long range part* of the effective interaction, because in this case the functions V_l become small for higher l -values. To obtain a similar description of the *short range part* one uses a different kind of expansion. We shall restrict ourselves to interactions between nucleons of the same type (for the treatment of short range correlations between protons and neutrons, see Sec. 7.5).

We now consider the general expression (4.3) of a not necessarily local force $V(r_1, r_2, r'_1, r'_2)$. In the case of a local force, we have $r_1 = r'_1$ and $r_2 = r'_2$, and the expansion (4.124) is made in the variables r_1, r_2 . Now we require

*In such calculations, the exchange term (5.43) to the HF potential is usually neglected because it is small [BK 68, Ma 74].

instead $\mathbf{r}_1 = \mathbf{r}_2$ and $\mathbf{r}'_1 = \mathbf{r}'_2$. We expand in $\mathbf{r}_1, \mathbf{r}'_1$ and obtain expressions similar to (4.124) and (4.125).

$$\begin{aligned} & \delta(\mathbf{r}_1 - \mathbf{r}_2)\delta(\mathbf{r}'_1 - \mathbf{r}'_2)V(\mathbf{r}_1, \mathbf{r}'_1) \\ &= \delta(\mathbf{r}_1 - \mathbf{r}_2)\delta(\mathbf{r}'_1 - \mathbf{r}'_2)\sum_{lm} V_l(r_1, r'_1)Y_{lm}(\theta_1\phi_1)Y^*_{lm}(\theta'_1\phi'_1). \quad (4.131) \end{aligned}$$

The requirements $\mathbf{r}_1 = \mathbf{r}_2$ and $\mathbf{r}'_1 = \mathbf{r}'_2$ already restrict us to a short range because it is only true if the two nucleons are at the same place. (This does not necessarily mean a δ -force, because we are allowing for nonlocal forces). At a first glance, the expansion (4.131) seems to be as poor as Eq. (4.124) for a short range force. However, we have to calculate matrix elements between two-particle wave functions. As we shall demonstrate in a moment, the l th term in (4.131) gives a contribution only to the matrix element when the two particles are coupled to spin $I=l$. For two particles in a single j -shell, for instance, we find that their wave functions have maximal spatial overlap for $I=0$. In this case, the angular part of their wave function takes the form:

$$\langle \Omega_1 \Omega_2 | jjI=0, M=0 \rangle \propto \sum_{m=-l}^l (-)^m Y_{lm}(\Omega_1) Y_{l-m}(\Omega_2) \propto P_l(\cos \theta_{12}). \quad (4.132)$$

(Because of the short range force, we assume only the spin singlet to be important.) Therefore, we find maximal interaction for $I=0$, where the angular momenta j_1 and j_2 are antiparallel, and we can thus understand that the expansion (4.131) is meaningful for short range interactions.

Again, if we replace the non-separable radial term in (4.131) by a separable ansatz as in (4.129), we obtain

$$V_l(r_1, r'_1) = -G_l r_1^l \cdot r_1'^l. \quad (4.133)$$

$$V = -\sum_{lm} G_l P_{lm}^+ P_{lm}^- = -\sum_l G_l P_l^+ \cdot P_l^-, \quad (4.134)$$

with

$$P_{lm}^+ = \frac{1}{2} \sum_{k_1 k_2} \langle k_1 | r' Y_{lm} | k_2 \rangle a_{k_1}^+ a_{k_2}^+, \quad (4.135)$$

where $|\bar{k}\rangle$ is the time-reversed state to $|k\rangle$. In deriving Eq. (4.134) from (4.131) we must take care in handling the spin coordinate s , because the operator (4.133) is not separable in spin space a priori. Because of the δ -force character, however, we always have $s_1 = -s_2$, $s'_1 = -s'_2$, which makes it possible to derive (4.134).

We are now able to calculate the matrix elements of a δ -force in a single j -shell, where the single-particle wave functions are given by $\langle \mathbf{r}|nljm\rangle = R_{nl}(r)\langle \Omega|ljm\rangle$. We construct pair operators A_{IM}^+ with angular momentum I, M :

$$A_{IM}^+ = \frac{1}{\sqrt{2}} \sum_{m_1 m_2} C_{m_1 m_2 M}^{I J I} a_{jm_1}^+ a_{jm_2}^+ \quad (4.136)$$

and use Eqs. (4.124) and (4.126) to obtain

$$V_\delta = - \sum_{I=0,2,\dots} V_\delta(I) \sum_M A_{IM}^+ A_{IM},$$

with*

$$V_\delta(I) = V_0 \cdot R_4 \frac{1}{2} \frac{1}{2I+1} |\langle j||Y_I||j\rangle|^2 = \frac{V_0}{8\pi} R_4 \frac{(2I+1)^2}{2I+1} |C_{1/2}^{I/2} \langle -1/2|_0^I|^2, \quad (4.137)$$

where R_4 is the radial integral

$$R_4 = \int_0^\infty dr r^2 R_{nl}^4(r).$$

From (4.137) we see that only the I th term in the expansion (4.131) goes into the matrix element coupled to spin $I = I$. In the case of a δ -force, $V_\delta(I)$ is maximal for $I = 0$ and drops off rapidly with increasing I (Table 4.5).* The most important part of the force (4.134) is therefore the $I = I = 0$ part.

Table 4.5 The relative magnitude of the matrix elements $V_\delta(I)$ (4.137) in a single j -shell

$V_\delta(I)/V_\delta(0)$	$I=0$	2	4	6	8	10	12
$j = 7/2$	1	0.238	0.117	0.058	—	—	—
9/2	1	0.242	0.126	0.075	0.040	—	—
11/2	1	0.245	0.131	0.082	0.053	0.025	—
13/2	1	0.246	0.133	0.087	0.060	0.038	0.019

To avoid complicated formulas, one usually introduces a slight modification of the Condon-Shortley phases (see [Ed 57]), the so-called BCS phases, and defines for $m > 0$:

$$|nljm\rangle_{\text{BCS}} = |nljm\rangle_{\text{CS}},$$

$$|nlj-m\rangle_{\text{BCS}} = (-)^{l+j-m} |nlj-m\rangle_{\text{CS}}. \quad (4.138)$$

The time reversal operator T [Eq. (2.45)] has a very simple form in this case. For $m > 0$, we find

$$|\overline{nljm}\rangle = T|nljm\rangle = |nlj-m\rangle; \quad T|nlj-m\rangle = -|nljm\rangle. \quad (4.139)$$

The $I=0$ part of Eq. (4.134), the so-called *pure pairing force*, has the form

$$V^P = -G \frac{1}{4} \sum_{\substack{kk' \\ \leq 0}} a_k^+ a_{k'}^+ a_{\bar{k}} a_k, \quad (4.140)$$

where \bar{k} is again the time reversed state to k and the sum runs over all

*In the limit of large I - and j -values we find, by a semiclassical expansion [MJB 75],

$$|C_{1/2}^{I/2} \langle -1/2|_0^I|^2 \approx \frac{2}{\pi \cdot j} \sqrt{1 - \left(\frac{I}{2j}\right)^2}.$$

values of k, k' . This force has been widely used to describe short range correlations in nuclei within the BCS-formalism (see Chap. 6). It is again important to notice that it should only be applied in a restricted configuration space. The value of the force constant is connected with the size of this space. It is easy to generalize this simple model force and to take into account higher l -values in the expansion (4.131). They are called *multipole pairing forces*. They are separable in particle-particle direction and play an important role in the description of pairing vibrations (see Chap. 8 and [BB 71, BBN 74b]).

A very simple model force for heavy nuclei has been obtained by combining a quadrupole-quadrupole force and a pure pairing force to the pairing-plus-quadrupole force [KS 63, BK 68]:

$$V^{QP} = -\frac{1}{2}\chi :Q_2^+ \cdot Q_2^- - GP_0^+ \cdot P_0^-, \quad (4.141)$$

which takes into account the most important long-range correlations and the most important short-range correlations, and is very easy to handle (see Sec. 7.4). It contains basically three constants: χ and two different constants G_p and G_n for protons and neutrons. It should only be applied in a configuration not larger than one major shell. For actual values of χ and G , see [KS 60] or [BK 68].

4.4.8 Experimentally Determined Effective Interactions

Since the derivation of the effective interaction from a bare nucleon-nucleon force is rather complicated, some authors have tried to determine the matrix elements of the nucleon-nucleon force in a certain basis directly from the experimental data (for a review, see [ST 76] and [BPO 76]).

Elliott et al. [EJM 68] used the experimental phase shifts of nucleon-nucleon scattering to derive the matrix elements of an effective interaction directly in an oscillator basis (*Sussex force*). In this way, the problem of the hard core is avoided completely.

Less ambitious are attempts to derive special matrix elements from the spectra of "simple" nuclei. These are nuclei in which one has good reason to believe that their structure is determined only by a few matrix elements whose number does not exceed the number of the observed levels [Ta 62]. We may take, for example, the $1f7/2$ shell nuclei, where the $f7/2$ shell is well separated in the simple particle spectrum. One assumes in this case that there exist many pure $f7/2$ configurations in nuclei close to the double magic core ${}^{40}\text{Ca}$ with $N > 20$ and $Z > 20$. These levels are completely determined by the eight matrix elements $\langle (f7/2)^2IT | V | (f7/2)^2IT \rangle$ for $I = 0, 1, \dots, 7$ ($T = 1$ for I even, $T = 0$ for I odd).

McCullen et al. [MBZ 64] have determined these matrix elements from the spectrum of the nucleus ${}^{42}\text{Sc}$. It contains one neutron and one proton outside the ${}^{40}\text{Ca}$ core. Coupling to angular momentum I gives the interaction energy

$$\begin{aligned} V(I) &= \langle j_1 j_2 I | V | j_1 j_2 I \rangle \\ &= B(I, {}^{42}\text{Sc}) - B(I, {}^{41}\text{Sc}) - B(I, {}^{41}\text{Ca}) + B(I, {}^{40}\text{Ca}), \end{aligned} \quad (4.142)$$

where B are the experimental binding energies of the level with spin I in ^{42}Sc and of the ground state of the other nuclei. Using these matrix elements, many energy levels and electromagnetic properties of the other $f7/2$ nuclei with more valence nucleons can be reproduced quite well. However, levels with a more complicated structure (e.g., holes in the ^{40}Ca core) are also encountered and it is not known how much they mix with the pure $f7/2$ configurations.

Schiffer [Sch 71b, 72b] and Molinari et al. [MJB 75] have made a more general investigation of many such simple nuclei with pure configurations where one nucleon is in a shell j_1 and the other in a shell j_2 . The coupling of angular momentum yields multiplets with $|j_1 - j_2| \leq I \leq j_1 + j_2$. The interaction produces a splitting of the multiplets. It is convenient to plot not $V(I)$ (Eq. 4.137) versus I but rather the dimensionless ratio $V(I)/\bar{V}$ as a function of the "overlap angle" θ_{12} where \bar{V} is the average two-body interaction energy

$$F = \sum_I (2I+1) V(I) / \sum_I (2I+1). \quad (4.143)$$

This angle is the angle between the classical orbits of the two valence nucleons

$$\cos \theta_{12} = \frac{j_1 \cdot j_2}{|j_1||j_2|} = \frac{I(I+1) - j_1(j_1+1) - j_2(j_2+1)}{2[j_1(j_1+1)]^{1/2} \cdot [j_2(j_2+1)]^{1/2}} \quad (4.144)$$

and it measures the spacial overlap of the two wave functions. In this plot (Fig. 4.10), the points for many different nuclei lie nearly on the same curves. As an example we show the plots for nuclei where the two valence nucleons are in the same orbit (Fig. 4.10) and compare them with the corresponding values for a pure δ -force. For identical particles ($T=1$) we again find that the absolute interaction

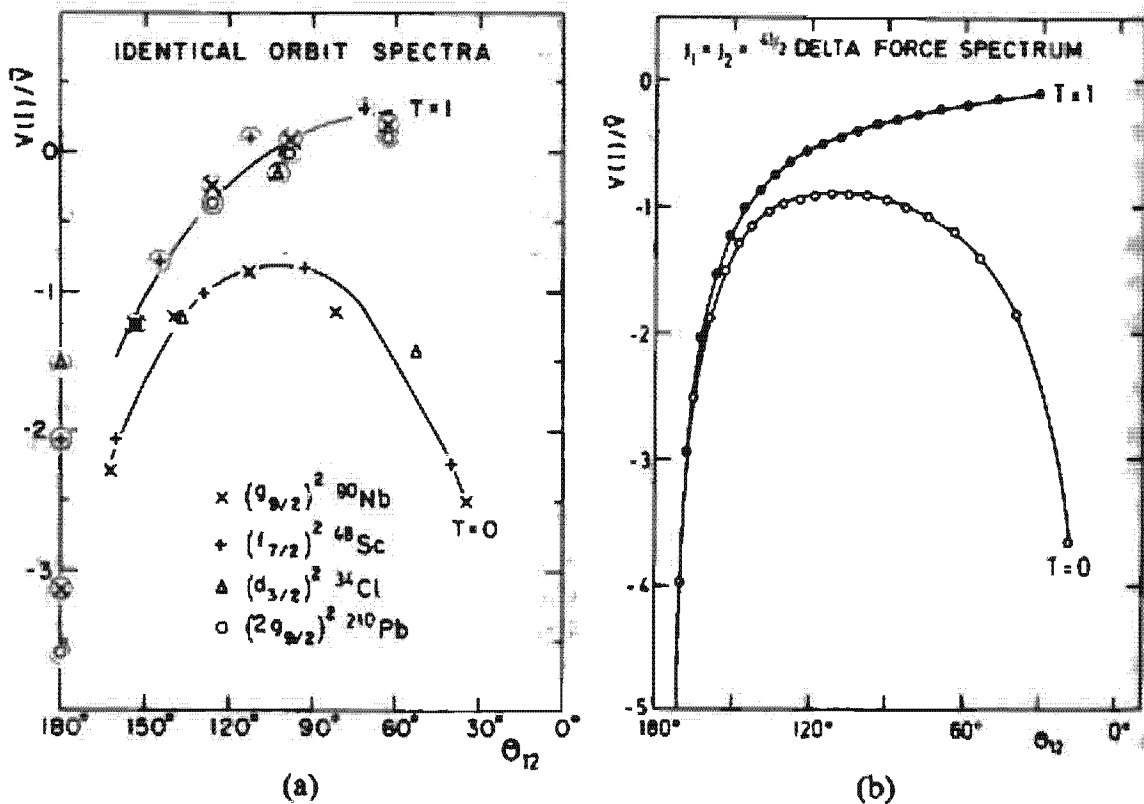


Figure 4.10. The relative interaction matrix elements $V(I)/\bar{V}$ as a function of the overlap angle θ_{12} . Experimental values for (a) four nuclei, (b) a pure δ -force spectrum and $j=41/2$. (From [AS 71].)

matrix elements are strongest for $\theta_{12} = 180^\circ$, that is, for antiparallel spins ($I=0$) and they drop off rapidly. For nonidentical particles in the case $T=0$ they also raise for $\theta_{12} = 0$, that is, for parallel spins. For identical particles this configuration is prevented by the Pauli principle. This expresses the fact that a short-range force requires a large spacial overlap of the wave functions and it seems that an effective interaction of the δ -type can reproduce qualitatively the "experimentally" determined matrix elements. However, a quantitative comparison [Sch 72b, GSZ 74, AEE 78] shows that a long-range part is also needed to reproduce properties of odd-odd nuclei. The origin of this long-range part is as yet not completely understood. For a discussion of this point see [Mo 76c].

4.5 Concluding Remarks

In the second section of this chapter we discussed the bare forces acting between nucleons. We first restricted their analytical form, observing that they have to obey a certain number of invariance principles. It is well known that the long-range part of the nucleon-nucleon interaction is given by the one-pion exchange; at shorter distances, exchanges of two pions and heavier mesons become important. We have not presented recent results of such investigations because the bare nucleon-nucleon forces within nuclear physics represent a discipline all its own involving intermediate and high energy physics [BJ 76a]. We have discussed some of the more conventional phenomenological ansätze (which usually involve between 40 and 50 fit parameters), but which achieve perfect reproduction of the nucleon-nucleon scattering data. However, this fit gives us information only about the on-shell behavior of the nuclear force, the off-shell part which enters into many-nucleon systems remaining indeterminate (see, for instance, [SS 76]). Three-body calculations show, however, that the currently used two-body interactions like the Hamada-Johnston potential or the Reid soft core potential in their off-shell behavior should not be very different from one another. We thus have phenomenological bare nucleon-nucleon potentials which are, in fact, quite reliable.

These potentials have, however, the inconvenient feature of being very repulsive at short distances and they can thus not be directly applied in nuclear structure calculations. Many-body theory teaches us to use effective forces instead of bare ones, the former being already an infinite sum of the latter. This procedure not only sums up higher order many-body effects in a consistent manner, but at the same time gets rid of the hard core problem, since it turns out that the effective forces are well-behaved. We shall see in the next chapter that the application of the concept of effective forces is quite successful for the calculation of ground state properties of nuclei, although the most advanced purely microscopic calculations in this field (consistently taking three-body correlations into account [KLZ 78]) are still not able to get quantitative agreement with experimental binding energies. In all other calculations, some phenomenol-

ogy enters at a certain step. Nevertheless, we can say that for the ground state properties the theory gives very good results.

Far less satisfying is the situation for the case of effective forces between valence nucleons. For example, shell model calculations within a two-particle model space and with a phenomenological two-body force are able to reproduce the low-lying spectrum of, for example, ^{18}O very well, and we may suppose that this success can be microscopically justified by calculating the effective force between the two valence nucleons. Unfortunately, these attempts have met with only partial success and show that at a certain stage in the perturbative expansion of the interaction, good agreement with experiment is achieved; but going further with the expansion worsens the results again. Until now, the reasons for this agreement at an intermediate step have not been explained.

After these numerically very involved theories of effective interactions with their moderate success, in Section 4.4 we passed to the treatment of the phenomenological effective forces. There the situation is quite satisfying. A number of phenomenological ansätze exist which have been very successful in explaining much more nuclear data than there are fit parameters. One of these forces is the Skyrme force, whose success for the ground state properties of nuclei will be discussed in more detail in the next chapter. For nuclear structure calculations we have to mention the very simple but highly successful pairing-plus-quadrupole force. In the lead region the quasi-particle concept seems to work well, as shown by the quite impressive success of calculations using the Migdal force. But other very simple forces, like the surface-delta force, also do surprisingly well. In view of their successes, it appears to be a difficult but challenging task to give an explanation from a microscopic point of view.

good
pairing
plus
quadrupole
force
in nucleus
works
surprisingly
well
but
other
simple
forces
also
do
surprisingly
well
in
nucleus
but
why?

good
pairing
plus
quadrupole
force
in nucleus
works
surprisingly
well
but
other
simple
forces
also
do
surprisingly
well
in
nucleus
but
why?

CHAPTER 5

The Hartree–Fock Method

5.1 Introduction

The success of the phenomenologically introduced shell model justifies the assumption that nucleons move independently in an average potential produced by all of the nucleons. The question now is how to extract such a single-particle potential out of the sum of two-body interactions

$$V(1 \dots A) = \sum_{i < j=1}^A V(i, j) \approx \sum_{i=1}^A V(i), \quad (5.1)$$

and how well this single-particle potential will agree with those used up to now, for example, the harmonic oscillator, the square well, or the Woods–Saxon potential. It will be shown that we can derive a single-particle potential from the two-body interaction by a variational principle using Slater determinants as trial wave functions.

In Section 5.2 we will discuss in general the variational method, which will be important in many of the following chapters. In Section 5.3, we describe the Hartree–Fock method in detail and in Section 5.4 we give an application to a very simple model. In Section 5.5 we treat symmetries in connection with the Hartree–Fock method, and in Section 5.6 we present the Hartree–Fock theory with density dependent forces.

5.2 The General Variational Principle

We first want to show that the exact Schrödinger equation

$$H|\Psi\rangle = E|\Psi\rangle \quad (5.2)$$

is equivalent to the variational equation

$$\delta E[\Psi] = 0, \quad (5.3)$$

with

$$E[\Psi] = \frac{\langle \Psi | H | \Psi \rangle}{\langle \Psi | \Psi \rangle}. \quad (5.4)$$

The variation (5.3) can be obtained from (5.4):

$$\langle \delta \Psi | H - E | \Psi \rangle + \langle \Psi | H - E | \delta \Psi \rangle = 0. \quad (5.5)$$

Since $|\Psi\rangle$ is, in general, a complex function, we can carry out the variation over the real and imaginary part independently, which is equivalent to carrying out the variation over $|\delta \Psi\rangle$ and $\langle \delta \Psi|$ independently. To see this we use the fact that Eq. (5.5) is valid for arbitrary infinitesimal $|\delta \Psi\rangle$. We can replace $|\delta \Psi\rangle$ by $i|\delta \Psi\rangle$ and get

$$-i\langle \delta \Psi | H - E | \Psi \rangle + i\langle \Psi | H - E | \delta \Psi \rangle. \quad (5.6)$$

Together with Eq. (5.5), we find

$$\langle \delta \Psi | H - E | \Psi \rangle = 0 \quad (5.7)$$

and the complex conjugate equation. Since $|\delta \Psi\rangle$ is arbitrary, Eq. (5.7) is equivalent to the eigenvalue problem (5.2).

The approximation of such variational methods consists of the fact that $|\Psi\rangle$ is usually restricted to a set of mathematically simple trial wave functions. As soon as the true function is not in this set, the minimal solution is no longer the exact eigenfunction, but only an approximation. The variational method is especially well suited for determining the ground state, since for any trial wave function $|\Psi\rangle$ we can show that

$$E[\Psi] \geq E_0, \quad (5.8)$$

and thus E_0 will always be the lower bound of a variational calculation. To prove this, we develop the trial wave function in terms of the exact eigenfunctions of the Hamiltonian:

$$|\Psi\rangle = \sum_{n=0}^{\infty} a_n |\Psi_n\rangle \quad (5.9)$$

with

$$H|\Psi_n\rangle = E_n|\Psi_n\rangle. \quad (5.10)$$

This yields

$$E[\Psi] = \frac{\sum_{nn'} a_n^* a_{n'} E_n \delta_{nn'}}{\sum_n |a_n|^2} \rightarrow \frac{\sum_n |a_n|^2 E_0}{\sum_n |a_n|^2} = E_0. \quad (5.11)$$

which is precisely Eq. (5.8). In cases where the ground state energy is not degenerate, the equality sign in (5.11) is valid, if and only if all the coefficients a_n with $n \neq 0$ vanish, that is, $|\Psi\rangle$ is proportional to $|\Psi_0\rangle$. If we are interested in the first excited state, we then have to carry out the variation within the subspace entirely orthogonal to $|\Psi_0\rangle$, that is, over all the wave functions $|\Psi\rangle$ with $a_0 = 0$. Within this subspace $|\Psi_1\rangle$ has the minimal expectation value of H . To find $|\Psi_1\rangle$, we must carry out the variation with the subsidiary condition $\langle \Psi_1 | \Psi_0 \rangle = 0$. In principle we can continue and calculate the whole spectrum using this method.

In practice, however, we do not know $|\Psi_0\rangle$ exactly. From a variation in a restricted subset of the Hilbert space, we find only an approximation $|\Phi_0\rangle$. For the calculation of an approximation $|\Phi_1\rangle$ to the first excited state $|\Psi_1\rangle$, we have to solve the variational equation (5.3) with the supplementary condition that $|\Phi_1\rangle$ is orthogonal to $|\Phi_0\rangle$:

$$\langle \Phi_1 | \Phi_0 \rangle = 0. \quad (5.12)$$

For the second excited state, we must have two supplementary conditions, namely:

$$\langle \Phi_2 | \Phi_1 \rangle = 0; \quad \text{and} \quad \langle \Phi_2 | \Phi_0 \rangle = 0. \quad (5.13)$$

These supplementary conditions are coupled to the problem via Lagrange parameters. We thus see that for higher excited states this method quickly gets rather complicated, therefore it has been applied mainly for the calculation of the ground state. Sometimes, however, these conditions are simply fulfilled because of symmetry properties, as, for example, is the case for states with different angular momentum quantum numbers. We will see in Chapter 7 how to calculate a whole rotational band where the determination of each level is no more complicated than that of the ground state.

So far we have shown that for a certain trial wave function, the ground state energy is always larger than or equal to the exact ground state energy and corresponds to an extremum. In actual calculations, we have to make sure that this extremum actually corresponds to a *minimum*, that is, we must calculate the second derivative of the energy functional, for example, with respect to certain parameters. In the case of the Hartree-Fock or Hartree-Fock-Bogoliubov theory, we will come back to this point (in Chapter 7).

In order to decide which of two variational approaches (i.e., two sets of trial wave functions) is the better one, we have two criteria:

- (i) If one set of the trial wave functions is a subset of the other, the larger set is usually the better one, because it contains the first's set minimum.
- (ii) Since the exact E_0 is a lower bound, we may hope that out of two trial wave functions, the one for which the corresponding energy is closest to E_0 is better.

Both criteria are, however, not exact statements. Pathological examples can be found which contradict them.

We finish this section with the remark that the variation principle is only valid in this form for a linear eigenvalue problem of the type (5.2). In cases where the Hamiltonian itself depends on the wave function we want to determine, we have to be very careful in applying this principle.

5.3 The Derivation of the Hartree-Fock Equation

5.3.1 The Choice of the Set of Trial Wave Functions

Using the fact that the shell model has provided a suitable approximation for the qualitative explanation of many nuclear properties, we shall assume that there is an average single-particle potential (later to be called the *Hartree-Fock potential*)

$$H^{\text{HF}} = \sum_{i=1}^A h(i) \quad (5.14)$$

whose eigenfunction having the lowest eigenvalue E_0^{HF} is an approximation to the exact ground state function. This eigenfunction $\Phi(1\dots A)$ is, as we have seen in Chapter 2, a *Slater determinant*

$$|\text{HF}\rangle = |\Phi(1\dots A)\rangle = \prod_{i=1}^A a_i^+ |-\rangle \quad (5.15)$$

in which the Fermion operators a_k^+, a_k correspond to the single-particle wave functions φ_k , which are themselves eigenfunctions of the single-particle Hamiltonian h , viz:

$$h(i)\varphi_k(i) = \epsilon_k \varphi_k(i), \quad i = \{r_i, s_i, t_i\}. \quad (5.16)$$

As we have seen in Section 2.5, we obtain the lowest eigenvalue of H^{HF} if one occupies the A lowest levels in the state $|\text{HF}\rangle$ (Eq. 5.15). In the following, we will characterize the occupied levels in $|\text{HF}\rangle$ by the letters i, j (hole states) and the empty levels by m, n (particle states). If we do not distinguish, we use the letters k, l, p, q .

The wave functions $\varphi_k(r, s, t)$ are a coordinate space representation of the eigenstates $|k\rangle$ of the single-particle Hamiltonian h . Very often, we work in a configuration space based on some arbitrary complete and orthogonal set of single-particle wave functions $\{\chi_i\}$ (an example is the set of spherical harmonic oscillator wave functions). The function φ_k can be

expanded on this basis:

$$\varphi_k = \sum_i D_{ik} \chi_i. \quad (5.17)$$

If, for each wave function χ_i , we define corresponding fermion creation and annihilation operators c_i^+, c_i (see Section C.1), we can similarly express the operators a_k^+ by the operators c_i^+ :

$$a_k^+ = \sum_i D_{ik} c_i^+. \quad (5.18)$$

Since both sets $\{\varphi_k\}$ and $\{\chi_i\}$ are complete and orthogonal, the transformation D has to be unitary:

$$D^\dagger D = DD^\dagger = 1. \quad (5.19)$$

This fact also guarantees that the operators (a_k^+, a_k) and (c_i^+, c_i) both obey separate Fermi commutation relations.

As discussed in Section D.2, there is no one-to-one correspondence between a Slater determinant Φ of the form (5.15) and the set of single-particle states φ_k . Any unitary transformation which does not mix particle and hole states leaves Φ unchanged (at least up to an unimportant phase).

It is therefore more convenient to represent a Slater determinant $|\Phi\rangle$ by its single-particle density matrix (D.9):

$$\rho_H = \langle \Phi | c_i^+ c_i | \Phi \rangle. \quad (5.20)$$

From Eqs. (5.18) and (5.19), we get

$$\rho_H = \sum_{kk'} D_{ik} D_{i'k'}^* \langle \Phi | a_k^+ a_k | \Phi \rangle = \sum_{i=1}^A D_{ii} D_{ii}^* \quad (5.21)$$

because ρ is diagonal in the basis a_k^+, a_k with the eigenvalues (occupation numbers) 1 for $i < A$ (holes) and 0 for $i > A$ (particles). The trace of ρ is equal to the particle number.

As we show in Appendix D.2, there is a one-to-one correspondence between the Slater determinant Φ and its single-particle density ρ . Single-particle densities ρ of Slater determinants are characterized by the fact that they have only eigenvalues 0 or 1, that is,

$$\rho^2 = \rho. \quad (5.22)$$

ρ is therefore a projector in the space of single-particle wave functions onto the subspace spanned by the hole states φ_i .

In the same way, we can define a projector σ

$$\sigma = 1 - \rho \quad (5.23)$$

onto the subspace spanned by the particle states φ_i .

The *Hartree-Fock method* [Ha 28, Fo 30] is now defined in the following way. We use the set of Slater determinants $\{\Phi\}$ of the form (5.15) consisting of A arbitrary but orthogonal single-particle wave functions φ_i as trial wave functions and minimize the energy within this set. An equivalent statement would be that we use the set of all wave functions

(Φ) whose single particle density (5.20) has the property $\rho^2 = \rho$ and $\text{Tr } \rho = A$.

As we will see in the following sections, this variation will give us the possibility of determining the single-particle operator H^{HF} .

5.3.2 The Hartree-Fock Energy

Before we are able to carry out the variation which allows us to determine the HF-wave function Φ , we have to calculate the HF-energy

$$E^{\text{HF}} = \langle \Phi | H | \Phi \rangle. \quad (5.24)$$

We start with the many-body Hamiltonian H and represent it in second quantization by the basis operators c_i^+, c_i (see Section C.1):

$$H = \sum_{I_1 I_2} t_{I_1 I_2} c_{I_1}^+ c_{I_2} + \frac{1}{4} \sum_{I_1 I_2 I_3 I_4} \bar{v}_{I_1 I_2 I_3 I_4} c_{I_1}^+ c_{I_2}^+ c_{I_3} c_{I_4}, \quad (5.25)$$

where

$$\bar{v}_{I_1 I_2 I_3 I_4} = v_{I_1 I_2 I_3 I_4} - v_{I_1 I_2 I_4 I_3}. \quad (5.26)$$

Wick's theorem (Sec. C.4) allows us to calculate the energy (5.24) as a functional of the single-particle density

$$\begin{aligned} E^{\text{HF}}[\rho] &= \sum_{I_1 I_2} t_{I_1 I_2} \langle \Phi | c_{I_1}^+ c_{I_2} | \Phi \rangle + \frac{1}{4} \sum_{I_1 I_2 I_3 I_4} \bar{v}_{I_1 I_2 I_3 I_4} \langle \Phi | c_{I_1}^+ c_{I_2}^+ c_{I_3} c_{I_4} | \Phi \rangle \\ &= \sum_{I_1 I_2} t_{I_1 I_2} \rho_{I_1 I_2} + \frac{1}{2} \sum_{I_1 I_2 I_3 I_4} \rho_{I_1 I_2} \bar{v}_{I_1 I_2 I_3 I_4} \rho_{I_3 I_4} \end{aligned} \quad (5.27)$$

$$= \text{Tr}(\rho) + \frac{1}{2} \text{Tr}_1 \text{Tr}_1(\rho \bar{v} \rho), \quad (5.28)$$

where $\text{Tr}_1 \text{Tr}_1 \dots$ is an obvious shorthand notation. Eq. (5.28) does not depend on the basis. We can therefore use it to give an expression for the HF-energy in the HF-basis $\{\varphi_k\}$ in which ρ is diagonal with the eigenvalues 0 and 1

$$E^{\text{HF}} = \sum_{i=1}^A t_{ii} + \frac{1}{2} \sum_{i,j=1}^A \bar{v}_{ij} \delta_{ij}. \quad (5.29)$$

5.3.3 Variation of the Energy

To determine the HF-basis, we have to minimize the energy (5.28) for all product wave functions $|\Phi\rangle$ or for all densities ρ with the property $\rho^2 = \rho$. Since a small variation $\rho + \delta\rho$ has to be a projector again, we get

$$(\rho + \delta\rho)^2 = \rho + \delta\rho$$

or, up to linear terms in $\delta\rho$,

$$\delta\rho = \rho \delta\rho + \delta\rho \rho.$$

In the HF-basis, where ρ is diagonal, this means that the particle-particle (pp) and hole-hole (hh) matrix elements of $\delta\rho$ have to vanish, that is,

$$\rho \delta\rho \rho = \sigma \delta\rho \sigma = 0. \quad (5.30)$$

To make sure that we stay within the set of Slater determinants, therefore, we can only allow for variations $\delta\rho_{mi}$ and $\delta\rho_{im}$ of the ph and hp matrix elements of ρ in the HF-basis.

The variation of the energy (5.27) is then given by

$$\delta E = E[\rho + \delta\rho] - E[\rho] = \sum_{kk'} h_{kk'} \delta\rho_{k'k} = \sum_{mi} h_{mi} \delta\rho_{im} + c.c., \quad (5.31)$$

where the Hermitian matrix h is defined as

$$h_{kk'} = \frac{\partial E^{\text{HF}}[\rho]}{\partial \rho_{k'k}}. \quad (5.32)$$

From Eq. (5.27), we obtain

$$h = t + \Gamma \quad (5.33)$$

with the *self-consistent field*

$$\Gamma_{kk'} = \sum_{II'} \bar{v}_{kI'k'I} \rho_{II'}. \quad (5.34)$$

Since arbitrary values of $\delta\rho_{mi}$ are allowed, we see from Eq. (5.31), that the condition $\delta E = 0$ for the HF-solution means that the ph matrix elements of h have to vanish,

$$h_{mi} = t_{mi} + \sum_{j=1}^A \bar{v}_{mjj} = 0 \quad (\text{for } i < A, m > A), \quad (5.35)$$

in the basis where ρ is diagonal, that is, h does not mix particle and hole states of ρ and Eq. (5.35) is equivalent to

$$[h, \rho] = [t + \Gamma[\rho], \rho] = 0. \quad (5.36)$$

This is a nonlinear equation, and not easy to solve. It also states that h and ρ can be diagonalized simultaneously. Since the basis in which ρ is diagonal is determined only up to unitary transformations among the occupied levels or among the empty levels, we use this freedom and require that h shall be diagonal. This defines the *Hartree-Fock basis* and converts (5.36) into an eigenvalue problem.

$$h_{kk'} = t_{kk'} + \sum_{i=1}^A \bar{v}_{kik'i} = \epsilon_k \delta_{kk'}. \quad (5.37)$$

Considering the fact that this basis is given by the transformation D (5.18), we obtain the set of *Hartree-Fock equations*

$$\sum_P h_{Pi} D_{P'k} = \sum_{P'} \left(t_{P'} + \sum_{i=1}^A \sum_{pp'} \bar{v}_{pp'i} D_{pi} D_{p'i}^* \right) D_{P'k} = \epsilon_k D_{ik}, \quad (5.38)$$

which represent a Hermitian eigenvalue problem. It is nonlinear because the matrix h depends on the density ρ , that is, on the solution of the

problem. The coefficients $D_{kk'}$ found by the solution of these equations determine the single-particle wave functions φ_k [Eq. (5.17)].

We have thus derived a single-particle Hamiltonian

$$\begin{aligned} H^{\text{HF}} &= \sum_{kk'} h_{kk'} a_k^\dagger a_{k'} = \sum_{kk'} (t + \Gamma)_{kk'} a_k^\dagger a_{k'} \\ &= \sum_{kk'} \left(t_{kk'} + \sum_{j=1}^A \bar{v}_{kj} c_j \right) a_k^\dagger a_{k'} = \sum_k \epsilon_k a_k^\dagger a_k \end{aligned} \quad (5.39)$$

with the properties required in Section (5.3.1): The Slater determinant $|\text{HF}\rangle$, where the lowest A levels are occupied, corresponds to an energy E which is stationary against small variations of the wave function.

The single-particle Hamiltonian h contains, besides the kinetic energy t , a self-consistent field Γ (Eq. (5.34)), which depends on the density of the nucleus. It is a one-body field and averages over all two-body interactions. This point will become even clearer in the coordinate representation (Sec. 5.3.4). The energy expectation value of the HF-wave function $|\text{HF}\rangle$ is given by Eqs. (5.29) and (5.37):

$$E_0^{\text{HF}} = \sum_{i=1}^A \epsilon_i - \frac{1}{2} \sum_{ij=1}^A \bar{v}_{ij}. \quad (5.40)$$

It is therefore not equal to the sum of single-particle energies [compare the discussion of this point in Sec. (2.8.6)].

5.3.4 The Hartree-Fock Equations in Coordinate Space

To give a better interpretation of the structure of Eq. (5.38), we write it down in the coordinate space. Assuming a local two-body potential which does not depend on spin or isospin, that is, a pure Wigner force (see Sec. 4.2), we find instead of Eq. (5.38):

$$\begin{aligned} -\frac{\hbar^2}{2m} \Delta \varphi_k(\mathbf{r}) + \sum_{j=1}^A \int d\mathbf{r}' v(\mathbf{r}, \mathbf{r}') \cdot \varphi_j^*(\mathbf{r}') \{ \varphi_j(\mathbf{r}') \varphi_k(\mathbf{r}) - \varphi_j(\mathbf{r}) \varphi_k(\mathbf{r}') \} \\ = \epsilon_k \varphi_k(\mathbf{r}). \end{aligned} \quad (5.41)$$

Defining the local Hartree potential

$$\Gamma_H(\mathbf{r}) = \int d\mathbf{r}' v(\mathbf{r}, \mathbf{r}') \sum_{j=1}^A |\varphi_j(\mathbf{r}')|^2 = \int d\mathbf{r}' v(\mathbf{r}, \mathbf{r}') \rho(\mathbf{r}') \quad (5.42)$$

and the nonlocal or exchange potential

$$\Gamma_{Ex}(\mathbf{r}, \mathbf{r}') = -v(\mathbf{r}, \mathbf{r}') \sum_{j=1}^A \varphi_j^*(\mathbf{r}') \varphi_j(\mathbf{r}) = -v(\mathbf{r}, \mathbf{r}') \rho(\mathbf{r}, \mathbf{r}'), \quad (5.43)$$

we find that $\varphi_k(\mathbf{r})$ is the solution of a nonlocal Schrödinger equation

$$\left\{ -\frac{\hbar^2}{2m} \Delta + \Gamma_H(\mathbf{r}) \right\} \varphi_k(\mathbf{r}) + \int d\mathbf{r}' \Gamma_{Ex}(\mathbf{r}, \mathbf{r}') \varphi_k(\mathbf{r}') = \epsilon_k \varphi_k(\mathbf{r}). \quad (5.44)$$

Equations (5.38) and (5.44) contain a self-consistency problem, since the potentials Γ , Γ_H and Γ_{Ex} depend on the local and nonlocal density $\rho(\mathbf{r})$ and $\rho(\mathbf{r}, \mathbf{r}')$ of the solution. The equations can be solved by iteration, starting with a set of phenomenological shell model wave functions to calculate Γ_H and Γ_{Ex} as a first step. Another convenient first guess is the Thomas-Fermi expression for the density (see Sec. 13.2.1). From (5.44) we then get new single-particle wave functions, and so on. This procedure is continued until convergence is obtained, that is, the potentials stay constant in two consecutive steps. In this case, Γ is the self-consistent average potential felt by one particle through interactions with all the other particles.

It should be noticed that, starting with a local two-body interaction, the Fock potential Γ_{Ex} (5.43) is nonlocal. This is caused by the Pauli principle and the antisymmetrization of the matrix element (5.26). A variation of simple product wave functions without antisymmetrization yields only the local Hartree potential. Of course, nonlocal two-body interactions give a nonlocal Hartree term, too. On the other hand, if we use a δ -force, then the Fock term is also local^{*} [see Eq. (5.99)].

Since many of the more formal discussions on HF theory will be taken up in Chapter 7, we will not go into more detail here; we wish only to mention that we will treat there the stability of the Hartree-Fock equations, that is, the question of whether the Hartree-Fock solutions correspond to a minimum or a maximum in the energy. We will also present the so-called gradient method for the solution of the HF equations.

In order to familiarize the reader with the concept of the theory presented in this chapter, we will now present a simple model in which all equations can be solved analytically.

5.4 The Hartree-Fock Method in a Simple Solvable Model

As we will discuss in the last section of this chapter, all realistic HF calculations are very difficult numerical problems. In order to get some feeling about how this method works, we want to apply it to a very simple, exactly solvable model first proposed by Lipkin, Meshkov, and Glick [LMG 65], and which has been widely used to test all kinds of many-body theories (as we shall see later on). Let us imagine two levels in a fixed shell model potential having the same j -value, one situated just below the Fermi level, the other just above. The level below the Fermi level is filled with $2j+1$ nucleons (of one kind, for simplicity). The fixed single-particle potential can be thought of as being produced by an especially stable core formed out of the rest of the nucleons. It is then conceivable to calculate solely that part of the average potential coming from the nucleons in the last j -shell, in a self-consistent manner, such that the mutual influence of the core and the last j -shell is neglected. Of course, the idea that there is only one level with the same j above the Fermi level is very unrealistic and serves only to schematize the problem.

* For numerical methods to solve the HF-equations (5.38) or (5.41), see also [QF 78].

[†]In this case, however, we also have to take into account spin degrees of freedom, otherwise the exchange term cancels the direct term.

Furthermore, it is assumed that in the basis produced by the fixed potential of the core, the residual interaction of the nucleons in the two shells is of a very special form, being of the monopole-monopole type (see Chap. 4) and having essentially only one matrix element different from zero (a particle-hole matrix element of the RPA type (see Chap. 8)). The *model Hamiltonian* is then of the form

$$H = \epsilon K_0 - \frac{1}{2} V(K_+ K_+ + K_- K_-), \quad (5.45)$$

with

$$K_0 = \frac{1}{2} \sum_{m=1}^{\Omega} (c_{+m}^+ c_{+m}^- - c_{-m}^+ c_{-m}^-); \quad K_+ = \sum_{m=1}^{\Omega} c_{+m}^+ c_{-m}^-; \quad K_- = (K_+)^+, \quad (5.46)$$

where $\Omega = 2j + 1$ and c_{+m}^+, c_{-m}^+ create a particle in the upper and lower levels, respectively, and ϵ is the energy difference between the two levels (see Fig. 5.1). The operators K_0, K_{\pm} fulfill the commutation relations of angular momenta.

$$[K_+, K_-] = 2K_0; \quad [K_0, K_{\pm}] = \pm K_{\pm}. \quad (5.47)$$

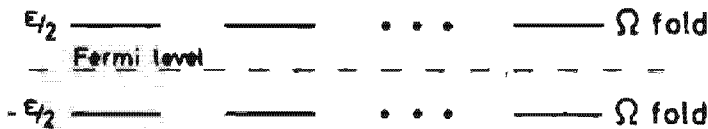


Figure 5.1. Level scheme in the schematic model.

However, it must be emphasized that the operators K_0, K_{\pm} have nothing to do with rotations in coordinate space. They are often referred to as quasi-spin operators. In order to apply the Hartree-Fock method, we have to construct the general Slater determinant $|\Phi\rangle$. The Hamiltonian (5.45) is invariant under a permutation of the Ω levels below and corresponding levels above the Fermi surface. Therefore, in the following, we restrict ourselves to those solutions of the problem which are completely symmetric under such a permutation. In this case, there is only one possibility of exciting *ph*-pairs, and the most general Slater determinant $|\Phi\rangle$ is characterized by the complex number z :

$$|\Phi\rangle = \mathcal{D} \exp(zK_+) |\Phi_0\rangle = \prod_{m=1}^{\Omega} a_{0m}^+ |-\rangle, \quad (5.48)$$

with

$$|\Phi_0\rangle = \prod_{m=1}^{\Omega} c_{-m}^+ |-\rangle \quad (5.49)$$

and

$$a_{0m}^+ = D_{-0} c_{-m}^+ + D_{+0} c_{+m}^+ \quad (5.50a)$$

$$a_{1m}^+ = D_{-1} c_{-m}^+ + D_{+1} c_{+m}^+, \quad (5.50b)$$

where we denote the new lower and upper levels by 0 and 1. With the aid of relations (5.50a) and (5.50b), we can express the Hamiltonian (5.45) in the new operators a_{0m}^+, a_{1m}^+ . Then, varying $\langle\Phi|H|\Phi\rangle$ with respect to D_{-0}^* and D_{+0}^* yields* the Hartree-Fock equations in the Lipkin model (this is, in fact, just another way

* Under the subsidiary condition that the D s are normalized [see Eq. (5.96)].

to derive the HF eqs.):

$$\begin{pmatrix} -\frac{1}{2} & -Q \\ -Q^* & \frac{1}{2} \end{pmatrix} \begin{pmatrix} D_{-0} \\ D_{+0} \end{pmatrix} = \frac{\epsilon_0}{\epsilon} \begin{pmatrix} D_{-0} \\ D_{+0} \end{pmatrix}, \quad (5.51)$$

where

$$\chi = \frac{\nu}{\epsilon} (\Omega - 1), \quad Q = \chi D_{+0} D_{-0}^*,$$

which is of the usual nonlinear type and can be solved by iteration. The new single-particle energies are given by

$$\begin{aligned} \epsilon_{0,1} &= \mp \epsilon \sqrt{\frac{1}{4} + |Q|^2} \\ &= \mp \frac{\epsilon}{2} \sqrt{1 + \chi^2 \sin 2\alpha}, \end{aligned} \quad (5.52)$$

where we put $D_{-0} = \cos \alpha$ and $D_{+0} = \sin \alpha \cdot e^{-i\varphi}$. Solving Eq. (5.51) for D_{-0} and D_{+0} and inserting these into the expression for Q yields, with (5.52) in the case $Q \neq 0$, the following equation for the "deformation" potential Q :

$$1 = \frac{\chi}{2} \frac{1}{\sqrt{\frac{1}{4} + Q^2}}. \quad (5.53)$$

This equation has only real solutions for $\chi > 1$ corresponding to the deformed HF solution given below. (The fact that Eq. (5.53) is very similar to the gap equation of BCS theory [Eq. (6.60)] is not accidental, as will be discussed in more detail in Sec. 11.2 and Appendix F.5.)

In the coordinates α, φ , we then obtain for the ground state energy

$$E_0^{\text{HF}} = -\frac{\epsilon}{2} \Omega \left(\cos 2\alpha + \frac{1}{2} \chi \sin^2 2\alpha \cdot \cos 2\varphi \right) \quad (5.54)$$

and the self-consistency condition

$$\frac{\partial E_0^{\text{HF}}}{\partial \alpha} = 0 = \epsilon \Omega \sin 2\alpha (1 - \chi \cos 2\alpha \cdot \cos 2\varphi), \quad (5.55)$$

$$\frac{\partial E_0^{\text{HF}}}{\partial \varphi} = 0 = \epsilon \Omega \frac{1}{2} \sin 2\alpha \cdot \sin 2\varphi.$$

From Eq. (5.55), we see that we have to distinguish two cases, depending on whether χ is greater than or smaller than one. In the latter case, we have only one solution:

$$\varphi_{\text{HF}} = 0, \quad \alpha_{\text{HF}} = 0, \quad \chi < 1. \quad (5.56)$$

For $\chi > 1$ we have a second solution,

$$\varphi_{\text{HF}} = 0, \quad \chi \cdot \cos 2\alpha_{\text{HF}} = 1, \quad \chi > 1, \quad (5.57)$$

which turns out to correspond to the minimum in the energy, the first solution having been a maximum. This can be seen from the curvature of the energy at this point:

$$\left. \frac{\partial^2 E_0^{\text{HF}}}{\partial \alpha^2} \right|_{\alpha=\alpha_{\text{HF}}} = 2\epsilon \Omega \left(\chi - \frac{1}{\chi} \right) > 0 \quad \text{for } \chi > 1. \quad (5.58)$$

In Fig. 5.2 we show a cut ($\varphi = 0$) through the two-dimensional energy surface (5.54) for $\chi \leq 1$.

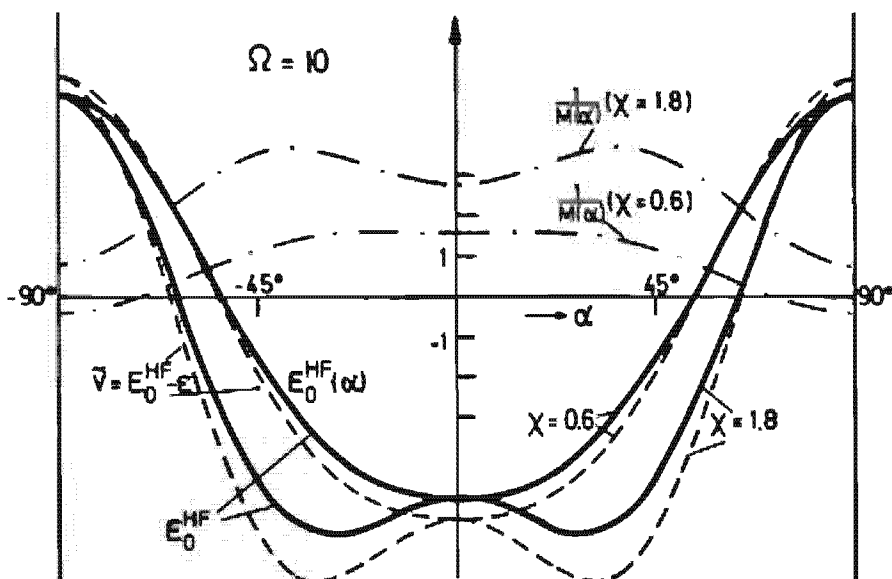


Figure 5.2. E_0^{HF} as a function of α for $x \leq 1$ (full lines). The other four curves correspond to quantities calculated within the generator coordinate method (see Sec. 10.7.5). (From [Ho 73].)

From the critical value

$$\chi_c = \frac{V_c(\Omega - 1)}{\epsilon} = 1 \quad (5.59)$$

on, the solution at $\alpha=0, \varphi=0$ becomes unstable and then we have to use a different single-particle basis. In Fig. 5.3, we show for $x=6$ how the iterative solution of equation (5.51) works. Starting with $\alpha_1 = 80^\circ, \varphi_1 = 30^\circ$ we find in the subsequent steps (full lines in Fig. 5.3): $\alpha_2 = 32.01^\circ, \varphi_2 = -30^\circ$; $\alpha_3 = 39.75^\circ, \varphi_3 = 30^\circ$; $\alpha_4 = 40.19^\circ, \varphi_4 = -30^\circ$; With respect to α we get a rapid convergence to the solution $\alpha_{\text{HF}} = 40.20$ [Eq. (5.57)]; with respect to the variable φ , however, we do not get convergence, the solution jumping back and forth between $+30^\circ$ and

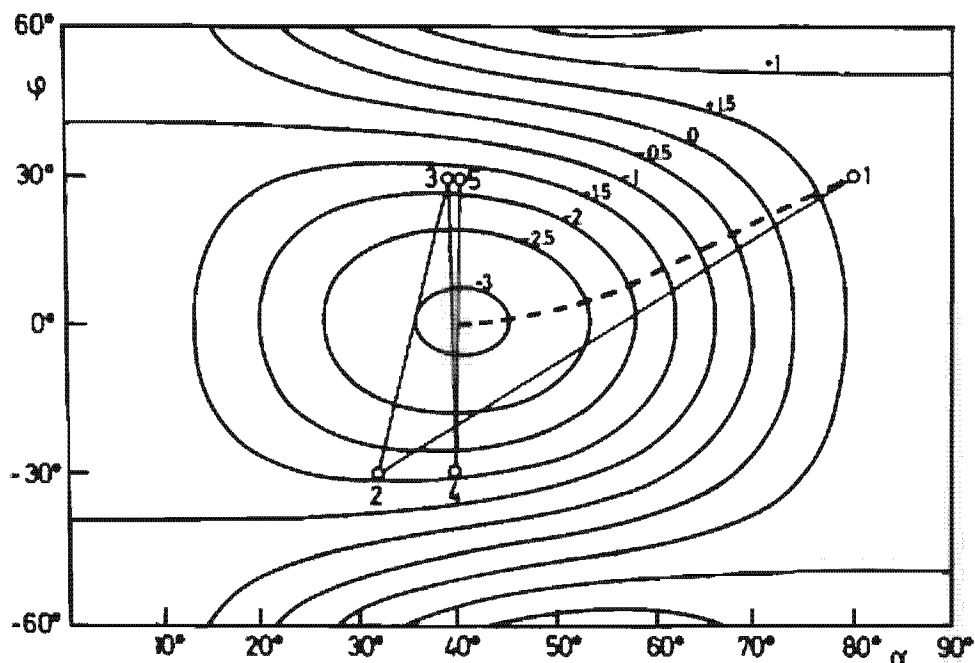


Figure 5.3. Numerical comparison of solution of the HF equations by iterative diagonalization (solid line) and the gradient method (dashed line).

–30°. Our model is certainly a very special case in the sense that in the general case the iterative diagonalization converges to a minimum in the energy surface. However, one sometimes also encounters in realistic calculations cases where, within a certain degree of freedom, the solution oscillates back and forth, as in our model. It is therefore preferable to use another method to find the minimum which can, in general, also give faster convergence. This is the gradient method, which will be explained in Section 7.3.3. The way in which the gradient method would converge to the minimum in our model is also indicated in Fig. 5.3 by the dashed line.

5.5 The Hartree-Fock Method and Symmetries

The HF equations (5.38) are nonlinear, which means that the self-consistent potential Γ [Eq. (5.34)] depends not only on the original Hamiltonian, but also on the solution [which is represented by its density matrix ρ (5.21)]. Therefore, this potential does not necessarily show the same symmetries as the Hamiltonian. We then say that the solution has a broken symmetry. The loss of translational invariance is one which we have already encountered, but, as we shall see, there are others—such as, for example, the rotational invariance and particle number conservation (see Chs. 6 and 7). Usually one calls a transition from a symmetry-conserving solution to a symmetry-broken solution a phase transition. The great advantage of this symmetry breaking is the fact that it allows us to take into account, in an approximate way, many-body correlations without losing the simple picture of independent particles. A more detailed discussion of this point will be given in Chapters 7 and 11 and in Appendix F, but let us give here the following argument: Let us suppose that we have a Slater determinant $|\Phi\rangle$ which consists of deformed single-particle wave functions $\{a_k^+\}$. We express them in a spherical basis $\{c_q^+\}$ through the linear transformation

$$a_k^+ = \sum_q D_{qk} c_q^+. \quad (5.60)$$

We thus obtain a sum of Slater determinants in the spherical basis which differs in the occupation numbers of the level q :

$$a_{i_1}^+ \dots a_{i_N}^+ |-\rangle = \sum_{q_1 \dots q_N} d_{q_1 \dots q_N}^{i_1 \dots i_N} c_{q_1}^+ \dots c_{q_N}^+ |-\rangle. \quad (5.61)$$

Here the coefficients $d_{q_1 \dots q_N}^{i_1 \dots i_N}$ are the corresponding minors of the matrix D_{qk} . They are of a special form; had we allowed them to be of the most general form, the ansatz (5.61) would contain the exact answer; however, this can never be the case in an independent particle (HF) description. Nevertheless, we see that a Slater determinant in one basis can be a complicated superposition of Slater determinants in another.

Of course, the exact wave function should have the symmetries of the Hamiltonian, and their violation is a matter of convenience in order to maintain the independent particle picture for as long as possible. Neverthe-

less, we should try at a later stage to restore the symmetries. How this can be achieved will be discussed in Chapter 11. However, certain symmetries are conserved in the HF theory, the so-called *self-consistent symmetries*. They depend on the symmetries of the initial density $\rho^{(0)}$ of the iteration, and are based on the property of the HF field Γ viz:

$$S\Gamma[\rho]S^+ = \Gamma[S\rho S^+] \quad (5.62)$$

for any matrix S of a unitary* symmetry operator

$$\hat{S} = \sum_{ll'} S_{ll'} c_l^+ c_{l'} \quad (5.63)$$

which commutes with the many-body Hamiltonian (5.25)

$$[H, \hat{S}] = 0.$$

The property (5.62) is easy to show for the definition (5.34) of Γ :

$$(S\Gamma S^+)_{kk'} = \sum_{ll'qq'pp'} S_{kp} S_{k'p'}^* \langle pq|V|p'q\rangle_{aa} S_{lq}^* S_{l'q'} (S\rho S^+)_{ll'} \quad (5.64)$$

$$= \sum_{ll'} \langle kl'| \hat{S} V \hat{S}^+ | p'q \rangle_{aa} (S\rho S^+)_{ll'}. \quad (5.65)$$

From the invariance of the two-body interaction

$$\hat{S}V\hat{S}^+ = V \quad (5.66)$$

we finally get (5.62) and

$$Sh[\rho]S^+ = h[S\rho S^+]. \quad (5.67)$$

This means that if the initial density $\rho^{(0)}$ has a certain symmetry S of the Hamiltonian H , then the field $h[\rho^{(0)}]$ for the first step of the iteration has it also. The density $\rho^{(1)}$ is found by a diagonalization of $h[\rho^{(0)}]$. It therefore has to have the same symmetry again, and so on. In each step of the iteration, the symmetry S is conserved.

The existence of these self-consistent symmetries has the following implications for practical calculations [Ri 68].

- (i) If we expect a certain symmetry for the solution, we can start with an initial density $\rho^{(0)}$ which has this symmetry and therefore reduce the computational effort by working in a basis consisting of eigenstates of this symmetry.
- (ii) If we start with a certain symmetry, we will always stay within this symmetry, and the minimum of energy can only be found among the wave functions that have this symmetry. If, for instance, the deepest minimum is a deformed Slater determinant, we will never get to it starting with a spherically symmetric density matrix, though it may happen that small numerical errors cause small deviations from the initial symmetry, which grow during the iteration.

*The following considerations also apply, with small modifications, for antilinear unitary symmetries [Me 61].

(iii) If we have a solution with a broken symmetry S

$$S\rho S^+ = \rho_1 \neq \rho, \quad (5.68)$$

then from Eq. (5.67) we obtain the HF-Hamiltonian $h[\rho_1]$, which belongs to the transformed density and has the form

$$h[\rho_1] = S^+ h[\rho] S. \quad (5.69)$$

This shows that ρ_1 is also a solution of the HF-equation (5.36)

$$[h[\rho_1], \rho_1] = 0. \quad (5.70)$$

In the case of a continuous symmetry, like that of translation or rotation, we therefore have, to each symmetry-breaking solution, an infinite number of degenerate solutions.

In the next section, we shall see that it is useful to do HF calculations with density dependent two-body forces. In this case, the force does not necessarily exhibit the same symmetry properties as the bare nucleon-nucleon force. Nevertheless, it is clear that the usual properties of HF solutions with respect to symmetry transformations, as previously discussed, are also retained for density dependent forces, if we require that the interaction satisfies the very plausible condition [BG 77]

$$\hat{S}V[\rho]\hat{S}^{-1} = V[S\rho S^{-1}]. \quad (5.71)$$

This means, for instance, that in the case of rotations the two-body interaction in a rotated system is the same as the interaction calculated with a rotated density. This condition is fulfilled for the Skyrme force (4.109).

5.6 Hartree-Fock with Density Dependent Forces

5.6.1 Approach with Microscopic Effective Interactions

5.6.1. Brückner-Hartree-Fock. One of the main obstacles to a direct application of the Hartree-Fock method, outlined in the preceding sections, is the fact that most bare nucleon-nucleon forces have an infinite or at least very repulsive core (see Chap. 4). As is easily verified, the two-body matrix elements entering the Hartree-Fock potential (5.34) all become infinite for a hard core potential. The way to solve this problem is to replace the bare interaction in (5.34) by the Brückner G -matrix discussed in Section 4.3.1. This, as a matter of fact, is not only convenient because it solves the hard core problem, but it can also be shown that it is a consistent resummation of certain higher order terms of the full many body problem. Since we do not have the technical many-body apparatus at hand here, we leave the demonstration to Appendix F.4.

The Brückner Hartree-Fock equations are given in analogy to Eq. (5.38) by (see also the review articles on the subject treated in this section by H.

S. Köhler [Kö 75] and W. Wild [Wi 77]):

$$\sum_{I'} \left\{ t_{I'} + \sum_{i=1}^A \sum_{pp'} G_{ip}^{*+*} D_{pi} D_{p'i}^* \right\} D_{Ik} = \epsilon_k D_{Ik}. \quad (5.72)$$

Here G is the Brückner G -matrix as defined in Eq. (4.39), written in terms of the basis of a definite single-particle potential. The corresponding ground state energies given in the basis, which are solutions of (5.72), are

$$E_0^{\text{BHF}} = \sum_{i=1}^A t_i + \frac{1}{2} \sum_{i,j=1}^A G_{ij}^{*+*} \quad (5.73)$$

$$= \sum_{i=1}^A \epsilon_i - \frac{1}{2} \sum_{i,j=1}^A G_{ij}^{*+*}. \quad (5.74)$$

For the ground state energy, it seems that we need only the hole solutions of (5.72). The particle solutions of (5.72), however, enter the Bethe-Goldstone equation (4.39) through the intermediate particle energies ϵ_n, ϵ_m . The Brückner Hartree-Fock solution then consists of a complicated doubly self-consistent procedure. It can be solved, for example, by the following iteration cycle: (i) Calculate the G -matrix via (4.39) in a suitable basis of first choice (e.g., harmonic oscillator); (ii) diagonalize once (5.72) in this basis, which gives a new basis; (iii) calculate in this new basis a new G -matrix; and so on until the convergence is achieved. In this iteration cycle there arises, however, a small ambiguity concerning the energy dependence of the G -matrix in (5.72). Since we do not know the solution a priori, we have to include the energy dependence of G_{ip}^{*+*} into the iteration cycle. We thus have to take for ϵ_k the energy corresponding to the basis in which we have actually written Eq. (5.72) for each step of the iteration, that is, we can take ϵ_k equal to ϵ_i or ϵ_j . No ambiguity arises for ϵ_i because the D_{pi} are taken to be diagonal in the iteration process. The conventional choice for the BHF potential energy matrix [see Eq. (5.34)] is (see e.g. [Ba 69a]) (of course, the final answer does not depend on any specific convention):

$$\Gamma_{kk'}^{\text{BHF}} = \begin{cases} \frac{1}{2} \sum_{i=1}^A (G_{kik'i}^{*+*} + G_{kik'i}^{*+*}) & \text{for } k, k' \leq \epsilon_F, \\ \sum_{i=1}^A G_{kik'i}^{*+*} & \text{for } k \leq \epsilon_F, k' > \epsilon_F, \\ \sum_{i=1}^A G_{kik'i}^{*+*} & \text{for } k' \leq \epsilon_F, \\ & k > \epsilon_F. \end{cases} \quad (5.75)$$

The particle-particle matrix elements of Γ^{BHF} are a somewhat controversial matter. For a fixed G -matrix, the particle-particle matrix elements of Γ^{BHF} do not influence the hole solutions of Eq. (5.72); they do influence, however, the particle solutions, and via (4.39) in the doubly self-consistent cycle, indirectly also the hole solutions. We can argue (see discussions in

(Ba 69a, Ne 70]) that if the particle-particle matrix elements of Γ^{BHF} are equal to zero,

$$\Gamma_{kk'}^{\text{BHF}} = 0, \quad \text{for } k, k' > \epsilon_F, \quad (5.76)$$

three-body correlations are effectively summed, which were originally not present in our formulation (5.72) and (4.39).

Equation (5.72) is not only different from the ordinary HF equation (5.38) because the two body operator is more complicated, but also because Γ^{BHF} now depends on the energy which we want to calculate. Therefore, it is a nonlinear problem in which the solutions to different energies are, in general, no longer orthogonal (solutions with different angular momentum are, though, still orthogonal for the spherically symmetric case). However, for the iterative solution this is of no special importance.*

As we discussed in Section 4.3.1, the G -matrix sums up two-particle scattering processes in the nuclear medium. One can show that (5.74) contains all contributions of this type to the ground state energy [Ma 67b]. In Table 5.1 we show the results of Brückner-Hartree-Fock calculations for the rms radius and the binding energy per particle in the case of ^{16}O , ^{40}Ca , and ^{208}Pb ; the bare force was the Reid soft core potential (4.35).

Table 5.1 Results of BHF calculations with the Reid soft core potential compared with experiment (from [DMS 73])

		BHF	Experiment
^{16}O	$-E_0/A$ (MeV)	3.91	7.98
	rms (fm)	2.50	2.73
^{40}Ca	$-E_0/A$	3.88	8.55
	rms	3.04	3.48
^{208}Pb	$-E_0/A$	2.52	7.87
	rms	4.51	5.50

The results in Table 5.1 are deceiving. The calculations do not give even half the experimental binding energy and the rms radii are about 10–20% off. The bad result for the binding energy is not too surprising, however, in view of the fact that it is a difference between two very large numbers, that for kinetic and that for potential energy.

Nevertheless, in view of the unsatisfying result, one has to envisage taking into account more complicated processes.* Next in the hierarchy are three-particle scattering terms whose importance should depend on the density of the system. As we have seen in Section 4.3, the healing distance, which characterizes the range of the two-particle correlations, is appreciably smaller than the average interparticle distance. Thus the probability

*One should nevertheless make sure that the energy dependence of Γ^{BHF} is not too strong, otherwise the independent particle picture may no longer be valid.

†In this context, see also the hypernetted chain formalism [PB 73, FR 75, 76a, LS 77, Ri 79].

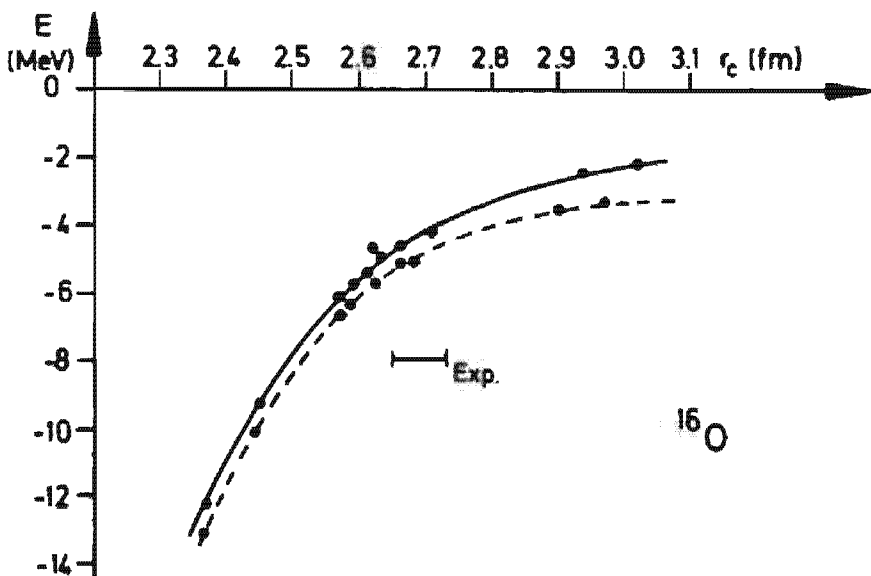


Figure 5.4. Comparison of BHF calculations with different nucleon-nucleon potentials (dots on full line) with calculations including 3-body correlations (broken line) and with experiment (from [Wi 77]).

that three particles are simultaneously within the range of the healing distance should be quite small. This is, however, a rather qualitative argument [Be 71, p. 161]. In fact, Kummel and co-workers have been able to include three-body correlations in a completely self-consistent manner into the calculations for the ground state energy (see, e.g., [KLZ 75, 78] and further references cited therein). They also give strong arguments that four-body correlations should be negligible. Their results are very interesting in the sense that agreement with experiment is improved, though not very dramatically. For different nucleon-nucleon potentials, the results lie roughly on a smooth line in the $-E_0/A$ versus rms-radius plane, as shown in Fig. 5.4. This line is called the *Coester line*. The results of the Reid soft core potential are located approximately at the point where the curve is closest to the experimental value. In view of the claim [KLZ 75] that the results have converged, the remaining difference must be attributed to relativistic effects or to mesonic degrees of freedom.

5.6.1.2. The Local Density Approximation and the Variational Principle. In Section 4.3 we saw that the influence of a hard core potential on a two-nucleon wave function is effective over relative distances of the two nucleons ranging from 0 to about 1 fm, that is, only over very short distances, compared to the nuclear radius of about 10 fm. This means that the Brückner G -matrix is only different from the bare interaction $\phi(r)$ within the same range of r -values. However, in general, variations of about 1 fm in the relative variable $r = |\mathbf{r}_1 - \mathbf{r}_2|$ of the two nucleons imply a similar variation in the center of mass coordinate. The nuclear density $\rho(\mathbf{R}) = \rho(\frac{1}{2}(\mathbf{r}_1 + \mathbf{r}_2))$ does not (at least, not in the interior of the nucleus) change very much over such a range of \mathbf{R} -values. It therefore seems a reasonable assumption to calculate the nuclear G -matrix at each value of $\rho(\mathbf{R})$ as if the nucleus locally around \mathbf{R} were a piece of nuclear matter* with the density $\rho(\mathbf{R})$. Actually, this reasoning is

* For the theory of nuclear matter, see the reviews [Be 71, Sp 72, JLM 76].

very close to the Thomas-Fermi approximation (see Chap. 13). More explicitly, this means that in the Bethe-Goldstone equation (4.39), which can be written using (5.76) as

$$G^W = \delta + \delta \frac{Q_F}{W - Q_F \Gamma Q_F} G^W, \quad (5.77)$$

we replace the projector Q_F by its expression Q_F^{NM} in nuclear matter of density $\rho(R)$. Since Q_F (4.41) can be expressed by the nonlocal single-particle density $\rho(r, r') = \sum_{i=1}^4 \varphi_i(r)\varphi_i^*(r')$,

$$\langle r_1 r_2 | Q_F | r'_1 r'_2 \rangle = [\delta(r_1 - r'_1) - \rho(r_1, r'_1)][\delta(r_2 - r'_2) - \rho(r_2, r'_2)], \quad (5.78)$$

this means that in (5.78) ρ has to be replaced by its nuclear matter value [see Eq. (13.20)]

$$\rho^{NM}(r, r') = \frac{3}{k_F(R)s} j_1(k_F(R)s) \rho(R), \quad (5.79)$$

where $s = r - r'$, $R = \frac{1}{2}(r + r')$, and j_1 is a Bessel function. The R -dependence of (5.79) comes from the fact that we have only treated the nucleus locally around R as nuclear matter. The relationship between k_F and ρ is given, as usual, by [see Eqs. (5.91), (13.22), and (13.23)]

$$\rho(R) = \frac{2}{3\pi^2} k_F^3(R). \quad (5.80)$$

Numerical comparison with exact density matrices of finite nuclei have shown [Ne 75] that the nonlocal behavior of ρ is very well approximated by (5.79) in the nuclear interior, and reasonably well represented throughout the nuclear surface. We can therefore conclude that the local density approximation to the G -matrix as described here is quite good.

In principle, the G -matrix thus calculated depends on the three variables $r = r_1 - r_2$; $r' = r'_1 - r'_2$ and on $R = \frac{1}{2}(r_1 + r_2 - r'_1 - r'_2)$; $G = G_{r, r', R}$. It turns out, however, that the dependence of G on the total momentum P (the conjugate variable to R) is weak, and we usually put it equal to some average value [BGW 58]:

$$G_{r, r', P} \approx G_{r, r', P_\infty}.$$

Negele [Ne 70] further simplifies the expression for G . He replaces the starting energy $W = \epsilon_i + \epsilon_j$ appearing in the G -matrix of Eq. (5.73) by an average value obtained as twice the average hole energy in nuclear matter. In this way, we get rid of the state dependence of the single-particle potential in Eq. (5.72) and the corresponding eigenfunctions form a complete orthonormal set. The next step consists of representing $G_{r, r'}$ by an effective local operator $v^{eff}(r)$; (we omit the details of how this is achieved and refer to [Ne 70]*). Furthermore, this effective interaction is renormalized phenomenologically to give the correct volume of nuclear matter [see the Bethe-Weizsäcker formula (1.4)]. In this sense, the "density dependent HF" (DDHF) method of Negele is still a semi-phenomenological procedure.

One further very important ingredient of Negele's theory we have not spoken of until now: In Table 5.1, we have seen that a pure BHF calculation does not give very good results; therefore, something better has to be invented. It turns out that

* Other applications of the 'local' density approximation can be found in [Kö 65, NV 70, CS 72, NR 72].

the intuitively appealing idea to vary the ground state energy (5.73) with G replaced by the local density approximation, with respect to the single-particle wave functions, as in the pure HF case (Eq. 5.29), yields very good results. The Hartree-Fock Hamiltonian becomes, in this case, [see Eq. (5.32)]

$$h_{kk'}^{\text{HF}} = \frac{\delta E[\rho]}{\delta \rho_{kk'}} = t_{kk'} + \sum_{qq'} \tilde{v}_{kq'k'q}^{\text{eff}} \rho_{qq'} + \langle \Phi | \frac{\delta v^{\text{eff}}}{\delta \rho_{kk'}} | \Phi \rangle, \quad (5.81)$$

where $|\Phi\rangle$ is a Slater determinant corresponding to the density ρ . For density independent forces, (5.81) just reduces to the usual HF-Hamiltonian. For density dependent forces, however, we have an additional term $\delta v^{\text{eff}}/\delta \rho$, usually called the *rearrangement* or *saturation potential*. It results from the density dependence in $v^{\text{eff}}(\rho)$ and plays a very important role in practical calculations. It has to be emphasized, however, that the variational method just described is not equivalent to the variation of a trial wave function minimizing the expectation value of the original many-body Hamiltonian (5.25). This implies that, at least in principle, the ground state energy calculated with (5.81) could be lower than the exact one. The method is justified in the first place by its success; theoretically, we can say that the additional term $\delta v^{\text{eff}}/\delta \rho$ somehow takes into account three-body scattering terms [Ne 75] ($\delta v^{\text{eff}}/\delta \rho$ has six indices in the shell model space). In Table 5.2, we show the big improvement over BHF which is obtained when using the DDHF method [Ne 70, NV 75].

Table 5.2 Binding energies (in MeV) and rms radii (in fm) with the density dependent Hartree-Fock method (DDHF)

		BHF	DDHF	Exp.
$^{16}_{8}\text{O}$	$-E_0/A$	3.91	7.59	7.98
	rms	2.50	2.75	2.73
$^{40}_{20}\text{Ca}$	$-E_0/A$	3.88	7.99	8.55
	rms	3.04	3.46	3.48
$^{208}_{82}\text{Pb}$	$-E_0/A$	2.52	7.83	7.87
	rms	4.51	5.49	5.50

The solution of the DDHF equations is a very complicated task because of the fact that the exchange term (5.43) implies that an integrodifferential equation must be solved. The fact that the nuclear force is of rather short range can, however, be exploited to simplify the problem so that the nonlocal exchange term can be expanded in powers of the nonlocality around its local value. This procedure leads in a rather natural way to a justification of the very successful HF scheme using the phenomenological Skyrme forces, which we will study next [Ne 75].

5.6.2 Hartree-Fock Calculations with the Skyrme Force

5.6.2.1. General Remarks. There have been many applications of the Hartree-Fock method over the years using different forces. It lies beyond the scope of this book to give a review of them (for a recent review, see [QF 78]). Many of them—in particular, those that do not use density

dependent forces—have the shortcoming that they are not able to simultaneously produce the binding energies, the radii, and the proper single-particle spectrum for light and heavy nuclei (see, for instance, [Vo 65, MB 65, BB 67, NDK 68, PS 68, SFW 69, SP 70]).

The use of the Skyrme force (4.104) as a phenomenological interaction in HF calculations has the important merit of being able to very well reproduce binding energies and nuclear radii over the entire periodic table.* Like the Negele force, obtained from the local density approximation, the Skyrme force is density dependent and, as discussed in the last section, cannot simply be used in the variation principle (5.3), which is based on a linear Hamiltonian. Formally, this difficulty can be overcome by considering the Skyrme force as a three-particle force (4.104).

5.6.2.2. The Energy Calculated with the Skyrme Force. We start with the Skyrme force as given in Eq. (4.104) and calculate the expectation value of the corresponding Hamiltonian with respect to a Slater determinant $|\Phi\rangle$ containing the single-particle wave functions $\varphi_i(\mathbf{r}, s, t)$. For the sake of simplicity we require time reversal invariance. This is not essential [Pa 76], but simplifies the equations considerably. Furthermore, we regard only nuclei with $N = Z$ and neglect the Coulomb field.[†] (For the case $N \neq Z$ with Coulomb interaction, and for more details of the following derivation, see the paper of Vautherin and Brink [VB 72]).

The energy is given by:

$$\begin{aligned} E_0 &= \langle \Phi | T + V^{(2)} + V^{(3)} | \Phi \rangle \\ &= \sum_{i=1}^A \langle i | \frac{p_i^2}{2m} | i \rangle + \frac{1}{2} \sum_{i,j=1}^A \langle ij | \bar{v}^{(2)} | ij \rangle + \frac{1}{6} \sum_{ijk=1}^A \langle ijk | \bar{v}^{(3)} | ijk \rangle. \end{aligned} \quad (5.82)$$

Because of the δ -function character of the Skyrme force (4.104), it is possible to express E by an integral over an energy density $H(\mathbf{r})$

$$E_0 = \int H(\mathbf{r}) d^3r, \quad (5.83)$$

in which $H(\mathbf{r})$ is an algebraic function of three quantities:

(i) the nucleon density

$$\rho(\mathbf{r}) = \sum_{i,s,t} |\varphi_i(\mathbf{r}, s, t)|^2; \quad (5.84)$$

(ii) the kinetic energy density

$$\tau(\mathbf{r}) = \sum_{i,s,t} |\nabla \varphi_i(\mathbf{r}, s, t)|^2; \quad (5.85)$$

* There is a large number of similar phenomenological density dependent forces with zero range [Mo 70, LV 71, La 72, EM 72, BJS 75, Kō 76, LB 76, TK 76, KKS 77, SM 78] or finite range [Kr 70, ZR 71, RPS 72, LMV 73, Go 75b, RBP 77] which show properties similar to the Skyrme force in HF calculations.

[†] For the treatment of the Coulomb field, see [Qu 72, GVL 73, SI 51, Go 52, KS 72, TQ 74].

(iii) the so-called spin orbit densities

$$\mathbf{J}(\mathbf{r}) = (-i) \sum_{i, s, s'} \varphi_i^*(\mathbf{r}, s, t) [\nabla \varphi_i(\mathbf{r}, s', t) \times \boldsymbol{\sigma}_{s'}]. \quad (5.86)$$

The sums are taken over all occupied single-particle states. A lengthy but straightforward calculation [VB 72] for $N = Z$ nuclei gives

$$\begin{aligned} H(\mathbf{r}) = & \frac{\hbar^2}{2m} \tau(\mathbf{r}) + \frac{3}{8} t_0 \rho^2 + \frac{1}{16} t_3 \rho^3 + \frac{1}{16} (3t_1 + 5t_2) \rho \tau \\ & + \frac{1}{64} (9t_1 - 5t_2) (\nabla \rho)^2 - \frac{3}{4} W_0 \rho \nabla \mathbf{J} + \frac{1}{32} (t_1 - t_2) \mathbf{J}^2. \end{aligned} \quad (5.87)$$

Besides the kinetic energy τ , we also have contributions from the two-body δ -force $\sim \rho^2$ and the three-body δ -force $\sim \rho^3$. The nonlocal p^2 -terms give contributions $\sim \rho \tau$ and $\sim \nabla \rho^2$. The latter has its largest contributions at the nuclear surface. The term $\frac{1}{32}(t_1 - t_2)\mathbf{J}^2$ is usually neglected because it is difficult to handle in deformed nuclei and its contribution to the spin orbit part does not reproduce the experimental spin-orbit splitting.

We could also have derived the three-body term $\sim \rho^3$ from a density dependent two-body interaction

$$\frac{1}{16} t_3 \rho^3 = \frac{1}{2} \sum_{i, j \leq A} \langle ij | \frac{1}{6} t_3 \delta(\mathbf{r}_1 - \mathbf{r}_2) \rho(\mathbf{r}_1) (1 + P^\alpha) | ij - ji \rangle. \quad (5.88)$$

In Section (5.6.1.1) we saw that when using density dependent interactions we have first to calculate the energy and only afterwards vary with respect to the density. In that sense, the three-body contact force of Skyrme is equivalent to the two-body interaction (5.88). This equivalence, however, is only valid in even-even nuclei with time reversal symmetry.

Using (5.87), we are able to calculate the binding energy per particle in nuclear matter without Coulomb interaction. In this case we have translational invariance and the single-particle wave functions are given by plane waves normalized to a δ -function

$$\varphi_{ksr} = \frac{1}{(2\pi)^{3/2}} e^{i\mathbf{k}\cdot\mathbf{r}} X_s^{1/2} X_r^{1/2} \quad (5.89)$$

and in Eqs. (5.84)–(5.86) we have to replace

$$\sum_{i=1}^A \dots \quad \text{by} \quad \int_{|k| \leq k_F} d^3 k \dots, \quad (5.90)$$

where all the levels with $|k|$ smaller than the Fermi momentum k_F are occupied. From (5.84), we get the usual relation between ρ and k_F [see also Eqs. (13.22) and (13.23)]

$$\rho = \frac{4}{(2\pi)^3} \frac{4\pi}{3} k_F^3 = \frac{2}{3\pi^2} k_F^3 \quad (5.91)$$

and from (5.85),

$$\tau = \frac{2}{3\pi^2} \frac{3}{5} k_F^5 = \frac{3}{5} \rho k_F^2 = \frac{3}{5} \left(\frac{3\pi^2}{2} \right)^{2/3} \rho^{5/3}. \quad (5.92)$$

Because of translational invariance, we have $\nabla\rho = \nabla J = 0$ and obtain for the binding energy per particle in nuclear matter

$$\frac{E_0}{A} = \frac{H}{\rho} = \frac{3}{5} \frac{\hbar^2}{2m} k_F^2 + \frac{3}{8} \iota_0 \rho + \frac{1}{16} \iota_3 \rho^2 + \frac{3}{80} (3\iota_1 + 5\iota_2) \rho k_F^2. \quad (5.93)$$

The saturation property means that there is an equilibrium density ρ_0 for which

$$\left. \frac{\partial}{\partial \rho} \left(\frac{E_0}{A} \right) \right|_{\rho=\rho_0} = 0 = \frac{2}{5} \frac{\hbar^2}{2m} k_F^2 \rho^{-1} + \frac{3}{8} \iota_0 + \frac{1}{8} \iota_3 \rho + \frac{1}{16} (3\iota_1 + 5\iota_2) k_F^2. \quad (5.94)$$

The incompressibility of nuclear matter K is defined as the curvature of the binding energy E_0/A with respect to the Fermi momentum k_F at this minimum:

$$K = k_F^2 \left. \frac{\partial^2 (E_0/A)}{\partial k_F^2} \right|_{\rho=\rho_0} = \frac{6}{5} \frac{\hbar^2}{2m} k_F^2 + \frac{9}{4} \iota_0 \rho + \frac{15}{8} \iota_3 \rho^2 + \frac{3}{4} (3\iota_1 + 5\iota_2) \rho k_F^2. \quad (5.95)$$

Equations (5.93)–(5.95) allow us to express the two constants ι_0 and ι_3 and the combination $3\iota_1 + 5\iota_2$ by the nuclear matter constants E_0/A , ρ_0 , and K . From Eq. (5.95), we see that ι_3 is strongly correlated with the incompressibility K .* From the Bethe-Weizsäcker Formula (1.4), we know that the value of $E_0/A = a_V = 15.9$ MeV. Less well determined is the equilibrium density $\rho_0 = 3/4\pi r_0^3 \approx 0.14$ fm⁻³. Therefore, it is not possible to adjust the force parameters of a phenomenological force to nuclear matter data alone. We first have to carry out the calculation for finite nuclei.

5.6.2.3. The Derivation of the Density Dependent Hartree-Fock Equations. According to the concept of Section 5.6.1, we have to vary the functional $E_0[\rho]$ with respect to the density in order to gain the Hartree-Fock Hamiltonian. Unfortunately, (5.95) does not have the form of a functional of ρ . It also depends on τ and J , and it is very hard to express τ and J in terms of ρ . In our case, however, this is no real problem, since the HF-density is uniquely defined by the single-particle wave functions φ_k (5.84), and we can also carry out the variation with respect to φ_k under the condition that they are normalized to unity. We use Lagrange multipliers ϵ_k for these subsidiary conditions and find

$$\frac{\delta}{\delta \varphi_k} \left(E_0[\rho] - \sum_i \epsilon_i \int d^3r |\varphi_i(\mathbf{r})|^2 \right) = 0. \quad (5.96)$$

The variation of the energy (5.83), after integrating by parts, can be written

$$\delta E = \int d^3r \left[\frac{\hbar^2}{2m^*(\mathbf{r})} \delta \tau(\mathbf{r}) + U(\mathbf{r}) \delta \rho(\mathbf{r}) + W(\mathbf{r}) \delta J(\mathbf{r}) \right] \quad (5.97)$$

* Nuclear matter calculations give values between 150 and 250 MeV and, from recent measurements of the breathing mode in ^{208}Pb , we deduce the value $K \approx 200$ MeV for the incompressibility of heavy, finite nuclei.

with an effective mass

$$m^*(r) = m \left(1 + \frac{2m}{\hbar^2} \frac{1}{16} (3t_1 + 5t_2)\rho \right)^{-1}, \quad (5.98)$$

an average field

$$\begin{aligned} U(r) &= \frac{3}{4} t_0 \rho + \frac{3}{16} t_3 \rho^2 + \frac{1}{16} (3t_1 + 5t_2) r \\ &\quad + \frac{1}{32} (5t_2 - 9t_1) \nabla^2 \rho - \frac{3}{4} W_0 \nabla J, \end{aligned} \quad (5.99)$$

and a one-body spin-orbit potential [we neglect the term $\frac{1}{32}(t_1 - t_2)J^2$]

$$W(r) = \frac{3}{4} W_0 \nabla \rho. \quad (5.100)$$

We now have to insert into Eq. (5.96) the variations δr , $\delta \rho$, and δJ with respect to φ_i . From definitions (5.84)–(5.86) we get

$$\delta E = 2 \sum_{i=1}^A \int d^3r \delta \varphi_i^* \left\{ -\nabla \frac{\hbar^2}{2m_r^*} \nabla + U + W \frac{1}{i} (\nabla \times \sigma) \right\} \varphi_i \quad (5.101)$$

and, using Eq. (5.96), we finally find the HF-equation in coordinate space viz:

$$\left\{ -\nabla \frac{\hbar^2}{2m^*(r)} \nabla + U(r) + W \frac{1}{i} (\nabla \times \sigma) \right\} \varphi_i(r) = \epsilon_i \varphi_i(r). \quad (5.102)$$

The exchange term in the HF-equation (5.44) is now local and is included in the potential $U(r)$, so that (5.102) is a pure differential equation. The nonlocality is expressed only in the r -dependence of the effective mass $m^*(r)$. In the case of spherical symmetry, we end up with a one-dimensional differential equation of second order in the radial coordinate r . In particular, the spin-orbit term (5.100) takes the form

$$\frac{3}{2} W_0 \left(\frac{1}{r} \frac{\partial}{\partial r} \rho \right) \text{is} \quad (5.103)$$

and, as we have already discussed in Section 2.4, this is concentrated mainly at the nuclear surface.

5.6.2.4. Discussion of the Results. Vautherin and Brink [VB 72] originally solved the HF equation (5.102) for the spherical closed shell nuclei ^{16}O , ^{40}Ca , ^{48}Ca , ^{90}Zr , and ^{208}Pb , and were able to adjust the six parameters t_0 , t_1 , t_2 , t_3 , W_0 , and x_0 so as to reproduce the radii and binding energies of these nuclei. They presented two sets of force constants (Skyrme I and II) which gave a good description of these closed shell nuclei. Both have large values of t_3 , which means a strong density dependence. This is a very crucial point, because for density dependent forces the binding energy E_0^{HF}

is given by (5.28) and (5.81)

$$\begin{aligned} E_0^{\text{HF}} &= \text{Tr}[\rho] + \frac{1}{2} \text{Tr}_1 \text{Tr}_1 \rho \bar{\rho} \rho \\ &= \frac{1}{2} \text{Tr}\{(\epsilon + \epsilon_i)\rho\} - \frac{1}{2} \text{Tr}\left(\langle \text{HF} | \frac{\delta V}{\delta \rho} | \text{HF} \rangle \rho\right) \end{aligned} \quad (5.104)$$

which, in the case of the Skyrme force (5.88), is

$$E_0^{\text{HF}} = \frac{1}{2} \sum_{i=1}^A (\epsilon_i + \epsilon_i) - \frac{1}{32} t_3 \int d^3r \rho^3. \quad (5.105)$$

The last term in Eqs. (5.104) and (5.105) is, as discussed in Section 5.6.1.2, called the rearrangement term. For a density independent force it vanishes, and it is not possible to simultaneously reproduce the binding energy E_0 , the radii, and the experimental single-particle energies ϵ_i of a nucleus, as the last two quantities already determine (more or less) the first part of Eq. (5.105). Only the rearrangement term makes it possible to reproduce the binding energy so well. This term is always negative because of the repulsion of the nuclear forces at short distances or large densities.

Later, the density dependence in many other spherical nuclei was investigated [BFG 75] and other sets of force parameters were determined (Skyrme III–VI). They differ in their density dependence, and it turns out that t_3 is not determined by the radii and binding energies alone. With rather different values of t_3 , we can, in fact, reproduce these values. However, the single-particle energies ϵ_i do depend dramatically on t_3 . Skyrme III [Eq. (4.108)] gives reasonable values for all these quantities.

Table 5.3 lists binding energies and root mean square radii r_c for several spherical closed-shell nuclei as calculated by the most sophisticated

Table 5.3 Experimental and calculated root mean square radii (in fm) and binding energies (in MeV) per nucleon

		Experiment	Negele [Ne 70]	Campi and Sprung [CS 72]	Nemeth et al. [NMH 73]	Skyrme III [BFG 75]
¹⁶ O	<i>E</i>	-7.98	-6.75	-7.68	-7.98	-7.96
	<i>r_c</i>	2.73	2.80	2.75	2.77	2.69
⁴⁰ Ca	<i>E</i>	-8.55	-7.49	-8.33	-8.47	-8.54
	<i>r_c</i>	3.49	3.49	3.49	3.40	3.48
⁴⁸ Ca	<i>E</i>	-8.67	-7.48	-8.40	-8.55	-8.71
	<i>r_c</i>	3.48	3.52	3.51	3.44	3.53
⁹⁰ Zr	<i>E</i>	-8.71	-7.85	-8.63	-8.70	-8.71
	<i>r_c</i>	4.23	4.25	4.27	4.13	4.32
²⁰⁸ Pb	<i>E</i>	-7.87	-7.53	-7.87	-7.87	-7.87
	<i>r_c</i>	5.50	5.44	5.45	5.22	5.57

Hartree-Fock calculations with effective interactions derived from the bare nucleon-nucleon force and also with Skyrme III.

One has also calculated angular distributions for electron scattering and found good agreement with the experimental data. This shows that the calculations produce the proper charge distributions. For example, in Fig. 5.5(a) we show the charge distribution of ^{208}Pb compared with a phenomenological curve determined from electron scattering. Figure 5.5(b) gives the corresponding average potential U_p and U_n for protons and neutrons and the effective mass m^*/m . The HF-charge density is not completely constant in the nuclear interior, but shows some oscillations which have their origin in the shell effects. They are smaller than the oscillations that would be obtained for a shell model charge density in a phenomenological Wood-Saxon potential, but are still larger than the experimentally observed wiggles. The corresponding self-consistent fields also show deviations from a Wood-Saxon shape. For lighter nuclei, they are more important. Figure 5.5(b) also gives the ratio m^*/m , which measures the nonlocality of the Skyrme potential. It is given by the parameter combination $3t_1 + 5t_2$ [see Eq. (5.98)]. For Skyrme II, the nonlocality is well pronounced.

The effective mass has a strong influence on the single particle energies ϵ_i . If we assume the single-particle wave functions of the A and the $A-1$ system to be identical, that is, if we neglect the polarization of the core by the hole in the level i , then we get for the energy difference

$$E(A) - E_i(A-1) = t_{ii} + \sum_{j < A} \bar{v}_{jj}^{(2)} + \frac{1}{2} \sum_{jk < A} \bar{v}_{ijk,jk}^{(3)}. \quad (5.106)$$

The evaluation of the right-hand side shows [VB 72] that (5.106) is exactly the single-particle energy ϵ_i , the eigenvalue of the HF-Hamiltonian. In Fig. 5.6, therefore, we compare the experimental single-particle levels in ^{208}Pb with the calculated single-particle energies ϵ_i . Essentially, we obtain the

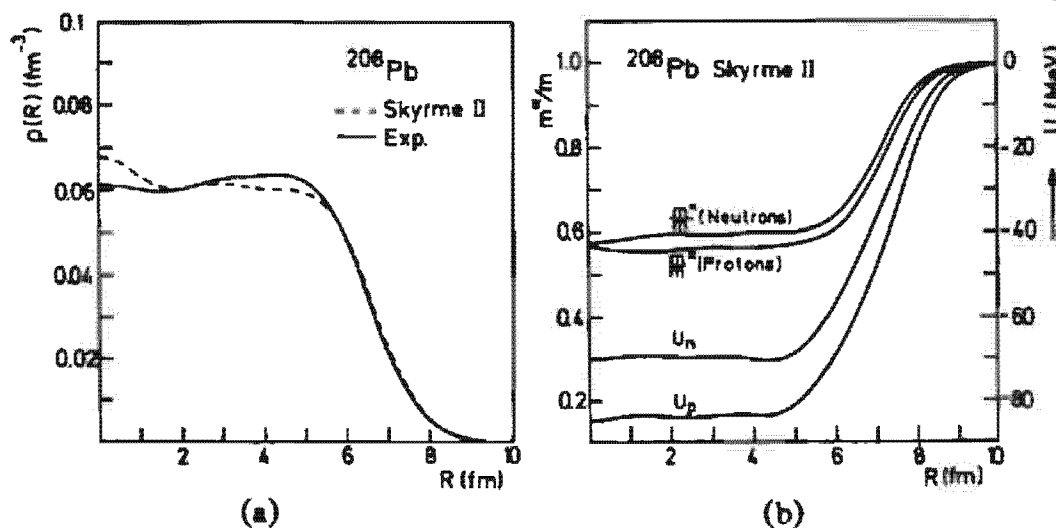


Figure 5.5. Hartree-Fock results for ^{208}Pb with the interaction Skyrme II. (a) Charge distribution. (b) Effective mass m^*/m and HF-potential $U(r)$ (the proton single-particle potential does not include the Coulomb term). (From [VB 72].)

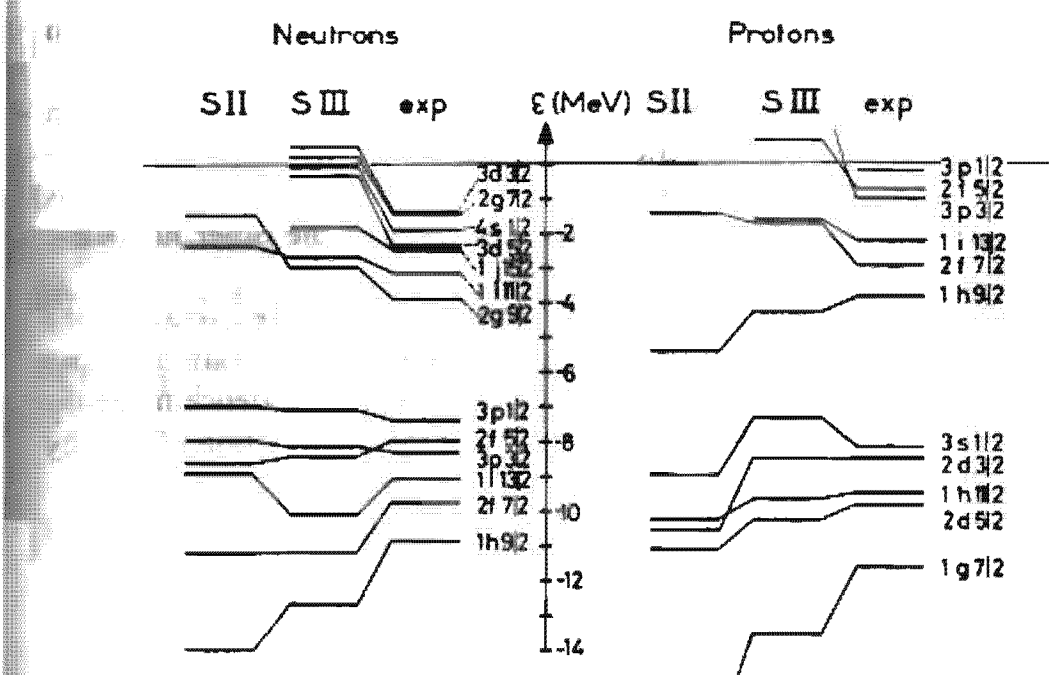


Figure 5.6. Experimental and calculated single-particle energies in the lead region. The calculated values were obtained with two different versions of the Skyrme force. With increasing effective mass, we recognize a compression of the spectrum ($m^*/m \approx 0.6$ for SII and ≈ 0.75 for SIII). (From [BFG 75].)

correct ordering of the single-particle levels, although quantitatively the different sets of parameters show rather different spectra. However, it should be emphasized that we cannot expect a priori complete agreement, because polarization effects play a certain role that have not yet been taken into account [RW 73].

5.7 Concluding Remarks

Summarizing the results of this chapter, we can say that there is a microscopic foundation of the spherical shell model as discussed in Chapter 2. The Hartree-Fock method provides a tool for calculating the average potential from an effective nucleon interaction. It becomes very important to use density dependent effective interactions to get quantitative agreement. In this case, we are able to reproduce the ground state properties of spherical nuclei very well. In most cases, the calculated single-particle levels show the correct ordering; however, they deviate in detail from the experimental single-particle excitations of neighboring odd mass nuclei.

So far we discussed only applications of the HF method to nuclei with closed shells. In fact, these are the only cases where the self-consistent field can have spherical symmetry. As soon as one or several particles are put in an unfilled j -shell (*open shell* HF [Ke 63]) we have to decide which one of the originally degenerate magnetic quantum numbers m needs to be occu-

plied and we get a slightly deformed density distribution (oblate with respect to the quantization axis for large values of $|m|$ and prolate for small values of $|m|$). This deformed density produces a deformed mean field in the next step of the iteration, which also changes the single-particle wave functions in the core. In this way, we take into account the correlations caused by the interaction of the external particle with the other nucleons. We call this effect a *polarization* of the core.

As long as we have only one or a few external particles, we can also treat this interaction in the spherical basis by a shell model configuration mixing calculation allowing for *ph excitations*. In this picture, the valence nucleons excite virtual vibrations in the core and we treat the polarization effects by a particle vibrational coupling technique (see Sec. 9.3).

In many practical applications, this effect has been taken into account only in an averaged way by distributing the external particle over all the m -quantum numbers of the next higher j -shell with equal probability $v_m^2 = 1/(2j+1)$. The wave function is then, in a sense, a HFB state (see Chap. 7) with a spherical density distribution.

In principle, the mean field approach is only justified if there is a well pronounced energy gap between the highest occupied level and the first empty level. If that is not the case (subshell closures), it is easy to excite virtual *ph-pairs*, and we can expect a more complicated wave function than a Slater determinant [see Eq. (2.36)]. From these arguments, we expect that the HF method yields a better approximation to the exact ground state for magic nuclei than for nuclei with a few particles away from the closed shell configuration. These nuclei show a small deformation in HF and have many nearly degenerate levels in the vicinity of the Fermi surface.

We call such nuclei transitional nuclei, and in the Chapters 9 and 10 we will discuss some methods for investigating their structure. For nuclei far from closed magic configurations, however, the correlation among the quasi-particles becomes so strong that they can again be treated in an extended mean field approach. Depending on the kind of correlations, we have to use a *deformed HF potential*—which is again a very good approximation for cases where new magic numbers develop in the deformed region (see Fig. 2.25). We will discuss these methods together with the nuclear pairing phenomenon in more detail in Chapters 6 and 7, and we will see then that nuclear deformations with density dependent forces can be explained rather nicely.

CHAPTER 6

Pairing Correlations and Superfluid Nuclei*

© Springer-Verlag Berlin Heidelberg 1970

6.1 Introduction and Experimental Survey

In Chapter 5 we looked for a wave function describing the ground state of the nucleus. Restricting ourselves to a product ansatz and minimizing the total energy of the system has led us to the Hartree-Fock method. As we have seen, the solution of the corresponding equation yields a transformation from a given single-particle basis to a new, better one. The variational principle is equivalent to the requirement that there are no matrix elements between the ground state and the most simple excitations, the particle-hole excitations. Therefore, the Hartree-Fock method partially takes into account the particle-hole part of the interaction, that is, the long-range part of the force, as we have seen in Chapter 4. Before we turn to the excitations caused by these correlations, we want to consider the short-range part of the force which causes particle-particle correlations (cf. Chap. 4). It will turn out that this can be done formally very similarly to the particle-hole part of the force by introducing generalized product wave functions consisting of "quasi-particles."

Of course we usually have to take into account both correlations at the same time. This will be done in the next chapter within the framework of Hartree-Fock-Bogoliubov theory. Here we restrict ourselves to pure

* We are glad to see that the original version of this chapter (in the book by Baumgartner and Schuck) [BS 68a] has partly been adopted by other authors [EG 70]. We have also incorporated some of their changes.

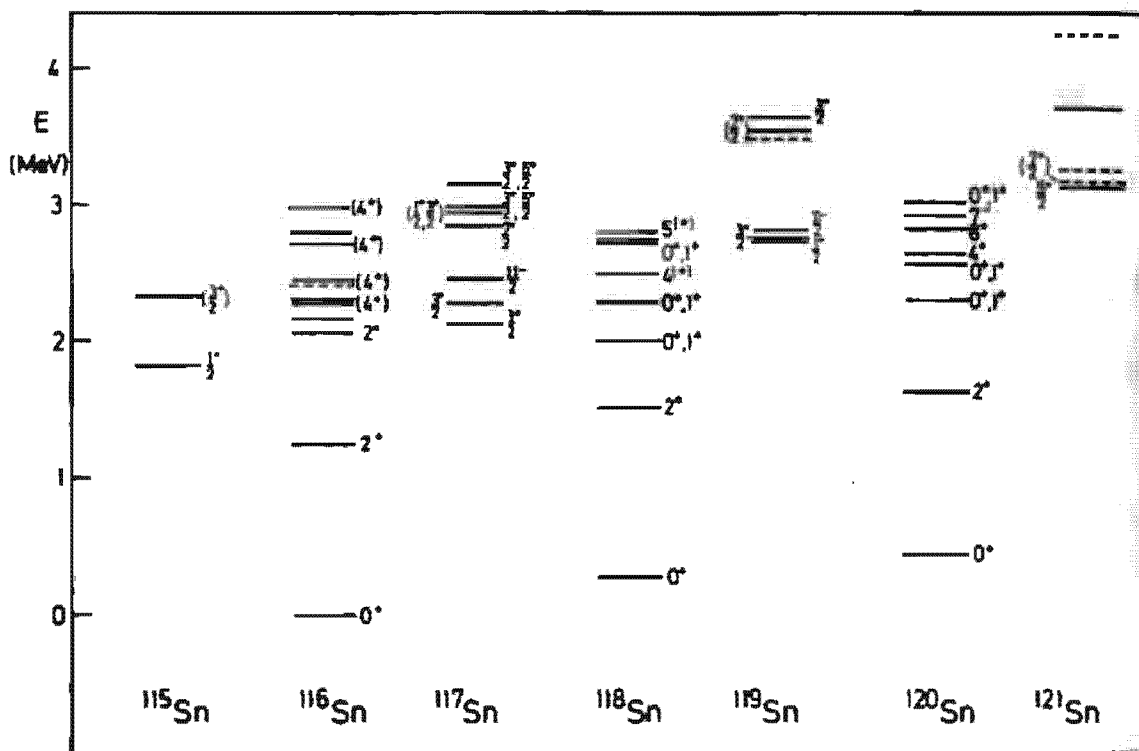


Figure 6.1. Excitation spectra of the $_{50}\text{Sn}$ isotopes.

short-range (particle-particle or pairing) correlations. This allows us to understand many important effects which cannot be explained within a pure Hartree-Fock picture.

Let us briefly summarize the essential experimental facts which lead to the idea of pairing correlations:

- (i) *The energy gap.* The spectra of deformed nuclei show a characteristic difference between even and odd nucleon number. Even-even nuclei have only few (collective) levels up to 1.5 MeV excitation energy. They can be nicely interpreted as rotational and vibrational bands. The situation is very different for even-odd nuclei, which have many collective and single-particle states in the same energy interval. Figure 6.1 shows the spectra of some tin isotopes as an example.
- (ii) *The level density.* If we assume that there are only a few nucleons in a shell of given j , many states can be constructed which are all energetically degenerate corresponding to the various possibilities of coupling angular momentum. The number of states per energy unit can easily be estimated, and it is found that in the low-lying excitation region the level density exceeds that found experimentally by roughly a factor of two.
- (iii) *Odd-even effect.* The total binding energy of an odd-even nucleus is found to be smaller than the arithmetic mean of the binding energies of the two neighboring even-even nuclei. Therefore, we

have the following relation for the masses of neighboring nuclei:

$$M_{(A \text{ odd})} > \frac{M_{A-1} + M_{A+1}}{2}.$$

This is called the odd-even effect.

- (iv) The *moments of inertia* of deformed nuclei can be measured from the level structure of rotational bands. Calculations based on the pure single-particle model (see Sec. 3.4.2) deviate by a factor of two from the experimental values. If pairing is included, theory and experiment are in much better agreement.
- (v) *Deformations.* If, in the pure shell model, we calculate the density distribution of the nucleons as a function of the nuclear mass number, we find that there is a steady transition from spherically symmetric shapes for closed shell nuclei to strong deformations for nuclei with half-filled shells. Nuclei whose mass numbers do not deviate very much from the closed shell configuration, however, stay at least in their ground state, spherically symmetric. Filling more nucleons into the shell, one enters a region in which nuclei undergo rapid changes in deformation, reaching its maximum value in the middle of the shell.
- (vi) *Low-lying 2^+ states.* We find in even nuclei, in the neighborhood of closed shell nuclei, a low-lying level with angular momentum 2 and positive parity (Fig. 6.1). These levels can be interpreted neither as rotations nor as single-particle excitations. In fact, they are vibrational in character (see Chap. 8), having a strong interplay with pairing correlations.

To understand all these phenomena we have to take into account the correlations due to the short-range part of the nucleon-nucleon interaction (see Chap. 4). As indicated in Chapter 2, even-even nuclei have ground state spin $I_0 = 0$, and the spin of odd-even nuclei is determined by the angular momentum of the odd nucleon. These observations led Göppert-Mayer [Ma 50] to a very early calculation showing that for *short-ranged, attractive, two-nucleon forces*, the coupling of two nucleons in a shell of given j to a ($I=0$)-pair is energetically favored over all other possible couplings. This can be understood very easily by neglecting the spin for a moment and by considering the density distribution of states $|lm\rangle$ and $|l-m\rangle$, as shown schematically in Fig. 6.2 (see also the discussion on this point in Section 4.4.7). From these density distributions, it is clear that the spatial overlap of two-nucleon densities is maximal if the two nucleons have the same $|m|$. For a short-range force the configuration in which the two nucleons orbit the nucleus with equal $|m|$ but in an opposite sense is therefore energetically very much favored (the case where they turn around in equal sense is obviously unfavored by the Pauli principle; see, however, the case of angular alignment in Chap. 3). Here, orbiting in opposite sense means coupling to $I=0$. The angular part of a pair coupled to $I=0, M=0$

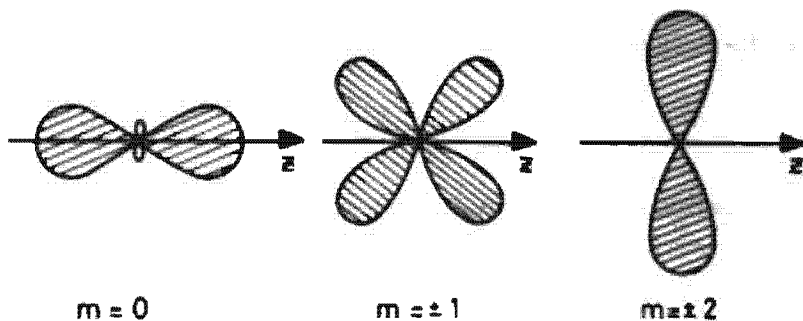


Figure 6.2. Density distributions for a nucleon in a given magnetic substate.

is, to within some factors, given by (4.132):

$$\begin{aligned} \langle \theta_1 \varphi_1, \theta_2 \varphi_2 | nljjI=0, M=0 \rangle &\propto \sum_{m=-l}^l (-1)^m Y_{lm}(\theta_1 \varphi_1) Y_{l-m}(\theta_2 \varphi_2) \\ &= \frac{2l+1}{4\pi} P_l(\cos \theta_{12}), \end{aligned} \quad (6.1)$$

where θ_{12} is the angle between the two nucleons. From (6.1), we see that the pair wave function depends only on the relative angle θ_{12} . For a fixed θ_{12} , the pair wave function is therefore uniformly distributed around a (spherical) nucleus. Since the radial functions of the two nucleons are the same, the position of the pair in space cannot, in general, be given in more detail, the radial dependence being very much a question of the nodal structure of the nucleon wave functions. As we have already seen in Fig. 4.9, $P_l(\cos \theta_{12})$ is peaked at $\theta_{12}=0$ with a width of $1/l$. Therefore, the two nucleons have a tendency to stay close in angle, which is necessary for their *spatial overlap* to be *maximal* imposed by the short range of the force. On the other hand, the two nucleons cannot get too close because this is forbidden by the uncertainty principle [it can be easily verified that the kinetic energy would be infinite for the pair wave function $\psi(r_1, r_2) \sim \delta(r_1 - r_2)$]. We can therefore say that the nucleons want to stay as close as possible according to their short-range interaction, but that the pair has to make a compromise with its kinetic energy, which would like to keep the nucleons apart.

If there is *more than one pair* in the j -shell, the formation of ($I=0$)-pairs is somewhat hindered by the Pauli principle. Some m -states necessary to achieve the coupling (6.1) of one pair are already occupied by another pair. This mutual interaction of pairs gives rise to certain special features which we will study later on but which do not destroy the pair-state character of a j -shell. On the other hand, some typical features, like transition probabilities, are proportional to the number of pairs we have in a given j -shell. If we take account of the symmetry between particles and holes, that is, of the fact that we have particle-particle as well as hole-hole pairs, we see that the effect of collectivity is largest for half-filled j -shells. On the other hand, for closed shell nuclei, no formation of pairs like (6.1) is possible.

For nuclei between closed shells, the energetically most favored configuration will be the one in which all nucleons (except the last one in the case

of odd-even nuclei) are paired off. To excite even-even nuclei, therefore, we have to break at least one pair, whereas for odd-even nuclei an excitation can be achieved by putting the odd nucleon in a very low energy level. Since the binding energy of a pair is of the order 1–2 MeV, the different energy spacing between the ground and first excited state in even-even and odd-even nuclei is thus qualitatively explained (see Fig. 6.1).

Other features mentioned above can also be understood with the pairing model. Because of the energy gap in the low-lying part of the spectrum of even-even nuclei, the level density agrees much better with the experimental one. Also the odd-even effect becomes obvious. The existence of ($I=0$)-pairs favors—as we have seen (6.1)—a spherical nuclear shape (no direction is preferred). Nuclei in the neighborhood of closed shells will therefore still have spherical symmetry, since the influence of the pairing force overcomes the tendency to deform. Further away from the closed shells we will have the opposite situation. However, this depends very sensitively on the strength of the pairing force versus the long-range ($p-h$) force; nevertheless, in this way the rather sudden change from sphericity to deformation can be understood.

Closely connected is the existence of *low-lying* 2^+ levels for open shell even-even nuclei. Nuclei in the neighborhood of closed shells that are still spherical can easily be excited to shape vibrations around their spherical equilibrium position, since the restoring force, which is the difference between pairing and deformation effects, is rather small. The nucleus will therefore become deformed into an ellipsoid and vibrate about its spherical shape with a low frequency (quadrupole oscillations, 2^+ -levels).

The diagonalization of the pair interaction cannot be interpreted as a contribution to the average static potential of the Hartree-Fock type. It is a completely new effect which gives rise to the so-called pairing potential. It is analogous to superconductivity in metals. This is the reason why Bohr, Mottelson, and Pines [BMP 58] and Belyaev [Be 59] successfully applied the methods of the theory of superconductivity by Barden, Cooper, and Schrieffer [BCS 57] to nuclei.

6.2 The Seniority Scheme

As we said in the introduction, pairing correlations are due to the short-range part of the nucleon-nucleon interaction, and this interaction is most effective between ($I=0$)-coupled pairs. In Section 4.4.7 we studied this problem to some length; to investigate the pairing phenomena in more detail we reconsider the model force derived in (4.140) and consider N particles in a single $(2j+1)$ -fold degenerate j -shell interacting through this pairing force. If we place this j -shell at zero energy, the corresponding

Hamiltonian is of the form*:

$$H = -G \sum_{m, m' > 0} a_m^+ a_{-m'}^+ a_{-m} a_m = -GS_+ S_-, \quad (6.2)$$

with

$$S_+ = \sum_{m > 0} a_m^+ a_{-m}^+; \quad S_- = (S_+)^+. \quad (6.3)$$

We introduced the operators of Eq. (6.3) because it turns out that they can be considered as the raising and lowering operators of a fictitious angular momentum, which we will call (as in the case of the Lipkin model; see Chap. 5) *quasi-spin*, which has nothing to do with real spin, but its introduction greatly facilitates the solution of (6.2) [Ke 61]. For this purpose we introduce the following three quantities for each substate m ($m > 0$):

$$\begin{aligned} s_+^{(m)} &= a_m^+ a_{-m}^+; \\ s_-^{(m)} &= a_{-m} a_m; \\ s_0^{(m)} &= \frac{1}{2}(a_m^+ a_m + a_{-m}^+ a_{-m} - 1). \end{aligned} \quad (6.4)$$

Using the commutation rules of the operators a_m and a_m^+ , we can derive the corresponding commutation rules:

$$\begin{aligned} [s_+^{(m)}, s_-^{(m)}] &= 2s_0^{(m)}; \\ [s_0^{(m)}, s_+^{(m)}] &= s_+^{(m)}; \\ [s_0^{(m)}, s_-^{(m)}] &= -s_-^{(m)}. \end{aligned} \quad (6.5)$$

Therefore, we see that the triad of operators $s_+^{(m)}, s_-^{(m)}, s_0^{(m)}$ has the commutation properties of angular momentum operators [Ed 57]. The $s_+^{(m)}, s_-^{(m)}$ are, respectively, the raising and lowering operators analogous to the angular momentum operators j_+ and j_- . Similarly, $s_0^{(m)}$ corresponds to the z-component of the angular momentum j_0 . We thus see the reason why we call $s^{(m)}$ the quasi-spin operator corresponding to the level m .

Furthermore, we can see from the definition of $s_0^{(m)}$ that it has eigenvalues $\pm \frac{1}{2}$ depending on whether the pair $(m, -m)$ is full or empty. The vector $s^{(m)}$, therefore, has a spin of $\frac{1}{2}$ angular momentum for 0, or two particles in the j -level. [If only one particle is present, all the components of $s^{(m)}$ are zero, so that $s^{(m)}$ has spin zero in this subspace.]

The total spin vector \mathbf{S} is defined by

$$\mathbf{S} = \sum_{m > 0} s^{(m)}. \quad (6.6)$$

This, of course, is also an angular momentum, and the pairing Hamiltonian (6.2) is conveniently written in the form:

$$H = -G(\mathbf{S} \cdot \mathbf{S} - S_0^2 + S_0). \quad (6.7)$$

* Note that we use BCS-phases (4.138) in the following.

We note also that

$$S_0 = \frac{1}{2} \sum_{m>0} (a_m^+ a_m + a_{-m}^+ a_{-m} - 1) = \frac{1}{2} (\hat{N} - \Omega), \quad (6.8)$$

where $\Omega = j + \frac{1}{2}$ is the number of pairs. Thus the eigenvalues of S_0 are integers or half integers, depending on whether S_0 is an integer or a half integer. Furthermore, it follows from the properties of angular momentum operators that

$$S > |S_0| = \frac{1}{2} |\Omega|. \quad (6.9)$$

Since, according to Eq. (6.6), the maximum value of S is $S = \Omega/2$, we see that S can take on all values $\Omega/2, (\Omega/2)-1, (\Omega/2)-2, \dots, |(\Omega/2)-(N/2)|$. The states will then be labeled by S and S_0 , and the energy eigenvalues of H (6.6) are given by

$$E(S) = -G \{ S \cdot (S+1) - \frac{1}{4}(N-\Omega)^2 + \frac{1}{2}(N-\Omega) \}. \quad (6.10)$$

As an alternative quantum number to the total quasi-spin S , we can introduce the so-called *seniority quantum number* s [Ra 43] given by the relation

$$S = \frac{1}{2}(\Omega - s), \quad (6.11)$$

where

$$\begin{aligned} s &= 0, 2, 4, \dots, N && \text{for } N \text{ even,} \\ s &= 1, 3, 5, \dots, N && \text{for } N \text{ odd.} \end{aligned}$$

The total energy (6.10) as a function of seniority is then given by

$$\begin{aligned} E(N, s) &= -\frac{G}{4}(N-s)(2\Omega-s-N+2) \\ &= -\frac{G}{4}(s^2 - 2s(\Omega+1) + 2N(\Omega+1) - N^2). \end{aligned} \quad (6.12)$$

The characteristic feature of the force is that the energy is labeled only by the seniority and is degenerate in all other quantum numbers except N . Although the absolute value of the energy depends strongly on the number of particles, the spectrum does not. Since the total quasi-spin changes by units of one, we have [from (6.10)] for the energy difference of two neighboring levels

$$E(S-1) - E(S) = 2G \cdot S. \quad (6.13)$$

The binding energy increases for a given N with S ; the ground state is therefore obtained when all quasi-spins are aligned, that is, $S = \frac{1}{2}\Omega$ or $s = 0$. For an even system, the first excited state has $s = 2$; and from (6.12) or (6.13) we have, for the excitation energy of the first excited state,

$$E(N, s=2) - E(N, s=0) = G \cdot \Omega. \quad (6.14)$$

The excitation energies are thus independent of the number of particles in the j -shell.

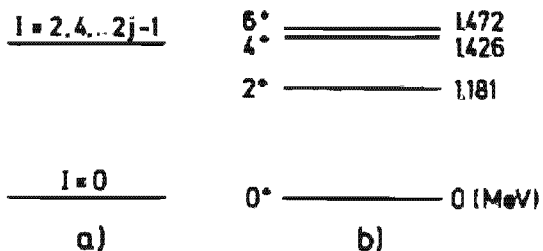


Figure 6.3. (a) Two-particle spectrum of a pure pairing force. (b) Spectrum of ^{210}Po (2p in the $1h9/2$ shell).

If we have only two particles in the j -shell, the seniority can take on only the values $s=0, 2$. The two (identical) nucleons can couple to $I=0, 2, 4, \dots, 2j-1$. Only the state with $I=0$ is affected—that is, lowered—by the pairing interaction (6.2). The other states are unaffected and therefore degenerate. Thus we see that the ground state ($s=0$) has $I=0$ and the excited states ($s=2$) have $I=2, 4, 6, \dots$, that is, in the ground state the two nucleons are “paired,” whereas in the excited states the pair is “broken.” This fact is represented schematically in Fig. 6.3, where we also show for comparison the low-lying spectrum of ^{210}Po (two protons in a $1h9/2$ shell). In the general case, the binding energy of the ground state as a function of N can be written as:

$$E(N, s=N) - E(N, s=0) = -E(N, s=0) = G\Omega \frac{N}{2} \left(1 - \frac{N-2}{2\Omega}\right). \quad (6.15)$$

We see that for cases in which the particle number is much smaller than the degeneracy of the shell ($N \ll \Omega$), the binding increases linearly with the number ($n = N/2$) of pairs, that is, the total energy is just the binding energy of one pair (6.14) multiplied by the number of pairs. If we draw the ground state energies as a function of n , we obtain a “harmonic spectrum” (Fig. 6.4). This is the *pair vibrational spectrum*, which is found, for example, in the lead region and which we will consider in more detail in Section 8.3.5. All the states of the spectrum in Fig. 6.4 have maximal quasi-spin ($s=0$), that is, they are *ground states*. We speak then of the $s=0$ band; there are, of course, $s=2$ bands, etc. It has been found that two-particle transfers between two states of a given band are enhanced with respect to those between two states belonging to different bands. If the number of pairs increases, the mutual disturbance of $I=0$ pairs due to the Pauli principle (see introduction) becomes important and the spectrum (6.15) becomes anharmonic.

We see that the excitation energy of the *first excited state* (6.14) is equal to the binding energy of one pair (6.15). Alternatively, we can say that in

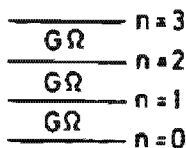


Figure 6.4. Harmonic spectrum of pair vibrations.

the first excited state ($s = 2$) two nucleons are unpaired. (The possibility of creating the first excited state by putting the bound pair into a higher level is excluded in our model, since there is only one level.) This classification scheme straightforwardly generalizes to the statement that a state of seniority s has s unpaired particles (s even and odd).

The ground state is apparently never degenerate, since there is only one way to make a total quasi-spin of $S = \Omega/2$ out of Ω spins $\frac{1}{2}$. There are $\Omega - 1$ ways for the $s = 2$ state:

$$\iota_2 = \Omega - 1 = \binom{\Omega}{1} - \binom{\Omega}{0}. \quad (6.16)$$

This can be easily checked by considering a definite example, say $\Omega = 4$; the $s = 2$ state can then be represented as: $\rightarrow \rightarrow \overset{3}{\rightarrow} \leftarrow \overset{a}{\leftarrow}$. There are $4 - 1 = 3$ possibilities of grouping a with one of the quasi-spins, namely $a1, a2, a3$.

It can be verified that for an arbitrary, even s the degree of degeneracy is given by [BS 68a]:

$$\iota_s = \binom{\Omega}{s/2} - \binom{\Omega}{s/2-1}, \quad s < N. \quad (6.17)$$

The wave function corresponding to Eq. (6.2) can also be obtained easily using the quasi-spin formalism. For $N = 0$ (a completely empty shell) and $N = 2\Omega$ (a completely full shell), the third component of each of the quasi-spins is $-\frac{1}{2}$ or $+\frac{1}{2}$, respectively. Therefore, the vacuum is the state $S = \frac{1}{2}\Omega$, $S_0 = -\frac{1}{2}\Omega$,

$$|-\rangle = |\frac{1}{2}\Omega, -\frac{1}{2}\Omega\rangle, \quad (6.18)$$

and the full shell is the state $S = \frac{1}{2}\Omega$; $S_0 = \frac{1}{2}\Omega$; $|\Omega/2, \Omega/2\rangle$. If we represent a general quasi-spin state by $|SS_0\rangle$, where $S_0 = \frac{1}{2}(N - \Omega)$, the ground states ($S = \Omega/2$) for different even N can be written as

$$|\frac{1}{2}\Omega, S_0\rangle = |\frac{1}{2}\Omega, \frac{N-\Omega}{2}\rangle \propto S_+^{N/2} |-\rangle. \quad (6.19)$$

The application of the raising operator S_+ (6.3) increases the number of particles by two. The ground states are eigenstates of S^2 , S_0 , and H and are just the products of $n = N/2$ pair states. Therefore, we also say that the ground state is a *pair condensate*.

For odd N -systems, the last particle cannot be paired and one of the quasi-spins will necessarily be zero. The largest possible value of S will therefore be $\frac{1}{2}(\Omega - 1)$ and the ground states are given by:

$$|\frac{\Omega-1}{2}, S_0\rangle \propto S_+^{\frac{1}{2}(N-1)} a_m^+ |-\rangle. \quad (6.20)$$

Since m can take on the 2Ω different values $-j \leq m \leq j$, the ground state of an N -odd system is 2Ω -fold degenerate (in contrast to the nondegenerate ground state of even systems). This is the explanation of why the level density for odd systems close to the ground state is high, whereas for even systems there is always an energy gap.

As we have seen, the seniority 2 states ($S = \frac{1}{2}\Omega - 1$) are the *first excited states* for even N systems. They can also be easily constructed within the quasi-spin formalism.

We first consider the case $N=2$ and construct eigenstates with good angular momentum by applying the operators

$$A_{IM}^+ = \frac{1}{\sqrt{2}} \sum_{m_1 m_2} C_{m_1 m_2 M}^{I \quad J} a_{m_1}^+ a_{m_2}^+ \quad (6.21)$$

on the vacuum

$$|IM\rangle = A_{IM}^+ |-\rangle. \quad (6.22)$$

Since $A_{00}^+ \propto S_+$ [we use BCS phases, Eq. (4.138)], they are eigenstates of the quasi-spin with $S = \Omega/2$ for $I=0$ and with $S = \frac{1}{2}\Omega - 1$ for $I \neq 0$. To see this, we calculate

$$\mathbf{S}^2 |IM\rangle = [\mathbf{S}^2, A_{IM}^+] |-\rangle + \frac{1}{2}\Omega(\frac{1}{2}\Omega + 1) |IM\rangle. \quad (6.23)$$

The first term on the r.h.s. is:

$$\begin{aligned} [\mathbf{S}^2, A_{IM}^+] |-\rangle &= [S_+, S_-, A_{IM}^+] |-\rangle + [S_0^2 - S_0, A_{IM}^+] |-\rangle \\ &= S_+ [S_-, A_{IM}^+] |-\rangle + [S_0^2 - S_0, A_{IM}^+] |-\rangle. \end{aligned} \quad (6.24)$$

Since S_- is proportional to A_{00} , it follows from the orthogonality relations for the Clebsch-Gordon coefficients [Ed 57] that for $I \neq 0$,

$$[S_-, A_{IM}^+] |-\rangle = 0. \quad (6.25)$$

Using (6.8), we finally find for $I \neq 0$:

$$\begin{aligned} \mathbf{S}^2 |IM\rangle &= -\Omega |IM\rangle + \frac{\Omega}{2} \left(\frac{\Omega}{2} + 1 \right) |IM\rangle \\ &= \left(\frac{\Omega}{2} - 1 \right) \frac{\Omega}{2} |IM\rangle. \end{aligned} \quad (6.26)$$

Therefore, the two-particle states (6.22) are, for $I \neq 0$, eigenstates of \mathbf{S}^2 with $S = (\Omega/2) - 1$ or $s = 2$, that is, the two particles are unpaired in the $I \neq 0$ states.

Since the operator S_+ cannot change S and only serves to add two particles, it is easy to construct the first excited states for an even N system with $N > 2$:

$$|\frac{1}{2}\Omega - 1, S_0\rangle \propto S_+^{1(N-2)} A_{IM}^+ |-\rangle. \quad (6.27)$$

Since S_+ is a spherical tensor operator of rank zero, these states have the angular momentum quantum numbers I, M and seniority two for $I \neq 0$.

The states (6.27) are, of course, eigenstates of the Hamiltonian (6.2) with the energy (6.12), and we see that it does not depend on I, M . As we have previously stated, the higher excited states are characterized by the number of unpaired particles, that is, the seniority number s . Such states can be constructed using multiple application of the A_{IM}^+ operators, but the

orthogonality to lower states as well as the construction of states with good angular momentum is then nontrivial.

In many cases, the explicit construction of the wave function, however, is not needed (e.g., many matrix elements can be obtained using angular momentum coupling techniques), which is one of the advantages of the quasi-spin formalism.

Let us calculate, for example, the *matrix elements of the quadrupole operator*:

$$Q_{20} = \sum_{m=-j}^j q_m a_m^+ a_m = \sum_{m>0} q_m s_0^{(m)} \\ q_m = \langle jm | r^2 Y_{20} | jm \rangle. \quad (6.28)$$

From (6.28) we see that \hat{Q}_{20} is a vector in quasi-spin space. This fact implies that the dependence of any quadrupole matrix element on $S_0 = \frac{1}{2}(N - \Omega)$, that is, on the particle number, is given by the Wigner-Eckart theorem [Ed 57]:

$$\langle SS_0 | Q_{20} | S'S_0 \rangle = (-)^{S-S_0} \begin{pmatrix} S & 1 & S' \\ -S_0 & 0 & S_0 \end{pmatrix} \langle S || Q_2 || S' \rangle. \quad (6.29)$$

Since quadrupole transitions go from the ground state with seniority zero to an excited state with $s = 2$ [selection rule given by (6.29)], we get for the quadrupole transition probability

$$|\langle s=2 | Q_{20} | s=0 \rangle|^2 \propto \begin{pmatrix} \Omega/2 & 1 & \Omega/2-1 \\ -S_0 & 0 & S_0 \end{pmatrix}^2 \propto \left(\frac{\Omega}{2} - S_0\right) \left(\frac{\Omega}{2} + S_0\right) \\ - \frac{N}{2} \left(\Omega - \frac{N}{2}\right). \quad (6.30)$$

From (6.30) we see the *collective effect* for transition probabilities which we mentioned in the introduction: It is proportional to the product of the number of particle pairs $N/2$ and the number of hole pairs $(\Omega - N/2)$. The collective effect is therefore most pronounced in the middle of closed shells and due to the aforementioned condensation of pairs in the ground state. This is in agreement with the experimental finding that the quadrupole transition probabilities for nuclei in the middle of closed shells are enhanced with respect to their pure shell model values.

The model we presented in this section is indeed very simple and in reality things will be much more complicated. We will have to consider, for instance, more levels and more realistic forces. Nevertheless, we wish to stress the point that many features of the seniority model remain valid in more realistic cases, and in a certain sense the mathematical and physical transparency of this model reflects reality better than the quite abstract formalism of quasi-particles, which we introduce in the next section, used to handle more complex situations.

6.3 The BCS Model

6.3.1 The Wave Function

The applicability of the seniority model is not limited to j^N configurations. If there exist several almost degenerate j -shells above the closed core, the model can be generalized [Ta 71, 76, LA 74, Lo 75]. Far away from closed shells, however, where nuclei are deformed and the levels more or less uniformly separated, the seniority model breaks down completely.

However, the results of the seniority model show that pairing correlations are very important in nuclei with open shells, and there is no reason to believe that this is no longer true still further from closed shells. In the following we therefore present a method which allows us to treat all the nucleons in the nucleus and which can easily be generalized for different types of interactions. This method no longer provides an exact solution of the eigenvalue problem, but, like the Hartree-Fock method, it can be derived from a variational principle. Therefore, it will be important to make the right ansatz for the ground state wave function. In analogy to Bardeen, Cooper, and Schrieffer [BCS 57], who determined the ground state of a superconductor, we try to represent the wave function for even-even nuclei in the following way.

$$|\text{BCS}\rangle = \prod_{k>0} (u_k + v_k a_k^\dagger a_k^\dagger) |-\rangle, \quad (6.31)$$

where u_k and v_k represent variational parameters. The product runs only over half the configuration space, as indicated by $k>0$. For each state $k>0$ there exists a "conjugate" state $\bar{k}<0$ and the states (k, \bar{k}) generate the whole single-particle space.

The v_k^2 and u_k^2 represent the probability that a certain pair state (k, \bar{k}) is or is not occupied, which has to be determined in such a way that the corresponding energy has a minimum. They are not, however, independent, as the norm of the state (6.31) requires

$$|u_k|^2 + |v_k|^2 = 1. \quad (6.32)$$

Since the BCS wave function is only fixed to within a phase factor, it is always possible to choose the coefficients u_k real and positive. In principle, the phase of v_k has to be determined by the variation of the energy expectation value. It can be shown, however (see Sec. 6.3.4), that for certain reasonable assumptions for the interaction, real positive values v_k yield the deepest energy. The ansatz (6.31) contains the coefficients u_k and v_k only for $k>0$. In the following it is sometimes convenient to also use coefficients $u_{\bar{k}} := u_k$ and $v_{\bar{k}} := -v_k$ for the values $\bar{k}<0$.

In many cases, especially if the Hamiltonian is invariant under time reversal, the conjugate state can be chosen as the time-reversed state [Me 61 Ch. XVI]:

$$|\bar{k}\rangle = T|k\rangle. \quad (6.33)$$

An example is a spherical basis [in BCS phases, Eq. (4.138)]:

$$|k\rangle = |nljm\rangle, \quad |\bar{k}\rangle = |nlj-m\rangle, \quad m > 0. \quad (6.34)$$

The following formulae, however, apply also for cases of Hamiltonians without time reversal symmetry (see Sect. 7.7).

At this point in the discussion, the *variational ansatz* (6.31) for the wave function seems rather arbitrary. It will become clear in the next chapter that it emerges quite naturally by a slight modification of the Hartree-Fock ansatz. Let us simply make the observation that the particles appear in mutually conjugate pairs similar to the ground state (6.19) of the seniority model, but with the important difference that $|\text{BCS}\rangle$ is a superposition of different numbers of pairs, that is, (6.31) no longer has a sharp particle number. This is actually a great disadvantage of (6.31) in nuclear physics.

The product can be written as

$$|\text{BCS}\rangle \propto |-> + \sum_{k>0} \frac{v_k}{u_k} a_k^+ a_k^+ |-> + \frac{1}{2} \sum_{kk'>0} \frac{v_k v_{k'}}{u_k u_{k'}} a_k^+ a_{k'}^+ a_{k'}^+ a_k^+ |-> + \dots \quad (6.35)$$

In solid state physics, where $N \approx 10^{23}$, the violation of particle number has no influence on any physical quantity. In nuclei, however, the violation of the invariance corresponding to the particle number in many cases gives rise to serious errors. One then has to use improved methods to deal with such problems (PBCS, FBCS; see Sec. 11.4.3).

To give an impression of the flexibility of the ansatz (6.31), we rewrite it in a different way: It can be expressed by a *generalized pair creation operator* (6.3)

$$A^+ = \sum_{k>0} \frac{v_k}{u_k} a_k^+ a_{\bar{k}}^+ \quad (6.36)$$

as

$$|\text{BCS}\rangle \propto \exp(A^+)|-> = \sum_{\nu=0}^{\infty} \frac{1}{\nu!} (A^+)^{\nu} |->. \quad (6.37)$$

The component having the particle number N is therefore $(A^+)^{N/2}$. This corresponds to the seniority zero state ($s=0$) of Eq. (6.19); in fact, this component is exactly the ground state wave function of the seniority model, since in this case all v_k 's and u_k 's are equal, as we shall see later on. In that sense, the BCS-ansatz contains the $s=0$ state of independent pairs, that is, it is a condensate of bound pairs (boson-like entities; see Chap. 9), which are in the same quantum state ($I=0$, $T=1$). In infinite matter this leads to a Bose-Einstein condensation of the pairs (superconductivity). In finite systems like nuclei there exists no real phase transition. Nevertheless, it can come quite close to it and in any case (6.37) should be a good ansatz.

6.3.2 The BCS Equations

We assume that a many-body system is described by the Hamiltonian

$$H = \sum_{k_1, k_2 \leq 0} t_{k_1 k_2} a_{k_1}^+ a_{k_2} + \frac{1}{4} \sum_{\substack{k_1, k_2, k_3, k_4 \\ \leq 0}} \bar{v}_{k_1 k_2 k_3 k_4} a_{k_1}^+ a_{k_2}^+ a_{k_3} a_{k_4}. \quad (6.38)$$

The parameters u and v of the trial wave function (6.31) are determined by variation of the energy. However, this variation is *restricted* by the subsidiary condition that the expectation value of the particle number has the desired value N

$$\langle \text{BCS} | \hat{N} | \text{BCS} \rangle = 2 \sum_{k > 0} v_k^2 = N. \quad (6.39)$$

This can be achieved by adding the term $-\lambda \hat{N}$ to the variational Hamiltonian

$$H' = H - \lambda \hat{N}. \quad (6.40)$$

The *Lagrange multiplier* λ is fixed by the condition (6.39). It is called the *chemical potential* or the *Fermi energy* because it represents the increase of the energy $E = \langle \text{BCS} | H | \text{BCS} \rangle$ for a change in the particle number

$$\lambda = \frac{dE}{dN}. \quad (6.41)$$

To see this, we use the fact that the expectation value of H' is a minimum with respect to an arbitrary variation of the BCS wave function (6.31). One special variation is a change of the parameter λ . Therefore, we get [see also Eq. (3.81)]

$$\frac{d}{d\lambda'} \{ \langle \text{BCS}(\lambda') | H | \text{BCS}(\lambda') \rangle - \lambda \langle \text{BCS}(\lambda') | \hat{N} | \text{BCS}(\lambda') \rangle \}_{\lambda=\lambda'} = 0 \quad (6.42)$$

or

$$\frac{dE}{d\lambda} = \lambda \frac{dN}{d\lambda}. \quad (6.43)$$

In the following we will always use H' instead of H . For the calculation of actual energy, however, we have to remember that we have to add the term λN at the end.

Another interesting quantity in this connection is the particle-number uncertainty

$$(\Delta N)^2 := \langle \text{BCS} | \hat{N}^2 | \text{BCS} \rangle - N^2 = 4 \sum_{k > 0} u_k^2 v_k^2. \quad (6.44)$$

which we will discuss later on.

From (6.31) and (6.38), we gain for the BCS expectation value of H' :

$$\begin{aligned} \langle \text{BCS} | H' | \text{BCS} \rangle = & \sum_{k \geq 0} \left\{ (t_{kk} - \lambda) v_k^2 + \frac{1}{2} \sum_{k' \geq 0} \bar{v}_{kk'kk'} v_k^2 v_{k'}^2 \right\} \\ & + \sum_{kk' > 0} \bar{v}_{kk'kk'} u_k v_k u_{k'} v_{k'}. \end{aligned} \quad (6.45)$$

Since the BCS wave function is completely determined by the parameters v_k and the condition (6.32), the variation

$$\delta\langle\text{BCS}|H'|\text{BCS}\rangle=0 \quad (6.46)$$

yields

$$\left(\frac{\partial}{\partial v_k} + \frac{\partial u_k}{\partial v_k} \frac{\partial}{\partial u_k} \right) \langle\text{BCS}|H'|\text{BCS}\rangle = 0. \quad (6.47)$$

After differentiating, we finally obtain the set of BCS equations

$$2\tilde{\epsilon}_k u_k v_k + \Delta_k (v_k^2 - u_k^2) = 0, \quad k > 0, \quad (6.48)$$

with

$$\tilde{\epsilon}_k = \frac{1}{2} \left(I_{kk} + I_{\bar{k}\bar{k}} + \sum_{k' \geq 0} (\bar{v}_{kk'kk'} + \bar{v}_{\bar{k}\bar{k}\bar{k}\bar{k}}) v_{k'}^2 \right) - \lambda \quad (6.49)$$

and the gap parameters (for real matrix elements)

$$\Delta_k = - \sum_{k' > 0} \bar{v}_{kk'k'k} u_{k'} v_{k'}. \quad (6.50)$$

For fixed values $\tilde{\epsilon}_k$ and Δ_k , (6.32) and (6.48) yield two quadratic equations for u_k^2 and v_k^2 , respectively, having the solutions

$$\begin{aligned} v_k^2 &= \frac{1}{2} \left[1 \pm \frac{\tilde{\epsilon}_k}{\sqrt{\tilde{\epsilon}_k^2 + \Delta_k^2}} \right] \\ u_k^2 &= \frac{1}{2} \left[1 \pm \frac{\tilde{\epsilon}_k}{\sqrt{\tilde{\epsilon}_k^2 + \Delta_k^2}} \right]. \end{aligned} \quad (6.51)$$

In the case of no interaction one has $\Delta = 0$ and $v_k^2 = 1$, $u_k^2 = 0$ for occupied orbits ($\tilde{\epsilon} < 0$). The only possible solutions of (6.51) are therefore:

$$\begin{aligned} v_k^2 &= \frac{1}{2} \left[1 - \frac{\tilde{\epsilon}_k}{\sqrt{\tilde{\epsilon}_k^2 + \Delta_k^2}} \right], \\ u_k^2 &= \frac{1}{2} \left[1 + \frac{\tilde{\epsilon}_k}{\sqrt{\tilde{\epsilon}_k^2 + \Delta_k^2}} \right]. \end{aligned} \quad (6.52)$$

Thus the variational principle (6.46) yields the set of equations (6.49), (6.50), and (6.52). Together with the *particle-number condition*

$$2 \sum_{k > 0} v_k^2 = N \quad (6.53)$$

they allow calculation of the BCS parameters u_k, v_k . In general, these equations are nonlinear and have to be solved by iteration.

For discussion of the properties of these equations it is often useful to

insert (6.52) into (6.50) and obtain the so-called *gap equation*:

$$\Delta_k = -\frac{1}{2} \sum_{k' > 0} \bar{v}_{kk'k'} \cdot \frac{\Delta_{k'}}{\sqrt{\epsilon_{k'}^2 + \Delta_{k'}^2}}. \quad (6.54)$$

6.3.3 The Special Case of a Pure Pairing Force

As we have seen in Section 6.2, the pure pairing force provides a very simple and powerful model for the description of pairing properties in nuclei. It is therefore widely used in the BCS description of nuclei. In the following, we therefore present the most important formulae of this theory for this special case.

The Hamiltonian here has the form,

$$H = \sum_{k > 0} \epsilon_k (a_k^\dagger a_k + a_k^\dagger a_k) - G \sum_{kk' > 0} a_k^\dagger a_{k'}^\dagger a_{k'} a_k. \quad (6.55)$$

The expectation value of H' [Eq. (6.45)] is

$$\langle \text{BCS} | H' | \text{BCS} \rangle = 2 \sum_{k > 0} \left(\tilde{\epsilon}_k v_k^2 + \frac{1}{2} G v_k^4 \right) - \frac{\Delta^2}{G}. \quad (6.56)$$

In this case the gap parameter Δ does not depend on k :

$$\Delta = G \sum_{k > 0} u_k v_k. \quad (6.57)$$

$\tilde{\epsilon}_k$ is given by

$$\tilde{\epsilon}_k = \epsilon_k - \lambda - G \cdot v_k^2. \quad (6.58)$$

The term Gv_k^2 in (6.56) and Gv_k^2 in (6.58) is often neglected, because it is not very important and its only effect is a renormalization of the single-particle energies. These are, in fact, influenced far more by particle-hole correlations, which are in any case not described in the proper way by the pairing force. In this case we have

$$\left. \begin{array}{l} u_k^2 \\ v_k^2 \end{array} \right\} = \frac{1}{2} \left[1 \pm \frac{\epsilon_k - \lambda}{\sqrt{(\epsilon_k - \lambda)^2 + \Delta^2}} \right]. \quad (6.59)$$

The $v_k^2 = \langle \text{BCS} | a_k^\dagger a_k | \text{BCS} \rangle$ are the *occupation probabilities* for the different single-particle states.

Again, from (6.59) we see that in the limit $G \rightarrow 0$, that is, $\Delta \rightarrow 0$, the $v_k^2 = 1$ for occupied levels and $v_k^2 = 0$ for unoccupied ones. In this case, v_k^2 is a step function (Fig. 6.5), whereas in the interacting case ($\Delta \neq 0$) the step function is somewhat smeared out. Due to the interaction, particles are scattered from below to above the Fermi surface. This yields a partial depletion of the states below and a partial filling of the states above the Fermi level

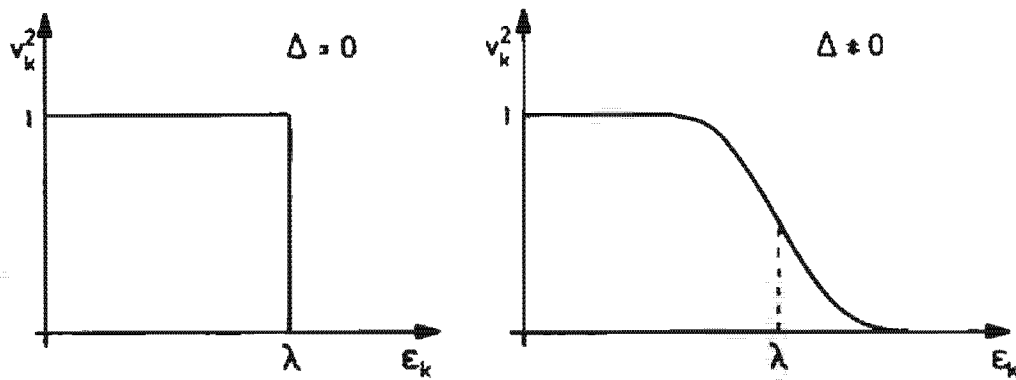


Figure 6.5. The occupation probabilities v_k^2 in the noninteracting case ($\Delta = 0$) and in the interacting case ($\Delta \neq 0$).

(Fig. 6.5). The *gap equation* (6.54) takes the simple form

$$\Delta = \frac{G}{2} \sum_{k>0} \frac{\Delta}{\sqrt{(\epsilon_k - \lambda)^2 + \Delta^2}}. \quad (6.60)$$

In the special case of a single j -shell, all ϵ_k are equal. From (6.58), (6.59), and (6.52) we see that in this case (even taking into account the term $G \cdot v^2$) all v_k^2 are equal. From the particle-number condition (6.39), we find

$$v_k = \sqrt{\frac{N}{2\Omega}}, \quad u_k = \sqrt{1 - \frac{N}{2\Omega}}. \quad (6.61)$$

The corresponding energy is ($\epsilon_k = 0$):

$$E_{\text{BCS}}^{(N)} = -\frac{1}{2} G \cdot N \cdot \Omega \left(1 - \frac{N}{2\Omega} + \frac{N}{2\Omega^2} \right). \quad (6.62)$$

This expression agrees for large N up to order $1/\Omega$ with the exact formula of Eq. (6.15). Therefore, we see that the BCS ansatz is a good approximation, well suited to treat the nuclear pairing correlations.

The uncertainty in the particle number can also be obtained according to (6.44) and (6.61):

$$\frac{\Delta N}{N} = \frac{1}{\sqrt{N}} \sqrt{2 - \frac{N}{\Omega}}. \quad (6.63)$$

The gap in this model is given using (6.57) and (6.61) as

$$\Delta = G \cdot \sqrt{\frac{N}{2} \left(\Omega - \frac{N}{2} \right)}. \quad (6.64)$$

The gap thus has a parabolic dependence on the number of particles in the shell and is zero for empty or filled shells. For $N = \Omega$, (half-filled shells), we find

$$2\Delta = G \cdot \Omega. \quad (6.65)$$

As we will see later (Sect. 6.3.4), it is not by accident that 2Δ is equal to the excitation energy (6.14) of the first excited state and it will become clear why Δ is called the (energy) gap.

6.3.4 Bogoliubov Quasi-particles—Excited States and Blocking

The main advantage of writing the ground state in the form (6.31) or (6.35) is that despite being very similar to the exact ground state of the seniority model (condensate of pairs), and therefore containing correlations between pairs of particles, $|\text{BCS}\rangle$ can at the same time be written as a product state of a new type of fermions: the *Bogoliubov quasi-particles*. The concept of quasi-particles as a general concept in many-body physics will be discussed in Chapter 7. In fact, it is easily verified that

$$|\text{BCS}\rangle \propto \prod_{k \geq 0} |\alpha_k|^{-1} \quad (6.66)$$

with

$$\begin{aligned} \alpha_k^+ &= u_k a_k^+ - v_k a_k^- \\ \alpha_k^- &= u_k a_k^+ + v_k a_k^- \end{aligned} \quad (6.67)$$

and the following fermion commutation relations hold:

$$\{\alpha_k, \alpha_{k'}\} = 0; \quad \{\alpha_k, \alpha_{k'}^+\} = \delta_{kk'}, \quad (6.68)$$

where we have used (6.34) and the usual phase convention

$$u_k = u_k > 0; \quad v_k = -v_k < 0; \quad k > 0. \quad (6.69)$$

The ansatz (6.67) for quasi-particles is very similar to the ansatz for HF-quasi-particles in the Lipkin model (5.50) and we could therefore have used the same techniques for their solution. In the latter case, we can show that real coefficients ($\varphi = 0$) give the lowest energy. The same is also possible here if the force has only matrix elements $\bar{v}_{kk'k'k} < 0$. Since this condition is very reasonable, we shall use only real coefficients u_k and v_k .

From Eqs. (6.67) and (6.52) we see that a quasi-particle has some properties of a bare particle and some of a bare hole: Above the Fermi surface (α_k^2 small) it is nearly a particle, while below the Fermi surface (u_k^2 small) it is nearly a hole.

We see from Eq. (6.67) that by using this very useful trick of a linear "Bogoliubov" transformation we have achieved a representation of the ground state of pairwise interacting particles in terms of a gas of non-interacting quasi-particles. This is, of course, in many practical cases a very helpful feature. The price we have to pay is that the transformation (6.67) clearly does not conserve particle number because we mix creation and annihilation operators. If we assume that not only the ground state is well

represented by a product state of quasi-particles, but also *excited states*, then the Hamiltonian H_{φ} , which corresponds to this gas of non-interacting gas of quasi-particles, is given by

$$H_{\varphi} = \langle \text{BCS} | H' | \text{BCS} \rangle + \sum_{k \geq 0} E_k \alpha_k^+ \alpha_k, \quad (6.70)$$

where the constant $\langle H' \rangle$ takes account of the fact that we have

$$\alpha_k | \text{BCS} \rangle = 0 \quad \text{for all } k \geq 0, \quad (6.71)$$

therefore H_{φ} has the right ground state expectation value. The quasi-particle energies E_k are a straightforward generalization of the definition of those for real particles (for details of the calculations see Chap. 7)

$$\begin{aligned} E_k &= \langle \text{BCS} | \alpha_k H' \alpha_k^+ | \text{BCS} \rangle - \langle \text{BCS} | H' | \text{BCS} \rangle \\ &= \sqrt{\epsilon_k^2 + \Delta_k^2}. \end{aligned} \quad (6.72)$$

The one-quasi-particle states

$$\alpha_{k_1}^+ | \text{BCS} \rangle = a_{k_1}^+ \prod_{k \neq k_1} (u_k + v_k a_k^+ a_k^+) | - \rangle, \quad (6.73)$$

$$\alpha_{k_1}^+ | \text{BCS} \rangle = a_{k_1}^+ \prod_{k \neq k_1} (u_k + v_k a_k^+ a_k^+) | - \rangle \quad (6.74)$$

obviously have the energy $\langle H' \rangle + E_k$. They are a superposition of states with odd particle number and describe a nucleus with an odd number of nucleons. According to the quantum number k , this state can be either the ground state or an excited state.

The two-quasi-particle states

$$\alpha_{k_1}^+ \alpha_{k_2}^+ | \text{BCS} \rangle = a_{k_1}^+ a_{k_2}^+ \prod_{k \neq k_1, k_2} (u_k + v_k a_k^+ a_k^+) | - \rangle, \quad k_2 \neq \bar{k}_1, \quad (6.75)$$

$$\alpha_{k_1}^+ \alpha_{\bar{k}_1}^+ | \text{BCS} \rangle = (-v_{k_1} + u_{k_1} a_{k_1}^+ a_{\bar{k}_1}^+) \prod_{k \neq k_1} (u_k + v_k a_k^+ a_k^+) | - \rangle, \quad k_2 = \bar{k}_1,$$

have the energy $\langle H' \rangle + E_{k_1} + E_{k_2}$. They describe excited states in the even system. In this case one pair is broken and the excitation energy is

$$E_{k_1} + E_{k_2} > 2\Delta. \quad (6.76)$$

The first excited state in the even system thus lies at least 2Δ higher than the ground state.

In the special case of a single j-shell, the excitation energy is given by

$$E_k + E_{\bar{k}} = 2\sqrt{\epsilon_k^2 + \Delta^2}. \quad (6.77)$$

With (6.58), (6.41), and (6.62) we find ($\epsilon_k = 0$)

$$\tilde{\epsilon} = G \frac{\Omega - N}{2}, \quad (6.78)$$

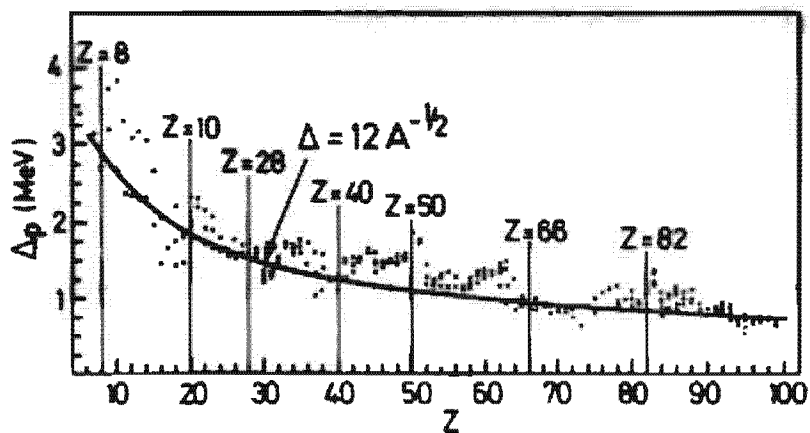


Figure 6.6. Dependence of the proton gap on the proton number. (From [BM 69].)

which, together with (6.64), gives

$$E_k + E_{k'} = G \cdot \Omega, \quad (6.79)$$

in accordance with the result (6.14) of the seniority model. From (6.78) we see that only in the middle of the shell is the excitation energy 2Δ .

In the odd system with the ground state k_0 ($\tilde{\epsilon}_{k_0} \approx 0$), the excitation energy is

$$E_k - E_{k_0} = \sqrt{\tilde{\epsilon}_k^2 + \Delta^2} - \Delta. \quad (6.80)$$

For small excitation energy ($\tilde{\epsilon}_k \ll \Delta$) we therefore find a high level density in these odd systems.

We also can explain the odd-even mass difference by the following consideration: The ground state energies E_N^{GS} are given for any N by

$$E_{N+2}^{GS} = E_N^{GS} + 2\lambda; \quad E_{N+1}^{GS} = E_N^{GS} + \lambda + E_{k_0},$$

and therefore the odd-even mass difference is given by:

$$\frac{1}{2} (E_{N+2}^{GS} - E_{N+1}^{GS} - (E_{N+1}^{GS} - E_N^{GS})) = -E_{k_0} \approx -\Delta. \quad (6.81)$$

Equation (6.81) is often exploited to determine the gap empirically from the measured binding energies. It has been found that on the average the gap follows the relation $\Delta = 12 \cdot A^{-1/2}$ as a function of nucleon number A [NA 62, ZGS 67] (Fig. 6.6).

The above considerations give a qualitative understanding of the structure of many states in superfluid nuclei. There remain, however, a few important points to take into account in a more detailed investigation:

- (I) The Chemical Potential. As we have seen in (6.53), the chemical potential λ is determined in such a way that the average particle number in the BCS ground state has the correct value. With the same λ , we find for a

one-quasi-particle state $|k\rangle = \alpha_k^+ |BCS\rangle$

$$\langle k|\hat{N}|k\rangle = N + u_k^2 - v_k^2. \quad (6.82)$$

This is $N \pm 1$ only for levels k which are far away from the Fermi surface. For the levels in the vicinity of the Fermi surface the average particle number is wrong. Since the energy depends strongly on the average particle number, one should readjust the chemical potential λ for the different levels in odd nuclei and also for the excited levels in even nuclei. As long as we have not done this, we should use the operator $H' = H - \lambda \hat{N}$ instead of H for the calculation of excitation energies (as we have done so far). This can, for instance, be seen if we correct for the wrong particle number in the state $|k\rangle$ of Eq. (6.82):

$$\begin{aligned} E_{N+1}^k &= \langle k|H|k\rangle + \frac{dE}{dN}(N+1 - \langle k|\hat{N}|k\rangle) \\ &= \langle k|H - \lambda \hat{N}|k\rangle + \lambda(N+1) \\ &= E_N^{GS} + \lambda + E_k. \end{aligned}$$

(II) The Blocking Effect. The occupation probabilities v_k^2 of the BCS ground state [Eq. (6.52)] were determined by the variational principle. The ground state of an odd system is described by the wave function

$$\alpha_{k_1}^+ |BCS\rangle = a_{k_1}^+ \prod_{k \neq k_1} (u_k + v_k a_k^+ a_k^+) |-\rangle. \quad (6.83)$$

The unpaired particle sits in the level k_1 , and blocks this level. The Pauli principle prevents this level from participating in the scattering process of nucleons caused by the pairing correlations. The level k_1 always stays occupied and the level \bar{k} always stays empty. Only for $k \neq k_1$ do we have $v_k^2 = v_{\bar{k}}^2$ (Fig. 6.7). Using the blocked wave function (6.83) as a trial wave function in the variational principle, we find the same equations for v_k^2 as before. The only difference is that in the calculation of the gap one level is

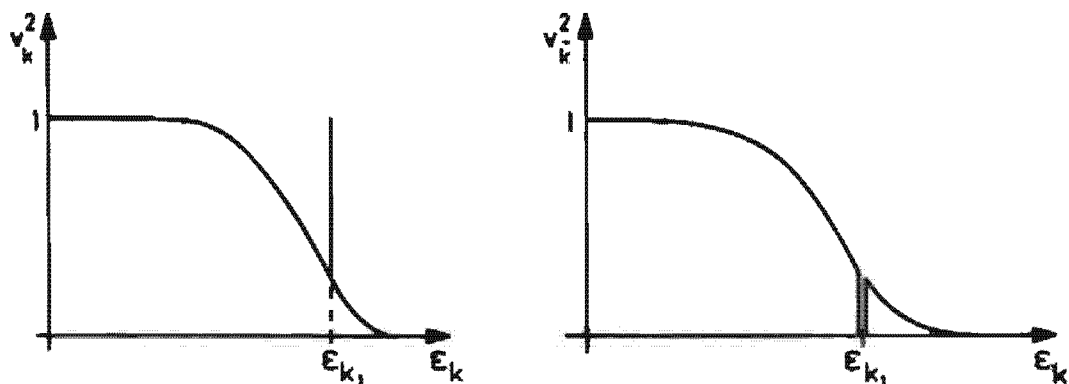


Figure 6.7. Blocking of the state k_1 .

"blocked":

$$\Delta = G \sum_{k \neq k_1} u_k v_k. \quad (6.84)$$

The level k_1 has to be excluded from the sum because it cannot contribute to the pairing energy. The chemical potential is determined by

$$N = 1 + 2 \sum_{k \neq k_1} v_k^2. \quad (6.85)$$

Similar equations hold for the case of a higher number of blocked levels, as in the case of two-quasi-particle states.

The change in Δ and in the u_k s and v_k s is called the blocking effect. These blocking correlations are of the order Ω^{-1} and can often be neglected. However, as pointed out by Soloviev [So 61, Wa 62b] and Nilsson and Prior [NP 61], the correction may be large in some cases. This can happen particularly for deformed nuclei where, although there may be 20 levels in the spectrum, only 4 or 5 contribute appreciably to the sum of Eq. (6.50). Clearly the blocking of one or two such levels in such a case has a big effect so that one cannot simply equate the excitation energies to quasi-particle energies, but must evaluate the total energy of the excited state and subtract it from the vacuum energy. For two-quasi-particle states the corrected energy (≈ 1.4 MeV) is always smaller than the quasi-particle energy (≈ 1.7 MeV), but much larger than the free-particle energy (≈ 0.15 MeV). One problem that arises in this corrected theory, in which the v_k can be appreciably different in the ground state and the excited states, is that these states are no longer automatically orthogonal, although sometimes a different quantum number, such as the spin or the parity, guarantees the orthogonality. In particular, two-quasi-particle states of spin 0^+ are not orthogonal to the ground state in such cases.

6.3.5 Discussion of the Gap Equation

For all practical cases, the BCS-equations have to be solved on a computer and the question arises of how many levels one should include for such calculations, that is, we have to investigate which states contribute most to the sum appearing in the gap equation (6.54). For this purpose, let us first consider the gap Δ_k for a state close to the Fermi level. In this case the main contributions to the sum come from states in the vicinity of the Fermi level. The reason for this is that (i) in this case the expression $\Delta_{k'}/(\tilde{\epsilon}_k^2 + \Delta_k^2)^{1/2} \approx 1$ ($\tilde{\epsilon}_k \approx 0$), and (ii) the matrix elements $v_{kk'k''}$ for $k' \approx k$ (strongly overlapping wave functions) are larger than the other matrix elements.

Conversely, if k is far from the Fermi surface, all the terms in the sum of Eq. (6.54) are small. For $k' \approx k$, the overlap of the wave functions is still large, but the factor $\Delta_{k'}/(\tilde{\epsilon}_k^2 + \Delta_k^2)^{1/2}$ is now small because of $\tilde{\epsilon}_k^2 \gg \Delta_k^2$. For

states k' at the Fermi surface it is just the other way around, since there the matrix elements are very small (k and k' usually belonging to different principal quantum numbers).

The effect of the pairing force is therefore restricted to the neighborhood of the Fermi surface, that is, only there is Δ_k different from zero. We may now understand why it might be a valid approximation to take a constant pairing force in the vicinity of the Fermi surface and have zero matrix elements elsewhere. On the other hand, if we had taken a constant matrix element over the whole configuration space, the gap would have diverged.

For spherical, only weakly deformed nuclei the single-particle levels exhibit a pronounced shell structure. The main contribution to the sum in the gap equation comes from transitions within the same shell. We can therefore more or less treat each shell separately. From our discussion above we expect for inner shells $\Delta_k \approx 0$. The pairing force will therefore only be effective in the partially filled shell, which is often called the Λ -shell. This leads back to the seniority model. For strongly deformed nuclei the shell structure is completely washed out, nevertheless, the sum only runs over a group of levels in the neighborhood of the Fermi surface, also called the Λ -shell.

The restriction of the pairing to the vicinity of the Fermi level is also the reason that neutrons and protons can be treated separately (at least for heavy nuclei). For nuclei with $A \sim 150$, the neutron excess is $(N - Z) > 20$. The neutron and proton levels close to the Fermi energy, therefore, have very small overlap compared to that of protons or neutrons alone. Therefore, neglecting the proton-neutron pairing, the total wave function may be represented as a product of the proton and neutron functions:

$$|\text{BCS}\rangle = \prod_{k_1 > 0} (u_{k_1}^{(P)} + v_{k_1}^{(P)} a_{k_1}^{(P)} + a_{k_1}^{(P)\dagger}) \prod_{k_2 > 0} (u_{k_2}^{(n)} + v_{k_2}^{(n)} a_{k_2}^{(n)} + a_{k_2}^{(n)\dagger}) |-\rangle. \quad (6.86)$$

In spite of these simplifying assumptions, the BCS equations can only be solved numerically. In order to study the influence of the interaction between pairs of nucleons in a qualitative manner we restrict ourselves to a pure pairing force (6.55) within the Λ -shell. In the following considerations, we therefore neglect the other shells. The gap equation is then of the form

$$\Delta = \frac{1}{2} G \sum_{k > 0}^{\Lambda} \frac{\Delta}{\sqrt{\epsilon_k^2 + \Delta^2}}, \quad (6.87)$$

where the sum runs over the Λ -shell only. Equation (6.87) always has the trivial solution $\Delta = 0$, that is, $u_k \cdot v_k = 0$, which for no or sufficiently weak pairing force is the only solution. However, for

$$\frac{1}{2} G \sum_{k > 0}^{\Lambda} \frac{1}{|\tilde{\epsilon}_k|} > 1 \quad (6.88)$$

there exists a second nontrivial solution $\Delta > 0$. This always happens if the pairing force is sufficiently strong or if the Λ -shell is sufficiently large. However, this sharp transition is a consequence of particle number violation and it is somewhat smeared out in a more extended theory [MPR 65]. For an infinite system, particle number violation is negligible, and the transition is always sharp.

On the other hand, (6.87) can also be used to determine the strength G of the pairing force since, and, as we have already said, Δ can be determined empirically from the odd-even effect. It still, however, depends on the "cutoff" Λ .

6.3.6 Schematic Solution of the Gap Equation

It is very instructive to have an *analytic solution* of the gap equation [Be 59]. This can only be achieved in a very schematic model. We image a well deformed nucleus for which the level density is almost uniform and the average level spacing $\Delta\epsilon$ is very small compared with Δ (for deformed nuclei in the rare earth region $\Delta \approx 1$ MeV and $\Delta\epsilon \approx 0.1-0.2$ MeV). We can then replace the sum in Eq. (6.87) approximatively by an integration over the Λ shell: $\epsilon' < \epsilon < \epsilon''$; $a = \epsilon' - \lambda$; $b = \epsilon'' - \lambda$,

$$1 - \frac{1}{2} G \int_a^b \frac{1}{\sqrt{\epsilon^2 + \Delta^2}} \rho(\epsilon) d\epsilon, \quad (6.89)$$

where $\rho(\epsilon)$ is the level density. We furthermore assume that $\rho(\epsilon)$ is approximately constant within the Λ -Shell ($\rho \approx \bar{\rho}$). We introduce the dimensionless quantity

$$\eta = \frac{1}{\bar{\rho}G} \quad (6.90)$$

and obtain after integration

$$2\eta = \operatorname{arsinh} \frac{b}{\Delta} - \operatorname{arsinh} \frac{a}{\Delta}. \quad (6.91)$$

Solving for Δ yields

$$\Delta = \frac{1}{\sinh 2\eta} \sqrt{b^2 + a^2 - 2ab \cosh 2\eta}. \quad (6.92)$$

The average particle number in the BCS model is given by Eq. (6.39) and determines the chemical potential λ . The number of particles in the Λ shell is given by (again we replace the sum in (6.39) by an integral):

$$N = 2 \int_a^b \frac{1}{2} \left(1 - \frac{\epsilon}{\sqrt{\epsilon^2 + \Delta^2}} \right) \bar{\rho} d\epsilon. \quad (6.93)$$

The number of levels in the Λ -shell is given by

$$\Omega = \bar{\rho}(b - a). \quad (6.94)$$

Introducing the occupation factor

$$\chi_N = 1 - \frac{N}{\Omega}, \quad (6.95)$$

we get, after a lengthy but straightforward calculation using (6.92),

$$\lambda = \frac{\epsilon' + \epsilon''}{2} - \frac{\epsilon'' - \epsilon'}{2} \chi_N \cdot \operatorname{ctgh} \eta. \quad (6.96)$$

Inserting (6.96) in (6.92), we get:

$$\Delta = \frac{\epsilon'' - \epsilon'}{2 \sinh \eta} \sqrt{1 - \chi_N^2}. \quad (6.97)$$

In the limit of weak coupling, that is, for $G \cdot \bar{\rho} \ll 1$, we find:

$$\Delta \propto e^{-(1/\rho G)}. \quad (6.98)$$

We therefore have from (6.98) the important result that the gap cannot be developed as a power series in the interaction strength.

Equation (6.97) has been derived under the condition that Δ is not smaller than the level distance, that is,

$$\Delta \cdot \bar{\rho} > 1 \quad (6.99)$$

or

$$\frac{1}{2 \sinh \eta} \sqrt{N(2\Omega - N)} > 1. \quad (6.100)$$

For $\eta \ll 1$ (strong pairing correlations), this inequality is always fulfilled. For $\eta \gg 1$, Eq. (6.100) is only satisfied for large enough values of $N(2\Omega - N)$.

The ground state energy in the BCS-theory is given by (6.56). Its contribution to the ground state expectation value of H' is

$$\langle \text{BCS} | H' | \text{BCS} \rangle = 2 \int_a^b \frac{1}{2} \left(1 - \frac{\epsilon}{\sqrt{\epsilon^2 + \Delta^2}} \right) \epsilon \bar{\rho} d\epsilon - \frac{\Delta^2}{G}. \quad (6.101)$$

Since H' differs from H by $\lambda \cdot N$, using (6.96) and performing the integral in (6.101) we get for the ground state energy:

$$E_{\text{BCS}} = \langle \text{BCS} | H | \text{BCS} \rangle = \frac{1}{2} (\epsilon' + \epsilon'') N - \frac{1}{4} \Omega (\epsilon'' - \epsilon') (1 - \chi_N^2) \operatorname{ctgh} \eta. \quad (6.102)$$

We are interested in that part of the ground state energy which comes from the pairing force alone. For this purpose, we first calculate the energy for $G = 0$ which corresponds to the limit $\eta \rightarrow \infty$:

$$E^0 = \frac{1}{2} (\epsilon' + \epsilon'') \cdot N - \frac{1}{4} \Omega (\epsilon'' - \epsilon') (1 - \chi_N^2). \quad (6.103)$$

The contribution E^P of the pairing force to the ground state energy is therefore given by:

$$E^P = E_{\text{BCS}} - E^0. \quad (6.104)$$

In the case of a half-filled shell where $N = \Omega$, we find, using Eqs. (6.102),

(6.103), (6.94), and (6.97),

$$E^P = -\frac{1}{4}\Omega(\epsilon'' - \epsilon)(1 - \chi_N^2)(\operatorname{ctgh} \eta - 1) = -\frac{1}{2}\Delta^2 \bar{\rho}(1 - e^{-2\eta}). \quad (6.105)$$

This is the *pairing energy* for neutrons or protons. For heavy nuclei it is possible to estimate G and Δ from the odd-even effect. Nilsson and Prior [NP 61] found for protons $G_p \approx 17/A$ MeV and for neutrons $G_n \approx 25/A$ MeV. The energy gap Δ is roughly 1 MeV. Assuming a characteristic level density $1/\bar{\rho} \approx 0.5$ MeV, we get $\eta \approx A/100$. In this case we can neglect the term $e^{-2\eta}$ in (6.105) and obtain for the total pairing energy, which is more or less the same for protons and neutrons,

$$E_{\text{total}}^P = E_{(p)}^P + E_{(n)}^P \approx -\bar{\rho}\Delta^2 \approx -2[\text{MeV}]. \quad (6.106)$$

The total pairing energy is therefore extremely small compared to the total binding energy. This is a general feature of all kinds of correlation energies, which does not mean, however, that they cannot play a decisive role in the explanation of many problems.

As we have seen, the BCS wave function represents a state which is not an eigenstate of the particle number operator. The whole theory is only valid if $|\text{BCS}\rangle$ is well localized around the actual particle number. In order to get an estimate, we therefore calculate the *mean square deviation of the particle number* (6.44):

$$(\Delta N)^2 = \sum_{k>0} \frac{\Delta_k^2}{\tilde{\epsilon}_k^2 + \Delta_k^2}. \quad (6.107)$$

Within the schematic model it follows that

$$(\Delta N)^2 = \bar{\rho}\Delta \left(\operatorname{arc tan} \frac{b}{\Delta} - \operatorname{arc tan} \frac{a}{\Delta} \right). \quad (6.108)$$

In the limit of weak pairing correlations or small level density we get

$$(\Delta N)^2 = \bar{\rho} \cdot \Delta \cdot \pi. \quad (6.109)$$

This approximation is roughly fulfilled for strongly deformed nuclei. Taking characteristic values for $\bar{\rho}$ and G , we obtain $\eta \approx 4, \dots, 5$ and for the mean deviation $\Delta N \approx \sqrt{6}$.

In the other limit of strong pairing ($\eta \ll 1$), we take only the leading terms of (6.108) with respect to η :

$$(\Delta N)^2 = \Omega(1 - \chi_N^2) = 2N \left(1 - \frac{N}{2\Omega} \right). \quad (6.110)$$

Consequently, for a half-filled shell ($N = \Omega$) one finds $\Delta N = \sqrt{N}$, whereas for only one pair ($N = 2$) we obtain $\Delta N \approx 2$. A typical example for a half-filled shell with $\eta \ll 1$ is ^{202}Pb . Its BCS wave function contains large amounts of ^{204}Pb and ^{200}Pb and also of ^{206}Pb and ^{198}Pb . We have to keep in mind, however, that the Fermi surfaces λ and the gap Δ are quite the same for all these nuclei, and therefore the uncertainty in the particle number is not as bad as it appears.

As we have seen, the very simple BCS model allows us to explain many features in nuclei arising from the short-range correlations of nucleons. We have only treated the pairing of neutrons and protons separately, neglecting the neutron-proton interaction. For heavy nuclei this was valid because the proton and neutron wave functions usually belong to different principal quantum numbers and the pairing matrix elements are small. For light nuclei ($s-d$ shell!), however, this is no longer true, and we also have to include neutron-proton pairing. Before we mention very briefly some of those calculations, we want to reconsider Hartree-Fock theory and deformations and pairing from the more general Hartree-Fock-Bogoliubov theory which, as we will see, embraces all the models we have treated so far.

CHAPTER 7

The Generalized Single-Particle Model (HFB Theory)

7.1 Introduction

As we have seen in the last two chapters, many properties of nuclei can be described in terms of a model of independent particles moving in an average potential whose space dependence closely follows the matter distribution. With unfilled shells, we find additional correlations between these particles. In the BCS model we have learned to treat these correlations in a generalized single-particle picture by introducing quasi-particles and a new type of field, the “pairing potential.”

The Hartree–Fock–Bogoliubov (HFB) theory generalizes and unifies both methods. Within this theory we look for the most general product wave functions consisting of independently moving quasi-particles. They are determined by a variational principle and take into account as many correlations as possible staying within a static single-particle picture. It turns out that within this approximation, the Hamiltonian reduces to two average potentials, the self-consistent field Γ , which we already know from the Hartree–Fock theory, and an additional pairing field Δ , known from the BCS theory. The field Γ contains all the long range $p\bar{n}$ -correlations which eventually lead to a deformed ground state (phase transition). On the other hand, Δ sums up the short-range pairing correlations that can lead to a phase transition and a superfluid state. HFB theory now mixes both descriptions and handles their interdependence. It is therefore capa-

ble of simultaneously describing all kinds of phase transition within the mean field approximation.

Since the HFB theory is a combination of both Hartree–Fock and BCS theory, many of the relevant problems have already been discussed in the foregoing chapters. We can therefore stay rather formal in deriving the necessary formulae appearing at the beginning of this chapter. In Section 7.2 we introduce a general quasi-particle picture. The nuclear wave function $|\Phi\rangle$ under consideration is defined as a vacuum of suitable quasi-particle operators, and its formal properties are discussed. Many of the formulae and some important theorems in this context are proved in Appendix E. In Section 7.3 we derive the HFB equations that determine the wave function $|\Phi\rangle$ and present several methods for solving them. The pairing-plus-quadrupole model is introduced in Section 7.4 as an example, which shows many important features of realistic calculations. Several applications of the theory are discussed in the last sections, namely, calculations of the ground state properties of deformed nuclei constrained Hartree–Fock theory (CHF) for the investigation of energy surfaces in the context of fission and the calculation of rotational spectra within the self-consistent cranking (SCC) model.

7.2 The General Bogoliubov Transformation

7.2.1 Quasi-particle Operators

The basic idea of any quasi-particle concept is to represent the ground state of a nucleus as a *vacuum* with respect to *quasi-particles*, which are defined by the low-lying excitations of neighboring nuclei. This is precisely the concept of Landau and Migdal [La 59, Mi 67], who defined the vacuum and the quasi-particles in terms of exact eigenstates of the many-body system. This theory of Fermi liquids is therefore, in principle, an exact one; however, it has the disadvantage that there is no simple mathematical relationship between these Landau–Migdal quasi-particles and the “bare” particles of the system (given by some basic operators c_i^+, c_i which may, for instance, be plane waves or harmonic oscillator states).

In this chapter, we use the so-called Bogoliubov quasi-particles [Bo 58, Bo 59a+b, BS 59, Va 61] which have a linear connection to the bare particles. They are easy to handle, but the corresponding vacuum $|\Phi\rangle$ and the one-quasi-particle states are now only approximations of the exact eigenfunctions of the many-body Hamiltonian.

We have already defined quasi-particles of a very special type within the BCS model (Eq. 6.67). In the limit of vanishing pairing correlations ($u_k, v_k = 0$), they are either particles ($\epsilon_k > \epsilon_F$) or holes ($\epsilon_k < \epsilon_F$). A very natural extension of these BCS quasi-particles is given by the most general linear transformation from the particle operators c_i^+, c_i to the *quasi-particle*

operators β_k^+ , β_k of the form:

$$\beta_k^+ = \sum_l U_{lk} c_l^+ + V_{lk} c_l. \quad (7.1)$$

The indices k and l both run over the whole configuration space ($k = 1, \dots, M$). The Hermitian conjugation of Eq. (7.1) gives us the operator β_k . We therefore have a transformation of the operators $(c_1, \dots, c_M, c_1^+, \dots, c_M^+) \rightarrow (\beta_1, \dots, \beta_M, \beta_1^+, \dots, \beta_M^+)$ which acts in a $2M$ -dimensional space*

$$\begin{pmatrix} \beta \\ \beta^+ \end{pmatrix} = \begin{pmatrix} U^+ & V^+ \\ V^T & U^T \end{pmatrix} \begin{pmatrix} c \\ c^+ \end{pmatrix} = \mathfrak{W}^+ \begin{pmatrix} c \\ c^+ \end{pmatrix} \quad (7.2)$$

and which is represented by the matrix \mathfrak{W} :

$$\mathfrak{W} = \begin{pmatrix} U & V^* \\ V & U^* \end{pmatrix}. \quad (7.3)$$

The coefficients U, V are not completely arbitrary. We require the new operators β_k, β_k^+ to obey the same fermion commutation relations as the old ones. This restricts the matrix \mathfrak{W} to being unitary.

$$\mathfrak{W}^+ \mathfrak{W} = 1 \quad \text{and} \quad \mathfrak{W} \mathfrak{W}^+ = 1, \quad (7.4)$$

or

$$\begin{aligned} U^+ U + V^+ V &= 1, & U U^+ + V^* V^T &= 1, \\ U^T V + V^T U &= 0, & U V^+ + V^* U^T &= 0, \end{aligned} \quad (7.5)$$

and allows us to invert Eq. (7.1):

$$c_l^+ = \sum_k U_{lk}^* \beta_k^+ + V_{lk} \beta_k. \quad (7.6)$$

There is a famous *theorem of Bloch and Messiah* [Zu 62, BM 62] which states that a unitary matrix \mathfrak{W} of the form (7.3) can always be decomposed into three matrices of very special form:

$$\mathfrak{W} = \begin{pmatrix} D & 0 \\ 0 & D^* \end{pmatrix} \begin{pmatrix} \bar{U} & \bar{V} \\ \bar{V} & \bar{U} \end{pmatrix} \begin{pmatrix} C & 0 \\ 0 & C^* \end{pmatrix} \quad (7.7)$$

or

$$U = D \bar{U} C, \quad V = D^* \bar{V} C. \quad (7.8)$$

*The definition of the matrix \mathfrak{W} in Eq. (7.2) seems somewhat unusual; it is, however, consistent with the definition (7.1) and has the advantage that we can use the rules of matrix multiplication in the following.

D and C are unitary matrices and \bar{U}, \bar{V} are real matrices of the general form

$$\bar{U} = \begin{pmatrix} 0 & & & & \\ & \ddots & & & \\ & & 0 & & \\ & & & \boxed{\begin{matrix} u_1 & 0 \\ 0 & u_1 \end{matrix}} & \\ & & & & \boxed{\begin{matrix} u_n & 0 \\ 0 & u_n \end{matrix}} \\ & & & & 1 \\ & & & & \\ & & & & 1 \end{pmatrix}, \quad (7.9)$$

$$\bar{V} = \begin{pmatrix} 1 & & & & & \\ & \ddots & & & & \\ & & 1 & & & \\ & & & \boxed{\begin{matrix} 0 & v_1 \\ -v_1 & 0 \end{matrix}} & & \\ & & & & \boxed{\begin{matrix} 0 & v_n \\ -v_n & 0 \end{matrix}} & \\ & & & & & 0 \\ 0 & & & & & \\ & & & & & 0 \end{pmatrix}$$

The proof of this theorem is given in Section E.1. Its meaning is that the transformation (7.1) can be decomposed into three parts

$$\left. \begin{array}{l} c \rightarrow a \\ c^+ \rightarrow a^+ \end{array} \right\} \rightarrow \left\{ \begin{array}{l} \alpha \rightarrow \beta \\ \alpha^+ \rightarrow \beta^+ \end{array} \right. \quad (7.10)$$

$$D \quad \bar{U}, \bar{V} \quad C$$

- (i) a unitary transformation of the particle operators c^+ among themselves

as in the HF case [Eq. (5.18)]

$$a_k^+ = \sum_l D_{lk} c_l^+. \quad (7.11)$$

It defines a new basis, called the “*canonical*” basis,* which is explained in more detail in Appendix E. It is convenient to use because, as we shall see, the density matrix ρ is diagonal in this basis;

- (ii) a *special Bogoliubov transformation*, which distinguishes between “*paired*” levels ($u_p > 0, v_p > 0$)

$$\begin{aligned} \alpha_p^+ &= u_p a_p^+ - v_p a_{\bar{p}}^+, \\ \alpha_{\bar{p}}^+ &= u_p a_{\bar{p}}^+ + v_p a_p^+, \end{aligned} \quad (7.12)$$

where (p, \bar{p}) are defined by the 2×2 boxes in Eq. (7.9) (see also Chap. 6), and “*blocked*” levels, which are either occupied ($v_i = 1; u_i = 0$) or empty ($v_m = 0; u_m = 1$):

$$\begin{aligned} \alpha_i^+ &= a_i, & \alpha_m^+ &= a_m^+, \\ \alpha_i^- &= a_i^+, & \alpha_m^- &= a_m. \end{aligned} \quad (7.13)$$

(7.12) corresponds to the BCS-transformation (6.67). The orthogonality relations (7.5) guarantee that the real occupation numbers v_p and u_p are normalized;

- (iii) a *unitary transformation of the quasi-particle operators* α_k^+ among themselves

$$\beta_k^+ = \sum_{k'} C_{kk'} \alpha_{k'}^+. \quad (7.14)$$

From this theorem we see that a general Bogoliubov transformation (7.1) is nothing but a BCS transformation in an appropriate basis, the canonical basis, defined by the transformation D in Eq. (7.11). In particular, the decomposition (7.7) defines fully occupied levels (i), completely empty levels (m), and paired levels (p) with canonical conjugate states p, \bar{p} . In many problems with time reversal symmetry it turns out that one can choose the time reversal operation as canonical conjugation. However, there are cases (for example, the HFB-theory in a rotating frame; see Sec. 7.7) where we do not know a priori what the canonical conjugation is. First we have to determine the full HFB transformation (7.1) and afterwards we can apply the Bloch-Messiah theorem (7.7) for the calculation of the canonical basis. We will see in Sec. 7.2.2, how this decomposition can be achieved in practical cases, which will be useful for a deeper insight into the physical content of the wave function.

* It has this name because the skew symmetric pairing tensor κ (7.24) is in the canonical form in this basis.

7.2.2 The Quasi-particle Vacuum

The definition of quasi-particle operators in the last section has up to now been highly mathematical. To get physical information from the transformation, we have to calculate a wave function. As discussed above, the ground state of the many-body system $|\Phi\rangle$ shall be represented as the vacuum with respect to these quasi-particles:

$$\beta_k |\Phi\rangle = 0 \quad \text{for all } k = 1, \dots, M. \quad (7.15)$$

Wave functions which fulfill this condition for a corresponding set of quasi-particle operators (7.1) will, in the following, be called HFB wave functions.

Before we can study the structure of such wave functions in more detail, we want to show that this definition is always possible and unique: It is easy to construct a wave function which fulfills Eq. (7.15). We start with the bare vacuum $|-\rangle$ and multiply it by a product of annihilation operators β_k :

$$|\Phi\rangle = \prod_k \beta_k |-\rangle. \quad (7.16)$$

If k runs over all values $k = 1, \dots, M$, the condition (7.15) is certainly fulfilled. In many cases, however, such a function vanishes identically. In a HF state, for instance, the product can run only over the annihilation operators of all hole states

$$|\Phi_{\text{HF}}\rangle = \prod_i \alpha_i |-\rangle = \prod_i a_i^+ |-\rangle. \quad (7.17)$$

Any annihilation operator of a particle state $a_m = a_m^\dagger$ would make $|\Phi\rangle$ vanish identically. Therefore, in Eq. (7.16) we define \prod as the product of the maximal number of k -values, such that the multiplication of any additional operator β_q would annihilate $|\Phi\rangle$. This maximal number turns out to depend on the physical situation. It is determined, as we shall see later on, by the blocking structure (7.18). It may happen that this number is even; then the wave function $|\Phi\rangle$ describes an even nucleus (ground state or excited state; see below). If this number is odd, one deals with an odd nucleus. From this definition, we can always construct a function $|\Phi\rangle$ which fulfills Eq. (7.15). Since the basis sets $c_{l_1}^+, \dots, c_{l_N}^+ |-\rangle$ ($N = 0, \dots, M$) and $\beta_{k_1}^+, \dots, \beta_{k_N}^+ |\Phi\rangle$ ($N = 0, \dots, M$) are both orthogonal complete sets in the many-body Hilbert space, the definition of $|\Phi\rangle$ by the operators β_k ($k = 1, \dots, M$) in Eq. (7.15) is certainly unique.

The opposite is not true: $|\Phi\rangle$ does not uniquely define the quasi-particle operators β_k . Any transformation of these operators amongst themselves [as in the C-transformation in Eq. (7.14)] leaves $|\Phi\rangle$ invariant. This means, in particular, that we could have also used the quasi-particle operators α_k [Eqs. (7.12) and (7.13)] in the canonical basis for the definition of $|\Phi\rangle$.

Therefore, $|\Phi\rangle$ is fully determined by the single-particle operators a_k in the canonical basis, and the occupation probabilities v_k^2 .

In particular, we can now use the prescription (7.16) to construct a more explicit form of $|\Phi\rangle$. It is clear that we have to leave out any operator a of unoccupied levels in Eq. (7.13). After proper normalization, we find

$$|\Phi\rangle = \mathcal{N} \prod_k a_k |-\rangle = \prod_i a_i^+ \prod_p (u_p + v_p a_p^+ a_p^+) |-\rangle, \quad (7.18)$$

where, by definition, none of the numbers u_p vanishes. Depending on whether the number of occupied levels i is even or odd, the function (7.18) is a superposition of states with an even or odd particle number. We call this quantum number the *number parity* [BMR 73]. It is evident that a wave function $|\Phi\rangle$ with even number parity can only describe a system with even particle number, and vice versa.

We usually assume that $|\Phi\rangle$ describes the ground state of an even system, but we have not used this fact in the derivation. We now see that, dependent on the coefficients U and V in the Bogoliubov transformation (7.1) which completely determine our wave function, we get even or odd number parity. These coefficients are determined by a variation of the energy expectation value and we will derive the corresponding (HFB) equations in Section 7.3.1. They are nonlinear and can have several solutions. Usually, the solution of these equations with the deepest energy will provide us with such coefficients U and V that the corresponding vacuum $|\Phi\rangle$ describes the ground state of an even nucleus, that is, the state (7.18) can be represented as a BCS state (6.31) in the canonical basis. Sometimes, however, we want to calculate the ground state of an odd mass nucleus. In such a case, we have to make sure that we use coefficients U and V which guarantee odd number parity for the wave function $|\Phi_1\rangle$; that is, $|\Phi_1\rangle$ can be written as a one quasi-particle state based on a properly chosen ground state $|\Phi_0\rangle$ with even number parity.

In practice, this is very simple to accomplish [BMR 73, Ma 75a]. We start, for instance, with a fully paired vacuum $|\Phi_0\rangle = \beta_1 \beta_2 \dots \beta_M |-\rangle$ with even number parity. The one-quasi-particle state

$$|\Phi_1\rangle = \beta_1^+ |\Phi_0\rangle \quad (7.19)$$

is a vacuum to the operators $(\tilde{\beta}_1, \tilde{\beta}_2, \dots, \tilde{\beta}_M)$ with

$$\tilde{\beta}_1 = \beta_1^+, \tilde{\beta}_2 = \beta_2, \dots, \tilde{\beta}_M = \beta_M. \quad (7.20)$$

The exchange of a quasi-particle creation operator β_1^+ with the corresponding annihilation operator β_1 means that we have replaced columns 1 in the matrices U and V by the corresponding columns in the matrices V^*, U^* :

$$(U_{II}, V_{II}) \leftrightarrow (V_{II}^*, U_{II}^*). \quad (7.21)$$

Thus by making such a replacement we change the number parity of the corresponding vacuum and go over to a one-quasi-particle state. This can be continued—starting from the fully paired ground state we can come to

many-quasi-particle states by simply interchanging the corresponding columns in the HFB coefficients. With this trick we represent *quasi-particle excitations* as HFB *vacua* for properly defined new quasi-particle operators.

Of course, the transformations C , \bar{U} , \bar{V} , and D of Eq. (7.7) are changed by the replacement (7.20). In particular, the canonical basis for $|\Phi_1\rangle$ is, in general, different from that for $|\Phi_0\rangle$ in Eq. (7.18). Only in cases where the C transformation is equal to unity (i.e., if $|\Phi_1\rangle = \alpha_1 |\Phi_0\rangle$) do the two wave functions have the same canonical basis.

7.2.3 The Density Matrix and the Pairing Tensor

As we saw in the last section, the general Bogoliubov transformation (7.1) or the coefficients U_{ik} and V_{ik} are not uniquely defined by the HFB wave function $|\Phi\rangle$ to within a C transformation (7.14).

We now define two quantities which contain no redundant information and which determine the wave function $|\Phi\rangle$ uniquely. They are called the *normal* and *abnormal density* (or density matrix and pairing tensor), and are given by their matrix elements in the particle basis

$$\rho_{ii'} = \langle \Phi | c_i^+ c_{i'} | \Phi \rangle, \quad \kappa_{ii'} = \langle \Phi | c_i c_{i'} | \Phi \rangle, \quad (7.22)$$

or in matrix notation

$$\rho = V^* V^T, \quad \kappa = V^* U^T = -UV^+. \quad (7.23)$$

ρ is hermitian ($\rho^* = \rho$) and κ is skew symmetric ($\kappa^T = -\kappa$).

Using the decomposition of the Bloch–Messiah theorem [Eq. (7.9)] and the unitarity of C , we find

$$\rho = D \bar{V}^2 D^+, \quad \kappa = D \bar{U} V D^T. \quad (7.24)$$

This means that ρ is diagonal in the canonical basis. The eigenvalues of ρ are the occupation probabilities v_k^2 and the eigenvectors are the coefficients D_{ik} of the wave functions a_k (7.11) in the canonical basis.* At the same time, κ is in its canonical form: it decomposes into 2×2 matrices:

$$\begin{pmatrix} 0 & u_k v_k \\ -u_k v_k & 0 \end{pmatrix}. \quad (7.25)$$

Two important relations hold for ρ and κ . They follow from Eqs. (7.5) and (7.23):

$$\rho^2 - \rho = -\kappa \kappa^+, \quad \rho \kappa = \kappa \rho^*. \quad (7.26)$$

Sometimes it is useful to define a $2M$ -dimensional generalized density

* Equation (7.24) shows that ρ behaves under a unitary transformation like a linear operator and κ behaves like the matrix part of an antilinear operator. For the connection between HFB theory and the theory of antilinear operators, see [HV 68, VH 70].

matrix [Sch 61, Va 61]

$$\mathcal{R} = \begin{pmatrix} \langle \Phi | c_r^+ c_i | \Phi \rangle & \langle \Phi | c_r c_i | \Phi \rangle \\ \langle \Phi | c_r^+ c_i^+ | \Phi \rangle & \langle \Phi | c_r c_i^+ | \Phi \rangle \end{pmatrix} = \begin{pmatrix} \rho & \kappa \\ -\kappa^* & 1 - \rho^* \end{pmatrix}, \quad (7.27)$$

which is Hermitian and idempotent:

$$\mathcal{R}^2 = \mathcal{R}. \quad (7.28)$$

Its eigenvectors are the HFB coefficients (U_ν) for quasi-particle creation operators with eigenvalue 0, and (V_ν) for quasi-particle annihilation operators with eigenvalue 1:

$$\mathcal{W}^\dagger \mathcal{R} \mathcal{W} = \begin{pmatrix} \langle \Phi | \beta_k^+ \beta_k | \Phi \rangle & \langle \Phi | \beta_r \beta_i | \Phi \rangle \\ \langle \Phi | \beta_k^+ \beta_k^+ | \Phi \rangle & \langle \Phi | \beta_r \beta_i^+ | \Phi \rangle \end{pmatrix} = \begin{pmatrix} 0 & 0 \\ 0 & 1 \end{pmatrix}. \quad (7.29)$$

Both sets of eigenvectors are determined only up to a unitary transformation in the corresponding eigenspace, that is, up to the C transformation (7.14), and this shows that ρ and κ uniquely determine $|\Phi\rangle$.

In the following chapters we will see that many theories developed originally in the HF picture of pure Slater determinants ($\rho^2 = \rho$) can be immediately generalized to the HFB case with pairing correlations simply by working in the $2M$ -dimensional formalism with the matrix \mathcal{R} .

7.3 The Hartree–Fock–Bogoliubov Equations

7.3.1 Derivation of the HFB Equation

Until now we have investigated only the formal structure of the HFB transformation (7.1) and the corresponding vacuum $|\Phi\rangle$. In this section we derive an equation for the coefficients U_{ik} and V_{ik} which defines the quasi-particles and the wave function $|\Phi\rangle$.

We assume that $|\Phi\rangle$ is an approximation for the exact ground state of the Hamiltonian

$$H = \sum_{l_1 l_2} t_{l_1 l_2} c_{l_1}^+ c_{l_2} + \frac{1}{4} \sum_{l_1 l_2 l_3 l_4} \bar{v}_{l_1 l_2 l_3 l_4} c_{l_1}^+ c_{l_2}^+ c_{l_3} c_{l_4}, \quad (7.30)$$

and use the variation principle of Ritz (see Sec. 5.2). In our case, the trial wave functions are the set of all generalized product states $|\Phi\rangle$ of the HFB type.

As in the BCS model these wave functions violate the symmetry connected with the particle number (see Sec. 6.3). Again we have to use a constraint on the particle number N and vary the Hamiltonian $H' = H - \lambda N$. To simplify the notation, we neglect the prime in the following and come back to the problem of a variation with constraint in Section 7.6.

Starting from the variational principle

$$\delta \frac{\langle \Phi | H | \Phi \rangle}{\langle \Phi | \Phi \rangle} = 0. \quad (7.31)$$

we have to investigate small variations $|\delta\Phi\rangle$ in the vicinity of the solution $|\Phi\rangle$. Since we consider only wave functions of the HFB type, we can use a theorem of Thouless (see Appendix E) and express the function $|\Phi'\rangle = |\Phi\rangle + |\delta\Phi\rangle$, which is not orthogonal to $|\Phi\rangle$ [MW 68, Ma 75a] by:

$$|\Phi'\rangle = \exp\left(\sum_{k < k'} Z_{kk'} \beta_k^+ \beta_{k'}^+\right) |\Phi\rangle. \quad (7.32)$$

In contrast to the coefficients U_{kk} and V_{kk} , which obey orthogonality relations (7.5), the variables $Z_{kk'}$ (with $k < k'$) are independent variables. The solution $|\Phi\rangle$ of variational equation (7.31) corresponds to $Z_{kk'} = 0$. For infinitesimal variations, we can expand up to second order. Using quasi-particle representation (E.18) for the Hamiltonian

$$H = H^0 + \sum_{k_1 k_2} H_{k_1 k_2}^{11} \beta_{k_1}^+ \beta_{k_2} + \sum_{k_1 < k_2} (H_{k_1 k_2}^{20} \beta_{k_1}^+ \beta_{k_2}^+ + \text{h.c.}) + H_{\text{int}}, \quad (7.33)$$

we get

$$\frac{\langle \Phi' | H | \Phi' \rangle}{\langle \Phi' | \Phi' \rangle} = H^0 + (H^{20} H^{20}) \begin{pmatrix} Z \\ Z^* \end{pmatrix} + \frac{1}{2} (Z^* Z) \begin{pmatrix} A & B \\ B^* & A^* \end{pmatrix} \begin{pmatrix} Z \\ Z^* \end{pmatrix}, \quad (7.34)$$

where the index of the vectors and matrices runs over all pairs ($k < k'$) and

$$\begin{aligned} H^0 &= \langle \Phi | H | \Phi \rangle, & A_{kk''} &= \langle \Phi | [\beta_{k'} \beta_k, [H, \beta_r^+ \beta_{r'}^+]] | \Phi \rangle; \\ H_{kk'}^{20} &= \langle \Phi | [\beta_{k'} \beta_k, H] | \Phi \rangle, & B_{kk''} &= -\langle \Phi | [\beta_{k'} \beta_k, [H, \beta_r \beta_{r'}]] | \Phi \rangle. \end{aligned} \quad (7.35)$$

Equation (7.34) gives a quadratic approximation of the multidimensional energy surface in the vicinity of $|\Phi\rangle$. The variation with respect to $Z_{kk'}^*$ yields* [Be 59]

$$\frac{\partial}{\partial Z_{kk'}^*} \frac{\langle \Phi' | H | \Phi' \rangle}{\langle \Phi' | \Phi' \rangle} \Big|_{Z=0} = H_{kk'}^{20} = 0, \quad (7.36)$$

which means that the linear terms in Eq. (7.34) vanish at the stationary point. To see if it is a minimum or a saddle point, the quadratic terms in Eq. (7.34) must be investigated. The matrix

$$S = \begin{pmatrix} A & B \\ B^* & A^* \end{pmatrix} \quad (7.37)$$

is called the *stability matrix* (or *curvature tensor*). At a minimum it has to be positive definite.

The variational equations (7.36) are not affected by a C-transformation of the quasi-particles among themselves [Eq. (7.14)]. The requirement $H^{20}=0$ determines, therefore, only the first two of the Bloch-Messiah transformations. The third transformation can be used to diagonalize the H^{11} part in Eq. (7.33). Together with (7.36), this corresponds to the

* Variation with respect to Z_{kk} gives the complex conjugate equation.

diagonalization of the supermatrix

$$\begin{pmatrix} H^{11} & H^{20} \\ -H^{20*} & -H^{11*} \end{pmatrix} = \begin{pmatrix} \langle \Phi | \{ [\beta_k, H], \beta_k^+ \} | \Phi \rangle & \langle \Phi | \{ [\beta_k, H], \beta_{k'}^+ \} | \Phi \rangle \\ \langle \Phi | \{ [\beta_k^+, H], \beta_k^+ \} | \Phi \rangle & \langle \Phi | \{ [\beta_k^+, H], \beta_{k'}^+ \} | \Phi \rangle \end{pmatrix} \quad (7.38)$$

In the space of the basis operators c_i, c_i^+ this matrix has the form

$$\mathcal{K} = \mathfrak{A} \begin{pmatrix} H^{11} & H^{20} \\ -H^{20*} & -H^{11*} \end{pmatrix} \mathfrak{A}^+ = \begin{pmatrix} h & \Delta \\ -\Delta^* & -h^* \end{pmatrix} \quad (7.39)$$

with

$$h_H = \langle \Phi | \{ [c_i, H], c_i^+ \} | \Phi \rangle, \quad \Delta_H = \langle \Phi | \{ [c_i, H], c_i \} | \Phi \rangle. \quad (7.40)$$

Applying Wick's theorem (Sec. C.4), we get*

$$h = \epsilon + \Gamma - \lambda; \quad \Gamma_H = \sum_{qq'} \bar{v}_{iq'q} p_{qq}; \quad \Delta_H = \frac{1}{2} \sum_{qq'} \bar{v}_{Hq'q} K_{qq'}. \quad (7.41)$$

We therefore end up with a diagonalization problem for the matrix \mathcal{K} , the so-called HFB equations [Ba 61, 63a+b]:

$$\begin{pmatrix} h & \Delta \\ -\Delta^* & -h^* \end{pmatrix} \begin{pmatrix} U_k \\ V_k \end{pmatrix} = \begin{pmatrix} U_k \\ V_k \end{pmatrix} \cdot E_k, \quad (7.42)$$

where the columns U_k, V_k of the matrices U and V determine the quasi-particle operator β_k^+ (7.1). In the basis corresponding to the operators β_k , both matrices \mathcal{K} and \mathfrak{A} [see Eq. (7.29)] are diagonal. We therefore get as an equivalent condition to Eq. (7.36) [BS 59]:

$$[\mathcal{K}, \mathfrak{A}] = 0 \quad (7.43)$$

which corresponds exactly to the formulation (5.36) of the HF equation.

The Hamiltonian (7.33) now takes the form

$$H = H^0 + \sum_k E_k \beta_k^+ \beta_k + H_{\text{int}}. \quad (7.44)$$

H_{int} (E.18) contains the terms H^{40}, H^{31} , and H^{22} . They are neglected in the HFB approach. In this case, H is diagonal. Its eigenstates are the quasi-particle vacuum $|\Phi\rangle$ (with the eigenvalue H^0), one-quasi-particle states

$$|\Phi_k\rangle = \beta_k^+ |\Phi\rangle, \quad (7.45)$$

with the quasi-particle energies E_k , two-quasi-particles states, and so on. The excited states to $|\Phi\rangle$ are states with an even number of quasi-particles. The states with an odd number of quasi-particles describe the neighboring nuclei ($A \pm 1$).

These considerations, however, give only a rough overview of the structure of excited states. In particular, the one-quasi-particle states (7.45) are not determined self-consistently. We will see in the next section how this point can be improved.

*The chemical potential λ is determined by the particle number: $\text{Tr } \rho = N$.

Before we discuss the properties of the HFB equations (7.42), let us give a different derivation which shows some interesting aspects of the theory and requires less calculation [Bl 62].

Using the theorem of Wick (see Sec. C.4), we expand the Hamiltonian in normal order ($: \cdot :)$ with respect to the ground state $|\Phi\rangle$. We then get for the one-particle operator

$$\begin{aligned} c_i^+ c_i = & \langle \Phi | c_i^+ c_i | \Phi \rangle + : c_i^+ c_i : \\ = & \rho_{ii} + : c_i^+ c_i :, \end{aligned} \quad (7.46)$$

and for the two-particle operator

$$\begin{aligned} c_{i_1}^+ c_{i_2}^+ c_{i_4} c_{i_3} = & \rho_{i_3 i_4} \rho_{i_1 i_2} - \rho_{i_2 i_3} \rho_{i_4 i_1} + \kappa_{i_1 i_2}^* \kappa_{i_3 i_4} \\ & + \rho_{i_3 i_4} : c_{i_2}^+ c_{i_4} : + \rho_{i_4 i_3} : c_{i_1}^+ c_{i_3} : - (i_3 \leftrightarrow i_4) \\ & + \kappa_{i_1 i_2}^* : c_{i_4} c_{i_3} : + \kappa_{i_3 i_4} : c_{i_1}^+ c_{i_2}^+ : \\ & + : c_{i_1}^+ c_{i_2}^+ c_{i_4} c_{i_3} : . \end{aligned} \quad (7.47)$$

Using the definitions (7.41) for Γ and Δ , we immediately find

$$H = H^0 + \frac{1}{2} : (c^+ c) \begin{pmatrix} h & \Delta \\ -\Delta & -h^* \end{pmatrix} \begin{pmatrix} c^+ \\ c \end{pmatrix} : + \frac{1}{4} \sum_{i_1 i_2 i_3 i_4} \bar{v}_{i_1 i_2 i_3 i_4} : c_{i_1}^+ c_{i_2}^+ c_{i_4} c_{i_3} : . \quad (7.48)$$

The last term contains only products of four-quasi-particle operators. It corresponds to H^{40} , H^{31} , and H^{22} in the quasi-particle representation (E.18). In the generalized single-particle model, this interaction between the quasi-particles is neglected. The rest is a quadratic form in the operators c , c^+ , which can be diagonalized exactly by the general Bogoliubov transformation (7.1). Again we find the HFB equations (7.42) with the solution (7.44).

7.3.2 Properties of the HFB Equations

The HFB-equations (7.42) are a $2M$ -dimensional set of nonlinear equations. They show more or less the same properties as the HF equations (5.38). Many points of the discussion in Chapter 5 are therefore also valid for the HFB equations. In particular, we can also derive them for density dependent forces by a variation with respect to both densities, ρ and κ (see Sec. 7.5). The theorem of self-consistent symmetries (Chap. 5) applies here also [Sa 68, Go 79]. They can be solved either by iterative diagonalization of the matrix X in Eq. (7.39) or by the gradient method, which will be described in the next section.

There are, however, some basic differences to the HF case, which we will discuss in the following.

The equations contain a chemical potential λ which has to be determined by the particle number subsidiary condition. Therefore, we must always constrain HFB-equations; for the method of treating such problems, see Sections (7.3.3) and (7.6).

In addition, the HFB equations contain two potentials, Γ and Δ . The Γ corresponds to the HF potential, which describes the shape of the nucleus (spherical or deformed), whereas Δ determines the pairing correlations. In contrast to the BCS-theory, Δ is now no longer given by one number Δ_k [Eq. (6.50)], but is a matrix which mixes different levels. Since we have seen that the HFB wave functions $|\Phi\rangle$ have the structure of BCS wave functions in the canonical basis

(7.11), it is interesting to investigate the HFB equations (7.42) in this basis. We therefore use the matrices \bar{U} and \bar{V} (7.9), for example, in a fully paired case, and obtain from Eq. (E.22), for the diagonal matrix elements of H_{kk}^{20} in the canonical basis (for real matrix elements Δ_{kk}),

$$u_k v_k (h_{kk} + h_{kk}) + \Delta_{kk} (u_k^2 - v_k^2) = 0, \quad (7.49)$$

which has a similar solution to Eq. (6.52) viz:

$$\begin{pmatrix} u_k^2 \\ v_k^2 \end{pmatrix} = \frac{1}{2} \left[1 \pm \frac{\frac{1}{4}(h_{kk} + h_{kk})}{\sqrt{\frac{1}{4}(h_{kk} + h_{kk})^2 + \Delta_{kk}^2}} \right]. \quad (7.50)$$

We see that the important quantities, which determine the occupation numbers, are the diagonal matrix elements h_{kk} , h_{kk} , and Δ_{kk} in the canonical basis. This does not, however, mean that the other matrix elements of h and Δ in general vanish, and a nontrivial C-transformation is needed to diagonalize H^{11} .

There is a special case when H^{11} is already diagonal in the canonical basis. As we see from Eq. (E.22) for H^{20} , this happens in cases of time reversal symmetry, whenever the only non-vanishing matrix elements of Δ in the canonical basis are the elements Δ_{kk} . In such cases, the off-diagonal matrix elements of h in the canonical basis also vanish, and we get for the quasi-particle energies

$$E_k = \sqrt{h_{kk}^2 + \Delta_{kk}^2}. \quad (7.51)$$

This happens, for instance, in all cases where there is time reversal invariance together with a monopole pairing force for the calculation of the pair field Δ (see Sec. 7.4). In such cases, the full HFB equations (7.42) can be solved by a solution of HF equations (5.39), including the appropriate occupation factors v_k^2 , which themselves are determined by the BCS equations in each step of the iteration. In the general case this is, however, not true: The Bloch–Messiah theorem (Sec. 7.2.1.) does not imply that HFB can be replaced by coupled HF–BCS equations (see also [Go 79]).

We want to stress that for the derivation of the HFB equations we have only used the general product structure of the function $|\Phi\rangle$ and the stationarity condition (7.31). Whether the solution corresponds to the absolute minimum in the multidimensional energy surface (see Sec. 7.3.3) or only to a local one, or perhaps only to a saddle point, depends on how we solve these equations and, in particular, on the initial conditions of the iterative solution. For instance, if we use a self-consistent symmetry (see Sec. 5.5), we can never get an eventual absolute minimum which breaks this symmetry. In such a case, the solution of the HFB equations will therefore be a local minimum or a saddle point.

This fact is often used to approximate functions other than the ground state wave function of the system. If there is a symmetry operator (for instance, angular momentum or the K -quantum number), the many-body Hamiltonian H can be diagonalized in each eigenspace of this symmetry separately, and we can apply the HFB approximation in each case. In such cases, the separate solution of the HFB equations in each subspace provides us with approximations for the lowest eigenstates with the corresponding symmetry.

An example is the number parity (see Sec. 7.2.2). If we run the iteration in such a way that $|\Phi\rangle$ has at each step an odd number parity, we get an approximation to the wave function for an odd mass nucleus. This corresponds to the self-consistent solution of the HFB equations for odd mass nuclei [RBM 70, RMB 74]. It includes,

in particular, the blocking effect (see Sec. 6.3.4) and the change of the average potential due to the odd particle (polarization). How such calculations are achieved in practice will be discussed later in this section.

Another example is two-quasi-particle states in the even system with axial symmetry. If the K -value of such a state does not vanish, it is automatically orthogonal to the ground state with $K=0$. For the calculation of $K=0$, two-quasi-particle states, we have to realize that such states correspond to different stationary points in the energy surface of the ground state. They can be found by a variation under the constraint that the wave function is orthogonal to the ground state wave function [MSR 76, EMR 80a]. Only in cases where they lie in the minimum of a well separated valley with approximately orthogonal wave functions, can we neglect this constraint.

We see that the HFB equations (7.42), in principle, can be used for the self-consistent approximation of all eigenstates of H whose wave functions have the structure of generalized products.

In an actual solution by iterative diagonalization of Eq. (7.42), we encounter the problem that the equations are $2M$ -dimensional and have $2M$ eigenvalues and eigenvectors. To construct a set of quasi-particle operators $\{\beta_1^+ \dots \beta_M^+\}$, and for the calculation of ρ and κ in Eq. (7.23), we have to choose M of them. However, as is easily recognized, to each eigenvector (V_k, U_k) with eigenvalue E_k there corresponds an eigenvector (V_k^*, U_k^*) with eigenvalue $-E_k$. We saw in Section 7.2.2 that an exchange of these two eigenvectors corresponds to a replacement of one operator β_k^+ by β_k and vice versa. It is forbidden to choose E_k and $-E_k$ at the same time (otherwise it is impossible to fulfill the Fermi commutation relations for the operators β , β^+). Therefore, we have to decide for each k ($k=1 \dots M$) whether one takes the eigenvalue E_k with the eigenvector (U_k, V_k) or $-E_k$ with the eigenvector (V_k^*, U_k^*) .

In the pure HF case, this choice corresponds to the freedom of keeping a level occupied or empty in the calculation of the density matrix ρ . Of course, in such a calculation the levels are usually filled according to their energy to get the lowest total energy. This corresponds to the case where all the excitation energies of the system are positive.

In the same way, we usually choose the M positive eigenvalues E_k in the HFB case for *even particle number*. Then the excited states of the system, whose lowest are the two-quasi-particle states, have a positive energy. With this choice at each step of the iteration we usually find a fully paired state which corresponds to the deepest minimum in the energy surface.

If we want to solve the HFB equations for an *odd nucleus*, we can start with the solution of the neighboring even system and a pure quasi-particle state as the input for the iteration. As we have already seen in Section 7.2.2, such a state can be interpreted as a "vacuum" to a new set of quasi-particle operators $\tilde{\beta}$ [see Eq. (7.20)] by interchanging one of the eigenvectors (U_k, V_k) by (V_k^*, U_k^*) . We therefore have, in the solution of the HFB equation of an odd system after each diagonalization, to choose one of the negative energies $-E_k$ with the corresponding eigenvector (V_k^*, U_k^*) to get a blocked HFB function. Which value of k we take depends on the quasi-particle state we want to describe. They represent different local minima in the energy surface. By such an exchange we therefore jump from one valley to another.

In cases where such valleys are no longer well separated (for instance, in band crossing phenomena in even nuclei), it may happen that one of the quasi-particle energies becomes very small and even *negative* (see Fig. 7.8d). In such cases we

must even use a negative quasi-particle energy for the even system. We are not allowed to choose only positive ones, because the latter would correspond to a jump into a different valley with odd number parity. Consequently, we must investigate the blocking structure of the system in each step of the iteration [BMR 73]. In the next section we will study a method that avoids such problems.

7.3.3 The Gradient Method

The HFB equations (7.42) are often solved by iterative diagonalization. In the last subsection we discussed the problems that can arise in such a method. The procedure is often rather time-consuming and convergence is not always guaranteed (see, for instance, Sec. 5.4), and it gets particularly complicated in cases with one or several subsidiary conditions.

In the following we will present the gradient method for the solution of the HF or the HFB equations [MSR 76, EMR 80a]. It is based on the fact that we are interested in a local minimum of the multidimensional energy surface.* Starting from an arbitrary initial wave function $|\Phi_0\rangle$, which corresponds to one point on this surface, it searches for the direction of steepest descent and follows it in iterative steps until the minimum is reached.

What we need, therefore, is a suitable and unique parametrization of the energy surface, at least in the vicinity of the point $|\Phi_0\rangle$. We use the theorem of Thouless (see Sec. E.3), which states that each wave function of the HFB type which is not orthogonal to $|\Phi_0\rangle$ can be represented as

$$|\Phi(Z)\rangle \propto \exp\left(\sum_{k < k'} Z_{kk'} \beta_k^* \beta_{k'}^*\right) |\Phi_0\rangle, \quad (7.52)$$

where the operators β_k annihilate $|\Phi_0\rangle$ and there is a one-to-one correspondence between the $M(M-1)/2$ parameters $Z_{kk'} (k < k')$ and the HFB functions $|\Phi(Z)\rangle$. As discussed in Sec. E.3, functions $|\Phi\rangle$ orthogonal to $|\Phi_0\rangle$ have, in a sense, the structure of quasi-particle excitations with a diverging matrix Z . They are therefore "far away" from $|\Phi_0\rangle$ on the energy surface and cannot be reached using a finite Z . Within this method it is therefore impossible to jump in one step to a state which is orthogonal to $|\Phi_0\rangle$, as is sometimes done in the diagonalization method. Nevertheless it is possible to reach all HFB wave functions in several steps, because at each point of the iteration the Thouless theorem is again applied. This corresponds to a new parametrization of the energy surface at each step.

Starting from $|\Phi_0\rangle$ (given, for instance, by the HFB coefficients U_0, V_0), we go as a first step to a function $|\Phi_1\rangle$ which corresponds to the parameters Z_1 chosen in the direction of the steepest descent, that is, parallel to the gradient of the energy [see Eq. (7.36)]

$$Z_{1kk'} = -\eta \frac{\partial}{\partial Z_{kk'}} E(Z) \Big|_{Z=0} = -\eta H_{kk'}^{(0)}. \quad (7.53)$$

The parameter η determines the size of the step. It is somewhat arbitrary at the beginning and reduced or increased in the following iterations, depending on the actual values of the energies $E(Z_i)$. To get the new coefficients U_1, V_1 that

* See also [Mc 56, 60, BTR 77].

correspond to the function $|\Phi_1\rangle = |\Phi(Z_1)\rangle$, we use Eq. (E.30) and calculate

$$\begin{aligned} U_1 &= U_0 + V_0^* Z_1^*, \\ V_1 &= V_0 + U_0^* Z_1^*. \end{aligned} \quad (7.54)$$

For general values of $Z_{1kk'}$ the coefficients U_1 and V_1 correspond to quasi-particle operators γ_k which annihilate $|\Phi(Z_1)\rangle$ but do not fulfil Fermi commutation relations

$$\{\gamma_k, \gamma_{k'}\} = 0; \quad \{\gamma_k, \gamma_{k'}^+\} = \delta_{kk'} - (Z_1 Z_1^*)_{kk'}. \quad (7.55)$$

Therefore, we have to orthogonalize the vectors $(\begin{smallmatrix} U_1 \\ V_1 \end{smallmatrix})$ by a C -transformation (7.14) in each step of the iteration.

This procedure is continued until convergence is achieved, that is, until the gradient H^{20} vanishes identically, which corresponds to the condition (7.36).

The method is extremely useful in cases where we must fulfill a subsidiary condition—for instance, the particle number condition $\langle \hat{N} \rangle = N$. Starting from $|\Phi_0\rangle$ with arbitrary particle number N_0 , we do not proceed in the direction of the gradient H^{20} alone, but we admix the gradient of the particle number N^{20}

$$Z_1 = -\eta(H^{20} - \lambda N^{20}). \quad (7.56)$$

The parameter λ is determined in such a way that $\Phi(Z_1)$ has the right particle number N up to linear order in Z_1 . This gives

$$N - N_0 = \sum_{k < k'} Z_{1kk'}^* N_{kk'}^{20} + \text{c.c.} = Z_1 \cdot N^{20} = -\eta(H^{20} \cdot N^{20} - \lambda N^{20} \cdot N^{20}) \quad (7.57)$$

or

$$\lambda = \frac{H^{20} \cdot N^{20}}{N^{20} \cdot N^{20}} + \frac{N - N_0}{\eta \cdot N^{20} \cdot N^{20}}, \quad (7.58)$$

where $Z \cdot N$ is the scalar product of the vectors (Z, Z^*) and (N, N^*) . In cases where $|\Phi_0\rangle$ already has the right particle number N , we get

$$Z_1 = -\eta \left(H^{20} - \frac{H^{20} \cdot N^{20}}{N^{20} \cdot N^{20}} N^{20} \right), \quad (7.59)$$

that is, we choose the direction of the gradient projected onto the hypersurface orthogonal to the gradient of N , which means that it has constant particle number. If convergence is achieved, we find, as in a variation with a Lagrange parameter λ ,

$$(H - \lambda N)^{20} = 0. \quad (7.60)$$

It is easy to extend the method to several subsidiary conditions.

The path on the energy surface to choose in the gradient method can be quite different from that of the diagonalization method. An example is given in Fig. 5.3.

7.4 The Pairing-plus-Quadrupole Model

In deriving the HFB equation (7.42) we started from the Hamiltonian (7.30) and obtained the two potentials Γ and Δ [Eq. (7.41)]. Both potentials are calculated from the same nuclear interaction $v(1,2)$. We saw in Chapter 5 that the bare nucleon–nucleon force cannot be used for the calculation of the HF potential Γ . The Brückner formalism (Chap. 4)

shows that we have to apply an effective interaction, that is, the G -matrix, which sums up part of the higher order processes. It is evident that similar arguments hold for the pairing field. Green's function techniques (see Appendix F) allow the derivation of the HFB equations, too [Go 58, AGD 63, Mi 67], and from there we see that the effective interactions for the calculation of the self-consistent field Γ and the pairing field Δ may be different. Therefore, it seems to be meaningful to also use different effective forces for both potentials in phenomenological models.

The *pairing-plus-quadrupole model* was first suggested by Bohr and Motelson and afterwards widely used by Kisslinger and Sorenson [KS 60], Baranger and Kumar [BK 65, 68], and many other authors (for a review, see [BS 69]). It distinguishes three important effects in any mean field theory of the nuclear many-body system.

- (i) The interaction between the particles can be summed up, as a first approach, by an average spherical single-particle potential which is localized in space and breaks the translational invariance.
- (ii) In open shell nuclei, there are two types of additional correlations: long-range ph -correlations can be taken into account by a deformation of the mean field. At this point the rotational symmetry is lost.
- (iii) Short-range pp -correlations are treated by a self-consistent pairing potential Δ which violates particle number symmetry.

These three effects are included most simply in the pairing-plus-quadrupole model. The average spherical potential is approximated by a spherical harmonic oscillator with $I \cdot s$ and I^2 term, that is, by a Nilsson potential (Chap. 2) at zero deformation with corresponding single-particle energies ϵ_k . Only nucleons within one major shell of each parity feel the residual interaction. The residual interaction has two parts, one contributing to Γ (which here is only that part of the field going beyond the spherical part already contained in the single-particle energies ϵ_k), and the second which contributes to Δ .

Both parts of the interaction are chosen to be separable in the appropriate indices. Since the most important deformations are of a quadrupole nature, and since the most important pairing correlations are the ones for $I=0$ pairs, the most simple Hamiltonian of this kind has the form (see also Sec. 4.4.7):

$$H = \sum_k \epsilon_k c_k^\dagger c_k - \frac{1}{2} x \sum_{\mu=-2}^2 :Q_\mu^+ Q_\mu^- : - GP^+ P, \quad (7.61)$$

with the quadrupole operator

$$Q_\mu = \sum_{kk'} \langle k | r^2 Y_{2\mu} | k' \rangle c_k^\dagger c_{k'}, \quad (7.62)$$

and the creation operator for a Cooper pair

$$P^+ = \sum_{k>0} c_k^\dagger c_k^\dagger. \quad (7.63)$$

Here \bar{k} is the time reversed state of k . BCS phases are used [see (Eq. 4.138)]. The actual values of the force constants χ and G depend on the configuration space under consideration (see, for instance, [BK 68]) and are adjusted from experimental data.

In the following, we neglect (by definition of the model) the single-particle part of $Q^+ \cdot Q$, the contributions of the pairing force to the potential Γ , and those parts of the QQ -force which contribute to the potential Δ and the Fock term in Γ . The latter terms are usually rather small. From (7.41) and (7.48) we then obtain the HFB single-particle Hamiltonian of the form:

$$H_{\text{HFB}} = \sum_k \epsilon_k c_k^+ c_k - \frac{1}{2} \sum_{\mu=-2}^2 q_\mu (Q_\mu^+ + Q_\mu) - p_0 (P^+ + P) \quad (7.64)$$

with

$$q_\mu = \chi \langle \Phi | Q_\mu | \Phi \rangle \quad \text{and} \quad p_0 = G \langle \Phi | P | \Phi \rangle \quad (7.65)$$

where we have assumed that the parameters q_μ and p_0 are real. The HFB Hamiltonian operator is a particle-number and rotation symmetry violating single-particle operator. With fixed "deformation" parameters q_μ and p_0 it is similar to a Nilsson Hamiltonian. In Eq. (7.65), q_μ and p_0 , however, depend on the solution $|\Phi\rangle$, that is, on ρ and κ . They have to be determined by iteration, or by what is equivalent in the case of separable forces—minimizing the energy $E(q_\mu, p_0)$ with respect to those parameters.

It becomes convenient to choose the principal axis of the density distribution as the axis of our coordinate frame (this implies $q_1 = q_{-1} = 0$ and $q_2 = q_{-2}$) and to work in a basis which is symmetrized with respect to a rotation of 180° around the x -axis ([RBM 70, Go 74]; see also Eq. (1.57)):

$$|k\rangle = \frac{1}{\sqrt{2}} (|nljm\rangle - ie^{i\pi J_x} |nljm\rangle); \quad |\bar{k}\rangle = T|k\rangle. \quad (7.66)$$

Assuming $R_x = e^{i\pi J_x}$ as a self-consistent symmetry in the sense of Section 5.5 and arranging the levels in the order $(k_1, k_2, \dots, \bar{k}_1, \bar{k}_2, \dots)$ we find in general for the densities ρ and κ and for the potentials Γ and Δ , the form:

$$\rho = \begin{pmatrix} \rho_1 & 0 \\ 0 & \rho_2 \end{pmatrix}, \quad \kappa = \begin{pmatrix} 0 & \kappa_2 \\ \kappa_1 & 0 \end{pmatrix}, \quad \Gamma = \begin{pmatrix} \Gamma_1 & 0 \\ 0 & \Gamma_2 \end{pmatrix}, \quad \Delta = \begin{pmatrix} 0 & \Delta_2 \\ \Delta_1 & 0 \end{pmatrix}, \quad (7.67)$$

with $\rho_i^+ = \rho_i$, $\Gamma_i^+ = \Gamma_i$; $\kappa_2 = -\kappa_1^T$, and $\Delta_2 = -\Delta_1^T$. The diagonalization of ρ gives the first transformation of the Bloch-Messiah theorem (7.7):

$$D = \begin{pmatrix} D_1 & 0 \\ 0 & D_2 \end{pmatrix}. \quad (7.68)$$

The Hamiltonian (7.61) is time reversal invariant, which implies

$$\begin{aligned} \rho_2 &= \rho_1^*; & \kappa_1^+ &= \kappa_1; & \Gamma_2 &= \Gamma_1^*; \\ D_2 &= D_1^*; & \Delta_1^+ &= \Delta_1. \end{aligned} \quad (7.69)$$

For a pure pairing force, since $\Delta_1 = p_0 \cdot 1$ is a multiple of unity, we find in the canonical basis $\Delta \rightarrow D^* \Delta D^*$ or $\Delta_1 \rightarrow D_2^T \Delta_1 D_1^* = p_0 \cdot 1$, that is, Δ is invariant under the first Bloch-Messiah transformation.

To determine the transformation D it is therefore sufficient to diagonalize the self-consistent field:

$$h = \epsilon - \lambda + \Gamma = \epsilon - \lambda - q_0 Q_0 - q_2 (Q_2 + Q_{-2}). \quad (7.70)$$

This is exactly a Nilsson Hamiltonian (2.89) for fixed deformation parameters q_0, q_2 . The canonical basis in this case is therefore the Nilsson basis with the eigenvalues $\tilde{\epsilon}_k$. In this basis the HFB equations (7.42) split into (2×2) matrices:

$$\begin{pmatrix} \tilde{\epsilon}_k & \Delta \\ -\Delta & -\tilde{\epsilon}_k \end{pmatrix} \begin{pmatrix} u_k \\ v_k \end{pmatrix} = \begin{pmatrix} u_k \\ v_k \end{pmatrix} \cdot E_k \quad (7.71)$$

with the gap parameter (7.75) $\Delta = p_0$, which have the BCS solutions (6.59).

To summarize, then, the complete solution of the HFB equations in the pairing-plus-quadrupole model corresponds to a Nilsson diagonalization with variable deformation parameters q_0 and q_2 , a subsequent BCS calculation with constant gap parameter $\Delta = p_0$, and a minimization of the total energy

$$E(q_0, q_2, \Delta) = \langle \Phi | H | \Phi \rangle = \sum_k \tilde{\epsilon}_k v_k^2 + \frac{1}{2\chi} (q_0^2 + 2q_2^2) - \frac{\Delta^2}{G} \quad (7.72)$$

with respect to parameters q_0, q_2 , and Δ . The term $(1/2\chi) \cdot (q_0^2 + 2q_2^2)$ has to be added, since in summing up single-particle energies we have counted the (negative) interaction energy twice [Eq. (5.40)].

This force explains the Nilsson model with BCS occupation probabilities very nicely and by a suitable choice of the constants G and χ one can therefore reproduce all its results. We have to emphasize, however, that it is only a model constructed for certain phenomena, namely quadrupole deformations and $I=0$ pairing correlations and the interplay between these degrees of freedom. For these phenomena it contains all the gross features of a more realistic approach.

7.5 Applications of the HFB Theory for Ground State Properties

There are many HFB studies on *light nuclei* (see, for instance, [WFS 71, BKD 73]). A variety of interactions have been used. In many cases it is necessary to use projection of angular momentum and particle number (for instance [GGF 73] or [GGA 74]; see also Chap. 11). We will not go into the details, but mention here the so-called *proton-neutron pairing* (for a review, see [Go 79]).

In light nuclei protons and neutrons occupy the same levels. We can therefore construct not only pp - and nn -pairs with a large spacial overlap of their density distributions, but also pn -pairs [Go 64]. We thus have two types of pairing

correlations: $T=0$ pairing for $p\bar{n}$ -pairs only and $T=1$ pairing for $p\bar{p}$, $n\bar{n}$ - and $p\bar{n}$ -pairs. In heavy nuclei, only $T=1$ pairing is important. The full HFB equations (7.42) with a general force include all these types of pairing at the same time. This, however, requires complex potentials Γ and Δ and complex HFB coefficients U and V [GSB 70]. In $N=Z$ nuclei, not only is there time reversal, but also charge conjugation invariance. In this case it can be shown analytically [Go 72] that there are three possibilities for each particle. The proton can be paired with (i) a particle of the same kind in the time reversed state ($p\bar{p}$), (ii) a particle of different kind in the time reversed state ($p\bar{n}$), and (iii) a different particle in the same state ($p\bar{n}$). The last possibility is not excluded by the Pauli principle; it does, however, violate the axial symmetry because it mixes states with different K -values (+ K and $-K$). The different modes have three different gap parameters, whose absolute squares add up to the square of the total gap.

Several authors have investigated different types of such pairing correlations in light nuclei, with many different kinds of forces [GK 65, CCJ 65 + 66, CG 67, GSG 68, BGG 69, WFS 70, WFS 71]. These calculations have demonstrated that $T=0$ pairing is significant in determining the equilibrium shapes. We find that for $N=Z$ nuclei, $T=0$ pairing is most important. For a small neutron excess, we have a competition between $T=0$ and $T=1$ pairing. For heavy nuclei with large neutron excess, where the protons and neutrons at the Fermi surface occupy different shells, $T=0$ pairing is no longer important and there remains the usual $T=1$ pairing in $p\bar{p}$ and $n\bar{n}$ pairs as discussed in Chapter 6.

To discuss further applications, we will restrict ourselves to a few examples in *heavy deformed nuclei*. According to the amount of phenomenology used in such calculations, we must distinguish among the following.

(a) **Calculations in a Model Space.** In this case, one starts with a finite configuration space and spherical single-particle energies. A phenomenological residual interaction is introduced which produces deformations and pairing correlations. Such theories are never able to give correct ground state energies.

The simplest model of this type is the pairing-plus-quadrupole model discussed in Section 7.4. By adjusting the force parameters it is possible to reproduce the deformation and the gap parameter in this way.

In the next step, Dietrich, Mang, and Pradal [DMP 66] used a more realistic residual interaction with finite range and spin-isospin exchange. They applied two methods to determine a HFB wave function $|\Phi\rangle$. In the first case they used Nilsson + BCS wave functions $|\Phi(\beta, \Delta)\rangle$ depending on the two parameters β and Δ and minimized the energy $\langle\Phi(\beta, \Delta)|H|\Phi(\beta, \Delta)\rangle$ with respect to these two parameters. In Fig. 7.1 we show the "energy surface" as a function of β . We see two minima for prolate and oblate deformations, which are rather similar in energy.

In the second case, they solved the full HFB equations $H^{(2)}=0$. Since this procedure allows for more general wave functions $|\Phi\rangle$, the resulting energies are lower (given by horizontal lines in Fig. 7.1). The energy difference is not very large in either case and a closer inspection of the wave function shows that the full HFB wave functions are rather well approximated by the "Nilsson + BCS" functions.

Although deformation parameters calculated by the second method give the trend quite nicely, they do not agree completely with experimental data, because of the restricted configuration space. On taking into account a contribution of the inert core, one finds full agreement.

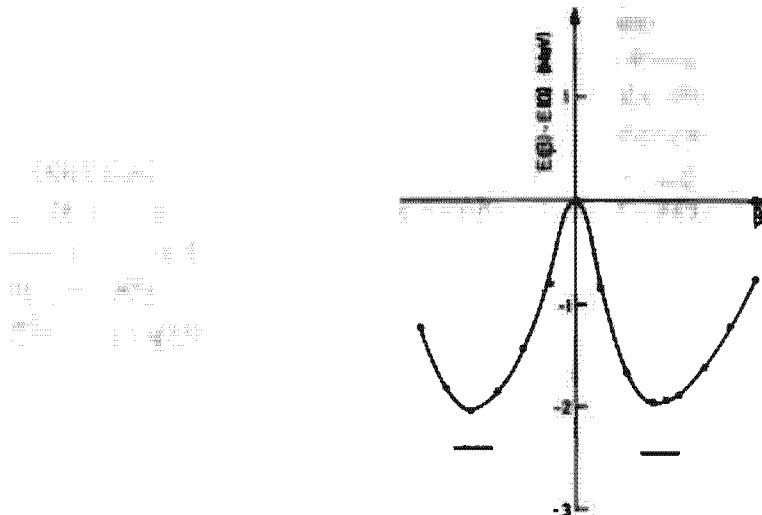


Figure 7.1. Binding energy as a function of deformation for ^{152}Sm . The lines beyond the minima are the solutions of the self-consistent calculations. (From [DMP 66].)

(b) **Calculations with Skyrme Forces.*** We saw in Section 5.6.2 that HF theory with density dependent Skyrme forces is able to reproduce the ground state properties of spherical nuclei. They have therefore also been applied to deformed cases [Va 73]. As discussed in Section 7.4, there is no a priori reason to use the same force for the calculation of Γ and Δ . The first step is therefore to use the pure pairing force (4.140) for the calculation of Δ . In the case of time reversal invariance, we again find (as in the pairing plus quadrupole model) that the canonical basis agrees with the HF basis, in which h is diagonal. It is thus sufficient to diagonalize h at each step of the iteration. The only difference to a normal HF calculation is that we have to take into account the pairing energy and occupation probabilities c_k^2 in the calculation of the densities ρ , τ , J . Instead of (5.84), we thus get, for instance,

$$\rho(\mathbf{r}) = \sum_{i,s}^{\infty} c_i^2 |\psi_i(\mathbf{r}, s, t)|^2, \quad (7.73)$$

with

$$c_i^2 = \frac{1}{2} \left(1 - \frac{\epsilon_i - \lambda}{\sqrt{(\epsilon_i - \lambda)^2 + \Delta^2}} \right). \quad (7.74)$$

Here λ is again fixed by the particle number condition. In principle, Δ should be determined by the gap equation (6.60). Vautherin went the opposite way and used a fixed gap Δ which he took from experiment and calculated the corresponding force constant using Eq. (6.60). The great difference from the HF calculations in spherical nuclei comes from the fact that in deformed nuclei the differential equation (5.100) is no longer separable in a radial coordinate r and angles θ, ϕ . It is now a partial differential equation. Vautherin has solved it by a diagonalization in an anisotropic harmonic oscillator basis. Only the matrix elements are calculated by a Gaussian integration in coordinate space. Axial symmetry allows a decompo-

* Similar calculations have been performed with the Negele force discussed in Section 5.6.1.2. [NR 77].

sition into subspaces with good quantum numbers Ω . Nevertheless, these calculations require a large computational effort.*

The results show a satisfactory agreement with the experimental binding energies and radii. In particular one can reproduce the measured quadrupole and hexadecupole moments of the deformed heavy nuclei [FQV 73].

(c) Full HFB Calculations. As we saw in Chapter 6, the pairing correlations depend not only on the properties of the effective pairing force, but also on the single-particle level density. A full HFB calculation, in which the self-consistent field and the pairing field are derived from the same force, is therefore only meaningful if the HF field yields a reasonable single-particle spectrum. As discussed in Chapter 5, one needs density dependent effective forces for such a task. On the other hand the present versions of the Skyrme force are not useful for complete HFB calculation because of their δ -character. Gogny [Go 73, 75b, DGG 75, DG 80] therefore introduced a new density dependent force (see Sec. 4.4.4) with a finite range part. The Gaussian form of this force allows a fast calculation of the matrix elements in a harmonic oscillator basis [Go 75a].

In the derivation of the HFB equations, we have not used density dependent forces until now. In analogy to Section 5.6 in such a case we have to calculate the energy as a functional of the densities ρ and κ (we use the conventions Tr_1 and Tr_2 defined in Eq. (E.19)).

$$E'(\rho, \kappa) = \langle \Phi | T + V(\rho) - \lambda \hat{N} | \Phi \rangle = \text{Tr} (\iota - \lambda) \rho + \frac{1}{2} \text{Tr}_1 \text{Tr}_2 \rho \bar{\rho} \rho + \frac{1}{4} \text{Tr}_2 \text{Tr}_2 \kappa^* \bar{\kappa}, \quad (7.75)$$

and derive the HFB equations from the variational principle. This is most easily achieved by working with the supermatrix \mathfrak{R} (7.27). We use $\rho_{ik}, \rho_{ik}^*, \kappa_{ik}^*, \kappa_{ik}^{**}$ for ($i < k$) as independent variables and impose the relations (7.28) as subsidiary conditions by a matrix of Lagrange parameters (this procedure could have also been adopted to derive the ordinary HF Eqs., Chap. 5)

$$\delta(E'(\rho, \kappa) - \text{Tr}(\Lambda(\mathfrak{R}^2 - \mathfrak{R}))) = 0. \quad (7.76)$$

We find

$$\delta E' = \text{Tr}(\mathcal{X} \cdot \delta \mathfrak{R}) \quad (7.77)$$

with

$$\delta \mathfrak{R} = \begin{pmatrix} \delta \rho & \delta \kappa \\ -\delta \kappa^* & -\delta \rho^* \end{pmatrix}, \quad \mathcal{X} = \begin{pmatrix} h & \Delta \\ -\Delta^* & -h^* \end{pmatrix} \quad (7.78)$$

and

$$h_{ik} = \frac{\delta E'}{\delta \rho_{ki}}, \quad \Delta_{ik} = \frac{\delta E'}{\delta \kappa_{ik}^*} \quad (7.79)$$

in agreement with Eq. (7.41) in the case of density independent forces.

From (7.76), it follows that

$$\text{Tr}((\mathcal{X} - \Lambda \mathfrak{R} - \mathfrak{R} \Lambda + \Lambda) \delta \mathfrak{R}) = 0. \quad (7.80)$$

Since $\delta \mathfrak{R}$ is an independent variation, this is equivalent to

$$\mathcal{X} = \Lambda \mathfrak{R} + \mathfrak{R} \Lambda - \Lambda. \quad (7.81)$$

* For a solution of deformed HF-equations in the coordinate space, see [HN 77].

Λ is eliminated by the condition $\mathcal{R}^2 = \mathcal{R}$ with the result:

$$[\mathcal{X}, \mathcal{R}] = 0. \quad (7.82)$$

This is exactly equation (7.43). It is equivalent to Eq. (7.36) and can be solved in the same way as the solution of the HFB equations (7.42). However, in cases where the interaction $v(1, 2)$ depends on ρ , we get additional terms contributing to the self-consistent field Γ . From Eqs. (7.75) and (7.79) we see that they have the form:

$$\frac{1}{4} \frac{\partial}{\partial \rho_{kl}} \text{Tr}_2 \text{Tr}_2 (\kappa^* U[\rho] \kappa). \quad (7.83)$$

By adjusting the force parameters in a suitable way (Table 4.4), Gogny was able to reproduce the properties of spherical as well as deformed nuclei. In particular, he got the proper deformations and gap parameters (see Table 7.1).

Table 7.1 Comparison between experimental and calculated values for the binding energy E , the charge quadrupole moments Q , and the gap parameters Δ for protons and neutrons (from [Go 75b])

	$E[\text{MeV}]$		$Q[\text{fm}^2]$		$\Delta_p[\text{MeV}]$		$\Delta_n[\text{MeV}]$	
	HFB	EXP	HFB	EXP	HFB	EXP	HFB	EXP
^{150}Sm	1235.8	1239.3	383	367	1.24	1.43	1.13	1.13
^{152}Sm	1249.0	1253.1	572	590	1.14	1.08	1.09	1.24
^{166}Er	1348.1	1351.6	770	770	1.10	0.97	1.02	1.00
^{184}W	1468.2	1472.9	631	627	0.90	0.86	0.86	0.73

The binding energies should still be corrected for the spurious contribution due to the violation of the rotational symmetry and particle number (see Chap. 11). These corrections can be of the order 5 MeV [FQV 73].

Summarizing these results we find that HFB theory with density dependent forces is able to reproduce all the essential ground state properties of spherical and deformed nuclei over the whole range of the periodic table. In the next section we will see how this theory can be extended to a microscopic calculation of energy surfaces for the fission process.

7.6 Constrained Hartree-Fock Theory (CHF)

Unrestricted HF and HFB calculations give only one point on the energy surface, namely the local minimum. We are often interested in other points on the surface, too: We can impose certain subsidiary conditions and ask for a minimum of the energy on the hypersurface defined by them. Sometimes we want to calculate the energy surface as a function of one (or several) collective parameters q , such as quadrupole or hexadecupole deformations. As we saw in Chapter 1, this is a first step toward a derivation of a collective Hamiltonian, as we use it in descriptions of collective vibrations or of the fission process. We will discuss this in more detail in Chapter 10 in connection with the generator coordinate method.

In all these cases, we are interested in a wave function $|\Phi(q)\rangle$, which minimizes the total energy under the *constraint* that a certain single-particle operator \hat{Q} has a fixed expectation value

$$q = \langle \Phi | \hat{Q} | \Phi \rangle. \quad (7.84)$$

The simplest method for solving this problem is adding the condition (7.84) with a Lagrange multiplier λ to the Hamiltonian H and minimizing

$$\langle H' \rangle = \langle H \rangle - \lambda \langle \hat{Q} \rangle. \quad (7.85)$$

After the solution of this problem, λ is determined by the condition (7.84). This method is also called variation with a *linear constraint*. It corresponds to the investigation of the many-body system in an external field \hat{Q} which deforms it in a proper way.

This method has already been applied in the BCS theory (Sec. 6.3.2) to get wave functions with the right expectation value of the particle number. In analogy to Eq. (6.41), we find that the Lagrange multiplier λ is the derivative of the energy $E = \langle \Phi | H | \Phi \rangle$ with respect to q

$$\lambda = \frac{dE}{dq}. \quad (7.86)$$

As we see from Fig. 7.2, the method of linear constraint means that we have to draw the tangent to the energy surface $E(q)$ at the point $q = q_0$ and use this line as the x -axis of a new coordinate system rotated by the angle α with $\tan \alpha = \lambda$. The y -axis in the new frame corresponds to $\langle H' \rangle$. An unrestricted variation on $\langle H' \rangle$ gives the extremum of the energy surface in the rotated system.

It is evident that this procedure can only work as long as the function $E(q)$ has a positive second derivative. In cases where the curve is concave downwards—as, for instance, in the neighborhood of a saddle point on the fission path or in the backbending region (Fig. 3.4)—this method will no longer work. In such cases, the energy in the rotated frame has a maximum at the point q_1 which will never be a stable solution of the HF equations.

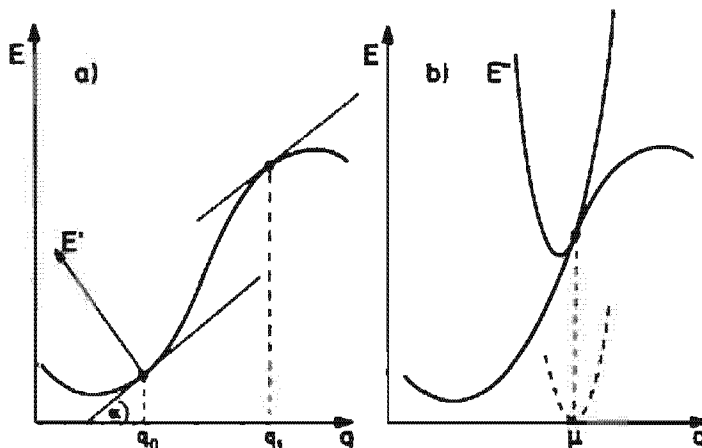


Figure 7.2. Schematic representation of an energy surface showing the methods of linear (a) and (b) quadratic constraint.

We also recognize that in the vicinity of inflection points there are always several points with parallel tangents (that is, with the same λ , but different values of q), that is, q is no longer a unique function of the Lagrange parameter (see Fig. 3.6).

There are several ways to avoid this problem and to find the wave function for such points in the energy surface.

- (i) The gradient method (as discussed in Sec. 7.3) allows us to follow the line of steepest descent perpendicular to the gradient with respect to \hat{Q} . Therefore, for each value of q we find the corresponding minimum in the energy.
- (ii) The method of quadratic constraint [GLW 70, FQK 73] uses an unrestricted variation of the function

$$E'' = \langle H \rangle + \frac{1}{2}C(\langle \hat{Q} \rangle - \mu)^2. \quad (7.87)$$

As in Fig. 7.2b, here we add a parabola with the symmetry axis $q = \mu$ to the energy surface. It produces a new surface E'' with an extremum in the vicinity of μ . If its width is sufficiently small ($C > |d^2 E / dq^2|$), this is always a real minimum.

The variation of E'' gives

$$\delta\langle H \rangle - C(\mu - \langle \hat{Q} \rangle)\delta\langle \hat{Q} \rangle = 0. \quad (7.88)$$

This means the quadratic constraint is equivalent to a linear constraint with $\lambda = C(\mu - \langle \hat{Q} \rangle)$. In both cases, we obtain the same energy surface. This is true for any constraint that is a function of $\langle \hat{Q} \rangle$. With the quadratic constraint, the effective value of λ is automatically changed during the iteration.

- (iii) A third method [BW 71] uses a linear constraint but changes the value of λ at each step of the iteration in such a way that the condition (7.84) is fulfilled. This method is applied in BCS calculations with a constraint on the particle number. However, it requires an additional iteration at each step.

Constrained Hartree-Fock theory (CHF) has been used to calculate the energy surfaces of nuclei in the vicinity of the ground state [BKS 67, CLF 73, CS 73, FQK 73, GG 78] and for fission processes [FQV 74, KCS 74, BFV 74].

In the latter case usually the question has to be faced of which constraining operator \hat{Q} should be used. It is easy to show that we can find any product wave function $|\Phi\rangle$ by CHF calculation using a suitable constraining operator \hat{Q}_* . We have only to use an operator whose two-quasi-particle part $Q_*^{(2)}$ is defined as a multiple of $H^{(2)}$. We then get

$$H^{(2)} - \lambda Q_*^{(2)} = 0, \quad (7.89)$$

that is, $|\Phi\rangle$ as a solution of the corresponding CHF equation. Of course, this is not of much practical use for a calculation of $|\Phi\rangle$, but it shows that there is a large variety of constraining operators that produce the same wave function and are different in their $Q^{(1)}$ -matrix elements.

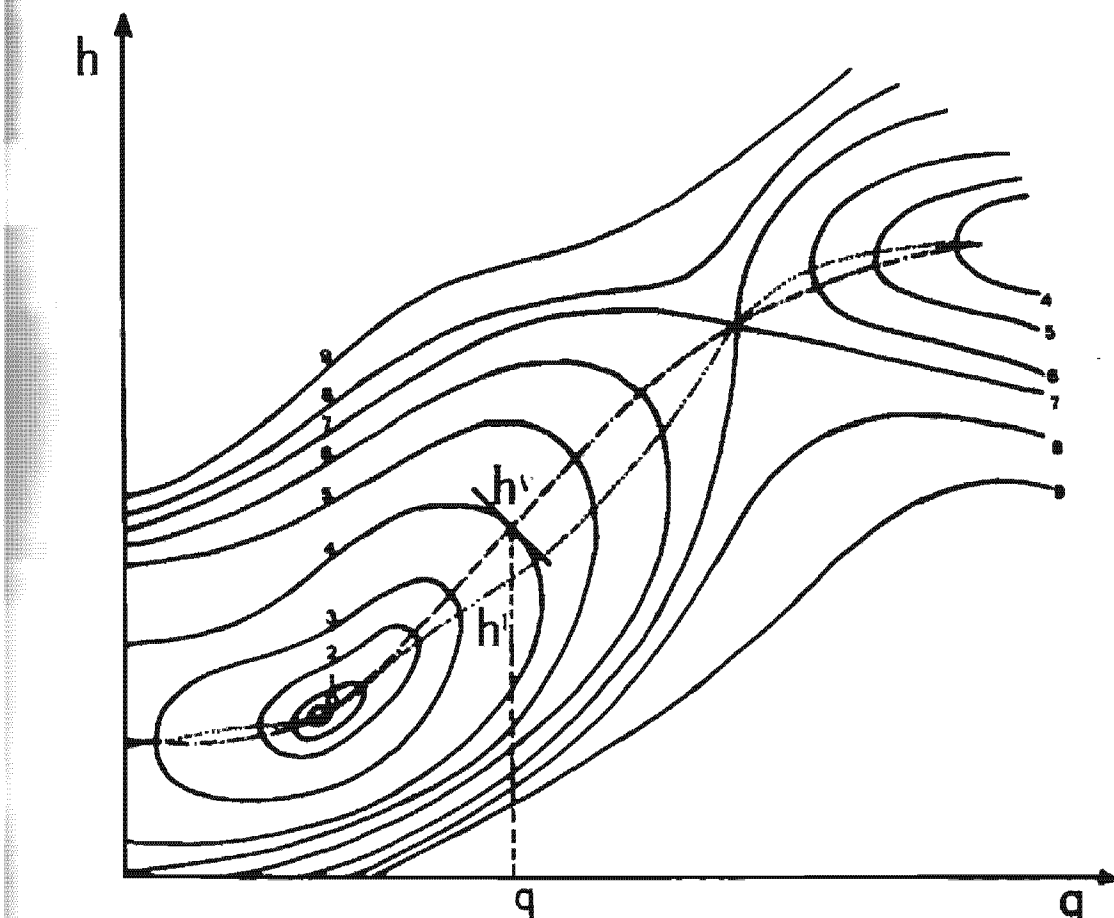


Figure 7.3. Example of an energy surface in the (q, h) plane showing that we do not follow the fission valley exactly with a constraint only on q . (From [FQK 73].)

On the other hand, a constraint on one deformation (for instance, the quadrupole deformation $q = \langle \Phi | Q_{20} | \Phi \rangle$) does not mean that another deformation (for instance, the hexapole deformation $h = \langle \Phi | Q_{40} | \Phi \rangle$) stays constant. This is shown schematically in Fig. 7.3. As long as we use a constraint on q , we follow the line $h'(q) = \langle \Phi(q) | Q_{40} | \Phi(q) \rangle$. It connects the points of a vertical tangent on each equipotential surface, because E has to be a minimum for constant q with respect to all other degrees of freedom, which means, in particular, $dE/dh|_{q=\text{const}} = 0$. This line $h'(q)$ is, in general, different from the bottom of the fission valley, which corresponds to a line of steepest descent $h''(q)$. Both lines go through the stationary points of the surface, such as the ground state minimum or the saddle point. Both lines are very close if the fission valley is parallel to the q axis, but they can deviate quite drastically if the valley is parallel to the h -axis. Nevertheless, we recognize an enormous advantage of CHF calculations compared to the liquid drop and Strutinsky-type calculations (see Sec. 2.9): In the CHF calculation we need only follow a one-parameter line and obtain a wave function which, in many cases, follows quite closely the bottom of the fission valley, whereas in the other methods we must calculate multidimensional energy surfaces.

We should certainly optimize the choice of the constraining operator in CHF calculation. In Chap. 10 we shall study a method for achieving this.

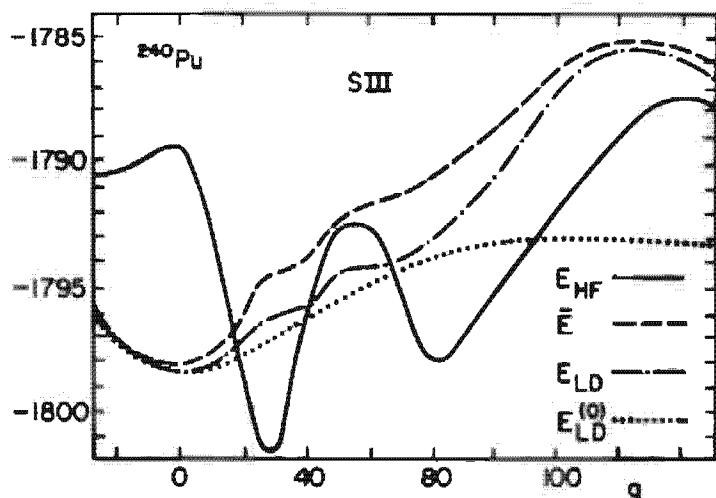


Figure 7.4. Deformation energy curves of ^{240}Pu obtained with the Skyrme III interaction as a function of the mass quadrupole moment q . The details are explained in the text. (From [BQ 75a].)

Figure 7.4 shows the deformation energy for the nucleus ^{240}Pu calculated with a Skyrme force with a constraint on the mass quadrupole moment q (full line [FQV 74]). Pairing correlations are taken into account by a simple pairing force, whose constant G is chosen to be proportional to the surface. The calculation reproduces the ground state minimum and a second minimum. The heights of the barriers do not agree quantitatively with experimental data, but we must bear in mind that axial symmetry and parity are conserved in the calculation, whereas there are indications that the actual fission path violates axial symmetry at the inner and parity at the outer saddle.

To compare these results with a liquid drop calculation, a Strutinski averaged HF energy (dashed line) is calculated and shown in Fig. 7.4. It shows small wiggles. These are, however, not caused by shell effects but are also present in the liquid drop energy which corresponds to the same deformation q and h (dashed-dotted line), because the curve intersects with side valleys. The liquid drop energy at the bottom of the fission valley (dotted line) is very smooth.

Figure 7.5 shows density distributions for the same nucleus at different deformations.

Several authors [FS 76, BSV 76] have pointed out that CHF calculations of this type with constraining operators with unbounded spectra (like $Q \sim r^2 Y_{20}$, which diverges for $r \rightarrow \infty$) can give very spurious results if wave functions $|\Phi\rangle$ are allowed to spread out very far in space. All the practical applications of the CHF method, however, have been carried out in finite configuration spaces, which ensures that the wave functions $|\Phi\rangle$ are somehow concentrated in the region of the nucleus.

In the choice of the configuration space, therefore, we are limited from two sides. To get convergence in the binding energy, a large configuration space is often needed, but on the other hand we should not be able to represent the spurious solutions mentioned above. It seems that the CHF calculations made up to the present time stay within these limits.

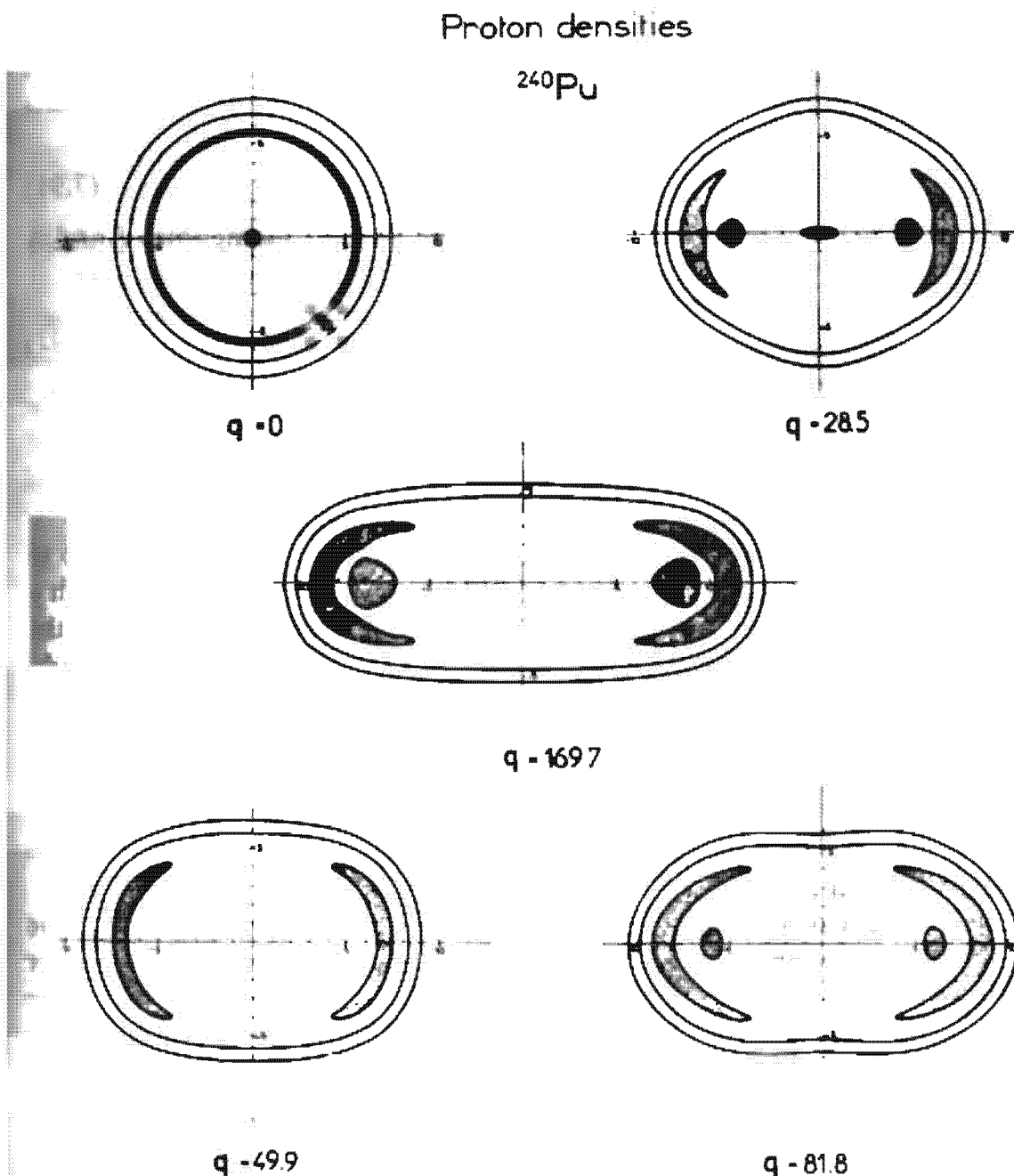


Figure 7.5. Density distributions of ^{240}Pu at different deformations $q = \langle Q_{20} \rangle$. (From [FQV 74].)

A different possible way of keeping the nuclear wave function concentrated is to introduce a second constraint [GL 77]:

$$\hat{H}' = \hat{H} - \lambda \hat{Q} + \mu \hat{Q}^2. \quad (7.90)$$

The Lagrange parameter μ would allow us to vary the $\langle \Delta \hat{Q}^2 \rangle$ fluctuation in the wave function.

7.7 HFB Theory in the Rotating Frame (SCC)

In Chapter 3 we discussed the cranking model within the framework of the pure single-particle shell model. It gave us the possibility of calculating the moment of inertia microscopically. It is evident how to generalize this

theory to the self-consistent many-body case: we must vary the expectation value of the many-body Hamiltonian H with the subsidiary condition that the angular momentum operator J_x has a certain expectation value. This gives the equation (see also Sec. 11.4)

$$\delta \langle \Phi | H - \omega J_x | \Phi \rangle = 0. \quad (7.91)$$

The cranking frequency ω depends on the angular momentum I and is determined by

$$\langle \Phi_\omega | J_x | \Phi_\omega \rangle = \sqrt{I \cdot (I+1)}. \quad (7.92)$$

In Chapter 11 we will see that the solution $|\Phi_{\omega(I)}\rangle$ of this problem must be understood as an internal wave function, from which the eigenfunction of \mathbf{J}^2 can be obtained in the laboratory system by a projection onto good angular momentum.

Within the HFB theory, we restrict the set of variational functions $|\Phi\rangle$ to generalized product functions of the HFB type, and we are then left with a constrained HFB problem. In analogy to the cranking model in the single-particle case, this method is called the *self-consistent cranking model* (SCC). We have already discussed in great detail the problems of the constrained HF method in the last section. In the backbending region (see Chap. 3 and [CMR 75]), the solution of (7.91) corresponds to a saddle point in the energy surface with constant ω . Therefore, we have to apply the gradient method or a quadratic constraint to obtain the solution on the backward-going branch.

In contrast to the applications of the HFB theory discussed so far, the time reversal symmetry of the wave function $|\Phi\rangle$ is broken by the operator ωJ_x . Therefore, we do not know a priori the conjugate states in the canonical basis and thus we must solve the full HFB problem in the rotating frame [RBM 70] viz:

$$\begin{pmatrix} h - \omega j_x & \Delta \\ -\Delta^* & -h^* + \omega j_x^* \end{pmatrix} \begin{pmatrix} U_k \\ V_k \end{pmatrix} = \begin{pmatrix} U_k \\ V_k \end{pmatrix} E_k. \quad (7.93)$$

Using the symmetry $e^{i\omega J_x}$, which is conserved by the cranking Hamiltonian, the matrices ρ , κ , Γ , and Δ take the form (7.67). Since the time reversal symmetry T is violated, we have, instead of Eq. (7.69),

$$\rho_2 \neq \rho_1^*; \quad \Gamma_2 \neq \Gamma_1^*; \quad D_2 \neq D_1^*; \quad \kappa_1^+ \neq \kappa_1^-; \quad \Delta_1^+ \neq \Delta_1^-. \quad (7.94)$$

The densities and the potentials thus have a time-even and a time-odd part, as, for example,

$$\rho^{(+)} = \rho_1 + \rho_2^*; \quad \rho^{(-)} = \rho_1 - \rho_2^*. \quad (7.95)$$

The quasi-particle energies E_k which, for $\omega=0$, are twofold degenerate (see Sec. 2.8), split up at finite cranking frequencies (Fig. 7.8d) and are no longer given by formula (7.51). According to the Bloch-Messiah theorem (7.7), however, there exists a canonical basis, which can be found by a diagonalization of the density ρ . As we can see from Eq. (7.50), the

occupation probabilities v_k^2 in this basis are given by

$$v_k^2 = \frac{1}{2} \left[1 - \frac{\epsilon_k - \omega j_{x_k}}{\sqrt{(\epsilon_k - \omega j_{x_k})^2 + \Delta_{kk}^2}} \right], \quad (7.96)$$

with $\epsilon_k = \frac{1}{2}(h_{kk} + h_{\bar{k}\bar{k}})$ and $j_{x_k} = \frac{1}{2}(j_{x_{kk}} + j_{x_{\bar{k}\bar{k}}})$.

This shows that the diagonal matrix elements h_{kk} , $j_{x_{kk}}$, $h_{\bar{k}\bar{k}}$, $j_{x_{\bar{k}\bar{k}}}$, and Δ_{kk} in the canonical basis are the crucial quantities that determine the occupation probabilities. The matrices h , j_x , and Δ themselves are in general not diagonal in this basis. One also notices that levels with large positive matrix elements j_{x_k} have a greater occupation probability than those with large negative values.

The self-consistent cranking model is useful for the description of the

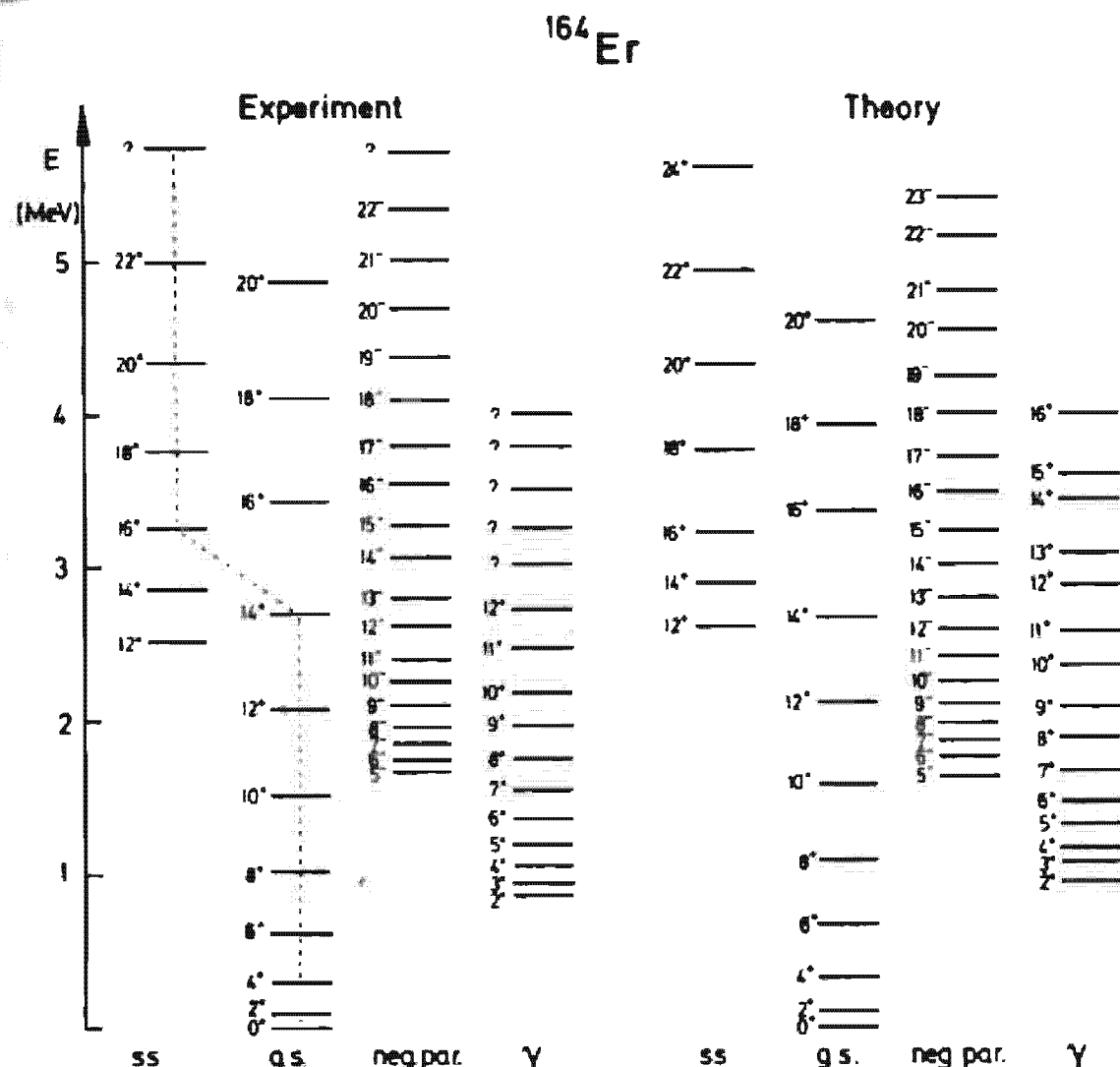


Figure 7.6. Spectra of rotational bands in ^{164}Er . Besides the ground state band (gs), we see a Stephens-Simon band (ss) of an aligned $i13/2$ neutron pair, a negative parity band, and a γ -band [KSM 78]. The yrast line (indicated by a dashed line) follows the lowest-energy levels for each J -value. The r.h.s. gives theoretical calculations within the SCC method [MSR 76, EMR 80a+b].

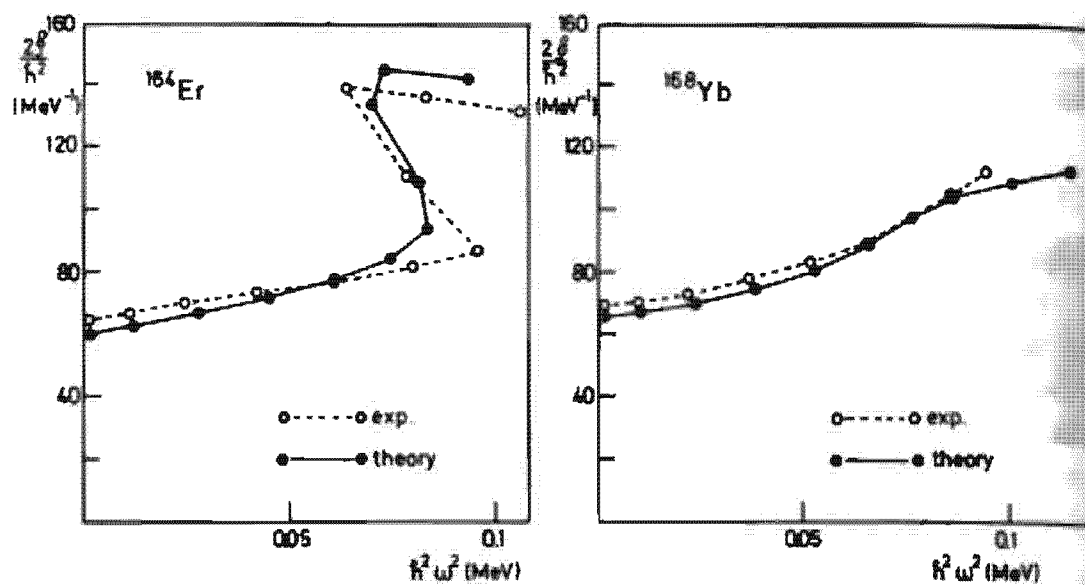


Figure 7.7. Backbending plots for the nuclei ^{164}Er and ^{168}Yb . Dashed lines represent experimental data and full lines show a calculation within the SCC theory [MSR 76]. In both cases, Eq. (3.3) was used to define the moment of inertia β and the angular frequency ω .

type of anomalies found in the high spin region,* which were discussed in Chapter 3. It is general enough to embrace a great variety of physical effects. To illustrate, we will discuss some of these effects for the nucleus ^{164}Er , which has been very well experimentally investigated in the last few years [LCS 76, KSM 78]. Several rotational bands have been found (see Fig. 7.6) which go up to rather high spin values.

A variation of Eq. (7.91) yields the lowest energy for each I -value. This is, by definition, the yrast line (dashed line in Fig. 7.6). As we see, it follows the ground state band only up to $I = 14$. Between $I = 14$ and $I = 16$, we have a band-crossing, that is, we get backbending if we follow the yrast line (see Fig. 7.7). The crossing band has the structure of a two-quasi-particle band with two aligned $i_{13/2}$ neutrons. Therefore, the yrast line changes its character. It follows the ground state band up to $I = 14$ and then corresponds to the aligned band for all I values $I > 16$. The calculation of levels along the yrast line within the self-consistent cranking model shows the following features.

(I) **The Stretching Effect** represents the possible change of the nuclear deformation during the rotation. It is described by the self-consistent potential Γ , which depends on the density and therefore on the cranking frequency. Figure 7.8a shows the effective nuclear deformations β and γ found in the SCC calculation for ^{164}Er . The change in the deformation β is rather small in this spin region. The same is true for many of the well-deformed rare earth nuclei. On the other hand, the γ -deformation

* Recently, the validity of the cranking model for the description of bandcrossings has become an object of discussion [Ha 76, 77, MG 78, GSF 78b, CDS 78].

goes up to $\gamma \sim 10^\circ$, but this depends strongly on the particular nucleus, and other nuclei can be rather stiff against γ -deformations.

(ii) The Coriolis Antipairing Effect (CAP) means that the pairing correlations within the nucleus are weakened by the Coriolis force. In Chapter 6 we saw that the pairing correlations come mostly from nucleon pairs of opposite spin (Cooper pairs), which feel a strong interaction because of their large spatial overlap. Since the Coriolis force acts on both angular momenta in the opposite direction (Fig. 7.9), we should expect at least a partial alignment and a lowering of the corresponding pair energy Δ with increasing spin. This is observed in the calculations (Fig. 7.8b) and is responsible for the moderate increase of the moment of inertia at low spin

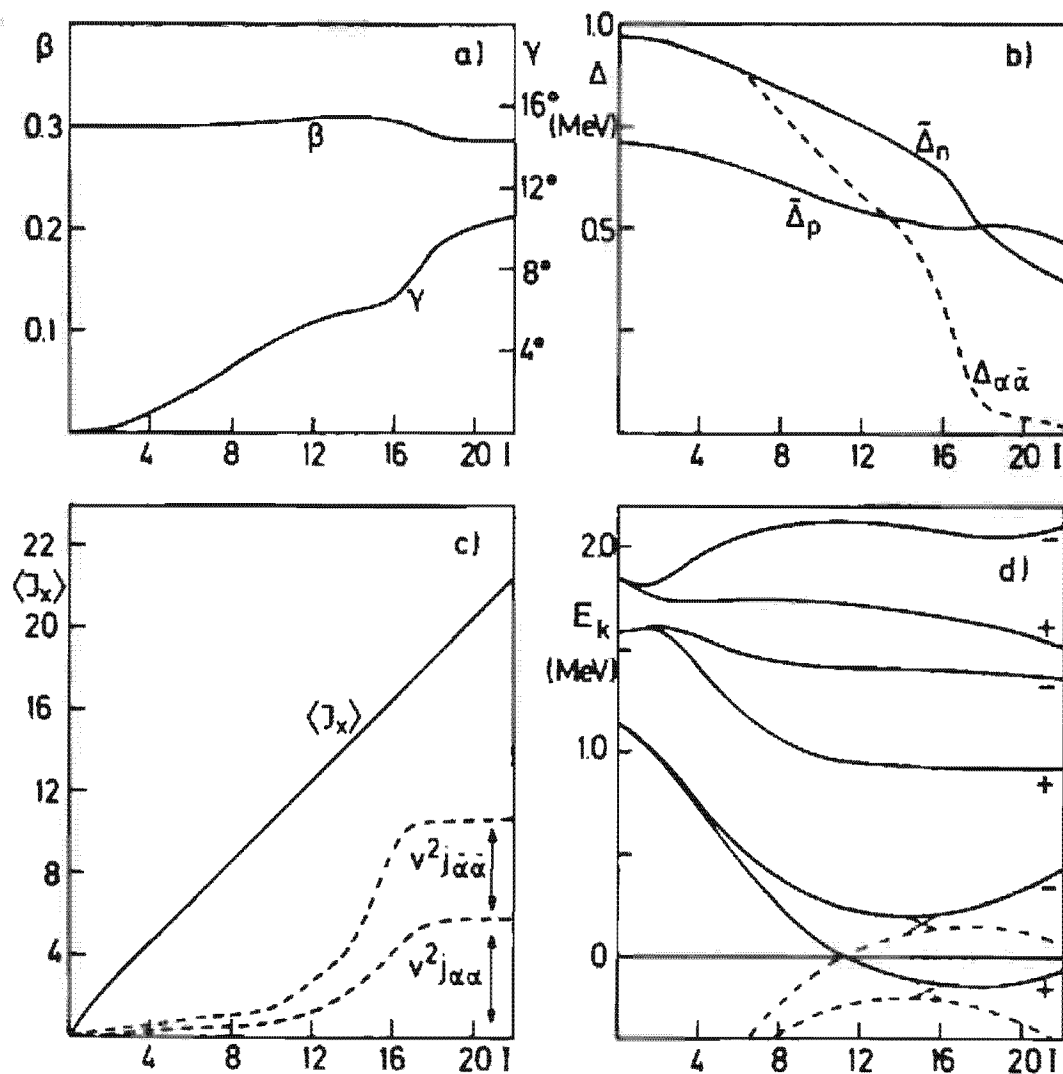


Figure 7.8. Calculated deformation parameters (a), gap parameters (b), expectation values of the angular momentum J_x (c), and quasi-particle energies E_k in the rotating frame (d) as a function of the angular momentum for the case of the nucleus ^{164}Er . (From [MSR 76].) The value of the β -deformation is normalized to 0.3 for $I=0$. Part (b) shows the averaged gap parameters $\tilde{\Delta}_p$ and $\tilde{\Delta}_n$ in the canonical basis [Eq. (7.97)] for protons and neutrons and the gap parameter $\Delta_{\alpha\bar{\alpha}}$ of the aligned pair (dashed line). Further details are explained in the text.

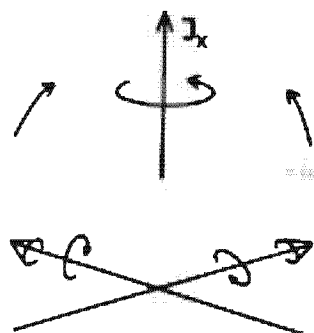


Figure 7.9. Schematic representation of the Coriolis antipairing effect.

values. As in a superconductor within a magnetic field, for a certain critical angular momentum we find a transition to a normal fluid state. This *nuclear Meissner effect* was predicted by Mottelson and Valatin [MV 60] and found in many calculations (for instance, [CV 66, RBM 70, Wa 70a, Ku 72, Fr 76]) at rather different spin values.

The backbending phenomenon has been assumed to be caused by such a phase transition [KS 73]. More realistic calculations, however, which allow decoupling processes of one or several pairs of nucleons, showed that the pairing gap Δ does not vanish completely in the backbending region (Fig. 7.8b, between $I = 12$ and $I = 16$). It is only reduced because of the alignment process. This corresponds to a transition to a two-quasi-particle band with the corresponding blocking effect (see Sec. 6.3.4). In Fig. 7.8b, we show the averaged gap

$$\tilde{\Delta} = \frac{1}{M'} \sum_{k>0}^{M'} \Delta_{kk}. \quad (7.97)$$

($M' = M/2$ is the number of levels $k > 0$ in the configuration space.) Even for a constant pairing force with the constant pairing matrix element Δ in the original basis, not all of the matrix elements Δ_{kk} in the canonical basis are equal. In particular, the matrix element of the aligned pair Δ_{aa} goes to zero (dashed line in Fig. 7.8b). This effect is most drastically pronounced for a pure pairing force, which acts only on $I=0$ pairs (see Sec. 4.4.7). Realistic calculations for very high spin states still have to be done. Model calculations and experimental data [BSC 75], however, indicate that the remaining pairing correlations still persist, sometimes up to rather high spin values ($I \sim 40-50\hbar$).

(iii) Alignment Processes. (Stephens–Simon Effect, [SS 72a]; see Sec. 3.2). Since HFB wave functions $|\Phi\rangle$ are products of the most general single-particle states (with corresponding occupation probabilities), they can represent the ground state band as well as states of partially or totally aligned two-quasi-particle bands. Therefore, they are the appropriate tools for investigating such decoupling processes microscopically. It is clear, however, that we must allow for a violation of axial symmetry to describe

such aligned states, which are a mixture of many different Ω values (see Sec. 3.3). This is no problem in a cranking calculation, since the Coriolis term ω_j destroys this symmetry anyway.

The degree of alignment is measured by the matrix elements j_{x_1} and j_{x_2} of the two particles in the canonical basis. Figure 7.8c shows these values [multiplied by the corresponding occupation probability (7.96) which are, in fact, very close to 1] and the total expectation value of J_x . One notices that in the back-bending region more than the total increment in J_x comes from this pair. The contribution from the rest of the particles decreases, which corresponds to a decrease in the angular frequency ω in this region. For higher spin values, the contribution of the aligned pair is rather constant $5.8 + 4.8 \approx 10.6$, whereas a fully aligned $i_{13/2}$ pair would give $13/2 + 11/2 = 12$.

(iv) Finally, Fig. 7.8d shows some quasi-particle energies E_k in the rotating frame, which are the eigenvalues of Eq. (7.93) as a function of angular momentum. They are no longer twofold degenerate, as is the case with time reversal invariance. At large angular momentum it may happen that one of these energies goes to zero and becomes negative. Since the pairing potential does not vanish in this region, this phenomenon is called *gapless superconductivity** [GLS 67, Gr 74, CMR 75]. It does not mean, however, that there is an excited state with lower energy, because the excitation energy in the even system is always the sum of two quasi-particle energies. We have seen that for each eigenvalue E_k of Eq. (7.93) we also have an eigenvalue $-E_k$ (dashed lines). One of these "unphysical" eigenvalues becomes positive in the backbending region. However, we are not allowed to choose this positive eigenvalue, because (as discussed in Sec. 7.3.2) this would correspond to a transition to a wave function in a system with odd particle number. We also indicated in Fig. 7.8d (by the thin lines) the band-crossing phenomenon, which is connected with the transition from the ground state band to a two-quasi-particle band in the backbending region.

Similar features are found in all nuclei in the rare earth region.[†] There are, however, drastic differences in the backbending plots (see Fig. 7.7), because this kind of plot is very sensitive to small changes in the level spacings of the spectra. In many cases such alignment processes do take place without the backbending phenomenon. As model calculations [CMR 75] show, whether backbending occurs depends on the underlying single-particle level density and on the residual interaction between the two crossing bands: small interaction and low level density give sudden alignment and therefore backbending. In other cases (for instance, ^{168}Yb) we have a smooth alignment process without backbending (see also footnote on p. 122).

* An analogous phenomenon occurs in metallic superconductors [AG 61].

[†] For applications of the SCC theory for light nuclei see [PM 76, NS 78, Zi 78].

The first calculations of this type were carried out by the Munich group [BMR 73] with a pairing-plus-quadrupole interaction in a restricted configuration space. In the meantime, the theory has been improved by particle number projection [DBM 73, FDG 76]. As discussed in Chapter 11, this seems to be necessary in regions in which the pairing correlations undergo drastic changes. The quantitative agreement with experiment is somewhat improved by such calculation, but nothing has changed in the qualitative picture discussed above. The same holds for the inclusion of quadrupole pairing forces [WF 78a].

Realistic forces have also been used, like the G -matrix in a restricted space derived from the Reid soft core potential [GVS 76, Go 76a] or forces of the Skyrme type [FMR 79]. Qualitatively similar results are found.

In Section 7.3.2 we saw that we can use the functions $|\Phi\rangle$ of the HFB type not only for the ground state of even nuclei and for states along the yrast line, but also for all kinds of quasi-particle states in even and odd nuclei. Therefore, we can also describe, in the SCC method, rotational bands in odd nuclei and general two-quasi-particle bands in even nuclei. In particular, we can study all types of alignment processes.

A more fundamental derivation of the cranking model in Chapter 11 shows that we should use the subsidiary condition

$$\langle J_x \rangle = \sqrt{I \cdot (I+1) - \langle J_z^2 \rangle} \quad (7.98)$$

instead of Eq. (7.92). For the ground state band in even nuclei, which are to a good approximation axially symmetric, $\langle J_z^2 \rangle$ is rather small. In such cases (7.98) is equivalent to (7.92). With this subsidiary condition very disturbed rotational bands in odd nuclei have been calculated [RMB 74, FDB 77] and been found in good agreement with the experimental spectra (Fig. 3.11). In particular, there is no need for any attenuation of the Coriolis interaction in this model [RM 74, Ri 77].

Figure 7.6 shows an example of a two-quasi-particle band with negative parity. Here one neutron sits in the $i_{13/2}$ shell and the other in negative parity shells. We again observe an alignment process of one $i_{13/2}$ neutron, which causes a small level spacing for the lower members of this band. Because of the parity selection rule, the corresponding wave functions are automatically orthogonal to the ground state. This is different in the calculation of the so-called "second" band, which causes the backbending phenomenon. It is an excited band which changes its character at the backbending point from the aligned two-quasi-particle band to the ground state band. This band has the same symmetries as the yrast band. Therefore, we have to apply the additional constraint that its wave functions are orthogonal to the corresponding wave functions of the yrast band [EMR 80a].

Figure 7.6 also shows a γ -band. As we shall see in the next chapter, such collective vibrations cannot be described by pure product wave functions. This does not, however, mean that the rotational band built upon such a vibration cannot be investigated by the cranking model. We need only use,

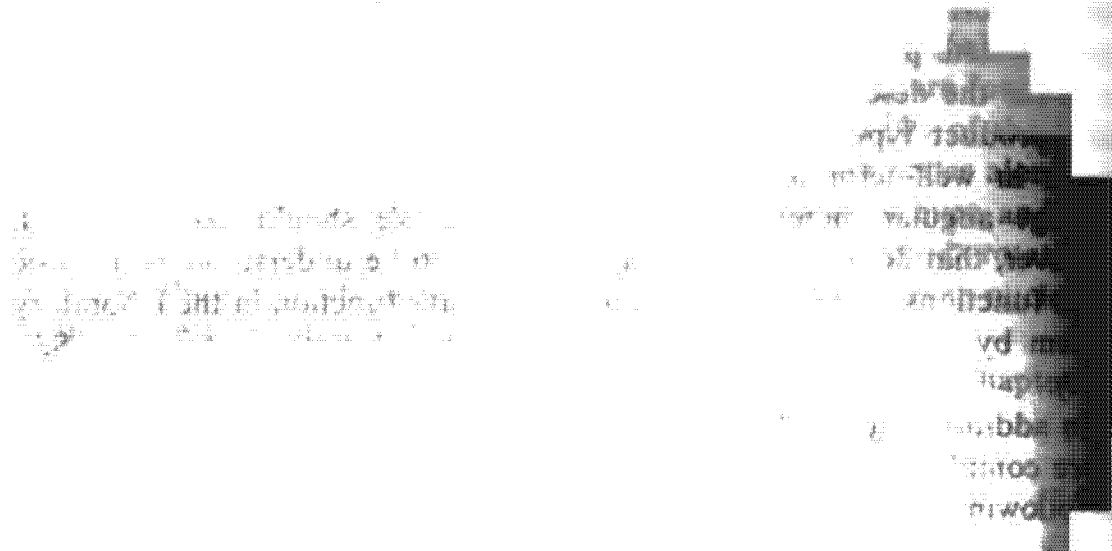
for $|\Phi\rangle$, wave functions of a more complicated structure (like TDA or RPA wave functions which are discussed in the next chapter; [Ho 68, CMR 75, Ma 77a, ERM 78, 80b]).

Let us finish this chapter with the following concluding remarks: HFB theory is a method which includes as many correlations as possible in a generalized static single-particle picture. It therefore defines two self-consistently determined fields [the order parameters (see Chap. 11)], an averaged potential Γ for the ph correlations, and a pairing potential Δ for the pp correlations. Within this theory, we are able to reproduce the ground state properties of spherical and deformed nuclei. It also can be used for the description of excited states with wave functions of generalized product type, such as pure quasi-particle excitations or rotational states in well-deformed nuclei. In the latter case a constraint on the average angular momentum must be used. We should keep in mind, however, that deformed wave functions have to be understood as intrinsic wave functions, from which we can get the wave function in the laboratory system by a projection onto eigenstates of angular momentum (see Sec. 11.4).

In addition, the HFB theory can be used to provide an optimal basis for more complicated methods to treat further correlations. This will be done in following chapters.

CHAPTER 8

Harmonic Vibrations



8.1 Introduction

In giving a microscopic description of the nuclear properties, until now we have used only static independent particle models. We have seen that by a proper definition of the particles or quasi-particles and by using an effective interaction, we are able within such a picture to explain the basic properties of the groundstates of many nuclei. Spectra of nuclear excitations are also very important for an understanding of the nuclear structure. If we perform an analysis of such spectra within the nuclear shell model or within the more elaborated independent particle models such as Hartree-Fock or Hartree-Fock-Bogoliubov, we find that a series of excited states can be very adequately explained by such models as *ph*- or two-quasi-particle excitations. But there are also many excited states with features that cannot be reproduced within the framework of shell model excitations, in spite of the fact that by introducing sophisticated methods involving the breaking of symmetries we are able to take into account important correlations among the nucleons.

If, for example, we restrict ourselves to spherically symmetric doubly magic nuclei like ^{16}O , ^{40}Ca , or ^{208}Pb , then the lowest excitations according to the harmonic oscillator approximation of the nuclear shell model should lie at about $\hbar\omega_0$. For ^{16}O the experimental shell difference between $1p$ and $2s-1d$ shells is roughly 11.5 MeV. In the spectrum of ^{16}O , however, we see amongst other states a ($J^\pi = 3^+$, $T=0$)-state at 6.14 MeV, and around 22

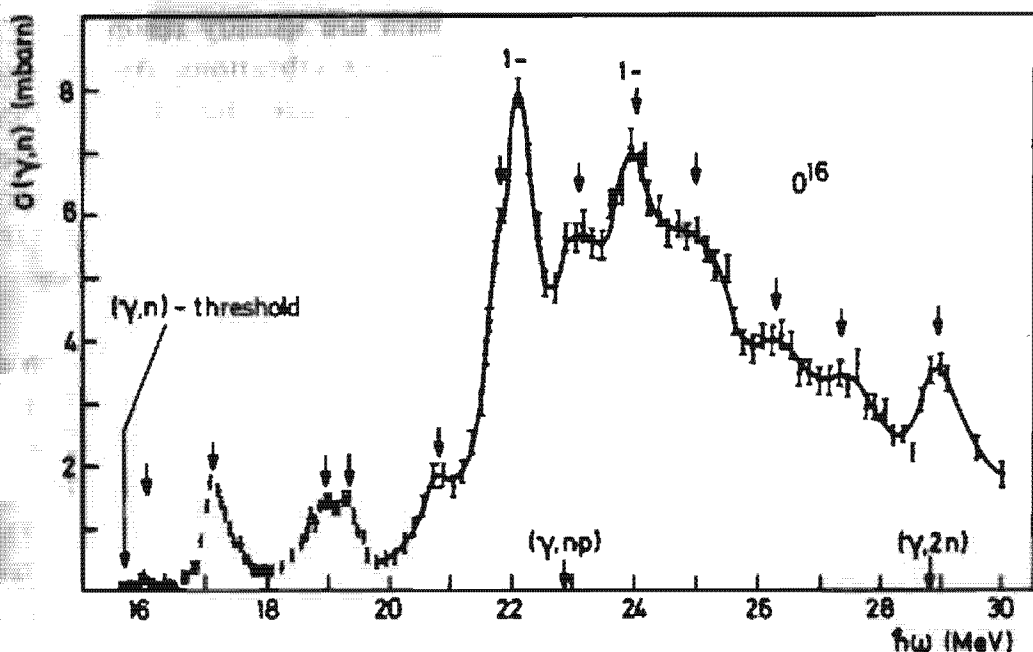


Figure 8.1. The cross section for (γ, n) processes as a function of the γ -energy (from [BCH 64]).

MeV a 5 MeV broad resonance which is usually called the giant dipole resonance (see Fig. 8.1) having the quantum numbers $J^\pi = 1^+$, $T = 1$.

It can be shown (see Sec. 8.3.3) that mainly $1\hbar\omega$ excitations are involved in this resonance. Therefore, the pure shell model also fails to explain the high energy of the giant dipole resonance.

It will turn out that these excitations can only be explained if we suppose that coherent participation by many nucleons takes place in the nucleus. What we understand by "coherent" can at the moment only be expressed in terms of the classical liquid drop approach to the nucleus (Chap. 1): Many nucleons are believed to take part in similar fashion to the shape vibrations of the nuclear drop. We will learn below what coherent means in the quantum mechanical sense. Such collective excitations furthermore generally fulfill the following criteria.

- Their electromagnetic transition probabilities have a collective strength such that they are one to two orders of magnitude larger than the single-particle transitions (see Sec. 2.7.2).
- They show up in the spectra of different nuclei over entire regions of the periodic table with great regularity. The giant dipole resonance, for instance, has been observed throughout the periodic table and its excitation energy varies slowly with mass number [$\propto 80A^{-1/3} + -1/6$, see Eq. (1.44)].

The spectra of spherical as well as deformed nuclei contain a variety of states that fulfill these criteria. We will restrict ourselves to the general methods which, within the context of the *residual interaction* Eq. (2.35)

$$V_R = \frac{1}{4} \sum_{kk', ll'} \bar{v}_{kk' ll'} a_k^+ a_{k'}^+ a_l a_{l'} - V_{HF}, \quad (8.1)$$

allow an explanation of the high-lying (which are usually resonances) as well as low-lying (usually bound states) collective vibrations. As indicated by Eq. (8.1), we will in the following mostly use the Hartree-Fock single-particle picture because it makes things somewhat less complicated. It should be emphasized, however, that all methods which we will present in the following sections generalize straightforwardly when using HFB quasi-particles (see Chap. 7) instead of particles. In certain cases we will also show this explicitly.

In Section 8.2, we study the interaction between *ph*-pairs based on an uncorrelated HF ground state (Tamm-Dancoff approximation TDA). In Section 8.3, different types of collective excitations are presented. Ground state correlations are taken into account in Section 8.4 within the random phase approximation (RPA) and it is shown that some problems inherent to the TDA method can be solved in this way. In Section 8.5, we show how the same equations can be derived with the formalism of linear response theory and what kind of features come into play when treating density dependent interactions. In Section 8.6 we present some numerical applications of the theory. Sum rules are an interesting means of extracting general properties of such resonances and of clarifying the relations between the quantum mechanical eigenstates of the RPA-Hamiltonian and the classical picture of surface vibrations. They are discussed in Section 8.7. Finally, Sections 8.8 and 8.9 are devoted to special extensions of the RPA, such as particle-particle RPA and quasi-particle RPA.

8.2 Tamm-Dancoff Method

8.2.1 Tamm-Dancoff Secular Equation

If we fill up the shell model potential with A nucleons up to a certain Fermi level, as shown in Fig. 8.2, then all zero, single, two, three, four, ..., N particle shell model excitations form a complete orthogonal set which can be used to expand the true many-nucleon wave functions of the ground state $|0\rangle$ or the excited states $|\nu\rangle$. The exact solution of the Schrödinger equation would then be obtained by a diagonalization of H in the full shell model space or, equivalently, by a variation of the following expansion coefficients. [In the following we restrict the indices m, n (i, j) to above (below) the Fermi level.]

$$|0\rangle = C_0^0 |\text{HF}\rangle + \sum_{mi} C_{mi}^0 a_m^+ a_i |\text{HF}\rangle + \frac{1}{4} \sum_{mnij} C_{mn,ij}^0 a_m^+ a_n^+ a_i a_j |\text{HF}\rangle + \dots \quad (8.2)$$

$$|\nu\rangle = C_0^\nu |\text{HF}\rangle + \sum_{mi} C_{mi}^\nu a_m^+ a_i |\text{HF}\rangle + \frac{1}{4} \sum_{mnij} C_{mn,ij}^\nu a_m^+ a_n^+ a_i a_j |\text{HF}\rangle + \dots \quad (8.3)$$

Ideally, the determinant $|\text{HF}\rangle$ would be given by filling up the N lowest single-particle levels of the Hartree-Fock potential. However, the latter is

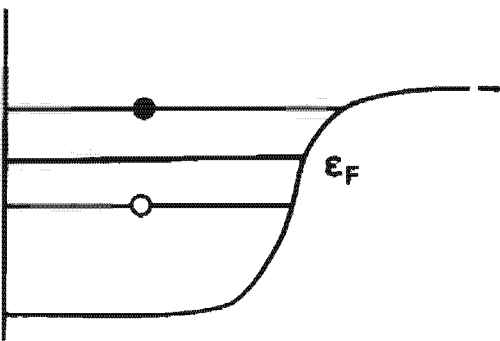


Figure 8.2. A *ph*-excitation in the shell model.

usually approximated by a phenomenological single-particle potential. The operator $a_m^+ a_i$ consequently annihilates a particle below ϵ_F (creates a hole) and creates a particle above ϵ_F . It is therefore called a particle-hole creation operator (Fig. 8.2).

The exact diagonalization of H within the full shell model space is a task which cannot be solved. Let us, however, suppose that it is reasonable in the expansion of the excited states $|\nu\rangle$ in Eq. (8.3) to go up to 1 particle-1 hole excitations only. We will see later that for certain kind of states this is indeed a very good approximation. *A priori* there are also reasons why this should be so. The subset of $1\Delta\omega$ particle-hole excitations are the shell model configurations lowest in energy and should therefore be important for low-lying states of negative parity. Transition probabilities of states which are excited by an electromagnetic field $F = \sum_{pp'} F_{pp'} a_p^+ a_{p'}$ are proportional to $|\langle 0|F|\nu\rangle|^2$ and these states are therefore believed to have dominant particle-hole contributions. We can thus hope to get a fair approximation for at least a certain class of states if we retain from the expansion (8.3) only the following terms

$$|\nu\rangle \approx C_0^* |\text{HF}\rangle + \sum_{mi} C_{mi}^* a_m^+ a_i |\text{HF}\rangle. \quad (8.4)$$

Since $\langle \text{HF} | H a_m^+ a_i | \text{HF} \rangle = 0$ [Eq. (5.35)], we see that the ansatz (8.4) implies that the ground state remains a determinant, whereas it is sufficient for the excited state to retain only

$$|\nu\rangle = \sum_{mi} C_{mi}^* a_m^+ a_i |\text{HF}\rangle. \quad (8.5)$$

The main drawback of this procedure is the fact that correlations are only taken into account for the excited states, whereas the ground state will be unchanged. Later we will see how we can build correlations into the ground state also.

Since the Hamilton operator commutes with the operator of total angular momentum I and in many cases also with the operator of total isospin T , we should use the ansatz (8.5) in a Clebsch-Gordon coupled form [see Eq. (2.46)]. In order not to spoil the simplicity of our formulae we shall omit them in the following unless they are absolutely necessary.

Using (8.5) as a variational ansatz, we obtain with

$$|\delta v\rangle = \sum_{mi} a_m^+ a_i |\text{HF}\rangle \delta C_{mi}' \quad (8.6)$$

as usual a secular equation for the determination of eigenvalues and expansion coefficients:

$$\sum_{nj} (\langle \text{HF} | a_i^+ a_m H a_n^+ a_j | \text{HF} \rangle - E_r \langle \text{HF} | a_i^+ a_m a_n^+ a_j | \text{HF} \rangle) C_{nj}' = 0. \quad (8.7)$$

With (5.35), we can get a more convenient form of Eq. (8.7):

$$\sum_{nj} \langle \text{HF} | a_i^+ a_m [H, a_n^+ a_j] | \text{HF} \rangle C_{nj}' = (E_r - E_0^{\text{HF}}) C_{mj}' \quad (8.8)$$

The commutator in (8.8) can easily be calculated with the use of Eqs. (5.25)

$$\begin{aligned} [H, a_n^+ a_j] &= \sum_r (i_m a_r^+ a_j - i_j a_n^+ a_r) \\ &\quad + \frac{1}{2} \sum_{rsi} \bar{v}_{rsni} a_r^+ a_s^+ a_i a_j - \frac{1}{2} \sum_{rsi} \bar{v}_{jrsi} a_n^+ a_r^+ a_i a_s. \end{aligned} \quad (8.9)$$

With the definition (5.37) of the Hartree-Fock single-particle energies ϵ_p and the rules for calculating the ground state expectation values of field operators (Appendix C) we finally obtain the so-called *Tamm-Dancoff equation*:

$$\sum_{nj} ((\epsilon_m - \epsilon_i) \delta_{mj} \delta_{ij} + \bar{v}_{mjln}) C_{nj}' = E_r^{\text{TDA}} C_{mj}' \quad (8.10)$$

[E_0^{HF} has been set to zero by a suitable choice of the energy scale and E_r^{TDA} is the excitation energy of $|v\rangle$ in Tamm-Dancoff approximation (TDA)].

For many purposes it has turned out to be useful to represent the matrix elements of the interaction \bar{v} graphically (Fig. 8.3):

$$\begin{aligned} \bar{v}_{mjln} &= \int \varphi_m^*(\xi_1) \varphi_l^*(\xi_2) v(\xi_1, \xi_2) \varphi_i(\xi_1) \varphi_n(\xi_2) d\xi_1 d\xi_2 \\ &\quad - \int \varphi_m^*(\xi_1) \varphi_j^*(\xi_2) v(\xi_1, \xi_2) \varphi_n(\xi_1) \varphi_i(\xi_2) d\xi_1 d\xi_2. \end{aligned} \quad (8.11)$$

The variable ξ stands symbolically for all coordinates and the integration shall include summation over spin and isospin. The rules for graphs are explained in many text books [AGD 63, Ma 67b] and since we do not want to present the graphical method as a tool by itself but rather as a pictorial representation of what we have derived analytically, we do not go into much detail here and simply give the prescription used to draw them. A wavy line shall stand for v and lines with arrows for the single-particle functions (arrow up-particle; arrow down-hole) which, according to their coordinates, are linked to the interaction points 1 and 2 of the wavy line. Furthermore, we usually agree that lines which are to the right of the interaction v in formula (8.11) point towards it, and that those lines to the left point away from it. With these conventions, \bar{v}_{mjln} can be displayed graphically, as shown in Fig. 8.3.

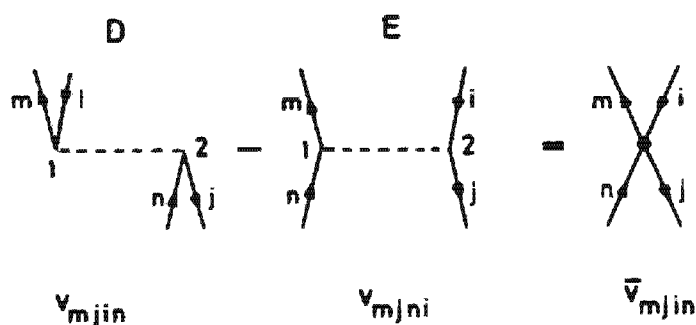


Figure 8.3. Graphical representation of the matrix elements v_{mjn} and v_{mjni} .

If we imagine a time scale perpendicular to the wavy line, a particle-hole pair nj is annihilated and another one created in the direct term D , whereas in the exchange term E a pair nj is scattered in a new one mi . Thinking of the wavy line as a pion, the meaning of "direct" and "exchange" becomes even clearer; process D being a pair creation and annihilation process (as in electrodynamics, in which the wavy line stands for the photon, the hole for the positron, and the particle for the electron). The graph E then represents a process in which a pion is exchanged between a particle-hole pair. Very often the direct plus exchange term is combined into one graph (Feynman graph), indicated in Fig. 8.3.

8.2.2 The Schematic Model

The solution of the Tamm-Dancoff equation is, in general, not obtained in the full particle-hole space, since this is a very big numerical task. Therefore, in most cases, only a "model" space is retained which includes several levels above and below ϵ_F . These calculations are also often called configuration mixing or shell model calculations. Before we go into more details, we want to study the qualitative features of the solutions of the TDA equation in a very simple model for which we can obtain the solution in an analytic form.

8.2.2.1. Solution of the TDA Equation with a Separable Interaction. The solution of Eq. (8.10) is greatly simplified if we assume that the matrix elements of the residual interaction are separable in the particle-hole indices (see Sec. 4.4.7 and [BB 59, BET 61])

$$\bar{v}_{mjn} = \lambda \cdot D_{mi} D_{nj}^*. \quad (8.12)$$

Further, it is assumed that the D_{mi} are matrix elements of a multipole operator as, for example, the quadrupole operator

$$D_{mi} = \langle m | r^2 Y_{2\mu}(\theta, \varphi) | i \rangle. \quad (8.13)$$

The multipolarity agrees, of course, with the angular momentum to which the particle-hole pair (m, i) is coupled. The matrix element (8.12) is certainly not antisymmetric as it should be. However, it turns out that the exchange term is small and neglecting it is a good approximation [BK 68,

Ma 74]. In general, the residual interaction is attractive for $T=0$ states (they are pushed down in energy as, for example, the $3^- T=0$ state in ^{16}O), and repulsive for $T=1$ states [BB 59]. Therefore, we have to choose

$$\begin{aligned} \lambda < 0 & \quad \text{for } T=0; \\ \lambda > 0 & \quad \text{for } T=1. \end{aligned} \quad (8.14)$$

There are reasons to believe that the ansatz (8.12) for the interaction is not as bad as it might look, but here we do not want to go into the philosophy of a separable force (see Sec. 4.4.7). Rather, we wish to consider (8.12) as a convenient simplification which allows us to study the qualitative features of the TDA solution.

With the ansatz (8.12), the secular equation (8.10) has the following form.

$$(E_r^{\text{TDA}} - \epsilon_m + \epsilon_i) C_{mi}' = \lambda D_{mi} \sum_{nj} D_{nj}^* C_{nj}'. \quad (8.15)$$

The states $|r\rangle$ should, of course, be normalized and with Eq. (8.5) we therefore have:

$$\sum_{mi} C_{mi}' C_{mi}' = \delta_{rr}. \quad (8.16)$$

With $\sum_{nj} D_{nj}^* C_{nj}' = \text{const.}$, we can solve Eq. (8.15) for the coefficients C_{mi}' :

$$\begin{aligned} C_{mi}' &= N \cdot \frac{D_{mi}}{E_r^{\text{TDA}} - \epsilon_m + \epsilon_i}; \\ N^{-2} &= \sum_{mi} \frac{|D_{mi}|^2}{(E_r^{\text{TDA}} - \epsilon_m + \epsilon_i)^2} \end{aligned} \quad (8.17)$$

Multiplying Eq. (8.15) by $D_{mi}^* (E_r^{\text{TDA}} - \epsilon_m + \epsilon_i)^{-1}$ and summing over m, i , we obtain an eigenvalue equation for the excitation energies E_r^{TDA} :

$$\frac{1}{\lambda} = \sum_{mi} \frac{|D_{mi}|^2}{E_r^{\text{TDA}} - \epsilon_m + \epsilon_i}. \quad (8.18)$$

We can solve Eq. (8.18) graphically by plotting the r.h.s. as a function of E_r^{TDA} . We thus obtain the eigenvalues from the intersection of this function with the straight line $1/\lambda$. All solutions are sandwiched between the original shell model excitations $\epsilon_{mi} = \epsilon_m - \epsilon_i$, only one solution being pushed up (if $1/\lambda > 0$) or down (if $1/\lambda < 0$). The assumption of a finite particle-hole space seems to enter into this argumentation, but we have to remember that *ph* shell model excitations of definite parity are grouped into bunches roughly $2\hbar\omega_0$ apart. Figure 8.4 thus represents just one of these bunches.

The one excitation which is pushed down ($T=0$) or up ($T=1$) is a state formed by a *coherent* superposition of all matrix elements of the residual interaction, as can easily be shown for the degenerate case to be discussed

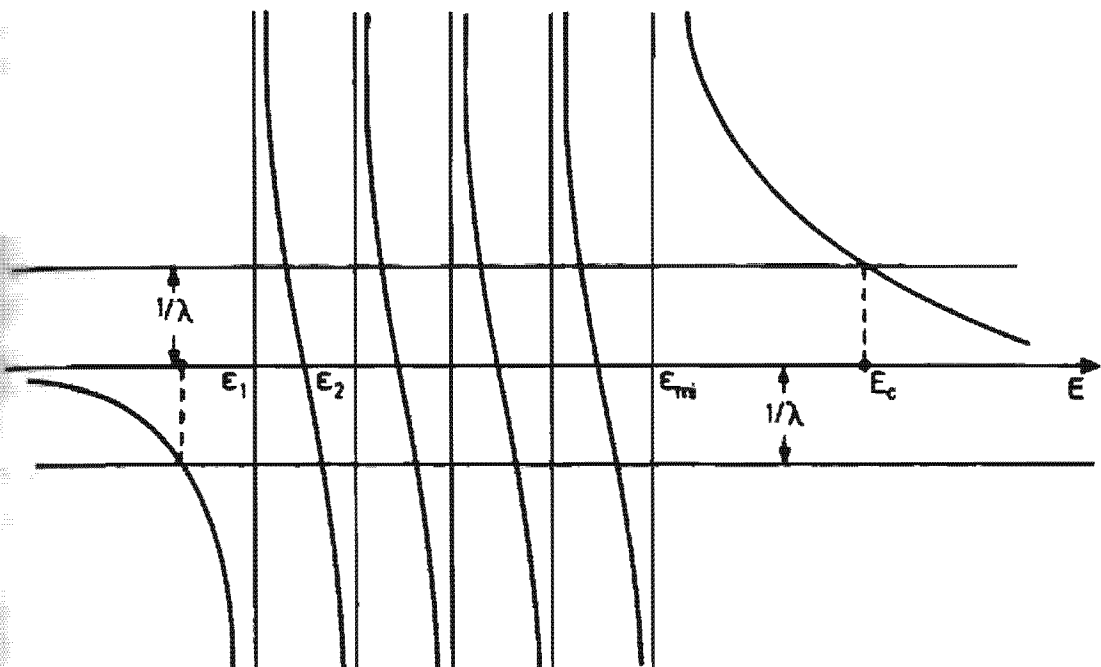


Figure 8.4. Graphical solution of Eq. (8.18).

next. By "coherent" we now mean that all matrix elements contribute with the same sign. Examples for such states are the first octupole states ($T=0$) appearing in ^{16}O , ^{40}Ca , and ^{208}Pb at low excitation energies and the giant dipole resonance ($T=1$), which we will turn to later.

8.2.2.2. Degenerate Case. If we set all ϵ_{mi} equal to ϵ , it follows from Eqs. (8.17, 8.18) that

$$C_{mi} = \left(\sum_{mi} |D_{mi}|^2 \right)^{-1/2} \cdot D_{mi}, \quad (8.19)$$

$$E_c^{\text{TDA}} = \epsilon + \lambda \sum_{mi} |D_{mi}|^2,$$

which means that collective state is being pushed up (down) by the sum of all diagonal elements of the interaction.

This degenerate case is realized, for example, if we take into account only one major shell for particles and another major shell for holes in a spherical oscillator potential without a spin orbit term. In reality things will not be so pronounced, but the essential features are likely to be preserved.

The collectivity of the shifted state can be demonstrated for the degenerate case by studying the partitioning of the total transition probability for the different excitations. For the collective state we have

$$|\psi_c\rangle = \left(\sum_{mi} |D_{mi}|^2 \right)^{-1/2} \sum_{mi} D_{mi} a_m^+ a_i |\text{HF}\rangle. \quad (8.20)$$

We therefore get, for the transition probability,

$$|\langle \psi_c | D | \text{HF} \rangle|^2 = \sum_{mi} |D_{mi}|^2, \quad (8.21)$$

a coherent superposition of the expansion coefficients (where the transition operator $D = \sum_{kk'} D_{kk'} a_k^* a_{k'}$ shall correspond to that for the separable interaction).

For the so-called sum rule (see Sec. 8.7), we get

$$\begin{aligned} \sum_{\nu} |\langle \nu | D | HF \rangle|^2 &= \sum_{\nu \neq \nu_c} \dots + |\langle \nu_c | D | HF \rangle|^2 \\ &= \sum_{\nu} \langle HF | D^+ | \nu \rangle \langle \nu | D | HF \rangle \\ &= \sum_{mi} \langle HF | D^+ | mi \rangle \langle mi | D | HF \rangle = \sum_{mi} |D_{mi}|^2. \end{aligned} \quad (8.22)$$

Here we replaced the complete set $|\nu\rangle$ in the ph space by the complete set $|mi\rangle$. Because of (8.21), we see that the total sum rule is exhausted by the collective state

This means that in the degenerate case there is no transition probability from the ground state to any non-collective state. On the other hand, the transition probability to the collective state (8.21) is drastically enhanced. We thus have a qualitative explanation for the strong 1^- resonance shown in Fig. 8.1.

8.2.3 Particle–Particle (Hole–Hole) Tamm–Dancoff Method

As we have seen in the case of doubly magic nuclei, the simplest correlations beyond Hartree–Fock can only be taken into account by breaking the HF core and raising a nucleon from below to above the Fermi level. In moving away from doubly magic nuclei, that is, by filling nucleons into the next open shell, a quite different type of correlation may be viewed as important. Since a magic nucleus is supposed to be quite a stable entity, the correlations among the valence nucleons alone seem to be responsible for a variety of experimental facts known about these nuclei. The $s-d$ shell nuclei ranging from ^{16}O to ^{40}Ca are perhaps the most studied examples of such “open shell” nuclei. A whole theory has been developed to treat such nuclei, known most widely under the heading of *shell model configuration mixing* calculations. Many ingredients of this theory can be found in the textbook of de Shalit and Talmi [ST 63], and the most advanced calculations within this theory have been performed by the Oak Ridge group [HMW 71] and by Whitehead [Wh 72]. In this section we only want to treat the simplest possible case of such nuclei, that is, we move away from the closed shell by only two particles, thus filling in two nucleons or removing two (creating two holes). In accordance with what we have said above, and by analogy to the ph -case, we may therefore try the following variational ansatz (*pp-TDA method*).

$$|\tau, A+2\rangle = \sum_{m < n} C'_{mn} a_m^* a_n^* |HF\rangle. \quad (8.23)$$

The coefficients C'_{mn} are supposed to be antisymmetric, that is, $C'_{mn} = -C'_{nm}$. In complete analogy to the ph -TDA case, we obtain the *pp-TDA* secular equation:

$$(E_{\tau}^{\text{TDA}} - \epsilon_m - \epsilon_n) C'_{mn} = \sum_{m' < n'} \delta_{mm'n'n'} C'_{m'n'}. \quad (8.24)$$

This is a linear Hermitian eigenvalue problem. The eigenvectors have to fulfill the norm and closure relations ($n < m$, $n' < m'$)

$$\sum_{m < n} C_{mn}^{T^*} C_{mn}^T = \delta_{rr}, \quad (8.25)$$

$$\sum_r C_{mn}^T C_{m'n'}^T = \delta_{mm'} \delta_{nn'}. \quad (8.26)$$

As indicated, the sum in principle runs over all levels $> \epsilon_F$ and therefore includes bound and continuum states. Since this generally gives rise to matrices too big for present day computers, we usually work in a restricted subspace, taking into account one or two major shells above the Fermi level. In order to account for the levels not included, we must take a suitably "renormalized" interaction (see Sec. 4.3.2). Equation (8.24) looks just the same for the hh -TDA case but the particle indices (m, n) are replaced by hole indices (i, j) and the sign of the single particle energies is reversed. The solutions of the $pp(hh)$ equation can exhibit features similar to the ph case. For instance, we can also get collective low-lying states, known mostly as *pairing vibrations* (see Sec. 8.3.5). Since the qualitative discussions would be very much the same as in the ph case, we will not go into greater detail. (For calculations in the lead region, see, for instance, [HK 72, MT 73] and references therein.)

8.3 General Considerations for Collective Modes

8.3.1 Vibrations in Quantum Mechanics

Perhaps this is the right place to interrupt our more or less formal discussion of the TDA method for a while and consider the nature of the collective states in more detail. In Chapter I we described states such as vibrations of a liquid drop. The word vibration may be puzzling in the quantum mechanical context, since we are in fact only dealing with stationary states. The density $\rho(r)$ of such a stationary state is time independent. The correspondence is roughly the same as talking about oscillations in the quantum mechanical harmonic oscillator problem. To get a time dependent density distribution $\rho(r, t)$ which vibrates around the ground state density $\rho^{(0)}(r)$ we have to investigate a *wavepacket*

$$|\Psi(t)\rangle = |0\rangle + \sum_\nu c_\nu |\nu\rangle e^{-iE_\nu t/\hbar} \quad (8.27)$$

which contains the ground state $|0\rangle$ and small admixtures of excited states $|\nu\rangle$. Up to first order in the coefficients c_ν the corresponding density is (see Appendix D):

$$\begin{aligned} \rho(r, t) &= \langle \Psi(t) | \sum_{i=1}^A \delta(r - r_i) | \Psi(t) \rangle \\ &= \rho^{(0)}(r) + \delta\rho(r, t) \end{aligned} \quad (8.28)$$

with

$$\delta\rho(r, t) = \sum_\nu c_\nu \langle 0 | \sum_{i=1}^A \delta(r - r_i) | \nu \rangle e^{-iE_\nu t/\hbar} + \text{c.c.} \quad (8.29)$$

A Fourier analysis of this density gives the contributions of the different excited states

$$\rho^{(1)\nu}(\mathbf{r}) = \langle 0 | \sum_{i=1}^A \delta(\mathbf{r} - \mathbf{r}_i) | \nu \rangle. \quad (8.30)$$

These quantities are called *transition densities*.

In general, we expect oscillations not only in the local part of the density as given in Eq. (8.28), but also in the nonlocal part, that is, we are interested in the transition density matrix. As discussed in Appendix D, in a shell model basis, it has the form

$$\rho_{pq}^{(1)\nu} = \langle 0 | a_q^\dagger a_p | \nu \rangle. \quad (8.31)$$

In the TDA approach these matrix elements are given by the coefficients $C_{\nu\nu}$ in Eq. (8.5), that is, in TDA we have

$$\rho_{nn}^{(1)\nu} = C_{\nu\nu}, \quad \rho_{ii}^{(1)\nu} = \rho_{nnn}^{(1)\nu} = \rho_{im}^{(1)\nu} = 0. \quad (8.32)$$

There are many different types of modes a nucleus can assume according to its various degrees of freedom: A nucleus can be deformed, displaced, or compressed; the densities of the protons and neutrons can vibrate *in* and *out* of phase; there can be vibrations in spin and isospin; we have pairing modes and many more things of which only a few elementary features will be discussed here (see also Chap. 13).

8.3.2 Classification of Collective Modes

Since we are dealing with harmonic vibrations in this chapter, in the following we want to investigate their qualitative properties in more detail. To see the basic structures we restrict our discussion to spherical closed shell nuclei. The best suited example is ^{208}Pb . These considerations do, however, also apply for the other regions in the periodic table. In fact, as we saw in the introduction, many of these collective excitations show rather classical properties which depend smoothly on the mass number.

Collective *ph*-vibrations can be characterized by the properties of the corresponding pair operators [Mo 76a+b]

$$(a^\dagger a). \quad (8.33)$$

There are a number of exact symmetries of the Hamiltonian such as rotational invariance, parity conservation, and charge conservation with the corresponding quantum numbers J , π and T . In addition, we have (as discussed in Sec. 2.6.3) the approximate isospin symmetry for light and heavy nuclei with the quantum number T . Since we start with a spherical closed shell nucleus in its ground state ($J^* = 0^+$), the angular momentum and the parity of the excitation are determined by the corresponding quantum numbers of the coupled pair $(a^\dagger a)_{J,\pi}$. The same also holds true in light ($N = Z$) nuclei (with $T = 0$ in the ground state) for the isospin. For

heavy nuclei, the isospin of the ground state is $T_0 = (N - Z)/2$ and it has to be coupled to the isospin of the ph pair to the total isospin $T = T_0$ or $T = T_0 + 1$.^{*} We usually classify the excitation by the numbers ΔT of the ph pairs $a^\dagger a$. Therefore, we have $\Delta T = 0$ or $\Delta T = 1$ excitations, and a $\Delta T = 1$ excitation does not necessarily mean $T = T_0 + 1$.

In addition to these general considerations about symmetries, which give, for instance, information about the angular distributions, we want to classify the collective motion more precisely according to the different degrees of freedom in the ph pair

$$a^\dagger(\mathbf{r}, s, t) a(\mathbf{r}', s', t'). \quad (8.34)$$

(a) In the first place, there are vibrations of the *local* density $\rho(\mathbf{r})$ of the nucleus in space. Since the angular dependence of such vibrations is already completely determined by the angular momentum, we only can allow for different *radial shapes*. The simplest examples in this context are the surface vibrations of a sphere with a sharp surface, which we have discussed in Section 1.4 in great detail. From Eq. (1.7) we find that the transition density (8.30) for such a surface vibration with a sharp surface is given by

$$\rho^{(1)}(r) = \begin{cases} \pm \rho_0 & \text{for } r \text{ between } R_0 \text{ and } R(\vartheta, \varphi), \\ 0 & \text{elsewhere,} \end{cases} \quad (8.35)$$

that is, the density in the nuclear interior stays constant. The entire transition is concentrated in the surface region.

We can also imagine other radial dependences of $\rho^{(1)}$, where the density in the interior is also changed. Such excitations are called *breathing modes*.

(b) A quite different type of motion, which also involves only the spatial degrees of freedom is given by vibrations in the nonlocal part of the transition density matrix $\rho^{(1)}(\mathbf{r}, \mathbf{r}')$. An example is the *nuclear twist* mode, where the local density of the nucleus stays unchanged and only the intrinsic velocity distribution oscillates (see [HE 77]).

(c) The isospin is an additional degree of freedom. There we have to distinguish between excitations in the same nucleus $\Delta T_z = 0$ and isospin flip processes $\Delta T_z = -1$, which belong to the neighboring nucleus with the charge $Z + 1$ and the neutron number $N - 1$. In the first case, the ph pair can be coupled to either $\Delta T = 0$ or to $\Delta T = 1$. For all the modes discussed so far, we therefore have two options: The protons can vibrate in phase ($\Delta T = 0$) or out of phase ($\Delta T = 1$) with the neutrons. At a fixed point \mathbf{r} we then eventually have an oscillating charge distribution. This corresponds to *polarization waves* in the nucleus. A case of vibrations with $\Delta T_z = -1$ is the analog resonances, which will be discussed in Section 8.3.4.

* $T = T_0 + 1$ is only possible in proton particle-neutron hole excitations that correspond to states in the neighboring odd-odd nucleus.

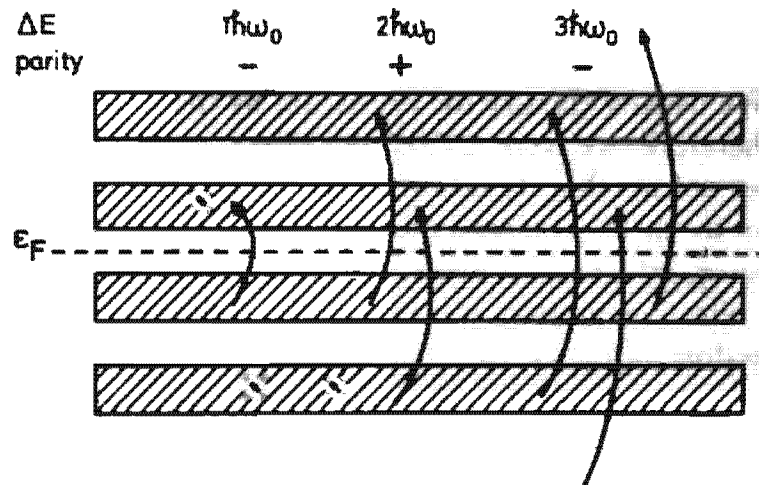


Figure 8.5. Schematic picture of the shell structure in a closed shell nucleus and possible $1p - 1h$ excitations.

(d) Finally, we also have the *spin* degree of freedom. The corresponding vibrations produce spin waves.

The classification of different modes given so far was, to a large extent, based on considerations within the coordinate space and emphasized its classical aspects. In finite realistic nuclei however, these modes are not precisely realized. There are always more or less drastic admixtures of less collective states. Therefore, it is often very useful to apply quite a different classification, based on the *shell model* in its simplest version—the harmonic oscillator.

Figure 8.5 shows schematically the shell structure for a closed shell nucleus (as ^{208}Pb). We have alternating shells with positive and negative parities separated by an energy distance of roughly $\hbar\omega_0$. For a closed shell nucleus, the Fermi surface lies just between two shells and we therefore find *ph*-pairs of a $1\hbar\omega_0$ excitation with negative parity, or a $2\hbar\omega_0$ excitation with positive parity, or a $3\hbar\omega_0$ excitation with negative parity, and so on. For nuclei between closed shells we also have, in addition, $0\hbar\omega_0$ excitations within the shell.

In realistic nuclei, the degenerate oscillator shells split up and a few levels with the wrong parity are shifted down into a lower shell by the $1s$ term. This also causes $1\hbar\omega_0$ excitations with positive parity for closed shell nuclei such as ^{208}Pb . But the basic features of this pictures also hold in realistic cases.

Although we have superpositions of many *ph* pairs in the collective excitation and drastic energy shifts due to the correlations as discussed in Section 8.2.2.2, this gross structure is conserved to a large extent.* For $j^* = 3^-$, for instance, we find a very collective state consisting mainly of $1\hbar\omega_0$ excitations and a second one consisting mainly of $3\hbar\omega_0$ excitations [MNS 76, St 79].

*One can also show this analytically in a schematic model with several bunches of degenerate levels in analogy to Sec. 8.2.2.2.

It is evident that this shell structure has a great influence on the excitation energy of the low-lying collective states (shown schematically in Fig. 1.6), because they depend closely on the ph energy of the lowest ph pair. In fact, here we observe drastic shell effects (see Fig. 1.7). For the high-lying states, the giant resonances, this is no longer the case. The energy distance between two major shells varies only smoothly over the periodic table [$\Delta\omega_0 \propto A^{-1/3}$; see Eq. (2.12)]. We therefore expect a similar smooth A -dependence of the resonance energy for giant resonances.

8.3.3 Discussion of Some Collective ph -Vibrations

In a sense the most trivial collective motion is a *translation* of the whole nucleus, generated by the linear momentum P . Since it commutes with the two-body Hamiltonian H , the exact ground state $|0\rangle$ is an eigenfunction of P . However, if we use an approximation $|0\rangle_{app}$ for the ground state which violates this symmetry, $P|0\rangle_{app}$ are new states. They look like collective excitations. We call them *spurious*, because they do not correspond to physical excitations. Within the angular momentum coupling scheme, their quantum numbers are $J=1^-$, $T=0$ (P is a vector operator that does not depend on the isospin). They correspond to a translation of the whole nucleus. There is no restoring force against this motion and therefore they should have zero excitation energy

$$HP|0\rangle_{app} = PH|0\rangle_{app} \approx E_0 P|0\rangle_{app}. \quad (8.36)$$

However, this depends on the approximation. For instance, in the TDA, $P|HF\rangle$ is a superposition of particle-hole states, which is generally not an eigenstate of the TDA equations (8.10). Instead, it is a mixture of all the TDA eigenstates, which form a complete set in the $1p - 1h$ space. Since its energy is nevertheless close to E_0 (Eq. 8.36), it has large components of the low-lying TDA states. This means some low-lying solutions of the TDA equation (8.10) have large spurious contributions. As long as we are working in a spherical basis with good spin and isospin, only the $J=1^-$, $T=0$ states are influenced. They have to be treated separately in order to extract the spurious components. For details, see Chapter 11.

The best known and the most thoroughly investigated giant resonance is the *giant dipole state* (see for instance [Sp 68]). It is a several MeV broad resonance, which has been observed over the whole periodic table at an energy of roughly

$$E_{1^-} \propto 80A^{-1/3+ -1/6} [\text{MeV}]. \quad (8.37)$$

A typical case is shown in Fig. 8.1. The experimental spectrum usually shows some fine structure. It has its origins in the specific properties of nuclei and is not constant over the periodic table. Particular ph -components may show up—as in ^{16}O [EF 57]—or shell effects may cause a splitting of the resonance. For instance, passing from spherical to de-

formed nuclei, we observe two kinds of dipole vibrations, one parallel to the symmetry axis and one orthogonal to it. The splitting of the energies allows an experimental determination of the deformation parameter [Da 58, Ok 58, BBC 71].

The giant dipole resonance is excited, for instance, by photo-absorption of γ -radiation. In Section B.7 we derive the cross section for the excitation of a final state $|\nu\rangle$ by a photon of energy E

$$\sigma_\nu(E) = \frac{4\pi^2 e^2}{\hbar c} (E - E_0) |\langle \nu | D | 0 \rangle|^2 \delta(E - E_\nu + E_0). \quad (8.38)$$

D is the dipole operator (B.88) for $E1$ -radiation in the z -direction.

$$D = \frac{NZ}{A} \left(\frac{1}{Z} \sum_{p=1}^Z z_p - \frac{1}{N} \sum_{n=1}^N z_n \right) = - \sum_{i=1}^A t_3^{(i)} (\mathbf{r}_i - \mathbf{R})_z. \quad (8.39)$$

It is proportional to the z -component of the distance between the two centers of gravity for protons and neutrons.

The total cross section for dipole absorption σ_{total} is obtained from (8.38) by summing over all final states $|\nu\rangle$ and integrating over the energy:

$$\sigma_{\text{total}} = \sum_\nu \int_0^\infty \sigma_\nu(E) dE = \frac{4\pi^2 e^2}{\hbar c} \sum_\nu (E_\nu - E_0) |\langle \nu | D | 0 \rangle|^2. \quad (8.40)$$

It is proportional to the energy-weighted dipole sum rule (see also Sec. 8.7)

$$S_1(D) = \sum_\nu (E_\nu - E_0) |\langle \nu | D | 0 \rangle|^2 \quad (8.41)$$

and can be evaluated in closed form:

$$S_1(D) = \frac{1}{2} \langle 0 | [D, [H, D]] | 0 \rangle,$$

where H is the exact two-body Hamiltonian and $|0\rangle$ is the exact ground state. If we assume that the two-body potential has no velocity dependence and no exchange mixtures (Wigner force), we easily calculate in analogy to (8.158):

$$\langle 0 | [D, [H, D]] | 0 \rangle = \frac{NZ}{A} \frac{\hbar^2}{m}. \quad (8.42)$$

For the dipole sum we therefore have the Thomas-Reiche-Kuhn sum rule:

$$\sigma_{\text{total}} = \int_0^\infty \sigma(E) dE = \frac{2\pi^2 e^2 \hbar}{mc} \frac{NZ}{A} \simeq 0.06 \frac{NZ}{A} [\text{MeV} \cdot \text{barn}]. \quad (8.43)$$

This value is enlarged by 40–80% if the two-body interaction contains exchange mixtures (see, e.g., Brenig [Br 65b]) and tensor forces [WKB 73], which then seems to yield roughly the right magnitude of the overall energy integrated cross section. It thus turns out that in ^{16}O approximately 3% of the dipole sum lies in low-lying 1^- states, which are almost pure shell model $p-h$ resonances below 20 MeV, whereas the giant resonance peak contains about 50%, clearly reflecting its collective character. The rest of the dipole sum is to be found beyond 30 MeV [ABC 63, FH 62a, b, Ha 65b, BS 64, ADW 78]. For heavy nuclei the giant dipole resonance can

exhaust up to 100% of the sum rule. The experiment therefore shows that a very large part of the dipole sum (8.43) is exhausted by the giant dipole resonance, and this means that this resonance has a large overlap with the state

$$|D\rangle = D|0\rangle = \frac{NZ}{A} \left\{ \frac{1}{Z} \sum_{pp'} \langle p|z|p'\rangle a_p^+ a_{p'} - \frac{1}{N} \sum_{nn'} \langle n|z|n'\rangle a_n^+ a_{n'} \right\} |0\rangle, \quad (8.44)$$

which has become known as the Goldhaber-Teller state [GT 48] (see Sec. 13.3.3).

The quantum numbers of the state are identical with those of the giant resonance $I^\pi = 1^-$. In the case of the isospin, we have to distinguish two cases.

- (a) For light $N = Z$ nuclei the Coulomb force can be neglected. The ground state $|0\rangle$ then has $T = 0$. The operator D is a vector in isospin space, as we see from Eq. (B.88). Angular momentum coupling rules therefore show that $D|0\rangle$ has $T = 1$.
- (b) For heavy nuclei the isospin is again conserved. The ground state has $T_0 = (N - Z)/2$. Using similar arguments as in Sec. 2.6.3 we can convince ourselves that the dipole state $|D\rangle$ has the same isospin T_0 by showing that

$$T_+ |D\rangle \approx 0. \quad (8.45)$$

This does not, however, mean that there are no other 1^- states with $T = T_0 + 1$ in the excitation spectrum of the nucleus. We simply do not excite them by dipole γ -rays.

The structure of the operator D shows that the giant dipole resonance consists mainly of $1\hbar\omega_0$ excitations. Because of the repulsive character of the residual interaction it is shifted to higher energies.

Besides this well known dipole state, in the last ten years a number of other giant resonances of higher multipolarity have been found. The *giant quadrupole resonance* is especially well established over the whole periodic table at an energy somewhat less than the giant dipole resonance [PW 71, FT 72, LB 72, HGA 74, Sa 74, KWB 75, YMR 76, Be 76]

$$E_{2+} \approx 60 - 65 A^{-1/3} [\text{MeV}]. \quad (8.46)$$

It exhausts 40–100% of the energy weighted sum rule of the isoscalar quadrupole operator*

$$r^2 Y_{20}. \quad (8.47)$$

* Unfortunately, in a direct comparison with experiment we cannot use photo-absorption, as in the dipole case, because (i) the photon field does not contain the isovector part for $\lambda > 1$, and (ii) in practice the photonuclear reactions proceed primarily through the dipole mode. The most important experimental tool used to excite such vibrations is inelastic scattering of electrons and heavier particles such as protons, deuterons, and alpha particles [Sa 76]. The corresponding excitation operators have a more complicated structure (see, for instance, [Ue 71, Sa 72a + b, 74, HMS 75] and the sum rules are no longer model independent. Therefore, we will not go into the details of the analysis of such experiments.

It consists, as numerical calculations show [RS 74a], mainly of $2\hbar\omega_0$ excitations, and is shifted downwards in energy by the residual interaction to around $1.4\hbar\omega_0$.* (The corresponding isovector mode is expected at $3.3\hbar\omega_0$ [Ha 72].) The rest of the isoscalar quadrupole strength lies in the low-lying collective 2^+ state, which shows drastic shell effects (Fig. 1.7) and consists mainly of $0\hbar\omega_0$ excitations.

Recently, a *breathing mode* was also observed [MMW 75, ST 77, HBI 77, YRM 77, BBL 80], a spherical density oscillation with the quantum number $J^\pi = 0^+$, $T=0$. As we shall see in Fig. 8.14, its transition density is not only concentrated on the nuclear surface but involves changes of the nuclear density over the whole volume. Its excitation energy lies at

$$E_0 \simeq 80A^{-1/3} \text{ MeV.} \quad (8.48)$$

This energy is a direct measure of the nuclear incompressibility (5.95) [Wa 62a, BGG 76]. In ^{208}Pb the experimental breathing mode lies at 13.8 MeV, a value corresponding to $K \simeq 200$ MeV, which is in good agreement with theoretical predictions [RS 74a, SZR 74, WMR 77].

* In deformed regions we observe a splitting of the giant quadrupole resonance into three components with $K=0, 1$ and 2 [KMY 75].

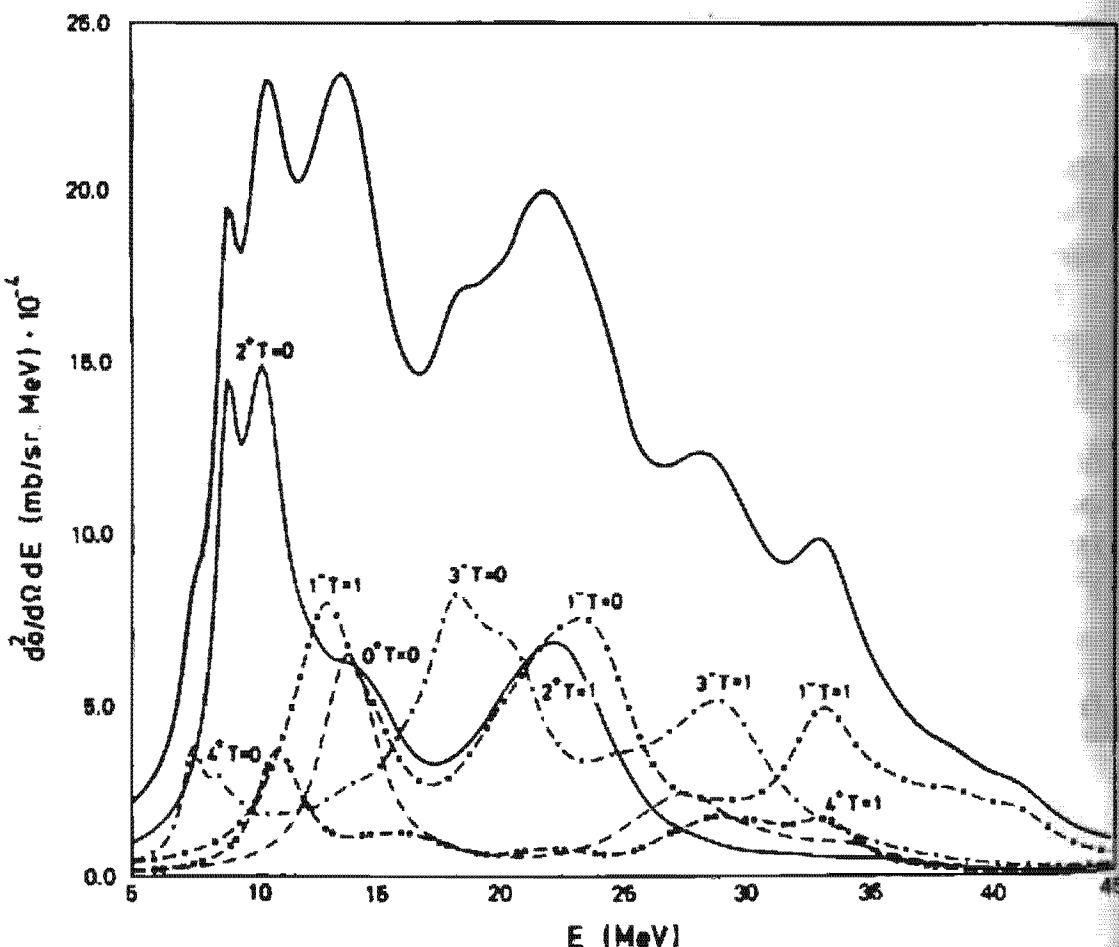


Figure 8.6. The electron spectrum for 90 MeV (e, e') at 75° calculated with microscopic RPA wave functions. The numbers in the figure denote the angular momentum parity and isospin of the corresponding cross-section contribution. The thick line is the sum of all the different contributions. (From [WKS 78].)

Magnetic resonances are excited by operators which involve the spin and the orbital angular momentum operators. They have the quantum numbers $1^+, 2^-, 3^+, \dots$ and have been predicted by several calculations (see, for instance, [RS 74a, SWK 76, FRS 78]). Their experimental evidence, however, is still an object of discussion.

Further giant resonances in the spectra have been observed in various experiments (see, for instance, [PBD 74, TIS 75, Pa 75a, SEB 74]), but the spin and parity assignments are not completely established. As an illustrative picture we show in Fig. 8.6 a calculation of the (e, e') spectrum for the giant resonance region of ^{208}Pb . We see clearly that the total spectrum can only be obtained by a complicated superposition of rather different resonances.

8.3.4 Analog Resonances

Nuclear reactions for heavy nuclei ($N > Z$), like, for example, $^{208}\text{Pb} (p, n) ^{208}\text{Bi}$, exhibit strong collective resonances called *analog states* for reasons we will learn about in a moment.*

To explain the structure of these states we use the fact that the nuclear wave functions in heavy nuclei are, to a rather good approximation, eigenstates of the isospin operator T^2 (see Sec. 2.6.3). The ground state and the low-lying excited states have the quantum numbers $T = T_3 = (N - Z)/2$.

Starting from such a state $|I, T, T_3 = T\rangle$ at an energy E , we can define its *analog state* by the application of the isospin lowering operator T_- .

$$T_- |I, T, T_3 = T\rangle = \sqrt{2T} |I, T, T_3 = T-1\rangle. \quad (8.49)$$

It belongs to the "daughter" nucleus ($N - 1, Z + 1$) and is again an eigenstate of H with the energy

$$E_a = E + \Delta_c. \quad (8.50)$$

To see this we decompose the exact Hamiltonian H into the nuclear part H_{nuc} which commutes with T_- and the Coulomb interaction V_c

$$HT_- = (H_{\text{nuc}} + V_c)T_- = T_- H + [V_c, T_-]. \quad (8.51)$$

The commutator $[V_c, T_-]$ is of the form

$$\begin{aligned} [V_c, T_-] &= \sum_{i < j} V_c(i, j) \left[\left(\frac{1}{2} - t_i^{(0)} \right) \left(\frac{1}{2} - t_j^{(0)} \right), T_- \right] \\ &= \sum_i V_c(i) t_i^{(0)} \end{aligned} \quad (8.52)$$

with the average Coulomb field

$$V_c(i) = \sum_{j \neq i} V_c(i, j) \left(\frac{1}{2} - t_j^{(0)} \right). \quad (8.53)$$

Under the assumption that this single-particle potential in the interior of the nucleus has a constant value of roughly Δ_c (see Fig. 2.7), we obtain for each eigenstate $|n\rangle$ of the "parent" nucleus (N, Z) an analog state $T_-|n\rangle$ in the

* For the literature, see, for instance, [AHK 72].



Figure 8.7. Schematic representation of the spectrum of analog states.

"daughter" nucleus ($N - 1, Z + 1$)

$$HT_-|n\rangle = E_n T_-|n\rangle + [H, T_-]|n\rangle \approx (E_n + \Delta_e)T_-|n\rangle. \quad (8.54)$$

This means that in the daughter nucleus there is a sequence of states with the same energy spacings as the low-lying levels of the parent nucleus itself, having isospin

$$T = \frac{N - Z}{2} = \frac{N - Z - 2}{2} + 1, \quad (8.55)$$

which is one unity larger than the isospin of the daughter nucleus ground state (Fig. 8.7).

In order to learn more about the structure of the analog resonances we will forget for the moment the residual interaction used in the description of the ground state of the parent nucleus (N, Z). This will be given by a pure shell model description, represented graphically in Fig. 8.8.

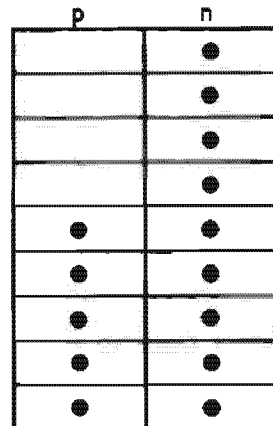


Figure 8.8. Schematic representation of a pure shell model determinant.

We assume that the protons and neutrons, which occupy the states with the same quantum numbers (besides I_3 , of course) form an inert core and are coupled to $T=0$. In the following, we shall neglect this inert core, so that the ground state of the mother nucleus is given by

$$|I, T, I_3 = T\rangle = \begin{array}{c} \text{p} \\ \hline \text{n} \end{array} \quad . \quad (8.56)$$

p	n
	●
	●
	●
	●

With $T_- = \sum_i \mu_i^{(0)}$, we obtain for the analog state of the daughter nucleus:

$$\begin{aligned} |I, T, T=1\rangle &= \frac{1}{\sqrt{2T}} \left\{ \begin{array}{c} \text{Diagram 1: } \begin{array}{|c|c|c|} \hline & \bullet & \\ \hline \bullet & & \\ \hline & \bullet & \\ \hline \end{array} \\ + \begin{array}{|c|c|c|} \hline & \bullet & \\ \hline \bullet & & \\ \hline & \bullet & \\ \hline \end{array} + \begin{array}{|c|c|c|} \hline & \bullet & \\ \hline \bullet & & \\ \hline & \bullet & \\ \hline \end{array} + \begin{array}{|c|c|c|} \hline \bullet & & \\ \hline & \bullet & \\ \hline & \bullet & \\ \hline \end{array} \end{array} \right\} \\ &= \frac{1}{\sqrt{2T}} \sum_{\mu} |\mu\rangle. \end{aligned} \quad (8.57)$$

The analog state in Eq. (8.57) is a coherent superposition of certain *ph*-states formed by replacing, in (8.56), the neutrons by protons one by one in the corresponding states.

There are, of course, other linear combinations of the states $|\mu\rangle$ orthogonal to the analog state $|I, T, T_3 = T-1\rangle$:

$$\sum_{\mu} c_{\mu} |\mu\rangle \quad \text{with} \quad \sum_{\mu} c_{\mu} = 0.$$

The operator T_+ annihilates them

$$T_+ \sum_{\mu} c_{\mu} |\mu\rangle \propto \left(\sum_{\mu} c_{\mu} \right) \cdot |I, T, T_3 = T\rangle = 0. \quad (8.58)$$

Therefore, they must have isospin $T-1$, which is the isospin of the ground state of the daughter nucleus. Without residual interaction they lie at the same energy as the analog state and have equal spin and parity.

Experimentally, the analog states are observed as very sharp resonances at high energies [AW 61]. Their width is so small, because the isospin selection rule forbids a rapid decay into the other states which form a continuous background.

To see how they can be treated with the TDA, we start with a HF potential which is the same for protons and neutrons. Only the energy levels of protons and neutrons are shifted with respect to one another by an amount $\Delta_s = \Delta_c - \Delta_n$ [see Eq. (2.27)]. The quantity Δ_s has its origin in the symmetry energy. In our approximation this is the only difference in the self-consistent potential of protons and neutrons resulting from the nuclear force.

If we diagonalize the residual interaction in the space of the states $|\mu\rangle$ we obtain a splitting between the analog resonance and the other states. Assuming a separable force we end up with the degenerate model of Section 8.2.2.2. Again, it concentrates all strength in the analog state and shifts its energy from the unperturbed value $\Delta_c = \Delta_c - \Delta_n$ to its proper value Δ_c , because it is exactly the proton-neutron interaction which causes the symmetry energy Δ_s . For details, see the textbook of G. E. Brown [Br 64, (second edition 1967)] and other references cited in the review article [AHK 72].

8.3.5 Pairing Vibrations

As indicated in the treatment of the $pp(hh)$ -TDA method, there is a great formal similarity between the *ph* and $pp(hh)$ cases. In fact, it also turns out that there are collective $pp(hh)$ solutions of the corresponding TDA equation (8.24). A good example is the 0^+ ground state of ^{206}Pb . The amplitudes C'_{mn} according to Eq. (8.23) enter directly into the expression of, for

example, a ^{208}Pb (p, t) ^{206}Pb pickup or a ^{208}Pb (t, p) ^{210}Pb stripping cross section [Gl 65]. The fact that the 0^+ ground state of ^{206}Pb is populated by such a reaction an order of magnitude larger than the other 0^+ states of ^{206}Pb , clearly indicates the coherent contribution of the C_p^{0+} amplitudes and therefore the collectivity of this state. Similar to this is the situation for ^{210}Pb . These rather strongly bound entities of two particles in (0^+) states is due to the short-range part of the interaction and has already been discussed at the beginning of Chapter 6. Two particles form such a stable entity that they can be multiplied, added to, or removed from a nucleus (like, for example, ^{208}Pb) almost like independent particles (which behave very much like bosons because of their integer spin). The spectrum should therefore be approximately harmonic which, in fact, is the case for the lead isotopes (Fig. 8.9) [BM 75]. This harmonic spectrum is what has been termed the spectrum of "pairing vibrations." We can also produce excited 0^+ pairing vibrations in these nuclei. For example, let us remove from ^{208}Pb a 0^+ pairing phonon, which leads us to ^{206}Pb . At the same time, let us add a phonon leading from the ^{208}Pb to the ^{210}Pb ground state; this clearly gives an excitation in ^{208}Pb $2\Delta\Omega$ apart and indeed such a strongly excited state in ^{210}Pb (p, t) ^{208}Pb and ^{206}Pb (t, p) ^{208}Pb reactions is very well known and lies at 4.9 MeV in ^{208}Pb .

The fact that particle-particle correlations lead to collective nuclear modes—now usually called pairing vibrations—was recognized by H. Schmidt [Sch 64a, b] and Bohr [Bo 64] and worked out in much detail later on by Bès and Broglia [BB 66] (for a review see [BHR 73] and the references therein).

It is a quite general concept which describes the pairing correlations on the same level as the deformations. Starting from a spherical closed shell nucleus, we can excite *quadrupole vibrations*, which have an *angular momentum* different from the ground state, and *pairing vibrations*, which belong to nuclei with a different *particle number*. Ground state correlations induced by such vibrations (see Sec. 8.4.6) give in the first case a virtual quadrupole deformation and in the second case a virtual excitation of collective $2p - 2h$ states. As we go away from a closed shell, the nuclei get softer, that is, the correlations get larger. Finally we get a phase transition to deformed states—induced by the *ph*-correlations; or to superfluid states—induced by

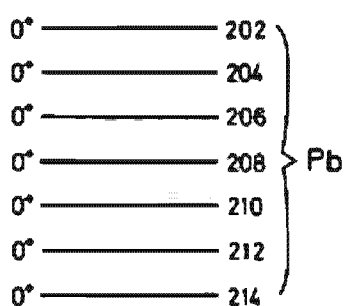


Figure 8.9. Schematic representation of the ground state energies in the even Pb isotopes.

the pp -correlations. In such a case, we have a condensate of quadrupole or pairing bosons (see Sec. 8.8.2).

We know that we have surface vibrations in deformed nuclei. These are oscillations around a stable deformation. In the same way, we can have pairing vibrations in superfluid nuclei. They correspond to oscillations of the gap parameters around their ground state values.

8.4 Particle-Hole Theory with Ground State Correlations (RPA)

One feature of our approximate ansatz (8.5) was the fact that we could build correlations into the excited states; the ground state however, remains unchanged in the TDA method. This complete neglect of the residual interaction V_R in the ground state certainly influences the results. To remove this drawback of the TDA method, we could think of retaining also the $(2p - 2h)$ components in Eq. (8.2). This is not practicable, since the corresponding matrices would become prohibitively large. One way out is a generalization of the TDA method in which we take, instead of the HF ground state, one in which a certain class of correlations has been summed. Although the discussion of the problem stays more or less the same as for the TDA method, we will have to pay a certain price for this refinement of our theory. Our new equations will no longer follow out of a variational principle, and thus we can generally get imaginary solutions. We will derive the new equations [random-phase approximation (RPA)]* in close analogy to the TDA method using a different technique which will suggest quite naturally the necessary generalizations leading to the RPA.

8.4.1 Derivation of the RPA Equations

To get a better understanding of what is done in the random phase approximation, we will first re-derive the TDA equations using a different technique, the so-called equation of motion method [Ro 68a, 70]. We start with a set of exact eigenstates of the Hamiltonian H

$$H|\nu\rangle = E_\nu |\nu\rangle. \quad (8.59)$$

It is possible to define operators[†] Q_ν^+ and Q_ν in such a way that

$$|\nu\rangle = Q_\nu^+ |0\rangle \quad \text{and} \quad Q_\nu |0\rangle = 0. \quad (8.60)$$

*This approximation has been introduced by Bohm and Pines [BP 53] in the theory of plasma oscillations. Other derivations have been given by several authors [GB 57, Hu 57, Sa 57, An 58].

[†]The frequent use later on of the letter Q in the sense of a coordinate should not be confused with its present meaning.

Q_v^+ , for example, can be chosen as

$$Q_v^+ = |v\rangle\langle 0|.$$

From the Schrödinger equation (8.59) we get the equation of motion

$$[H, Q_v^+]|0\rangle = (E_v - E_0)Q_v^+|0\rangle. \quad (8.61)$$

Multiplying from the left with an arbitrary state of the form $\langle 0|\delta Q$ we get*

$$\langle 0|[\delta Q, [H, Q_v^+]]|0\rangle = (E_v - E_0)\langle 0|[\delta Q, Q_v^+]|0\rangle. \quad (8.62)$$

We can use the commutator, because $\langle 0|Q_v^+ = \langle 0|HQ_v^+ = 0$. Until now we were exact and, since the variation of $\delta Q|0\rangle$ exhausts the whole Hilbert space, (8.62) corresponds to the full Schrödinger equation (8.59). First we re-derive the TDA equation (8.10) by approximating the exact ground state $|0\rangle$ by the HF state $|\text{HF}\rangle$ and the operator Q_v by the collective ph -operator

$$Q_v^+ = \sum_{mi} C'_{mi} a_m^+ a_i. \quad (8.63)$$

By this approximation, we restrict ourselves to the space of $1p-1h$ excitations, that is, we set, $\delta Q|0\rangle = \sum_{mi} a_m^+ a_i |\text{HF}\rangle \delta C_{mi}$ and from (8.62) get

$$\sum_{nj} \langle \text{HF} | [a_m^+ a_i, [H, a_n^+ a_j]] | \text{HF} \rangle C'_{nj} = E_v^{\text{TDA}} C'_{nn}, \quad (8.64)$$

where E_v^{TDA} is the excitation energy in TDA approximation. This is exactly the TDA equation we derived earlier (8.10). In deriving this equation we have not used a variational principle this time. The above procedure has, however, the advantage that it can be generalized in a straightforward way. There is no reason why we should not use, in Eq. (8.63), a more general vibration creation operator which then also implies, as we shall see, a more general ground state. If we think of a ground state containing $2p-2h$ correlations, as indicated by Eq. (8.2), we can not only create a ph pair but also destroy one. The most straightforward generalization of Eq. (8.63) is therefore:

$$Q_v^+ = \sum_{mi} X'_{mi} a_m^+ a_i - \sum_{mi} Y'_{mi} a_i^+ a_m, \quad (8.65)$$

where the minus sign has been chosen for convenience. The RPA ground state $|\text{RPA}\rangle$ is defined by analogy to (8.60) by†

$$Q_v^+ |\text{RPA}\rangle = 0. \quad (8.66)$$

We will later on deduce from this condition an explicit expression for the ground state. Instead of only one matrix C'_{mi} we now have two matrices X'_{mi} and Y'_{mi} . We also have two kinds of variations $\delta Q|0\rangle$, namely $a_m^+ a_i|0\rangle$ and

* If we express Q by the operators $a_p^+ a_q$, $a_p^+ a_q^+ a_r a_s$ with coefficients C_{pq} and C_{pqrs} , then δQ is given by $\partial Q / \partial C \cdot \delta C$ for arbitrary variations δC .

† One usually assumes $|\text{RPA}\rangle$ to be the ground state of an even system with closed shells ($J'' = 0^+$). Rowe et al. also investigated the possibility of constructing an RPA based on an open shell configuration (open shell RPA; see [RW 69, 70, NR 71, RN 75]).

$a_i^+ a_m |0\rangle$. Therefore, from (8.62) we get two sets of equations:

$$\begin{aligned}\langle \text{RPA} | [a_i^+ a_m, [H, Q_r^+]] | \text{RPA} \rangle &= \hbar\Omega_r \langle \text{RPA} | [a_i^+ a_m, Q_r^+] | \text{RPA} \rangle, \\ \langle \text{RPA} | [a_m^+ a_i, [H, Q_r^+]] | \text{RPA} \rangle &= \hbar\Omega_r \langle \text{RPA} | [a_m^+ a_i, Q_r^+] | \text{RPA} \rangle, \quad (8.67)\end{aligned}$$

where $\hbar\Omega_r$ is the excitation energy of the state $|\nu\rangle$. These equations contain only expectation values of four Fermion operators, which are still very complicated to calculate, because we do not as yet know the ground state $|\text{RPA}\rangle$.

We content ourselves with an approximation usually known as the "quasi-boson approximation" [BET 61, Br 64]. If we assume that the correlated ground state does not differ very much from the HF ground state, we can calculate all expectation values in the HF approximation, for example,

$$\begin{aligned}\langle \text{RPA} | [a_i^+ a_m, a_n^+ a_j] | \text{RPA} \rangle &= \delta_{ij} \delta_{mn} - \delta_{mn} \langle \text{RPA} | a_j a_i^+ | \text{RPA} \rangle \\ &\quad - \delta_{ij} \langle \text{RPA} | a_n^+ a_m | \text{RPA} \rangle \\ &\simeq \langle \text{HF} | [a_i^+ a_m, a_n^+ a_j] | \text{HF} \rangle = \delta_{ij} \delta_{mn}. \quad (8.68)\end{aligned}$$

The name "quasi-boson" approximation comes from the fact that Eq. (8.68) would be an exact relation if the *ph* creation and annihilation operators obeyed the commutation relations for boson field operators. Equation (8.68), however, violates the Pauli principle because we have neglected terms coming from the commutator. The quality of this approximation can only be checked from realistic calculations (see also Chap. 9).

Within the quasi-boson approximation, the amplitudes X'_{mi} and Y'_{mi} have a very direct meaning: their absolute squares give the probability of finding the states $a_m^+ a_i |0\rangle$ and $a_i^+ a_m |0\rangle$ in the excited state $|\nu\rangle$, that is, the *ph* and *hp* matrix elements of the transition density $\rho^{(1)}$ of equation (8.31):

$$\begin{aligned}\rho_{mi}^{(1)*} &= \langle 0 | a_i^+ a_m | \nu \rangle \simeq \langle \text{HF} | [a_i^+ a_m, Q_r^+] | \text{HF} \rangle = X'_{mi}, \\ \rho_{im}^{(1)*} &= \langle 0 | a_m^+ a_i | \nu \rangle \simeq \langle \text{HF} | [a_m^+ a_i, Q_r^+] | \text{HF} \rangle = Y'_{mi}. \quad (8.69)\end{aligned}$$

Equations (8.67) can now be written in a very compact form:

$$\begin{pmatrix} A & B \\ B^* & A^* \end{pmatrix} \begin{pmatrix} X' \\ Y' \end{pmatrix} = \hbar\Omega_r \begin{pmatrix} 1 & 0 \\ 0 & -1 \end{pmatrix} \begin{pmatrix} X' \\ Y' \end{pmatrix} \quad (8.70)$$

with $(X')_{mi} = X'_{mi}$; $(Y')_{mi} = Y'_{mi}$; and

$$\begin{aligned}A_{minj} &= \langle \text{HF} | [a_i^+ a_m [H, a_n^+ a_j]] | \text{HF} \rangle = (\epsilon_m - \epsilon_i) \delta_{mn} \delta_{ij} + \bar{\epsilon}_{mijn}, \\ B_{minj} &= -\langle \text{HF} | [a_i^+ a_m [H, a_j^+ a_n]] | \text{HF} \rangle = \bar{v}_{mijn}. \quad (8.71)\end{aligned}$$

The matrix A is Hermitian and the matrix B is symmetric.

Equation (8.70), together with (8.71), is called the *RPA equation*. We get back the TDA equation by putting all Y'_{mi} equal to zero. They are therefore a measure for the correlations in the ground state.

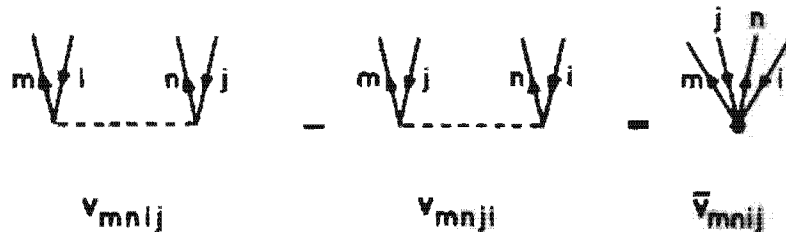


Figure 8.10. Graphical representation of the matrix elements B in Equation (8.71).

As we can see by looking at matrix B of Eq. (8.71), the RPA contains, in addition to the graphs of Fig. 8.3, the graphs shown in Fig. 8.10, which have the meaning of virtual $2p - 2h$ excitations.

In general, we can say that the quasi-boson approximation (8.68) is valid for very collective states, that is, if we have many coefficients X'_{mi} of the same order of magnitude. In such cases each single ph -component has only a small probability of being excited and the violation of the Pauli principle can be neglected. We will discuss this point again later in Chapter 9.

On the other hand, the amplitudes Y'_{mi} should be small compared to the coefficients X'_{mi} because they describe ground state correlations. If they are too strong, the replacement of the correlated ground state $|RPA\rangle$ by the $|HF\rangle$ state in Eq. (8.67) is not justified.

In cases where the coefficients Y'_{mi} can be neglected completely, we get back to the TDA. This is the reason that we can describe collective states very well using the RPA, where the quasi-boson approach is justified, and also rather pure ph -states, where the coefficients Y'_{mi} are negligible. The RPA equation (8.70) looks like the diagonalization of the Hamiltonian in a basis with a metric tensor (\perp) which is no longer positive definite. In fact, in Section 8.4.4 we will show that the eigensolutions of Eq. (8.70) are orthogonal with respect to this metric. Another consequence of this metric is that the eigenvalues $\Delta\Omega_i$ are not necessarily real.

To calculate transition probabilities (B.62) between the excited state $|\nu\rangle$ and the ground state $|0\rangle$ we only need matrix elements of the type $\langle 0|F|\nu\rangle$ for a Hermitian one-body operator F .

In the RPA approximation they are given by

$$\langle 0|F|\nu\rangle = \sum_{kk'} F_{kk'} \rho_{k'k}^{(1)\dagger} = \sum_{mi} F_{im} X'_{mi} + F_{mi} Y'_{mi}.$$

In the following sections we will frequently use the notation

$$\langle 0|F|\nu\rangle = f^+ \cdot \chi^\nu \quad (8.72)$$

with the column vectors

$$f = \begin{pmatrix} F_{mi} \\ F_{mi}^* \end{pmatrix} \quad \text{and} \quad \chi^\nu = \begin{pmatrix} X'_{mi} \\ Y'_{mi} \end{pmatrix}.$$

8.4.2 Stability of the RPA

The matrix

$$\mathbf{S} = \begin{pmatrix} A & B \\ B^* & A^* \end{pmatrix} \quad (8.73)$$

is exactly the *stability matrix* of the HF theory derived in Eq. (7.37). It is a Hermitian matrix and its real eigenvalues characterize the nature of the HF solution. If \mathbf{S} is positive definite it corresponds to a minimum in the energy surface. In this case, we can calculate the square root of the matrix \mathbf{S} and bring the eigenvalue problem (8.70) into a more symmetric form:

$$\mathbf{S}^{1/2} \begin{pmatrix} 1 & 0 \\ 0 & -1 \end{pmatrix} \mathbf{S}^{1/2} \begin{pmatrix} \tilde{X} \\ \tilde{Y} \end{pmatrix} = \begin{pmatrix} \tilde{X} \\ \tilde{Y} \end{pmatrix} \hbar\Omega$$

with

$$\begin{pmatrix} \tilde{X} \\ \tilde{Y} \end{pmatrix} = \mathbf{S}^{1/2} \begin{pmatrix} X \\ Y \end{pmatrix},$$

which is a Hermitian eigenvalue problem having only real solutions. In other words, if the HF solution corresponds to a minimum in the energy surface and not to a saddle point or a maximum, then the corresponding RPA equation has only real frequencies [Th 61a]. The opposite is not necessarily true. In the following we will assume that we only have real non-vanishing eigenvalues Ω_ν .

8.4.3 Normalization and Closure Relations

Since the RPA matrix is not Hermitian, its eigenvectors cannot be orthogonal in the usual sense. We would also expect a different kind of orthogonality relations from the condition, that the excited states $|\nu\rangle = Q_\nu^\dagger |RPA\rangle$ should be mutually orthogonal

$$\langle \nu | \nu' \rangle = \delta_{\nu\nu'} = \langle RPA | [Q_\nu, Q_{\nu'}^\dagger] | RPA \rangle \simeq \langle HF | [Q_\nu, Q_{\nu'}^\dagger] | HF \rangle$$

or

$$\delta_{\nu\nu'} = \sum_{mi} (X_{mi}^{\nu\dagger} X_{mi}^{\nu'} - Y_{mi}^{\nu\dagger} Y_{mi}^{\nu'}). \quad (8.74)$$

In fact, we can show that the solutions of the RPA equations for $\nu \neq \nu'$ fulfill this relation exactly. For $\nu = \nu'$ this gives us the possibility of normalizing the vector (X^ν, Y^ν) if the norm is positive [Th 61a].

To show the orthogonality of the RPA solutions in the sense of (8.74) we first notice that to each eigenvector (X^ν, Y^ν) with eigenvalue Ω_ν , we have another eigenvector $(Y^{\nu'}, X^{\nu'})$ with the eigenvalue $-\Omega_\nu$. Both eigenvectors have the same absolute norm in the sense of (8.74) but with different sign.

It is useful to introduce the matrices

$$\mathcal{X} = \begin{pmatrix} X & Y^* \\ Y & X^* \end{pmatrix}; \quad \mathcal{R} = \begin{pmatrix} 1 & 0 \\ 0 & -1 \end{pmatrix}. \quad (8.75)$$

Together with (8.75), the RPA equation (8.70) has the form

$$S\mathcal{X} = \mathcal{R}\mathcal{X}\Omega, \quad (8.76)$$

where the diagonal matrix Ω contains the real eigenvalues $(\hbar\Omega_\mu, -\hbar\Omega_\mu)$. Simple matrix algebra shows that

$$[\Omega, \mathcal{X}^* \mathcal{R} \mathcal{X}] = (\mathcal{R} \mathcal{X} \Omega)^* \mathcal{X} - \mathcal{X}^* (\mathcal{R} \mathcal{X} \Omega) = \mathcal{X}^* (S^* - S) \mathcal{X} = 0 \quad (8.77)$$

that is, Ω commutes with $\mathcal{X}^* \mathcal{R} \mathcal{X}$, and thus $\mathcal{X}^* \mathcal{R} \mathcal{X}$ is diagonal together with Ω . Since the norm of the vectors (X, Y) is open, we choose*

$$\mathcal{X}^* \mathcal{R} \mathcal{X} = \mathcal{R}. \quad (8.78)$$

These are exactly the orthogonality conditions (8.74).

The closure condition is obtained by multiplying (8.78) with \mathcal{R} , which shows that $\mathcal{R} \mathcal{X} \mathcal{R}$ is the inverse matrix of \mathcal{X}^* , or

$$\mathcal{X} \mathcal{R} \mathcal{X}^* = \mathcal{R} \quad (8.79)$$

which gives explicitly

$$\sum_p X_{mi}^* X_{m'i'}^* - Y_{mi}^* Y_{m'i'}^* = \delta_{mm'} \delta_{ii'}. \quad (8.80)$$

8.4.4 Numerical Solution of the RPA Equations

In many practical cases the RPA-matrices A and B are real. For real frequencies Ω , the problem can be reduced to the diagonalization of a real symmetric matrix of *half the dimension*.

We define the vectors (see footnote page 301)

$$P^* = i \cdot \sqrt{\frac{\hbar\Omega_\nu}{2}} (X^* + Y^*); \quad Q^* = \sqrt{\frac{\hbar}{2\Omega_\nu}} (X^* - Y^*). \quad (8.81)$$

From (8.70) it is easy to deduce

$$\begin{aligned} i \cdot (A - B) Q^* &= \hbar P^*, \\ -i \cdot (A + B) P^* &= \hbar \Omega_\nu^2 Q^*. \end{aligned} \quad (8.82)$$

and

$$(A + B)(A - B)Q^* = \hbar^2 \Omega_\nu^2 Q^*. \quad (8.83)$$

Together with the stability matrix S (8.73), the matrices $(A \pm B)$ are positive definite. We can decompose $A - B$ into a product of two triangular matrices (Orthogonalization of Gram-Schmidt [Wi 65, Ch 70]), we

* For a positive definite stability matrix S this is always possible, because Ω , then has the same sign as $(\mathcal{X}^* \mathcal{R} \mathcal{X})_{\mu\nu}$.

could also search for the square root of the matrix $(A - B)$ [UR 71])

$$(A - B) = T^T T \quad \text{with } T_{ik} = 0 \text{ for } i > k \quad (8.84)$$

and be left with the real symmetric eigenvalue problem

$$T(A + B)T^T R' = \hbar^2 \Omega^2 R'. \quad (8.85)$$

Its solution gives the eigenvalues Ω , and the normalized eigenvectors R' . Finally, we get the properly normalized RPA amplitudes from

$$\begin{pmatrix} X' \\ Y' \end{pmatrix} = \frac{1}{2} ((\hbar \Omega_s)^{-1/2} T^T R' \pm (\hbar \Omega_s)^{1/2} T^{-1} R'). \quad (8.86)$$

8.4.5 Representation by Boson Operators

For the derivation of the RPA equations (8.70) we have used the quasi-boson approximation (8.68), that is, we have replaced the ph operators $a_m^+ a_i$ by boson operators B_{mi}^+

$$a_m^+ a_i \rightarrow B_{mi}^+, \quad a_i^+ a_m \rightarrow B_{mi}, \quad (8.87)$$

which fulfill exact boson commutation relations

$$[B_{mi}, B_{m'i}] = [B_{mi}^+, B_{m'i}^+] = 0; \quad [B_{mi}, B_{m'i}^+] = \delta_{ii} \delta_{mm'}. \quad (8.88)$$

This replacement is an approximation. In fact we will see in Chapter 9 that we can expand the Fermion pair operators $a_m^+ a_i$ in a series of boson operators, in which the first term is B_{mi}^+ . In the quasi-boson approximation we neglect all higher terms.

Since we use this approximation within the RPA theory it is very convenient to represent other operators, such as the Hamiltonian H or transition operators, by the B 's and B s. How this can be done is discussed in Chapter 9.

Here we shall go to harmonic order only, that is, we take into account in the Hamiltonian H_B only terms quadratic in B, B^+ as $B^+ B$, BB , and $B^+ B^+$. This is consistent with the approach (8.87) because we need only terms of the form $[H, B^+]$, $[H, B]$ (see Eq. 8.67) in the derivation of the RPA equations. In particular, we determine the coefficients of the terms $B^+ B$, BB , and $B^+ B^+$ of the Hamiltonian by the requirement* (8.71):

$$\begin{aligned} \langle HF | [B_{mi}, [H_B, B_{nj}^+]] | HF \rangle &= \langle HF | [a_i^+ a_m, [H, a_n^+ a_j]] | HF \rangle = A_{minj}, \\ \langle HF | [B_{mi}, [H_B, B_{nj}]] | HF \rangle &= \langle HF | [a_i^+ a_m, [H, a_j^+ a_n]] | HF \rangle = -B_{minj}, \end{aligned} \quad (8.89)$$

* To be precise, we must remark that $|HF\rangle$ is not exactly the ground state of the Boson operators B_{mi}^+ , since they coincide only approximately with the operators $a_i^+ a_m$. In Chapter 9, we define the ground states of Boson operators by round parenthesis $B_{mi}|HF\rangle = 0$. There is no difference between $|HF\rangle$ and $|HF\rangle$ in RPA order; we do not distinguish between these two states in the present chapter and always use $B_{mi}|HF\rangle = 0$.

and find*

$$\begin{aligned} H_B &= E_{HF} + \sum_{m \neq n} A_{mnij} B_{mi}^+ B_{nj} + \frac{1}{2} \sum_{m \neq n} (B_{mnij} B_{mi}^+ B_{nj}^+ + h.c.) \\ &= E_{HF} - \frac{1}{2} \sum_{mi} A_{mmii} + \frac{1}{2} (B^+ - B) \begin{pmatrix} A & B \\ B^* & A^* \end{pmatrix} \begin{pmatrix} B \\ B^+ \end{pmatrix}. \end{aligned} \quad (8.90)$$

The constant E_{HF} corresponds to the expectation value of the Hamiltonian in the HF ground state, as can be seen by switching Eq. (8.90) between $|HF\rangle$. In Chapter 9, it is shown that the higher order terms in B give no contributions. There are no linear terms in the operators B, B^+ because we start with a self-consistent solution [$H^{20} = 0$, Eq. (7.36)]. A Hamiltonian of this form can also be derived in second order by the method of generator coordinates, which has been introduced in this context by Jancovici and Schiff [JS 64] (see also Chap. 10).

The diagonalization of (8.90) is straightforward if we introduce a Bogoliubov transformation [see (E.60)] amongst the Boson operators corresponding to (8.65) and replace the operators Q_i by pure Boson operators O_i ,

$$O_i^+ = \sum_{mi} X_{mi}^* B_{mi}^+ - Y_{mi}^* B_{mi}. \quad (8.91)$$

The requirement that the operators O_i^+, O_i now fulfill exact boson commutation relations is equivalent to the unitarity of this transformation and immediately yields the orthogonality relations (8.78) and (8.79).

The Hamiltonian expressed in terms of the operators O_i^+, O_i is found to be diagonal after taking into account the RPA equation (8.76) viz:

$$\begin{aligned} H_B &= E_{HF} - \frac{1}{2} \text{Tr } A + \frac{1}{2} (O^+ - O) \mathcal{X}^+ \mathcal{S} \mathcal{X} \begin{pmatrix} O \\ O^+ \end{pmatrix} \\ &= E_{RPA} + \sum_r \hbar \Omega_r O_r^+ O_r \end{aligned} \quad (8.92)$$

with

$$E_{RPA} = E_{HF} - \frac{1}{2} \text{Tr } A + \frac{\hbar}{2} \sum_{r>0} \Omega_r \quad (8.93a)$$

$$= E_{HF} - \sum_r \hbar \Omega_r \sum_{mi} |Y_{mi}^*|^2. \quad (8.93b)$$

In Eq. (8.93) we have used the inverse of the RPA equation (8.76)

$$\begin{aligned} A &= X \Omega X^+ + Y^* \Omega Y^T, \\ -B &= X \Omega Y^+ + Y^* \Omega X^T. \end{aligned} \quad (8.94)$$

The Hamiltonian (8.92) corresponds to the Hamiltonian of harmonic oscillators. Therefore, the RPA is called the harmonic approximation. It

* We should not, in the following matrix notation, confuse the operators B_{mi} with the matrix B_{mnij} .

determines uncoupled eigenmodes of the system. The eigenfunctions of H_B are the ground state $|RPA\rangle$ (it will be constructed in Section 8.4.6), one-boson states $O_r^+|RPA\rangle$, two-boson states $O_r^+O_s^+|RPA\rangle$, and so on.

Since A is just the matrix, which is diagonalized in the TDA equation (8.10), we see from Eq. (8.93) that the RPA ground state energy E_{RPA} is lowered compared to the Hartree-Fock energy E_{HF} by the amount

$$E_{HF} - E_{RPA} = \frac{1}{2} \sum_{r>0} (E_r^{TDA} - E_r^{RPA}).$$

It is just half the sum of all differences in the excitation energies between the RPA and the TDA approach.

As we know from the theory of the harmonic oscillator, we may also represent the eigenmodes by generalized coordinates φ_r and moments ϱ_r , defined by [MW 69b]

$$\varphi_r = \frac{\hbar}{i} \sqrt{\frac{M_r \Omega_r}{\hbar}} \frac{1}{\sqrt{2}} (O_r - O_r^+); \quad \varrho_r = \sqrt{\frac{\hbar}{M_r \Omega_r}} \frac{1}{\sqrt{2}} (O_r + O_r^+). \quad (8.95)$$

The numbers M_r are arbitrary at this point. The operators φ_r, ϱ_r fulfill the commutation relations of conjugate momenta and coordinates

$$[\varphi_r, \varphi_s] = [\varrho_r, \varrho_s] = 0; \quad [\varphi_r, \varrho_s] = \frac{\hbar}{i} \delta_{rs}. \quad (8.96)$$

The Hamiltonian (8.92) can be expressed in these operators:

$$H_B = E_{HF} - \frac{1}{2} \text{Tr } A + \sum_r \left(\frac{1}{2M_r} \varphi_r^2 + \frac{M_r}{2} \Omega_r^2 \varrho_r^2 \right). \quad (8.97)$$

The operators φ_r, ϱ_r , therefore, obey the equations of motion

$$[H_B, \varphi_r] = i\hbar \Omega_r^2 M_r \varrho_r; \quad [H_B, \varrho_r] = -\frac{i\hbar}{M_r} \varphi_r. \quad (8.98)$$

Using the representation

$$\varphi_r = \sum_{mi} P_{mi}^r B_{mi}^+ + P_{mi}^{r*} B_{mi} \quad \text{with } P_{mi}^r = i\hbar \sqrt{\frac{M_r \Omega_r}{2\hbar}} (X + Y^*)_{mi}^r,$$

$$\varrho_r = \sum_{mi} Q_{mi}^r B_{mi}^+ + Q_{mi}^{r*} B_{mi} \quad \text{with } Q_{mi}^r = \sqrt{\frac{\hbar}{2M_r \Omega_r}} (X - Y^*)_{mi}^r,$$

we get an explicit form for the Eqs. (8.98):

$$\begin{pmatrix} A & B \\ B^* & A^* \end{pmatrix} \begin{pmatrix} P \\ -P^* \end{pmatrix}_r = i\hbar \Omega_r^2 M_r \begin{pmatrix} Q \\ Q^* \end{pmatrix}_r; \quad (8.99)$$

$$\begin{pmatrix} A & B \\ B^* & A^* \end{pmatrix} \begin{pmatrix} Q \\ -Q^* \end{pmatrix}_r = \frac{\hbar}{i} \frac{1}{M_r} \begin{pmatrix} P \\ P^* \end{pmatrix}_r.$$

Neither the normalization of the vectors P_{mi}^* and Q_{mi}^* nor the parameter M_s is determined from the solution of this equation. The condition (8.96),

$$(P^* \quad P)_s \begin{pmatrix} Q \\ -Q^* \end{pmatrix}_s = \frac{\hbar}{i} \delta_{ss}, \quad (8.100)$$

can be used to determine either the parameter M_s (for fixed normalization of P_{mi}^* or Q_{mi}^*) or the normalization of these vectors (for fixed parameter M_s).

So far we have only treated the case of non-vanishing real RPA frequencies ($\Omega_i^2 > 0$). In principle, the RPA matrix can also have complex eigenvalues. (An example is $A = \begin{pmatrix} 1 & 0 \\ 0 & -1 \end{pmatrix}$, $B = \begin{pmatrix} 0 & 1 \\ 1 & 0 \end{pmatrix}$, with the eigenvalues $\Omega_i = \pm 1 \pm i$.) Until now such general cases have not been investigated. In the context of adiabatic time-dependent Hartree-Fock theory (see Sec. 12.3), it happens sometimes that we must diagonalize a matrix of the RPA type with a pure imaginary eigenvalue $\Omega_i = i|\Omega_i|$. The corresponding eigenvector \mathcal{X}_i has zero norm:

$$i|\Omega_i| \mathcal{X}_i^* \mathcal{X}_i = \mathcal{X}_i^* S \mathcal{X}_i = (\mathcal{X}_i^* S \mathcal{X}_i)^+ = -i|\Omega_i| \mathcal{X}_i^* \mathcal{X}_i.$$

In such a case there exists no boson of the form (8.91), which corresponds to this eigenvalue. Nevertheless, we can construct operators \mathcal{O}_i and \mathcal{O}_i^+ with the properties (8.96) and (8.98). We have only to solve the system (8.99) for an arbitrary positive value of M_s and a negative value of Ω_i^2 . In order to obtain a complete set of boson operators, we can then define corresponding bosons O_i , O_i^+ by Eq. (8.95) using the absolute value $|\Omega_i|$ instead of Ω_i [RB 76]. The Hamiltonian H_B (8.97) is not diagonal in this basis, but "maximally" off diagonal:

$$-\frac{\hbar}{2} |\Omega_i| (O_i^+ O_i^+ + O_i O_i).$$

8.4.6 Construction of the RPA Ground State

The RPA ground state was originally defined by Eq. (8.66) as the vacuum of the operators Q_s . Within the quasi-boson approximation it is now equivalent to the vacuum $|\text{RPA}\rangle$ of the boson operators O_s :

$$O_s |\text{RPA}\rangle = 0.$$

We can construct it explicitly from the vacuum $|\text{HF}\rangle$ of the bosons B_{mi} [Eq. (8.87)] in analogy to Chapter 7, where we constructed the vacuum of quasi-particle operators, by the theorem of Thouless [Th 60] (see also Sec. E.5):

$$|\text{RPA}\rangle = N_0 e^{\hat{Z}} |\text{HF}\rangle \quad (8.101)$$

where

$$\hat{Z} = \frac{1}{2} \sum_{minj} Z_{minj} B_{mi}^+ B_{nj}^+$$

and N_0 is a normalization (see Eqs. E.69 and E.75). In Appendix E we get, for the matrix Z , from (8.91) and the commutation relations (8.88),

$$Z = Y^* X^{*-1}.$$

The inversion of the matrix X is, in principle, possible, but more practicable methods have been proposed by Sanderson [Sa 65] and by da Providencia [Pr 66]. Actual calculations have been performed by Goswami and Pal [GP 63]. It turns out that the RPA ground state has to be taken with care, since the quasi-boson approximation probably overestimates the ground state correlations in many cases [IUY 65, PR 68, UR 69].

The energy of the ground state is given by Eq. (8.93). Obviously, it is always lower than the Hartree-Fock energy E_{HF} . The reason is that it takes into account higher correlations. However, we have to keep in mind that the RPA does not follow from a variational principle. It may, therefore, happen that its energy can even be deeper than the exact energy.

Since we are now able to calculate the RPA ground state, we could use it to evaluate Eq. (8.67), avoiding the quasi-boson approximation (8.68) in the calculation of the matrices A and B . Diagonalizing the new RPA equations gives a better ground state, and so on. This yields a self-consistent prescription which avoids the shortcomings of the quasi-boson approximation [Ro 70, SE 73, Ma 76a]. We will come to this method in more detail in Section 9.2.3.

Over the years, several other extensions of the RPA theory have been proposed (so-called *higher random phase approximations*; see, for instance, [Sa 62, TU 64, Ro 68a, MYM 68, GNS 70, DDK 71]). We do not want to discuss these methods in the framework of this book, since in Chapter 9 we present a systematic way of treating collective phenomena in nuclei, the so-called boson expansion technique.

8.4.7 Invariances and Spurious Solutions

We assume in the following that the exact two-body Hamiltonian H is invariant under a continuous symmetry operation generated by a Hermitian one-body operator \hat{P} , as there is, for instance, the case of translation; we assume further that the HF solution violates this symmetry. This means, in particular, that the HF single-particle density $\rho^{(0)}$ does not commute with \hat{P}

$$[\rho^{(0)}, \hat{P}] \neq 0. \quad (8.102)$$

Since $\rho^{(0)}$ is diagonal in the HF basis (0 for particles and 1 for holes) this means that not all the ph matrix elements P_{mn} vanish.

The exact Hamiltonian commutes with \hat{P} :

$$[H, \hat{P}] = 0. \quad (8.103)$$

\hat{P} is therefore an exact but *spurious solution* of the RPA equation $\langle HF | [SO, [H, \hat{P}]] | HF \rangle = 0^*$ or, in matrix language,

$$\begin{pmatrix} A & B \\ B^* & A^* \end{pmatrix} \begin{pmatrix} P \\ -P^* \end{pmatrix} = 0, \quad (8.104)$$

* The pp and hh matrix elements of \hat{P} do not contribute to this equation because of (5.35).

where P is the vector P_m in particle-hole space. The corresponding state is

$$|P\rangle = \sum_{mi} (P_{mi} a_m^+ a_i + P_{mi}^* a_i^+ a_m) |RPA\rangle. \quad (8.105)$$

We realize that the RPA equation (8.70) has such a solution only for the case in which the symmetry is, in fact, broken by the HF solution. Otherwise the matrix elements P_{mi} vanish identically.

Thus, we see that to the extent that we calculate the RPA exactly and use self-consistent single-particle energies and wave functions* the spurious excitations that correspond to a broken symmetry in the HF state—as, for example, in translation of the nucleus as a whole—separate out. They are orthogonal to the other excitations and lie at zero excitation energy. We have derived this for density-independent interactions. However, in Section (8.5) we will see that this also holds for density-dependent interactions that obey the condition (5.71).

This fact is a major advantage of the RPA over the TDA where, as we have seen in Section 8.3.3, the spurious and physical solutions become mixed up with one another.

As we stated at the beginning of Section 8.4.3, the RPA always has two symmetric solutions, Ω , and $-\Omega$. For \hat{P} , however, we have no adjoint partner, since \hat{P} is Hermitian and the adjoint is simply a repetition of itself. In fact, the state $|P\rangle$ in Eq. (8.105) is not normalizable in the sense of Eq. (8.74). There exists no corresponding boson. Since the RPA matrix has even dimensions and all non-spurious solutions are paired off, the RPA solutions are one short of forming a complete set.

To see what is going on, we follow Marshalek and Weneser [MW 69b, MW 70], and use the representation (8.95) for the spurious state. Obviously, the ph and the hp parts of \hat{P} are now identical to the Hermitian operator \mathcal{P}_0 (the canonical momentum) up to a constant M_0 which, in the definition (8.95) is open in any case. In order to obtain complete sets of operators O_v^+, O_v ($v > 0$) and $\mathcal{P}_0, \mathcal{Q}_0$ we only have to determine the canonical coordinate \mathcal{Q}_0 . It is given by the solution of Eq. (8.99):

$$\begin{pmatrix} A & B \\ B^* & A^* \end{pmatrix} \begin{pmatrix} -\mathcal{Q} \\ -\mathcal{Q}^* \end{pmatrix}_0 = -\frac{i\hbar}{M_0} \begin{pmatrix} P \\ P^* \end{pmatrix}, \quad (8.106)$$

which is a linear inhomogeneous problem. Since the matrix S is singular, this equation only has a solution if the inhomogeneous part is perpendicular to the spurious solution. But this is exactly the case (8.104). The equations (8.106) were first derived by Thouless and Valatin in the context of nuclear rotations [TV 62].

The constant M_0 is finally determined by the commutation relation (8.96):

$$\sum_{mi} (P_{mi}^* Q_{mi} - P_{mi} Q_{mi}^*)_0 = (P^* \quad P)_0 \begin{pmatrix} -\mathcal{Q} \\ -\mathcal{Q}^* \end{pmatrix}_0 = \frac{\hbar}{i}. \quad (8.107)$$

* In a case where this is not true, for instance, in RPA calculations based on a phenomenological Woods-Saxon potential, special methods have been developed to remove the spurious components [PS 77, Me 79].

Inverting (8.106), we find

$$\frac{\hbar^2}{2M_0} - \frac{1}{2}(Q^* - Q)_0 \begin{pmatrix} A & B \\ B^* & A^* \end{pmatrix} \begin{pmatrix} -Q \\ -Q^* \end{pmatrix}_0 = \frac{1}{2} \langle \text{HF} | [\varrho_0, [H, \varrho_0]] | \text{HF} \rangle \quad (8.108)$$

In practical cases it is often possible to choose the phases in such a way that A and B are real. In a case where Q_{mi} is also real, P_{mi} has to be purely imaginary and we get, for instance,

$$M_0 = 2P_0^*(A - B)^{-1}P_0 \quad (8.109)$$

We can now write down the Hamiltonian H_B in RPA order in the following way (8.97).

$$H_B = E_{\text{RPA}} + \sum_{r>0} \hbar\Omega_r O_r^+ O_r + \frac{\hat{P}_0^2}{2M_0}. \quad (8.110)$$

The constant E_{RPA} no longer has the form (8.93b) because of the zero frequency mode. However, we can give it easily by constructing the HF expectation value of (8.110):

$$E_{\text{RPA}} = E_{\text{HF}} - \sum_{r>0} \hbar\Omega_r \sum_{ml} |Y'_{ml}|^2 - \frac{\langle \text{HF} | \hat{P}_0^2 | \text{HF} \rangle}{2M_0}. \quad (8.111)$$

The subtraction of the term $\langle \hat{P}^2 \rangle / 2M_0$ is often used in the recipes (Chap. 11) for doing HF calculations in nuclei in order to correct for spurious translational motion of the centre of mass. We see that this correction is included automatically in the RPA.

The form of the operator (8.110) also gives us an interpretation of the constant M_0 . It is the inertial parameter corresponding to the motion characterized by \hat{P} .

Let us consider two examples:

- (i) *Translation.* Here we can use the Galilean invariance for the exact Hamiltonian

$$[H, X] = -\frac{i\hbar}{Am} P, \quad (8.112)$$

where X is the center-of-mass coordinate, and find by calculating the matrix elements $\langle \text{HF} | [a_i^+ a_m^-] | \text{HF} \rangle$ of this equation an equation identical to (8.106). This shows that in this case $M_0 = Am$ is the total mass of the nucleus.

- (ii) *Rotation.* Starting with a deformed HF calculation, a violated symmetry is a rotation perpendicular to the symmetry axis, let us say a rotation around the x -axis—the operator \hat{P} is now the angular momentum operator \hat{J}_x . Equation (8.106) determines the ph -matrix element of a corresponding coordinate, an angle θ_x . M_0 is now a moment of inertia \mathfrak{I}_{TV} corresponding to a rotation around the x -axis. We get for real matrix elements J_{x_m} in analogy to Eq. (8.109)

$$\mathfrak{I}_{\text{TV}} = 2 \sum_{ml} J_{x_m}^* (A + B)^{-1} J_{x_l}. \quad (8.113)$$

with

$$(A + B)_{mnj} = \delta_{mn} \delta_{ij} (\epsilon_m - \epsilon_i) + \bar{v}_{mjn} + \bar{v}_{mnj}.$$

Neglecting the residual interaction \bar{v} we again find the well-known cranking formula (3.89). For a discussion of the numerical application of this formula see Chap. (3.4.2).

In the next step, we would like to construct wave functions corresponding to these "spurious" excitations. We can define a ground state $|0\rangle$ by

$$O_\nu |0\rangle = 0 \quad \text{for } \nu > 0; \quad \mathcal{P}_0 |0\rangle = 0;$$

and excited states

$$|p\rangle = O_p^+ |0\rangle \quad \text{for } p > 0; \quad |p\rangle = \exp\left(i \frac{p}{\hbar} \Omega_0\right) |0\rangle.$$

These wave functions give the proper excitation energies Ω_p and $p^2/2M_0$, but it turns out that they are no longer normalizable. [MW 70]. The reason for this is that the RPA is a small amplitude approximation. Therefore, we describe the wave function of a rotational state, for instance, properly only for small angles. We can deduce therefore, energies, but not the full wave function. In particular, we do not recover the quantization of the angular momentum.

Summarizing, we can say that the RPA theory treats the inherent symmetries of the problem consistently. It separates the so-called spurious motions from the vibrations. In fact, these excitations are not really spurious, but they represent a different type of motion which has to be treated separately. At least their energies (which are not given by $\Omega_0 = 0$ but by $p^2/2M_0$) are reproduced properly, since they are characterized by the right mass parameters.

8.5 Linear Response Theory

In calculating collective excitations of the nuclear system, we have so far used the stationary Schrödinger equation (8.59) and tried to diagonalize the Hamiltonian at least in some approximation.

We shall now begin from quite a different starting point. We investigate the influence of an external time-dependent field

$$F(t) = F e^{-i\omega t} + F^+ e^{i\omega t} \quad (8.114)$$

on the system. We assume that F is a one-body operator, that is,

$$F(t) = \sum_{kl} f_{kl}(t) a_k^+ a_l,$$

and that the field is weak, that is, it introduces only small changes of the nuclear density, which we can treat in linear order.

As we will see, the nuclear density oscillates with this external field and we obtain resonances whenever the frequency ω is close to an excitation energy of the system. In this way:

- (i) We get information about the excited states of the system. In particular, we find an equation for the amplitudes $\langle 0|a_i^+a_m|r\rangle$, which corresponds precisely to the RPA equations.
- (ii) We are able to calculate the response of the system to the external field, that is, changes in its density, energy, and so on.
- (iii) We find a method to derive the RPA equations for density-dependent forces.

8.5.1 Derivation of the Linear Response Equations

The wave function $|\Phi(t)\rangle$ of a nuclear system in an external, time-dependent field is no longer stationary. It is a wave packet, and its one-body density

$$\rho_{kl}(t) = \langle \Phi(t) | a_l^+ a_k | \Phi(t) \rangle \quad (8.115)$$

is now time dependent. We want to calculate this density explicitly under the following approximations.

- (i) We assume that at any time $\rho(t)$ corresponds to a *Slater determinant** (i.e., $\rho^2 = \rho$). Then ρ obeys the following equation of motion.

$$i\hbar\dot{\rho} = [h[\rho] + f(t), \rho]. \quad (8.116)$$

This is the *time-dependent Hartree-Fock (TDHF) equation*. It will be derived in Section 12.2. Here $h[\rho]$ is the single-particle Hartree-Fock (HF) field as defined in Eq. (5.33) and f is the time-dependent external field of Eq. (8.114).

- (ii) We assume that the external field $f(t)$ is weak, that is, it introduces only oscillations with *small amplitudes* around the stationary density $\rho^{(0)}$, which is itself a solution of the stationary Hartree-Fock equation (5.36) $[h[\rho^{(0)}], \rho^{(0)}] = 0$. Therefore, the density has the form

$$\rho(t) = \rho^{(0)} + \delta\rho(t), \quad (8.117)$$

where

$$\delta\rho = \rho^{(1)}e^{-i\omega t} + \rho^{(1)*}e^{i\omega t} \quad (8.118)$$

is linear in the field f . In the following we work in the basis in which $\rho^{(0)}$ and $h[\rho^{(0)}]$ are diagonal, that is, in the HF-basis:

$$\rho_{kl}^{(0)} = \delta_{kl} \cdot \rho_k^{(0)} = \begin{cases} 0 & \text{for particles,} \\ 1 & \text{for holes,} \end{cases} \quad (8.119)$$

and

$$(h_0)_{kl} = (h[\rho^{(0)}])_{kl} = \delta_{kl} \cdot \epsilon_k. \quad (8.120)$$

* In this sense, the following derivation of the RPA shows that it is just a time dependent generalization of the independent particle picture (see Chap. 12).

In Section 5.3.3 we saw that the condition $\rho^2 = \rho$ implies that the only non-vanishing matrix elements of $\rho^{(1)}$ are ph and hp matrix elements $\rho_{mi}^{(1)}$ and $\rho_{im}^{(1)}$. They are determined by the solution of the TDHF equation (8.116). We insert Eq. (8.117) and expand up to linear order in the external field f ,

$$i\hbar\delta\rho = [\hbar_0, \delta\rho] + \left[\frac{\partial h}{\partial \rho} \cdot \delta\rho, \rho^{(0)} \right] + [f, \rho^{(0)}], \quad (8.121)$$

where $\delta h / \delta\rho \cdot \delta\rho$ is a shorthand notation for

$$\sum_{im} \left(\frac{\partial h}{\partial \rho_{im}} \Big|_{\rho=\rho^{(0)}} \cdot \delta\rho_{mi} + \frac{\partial h}{\partial \rho_{mi}} \Big|_{\rho=\rho^{(0)}} \cdot \delta\rho_{im} \right). \quad (8.122)$$

Using the rules for the calculation with HF densities, as given in Appendix D, [Eq. (D.30)ff] we find that the pp and the hh matrix elements of Eq. (8.121) vanish identically. From (8.118) we obtain for the ph and hp elements the *linear response equation*

$$\left\{ \begin{pmatrix} A & B \\ B^* & A^* \end{pmatrix} - \hbar\omega \begin{pmatrix} 1 & 0 \\ 0 & -1 \end{pmatrix} \right\} \begin{pmatrix} \rho^{(1)ph} \\ \rho^{(1)hp} \end{pmatrix} = - \begin{pmatrix} f^{ph} \\ f^{hp} \end{pmatrix} \quad (8.123)$$

with

$$A_{mnj} = (\epsilon_m - \epsilon_j) \delta_{mn} \delta_{ij} + \frac{\partial h_{mj}}{\partial \rho_{nj}}; \quad B_{mnj} = \frac{\partial h_{mi}}{\partial \rho_{nj}}.$$

These matrices correspond exactly to the matrices A and B of the RPA method, if we use as a residual interaction [see Eq. (5.32)]

$$\tilde{v}_{pqrs} = \frac{\partial h_{pq}}{\partial \rho_{rs}} = \frac{\partial^2 E}{\partial \rho_{pq} \partial \rho_{rs}}. \quad (8.124)$$

In the case of HF theory without density dependent forces, we can use the expression (5.28) for the energy and thus we get back the RPA matrices (8.71). However, the above derivation is more general. It can also be applied to theories with *density dependent forces* (see Sec. 5.6). In this case, for the calculation of excited states we have to use the force defined by Eq. (8.124) as the second derivative of the ground state energy with respect to the density. In particular, this force is no longer necessarily antisymmetric in the indices q and r .

The linear response equation (8.123) is an inhomogeneous equation and can be solved by inverting the matrix on the left-hand side. We then find a linear connection between the external field f and the change in the nuclear density (i.e., the response of the system):

$$\rho_{kl}^{(1)} = \sum_{pq} R_{klpq}(\omega) f_{pq}. \quad (8.125)$$

The function $R_{klpq}(\omega)$ is called the *response function* [see Eqs. (F.51) and (F.68)]. We have calculated it here only in the mean field approach (i.e., in "RPA order"), because we restrict ourselves to product wave functions

with $\rho^2 = \rho$. Therefore, the indices kl and pq run only over ph and hp indices. This is no longer true in the general case.

The response function R depends on the frequency of the external field. It has poles at the eigenfrequencies of the system, where already an infinitesimal field f is sufficient to excite the corresponding eigenmode.

To find these resonances ($\omega = \Omega_s$), we have to look for the solutions of the homogeneous equation (8.123) with vanishing external field. With the notation of Eqs. (8.73) and (8.75) we obtain

$$(\mathcal{S} - \mathcal{M}\Omega_s \mathcal{R})\rho^{(1)*} = 0. \quad (8.126)$$

This is exactly the RPA equation (8.70). Its solution gives the transition densities (8.69)

$$\rho_{pq}^{(1)}(\Omega_s) = \langle 0 | a_q^+ a_p | \nu \rangle \quad (8.127)$$

The derivation of the RPA equations is more general than the one given in Section 8.4.1, because it can also be used in the case of density-dependent forces, which is a crucial point for the validity of the mean field approach in nuclear physics.

On the other hand, the derivation shows us also very clearly the connection of the random phase approximation to the Hartree-Fock theory. We allow the average nuclear potential to oscillate around its stationary value, which corresponds to a minimum in the energy surface of all possible product wave functions (see Sec. 7.3.1). In the limit of small amplitudes we thus get a linear eigenvalue problem for the determination of the normal modes of the system (see also Sec. 12.3.2). The *RPA approximation* is therefore nothing but the *small amplitude limit of the time-dependent mean field approach*.

The energy surface in the vicinity of the stationary point ρ_0 can be obtained by expanding the HF energy $E[\rho]$, up to second order in $\delta\rho^*$ [BG 77]:

$$\begin{aligned} E[\rho] &= E[\rho^{(0)}] + \text{Tr} \left(\frac{\delta E}{\delta \rho} \delta \rho \right) + \frac{1}{2} \text{Tr} \text{Tr} \left(\delta \rho + \frac{\delta^2 E}{\delta \rho \delta \rho} \delta \rho \right) \\ &= E[\rho^{(0)}] + \frac{1}{2} \rho^{(1)*} \mathcal{S} \rho^{(1)}. \end{aligned} \quad (8.128)$$

We find that the stability matrix \mathcal{S} has again the form (7.37), but now the matrices A and B (8.123) are also defined for density-dependent forces.

It is easy to show also for such forces that we eventually obtain *spurious solutions* at zero frequency in the case of a broken symmetry \hat{P} . We have only to use the condition (5.68), which states that

$$\bar{\rho} = e^{i\alpha P} \rho^{(0)} e^{-i\alpha P},$$

* In deriving Eq. (8.128) we must be aware of the fact that $\delta\rho$ has in second order also pp - and hh matrix elements. They are, however, not independent variables, because any Slater determinant can be expressed by the ph and hp matrix elements of $\delta\rho$. We can use the relation $\rho^2 = \rho$ to eliminate them. Thus, the term $\text{Tr}(h_0 \delta\rho)$ gives a quadratic contribution, namely, just the ph energies $\epsilon_m - \epsilon_i$ in the matrix A .

as well as $\rho^{(0)}$, also fulfills the equation

$$[h(\bar{\rho}), \bar{\rho}] = 0.$$

Infinitesimal changes $\bar{\rho} = \rho^{(0)} + \rho^{(1)}$, with $\rho^{(1)} \propto [P, \rho^{(0)}]$, gives

$$[h_0, \rho^{(1)}] + \left[\frac{\delta h}{\delta \rho} \cdot \rho^{(1)}, \rho^{(0)} \right] = 0, \quad (8.129)$$

which shows that $\rho^{(1)}$, that is, just the ph and hp matrix elements of P , correspond to a spurious solution at zero energy analogous to Eq. (8.104) in the case of density-independent forces.

Knowing the eigenmodes of the system, that is, the frequencies Ω , and the RPA amplitudes X and Y , makes it possible to solve the linear response equation (8.123). Using (8.76ff), we find

$$\mathcal{S} - \hbar\omega\mathcal{R} = \hbar\mathcal{R}\mathcal{X}(\Omega - \omega)\mathcal{R}\mathcal{X}^+ \mathcal{R}$$

which can easily be inverted:

$$\rho^{(1)} = \frac{1}{\hbar} \mathcal{X}(\omega - \Omega)^{-1} \mathcal{R} \mathcal{X}^+ f.$$

This is equivalent to Eq. (8.125)—we have now an explicit expression for the response function,* namely its *spectral representation*:

$$R_{pq,p'q'}(\omega) = \frac{1}{\hbar} \sum_{\nu > 0} \left(\frac{\langle 0 | a_q^+ a_p | \nu \rangle \langle \nu | a_{p'}^+ a_{q'} | 0 \rangle}{\omega - \Omega_\nu + i\eta} - \frac{\langle 0 | a_p^+ a_q | \nu \rangle \langle \nu | a_{q'}^+ a_{p'} | 0 \rangle}{\omega + \Omega_\nu + i\eta} \right). \quad (8.130)$$

Again, the index pairs pq and $p'q'$ run only over ph and hp pairs. All other matrix elements of R vanish in RPA order. The form (8.130), however is *more general*. If we use exact eigenfunctions $|\nu\rangle$ and exact energies $\hbar\Omega_\nu$ of the system, $R_{pq,p'q'}(\omega)$ in Eq. (8.130) is just the exact response function. This can easily be seen by using time-dependent perturbation theory (see [No 64a, Chap. 2]) for the calculation of the change in the exact wave function produced by the external field F :

$$|\Psi(t)\rangle = |0\rangle + \sum_{\nu > 0} |\nu\rangle \left\{ \frac{\langle \nu | F | 0 \rangle}{\hbar(\omega - \Omega_\nu) + i\eta} e^{-i\omega t} - \frac{\langle \nu | F^+ | 0 \rangle}{\hbar(\omega + \Omega_\nu) - i\eta} e^{i\omega t} \right\}.$$

The states $|0\rangle$ and $|\nu\rangle$ are the stationary eigenstates of the system without perturbation. The transition density corresponding to this wave function $\rho^{(1)}$ is then given by Eq. (8.125) with the exact response function (8.130).

If we introduce the response function R^0 of the free system (without residual interaction \tilde{v} in (8.124)),

$$R_{pq,p'q'}^0(\omega) = \frac{\rho_q^{(0)} - \rho_p^{(0)}}{\hbar\omega - \epsilon_p + \epsilon_q + i\eta} \delta_{pp'} \delta_{qq'},$$

* For the sake of completeness we have added the infinitesimal positive parameter η , which determines the boundary condition in the case of unbound states (see Sec. 8.5.4). In a bound state problem η can be set equal to zero.

we can finally, in RPA approximation, derive another equation for $R(\omega)$, the so-called *linearized Bethe-Salpeter* equation (F.75), viz.

$$R_{pq,p'q'} = R_{pq,p'q'}^0 + \sum_{\substack{p_1 q_1 \\ p_2 q_2}} R_{pq,p_1 q_1}^0 \tilde{v}_{p_1 q_1 q_2 p_2} R_{p_2 q_2,p'q'} \quad (8.131)$$

The correctness of this equation can be verified simply by multiplying by $(\hbar\omega - \epsilon_p + \epsilon_q)$ and using the definition of R^0 , the spectral representation (8.130) for R and the RPA equation (8.126).

8.5.2 Calculation of Excitation Probabilities and Schematic Model

Another useful property of the linear response function lies in the fact that its imaginary part is related to the total transition probability (8.72). We define

$$R_F(\omega) := \text{Tr}(f^+ \rho^{(1)}(\omega)) = \sum_{p q p' q'} f_{pq}^* R_{pq p' q'}^{(\omega)} f_{p' q'} \quad (8.132)$$

and use the relation $1/(\omega + i\eta) = P(1/\omega) - i\pi\delta(\omega)$ in Eq. (8.130) to obtain

$$\text{Im}R_F(\omega) = -\pi \sum_{p>0} |\langle p | F | 0 \rangle|^2 \delta(\hbar\omega - \hbar\Omega_p), \quad \omega > 0. \quad (8.133)$$

We get the energy-weighted sum rule (8.154) by integrating this function,

$$-\frac{\hbar^2}{\pi} \int_0^\infty \omega \text{Im}R(\omega) d\omega = \sum_p \hbar\Omega_p |\langle p | F | 0 \rangle|^2 \equiv S_1, \quad (8.134)$$

and the transition matrix element $|\langle p | F | 0 \rangle|^2$ as the residue of $R_F(\omega)$ at the pole $\omega = \Omega_p$.

The solution becomes extremely simple in the schematic model, where the separable ansatz for the ground state correlation matrix element is now:

$$\tilde{v}_{mijn} = \lambda D_{mi} D_{nj}^*, \quad \tilde{v}_{mnij} = \lambda D_{ni} D_{mj},$$

where D is identical with the external field operator F . From the Bethe-Salpeter equation (8.131), we get

$$R_D(\omega) = R_D^0(\omega) [1 + \lambda R_D(\omega)]$$

with

$$R_D^0(\omega) = \sum_{p q p' q'} D_{pq}^* R_{pq p' q'}^0 D_{p' q'} = \sum_m |D_{mi}|^2 \left(\frac{1}{\hbar\omega - \epsilon_m + \epsilon_i + i\eta} - \frac{1}{\hbar\omega + \epsilon_m - \epsilon_i + i\eta} \right).$$

Solving for $R_D(\omega)$ yields

$$R_D(\omega) = \frac{R_D^0}{1 - \lambda R_D^0}.$$

The poles of $R_D(\omega)$ give the excitation energies Ω , and thus in the schematic model

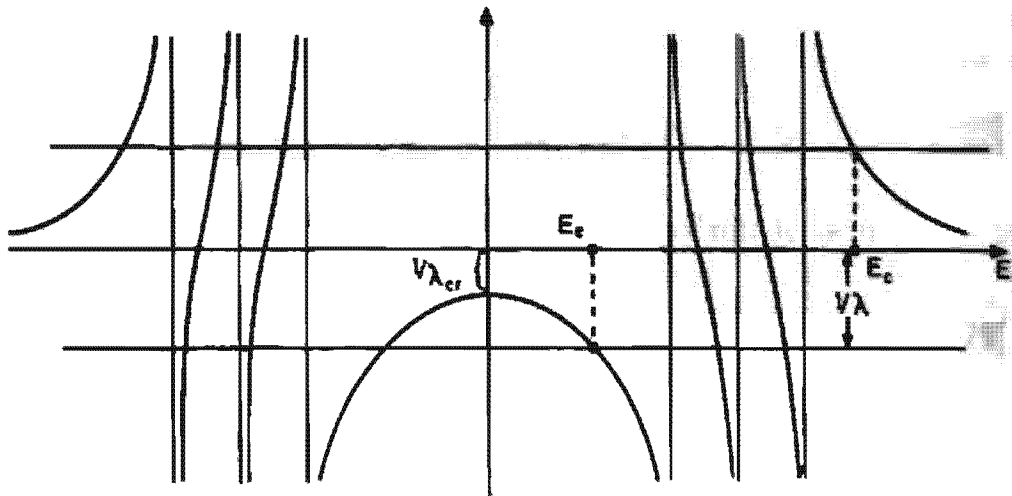


Figure 8.11. Graphical solution of the dispersion relation (8.135).

we have the following dispersion relation.

$$\frac{1}{\lambda} = R_D^0(\Omega_r) = \sum_{mi} |D_{mi}|^2 \frac{2\epsilon_{mi}}{\Lambda^2 \Omega_r^2 - \epsilon_{mi}^2}; \quad \epsilon_{mi} = \epsilon_m - \epsilon_i. \quad (8.135)$$

(We can drop the infinitesimal η because we are only interested in bound states for which $\Omega_r \neq \epsilon_{mi}$.)

Equation (8.135) can be solved graphically as in the TDA case. Comparing Fig. 8.11 with Fig. 8.4, we notice two qualitative differences which are due to the RPA ground state correlations:

- (i) In the case where the residual interaction becomes stronger than the critical value (i.e., $\lambda < \lambda_{\text{crit}}$) the energy of the low-lying collective state becomes imaginary.
- (ii) The ($T=0$)-RPA state is shifted further down than its corresponding TDA state for a comparable interaction strength λ .

We can study this more closely in the degenerate case. If we put all ϵ_{mi} equal to ϵ we have, from Eq. (8.135),

$$E_{\text{coll}}^2 = \epsilon^2 + 2\epsilon\lambda \sum_{mi} |D_{mi}|^2.$$

In the degenerate case, therefore, we have for λ_{crit}

$$\lambda_{\text{crit}} = -\frac{\epsilon}{2 \sum_{mi} |D_{mi}|^2}.$$

This is the point where the chosen HF-basis no longer gives the minimum for the ground state energy. The true minimum now occurs in a different HF-solution, which turns out to be deformed. We therefore often call λ_{crit} the point at which a phase transition from spherical state into a deformed shape of the nucleus occurs (for example, $D \sim r^2 Y_{20}$). In a comparison with the TDA case, we see that

$$E_{\text{coll}}^{\text{TDA}}(\lambda_{\text{crit}}) = \frac{\epsilon}{2}$$

and

$$E_{\text{coll}}^{\text{TDA}}(2\lambda_{\text{crit}}) = 0,$$

that is, in the schematic model the "phase transition" occurs in the TDA case at only twice the interaction strength.

We now want to turn to the calculation of transition matrix elements. We have to calculate the residue of $R_D(\omega)$ at the pole $\omega = \Omega_p$. In the vicinity of Ω_p , $R_D(\omega)$ has the form:

$$R_D(\omega) = \frac{R_D^0(\Omega_p)}{-\lambda(dR^0/d\omega)|_{\omega=\Omega_p} \cdot (\omega - \Omega_p)}.$$

We therefore get

$$|\langle p | D | 0 \rangle|^2 = -\frac{\hbar}{\lambda^2} \left(\frac{dR^0}{d\omega} \right)_{\Omega_p}^{-1} = \left(\lambda^2 \sum_{mi} |D_{mi}|^2 \frac{4\epsilon_{mi}\Delta\Omega_p}{(\hbar^2\Omega_p^2 - \epsilon_{mi}^2)^2} \right)^{-1}.$$

In the degenerate case this yields

$$|\langle p | D | 0 \rangle|^2 = \frac{\epsilon}{E_{coll}} \sum_{mi} |D_{mi}|^2.$$

We see that for the low-lying states the transition probability is enhanced as compared to the TDA value (8.21) by a factor ϵ/E_{coll} . For the collective octupole and quadrupole states this factor can be as large as two. Similar but less pronounced results are found in realistic calculations (see Sec. 8.6).

8.5.3 The Static Polarizability and the Moment of Inertia

We can apply linear response theory to calculate the change of the nuclear energy and the nuclear deformation in a static external field $-\lambda F$. This corresponds to the solution of the constrained HF equation

$$[h[\rho] - \lambda f, \rho] = 0 \quad (8.136)$$

in linear response theory. For the change of the density, we get from Eq. (8.118) and (8.125),

$$\rho^{(1)} = -\lambda R(\omega=0)f = \lambda \delta^{-1}f. \quad (8.137)$$

The static polarizability α is defined by the change of the expectation value of F :

$$\langle \lambda | F | \lambda \rangle = \langle 0 | F | 0 \rangle + \lambda \cdot \alpha; \quad (8.138)$$

and the change in energy is given by

$$\langle \lambda | H | \lambda \rangle = \langle 0 | H | 0 \rangle + \frac{1}{2} \lambda^2 \cdot \alpha. \quad (8.139)$$

The fact that we have the same constant α in both cases is called *Feynman's theorem* [Fe 39] and can be derived in analogy to Eq. (3.81) for density dependent forces also.

Finally, for the curvature of the energy function at the stationary point $\lambda=0$, which is equivalent to the static polarizability, the compression

modulus [BGG 76], or the spring constant [MP 73], we get

$$\alpha = \frac{d^2 E}{d \lambda^2} = \frac{d}{d \lambda} \langle \lambda | F | \lambda \rangle = \frac{d}{d \lambda} \text{Tr}(f^+ \rho^{(1)}) = f^+ S^{-1} f. \quad (8.140)$$

From Eq. (8.132) we have

$$\alpha = -R_F(\omega=0) = 2 \sum_{\nu>0} \frac{|\langle \nu | F | 0 \rangle|^2}{E_\nu - E_0}, \quad (8.141)$$

which shows that the static polarizability is closely connected to the sum rule S_{-1} [see Eq. (8.150)]. Using the exact states $|\nu\rangle$ and exact energies we obtain Eq. (8.141) by calculating the exact polarizability α_{exact} from first-order perturbation theory. The derivation shows that we get the polarizability in HF-approximation α_{HF} by using RPA wave functions and energies on the r.h.s. of Eq. (8.141). This can also be generalized to the dynamic polarizability [SLO 78].

The calculation of the *moment of inertia* within the self-consistent cranking theory (see Sec. 7.7) provides a simple application of these considerations. In this case, the external field λF is given by the cranking operator ω_x . An exact solution of Eq. (8.136) has been discussed in Section 7.7. Thouless and Valatin [TV 62] proposed to solve it in linear response theory. In this case, from Eq. (8.123) we get the Thouless–Valatin equation:

$$S \rho^{(1)} = \omega_x,$$

which is equivalent to Eq. (8.106). As discussed there, we have to be a little careful with the solution, since in this case S is a singular matrix. Nevertheless, we get the result for the moment of inertia from

$$g_{\text{TV}} = \left. \frac{d^2 E}{d \omega^2} \right|_{\omega=0} = 2 \sum_{\nu>0} \frac{|\langle \nu | J_x | 0 \rangle|^2}{E_\nu - E_0}, \quad (8.142)$$

where the sum over ν does not include the spurious state. This is a very general expression. It contains, as special cases, the Inglis formula (3.89) ($|\nu\rangle$ pure *ph* states) and the Belyaev formula (3.93) ($|\nu\rangle$ pure 2-quasi-particle states). But it also contains the more general case in which pairing correlations are included into the RPA theory (see Sec. 8.9). In this case, $|\nu\rangle$ are solutions of the quasi-particle RPA equations.

8.5.4 RPA Equations in the Continuum

Up to now we have always assumed a discrete spectrum of excited states $|\nu\rangle$. In fact, only the low-lying excited states are really discrete levels. All higher excitations lie in the continuum, that is, they are resonances. As discussed in Section 8.3, they are observed as maxima in the cross section of a suitable reaction.

The simplest way to overcome this problem is to work in a truncated oscillator basis. In such a basis there are only discrete levels. Single-particle resonances of the HF potential are approximated by bound single-particle states. Since the residual

interaction has a short range, and since the matrix elements entering the RPA matrix always contain two hole indices which correspond to exponentially decreasing single-particle wave functions, we need the wave functions of the unbound particle states only in the region of the nucleus, and we can approximate them there by a bound state. As a result of such a discretization, we get no giant resonances from the solution of the RPA equations (8.70), but groups of discrete states in this region (see Fig. 8.12) which show an enhanced strength $|\langle \nu | F | 0 \rangle|^2$ for the appropriate transition operator (as, for instance, $F = r^\lambda Y_{\lambda\mu}$ in the case of surface vibrations of multipolarity λ).

This method, however, provides only an approximative solution to the problem which becomes rather poor in cases where the single-particle resonances are spread out over a wide energy range. In reality, the problem is not a bound state problem. There is a solution for each energy ω , and the interesting quantity is now the excitation strength

$$S(\omega) = \sum_{\nu > 0} |\langle \nu | F | 0 \rangle|^2 \delta(\hbar\omega - \hbar\Omega_\nu), \quad (8.143)$$

which shows poles of discrete values of ν (bound states) and has a resonance behavior for continuous quantum numbers ν . In fact we have already seen in Eq. (8.38) that for the example of the giant dipole resonance this is exactly the measurable quantity. From Eq. (8.133) we get:

$$S(\omega) = -\frac{1}{\pi} \text{Im} R_F(\omega).$$

Therefore, we have to calculate the response function $R_F(\omega)$ of Eq. (8.130).

It turns out that the width of the giant resonances has two origins:

- (i) The wave function of the giant resonance is given as a superposition of ph states, where the p -state is a scattering solution of the single-particle HF potential. This means that there is always a certain probability that the state will decay into a free particle and a hole state in the $A - 1$ nucleus. This part of the width is called the *decay width* [MW 69a]. We are able, as we shall see in a moment, to describe this if we use scattering solutions of the single-particle HF equations in the calculation of $R(\omega)$.
- (ii) There are more complicated states, for instance, $2p - 2h$ excitations, which can also contribute to the wave function. They are neglected in the RPA approximation. It means that in reality a ph -component of the wave function is spread out over many $2p - 2h$ components. Therefore this part is called the *spreading width*. We are not able to calculate this in the present approximation (see for example [WS 72, HA 76, SSV 77, DKS 77, AY 78, BBB 79b].)

Several authors have treated the continuum within the TDA or the RPA [BG 65, DH 68, LV 68]. Because of the continuous variable ϵ of the single-particle energy in the continuum, we find a set of integrodifferential equations that are similar to the continuum shell model equations [We 67, MW 69a]. Their solution requires a big numerical effort [RMS 67, BH 67, Bi 72, KKS 77]. We do not want to present this matter further here but will instead discuss a method for calculating $R(\omega)$ for the case of zero range forces.

In cases in which the residual interaction consists only of a δ -force or derivatives of it [such as the Skyrme force (4.104ff)], Bertsch et al. [Be 73,

SB 75, BT 75, LG 76b, Ts 78] have developed a method of solving the Bethe-Salpeter equation (8.131) for the response function R in coordinate space. We present it here for the simple case of a pure δ -force $v(r_1, r_2, r_3, r_4) = V_0 \cdot \delta(r_1 - r_2)\delta(r_2 - r_3)\delta(r_3 - r_4)$ and neglect spin variables.

Using Eq. (8.131) and transforming it into coordinate space, we get, for the shell model response function R^0 ,

$$R^0(r_1, r_2, r'_1, r'_2, \omega) = \sum_{mi} \frac{\varphi_m(r_1)\varphi_i^*(r_2)\varphi_m^*(r'_1)\varphi_i(r'_2)}{\hbar\omega - \epsilon_m + \epsilon_i + i\eta} - \frac{\varphi_i(r_1)\varphi_m^*(r_2)\varphi_i^*(r'_1)\varphi_m(r'_2)}{\hbar\omega + \epsilon_m - \epsilon_i + i\eta}, \quad (8.144)$$

where $\varphi_i(r)$ are eigenfunctions of the single-particle HF Hamiltonian h^0 with eigenvalue ϵ_i . Because of the δ -character of the force, we will only need the function R^0 for $r_1 = r_2$ and $r'_1 = r'_2$:

$$R^0(r, r', \omega) = \sum_i \left\{ \varphi_i^*(r)\langle r| \frac{1}{\hbar\omega + \epsilon_i + i\eta - h^0} |r'\rangle \varphi_i(r') + \varphi_i^*(r')\langle r'| \frac{1}{-\hbar\omega + \epsilon_i + i\eta - h^0} |r\rangle \varphi_i(r) \right\}. \quad (8.145)$$

To see that (8.145) follows from (8.144), we must insert a complete set $\sum_s |s\rangle\langle s|$ and realize that the hole contributions vanish.

In the case of a pure δ -force, h^0 contains the kinetic energy and a local one-body potential. We can apply scattering theory in a one-body potential (see [Me 61, Vol. II, Chap. XII.13]) and derive for a given partial wave the radial part of the single-particle Green's function viz:

$$G(r, r', \omega) \equiv \langle r| \frac{1}{\hbar\omega + i\eta - h^0} |r'\rangle = \frac{2m}{\hbar^2} \frac{v(r_>)w(r_<)}{W(v, w)}. \quad (8.146)$$

Here $r_>$ and $r_<$ denote the greater and the lesser of r and r' and v and w are two linear independent solutions of $(h^0 - \omega)v = 0$ with the boundary conditions:

- $r=0$: $v(r)$ regular, $w(r)$ irregular;
- $r \rightarrow \infty$: $\omega < 0$, $v(r)$ increases and $w(r)$ decreases exponentially;
- $\omega > 0$, $v(r)$ standing wave $w(r)$ outgoing wave.

Finally, $W(v, w)$ is the Wronskian of v and w .

Having a solution of the HF problem, we know the radial part of the bound state wave function $\varphi_i(r)$, and the functions v and w at a set of mesh points in coordinate space. For each ω , we can therefore get the function $R^0(r, r', \omega)$ from Eq. (8.145) and (8.146) with the aid of some angular momentum coupling.

For the local response function $R(r, r') = R(rr, r'r')$ with a pure δ -force, we get from (8.131)

$$R(r, r', \omega) = R^0(r, r', \omega) + V_0 \int d^3r'' R^0(r, r'', \omega) R(r'', r', \omega). \quad (8.147)$$

Using angular momentum coupling techniques [BT 75], the three-dimensional integral can be reduced to a one-dimensional integral over the radial coordinate. Introducing mesh points in r -space, we find an inhomogeneous linear matrix equation whose solution gives $R(\mathbf{r}, \mathbf{r}')$.

For a local operator $F(\mathbf{r})$ (for instance, a multipole operator), we are now able to calculate the transition density $\rho^{(1)}(\mathbf{r})$ from Eq. (8.125), which is sometimes also called the *form factor*:

$$\rho^{(1)}(\mathbf{r}, \omega) = \int d^3r' R(\mathbf{r}, \mathbf{r}', \omega) F(\mathbf{r}'); \quad (8.148)$$

and the strength function (8.142)

$$S(\omega) = -\frac{1}{\pi} \text{Im} \int d^3r d^3r' F^*(\mathbf{r}) R(\mathbf{r}, \mathbf{r}', \omega) F(\mathbf{r}'). \quad (8.149)$$

(An example of such a calculation is given in Fig. (8.13).)

8.6 Applications and Comparison with Experiment

Over the years, there has been an enormous number of applications of the TDA and RPA approximations in nuclei starting with simple configuration mixing of a few *ph* levels in O^{16} up to the extended RPA calculations with inclusion of the continuum in heavy nuclei. It goes far beyond the scope of this book to give a review of this work. We wish only to pick a few examples to demonstrate certain essential points. We therefore restrict ourselves to spherical closed-shell nuclei such as ^{16}O , ^{40}Ca , ^{50}Zr , and ^{208}Pb . In a spherical basis, we can use angular momentum coupling techniques [Ed 57] to diagonalize the Hamiltonian in the eigenspaces of angular momentum and parity. This fact reduces the dimension of the corresponding matrices enormously. In $N = Z$ nuclei, we can furthermore neglect the Coulomb force to a good approximation and use the isospin symmetry.

8.6.1 Particle–Hole Calculations in a Phenomenological Basis

In most of the calculations the self-consistent HF potential has been replaced by a phenomenological shell model potential, such as an oscillator potential whose oscillator length was adjusted to the empirical rms radius. This potential provides single-particle wave functions for the calculation of the *ph*-matrix elements (8.71) of a residual interaction. Since the final energy levels—at least for the non-collective states—depend very sensitively on the particle–hole energies $\epsilon_m - \epsilon_i$, in fact, usually not the single-particle energies of the phenomenological potential have been used, but instead taken the measured single-particle spectrum energies determined from neighboring odd nuclei

$$\epsilon_m = E(m, A+1) - E(0, A),$$

$$\epsilon_i = E(0, A) - E(i, A-1).$$

One of the oldest calculations of this type is the TDA calculation of Elliot and Flowers [EF 57] for the negative parity levels in ^{16}O . They used one shell below the Fermi surface ($1p$) and one shell above the Fermi surface ($2s - 1d$ shell). This gives

five ph -states for the 1^- channel and three ph states for the 3^- channel. With a Yukawa interaction and a Rosenfeld exchange mixture [EF 57, Table 4.3], they found a highly collective $3^- T=0$ state at ≈ 7 MeV and two collective $1^- T=1$ states at 22.6 and 25.2 MeV. The octupole state exhausted 68% and the two dipole states exhausted 97% of the S_0 sum rule in this configuration space. This agrees qualitatively with the results of the schematic model (Sec. 8.2.2). The strength is concentrated mainly in one level shifted away from the unperturbed single-particle energies (~ 11.5 MeV).

The position of the energy levels is in good agreement with experiment—the two dipole states, which are discrete levels in this calculation, correspond to the two peaks in the dipole-resonance (Fig. 8.1). The absolute value of the excitation probability of the 3^- state is, however, a factor of 3–6 too small. One reason for this is the neglect of ground state correlations in the TDA; another reason is that the configuration space which includes only $1\hbar\omega_0$ excitations is probably too small (see below).

Gillet et al. [Gi 64, GV 64, GS 64, GGS 66] investigated the influence of ground state correlation by comparing TDA with RPA calculations in the closed shell nuclei ^{12}C , ^{16}O , ^{40}Ca , and ^{208}Pb . They again used a harmonic oscillator basis and a Gaussian force [Eq. (4.100)]. The parameters of the exchange mixture (Tab. (4.3)) were adjusted by extensive least-square fits to the ^{12}C and ^{16}O data. They found that the RPA leaves the TDA more or less unchanged for $T=1$ levels. The low-lying $T=0$ states, however, were reproduced better by the RPA. In particular, the RPA excitation probabilities were considerably larger than the TDA ones, although actually not reaching the experimental value. The reason is again the size of the configuration space, which included only $1\hbar\omega_0$ excitations. This fact in particular causes very poor results for positive parity states.

In detail, the results depend very much on the residual interaction. As we have already seen in Chapter 4, there have been attempts to derive such an interaction from the bare nucleon force. It is therefore very interesting to apply such forces to RPA calculations also. In this case, we have no free parameter and cannot necessarily expect the same agreement with the experimental data as with a phenomenologically adjusted force. Several groups [MMG 67, BK 69, KBB 70] have used the Kuo–Brown effective interaction [KB 66]. As discussed in Chapter 4, there are still many open problems inherent in the derivation of this force, and it is not absolutely clear how to modify an effective interaction originally deduced for pp -calculations for a ph theory. Nevertheless, the results are encouraging. Many of the collective energies are reproduced quite well. It turns out that the screening term (Fig. 4.7) plays an important role. Without it, the energy of the collective 3^- state in ^{208}Pb becomes imaginary [KBB 70]. The calculations have again been carried out in an oscillator basis and the configuration space includes only $1\hbar\omega_0$ excitations. Therefore, the absolute strength of the excitation probabilities is again too small.

Ring and Speth [RS 74a] used the theory of finite Fermi systems developed by Migdal [Mi 67]. This theory starts from quite a different point of view. It describes the interaction between quasi-particles and quasi-holes by a renormalized effective interaction which is short ranged and density dependent (Eq. (4.113)) and ends up with the RPA equations for the calculation of collective states. The force is phenomenological in as far as its parameters have to be adjusted to experimental values (such as energies and transition probabilities of collective states in even nuclei and electromagnetic moments and transitions probabilities in neighboring odd nuclei (see Sec. 9.3.5). This has been done in the lead region [RBS 73, BSK 73,

NW 74, BER 75, SWW 77] and the force has been applied in extensive RPA calculations in ^{208}Pb [RS 73, RS 74a, ERW 78] and other doubly closed shell nuclei [KS 74].

These calculations are different from the work discussed above in so far as they use (i) a Woods-Saxon basis, which is particularly important and more realistic than the harmonic oscillator for heavy nuclei, (ii) a large configuration space: two shells below and two shells above the Fermi surface, and (iii) a density-dependent interaction, which is slightly repulsive in the nuclear interior and attractive outside. The results are very encouraging. With six parameters adjusted once and for all, it is possible to reproduce nearly all of the experimental measured effective charges in

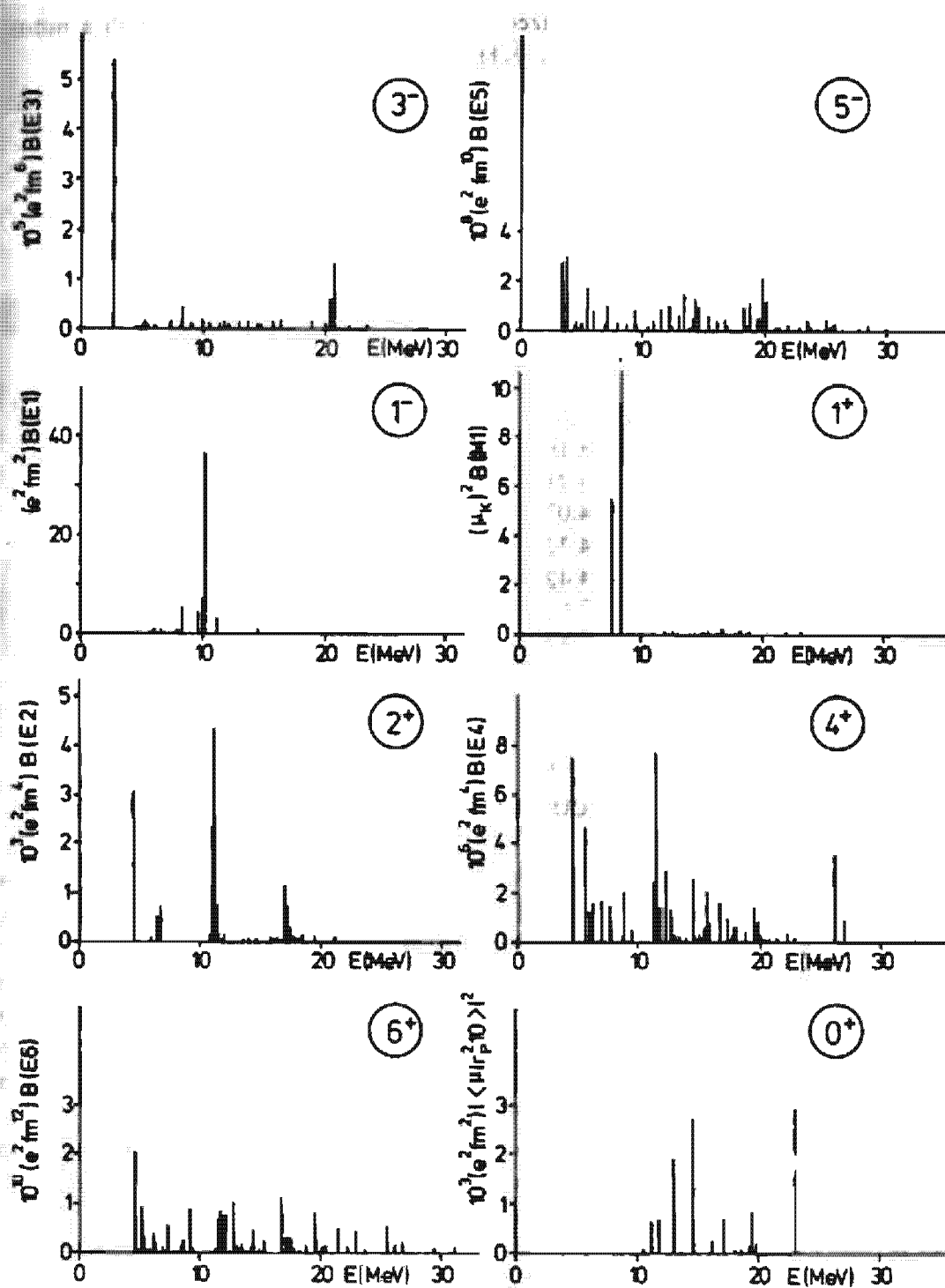


Figure 8.12. Distribution of multipole strength in ^{208}Pb (from [RS 74a]).

odd nuclei as well as the energies and the excitation probabilities of the excited states in even nuclei (see Table 8.1). Since the configuration space includes $2\hbar\omega$ excitations it is now also possible to reproduce positive parity states.

These calculations have been carried out in a discretized basis (the Woods-Saxon potential is expanded in a harmonic oscillator basis). The giant resonance therefore consists of discrete lines. Figure 8.12 shows the distribution of the strength. In particular, it shows the low-lying 3^- , 2^+ , 4^+ , 6^- collective states, but also the giant resonances, such as 1^- (which lies too low in energy), 2^+ (which is split into a $T=0$ part and a $T=1$ part), a breathing mode (0^+) at ~ 14 MeV, and higher resonances. To get a continuous resonance an RPA must be calculated fully in the continuum, as has been discussed in Sec. 8.5.4 [KBF 74, TW 78].

Similar calculations in a discretized basis have been carried out with a momentum dependent residual interaction [KH 76].

Table 8.1. Energies and excitation probabilities of low-lying collective states in ^{208}Pb , calculated with the Migdal force in RPA theory [RS 74a].

$E(I)$ [MeV]		$B\left(\frac{E}{M}\right)_I$ [$e^2 \text{ fm}^{2J}$] [$\mu^2 \text{ fm}^{2J-2}$]	
theory	exp.	theory	exp.
3^-	2.63	2.61	546 $540 \pm 30 \times 10^3$
5^-	3.39	3.19	285 $462 \pm 55 \times 10^6$
5^-	3.82	3.71	301 330×10^6
2^+	4.49	4.07	3070 2965
4^+	4.69	4.32	757 1287×10^4
6^+	4.77	4.42	210 230×10^8
1^+	7.50	7.56	568 5.9
1^+	8.30	7.99	11.00 10.0
2^-	7.51		11.00×10^3

8.6.2 Particle–Hole Calculations in a Self-Consistent Basis

As we have seen, RPA calculations with phenomenological density-dependent forces are able to describe many of the excited states in spherical closed shell nuclei. In Chapter 5 we learned that ground state properties are reproduced rather well in HF theory with Skyrme forces, and in Section 8.5 we constructed a method of deriving RPA theory from the density dependent HF theory: we have only to use the second derivative of the total energy with respect to the density as the *ph*-force [see Eq. (8.124)]. In the last few years this concept has been used by several groups [BT 75, LB 76, BGG 76, KKS 77, BG 77].

Starting from an HF calculation in coordinate space they either diagonalize the resulting HF single-particle Hamiltonian in an oscillator basis with nine or ten major shells to obtain discrete single-particle levels for a discretized RPA calculation or use the HF wave function and calculate in coordinate space. In the first case, we get discrete eigenvalues of the RPA equation, in particular the low-lying bound states and discretized resonances. In the other case, the continuum is taken

fully into account and we immediately get the strength function $S(\omega)$ [Eq. (8.149)], which has poles at the bound states.

The result of this calculation is that the usual Skyrme force—in its different versions [BFG 75]—which reproduces ground state properties very nicely, is not able to describe all the excited states [SLR 73, SZ 73, Ch 75, BJS 75]. This fact is not very disturbing, as the Skyrme force was adjusted so as to give the right energy and the right density at the equilibrium point of the functional $E[\rho]$. In particular, this means that the minimum is at the right value ρ_0 and has the right energy $E[\rho_0]$. However, it is not necessary that the curvature of the energy surface, $\delta^2 E / \delta \rho^2$, which gives the $p\bar{n}$ force, also be reproduced.

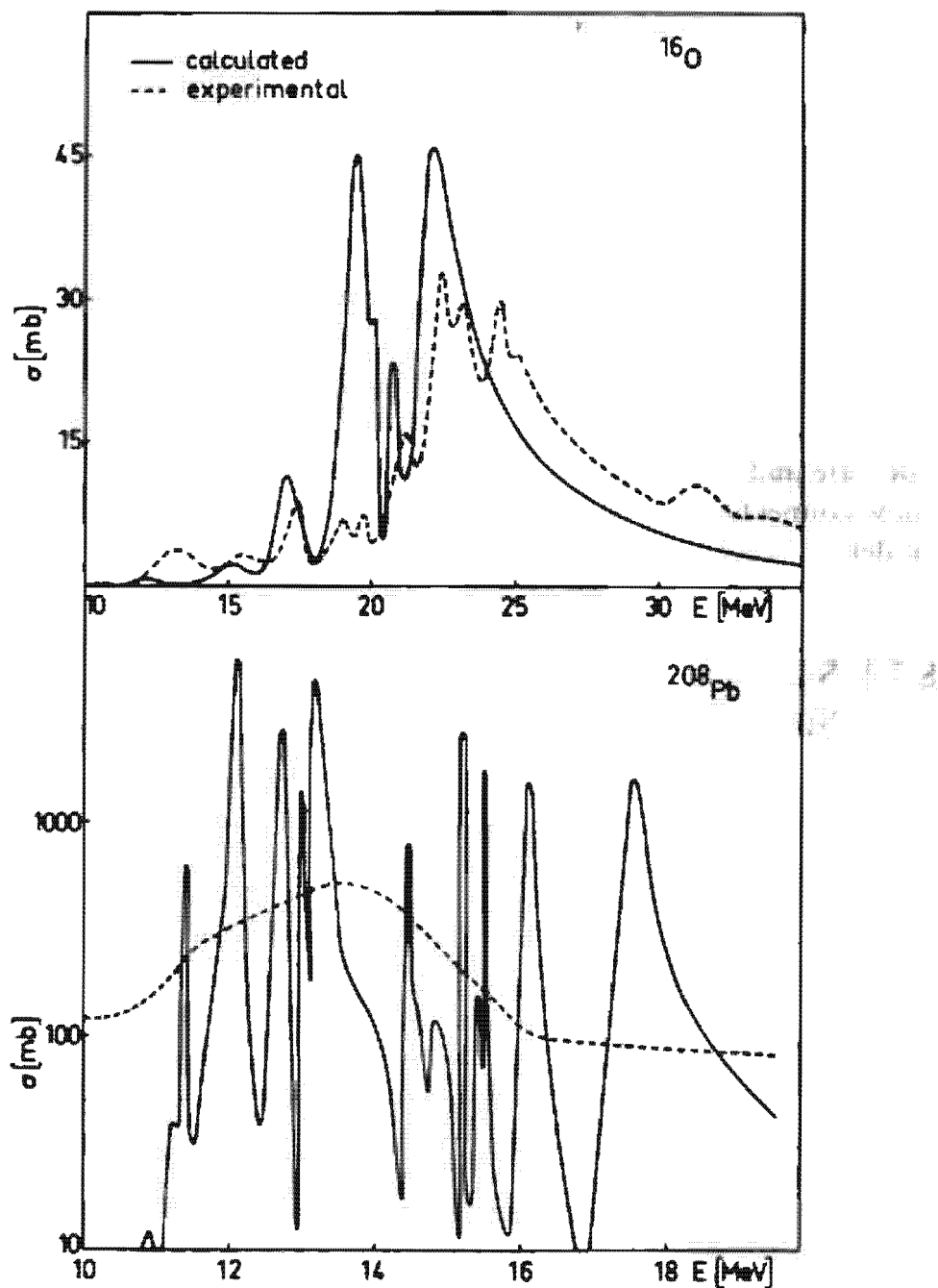


Figure 8.13. The photo cross section of the giant dipole resonance in ^{16}O and ^{208}Pb calculated with a continuum RPA calculation. The dashed lines correspond to experimental values. (From [LG 76b].)

The different groups, therefore, proposed generalizations of the Skyrme force that will not spoil their properties in HF calculations, such as a momentum-dependent three-body term [LB 76] $k^2 \cdot \delta(\mathbf{r}_{12})\delta(\mathbf{r}_{13})$ or density dependence of the momentum dependent *S*- and *P*-wave interaction [KKS 77]. In this way, one is able to reproduce the low-lying bound states more or less correctly and, in general, gets the right positions of the giant resonances. However, one is not able—even with the continuum calculations—to reproduce the proper width and the fine structure of the giant resonances. The reason is that only the decay width has been calculated (see Sec. 8.5.4) and not the spreading width. To do this we must include higher configurations such as $2p - 2h$ or $3h - 3h$ states [WS 72]. This goes beyond the RPA approach. In Fig. 8.13, we observe that in ^{208}Pb , in particular, the theoretical curve for the giant resonance is split into many sharp peaks and coupling to higher configurations should wash this out.

8.7 Sum Rules

We have already seen that in the calculation of the total cross-section of the giant dipole resonance in Section (8.3.3), the sum rules form a very important tool in the theory of collective excitations. In many cases, they allow a calculation of global properties in a simple way and are therefore useful in testing different approximation schemes. Sum rules give less detailed information than the RPA solutions, but they are much easier to calculate and easier to interpret [No 78, BLM 79]. More particularly, they allow connections to be made to the older macroscopic or hydrodynamical models.

8.7.1 Sum Rules as Energy Weighted Moments of the Strength Functions

In general, a sum rule is related to a Hermitian single-particle operator $F = \sum f_{pq} a_p^+ a_q$ and given by

$$S_k \equiv \sum_{\nu} (E_{\nu} - E_0)^k |\langle \nu | F | 0 \rangle|^2. \quad (8.150)$$

It gives the k th moment of the distribution of the excitation strength produced by the one-body operator F . The $|\nu\rangle$ s represent the complete set of eigenstates of the exact Hamiltonian H with the energies E_{ν} . Using the completeness relation, we find

$$S_k = \langle 0 | F(H - E_0)^k F | 0 \rangle. \quad (8.151)$$

We will see that in some cases this expression can be calculated in a rather simple way.

Following Lane et al. [MBF 76, BML 76, BLM 79], we can define a set

of energies

$$\varepsilon_k = \left(\frac{S_k}{S_{k-2}} \right)^{1/2} \quad (8.152)$$

which characterizes the strength distribution (8.150). If it is sharply peaked at a certain energy, then all the ε_k coincide. The degree to which they are different reflects the width of the distribution.

Using the Schwarz inequality for the moments $S_{k+2} \cdot S_k \geq S_{k+1} \cdot S_{k+1}$, we deduce [La 75] that

$$\varepsilon_{-1} < \varepsilon_0 < \varepsilon_1 < \bar{E} \equiv \frac{S_1}{S_0} < \varepsilon_2 < \dots$$

and get for the mean square fluctuation about the mean energy [BLM 79]

$$\rho^2 \equiv \varepsilon_2^2 - \bar{E}^2 < \frac{1}{4} (\varepsilon_3^2 - \varepsilon_1^2). \quad (8.153)$$

As we shall see, we can evaluate the moments S_{-1} , S_1 , and S_3 rather generally. Therefore, in this way we can gain information about the energy of a resonance and its width.

8.7.2 The S_1 -Sum Rule and the RPA Approach

The most important sum rule is the energy weighted sum rule S_1 . It can be written as a double commutator [see Eq. (8.42)]

$$S_1 = \sum_{\nu} (E_{\nu} - E_0) |\langle \nu | F | 0 \rangle|^2 = \frac{1}{2} \langle 0 | [F, [H, F]] | 0 \rangle. \quad (8.154)$$

This relation holds for a set of exact eigenstates $|\nu\rangle$ of H . We usually have only approximative states $|\nu\rangle$ and approximative energies E_{ν} . It is a test of the validity of any approximation to see whether it fulfills the sum rules.

Thouless [Th 61a] showed that the sum rule (8.154) is satisfied if the left-hand side is evaluated with RPA wave functions and energies and the right-hand side is calculated using the HF ground state wave function. In the following we give a proof of this theorem for the case of Hermitian one-body operators F and G [La 75]. Using the notation of Eq. (8.72), we find for density independent forces with (8.76) and (8.79)

$$\begin{aligned} \langle HF | [F, [H, G]] | HF \rangle &= (F^* - F) \begin{pmatrix} A & B \\ B^* & A^* \end{pmatrix} \begin{pmatrix} G \\ -G^* \end{pmatrix} \\ &= f^+ \mathcal{X} \Omega \mathcal{X}^+ g. \end{aligned} \quad (8.155)$$

Finally, expression (8.72) for the strengths $\langle 0 | F | \nu \rangle$ yields

$$\langle HF | [F, [H, G]] | HF \rangle = \sum_{\nu} \hbar \Omega_{\nu} (\langle 0 | F | \nu \rangle \langle \nu | G | 0 \rangle + \langle 0 | G | \nu \rangle \langle \nu | F | 0 \rangle). \quad (8.156)$$

It is easy to generalize this relation [GLM 78]:

$$\int^+ \begin{pmatrix} A & B \\ -B^* & -A^* \end{pmatrix}^n \mathcal{R} g = \sum_s (\hbar\Omega_s)^n (\langle 0|F|s\rangle \langle s|G|0\rangle + (-)^{s+1} \text{c.c.}). \quad (8.157)$$

In the case of *density dependent* forces, however, the matrices A and B are defined by Eq. (8.124), and this proof does not apply.

In fact, in general we get additional terms on the rhs of Eq. (8.154). Nevertheless, it can be shown that the theorem also applies to local operators $F(r)$ and interactions whose density-dependent parts do commute with F [BG 77], as is the case for the usual Skyrme force (4.104).

From Eq. (8.155) we also recognize immediately that the sum rule S_1 is violated in the TDA approach, which is obtained by simply setting $B=0$, and conversely the TDA approximation conserves the sum rule S_0 , which is violated by the RPA. The pure shell model without residual interaction fulfills both sum rules S_0 and S_1 .

The sum rule S_1 is of special importance because it can be reduced to an expectation value of a one-body operator which can be evaluated rather easily, as will be seen in the following section.

8.7.3 Evaluation of the Sum Rules S_1 , S_{-1} , and S_3

To evaluate the energy weighted sum rule, we shall restrict ourselves here to an isoscalar single-particle operator $F = \sum_i f(r_i)$ and neglect momentum dependent parts in the residual interaction.*

In this case we have only a contribution coming from the kinetic energy, thus

$$S_1 = \frac{1}{2} \langle 0 | [F, [H, F]] | 0 \rangle = \frac{\hbar^2}{2m} A \langle 0 | (\nabla f)^2 | 0 \rangle. \quad (8.158)$$

However, the dipole case is extremely simple, because F is linear and ∇f no longer depends on r (8.39). This part of the calculation is therefore model independent. In all other cases $(\nabla f)^2$ is still a single-particle operator which should not be too sensitive to correlations in the ground state $|0\rangle$. It can therefore be easily calculated within a model.

For surface vibrations we have already seen that $F = r^\lambda Y_{\lambda 0}$. Using the gradient formula [Ed 57], we may derive†

$$S_1(r^\lambda Y_{\lambda 0}) = \frac{\hbar^2}{2m} A \langle 0 | (\nabla r^\lambda Y_{\lambda 0})^2 | 0 \rangle = \frac{\hbar^2}{2m} \frac{(2\lambda+1)\lambda}{4\pi} \cdot A \cdot \langle r^{2\lambda-2} \rangle. \quad (8.159)$$

* We can show [BL 76] that Eq. (8.158) holds for the Skyrme force, too, because of the δ -character of the p^2 -terms. This is, however, no longer true for isovector operators such as the dipole operator (8.39). We also gain contributions to the dipole sum rule from exchange forces, as discussed in Section 8.3.3 (see also [Ki 78]).

† For a nucleus with a constant density and a sharp surface we obtain:

$$\langle r^L \rangle = \frac{3}{L+3} R^L.$$

In the quadrupole case, S_3 is proportional to the mean square radius $\langle r^2 \rangle$. The same is true for $E0$ excitations—breathing modes—in which $F \propto r^2$ must be used (see [SF 74]).

We have already seen in Section 8.5.3 that the static polarizability α is proportional to the inverse energy-weighted sum rule S_{-1} ; this fact can be used to calculate it in the RPA approximation using the solution of a constrained HF calculation ($H - \lambda F$) in the limit of small λ -values (see also [SLO 78]).

$$S_{-1}^{\text{RPA}} = \frac{1}{2} \frac{\partial^2}{\partial \lambda^2} \langle \Phi(\lambda) | H | \Phi(\lambda) \rangle_{\lambda=0}. \quad (8.160)$$

To calculate the sum rule S_3 , we can use the identity [La 75, MBF 76, LOL 76]:

$$S_3 = \langle 0 | F(H - E_0)^3 F | 0 \rangle = -\frac{1}{2} \left(\frac{2\hbar^2}{m} \right)^2 \langle 0 | [G, [H, G]] | 0 \rangle \quad (8.161)$$

with $-(2\hbar^2/m)G = [H, F] = [T, F]$, which is a one-particle operator if the potential energy commutes with F . In this case, we can calculate the energy-weighted sum rule for the operator G . It can be obtained as the second derivative

$$S_3 = \frac{1}{2} \left(\frac{2\hbar^2}{m} \right)^2 \frac{\partial^2}{\partial \eta^2} E(\eta) \Big|_{\eta=0} \quad (8.162)$$

of the energy

$$E(\eta) = \langle 0 | e^{-\eta G} H e^{\eta G} | 0 \rangle. \quad (8.163)$$

This equation is also true if we replace the exact ground state $|0\rangle$ on the r.h.s. by the $|\text{HF}\rangle$ ground state and S_3 by S_3^{RPA} on the left-hand side.

In the following, we shall restrict ourselves to isoscalar multipole vibrations ($f = r^\lambda Y_{\lambda 0}$) and breathing modes ($f = r^2$). Similar calculations have also been made for the isovector modes [BL 76].

For the operator G , we find

$$G = \frac{1}{2} (\nabla r^\lambda Y_{\lambda 0}) \cdot \nabla (\lambda \neq 0) \quad \text{and} \quad G = \frac{3}{2} + r \frac{\partial}{\partial r} (\lambda = 0), \quad (8.164)$$

where we have used $\Delta r^\lambda Y_{\lambda 0} = 0$. We see that $e^{\eta G}$ is, in fact, a *scaling operation*.

$$e^{\eta/2(\nabla r^\lambda Y_{\lambda 0}) \cdot \nabla} \Phi(r) \propto \Phi\left(r + \frac{\eta}{2} \nabla r^\lambda Y_{\lambda 0}\right). \quad (8.165)$$

In the case $\lambda = 0$ and $\lambda = 2$, we get

$$e^{\eta G} \Phi(x_i, y_i, z_i) = \begin{cases} e^{3/2\eta^2} \Phi(x_i e^\eta, y_i e^\eta, z_i e^\eta), & (\lambda = 0), \\ \Phi(x_i e^{-\eta'}, y_i e^{-\eta'}, z_i e^{2\eta'}), & (\lambda = 2), \end{cases}$$

with $\eta' = \eta \cdot (5/16\pi)^{1/2}$. The factor $e^{3/2\eta}$ in the case $\lambda = 0$ shows the difference between the breathing modes, which change the density over the

whole volume, and the higher multipolarities, which involve only the nuclear surface. It is easy to calculate the contributions to $E(\eta)$ of the different parts of simple forces:

	$\lambda = 0$	$\lambda = 2$
Kinetic energy T	$e^{2\eta} \langle T \rangle$	$1/3(2e^{-2\eta} + e^{+2\eta}) \langle T \rangle$
$V_0 \propto \delta(r - r')$	$e^{3\eta} \langle V_0 \rangle$	$\langle V_0 \rangle$
$V_p \propto \rho \delta(r - r')$	$e^{6\eta} \langle V_p \rangle$	$\langle V_p \rangle$

and to derive the contributions to the sum rule S_3 . As an example, we present the case of quadrupole vibrations ($\lambda = 2$):

$$S_3(\lambda = 2) = \frac{1}{2} \left(\frac{2\hbar^2}{m} \right)^2 \frac{5}{16\pi} 8 \langle T \rangle.$$

Together with (8.159), we find for the energy ξ_3 , (8.152)

$$\xi_3(\lambda = 2) = \left(\frac{S_3}{S_1} \right)^{1/2} = \left(\frac{\hbar^2}{m} \frac{4 \langle T \rangle}{A \langle r^2 \rangle} \right)^{1/2}. \quad (8.166)$$

In the harmonic oscillator model, the expectation value of T is equal to the potential energy $\langle T \rangle = \frac{1}{2} m \omega_0^2 \langle r^2 \rangle A$. If we furthermore assume that all the strength is concentrated in a small energy interval, all the ξ_k should be roughly equal, and we then find for the energy of the giant quadrupole resonance ($T = 0$) with $\hbar\omega_0 \approx 41 A^{-1/3}$ [MeV],

$$E(2^+) = \sqrt{2} \hbar\omega_0 \approx 58 \cdot A^{-1/3} [\text{MeV}] \quad (8.167)$$

a formula which is in good agreement with experiment [Eq. (8.46)] and which has also been derived in a similar model by Mottelson and Suzuki [BM 75, Su 73]. It can be extended to higher isoscalar surface vibrations and gives

$$E(\lambda) = \sqrt{\lambda} \cdot 41 \cdot A^{-1/3} [\text{MeV}] \quad (\lambda > 2). \quad (8.168)$$

Zamick [Za 73, Za 74a] has shown that the breathing mode is not well described by zero range forces which are unable to give saturation. One has to include finite range terms, or at least the p^2 -terms, in the Skyrme force. With reasonable values for the force constants, we get

$$E(0^+) \approx 2\hbar\omega_0 \approx 82 A^{-1/3} [\text{MeV}]. \quad (8.169)$$

We find that the energy of all the surface vibrations is $\propto A^{-1/3}$, which is in agreement with the experiment. From the simple hydrodynamical model, as discussed in Section 1.4, we find $E_\lambda = (C_\lambda / B_\lambda)^{1/2} \propto A^{-1/2}$. The reason for this discrepancy will be discussed in Section 13.3.

8.7.4 Sum Rules and Polarizabilities

In Eq. (8.160) we expressed the sum rule $S_{-1}(F)$, that is, the -1st moment of the strength distribution in a RPA calculation, by the RPA polarizability of the system in an external field F . This can be extended [GLM 78]. The RPA sum rules $S_{2n-1}(F)$ for arbitrary n can be expressed as the polarizability in a suitable single-particle field $F^{(n)}$.

We therefore start with the operator F and define

$$F^{(0)} = \sum_{mi} f_{mi} a_m^+ a_i + f_{im} a_i^+ a_m \quad (8.170)$$

$$F^{(1)} = i[H, F^{(0)}]'$$

$$F^{(2)} = i[H, F^{(1)}]'$$

⋮

where the prime means only the ph and hp part of the corresponding operator $F^{(n)}$. The $F^{(n)}$ is therefore a single-particle operator with vanishing pp and hh matrix elements.

Using the definitions (8.72) we get for the ph and hp matrix elements

$$f^{(n+1)} = iS\mathcal{R}f^{(n)}. \quad (8.171)$$

With this relation we may also define the operators $F^{(n)}$ for negative values of n . From Eq. (8.157) we find that

$$\begin{aligned} S_{2n-1}(F) &= \frac{1}{2} f^{(0)} + (\mathcal{R}S)^{2n-1} \mathcal{R}f^{(0)} = \frac{1}{2} f^{(n)} + S^{-1}f^{(n)} \\ &= \frac{1}{2}\alpha(F^{(n)}) = S_{-1}(F^{(n)}) \end{aligned} \quad (8.172)$$

corresponds to the polarizability with respect to the operator $F^{(n)}$. In cases where the operator $F^{(n)}$ has a simple form, we can find the corresponding sum rules very easily. In the last section we had examples of such cases.

8.7.5 Calculation of Transition Currents and Densities

A generalization of the usual sum rule (8.150) for the nuclear *density* (D.1) has been derived by Kao and Fallieros [KF 70, No 71, DF 73]:

$$S_\rho(\mathbf{r}) = \sum_p (E_p - E_0) \langle 0 | \hat{\rho}(\mathbf{r}) | p \rangle \langle p | F | 0 \rangle. \quad (8.173)$$

If we assume that F is a local, spin-independent operator of the form $F = \sum_i f(\mathbf{r}_i)$, it can be evaluated for velocity-independent forces:

$$S_\rho(\mathbf{r}) = \frac{1}{2} \langle 0 | [\hat{\rho}(\mathbf{r}), [H, F]] | 0 \rangle = -\frac{\hbar^2}{2m} \nabla (\rho^{(0)}(\mathbf{r}) \nabla f(\mathbf{r})), \quad (8.174)$$

where $\rho^{(0)}(\mathbf{r})$ is the density of the time reversal invariant ground state.

In the case where one state exhausts the total sum rule $S_p(r)$ (the "classical case"), $S_p(r)$ is proportional to the transition density (8.31) $\langle 0|\hat{\rho}(r)|\nu\rangle$. In such a case we have a connection between the quantum mechanical RPA calculation and the classical interpretation of a vibrating liquid drop, and we can study the actual form of the vibration which we have calculated in the RPA theory.

From Eqs. (8.173) and (8.174) we see that this form depends crucially on the transition operator F . It is determined by the requirement that *one* state exhausts a major part of the corresponding sum. As an example, we take

$$f(r) = r^\lambda Y_{\lambda 0} \quad \text{for } \lambda > 0 \quad \text{and} \quad f(r) = r^2 \quad \text{for } \lambda = 0.$$

In this case, we get

$$\rho^{(\nu)}(r) = \langle 0|\hat{\rho}(r)|\nu\rangle \propto \begin{cases} \lambda r^{\lambda-1} Y_{\lambda 0} \frac{d}{dr} \rho^{(0)}, & \lambda \neq 0, \\ 3\rho^{(0)} + r \frac{d}{dr} \rho^{(0)}, & \lambda = 0. \end{cases} \quad (8.175)$$

We have seen that with these transition operators the giant resonances exhaust to a large extent the sum rules. We then get transition densities (8.175) which correspond exactly to hydrodynamic models, which will be discussed in Section 13.3. In the case of $\lambda > 0$, we get the *Bohr-Tassie model* [Bo 52, Ta 56a] of an incompressible irrotational fluid, and in the case $\lambda = 0$ we get the *Wertz-Überall model* [WU 66] of a compressible irrotational fluid.

Figure 8.14 shows transition densities for the case $\lambda = 0$ and $\lambda = 2$ in the nucleus ^{208}Pb . The simple expression (8.175) (dotted curves) are in very good agreement with the transition densities obtained from a continuum RPA calculation with the Skyrme I force (full lines). This shows that the giant resonances ($\lambda > 0$) to a large extent correspond to the surface vibrations of a liquid drop discussed in Chapter 1.

Suzuki and Rowe [SR 76, SR 77] derived a similar sum rule for the current density

$$\hat{j}(r) = \frac{\hbar}{2mi} \sum_{i=1}^A (\delta(r-r_i) \nabla_i + \nabla_i \delta(r-r_i)). \quad (8.176)$$

$$\begin{aligned} S_j(r) &= \sum_\nu \langle 0|\hat{j}(r)|\nu\rangle \langle \nu|F|0\rangle \\ &= \frac{1}{2mi} \rho^{(0)}(r) \nabla f(r). \end{aligned} \quad (8.177)$$

In the "classical" case, where one state exhausts the entire sum, we can calculate the *transition current density*

$$j^{(\nu)}(r) = \langle 0|\hat{j}(r)|\nu\rangle \propto \rho^{(0)}(r) \nabla f(r). \quad (8.178)$$

This is the current which is connected to the collective motion in the same sense as the transition density (8.30) corresponds to the change in the density in the collective motion (see Sec. 13.3). We then can also define the

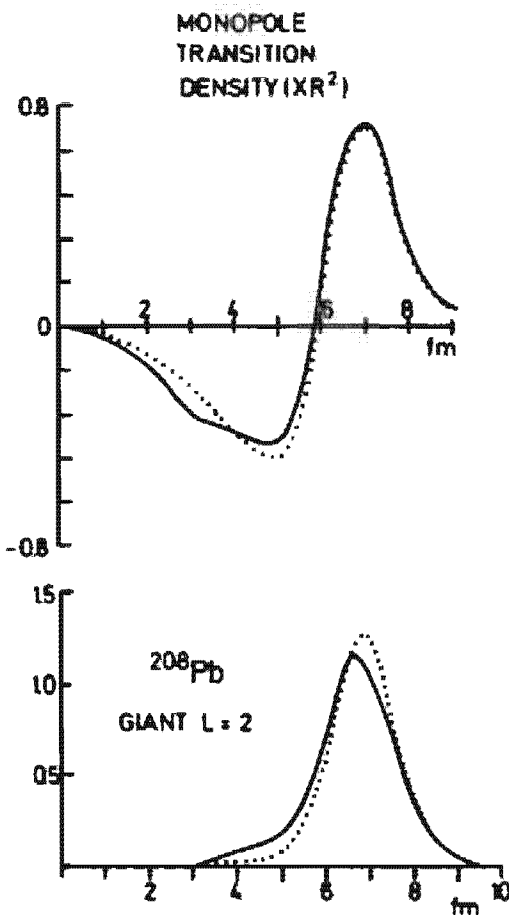


Figure 8.14. Isoscalar monopole and quadrupole transition densities in ^{208}Pb . (From [BT 75].)

velocity field

$$\mathbf{v}^{(\nu)}(\mathbf{r}) = \frac{\langle 0|\hat{\mathbf{j}}(\mathbf{r})|\nu\rangle}{\rho^{(0)}(\mathbf{r})} \propto \nabla f(\mathbf{r}). \quad (8.179)$$

It is irrotational—

$$\nabla \times \mathbf{v}^{(\nu)} = 0 \quad (8.180)$$

—for arbitrary, local one-body operators F . Furthermore, in the case of $f \sim r^\lambda Y_{\lambda 0}$, we get incompressibility (1.25) viz:

$$\nabla \cdot \mathbf{v}^{(\nu)} = 0.$$

We have to emphasize, however, that the simple classical picture of a local transition operator, which exhausts the entire sum rule, is only an approximation. Usually a part of the total strength is distributed also over some low-lying collective states (see Fig. 8.12).

In general, the excited state $|\nu\rangle$ can be written in the form*

$$|\nu\rangle = O_\nu^+ |0\rangle \quad \text{with } O_\nu |0\rangle = 0,$$

* As long as we allow a general operator for O_ν^+ , the following considerations are exact [St 79]. If we restrict ourselves to one-particle operators O_ν^+ , we end up with the RPA approach.

and we obtain for the wave packet (8.27) in the limit of small amplitudes ($\epsilon \ll 1$):

$$\begin{aligned} |\Psi(t)\rangle &= |0\rangle + \epsilon O_s^+ |0\rangle e^{-i\Omega_s t} \\ &= e^{iA(t)} |0\rangle \end{aligned}$$

with the Hermitian operator

$$A(t) = -i\epsilon(O_s^+ e^{-i\Omega_s t} - O_s e^{i\Omega_s t}).$$

We can also express $|\Psi(t)\rangle$ by the generalized coordinate \mathcal{Q}_s and the momentum \mathcal{P}_s , as defined in Eq. (8.95), with $\epsilon' = \epsilon(2/M_s \Omega_s \hbar)^{1/2}$:

$$|\Psi(t)\rangle = \exp[-i\epsilon'(\Omega_s M_s \mathcal{Q}_s \sin \Omega_s t + \mathcal{P}_s \cos \Omega_s t)] |0\rangle.$$

If the ground state $|0\rangle$ and the operator O_s^+ is time even,

$$TO_s^+ T^+ = O_s^+ \quad \text{and} \quad T|0\rangle = |0\rangle,$$

this representation corresponds to the separation of time-even (\mathcal{Q}_s) and time-odd parts (\mathcal{P}_s) in $A(t)$. They induce physically different effects in the nucleus: The transformation $\exp(-i\epsilon' \mathcal{P}_s \cos \Omega_s t)$ is time even. It causes "static"^{*} deformations. On the contrary, the operation $\exp(-i\epsilon' M_s \Omega_s \mathcal{Q}_s \sin \Omega_s t)$ is time odd and induces currents. Both effects oscillate with the frequency Ω_s .

The expectation value of any operator \hat{T} in the state $|\Psi(t)\rangle$ is given by:

$$\begin{aligned} \langle \Psi(t) | \hat{T} | \Psi(t) \rangle &= \langle 0 | \hat{T} | 0 \rangle - i\epsilon' \langle 0 | [\hat{T}, \mathcal{Q}_s] | 0 \rangle M_s \Omega_s \sin \Omega_s t \\ &\quad - i\epsilon' \langle 0 | [\hat{T}, \mathcal{P}_s] | 0 \rangle \cos \Omega_s t. \end{aligned}$$

Considering for the operator \hat{T} either the density $\hat{\rho}(r)$ or the current $\hat{j}(r)$, we obtain for the transition density and the transition current:

$$\rho''(r) = -\frac{i}{\hbar} \sqrt{\frac{\hbar}{2M_s \Omega_s}} \langle 0 | [\hat{\rho}(r), \mathcal{Q}_s] | 0 \rangle,$$

$$j''(r) = \sqrt{\frac{M_s \Omega_s}{2\hbar}} \langle 0 | [\hat{j}(r), \mathcal{Q}_s] | 0 \rangle,$$

respectively. The state $|\nu\rangle$ is completely determined by the "coordinate" \mathcal{Q}_s . The corresponding "momentum" \mathcal{P}_s can be calculated from Eq. (8.98). As an example, we obtain for a velocity independent single-particle operator

$$\mathcal{Q}_s = \sum_i f(r_i),$$

and for a local two-body interaction the corresponding momentum

$$\mathcal{P}_s = \frac{1}{2} \frac{M_s}{m} \sum_i (\hat{p}_i \nabla f(r_i) + \text{h.c.})$$

^{*} We use here the word "static" in the sense of Section 12.3.1.

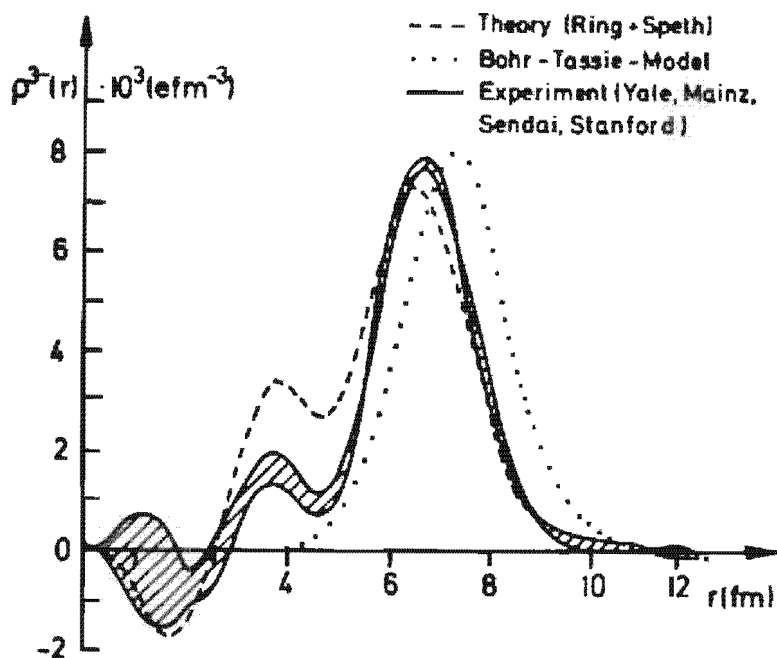


Figure 8.15. Theoretical and experimental radial transition density of the lowest 3^- state of ^{208}Pb . The full lines indicate the experimental errors [RFM 74], the dashed line [TW 73] is based on RPA calculations with the Migdal force, and the dotted line corresponds to the Bohr-Tassie model. (From [St 79].)

The constant M_+ is determined from the commutation relation (8.96). Again the velocity field is irrotational.

In general, we do not know \mathcal{Q} , a priori and obtain this operator only after the solution of the RPA equation. It then turns out that the low-lying collective states have large nonlocal components in \mathcal{Q} [St 79]. They cannot be represented by the simple hydrodynamical models discussed above.

An example is the low-lying collective 3^- state in ^{208}Pb . Figure 8.15 shows experimental and theoretical transition densities $\rho^3(\mathbf{r})$. The experimental values deviate rather dramatically from the predictions of the Bohr-Tassie model. The fully microscopic calculation obtained by the solution of the RPA equation with a density dependent force is in much better agreement. Again for the high lying 3^- state the agreement with the Bohr-Tassie model is good [St 79].

8.8 Particle-Particle RPA

8.8.1 The Formalism

As in the Tamm-Dancoff case, where we distinguished between ph and pp TDA (Sec. 8.2.3), we have a pp RPA corresponding to the ph RPA. The pp TDA and the pp RPA give us states in the $A \pm 2$ systems. If they are collective, they are called *pairing vibrations* (see Sec. 8.3.5). Since many formal features of the pp RPA will be almost identical to those in the ph RPA, we will be quite brief in this section.

Corresponding to the *ph*-ansatz (8.65), in the *pp* case for the eigenstate τ of the $A+2$ system we have

$$\begin{aligned} |A+2, \tau\rangle &= \left(\sum_{m < n} X_{mn}^{\tau} a_m^+ a_n^+ - \sum_{i < j} Y_{ij}^{\tau} a_i^+ a_j^+ \right) |A, 0\rangle \\ &= R_{\tau}^+ |A, 0\rangle. \end{aligned} \quad (8.181)$$

The ground state (belonging to the A -system) is defined by

$$R_{\tau} |A, 0\rangle = 0$$

and we get in the same approximation as in Eq. (8.69):

$$X_{mn}^{\tau} = \langle A, 0 | a_m a_n | A+2, \tau \rangle; \quad Y_{ij}^{\tau} = \langle A, 0 | a_i a_j | A+2, \tau \rangle. \quad (8.182)$$

Proceeding as in the *ph* case (Sec. 8.4.1), and using the equation of motion for R_{τ}^+ , we obtain* [FIS 64, Sch 64b, MLE 67, Ro 68a+b, RP 69]

$$\begin{aligned} (\hbar\Omega_{\tau} - \epsilon_m - \epsilon_n) X_{mn}^{\tau} &= \sum_{m' < n'} \bar{v}_{mm'n'n'} X_{m'n'}^{\tau} - \sum_{i' < j'} \bar{v}_{mm'ij'} Y_{ij'}^{\tau}, \\ (-\hbar\Omega_{\tau} + \epsilon_i + \epsilon_j) Y_{ij}^{\tau} &= - \sum_{m' < n'} \bar{v}_{ijm'n'} X_{m'n'}^{\tau} + \sum_{i' < j'} \bar{v}_{ijrj'} Y_{rj'}^{\tau}. \end{aligned} \quad (8.183)$$

$\hbar\Omega_{\tau} = E_{\tau}^{A+2} - E_0^A$ is the excitation energy of the $A+2$ nucleus related to the ground state of the A -system.

We get identical equations for the $A-2$ particle system

$$(-\hbar\Omega_{\lambda} + \epsilon_i + \epsilon_j) X_{ij}^{\lambda} = \sum_{i' < j'} \bar{v}_{ijrj'} X_{rj'}^{\lambda} - \sum_{n' < m'} \bar{v}_{ijn'm'} Y_{n'm'}^{\lambda}, \quad (8.184)$$

$$(\hbar\Omega_{\lambda} - \epsilon_n - \epsilon_m) Y_{nm}^{\lambda} = - \sum_{i' < j'} \bar{v}_{nmij'} X_{ij'}^{\lambda} + \sum_{n' < m'} \bar{v}_{nmn'm'} Y_{n'm'}^{\lambda},$$

with $\hbar\Omega_{\lambda} = E_0^A - E_{\lambda}^{A-2}$,

$$X_{ij}^{\lambda} = \langle A-2, \lambda | a_i a_j | A, 0 \rangle, \quad Y_{nm}^{\lambda} = \langle A-2, \lambda | a_m a_n | A, 0 \rangle. \quad (8.185)$$

We can therefore combine Eqs. (8.183) and (8.184) into one matrix equation similar to that in the *ph* case:

$$\begin{pmatrix} A & B \\ B^+ & C \end{pmatrix} \begin{pmatrix} R_{\tau}^{\tau, \lambda} \\ R_h^{\tau, \lambda} \end{pmatrix} = \begin{pmatrix} 1 & 0 \\ 0 & -1 \end{pmatrix} \begin{pmatrix} R_p^{\tau, \lambda} \\ R_h^{\tau, \lambda} \end{pmatrix} \cdot \hbar\Omega_{\tau, \lambda}, \quad (8.186)$$

with

$$A_{mm'n'n'} = \delta_{mn} \delta_{n'n} (\epsilon_m + \epsilon_n) + \bar{v}_{mm'n'n'},$$

$$C_{ijrj'} = - \delta_{ii'} \delta_{jj'} (\epsilon_i + \epsilon_j) + \bar{v}_{ijrj'},$$

$$B_{nmij} = - \bar{v}_{nmij}.$$

* The Eqs. (8.183) can also be derived from the time-dependent HF Eq. (8.116) generalized to include pair correlations. In application to nuclear physics this theory has been set up by H. Schmidt [Sch 64a+b].

and

$$\begin{aligned} (R_p^r)_{mn} &= X_{mn}^r, & (R_p^\lambda)_{mn} &= Y_{mn}^\lambda, \\ (R_h^r)_{ij} &= Y_{ij}^r, & (R_h^\lambda)_{ij} &= X_{ij}^\lambda. \end{aligned} \quad (8.187)$$

Note that, in general, the hermitian matrices A and C have different dimensions and that B is a rectangular matrix.

Equation (8.187) thus simultaneously yields the eigenstates of the $A \pm 2$ system, which are different from the ph case in which we had only solutions belonging to the same particle number. This, however, does not mean that the particle number is violated in pp RPA as it is in the BCS model (Chap. 6). The ansatz (8.181) conserves particle number. In practice, we recognize the solutions of Eq. (8.186), which belong to the pp system according to their wave functions: They have large pp components X_{mn} and small hh components Y_{ij} , and energies in the region of the pp -energies $\epsilon_m + \epsilon_n$. In cases where the pp and the hh components are of the same order of magnitude, we are, as in the ph -RPA, close to a phase transition, and the RPA approximation is not justified in any case.

Most of the other RPA features remain the same as in the ph -case. We list here, without proof, the normalization conditions:

$$\begin{aligned} \sum_{m < n} X_{mn}^{r*} X_{mn}^r - \sum_{i < j} Y_{ij}^{r*} Y_{ij}^r &= \delta_{rr}, \\ \sum_{i < j} X_{ij}^{\lambda*} X_{ij}^{\lambda} - \sum_{m < n} Y_{mn}^{\lambda*} Y_{mn}^{\lambda} &= \delta_{\lambda\lambda}. \end{aligned} \quad (8.188)$$

and the closure relation ($r < s, r' < s'$)

$$\sum_r X_{rs}^r X_{r's'}^{r*} - \sum_\lambda Y_{rs}^{\lambda*} Y_{r's'}^{\lambda} = \delta_{rr'} \delta_{ss'}. \quad (8.189)$$

The pp -RPA has been applied with success for closed shell ± 2 -nucleons nuclei [VG 71, BV 71, KS 76]. It turns out, however, that in most cases a simple pp TDA calculation gives similar results. The $A \pm 2$ states are usually much less collective than the low-lying ph states. Therefore, the violation of the Pauli principle in the RPA approximation seems to be less justified than in the ph case. Therefore, the TDA approach is used in most of the $A \pm 2$ nuclei.

8.8.2 Ground State Correlations Induced by Pairing Vibrations

We have already seen that the ground state of the A -system is defined as the vacuum with respect to the boson operator O , (8.91), and in Eq. (8.101) we derived an explicit expression for it. By analogy, we now require that

$$R_r|RPA\rangle = R_\lambda|RPA\rangle = 0. \quad (8.190)$$

This yields an exponential factor of the form

$$|\text{RPA}\rangle = N_0 \exp\left(\sum_{m < n, i < j} Z_{maji} A_m^+ A_n^+ A_i^+ A_j^+\right) |\text{HF}\rangle, \quad (8.191)$$

with

$$A_m^+ = a_m^+ a_n^+; A_i^+ = a_i a_j \quad \text{and} \quad Z^T = Y^* X^{*-1}.$$

If pp as well as ph correlations are important, the ground state has to be simultaneously the vacuum of the ph and pp bosons. We then gain an expression for the ground state having two exponential factors. These factors commute in the quasi-boson approximation.

Expanding Eq. (8.191), we see that the correlated ground state contains, besides the $|\text{HF}\rangle$ state, contributions with two bosons, four bosons, and so on. The particle number is conserved, because the number of pp bosons is always equal to the number of the hh bosons.

To study the pp correlations in more detail, we restrict ourselves to a pure pairing force [see Eq. (4.140)] and a spherical closed shell nucleus. Since the pure pairing force is separable in the pp direction, we can again get the schematic model. In analogy to Eq. (8.135), we may derive from Eq. (8.184) the following dispersion relation.

$$\frac{2}{G} = \sum_n \frac{2j_n + 1}{2\epsilon_n - \hbar\Omega} + \sum_i \frac{2j_i + 1}{2\epsilon_i + \hbar\Omega}, \quad (8.192)$$

where n and i run over the particle and hole shells, respectively, and $2j + 1$ is the number of levels in each of these shells. The single-particle energies are counted from the Fermi level, that is, $\epsilon_n > 0$, $\epsilon_i < 0$. The ground state has the form

$$|\text{RPA}\rangle = N_0 \cdot \exp\left(\sum_{ni} Z_{ni} A_n^+ A_i^+\right) |\text{HF}\rangle = N_0 \sum_{\tau=0}^{\infty} \frac{1}{\tau!} \left(\sum_{ni} Z_{ni} A_n^+ A_i^+\right)^{\tau} |\text{HF}\rangle, \quad (8.193)$$

where $A^+ = \sum_{m>0} a_m^+ a_{-m}^+$ is a 0^+ pair in the corresponding shell and the matrix Z is given by the equations

$$\sum_n Z_{ni} \frac{j_n + 1/2}{\hbar\Omega_n - 2\epsilon_n} = \frac{1}{\hbar\Omega_i + 2\epsilon_i} \quad \text{for all } \tau \text{ values.}$$

For an increasing force constant, the number of virtual bosons becomes larger and we come to a phase transition as

$$G = G_c = 2 \left(\sum_n \frac{2j_n + 1}{2\epsilon_n} + \sum_i \frac{2j_i + 1}{2\epsilon_i} \right)^{-1}, \quad (8.194)$$

the excitation energy Ω goes to zero, and the RPA approach breaks down [Hö 61, BRS 68].

It is instructive to write down the BCS ground state in the form

$$|\text{BCS}\rangle = N'_0 \exp\left(\sum_n \frac{v_n}{u_n} A_n^+ + \sum_i \frac{u_i}{v_i} A_i^+\right) |\text{HF}\rangle. \quad (8.195)$$

It violates the particle number. If we project onto a good particle number, that is, if we neglect all components in which the number of pp bosons is different from the number of hh bosons, we get

$$|\text{PBCS}\rangle = N' \sum_{\nu=0}^{\infty} \frac{1}{\nu!} \frac{1}{\nu!} \left(\sum_m \frac{u_n u_\nu}{u_n v_\nu} A_n^\dagger A_\nu^\dagger \right) |\text{HF}\rangle. \quad (8.196)$$

On the other hand, we know that for small values of the force constant G , the gap equation (6.60)

$$\frac{2}{G} = \sum_n \frac{2j_n + 1}{2\sqrt{\epsilon_n^2 + \Delta^2}} + \sum_i \frac{2j_i + 1}{2\sqrt{\epsilon_i^2 + \Delta^2}} \quad (8.197)$$

has no solution ($\Delta = 0$). We find the same critical value G_c as in Eq. (8.194). For $G < G_c$ we use the correlated RPA ground state, and for $G > G_c$ we use the $|\text{BCS}\rangle$ state. Both approximations become poor in the vicinity of G_c . A way to avoid this problem would be a variation with respect to the occupation probabilities v^2 after projecting the particle number (see Chap. 11).

8.9 Quasi-particle RPA

Away from the closed shells, pair correlations become so important that the "feedback" of these correlations on the single-particle motion cannot be neglected any more. We have already seen in Chapters 6 and 7 that instead of $|\text{HF}\rangle$, the BCS or HFB ground state is appropriate in such cases. Since it is also a determinantal wave function, we can construct TDA and RPA theory in complete analogy to the normal case* [Ba 60a]. It will thereby turn out that ph and pp RPA (TDA) may be encapsulated in one concise equation (see, for instance, [So 71]).

To derive these equations, we have to start with the quasi-particle representation (E.18)

$$H = H^0 + H^{11} + H^{31} + H^{40} + H^{22}. \quad (8.198)$$

Instead of Eq. (8.65), we now use the ansatz

$$Q_s^\dagger = \frac{1}{2} \sum_{kk'} (X'_{kk'} a_k^\dagger a_{k'}^\dagger - Y'_{kk'} a_{k'} a_k) \quad (8.199)$$

and find, in analogy to the derivation of Section 8.4.1 the quasi-particle RPA equation whose matrix form is identical to Eq. (8.70). Only the matrix indices run through all pairs ($k < k'$) of the configuration space. In particular, this means ph indices (mi) and pp , and hh indices (mn), (ij). The

*The same equations have been derived by Bogoliubov within the Green's function formalism [Bo 59b].

matrices A and B are now given by ($k < k'$, $l < l'$)^{*}

$$\begin{aligned} A_{kk'H'} &= \langle \text{HFB} | [a_k a_k, [H, a_l^+ a_{l'}^+]] | \text{HFB} \rangle \\ &= (E_k + E_{k'}) \delta_{kl} \delta_{k'l'} + H_{kk'H'}^{22}, \\ B_{kk'H'} &= -\langle \text{HFB} | [a_k a_k, [H, a_l a_{l'}]] | \text{HFB} \rangle = 4! \cdot H_{kk'H'}^{40}. \end{aligned} \quad (8.200)$$

Together they form the stability matrix (7.37) of the HFB theory, where we have used the representation of Eq. (E.18). In the canonical basis (in the case of a Nilsson + BCS calculation, this means the Nilsson basis; see Sec. 7.4) we find, for a time reversal invariant $|\text{HFB}\rangle$ ground state with real matrix elements,

$$\begin{aligned} A_{kk'H'} &= (E_k + E_{k'}) \delta_{kl} \delta_{k'l'} + \bar{v}_{kk'H'} \frac{1}{2} (\xi_{kk'}^+ \xi_{ll'}^+ + \xi_{kk'}^- \xi_{ll'}^-) \\ &\quad + \bar{v}_{k\bar{l}k'\bar{l}'} \frac{1}{2} (\eta_{kk'}^+ \eta_{ll'}^+ + \eta_{kk'}^- \eta_{ll'}^-) \\ &\quad - \bar{v}_{k\bar{l}k'\bar{l}'} \frac{1}{2} (\eta_{kk'}^+ \eta_{ll'}^+ - \eta_{kk'}^- \eta_{ll'}^-); \\ B_{kk'H'} &= \bar{v}_{kk'H'} \frac{1}{2} (\xi_{kk'}^+ \xi_{ll'}^+ - \xi_{kk'}^- \xi_{ll'}^-) \\ &\quad + \bar{v}_{k\bar{l}k'\bar{l}'} \frac{1}{2} (\eta_{kk'}^+ \eta_{ll'}^+ + \eta_{kk'}^- \eta_{ll'}^-) \\ &\quad - \bar{v}_{k\bar{l}k'\bar{l}'} \frac{1}{2} (\eta_{kk'}^+ \eta_{ll'}^+ - \eta_{kk'}^- \eta_{ll'}^-); \end{aligned} \quad (8.201)$$

where

$$\xi_{kk'}^\pm = u_k u_{k'} \mp v_k v_{k'}, \quad \eta_{kk'}^\pm = u_k v_{k'} \pm v_k u_{k'}. \quad (8.202)$$

In the HF-limit we get

$$\xi_{mm}^\pm = 0; \quad \xi_{mm}^\pm = 1; \quad \xi_{jj}^\pm = \mp 1; \quad \eta_{mm}^\pm = 1; \quad \eta_{mm}^\pm = \eta_{jj}^\pm = 0; \quad \eta_{lm}^\pm = \pm 1$$

which means that the set of *quasi-particle RPA equations* is decomposed, in this case, into the set of *ph* RPA equations (8.70), the set of *pp* RPA equations (8.186), and a set of *hh* RPA equations [the complex conjugate of (8.186)].

Furthermore, we see that the matrices A and B contain two types of matrix elements: *pp*-matrix elements $v_{kk'H'}$ multiplied by the factors ξ , which are close to one for *pp* or *hh* pairs; and the *ph* matrix elements $v_{k\bar{l}k'\bar{l}'}$ multiplied by factors η , which are close to one for *ph* pairs. In our derivation, both must be calculated with the same density-independent interaction. For density dependent interactions, however, we get the *ph* force [terms with η in Eq. (8.201)] as the derivative of the self-consistent field Γ with respect to the density ρ . The formalism of linear response theory can also be extended to the HFB case, working with the generalized densities \mathfrak{A} [Eq. (7.27)]. In this case, we get the *pp* force [terms with ξ in

* As we will see in Sec. 9.2.3.1, we can derive the quasi-particle RPA from a perturbative boson expansion, too. We have to be aware, however, that the matrix B obtained in Eq. (9.48) deviates from the matrix B in Eq. (8.200) by a factor of 3. This has its origin in the fact that higher order terms in the boson expansion are neglected [see also the discussion after Eq. (9.134)].

Eq. (8.201)] as a derivative of the pairing field Δ with respect to the pairing tensor κ [Mi 59, 60, ML 64, Mi 67, Bi 68, Ka 69, BEL 70].

The quasi-particle RPA equations have been widely used in connection with *separable forces*, such as the pairing-plus-quadrupole or the surface-delta interaction (see Secs. 4.4.6 and 4.4.7). As in the case of the schematic model (Sec. 8.5.2), the diagonalization problem is then reduced to a root search for relatively simple functions. This method provides a microscopic description of a large number of low-lying collective states, such as vibrations in spherical superconducting nuclei [Ar 63, ABV 63, AV 63, ASV 64]. It also has been successfully applied in the deformed rare earth and actinides nuclei for the description of β , γ , octupole, and pairing vibrations [SV 63, Be 63, So 65, FPM 67, MSU 67]. To each of these states belongs a rotational band, which can be calculated in the framework of the cranking model: We simply have to solve the RPA equations in a basis of rotating quasi-particles provided by a solution of the self-consistent cranking model as discussed in Section 7.7 [Ma 76b, MJ 78, EMR 80b]. Most of these calculations were concerned with the low-lying collective states. In recent years giant resonances in deformed regions in the framework of the quasi-particle RPA [KMY 75, ZS 75, MNS 76, ZS 76] were also investigated. Calculations with *realistic density-dependent forces* [ZSP 78] show again (as in spherical nuclei) that only a small fraction of the multipole sum rule is exhausted by the low-lying collective states. The giant resonances are much more collective and correspond to the classical surface oscillation (for instance, β or γ vibrations).

CHAPTER 9

Boson Expansion Methods

9.1 Introduction

In the last chapter we studied collective vibrations within the harmonic approximation. Harmonic oscillations are characterized by an equidistant spectrum. As shown in Fig. 1.5, in the quadrupole case we expect a one-boson 2^+ excitation at energy $\hbar\omega$, a two-boson triplet $0^+, 2^+, 4^+$ at twice this energy, a three-boson quintet $0^+, 2^+, 3^+, 4^+, 6^+$ at three times this energy, and so on. Experimental spectra of spherical nuclei (see, for instance, Fig. 9.4) in some regions of the periodic table qualitatively show this structure. In detail, however, we always find some more or less dramatic deviations from this simple picture, as, for instance, splitting of the higher multiplets and a shift in the position of the energy centroid.

Such anharmonicities are caused by two effects:

(i) **The collective fermion pairs***

$$\sum_{ml} C_{ml} a_m^+ a_l \quad (9.1)$$

are not exact bosons. Applying this operator twice, in the description of a two-phonon state, we do not obtain two uncoupled bosons,

* For the sake of simplicity, in this chapter we investigate mainly bosons based on TDA wave functions. In principle, we could also use RPA bosons of the form (8.65). This has not been done very often in the literature [Se 70], because in the method of boson expansions higher correlations are taken into account anyway.

because the Pauli principle excludes all configurations, where the same level is occupied by more than one particle (or hole). We call such effects *kinematic effects* because they will be connected with the basis used in the following sections.

- (ii) The exact many-body Hamiltonian contains not only second-order terms in the bosons, which are diagonalized in the TDA approach (or the RPA method), but also higher-order terms. Such terms are neglected in the harmonic approximation and provide a coupling between the different collective modes and also a coupling to non-collective states, such as rather pure two-quasi-particle states. We call such effects *dynamic effects*, because they are determined by the properties of the Hamiltonian.

If we start with a double magic nucleus with a rather pure harmonic spectrum and add more and more particles, we observe larger and larger *anharmonicities*. We come into a transitional region where the vibrational character of the spectrum is lost and a rotational structure develops. Finally, we end up in the region of well-deformed nuclei with pure rotational bands.

We are able to describe such anharmonicities and, in principle, also the transition to deformed nuclei by the methods discussed in this chapter. The basic idea of such methods is to represent the fermion Hamiltonian by pure boson operators B_μ, B_μ^+ and to diagonalize it in a boson space. Mathematically, this corresponds to a mapping of the Fock space of many fermion states into a space of boson states. This will be discussed in detail in Section 9.2.

The advantage of such a boson representation is that very collective modes—for instance, the quadrupole mode—can be approximated by rather simple wave functions, namely one-boson states $B_\mu^+|0\rangle$. For such states the quadratic approximation of the Hamiltonian is already very good, as we saw in the last chapter. We can therefore hope that higher terms in the boson representation of the Hamiltonian drop off rapidly. In Section 9.2 we shall see that this is, in fact, the case for collective modes. It is often sufficient to take into account only fourth- or sixth-order terms.

On the other hand, pure *ph* operators $a_m^+a_n$, which are needed for the description of non-collective modes, have a complicated structure in the boson space. The basic idea of all boson expansions is therefore to restrict ourselves to a few collective bosons which span a *collective subspace* of the full Hilbert space, and to diagonalize the Hamiltonian within this subspace. If there are eigenstates of the exact Hamiltonian in this subspace, that is, if we can neglect their coupling to non-collective states in the Hilbert space, we obtain a rather simple description of these states.

This assumption is certainly not fulfilled for all states or for all nuclei. In many problems we must explicitly take into account the coupling to non-collective few-quasi-particle states. This is in particular always the case for odd systems. In Section 9.3 we will therefore treat techniques that

deal with the coupling of collective modes (described by the boson picture) to single-particle states. One of the simplest models of this kind is the *vibration particle coupling* (VPC) model of Bohr and Mottelson.

9.2 Boson Representations in Even–Even Nuclei

9.2.1 Boson Representations of the Angular Momentum Operators

The problem of representing a fermion system by Boson operators has been investigated in many fields of physics (for a review see [Ga 78]). Since such representations are in general highly mathematical, in this section we shall start with some simple examples that already show the basic features of such methods.

The *angular momentum operators* can be represented by bosons. In the theory of spin waves in a ferromagnet, several techniques of this type have been developed, and it has turned out that some of them can be extended to the case of general many-fermion systems.

We shall start with the algebra of the angular momentum operators $J_{\pm} = J_x \pm iJ_y$ and J_z , which obey the commutation relations of the group $SU(2)$:

$$[J_+, J_-] = 2J_z, \quad [J_z, J_+] = J_+. \quad (9.2)$$

The corresponding Hilbert space is spanned by the eigenvectors $|IM\rangle$ of J^2 and J_z . This Hilbert space is now mapped onto a space of bosons, given by the boson vacuum* $|0\rangle$ and boson operators B, B^+ , which fulfill the relations

$$[B, B^+] = 1, \quad B|0\rangle = 0. \quad (9.3)$$

There are several ways to carry out this mapping, that is, to represent the operators J_i by the boson operators B, B^+ .

(I) **The Holstein Primakoff Representation** [HP 40]. Restricting ourselves to the subspace characterized by the angular momentum quantum number I , we can map the operators J_{\pm} and J_z in the following way.

$$\begin{aligned} J_+ &\rightarrow (J_+)_B = \sqrt{2I} \cdot B^+ \sqrt{1 - \frac{1}{2I} \cdot B^+ B}, \\ J_- &\rightarrow (J_-)_B = (J_+)_B^+ = \sqrt{2I} \cdot \sqrt{1 - \frac{1}{2I} B^+ B} \cdot B, \\ J_z &\rightarrow (J_z)_B = -I + B^+ B. \end{aligned} \quad (9.4)$$

*In the following we always use sharp brackets $| \rangle$ for the original angular momentum and fermion states, and round brackets $| \rangle$ for the states in the boson space.

The square roots are formal abbreviations for the corresponding Taylor series. It is easy to show that the operators $(J_{\pm})_B$ and $(J_z)_B$ in the boson space satisfy the angular momentum algebra (9.2).

The boson space is spanned by the n -boson states

$$|n\rangle = \frac{1}{\sqrt{n!}} (B^+)^n |0\rangle \quad \text{for } n = 0, 1, 2, \dots \quad (9.5)$$

In contrast to the subspace with angular momentum J , which has the dimension $2J+1$, the boson space may have infinite dimension ($n \rightarrow \infty$). On the other hand, because B^+B counts the number of bosons (n), the square roots in Eq. (9.4) are not defined in the whole boson space. Thus we have the condition

$$n < 2J. \quad (9.6)$$

The subspace which, at maximum, contains $2J$ bosons is called the *physical subspace* of the infinitely dimensional boson space. It is spanned by the $2J+1$ states

$$|0\rangle, B^+|0\rangle, \dots, (B^+)^{2J}|0\rangle \quad (9.7)$$

and has therefore the same dimension as the angular momentum space. The mapping (9.4) provides a one-to-one correspondence between the angular momentum space characterized by J and the physical subspace. Since it conserves the commutation relations, it is a matter of convenience in which space we want to carry out actual calculations. All physically important properties are not influenced by this mapping.

This is the basic idea of all boson representations, and we already see the two basic ingredients that have to be fulfilled for this concept:

- (i) We have to be sure that the algebraic rules for calculations, that is, the underlying *algebra*, are conserved by the mapping
- (ii) One is only allowed to work in the physical subspace, i.e., in our example all the vectors have to belong to the eigenspace of the operator J^2 with the eigenvalue $J \cdot (J+1)$. In general one can express this fact in the following way: One can only work with vectors, which are eigenstates to the *Casimir operators* of the underlying symmetry group [Ya 74]

As an example, we express the eigenvectors of the angular momentum states by boson states:

$$|JM\rangle \rightarrow |JM\rangle = [(I+M)!]^{-1/2} (B^+)^{I+M} |0\rangle. \quad (9.8)$$

In practical applications we have to use the Taylor expansion of Eq. (9.4). It converges well, if the number of bosons is small compared to $2J$. It is a disadvantage of this type of boson representation that, in principle, an infinite number of terms is needed to fulfill the commutator algebra (9.2). There are, however, other ways to avoid this difficulty:

(II) The Dyson Representation [Dy 56]. Dyson proposed the following mapping.

$$\begin{aligned} J_+ \rightarrow (J_+)_B &= \sqrt{2I} B^+ \left(1 - \frac{1}{2I} B^+ B \right), \\ J_- \rightarrow (J_-)_B &= \sqrt{2I} B, \\ J_z \rightarrow (J_z)_B &= -I + B^+ B. \end{aligned} \quad (9.9)$$

This representation is very simple, but it violates Hermiticity because $(J_+)_B^+$ is different from $(J_-)_B$, and leads to a non-Hermitian Hamiltonian. However, as we shall see in the following sections, it has certain advantages and can also be used in the many-body problem.

(III) The Schwinger Representation [Sch 65]. Schwinger introduced a boson representation of the angular momentum operators which, as well as being finite, is also Hermitian. He used two bosons A and B ,

$$[A, A^+] = 1, \quad [B, B^+] = 1, \quad [A, B] = [A, B^+] = 0, \quad (9.10)$$

which act in a space of two-dimensional oscillator states

$$|n_A n_B\rangle = \frac{1}{\sqrt{n_A! n_B!}} (A^+)^{n_A} (B^+)^{n_B} |0, 0\rangle. \quad (9.11)$$

The Schwinger representation is given by

$$\begin{aligned} J_+ \rightarrow (J_+)_B &= B^+ A, \\ J_- \rightarrow (J_-)_B &= (J_+)_B^+ = A^+ B, \\ J_z \rightarrow (J_z)_B &= \frac{1}{2}(B^+ B - A^+ A). \end{aligned} \quad (9.12)$$

The eigenstates of the angular momentum operators can be written as

$$|IM\rangle = [(I-M)!(I+M)!]^{-1/2} (B^+)^{I+M} (A^+)^{I-M} |0, 0\rangle. \quad (9.13)$$

The boson number operator

$$N = B^+ B + A^+ A = 2I \quad (9.14)$$

is proportional to I . Rotational invariant Hamiltonians must therefore conserve the boson number. This is different in the Holstein-Primakoff representation, which yields boson number violating terms. On the other hand, it can be shown that there is a nearly unitary transformation between both representations [BM 78].

It is evident that these simple representations of the angular momentum operators can be used in *models*, in which the Hamiltonian is expressed by spin or quasi-spin operators, like the Lipkin model (see Sec. 5.4) or the seniority model (see Sec. 6.2). In such cases, we immediately obtain a boson representation of the Hamiltonian. Such models have therefore been widely used to study the properties of boson representations [PKD 68, BS 68b, KI 69], and we will come back to some of them in the following sections.

Such boson representations of the angular momentum operators have also been used in the *rotor model* (see Sec. 1.5). Marshalek [Ma 75b] introduced a generalization of Eq. (9.4) with three bosons corresponding to the three degrees of freedom usually described by the Euler angles. Yamamura et al. [YSI 78, IY 78] used an extension of the Schwinger representation with four bosons.

These methods are most useful in the limit of larger angular momenta, where there is essentially a classical rotation around a fixed axis. In a boson picture, deviations from this rotation may be described as small oscillations of the rotational axis, so-called wobbling bosons [BM 75, Ma 79].

9.2.2 Concepts for Boson Expansions

In the last section we discussed several examples of boson representations of the angular momentum operators. These methods can be generalized to the case of a many-fermion system. We shall first restrict ourselves to systems with *even particle number*, systems with odd particle number will be described in Section 9.3.

As in the angular momentum case, there are many types of boson representations. Some of them are equivalent in certain limits. Before we go into the details, we want to discuss a few basic concepts which so far have been used in the theory of boson representations.

All these methods start with a many-fermion Hilbert space \mathfrak{Q}_F , which contains vectors and operators. In second quantization the space is completely specified by the vacuum $|0\rangle$ and a set of fermion operators α_k, α_k^+ . In the following we always work in the quasi-particle picture, that is, the operators are the Bogoliubov quasi-particle operators in the sense of Chapter 7; the HF-quasi-particles are just a special case of them.

Since bosons have integer spin values we prefer to use pairs of fermion operators

$$\alpha_k^+ \alpha_i^+, \quad \alpha_i \alpha_k, \quad \alpha_i^+ \alpha_k. \quad (9.15)$$

In fact, we can describe all wave functions and operators in an even system by such fermion pairs and the corresponding quasi-particle vacuum $|0\rangle$.*

This fermion space is now mapped onto a different Hilbert space, a space of bosons \mathfrak{Q}_B

$$\mathfrak{Q}_F \rightarrow \mathfrak{Q}_B. \quad (9.16)$$

* If we start with a vacuum $|0\rangle$ corresponding to an odd system, we are, in principle, also able to describe odd systems completely by the pair operators (9.15). Single-fermion operators are only needed for transfer processes. For practical reasons (non-degenerate vacuum), however, we prefer to use only quasi-particle vacua with even particle number.

The boson space is given by a boson vacuum $|0\rangle$ and boson creation and annihilation operators* B_μ, B_μ^+ :

$$B_\mu |0\rangle = 0, \quad [B_\mu, B_\nu^+] = \delta_{\mu\nu}, \quad [B_\mu, B_\nu] = 0. \quad (9.17)$$

As in the angular momentum case (Sec. 9.2.1), it generally turns out that the boson space \mathfrak{H}_B is much larger than the fermion space \mathfrak{H}_F . Therefore, the mapping (9.16) is only unique in a certain subspace $\mathfrak{H}_{\text{phys}}$ of the boson space

$$\mathfrak{H}_F \leftrightarrow \mathfrak{H}_{\text{phys}} \subset \mathfrak{H}_B.$$

There are now two basic concepts to introduce this mapping† explicitly:

(i) Belyaev and Zelevinskii [BZ 62] propose to map the operators in such a way that the *commutation relations* are preserved. Usually all important operators can be constructed from a set of *basic operators* whose commutation relations form an *algebra*. An example is the set (9.15) and another example is the operators K_\pm and K_0 in the case of the Lipkin model (Sec. 5.4). It is then sufficient to map only these basic operators onto operators in the boson space in such a way that this algebra is preserved.‡ All other operators can be represented as polynomials of these basic operators and their boson image is obtained as the same polynomial in the images of the basic operators.

To obtain the mapping of the vectors one only has to define a correspondence between the vacuum in the boson space $|0\rangle$ and the quasi-particle vacuum $|0\rangle$ in the fermion space. All other states can be found by successive application of the basic operators.

It is evident that the vectors obtained in this way do not span the whole boson space but only the physical subspace. It is an eigenspace to the Casimir operators of the corresponding commutator algebra, as discussed in Section 9.1. In cases where the commutator algebra is fulfilled only approximatively, we can have admixtures of unphysical states. To avoid them, we have to ensure at least that one works in eigenspaces of the Casimir operators [Ya 74].

(ii) Marumori [MYT 64a and b] proposed to *map vectors* in the Hilbert spaces \mathfrak{H}_F and \mathfrak{H}_B and to define the operators in such a way that the

* In the following we shall always use sharp brackets $| \rangle$ for states in the fermion space \mathfrak{H}_F and round brackets $| \)$ for states in the boson space \mathfrak{H}_B . We also use small Greek letters for fermion operators and capital Latin letters for bosons. The fermion indices are given by Latin letters k, l, \dots ; the boson indices are Greek letters μ, ν, \dots . Sometimes a boson index corresponds to a fermion pair (k, l) .

† We also can use the generator coordinate method to introduce boson representations [JS 64, JDF 71, Ho 72, HL 72b]. We will study this technique in more detail in Section 10.4.

‡ In the case of the Lipkin model, for instance, this is achieved by one of the prescriptions discussed in Section 9.2.1.

matrix elements are conserved by the mapping. In practice, one starts with a full orthogonal set of basis states $|n\rangle$ in the boson space:

$$(n|n') = \delta_{nn'}; \quad \sum_n |n\rangle\langle n| = I_B$$

and maps them onto states $|n\rangle$ in the Fermion space.

The image of an operator O_F in the fermion space is then given by

$$O_F \rightarrow O_B = \sum_{nn'} \langle n|O_F|n'\rangle \cdot |n\rangle\langle n'|. \quad (9.18)$$

This definition obviously conserves the matrix elements. The mapping of Fermion states $|n\rangle$ to boson states by this prescription, however, is not unique. In Section 9.2.6 we will see in some detail how this mapping can be carried out in a unique manner by restricting ourselves to the physical subspace.

These two concepts of mapping *operators* (Belyaev-Zelevinskii) or *states* (Marumori) have been applied in different ways. Before we discuss some of the methods (in the following sections), we wish to stress that in all the applications we must, to a greater or lesser extent, use drastic approximations, which are justified only in special physical cases. For instance, an expansion of Eq. (9.4) in a Taylor series with only a few terms is only meaningful for large values of J , that is, in a case where J_+ already has well-pronounced boson properties. It is therefore important to choose the basic fermion operators that are to be mapped in a first approximation onto a boson in a proper way, such that rapid convergence is guaranteed. Mathematically it is possible to start with pure two-quasi-particle operators $a_k^+ a_l^+$ (see Sec. 9.2.6). Since they only fulfill the boson commutation relations to a very poor approximation, the corresponding boson expansion does not converge rapidly and is useless in practical applications.

Boson representations are therefore only meaningful if we start with linear combinations of fermion pairs

$$b_\mu^+ = \sum_{k < l} C_{kl}^\mu a_k^+ a_l^+, \quad (9.19)$$

which in the following we call *collective fermion pair operators*.* The coefficients $C_{kl}^\mu = -C_{lk}^\mu$ can be obtained, for instance, from TDA calculations (see Sec. 8.2), or we can use operators of a given type, such as the five quadrupole operators

$$b_\mu^+ = \frac{1}{2} \sum_{kl} Q_{kl}^{2\mu} a_k^+ a_l^+ \quad (\mu = -2, \dots +2). \quad (9.20)$$

* For a discussion of the term "collective," see Section 8.2.2.

They are easy to handle because of their group theoretical properties, and have been widely used in the literature. We have to be aware, however, that whenever we restrict the number of given operators b_μ^+ , the operators (9.19) no longer form a complete system in the two-quasi-particle space, and we fail to describe certain states not taken into account. For instance, it is impossible to approximate a pure two-quasi-particle state in the space spanned by pure quadrupole bosons.

So far we have considered the collective low-lying excitations of a many-fermion system as approximate bosons and used them to construct a theory based on the corresponding ideal bosons. A different system, in which we have had to deal with approximate bosons, is that of the superfluid system of Cooper pairs studied in Section 6.2. In this case, we do not start with an HF ground state as quasi-particle vacuum and ph excitation as quasi-bosons. We start with the bare vacuum and couple pairs of particles to the quasi-bosons. As we shall see in Section 9.2.7, such an approach is closely connected to the idea of the *Schwinger representation* [see Eq. (9.12)]. It has the advantage that symmetries, such as the particle number conservation, are guaranteed from the beginning, but also has the disadvantage that we have to construct the ground state of the system out of many bosons, which might be a very complicated task in the general case.

After these general remarks, in the following sections we shall use bosons based on collective ph (or two-quasi-particle states) and discuss in more detail a few methods used to describe the many-fermion system in this way.

9.2.3 The Boson Expansion of Belyaev and Zelevinskii

We begin our discussion with a quasi-particle representation of the many-fermion space. It is based on a generalized Slater determinant $|0\rangle$, which represents the vacuum of the quasi-particle operators $(\alpha_1 \dots \alpha_M)$. The Hamiltonian has the form* (E.18)

$$H = H^0 + H^{11} + H^{22} + H^{31} + H^{40}. \quad (9.21)$$

In an even system it is sufficient to consider only the fermion pair operators†

$$b_{kl}^+ = \alpha_k^+ \alpha_l^+; \quad b_{kl} = \alpha_l \alpha_k; \quad a_{kl} = \alpha_l^+ \alpha_k. \quad (9.22)$$

* H^{20} does not occur, since we assume that the ground state $|0\rangle$ is a self-consistent solution of the variational principle (7.31). This fact is, however, not essential for the following discussions.

† In the following we will always use small Latin letters for fermion pair operators and capital Latin letters for bosons. They take the pair index (l, k) in the non-collective case and the Greek indices μ, ν, \dots in the collective case.

They form an algebra [which belongs to the group $SO(2M)$]:

$$[b_{kl}, b_{k'l'}] = 0, \quad (9.23a)$$

$$[b_{kl}, b_{k'l'}^+] = \delta_{kk'}\delta_{l'l} + \delta_{kl'}a_{lk'} + \delta_{lk}a_{kl'} - (k \leftrightarrow l), \quad (9.23b)$$

$$[b_{kl}, a_{k'l'}] = \delta_{ll'}b_{kk'} - (k \leftrightarrow l), \quad (9.23c)$$

$$[a_{kl}, a_{k'l'}] = \delta_{kl'}a_{k'l} - \delta_{lk}a_{kl'}. \quad (9.23d)$$

In principle, non-collective fermion pair operators can be represented by corresponding bosons, and we will show how to do this in more detail in section 9.2.6. However, as discussed in the last section, for all practical applications we need collective bosons. We therefore start with the collective fermion pair operators

$$b_\mu^+ := \sum_{k < l} C_{kl}^\mu a_k^+ a_l^+, \quad (9.24)$$

$$a_{\mu\nu} := \sum_{k'l} C_{kl}^\mu C_{l'm}^\nu a_{kl} = a_{\mu\nu}^+. \quad (9.25)$$

The coefficients $C_{kl}^\mu = -C_{lk}^\mu$ characterize the kind of bosons we will use for our representation. We shall assume that they obey the orthogonality and completeness relations (8.26)

$$\sum_{k < l} C_{kl}^\mu C_{kl}^{\mu'} = \delta_{\mu\mu'}, \quad \sum_\mu C_{kl}^\mu C_{k'l'}^{\mu'} = \delta_{kk'}\delta_{l'l} - (k \leftrightarrow l). \quad (9.26)$$

As long as we take into account all μ -values, Eq. (9.24) represents a unitary transformation in the space of fermi pair operators. In practical applications we often use only one or a few bosons, which means that care has to be taken in using the completeness relations (9.26).

We can now use Eq. (9.24) to derive the commutator algebra for the collective fermion pair operators (9.24) and (9.25):

$$[b_\mu, b_{\mu'}] = [b_\mu^+, b_{\mu'}^+] = 0, \quad (9.27a)$$

$$[b_\mu, b_{\mu'}^+] = \delta_{\mu\mu'} - a_{\mu\mu'}, \quad (9.27b)$$

$$[b_\mu, a_{\mu'\nu}] = \sum_\rho \Gamma_{\nu\rho}^{\mu\mu'} b_\rho, \quad (9.27c)$$

$$[b_\mu^+, a_{\mu'\nu}] = - \sum_\rho \Gamma_{\mu'\rho}^{\nu\nu'} b_\rho^+, \quad (9.27d)$$

$$[a_{\mu\nu}, a_{\mu'\nu'}] = \frac{1}{M-2} \sum_{\rho\sigma} (\Gamma_{\nu\rho}^{\mu\mu'} \Gamma_{\nu'\rho}^{\nu\nu'} - \Gamma_{\nu\rho}^{\mu\nu'} \Gamma_{\nu'\rho}^{\mu\mu'}) a_{\rho\sigma}, \quad (9.27e)$$

where M is the dimension of the single-particle configuration space. (This factor drops out in the final formulae, so there need be no worry about an infinite space.) The coefficients $\Gamma_{\mu'\nu}^{\mu\nu'}$, $\Gamma_{\mu'\nu\rho}^{\mu\nu'}$, and other quantities $\Gamma_{\mu'k}^{\mu k'}$,

which we shall need later on, are defined by

$$\Gamma_{\mu\nu}^{\alpha\beta} = \sum_{klpq} C_{kl}^{\alpha} C_{lp}^{\beta} C_{pq}^{\gamma} C_{qk}^{\delta}, \quad (9.28a)$$

$$\Gamma_{\mu\nu\rho}^{\alpha\beta\gamma} = \sum_{klpqrs} C_{kl}^{\alpha} C_{lp}^{\beta} C_{pq}^{\gamma} C_{qr}^{\rho} C_{rs}^{\sigma} C_{sk}^{\delta}, \quad (9.28b)$$

$$\Gamma_{\mu\nu\rho\sigma}^{\alpha\beta\gamma\delta} = \dots$$

$$\Gamma_{\mu'k'}^{\mu k} = \sum_l C_{k'l}^{\mu} C_{kl}^{\mu'}. \quad (9.29)$$

Figure 9.1 shows an obvious graphical representation of Eqs. (9.28). The quantities Γ are closely related to the fact that the fermion pair operators b_μ are not real bosons. They take into account the Pauli principle by taking care of exchange corrections. Using Eqs. (9.26), we can prove many useful relations, as, for example,

$$\begin{aligned} \sum_\tau \Gamma_{\nu\nu}^{\mu\mu\tau\tau} &= -(M-1)\Gamma_{\nu\nu}^{\mu\mu\tau\tau}, \quad \Gamma_\nu^\mu = -2\delta_{\mu\nu}; \\ \sum_\tau \Gamma_{\mu'\tau}^{\mu\mu} \Gamma_{\nu'\rho'}^{\nu\rho} &= -\Gamma_{\mu'\nu'\rho'}^{\mu\mu\nu\rho} - \Gamma_{\mu'\rho'\nu'}^{\mu\mu\nu\rho}; \\ \sum_{\sigma\rho} \Gamma_{\nu\rho}^{\mu\sigma} \Gamma_{\sigma\tau}^{\rho\lambda} &= (M-2)\Gamma_{\nu\tau}^{\mu\lambda} + 4\delta_{\mu\nu}\delta_{\lambda\tau}; \\ \sum_{\sigma\rho} \Gamma_{\sigma k}^{\rho i} \Gamma_{\rho q}^{\sigma p} &= (M-2)\delta_{pk}\delta_{qi} + \delta_{pq}\delta_{ki}. \end{aligned} \quad (9.30)$$

To get Eq. (9.27), we need the inverse of (9.25), which reads

$$a_{kl} = \frac{1}{M-2} \left\{ \sum_{\mu\nu} \Gamma_{\mu\nu}^{kk} a_{\mu\nu} - \delta_{kl} \frac{1}{M-1} \sum_\mu a_{\mu\mu} \right\}, \quad (9.31)$$

and can be verified by a simple insertion of Eq. (9.25). We can also represent the Hamiltonian (E.18) in terms of the collective fermion pair

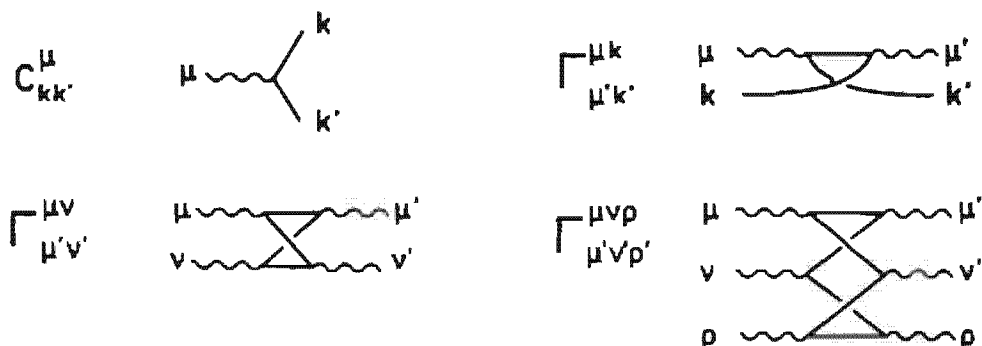


Figure 9.1. Graphical representation of the quantities C and Γ . (These kinds of graphs are not Feynman graphs in the sense of Appendix F.)

operators b_μ and $a_{\mu\nu}$:

$$\begin{aligned} H^{11} &= \sum_{\mu\nu} E_{\mu\nu} a_{\mu\nu}, \\ H^{22} &= \sum_{\mu\nu} V_{\mu\nu}^{22} b_\mu^+ b_\nu, \\ H^{31} &= \sum_{\mu\nu\rho} V_{\mu\nu\rho}^{31} b_\mu^+ a_{\nu\rho} + \text{h.c.}, \\ H^{40} &= \sum_{\mu\nu} V_{\mu\nu}^{40} b_\mu^+ b_\nu^+ + \text{h.c.}, \end{aligned} \quad (9.32)$$

with

$$\begin{aligned} E_{\mu\nu} &= \frac{1}{M-2} \sum_k \left(\Gamma_{\mu k}^{\nu k} - \frac{1}{M-1} \delta_{\mu\nu} \right) E_k, \\ V_{\mu\nu}^{22} &= \frac{1}{4} \sum_{klpq} H_{klpq}^{22} C_{kl}^{\mu*} C_{pq}^{\nu}, \\ V_{\mu\nu\rho}^{31} &= \frac{1}{M-2} \sum_{klpq} H_{klpq}^{31} C_{kl}^{\mu*} \left(\Gamma_{\nu p}^{\rho q} - \frac{1}{M-1} \delta_{\nu p} \delta_{\rho q} \right), \\ V_{\mu\nu}^{40} &= \sum_{klpq} H_{klpq}^{40} C_{kl}^{\mu*} C_{pq}^{\nu*}. \end{aligned} \quad (9.33)$$

A special case is the *Lipkin model* (see Sec. 5.4), which we shall discuss later on in some detail. In the following, we apply this model using the quasi-particle representation, in which the operator $\alpha_m^+ = c_m^+$ (and $\beta_m^+ = c_{-m}$) correspond to the creation of a particle in the upper shell (and a hole in the lower shell). In the HF state $|0\rangle$ the lower shell (Ω particles) is completely filled

$$\alpha_m|0\rangle = \beta_m|0\rangle = 0. \quad (9.34)$$

The Hamiltonian commutes with the quasi-spin operator K^2 (5.47). As long as we restrict ourselves to the subspace with eigenvalue $K = \Omega/2$, we only have one collective fermion pair operator (9.24)

$$b^+ = \frac{1}{\sqrt{\Omega}} K_+ = \frac{1}{\sqrt{\Omega}} \sum_m \alpha_m^+ \beta_m^+, \quad (9.35)$$

with *ph* amplitudes $C_{mm'} = (1/\sqrt{\Omega}) \delta_{mm'}$ ($m > 0$). The operator (9.25) is closely connected to K_0

$$a = \frac{1}{\Omega} \sum_m (\alpha_m^+ \alpha_m + \beta_m^+ \beta_m) = 1 + \frac{1}{\Omega} 2K_0. \quad (9.36)$$

The number of states is $M = 2\Omega$ and the quantities Γ (9.28a, b) are given by

$$\Gamma^{(2)} = +\frac{2}{\Omega}; \quad \Gamma^{(3)} = -\frac{2}{\Omega^2}; \quad \Gamma^{(4)} = +\frac{2}{\Omega^3}; \dots \quad (9.37)$$

The algebra (9.27) now corresponds to the angular momentum algebra.

The Hamilton operator of the model is given by Eq. (5.45). Expressed in terms of the operators b and a it takes the form

$$H = -\frac{\epsilon}{2}\Omega + \frac{\epsilon}{2}\Omega a - \frac{\nu}{2}\Omega(b^+ b^+ + bb). \quad (9.38)$$

From the consideration of Section 9.2.2 we could have immediately written down a boson expansion for the operators a and b ; however, first we want to study the general case further.

According to the prescription of Beliaev and Zelevinski in the *general case* [BZ 62], we have to start with a set of pure boson operators

$$[B_\mu, B_\nu^+] = \delta_{\mu\nu}, \quad [B_\mu, B_\nu] = 0, \quad (9.39)$$

and to expand the boson images of the operators b_μ^+ and $a_{\mu\nu}$ in the following way.*

$$(b_\mu^+)_B = \sum_\rho x_{\mu\rho}^{(1)} B_\rho^+ + \sum_{\rho\sigma\lambda} x_{\mu\rho\sigma\lambda}^{(3)} B_\sigma^+ B_\rho^+ B_\lambda + \dots, \quad (9.40a)$$

$$(a_{\mu\nu})_B = y^{(0)} + \sum_{\rho\lambda} y_{\mu\nu\rho\lambda}^{(2)} B_\rho^+ B_\lambda + \dots. \quad (9.40b)$$

The coefficients $x^{(i)}$ and $y^{(i)}$ are determined by the condition that the commutation relations (9.27) are satisfied.

Two methods have been developed in the literature to achieve this requirement:

9.2.3.1. The Perturbative Boson Expansion. This method is based on a “small parameter” and the commutator algebra is fulfilled order by order. This method was originally proposed by Belyaev and Zelevinskii [BZ 62] and later its properties were much investigated by Marshalek [Ma 71, MH 72, Ma 74]. In these papers the authors have concentrated themselves on fermion pair operators coupled to good angular momentum. The “small parameter” is then

$$\epsilon = \frac{1}{2j+1}, \quad (9.41)$$

where j is an averaged single-particle angular momentum of the levels in the vicinity of the fermi surface. In fact, this parameter is not very small and the method works much better if one treats collective fermion pairs as in Eq. (9.24). As we shall see, the “small parameter” is in this case the quantity $\Gamma_{\mu\nu}^{(0)}$ of Eq. (9.28a). If the bosons, which one uses for the expansion, are really collective, that is, if there are many small values of the coefficients C_{kl}^n , the value of $\Gamma^{(2)}$ becomes very small. An example occurs in the Lipkin model [see Eq. (9.37)], where we have $\Gamma^{(2)} \propto \epsilon = 1/\Omega$. In such cases, the higher vertices $\Gamma^{(3)}, \Gamma^{(4)}$ of Eq. (9.28b) are of the order $\epsilon^2, \epsilon^3, \dots$

The commutator algebra (9.27) is now fulfilled in two steps. First, we can show by a straightforward application of the relations (9.29) or (9.30) that the subalgebra (9.27e) can already be satisfied with a finite expansion

* The following ansatz is certainly not unique, but it is reasonable to assume that the application of a fermion pair operator b_μ^+ increases the number of bosons by just one and that the application of the operator $a_{\mu\nu}$ does not change the boson number.

of Eq. (9.40b):

$$(a_{\mu\nu})_B = \sum_{\rho\sigma} \Gamma_{\mu\rho}^{\nu\sigma} B_{\rho}^{+} B_{\sigma}, \quad (9.42)$$

that is, $y_{\mu\nu\rho\lambda}^{(2)} = \Gamma_{\rho\lambda}^{\nu\sigma}$ and all other coefficients $y^{(n)}$ vanish. In the next step we try to satisfy Eq. (9.27b) at each order in Γ . The zero'th order gives $x_{\mu\nu}^{(0)} = \delta_{\mu\nu}$, the first order is fulfilled by $x_{\mu\nu\rho\sigma}^{(1)} = -\frac{1}{4} \Gamma_{\rho\sigma}^{\nu\mu}$, and so on. After a rather lengthy calculation, which we do not want to present here, because the result can be obtained in a much simpler way by the methods discussed in Section 9.2.6, we end up with the infinite expansion

$$(b_{\mu}^{+})_B = B_{\mu}^{+} - \frac{1}{4} \sum_{\rho\sigma\rho'} \Gamma_{\mu\rho}^{\nu\sigma} B_{\nu}^{+} B_{\rho}^{+} B_{\sigma} + \frac{1}{16} \sum_{\substack{\nu\rho_1\sigma_1 \\ \rho_2\sigma_2}} \Gamma_{\mu\rho_1\sigma_1}^{\nu\rho_2\sigma_2} B_{\nu}^{+} B_{\rho_1}^{+} B_{\sigma_1} B_{\rho_2}^{+} B_{\sigma_2} + \dots, \quad (9.43)$$

which is of the form (9.40a) with

$$x_{\mu\nu\rho_1\sigma_1\rho_2\sigma_2\dots\rho_n\sigma_n}^{(2n+1)} = -\frac{1}{2} \binom{1/2}{n} \cdot \Gamma_{\mu\sigma_1\sigma_2\sigma_3\dots\sigma_{n-1}}^{\nu\rho_1\rho_2\rho_3\dots\rho_n\dots}. \quad (9.44)$$

We can also verify that the expression obeys the relations (9.27c and d) in each order. The boson expansion obtained in this way is not in normal order with respect to the boson vacuum.

In deriving these expressions, at many places we use the completeness relations (9.26) for the coefficients C_{kl}^{μ} and similar equations of the type (9.30). This means that, in principle, we have to include all indices μ with corresponding solutions of the TDA equation (8.10). Among them there are many non-collective bosons for which the higher terms $\Gamma^{(n)}$ do not drop off rapidly. The whole expansion is therefore only meaningful if we restrict ourselves to a few collective bosons (the subspace spanned by them is called the *collective subspace*), and also if the coefficients Γ have the property that they do not mix these collective bosons very much with the rest of the Hilbert space. For instance, this is the case in the Lipkin model [see Eq. (9.37)], where $SU(2)$ symmetry provides a complete decoupling of the collective subspace. In the general case, it is not always possible to find such a collective subspace.

On the other hand the condition that Γ provides no coupling of the collective subspace and the rest of the Hilbert space is only a *kinematic condition*, that is, it depends only on the property of the underlying boson basis. It is not sufficient to guarantee a meaningful boson expansion. In the introduction we saw that the restriction to a collective subspace is meaningful only in cases where the Hamiltonian provides no serious coupling to the rest of the Hilbert space, that is, in cases where the collective subspace contains to a good approximation some eigenstates of the system. Since this condition depends on the Hamiltonian, it is called a *dynamic condition*.

Both conditions are sometimes fulfilled for group theoretical reasons. Again, an example is the Lipkin model, where we can restrict ourselves to

the collective subspace with quasi-spin $\Omega/2$. In this case we only have one boson B and get from Eq. (9.35ff) and (9.42ff)

$$\begin{aligned} a &= \frac{2}{\Omega} B^+ B, \\ b^+ &= B^+ - \frac{1}{2\Omega} B^+ B^+ B - \frac{1}{8\Omega^2} B^+ B^+ B B^+ B - \dots, \end{aligned} \quad (9.45)$$

which can be summed up to

$$b^+ = B^+ \sqrt{1 - \frac{1}{\Omega} B^+ B}. \quad (9.46)$$

This corresponds exactly to the Holstein–Primakoff representation (9.4) of the angular momentum operators K_{\pm}, K_0 . The perturbative boson expansion of Belyaev and Zelevinskii is therefore often called a Holstein–Primakoff expansion. If we expand the Hamiltonian (9.38) up to order $1/\Omega$ we get, after normal ordering,

$$H_B = -\frac{\epsilon}{2}\Omega + \epsilon B^+ B - V \frac{\Omega}{2} \left(\left(1 - \frac{1}{2\Omega}\right) B^+ B^+ - \frac{1}{\Omega} B^+ B^+ B^+ B + \text{h.c.} \right). \quad (9.47)$$

The perturbative boson expansion has the advantage that in lowest order it corresponds exactly to the *RPA approximation* of Section 8.4. To see this, we use non-collective boson operators and stop after the first term in Eq. (9.43), which means that

$$(a_k^+ a_l^+)_{\mathcal{B}} = B_{kl}^+, \quad (a_k^+ a_l)_{\mathcal{B}} = \sum_p B_{kp}^+ B_{lp}.$$

Inserting these expressions into the Hamiltonian (E.18) and taking into account only terms up to $B^+ B$, $B^+ B^+$, and BB , we find the RPA Hamiltonian of Eq. (8.90) in the quasi-particle representation (8.200):

$$\begin{aligned} H &= E_{HF} + \sum_{\substack{k < l \\ k' < l'}} \{ (E_k + E_{l'}) \delta_{kk'} \delta_{ll'} + H_{kik'l'l'}^{22} \} B_{kl}^+ B_{k'l'l}^+ \\ &\quad + 4 \sum_{\substack{k < l \\ k' < l'}} \{ H_{kik'l'l'}^{40} B_{kl}^+ B_{k'l'l}^+ + \text{h.c.} \} \end{aligned} \quad (9.48)$$

(see, however, footnote on p. 344).

We can now also understand, in a very simple way, why the RPA approach preserves the symmetries [Ma 74]. Since the boson expansion (9.43) is constructed so as to satisfy the commutation relations in each order separately, we find for two arbitrary operators A, B with

$$[A, B] = C, \quad (9.49)$$

$$[A^{(n)}, B^{(1)}] + [A^{(n-1)}, B^{(2)}] + \dots + [A^{(1)}, B^{(n)}] = C^{(n-1)}, \quad (9.50)$$

where $A^{(n)}$, $B^{(n)}$, and $C^{(n)}$ are the n th order terms of the boson parts of the operators A, B, C , which contain n operators B or B^+ . Since the order

is determined by the expansion parameter ϵ , these operators are not in normal order. Reordering them would imply that terms with a fixed number of operators B or B^+ contain contributions in a different order in ϵ .

For a symmetry operator P which commutes with H , we find from Eq. (9.50) in the case $n=2^*$

$$[H^{(2)}, P^{(1)}] = 0, \quad (9.51)$$

which is exactly the RPA equation (8.104) for the zero frequency mode $P^{(1)}$. These arguments can easily be extended to higher order in the boson expansion. The practical applicability of this advantage, however, is restricted by the fact that it is only true if the commutator algebra is fulfilled exactly. In higher orders we usually need additional drastic approximations—for instance, the restriction to only a few collective bosons—which destroy this property.

Mathematically, the RPA Hamiltonian (9.48) has the same structure for bosons as the general single-particle Hamiltonian of Eq. (7.59) for fermions. Both are diagonalized by Bogoliubov transformations [Eqs. (7.1) and (8.91); see also Appendix E.5] resulting in the HFB equations (7.42) and the RPA equations (8.70). The only difference is that the HFB equations are nonlinear. They contain a part of the fourth-order term in the fermion Hamiltonian (i.e., of the two-body interaction). Going to higher orders in the boson expansion in Eq. (9.48), we can proceed as in Eqs. (7.57f.) and bring all terms that we want to take into account into normal order with respect to the new boson vacuum. All quadratic terms B^+B , B^+B^+ , and BB can be brought into the form (8.90) with single-boson fields depending on the boson densities. We thus end up with a *self-consistent random phase approximation* (SCRPA) [SE 73, Ma 76a].

*The term $H^{(1)}$ corresponds to $H^{(2)}$ in Eq. (7.36) and is assumed to vanish.

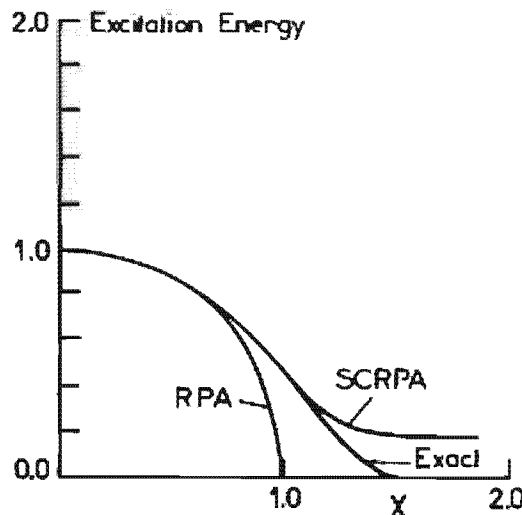


Figure 9.2. The self-consistent RPA is compared to the usual RPA and the exact solution of the Lipkin model as a function of the coupling strength x . (From [SE 73].)

Figure 9.2 shows its solution in the case of the Lipkin model (see Sec. 5.4). We see clearly how the breakdown of RPA in the region of the phase transition (as discussed in Sec. 8.8.2) is avoided by the treatment of higher terms in the boson expansion. For very large particle numbers, SCRPA and RPA begin to coincide, indicating that in very large systems there can be sharp phase transitions, whereas in finite systems the phase transition is always smeared out to a certain extent (see Chap. 11).

9.2.3.2. Restriction to a Few Collective Bosons. In some cases there are physical reasons for restrictions to a few collective bosons, such as quadrupole oscillations and pairing vibrations. The expansion (9.43) does not then satisfy the commutator algebra exactly. Following Sørensen [Sø 67], we can nevertheless use the ansatz (9.40) up to a fixed number of boson operators with variable parameters $x^{(1)}$, $x^{(3)}, \dots, x^{(2n+1)}$ and $y^{(0)}, y^{(1)}, \dots, y^{(2n)}$ as unknowns. By inserting this ansatz into the algebra, evaluating the commutators and then equating the coefficients of the same types of operators, we get a set of equations (which are generally nonlinear) for the coefficients $x^{(i)}$ and $y^{(i)}$. For example, in the case of only one boson,

$$\begin{aligned} 1 - y^{(0)} &= |x^{(1)}|^2, \\ -y^{(2)} &= 2(|x^{(1)}|^2 + x_1^* x_3 + x_3^* x_1), \\ &\vdots \quad \vdots \end{aligned} \tag{9.52}$$

The evaluation of these equations is possible, and has been carried out by Sørensen [Sø 67, 68a+b, 69, 70, 71, 73] to fourth order and also by Kishimoto and Tamura [KT 72, 76] to sixth order in the Hamiltonian (see also [SP 77b]). However, the parameter $y^{(0)}$ is always open. A change of this parameter corresponds to a unitary transformation within the boson space [Sø 68b]. It has an influence on the convergence properties and has been used in different ways.

This kind of boson expansion is not a perturbative expansion, in the sense that the coefficients in a certain order are not changed if further terms are included. In this sense it may be better adapted to the collective bosons under consideration. The dynamical condition that the Hamiltonian should not couple the collective subspace with the rest of the Hilbert space is not touched by these considerations.

9.2.4 The Boson Expansion of Marumori

Marumori et al. [MYT 64a+b] propose a method which starts with a one-to-one mapping of states in the fermion space to states in the physical subspace of the boson space. The procedure is carried out for non-collective bosons, and we shall give a short discussion of the mathematical details in Section 9.2.6. Since, in this case, the convergence properties are very poor, Holzwarth et al. [LH 75] have used, in practical applications, a somewhat modified version using a few collective bosons. The same method has also been applied to exactly solvable models [PKD 68, KI 69]. Starting from collective fermion pair operators b_μ^+ of the form (9.24), we

introduce the normalized $2n$ -fermion states

$$|n\rangle = \mathcal{N}_F(n)|\mu_1 \dots \mu_n\rangle = \mathcal{N}_F(n)b_{\mu_1}^+ \dots b_{\mu_n}^+ |0\rangle, \quad (9.53)$$

where $\mathcal{N}_F(n)$ is a normalization constant. These states are, in general, not orthogonal. We will assume, however, that they are linearly independent, which is certainly true if only a few collective operators are taken into account and the number n is not too large (i.e., the whole number must not exceed the corresponding fermion space). The norm matrix $N_{nn'}$ is given by

$$N_{nn'} = \langle \mu_1 \dots \mu_n | \mu'_1 \dots \mu'_{n'} \rangle. \quad (9.54)$$

It is closely related to the quantities Γ of Eq. (9.28).

$$\begin{aligned} N_{11}: \quad & \langle \mu | \mu' \rangle = \delta_{\mu\mu'}, \\ N_{22}: \quad & \langle \mu\nu | \mu'\nu' \rangle = \delta_{\mu\mu'}\delta_{\nu\nu'} + (\mu \leftrightarrow \nu) - \Gamma_{\mu\nu}^{\mu'\nu'}, \\ N_{33}: \quad & \langle \mu\nu\rho | \mu'\nu'\rho' \rangle = \delta_{\mu\mu'}\delta_{\nu\nu'}\delta_{\rho\rho'} - \delta_{\rho\rho'}\Gamma_{\mu\nu}^{\mu'\nu'} - \Gamma_{\mu\nu}^{\mu'\nu'}\delta_{\rho\rho'} \\ & (+ \text{several permutations}). \end{aligned} \quad (9.55)$$

The diagonal matrix elements define the norm factors; for instance, we get for the two phonon norm

$$\mathcal{N}_F(2) = (1 + \delta_{\mu\nu} - \Gamma_{\mu\nu}^{\mu\nu})^{-1/2}. \quad (9.56)$$

Marumori now introduces a boson space spanned by the normalized orthogonal states

$$|n\rangle = \mathcal{N}_B(n)|\mu_1 \dots \mu_n\rangle = \mathcal{N}_B(n)B_{\mu_1}^+ \dots B_{\mu_n}^+ |0\rangle. \quad (9.57)$$

\mathcal{N}_B is a trivial factor of the form $(n_1! n_2! \dots)^{-1/2}$ (see C.19). The unitary operator

$$U = \sum_{nn'} |n\rangle N_{nn'}^{-1/2} \langle n'| \cdot \mathcal{N}_F^{-1}(n') \quad (9.58)$$

maps the space of fermions into this space.

In many practical applications (see Sec. 9.2.8), the matrix N is diagonal, otherwise the application of $N^{-1/2}$ means an orthogonalization. We therefore restrict ourselves to this case and gain, for the transformation of operators to the boson space,

$$H_B = U H U^\dagger = \sum_{nn'} \langle n | H | n' \rangle |n\rangle \langle n'|. \quad (9.59)$$

The operators $|n\rangle \langle n'|$ in the boson space can be expressed by the projector onto the boson vacuum*

$$|0\rangle \langle 0| = : \exp \left(- \sum_\mu B_\mu^+ B_\mu \right) := 1_B - \sum_\mu B_\mu^+ B_\mu + \frac{1}{2!} \sum_{\mu\nu} B_\mu^+ B_\nu^+ B_\mu B_\nu \dots \quad (9.60)$$

* The dots : mean normal ordering of the operators. The relation (9.60) is easy to prove in the case of one boson:

$$B |0\rangle \langle 0| = B (1 - B^+ B + \frac{1}{2} B^+ B^+ B B - \dots) = B - B + B^+ B B - B^+ B B + \dots = 0.$$

in an obvious shorthand notation

$$|n\rangle\langle n'| = \mathcal{N}_B(n)\mathcal{N}_B(n')(B^+)^n(1 - \dots B^+B + \dots B^+B^+BB - \dots)(B^+)^{n'}. \quad (9.61)$$

If $|n\rangle$ represent only a few collective states, the Hamiltonian (9.59) corresponds only to the collective part of the many-body Hamiltonian, and its eigenstates have a physical meaning only in cases where the full Hamiltonian does not couple the collective subspace to the rest of the Hilbert space. Therefore, the choice of proper bosons requires physical intuition.

In Eq. (9.59), the collective Hamiltonian is expressed as a normal ordered power series of boson operators. It contains the fermion matrix elements of the Hamiltonian in the collective subspace and the expansion of the boson-vacuum projector (9.60). As we shall see, it is usually a good approximation to take into account, in the sum (9.59), only low values of n and n' : $n + n' < n_{\max}$. Therefore, for practical application we need only low-order fermion matrix elements $\langle n|H|n'\rangle$. This is actually the *main practical advantage* of the boson theories (see below). They are calculated in the basis of collective fermion pairs b_μ^+ using the representation (9.32) of the Hamiltonian. Considering, for example, the matrix element $\langle n+2|H|n\rangle$, we find

$$\langle \mu_1 \dots \mu_{n+2} | H | \nu_1 \dots \nu_n \rangle = \sum_{\rho\sigma} V_{\rho\sigma}^{40} \langle \mu_1 \dots \mu_{n+2} | \rho\sigma \nu_1 \dots \nu_n \rangle. \quad (9.62)$$

With the assumption that the Hamiltonian does not scatter out of the collective space, the sum over ρ and σ is restricted to the few collective indices only, and we are left with the problem of calculating the norm matrix elements (9.54), which in practical applications is a rather tedious problem, because they take into account the corrections of the Pauli principle in the form of the quantities Γ in Eqs. (9.28).

At this step one often uses the additional approximation that the commutation relation (9.27c) is already fulfilled within the collective space, if the sum over ρ on the r.h.s. only runs over states in this space. It means that the double commutator

$$[b_\mu, [b_{\mu'}, b_{\nu'}^+]] = - \sum_{\rho} \Gamma_{\nu\rho}^{\mu'} b_\rho \quad (9.63)$$

does not scatter out of the collective space, an approximation which we have already used in the framework of the Belyaev-Zelevinskii approximation.

Using Eqs. (9.27b, c) we then can derive a *recursion relation* (see also [HJJ 76, IST 77, SP 78]):

$$\begin{aligned} \langle \mu_1 \dots \mu_n | \nu_1 \dots \nu_n \rangle &= \delta_{\mu_1 \nu_1} \langle \mu_2 \dots \mu_n | \nu_2 \dots \nu_n \rangle \\ &+ \sum (\mu_1 \text{ exchanged with all } \mu_2 \dots \mu_n) \\ &- \sum_{\lambda} \Gamma_{\nu_1 \lambda}^{\mu_1} \langle \lambda \mu_3 \dots \mu_n | \nu_2 \dots \nu_n \rangle \\ &- \sum [\mu_1 \mu_2 \text{ exchanged with all pairs in } (\mu_1 \dots \mu_n)]. \end{aligned} \quad (9.64)$$

Starting from the two-phonon norm (9.55) we are therefore able to express all higher norm matrix elements by $\Gamma^{(2)}$. Holzwarth et al. [HJJ 76] have checked the validity of this approximation in realistic transitional nuclei and found very good agreement with exact expressions for the norm matrix elements.

We will see in Section 9.2.6 that the quantities $\langle \mu_1 \dots \mu_n | \nu_1 \dots \nu_n \rangle$ are proportional to the matrix elements of the projection operator \hat{P} onto the physical subspace (see Eq. 9.99). They take into account the fact that the collective two-quasi-particle operators b_μ^+ are not real bosons. The fermion spaces spanned by these operators are finite, whereas the boson space spanned by the corresponding boson operators is infinite. Therefore, we find that the quotient of fermion to boson norm,

$$\nu(n) = \frac{\langle \mu_1 \dots \mu_n | \mu_1 \dots \mu_n \rangle}{(\mu_1 \dots \mu_n | \mu_1 \dots \mu_n)}, \quad (9.65)$$

becomes very small for large n -values. This means that the effective fermion space is truncated drastically by the Pauli principle. In particular, we find that the matrix elements $(n+2|H|n)$, which couple states with different boson numbers, become small for large n -values. As a consequence, we can restrict the sum in Eq. (9.59) to low values of n and n' . In many cases [HJJ 76, SP 77c], a Marumori expansion of the Hamiltonian up to fourth or sixth order is therefore a very good approximation.

Summarizing these results, we see two conditions under which the collective Marumori expansion is valid:

- (i) The first condition is a purely *kinematic* one (i.e., it has only to do with the collective operators b_μ^+ and the quantities Γ): The fermion norm matrix elements have to drop dramatically for large values of n , with the consequence that higher-order terms are cut down by the Pauli principle
- (ii) The second condition is a *dynamic* one (i.e., it has to do with the properties of the Hamiltonian H): The collective subspace spanned by the vectors $|\mu_1 \dots \mu_n\rangle$ under consideration has to coincide with an approximate eigenspace of the many-body Hamiltonian, that is, H should couple only weakly to the rest of the Hilbert space.

The first condition seems to be in contradiction to the condition of very collective bosons and small Γ -values in the case of perturbative boson expansions (see Sec. 9.2.3). For small Γ -values, the effective fermion space is indeed rather large. In fact, the first condition would be best fulfilled for a few pure two-quasi-particle operators, where the effective fermion space is very small. In this case, however, the second condition is hardly fulfilled. Only for *collective* bosons is the corresponding fermion space large enough that we can find cases where the exact eigenstates of the Hamiltonian can be represented in this way. It turns out, however, that the effects of the Pauli principle are still strong enough in these cases to guarantee rapid convergence (see [HJJ 76]).

As an example, we again investigate the *Lipkin model* of Section 5.4 (for

details, see [PKD 68]). From Eqs. (9.37) and (9.64), we gain the recursion relation for the norm,

$$\langle (b)^n (b^+)^n \rangle = \langle (b)^{n-1} (b^+)^{n-1} \rangle \left(n - \frac{n}{2} (n-1) \frac{2}{\Omega} \right), \quad (9.66)$$

which in this case is exact. For the normalization factors it yields

$$\mathcal{N}_F(n) = \sqrt{\frac{(\Omega-n)!}{\Omega! n!}} \Omega^n, \quad \mathcal{N}_B = \frac{1}{\sqrt{n!}}, \quad (9.67)$$

and for the Hamilton (9.38) up to four boson terms we have, from Eqs. (9.59f),

$$H_B = -\frac{\epsilon}{2}\Omega + \epsilon B^+ B - V \frac{\Omega}{2} \left[\sqrt{1 - \frac{1}{\Omega}} B^+ B^+ - \left(\sqrt{1 - \frac{1}{\Omega}} - \sqrt{\left(1 - \frac{1}{\Omega}\right)\left(1 - \frac{2}{\Omega}\right)} \right) B^+ B^+ B^+ B + \text{h.c.} \right]. \quad (9.68)$$

We see that the Marumori representation does not correspond to an expansion in $1/\Omega$. Each coefficient contains all orders in $1/\Omega$. If we expand them to a certain order in $1/\Omega$, we get the equivalent Belyaev-Zelevinskii terms of Eq. (9.47). On the other hand, we get the Marumori Hamiltonian by taking all orders of the Belyaev-Zelevinskii expansion, bringing them into normal order, and summing up the coefficients belonging to a fixed number of boson operators, because both expansions are equivalent in infinite order (see Sec. 9.2.6). The advantage of the Marumori expansion is that it takes the Pauli principle into account exactly in each order n .

In fact, the diagonalization of the Marumori operator in a boson space with a maximal number of N_{\max} bosons corresponds to the diagonalization of the fermion Hamiltonian in the space spanned by the fermion states $|n\rangle$, with $n < N_{\max}$. In the latter case, we would have to calculate the matrix elements $\langle n|H|n'\rangle$. From Eq. (9.59), we see that they are obtained as matrix elements $\langle n|H_B|n'\rangle$ of the Marumori operators in a boson space. The advantage of the transcription to a boson picture is the fact that the sum over n can be restricted to a small value n_{\max} under the conditions discussed above. This means that the higher order matrix elements $\langle n|H_B|n'\rangle$ are expressed by sums containing only the low-order fermion matrix elements.

If we include all fermion pairs b_μ^+ (also non-collective ones) the Marumori method corresponds exactly to a shell model calculation in an $2N_{\max}$ -quasi-particle space. In lowest order, therefore, we get not the RPA, but the TDA approximation.

9.2.5 The Boson Expansion of Dyson

The boson representations discussed so far are infinite expansions which converge only under certain conditions, such as a high collectivity of the underlying fermion pairs. In some cases—in particular, near closed shells—we must also take into account other types of less collective two-fermion pairs and their mixing with the collective subspace. In such cases, we must allow for several types of bosons with a different degree of collectivity. Nevertheless we hope that, at least for low-lying states, convergence can be found in the number m of different bosons.

This is quite a different type of convergence [(vertical direction in Fig. 9.3)]. It can be investigated by the boson representation of Dyson, because this method ends up with a finite boson Hamiltonian. Figure 9.3 also shows the cases that have been under investigation up to the present. Horizontal convergence with a few collective bosons [HJJ 76] in the transition region of soft nuclei has been tested, as has vertical convergence for many different Bosons—but only a few of them at one time have been tested in the region of the magic nucleus ^{208}Pb [IRS 80].

In general, there will most probably be cases in which many different types of bosons, as well as large numbers of them, are also needed, a region (characterized by a question mark in Fig. 9.3) which is difficult to investigate.

The Dyson representation is based on the fact that the commutator algebra (9.27) can be satisfied by the mapping* [RS 77a].

$$b_\mu^+ \rightarrow \tilde{B}_\mu^+ = B_\mu^+ - \frac{1}{2} \sum_{\nu\rho\sigma} \Gamma_{\mu\nu}^\rho B_\nu^+ B_\rho^+ B_\sigma, \quad (9.69a)$$

$$b_\mu \rightarrow B_\mu, \quad (9.69b)$$

$$a_\mu \rightarrow \sum_{\rho\sigma} \Gamma_{\mu\rho}^\sigma B_\rho^+ B_\sigma. \quad (9.69c)$$

It is a generalization of the Dyson representation (9.9) of the angular momentum algebra. By mapping the fermion vacuum $|0\rangle$ onto the boson vacuum $|0\rangle$, we obtain the corresponding representation of the vectors in the Hilbert space.

From the finite expressions (9.32) and (9.69) we get a finite boson Hamiltonian, which contains terms up to sixth order in the operators B and B^+ . The operators H^{11} and H^{22} conserve the boson number. If we assume that the coefficients $C_{kl}^{\mu\nu}$ of Eq. (9.24) are determined by the TDA equation (8.10), we get after a straightforward calculation,

$$V_{\mu\nu}^{22} = \delta_{\mu\nu} \Omega_\mu - \sum_k \Gamma_{\mu k}^{\mu k} \cdot E_k \quad (9.70)$$

and

$$H^{11} + H^{22} = \sum_\mu \Omega_\mu B_\mu^+ B_\mu + \frac{1}{4} \sum_{\mu\nu\rho\sigma} W_{\mu\nu\rho\sigma} B_\mu^+ B_\nu^+ B_\rho B_\sigma, \quad (9.71)$$

* For an early version of this representation, see also [Am 67].

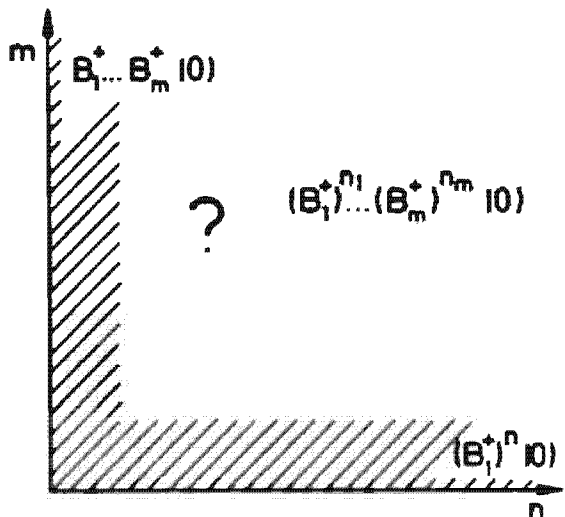


Figure 9.3. Schematic representation of the two kinds of convergence we are faced with in boson expansions. m gives the number of different boson types $B_1^+ \dots B_m^+$ and n gives the number of bosons of one type $(B_1^+)^n$.

with the matrix elements

$$W_{\mu\nu\rho\sigma} = \sum_{klpq} C_k^\mu C_l^\nu C_p^\rho C_q^\sigma (E_k + E_l + E_p + E_q - \Omega_\rho - \Omega_\sigma). \quad (9.72)$$

The other terms of the Hamiltonian violate the boson number and can be found in [RS 77a].

A disadvantage of the Dyson-representation is the fact that it violates Hermiticity, as we see, for instance, from the operator W in Eq. (9.71). The images of the bra and ket vectors

$$|\mu_1 \dots \mu_n\rangle \rightarrow \tilde{B}_{\mu_1}^+ \dots \tilde{B}_{\mu_n}^+ |0\rangle, \quad \langle \mu_1 \dots \mu_n| \rightarrow \langle 0| B_{\mu_1} \dots B_{\mu_n}$$

no longer form an orthogonal set.

In analogy to (9.54), we get for the norm matrix N :

$$N(\mu_1 \dots \mu_n, \mu'_1 \dots \mu'_n) = \langle 0| B_{\mu_1} \dots B_{\mu_n} \tilde{B}_{\mu'_1}^+ \dots \tilde{B}_{\mu'_n}^+ |0\rangle. \quad (9.73)$$

Since there are fast computer programs for the diagonalization of non-Hermitian matrices, this is not an essential shortcoming [RS 74b, SWR 76, Sch 76]. We will discuss some of the mathematical details in Section 9.2.6 and 9.3.6.

The method is extremely simple if one can neglect the coupling of subspaces with different boson numbers. In such cases the Hamiltonian is represented by $H^{11} + H^{22}$. It can be expressed entirely by the TDA amplitudes C_{kl}^μ , the TDA energies Ω_μ , and the quasi-particle energies E_k .

9.2.6 The Mathematical Background

In this section we want to discuss some mathematical properties of the boson representations treated so far. We can thus clarify the mathematical connections between the different methods. The reader who is not interested in such details may skip this section, which is highly mathematical. On the other hand, we are not

able to present all steps in the calculations, which are often rather lengthy, but refer the reader to the corresponding literature.

To understand the mathematical structure of the boson representations it is useful to work with "non-collective" bosons $B_{kl} = -B_{lk}$. Their index is the index of a fermion pair (9.22) and they obey the boson commutation relations

$$[B_{kl}, B_{k'l'}] = 0; \quad [B_{kl}, B_{k'l'}^+] = \delta_{kk'}\delta_{ll'} - (k \leftrightarrow l). \quad (9.74)$$

Starting from a complete orthogonal basis in the many-fermion space

$$|n\rangle = |k_1 l_1 \dots k_n l_n\rangle = \alpha_{k_1}^+ \alpha_{l_1}^+ \dots \alpha_{k_n}^+ \alpha_{l_n}^+ |0\rangle, \quad (9.75)$$

we can define a corresponding orthogonal set of states in the boson space [MYT 64a]

$$|n\rangle = \frac{1}{\sqrt{(2n-1)!!}} \sum_P (-)^P P B_{k_1 l_1}^+ \dots B_{k_n l_n}^+ |0\rangle, \quad (9.76)$$

where P runs over all permutations of the indices $k_1 \dots l_n$, which provide new combinations of bosons $B_{k_1 l_1}^+ \dots B_{k_n l_n}^+$ (i.e., $B_{12}^+ B_{34}^+$ and $B_{34}^+ B_{21}^+$ are each counted only once); there are $(2n)!/(n!2^n) = (2n-1)!!$ terms.

The states $|n\rangle$ of Eq. (9.76) span a linear subspace of the boson space, the so-called *physical subspace*. As we shall see, there is a one-to-one correspondence between this subspace and the fermion space. The rest of the boson space contains states $B_{k_1 l_1}^+ \dots B_{k_n l_n}^+ |0\rangle$, which are not completely antisymmetrized in the indices $k_1 \dots l_n$. They therefore violate the Pauli principle. States that have components of this type can provide spurious contributions to the expectation values of physical operators.

Janssen et al. [JDF 71] have shown that the basis states in Eq. (9.76) can also be written as

$$|n\rangle = \frac{1}{\sqrt{(2n-1)!!}} \langle 0 | \exp \left\{ \frac{1}{2} \sum_{kl} B_{kl}^+ \alpha_l \alpha_k \right\} \alpha_{k_1}^+ \alpha_{l_1}^+ \dots \alpha_{k_n}^+ \alpha_{l_n}^+ |0\rangle |0\rangle \quad (9.77)$$

$$= \frac{1}{\sqrt{(2n-1)!!}} \tilde{B}_{k_1 l_1}^+ \dots \tilde{B}_{k_n l_n}^+ |0\rangle, \quad (9.78)$$

with the non-collective Dyson operators (9.69a)

$$\tilde{B}_{kl}^+ = B_{kl}^+ - \sum_{pq} B_{kp}^+ B_{lq}^+ B_{pq}. \quad (9.79)$$

An example is the two-boson state

$$|2\rangle = \frac{1}{\sqrt{3}} \tilde{B}_{k_1 l_1}^+ \tilde{B}_{k_2 l_2}^+ |0\rangle = \frac{1}{\sqrt{3}} (B_{k_1 l_1}^+ B_{k_2 l_2}^+ - B_{k_1 k_2}^+ B_{l_1 l_2}^+ + B_{l_1 k_2}^+ B_{k_1 l_2}^+) |0\rangle. \quad (9.80)$$

The projector \hat{P} onto the physical subspace has the form

$$\hat{P} = \sum_n |n\rangle \langle n| = \sum_{n=0}^{\infty} \frac{1}{(2n)!} \frac{1}{(2n-1)!!} \sum_{\substack{k_1 \dots k_n \\ l_1 \dots l_n}} \tilde{B}_{k_1 l_1}^+ \dots \tilde{B}_{k_n l_n}^+ |0\rangle \langle 0| \tilde{B}_{k_n l_n} \dots \tilde{B}_{k_1 l_1}. \quad (9.81)$$

After a straightforward application of the relations

$$\begin{aligned} & \sum_{\substack{k_1 \dots k_n \\ l_1 \dots l_n}} \tilde{B}_{k_1 l_1}^+ \dots \tilde{B}_{k_n l_n}^+ |0\rangle \langle 0| \tilde{B}_{k_n l_n} \dots \tilde{B}_{k_1 l_1} \\ & = (2n-1)!! \sum_{\substack{k_1 \dots k_n \\ l_1 \dots l_n}} \tilde{B}_{k_1 l_1}^+ \dots \tilde{B}_{k_n l_n}^+ |0\rangle \langle 0| B_{k_n l_n} \dots B_{k_1 l_1} \end{aligned} \quad (9.82)$$

and

$$\langle 0 | \tilde{B}_{p_1 q_1} \dots \tilde{B}_{p_n q_n} \tilde{B}_{k_1 l_1}^+ \dots \tilde{B}_{k_m l_m}^+ | 0 \rangle = (2n - 1)!! \langle 0 | B_{p_1 q_1} \dots B_{p_n q_n} \tilde{B}_{k_1 l_1}^+ \dots \tilde{B}_{k_m l_m}^+ | 0 \rangle, \quad (9.83)$$

we obtain for the quantities

$$(B^+ B)_{kl} = \sum_q B_{ql}^+ B_{qk} \quad \text{and} \quad \hat{N} = \frac{1}{2} \sum_{kl} B_{kl} B_{kl} \quad (9.84)$$

the following properties

$$[\hat{P}, \tilde{B}_{kl}^+] = 0, \quad \hat{P} B_{kl} \hat{P} = B_{kl} \hat{P}, \quad [\hat{P}, (B^+ B)_{kl}] = 0, \quad (9.85)$$

$$\tilde{B}_{kl}^+ \hat{P} = \hat{P} B_{kl}^+ (1 + 2\hat{N}), \quad 2\hat{P} B_{kl}^+ \hat{N} = -\hat{P} (B^+ \cdot (B^+ B))_{kl} \quad (9.86)$$

There are several possible ways of mapping the fermion space onto the physical subspace of the bosons. Usui [Us 60] used the operator

$$U = \langle 0 | \exp \left(\frac{1}{2} \sum_{kl} B_{kl}^+ \alpha_l \alpha_k \right) | 0 \rangle. \quad (9.87)$$

Inserting a complete set (9.75) in the fermion space and using Eq. (9.77), it can be written as

$$U = \sum_n \sqrt{(2n - 1)!!} | n \rangle \langle n |. \quad (9.88)$$

It is obviously not unitary. We therefore have to define a conjugate operator

$$\tilde{U} = \sum_n \frac{1}{\sqrt{(2n - 1)!!}} | n \rangle \langle n | = U^* ((2\hat{N} - 1)!!)^{-1}, \quad (9.89)$$

where \hat{N} is the boson number operator (9.84). If I_F is the unity operator in the fermion space, we have

$$\tilde{U}U = I_F \quad \text{and} \quad \tilde{U}\tilde{U} = \hat{P}. \quad (9.90)$$

The fermion pair operators (9.22) are mapped in the following way.

$$\begin{aligned} b_{kl}^+ &\rightarrow \tilde{U} \alpha_k^+ \alpha_l^+ \tilde{U} = \tilde{B}_{kl}^+ \cdot \hat{P}, \\ b_{kl}^- &\rightarrow \tilde{U} \alpha_l \alpha_k \tilde{U} = B_{kl} \cdot \hat{P}, \\ a_{kl} &\rightarrow \tilde{U} \alpha_l^+ \alpha_k \tilde{U} = (B^+ B)_{kl} \cdot \hat{P}. \end{aligned} \quad (9.91)$$

This transformation obviously corresponds to the Dyson representation discussed in Section 9.2.5. The corresponding Hamiltonian has the form

$$U H_B \tilde{U} = H_B \cdot \hat{P} \quad (9.92)$$

with

$$\begin{aligned} H_B = & \sum_k E_k (B^+ B)_{kk} + \sum_{klpq} (H_{klpq}^{40} \tilde{B}_{kl}^+ \tilde{B}_{pq}^+ + H_{klpq}^{40*} B_{kl} B_{pq}) \\ & + \sum_{klpq} (H_{klpq}^{31} \tilde{B}_{kl}^+ (B^+ B)_{pq} + H_{klpq}^{31*} (B^+ B)_{pq} B_{kl}) \\ & + \frac{1}{4} \sum_{klpq} H_{klpq}^{22} \tilde{B}_{kl}^+ B_{pq}. \end{aligned} \quad (9.93)$$

As long as we restrict ourselves to physical wave functions we can neglect the projector and solve the Schrödinger equation

$$H_B |\Psi\rangle = E |\Psi\rangle. \quad (9.94)$$

However, we have to be aware that there are also spurious solutions $|\Psi\rangle$ which come from a violation of the Pauli principle. Since \hat{P} does not commute with H_B , they can have components in the physical subspace, that is, $\hat{P}|\Psi\rangle \neq 0$. To recognize them we have to apply the criterion $(I - \hat{P})|\Psi\rangle \neq 0$. In cases where the eigenvalue problem is approximated by restricting the number of collective bosons they can mix with the physical solutions. It is therefore often meaningful to decompose

$$H_B = H_B^0 + V_B, \quad (9.95)$$

with $H_B^0 = \sum_k E_k (B^\dagger B)_{kk}$. From Eq. (9.85) we see that H_B^0 commutes with \hat{P} . The physical solutions of Eq. (9.94) therefore also obey the equation

$$(H_B^0 + \hat{P}V_B)|\Psi\rangle = E|\Psi\rangle. \quad (9.96)$$

From a decomposition of any solution $|\Psi\rangle = \hat{P}|\Psi\rangle + (I - \hat{P})|\Psi\rangle$ into a physical and a spurious part, we see that its spurious part is an eigenvector of H_B^0 with the eigenvalue E .

$$H_B^0(I - \hat{P})|\Psi\rangle = E(I - \hat{P})|\Psi\rangle, \quad (9.97)$$

that is, the unphysical solutions of Eq. (9.96) have the eigenvalues of H_B^0 . They are given by

$$E_{k_1} + E_{l_1} + E_{k_2} + E_{l_2} + \dots \quad (9.98)$$

The lowest spurious eigenfunctions of H^0 are two boson states of the type $B_{12}^\dagger B_{12}^\dagger |0\rangle$. The lowest spurious solutions of (9.96) therefore lie at the free four-quasi-particle energies. This is usually much higher than the interesting low-lying part of the spectrum and an approximate solution of Eq. (9.96) does not provide serious mixing between physical and unphysical states.

In practical applications, it is meaningful to start with collective bosons. The form of the Hamiltonian H_B has already been derived in Section 9.2.5. To apply Eq. (9.96) we only need the matrix elements of the projector \hat{P} . We see from Eq. (9.81f) that they are given by the norm (9.54) or (9.73).

$$\begin{aligned} \langle \mu_1, \dots, \mu_n | \hat{P} | \mu'_1, \dots, \mu'_n \rangle &= \langle 0 | B_{\mu_1} \dots B_{\mu_n} \hat{P} B_{\mu'_1}^\dagger \dots B_{\mu'_n}^\dagger | 0 \rangle \\ &= \frac{1}{(2n-1)!!} \langle \mu_1, \dots, \mu_n | \mu'_1, \dots, \mu'_n \rangle. \end{aligned} \quad (9.99)$$

If we have physical eigensolutions of Eq. (9.94) or (9.96) we can calculate the matrix elements of a transition operator Q by transforming to the boson space

$$\bar{U}Q\bar{U} = Q_B \cdot \hat{P} \quad (9.100)$$

and get

$$\begin{aligned} \langle \Psi | Q | \Psi \rangle &= \langle \Psi | \bar{U}UQ\bar{U}U | \Psi \rangle (\Psi | Q_B \hat{P} | \Psi) \\ &= (\Psi | Q_B | \Psi). \end{aligned} \quad (9.101)$$

This shows that we can calculate all interesting quantities in the boson space without transforming back to the fermion space as long as we know that $|\Psi\rangle$ contains no spurious components. This can be achieved by diagonalizing the norm matrix (9.99) and restricting to the space with non-vanishing eigenvalues.

Marumori avoids non-Hermitian operators by a unitary mapping

$$U = \sum_n |n\rangle \langle n| = ((2N-1)!!)^{-1/2} \bar{U} \quad (9.102)$$

and obtains from Eqs. (9.91) and (9.86),

$$\begin{aligned} b_{kl}^+ &\rightarrow U a_k^+ a_l^+ U^+ = \tilde{B}_{kl}^+ (1 + 2\hat{N})^{-1/2} \hat{P} = \hat{P} (B^+ \sqrt{1 - B^+ B})_{kl} \hat{P}, \\ b_{kl} &\rightarrow U a_k a_l U^+ = (1 + 2\hat{N})^{-1/2} \tilde{B}_{kl} \hat{P} = \hat{P} (\sqrt{1 - B^+ B} \cdot B)_{kl} \hat{P}, \\ a_{kl} &\rightarrow U a_k^+ a_l U^+ = \hat{P} (B^+ B)_{kl} \hat{P}. \end{aligned} \quad (9.103)$$

In all practical applications, the square roots in Eq. (9.102) have to be replaced by a Taylor series. Therefore, the Marumori theory ends up with an infinite series, even if we restrict ourselves to the physical subspace.

The expansion coefficients of the square root are $(-)^n \binom{1/2}{n}$. Equation (9.103) therefore corresponds exactly to the *perturbative boson expansion* in Eq. (9.43). If we go to infinite order it is equivalent to the method of Marumori. The latter is obtained after normal ordering. Stopping at a finite order gives differences between both these cases [see, e.g., the Lipkin model in Eqs. (9.47) and (9.68)].

We also see that a formal expansion of $\sqrt{1 - B^+ B}$ does not converge in the case of non-collective bosons [Ok 74]. Only by introducing collective bosons and an appropriate decoupling of the corresponding subspace can convergence as discussed in Section 9.2.4 be achieved.

9.2.7 Methods Based on pp -Bosons

So far we have discussed several methods based on bosons in the vicinity of the fermi surface. These bosons were, to a good approximation, given by ph pairs or two-quasi-particle pairs. As a natural consequence, the boson number was not conserved in all these methods. The corresponding Hamiltonians included terms of the form $B^+ B^+$, $B^+ B^+ B$.

We now start from quite a different approach, namely from the bare vacuum $|-\rangle$ (or, in practical cases, also from a completely inert core) and add pairs of two particles coupled to an approximate boson. An example are Cooper pairs in a single j -shell* [Eq. (6.3)]

$$S_+ \propto \sum_m C_m^{j,j} a_{jm}^+ a_{j-m}^+ \quad (9.104)$$

or quadrupole pairs

$$D_\mu^+ \propto \sum_{mm'} C_{mm'}^{j,j/2} a_{jm}^+ a_{jm'}^+. \quad (9.105)$$

In the seniority scheme (Sec. 6.2), we can represent the ground state as a product of Cooper pairs [Eq. (6.19)]

$$|0\rangle \propto (S_+)^{N/2} |-\rangle$$

and some excited states by replacing one S_+ operator by a D_μ^+ [Eq. (6.27)]:

$$|2\mu\rangle \propto (S_+)^{N/2-1} D_\mu^+ |-\rangle. \quad (9.106)$$

In the general case, we can start with collective two-particle pairs

$$b_r^+ = \frac{1}{2} \sum_{kl} C_{kl}^r a_k^+ a_l^+ \quad (9.107)$$

*This contrasts with our convention of using capital letters for bosons; S_+ (9.104) and D_μ^+ (9.105) are collective fermion pairs. On the other side, the operators s^+ and d^+ in Eq. (9.119) are pure bosons.

and apply one of the methods discussed in the foregoing sections to construct a boson representation. Since the particle number is conserved, we now have only terms that conserve the boson number. In the Dyson method, for instance, we get a finite Hamiltonian of fourth order [see Eq. (9.71)]:

$$H_B = \sum_i \Omega_i B_i^+ B_i + \frac{1}{4} \sum_{\tau_1 \tau_2 \tau_3 \tau_4} W_{\tau_1 \tau_2 \tau_3 \tau_4} B_{\tau_1}^+ B_{\tau_2}^+ B_{\tau_3} B_{\tau_4}. \quad (9.108)$$

The coefficients C_{kl}' are now the pp -TDA amplitudes, and the quantities Ω_i are given by the corresponding energies. In the other methods we end up with similar Hamiltonians (perhaps infinite and Hermitian but *boson number conserving*).

The disadvantage of this method is that it can be applied microscopically only for very few bosons, for instance, in the vicinity of a magic nucleus with a really inert core. For nuclei far away from magic shells we need a large number of pp -bosons whose corresponding C_{kl}' coefficients are determined on the basis of a completely inert core. For a large number of active particles this need not be a very good basis, however, as we can easily imagine in considering the extreme case of a ^{16}O core for the description of nuclei in the ^{208}Pb region. Thus, for nuclei far from being magic, the pp -boson description might not be valid if the amplitudes are restricted to the inert core basis. We may, however, try to consider the amplitudes C_{kl}' as adjustable parameters to be determined, for example, by a variational calculation.

On the other hand, configurations consisting of a large number of bosons can only be treated by group theoretical methods. So far, one has investigated only phenomenological models. One of this models is the *interacting boson model* ($SU(6)$ -model) of Arima and Iachello [AI 75a and b]. It includes two types of bosons, an s -boson corresponding to a Cooper pair of Eq. (9.104), and five d -bosons corresponding to the five quadrupole pairs in Eq. (9.105). The Hermitian Hamiltonian has only boson number conserving terms up to fourth order [see Eq. (9.119)]:

$$s^+ s, \quad d^+ d, \quad d^+ d^+ dd, \quad s^+ s^+ ss, \quad d^+ d^+ ss, \quad d^+ d^+ ds \quad + \text{h.c.}$$

Neglecting the fourth-order terms which describe the interaction between the bosons, we have an unperturbed ground state as a product of $A/2$ s -bosons and excited states, where some of the s -bosons are replaced by d -bosons. Originally, the model was introduced on purely phenomenological grounds. For one j -shell with a pairing-plus-quadrupole interaction (4.141), however, it can be motivated from a microscopic point of view by mapping pp -fermion pairs onto a suitable boson representation [AOI 77]. We shall discuss a few applications of this model in the next section.

Another example for pp -bosons is the *Schwinger representation* [BM 78]. Working in a single-particle basis, where a_m^+ and a_i^+ create particles above and below the fermi surface, we can introduce two types of bosons: B -bosons B_{mi}^+ , which correspond to the creation of a pp -pair $a_m^+ a_i^+$ (with one particle above and one below the fermi surface); and A -bosons A_{ij}^+ , which correspond to the creation of pp -pair $a_i^+ a_j^+$ (with both particles below the fermi surface). Both types of bosons are ideal bosons with the commutation relations

$$[B_{mi}, B_{m'i'}^+] = \delta_{mm'} \delta_{ii'}, \quad [A_{ij}, A_{ij'}^+] = \delta_{ii'} \delta_{jj'} - \delta_{ij} \delta_{j'i'}. \quad (9.109)$$

For the description of even systems we need only the density operators $a_k^+ a_i$. They

are mapped in the following way.

$$\begin{aligned} a_m^+ a_m \rightarrow (a_m^+ a_m)_B &= \sum_i B_{mi}^+ B_{mi}, \\ a_r^+ a_i \rightarrow (a_r^+ a_i)_B &= \sum_j A_{rj}^+ A_{ij}, \\ a_m^+ a_i \rightarrow (a_m^+ a_i)_B &= \sum_j B_{mj}^+ A_{ij}, \\ a_i^+ a_m \rightarrow (a_i^+ a_m)_B &= (a_m^+ a_i)_B^+. \end{aligned} \quad (9.110)$$

This mapping conserves the corresponding commutation relations for the density operators $a_k^+ a_i$, Hermiticity, and furthermore ends up with finite expressions in the boson space. Starting from the boson vacuum $|-\rangle$,

$$A_y|-\rangle = B_{my}|-\rangle = 0, \quad (9.111)$$

which corresponds to the bare vacuum in the fermion space we can construct the HF ground state $|\Phi_0\rangle$ in the boson space by the conditions

$$(a_m^+ a_m)_B |\Phi_0\rangle = 0, \quad [\delta_{ir} - (a_r^+ a_i)_B] |\Phi_0\rangle = 0. \quad (9.112)$$

They are satisfied by

$$|\Phi_0\rangle = \frac{1}{\sqrt{N!}} \det A^+ |-\rangle = \frac{1}{\sqrt{N!}} \begin{vmatrix} A_{11}^+ & \dots & A_{N1}^+ \\ \vdots & \ddots & \vdots \\ A_{1N}^+ & \dots & A_{NN}^+ \end{vmatrix} |-\rangle. \quad (9.113)$$

Excited *ph*-states are constructed by successive applications of the operators $(a_m^+ a_i)_B$. From Eq. (9.110), we see that the effect of such an operation is to replace the *i*th column of the operators A_y^+ by a column of B_{mj}^+ in the determinant (9.113).

This boson representation is a straightforward generalization of the *Schwinger representation* (9.11) in the angular momentum case. A problem connected with this type of representations is the fact that we have introduced too many boson operators.

The state $|\Phi_0\rangle$ and the many-particle-many-hole states built from it form a basis in the physical subspace of the bosons. We can show that the operator

$$L_{ii'} = \sum_j A_{ji}^+ A_{ji'} + \sum_m B_{mi}^+ B_{mi'} = (A^+ A + B^+ B)_{ii'} \quad (9.114)$$

annihilates all these states for $i \neq i'$ and leaves them unchanged for $i = i'$; that is, we have the constraint

$$L_{ii'} = (A^+ A + B^+ B)_{ii'} = \delta_{ii'} \quad (9.115)$$

in the physical subspace. It corresponds to the constraint (9.14) in the angular momentum case. Introducing the boson operators A and B enlarges the boson space drastically. As a result, we get a new class of additional spurious solutions violating the condition (9.115).

In principle, we can use the constraint (9.115) to eliminate the operators A_y, A_y^+ . This is done formally by writing

$$A \sim \sqrt{1 - B^+ B}. \quad (9.116)$$

Inserting the expression into Eq. (9.110), we again end up with the Holstein-Primakoff expression (9.4) in the physical subspace. A detailed analysis shows that the elimination (9.116) corresponds to a canonical transformation within the boson space [BM 78].

In a similar way we can eliminate the s -boson in the $SU(6)$ model of Arima and Iachello. We then end up with a Holstein-Primakoff representation of this model containing only d -bosons with square root factors of the type (9.116). In this form the $SU(6)$ model has been first investigated by Janssen et al. [JJD 74].

So far we have used only the particle representation to discuss the *Schwinger bosons*. There have been also attempts to introduce a general *Schwinger representation* based on quasi-particles [YN 76, MNY 77, FYN 77, Fu 77].

9.2.8 Applications

Several groups have applied the method of boson expansions to the description of transitional nuclei, starting with weakly anharmonic vibrators through strong anharmonicities, to the rotational limit in well deformed nuclei. Basically, we have to distinguish between two types of work, namely *phenomenological approaches*, which parametrize boson Hamiltonians of a simple structure and *microscopic approaches*, where the parameters in the boson Hamiltonian are derived from an underlying fermion many-body Hamiltonian.

9.2.8.1. Phenomenological and Interacting Boson Models. We can express the Hamiltonian by phenomenological boson operators whose physical structure need not be specified in detail. According to the number of different bosons and the order to which we go, it contains a number of parameters h_{lm} . An example is provided by the quadrupole bosons d_μ^+ up to fourth order. (The word quadrupole in this context only means that these operators are spherical tensors of rank 2. It does not specify the radial dependence of a corresponding fermion operator.)

$$\begin{aligned} H = & h_{00} + h_{11} [d^+ d]_0 + h_{20} [d^+ d^+]_0 + h_{30} [[d^+ d^+]_2 d^+]_0 + h_{21} [[d^+ d^+]_2 d]_0 \\ & + h_{40} [d^+ d^+]_0 [d^+ d^+]_0 + h_{31} [d^+ d^+]_0 [d^+ d]_0 \\ & + \sum_{L=0,2,4} h_{22}^L [[d^+ d^+]_L [dd]_L]_0. \end{aligned} \quad (9.117)$$

The brackets indicate the coupling of the angular momenta. The diagonalization of such an operator is a nontrivial problem. One usually calculates its matrix elements between multi-boson states and diagonalizes the corresponding matrix. However, the size of this matrix can only be kept within reasonable limits by using the group theoretical properties of the underlying Hamiltonian. For instance, the quadrupole bosons obey the $SU(5)$ symmetry, which has been studied in great detail in the literature [WHG 66, KPW 68, WP 68, KT 71].

The diagonalization of the phenomenological Hamiltonian (9.117) gives a spectrum that depends on the constants h_{lm} . In the calculation of *transition probabilities*, we need a boson representation of the transition operator containing additional constants. The fitting of all these parameters to experimental data allows a test, to see if the observed physical phenomena can be described by the corresponding bosons. If they can, we

also get information about the Hamiltonian, such as statements concerning the parameters. On the other hand, as we have no microscopic derivation, we have to be very careful, because if we use enough parameters sometimes quite different physical phenomena may be fitted.

The simplest version of such phenomenological approaches uses only the five quadrupole bosons and a fourth-order coupling term diagonal in the boson number. In such cases, we can fit the highest angular momentum members of the different quadrupole multiplets reasonably well [BTK 65, DDK 70, HR 74, IA 74]. To describe the other members we also need a more general ansatz, like (9.117) [KS 62, GG 71, HL 72a].

Starting from the boson operators B, B^+ , we can define corresponding coordinates Q and momenta P [see, for instance, Eq. (8.95)] and formally divide the Hamiltonian into a potential and kinetic energy part

$$H(P, Q) = \frac{1}{2M} P^2 + V(Q). \quad (9.118)$$

The requirement that the "mass parameter" depends on neither P nor Q leads to simple relations between the parameters of the boson Hamiltonian [Ho 71a]. In the quadrupole model, the potentials in the internal frame depend on the deformation parameters (see Eq. (1.13)). Figure 9.4 shows such a potential curve as a function of β and the corresponding spectrum in the nucleus ^{76}Se . The constants of the boson Hamiltonian were obtained using a fit of four phenomenological parameters.

One is also able to describe the transition from a spherical vibrator spectrum, through anharmonicities to spectra with a rotational band struc-

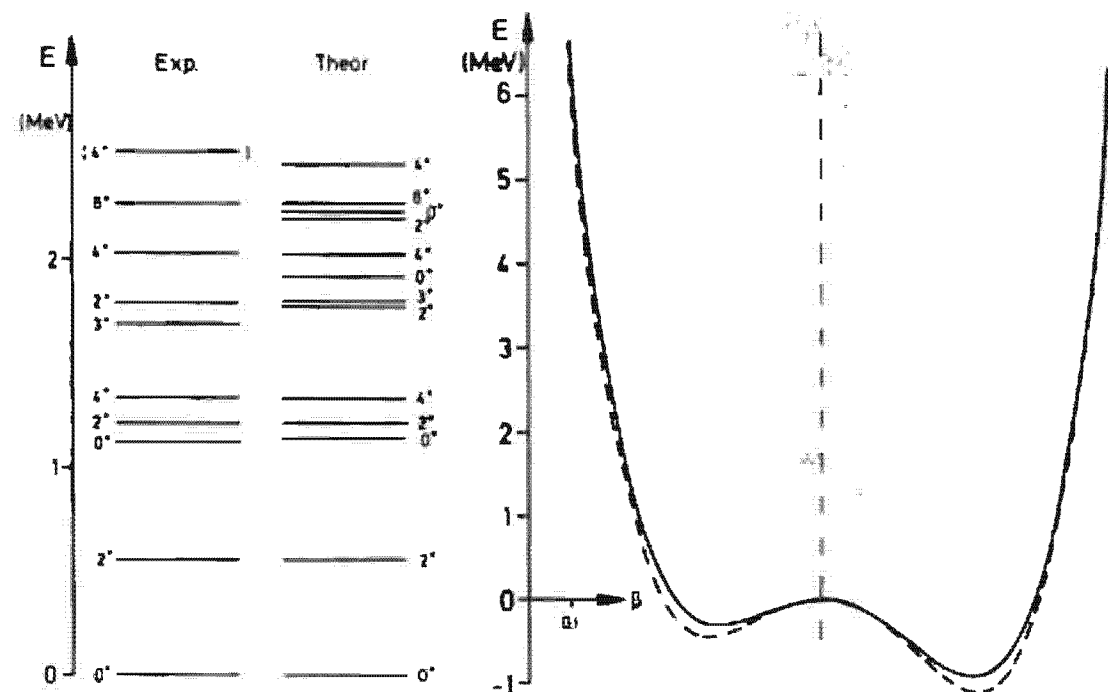


Figure 9.4. The experimental energy levels of ^{76}Se compared to the eigenvalues of a phenomenological boson Hamiltonian. The full curve shows the corresponding potential energy in the intrinsic $\beta - \gamma$ frame at $\gamma = 0^\circ$. The dashed curve is the potential arising from a microscopic calculation. (From [LH 75].)

ture using an appropriate choice of the parameters in the Hamiltonian [Ho 70, GMG 69, 70, DB 70, GG 71, Ho 71a]. A rotational band structure develops if the potential $V(Q)$ has a well-pronounced deformed minimum (see Fig. 9.5). However, for such cases a large number of bosons (up to 30) is needed. Besides the tremendous numerical effort brought about by the components with high boson numbers, also serious doubts from a physical point of view may exist, since they strongly violate the Pauli principle and we do not know if the phenomenological Hamiltonian really takes care of this fact.

Over the years, a large number of phenomenologically based models have been developed whose diagonalizations are considerably simplified by the use of group theoretical techniques (see, for instance, [HNL 70, DDK 70, VNR 75, RD 76, RGB 77]). Of these, probably the best known is the *interacting boson model* ($SU(6)$ -model), which was first proposed by Janssen et al. [JJD 74] and later on much investigated by Arima and Jachello [AI 75a, b]. Its six basic blocks are five quadrupole bosons d_μ^+ ($\mu = -2, \dots, +2$) and one pairing boson s^+ . The boson number is conserved, and it is a model having pp -bosons (a boson representation of the Schwinger type) as discussed in Section 9.2.7. The Hamiltonian has the form

$$\begin{aligned} H = & \epsilon_s s^+ s + \epsilon_d [d^+ d]_0 + \sum_{L=0,2,4} c_L [[d^+ d^+]_L [dd]_L]_0 + u_0 s^+ s^+ ss \\ & + (v_2 [[d^+ d^+]_2 [ds]_2]_0 + v_0 [d^+ d^+]_0 ss + u_2 [[d^+ s^+]_2 [ds]_2]_0 + \text{h.c.}). \end{aligned} \quad (9.119)$$

It contains eight parameters $\epsilon = \epsilon_d - \epsilon_s$, $c_0, c_2, c_4, u_0, u_2, v_0, v_2$ which are fitted to experimental data. In addition, we need two further constants to define the $E2$ -transition operator

$$T_{2\mu} = q_0 ([d^+ s]_{2\mu} + \text{h.c.}) + q_1 [d^+ d]_{2\mu}. \quad (9.120)$$

In the case of a vanishing interaction ($c_L = v_L = u_L = 0$), the ground state consists only of s -bosons:

$$|0\rangle = \frac{1}{\sqrt{n!}} (s^+)^n |-\rangle,$$

in which $|-\rangle$ is the bare vacuum and $2n$ the number of nucleons. Successively replacing one or several s -bosons by d -bosons, we obtain quadrupole excitations in the same nucleus with the excitation energies $\epsilon = \epsilon_d - \epsilon_s$,

$$|\mu\rangle = \frac{1}{\sqrt{(n-1)!}} d_\mu^+ (s^+)^{n-1} |-\rangle.$$

The unperturbed spectrum is therefore a purely harmonic quadrupole spectrum, as shown in Fig. 1.5.

Adding further s -bosons, we obtain states in the neighboring even nuclei with particle numbers $2n+2, 2n+4, \dots$, etc., as was discussed in the seniority model (see Sec. 8.2).

The boson-boson interaction induces correlations. The Hamiltonian (9.119) then has to be diagonalized in a multi-boson basis containing states with n_s s-bosons and $n_d = n - n_s$ d-bosons $|n_s, n_d, \alpha\rangle$. (α contains all remaining quantum numbers needed for the unique specification of the states.) The evaluation of the corresponding matrix elements is greatly simplified by group theoretical methods.

The relation

$$n = \hat{n}_s + \hat{n}_d = s^+ s + \sum_{\mu} d_{\mu}^+ d_{\mu}$$

can be used to *eliminate the operators s and s^+* . For a fixed value of n the basis states are completely characterized by the quantum numbers of the d-bosons, and we obtain the proper matrix elements of the Hamiltonian if we replace the operators s by

$$s \rightarrow \sqrt{n - \sum_{\mu} d_{\mu}^+ d_{\mu}} . \quad (9.121)$$

For example, we have

$$\begin{aligned} s|n_s = n - n_d, n_d, \alpha\rangle &= \sqrt{n_s} |n - n_d - 1, n_d, \alpha\rangle \\ &= \sqrt{n - \sum_{\mu} d_{\mu}^+ d_{\mu}} |n - n_d - 1, n_d, \alpha\rangle. \end{aligned}$$

Applying these rules to the operator (9.119), we end up with a Hamiltonian containing only the quadrupole bosons d_{μ}^+ . However, it no longer conserves the boson number, and by expanding the square roots in Eq. (9.121) we obtain an infinite series of terms $d^+ d \dots$. This is the Holstein-Primakoff version of the $SU(6)$ -model [JJD 74]. The introduction of the s-boson is therefore a very elegant tool for treating the square root factors introduced by the Pauli principle and ending up with a finite boson representation. We emphasize, however, that the s-boson does not introduce a new degree of freedom for a fixed particle number. It is only used to construct the unperturbed ground state. The model contains no 0^+ pairing vibrations of the $2p - 2h$ type as discussed in Section 8.3.5. On the other hand, the introduction of the s-boson allows us to treat states in the adjacent $A + 2, A + 4, \dots$ nuclei.

Depending on the actual values of the parameters, the model has several *limits*, which correspond to various subgroups of $SU(6)$ [CCF 79] and are sometimes analytically soluble. They also represent very important physical mechanisms in actual nuclei:

- (i) For $c_L = v_L = 0, u_2 = 0$ (i.e., without coupling to d-bosons), we obtain the *seniority scheme* in a single j -shell ($SU(2)$) as discussed in Section 6.2:

$$H = \epsilon_s s^+ s + u_0 s^+ s^+ s s = -G S_+ S_- ,$$

with the quasi-spin operators

$$S_+ = \sqrt{\Omega} \cdot s^+ \sqrt{1 - \frac{s^+ s}{\Omega}}$$

and

$$\mu_0 = -G, \quad \epsilon_s = G \cdot \Omega.$$

- (ii) For weak interaction $\mu_L = 0$; $v_L, c_L \ll \epsilon_d - \epsilon$, we have the *vibrational limit* [AI 76] with the symmetry $SU(5)$. The s -bosons play no role in this limit, and in the extreme case we have only interacting quadrupole bosons (see also [BTK 65, DDK 70, IA 74]) with the Hamiltonian

$$H = \sum_{\mu} \epsilon_d d_{\mu}^+ d_{\mu} + \sum_{L=0,2,4} c_L [[d^+ d^+]_L [dd]_L]_0. \quad (9.122)$$

Its eigenvalues and transition rates can be given in analytic form.

- (iii) If certain relations between the parameters of the model are fulfilled, we can rewrite the Hamiltonian (9.119) in the form

$$H = \epsilon \sum_{\mu} d_{\mu}^+ d_{\mu} - \kappa' [L \cdot L]_0 - \kappa [Q \cdot Q]_0, \quad (9.123)$$

with the parameters $\epsilon, \kappa, \kappa'$, the three angular momenta

$$L_{\mu} = \sqrt{10} [d^+ d]_{1\mu}$$

and the five quadrupole operators

$$Q_{\mu} = d_{\mu}^+ s + s^+ d_{\mu} - \frac{\sqrt{7}}{2} [d^+ d]_{2\mu}.$$

For $\epsilon = \kappa' = 0$, we obtain the *rotational limit* [AI 78a] based on the group $SU(3)$. It is an extension of the Elliot model [El 58], which was widely used for fermions and whose group theoretical properties are discussed in the literature [Ha 68, Ve 68, JDJ 75]. It has the spectrum of an axially symmetric rigid rotor (with degenerate 2_{β}^+ and 2_{γ}^+ levels)

$$E(\lambda, \mu, K, L, M) = \frac{3}{4}(\kappa - \kappa')L \cdot (L + 1) - \kappa(\lambda^2 + \mu^2 + \lambda\mu + 3(\lambda + \mu)),$$

where (λ, μ, K, L, M) are the quantum numbers of the group $SU(3)$.

- (iv) At the end of each major shell, another subgroup of the $SU(6)$, the $O(6)$ seem to play an important role for the classification of the spectra [AI 78b, CC 78, CBP 78]. Again, the eigenvalues can be given in analytic form. In a certain limit they are identical to those of a deformed, completely γ -soft oscillator, the Wilets-Jean model [WJ 56, Me 78].

Since the $SU(6)$ model incorporates so many important physical effects and also has a rather large number of free parameters (up to eleven), we can get excellent agreement with many experimental spectra in spherical, and weakly and strongly deformed nuclei (see also [Ia 77, AOI 78, Ia 78]). We can also give a microscopic justification for the case of a pairing-plus-quadrupole interaction within a single j -shell [OAI 78]. A full microscopic derivation, which also includes *single-particle degrees of freedom* is, however, still missing.

9.2.8.2. Microscopic Calculations. Although the phenomenological boson models have had great success in fitting experimental spectra and transition probabilities, we can never be sure that they do not simulate quite different physical mechanisms having nothing to do with bosons, by a suitable choice of parameters. It is therefore crucial in this kind of theory to demonstrate that we can, in principle, derive the parameters entering the Hamiltonian from a microscopic point of view.

Lee and Holzwarth [LH 75] have used the Marumori method (Sec. 9.2.4) with collective bosons for the description of anharmonic nuclei with a rather pure quadrupole structure. They expanded the Hamiltonian of a surface delta interaction [see Eq. (4.117)] up to fourth order in TDA bosons with angular momentum two and found that the resulting expansion coefficients h_{lm} in Eq. (9.117) are generally in good agreement with the parameters determined by fitting the experimental levels [HL 72a]. Figure (9.4) shows the corresponding microscopically determined boson potential $V(Q)$ (dashed line).

B. Sørensen used the Belyaev-Zelevinskii method described in Section 9.2.3.2. In several papers [Sø 67, 68a+b, 69, 70] he investigated pairing modes near closed shells and quadrupole modes in transitional nuclei. He used a slightly modified pairing-plus-quadrupole interaction [see Eq. (4.141)] and expanded the Hamiltonian to fourth order. He successfully reproduced, at least semiquantitatively, the main features of such nuclei. However, he had difficulties in cases where the coupling to non-collective two-quasi-particle states are important.

More complete investigations based on the same method have been

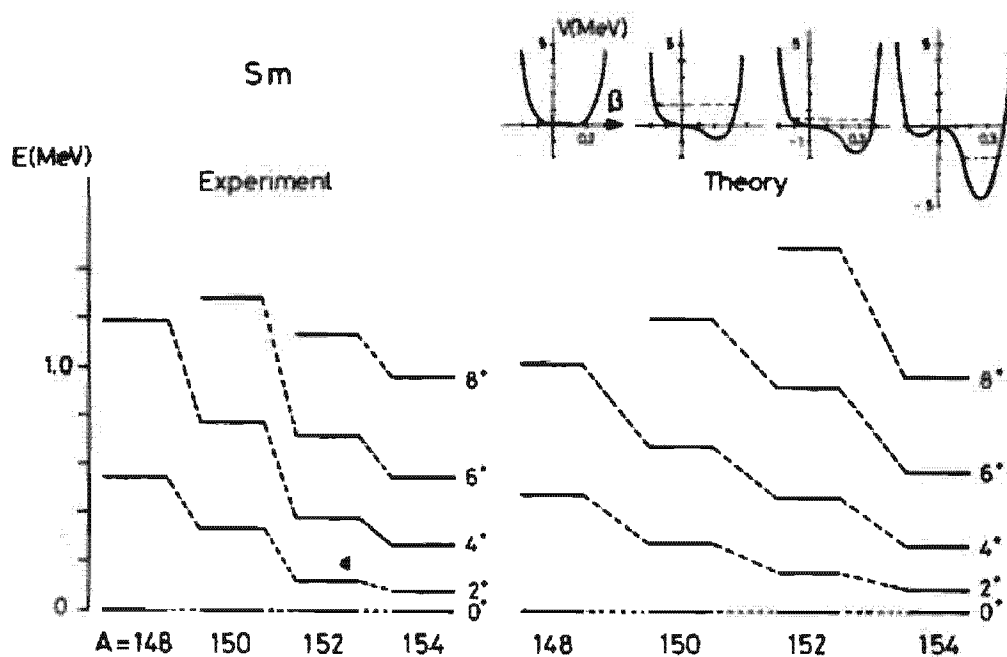


Figure 9.5. The phase transition spherical-deformed in the Samarium nuclei. The structure of the spectrum changes from a vibrator to a rotator. Also shown are corresponding potentials of the boson Hamiltonian as a function of the deformation parameter. (From [KT 76].)

carried out by Kishimoto and Tamura [KT 72, 76]. In addition to the pairing-plus-quadrupole interaction they used a quadrupole pairing force [see Eq. (4.134)] and expanded the Hamiltonian to sixth order in the collective branch of ($I=2$)-bosons. The coupling to the non-collective branches turned out to be very important in many nuclei. It was taken into account by a projector formalism in the sense of Feshbach [Fe 58, 62], which ends up with an effective Hamiltonian in the collective subspace. Thus the parameters h_{lm} had to be replaced by energy-dependent renormalized parameters \tilde{h}_{lm} . The results of these complicated calculations show extremely good agreement with experimental data not only for vibrational, but also for transitional and even purely rotational nuclei. Figure 9.5 gives an example for the transition from spherical to deformed shapes in the Sm region. Table 9.1 gives the corresponding electric properties.

Table 9.1. Spectroscopic quadrupole moments and $BE2$ values of the first excited 2^+ state calculated with the boson expansion method and compared with experimental data (from [TK 73])

	$Q [e \cdot b]$		$BE2(2^+ \rightarrow 0^+) [e^2 \cdot b^2]$	
	Experiment	Theory	Experiment	Theory
^{148}Sm	-0.97 ± 0.27	-0.91	0.141 ± 0.005	0.152
^{150}Sm	-1.31 ± 0.19	-1.17	0.274 ± 0.006	0.270
^{152}Sm	-1.73 ± 0.20	-1.72	0.666 ± 0.014	0.697
^{154}Sm	—	-1.91	0.922 ± 0.040	0.884

9.3 Odd Mass Nuclei and Particle Vibration Coupling

Until now we have considered only systems with an even number of particles. Systems with odd particle number also, of course, have collective states. Historically, one of the most famous examples is the septuplet of ^{209}Bi , where the $1h_{9/2}$ proton of ^{209}Bi couples to the 3^- vibration at 2.61 MeV of the ^{208}Pb core. The proton perturbs this vibration only very slightly, giving rise to a very small splitting of the seven different spin states (see Fig. 9.6). These states are very often treated in the vibration-

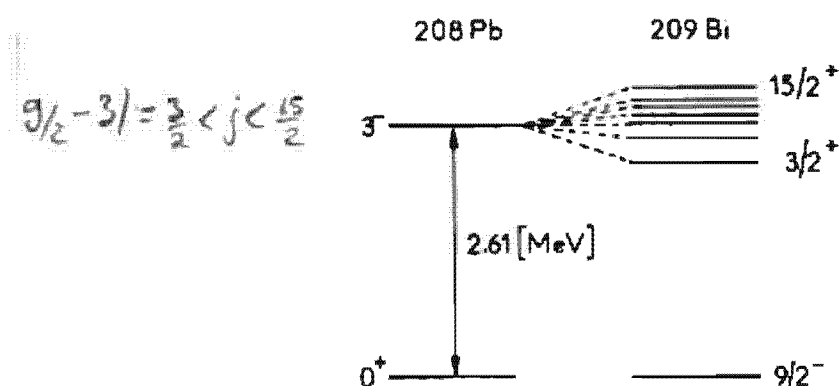


Figure 9.6. Schematic comparison of the experimental spectra of ^{208}Pb and ^{209}Bi .

particle coupling (VPC) model [BM 75]. It turns out that this is closely connected to the boson expansion in odd systems.

9.3.1 Boson Expansion for Odd Mass Systems

All different kinds of boson theories considered in the last section can be generalized to odd mass systems [Ya 65, DJ 73, Ma 73, Ma 74, Pr 74, RS 77a, BM 78]. Since the principle is not very different from the even case, we only want to sketch briefly the Belyaev-Zelevinskii and Dyson methods.

In the Belyaev-Zelevinskii method we now consider, in addition to the fermion pair operators b_μ^+ , $a_{\mu\nu}$ [Eqs. (9.24) and (9.25)], the fermion operators α_k^+ , and map these operators into an enlarged space, namely the direct product of the usual boson space of the B_μ^+ and a space of one ideal fermion β_k^+ which commutes with the bosons.

$$[B_\mu, \beta_k^+] = [B_\mu^+, \beta_k^+] = 0. \quad (9.124)$$

Since there is only one ideal fermion at a time, the operators β_k obey the relations [Ok 74]

$$\beta_k \beta_l = \beta_k^+ \beta_l^+ = 0, \quad \beta_k \beta_l^+ = \delta_{kl}. \quad (9.125)$$

The vacuum projector in this space is given by

$$|0\rangle\langle 0| = : \exp\left(-\sum_\mu B_\mu^+ B_\mu\right) : \left(1 - \sum_k \beta_k^+ \beta_k\right), \quad (9.126)$$

which again means

$$B_\mu |0\rangle = \beta_k |0\rangle = 0. \quad (9.127)$$

The basis states in the product space are therefore given by

$$|k, N\rangle = \mathcal{R}_B \cdot \beta_k^+ B_{\mu_1}^+ \dots B_{\mu_N}^+ |0\rangle \quad N = 0, 1, \dots. \quad (9.128)$$

In addition to the algebra (9.27) of the operators b_μ^+ and $a_{\mu\nu}$, we now also have to consider commutation relations between single-fermion and fermion pair operators:

$$\begin{aligned} \{\alpha_k, \alpha_l\} &= \{\alpha_k^+, \alpha_l^+\} = 0, \quad \{\alpha_k, \alpha_l^+\} = \delta_{kl}, \\ [\alpha_k, b_\mu] &= 0, \quad [\alpha_k, b_\mu^+] = \sum_l C_{kl}^\mu \alpha_l^+, \\ [\alpha_k, a_{\mu\nu}] &= \sum_l \Gamma_{\mu\nu}^{lk} \alpha_l, \end{aligned} \quad (9.129)$$

with $\Gamma_{\mu\nu}^{lk}$ defined by Eq. (9.29).

We now proceed as in Section 9.2.3.1 and make the following ansatz for the boson image of the different operators (arguments for the specific choice of the ansatz are given in [Ma 74]); here we want to content ourselves with the fact that the commutation rules are satisfied order by

order*:

$$\begin{aligned}
 (a_{\mu\nu})_B &= \sum_{\rho\sigma} \Gamma_{\nu\rho}^{\mu\sigma} B_{\rho}^{+} B_{\sigma} + \sum_{kl} \Gamma_{\nu l}^{\mu k} \beta_k^{+} \beta_l, \\
 (b_{\mu}^{+})_B &= B_{\mu}^{+} - \frac{1}{4} \sum_{\rho\sigma} \Gamma_{\mu\rho}^{\nu\sigma} B_{\nu}^{+} B_{\rho}^{+} B_{\sigma} \\
 &\quad + \dots - \frac{1}{2} \sum_{\rho kl} \Gamma_{\mu l}^{\nu k} B_{\nu}^{+} \beta_k^{+} \beta_l + \dots, \\
 (\alpha_k^{+})_B &= \beta_k^{+} - \frac{1}{2} \sum_{\rho l} \Gamma_{\rho k}^{\nu l} B_{\rho}^{+} B_{\sigma} \beta_l^{+} + \dots + \sum_{\rho l} C_{kl}^{\rho} B_{\rho}^{+} \beta_l.
 \end{aligned} \tag{9.130}$$

With these formulas we can construct the boson image of the Hamiltonian operator (9.32).

9.3.2 Derivation of the Particle-Vibration Coupling (Bohr) Hamiltonian

Insertion of (9.130) into the Hamiltonian (9.32), (9.33) yields to first order in the Γ 's if we neglect for the moment ground state correlations, that is, $H^{(0)}$:

$$\begin{aligned}
 H &= \sum_{\mu} \Omega_{\mu} B_{\mu}^{+} B_{\mu} + \sum_k E_k \beta_k^{+} \beta_k + \dots + H_{\text{coupl}}, \\
 H_{\text{coupl}} &= \sum_{\mu, k, l} \frac{1}{2} (\gamma_{kl}^{\mu} B_{\mu}^{+} \beta_k^{+} \beta_l + \text{h.c.}) \\
 &\quad - \frac{1}{2} \sum_{\substack{\mu\lambda \\ kl}} V_{\mu\lambda}^{22} \cdot (\Gamma_{\nu k}^{\lambda\mu} B_{\mu}^{+} B_{\lambda} + \Gamma_{\mu l}^{\lambda k} B_{\lambda}^{+} B_{\nu}) \beta_k^{+} \beta_l,
 \end{aligned} \tag{9.131}$$

with

$$\gamma_{kl}^{\mu} = 2 \sum_{rs} H_{rs kl}^{31} C_{rs}^{\mu}, \tag{9.132}$$

where C_{kl}^{μ} are the TDA amplitudes and Ω_{μ} the corresponding energies. In Eq. (9.131) we neglected $B^{+}B$ terms containing two Γ 's, since they are usually smaller than those with only one Γ . The first term of the particle-vibration coupling H_{coupl} is known as the Bohr coupling Hamiltonian [BM

* In the non-collective case we can, in analogy to Eq. (9.103), sum up the infinite series for $(b_{kl}^{+})_B$ and $(\alpha_k^{+})_B$:

$$\begin{aligned}
 (a_{kl})_B &= \sum_{\nu} B_{\nu}^{+} B_{kl} + \beta_l^{+} \beta_k, \\
 (b_{kl}^{+})_B &= (B^{+} \sqrt{1 - B^{+} B})_{kl} + \sum_{pq} \left[(\sqrt{1 - B^{+} B})_{pq} B_{kl}^{+} \right] \beta_p^{+} \beta_q, \\
 (\alpha_k^{+})_B &= \sum_l (\sqrt{1 - B^{+} B})_{kl} \beta_l^{+} + B_{kl}^{+} \beta_k.
 \end{aligned}$$

[†] Since we neglect $H^{(0)}$, terms like $B^{+}B^{+}$ and BB are missing. We could take them into account by transforming to RPA bosons with (see Appendix E.5)

$$B_{\mu} = \sum_{mi} C_{mi}^{\mu} (X_{mi}^{\mu} Q_{\mu} + Y_{mi}^{\mu} Q_{\mu}^{+}).$$

75], since it has also been derived within the liquid drop model (see Sec. 9.3.4). The second term in H_{coupl} comes from a systematic and microscopic treatment of the boson expansion and corrects for the Pauli principle, as we shall see. The matrix element H^{31} can be calculated in the canonical basis (see Chap. 7) from Eq. (E.25) for systems with time reversal invariance:

$$\begin{aligned} H_{rskl}^{31} = & \frac{1}{3} \cdot \frac{1}{4} \left(-\bar{v}_{rksi} (\eta_{rs}^+ \xi_{kl}^+ + \eta_{rs}^- \xi_{kl}^-) \right. \\ & + \bar{v}_{skri} (\eta_{rs}^+ \xi_{kl}^+ - \eta_{rs}^- \xi_{kl}^-) \\ & \left. + \bar{v}_{rskl} (\xi_{rs}^+ \eta_{kl}^+ - \xi_{rs}^- \eta_{kl}^-) \right), \end{aligned} \quad (9.133)$$

where the occupation factors ξ, η are defined in Eq. (8.202). In the following we investigate, in more detail, cases without pairing correlations. The quasi-particle operators β_k^\pm then have to be replaced by particle operators (see Chap. 2) c_m^\pm or hole operators c_i (we use the indices m, n for particles and i, j for holes). Instead of quasi-particle energies we find ϵ_m or $-\epsilon_i$ (where the energy scale $\epsilon_F = 0$ is used). We obtain two types of vertices, because in our quasi-particle formalism we can represent a *ph*-vibration (indices ν, ν', \dots) or a *pp* (*hh*) vibration (indices τ, τ', \dots). Neglecting pairing correlations, therefore, if we consider a particle coupled to a $1p - 1h$ state (note that the original C_{rs}^a are antisymmetric) we obtain for the first term of H_{coupl} :

$$\begin{aligned} H_{\text{coupl}} = & \frac{1}{3} \sum_\nu \sum_{mn} \sum_{m'n'} C_{m'n'}^{\nu*} \bar{v}_{m'mn} B_\nu^+ c_m^+ c_n + \text{h.c.} \\ = & \frac{1}{3} \frac{1}{2} \sum_\tau \sum_{jn} \sum_{m'n'} C_{m'n'}^{\tau*} \bar{v}_{m'n'jn} B_\tau^+ c_j c_n + \text{h.c.} \end{aligned} \quad (9.134)$$

The origin of the factor $\frac{1}{3}$ comes from the fact that our fermion-boson basis is three times as large as our original basis, having included two possibilities of coupling a particle to a *ph*-vibration and one possibility of coupling a hole to a *pp* vibration (see also below). Using our graphical rules (Chap. 8 and Appendix F), we can represent the two vertices $\gamma_{mn}^{\nu*}$ and $\gamma_{jn}^{\tau*}$ as shown in Fig. 9.7. In order to facilitate the discussion somewhat we want to disregard the possibility of *pp* vibrations for the moment, that is, the second term of (9.134) will drop out. Of course, we should rederive our boson expansion from the beginning under this assumption; we do not want to do this here, but rather state that we find that the factor $\frac{1}{3}$ in Eq.



Figure 9.7. Vertices for the coupling of a particle to a particle plus *ph* vibration and the coupling of a particle to a hole plus *pp* vibration.

(9.134) is changed to $\frac{1}{2}$, that is,*

$$H_{\text{coupl}} = \frac{1}{2} \sum_r (\gamma'_{mr} B_r^+ c_m^+ c_n + \text{h.c.}), \quad (9.135)$$

$$\gamma'_{kl} = \sum_{mi} C_{m'i}^{r*} \bar{v}_{m'kl}.$$

In order to treat collective vibrations of odd nuclei, we must formally diagonalize the Hamiltonian (9.131) in the multi-phonon-one-particle basis (9.128). Of course, in practice again, often only one phonon (for instance, the quadrupole or octupole phonon) will be taken into account. The more anharmonic the underlying vibrator is, the more multi-phonon components we need for the diagonalization of the Hamiltonian (9.131). This procedure has been pursued in a somewhat more phenomenological version by Alaga and collaborators (see, e.g., [Al 67, APS 75] and references therein). As we have seen in the case of even systems, the boson description works quite well even for rotational nuclei. The Hamiltonian (9.131) is therefore, in principle, capable of describing all the effects occurring if an odd particle is coupled to a rotor as, for instance, rotational alignment or the pattern of triaxial shapes. Few attempts in this direction have been made [AP 76, PVD 77]. Applications of this Hamiltonian [(9.131), (9.134)] have, however, been made mainly for rather harmonic vibrators, to which we shall now turn.

9.3.3 Particle Vibration Coupling (Perturbation Theory)

As we said previously, the Hamiltonian (9.131) is suitable for treating collective vibrations in odd nuclei. In the simplest case we consider the neighboring even-even nucleus to be a harmonic vibrator, and the first collective state is then a vibration particle state. Furthermore it sometimes happens that the vibration particle coupling (VPC) is so weak that H_{coupl} can be treated in perturbation theory (weak coupling situation). If we want to calculate, for example, the energy shift of the vibration particle state due to the coupling terms, we obtain to second order:

$$\Delta E = \Delta E_1 + \Delta E_2 = (p\mu | H_{\text{coupl}} | kN) (kN | H_{\text{coupl}} | p\mu) + \sum_{\substack{kN \\ \neq p\mu}} \frac{(p\mu | H_{\text{coupl}} | kN) (kN | H_{\text{coupl}} | p\mu)}{E_{p\mu} - E_{kN}}, \quad (9.136)$$

where $|p\mu\rangle = \beta_p^+ B_p^+ |0\rangle$ is the unperturbed configuration and the $|kN\rangle$ are defined in Eq. (9.128). In first order only the second term of H_{coupl} contributes, and we obtain from (9.33), (9.26), and (9.131):

$$(p\mu | H_{\text{coupl}} | p\mu) = -\frac{1}{2} \sum_r (V_{mr}^{22} \Gamma_{pr}^{*} + \text{c.c.})$$

$$= -\frac{1}{4} \sum_{klq} (H_{k\bar{p}q}^{22} C_{kl}^{r*} C_{pq}^{\mu} + \text{c.c.}), \quad (9.137)$$

with H^{22} defined by Eq. (8.200 and 8.201).

* The interaction that we use here is formally the bare one, as in all boson expansion theories we have used so far, since we started from the original fermion Hamiltonian. It can be shown, however (see Appendix F), that the bare interaction in the vertex (9.135) can be replaced by an effective $p\bar{h}$ hole force, which is not necessarily antisymmetric.

As we already mentioned, there are several other boson expansion techniques that can also be applied to odd systems (but which will not be presented here). A somewhat different but related method is *nuclear field theory* (NFT) (see also below), which has been introduced by Bohr and Mottelson [Mo 67, BM 75] and worked out in detail by Broglia et al. [BBB 77 and references therein] and has been applied to odd systems. In order to facilitate the comparison of our present treatment with NFT we introduce an additional rule: Whenever the two indices of a TDA amplitude like C_{pq}^* in Eq. (9.137) do not go to the same matrix element and are not summed over, we shall have to use the TDA equation (8.10)

$$\langle \text{---} \rangle = \langle \text{---} \rangle$$

in order to make this type of amplitudes change to ones in which both indices are on the same $\bar{\nu}$ and are summed over. Applying this rule to the first-order expression (9.137) and going over to the HF limit [see Eq. (8.202)], we obtain, if we restrict ourselves to $p\hbar$ vibrations only, with (9.135)

$$\Delta E_1 = - \sum_i \frac{|\gamma_{pi}^\mu|^2}{\Omega_\mu + \epsilon_p + \epsilon_i}. \quad (9.138)$$

In second order, only the first term of H_{coupl} contributes, and we obtain two terms coming from intermediate states $|k, N\rangle$ containing zero ($N=0$) and two ($N=2$) bosons. Again in the HF limit, we have*

$$\Delta E_2 = \sum_n \frac{|\gamma_{pn}^\mu|^2}{\Omega_\mu + \epsilon_p - \epsilon_n} + \sum_n \frac{|\gamma_{pq}^\mu|^2}{\epsilon_p - \epsilon_n - \Omega_\mu}. \quad (9.139)$$

According to our graphical rules (see Chap. 8 and Appendix F), the first and second term of ΔE_2 are represented by the graphs a and b, respectively, in Fig. 9.8 and ΔE_1 by graph c. The process shown in Fig. 9.8d clearly involves a matrix element of H^{40} (see Fig. 8.10), and we would have obtained it by taking into account H^{40} terms in Eq. (9.131) and transforming to RPA bosons, as previously mentioned. This quite lengthy procedure would have given a second first-order contribution corresponding to graph d. Neglecting the small RPA amplitudes, its analytic expression is given by

$$\sum_i \frac{|\gamma_{pi}^\mu|^2}{\Omega_\mu + \epsilon_p - \epsilon_i}. \quad (9.140)$$

The physical meaning of the different graphs is as follows.

* The strict application of perturbation theory (9.136) gives different weight factors for the various contributions than those we write down. [The first term in (9.139), for example, is multiplied by a factor $\frac{1}{2}$.] It is, however, quite a tricky point that in diagonalizing the second term of H_{coupl} in Eq. (9.131), that is, in summing its perturbation series to infinite order, additional terms like those given in (9.139) are generated (in addition to others, of course). Including them gives the factors (one) that we write down. Formally, then, this looks as if we had suppressed the factor $\frac{1}{2}$ in Eq. (9.135). It would go beyond the scope of this book to try to explain in detail how this comes about. This factor $\frac{1}{2}$ has, however, been a long-standing controversy in the literature [JDK 69, El 70] and we can make the following statements: Whenever a full diagonalization of the coupling term (9.131) is made, the factor $\frac{1}{2}$ must be kept; whenever we want to do only lowest-order perturbation theory this factor should be dropped. In any case, we should handle a perturbative treatment like, for instance, that of a collective boson Hamiltonian with great care, since the bosons, of course, contain an infinite number of interactions, making a consistent perturbative expansion in interactions and collective bosons quite a subtle question.

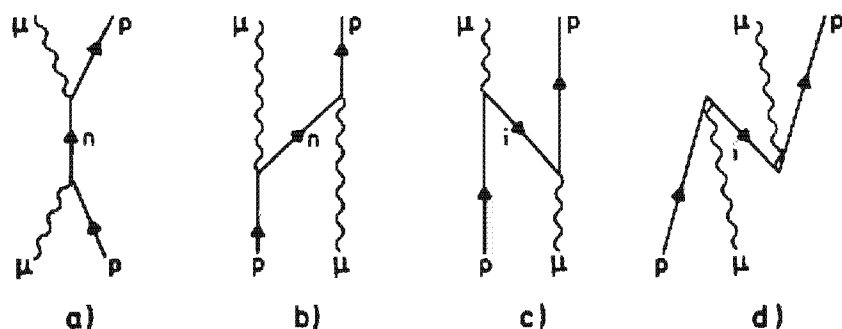


Figure 9.8. Four possible diagrams representing the second-order contribution to the particle— μh vibration coupling.

- (a) The vibration and particle combine into a particle which afterwards disintegrates once again into a particle and a vibration.
- (b) As the particle and vibration travel along, the particle excites a vibration and is itself scattered into another particle state which later on absorbs the incoming vibration.
- (c) The incoming vibration disintegrates into a particle-hole pair, the hole of which later combines with the incoming particle, forming an outgoing vibration. Since this represents nothing but an exchange of the hole from one particle partner to another, this process takes into account the Pauli principle. We also see that this term comes from a higher boson term in H_{coupl} , where we know from the discussions for the even system, they represent corrections to the Pauli principle.
- (d) This process is the same as the one in graph a, only the intermediate particle is changed to an intermediate hole. As we said, this process is due to correlations in the ground state.

The terms *a* and *b* have been taken into account by Kisslinger and Sorenson [KS 63], for example, but that the coupling to holes may also be quite important was pointed out for the first time by Hafele [Ha 67]. The relative importance of all these graphs for the particle 3^- phonon coupling in ^{209}Bi has been discussed by Mottelson [Mo 67].

9.3.4 The Nature of the Particle-Vibration Coupling Vertex

Before we go on, let us briefly discuss in some detail the vertex γ_{kl}^μ (9.135), which is the main ingredient in all four processes shown in Fig. 9.8. For this purpose we want to write the vertex in the r -representation viz:

$$\begin{aligned} \gamma_{kl}^\mu &= \int d^3r_1 d^3r_2 \varphi_k(r_1) \gamma^\mu(r_1, r_2) \varphi_l^*(r_2) \\ \gamma^\mu(r_2, r_4) &= \sum_m \int d^3r_1 d^3r_3 \bar{v}(r_1, r_2, r_3, r_4) \varphi_m^*(r_1) C_{ml}^\mu \varphi_l(r_3). \end{aligned} \quad (9.141)$$

For the purpose of this qualitative discussion we approximate the force for the direct term by a pure Wigner δ -interaction (see Chap. 4), neglect the exchange, and obtain

$$\gamma^\mu(r_1, r_2) = \delta(r_1 - r_2) \gamma^\mu(r_1), \quad \gamma^\mu(r) \propto \delta\rho^\mu(r). \quad (9.142)$$

where $\delta\rho''(\mathbf{r})$ is the transition density* discussed in Section 8.3.1. From the sum rule (see Sec. 8.7.5) and semiclassical [see Tassie model, Eq. (8.175)] considerations, we find the following form for the transition density expressed in terms of the spherical density ρ_0 :

$$\delta\rho^\lambda \propto \lambda^{\lambda-1} Y_{\lambda 0} \cdot \frac{d\rho_0}{dr}, \quad \lambda \neq 0. \quad (9.143)$$

We see, therefore, that the particle vibration coupling takes place predominantly in the surface region of the nucleus. It is interesting to study the very close relationship to the liquid drop model (see [BM 75] and Chap. 1): As usual, in this model the equipotential surfaces of the nuclear potential $V(r)$, for a fixed value of r , are supposed to be given for small deformations by Eq. (1.7) [Ha 74a]:

$$r_\Omega = r \cdot \left(1 + \sum_{\lambda\mu} \alpha_{\lambda\mu}^* Y_{\lambda\mu}(\Omega) \right). \quad (9.144)$$

This is equivalent to the equation

$$V(r_\Omega, \Omega) = V_0(r), \quad (9.145)$$

where $V_0(r)$ is the undeformed potential. For any r_Ω we can therefore express the actual potential simply by rescaling the coordinate:

$$V(r_\Omega, \Omega) = V_0 \left[\frac{r_\Omega}{1 + \sum_{\lambda\mu} \alpha_{\lambda\mu}^* Y_{\lambda\mu}(\Omega)} \right]. \quad (9.146)$$

For small deformations we can expand and obtain (we replace r_Ω by r):

$$V(r, \Omega) = V_0(r) - r \frac{dV_0(r)}{dr} \sum_{\lambda\mu} \alpha_{\lambda\mu}^* Y_{\lambda\mu}(\Omega) + O(\alpha^2). \quad (9.147)$$

The coupling term is therefore of the form:

$$H_{\text{coupl}} = -k(r) \sum_{\lambda\mu} \alpha_{\lambda\mu}^* Y_{\lambda\mu}(\Omega), \quad (9.148)$$

with

$$k(r) = r \frac{dV_0}{dr}. \quad (9.149)$$

After quantizing the surface modes, as in the liquid drop model (Chap. 1), we obtain an expression similar to H_{coupl} of Eq. (9.135). With the assumption that the potential roughly follows the density, we get for the form factor $k(r)$ the same expression for the quadrupole mode (up to a constant factor) within the Tassie (see Sec. 13.3.3) and the liquid drop model, but a different power for higher multipoles. This kind of phenomenological particle vibration coupling vertex has been used in numerous applications over the years for the coupling of a nucleon to either the 2^+ or 3^- surface vibration (see, for instance, the review articles by Arima and Hamamoto

* In this discussion we neglect the difference between RPA and TDA amplitudes.

[AH 71b] and Hamamoto [Ha 74a] and references cited therein, and the conference report on *Problems of Vibrational Nuclei*, by Alaga, Paar, and Sips [APS 75].

9.3.5 Effective Charges

In this section we apply the boson expansion method to systems with odd particle number to study the concept of the so-called "effective charge." For this purpose we start with the Hamiltonian [(9.131) and (9.135)], make a canonical transformation to RPA bosons (to lowest order in the coupling this is not difficult), and obtain the following expression.

$$\begin{aligned} H = E_{\text{RPA}} + \sum_k \epsilon_k c_k^+ c_k + \sum_\mu \Omega_\mu O_\mu^+ O_\mu \\ + \sum_{\mu k l} \gamma_{k l}^\mu O_\mu^+ c_k^+ c_l + \text{h.c.}, \end{aligned} \quad (9.150)$$

with

$$\gamma_{k l}^\mu = \sum_{m i} (X_{m i}^\mu \bar{v}_{m k l i} + Y_{m i}^\mu \bar{v}_{i k m l}). \quad (9.151)$$

(We have dropped the factor $\frac{1}{2}$, since we are going to apply lowest-order perturbation theory; see discussion in footnote on p. 386.) In first-order perturbation theory, the wave function of the odd system is given by:

$$|\tilde{k}\rangle = c_k^+ |0\rangle + \sum_\mu \frac{\gamma_{k l}^\mu}{\epsilon_k - \epsilon_l - \Omega_\mu} O_\mu^+ c_l^+ |0\rangle. \quad (9.152)$$

We are interested in the contribution of this "particle-phonon" correction to the matrix element of an electromagnetic multipole operator T . For this purpose, we first have to transform T into the boson representation (9.130). Using the formulas (E.11),

$$T = T^0 + \sum_{mn} T_{mn} c_m^+ c_n - \sum_{ij} T_{ij} c_i c_j^+ + \sum_{mi} (T_{mi} c_m^+ c_i + \text{h.c.}), \quad (9.153)$$

we find, to first order,^{*}

$$T_B = \sum_{mn} T_{mn} c_m^+ c_n - \sum_{ij} T_{ij} c_i c_j^+ + \sum_\mu (T^\mu O_\mu^+ + \text{h.c.}), \quad (9.154)$$

with

$$T^\mu = \sum_{mi} (T_{mi} X_{mi}^\mu + T_{im} Y_{mi}^\mu). \quad (9.155)$$

We now can calculate the effective matrix element, which is defined by

$$\begin{aligned} T_{kl}^{\text{eff}} &= (\tilde{k} | T_B | \tilde{l}) \\ &= T_{kl} + \sum_\mu \left(\frac{\gamma_{kl}^\mu T^\mu}{\epsilon_l - \epsilon_k - \Omega_\mu} + \frac{\gamma_{lk}^\mu T^\mu}{\epsilon_k - \epsilon_l - \Omega_\mu} \right). \end{aligned} \quad (9.156)$$

* In the following, we assume that the expectation value T^0 of the core vanishes.

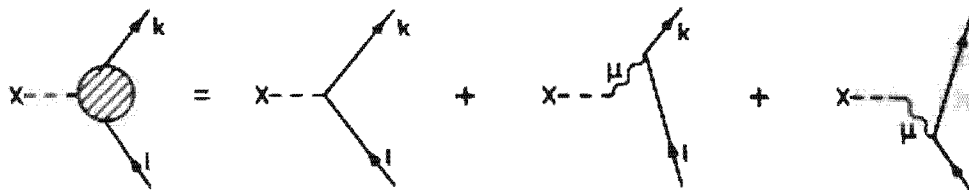


Figure 9.9. Graphical representation of the effective charge.

From this formula we see that the particle vibration coupling changes the bare matrix element T_{kl} to an effective matrix element T_{kl}^{eff} . This is caused by the fact that the external field can excite virtual vibrations of the core which interact with the external particle. If the vibration is very collective, this can give rise to substantial changes in the value of the matrix element. The effective matrix element is graphically represented in Fig. 9.9.

An example of the importance of this process is the effective charges of single-particle states near closed shells. In Section 2.7.2 we saw that it was necessary to introduce an effective charge for protons and neutrons ($e_p^{\text{eff}} \approx 2$; $e_n^{\text{eff}} \approx 1$) to reproduce the experimental electric moments and transition probabilities. The reason for this is, of course, the possibility of virtual phonon excitation as shown in Fig. 9.9. Our effective matrix element (9.156) can be written as

$$T_{kl}^{\text{eff}} = T_{kl} + \sum_{mn} e_{klmn}^{\text{pol}} T_{mn}, \quad (9.157)$$

where the polarization charge $e^{\text{pol}} = e^{\text{pol}}(\epsilon_k - \epsilon_i)$ is now an operator which depends on the energy difference $\epsilon_k - \epsilon_i$. Replacing this operator by a constant number corresponds to the concept of the effective charge:

$$e^{\text{eff}} = 1 + e^{\text{pol}}. \quad (9.158)$$

For instance, for the calculation of the effective charge of a quadrupole moment, we must sum up the contributions of all collective 2^+ states of the even core nucleus. In particular, this means that we must also include the giant quadrupole resonance (see Chap. 8). Calculations of this type have been carried out in the Pb region [RBS 73], for example, and the results show good agreement with experiment.

The calculation of the effective matrix elements requires the knowledge of RPA amplitudes X_{mi}^A , Y_{mi}^A and the corresponding energies Ω_μ . The RPA equation (8.131)  can be used to derive an equation for T^{eff} directly (see also [Mi 67]):

$$T_{kl}^{\text{eff}}(\omega) = T_{kl} + \sum_{pq} \bar{v}_{kqlp} \frac{n_q - n_p}{\omega - \epsilon_s + \epsilon_a} T_{pq}^{\text{eff}}(\omega). \quad (9.159)$$

9.3.6 Intermediate Coupling and Dyson's Boson Expansion

The perturbative treatment of the particle vibration coupling as described in the preceding sections is, of course, only valid in the extreme weak coupling limit where the off diagonal matrix elements of H_{coupl} are very

small compared to the diagonal ones. As a matter of fact, this situation is not completely fulfilled even in the prototype of weak coupling, namely the septuplet of ^{209}Bi (see discussion below). In order to resolve the problem, we could, of course, diagonalize the Hamiltonian [(9.130), (9.131)] in the basis of the unperturbed one ($H_{\text{coupl}} = 0$), but at the same time we should push the boson expansion (9.131) of the Hamiltonian further to be sure that horizontal (see Fig. 9.3) convergence has been achieved. This program has not, however, been carried out so far, and it is rather a different type of boson theory which has been applied mainly to odd nuclei; this is the nuclear field theory (NFT) (see, e.g., [Re 75b, BBB 77] and references cited therein). This theory is *nonlinear*, and it can be shown [IRS 79] that there is a simple mathematical relationship which reduces NFT to the *linear* theory of Dyson's boson expansion (DBE), which has itself also been applied to realistic cases [DJ 73, RS 74b, SWR 76, IRS 80]. Since linear theories are usually simpler to handle than nonlinear ones, we shall present only DBE here. We can also use the formalism which we derived for the even case to a large extent. It is not surprising, that the DBE is also finite in the odd case.

For collective bosons, the fermion pair operators are expressed in the following way (for the non-collective version, see [DJ 73]).

$$\begin{aligned} (b_p^+)_B &= B_p^+ - \frac{1}{2} \sum_{\nu\rho\sigma} \Gamma_{\mu\nu}^\rho B_\nu^+ B_\rho^+ B_\sigma - \sum_{kl\nu} \Gamma_{\mu\nu}^k B_\nu^+ \beta_k^+ \beta_l, \\ (b_\mu)_B &= B_\mu, \\ (a_{\mu\nu})_B &= \sum_{\rho\sigma} \Gamma_{\nu\sigma}^{\mu\rho} B_\rho^+ B_\sigma + \sum_{kl} \Gamma_{\nu l}^{\mu k} \beta_k^+ \beta_l. \end{aligned} \quad (9.160)$$

Inserting these expressions into the Hamiltonian (9.32) and diagonalizing it in the basis

$$|A+1, \nu\rangle = \sum_p C_p^{(\nu)} \beta_p^+ |0\rangle + \sum_{p\mu} C_{p\mu}^{(\nu)} \beta_p^+ \tilde{B}_\mu^+ |0\rangle \quad (9.161)$$

yields the following matrix equation.

$$\sum_{p'p} \begin{pmatrix} \delta_{pp'} E_p & \frac{1}{2} \gamma_{pp'}^{A''} \\ \frac{1}{2} \gamma_{pp'}^\mu & (\Omega_\mu + E_p) \delta_{pp'} \delta_{pp'} + B_{pp'p'\mu} \end{pmatrix} \begin{pmatrix} C_p^{(\nu)} \\ C_{p'p'}^{(\nu)} \end{pmatrix} = \omega^{(\nu)} \begin{pmatrix} C_p^{(\nu)} \\ C_{p'p'}^{(\nu)} \end{pmatrix}, \quad (9.162)$$

with $\gamma_{pp'}^{\mu''}$ defined in Eq. (9.132) and

$$B_{pp'p'\mu} = - \sum_l (\Omega_\mu - E_l - E_p) C_{p'l}^* C_{p'l}^{\mu''}. \quad (9.163)$$

In (9.162) we use the quasi-particle TDA equation [(8.10) and (9.70)]. The evaluation of the matrix elements (9.162) is straightforward, and only the treatment of H^{11} [see Eq. (9.32)] is somewhat lengthy. The summation over μ' , of course, includes ph and pp vibrations in the limit of no-pairing correlations. This can easily be worked out with (9.133), (8.201), and (8.202). As can be seen from (9.162), the matrix is, as in the case of even particle number, non-Hermitian. In order to study the significance of the

matrix B , we have to go over to the HF limit, where we can distinguish between ph and pp vibrations. We then see that B can couple $p-ph$ with $h-pp$ configurations as well as $p-ph$ with $p-ph$ states. According to Fig. 9.8c, the latter case takes care of the Pauli principle. The term $B_{h-pp, h-pp}$ is missing because, as is obvious, there is no problem with the Pauli principle.

The meaning of the coefficients $C_{pp}^{(\tau)}$ of course, indicates to what extent the collective vibration is built up by the uncorrelated motion of the odd quasi-particle and the collective vibration of the even nucleus (spectroscopic factor). The quasi-particle can be a particle or a hole. The coefficients $C_{pp}^{(\tau)}$, therefore, give the probability of, for example, how much the states of the septuplet in ^{209}Bi are built up from a particle coupled to the ph -vibrations of ^{208}Pb and how much they are built up from a hole coupled to pp vibrations of ^{210}Pb , ^{210}Po , and ^{210}Bi . It should be noted that Eq. (9.162) corresponds to a *nonorthogonal basis*, and therefore only statements about relative probabilities can be made.

The dimension of the matrix (9.162) is, of course, much larger than that for the original fermion space, but we can hope that it can be drastically truncated because of the collectivity of the bosons. Because of the over-completeness of our basis, spurious solutions are contained in (9.162), but, as in the even case [see Eq. (9.98)], they all lie at the free three-quasi-particle energies, and then are much higher than the interesting collective vibrations. Therefore, for cases where vertical convergence (see Fig. 9.3) has been achieved, these cause no trouble. In this case, all the eigenvalues are also real and the non-Hermiticity of the matrix causes no problem. For cases where we do not have very pronounced collective states and the spurious solutions are therefore intermingled with the physical ones, it is advantageous to transform (9.162) to a Hermitian problem in diagonalizing the norm matrix and eliminating its zero (i.e., practically smaller than a certain value ϵ) eigenvalues [IRS 80, BSL 79]. Taking the square root of the remaining diagonal matrix and inverting yields a Hermitian eigenvalue problem. This corresponds to an orthogonalization of the basis. The details of this procedure are explained in Section 10.2. The dimension of the Hermitian problem can, of course, never become larger than the original fermion space, and therefore no spurious solutions will enter the problem in this way. An orthonormalized basis is also preferable for the calculation of transition probabilities.

In studying these questions it is very instructive to treat an analytically solvable, though academic, model: In the case of no pairing correlations and three particles outside a closed shell core, the vertices γ in (9.162) vanish and we obtain the following simple matrix equation (p, m, n are particles and τ, τ' pp -vibrations):

$$\sum_{\tau' p'} B_{pp'\tau'} C_{p'\tau'}^{(\tau)} = (\omega^{(\tau)} - \Omega_\tau - \epsilon_p) C_{p\tau}^{(\tau)}, \quad (9.164)$$

with

$$B_{pp'\tau'} = \sum_n C_{p'n}^{\tau'} (\Omega_\tau - \epsilon_n - \epsilon_p) C_{np}^{\tau}, \quad (9.165)$$

where C_{mn}^{τ} and Ω_τ are solutions of a pp -TDA calculation. As our model, we take

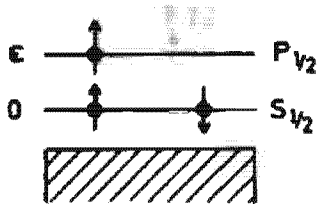


Figure 9.10. The three-particle configuration of the model.

the case of three valence nucleons in an $s_{1/2}$ and $p_{1/2}$ level (see Fig. 9.10). There exists only one state with negative parity and spin up:

$$|\alpha\rangle = a_+^+ \{ a_-^+ \} a_p^+ \{ |D\rangle .$$

The energy of this state can be readily calculated to be

$$\begin{aligned} \langle \alpha | H | \alpha \rangle - \langle D | H | D \rangle &= \epsilon + v_s \{ s_{-1/2} \} s_{1/2} \{ \} + v_p \{ p_{-1/2} \} p_{1/2} \{ \} + v_{sp} \{ s_{-1/2} p_{1/2} \} \\ &= \epsilon + G + F + H. \end{aligned}$$

We now have to calculate the two-particle states; we suppose that only the diagonal matrix elements are nonzero and obtain the following five relevant τ states:

$$\begin{aligned} C_s^{r1} \{ p \} &= 1, \quad \Omega_{r1} = \epsilon + F; \\ C_s^{r2} \{ p \} &= 1, \quad \Omega_{r2} = \epsilon + H; \\ C_s^{r3} \{ s_{-1/2} \} &= 1, \quad \Omega_{r3} = G; \\ C_s^{r4} \{ p_{-1/2} \} &= 1, \quad \Omega_{r4} = \epsilon + v_{sp} \{ s_{-1/2} p_{-1/2} \} := \epsilon + I; \\ C_p^{r5} \{ p_{-1/2} \} &= 1, \quad \Omega_{r5} = 2\epsilon + v_p \{ p_{-1/2} p_{-1/2} \} := 2\epsilon + J. \end{aligned}$$

The corresponding five $p\tau$ configurations are displayed in Fig. 9.11.

We can clearly see how neglecting the Pauli principle in the basis states enlarges the dimension of the space from one to five, that is, the space is now overcomplete. Let us now calculate the corresponding matrix (we abbreviate the different configurations $p\tau$ by I, II, ...):

$$B_{11} = \sum_n C_s^{r1} \{ n \} (\epsilon + F - \epsilon_n - 0) C_{n1}^{r1} \{ \} = 0,$$

$$B_{111} = \sum_n C_s^{r1} \{ n \} (\epsilon + H - \epsilon_n - 0) C_{n1}^{r2} \{ \} = -H,$$

$$B_{1111} = -G,$$

$$B_{11111} = B_{1111} = 0.$$

Continuing in this way for the entire matrix, we arrive at the following secular equation for the eigenvalues of Eq. (9.164).

$$\left| \begin{array}{ccccc} \epsilon + F - \omega^{(a)} & -H & -G & 0 & 0 \\ -F & \epsilon + H - \omega^{(a)} & G & 0 & 0 \\ -F & H & \epsilon + G - \omega^{(a)} & 0 & 0 \\ 0 & 0 & 0 & \epsilon - \omega^{(a)} & 0 \\ 0 & 0 & 0 & 0 & 2\epsilon - \omega^{(a)} \end{array} \right| = 0.$$

It is obvious that the corresponding matrix is non-Hermitian, and it can be readily checked that the eigenvalues are:

$$\omega^{(1)} = \omega^{(2)} = \omega^{(3)} = \epsilon; \quad \omega^{(4)} = 2\epsilon; \quad \omega^{(5)} = \epsilon + F + G + H.$$

We thus get back the physical eigenvalue and four unphysical ones which lie at the

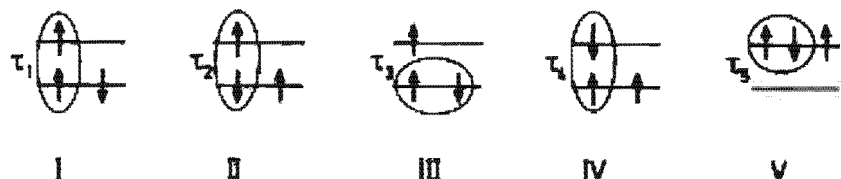
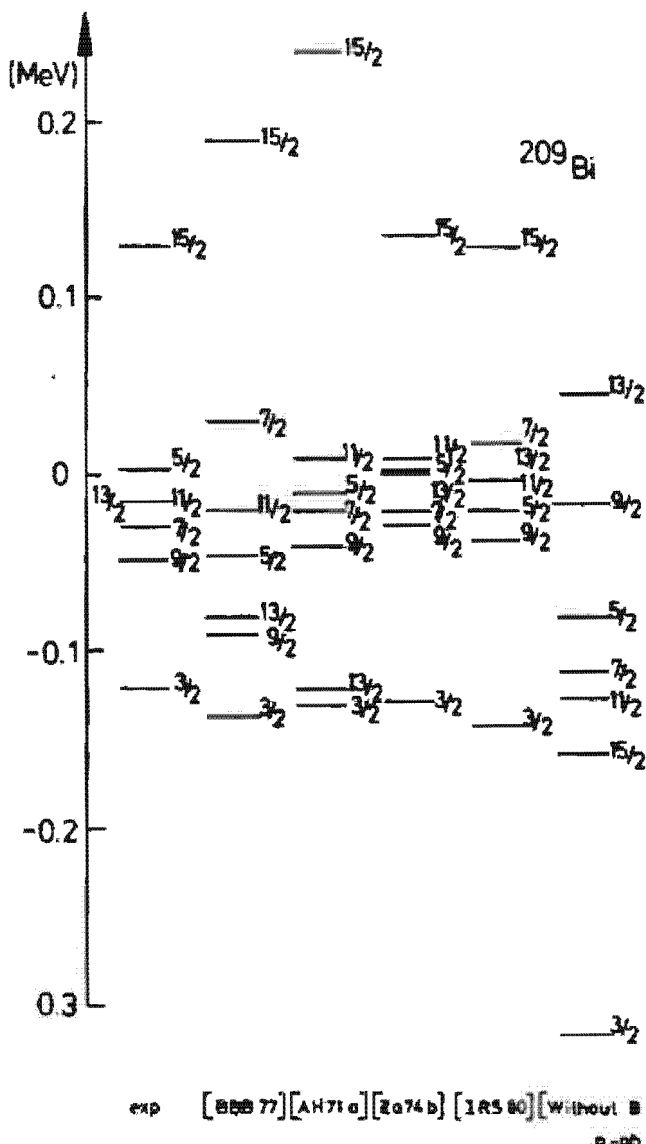


Figure 9.11. The five possible particle boson configurations.

unperturbed particle energies. This, of course, is the same as what we have already discussed in the case of the DBE for even systems. The unphysical states all lie at the unperturbed particle (hole) energies. Of course, our model has only had a pedagogic purpose in order to explain the principle involved. In realistic cases, where there may be quite collective states of the even system, the actual matrix to be diagonalized is much smaller than the one in the fermion space.



As an example, we show in Fig. 9.12 the septuplet of ^{209}Bi , which has been calculated solving Eq. (9.162) by enlarging the dimension successively until vertical convergence (see Fig. 9.3) is achieved. In Fig. 9.12 the spectra calculated with nuclear field theory are also given [BBB 77] together with calculations of other authors [AH 71a, Za 74b] using different approaches.

In Table 9.2 we give certain components $C_{\mu\mu}^{(\nu)}$ (spectroscopic factors) in order to see their relative importance and in Fig. 9.12 we show how relevant it is to treat the Pauli principle correctly. This can be checked by switching off the $p-ph$, $p-ph$ part of the matrix B of Eq. (9.162). The remaining discrepancies with the experimental spectrum can be due to several things. One obvious feature which has been omitted is the fact that the $2p - 1h$ components are the main components of the septuplet and we treated the weak coupling to the $1p$ space but neglected the coupling to the $3p - 2h$ configuration; by symmetry reasons the latter should then also be included, a task much harder to realize in practice.

Table 9.2. Wave functions of several particle vibrational coupling states in the septuplet of ^{209}Bi given by the spectroscopic factors $C_{\mu\mu}$. The largest component $\pi h_{9/2} \otimes ^{208}\text{Pb}(3^-)$ is normalized to unity. (From [IRS 80].)

p	μ	3/2	5/2	7/2	
Pure single particle		0.005	0.001	0.026	
$\pi h_{9/2} \otimes ^{208}\text{Pb}(3^-) \times$		1.0	1.0	1.0	—
$\pi h_{9/2} \otimes ^{208}\text{Pb}(6^-)$		-0.385	0.266	-0.233	
$\pi g_{9/2} \otimes ^{208}\text{Bi}(6_2^+)$		-0.406	0.356	-0.320	
$\pi i_{11/2} \otimes ^{208}\text{Bi}(6_1^+)$		0.100	-0.155	0.211	
$\pi i_{11/2} \otimes ^{208}\text{Bi}(7_1^+)$		-0.318	0.282	-0.232	
$(\pi d_{3/2})^{-1} \otimes ^{210}\text{Po}(0^+)$		0.326	—	—	
$(\pi d_{3/2})^{-1} \otimes ^{210}\text{Po}(2^+)$		0.233	0.231	0.095	
$(\pi d_{3/2})^{-1} \otimes ^{210}\text{Po}(4^+)$		—	0.200	0.282	
$(\pi p_{3/2})^{-1} \otimes ^{210}\text{Bi}(1^-)$		0.286	-0.128	—	
$(\pi p_{3/2})^{-1} \otimes ^{210}\text{Bi}(2^-)$		0.225	0.205	0.090	
$(\pi p_{3/2})^{-1} \otimes ^{210}\text{Bi}(3^-) \times$		0.151	0.234	0.191	
$(\pi p_{3/2})^{-1} \otimes ^{210}\text{Bi}(4^-)$		—	-0.181	-0.255	
$(\pi p_{3/2})^{-1} \otimes ^{210}\text{Bi}(5^-)$		—	—	-0.235	

9.3.7 Other Particle Vibration Coupling Calculations

As we said at the beginning, there are many applications of different weak coupling formalisms all of which we do not wish to present here. For instance, we have not treated any of the quasi-particle-phonon coupling theories [KS 63, DJ 73] for spherical open-shell nuclei, where pairing correlations have to be included. One of the most advanced theories in this respect which is, however, beyond the scope of this book is the one set up by Marumori and coworkers [KMM 72, 75(a+b)]. This theory is able to treat

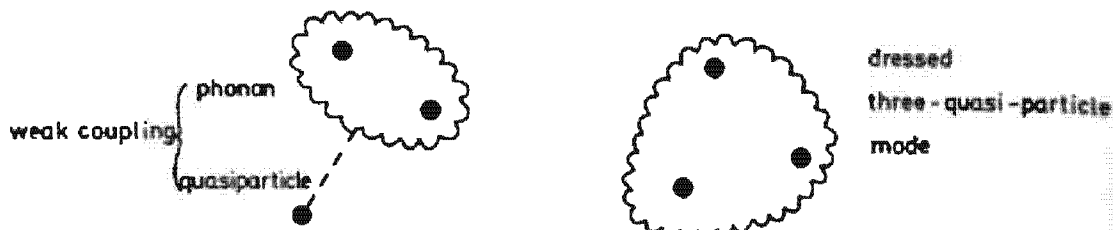


Figure 9.13. Schematic representation of a quasi-particle phonon and a dressed three-quasi-particle state.

not only the weak but also the strong coupling case where three quasi-particles are strongly interwoven (Fig. 9.13) (of course, this is also the case for the DBE) and takes into account ground state correlations as well as, for instance, a proper elimination of the spurious components due to particle number violation of the BCS theory. A nice application of this theory, in which can be seen a gradual transition from weak to strong coupling is the $h_{11/2}$ odd neutron coupled to the 2^+ phonon state for different Xe and Te isotopes, shown in Fig. 9.14. In Xe we see a gradual increase of the splitting in going from ^{133}Xe to ^{127}Xe —that is, towards the middle of the $h_{11/2}$ shell for ^{127}Xe the splitting has become so strong that the lowest member—that is, the $9/2$ (correlated three quasi-particles) state is lower than the single-particle state $11/2$ of the odd neutron. Such states are usually called *abnormal coupling states*, and are due to two effects:

- (i) a geometrical reason, which is that in a j -particle 2^+ -phonon coupling the $(j-1)$ state is always the lowest member of the multiplet (see [KMM 75a]); and
- (ii) the increase of the ground state (BCS) correlations as the middle of the shell is approached. It can be shown that graph c in Fig. 9.8 then becomes very important.

The coupling is less pronounced in the Te isotopes, and no abnormal coupling occurs. The experimental trends are nicely reproduced by the theory.

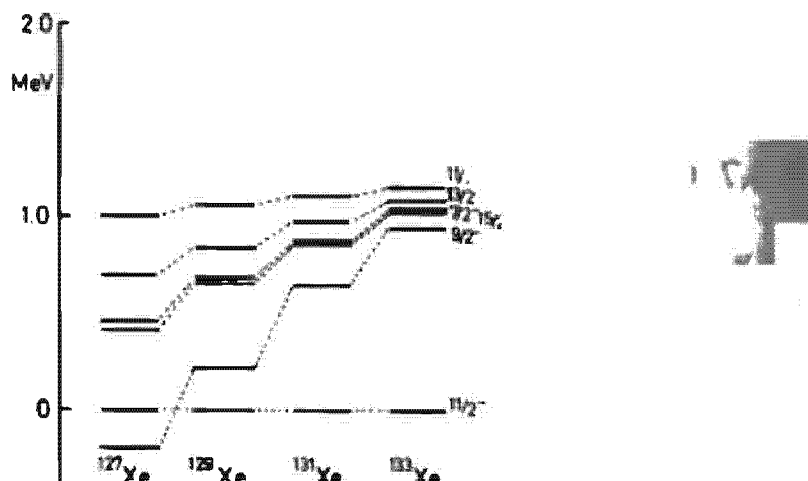


Figure 9.14. Energy systematics of particle vibrational coupling states for a series of Xe-isotopes. (From [KMM 75a].)

9.3.8 Weak Coupling in Even Systems

There are many other different kinds of weak coupling situations. A weak coupling need not necessarily occur only in odd mass nuclei—there are also weak coupling situations in even nuclei. For example, the two 3^- -phonon quadruplet in ^{208}Pb ($3^- \otimes 3^- \Rightarrow 0^+, 2^+, 4^+, 6^+$; only the 0^+ and 2^+ have been experimentally identified so far) is likely to be of the weak coupling type [BBN 74a, Sch 76]. On the other hand, it is preferable to treat such a problem with a formalism able to describe weak, intermediate, and strong coupling situations at the same time and we have seen above that the Dyson boson expansion (DBE) is such a formalism for the case of magic or close to magic nuclei. Treating the coupling of one- and two-phonon states, we can write for the wave function:

$$|\tilde{\nu}\rangle = \sum_{\mu} C_{\mu}^{(r)} \tilde{B}_{\mu}^+ |0\rangle + \sum_{\mu_1 \mu_2} C_{\mu_1 \mu_2}^{(r)} \tilde{B}_{\mu_1}^+ \tilde{B}_{\mu_2}^+ |0\rangle, \quad (9.166)$$

where the μ sums, of course, again include ph and pp vibrations. The corresponding DBE-matrix has the form

$$\begin{bmatrix} \Omega_{\mu} \delta_{\mu\mu'} & -\frac{1}{2} \sum_{kl} \gamma_{kl}^{\mu_1} \Gamma_{\mu'l}^{\mu_2 k} - (\mu'_1 \leftrightarrow \mu'_2) \\ -\frac{1}{2} \sum_{kl} \gamma_{kl}^{\mu_1} \Gamma_{\mu'l}^{\mu_2 k} - (\mu_1 \leftrightarrow \mu_2) & (\Omega_{\mu_1} + \Omega_{\mu_2}) \delta_{\mu_1 \mu_1'} \delta_{\mu_2 \mu_2'} + W_{\mu_1 \mu_2 \mu_1' \mu_2'} \end{bmatrix}, \quad (9.167)$$

with γ_{kl}^{μ} given in Eq. (9.132), $\Gamma_{\mu'l}^{\mu_2 k}$ in Eq. (9.29), and $W_{\mu_1 \mu_2 \mu_1' \mu_2'}$ in Eq. (9.72). This equation has been numerically solved for the $3^- \otimes 3^-$ quadruplet in ^{208}Pb [Sch 76]. Convergence in the vertical direction (see Fig. 9.3) has been achieved for about 10–20 configurations, and the splitting of the quadruplet found to be of the order of 100 keV, indicating quite a weak coupling situation.

In the case of superfluid nuclei, a more elaborate theory has to be set up due to particle number violation. This has been done by the Marumori group [IMS 76]. In this way, it has been possible to explain, for example, the anomalously low position of the second 0^+ state in some Ge isotopes which turns out to be due to a very anharmonic interplay between the pairing vibration and the 0^+ member of a $(2^+ \otimes 2^+)$ quadruplet. The fact that these Ge isotopes are very “soft” with respect to pair vibration can be understood from the very low-level density ($j=1/2$ states) below the fermi surface and the very high-level density just above the fermi level ($j=9/2$) in these nuclei. As discussed in Chapters 6 and 7, pairing correlations are favored by a high-level density, and the nucleons therefore have a strong tendency to exploit the phase space offered to them just above the fermi level. This makes the nucleus very anharmonic in the pairing mode. These considerations conclude our studies about anharmonic effects in nuclei, in which we have seen that the boson descriptions are adequate to describe even and odd nuclei. Further numerical applications have, however, to be carried out to justify the method in all its aspects from a practical point of view.

CHAPTER 10

The Generator Coordinate Method

10.1 Introduction

The microscopic description of collective motion has up to now been based on a generalized product state chosen so as to include as many correlations as possible. Using this picture as a basis, further correlations were then taken into account by including boson-like excitations. In principle, it is possible to obtain the exact eigenstates in the boson picture, but in practice we are restricted to a limited number of bosons. As a result, we are able to describe harmonic vibrations in nuclei that are stiff against deformations and anharmonic effects in the transition region. However, for nuclei that are so soft that they are just about to collapse (i.e., in the vicinity of a phase transition), boson expansion techniques up to a definite order may no longer be sufficient. We have to do at least a partial summation up to infinite order. It is clear, for example, that the nuclear fission process, where really *large amplitude collective motions* (LACM) are involved, is also a candidate for a theory that has to go beyond that considered so far. To handle these situations, essentially two theories have been proposed: the *generator coordinate method* (GCM) and the *time dependent Hartree–Fock theory* (TDHF). In this chapter, we will consider the GCM. It is a fully quantum mechanical method and consists of a construction of a linear superposition of many different product wave functions and is, in a sense, a generalization of the LCAO (linear combination of atomic orbital) method in molecular physics for the case of continuously labeled basis functions [MEL 76]. The method can be used for a variety of problems,

such as the proper treatment of symmetries in many-body wave functions (see Chap. 11), the cluster representation of nuclei [WM 66, BW 68], and the scattering of composite particles on nuclei [Fl 72, TRG 73, FHW 74, BBB 75]. Although in the back of our minds we shall restrict the application of the GCM to LACM, many of the problems we will discuss are equally valid for any other bound state problem. We will, however, omit all questions specifically concerning the treatment of unbound states (for a review, see [Wo 75]).

In Section 10.2 we will introduce the general concept and apply it in Section 10.3 to the Lipkin model. The close relationship between GCM and boson expansions is treated in Section 10.4. A very instructive example is the harmonic oscillator (Sec. 10.5). Complex generator coordinates are handled in Section 10.6. One of the reasons to apply the GCM to the theory of collective motion is the fact that we can derive in a fully quantum mechanical way a collective Hamiltonian which provides a microscopic connection to the collective model described in Chapter 1 (Sec. 10.7). In Section 10.8, a method is presented which allows determination of the optimal generating functions. Some applications of the GCM are discussed in Section 10.9.

10.2 The General Concept

10.2.1 The GCM Ansatz for the Wave Function

The generator coordinate method consists of a very general ansatz for a trial function. It is a continuous superposition of the so-called generating functions $|\Phi(a)\rangle$, which are labeled by an unlimited number of real or complex parameters $\{a\} = a_1, a_2, \dots, a_i$, the so-called generator coordinates; they depend, as does the wave function in the many-body Hilbert space, on the particle coordinates

$$|\Psi\rangle = \int da f(a) |\Phi(a)\rangle. \quad (10.1)$$

The integral is a multidimensional one going over all real and imaginary parts of the parameters a . The name “generator coordinate” is somewhat misleading, because the a s are not coordinates in the strict sense. The GCM does not introduce redundant coordinates. They are only a kind of continuous summation index in the expansion (10.1). The function $f(a)$ is a weight and is therefore called a *weight function*, although as we shall see, in the mathematical sense it is no wave function.

The set of generating functions $|\Phi(a)\rangle$ —as well as the limits of integration in Eq. (10.1)—can be chosen to be anything we like. Depending on the nature of the functions $|\Phi(a)\rangle$ and the number of parameters a_i , the ansatz (10.1) may eventually contain the exact solution of the Schrödinger equation. In many cases we use product wave functions $|\Phi(a)\rangle$. An example is

Nilsson wave functions in a potential of deformation β (see Chap. 2). In this case, β would be the generator coordinate.

Another example is the most general product HFB-type wave functions* $|\Phi(z^*)\rangle$, not orthogonal to some basic function $|\Phi_0\rangle$. They are given by the theorem of Thouless (Sec. E.3)

$$|\Phi(z^*)\rangle = N_0 \exp \left\{ \sum_{k < k'} z_{kk'}^* \alpha_k^+ \alpha_{k'}^+ \right\} |\Phi_0\rangle, \quad \langle \Phi | \Phi \rangle = 1 \quad (10.2)$$

where $z_{kk'} (k < k')$ are the complex numbers

$$z_{kk'} = x_{kk'} + iy_{kk'}, \quad \int dz = \int_{-\infty}^{+\infty} \prod_{k < k'} dx_{kk'} dy_{kk'}. \quad (10.3)$$

In Section 10.4 we will see that the exact eigenfunctions of the many-body Hamiltonian H can be described with generating functions of the type (10.2). However, the number of generator coordinates $z_{kk'}$ is extremely large in this case. For practical applications, we must reduce their number as much as possible, and it requires physical intuition to choose a set of generating functions $|\Phi(a)\rangle$ which is general enough to describe the physical situation and still simple enough to be treated by the following methods. In general, therefore, with a fixed set of generating functions we are only able to describe a certain class of eigenstates of the Hamiltonian H by an ansatz of the form (10.1).

10.2.2 The Determination of the Weight Function $f(a)$

The weight function $f(a)$ of the ansatz (10.1) is assumed to be a well behaved function of the variables a (in general square integrable), such that we can perform the following mathematical operations.[†] For a determination of the function $f(a)$ we use the variational principle:

$$\delta \frac{\langle \Psi | H | \Psi \rangle}{\langle \Psi | \Psi \rangle} = 0. \quad (10.4)$$

Variation with respect to $f(a)$ gives the integral equation

$$\int da' \langle \Phi(a) | H | \Phi(a') \rangle f(a') = E \int da' \langle \Phi(a) | \Phi(a') \rangle f(a'). \quad (10.5)$$

This equation has become known as the *Hill–Wheeler equation* [HW 53]. It may be formally written

$$\mathcal{K}f = E \mathcal{R}f \quad (10.6)$$

* For convenience, we use here z^* instead of z (see Eq. (10.79)).

[†] The reader who is interested in deeper mathematical foundations is referred to the references [La 74, La 76, TPG 77, TP 78], where the mathematical properties of the GCM techniques are treated with complete rigor.

with the overlap functions

$$\begin{aligned}\mathcal{K}(a, a') &= \langle \Phi(a) | H | \Phi(a') \rangle, \\ \mathcal{N}(a, a') &= \langle \Phi(a) | \Phi(a') \rangle\end{aligned}\quad (10.7)$$

as integral kernels.

Formally, it looks very similar to the diagonalization of the Hamiltonian in the nonorthogonal "basis" of the generator states $|\Phi(a)\rangle$ [Wo 70]. This is certainly true if the parameter a (we will restrict ourselves in the following to only one real parameter) has only a finite number of values a_1, \dots, a_M . In this case there is a finite number of functions $|\Phi_i\rangle = |\Phi(a_i)\rangle$ that are, in general, linearly dependent and not complete. In fact, the Hill-Wheeler equation (10.5) is often solved numerically by discretization. We then immediately get a matrix equation of the form (10.6). In the general case of a continuous parameter a , however, we have to be a little careful, as we shall see in the following.

The formal solution of Eq. (10.6) is easy. We could try to invert the operator \mathcal{N} and diagonalize $\mathcal{N}^{-1}\mathcal{K}$. This yields a non-Hermitian eigenvalue problem, and this is only possible if \mathcal{N} has no zero eigenvalues. However, this is very often the case, since the set of $|\Phi(a)\rangle$ is, in general, linearly dependent. Therefore, we solve the problem by an orthogonalization of the set $|\Phi(a)\rangle$. There are several methods by which to proceed. The best known is the procedure of Gram-Schmidt, which corresponds to a decomposition of the matrix \mathcal{N} into two triangular matrices (see Sec. 8.4.4). Another method which is also applicable to the continuous case is the so-called symmetric orthogonalization. It corresponds to a diagonalization of the Hermitian operator \mathcal{N} .

$$\int da' \mathcal{N}(a, a') u_k(a') = n_k u_k(a). \quad (10.8)$$

In the following, we assume that the spectrum n_k ($k = 1, 2, \dots$) is discrete.* Since \mathcal{N} is a norm, its eigenvalues are never negative ($n_k \geq 0$).

The functions $u_k(a)$ form a complete orthonormalized set in the space of the weight functions $f(a)$

$$\sum_k u_k(a) u_k^*(a') = \delta(a - a'); \quad \int da u_k^*(a) u_k(a) = \delta_{kk}. \quad (10.9)$$

The operator \mathcal{N} in this space can be decomposed ($\mathcal{N} = \mathcal{N}^{1/2} \cdot \mathcal{N}^{1/2}$) with

$$\mathcal{N}^{1/2}(a, a') = \sum_k u_k(a) \sqrt{n_k} u_k^*(a'). \quad (10.10)$$

*This is the case if \mathcal{N} is of the Hilbert-Schmidt type (i.e., Hermitian and with a finite trace of $\mathcal{N}^+ \mathcal{N}$ [RS 72]). In many practical cases the kernels \mathcal{N} and \mathcal{K} do not have this property (for instance, Eq. (10.49)). However, it has been shown that by a suitable change of the parametrization [TP 78] or by multiplication of the generating states with a suitable renormalization factor $r(a)$ [La 76], we can always achieve this property. The theory may also be developed more or less in the same way with weaker assumptions, in which there is a continuous spectrum [TP 78]; see also Sec. 10.5).

and we can formally deduce the Hermitian eigenvalue problem

$$\mathfrak{K}^{1/2} \mathfrak{H} \mathfrak{K}^{1/2} g = Eg \quad (10.11)$$

with

$$f = \mathfrak{K}^{-1/2} g. \quad (10.12)$$

The inversion of $\mathfrak{K}^{1/2}$ is impossible if \mathfrak{K} has zero eigenvalues ($n_k = 0$). Weight functions $f^0(a)$ which lie in the corresponding eigenspace produce many-body wave functions $|\Psi\rangle$ which vanish identically:

$$\langle \Psi | \Psi \rangle = \int da da' f^0(a) \mathfrak{K}(a, a') f^0(a') = 0. \quad (10.13)$$

If there exists a zero eigenvalue, the weight functions f corresponding to an HW state $|\Psi\rangle$ are not determined uniquely. We can always add a function f^0 and obtain the same $|\Psi\rangle$. To find a unique correspondence between $|\Psi\rangle$ and the weight function f , we should therefore at least restrict $f(a)$ to weight functions that are linear combinations of functions $u_k(a)$ with $n_k \neq 0$. For each of these functions, there exists a normalized vector in the Hilbert space

$$|k\rangle = \frac{1}{\sqrt{n_k}} \int u_k(a) |\Phi(a)\rangle da. \quad (10.14)$$

These vectors are called *natural states*. It is easy to show that they are orthogonal. They span a sub Hilbert space \mathfrak{H}_C , the so-called "collective" subspace. It is the smallest Hilbert space, which contains all the generating states $|\Phi(a)\rangle$. The projection onto this space is given by

$$P_C = \sum_{k, n_k \neq 0} |k\rangle \langle k|. \quad (10.15)$$

Instead of Eq. (10.11), we now diagonalize the Hamiltonian $P_C H P_C$ in the collective subspace

$$\sum_{k'} \langle k | H | k' \rangle g_{k'} = E g_k \quad (10.16)$$

with

$$(P_C H P_C)_{kk'} = \langle k | H | k' \rangle = \int da da' \frac{u_k^*(a)}{\sqrt{n_k}} \mathfrak{K}(a, a') \frac{u_{k'}(a')}{\sqrt{n_{k'}}}. \quad (10.17)$$

The eigenstates are given by

$$|\Psi\rangle = \sum_{k, n_k \neq 0} g_k |k\rangle. \quad (10.18)$$

From (10.14), we find the corresponding weight function

$$f(a) = \sum_{k, n_k \neq 0} \frac{g_k}{\sqrt{n_k}} u_k(a). \quad (10.19)$$

If there is only a finite number of eigenvalues $n_k \neq 0$ (or, more precisely, if zero is not a limit point of the n_k 's), the function $f(a)$ is always well defined by (10.19). In the continuous case, however, there are often infinitely many non-vanishing eigenvalues n_k with zero as a limit point. It therefore happens that the functions $f(a)$ diverge, even if $|\Psi\rangle$ (10.18) has a finite norm ($\sum |g_k|^2 < \infty$), as we see from Eq. (10.19). This means that there are vectors in the Hilbert space \mathfrak{H}_C that cannot be

represented as Hill-Wheeler states of the form (10.1) with well-behaved functions $f(a)$. The corresponding functions f have the character of distributions [see Eq. (10.58)]. It is obvious that we can never find such solutions of the Hill-Wheeler equation (10.5) by a discretization of the integration.*

Roughly speaking, the GCM ansatz (10.1) represents an expansion of the many-body wave functions $|\Psi\rangle$ in terms of the nonorthogonal generating functions $|\Phi(a)\rangle$: The expansion coefficients are given by the weight function $f(a)$: For a better understanding of the physical meaning of this function, it is useful to introduce the so-called *biorthogonal basis* [Wo 70]. It is given by the states $|\tilde{\Phi}(a)\rangle$, with the property

$$\langle \tilde{\Phi}(a)|\Phi(a')\rangle = \delta(a - a'). \quad (10.20)$$

If the norm has zero eigenvalues, we can obviously only require

$$\langle \tilde{\Phi}(a)|\Phi(a')\rangle = P_{\perp}(a, a') = \sum_{k, n_k \neq 0} u_k(a) u_k^*(a'), \quad (10.21)$$

where P_{\perp} is the projection onto the space orthogonal to the eigenvectors $u_k(a)$ of Eq. (10.8) with eigenvalues $n_k = 0$. We can construct vectors $|\tilde{\Phi}\rangle$ with this property by expanding them in natural states

$$|\tilde{\Phi}(a)\rangle = \sum_{k, n_k \neq 0} \frac{u_k^*(a)}{\sqrt{n_k}} |k\rangle. \quad (10.22)$$

The biorthogonal states $|\tilde{\Phi}(a)\rangle$ defined in this way, however, do not generally belong to the many-body Hilbert space, because their norm is not necessarily finite. Nevertheless, we can now express the weight function $f(a)$ belonging to the Hill-Wheeler state $|\Psi\rangle$ (10.1) in terms of

$$f(a) = \langle \tilde{\Phi}(a)|\Psi\rangle. \quad (10.23)$$

Therefore, $f(a)$ measures the overlap between the function $|\Psi\rangle$ and the state $|\tilde{\Phi}(a)\rangle$ in the biorthogonal basis. It is not the probability amplitude for finding the generating state $|\Phi(a)\rangle$ in the wave function $|\Psi\rangle$. The latter is given by $\langle \Phi(a)|\Psi\rangle$. The formula (10.23) again makes clear that $f(a)$ is not necessarily a well-behaved function.

So far, we treated only questions connected with the structure of the GCM representation (10.1). These properties were completely determined by the set of generating functions $|\Phi(a)\rangle$ used in this ansatz. In analogy to Chapter 9, we call them *kinematic properties*, because they have only to do with the underlying basis. We did not ask the question of whether the set $|\Phi(a)\rangle$ is useful for a description of the eigenstates of the Hamiltonian, that is, if $|\Psi\rangle$ can be represented at least in a good approximation as a linear superposition of these functions. This means that we did not investigate the *dynamic aspects* of the GCM ansatz.

We only can expect to obtain from Eq. (10.16) wave functions $|\Psi\rangle$ which are close to exact wave functions of the system, if the Hamiltonian

* The mathematical reason for these problems is the fact that the linear space formed by the Hill-Wheeler states (10.1) with mathematically well-behaved weight functions $f(a)$ is, in general, no Hilbert space, because it is not closed in the sense that for each converging set of vectors $|\Psi_i\rangle$ there exists a converging set of well-behaved weight functions $f_i(a)$.

commutes with P_C to a good approximation

$$[H, P_C] \approx 0. \quad (10.24)$$

In such a case, the collective space contains eigenstates of H . To what degree this condition is fulfilled depends on the choice of the set $|\Phi(a)\rangle$.

10.2.3 Methods of Numerical Solution of the HW Equation

Based on the above consideration, we shall discuss very briefly several numerical methods for solving the Hill-Wheeler equations (10.5).

(i) The most obvious method is a *discretization of the integrals* in the variable a . As we have seen, in this case we end up with a matrix equation. We diagonalize the norm matrix and obtain an orthogonal set of eigenvectors. In a second step, we restrict ourselves to vectors with nonzero eigenvalues and, for numerical reasons, eigenvalues larger than a small positive constant ϵ , and then diagonalize the matrix (10.17). This gives energies E and wave functions of the form (10.18). In principle, we can also determine weight functions by Eq. (10.19). They are well defined for each choice of the discretization. It may happen, however, that they are ill behaved for the continuous problem. Choosing more and more mesh points for the discretization, we find in such cases convergence for the energy E and for the wave function $|\Psi\rangle$ (10.18), but no convergence for the weight function $f(a)$.

Small eigenvalues of the norm matrix are connected with approximate linear dependence of the generating functions. It is therefore not meaningful to increase the number of mesh points too much. Usually we limit the number of mesh points in such a way that there is no eigenvalue of the corresponding norm matrix smaller than a positive constant ϵ .

(ii) In some physical problems we use generating functions that allow an analytic solution of the eigenvalue problem (10.8), such that an *expansion in natural states* of the type (10.18) can be carried out. The approximation now consists of cutting this expansion after a finite number of natural states. Again we obtain a finite diagonalization problem (10.17), where the matrix elements can be calculated analytically.

In the special case where the norm $\mathcal{N}(a, a')$ only depends on the difference $(a - a')$, we can determine the eigenfunctions $u_k(a)$ immediately. They are given by plane waves

$$u_k(a) \propto e^{-ika} \quad (10.25)$$

and the corresponding eigenvalues are

$$n_k = \int da \mathcal{N}(a, 0) e^{ika}. \quad (10.26)$$

In this case the expansion in natural states corresponds to a Fourier transformation and the limitation to eigenvalues larger than ϵ excludes the components of the wave function with high k -values.

If the norm cannot be diagonalized analytically, it is often possible to approximate $\mathcal{R}(a, a')$ by a function $\mathcal{R}_0(a, a')$ which has this property. In such a case, we can carry out an expansion in natural states with respect to \mathcal{R}_0 and treat the difference $\mathcal{R} - \mathcal{R}_0$ by perturbation theory [LL 77].

(iii) A third type of approximation uses special properties of the overlap kernels $\mathcal{K}(a, a')$ and $\mathcal{R}(a, a')$. They are often sharply peaked at $a = a'$. Using this fact, we can transform the HW equation (10.5) into a *differential equation* of second order. We will discuss these methods in more detail in Section 10.7.

10.3 The Lipkin Model as an Example

In order to fix our ideas on a specific example we apply the foregoing considerations to the well-known Lipkin model (see Sec. 5.4).

In this model, from Eq. (5.48) we have for Eq. (10.2)

$$|a\rangle = N_0 e^{a K_+} |\Phi_0\rangle \quad \langle a | a \rangle = 1 \quad (10.27)$$

and, with Eq. (E.51), obtain for the norm and Hamiltonian overlap

$$\mathcal{R}(a, b) = (1 + a^* b)^{\Omega} (1 + |a|^2)^{-\Omega/2} (1 + |b|^2)^{-\Omega/2} \quad (10.28)$$

and

$$\mathcal{K}(a, b) = -\frac{\epsilon \Omega}{2} \left\{ \frac{1 - a^* b}{1 + a^* b} + \chi \cdot \frac{a^{*2} + b^2}{(1 + a^* b)^2} \right\} \mathcal{R}(a, b). \quad (10.29)$$

Decomposing the integral equation

$$\int d(\text{Re } a') d(\text{Im } a') (\mathcal{K}(a, a') - E \mathcal{R}(a, a')) f(a') = 0 \quad (10.30)$$

into its real and imaginary part we obtain two coupled two-dimensional integral equations for the real and imaginary part of $f(a')$. As we shall see, this equation contains the exact answer. It even contains the exact answer if we restrict ourselves to only real parameters $a = i g(\varphi/2)$. This yields

$$\int_{-\pi}^{\pi} d\varphi' [\mathcal{K}(\varphi, \varphi') - E \mathcal{R}(\varphi, \varphi')] f(\varphi') = 0, \quad (10.31)$$

where we use the same letter $\mathcal{K}, \mathcal{R}, f$ for the transformed functions:

$$\begin{aligned} \mathcal{R}(\varphi, \varphi') &= \left(\cos \left(\frac{\Psi - \Psi'}{2} \right) \right)^{\Omega}, \\ \mathcal{K}(\varphi, \varphi') &= -\frac{\epsilon \Omega}{2} \left\{ \frac{\cos \Psi}{\cos(\varphi/2)} + \frac{1}{2} \chi \left[\frac{1 + \sin^2 \Psi}{\cos^2(\varphi/2)} - 1 \right] \right\} \mathcal{R}(\varphi, \varphi'), \end{aligned} \quad (10.32)$$

with

$$\Psi = \frac{1}{2}(\varphi + \varphi'); \quad \phi = \varphi - \varphi'. \quad (10.33)$$

In order to achieve the diagonalization of the norm overlap analytically, we use the

identity $\cos(x) = \frac{1}{2}(e^{ix} + e^{-ix})$ and apply the binomial expansion:

$$\begin{aligned}\mathcal{O}(\varphi, \varphi') &= \frac{1}{2^\Omega} \sum_{k=0}^{\Omega} \binom{\Omega}{k} e^{-ik\frac{1}{2}(\varphi-\varphi')} e^{i(\Omega-k)\frac{1}{2}(\varphi-\varphi')} \\ &= \sum_{k=-\Omega/2}^{\Omega/2} e^{-ik\varphi} \frac{1}{2^\Omega} \binom{\Omega}{k + \frac{\Omega}{2}} e^{ik\varphi'}. \end{aligned}\quad (10.34)$$

From the above form of the norm overlap, it becomes clear that it has the eigenfunctions $(1/\sqrt{2\pi})e^{-ik\varphi}$ with a finite number of non-vanishing eigenvalues

$$n_k = \frac{2\pi}{2^\Omega} \binom{\Omega}{k + \frac{\Omega}{2}}, \quad (10.35)$$

and that the Eq. (10.16) is a finite matrix equation

$$\sum_{k'} \tilde{H}_{kk'} g_{k'} = Eg_k, \quad (10.36)$$

with

$$\tilde{H}_{kk'} = \frac{1}{2\pi} \int_{-\pi}^{\pi} d\varphi d\varphi' \frac{e^{ik\varphi}}{\sqrt{n_k}} \mathcal{O}(\varphi, \varphi') \frac{e^{-ik'\varphi'}}{\sqrt{n_{k'}}}, \quad (10.37)$$

$$g_k = \sqrt{\frac{n_k}{2\pi}} \int_{-\pi}^{\pi} d\varphi e^{ik\varphi} f(\varphi). \quad (10.38)$$

The finiteness of the dimension in Eq. (10.36) clearly reflects the fact that in the Lipkin model containing Ω particles we cannot excite more than $\Omega + 1$ different $p\hbar$ states going from $0p - 0h$ up to the $\Omega p - \Omega h$ state. Since we started from a variational ansatz to arrive at Eq. (10.36), it is clear that the Hermitian eigenvalue problem (10.36) contains the exact answer for the Lipkin model.

It is very easy to evaluate the matrix elements (10.37); thus we have a straightforward method for solving the Lipkin model exactly. This shows us that, at least in this model, the GCM method is very powerful. We have to emphasize, however, that the structure of this model is extremely simple: There exists a collective subspace which coincides with the space spanned by the Hill-Wheeler representation (10.1). It is *finite* and, because of the quasi-spin symmetry, it *decouples exactly* from the rest of the Hilbert space. This is the optimal situation for the application of this method: In realistic cases we do not know a priori if similar conditions are fulfilled. Already in the case of the harmonic oscillator, which can still be treated analytically, but which has an infinite spectrum, we will run into some difficulties (see Sec. 10.5).

10.4 The Generator Coordinate Method and Boson Expansions

In the introduction we mentioned that the GCM is a method which is, in principle, capable of going beyond the boson expansion techniques. Nevertheless, in the limit of weak anharmonicities it should contain the Bose expansion theories. We will show in this section that this is actually the case [JDF 71, PUF 71].

We start from Eq. (10.2), that is, we use the most general product wave functions not orthogonal to $|\Phi_0\rangle$ as a set of generating functions. The formula of Onishi (E.51) and the quasi particle representation (E.18) gives us the overlap integrals for norm and Hamiltonian.*

$$\mathcal{U}(z, z'^*) = \langle \Phi(z^*) | \Phi(z'^*) \rangle = \exp\left\{\frac{1}{2} \text{Tr} \ln(1 - zz'^*)\right\}, \quad (10.39)$$

$$\mathcal{H}(z, z'^*) = \langle \Phi(z^*) | \Phi(z'^*) \rangle = h(z, z'^*) \cdot \mathcal{U}(z, z'^*),$$

where

$$\begin{aligned} h(z, z'^*) &= \sum_k E_k \rho_{kk} + 3 \sum_{klpq} \left(H_{klpq}^{40} \bar{\kappa}_{kl} \bar{\kappa}_{pq} + H_{klpq}^{40*} \kappa_{kl} \kappa_{pq} \right) \\ &\quad + 3 \sum_{klpq} \left(H_{klpq}^{31} \bar{\kappa}_{kl} \rho_{qp} + H_{klpq}^{31*} \rho_{pq} \kappa_{kl} \right) \\ &\quad + \frac{1}{4} \sum_{klpq} \left(H_{klpq}^{22} \bar{\kappa}_{kl} \kappa_{pq} + 2 H_{klpq}^{22*} \rho_{pk} \rho_{ql} \right) \end{aligned} \quad (10.40)$$

and

$$\bar{\kappa}_{kl} \mathcal{U}(z, z'^*) = \left\{ z \frac{1}{1 - z'^* z} \right\}_{kl} \mathcal{U}(z, z'^*) = \langle \Phi(z^*) | \alpha_k^+ \alpha_l^+ | \Phi(z'^*) \rangle, \quad (10.41)$$

$$\kappa_{kl} \mathcal{U}(z, z'^*) = \left\{ \frac{1}{1 - z'^* z} z'^* \right\}_{kl} \mathcal{U}(z, z'^*) = \langle \Phi(z^*) | \alpha_l \alpha_k | \Phi(z'^*) \rangle, \quad (10.42)$$

$$\rho_{kl} \mathcal{U}(z, z'^*) = - \left\{ z'^* z \frac{1}{1 - z'^* z} \right\}_{kl} \mathcal{U}(z, z'^*) = \langle \Phi(z^*) | \alpha_l^+ \alpha_k | \Phi(z'^*) \rangle. \quad (10.43)$$

If we use z_{kl} and z_{kl}^* ($k < l$) as independent variables in the sense of Section 5.2 we obtain the relation ($k < l, k' < l'$)

$$\left[\frac{\partial}{\partial z_{kl}}, z_{k'l'} \right] = \delta_{ll'} \delta_{kk'}, \quad \left[\frac{\partial}{\partial z_{kl}}, z_{k'l'}^* \right] = 0.$$

Then the quantities ρ_{kl} , κ_{kl} , $\bar{\kappa}_{kl}$, and therefore h , can be expressed as operators acting on $\mathcal{U}(z, z'^*)$:

$$\begin{aligned} \bar{\kappa}_{kl} \mathcal{U}(z, z'^*) &= \left(z_{kl} - \sum_{pq} z_{kp} z_{lq} \frac{\partial}{\partial z_{pq}} \right) \mathcal{U}(z, z'^*) \equiv \hat{\bar{\kappa}}_{kl} \mathcal{U}(z, z'^*), \\ \kappa_{kl} \mathcal{U}(z, z'^*) &= \frac{\partial}{\partial z_{kl}} \mathcal{U}(z, z'^*) \equiv \hat{\kappa}_{kl} \mathcal{U}(z, z'^*), \quad (10.44) \\ \rho_{kl} \mathcal{U}(z, z'^*) &= \sum_p z_{lp} \frac{\partial}{\partial z_{kp}} \equiv \hat{\rho}_{kl} \mathcal{U}(z, z'^*). \end{aligned}$$

The relations (10.44) are somewhat tedious but straightforward to verify in differentiating the norm overlap. For the reduced Hamiltonian (10.40), Eq. (10.44) means that the density operators κ , $\bar{\kappa}$ and ρ can be replaced by

The definition of the overlap functions $\mathcal{U}(z, z')$, $\mathcal{K}(z, z')$, $h(z, z')$ in this subsection deviates from Eq. (10.7) for complex values of z . It makes it clear that these functions depend actually on z and not on z^ (see also Sec. 10.6).

differential operators. In a shorthand notation we therefore get

$$\mathcal{H}(z, z'^*) = h(z, z'^*) \mathcal{R}(z, z'^*) \equiv \tilde{h} \left(z, \frac{\partial}{\partial z} \right) \mathcal{R}(z, z'^*). \quad (10.45)$$

With Eq. (10.5) and the definition

$$g(z) = \int dz' f(z') \mathcal{R}(z, z'^*), \quad (10.46)$$

we obtain the Schrödinger equation

$$\tilde{h} \left(z, \frac{\partial}{\partial z} \right) g(z) = E g(z). \quad (10.47)$$

It turns out that the operator \tilde{h} in Eq. (10.47) and the boson Hamiltonian (9.93) of the Dyson expansion are identical if we identify the operators z_{kl} and $\partial/\partial z_{kl}$ with the boson operators B_{kl}^+ , B_{kl} , respectively [JDF 71]. z and $\partial/\partial z$ are correspondingly the Bargmann representation of B^+ and B [Ba 62, JS 64]. At this point, this step is completely formal. Its mathematical background is discussed in Section 10.6.

Since we showed in Section 9.2.6 that, to infinite order, all boson expansions are equivalent and that they can be mutually transformed into one another, it is not astonishing that the Marumori and Belyaev-Zelevinskii boson expansions can also be derived with the GCM [Ho 72]. For instance, the RPA was deduced in this way in an early paper by Jancovici and Schiff [JS 64].*

We know from Chapter 9 that we can represent the exact eigenfunction of the Schrödinger equation within the boson space. It is therefore now clear that the ansatz (10.2) contains the exact solution not only in the Lipkin model (Sec. 10.3) but also in the general case. Contrary to the Lipkin model, however, the representation (10.2) is not necessarily unique in the general case, because there is no unique solution f of Eq. (10.47) if the integral operator $\mathcal{R}(z, z')$ has zero eigenvalues. In fact, this is usually the case, because $\mathcal{R}(z, z')$ is totally antisymmetric with respect to the indices $i_1 k_1, i_2 k_2, \dots$ in the arguments $z'_{i_1 k_1}, z'_{i_2 k_2}$, and projects all symmetric parts of the function $f(z')$ onto zero. To get a unique description, we shall therefore restrict ourselves to functions f , which are totally antisymmetric.

To solve the Hill-Wheeler equations for all generator coordinates z_{ik} exactly is certainly impossible. In practice, we are restricted to one or perhaps a few coordinates. It is a problem in itself to determine the optimal generator coordinates and wave functions. We will come back to this in Section 10.8.

In most cases we rely on phenomenology for the choice of a few collective parameters a_1, a_2, \dots as generator coordinates. Then the set of variational wave functions (10.1) contains only a small part of the many-body Hilbert space, but we hope that we are able to at least describe the collective modes a nucleus may undergo. It is clear that this is only

* See also [BW 68].

possible if the collective motion is well separated from all other degrees of freedom that are not taken into account by the ansatz (10.1).

10.5 The One-Dimensional Harmonic Oscillator

A model which is often used to show the problems that can arise in the GCM is the one-dimensional harmonic oscillator. It is also of great importance in the theory of collective motion, since we have seen that the collective excitations at low energy can be described quite well in the harmonic approximation (Chap. 8). Assuming only one collective degree of freedom, we get:

$$H = \frac{1}{2M} \dot{P}^2 + \frac{M\omega^2}{2} \dot{Q}^2. \quad (10.48)$$

We use *generating functions* of Gaussian form in the q -representation ($\hat{Q}|q\rangle = q|\hat{q}\rangle$):

$$\langle q|\Phi(a)\rangle = (\pi s^2)^{-1/4} e^{-(q-a)^2/2s^2}. \quad (10.49)$$

and obtain for the norm and Hamilton overlap functions

$$\mathcal{N}(a, a') = e^{-(a-a')^2/4s^2}, \quad (10.50)$$

$$\mathcal{K}(a, a') = \mathcal{N}(a, a') \left\{ \frac{\hbar^2}{2M} \left(\frac{1}{2s^2} - \frac{(a-a')^2}{4s^4} \right) + \frac{M\omega^2}{2} \left(\frac{s^2}{2} + \frac{(a+a')^2}{4} \right) \right\}. \quad (10.51)$$

An analytical solution of the corresponding Hill-Wheeler equation (10.5) can be given [GW 57]. But to construct the collective space \mathfrak{H}_C , we shall apply in the following the method (ii) described in Section 10.2.3.

The norm overlap has a Gaussian form and depends only on the difference $(a - a')$. As discussed in Section 10.2.3, it is diagonalized by the functions $u(k, a)$ with eigenvalues $n(k)$ *

$$u(k, a) = \frac{1}{\sqrt{2\pi}} e^{-ika}, \quad n(k) = \int_{-\infty}^{\infty} da e^{ika} \mathcal{N}(a, 0) = 2\sqrt{\pi s^2} e^{-k^2 s^2}, \quad (10.52)$$

where k is now a continuous index. As we see, the spectrum has no zero eigenvalues for finite k 's, but 0 is a limit point for $k \rightarrow \infty$. The representation of the Hamiltonian in this basis is

$$H_{kk'} = \frac{\hbar k^2}{2M} \delta(k - k') - \frac{M\omega^2}{2} \delta''(k - k'), \quad (10.53)$$

which is obviously the momentum space version of the standard harmonic oscillator. The important point is that the parameter s , which depends on the choice of the generator wave functions, has disappeared. This is the exact Hamiltonian, and we gain all the exact solutions from it.

The Schrödinger equation in the collective subspace is

$$\frac{\hbar^2 k^2}{2M} g(k) - \frac{M\omega^2}{2} \frac{d^2}{dk^2} g(k) = E g(k). \quad (10.54)$$

* The operator \mathcal{N} in Eq. (10.50) is not of Hilbert-Schmidt type. It therefore has no discrete spectrum.

The solution for the ground state is

$$g_0(k) = \left(\frac{b^2}{\pi} \right)^{1/4} e^{-\frac{1}{2} b^2 k^2}, \quad (10.55)$$

with

$$b = \sqrt{\frac{\hbar}{M\omega}}.$$

The corresponding weight function $f_0(a)$ can be found from Eqs. (10.19) and (10.52) or by an explicit solution of the HW equation (10.6). For $b > s$ we get:

$$f_0(a) = \int dk g_0(k) \frac{1}{\sqrt{n(k)}} u(k, a) = \frac{1}{\sqrt{2\pi}} \frac{1}{\sqrt{b^2 - s^2}} \sqrt{\frac{b}{s}} \cdot e^{-a^2/2(b^2 - s^2)}. \quad (10.56)$$

The ground state wave function $|\Psi_0\rangle$ in Q space is then given by

$$\Psi_0(q) = \int da f_0(a) \langle q | \Phi(a) \rangle = (\pi \cdot b^2)^{-1/4} e^{-q^2/2b^2}. \quad (10.57)$$

We have thereby found the correct ground state wave function of the harmonic oscillator. The functions f_i can also be explicitly constructed, yielding the excited states. In Eq. (10.57) we can see that the weight function f_0 has added to the width s of the generating function $|\Phi(a)\rangle$ just what was lacking to generate the width b of the harmonic oscillator ground state. However, this is only possible if the width of the generating function is smaller than that of the solution, since by a convolution the width can only increase. Eq. (10.56) is therefore only valid if $b > s$.

If, on the contrary, $b < s$, $f_0(a)$ is no longer given by an ordinary function, but by a distribution which is necessary in order to "sharpen" the generating function. However, we can derive $f_0(a)$ from the integral (10.56) by expanding the integrand in powers of $(s^2 - b^2)$; then:

$$f_0(a) = \sqrt{\frac{b}{s}} \sum_{n=0}^{\infty} \left(\frac{1}{2} (s^2 - b^2) \right)^n \frac{(-)^n}{n!} \delta^{(2n)}(a) \quad (10.58)$$

is a solution of the HW equation for $s > b$. It is obvious that we never could have obtained this solution by discretizing the integral equation.

This example shows very nicely that for $s > b$ it is not possible to express the exact ground state with a well-behaved weight function f_0 . The collective space \mathfrak{G}_C is, in this case, the whole Hilbert space. We have to emphasize, however, that a *numerical solution* with discrete mesh points converges to the right groundstate wave function $\Psi_0(q)$ (10.57) for all values of the width s (this can be shown from the general Tauberian theorem [Wi 33]). Only the weight function $f_0(a)$ remains undefined.

There is another way to avoid this difficulty. We can use the analytical behavior of $f(a)$ in choosing *complex* a . For example, we obtain the solution (10.57) for $s > b$ with the analytical $f(a)$ of Eq. (10.56) in integrating along the pure imaginary a -axis ($a = a_i + ia_j$):

$$\Psi_0(q) = \int_{-\infty}^{+\infty} da_i f_0(ia_i) \langle q | \Phi(ia_i) \rangle = (\pi b^2)^{-1/4} e^{-q^2/2b^2}. \quad (10.59)$$

Here we have only used the fact that in giving the generating function for real parameters we necessarily also have its analytic continuation into the complex plane. We then have to deform the path of integration in such a way as to enter a

domain where the weight function $f_0(a)$ is well behaved. For a numerical solution, however, this does not help very much, because in order to find the "good" integration path we already have to know the solution.

A way out of this problem is to introduce *complex generator coordinates* and integrate over the whole complex plane. We will see in the next section that this yields very well-behaved weight functions in the case of a Gaussian overlap. Introducing the complex space, however, renders the problem numerically much more laborious, since this means, as we have seen in Eq. (10.3), the introduction of a two-parameter GCM. On the other hand, it might not help to avoid ill-behaved weight functions f in the general case.

10.6 Complex Generator Coordinates

A formulation of quantum mechanics exists based on operators with a complex spectrum—the so-called *Bargmann representation* [Ba 62]. The corresponding basis functions are not orthogonal in the usual sense. The corresponding Schrödinger equation is therefore of the Hill-Wheeler type (10.5) with complex generator coordinates. The method of complex generator coordinates in the general sense is closely related to this representation of quantum mechanics and we will discuss its properties in this section. For the sake of simplicity we restrict our discussion to one dimension.

10.6.1 The Bargmann Space

The states of a quantum mechanical system $|\varphi\rangle$ are vectors in an abstract Hilbert space. For concrete calculation we need some representation, for instance, the wave functions in coordinate space

$$\varphi(q) = \langle q|\varphi\rangle, \quad (10.60)$$

that is, we use the eigenfunctions $|q\rangle$ of the self-adjoint operator \hat{Q} as a basis. We can also use the momentum operator \hat{P} and then have the representation in a Fourier space. The eigenvalues of these operators q or p are real, therefore we can work with real coordinates q or p . This is an advantage of such representations. A disadvantage is the fact that the eigenfunction $|q\rangle$ or $|p\rangle$ has an infinite norm. They can only be normalized to a δ function

$$\langle q|q'\rangle = \delta(q - q'); \quad \langle p|p'\rangle = \delta(p - p'). \quad (10.61)$$

Instead of \hat{Q} and \hat{P} , Fock [Fo 28] introduced the operators

$$O = \sqrt{\frac{M\omega}{2\hbar}} \left(\hat{Q} + \frac{i}{M\omega} \hat{P} \right); \quad O^+ = \sqrt{\frac{M\omega}{2\hbar}} \left(\hat{Q} - \frac{i}{M\omega} \hat{P} \right), \quad (10.62)$$

where the constants ω and M are arbitrary at this point. They obey the commutation relation

$$[O, O^+] = 1. \quad (10.63)$$

Bargmann [Ba 62] used the operator O to derive a new representation. The non-Hermitian operator O can be diagonalized and has all the complex numbers z as its eigenvalues

$$O|z\rangle = z|z\rangle. \quad (10.64)$$

The eigenfunctions are called *coherent states* [Gl 63] because they are of great use in the description of coherent phenomena of light.* They can be represented by the eigenstates $|n\rangle$ of the operator $\hat{N} = O^* O$ (which are oscillator functions)

$$\hat{N}|n\rangle = n|n\rangle \quad (10.65)$$

in the following way†

$$|z\rangle = \sum_{n=0}^{\infty} \frac{z^n}{\sqrt{n!}} |n\rangle = e^{z^* O^*} |0\rangle = e^{\frac{1}{2}|z|^2} e^{(z^* O^* - z^* O)} |0\rangle. \quad (10.66)$$

$|0\rangle$ is the ground state of the harmonic oscillator. It is easy to derive this relation from the property $O|n\rangle = \sqrt{n} |n-1\rangle$ [see Eq. (C.11)]. Similarly, we get

$$O^+|z\rangle = \frac{d}{dz}|z\rangle. \quad (10.67)$$

The orthogonality relation (10.61) now has the form

$$\langle z|z'\rangle = \exp(z^* z') := B(z^*, z'), \quad (10.68)$$

which means that these states have a finite norm, but are no longer orthogonal in the usual sense. However, it is possible to define a real positive *measure* $d\mu(z)$ in the complex plane.

$$d\mu(z) = \frac{1}{\pi} e^{-|z|^2} dx dy, \quad \text{where } z = x + iy, \quad (10.69)$$

which allows us to derive the closure relation

$$1 = \sum_n |n\rangle \langle n| = \int |z\rangle d\mu(z) \langle z|, \quad (10.70)$$

where the integral runs over the whole complex plane. Equation (10.70) can be proved with Eqs. (10.66) and (10.69) using polar coordinates $z = re^{i\varphi}$.

In analogy to Eq. (10.60), the wave functions in this representation are given by

$$\psi(z) = \langle z^* | \psi \rangle. \quad (10.71)$$

From (10.66) we see that they depend on z , not on z^* . The measure (10.69) allows us to define a scalar product

$$\langle \psi_1 | \psi_2 \rangle = \int d\mu(z) \psi_1^*(z) \psi_2(z) = \langle \psi_1 | \psi_2 \rangle, \quad (10.72)$$

* For a general group theoretical definition of coherent states, see [Pe 77].

† We use the Baker–Campbell–Hausdorff formula [Wi 67]

$$e^A \cdot e^B = e^{A + B + \frac{1}{2}[A, B]}$$

for operators A and B , that commute with $[A, B]$.

which means that the representation (10.71) is isometric with respect to the measure (10.69). We can now also derive a representation for the operators O, O^+ from (10.64) and (10.72):

$$\begin{aligned} O^+ \psi(z) &= \langle z^* | O^+ | \psi \rangle = z \langle z^* | \psi \rangle = z\psi(z), \\ O\psi(z) &= \langle z^* | O | \psi \rangle = \frac{d}{dz} \langle z^* | \psi \rangle = \frac{d}{dz} \psi(z), \end{aligned} \quad (10.73)$$

or

$$O^+ = z, \quad O = \frac{d}{dz}, \quad (10.74)$$

which obviously fulfills the commutation relation (10.63).*

Finally, with Eq. (10.70) it is easy to prove that the function $B(z^*, z')$ in Eq. (10.68) has with the metric (10.72) similar properties in the Bargmann space as the δ function in the usual space, namely

$$\psi(z) = \int B(z, z'^*) \psi(z') d\mu(z'). \quad (10.75)$$

This function is therefore often called Bargmann's complex δ function. In fact, it is an entire function and no distribution.

10.6.2 The Schrödinger Equation

We obtain the Schrödinger equation $H|\psi\rangle = E|\psi\rangle$ as represented in the Bargmann space by multiplying by $\langle z^* |$ and inserting the complete set (10.70)

$$\int H(z, z'^*) \psi(z') d\mu(z') = E\psi(z), \quad (10.76)$$

where

$$H(z, z'^*) = \langle z^* | H | z'^* \rangle \quad (10.77)$$

is a function of z, z'^* . It does not depend on z^* or z' .

We can rewrite Eq. (10.76) in two ways [UB 68]:

- (i) We can use Eq. (10.75) and gain an equation of the Hill-Wheeler form

$$\int (H(z, z'^*) - EB(z, z'^*)) \psi(z') d\mu(z') = 0. \quad (10.78)$$

This corresponds to the GCM ansatz

$$|\psi\rangle = \int d\mu(z) \psi(z) |z^*\rangle, \quad (10.79)$$

where the coherent states $|z^*\rangle$ of Eq. (10.66) have been used as generating functions with the complex generator coordinate z . The

* One should not be confused by the fact that (10.74) is different from (10.64) and (10.67). The reason is that there are two different representations of O^+, O acting in different Hilbert spaces.

advantage of these generating functions is that their overlap $B(z, z'')$ corresponds to the δ function in the Bargmann space. It has the more or less Gaussian form

$$B(z, z'') = e^{zz''} = e^{\frac{1}{2}z^2} e^{\frac{1}{2}z''^2} e^{-\frac{1}{2}(z-z'')^2}. \quad (10.80)$$

(ii) We can introduce the function $h(z, z'')$

$$H(z, z'') = h(z, z'') B(z, z'') \quad (10.81)$$

and use

$$\frac{\partial}{\partial z} B(z, z'') = z'' B(z, z'') \quad (10.82)$$

to transform to the differential equation

$$:h\left(z, \frac{\partial}{\partial z}\right) : \psi(z) = E\psi(z). \quad (10.83)$$

The dots mean normal ordering so that powers of z are always on the left side of $\partial/\partial z$. If we now use the operators (10.74) we can express the Hamiltonian H by boson operators and get a "boson expansion," as discussed in Section 10.4. There, however, we do not have coherent states because of the non-Gaussian form of the norm (10.39). Nevertheless, this may often be quite a good approximation (see Sec. 10.7).

Because of the δ function property of the function $B(z, z'')$ in Eq. (10.75) the function g of Eq. (10.12) now coincides with the weighting function, that is, the norm overlap is in this case just the identity operator. Therefore, the weight functions are now always well behaved, which was not true in the case of real generator coordinates. However, we have to emphasize that this holds only for overlap functions of a Gaussian form. In the general case the use of complex coordinates does not automatically yield well-behaved weight functions.

10.6.3 Gaussian Wave Packets in the Harmonic Oscillator

Gaussian wave packets in the harmonic oscillator are closely related to the theory of coherent states. Therefore, in the following we discuss some of their properties and, particularly, their time dependence. However, we do not need all of the following results in the context of the generator coordinate method, in which we treat only the stationary problem.

The coherent state $|z\rangle$ in Eq. (10.66) is represented by the boson operators O^+ and O of a harmonic oscillator Hamiltonian.

$$H_0 = \frac{\hat{P}^2}{2M} + \frac{M\omega^2}{2} \hat{Q}^2 = \hbar\omega(O^+O + \frac{1}{2}),$$

with the oscillator length $b = (\hbar/M\omega)^{1/2}$. The state $|z\rangle$ in Eq. (10.66) is not

normalized. In the following we therefore define normalized states:

$$|z, 0\rangle = e^{-\frac{1}{2}|z|^2} |z\rangle = \exp(zO^+ - z^*O)|0\rangle,$$

where $|0\rangle$ corresponds to the ground state of H_0 . The unitary operator

$$\hat{S}_z^+ = \exp(zO^+ - z^*O)$$

produces a shift in the boson operators by an amount z (see Sec. E.5)

$$\hat{S}_z^+ O^+ \hat{S}_z^- = O^+ - z^*, \quad \hat{S}_z^+ O \hat{S}_z^- = O - z.$$

Decomposing z into its real and imaginary parts

$$z = \frac{1}{\sqrt{2}} \frac{1}{b} \left(q_0 + i \frac{p_0}{M\omega} \right),$$

we can also express it by the operators \hat{P} and \hat{Q} ,

$$\hat{S}_z^+ = \exp \frac{i}{\hbar} (p_0 \hat{Q} - q_0 \hat{P}) = \exp \left(-\frac{i}{2\hbar} p_0 q_0 \right) \exp \left(\frac{i}{\hbar} p_0 \hat{Q} \right) \cdot \exp \left(-\frac{i}{\hbar} q_0 \hat{P} \right),$$

which shows that it produces a shift in the coordinate by an amount q_0 and in the momentum by an amount p_0 ,

$$\hat{S}_z^+ \hat{Q} \hat{S}_z^- = \hat{Q} - q_0, \quad \hat{S}_z^+ \hat{P} \hat{S}_z^- = \hat{P} - p_0.$$

The coherent state

$$|z, 0\rangle = \exp \frac{i}{\hbar} (p_0 \hat{Q} - q_0 \hat{P}) |0\rangle \quad (10.84)$$

is therefore nothing but the ground state of a shifted harmonic oscillator

$$H_z = \frac{(\hat{P} - p_0)^2}{2M} + \frac{M\omega^2}{2} (\hat{Q} - q_0)^2. \quad (10.85)$$

It is neither an eigenstate of \hat{P} nor \hat{Q} nor of the original Hamiltonian H_0 . We obtain for the mean value of the coordinate and the momentum operator

$$\langle z, 0 | \hat{Q} | z, 0 \rangle = q_0, \quad \langle z, 0 | \hat{P} | z, 0 \rangle = p_0,$$

and for the fluctuations

$$\langle z, 0 | \Delta \hat{Q}^2 | z, 0 \rangle = \frac{b^2}{2}, \quad \langle z, 0 | \Delta \hat{P}^2 | z, 0 \rangle = \frac{\hbar^2}{2b^2}. \quad (10.86)$$

This shows that $|z, 0\rangle$ minimizes the uncertainty

$$\langle z, 0 | \Delta \hat{Q}^2 | z, 0 \rangle \langle z, 0 | \Delta \hat{P}^2 | z, 0 \rangle = \frac{\hbar^2}{4}.$$

Therefore, the coherent states are the "most classical" wave functions that can be found.

We can represent the state $|z, 0\rangle$ in coordinate space by the wave function

$$\psi_0(x) = \langle x | z, 0 \rangle = e^{-\frac{1}{2}|x|^2} \langle x | e^{zO^+} | 0 \rangle.$$

Using $O^+ = O - i\sqrt{2} b\hat{P}/\hbar$ and $O|0\rangle = 0$, we obtain

$$\psi_0(x) = e^{-\frac{1}{2}(x^2 - z^2)} \langle x - \sqrt{2} bz | 0 \rangle.$$

This is a Gaussian wave function centered around $\sqrt{2} bz = q_0 + i(p_0/M\omega)$

$$\begin{aligned} \psi_0(x) &= (\sqrt{\pi} b)^{-1/2} e^{-\frac{1}{2}(x^2 - z^2)} e^{-(x/\sqrt{2}b - z)^2} \\ &= (\sqrt{\pi} b)^{-1/2} \exp \frac{i}{\hbar} \left\{ \frac{p_0 q_0}{2} + p_0(x - q_0) + i \frac{M\omega}{2} (x - q_0)^2 \right\}. \end{aligned} \quad (10.87)$$

Since this wave function is not an eigenfunction of the original Hamiltonian H_0 , the coherent state $|z, 0\rangle$ forms a wave packet. We obtain its time evolution by

$$|z, t, 0\rangle = e^{-\frac{i}{\hbar} H_0 t} |z, 0\rangle = e^{-\frac{i\omega}{2} t} |ze^{-i\omega t}, 0\rangle.$$

Decomposing $ze^{-i\omega t}$ into real and imaginary parts, we find

$$ze^{-i\omega t} = \frac{1}{\sqrt{2} b} \left(q(t) + i \frac{p(t)}{M\omega} \right),$$

where

$$q(t) = q_0 \cos \omega t + \frac{p_0}{M\omega} \sin \omega t,$$

$$p(t) = p_0 \cos \omega t - M\omega q_0 \sin \omega t$$

describes the classical path of a particle with the initial conditions q_0, p_0 at $t = 0$. To obtain the time-dependent wave function in coordinate space, we have only to replace p_0 and q_0 in Eq. (10.87) by $p(t)$ and $q(t)$, and to add the trivial phase $-\omega t/2$:

$$\psi_0(x, t) = (\sqrt{\pi} b)^{-1/2} \exp \frac{i}{\hbar} (S(x, t) - \epsilon_0 t),$$

with

$$S(x, t) = W(t) + p(t)(x - q(t)) + i \frac{M\omega}{2} (x - q(t))^2, \quad (10.88)$$

$$W(t) = \frac{1}{2} p(t) q(t), \quad \epsilon_0 = \frac{\hbar\omega}{2}.$$

It describes a Gaussian wave packet whose center $q(t)$ moves like a classical particle: It oscillates with constant frequency ω . The wave packet itself preserves its shape and shows no dispersion, that is, it moves "coherently."

We obtained this wave packet as the time evolution of the stationary ground state of a shifted harmonic oscillator Hamiltonian. We can also take internal excitations of this wave packet into account by starting with the excited states in the shifted oscillator (10.85)

$$|z, n\rangle = \hat{S}_z^+ |n\rangle = \frac{1}{\sqrt{n!}} (O^+ - z^*)^n |z, 0\rangle.$$

Again, their time dependence is given by

$$|z, t, n\rangle = e^{-\frac{i}{\hbar}Ht}|z, n\rangle = e^{-\frac{i}{\hbar}\epsilon_n t}|ze^{-i\omega t}, n\rangle,$$

with $\epsilon_n = \hbar\omega(n + \frac{1}{2})$.

For the corresponding wave function in the coordinate space a lengthy calculation gives

$$\psi_n(x, t) = \langle x | z, t, n \rangle = (2^n n! \sqrt{\pi} b)^{-1/2} H_n\left(\frac{x - q(t)}{b}\right) \exp\frac{i}{\hbar}(S(x, t) - \epsilon_n t),$$

where H_n are the Hermite polynomials and $S(x, t)$ is given in Eq. (10.88). Again, these Hermite wave packets $\psi_n(x, t)$ oscillate along the classical path $q(t)$, preserving their shape. At each time they represent a complete orthogonal set, which may be an efficient tool for the investigation of time-dependent processes. So far we started with stationary wave functions in a shifted oscillator (10.85) having the same frequency ω , that is, the same oscillator length b as the original Hamiltonian H_0 . We can go a step further still and start with the eigenstates in a harmonic oscillator potential

$$H_I = \frac{(\hat{P} - p_0)^2}{2M} + \frac{M\bar{\omega}^2}{2}(\hat{Q} - q_0)^2$$

with a different frequency $\bar{\omega} \neq \omega$ and the corresponding oscillator length \bar{b} . Its eigenstates are given by

$$|\bar{z}, n\rangle = \frac{1}{\sqrt{n!}} (\bar{O}^+ - \bar{z}^*)^n S_{\bar{z}}^+ |\bar{0}\rangle,$$

with

$$\bar{O}^+ = \frac{1}{\sqrt{2}} \frac{1}{\bar{b}} \left(\hat{Q} - \frac{i}{M\bar{\omega}} \hat{P} \right) \quad \text{and} \quad \bar{O} |\bar{0}\rangle = 0.$$

Without proof, we give the coordinate representation of the time-dependent wave function (for details, see [Bö 76, LR 69]):

$$\begin{aligned} \bar{\psi}_n(x, t) &= \langle x | e^{-\frac{i}{\hbar}H_I t} | \bar{z}, n \rangle \\ &= (2^n n! \sqrt{\pi} \bar{b}(t))^{-1/2} H_n\left(\frac{x - q(t)}{\bar{b}(t)}\right) \exp\left[-\frac{1}{2} \frac{(x - q(t))^2}{\bar{b}(t)^2} + \frac{i}{\hbar} \phi(x, t)\right], \end{aligned} \tag{10.89a}$$

with

$$\bar{b}(t) = b(\sigma + \tau \cos 2\omega t)^{1/2}$$

$$\begin{aligned} \phi(x, t) &= W(t) + p(t)(x - q(t)) - \frac{M\omega}{2} (x - q(t))^2 \frac{\tau \sin 2\omega t}{\sigma + \tau \cos 2\omega t} \\ &\quad - \hbar\left(n + \frac{1}{2}\right) \operatorname{arctg}\left(\frac{\bar{\omega}}{\omega} \operatorname{tg}(\omega t)\right) \end{aligned} \tag{10.89b}$$

and

$$\sigma = \frac{1}{2} \left(\frac{\omega}{\bar{\omega}} + \frac{\bar{\omega}}{\omega} \right), \quad \tau = \frac{1}{2} \left(\frac{\omega}{\bar{\omega}} - \frac{\bar{\omega}}{\omega} \right). \quad (10.89c)$$

10.6.4 Double Projection

In Section 10.5 we treated the case of a harmonic oscillator using generating wave functions, which were shifted in the configuration space by the amount α (10.49). Up to a factor $e^{1/2|\alpha|^2}$, these are coherent states of the form

$$|z\rangle = e^{\frac{i}{\hbar}|\alpha|^2} \exp \left\{ \frac{i}{\hbar} (\beta \hat{Q} - \alpha \hat{P}) \right\} |0\rangle,$$

$$\alpha = \sqrt{\frac{2\hbar}{M\omega}} \operatorname{Re} z, \quad \beta = \hbar \sqrt{\frac{2M\omega}{\hbar}} \operatorname{Im} z,$$

with a real parameter z : $\alpha = a$, $\beta = 0$. Using complex values of z means an analytic continuation of these functions into the complex plane or the introduction of a second generator coordinate $\beta \propto \dot{\alpha}$, which describes a shift in momentum.

Such a treatment—using generating functions $|\Phi(\alpha, \beta)\rangle$ depending not only on the coordinate α , but also on the corresponding momentum β —was first introduced by Thouless and Peierls [PT 62] in connection with projection onto eigenstates of linear momentum, and is therefore called the double projection technique (see Chap. 11). In the case of generating functions of the oscillator type, this method is useful insofar as it is equivalent to the use of coherent states as generating functions that are very well behaved in the Bargmann space. We do not run into trouble, even if their width s is larger than the width of the function $|\Psi\rangle$ we wish to represent (see Sec. 10.5).

However, as we have seen in Section 10.5, we already get the exact wave function with one real generator coordinate α if we construct the collective space \mathfrak{G}_C in a proper way. Only the weight functions are very ill behaved in some cases. This means that the collective space \mathfrak{G}_C spanned by the generating functions $|\Phi(\alpha, 0)\rangle$ is the same as the space \mathfrak{G}_C spanned by the functions $|\Phi(\alpha, \beta)\rangle$ in the harmonic oscillator case. The coordinate β is *redundant*.

In general, this may not always be the case. We might sometimes be tempted to introduce a two-parameter generator coordinate for physical reasons. For example, for the case of quadrupole oscillations, one might think that not only the quadrupole moment α is a good generator coordinate, but in addition also its time derivative $\dot{\alpha}$ (or the corresponding momentum β), thus forming a set of generator coordinates of two conjugate variables. We will see in Chapter 12 that in the time-dependent Hartree-Fock (TDHF) theory, we always have to deal with such wave

functions $|\Phi(\alpha, \beta)\rangle$. In the GCM, however, it often happens that the generating functions $|\Phi(\alpha, \beta)\rangle$ lie mostly in the space already formed by the $|\Phi(\alpha, 0)\rangle$. They are, therefore, almost redundant. The determination of the weight function $f(\alpha, \beta)$ through the variational principle becomes very insensitive in such cases, or, in other words, the norm overlap $\mathfrak{R}(\alpha\beta, \alpha'\beta')$ has a large eigenspace with vanishing norm.

The two parameters (α, β) are certainly redundant, if they only enter into the combination $\alpha + i\lambda\beta$, where λ is a real constant. From the relation

$$|\Phi(\alpha + i\lambda\beta)\rangle = \exp\left(i\lambda\beta \frac{\partial}{\partial\alpha}\right) |\Phi(\alpha, \beta)\rangle$$

and subsequent partial integration in the HW-ansatz (10.1), we can redefine new weight functions depending on only one real parameter.

A function $|\Phi(\alpha, \beta)\rangle$ only depends on the combination $\alpha + i\lambda\beta$ if

$$\left(\frac{\partial}{\partial\beta} - i\lambda \frac{\partial}{\partial\alpha} \right) |\Phi(\alpha, \beta)\rangle = 0. \quad (10.90)$$

This condition means local redundancy [Re 76a+b]: The change of the function $|\Phi\rangle$ by an infinitesimal variation of the coordinate β can be expressed by a corresponding change of the coordinate α . It is a sufficient condition for redundancy.

The double projection method in the GCM theory has not, up to the present, been studied in great detail. It is not clear whether there are cases in which it has great advantages.

10.7 Derivation of a Collective Hamiltonian

10.7.1 General Considerations

As we discussed in Section 10.2, the direct solution of the HW equation (10.5) can be quite cumbersome. In particular, the construction of the collective Hamiltonian (10.17) in analytical form is hardly possible in realistic cases. On the other hand, there are, at least for heavy nuclei, a number of suggestive approximations more or less based on the idea of transforming Eq. (10.5) into a differential equation, which looks similar to a Schrödinger equation in a collective variable q [FC 72, HW 72, BB 73, Ho 73, GG 75, Re 76a+b]. These theories have also been used to derive a collective Hamiltonian (as discussed in Chap. 1) from a microscopic point of view.

We start with a set of time-reversal invariant generating functions $|q\rangle = |\Phi(q)\rangle$, where q is a collective parameter; it characterizes, for instance, a certain deformation. The methods discussed in the following are based on two facts:

- (i) In many cases, the overlap function $\mathcal{N}(q, q') = \langle q | q' \rangle$ is very small unless the two parameters q and q' are very close to each other, that is, \mathcal{N} is a *rapidly decreasing* function with increasing distance $|q - q'|$. For instance, this is the case for the Lipkin model, where the function \mathcal{N} in Eq. (10.32) depends only on $\varphi - \varphi'$ and is sharply peaked at the origin for large values of Ω (large particle number). The same is true for large particle numbers in the general case of two Slater determinants which differ from one another in a collective parameter, for example, in the deformation [HW 74]. This case will be discussed in more detail later (Sec. 10.7.4), and it will be shown that in many cases \mathcal{N} has the form of a Gaussian in the variable $q - q'$. Only the width of this Gaussian may still depend on the center of mass $\frac{1}{2}(q + q')$.
- (ii) We assume that the overlap functions \mathcal{N} and \mathcal{K} are *well behaved*—that is, differentiable—many times. This seems reasonable for many physical cases, and in particular when we have to deal with collective phenomena. It is not justified, however, when level crossings occur. There the overlap functions of HF Slater determinants make sudden jumps if there is a change in the occupation numbers [Re 77]. The occupation numbers σ^2 in HFB functions are smeared out; this gives smoother but perhaps rapid changes of the functions \mathcal{N} and \mathcal{K} . However, we must realize that in the HFB case we have to readjust the chemical potential λ ; this is a nonlinear problem and causes additional difficulties. There may be more than one solution and sudden jumps between them. We shall therefore omit problems of level crossings in this section (see also Sec. 12.3.7).

There are essentially three different methods in order of increasingly simplifying assumptions: the *symmetric moment expansion* (SME), the *local approximation* (LA), and the *Gaussian overlap approximation* (GOA). We shall discuss them successively in this section. For the GOA we will present an independent derivation. Readers who are not interested in the details may therefore skip the next two subsections.

10.7.2 The Symmetric Moment Expansion (SME)

The two assumptions of differentiability and sharply peaked overlap functions can be used to transform the integral equation (10.5) into a second-order differential equation. In principle we have already applied similar techniques in Section 10.4 in the derivation of boson expansions. However, at that time it was a rather formal method and we ended up with a second-order differential equation in many hundreds of variables z_{ik} . We shall now restrict ourselves to one (or a few) collective variables q .

Using the identity

$$|q'\rangle =: e^{-i(q'-q)P/\hbar} |q\rangle \quad (10.91)$$

with*

$$P = -\frac{N}{I} \frac{\partial}{\partial q} \quad (10.92)$$

and the dots meaning normal ordering, so that powers of $(q' - q)$ are always to the left side of P , we can write for the integral equation (10.5) (we drop the normal ordering points in the following):

$$\int dq' (\mathcal{K}(q, q') - E \mathcal{A}(q, q')) e^{-i(q'-q)P/\hbar} f(q) = 0. \quad (10.93)$$

As we assume that the norm overlap is a rapidly decreasing function of $|q' - q|$, we see by inspection of the Onishi formula (10.39) that the Hamilton overlap $\mathcal{K}(q, q')$ should also be quite a rapidly decreasing function of $|q - q'|$. We are therefore allowed to develop the exponentials up to second order. We first introduce the variable

$$s = q - q' \quad (10.94)$$

and gain from (10.5)

$$\int_{-\infty}^{+\infty} ds \langle q | H - E | q - s \rangle e^{isP/\hbar} f(q) = 0. \quad (10.95)$$

As the second-order differential operator we will obtain on the left-hand side of Eq. (10.95) is not, term by term, a symmetric operator [BB 73], it is preferable to symmetrize this equation first [Ho 73]:

$$\int_{-\infty}^{+\infty} ds e^{isP/2\hbar} \langle q + s/2 | H - E | q - s/2 \rangle e^{isP/2\hbar} f(q) = 0. \quad (10.96)$$

The (still) exact equation (10.96) is now approximated by expanding the exponentials up to second order in s :

$$(H_0 - \frac{1}{2} \overline{H_2 P^2}) f = E (N_0 - \frac{1}{2} \overline{N_2 P^2}) f, \quad (10.97)$$

with the moments

$$\left. \begin{aligned} H_n(q) \\ N_n(q) \end{aligned} \right\} = \frac{1}{\hbar^n} \int_{-\infty}^{+\infty} ds s^n \langle q + s/2 | \overline{H} | q - s/2 \rangle \quad (10.98)$$

and the definition of a symmetric ordered product of operators [Re 76b], viz.

$$\begin{aligned} \overline{A(q)P^2} &:= \frac{1}{4} (AP^2 + 2PAP + P^2A) = \frac{1}{4} [P, [A, P]_+]_+ \\ &= \sum_{n=0}^{\infty} \frac{1}{2^n} \binom{n}{n} P^n A P^{n-n} \Big|_{n=2}. \end{aligned} \quad (10.99)$$

The odd moments vanish identically, $H_1 = N_1 = 0$, since we have assumed that the set of generating states $|\Phi(q)\rangle$ is invariant under time reversal, which means that the overlap functions \mathcal{A} and \mathcal{K} are real. The only quantities we have to know are the zeroth and second moments of the norm and the Hamiltonian overlap (10.98).

*The operator P acts on the parameter q and not on the particle coordinates (x) in the wave function $|\Phi(q)\rangle$. It is therefore convenient to use a minus sign in its definition. In the case of pure translation, where q is the origin of the new coordinate system, we get $|\Phi(x, q)\rangle = |\Phi(x, -q, 0)\rangle$ and $\sum (h/i)(\partial/\partial x_i) |\Phi\rangle = -(h/i)(\partial/\partial q) |\Phi\rangle$. In the present context the minus sign does not matter, since the Hamiltonian we are going to derive is quadratic in P .

Equation (10.97) is a Hermitian second-order differential equation for $f(q)$. However, it is still not of the usual Schrödinger type. To arrive at such an equation we have to decompose the operator $(N_0 - \frac{1}{2}N_2\overline{P^2})$ in the following way.

$$(N_0 - \frac{1}{2}N_2\overline{P^2}) = (K^{1/2})^+ (K^{1/2}). \quad (10.100)$$

Starting from the ansatz

$$K^{-1/2} = N_0^{-1/2}(1 + K_2(q)\overline{P^2} + K_4(q)\overline{P^4} + \dots), \quad (10.101)$$

we can insert into Eq. (10.100) and bring the result in each order to the symmetric form defined by Eq. (10.99). This allows us to determine the functions K_n . We will see that in most cases we only need them up to $n < 4$. In practice, the calculations are quite lengthy. Also, we usually neglect derivatives $(\partial^n/\partial q^n)N_0$ and $(\partial^n/\partial q^n)N_2$ for $n > 2$ and stop after second order. This is consistent with the quadratic approximation (10.97).

For the sake of simplicity, in the following we will neglect all derivatives of N_0 and N_2 . This is realized in all the cases where (q, q') depends only on the difference $(q - q')$. In this case, up to order P^2 we get:

$$K^{-1/2} = N_0^{-1/2}\left(1 + \frac{1}{4} \frac{N_2}{N_0} P^2\right). \quad (10.102)$$

In the next step we have to calculate the collective Hamiltonian $K^{-1/2+}(H_0 - \frac{1}{2}H_2\overline{P^2})K^{-1/2}$. Again, we have to bring all orders of P^2 into the symmetric form (10.99).* We usually neglect terms of order higher than P^2 and the derivatives $(\partial^n/\partial q^n)H$ for $n > 2$. At this point, this is certainly not well justified. We should calculate the corresponding higher-order coefficients and see if they are small. In fact, we can show, on the basis of the Lipkin model, that they are of the order $(1/\Omega)^2$ [Ho 73], but this is probably not very significant.

In general, we expect that this method is justified for motions with large amplitudes, but not very large velocities.

Under these conditions we get from Eq. (10.102) the following Schrödinger equation for the function $g(q) = K^{1/2}f(q)$.

$$\left(\frac{1}{2M(q)}\overline{P^2} + V(q)\right)g(q) = Eg(q), \quad (10.103)$$

with

$$V(q) = \frac{H_0}{N_0} - \frac{\hbar^2}{8} \frac{N_2}{N_0} \cdot \frac{H_0''}{N_0} \quad \text{and} \quad \frac{1}{M(q)} = \frac{H_0}{N_0} \frac{N_2}{N_0} - \frac{H_2}{N_0}, \quad (10.104)$$

where the primes mean differentiation with respect to q . We have also neglected in $1/M$ the derivatives H_0'', H_2'' consistent with the fact that P^2 is already of second order in the momentum.

Equation (10.103), together with Eq. (10.104) is the consistent transformation of Eq. (10.5) into a Hermitian second-order differential equation. This is a full quantum mechanical equation. Since the mass parameter M depends on the coordinate q , the relative order of P and M in Eq. (10.103) is important. Here we

* These calculations are rather simple if we use the formula [Re 76b] [for any function $X(q)$, X'' means $(\partial^2/\partial q^2)X$]:

$$P^l \overline{X P^m P^n} + P^n \overline{X P^m P^l} = 2 \overline{X P^{l+m+n}} + \frac{1}{2} ((n+l) - (n-l))^2 A^2 \overline{X'' P^{l+m+n-2}}.$$

have used the prescription (10.102), which is a result of the symmetric expansion (10.97). We should be aware, however, that this is not the only possibility, and to require the same ordering after the inversion (10.101) seems somewhat arbitrary. Flocard and Vautherin [FV 74], for example, give a slightly different formulation.

In the formulae (10.104) we neglected the coordinate dependence of N_0 and N_2 . This can be included [Re 76b] yielding rather lengthy expressions of the same structure.

In Eq. (10.103) the zeroth and second moments of the norm and Hamilton overlap are unknown. Since these functions must be known over their whole range of nonlocality, we call this the *global approximation*. It can be checked immediately that our harmonic oscillator model (Sec. 10.5) is exactly reproduced by Eq. (10.103). This is only true, however, in lowest order. Including higher orders in the expansion (10.97) adds small corrections. In fact, we have to go up to infinite order in the moment expansion (10.97) to get the proper weight function f of Eq. (10.56). Because of its global nature, for more realistic problems Eq. (10.103) is still quite complicated. Therefore, we try to reduce its complexity further by introducing the local approximation.

10.7.3 The Local Approximation (LA)

In Section 10.7.1 we put forward arguments that the Hamilton overlap should not be completely different in its q -dependence from the norm overlap (see also (10.32)). It should, for instance, also be a rapidly decreasing function if this is the case for the norm overlap. Therefore, it seems reasonable to stop the following (in principle, exact expansion) after second-order terms:

$$\mathcal{K}\left(q + \frac{s}{2}, q - \frac{s}{2}\right) = \left\{ A(q) + B(q) \frac{\partial^2}{\partial s^2} + \dots \right\} \mathcal{N}\left(q + \frac{s}{2}, q - \frac{s}{2}\right). \quad (10.105)$$

Because of time reversal invariance, there are no odd derivatives in Eq. (10.105). Expanding both sides of this equation in powers of s yields a system of equations for the coefficients A, B, \dots . To second order, we obtain the following expressions.

$$A(q) = \left. \frac{\mathcal{K} \cdot \mathcal{K}'' - \mathcal{K}' \cdot \mathcal{K}'}{\mathcal{N} \cdot \mathcal{N}'' - \mathcal{N}' \cdot \mathcal{N}'} \right|_{s=0}, \quad (10.106)$$

$$B(q) = - \left. \frac{\mathcal{K} \cdot \mathcal{K}'' - \mathcal{K}' \cdot \mathcal{K}'}{\mathcal{N} \cdot \mathcal{N}'' - \mathcal{N}' \cdot \mathcal{N}'} \right|_{s=0}. \quad (10.107)$$

The upper primes mean differentiation with respect to s . Using $\mathcal{N}(q, q) = 1$ and inserting the expression (10.105) with Eqs. (10.106) and (10.107) into the integrals (10.98), we obtain for the first two moments of the Hamiltonian ($\int ds \mathcal{N}'' = 0$):

$$H_0(q) = N_0 \cdot A, \quad (10.108)$$

$$H_2(q) = \frac{N_2}{N_0} \cdot H_0 + \frac{2}{N^2} N_0 \cdot B. \quad (10.109)$$

Using the approximate expressions (10.108) and (10.109) for H_0 and H_2 , we have achieved a reduction of the information we need about the Hamilton overlap to that of a knowledge of its local $\mathcal{K}(q, q)$ and "slightly nonlocal" values $\mathcal{K}''|_{s=0}$. This is naturally an advantage over the expression (10.98) where we had to know the Hamilton overlap over its entire range of nonlocality. Only for the norm overlap do we still have to know its nonlocality over the entire range, since its zeroth and

second moments enter Eq. (10.104). The theory developed so far [Re 76a+b] is equivalent to that of Giraud and Grammaticos [GG 74a, GG 75]. It still gives the exact result for the harmonic oscillator model (Sec. 10.5). However, it is a global approximation of the norm overlap. It may be that for specific cases where the norm overlap is easier to calculate than the Hamilton overlap, the local approximation is useful; however, in general, this is also a very difficult task. In the next section we will therefore develop an approximation scheme for the norm overlap.

10.7.4 The Gaussian Overlap Approximation (GOA)

In order to derive simple expressions for the parameters of the collective Hamiltonian, the Gaussian overlap approximation is widely used [HW 53, JS 64, Ka 68, Vi 75]: We assume that the norm overlap $\mathcal{N}(a, a')$ is in the center of mass coordinates

$$q = \frac{a + a'}{2}, \quad s = (a - a') \quad (10.110)$$

of the form

$$\mathcal{N}(a, a') = \mathcal{N}\left(q + \frac{s}{2}, q - \frac{s}{2}\right) = e^{-\frac{1}{2} \gamma(q)s^2}. \quad (10.111)$$

With the definition (10.92) for the operator $P = -(\hbar/i)(\partial/\partial q)$ we find ($|q\rangle \equiv |\Phi(q)\rangle$),

$$\hbar^2 \gamma(q) = \langle q | P^2 | q \rangle. \quad (10.112)$$

The expectation value of P vanishes because of time reversal invariance

$$\langle q | P | q \rangle = 0. \quad (10.113)$$

Before we apply the Gaussian approximation, we first have to discuss the conditions under which it is valid. To be more precise, we suppose for a moment that $|q\rangle$ is a set of Slater determinants depending on a collective parameter q , as may be obtained, for instance, by a constrained Hartree-Fock calculation (see Section 7.6).

Thouless' theorem tells us that we can represent a function in the vicinity of $|q\rangle$ as [(E.40) and (E.26)]

$$|q + \frac{s}{2}\rangle = e^{-i\hat{P}/2\hbar} |q\rangle = \mathcal{N}\left(q, q + \frac{s}{2}\right) \cdot e^{i\hat{Z}/2\hbar} |q\rangle, \quad (10.114)$$

where \hat{P} is a Hermitian operator with only ph and hp matrix elements. It is obviously a representation of the operator $-(\hbar/i)(\partial/\partial q)$ in the Hilbert space. The operator \hat{Z} has only ph matrix elements. As long as s is small, we can assume \hat{P} and \hat{Z} to be independent of s and find, from Eq. (E.48), that \hat{Z} is just the ph part of \hat{P} . Both operators depend on q .

Using the formula of Onishi (E.51), we find, up to a phase,

$$\mathcal{N}\left(q + \frac{s}{2}, q - \frac{s}{2}\right) = \exp\left\{\text{Tr}\left(-\text{Artanh}\frac{s^2}{2} A\right)\right\}, \quad (10.115)$$

where the matrix A is given by

$$A_{ij} = \sum_m \frac{Z_{im}^* Z_{mj}}{\hbar^2}. \quad (10.116)$$

For small values of s , we can expand the exponent of Eq. (10.115) and obtain the Gaussian overlap* (10.111)

$$\mathcal{N}\left(q + \frac{s}{2}, q - \frac{s}{2}\right) = \exp\left(-\frac{1}{2}\gamma(q)s^2\right), \quad (10.117)$$

with

$$\gamma(q) = \text{Tr } A = \sum_{mi} |P_{mi}|^2 / \hbar^2 = \frac{1}{\hbar^2} (\langle q | \hat{P}^2 | q \rangle - \langle q | \hat{P} | q \rangle^2). \quad (10.118)$$

We see that the crucial parameter in this approximation is the fluctuation of the operator \hat{P} in the Slater determinant $|q\rangle$. If it is large compared to \hbar/s , we can neglect higher terms in Eq. (10.117) and end up with the Gaussian shape. For a general collective operator, \hat{P} , γ grows roughly with the particle number. Therefore, the Gaussian overlap approach is justified for heavy systems.

The function $\gamma(q)$ determines some sort of a metric along the path $|q\rangle$. It turns out to be convenient to introduce a scale transformation for an absolute coordinate a in such a way that the norm has a constant width γ_0 . This is achieved by the transformation

$$\gamma_0(da)^2 = \gamma(a)(da)^2, \quad a = \int^a \sqrt{\gamma(a')/\gamma_0} da'. \quad (10.119)$$

In first order we then get, in the exponent of Eq. (10.117),

$$\gamma\left(\frac{a+a'}{2}\right)(a-a')^2 = \gamma_0(\alpha-\alpha')^2.$$

In the following we assume that we are working with this absolute coordinate.

In the case of a Gaussian overlap, it is rather simple to derive an equation of motion in the coordinate q [Vi 75, GG 75, Ka 73, OU 75], because we can now calculate $\mathcal{N}^{1/2}$ in Eq. (10.10) analytically. It is easy to show that $\mathcal{N}(a, a')$ can be written as

$$\mathcal{N}(a, a') = \int dq \sqrt{\gamma_0} \mathcal{N}^{1/2}(a, q) \mathcal{N}^{1/2}(q, a'),$$

with

$$\mathcal{N}^{1/2}(a, q) = \left(\frac{2}{\pi}\right)^{1/4} \exp(-\gamma_0 \cdot (a-q)^2). \quad (10.120)$$

The expectation values of the Hamiltonian H for the GCM function

$$|\Psi\rangle = \int da f(a)|a\rangle \quad (10.121)$$

* In the case where $|q\rangle$ also has time odd components, we gain an additional phase [see Eq. (11.79)].

are then given by:

$$\begin{aligned}\langle \Psi | H | \Psi \rangle &= \int da da' f^*(a) \mathcal{R}(a, a') h(a, a') f(a') \\ &= \int da da' f^*(a) \int dq \sqrt{\gamma_0} \mathcal{R}^{1/2}(a, q) h(a, a') \mathcal{R}^{1/2}(q, a') f(a').\end{aligned}\quad (10.122)$$

In the next step, we replace $h(a, a')$ by a differential operator, the collective Hamiltonian

$$h(a, a') \hat{=} \mathcal{H}_{\text{coll}}\left(q, \frac{\partial}{\partial q}\right), \quad (10.123)$$

which no longer depends on a and a' . To achieve this, we use the fact that $\mathcal{R}^{1/2}(a, q)$ is sharply peaked at $a = q$ and expand $h(a, a')$ at the point $a = a' = q$ up to second order in the differences $(a - q)$ and $(a' - q)$. Here we again use the property that $h(a, a')$ is a well-behaved smooth function:

$$\begin{aligned}h(a, a') &= h + h_x \cdot (a - q) + h_y \cdot (a' - q) + \frac{1}{2}(h_{xx} \cdot (a - q)^2 \\ &\quad + 2h_{xy} \cdot (a - q)(a' - q) + h_{yy} \cdot (a' - q)^2),\end{aligned}\quad (10.124)$$

where

$$\begin{aligned}h &= h(q, q) = \langle q | H | q \rangle, \quad h_x = \frac{\partial}{\partial a} h(a, a') \Big|_{a=a'=q}, \quad h_y = \frac{\partial}{\partial a'} h(a, a') \Big|_{a=a'=q} \\ h_{xx} &= \frac{\partial^2}{\partial a^2} h(a, a') \Big|_{a=a'=q}; \quad h_{xy} = \frac{\partial^2}{\partial a \partial a'} h(a, a') \Big|_{a=a'=q}; \quad h_{yy} = \dots.\end{aligned}\quad (10.125)$$

The linear derivations do not contribute to the final result because of time-reversal invariance. To see this and to get a simple expression for the second derivatives, we write the full Hamilton overlap as [see Eq. (10.91)],

$$\mathcal{K}(a, a') = \langle q | e^{i(a-q)\hat{P}/\hbar} H e^{-i(a'-q)\hat{P}/\hbar} | q \rangle, \quad (10.126)$$

and get [with a similar expression for $\mathcal{R}(a, a')$] ($\mathcal{R}(a, a) = 1$)

$$\begin{aligned}\frac{\partial}{\partial a} h(a, a') \Big|_{a=a'=q} &= \frac{\partial}{\partial a} \left(\frac{\mathcal{K}(a, a')}{\mathcal{R}(a, a')} \right) \Big|_{a=a'=q} \\ &= \frac{i}{\hbar} \langle q | \hat{P} H | q \rangle = 0\end{aligned}\quad (10.127)$$

and

$$h_x - h_y = \frac{i}{\hbar} \langle q | \hat{P} H + H \hat{P} | q \rangle = 0.$$

In the same way, we find

$$h_{xx} = \frac{1}{\hbar^2} \langle q | \hat{P}^2 H | q \rangle_L := -\frac{1}{\hbar^2} (\langle q | \hat{P}^2 H | q \rangle - \langle q | H | q \rangle \langle q | \hat{P}^2 | q \rangle), \quad (10.128)$$

$$h_{xx} = h_{yy}$$

and so on. The index L (linked) in this context* means that we have to subtract the product of the corresponding matrix elements for the norm and the expectation value of H . Similar expressions can be derived for h_{xy} and h_{yy} . In particular, we get

$$\frac{1}{4}(h_{xx} - 2h_{xy} + h_{yy}) := \frac{-1}{\hbar^2} \langle q | \hat{P}^2 H | q \rangle_L = \frac{-1}{4\hbar^2} \langle q | [\hat{P}, [H, \hat{P}]_+]_+ | q \rangle_L. \quad (10.129)$$

We now come back to Eq. (10.122) and insert (10.124). Since the functions $\mathcal{R}^{1/2}(a, q)$ have Gaussian form (10.120), we can express terms $(a - q) \cdots$ by

$$(a - q)\mathcal{R}^{1/2} = \frac{1}{2\gamma_0} \frac{\partial}{\partial q} \mathcal{R}^{1/2}; \quad (a - q)^2 \mathcal{R}^{1/2} = \left(\frac{1}{4\gamma_0^2} \frac{\partial^2}{\partial q^2} + \frac{1}{2\gamma_0} \right) \mathcal{R}^{1/2}. \quad (10.130)$$

After partial integrations we return to the general coordinates (10.119) and obtain, if we neglect higher than second-order derivatives of h (we have to realize that despite of (10.127) the term $\partial/\partial q h_x = h_{xx} + h_{xy}$ contributes):

$$\langle \Psi | H | \Psi \rangle = \int \sqrt{\gamma} dq g^*(q) \mathcal{K}_{\text{coll}} \left(q, \frac{\partial}{\partial q} \right) g(q), \quad (10.131)$$

where

$$g(q) = \int \mathcal{R}^{1/2}(q, a) f(a) da. \quad (10.132)$$

The collective Hamiltonian is given by

$$\mathcal{K}_{\text{coll}} = - \frac{1}{\sqrt{\gamma}} \frac{\partial}{\partial q} \sqrt{\gamma} \frac{\hbar^2}{2M(q)} \frac{\partial}{\partial q} + V(q) \quad (10.133)$$

with the inertial parameter

$$\frac{1}{M(q)} = \frac{-1}{2\gamma^2} (h_{xx} - h_{xy}) = \frac{\langle q | [\hat{P}, [H, \hat{P}]_+]_+ | q \rangle_L}{4\langle q | \hat{P}^2 | q \rangle^2} \quad (10.134)$$

and the potential energy

$$V(q) = \tilde{V}(q) - \epsilon_0(q), \quad \tilde{V}(q) = \langle q | H | q \rangle, \quad (10.135)$$

$$\epsilon_0(q) = \frac{h_{xy}}{2\gamma} = \frac{\langle q | \hat{P}^2 | q \rangle}{2M(q)} + \frac{\hbar^2}{8\langle q | \hat{P}^2 | q \rangle} \frac{\partial^2}{\partial q^2} \tilde{V}(q). \quad (10.136)$$

$$\hbar^2 \frac{\partial^2}{\partial q^2} \tilde{V}(q) = - \langle q | [\hat{P}, [\hat{P}, H]_-]_- | q \rangle.$$

We end up with a collective Hamiltonian in the variable q . Its potential energy $V(q)$ is not simply the static expectation value of the Hamiltonian, but is corrected for the value $\epsilon_0(q)$, which is called the zero-point energy [Re 75c, 78]; because an oscillating wave packet $|q\rangle$ of the form (10.84) in

* For the general definition of linked matrix elements see, for instance, [VS 71].

the vicinity of the minimum of $V(q)$ would have just this energy (in this case $\hbar^2/\langle q|\hat{P}^2|q\rangle = 4\langle q|\hat{Q}^2|q\rangle$). Equations (10.133)–(10.136) are again exact for our harmonic oscillator model of Section 10.5. They also turn out to be strictly equivalent to Eqs. (10.103)–(10.109), if we specialize to Gaussian norm.*

If we solve the equation of motion with (10.133) for an oscillation in a potential $\tilde{V}(q)$, we get a ground state having a zero-point energy higher than the HF minimum in the potential V . Calculations [Go 77] showed that the potential $V = \tilde{V} - \epsilon_0$ has a ground state which lies just below the HF value (see Fig. 12.6).

The inertia parameter M in Eq. (10.134) turns out to be coordinate dependent. It is usually called *Yoccoz-inertia* for reasons which we will see in Section 11.4. In the case of pure translations, it is not the bare mass of the nucleus. It is a great theoretical disadvantage of the primitive version of the GCM theory that it does not yield the proper mass. This does not, however, mean that the results of this theory are necessarily bad.

Several attempts have been made to improve the theory in order to obtain the proper mass. Peierls and Thouless [PT 62] proposed to use a GCM with two generator coordinates, a coordinate q and a momentum p . As discussed in Section 11.4, this procedure yields Galilei invariant wave functions in the translational case and the proper mass.

On the other hand, it is quite cumbersome to use two generator coordinates.[†] Holzwarth and Villars [Vi 75] therefore proposed to generalize the GCM ansatz in the following way:

$$|\Psi\rangle = \int dq e^{\hat{S}(q)} \frac{\partial}{\partial q} |\Phi(q)\rangle f(q),$$

where $\partial/\partial q$ acts only on the weight function $f(q)$, whereas the single-particle operator $\hat{S}(q)$ acts on the wave function. With an appropriate choice for the operator \hat{S} , we obtain in this way the proper mass parameter using only one generator coordinate.

10.7.5 The Lipkin Model

In order to give a demonstrative example of this theory, we again take the Lipkin model (Sec. 10.3). For large particle numbers Ω the norm overlap function (10.32) behaves like a Gaussian. With $\phi = \varphi - \varphi'$, $\Psi = \frac{1}{2}(\varphi + \varphi')$, we get

$$\mathcal{R}(\phi) = \exp\left(-\frac{1}{8}\Omega\phi^2\right) + O\left(\frac{1}{\Omega}\right) \quad (10.137)$$

*In order to verify this, we have to realize that $(\hbar^2/2\langle q|\hat{P}^2|q\rangle)\partial^2/\partial q^2\mathcal{R}|_{q=0} = -(1/2)\partial^2/\partial q^2\mathcal{C}|_{q=0}$.

[†]In this context, see also [HW 72, 74, GG 79].

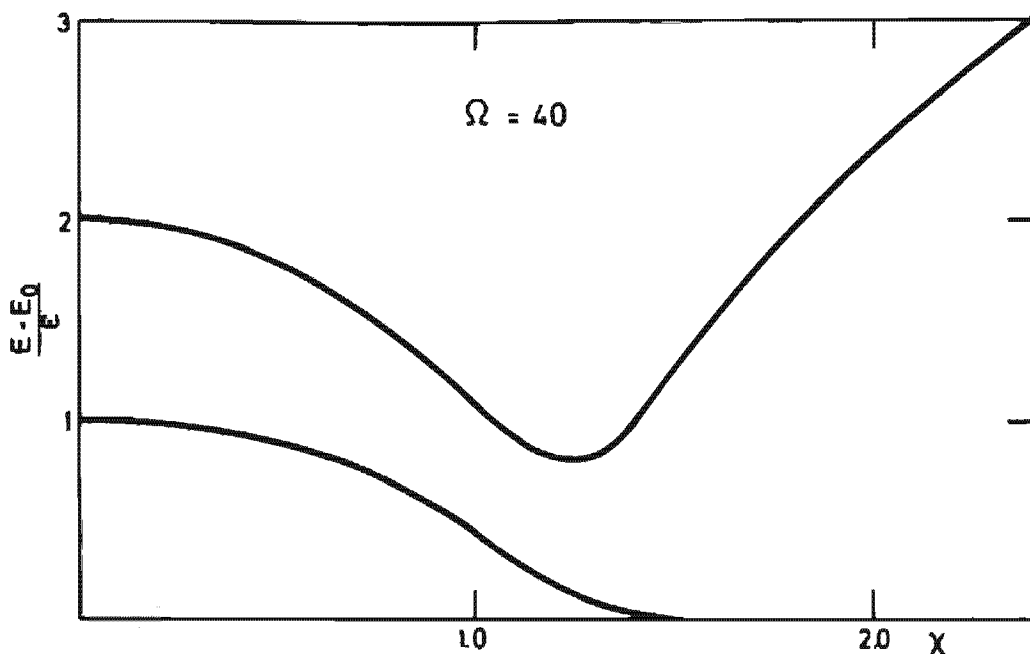


Figure 10.1. Excitation energies of the first and second excited states for $\Omega = 40$. (From [Ho 73].)

and

$$\mathcal{K}(\Psi + \frac{1}{2}\phi, \Psi - \frac{1}{2}\phi) = \left\{ \mathcal{K}(\Psi, \Psi) + \frac{\Omega}{4} B(\Psi) + B(\Psi) \frac{\partial^2}{\partial \phi^2} \right\} \mathcal{R}(\phi); \quad (10.138)$$

with

$$B(\Psi) = -\frac{\epsilon}{\Omega} (\cos \Psi + \chi(1 + \sin^2 \Psi)). \quad (10.139)$$

From Eqs. (10.104) and (10.108) or (10.134) and (10.135), we get for the mass

$$\frac{1}{M(\Psi)} = \frac{2\epsilon}{\Omega} (\cos \Psi + \chi(1 + \sin^2 \Psi)) \quad (10.140)$$

and for the potential

$$V(\Psi) = -\frac{\epsilon}{2} \Omega \left(\cos \Psi + \frac{1}{2} \chi \sin^2 \Psi \right) - \frac{\epsilon}{4} (2 \cos \Psi + 3 \chi \sin^2 \Psi) + O\left(\frac{1}{\Omega}\right). \quad (10.141)$$

These two quantities are shown as a function of $\alpha = \Psi/2$ in Fig. 5.2. The dashed lines give the potential V and the chain curves the inverse mass parameter $1/M$.

The solution of the collective equation for the two first excited states with these potentials are given in Fig. 10.1 and compared with the exact ones.

The approximate solutions and the exact ones cannot be distinguished. This is not very astonishing, since we know that the GCM is able to produce the exact result (Sec. 10.4) and the terms neglected in the symmet-

ric momentum expansion and the Gaussian overlap approach in this model are of the order $1/\Omega$.

10.7.6 The Multidimensional Case

For the sake of simplicity we have so far treated only one generator coordinate. In the general case of several coordinates $\mathbf{a} = (a_1, \dots, a_f)$, Kamiah [Ka 73] and Onishi et al. [OU 75] have used a general Gaussian ansatz for the norm overlap

$$\mathcal{A}(\mathbf{a}, \mathbf{a}') = \mathcal{A}\left(\mathbf{q} + \frac{\mathbf{s}}{2}, \mathbf{q} - \frac{\mathbf{s}}{2}\right) = \exp\left(-\frac{1}{2}s^2(\mathbf{q}, \mathbf{s})\right), \quad (10.142)$$

where $\mathbf{q} = \frac{1}{2}(\mathbf{a} + \mathbf{a}')$, $\mathbf{s} = \mathbf{a} - \mathbf{a}'$, and

$$s^2 = \gamma_{ij}(\mathbf{q}) \cdot s^i s^j \quad (10.143)$$

is the squared geodesic distance in a curved space characterized by the coordinates \mathbf{a} . Applying the theory of Riemann spaces one can proceed as in Section 10.7.4 and end up with a collective Hamiltonian

$$\mathcal{H}_{\text{coll}} = -\frac{1}{\sqrt{\gamma}} \frac{\partial}{\partial q^i} \sqrt{\gamma} \left(\frac{\hbar^2}{2M} \right)^{1/2} \frac{\partial}{\partial q^i} + \tilde{V}(\mathbf{q}), \quad (10.144)$$

where $\gamma(\mathbf{q})$ is the determinant of the metric tensor γ_{ik} defined by the ansatz (10.143). The inertia tensor and the potential have a form analogous to Eqs. (10.134 ff):

$$\left(\frac{\hbar^2}{2M(\mathbf{q})} \right)_{ij} = -\frac{1}{4} \left(\frac{\Delta}{\Delta q^i} \frac{\Delta}{\Delta q^j} h(\mathbf{q}, \mathbf{q}') - \frac{\Delta}{\Delta q^i} \frac{\Delta}{\Delta q'^j} h(\mathbf{q}, \mathbf{q}') \right)_{\mathbf{q}=\mathbf{q}'} \quad (10.145)$$

$$V(\mathbf{q}) = \tilde{V}(\mathbf{q}) - \epsilon_0(\mathbf{q}); \quad \tilde{V}(\mathbf{q}) = \langle \mathbf{q} | H | \mathbf{q} \rangle,$$

$$\epsilon_0(\mathbf{q}) = \gamma_{ij} \left(\frac{\hbar^2}{2M} \right)^{1/2} + \frac{1}{8} \gamma^{ij} \frac{\Delta}{\Delta q^i} \frac{\Delta}{\Delta q^j} V(\mathbf{q}),$$

where $\Delta/\Delta q^i$ are covariant derivations of the tensor fields as defined, for instance, in [LL 59, vol. II, Chap. 10]. The operator of the kinetic energy is similar to the operator we get from Pauli quantization [Eq. (1.53)]. In the latter case, however, the inertia tensor is identical with the metric tensor. Now we have to distinguish between the *metric* determined completely by the kinematical properties, that is, by \mathcal{A} , and the *inertia* given by the dynamical behavior of \mathcal{H} .

10.8 The Choice of the Collective Coordinate

In Section 10.4 we saw that the ansatz (10.2) contains, in principle, the exact answer to the many-body problem if we choose enough generator coordinates. Unfortunately, this is by far too large a problem to be handled exactly, and in practice we are restricted to the treatment of one or perhaps a few generator coordinates at a time. It is therefore very important to choose the proper generator coordinate, that is, the most suitable set $|\mathbf{q}\rangle = |\Phi(\mathbf{q})\rangle$. In the following, we again restrict ourselves to a real coordinate q with time even functions $|q\rangle$.

The set of generating functions $|\Phi(q)\rangle$ represents a path in the multidimensional energy surface

$$E[\Phi] = \langle\Phi|H|\Phi\rangle.$$

To determine this path, we again apply the variational principle and require that the expectation value of the energy in the state

$$|\Psi\rangle = \int f(q)|\Phi(q)\rangle dq \quad (10.146)$$

is stationary not only with respect to variations of the weight function f , but also with respect to the path $|\Phi(q)\rangle$. This *double variational method* gives us a set of coupled equations [HY 74, Vi 75]

$$\int dq' \langle\Phi(q)|H - E|\Phi(q')\rangle f(q') = 0, \quad (10.147a)$$

$$\int dq dq' f^*(q) \langle\delta\Phi(q)|H - E|\Phi(q')\rangle f(q') = 0, \quad (10.147b)$$

which, in principle, have to be solved by iteration.

At a point q , the variation $|\delta\Phi\rangle$ is not completely arbitrary. We can only allow for changes $|\delta\Phi\rangle_{\perp}$ that are orthogonal to the path itself. A variation parallel to the path could be absorbed in a variation of the weight function.

Since the length of $|\delta\Phi\rangle_{\perp}$ is arbitrary, Eq. (10.147b) may be written as

$$\int dq'_{\perp} \langle\delta\Phi(q)|H - E|\Phi(q')\rangle f(q') = 0. \quad (10.148)$$

In the next step, we make two essential assumptions:

- (i) We again use the fact that the overlap functions $\langle\Phi(q)|\dots|\Phi(q')\rangle$ are sharply peaked at $q = q'$, such that for fixed q only a certain q' region contributes to the integral (10.148).
- (ii) We assume that in this q' -region, the path does not bend too strongly, such that $|\delta\Phi(q)\rangle$ is orthogonal to the path in this whole region.

Under these conditions, the second equation (10.147b) decouples from the first one (10.147a), and for variations $|\delta\Phi\rangle_{\perp}$ that do not change the norm of $|\Phi\rangle$ [Vi 75] we find

$$_{\perp} \langle\delta\Phi|H|\Phi\rangle = 0. \quad (10.149)$$

The variation $|\delta\Phi\rangle_{\perp}$ is restricted to be orthogonal to the path. A variation parallel to the path is given by

$$|\delta\Phi\rangle_{\parallel} = |\Phi(q + \delta q)\rangle - |\Phi(q)\rangle = -\delta q \frac{i}{\hbar} \hat{P} |\Phi(q)\rangle. \quad (10.150)$$

The operator \hat{P} is a representation of $-(\hbar/i)\partial/\partial q$ in the many-body Hilbert space. It acts on the particle coordinates in $|\Phi\rangle$ but not on the parameter q . Variations orthogonal to the path now have the form

$$|\delta\Phi\rangle_{\perp} = |\delta\Phi\rangle - \hat{P}|\Phi\rangle \frac{\langle\Phi|\hat{P}|\delta\Phi\rangle}{\langle\Phi|\hat{P}^2|\Phi\rangle}, \quad (10.151)$$

where $|\delta\Phi\rangle$ is an unrestricted variation. Variations of the potential energy $V(q) = \langle\Phi(q)|H|\Phi(q)\rangle$ parallel to the path are given by

$$\frac{dV}{dq} = +\frac{i}{\hbar} \langle\Phi|[\hat{P}, H]|\Phi\rangle \quad (10.152)$$

and those orthogonal to it have to vanish:

$$_{\perp} \langle\delta\Phi|H|\Phi\rangle = \langle\delta\Phi|H - \frac{\hbar}{2i} \frac{dV}{dq} \frac{\hat{P}}{\langle\Phi|\hat{P}^2|\Phi\rangle}|\Phi\rangle = 0. \quad (10.153)$$

In deriving this equation, we have used (10.152) and the fact that $|\Phi\rangle$ is time even. The problem (10.153) is a constrained variational principle, but the constraining operator is not Hermitian; we therefore restrict ourselves to cases in which \hat{P} can be decomposed.

$$\hat{P} = i(A^+ - A) \quad \text{with } A|\Phi\rangle = 0. \quad (10.154)$$

Examples are Slater determinants $|\Phi(q)\rangle$, where we have $A^+ = (1/i) \sum_m P_{mi} a_m^+ a_i$, or RPA wave functions, where A^+ is a creation operator for a boson (see also [ABC 77b]).

In such cases, we can define a Hermitian constraining operator

$$\hat{Q} = \frac{\hbar}{2\langle\Phi|\hat{P}^2|\Phi\rangle} (A^+ + A) \quad (10.155)$$

and from Eqs. (10.152) and (10.153) get

$$\langle\delta\Phi|H - \frac{dV}{dq} \cdot \hat{Q}|\Phi\rangle = 0, \quad (10.156)$$

which gives us the optimal path. It is determined in such a way that the energy surface has a minimum with respect to all variations perpendicular to it. This means, for instance, that it follows the bottom of the fission valley (see Sec. 7.6). Equation (10.156) is a constrained variational problem. The constraining operator \hat{Q} is not imposed on the system, but is determined self-consistently by the system itself. It does not push the system into unphysical regions, but acts like an inertial force in the sense of d'Alembert [Vi 77].

The actual calculation of $|\Phi(q)\rangle$ requires a double iteration: Starting with some initial value \hat{Q}_0 for the constraining operator, we have to determine $|\Phi_0(q)\rangle$ by a constrained HF calculation. In a second step, we have to calculate the operator \hat{P} at each point q . It can be done, for instance, by a solution of Eq. (8.106) in linear response theory [see Eqs. (8.136) and (12.120)]. From the operator \hat{P} a new constraint \hat{Q} is determined. This has to be continued until convergence is achieved.

At the end, we have to solve the Hill-Wheeler equations (10.5) for the determined generating functions $|\Phi(q)\rangle$.

This double iteration, naturally, is extremely time consuming, and the prescription of a self-consistent constraint in the GCM has up to now been tested only on a three-level Lipkin model [HY 74] and in the $s-d$ shell [PL 77] with quite promising results. For heavier nuclei the gradient method described in Chapter 7 could facilitate the problem.

10.9 Application of the Generator Coordinate Method for Bound States

In the last few years, the GCM has been applied to many problems of nuclear structure, such as giant resonances and shape and pairing vibrations, and to coupling mechanisms between different modes. In most cases, generating functions with proper symmetries were used, such as Slater determinants projected onto good angular momentum or particle number (see Chap. 11). The Hill-Wheeler equation (10.5) is usually solved by discretization. In many cases, very few mesh points were chosen. Therefore, there were no problems with zero eigenvalues of the norm. We will discuss only a few examples in the following.

10.9.1 Giant Resonances

The breathing mode and quadrupole oscillations in *light nuclei* have been investigated using Slater determinants $\Phi_{JMP}(b, \delta)$ of deformed oscillator functions projected onto good angular momentum J, M and linear momentum $P=0$; they depend on the oscillator lengths $b = (b_x^2 b_y)^{1/3}$ and the deformation $\delta = b_x/b_y$ [CBA 73, AC 75]. For $\delta = 1$, the parameter b describes a scaling of the radial coordinate, and therefore a breathing mode. (It has already been used in a very early paper by Ferrell and Visscher [FV 56]). The coordinate δ describes the quadrupole oscillation. The Hill-Wheeler Eq. (10.5) is solved by discretization (up to 50 mesh points) with the interaction of Brink and Boeker [BB 67]. The lowest eigenstate for each value of J gives the ground state rotational band. It is in good agreement with projected HF wave functions. The excited states are vibrations. One finds anharmonicities in the spectra and for the moments and couplings between the different modes.

Faessler et al. [KRG 76] have investigated the monopole modes in the closed shell nuclei ^{16}O , ^{40}Ca , ^{90}Zr , and ^{208}Pb with constrained HF wave functions $\Phi(r_p, r_n)$ as generating states. The coordinates r_p, r_n are the rms radii for protons and neutrons, and the constraining operator (see Chap. 7) is given by

$$r^2 \left(1 + \exp\left(\frac{r - R}{a}\right) \right)^{-1}.$$

The fermi distribution makes sure that the constraining operator is bounded and the corresponding HF Hamiltonian has discrete eigenstates. The coupling to the continuum is neglected. The interaction is a modified δ -interaction of the Skyrme type, where the overlap integral \mathcal{K} can be calculated in a simple way. With the constrained HF calculation, the scaling prescription can be checked and one finds that it is well justified. Equation (10.5) is again solved by discretization. The ground state energy of the GCM agrees very well with the HF energy. The excited states are breathing modes. Table 10.1 gives some results.

The energy of the isoscalar breathing mode in ^{208}Pb is 13.32 MeV and corresponds quite well to the liquid drop model with an incompressibility (Eq. 5.95) $K \approx 200$ MeV and with the RPA calculation with the Migdal force [RS 74a].

The Skyrme interaction (see Sec. 4.4.3) in a basis of oscillator wave functions with variable oscillator parameters provides rather simple analytic expressions for \mathcal{K} and \mathcal{N} . They were used by Giraud and Grammaticos [GG 75] in connection

Table 10.1. Results of GCM calculations for breathing modes: Excitation energy E , reduced transition probabilities, fraction S of the energy weighted sum rule (8.154), proton and neutron transition amplitudes A_p and A_n , isospin expectation value $\langle T^2 \rangle$, and proton and neutron radii r_p and r_n . (From [KRG 76].)

Nucleus	E (MeV)	$B(E0)$ (fm^4)	S	A_p (fm^2)	A_n (fm^2)	$\langle T^2 \rangle$	r_p (fm)	r_n (fm)
^{16}O	0					0.00	2.70	2.67
	23.96	106	0.56	10.3	9.7	0.00	2.91	2.86
^{40}Ca	0					0.02	3.41	3.36
	20.73	502	0.55	22.4	20.4	0.14	3.50	3.44
^{90}Zr	0					30.12	4.22	4.30
	17.46	1530	0.45	39.1	49.8	30.12	4.25	4.33
^{208}Pb	0					506.38	5.46	5.66
	13.32	5749	0.36	75.8	127.4	506.41	5.47	5.67
	21.29	359	0.04	-19.0	130.6	506.59	5.45	5.71
	38.18	239	0.04	-15.4	26.3	506.68	5.44	5.79

with the moment expansion (see Sec. 10.7) for the description of monopole modes.

Flocard and Vautherin [FV 75, 76] solved the HW Eq. (10.5) for monopole, quadrupole, and dipole excitations with Slater determinants of oscillator wave functions and a Skyrme force by discretization (up to 143 mesh points). The ground state again agrees well with the HF state. Figure 10.2 shows weight functions g_i [Eq. (10.12)] for the ground state (g_0) and the first two excited breathing modes (g_1, g_2) in ^{16}O and the diagonal part of the energy overlap ($\mathcal{K}(r, r)$ in Eq. (10.135)), which corresponds more or less to the potential $V(r)$ of the collective coordinate. We see that the functions g behave qualitatively like oscillator functions in this potential.

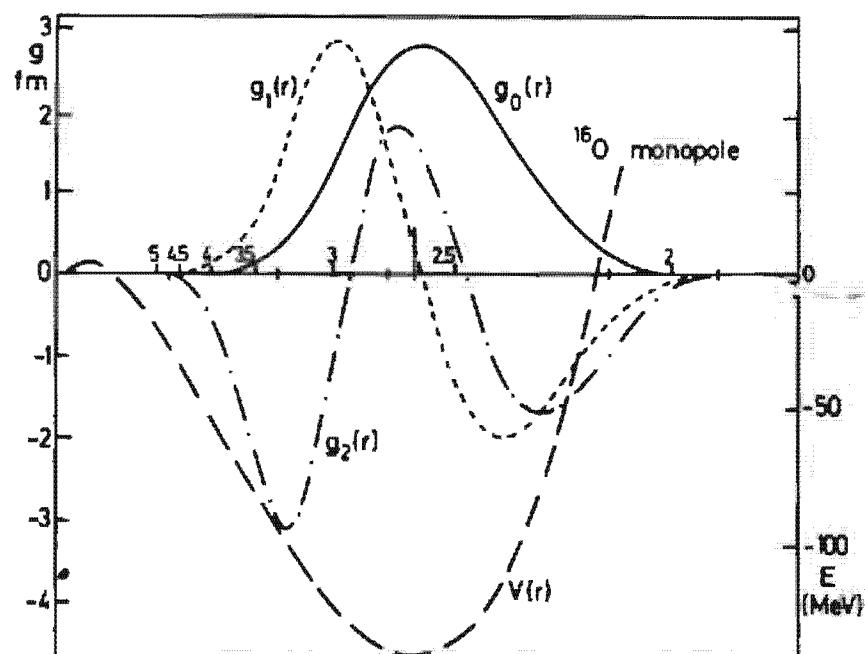


Figure 10.2. Weight functions g_i for the first three GCM states in ^{16}O in the case of monopole vibrations and the diagonal part of the energy overlap $V(r)$. (From [FV 76].)

For increasing mass number, the width of the function g_0 decreases. For heavy nuclei, it is sharply peaked at a certain value of the generator coordinate. This means that the GCM wave function is given, to a good approximation, by a Slater determinant with this parameter.

The GCM has also been applied to low-lying *shape vibrations* in light nuclei. As long as we restrict them to a configuration space which includes only an $s-d$ shell [IGMA 75, MMR 75], they can be compared to an exact diagonalization of the Hamiltonian in this subspace [PW 72, Wh 72, SZ 72], and one finds good agreement for many levels. In some cases, however, the agreement is rather poor. This means that the corresponding state does not lie in the space spanned by the generating functions. A pure quadrupole constraint [KK 74] is then less effective than a constraining operator determined by the system itself, as discussed in Section 10.8 [PL 77].

10.9.2 Pairing Vibrations

In Sec. 8.8 we saw that in the description of pairing vibrations by the RPA based on a normal fluid ground state, we find a phase transition for a critical coupling constant G_c . In this region, neither the RPA nor the BCS model works well. The GCM provides a method to overcome this difficulty.

Several authors [JMR 72, ISY 73] proposed the use of BCS wave functions [see Eq. (6.31)] projected onto good particle number (see Sec. 11.4) as generating states

$$|\Phi^N\rangle = P^N \prod_{\alpha, m} (u_\alpha + v_\alpha a_{\alpha m}^\dagger a_{\alpha -m}^\dagger) |-\rangle, \quad (10.157)$$

where P^N is the projection operator onto particle number N , and $\alpha = (nlj)$ are the quantum numbers of the different j -shells. For independent parameters $p_\alpha = u_\alpha/v_\alpha$, these states span the seniority-zero subspace of the full Hilbert space (see Sec. 6.2 and [JMR 69]). For occupation probabilities u_α, v_α of the BCS-form (6.59) that depend only on one parameter, Δ , this is still true to a good approximation. Since we expect the pairing vibrations with $J^* = 0^+$ to lie in this subspace (see Sec. 8.8), the ansatz (10.157) is particularly useful for describing them within the GCM. The second parameter, the chemical potential λ , can be determined by the BCS-number equation (6.53) for each point in the Δ mesh, or can be used as a second generator coordinate (Sorensen et al. [SS 72b]).

This method works equally well for superconducting nuclei, non-superconducting nuclei, and in the intermediate region. It has been applied with the pure pairing force [SS 72b, FGP 73] to simple models and to pairing vibrational spectra in the Pb, the Ni, and Sn regions.

Figure 10.3 shows the components of the GCM wave function for the ground state in ^{208}Pb and for the so-called pairing vibrational state at 4.87 MeV, which is to a large extent a $2p-2h$ state or a superposition of the $2p$ pairing vibration in ^{210}Pb and of the $2h$ -pairing vibration in ^{206}Pb . The $0p-0h$, $2p-2h$, and $4p-4h$ components are given as a function of the pairing strength G . The realistic value of G , which gives the right mass difference $M(^{206}\text{Pb}) + M(^{210}\text{Pb}) - 2M(^{208}\text{Pb})$, is $G = 0.1166$ (MeV). At this value, already 10% of the ground state is $2p-2h$ and the pairing vibration has roughly 12% $4p-4h$ admixtures.

More realistic forces have been used by Faessler et al. [AGM 74] in the $p-f$ shell. Here the BCS functions in Eq. (10.157) were replaced by constrained HFB

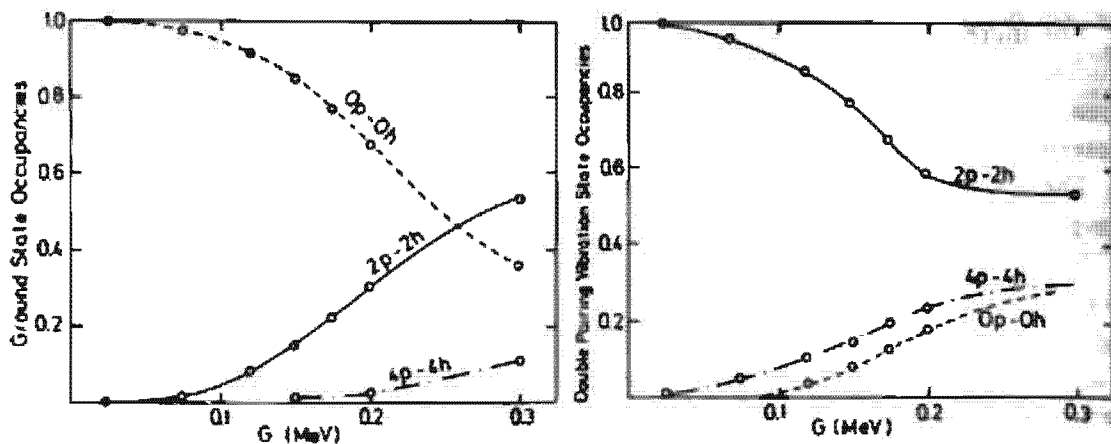


Figure 10.3. Percentage of ^{208}Pb ground state and pairing vibrational state at 4.87 MeV, which is $0p - 0h$, $2p - 2h$, and $4p - 4h$ as a function of G . (From [SS 72b].)

functions (see Sec. 7.6). The constraining operator is a pairing potential of variable strength and the generator coordinate is the resulting energy contribution $-\frac{1}{4}\text{Tr}(\kappa^* \delta \kappa)$. The generating functions were determined from these HFB functions by projection onto good particle number and angular momentum. The results are in good agreement with experimental energy levels and transfer cross sections.

This method provides a tool for investigating the dependence of the pairing correlations (measured by the energy gap Δ) on the effective pairing strength G_{eff} in the ground and pairing vibrational states (Fig. 10.4). In cases where the ground state is strongly paired (large G_{eff}), the pairing vibration has weak pairing correlations. This is the case, for instance, in the rare earth nuclei. The opposite is true for nuclei with weak pairing in the ground state, as in Ti (see also [KJ 70]). From Section 7.7 we know that the Coriolis antipairing effect (CAP) reduces the effective pairing strength with increasing angular momentum. This produces decreasing pairing correlations in the ground state of the rare earth nuclei, and increasing pairing correlations in the pairing vibrational mode. The same is no longer true, however, for lighter nuclei such as Ti.

Finally, we can describe various couplings between different modes by the GCM, if we introduce more generator coordinates, such as deformation parameters

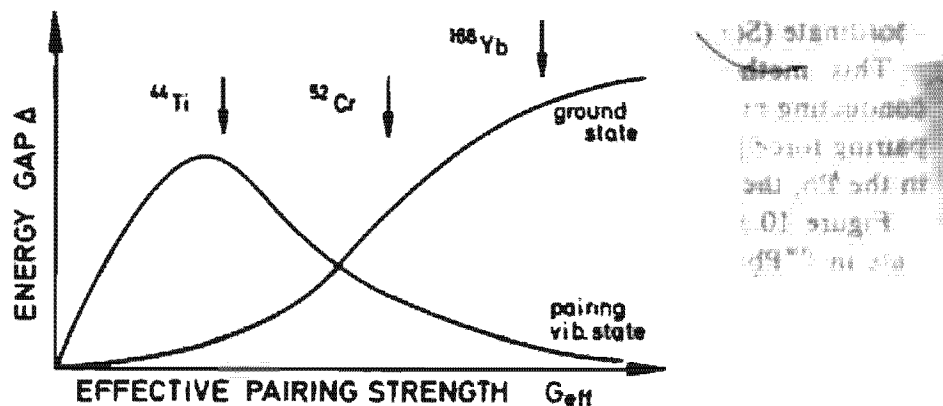


Figure 10.4. Schematic picture of the dependence of the energy gap Δ on the effective pairing strength G_{eff} . The position is indicated by arrows for a few nuclei. (From [GSF 75].)

β , pairing parameters Δ , and so on [MAG 75]. We can even include *single-particle degrees of freedom* by making the generalized ansatz [DMG 76, MGA 77]:

$$|\Psi\rangle = \int da f(a)|\Phi(a)\rangle + \sum_i \int da f^i(a)|\Phi_i(a)\rangle, \quad (10.158)$$

where $|\Phi(a)\rangle$ are, for instance, the ground states of a constrained HF calculation dependent on some deformation parameter a and $|\Phi_r(a)\rangle$ are the corresponding $1p - 1h$ states, and so on.

CHAPTER 11

Restoration of Broken Symmetries

11.1 Introduction

In the investigation of the properties of the nuclear interaction (Chap. 4), we showed that the exact many-body Hamiltonian H is invariant under a number of symmetry operations, that is, it commutes with the corresponding symmetry operator S :

$$[H, S] = 0. \quad (11.1)$$

Therefore, we can always find wave functions that are simultaneous eigenfunctions of H and S . Examples are the three components of the linear momentum \mathbf{P} , the particle number N , and the angular momentum operators \mathbf{J}^2, J_z .

We have also seen that this general property is very useful in cases of a few particles, where it can be used to reduce the size of the corresponding eigenvalue problem dramatically by working in appropriate eigenspaces of the symmetry operators. The elimination of the center of mass coordinate in a two-body system or angular momentum coupling techniques applied for a few particles outside a closed shell are examples.

In the general case of many particles and strong correlations, the proper treatment of symmetries is a serious problem: On the one hand, we want to describe the system by *simple wave functions*, such as product states of independently moving particles (or quasi-particles); on the other hand, we are not able to take into account *important correlations* between the nucleons by such simple wave functions if we require simultaneously the

proper symmetry behavior. The only translational invariant product wave functions, for example, are products of plane waves. They are certainly not able to describe the strong correlations among the nucleons, which cause their clustering into a finite nucleus.

In Chapter 2 we saw, however, that such correlations can be described by a mean field (the shell model) and that product states of shell model wave functions provide a very reasonable description of many nuclear properties. Such wave functions, however, break the translational symmetry.

It is a general procedure,* which is very important in nuclear physics, that correlations are treated by a *symmetry-violating mean field approach*. Whether such a description is possible and is a good approximation certainly depends on the nature of the correlations. The long-range particle-hole correlations which cause stable deformations, and the $p\bar{p}$ -correlations, which provide superfluid properties, are in any case of the mean field type. In Chapter 7 we saw that they can be treated by the HFB theory, a mean field approach that violates angular momentum and particle number. It turns out that the stronger the correlations, the better such an approximation. In analogy to solid state physics, we say that the system undergoes a *phase transition* to a symmetry-violating state, as, for instance, to a deformed state or to a superfluid phase. Of course, classical and macroscopic considerations enter our arguments when we say the nucleus is localized, is deformed, or has a superfluid phase. We will see later in this chapter that the mean field description of phase transition eventually becomes exact in very large (macroscopic) systems. This means that for certain measurable quantities it may be irrelevant as to whether we calculate them in the symmetry-broken mean field approach or in a symmetry-nonbreaking theory, which of course is, in principle, required by quantum mechanics. Imagine a droplet of the quantum fluid ^3He with various numbers of particles. Once the drop is so big that it can actually be "seen," it is certainly an exact description to consider the drop (or its mean field) as localized (wave packet), though quantum mechanics would still require a translationally invariant treatment for stationary states.

Nuclei are, of course, not macroscopic objects, but the heavier ones are big enough that a mean field treatment—which for a macroscopic drop would eventually become exact—is already a very good description for certain quantities. These quantities are, of course, those which are also macroscopically defined as, for instance, radius, deformation,[†] superfluid current, ground state energy, etc. Those quantities which are, however, of a quantum nature, as, for example, discrete energy spectra and transitions

* For a more detailed discussion of this point, see [Li 60a].

[†]The deformation of a nucleus is, of course, not a directly measurable quantity as in a macroscopic system, but it can be defined in a model-dependent way only rather indirectly over the "inner" quadrupole moment (see Secs. 1.5.2 and 11.4.6.4); once this relationship is established once and for all, the mean field theory also reproduces the nuclear deformation rather well over the whole periodic system.

between excited states, will not be describable in a pure mean field approach.

In particular, the product wave function is a very poor approximation of the exact many-body state. As we shall see, it has been tried to interpret the symmetry-violating wave function as a function in an "*intrinsic*" coordinate frame moving with the nucleus. All quantities which depend only on this internal function are eventually reproduced quite well in the mean field approach.

There are, however, two reasons to go beyond the mean field approach:

- (i) In nuclear physics we are also interested in quantities such as transition probabilities and electromagnetic moments, which can never be calculated from a symmetry-violating Nilsson wave function alone.
- (ii) The nucleus is a finite system. The phase-transition is therefore always smeared out. We often find a gradual transition from conservation to weak violation, and eventually a strong breaking of the symmetry. In cases of weak symmetry violation we have to go beyond the mean field approach and incorporate the symmetries properly.

In Section 11.2 we wish first to discuss in more detail the mechanism of symmetry breaking in the mean field approach. It gives us a better understanding of the methods used in Chapters 5, 6 and 7. We present this discussion here because in those chapters we did not yet have the techniques of Chapters 9 and 10.

To *restore the symmetries* broken in the mean field approach, there have been attempts to transform explicitly to an "*intrinsic*" system. Such attempts, however, are often intimately connected with basic difficulties. On the other hand, such ideas are used in many phenomenological models (see Sec. 1.5). We therefore discuss them briefly in Section 11.3. The usual means to develop a symmetry-conserving theory on the basis of wave functions obtained from a mean field approach is provided by *projection techniques* onto eigenspaces of the symmetry operator. These are discussed in Section 11.4.

We should also mention the RPA approximation, which goes beyond the static mean field approach. It includes higher correlations and provides an approximate restoration of the symmetry (see Sec. 8.4.7 and [UW 65, GW 68, MW 69b, MW 70, Bi 76, Ma 77a]). As we shall see in Section 12.3.2, we can also derive this method in a time-dependent mean field theory, which shows that this more general mean field approach can already restore some aspects of symmetry violation.

In this chapter we treat mainly the symmetry violations of *translational invariance* (transition to a *localized nucleus*), of *particle number* (phase transition to a *superfluid state*), and *angular momentum* (phase transition to a *deformed state*). There are, of course, also other symmetries, like the parity [BSB 69] (which is also broken in the context of pion condensation

[MKS 74, BF 74, BCD 75, BW 76]) or the isospin (which is only an approximate symmetry [GW 68]). They can be handled in a very similar fashion.

Investigations have also been carried out on the possibility of a crystalline structure of nuclear matter with a periodic long-range order described by non-plane-wave HF-states, which violate translational symmetry (Overhauser states [Ov 60, ALP 77, AAZ 77]). One finds that for realistic nuclear forces such wave functions generally yield a higher energy than plane waves. Only at very low subnuclear densities can a stable crystalline structure of α particles develop (see also [BC 73]).

Symmetry violations discussed in this chapter are based on the mean field approach. Certainly, there are also other symmetry breaking theories. They can sometimes be treated with similar techniques.

11.2 Symmetry Violation in the Mean Field Theory

As we saw in Section 4.3 and Chapter 7, in the nucleus there are very different correlations: On the one hand, there are the very short-range Brueckner correlations, which have nothing to do with symmetry violations. On the other hand, there are long-ranged correlations caused by ph and pp forces.* If they are weak, they can be treated by the RPA approximation and yield harmonic collective vibrations and a correlated ground state. If they become stronger we find anharmonicities and modes that are lowered drastically in energy (soft modes). The corresponding energy surface becomes very flat in one direction and, with sufficiently strong correlations, a sudden symmetry-violating minimum develops. In such cases the mean field approximation discussed in Chapter 7 yields non-vanishing deformation potentials Γ or pairing fields Δ as solutions of the nonlinear "gap equations" (7.41)

$$\Gamma_{lm} = \sum_{rs} v_{lmrs}^{ph} \rho_{rs}, \quad \Delta_{lm} = \sum_{rs} v_{lmrs}^{pp} \kappa_{rs} \quad (11.2)$$

where v^{ph} and v^{pp} are the effective forces in the ph and the pp channel and the densities ρ and κ [Eq. (7.22)] depend nonlinearly on Γ and Δ through the diagonalization of the HFB equations (7.42).

Since the densities ρ and κ are calculated with symmetry-breaking wave functions, they have a monopole part ρ_0, κ_0 , a quadrupole part ρ_2, κ_2 , and so on. They are obtained from coupling the indices r and s to angular momentum $I=0, 2, \dots$. ρ_0 corresponds to a spherical density distribution and yields the spherical part V_0 of the potential Γ . It is well pronounced for all nuclei and corresponds to the spherical shell model potential. In the following we shall work in this basis.

* We have to emphasize, however, that this does not mean that the range of the forces that produce these correlations is large.

Depending on the strength of the interactions v^{ph} and v^{pp} and on the level density in the vicinity of the fermi surface, the "gap" equations (11.2) may have non-vanishing solutions also for the quadrupole part Γ_2 , the monopole pairing field Δ_0 , and eventually for higher terms, which are less important in nuclei.* We can therefore divide the mean field into three parts, V_0 , Γ_2 , and Δ_0 . They are connected with the violation of translational symmetry, rotational symmetry, and particle number.

In Section 4.4.7 we saw that we can decompose the interactions v^{ph} and v^{pp} into components with different angular momentum. According to Eqs. (4.124) and (4.131), they are separable in the angles. Since the radial dependence only enters at the vicinity of the nuclear surface, we can replace it to a good approximation by a constant and get for the quadrupole part of v^{ph} , and from the monopole part of v^{pp} the well known pairing-plus-quadrupole model (see Sec. 7.4), which we shall use for the following discussion of phase transitions in the nucleus.

We first investigate the *quadrupole correlations*. In this case, the effective two-body Hamiltonian leading to the one body equation (11.2) can be written in the form

$$H = \sum_k \epsilon_k c_k^+ c_k - \frac{\chi}{2} \sum_\mu Q_\mu^+ Q_\mu; \quad \chi > 0. \quad (11.3)$$

c_k^+ , c_k are particle operators in the spherical shell model basis and ϵ_k are the corresponding eigenvalues of $T + V_0$. The quadrupole operators Q_μ are given by

$$Q_\mu = \sum_{k_1 k_2} \langle k_1 | r^2 Y_{2\mu} | k_2 \rangle c_{k_1}^+ c_{k_2}. \quad (11.4)$$

The "deformation" equation (11.2) now has the form (7.75) and determines the deformation parameters q_μ :

$$q_\mu = \chi \langle \Phi | Q_\mu | \Phi \rangle. \quad (11.5)$$

To avoid the problem of HF in open shells we furthermore assume that for vanishing interaction ($\chi=0$) the spherical subshells i with $\epsilon_i < \epsilon_F$ are occupied and the subshells ϵ_m with $\epsilon_m > \epsilon_F$ are empty.

For non-vanishing interactions the behavior of the system depends very much on the relation of the average level spacing in the vicinity of the fermi surface[†] to strength χ . For small level density, for instance, for magic nuclei, or for small values of χ we have the case of spherical nuclei. The "deformation" equation (11.5) only has the solution $q_\mu = 0$. It corresponds to a minimum in the energy surface and we can calculate vibrational states with the frequency Ω in the framework of the RPA [Eq. (8.135)]:

$$\frac{1}{\chi} = \sum_m \left| \langle m | r^2 Y_2 | i \rangle \right|^2 \frac{2(\epsilon_m - \epsilon_i)}{(\epsilon_m - \epsilon_i)^2 - (\hbar\Omega)^2}. \quad (11.6)$$

* For instance, octupole deformations (Γ_3) or quadrupole pairing (Δ_2); see also the multipole expansion in Sec. 4.4.7.

[†] See the analogous discussion of Δ in Section 6.3.5.

With increasing level density (i.e., if we go to nuclei far from closed major shells) or for increasing strength χ we come to a point where the RPA energy goes to zero, which is equivalent to the fact that the spherical solution $q_\mu = 0$ of Eq. (11.5) no longer corresponds to a minimum in the energy surface (see Sec. 8.4.3). There exists at least one deformed solution $|\Phi_0\rangle$ of Eq. (11.5), with

$$\langle \Phi_0 | Q_\mu | \Phi_0 \rangle \neq 0 \quad \text{for at least one } \mu. \quad (11.7)$$

It violates rotational symmetry. We are now able to define an *intrinsic coordinate system*, for instance, by the principal axis of the mass distribution in the function $|\Phi_0\rangle$. At the same time we see that there is now a whole set of solutions $|\Phi(\Omega)\rangle$ to the HF equations that are obtained from $|\Phi_0\rangle$ by an arbitrary rotation in space characterized by the Euler angles $\Omega = (\alpha, \beta, \gamma)$ [see Eq. (A.4)]

$$|\Phi(\Omega)\rangle = \hat{R}(\Omega)|\Phi_0\rangle \quad (11.8)$$

as it is schematically shown in Fig. 11.1.

Because of the rotational invariance of the Hamiltonian, all these solutions have the same energy

$$\langle \Phi(\Omega) | H | \Phi(\Omega) \rangle = \langle \Phi_0 | H | \Phi_0 \rangle. \quad (11.9)$$

In particular, this means that the deformed state does not correspond to a minimum but rather to a point of the bottom of a valley in the energy surface. In Section 11.4 we will see that this degeneracy in energy can be used to construct a linear superposition of all these wave functions $|\Phi(\Omega)\rangle$, which is then an eigenfunction of the symmetry operators J^2 and J_z .

The transition from spherical nuclei in the vicinity of closed major shells to deformed nuclei in the middle of major shells is often called a *phase transition*. This is analogous to a macroscopic system, where with increasing correlations we have the same mechanism: a soft mode connected to the violation of a symmetry. There are, however, two important differences between a usual phase transition in solid state theory and a "phase transition" in nuclear physics:

- (i) In a macroscopic system the transition is strictly *discontinuous*, that is, the different quantities (order parameters) change abruptly at a certain value of a continuous parameter. For a finite system the

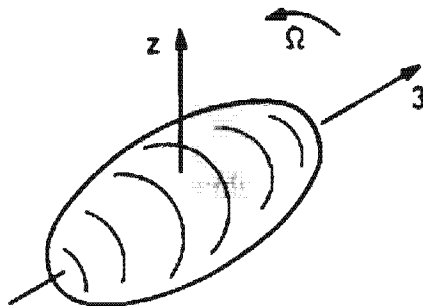


Figure 11.1. Schematic representation of the fact that the mean field approach defines an internal coordinate frame.

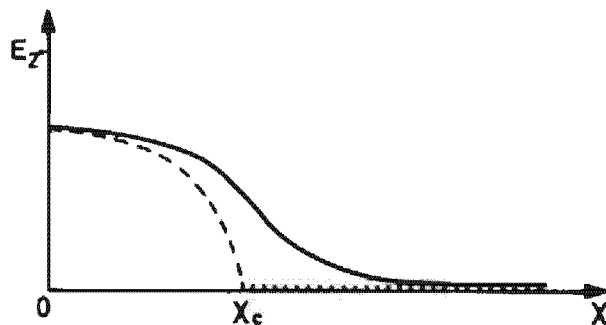


Figure 11.2. Schematic representation of the lowest excitation energy as a function of quadrupole coupling strength: exact solution (full line) and RPA approach in the spherical basis (dashed line) and in the deformed basis (dotted line). In the latter case, the lowest RPA solution is the spurious state, which corresponds to the rotation (see Sec. 8.4.7).

sharp transition is washed out and a more or less *gradual change* in the order parameters given by the deformations q_μ (or the gap Δ) is observed. This fact is somewhat hidden if our procedure is followed: If we calculate vibrations around a spherical shape in RPA we find that with increasing coupling strength x , one frequency goes to zero at a sharp critical value x_c . For all values $x > x_c$ we find a deformed solution. However, in a finite system both methods—the RPA in the spherical case and the deformed HF-method in the deformed case—break down in the vicinity of the critical point and do not provide a method for describing the transition quantitatively. In an exact solution, as shown schematically in Fig. 11.2, we find that the vibrational mode is lowered dramatically in energy in the transition region and goes over into the 2^+ rotational state in the deformed region, which goes to zero only in the limit of very large deformations or strong correlations.

- (ii) Whereas in the macroscopic case the mean field approximation can provide an *exact description* of many quantities, this is no longer the case in the finite nuclear system. As we shall see in Section 11.4.4, the approximation becomes good only in the limit of strong symmetry violations. There are many nuclei in the transition region, where a static mean field approach is not applicable. From that point of view, the three symmetry violations of linear momentum, angular momentum, and particle number are very different. The quality of the mean field approximation is very good in the translational case for all medium and heavy nuclei. In the rotational case it is good only for the well-deformed regions. However, we also observe spherical nuclei without rotational symmetry violations; there are also large transitional regions, where the mean field approach breaks down. BCS correlations in nuclei are usually quite weak, therefore the corresponding mean field approximation, the BCS theory, is often not good enough to reproduce the experimental data. We shall therefore investigate, in the following sections, methods of improving the deficiencies of the mean field approximation.

An *experimental measure* of the strength of the quadrupole correlations, and therefore also an indication of the validity of the mean field approximation, is given by the *fluctuation of the quadrupole operator* in the exact wave function $|\Psi\rangle$

$$\Delta Q^2 = \langle \Psi | Q \cdot Q | \Psi \rangle - \langle \Psi | Q | \Psi \rangle \cdot \langle \Psi | Q | \Psi \rangle. \quad (11.10)$$

(The dot means a scalar product of the five quadrupole operators.) Since the expectation values $\langle \Psi | Q_\mu | \Psi \rangle$ vanish in the ground state with $I=0$, we find that ΔQ^2 is proportional to the quadrupole correlation energy of the Hamiltonian (11.3)

$$\Delta Q^2 = \langle \Psi | \sum_\mu Q_\mu^+ Q_\mu^- | \Psi \rangle. \quad (11.11)$$

The quadrupole force is attractive, therefore the system wants to increase ΔQ^2 as far as possible in the spherical single-particle potential V_0 .

On the other hand, there is direct experimental information on the value of ΔQ^2 in realistic nuclei, because it is proportional to the non-energy weighted isoscalar quadrupole sum rule [see Eq. (1.43)].

$$\Delta Q^2 = \sum_s |\langle \Psi_s | Q | \Psi_s \rangle|^2 = 5 \cdot \sum_s BE2(2^+_s \rightarrow 0). \quad (11.12)$$

In contrast to the energy weighted sum rule [Eq. (8.159)], which is proportional to $\langle r^2 \rangle$ and is roughly a constant, the non-energy weighted sum increases dramatically during the transition from spherical to deformed: Whereas the contribution from the giant quadrupole resonance stays roughly constant, the $BE2$ -value of the lowest 2^+ state increases from ~ 20 single-particle units [see Eq. (B.85)] in the spherical case to ~ 100 in the deformed case, where the lowest 2^+ belongs to the ground state rotational band.

The quadrupole strength, which in the spherical case is concentrated in the giant resonance, increases in the deformed case and is then concentrated into two regions, the giant quadrupole resonance and the collective rotation. In the classical limit, therefore, we have, for the spherical case only vibrations, and in the deformed case vibrations as well as rotations.

Further experimental evidence for a phase transition is the existence of a "rotational" spectrum. In Section 11.4 we shall see that in the case of strong symmetry violations we gain, besides the deformed ground state, a whole band of excited states which differ from the ground state only in the quantum number of the symmetry operator S . There, excitation energies are proportional to the eigenvalue of S^2 . The simplest examples are rotational bands in deformed nuclei ($\sim I \cdot (I+1)/2\hbar$), pairing rotations ($\sim (N - N_0)^2 / 8S_N$ [Sch 71a, BB 76]), or translational excitations ($\sim P^2 / 2M$).

Phase transitions can also be described in the *boson picture*. On the one hand, we saw in Fig. 9.5 that we can, in principle, reproduce the transition from spherical to deformed shapes by a boson expansion of the fermion Hamiltonian. Most of these calculations have been carried out in a

spherical boson basis. To represent a deformed state in this basis requires very complicated wave functions, because we always work in the laboratory frame and do not violate rotational symmetry. On the other hand, we can try to represent the deformed wave function in the intrinsic frame by bosons: According to Thouless' theorem (E.26), we can represent a deformed Slater determinant in the following way.

$$|\Phi_0\rangle = \mathcal{N} \exp\left(\sum_{mi} Z_{mi} c_m^+ c_i\right) |0\rangle, \quad (11.13)$$

where $|0\rangle$ is the spherical HF solution and \mathcal{N} is a normalization constant. In a well-deformed case, we have many non-vanishing coefficients, that is, the collective fermion pair operator

$$B_0^+ = \frac{1}{c} \sum_{mi} Z_{mi} c_m^+ c_i, \quad (11.14)$$

with

$$c^2 = \sum_{mi} |Z_{mi}|^2,$$

is to a good approximation a boson (see Sec. 9.2), and the deformed state

$$|\Phi\rangle = \mathcal{N} \exp(c B_0^+) |0\rangle$$

is a coherent state (see Sec. 10.6.1) containing only the collective boson B_0^+ . Therefore, we call it a *condensate* of the bosons B_0^+ in analogy with the Bose-Einstein condensation describing certain classes of phase transition of condensed matter (see also [SP 77a]).

This interpretation of the deformed state again shows the *classical behavior* of the mean field approximation. The structure of the boson B_0^+ is determined by the solution of the variational equations (11.2), which, in general, changes with deformation. We can show, however, that in the limit of small deformations it corresponds exactly to the *ph* part of the RPA boson, which goes to zero frequency at the transition point. In that sense, we can say that during the phase transition one boson goes to zero energy and forms a condensate. We have already used this picture in the BCS-model, where we interpreted the BCS ground state as a condensate of Cooper pairs.

So far, our discussion has concentrated mainly on the violation of rotational symmetry. In the following we show that the same considerations can be applied to symmetry violation in connection with the *pairing correlations*. Here we investigate first the simple seniority model (see Sec. 6.2). The effective Hamiltonian in a single j -shell is given by

$$H = -GS_+S_- = -G(S \cdot S - S_z^2 + S_x), \quad (11.15)$$

where S_i are the quasi-spin operators defined in Eq. (6.6). They act in a three-dimensional quasi-spin space. S^2 and S_z commute with the Hamiltonian. We can therefore classify the eigenstates according to their senior-

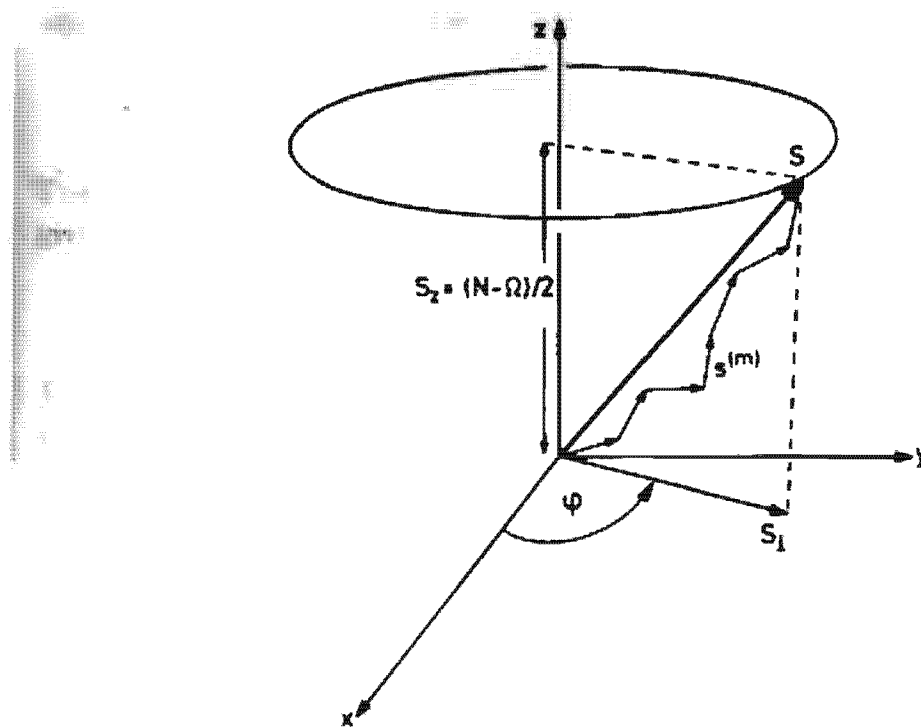


Figure 11.3. Schematic representation of the quasi-spin model.

ity s [Eq. (6.11)] and the particle number N

$$s = \Omega - 2S; \quad \hat{N} = 2S_z + \Omega \quad (11.16)$$

\mathbf{S} is composed by Ω quasi-spins $s^{(m)}$ [see Fig. 11.3 and Eq. (6.6)]. The length of this vector is determined by the seniority s , and we will restrict the following considerations to a fixed value of s .

The other quantum number S_z corresponds to the symmetry of rotation about the z -axis. In the following we will investigate this invariance of the Hamiltonian in more detail:

$$[H, \hat{N}] = 0. \quad (11.17)$$

The particle number operator \hat{N} is related to S_z (11.16) and therefore corresponds to an infinitesimal generator of rotations around the z -axis in the quasi-spin space. Such rotations are called *gauge transformations*. The corresponding angle φ is the *gauge angle*.

We can represent the operator \hat{N} by this gauge angle,

$$\frac{\hat{N}}{2} = -\frac{1}{i} \frac{\partial}{\partial \varphi} + \text{const.}, \quad (11.18)$$

in analogy to the representation of the angular momentum operators \mathbf{J} by Euler angles, as in Eq. (A.11).

For fixed values of N , that is, for all exact eigenstates $|\Psi\rangle$ of the Hamiltonian (11.15), the vector \mathbf{S} performs a precession around the symmetry axis with a frequency

$$\frac{d\varphi}{dt} = 2 \frac{dE}{dN} = 2\lambda. \quad (11.19)$$

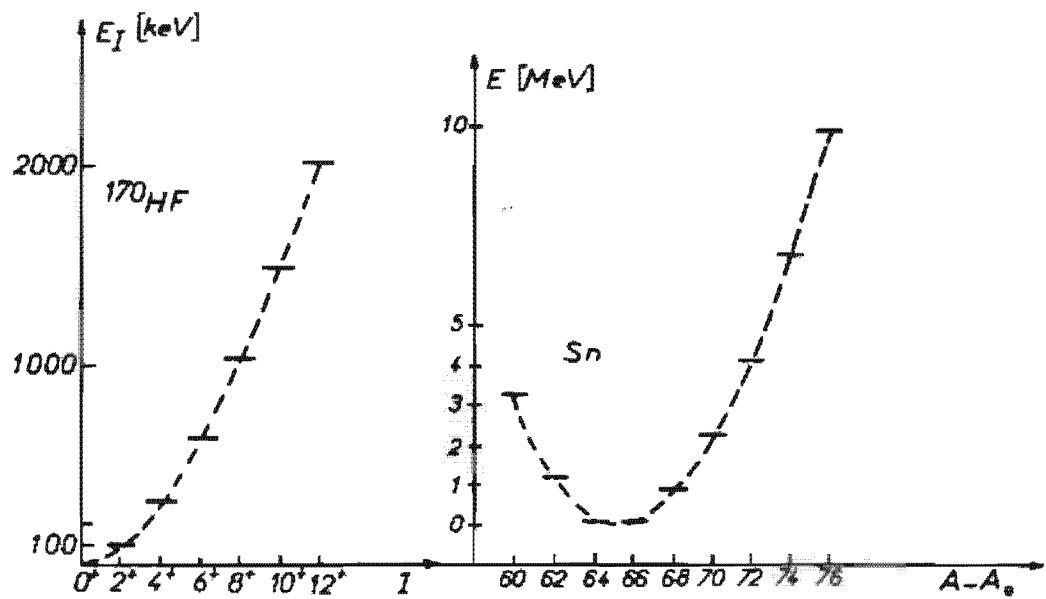


Figure 11.4. An experimental rotational spectrum (^{170}HF), where the excited levels correspond to states with different I -values and a pairing rotational spectrum (Sn), where the "excited" levels correspond to states with different A -values (i.e., the ground states in the neighboring nuclei). (From [BB 76].)

where λ is the chemical potential [Eq. (6.41)]. We call this motion a *pairing rotation*. For different values of the particle number, we obtain a rotational band (see Fig. 11.4).

The expectation values of S_x and S_y vanish,

$$\langle \Psi | S_x | \Psi \rangle = 0, \quad (11.20)$$

in the same way as the quadrupole moment of the exact ground state with $I=0$ in the case discussed above.

The length of the projection of \mathbf{S} onto the x, y plane is given by

$$S_\perp^2 = \langle \Psi | S_+ S_- | \Psi \rangle \quad (11.21)$$

and is proportional to the correlation energy. Since there is now no "spherical" single-particle part, the system always prefers the largest possible value of S_\perp in its ground state, in which all the quasi-spins $s^{(m)}$ are aligned. In this model, therefore, we have for all values of the force constant a "deformed" state. For large values of S , that is, for large Ω -values and $N \ll \Omega$, we can therefore expect to obtain a good approximation to the exact wave function by breaking the gauge symmetry. The symmetry-violating inner state $|\Phi\rangle$ is a BCS wave function. It is characterized by a fixed angle φ .

$$|\Phi(\varphi)\rangle = \prod_{m>0} (u + v e^{i\varphi} c_m^+ c_{-m}^+) |-\rangle = e^{i\varphi N/2} |\Phi(0)\rangle. \quad (11.22)$$

The usual ansatz (6.31) corresponds to $\varphi=0$, that is, we have fixed the angle in a classical way. Again, all the states $|\Phi(\varphi)\rangle$ are degenerate in energy. The symmetry violation is measured by the gap parameter Δ ,

which corresponds to the deformation Eq. (11.20) in the rotational case

$$\Delta = G\langle\Phi(0)|S_+|\Phi(0)\rangle = G \sum_{m>0} uv = G \cdot \Omega uv. \quad (11.23)$$

The coefficients u, v are determined by the variational principle, which yields the usual gap equation [(6.60) and (6.65)]

$$u = v = \frac{1}{\sqrt{2}}. \quad (11.24)$$

The BCS state can therefore also be represented in the quasi-boson approximation by a coherent state with quasi-boson S_+

$$|BCS\rangle = \mathcal{N} \exp(S_+) |-\rangle. \quad (11.25)$$

It violates the particle number, but its component with the proper particle number N corresponds to the exact eigenstate (6.19) of the system. The relative fluctuations $\Delta N/N$ (6.63) vanish for large particle numbers. In this case, the mean field approximation is therefore excellent.

In more realistic applications of the BCS theory, we have the model of a pure pairing force in addition to a single-particle part

$$H = \sum_k \epsilon_k c_k^+ c_k - G \cdot P^+ P, \quad (11.26)$$

$$P^+ = \sum_{k>0} c_k^+ c_k^+.$$

An exact analytic solution is now no longer possible [KLM 61, RS 64, Ri 66]. It can be solved with the help of a computer, and the solution shows that the BCS approach is still a reasonable approximation, particularly if we use only the component with proper particle number (see Sec. 11.4). The particle number \hat{N} commutes with the Hamiltonian; however, the corresponding gauge symmetry is broken by the BCS approximation and we find a phase transition. In all details the model works in full analogy to the quadrupole case (11.3). The only difference is that we now have to use a *constraint on the particle number* (by adding a term $-\lambda\hat{N}$ to the Hamiltonian), because we are not interested in a state with a vanishing expectation value of \hat{N} . In the case of rotational symmetry we also sometimes want wave functions with non-vanishing expectation values of J_x . We then end up with the Cranking model (see Sec. 3.4).

To show the close analogy between the transition from spherical to deformed and the transition from normal to superfluid systems, we give the following list of the quantities which correspond to one another [Sch 71a, BHR 73].

The model Hamiltonian in a spherical basis is

$$H_Q = \epsilon - \frac{\chi}{2} Q \cdot Q, \quad H_p = \epsilon - GP^+ P.$$

For small coupling strength the ground state is the uncorrelated spherical shell model state $|0\rangle$. The residual interaction, taken into account within the RPA, yields collective vibrations, namely

quadrupole vibrations
with $J = 2$

pairing vibrations in the
nuclei with mass $A \pm 2$.

They have enhanced

BE 2-value (in single-
particle units)

$$BE(2^+ \rightarrow 0^+) \approx 20B_p;$$

pair transfer cross section
(in $2p$ units)

$$\sigma(g.s.(A-2) \rightarrow g.s.(A)) \approx 10\sigma_p.$$

With increasing coupling strength, the lowest RPA frequency goes to zero. From this point on there exists a

deformed

superfluid

minimum in the energy surface. It is described by a product wave function based on the spherical (normal fluid) ground state $|0\rangle$

$$|\Phi\rangle = \prod_k \alpha_k |0\rangle$$

with the quasi-particle operators

$$\alpha_m^+ = \sum_k D_{km} c_k^+,$$

$$\alpha_m^+ = u_m c_m^+ - v_m c_m^-.$$

$$\alpha_i^+ = \sum_k D_{ki}^* c_k,$$

$$\alpha_i^+ = v_i c_i + u_i c_i^+.$$

The coefficients D_{kl} and u_k , v_k are determined from the diagonalization of the single-particle operator

$$\epsilon - q(Q + Q^+),$$

$$\epsilon - \Delta(P + P^+).$$

The strength of the single-particle field is the order parameter. It is determined self-consistently by the "deformation equation" and the gap equation

$$q = \chi \langle \Phi | Q | \Phi \rangle,$$

$$\Delta = G \langle \Phi | P | \Phi \rangle.$$

In the quasi-boson approximation, the wave function $|\Phi\rangle$ can be written as a coherent state (boson condensate)

$$|\Phi\rangle \propto \exp(c B_0^+) |0\rangle,$$

$$|\Phi\rangle \propto \exp(c A_0^+) |0\rangle,$$

with the boson

$$B_0^+ = \frac{1}{c} \sum_m Z_{mm} c_m^+ c_m,$$

$$A_0^+ = \frac{1}{c} \sum_m \frac{v_m}{u_m} c_m^+ c_m^+ + \frac{1}{c} \sum_i \frac{u_i}{v_i} c_i c_i^+.$$

The mean field approximation violates the symmetry.

$$[H, J] = 0,$$

$$[H, \hat{N}] = 0.$$

Its solutions $|\Phi\rangle$ characterize an orientation given by angles $\Omega = (\alpha, \beta, \gamma)$ in coordinate space, and φ in the quasi-spin space. The solutions are degenerate with respect to rotations

$$R(\Omega) = e^{i\alpha j_x} e^{i\beta j_y} e^{i\gamma j_z},$$

$$G(\varphi) = e^{i\varphi \hat{N}/2}.$$

In the deformed state, we have in the excitation spectrum

β, γ vibrations

(time-dependent deformation)

pairing vibrations

(time-dependent gap Δ)

and (as zero-frequency modes in the RPA, see Fig. 11.4)

rotations (states with $I \neq 0$)	pairing rotations (ground states in the nuclei $A \pm 2, A \pm 4, \dots$).
-------------------------------------	---

The transitions among the members of the ground state "rotational" bands are proportional to the square of the deformation parameter (q or Δ). Typical values are

$$\begin{aligned} B(E2, 2^+ \rightarrow 0^+) &\approx 100 B_{sp}, & \sigma(g.s.(A-2) \rightarrow g.s.(A)) &\approx 50\sigma_{sp}, \\ B(E2, 2'^+ \rightarrow 0^+) &\approx 3 B_{sp}, & \sigma(g.s.(A-2) \rightarrow p.v.(A)) &\approx 1\sigma_{sp}. \end{aligned}$$

The rotations can be treated (see Sec. 11.4) either classically by the Cranking model:

$$H - \omega J_x, \quad H - \lambda \hat{N};$$

or quantum mechanically by projection

$$P'_{MK} \propto \int D_{MK}^{I''}(\Omega) R(\Omega) d\Omega, \quad P^N \propto \int e^{-i(\varphi/2)^N} G(\varphi) d\varphi.$$

This list concludes our general considerations about symmetries and its violations within the mean field theory, and it is clear that a similar list can be produced for all kind of phase transitions connected with a symmetry violation, for instance, pion condensation. We shall now turn to methods that allow a restoration of the broken symmetries.

11.3 Transformation to an Intrinsic System

11.3.1 General Concepts

Symmetry violations in the many-body wave functions are strongly connected with *collective motion*. To explain this fact in more detail we again use the example of rotational symmetry. A deformed wave function $|\Phi\rangle$ defines a fixed orientation in space, characterized, for instance, by the principal axes of the mass distribution. All wave functions $|\Phi(\Omega)\rangle$ that differ from $|\Phi\rangle$ only in this orientation have the same internal structure and yield the same energy expectation value. They lie at the bottom of a valley in the energy surface. In the classical picture we therefore have a type of motion which stays, if it is slow enough, close to the bottom of this valley. It corresponds to rotational motion with an approximate preservation of the intrinsic structure. If the deformation is large, there are many particles involved in this motion and we call it collective. (For a further discussion of these quasi-classical considerations, see also Sec. 12.3.)

In quantum mechanics, the states $|\Phi(\Omega)\rangle$ span a subspace of the many-body Hilbert space, the collective subspace in the sense of the GCM method (see Chap. 10). If this subspace is large enough—that is, as we shall see in Section 11.4, if the overlap $\langle\Phi(\Omega)|\Phi(\Omega')\rangle$ is strongly peaked at $\Omega = \Omega'$, which happens for strong deformations—it contains not only the

ground state to a good approximation, but also low-lying excited states, with the same internal structure, which exhibit a rotational spectrum.

Since the intrinsic structure in such a wave function is preserved to a good approximation in the collective motion, many authors have tried to separate intrinsic and collective degrees of freedom by an appropriate coordinate transformation from the $3A$ particle coordinates \mathbf{r}_i to collective coordinates q_1, \dots, q_f and intrinsic coordinates ξ_1, \dots, ξ_{3A-f} [Vi 57a and b, Vi 58, SG 68, FKS 72]

$$(\mathbf{r}_1, \dots, \mathbf{r}_A) \rightarrow (q_1, \dots, q_f, \xi_1, \dots, \xi_{3A-f}). \quad (11.27)$$

The collective coordinates are usually well defined by the underlying symmetry as the canonical conjugate variables to the generators of the symmetry group. In the case of translations, there are the center of mass coordinates; in the case of rotations, there is a set of angles as the Euler angles; and in the case of superfluid systems, it is the Gauge angle ϕ .

The definition of the intrinsic variables ξ is a serious problem. It is only simple in the translational case of two particles, where it is the relative coordinate $\mathbf{r} = \mathbf{r}_1 - \mathbf{r}_2$. In the case of a few particles, we can introduce, for instance, Jacobi coordinates, but this procedure in the translational case and similar procedures in the rotational case get extremely complicated in the case of our many-particle system. Nevertheless as we shall see in some examples, we can sometimes deduce the structure of the Hamiltonian in the collective variables without explicitly specifying the intrinsic coordinates.

The main idea of these theories is to decompose the nuclear Hamiltonian into the following three parts

$$H = H_{\text{coll}}(q) + H_{\text{int}}(\xi) + H_{\text{coupl}}(q, \xi), \quad (11.28)$$

where H_{coll} describes the collective and H_{int} the intrinsic motion. The coupling term H_{coupl} , it is hoped, will be small or of a simple structure. The case of nuclear translations is an example of where this concept works well. Because of Galilean invariance, H_{coupl} vanishes identically.

If we can neglect H_{coupl} , we find the eigenfunctions of the total system as products of a collective wave function $\chi_c(q)$ and an intrinsic wave function $\varphi_n(\xi)$

$$\Psi_n^c = \chi_c(q) \cdot \varphi_n(\xi), \quad (11.29)$$

and the energies have the form

$$E_n^c = E_c + E_n. \quad (11.30)$$

For each intrinsic state φ_n there exists a collective band labelled with the index c .

In practical applications of this procedure, we are always faced with two problems:

- (i) The decomposition (11.28) is not unique. It depends on the actual choice of the intrinsic coordinates. It is evident that the size of the coupling term depends sensitively on this choice. Therefore, some-

times the variational principle of minimal coupling has been used to determine the intrinsic system [Co 56, BM 58, RV 69, Ru 73].

- (ii) The intrinsic Hamiltonian $H_{\text{int}}(\xi)$ does not depend on $3A$ coordinates of A particles, but only on $3A - f$ variables ξ . None of them can be identified with particle position coordinates. This is particularly unpleasant, if we want to describe the intrinsic motion within the independent particle picture. We already have this problem in the case of translations.

A series of authors have therefore used the concept of *redundant variables* [LST 55, Li 55, Ta 56b, Na 57, Li 58, VC 70]. Here it is attempted to combine the advantages of the method of canonical transformations with the advantages of dealing with $3A$ -particle coordinates to describe the intrinsic motion. This is achieved by embedding the A -body Hilbert space in the particle coordinates r_1, \dots, r_A (the physical subspace) into a larger space with the dimension $3A + f$, where f is the number of collective variables. We characterize these additional unphysical degrees of freedom by the coordinates g_1, \dots, g_f . The physical subspace is then characterized by the conditions

$$g_1 = g_2 = \dots = g_f = 0. \quad (11.31)$$

Physical operators, that is, operators which depend only on the coordinates r_1, \dots, r_A as, for instance, the Hamiltonian, have eigenfunctions of the form

$$\Psi_m(g, r) = h_m(g) \varphi_n(r), \quad (11.32)$$

where $h_m(g)$ is an arbitrary orthonormal set of functions in the redundant coordinates. Each eigenvalue E_n is therefore highly degenerate in the enlarged space, but the corresponding eigenfunctions are identical in the physical subspace (11.31).* We are now able to transform the coordinates $g_1, \dots, g_f, r_1, \dots, r_A$ in the redundant laboratory system into the redundant intrinsic system with the collective coordinates q_1, \dots, q_f and the particle coordinates x_1, \dots, x_A :

$$\begin{aligned} r_i &= r_i(q_1, \dots, q_f, x_1, \dots, x_A), \quad i = 1, \dots, A \\ g_i &= g_i(q_1, \dots, q_f, x_1, \dots, x_A), \quad i = 1, \dots, f. \end{aligned} \quad (11.33)$$

In this way we derive a Hamiltonian in the variables q and x of the form

$$H = H_{\text{coll}}(q) + H_{\text{int}}(x) + H_{\text{coupl}}(q, x). \quad (11.34)$$

In the next step we apply the usual approximation techniques for the diagonalization of H_{int} . The question remains, however, as to whether we can find an appropriate transformation (11.33) such that the coupling term is small, and also whether we can separate the admixture of spurious states obtained by such approximations in a proper way. Before we discuss these techniques in the context of translations and rotations, we wish to mention

* Further details concerning the calculation with redundant variables are given in the quantum mechanical case by Lipkin et al. [LST 55], and for the classical theory by Watanabe [Wa 56].

that similar methods have also been applied for more general collective motions such as surface vibrations, which are not connected with a broken symmetry [BP 53, Sü 54, MYT 55, To 55, MY 55, Co 55, MT 56, HM 57, Vi 57b], but for which one is also interested in deriving the collective Hamiltonian.

11.3.2 Translational Motion

In the following we will study translational motion in more detail. This simple case already shows many problems. In nuclear physics it is connected with a very strong symmetry violation. It is the only case where the collective motion decouples completely from the intrinsic degrees of freedom. The reason for this is Galilean invariance.

The intrinsic system in this case is given by the center of mass frame, and the collective coordinate is

$$\mathbf{R} = \frac{1}{A} \sum_i \mathbf{r}_i. \quad (11.35)$$

In a first step we do not use redundant coordinates. Without specifying the intrinsic coordinates ξ we gain from (11.27) for the derivatives

$$\frac{\partial}{\partial \mathbf{r}_i} = \frac{1}{A} \frac{\partial}{\partial \mathbf{R}} + \sum_j \frac{\partial \xi}{\partial \mathbf{r}_i} \frac{\partial}{\partial \xi_j}. \quad (11.36)$$

Since the intrinsic coordinates ξ depend only on the differences $\mathbf{r}_i - \mathbf{r}_j$, we get $\sum_i (\partial/\partial \mathbf{r}_i) \xi_j = 0$ and find a complete decoupling of the collective motion

$$H = -\frac{\hbar^2}{2m} \sum_i \left(\frac{\partial}{\partial \mathbf{r}_i} \right)^2 + V = \frac{1}{2Am} \mathbf{P}^2 + \sum_H D_H(\xi) \pi_i \pi_j + V(\xi), \quad (11.37)$$

with the center of mass momentum $\mathbf{P} = (\hbar/i) \partial/\partial \mathbf{R}$, the intrinsic momenta $\pi_i = (\hbar/i) \partial/\partial \xi_i$, and the intrinsic inertia functions

$$D_H(\xi) = \sum_i \frac{\partial \xi}{\partial \mathbf{r}_i} \cdot \frac{\partial \xi}{\partial \mathbf{r}_i}. \quad (11.38)$$

As discussed in the last section, we cannot approximate the intrinsic part of (11.37) by a shell model Hamiltonian. Therefore, we now apply the method of redundant coordinates. The coordinates \mathbf{x}_i are in this case the particle coordinates in the center of mass frame, and for the transformation (11.33) we get

$$\begin{aligned} \mathbf{r}_i &= \mathbf{x}_i + \mathbf{R} & \mathbf{x}_i &= \mathbf{r}_i - \frac{1}{A} \sum_j \mathbf{r}_j + \mathbf{g} \\ &&\text{or}& \\ \mathbf{g} &= \frac{1}{A} \sum_j \mathbf{x}_j & \mathbf{R} &= \frac{1}{A} \sum_j \mathbf{r}_j - \mathbf{g}. \end{aligned} \quad (11.39)$$

The physical subspace is characterized by $\mathbf{g} = 0$. For the momenta we find the transformation

$$\frac{\hbar}{i} \frac{\partial}{\partial \mathbf{r}_i} = \frac{1}{A} \mathbf{P} + \mathbf{p}_i - \frac{1}{A} \sum_j \mathbf{p}_j, \quad (11.40)$$

with

$$\mathbf{p}_i = \frac{\hbar}{i} \frac{\partial}{\partial \mathbf{x}_i}, \quad \mathbf{P} = \frac{\hbar}{i} \frac{\partial}{\partial \mathbf{R}}.$$

The Hamiltonian in the coordinates \mathbf{x} , \mathbf{R} takes the form

$$H = \frac{1}{2Am} \mathbf{P}^2 + \sum_i \frac{\mathbf{p}_i^2}{2m} + V(\mathbf{x}_i - \mathbf{x}_j) - \frac{1}{2Am} \left(\sum_i \mathbf{p}_i \right)^2. \quad (11.41)$$

Again we get a complete decoupling. The collective Hamiltonian $(1/2Am)\mathbf{P}^2$ has plane waves as eigenfunctions. To each internal eigenstate exists a continuum corresponding to the translational motion. Since we are only interested in intrinsic excitations, it is enough to investigate only H_{intr} :

$$H_{\text{intr}} = \sum_i \frac{\mathbf{p}_i^2}{2m} + V - \frac{1}{2Am} \left(\sum_i \mathbf{p}_i \right)^2. \quad (11.42)$$

It looks very similar to the original Hamiltonian H in the coordinates \mathbf{r}_i . Only the term $(1/2Am)\sum_{ij}\mathbf{p}_i\mathbf{p}_j$, which is sometimes called the "recoil term," is subtracted. We are now able to treat this intrinsic Hamiltonian with the usual techniques. We do not have to worry about translational invariance, because we are in the intrinsic system. Using, for instance, the Hartree-Fock method, we would get a localized potential and localized wave functions. There are only two things we have to take into account:

- (i) We have to subtract from the usual Hamiltonian the term $(1/2Am)\sum_{ij}\mathbf{p}_i\mathbf{p}_j$, which contains a two-body interaction. This is often done in HF calculations. In a pure phenomenological shell model, we sometimes subtract at least the expectation value of this operator from the final energy. It is the kinetic energy of the spurious center of mass motion.*
- (ii) We have to be aware that because we use redundant coordinates there are spurious solutions among our eigenfunctions. In cases in which we solve the problem in the center of mass frame exactly they do not mix with the physical solutions and can be separated out by special techniques. In the case of an approximate solution, however, they can mix with physical solutions and it is sometimes hard to decide which states are physical and which are not.

To understand the structure of these unphysical solutions a little better, we use a purely harmonic interaction [GS 57]

$$V = \frac{k}{2} \sum_{i < j} (\mathbf{r}_i - \mathbf{r}_j)^2. \quad (11.43)$$

In this case we can write

$$H_{\text{intr}} = H_0 + H_1, \quad (11.44)$$

with

$$H_0 = \sum_i \left(\frac{\mathbf{p}_i^2}{2m} + \frac{Ak}{2} \mathbf{x}_i^2 \right) \quad (11.45)$$

and

$$H_1 = -\frac{1}{2Am} \left(\sum_i \mathbf{p}_i \right)^2 - \frac{A^2k}{2} \left(\frac{1}{A} \sum_i \mathbf{x}_i \right)^2. \quad (11.46)$$

* The same term is automatically obtained, if we work with the Hamiltonian in the laboratory system (coordinates \mathbf{r}_i) and treat the ground state correlations in the framework of the RPA approach [see Eq. (8.111)]. It is the contribution of the zero-frequency mode connected with the translation to the ground state correlation energy. The RPA is a symmetry conserving theory. It is therefore not necessary to introduce redundant coordinates here. We also get the same term in other symmetry-conserving theories, like projection techniques [see Sec. (11.4.4)].

H_0 is a single-particle harmonic oscillator potential with corresponding Slater determinants as eigenfunctions. Since H_1 commutes with H_0 it can be simultaneously diagonalized, and the exact solution of H_{intr} is just the shell model wave function corrected for the center of mass motion. On the other hand, H_1 describes an oscillator of the center of mass $\mathbf{g} = (1/A)\sum \mathbf{x}_i$ of the intrinsic coordinates in an harmonic oscillator potential with the frequency $\omega = (Ak/m)^{1/2}$ of an individual particle. This motion is certainly spurious, because in the physical space we have the condition $\mathbf{g} = 0$. The spurious solutions correspond to oscillations of the nucleus as a whole in the shell model potential.

In shell model calculations based on an harmonic oscillator basis they can be separated by group theoretical methods [BR 37, ES 55, UT 58, Kr 60, Ve 60, KM 66, AMK 69, Mo 69, He 71, Sch 77b]. Since the center of mass problems are especially important in light nuclei, and since, on the other hand, the harmonic oscillator potential is a reasonable approximation for the self-consistent field in this region of the periodic table, this basis is preferred for many practical applications.

In the general case the problem is very complex. An exact separation of the spurious components is often hardly possible. It has been tried to remove the spurious components approximatively by adding an operator $S(\mathbf{g})$ to the Hamiltonian, which vanishes in the physical space ($\mathbf{g} = 0$) and is large and positive for $\mathbf{g} \neq 0$. It shifts the spurious eigenstates to high energies such that they do not mix with low-lying states even if they are only calculated approximately [Pa 67, SG 68, FKS 72].

In heavy nuclei the spurious center of mass motion can be neglected in all cases, where it gives an effect only of the order $1/A$. As an example, we calculate the orbital part of the magnetic moment in a nucleus with one odd nucleon outside a magic configuration (for instance, Pb²⁰⁹ or Bi²⁰⁹). The orbital angular momentum of the i th particle with respect to the center of mass of the whole system is given by

$$\mathbf{l}_i = \mathbf{x}_i \times \mathbf{p}_i = \left(\mathbf{x}'_i - \frac{1}{A} \mathbf{x}'_0 \right) \times \left(\mathbf{p}'_i - \frac{1}{A} \mathbf{p}'_0 \right), \quad (11.47)$$

where $\mathbf{x}'_i, \mathbf{p}'_i$ are the coordinates of the particles in the center of mass system of the magic core. The index 0 characterizes the odd particle. Only the protons contribute to the orbital part of the magnetic moment. If p characterizes the protons in the core, we get

$$\begin{aligned} \frac{\mu}{\mu_*} &= \sum_p \mathbf{l}_p + g_i \cdot \mathbf{l}_0 \\ &= \sum_p \mathbf{l}'_p - \frac{1}{A} \left(\sum_p \mathbf{x}'_p \right) \times \mathbf{p}'_0 - \frac{1}{A} \mathbf{x}'_0 \times \left(\sum_p \mathbf{p}'_p \right) + \left(\frac{Z}{A^2} + g_i \left(1 - \frac{2}{A} \right) \right) \mathbf{l}'_0. \end{aligned} \quad (11.48)$$

Depending on whether the odd particle is a proton or a neutron, g_i is one or zero, respectively. Within a shell model approach whose center coincides with the center of mass of the magic core, all the protons are in closed shells and the first three terms in Eq. (11.48) vanish and we are left with a g -factor corrected for the center of mass motion \bar{g}_i :

$$\bar{g}_i = g_i \left(1 - \frac{2}{A} \right) + \frac{Z}{A^2}. \quad (11.49)$$

This is a $1/A$ effect.

11.3.3 Rotational Motion

The rotational case has many formal similarities to the translational case; there are, however, some basic differences:

- (i) There is no counterpart to the Galilean invariance in the rotational case. Therefore, we cannot expect a priori decoupling between collective and intrinsic motion. We only can hope that the coupling terms become small at least for not-too-large angular momenta. How large they are depends on the choice of the intrinsic system.
- (ii) There is no well-defined center of mass angle. The most natural choice of the intrinsic system seems to be provided by the principal axis of the mass distribution. It turns out, however, that the spurious motion of the system around these axes yields very large coupling terms between intrinsic and collective degrees of freedom [VC 70].
- (iii) The underlying symmetry group, the rotational group, is no longer Abelian. Whereas the first two difficulties are already encountered in the one-dimensional rotations in a plane,* we have additional difficulties with non-commuting operators. This requires some lengthy calculations involving angular momentum algebra, which we do not want to go into here. The reader is referred to the literature for all the details [LST 55, Na 57, Vi 57a, b]. We shall present only the main results.

As collective coordinates, Euler angles $\Omega = (\alpha, \beta, \gamma)$ are chosen that connect the laboratory frame to the body-fixed system, whose precise definition is still open. In a first step, we can again try to use 3A – 3 intrinsic coordinates ξ . Villars [Vi 57a, b] in this case derived the following general structure of the Hamiltonian

$$H = \frac{1}{2} \sum_{ik=1}^3 (\mathfrak{I}^{-1}(\xi))_{ik} \hat{I}_i \cdot \hat{I}_k + \sum_{i=1}^3 B_i(\xi) \hat{I}_i + H_{\text{int}}(\xi). \quad (11.50)$$

The operators \hat{I}_i are the components of the angular momentum operator \mathbf{I} with respect to the intrinsic axis $i = (1, 2, 3)$ expressed by Euler angles [see Eq. (A.14)]. The rest of the Hamiltonian, particularly the tensor of inertia \mathfrak{I}_{ik} and the quantities B_i , depend only on the intrinsic coordinates ξ . They provide a coupling between the collective and the intrinsic motion.

If we determine the body-fixed system by the principal axis of the mass distribution, we find that the tensor \mathfrak{I}_{ik} is diagonal and that the moments of inertia are given by the hydrodynamical values (1.48) derived from an irrotational liquid drop motion. They are in strong disagreement with experimental evidence. Consequently, the coupling terms B_i have to be very large.

We can also give the general structure of the eigenfunctions to the Hamiltonian (11.50). Since it is rotational invariant, and since the Wigner functions $D_{MK}^{J''}(\Omega)$ provide a complete system in the variables Ω , we find for the eigenfunctions of Eq. (11.50):

$$\Psi^{JM}(\Omega, \xi) = \sum_K D_{MK}^{J''}(\Omega) \cdot g_K(\xi). \quad (11.51)$$

As in the translational case, the coordinates ξ are not very useful for practical

* The violation of gauge symmetry in the BCS wave function would correspond to such a one-dimensional rotation.

applications. Several authors therefore used the concept of redundant coordinates. Again we are faced with the problem of a proper choice of the body-fixed frame. If we choose the principal axes of the mass distribution, we again find the irrotational moments of inertia and large coupling terms. Several attempts have been made to remove them by a unitary transformation or a proper choice of the intrinsic system [Co 56, HM 57, BM 58, VC 70, Ru 73]. However, in general, in this way we end up with very complicated equations. Their solution is only possible with more or less drastic approximations. The most elaborate investigations of this kind have been carried out by Villars and Cooper [VC 70]. They obtain a renormalization of the irrotational moment of inertia and end up with the Thouless-Valatin value [Eq. (8.113)].

Summarizing all these investigations, we can say that the transformation to the intrinsic system and the construction of a collective Hamiltonian in this way encounters serious problems that have not yet been solved completely. It is only in the case of translations that complete separation of the collective and intrinsic degrees of freedom can be achieved, and where in the case of an harmonic oscillator basis an elimination of spurious results is possible by group-theoretical methods.

In view of the great success of the rotor model of Bohr and Mottelson (see Chaps. 1 and 3), however, we should expect that it is also possible in the rotational case to achieve at least an approximate decoupling of collective and intrinsic motion. The essential problem is the determination of the moments of inertia. In contradiction to the translational case, where the total mass is independent of the residual interaction, the inertia parameters of the rotational motion are influenced by the correlations. This is a dynamic effect which can hardly be taken into account by a pure coordinate transformation.

A much more general way to treat symmetry violations is given by the method of generator coordinates. In many cases these techniques correspond to a projection onto the corresponding eigenspace of the symmetry operator. We will treat these projection methods in the next section.

11.4 Projection Methods

11.4.1 Projection Operators

Projection techniques are a special case of the generator coordinate method (GCM) discussed in Chapter 10. The basic concept of this method is a diagonalization of the full many-body Hamiltonian H in the subspace spanned by a set of generating functions $|\Phi(\Omega)\rangle$, which depend on one or several continuous parameters Ω . This space is called the "collective subspace."

We now have a symmetry group, generated by the symmetry operators S_i , which commute with the Hamiltonian, and a symmetry-violating wave function* $|\Phi\rangle$. Applying all the elements $R(\Omega)$ of this group onto $|\Phi\rangle$, we

* In the following we always have product wave functions in mind, although the method can be generalized to other types of symmetry-breaking functions.

get a continuous set of generating functions

$$|\Phi(\Omega)\rangle = R(\Omega)|\Phi\rangle, \quad (11.52)$$

where Ω runs over the whole parameter space of the group.

All the wave functions $|\Phi(\Omega)\rangle$ have the same energy expectation value. Peierls and Yoccoz [PY 57] therefore proposed to use them as generating functions in the GCM technique, that is, to make the following ansatz for the wave function $|\Psi\rangle$ of the system*

$$|\Psi\rangle = \int d\Omega f(\Omega)|\Phi(\Omega)\rangle. \quad (11.53)$$

The variation of the energy with respect to the weight function $f(\Omega)$ corresponds to a diagonalization of H in the space spanned by the functions $|\Phi(\Omega)\rangle$ (see Sec. 10.2). This subspace is invariant under the elements of the symmetry group [Ze 67]:†

$$R(\Omega)|\Psi\rangle = \int d\Omega' f(-\Omega + \Omega')|\Phi(\Omega')\rangle, \quad (11.54)$$

which means that the projector P_Φ onto this subspace commutes with the symmetry operation $R(\Omega)$. Thus we see that we may find simultaneous eigenfunctions of $P_\Phi H P_\Phi$ and the symmetry operators. In other words, there exists a function $f(\Omega)$ which minimizes the energy and causes $|\Psi\rangle$ to have the proper symmetry.

To find such a function, we expand $f(\Omega)$ in a complete set of eigenfunctions of the symmetry operators expressed in the variables Ω . For all Abelian groups this corresponds to a Fourier decomposition. As an example, we use the case of the gauge group connected with particle number violation (see Sec. 11.2). It has one group parameter φ , and the symmetry operator $\hat{N}/2$ has the representation $i\partial/\partial\varphi$. Its eigenfunctions are exponentials

$$f(\varphi) = \sum_n \frac{1}{2\pi} e^{-in\varphi} \cdot g_n \quad (11.55)$$

with integer n because of the periodicity in φ . From Eqs. (11.53) and (11.55) we get

$$|\Psi\rangle = \sum_n g_n \hat{P}^{2n} |\Phi\rangle, \quad (11.56)$$

with

$$\hat{P}^A = \frac{1}{2\pi} \int_0^{2\pi} e^{i\varphi(\hat{N}-A)} d\varphi. \quad (11.57)$$

The operator \hat{P}^A is a projection operator in the mathematical sense ($\hat{P}^2 = \hat{P}$, $\hat{P}^+ = \hat{P}$), which projects onto the subspace with particle number

* For a review of projection methods based on the GCM ansatz, see also [Wo 75] and, for a review on more general projectors, see [Ma 70].

† Note that for non Abelian groups $-\Omega + \Omega'$ depends on the ordering and means the set of parameters corresponding to the transformation $R^{-1}(\Omega)R(\Omega')$.

A. To see this, we multiply \hat{P}^A from the left and from the right with the unity operator, expressed by a complete orthogonal set of wave functions $|N\alpha\rangle$ with the particle number N :

$$\begin{aligned}\hat{P}^A &= \sum_{N\alpha, N'\alpha'} |N\alpha\rangle\langle N\alpha| \frac{1}{2\pi} \int_0^{2\pi} e^{i\theta(\hat{N}-A)} |N'\alpha'\rangle\langle N'\alpha'| \\ &= \sum_{N\alpha, N'\alpha'} |N\alpha\rangle\langle N\alpha| N'\alpha'\rangle\langle N'\alpha'| \cdot \delta_{N,A} = \sum_{\alpha} |A\alpha\rangle\langle A\alpha|. \quad (11.58)\end{aligned}$$

Since we are only interested in a wave function $|\Psi\rangle$ with the proper particle number A , we find

$$g_n = 0 \quad \text{for } 2n \neq A.$$

$g_{A/2}$ is a normalization constant.

In the same way, in the case of translations we obtain a projector onto eigenstates of the linear momentum operators P with eigenvalues p :

$$\hat{P}^p = \frac{1}{(2\pi\hbar)^3} \int_{-\infty}^{+\infty} e^{(i/\hbar)q(P-p)} d^3q = \delta(P-p) \quad (11.59)$$

and

$$\hat{P}^p \Phi(r_1, \dots, r_A) = \int d^3q e^{ipq/\hbar} \Phi(r_1 - q, \dots, r_A - q).$$

For Abelian symmetry groups the weight function f is therefore completely determined by pure kinematics.

This is different for non-Abelian groups. Here we do not end up with a projector in the mathematical sense—though we also use the term “projection techniques” in this case. The weight function f is not completely determined by the symmetry. The most important example is the case of rotations in three dimensions. Since this symmetry group involves many details, and we do not want to interrupt the general discussion of projection techniques here, we will come back to three-dimensional rotations in Section 11.4.6.

11.4.2 Projection Before and After the Variation

So far we have not specified the symmetry-violating internal wave function $|\Phi\rangle$. In principle, there are two ways to determine this function

- (i) *Variation before the projection (VBP)* [PY 57]. In this case we proceed, for instance, as described in Chapter 7 and determine the optimal product wave function $|\Phi\rangle$ by the variational principle

$$\delta \frac{\langle \Phi | H | \Phi \rangle}{\langle \Phi | \Phi \rangle} = 0; \quad (11.60)$$

A “deformed” solution $|\Phi\rangle$ of this equation is a superposition of eigenstates of the corresponding symmetry operator, for instance, of

the angular momentum* \hat{J} : Applying the projection operator \hat{P}' , we get a wave function

$$|\Psi'\rangle = \hat{P}'|\Phi\rangle, \quad (11.61)$$

which contains only components with the angular momentum J . It is no longer a product wave function, but a complicated superposition of Slater-determinants as discussed in Section 5.5. Insofar it contains many more correlations than the function $|\Phi\rangle$. As we shall see in Section 11.4.4, it therefore has a lower energy expectation value and it is certainly a much better approximation of the exact wave function of the system.

The method is rather simple insofar as we get the whole rotational band based on the intrinsic wave function $|\Phi\rangle$ if we apply the projector \hat{P}' for different values of J . The variational equation (11.60) has to be solved only once. However, this method does violate the variational principle, since we do not vary the projected function $|\Psi'\rangle$ and it does not allow for changes of the self-consistent internal field within a rotational band. We can therefore improve the method in the following way.

- (ii) *Variation after projection (VAP)*: [Ze 65, RY 66, Yo 66]. Here we use the proper variational principle

$$\delta \frac{\langle \Psi' | H | \Psi' \rangle}{\langle \Psi' | \Psi' \rangle} = \delta \frac{\langle \Phi | \hat{P}' H \hat{P}' | \Phi \rangle}{\langle \Phi | \hat{P}' \hat{P}' | \Phi \rangle} = 0, \quad (11.62)$$

which means that we have to minimize the expectation value of the projected energy $\hat{P}' H \hat{P}'$ within the set of product wave functions $|\Phi\rangle$.

In principle, this method corresponds to a double variational GCM technique [see Eq. (10.147)], where we use the ansatz

$$|\Psi\rangle = \int d\Omega f(\Omega) R(\Omega) |\Phi\rangle \quad (11.63)$$

and vary the energy with respect to both the weight function f and the generating function $|\Phi\rangle$. Since the function f is determined more or less by the symmetry, only a variation of $|\Phi\rangle$ is left.

This method is certainly better than a variation before projection, but is also much more complicated. We must repeat the variation for each value of J again, and the operator $\hat{P}' H \hat{P}'$ is a multi-body operator.

Only in the case of particle number violation within the BCS model (Chap. 6) have both methods been carried out exactly. We will discuss these calculations in more detail in Section 11.4.3.

*Since in this section we give only a very qualitative discussion of different projection techniques, we use the angular momentum \hat{J} here only as an example, without going into the details of the rotational group. \hat{J} could be replaced in the following by any other symmetry operator.

In the BCS case we have only to vary with respect to the occupation probabilities c_k^2 . In the general case, where we must also vary the single-particle wave functions φ_k , the VAP methods become extremely complicated. In principle, we can write down (in analogy to Sec. 7.3.1) projected HFB equations in the most general case [Ze 65, On 68, SG 79], but in detail they correspond to a matrix of integral equations in several variables that have not been solved so far.

In all practical applications, therefore, one has used, to a greater or lesser extent, rather drastic approximations. There are two ways to solve Eq. (11.62) approximately:

- (i) We use the exact projection operator and restrict the set of trial functions $|\Phi\rangle$ drastically, allowing only very few important degrees of freedom. For instance, we can use a set of wave functions $|\Phi(\beta, \gamma)\rangle$ depending only on some deformation parameters, which we obtain from a diagonalization of the corresponding Nilsson potential. For each point in the (β, γ) plane we then have to calculate the projected energy and search for minima in this surface. This method is the complete analogy to the technique used in Fig. 7.1 for the determination of the unprojected HF solution. It has been applied in calculations in the high spin region, where particle number projection is important [DBM 73, FLW 73, FDG 76].
- (ii) We can use rather general assumptions for the wave functions $|\Phi\rangle$, such as large deformations and nearly Gaussian shape for the overlap kernels [see Eq. (11.79)] to approximate the projected energy without specifying the detailed structure of $|\Phi\rangle$. These techniques correspond to the momentum expansion in the GCM method (see Sec. 10.7). We will discuss them in Section 11.4.4.

Here we want only to anticipate the most important result [Ka 68, BMR 70, VS 71, Co 72]: In the limit of strong deformations, we find that the cranking model wave function $|\Phi_\omega\rangle$ (see Sec. 7.7) is an approximate solution of Eq. (11.62). This wave function is defined as a solution of the constrained variational principle

$$\delta \frac{\langle \Phi | H - \omega \hat{J}_x | \Phi \rangle}{\langle \Phi | \Phi \rangle} = 0, \quad \langle \Phi | \hat{J}_x | \Phi \rangle = \sqrt{I(I+1)}, \quad (11.64)$$

and ω is determined in such a way that the symmetry is, on the average, conserved. To each I -value we must therefore use a different internal wave function.*

* In the BCS case this result is rather trivial, because we adjust the chemical potential anyway for each value of N . This is necessary, because the simplest version of VBP without symmetry conservation on the average, would be a very poor approximation. The reason for that is given by the fact that the BCS wave function is not "strongly deformed," because BCS correlations are usually rather weak in nuclei. The first-order variation after the projection method, as it is given by the projection after variation from a BCS-function with proper particle number (PBCS), can therefore be improved by a full variation after projection (FBCS).

11.4.3 Particle Number Projection

The violation of the particle number in BCS wave functions is a nice example of a symmetry violation that can be treated by projection techniques.* Over the years a large number of methods have been developed in this field [Ba 60b, KLM 61, DMP 64, MPR 65, La 65, MRR 66, Ri 66, DK 66, IO 67, Fo 70, So 72, FHM 73, GGF 73, MMW 73, DMR 75, MR 77]. As an example, we present the *method of residues* proposed by Dietrich, Mang, and Pradal [DMP 64]. It starts with the projector (11.57). Introducing a complex variable $z = e^{i\pi}$, we can write it as an integral in the complex plane,

$$\hat{P}^A = \frac{1}{2\pi i} \oint \frac{z^{\hat{N}}}{z^{A+1}} dz. \quad (11.65)$$

When applied to a BCS wave function $|\Phi\rangle$ of the form (6.31), we get

$$|\Psi^A\rangle = \hat{P}^{A=2p} |\Phi\rangle = \frac{1}{2\pi i} \oint \frac{d\xi}{\xi^{p+1}} \prod_k (u_k + v_k \xi a_k^+ a_k^-) |-\rangle, \quad (11.66)$$

where we have replaced z by $\xi = z^2$ and used the fact that the pair of operators $a_k^+ a_k^-$ raises the particle number by two. $p = A/2$ is the number of pairs. The integrand in (11.66) is a Laurent series in ξ . The integration just picks the component with ξ^{-1} , that is, the component with p pairs.

Using the fermi commutation relations for the operators a_k, a_k^+ , we can express arbitrary matrix elements by the residues

$$R_r^m(k_1, \dots, k_m) = \frac{1}{2\pi i} \oint \frac{dz}{z^{(p-r)+1}} \prod_{\substack{k \neq k_1, \dots, k_m \\ >0}} (u_k^2 + z v_k^2). \quad (11.67)$$

The states listed in the argument of $R(\dots)$ are to be excluded from the product under the integral. As simple examples, we find the norm

$$\langle \Psi^A | \Psi^A \rangle = R_0^0 = \frac{1}{2\pi i} \oint \frac{dz}{z^{p+1}} \prod_{k>0} (u_k^2 + z v_k^2) \quad (11.68)$$

and the occupation probabilities for the level k in the wave function $|\Psi^A\rangle$

$$\frac{\langle \Psi^A | a_k^+ a_k | \Psi^A \rangle}{\langle \Psi^A | \Psi^A \rangle} = v_k^2 \cdot \frac{R_1^1(k)}{R_0^0}, \quad (11.69)$$

which shows that in the projected BCS theory the numbers v_k^2 no longer have the meaning of occupation probabilities. They are only variational parameters.

The residues R_r^m can be evaluated in a rather simple way from the recursion relations

$$R_r^m(k_1, \dots, k_m) = u_k^2 R_r^{m+1}(k_1, \dots, k_m, k) + v_k^2 R_{r+1}^{m+1}(k_1, \dots, k_m, k). \quad (11.70)$$

* A quite different method to treat particle number violation by two constraints on \hat{N} and \hat{N}^2 has been proposed by Lipkin and Nogami [Li 60b, No 64b, NZ 64, SR 78].

The projected expectation value of the energy takes the form*

$$\begin{aligned}
 E_{\text{proj}}^A &= \frac{\langle \Psi^A | H | \Psi^A \rangle}{\langle \Psi^A | \Psi^A \rangle} \\
 &= R_0^{0^{-1}} \cdot \left\{ \sum_{k \geq 0} \epsilon_k v_k^2 R_1^1(k) + \frac{1}{2} \sum_{kk' \geq 0} \bar{v}_{kk'kk'} v_k^2 v_{k'}^2 R_2^2(k, k') \right. \\
 &\quad \left. + \sum_{k, k' > 0} \bar{v}_{kk'kk'} v_k v_{k'} v_{k'} R_1^2(k, k') \right\}. \quad (11.71)
 \end{aligned}$$

We see that the expression (11.71) for the projected energy in this formalism is very similar to the analogous formula for the BCS energy (6.45). In the same way, we can calculate expectation values of arbitrary operators with particle number projected BCS functions (usually this method is called *PBCS theory*).

A bit more complicated is the *FBCS theory*, a variation after particle number projection. In this case, we must vary the projected energy with respect to the parameters v_k^2 . Proceeding in the same way as we have in the derivation of the BCS equations (6.48), we obtain a set of so-called FBCS equations [DMP 64]. They have a structure similar to the ordinary BCS equations and their solution provides no further difficulties.

Table 11.1 shows total energies of valence nucleons for even-even systems in the actinide region. As expected, the projected energies are always deeper by several hundred keV. The major part already comes from the elimination of spurious components in the BCS wave function by the PBCS procedure. The variation in the FBCS method causes an additional lowering.

The details depend strongly on the level density in the vicinity of the fermi surface. In general, with decreasing pairing correlations (i.e., with decreasing level density, which happens in Table 11.1 for increasing proton numbers) we observe an increase in the error of the PBCS method. In other words, for large correlations with strong symmetry violations, the mean field solution, which is obtained by a symmetry conservation on the average (in our case the simple BCS wave function) already provides a good approximation of the solution of the projected variational

Table 11.1. Total energies of valence nucleons for even proton systems in the actinide region calculated by different BCS techniques (25 orbitals outside a $Z = 76$ core). (From [MPR 65].)

Z	$-E_{\text{FBCS}}$ [MeV]	$E_{\text{BCS}} - E_{\text{FBCS}}$ [keV]	$E_{\text{PBCS}} - E_{\text{FBCS}}$ [keV]
88	91.433	264	2
90	106.005	330	28
92	120.340	400	36
94	134.312	427	51
96	147.956	553	72
98	160.829	494	84
100	173.210	496	77

* Residues with negative k -values should be set equal to the ones with the same positive indices in Eq. (11.71). For equal indices, we also have to use the rule

$$R_s^2(kk) = R_1^1(k).$$

problem. For small correlations the mean field approach does not give a satisfying internal wave function.

In particular, we know that below a critical level density (which is equivalent to a critical force strength G_c) the gap equation (6.60) only has the trivial solution with vanishing gap. This is no longer true in the FBCS method. It can also account for rather weak pairing correlations. As a measure of these correlations, we can no longer use the parameter Δ in a projected theory, since it describes a "deformation," which vanishes in the symmetry conserving wave function. Instead, we can use, for instance, the function

$$D^2 = \sum_{k, k' > 0} \langle a_k^\dagger a_k^\dagger a_{k'} a_{k'} \rangle, \quad (11.72)$$

which measures the number of Cooper pairs in the wave function. D coincides to leading order with Δ/\sqrt{G} in the BCS theory. In the projected theory it is given by

$$D^2 = \sum_{kk' > 0} R_1^2(k, k') \frac{u_k v_k u_{k'} v_{k'}}{R_0^2}. \quad (11.73)$$

Figure 11.5 shows the qualitative behavior of this quantity as a function of the coupling strength G . In the BCS and PBCS cases, the pairing correlation vanishes for $G < G_c$. The BCS solution, in particular, shows a rather sharp cusp at $G = G_c$. This sharp "phase transition," however, is washed out for finite systems. It disappears in the FBCS model and we find a gradual weakening of the pairing correlations as a function of G . In all cases of weak pairing correlations we should therefore go beyond PBCS theory. An example is calculations in the high spin region, where we expect a drastic reduction of the pairing field by either a decoupling mechanism or the Mottelson-Valatin effect in the rotating system (see Sec. 7.7).

As we saw in Sec. 7.7, in these cases we need the full HFB theory, that is, we also have to vary with respect to the single-particle wave functions φ_k . *Particle number projected HFB theory* after the variation can be obtained rather simply from the method discussed so far. Since general HFB wave functions in the canonical basis (see Sec. 7.2) have the structure of BCS functions, we have only to transform to the canonical basis and obtain in the same way the projected matrix elements.

An approximate method that avoids these transformations is based on the idea of Fomenko to replace the integral in Eq. (11.66) by a sum over L points $\xi_l = \exp(2\pi il/L)$ on the unity circle [Fo 70, So 72]. The approximate projector then

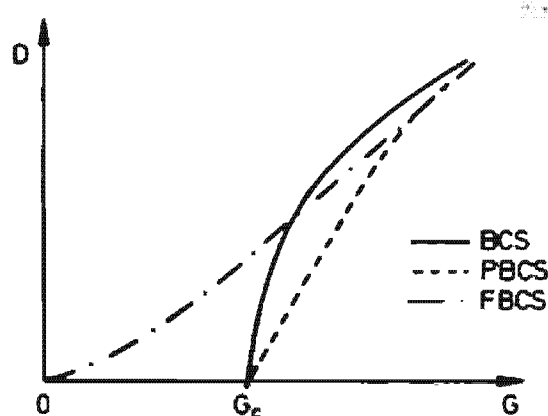


Figure 11.5. Pairing correlations as a function of the coupling strength G in the BCS (full), PBCS (dashed), and FBCS (dashed/dotted) method (qualitatively).

has the form

$$\hat{P}_L^A = \frac{1}{L} \sum_{l=1}^L (\zeta_l)^{(\hat{N}-A)/2}. \quad (11.74)$$

It is easy to see that $\hat{P}_L^{A+2m} \hat{P}_L^A |\text{BCS}\rangle$ vanishes unless $m=0, \pm L, \pm 2L, \dots$. This means that the wave function $\hat{P}_L^A |\text{BCS}\rangle$ contains only components with the particle numbers $A, A \pm 2L, A \pm 4L, \dots$. For instance, the approximate projector \hat{P}_2^A already annihilates the components with $A \pm 2, A \pm 6, A \pm 10, \dots$. The projected wave function ($A=2p$)

$$\hat{P}_L^{2p} |\text{BCS}\rangle = \frac{1}{L} \sum_{l=1}^L \zeta_l^{-p} \prod_{k>0} (u_k + c_k \zeta_l a_k^\dagger a_k^\dagger) |-\rangle \quad (11.75)$$

is a linear combination of L BCS wave functions rotated in the gauge space by the angle $\varphi_l = 2\pi l/L$; that is, c_k is replaced by $e^{i\varphi_l} c_k$. In the same way \hat{P}_L^A transforms an HFB function $|\Phi\rangle$ given by the coefficients (U_{kk}, V_{kk}) into a linear combination of HFB functions $|\Phi_i\rangle$ ($i=1, \dots, L$) with the coefficients $(U_{kk}, \zeta_i V_{kk})$. A transformation to the canonical basis is not necessary.

Since the BCS wave function is smeared out only over a few particle numbers, for small values of L , we already obtain a nearly exact projection.

A full HFB theory with variation after particle number projection has so far not been carried out. In any case, it is much more complicated than FBCS. In all practical calculations functions $|\Phi(\beta, \gamma, \Delta)\rangle$ depending on a limited number of parameters have been used to minimize the projected energy.

11.4.4 Approximate Projection for Large Deformations

A quite general method for approximate projection for the case of strong symmetry violations has been given by Kamalah [Ka 68] for the case of the rotational group (see also [Kü 72]). Since the rotational group shows many complicated special features, and since the method is also applicable to other cases, such as the particle number [DMR 75, Ma 75a], we shall present it here for the case of a one-dimensional rotation around a fixed axis only. It will be described by the operator \hat{J} and the angle α .

The projector onto eigenfunctions of \hat{J} has the form (11.57)

$$\hat{P}^j = \frac{1}{2\pi} \int_0^{2\pi} e^{i\alpha(j-1)} d\alpha \quad (11.76)$$

and for the projected energy we obtain

$$E_{\text{proj}}^j = \frac{\langle \Phi | H \hat{P}^j | \Phi \rangle}{\langle \Phi | \hat{P}^j | \Phi \rangle} = \frac{\int d\alpha h(\alpha) e^{-i\alpha j}}{\int d\alpha n(\alpha) e^{-i\alpha j}} \quad (11.77)$$

with overlap integrals

$$\begin{Bmatrix} h(\alpha) \\ n(\alpha) \end{Bmatrix} = \langle \Phi | \begin{Bmatrix} H \\ 1 \end{Bmatrix} e^{i\alpha j} | \Phi \rangle. \quad (11.78)$$

In the case of large particle numbers and strong deformations, we expect the functions $n(\alpha)$ and $h(\alpha)$ to be sharply peaked at $\alpha=0$ and to vanish elsewhere in such a way that the quotient $h(\alpha)/n(\alpha)$ is a rather smooth function. This is a general property of many-body wave functions (which was discussed in great detail in Sec. 10.7). Following the arguments of Section 10.7.4, we obtain*

$$n(\alpha) \approx \exp(i\langle \hat{J} \rangle \cdot \alpha - \frac{1}{2}\langle \Delta \hat{J}^2 \rangle \alpha^2), \quad (11.79)$$

with

$$\Delta \hat{J} = \hat{J} - \langle \hat{J} \rangle,$$

the only difference now being that we also allow for time odd components in the wave functions, which does not give a pure Gaussian, but an additional phase in Eq. (11.79) ($\langle \hat{J} \rangle \neq 0$). The idea of Kamlah is now to use the operator

$$\hat{I} := -\langle \hat{J} \rangle + \frac{1}{i} \frac{\partial}{\partial \alpha},$$

which is a representation of the symmetry operator in the space of the parameter α ,[†] and to expand the Hamilton overlap function $h(\alpha)$ in the following way.

$$h(\alpha) = \sum_{n=0}^M h_n \hat{I}^n n(\alpha). \quad (11.80)$$

Mathematically this essentially corresponds to a Taylor expansion of the Fourier transformed function $h(\alpha)/n(\alpha)$. Since we need $h(\alpha)$ only in the vicinity of $\alpha=0$ we can already hope to get a very good approximation for this function with a few non-vanishing constants h_0, h_1, \dots, h_M , if they are properly adjusted. The number M certainly depends on the width of the overlap (11.79), that is, on the fluctuation $\langle \Delta \hat{J}^2 \rangle$ of the symmetry operator \hat{J} in the wave function $|\Phi\rangle$. The larger the symmetry violation, the better the approximation will already be for low M -values.

The expansion (11.80) is not a perturbative expansion in the sense that the coefficients h_n are determined step by step one after the other, such that the coefficient h_0 does not change going from M to $M+1$, but for each M -value the whole set h_0, \dots, h_M is calculated at once: Operating with $1, \hat{I}, \hat{I}^2, \dots, \hat{I}^M$ on Eq. (11.80) we obtain, in the limit $\alpha \rightarrow 0$, the following inhomogeneous system for the unknowns h_0, \dots, h_M :

$$\langle H(\Delta \hat{J})^M \rangle = \sum_{n=0}^M h_n \langle (\Delta \hat{J})^{M+n} \rangle. \quad (11.81)$$

The solution of these equations gives us an expression for the projected

* In the following we use the symbol $| \rangle$ for the normalized intrinsic function $|\Phi\rangle$.

[†] In the case of three-dimensional rotations we therefore use, instead of $(1/i)\partial/\partial\alpha$, the representation of the angular momenta in Euler angles (see Appendix A).

energy. From (11.77) and (11.80), we get

$$E'_{\text{proj}} = \sum_{n=0}^M h_n \cdot (I - \langle \hat{j} \rangle)^n. \quad (11.82)$$

The simplest case is $M = 1$. Here we find

$$h_0 = \langle H \rangle, \quad h_1 = \frac{\langle H \Delta \hat{j} \rangle}{\langle \Delta \hat{j}^2 \rangle}, \quad (11.83)$$

and

$$E'_{\text{proj}} = \langle \Phi | H - h_1 \hat{j} | \Phi \rangle + h_1 \cdot I. \quad (11.84)$$

In a variation after projection method we get the variational equation

$$\frac{\delta}{\delta \Phi} \langle \Phi | H | \Phi \rangle - h_1 \frac{\delta}{\delta \Phi} \langle \Phi | \hat{j} | \Phi \rangle + (I - \langle \hat{j} \rangle) \frac{\delta h_1}{\delta \Phi} = 0. \quad (11.85)$$

It is solved by a solution of the cranking equations*

$$\frac{\delta}{\delta \Phi} \langle \Phi | H | \Phi \rangle - \omega \frac{\delta}{\delta \Phi} \langle \Phi | \hat{j} | \Phi \rangle = 0. \quad (11.86)$$

with

$$\langle \hat{j} \rangle = I$$

if the condition $h_1 = \omega$ is fulfilled. To see that this is always the case we use the fact that Eq. (11.86) has to hold for arbitrary variations $|\delta \Phi\rangle$ in the set of product wave functions. One such variation is given by $|\delta \Phi\rangle \propto \Delta \hat{j} |\Phi\rangle = \hat{j}^{20} |\Phi\rangle$ (in the sense of a quasi-particle representation of Chap. 7). Therefore, we get

$$\langle \Delta \hat{j} H \rangle - \omega \langle (\Delta \hat{j})^2 \rangle = 0,$$

which shows that $\omega = h_1$ in Eq. (11.83).

We now have proven the remarkable result that in the case of strong symmetry violations, where $M = 1$ is a sufficient approximation in the expansion (11.80), cranking model wave functions that preserve the average symmetry are a solution of the variational equations after projection. This result does not depend on the structure of the overlap functions in detail. One only needs the fact that they are sharply peaked around the origin.

So far we have shown this only in the case of a one-dimensional rotation, but the result (as we shall see in Sec. 11.4.4) can be transferred with minor changes also to the three-dimensional case.

Within this approximation, the projected energy is given by h_0 and equal to the unprojected energy. This justifies the self-consistent cranking model calculations for the rotational spectra (see Sec. 7.7). In particular, for the

* In some cases it turns out that this solution does not correspond to a minimum but to a flat maximum. Second-order terms ($M = 2$), however, guarantee that this maximum is changed to a minimum [BMR 70].

self-consistent moment of inertia we find

$$g_{sc}^{-1} = \frac{\omega}{\langle \hat{J} \rangle} = \frac{\langle H \Delta \hat{J} \rangle}{\langle \Delta \hat{J}^2 \rangle \langle \hat{J} \rangle}. \quad (11.87)$$

As discussed in Section 8.5.4, it is at the point $\omega=0$ identical with that of Thouless and Valatin.

This simple result, however, only applies for the energy expectation value. If we want to calculate moments and transition probabilities, we have to carry out an explicit projection from the intrinsic cranking functions (see Sec. 11.4.6.4).

In cases where the restriction to $M=1$ in the expansion (11.80) is not good enough, we have to go to higher M -values. For $M=2$ we neglect* $\langle \Delta \hat{J}^3 \rangle$, and get

$$h_0 = \langle H \rangle - \frac{\langle \Delta \hat{J}^2 \rangle}{2g_Y}, \quad h_1 = \frac{\langle H \Delta \hat{J} \rangle}{\langle \Delta \hat{J}^2 \rangle} = \frac{\langle \hat{J} \rangle}{g_{sc}}, \quad h_2 = \frac{1}{2g_Y}, \quad (11.88)$$

with

$$\frac{1}{2g_Y} = \frac{\langle H \Delta \hat{J}^2 \rangle - \langle H \rangle \langle \Delta \hat{J}^2 \rangle}{\langle \Delta \hat{J}^4 \rangle - \langle \Delta \hat{J}^2 \rangle^2}. \quad (11.89)$$

In the case of a Gaussian norm (11.79), we have $\langle \Delta \hat{J}^4 \rangle = 3\langle \Delta \hat{J}^2 \rangle^2$ and find

$$g_Y^{-1} = \frac{\langle (H - \langle H \rangle) \Delta \hat{J}^2 \rangle}{\langle \Delta \hat{J}^2 \rangle^2}. \quad (11.90)$$

The projected energy now has the form:

$$E'_{proj} = \langle H \rangle - \frac{\langle \Delta \hat{J}^2 \rangle}{2g_Y} + \frac{\langle \hat{J} \rangle}{g_{sc}} (I - \langle \hat{J} \rangle) + \frac{1}{2g_Y} (I - \langle \hat{J} \rangle)^2. \quad (11.91)$$

Let us first study the method of *variation before projection*, which was originally proposed by Peierls and Yoccoz [PY 57, Yo 57]. Here the wave function $|\Phi\rangle$ is obtained from a minimization of H without constraint. It is, therefore, time-reversal invariant and has vanishing expectation values $\langle \hat{J} \rangle$ and $\langle H \hat{J} \rangle$. The spectrum then has the form

$$E'_{proj} = \langle H - \frac{\hat{J}^2}{2g_Y} \rangle + \frac{I^2}{2g_Y}. \quad (11.92)$$

It is the spectrum of a one-dimensional rotor with the Yoccoz value g_Y for the moment of inertia (see Sec. 11.4.5).[†] The band head is obtained from the HF energy $\langle H \rangle$ by subtracting the spurious rotational energy in the

* $\langle \Delta \hat{J}^3 \rangle$ measures the asymmetry of the I distribution in $|\Phi\rangle$. In the case of a Gaussian norm overlap, it vanishes exactly.

[†] The method has also been investigated in great detail by Verhaar [Ve 63, Ve 64] for the three-dimensional rotation in even and odd nuclei for $K=0$ and $K \neq 0$ bands. Thus one can derive microscopic expressions for the B and C coefficients in Eq. (3.1) as well as for the decoupling parameters (3.31).

symmetry-violating wave function.* This produces a substantial lowering of the ground state energy. In well deformed nuclei this term is of the order of 4–6 MeV. We have already encountered this term several times, for instance, in the method of redundant coordinates (see Sec. 11.3.2) and in the treatment of symmetry violations within the RPA approach (Sec. 8.4.8).

Carrying out a *variation after projection*, we have to minimize the r.h.s. of Eq. (11.91) with respect to $|\Phi\rangle$. In the case where the spurious energy $\langle\Delta\hat{J}^2\rangle/2\gamma$ does not depend very much on $|\Phi\rangle$ we again find that the cranking model is a solution. Model calculations [BMR 70] in well-deformed nuclei of the rare earth region have shown that this term indeed gives a rather flat contribution to the energy surface.

The convergence of the Kamlah expansion (11.80) depends on how sharply the overlap functions are peaked at the origin. It is measured by the width $\langle\Delta\hat{J}^2\rangle$, that is, by the fluctuation of the symmetry operator. If this fluctuation is large, the expansion converges rapidly. We call such cases the limit of *large deformations*, and we want to emphasize that this limit is not necessarily connected with large deformation parameters of the corresponding mean field. In the case of large particle numbers, the fluctuation $\langle\Delta\hat{J}^2\rangle$ can have a very large value, even for small deformation parameters. In fact, the shape of “well deformed” heavy nuclei in the ground state does not differ very much from a sphere (see, for instance, Fig. 7.5). Because of the large particle numbers, however, the overlap functions are strongly peaked at the origin, which indicates that the assumption of a phase transition to a deformed mean field is well justified.

11.4.5 The Inertial Parameters

In all collective motions connected with the violation of a continuous symmetry, the potential energy $\langle H \rangle$ (11.9) does not depend on the collective coordinate. Therefore, there are no restoring forces and in most cases of the rotational type we always get motions with large amplitude. The crucial parameters of the collective Hamiltonian are therefore the inertial parameters.

There is one case where we know this parameter a priori: Because of Galilean invariance, the collective inertia of *translations* have to be equal to the total mass $A m$ of the system. This case therefore provides a very good test of the different approximation schemes used so far in the treatment of symmetry violations.

We start with the method of *variation after projection* [Ze 65, Vi 66, RY 66]. Equation (11.62) defines the intrinsic solution for a wave function with momentum p :

$$\langle \delta\Phi | (H - E^p) \hat{P}^p | \Phi \rangle = 0. \quad (11.93)$$

* For calculations concerning this contribution, see [ZN 77, VLS 79, ER 80].

Transforming from the laboratory system to a system which moves with the velocity $v = p/2Am$, we find (R is the center of mass coordinate):

$$|\Phi\rangle = e^{(i/\hbar)pR} |\Phi'\rangle \quad (11.94)$$

and

$$\langle \delta\Phi' | e^{-(i/\hbar)pR} (H - E^p) \hat{P}^p e^{(i/\hbar)pR} |\Phi'\rangle = 0. \quad (11.95)$$

Using the definition (11.59) of the projector \hat{P}^p , we obtain the transformation

$$e^{-(i/\hbar)pR} \hat{P}^p e^{(i/\hbar)pR} = \hat{P}^0. \quad (11.96)$$

For a local two-body interaction we get

$$e^{-(i/\hbar)pR} H e^{(i/\hbar)pR} = H + \frac{pP}{Am} + \frac{p^2}{2Am}. \quad (11.97)$$

Since \hat{P}^0 projects onto states with vanishing eigenvalue of the center of mass momentum P , Eq. (11.95) has the form

$$\langle \delta\Phi' | \left(H - E^p + \frac{p^2}{2Am} \right) \hat{P}^0 |\Phi'\rangle = 0. \quad (11.98)$$

It corresponds to the variational problem for vanishing momentum and energy E^0 . The energy of the system with momentum p is therefore given by

$$E^p = E^0 + \frac{p^2}{2Am}, \quad (11.99)$$

which shows that we obtain the proper total mass using the method of projection after variation. This property is conserved if we approximate the projection after variation by the *self-consistent cranking model* [Gr 60] (in the case of translations, we usually say "pushing" model):

$$\langle \delta\Phi | H - vP | \Phi \rangle = 0. \quad (11.100)$$

The inertia parameter of Thouless and Valatin (8.113) obtained in this way is the total mass. In principle, we have shown this already in Section 8.4.7, but it is easy to verify it once more if we use the admissible variation

$$|\delta\Phi\rangle \propto R|\Phi\rangle. \quad (11.101)$$

Subtracting Eq. (11.100) from its complex conjugate, we obtain

$$\langle \Phi | [H, R] - v \cdot [P, R] | \Phi \rangle = 0. \quad (11.102)$$

In the case of H containing only a local two-body interaction, we get

$$v = \frac{\langle \Phi | P | \Phi \rangle}{Am}, \quad (11.103)$$

which shows that the inertia parameter, which is given by the ratio of the expectation value of P to the velocity v , is again the total mass.

We can deduce the simple *Inglis formula* [see Eq. (3.89)] as the inertia parameter also from the variational equation (11.93) if we replace the

two-body interaction in the Hamiltonian H by a one-body potential (the variational principle in this case is equivalent to an exact diagonalization). This shows us that for a local one-body potential as, for instance, for a Woods-Saxon well, the Inglis formula also gives the exact total mass* [Vi 63].

It is a drawback of the method of *variation before projection*—which yields the inertia of Yoccoz[†] (11.90)—that it violates the Galilean invariance. It does not produce the exact mass. From Eqs. (11.90) and (10.134) we obtain for the inertia in the notation of Section 8.4.7 (see also [FW 70]):

$$\mathfrak{g}_Y^{-1} = \frac{1}{4\langle \Delta P^2 \rangle^2} \langle [P, [H, P]_+]_+ \rangle_L = \frac{(P^* P) \begin{pmatrix} A & B \\ B^* & A^* \end{pmatrix} \begin{pmatrix} P \\ P^* \end{pmatrix}}{\left(2 \sum_{mi} |P_{mi}|^2\right)^2}, \quad (11.104)$$

where P is the *ph* part of one component of the vector \mathbf{P} if the self-consistent basis ($H^{20}=0$) is used. In the limit of a vanishing residual interaction, it is equal to

$$\mathfrak{g}_Y(V=0) = \frac{2 \left(\sum_{mi} |P_{mi}|^2 \right)^2}{\sum_{mi} |P_{mi}|^2 (\epsilon_m - \epsilon_i)}. \quad (11.105)$$

It is obviously different from the Thouless-Valatin inertia (8.108),

$$\mathfrak{g}_{TV}^{-1} = \frac{1}{\hbar^2} \langle [R, [H, R]_-]_- \rangle = \frac{2}{\hbar^2} S_1(R)$$

or

$$\mathfrak{g}_{TV} = \frac{1}{2} (P^* P) \begin{pmatrix} A & B \\ B^* & A^* \end{pmatrix}^{-1} \begin{pmatrix} P \\ P^* \end{pmatrix} \quad (11.106)$$

which in the limit of vanishing interaction goes over into the Inglis formula (3.89),

$$\mathfrak{g}_{TV}^{-1}(V=0) = 2 \sum_{mi} \frac{|P_{mi}|^2}{\epsilon_m - \epsilon_i}. \quad (11.107)$$

* This is not a contradiction to the fact that the Thouless-Valatin mass (8.113) differs from the Inglis formula by the residual interaction, because for all forces that produce a local HF field, the residual interaction has no influence on the mass (the time odd part Γ_1 in Eq. (12.81) vanishes).

[†] The idea that the intrinsic wave function $|\Phi\rangle$ is a superposition of all the members of the rotational band Ψ' has also been used by Skyrme [Sk 57]: Assuming that the intrinsic Hamiltonian $H' = H - J^2/2\hbar$ has an eigenstate, which is not an eigenstate of J^2 , we can show [Li 60a] that H has a rotational spectrum with \mathfrak{g} as moment of inertia. To determine the optimal value of \mathfrak{g} , Skyrme minimized the expectation value $\langle (H' - \langle H' \rangle)^2 \rangle$ with respect to the parameter \mathfrak{g} , and found as a solution

$$\frac{1}{2\hbar_{\text{Skyrme}}} = \frac{\langle (H - \langle H \rangle) J^2 \rangle}{\langle J^2 \rangle - \langle J^2 \rangle^2}.$$

This expression is for time-even wave functions identical with Eq. (11.89), and therefore closely related to \mathfrak{g}_Y (see also [Wo 75]).

How large and how important this difference actually is, has not been investigated very much. It certainly depends on the interaction and on the single-particle energies ϵ_k . For all models with a constant level spacing $\epsilon = \epsilon_m - \epsilon_l$, both values are identical. In Sec. 10.7 we saw that we have the Yoccoz inertia (11.104) for all kinds of collective motions, if we use the simple GCM method with coordinate dependent generating functions. Only in theories in which we allow the intrinsic function $|\Phi\rangle$ to also have time-odd components that depend on the momentum do we eventually obtain the proper mass. This is the case in the *time-dependent Hartree-Fock method* (see Chap. 12) and in the variation-after-projection method.

To obtain the proper mass in a GCM method also, *Thouless and Peierls* [PT 62] proposed to superpose not only wave functions of different positions [see Eq. (11.59)],

$$|\Phi(\mathbf{q})\rangle = e^{(i/\hbar)\mathbf{q}\cdot\mathbf{P}}|\Phi\rangle, \quad (11.108)$$

but also those with different velocities,

$$|\Phi(\mathbf{q}, \mathbf{v})\rangle = e^{-(i/\hbar)\mathbf{M}\cdot\mathbf{v}\mathbf{R}}|\Phi(\mathbf{q})\rangle. \quad (11.109)$$

This yields a double projection method, in which the velocity dependence of the weight function $f(\mathbf{q}, \mathbf{v})$ has to be determined by variation. We can show that the wave functions obtained in this way do not violate Galilean invariance. The method itself, however, is rather complicated and up to now has not been applied very much [Ba 69b]. In practical calculations the method of variation after projection is usually preferred (see Sec. 11.4.2).

So far we have treated only the case of translations. In the case of rotations or other collective motions as discussed in Section 10.7 the situation is more complicated. The exact inertia is not known a priori. We can only argue in analogy to the translational case. Numerical calculations have shown, at least, that in the rotational case, the moments of inertia obtained by the method of Thouless and Valatin are, with proper handling of the pairing correlations, in good agreement with experimental data (see Fig. 3.14).

11.4.6 Angular Momentum Projection

11.4.6.1. Derivation of Projector-like Operators. The rotational group is usually parametrized by the three Euler angles* $\Omega = (\alpha, \beta, \gamma)$, and the general rotation is given in Eq. (A.4). We have to go back to the ansatz (11.53) of the wave function $|\Psi\rangle$. As in Eq. (11.55), we expand the weight function $f(\Omega)$ into a complete set of eigenfunctions of the corresponding symmetry operators: the angular momenta represented in Euler angles. As

* There have been used other representations also, for instance

$$R = \exp(i\mathbf{p}\cdot\hat{\mathbf{J}})$$

for a general rotation with the parameters $\varphi_x, \varphi_y, \varphi_z$ [KO 77].

discussed in Appendix A, such a set is given by the Wigner functions $D_{MK}^{I''}(\Omega)$. We therefore gain the ansatz

$$f(\Omega) = \frac{2I+1}{8\pi^2} \sum_{IMK} g_{IMK} D_{MK}^{I''}(\Omega) \quad (11.110)$$

and

$$|\Psi\rangle = \sum_{IMK} g_{IMK} \hat{P}_{MK}^I |\Phi\rangle. \quad (11.111)$$

The operators [RW 54, PY 57, Vi 66]

$$\begin{aligned} \hat{P}_{MK}^I &= \frac{2I+1}{8\pi^2} \int D_{MK}^{I''}(\Omega) R(\Omega) d\Omega \quad (11.112) \\ R(\Omega) &= e^{iaj_x} e^{ibj_y} e^{icj_z} \end{aligned}$$

can be written in analogy to (11.58) [LB 68, Co 71]

$$\hat{P}_{MK}^I = \sum_{\alpha} |IM\alpha\rangle \langle IK\alpha|, \quad (11.113)$$

where $|IM\alpha\rangle$ is a complete orthonormalized set in the Hilbert space and α characterizes all quantum numbers besides the rotational quantum numbers I and M .

From (11.113) we see that \hat{P}_{MK}^I are not projectors in the mathematical sense. We only have the relations

$$\hat{P}_{MK}^I \hat{P}_{M'K'}^{I'} = \delta_{II'} \delta_{M'K'} \hat{P}_{MK}^I; \quad (\hat{P}_{MK}^I)^* = \hat{P}_{KM}^I. \quad (11.114)$$

To show how they act on the "internal"^{*} symmetry-violating wave function $|\Phi\rangle$, we decompose $|\Phi\rangle$ with respect to eigenstates of the operator \hat{j}_z with quantum number K :

$$|\Phi\rangle = \sum_{K'} |\Phi_{K'}\rangle; \quad \hat{j}_z |\Phi_{K'}\rangle = K |\Phi_{K'}\rangle. \quad (11.115)$$

\hat{P}_{MK}^I transforms the component $|\Phi_K\rangle$ into an eigenfunction of \hat{j}^2 and \hat{j}_z with the quantum numbers I and M and annihilates all other components with $K' \neq K$.

In principle it is very simple to construct the precise mathematical projector onto the quantum numbers I, M . It is given by[†]

$$\hat{P}_{MM}^I = \sum_{\alpha} |IM\alpha\rangle \langle IM\alpha|. \quad (11.116)$$

* Actually, in the GCM method we introduce neither an intrinsic frame nor redundant coordinates. The connection between the "internal" wave function $|\Phi\rangle$ and the function $|\Psi\rangle$ in the laboratory frame is given not by a coordinate transformation, but by the GCM ansatz (11.111).

[†] This operator has been represented by Lowdin [Lo 64] in the following way.

$$\hat{P}_{MM}^I = \prod_{L \neq I} \frac{\hat{j}^2 - L(L+1)}{I(I+1) - L(L+1)} \prod_{K \neq M} \frac{\hat{j}_z - K}{M - K}.$$

In practical applications of this operator, we end up with a set of algebraic equations (see also [KL 64, Ke 66, Ul 71, 72, MKL 71, MM 76]) and do not have to perform integrals over the Euler angles.

From (11.115) we see, however, that this operator is rather unphysical. Acting, for instance, on an axial symmetric Nilsson function with $K=0$, we would get only wave functions $|\Psi^{IM}\rangle$ with $M=0$, which clearly violates the rotational symmetry.

We therefore have to use the general ansatz*

$$|\Psi^{IM}\rangle = \sum_K g_K \hat{P}_{MK}^I |\Phi\rangle = \sum_K g_K \frac{2I+1}{8\pi^2} \int d\Omega D_{MK}^{I*}(\Omega) R(\Omega) |\Phi\rangle. \quad (11.117)$$

In cases where the wave function $|\Phi\rangle$ has axial symmetry, only the K -value K_0 contributes to the sum (11.117), and the coefficient g_{K_0} is given by the normalization. In general, however, we have to minimize the Hamiltonian with respect to the coefficients g_K . The energy is given by

$$E'_{\text{proj}} = \frac{\langle \Psi^{IM} | H | \Psi^{IM} \rangle}{\langle \Psi^{IM} | \Psi^{IM} \rangle} = \frac{\sum_{KK'} g_K^* g_{K'} h'_{KK'}}{\sum_{KK'} g_K^* g_{K'} n'_{KK'}}, \quad (11.118)$$

with the kernels

$$\begin{aligned} h'_{KK'} &= \langle \Phi | H \hat{P}_{KK'}^I | \Phi \rangle, \\ n'_{KK'} &= \langle \Phi | \hat{P}_{KK'}^I | \Phi \rangle. \end{aligned} \quad (11.119)$$

The coefficients g_K are the solution of the generalized eigenvalue problem

$$\sum_{K'} h'_{KK'} g_{K'} = E' \sum_{K'} n'_{KK'} g_{K'}. \quad (11.120)$$

It corresponds to a diagonalization of the Hamiltonian H in the space spanned by the nonorthogonal system $\hat{P}_{MK}^I |\Phi\rangle$.

In Section 10.7 we saw how to proceed in order to end up with a Hermitian eigenvalue problem. We must either orthogonalize the set $\hat{P}_{MK}^I |\Phi\rangle$ or calculate the square root of the matrix $n'_{KK'}$. In the case of a Gaussian form of the overlap function $\langle \Phi | R(\Omega) | \Phi \rangle$, that is, for a strongly deformed wave function (see Sec. 11.4.4), we can do this analytically. Since we are faced with a three dimensional problem, we end up with a collective Hamiltonian like the one of Eq. (10.145). Une et al. [UIO 76] have shown that it has exactly the form of the rotor Hamiltonian (1.55) with moments of inertia given by the Yoccoz formula† (see Sec. 11.4.5).

The close analogy to the collective rotor model can be visualized rather easily if we define extremely deformed many-body wave functions‡ $|\Omega\rangle$, which point like a needle in the direction Ω . They are nearly localized in Ω -space. The overlap between these functions and the wave function $|\Psi^{IM}\rangle$ (11.117),

$$\langle \Omega | \Psi^{IM} \rangle \propto \sum_K g_K \int d\Omega' D_{MK}^{I*}(\Omega') \langle \Omega | R(\Omega') | \Phi \rangle, \quad (11.121)$$

* The coefficients g_K will certainly also depend on I , as we see from Eq. (11.120). However, we omit the index I .

† See also [ABC 77a].

‡ These functions correspond to the biorthogonal basis discussed in Eq. (10.20)ff.

measures the probability amplitude of finding the system at the angles Ω . In the limit where the wave function $|\Phi\rangle$ is well deformed, peaking at $\Omega=0$, the overlap $\langle\Omega|R(\Omega')|\Phi\rangle$ behaves like the δ -function $\delta(\Omega-\Omega')$ in Ω -space, and we get [Ze 67, FJM 71]

$$\langle\Omega|\Psi'^M\rangle \propto \sum_K g_K D_{MK}^I(\Omega), \quad (11.122)$$

which is exactly the wave function of a rotor (see Sec. 1.5.1). In this approximation, the deformed function $|\Phi\rangle$ moves in space like a rotor. We have to emphasize, however, that we use no redundant variables. The Euler angles Ω are only parameters used as generator coordinates.

In the same way as the symmetry behavior of the rotor, under certain operations of the group D_2 [as, for instance, \mathfrak{R}_1 or \mathfrak{R}_2 in Eqs. (1.57)ff.] causes relationships between the expansion coefficients $g_K^{(\text{rotor})}$, we can now derive corresponding relations for the coefficients g_K if our internal wave function has these symmetries.

As an example, we use a rotation of 180° around the x -axis. We assume* that the internal wave function $|\Phi\rangle$ is an eigenfunction with respect to this operation:

$$e^{i\pi j_x}|\Phi\rangle = r_x|\Phi\rangle, \quad (11.124)$$

The eigenvalue r_x is ± 1 for systems with even and $\pm i$ for systems with odd particle number. It is often called the *signature* [Bo 76b]. The ground state of an even-even nucleus in a deformed Nilsson well, for instance, always has $r_x = +1$, because a pair-wise occupation of the degenerate levels with $\pm i$ gives the lowest energy. The condition $r_x = +1$ for the ground state band is therefore a natural consequence of the variational principle. This fact provides a microscopic foundation for the assumption (1.58) of the rotor model—that the deformed core has the eigenvalue $+1$ with respect to the operation \mathfrak{R}_1 (1.57).

The symmetry (11.123) is rather general and also applies for cranking model wave functions. So far, no experimental evidence has been found that it is not valid. We shall therefore use this symmetry in the following.

If we decompose the internal wave function $|\Phi\rangle$ into its components $|\Phi_K\rangle$ with good K -quantum number, as in Eq. (11.115), we get from (11.123):

$$e^{i\pi j_x}|\Phi_K\rangle = r_x|\Phi_{-K}\rangle, \quad (11.125)$$

From Eq. (11.124) we can deduce

$$\hat{P}_{MK}^I e^{i\pi j_x} = (-)^I \hat{P}_{MK}^I, \quad (11.126)$$

which shows that the states

$$\hat{P}_{MK}^I |\Phi\rangle = \hat{P}_{MK}^I |\Phi_K\rangle \quad \text{and} \quad \hat{P}_{M-K}^I |\Phi\rangle = \hat{P}_{M-K}^I |\Phi_{-K}\rangle$$

correspond to the same state in the Hilbert space. We can therefore restrict the sum in Eq. (11.117) over $K > 0$.

*This assumption is compatible with rotational invariance of our method, because a rotation of the function $|\Phi\rangle$ by the Euler angles Ω can be expressed as a transformation of the coefficients g_K , as we may see from the relationship

$$\hat{P}_{MK}^I R(\Omega) = \sum_K D_{KK}^I(\Omega) \hat{P}_{MK}^I. \quad (11.123)$$

As long as we take into account arbitrary coefficients g_K , we are free in the choice of the orientation of $|\Phi\rangle$.

The representation

$$|\Psi'^M\rangle = \sum_{K>0} \frac{g_K}{1 + \delta_{K0}} (\hat{P}'_{MK} + (-)^I r_x^{-1} \hat{P}'_{M-K}) |\Phi\rangle \quad (11.127)$$

clearly shows that an axially symmetric wave function $|\Phi\rangle$ with $K=0$ and $r_x=1$ is projected onto zero for odd I -values. For the ground state band, we therefore get the spin sequence $I=0, 2, 4, \dots$.

In cases in which we have only approximate axial symmetry, as in the cranking model wave functions (see Secs. 7.7 and 11.4.6.3), the remaining $K \neq 0$ parts are not projected onto zero. They have their origin, however, in admixtures of two-quasi-particle states and more complicated configurations that lie at higher energies and contribute only to highly excited levels in the eigenvalue problem (11.120), in which we are not interested. For the ground state band, we should therefore impose the condition

$$r_x = (-)^I. \quad (11.128)$$

11.4.6.2. The Double Variational Method. So far, we have not specified the method of determining the intrinsic wave function $|\Phi\rangle$. As in the case of Abelian groups discussed in Section 11.4.2, we can carry out a variation either before or after projection. In the case without axial symmetry, the situation is now more complicated, however, since we must also determine the coefficients g_K . In the VBP method, they must be calculated by Eq. (11.120).

In the VAP method, we now end up with a coupled system similar to the system (10.147) [Ze 67]:

$$\begin{aligned} \sum_{K'} g_{K'} \langle \Phi | (H - E') \hat{P}'_{KK'} | \Phi \rangle &= 0, \\ \sum_{KK'} g_K^* g_{K'} \langle \delta \Phi | (H - E') \hat{P}'_{KK'} | \Phi \rangle &= 0. \end{aligned} \quad (11.129)$$

The first part corresponds to Eq. (11.120); the second part is a generalization of the VAP equation (11.62). In principle, this system has to be solved by iteration.

Besides the fact that the system (11.129) is much too complicated to be solved exactly, in many cases it also contains a high degree of redundancy. To see this, we again use the decomposition (11.115) of $|\Phi\rangle$ into its K -components. Using the fact that \hat{P}'_{MK} annihilates all components $|\Phi_{K'}\rangle$ with $K \neq K'$, we get

$$|\Psi'^M\rangle = \sum_K \hat{P}'_{MK} \sum_{K'} g_{K'} |\Phi_{K'}\rangle = \sum_K \hat{P}'_{MK} |\tilde{\Phi}\rangle. \quad (11.130)$$

The function

$$|\tilde{\Phi}\rangle = \sum_K g_K |\Phi_K\rangle \quad (11.131)$$

will, in general, no longer be a product wave function. However, there are

many cases in which it can be approximated by a function of this type.* In all such cases, the variation of g_K is redundant if we carry out a general variation of $|\Phi\rangle$. We then end up with the simple operator (originally proposed by Kamlah [Ka 68]):

$$\hat{P}'_M = \sum_K \hat{P}'_{MK}. \quad (11.132)$$

It has the property $\hat{P}^2 = \hat{P}$, but is not Hermitian. It also violates rotational symmetry [So 77] in the sense that it is not invariant under a rotation of the function $|\tilde{\Phi}\rangle$. Together with a full variation of $|\tilde{\Phi}\rangle$, however, the procedure stays rotationally invariant, because we always find $|\tilde{\Phi}\rangle$ at such an orientation that the energy has a minimum. By symmetry arguments, the quantization axis determined by the operator \hat{P}'_M should coincide with one of the principal axes of the mass distribution in $|\tilde{\Phi}\rangle$.

The operator (11.132) annihilates all components in the wave function $|\tilde{\Phi}\rangle$ that do not have the signature

$$r_x = (-)^I. \quad (11.133)$$

In even nuclei, this fact guarantees a spin sequence $I=0, 2, 4, \dots$ in the ground state band, even if it is no longer axially symmetric. In odd nuclei it causes the $\Delta I=2$ level sequence in favored and unfavored bands to have a different signature (see Sec. 3.3).

11.4.6.3. The Self-Consistent Cranking Model. In Section 11.4.4, we presented a method of deriving an approximate expression for the projected energy without specifying much about the internal wave function $|\Phi\rangle$. For pedagogical reasons, it was discussed in that section for the case of a one-dimensional rotor. It can also be applied to the general case of three-dimensional rotations [Ka 68, BMR 70, Ma 75a].

Since the three-dimensional case involves rather lengthy calculations, we give here only the main result: Under the following three assumptions for the "internal" wave function $|\Phi\rangle$ namely:

- (i) strong deformation ($\langle\langle\Phi|\hat{J}_y^2|\Phi\rangle\rangle \gg 1$),
- (ii) definite signature ($e^{i\pi J_z}|\Phi\rangle \propto |\Phi\rangle$),
- (iii) approximate axial symmetry for small I -values (i.e., in the ground state band $\langle\Phi|\hat{J}_x^2|\Phi\rangle \ll I(I+1)$),

we find up to second order in the Kamlah expansion (11.80) the following

* A simple example is a wave function of an odd nucleus

$$|\Phi\rangle = \sum_K C_K \beta_K^+ |\Phi_0\rangle,$$

where an arbitrarily strongly mixed particle sits on a core with $K=0$; another example is a wave function $|\Phi\rangle$ which deviates only slightly from axial symmetry.

expression for the projected energy* [BMR 70]

$$\begin{aligned} E_{\text{proj}}^I = \frac{\langle H \hat{P}_M^I \rangle}{\langle \hat{P}_M^I \rangle} &= \langle H \rangle - \frac{\langle \Delta \hat{J}^2 \rangle}{2g_Y} + \omega \left(\sqrt{I(I+1) - \langle \hat{J}_z^2 \rangle} - \langle \hat{J}_x \rangle \right) \\ &+ \frac{1}{2g_Y} \left(\sqrt{I(I+1) - \langle \hat{J}_z^2 \rangle} - \langle \hat{J}_x \rangle \right)^2, \end{aligned} \quad (11.134)$$

with

$$\frac{1}{2g_Y} = \frac{\langle (H - \langle H \rangle) \Delta \hat{J}^2 \rangle}{2(\langle \Delta \hat{J}_x^2 \rangle + \langle \hat{J}_y^2 \rangle + \langle \hat{J}_z^2 \rangle)}, \quad \omega = \frac{\langle H \Delta \hat{J}_x \rangle}{\langle \Delta \hat{J}_x^2 \rangle}.$$

These expressions are very similar to Eq. (11.91), and we can draw the same conclusions: In the case where the term $\langle \Delta \hat{J}^2 \rangle / 2g_Y$, which removes the spurious contributions in the energy, can be neglected in the variation, we end up with the cranking model

$$\delta \langle H - \omega \hat{J}_x \rangle = 0 \quad (11.135)$$

with the subsidiary condition

$$\langle \hat{J}_x \rangle = \sqrt{I(I+1) - \langle \hat{J}_z^2 \rangle}. \quad (11.136)$$

It differs from the usual constraint (7.97) by the term $\langle \hat{J}_z^2 \rangle$. In the ground state band of well-deformed nuclei, it does not play any role: For small I -values the nucleus is nearly axially symmetric with $K=0$, and for large angular momenta it can be neglected anyway. However, it is important to take it into account for cranking calculations in $K \neq 0$ bands, particularly in odd A nuclei [RMB 74, RM 74].

We thus have a microscopic derivation of the cranking model (Sec. 3.4) which was originally introduced by classical arguments. The cranking wave functions have to be understood as internal wave functions. The wave function in the laboratory frame is obtained by an angular momentum projection with the operator (11.132). This derivation is only based on the assumption of large particle numbers and large deformations, which guarantee a sharply peaked overlap function $\pi(\Omega)$. In that sense, it is a fully quantum mechanical derivation, which does not depend on classical arguments such as large angular momenta with $\langle \Delta \hat{J}^2 \rangle \ll I^2$; on the contrary, the derivation is based on the fact that we have large fluctuations $\langle \Delta \hat{J}^2 \rangle \gg 1$ (narrow overlap). This means also via the uncertainty relation that the spread in angle is small ($\langle \Delta \Omega^2 \rangle \ll 1$).

In Chapter 12 we will rederive these relations in a time-dependent formulation with wave packets. For example, in the case of translations it will also turn out that the physically realized fact that nuclei are rather

* \hat{P}_M^I is the operator defined in Eq. (11.132), and the wave function $|\Phi\rangle$ is replaced by a simple ket $| \rangle$.

localized in space ($\langle \Delta R^2 \rangle^{1/2}$ very small compared to the nuclear radius, that is, a small width of the wave packet) has the consequence that the momentum spread $\langle \Delta P^2 \rangle$ is large. Therefore, the self-consistent cranking model (pushing model in this case) will turn out to be a good approximation.

11.4.6.4. Electromagnetic Moments and Transition Probabilities. In Section 11.4.4 we saw that for the calculation of rotational spectra in well-deformed nuclei, we do not need an explicit angular momentum projection. The cranking model already provides a rather good approximation. The same is no longer true for matrix elements of operators, which do not behave like a scalar under rotations, such as electromagnetic multipole operators $\hat{Q}_{\lambda\mu}$.

For the reduced matrix element of the operator $\hat{Q}_{\lambda\mu}$ between normalized wave functions $|\Psi_1^{I_1 M_1}\rangle$ and $|\Psi_2^{I_2 M_2}\rangle$ of the type (11.117), we obtain

$$\begin{aligned} \langle \Psi_1^{I_1} | \hat{Q}_\lambda | \Psi_2^{I_2} \rangle &= \sum_{\substack{K_1 K_2 \\ K_2 \mu}} g_{K_1}^{(1)*} g_{K_2}^{(2)} (-)^{I_1 - K_1} \begin{pmatrix} I_1 & \lambda & I_2 \\ -K_1 & \mu & K_2 \end{pmatrix} ((2I_1 + 1)(2I_2 + 1))^{1/2} \\ &\cdot Q_{\lambda\mu}^{\text{intr}}(K_2, K_2), \end{aligned} \quad (11.137)$$

with

$$\begin{aligned} Q_{\lambda\mu}^{\text{intr}}(K_2, K_2) &= \mathcal{R}_1 \mathcal{R}_2 ((2I_1 + 1)(2I_2 + 1))^{1/2} \\ &\times \frac{1}{8\pi^2} \int d\Omega D_{K_2 K_2}^{I_2}(\Omega) \langle \Phi_1 | \hat{Q}_{\lambda\mu} R(\Omega) | \Phi_2 \rangle. \end{aligned} \quad (11.138)$$

The factors \mathcal{R}_i are normalization constants (i refers to the intrinsic wave function $|\Phi_i\rangle$)

$$\mathcal{R}_i^{-2} = \sum_{KK'} g_K^{*(i)} g_{K'}^{(i)} n_{KK'}^{I_i(i)}. \quad (11.139)$$

To evaluate the overlap integrals $\langle \Phi_1 | \hat{Q}_{\lambda\mu} R(\Omega) | \Phi_2 \rangle$, we can again use a sort of Kamlah expansion (11.80) and obtain, in zeroth order,

$$\langle \Phi_1 | \hat{Q}_{\lambda\mu} R(\Omega) | \Phi_2 \rangle = \langle \Phi_1 | \hat{Q}_{\lambda\mu} | \Phi_2 \rangle \langle \Phi_2 | R(\Omega) | \Phi_2 \rangle. \quad (11.140)$$

Using this approximation, we find

$$Q_{\lambda\mu}^{\text{intr}}(K_2, K_2) \propto \langle \Phi_1 | \hat{Q}_{\lambda\mu} | \Phi_2 \rangle \int d\Omega D_{K_2 K_2}^{I_2}(\Omega) n_2(\Omega). \quad (11.141)$$

The remaining integrals have to be carried out explicitly. Only in the limit of very large deformations do we obtain [Vi 66, Ze 67]

$$Q_{\lambda\mu}^{\text{intr}}(K_2, K_2) = \langle \Phi_1 | \hat{Q}_{\lambda\mu} | \Phi_2 \rangle \delta_{K_2, K_2} \quad (11.142)$$

and

$$\begin{aligned} \langle \Psi_1^{I_1} | \hat{Q}_\lambda | \Psi_2^{I_2} \rangle &= \sum_{\substack{K_1 K_2 \mu}} g_{K_1}^{(1)*} g_{K_2}^{(2)} ((2I_1 + 1)(2I_2 + 1))^{1/2} (-)^{I_1 - K_1} \begin{pmatrix} I_1 & \lambda & I_2 \\ -K_1 & \mu & K_2 \end{pmatrix} \\ &\times \langle \Phi_1 | \hat{Q}_{\lambda\mu} | \Phi_2 \rangle, \end{aligned} \quad (11.143)$$

a result which corresponds to Eq. (1.70) in the collective model. The only difference is that the intrinsic multipole moments can now be calculated microscopically. In

particular, we take into account differences between the intrinsic wave functions $|\Phi_1\rangle$ and $|\Phi_2\rangle$ by the overlap integral $\langle\Phi_1|\hat{Q}_{\lambda\mu}|\Phi_2\rangle$.

In cases where this first approximation is not good enough, we need explicit expressions for the norm overlap $n(\Omega)$ in the three-dimensional case. It can be expanded as [IMR 79]

$$n(\Omega) = \exp\left(\sum_{LKK'} C_{KK'}^L D_{KK'}^{L''}(\Omega)\right). \quad (11.144)$$

The Gaussian approximation corresponds to a restriction to $L < 2$. In analogy to Eq. (11.79), we can express the coefficients $C_{KK'}^L$ by expectation values of $\langle j_i\rangle$ and $\langle j_i j_k\rangle$. Using the relations (A.17), for large deformations and small K -admixtures [BMR 70, VS 71] we get

$$n(\Omega) \approx \exp\left\{-\frac{\langle j_z^2 \rangle}{2}\beta^2 + (\cos(\alpha + \gamma) - 1)\langle j_x^2 \rangle + \frac{i}{2}\langle j_x \rangle \beta (\sin \alpha - \sin \gamma)\right\}. \quad (11.145)$$

11.4.6.5. Exact Angular Momentum Projection. Calculations with exact angular momentum projected wave functions usually require a large numerical effort. The expectation value of each operator—for instance, the Hamiltonian—contains a sum over a series of three-dimensional integrals [see Eqs. (11.118) and (11.119)]. The integrands are proportional to the overlap functions $\langle\Phi|R(\Omega)|\Phi\rangle$ and $\langle\Phi|HR(\Omega)|\Phi\rangle$, which have to be calculated point by point using the formula of Onishi (E.49). Only in cases of axially symmetric intrinsic wave functions (with the quantum number K) do the α - and γ -dependences become trivial, and we end up with a one-dimensional integral:

$$\langle\Psi^{IM}|H|\Psi^{IM}\rangle = \frac{\int d\cos\beta d_{KK}'^I(\beta) \langle\Phi|e^{i\beta j_z} H |\Phi\rangle}{\int d\cos\beta d_{KK}'^I(\beta) \langle\Phi|e^{i\beta j_z} |\Phi\rangle}.$$

In this form, the angular momentum projection before or after the variation has been applied very often in the literature (for a review, see [Ri 68, Ma 70, Wo 75]). Many investigations have been carried out within the $1p$ and the $2s-1d$ shell, where we have deformed nuclei with spectra of rotational character [BBC 72]. In this region of the periodic table the angular momentum projected HF theory can be compared with exact shell model calculations [Re 58, KP 59, Wa 70b, MMW 73], and in many cases we find a perfect agreement. In detail, the projected HF theory has been applied in many versions in these light nuclei. In the simplest case one often projects after variation (see Sec. 11.4.2) from axially symmetric deformed product states [KL 64, BGR 65, WG 67b, GFW 72]. An improvement is obtained by a projection before variation with intrinsic wave functions that depend on several variables [BLD 67, DFG 68, ABC 69, LB 68, 69]. Sometimes one must also take pairing correlations into account. This is usually done in the framework of particle number projected BCS or HFB theory [GGF 73, GGA 74]. To treat further correlations, some authors finally have also superimposed several angular momentum projected wave functions [TG 69, CP 70, Da 70, Wa 71, MKL 71] in the sense of the GCM ansatz of Chapter 10.

In the $2s-1d$ shell of some nuclei, triaxial HF solutions have been found. In such cases one must carry out a full three-dimensional projection. The ansatz (11.112), however, seems to be too complicated for actual applications. So far, in all

practical calculations other representations of the projection operator have been used [Un 63, Sh 65, Ke 66, GS 69, Ra 70, GM 71, CL 73, MWW 74, Wa 74, KD 75, 76] which, however, seem to be restricted to applications in light nuclei.

In *heavy nuclei*, an exact angular momentum projection has so far only been carried out in axially symmetric cases. There, however, the method again yields very promising results for the ground state properties and for the low-lying members of the ground state rotational band* in deformed nuclei [OSY 70, AN 71].

We can conclude this section with the remark that projection methods in connection with the self-consistent field approach seem to be a very powerful tool for the description of collective rotational motion, though in detail they can be rather complicated.

11.4.7 The Structure of the Intrinsic Wave Functions

Until now, we have only investigated the problem of how to construct symmetry-conserving wave functions $|\Psi'\rangle$ from the intrinsic wave function $|\Phi\rangle$. We could also ask the opposite question: Is it possible to represent the symmetry-violating wave function $|\Phi\rangle$ as a superposition of the functions $|\Psi'\rangle$, and how large are the components with different I values, that is to calculate the spread $\langle \Delta J^2 \rangle$?†

In the case of Abelian groups, the operator P' (11.57) is a real projector. If $|I\alpha\rangle$ is a complete orthogonal set, we find

$$|\Phi\rangle = \sum_{I\alpha} C_{I\alpha} |I\alpha\rangle, \quad (11.146)$$

and the probability of finding a component with eigenvalue I in the symmetry violating function $|\Phi\rangle$ is given by

$$W_I = \sum_{\alpha} |C_{I\alpha}|^2 = \langle \Phi | \hat{P}' | \Phi \rangle = \frac{1}{2\pi} \int d\alpha e^{-iI\alpha} n(\alpha), \quad (11.147)$$

where W_I is the I th Fourier component of the norm overlap $n(\alpha)$. If $|\Psi'\rangle$ is normalized, we can write

$$|\Phi\rangle = \sum_I \sqrt{W_I} |\Psi'\rangle. \quad (11.148)$$

In the case of three-dimensional rotations, we can again decompose

$$|\Phi\rangle = \sum_{IM\alpha} C_{IM\alpha} |IM\alpha\rangle. \quad (11.149)$$

The probability of finding an eigenstate with eigenvalue $I(I+1)$ in the function Φ is given by [GSF 78a, IMR 79]:

$$W_I = \sum_{IM} |C_{IM\alpha}|^2 = \sum_M \langle \Phi | \hat{P}_{MM}^I | \Phi \rangle = \sum_M n_{MM}^I. \quad (11.150)$$

* For the description of excited states of vibrational character, a TDA approach based on projected two-quasi-particle states seems to be a very powerful method [OS 69, KI 70, AG 74, HIT 79].

† An early investigation of this type has been carried out in [AY 59].

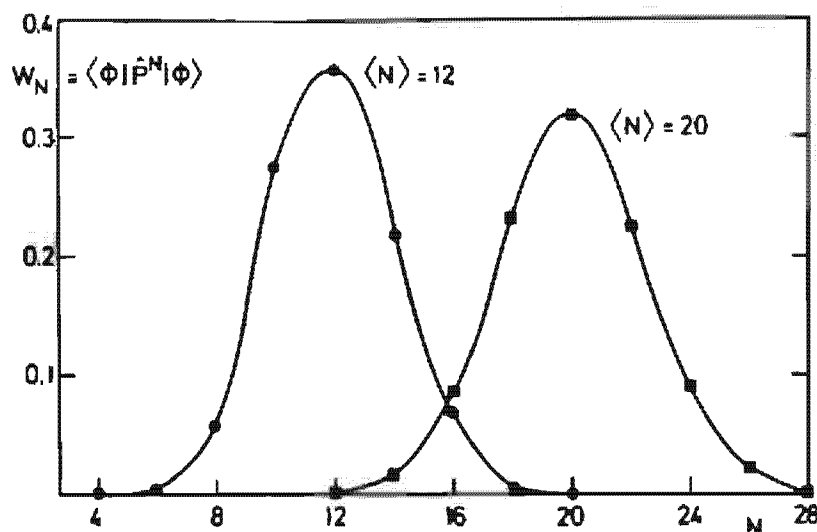


Figure 11.6. Probability components with N particles in the BCS ground state wave function with average numbers $\langle N \rangle = 12$ and $\langle N \rangle = 20$ for realistic nuclei in the rare earth region.

Figure 11.6 shows the decomposition of two BCS wave functions into their components having eigenvalue N for the *particle number*. They differ in the average value $\langle N \rangle$. We see that the violation of the particle number is rather weak. The distribution corresponds roughly to a Gaussian with a relatively small $\Delta N^2 \approx 4-6$. It is therefore crucial to conserve the particle number at least on the average ("cranking" approach). Consequently, the first approximation in the Kamlah expansion (11.80) is often not sufficient. In many cases an exact projection is important.

The situation is quite different in the case of *angular momenta*. Figure 11.7 shows the components W_I [Eq. (11.150)] of different angular momenta in the internal wave function of the well-deformed nucleus ^{164}Er , calculated by the self-consistent cranking model for different values of $\langle J_x \rangle$. We

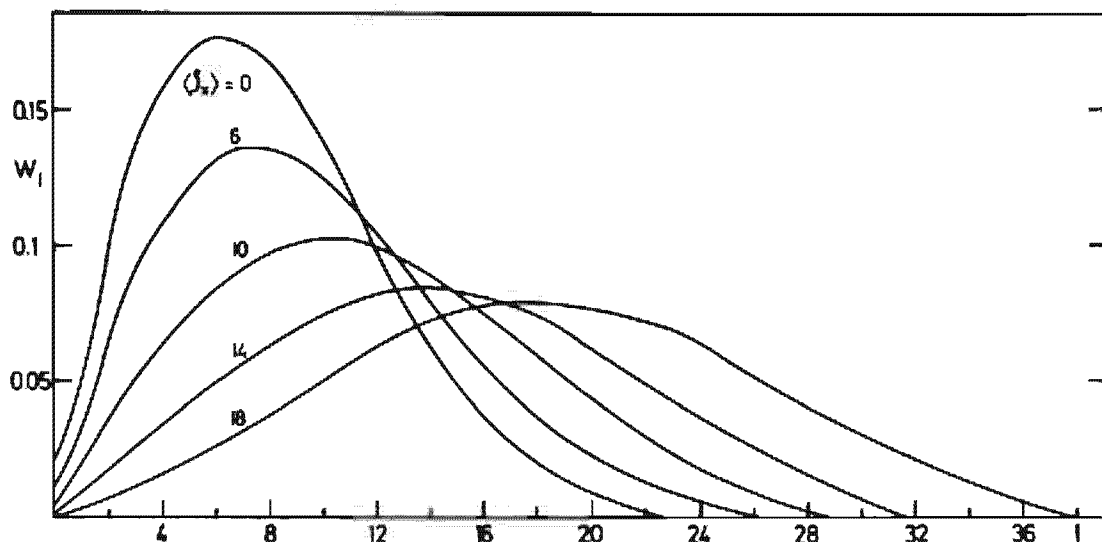


Figure 11.7. Probability components with angular momentum I in the HFB wave function of ^{164}Er for different values of $\langle J_x \rangle = \sqrt{I(I+1)}$. (From [IMR 79].)

now have a strong symmetry violation: $\langle \Delta J^2 \rangle \approx 100$, this corresponds to a spread in angle of roughly 10° , a rather sharp distribution indeed. In the ground state wave function $J=0$ is represented only by a relatively small component. The maximum lies at $J \approx 6$. The reason for this unexpected behavior is the fact that angular momenta are not additive quantities, and there is a much higher number of possibilities, in the configuration space under consideration, of coupling to $J=6$ than to $J=0$. Since we are interested in taking into account as many correlations as possible in the form of a generalized product state, we have to allow for such large spurious components. The projection puts all these components to zero. Only in the limit of high spins does the maximum of the distribution lie at the average value of J_x .

CHAPTER 12

The Time-Dependent Hartree–Fock Method (TDHF)

12.1 Introduction

On the way to describe processes in nuclei involving large amplitudes like anharmonic vibrations or fission and fusion processes, up to now we have only used stationary wave functions together with the Ritz variational principle.

On the other side, we can also formulate the problem in a time-dependent way. Let us start at time $t=0$ with a wave function $|\Psi(0)\rangle$ which is not an exact solution of the stationary many-body Schrödinger equation. Such a state represents a *wave packet*, and its behavior with increasing time is given by the time evolution operator:

$$|\Psi(t)\rangle = e^{-iHt/\hbar} |\Psi(0)\rangle, \quad (12.1)$$

where H is the full many-body Hamiltonian. The information contained in the time-dependent wave function $|\Psi(t)\rangle$ is, in principle, equivalent to the solution of the stationary Schrödinger equation, since a Fourier analysis of $|\Psi(t)\rangle$ gives us the spectrum of H and the corresponding eigenstates. On the other hand, the description of the system by a wave packet is much closer to our classical intuition. In the fission process, for instance, we have a classical droplet in mind which at each time has a fixed deformation. In a microscopic picture, such a deformed state would be represented by a Slater determinant in a deformed potential well, which is certainly no eigenstate of H , but a wave packet in the sense of Eq. (12.1). In fact, we

will see that in such a picture, under certain approximations, classical equations of motion can be derived.

The general ansatz (12.1) is certainly much too complicated for practical solutions. Therefore, in this chapter, we will make the following clear-cut approximations in two successive steps:

(i) Within the *time-dependent Hartree–Fock (TDHF)* theory we start with a Slater determinant $|\Phi(0)\rangle$ and assume that it stays a Slater determinant for all times. In general, this implies a drastic approximation and yields, as we shall see, serious problems in the interpretation of the results. On the other hand, in the static case we have seen that this assumption is based on the fact that because of the Pauli principle each particle does not interact with the other particles directly, but only with the wall of a self-consistent field. Together with the Brückner renormalization of the force and the inclusion of pairing correlation by HFB theory, this approximation yields an excellent description of ground states and single-particle energies throughout the periodic table. At least for energies per particle well below the Fermi energy, the Pauli principle should work in a similar way in the time-dependent case, and there is no reason why the HF approximation should break down in the dynamic case. There is a wide range of phenomena, such as low-lying collective excitations, nuclear fission, and heavy ion collisions at moderate energies, for which this approach seems reasonable. Therefore, we shall in Section 12.2 derive the TDHF equations, which are the basis of this theory, and discuss their properties and the problems involved. We will also present several applications. Naturally, density-dependent forces are used, and in many cases pairing correlations also have to be included [Be 66, BF 76]. Since it will become obvious how to do such calculations, we will present the whole theory for Slater determinants without pairing ($\rho^2 = \rho$) only.

(ii) In a second step, we use the adiabatic approximation, that is, we assume that the velocities in our systems are small. An expansion in these velocities up to second order yields the *adiabatic time-dependent Hartree–Fock (ATDHF)* theory. It results in equations that, in principle, are no easier to solve than the TDHF equations, but it gives much insight into the physical problems and allows the derivation of a collective Hamiltonian for all cases in which the motion may be described in terms of a few collective variables. This will be discussed in Section 12.3.

12.2 The Full Time-Dependent Hartree–Fock Theory

12.2.1 Derivation of the TDHF Equation

We start with an arbitrary wave packet $|\Psi(0)\rangle$. Its exact time evolution is given by Eq. (12.1) and its one-body density at time t is given by

$$\rho_{kl}(t) = \langle \Psi(t) | c_l^\dagger c_k | \Psi(t) \rangle. \quad (12.2)$$

To obtain an equation of motion, we calculate its time derivative:

$$i\hbar\dot{\rho}_{kl}(t) = \langle\Psi(t)|[c_l^+ c_k, H]|\Psi(t)\rangle. \quad (12.3)$$

For a two-body Hamiltonian [Eq. (5.25)] it can be written as

$$i\hbar\dot{\rho}_{kl} - \sum_p t_{kp}\rho_{pl} - \rho_{kp}t_{pl} = \frac{1}{2} \sum_{prs} \bar{v}_{kprs}\rho_{rspl}^{(2)} - \bar{v}_{rspl}\rho_{kprs}^{(2)}, \quad (12.4)$$

where we have introduced the two-body density

$$\rho_{klpq}^{(2)}(t) = \langle\Psi(t)|c_p^+ c_q^+ c_l c_k|\Psi(t)\rangle. \quad (12.5)$$

We can derive an equation of motion for this quantity in the same way as we did for the one-body density in Eq. (12.3). It connects the two-body density with the three-body density, and so on (see Appendix F). This system of equations [BG 49] is exact, but certainly not closed. In order to close it, we have to introduce some approximations. The l.h.s. of Eq. (12.4) describes the free motion of the system. It contains only the kinetic energy, whereas the r.h.s. contains the interaction between the particles. This interaction can be divided into two parts—a self-consistent one-body field, which averages over all particles, and individual collisions between two nucleons which cannot be taken into account by the mean field. The latter causes the two-body correlations.

To achieve this decomposition we define a correlation function $g^{(2)}$ by extracting the uncorrelated pairs of $\rho^{(2)}$,

$$\rho_{klpq}^{(2)} = \rho_{kp}\rho_{lq} - \rho_{kq}\rho_{lp} + g_{klpq}^{(2)}, \quad (12.6)$$

and gain, instead of Eq. (12.4),

$$i\hbar\dot{\rho}_{kl} - [i + \Gamma, \rho]_{kl} = \frac{1}{2} \sum_{prs} \bar{v}_{kprs}g_{rspl}^{(2)} - \bar{v}_{rspl}g_{kprs}^{(2)}, \quad (12.7)$$

with the density dependent HF potential

$$\Gamma_{kl} = \sum_{pq} \bar{v}_{kqlp}\rho_{pq}, \quad (12.8)$$

which is defined as in the static HF theory [Eq. (5.34)]. The only difference is that it now contains the exact time-dependent density $\rho(t)$; therefore, the self-consistent field Γ is time dependent.

Particles in this system can now undergo two kinds of interactions—collisions with the moving walls of the self-consistent field Γ or collisions with the other particles. Both types provide internal excitations of the system. We therefore have to distinguish between “one-body friction,” caused by the collisions with the wall (see [MSK 77]), and “two-body friction,” caused by two-body collisions on the r.h.s. of Eq. (12.7).

As we discussed in the Introduction, for the static case the two-body correlations can be neglected because of the Pauli principle. They can be summed up in a properly renormalized effective interaction of a Brückner theory. We therefore also expect that two-body scattering plays no essential role in the dynamical case, as long as the excitation energies per particle are less than the Fermi energy and $g^{(2)}$ may be neglected. In the

classical limit ($\hbar \rightarrow 0$) this corresponds to the neglect of the collision term in the Boltzmann equation, as we will discuss in more detail in Chapter 13. In this case, the two-body density $\rho^{(2)}$ in Eq. (12.6) factorizes and can be expressed completely by the one-body density ρ ; the wave function $|\Psi(t)\rangle$ then stays a Slater determinant $|\Phi(t)\rangle$ for all times. For $g^{(2)} = 0$ we therefore end up with the TDHF equation [Di 30]

$$i\hbar\dot{\rho} = [\hbar, \rho] \quad (12.9)$$

with $\hbar = t + \Gamma$. It is a nonlinear matrix equation for the one-body density matrix ρ and a first-order differential equation in time. Starting with an initial condition $\rho(0)$, it defines $\rho(t)$ for all times.*

In the case of an external field $F(t) = \sum_{kl} f_{kl}(t) c_k^* c_l$, we have the Schrödinger equation

$$i\hbar\dot{|\Psi(t)\rangle} = (H + F(t))|\Psi(t)\rangle \quad (12.10)$$

that is, we have to replace the Hamiltonian H in Eq. (12.3) by $H + F(t)$, or the matrix \hbar in Eq. (12.9) by $\hbar + f(t)$. This was used to derive linear response theory in a time-dependent external field (see Sec. 8.5).

In coordinate space (it is obvious how to also include spin and isospin variables) with a spin independent two-body potential $v(\mathbf{r}, \mathbf{r}')$ the TDHF equation (12.9) has the form

$$\begin{aligned} i\hbar\dot{\rho}(\mathbf{r}, \mathbf{r}', t) &= -\frac{\hbar^2}{2m} (\Delta_{\mathbf{r}} - \Delta_{\mathbf{r}'})\rho(\mathbf{r}, \mathbf{r}', t) + (\Gamma_H(\mathbf{r}) - \Gamma_H(\mathbf{r}')) \cdot \rho(\mathbf{r}, \mathbf{r}', t) \\ &\quad + \int d^3r'' (\Gamma_{Ex}(\mathbf{r}, \mathbf{r}'')\rho(\mathbf{r}'', \mathbf{r}', t) - \Gamma_{Ex}(\mathbf{r}'', \mathbf{r}')\rho(\mathbf{r}, \mathbf{r}'', t)); \end{aligned} \quad (12.11)$$

where Γ_H and Γ_{Ex} are defined as in Eq. (5.42)ff.

We see that we get a solution $\rho(t)$ of Eq. (12.9) if we decompose the Slater determinant $|\Phi(0)\rangle$ into A orthogonal single-particle wave functions $\varphi_i(\mathbf{r}, 0)$ ($i = 1, \dots, A$) and follow their time evolution by the TDHF equation for single-particle wave functions:

$$i\hbar \frac{\partial}{\partial t} \varphi_i(\mathbf{r}, t) = \left(-\frac{\hbar^2}{2m} \Delta + \Gamma_H(\mathbf{r}, t) \right) \varphi_i(\mathbf{r}, t) + \int d\mathbf{r}' \Gamma_{Ex}(\mathbf{r}, \mathbf{r}', t) \varphi_i(\mathbf{r}', t). \quad (12.12)$$

The density ρ is then given by

$$\rho(\mathbf{r}, \mathbf{r}', t) = \sum_{i=1}^A \varphi_i(\mathbf{r}, t) \cdot \varphi_i^*(\mathbf{r}', t). \quad (12.13)$$

This form of the TDHF equation is easier to handle for practical calculations, because it is simpler to solve A differential equations depending on four coordinates (\mathbf{r}, t) than one differential equation depending on seven coordinates $(\mathbf{r}, \mathbf{r}', t)$ as in Eq. (12.11).

* This equation has been explicitly used in nuclear physics for the first time by Ferrel [Fe 57].

Before we discuss the properties of the TDHF equations, we should mention that it can also be derived from a time-dependent variational principle [KK 76]. The Lagrangian is defined as

$$\mathcal{L} = \langle \Phi(t) | i\hbar \frac{\partial}{\partial t} - H | \Phi(t) \rangle. \quad (12.14)$$

Under the assumption that $|\Phi(t)\rangle$ is a Slater determinant* of the single-particle functions $\varphi_1(\mathbf{r}, t), \dots, \varphi_A(\mathbf{r}, t)$, \mathcal{L} is a functional of the $2A$ independent fields $\varphi_i(\mathbf{r}, t)$ and $\varphi_i^*(\mathbf{r}, t)$. Using them as classical field variables, we can define an action

$$I_{12} = \int_{t_1}^{t_2} \mathcal{L}[\varphi, \varphi^*] dt \quad (12.15)$$

with fixed endpoints 1 and 2. The Hamilton variational principle [Go 59]

$$\delta I_{12} = 0 \quad (12.16)$$

with independent variation of φ and φ^* gives the equations of motion (12.12).

12.2.2 Properties of the TDHF Equation

12.2.2.1. Conservation of Product Character. In the last section we assumed that the wave function $|\Phi(t)\rangle$ is a Slater determinant for all times and under this condition we derived the TDHF equations (12.9). Therefore, the first thing we have to show is that the theory is consistent, that is, if we start with a density of a Slater determinant ($\rho^2(0) = \rho(0)$) this property is conserved for all times:

$$i\hbar \frac{\partial}{\partial t} (\rho^2 - \rho) = i\hbar (\dot{\rho}\rho + \rho\dot{\rho} - \dot{\rho}) = [\hbar, \rho^2 - \rho]. \quad (12.17)$$

In Chapter 7 we discussed in great detail the energy surface which we get if all the Slater determinants are parameterized in a suitable way. The solution of the TDHF equation $|\Phi(t)\rangle$ therefore corresponds to a *trajectory* on this energy surface.

12.2.2.2. Conservation of Orthogonality. Closely connected to the property just discussed is the fact that single-particle wave functions $\varphi_i(\mathbf{r}, t)$ stay orthogonal for all times:

$$i\hbar \frac{\partial}{\partial t} \langle \varphi_i | \varphi_k \rangle = \langle \varphi_i | \hbar - \hbar^+ | \varphi_k \rangle = 0. \quad (12.18)$$

12.2.2.3. Conservation of Expectation Values of Symmetry Operators. For an arbitrary, time-independent, single-particle operator $F = \sum f_{lm} c_l^+ c_m$,

* This variational principle can be generalized. If $|\Phi\rangle$ is a general many-body wave function, the exact Schrödinger equation [KK 76] can be derived.

from Eq. (12.9) we obtain for the expectation values in the state $|\Phi(t)\rangle$

$$i\hbar \frac{d}{dt} \langle F \rangle = i\hbar \text{Tr}(f \cdot \dot{\rho}) = \text{Tr}(f \cdot [h, \rho])$$

or

$$i\hbar \frac{d}{dt} \langle F \rangle = \langle [F, H] \rangle, \quad (12.19)$$

in which the last expectation value was evaluated using Wick's theorem (Sec. C.4). Therefore, we find that all symmetries of the Hamiltonian are conserved, at least on the average. Examples are

$$(i) \text{ the particular number: } \langle d/dt \rangle \langle N \rangle = \langle d/dt \rangle \text{Tr} \rho = 0; \quad (12.20)$$

$$(ii) \text{ the total linear momentum: } \langle d/dt \rangle \langle \mathbf{P} \rangle = 0; \quad (12.21)$$

$$(iii) \text{ the total angular momentum: } \langle d/dt \rangle \langle \mathbf{J} \rangle = 0. \quad (12.22)$$

However, this does not mean that $|\Phi\rangle$ has to be an eigenstate of these symmetry operators. Any localized density distribution $\rho(\mathbf{r})$, for instance, violates translational invariance. We will discuss the problems of symmetry conservation in Section 12.2.2.5.

Furthermore, from (12.19), for velocity independent forces we get for the center of mass $\mathbf{R} = (1/A) \sum \mathbf{r}_i$,

$$\frac{d}{dt} \langle \mathbf{R} \rangle = \frac{1}{Am} \cdot \langle \mathbf{P} \rangle. \quad (12.23)$$

12.2.2.4. Conservation of Energy. The derivative of the energy with respect to time can be expressed by the change of the density. Since ρ always stays a Slater determinant, $\dot{\rho}$ only has ph matrix elements in the basis in which ρ is diagonal (see Sec. 5.3.3).

$$\begin{aligned} \frac{d}{dt} \langle H \rangle &= \frac{d}{dt} E = \sum_{mi} \left(\frac{\partial E}{\partial \rho_{mi}} \dot{\rho}_{mi} + \frac{\partial E}{\partial \rho_{im}} \dot{\rho}_{im} \right) \\ &= \text{Tr}(h \dot{\rho}) = \frac{i}{\hbar} \text{Tr}(h \cdot [\rho, h]) = 0. \end{aligned} \quad (12.24)$$

This means that the energy is conserved with time. The motion therefore has to take place on lines of constant energy in the multidimensional energy surface of Slater determinants. If, therefore, our initial conditions are inside a valley, such that the energy is smaller than the lowest saddle point, we can never leave that valley. The system runs on equipotential lines within the valley.

In Section 5.4 we discussed an example for such an energy surface in the Lipkin model. The HF energy $\langle H \rangle$ depends here on the two variables α and φ . One can transform them to a coordinate and a canonically conjugate momentum in such a way that the TDHF equations are classical equations of motion in the corresponding phase space [KLD 80].

12.2.2.5. Self-Consistent Symmetries. In Section 12.2.2.3 we have seen that symmetries of the exact Hamiltonian H are connected with conservation laws for the expectation values of the corresponding operators. It is one of the essential features of any mean field theory that the wave functions and densities can break these symmetries. With increasing time the deformation or the position of the nucleus may change drastically.

However, as we have seen in the static case, there may be self-consistent symmetries (Sec. 5.5). They occur in the dynamic case also: If S is a unitary symmetry operation which commutes with the Hamiltonian H and with the initial density $\rho(0)$, then ρ stays invariant under this operation for all times. With $\bar{\rho} = S\rho S^+$, we get

$$i\hbar \frac{\partial}{\partial t} (\bar{\rho} - \rho) = [h(\bar{\rho}) - h(\rho), \bar{\rho}] + [h(\rho), \bar{\rho} - \rho], \quad (12.25)$$

that is, if the symmetry is conserved $\bar{\rho} = \rho$ at a time t , it is also conserved at time $t + dt$.

This fact has numerical advantages, because the size of the matrices can be reduced. However, in imposing symmetries we restrict the possible motions drastically and they hinder the development of many correlations. Even in cases where symmetry breaking has not much influence on the *macroscopic shape* of the nucleus, the internal single-particle motion can change drastically, because self-consistent symmetries restrict the freedom of each individual single-particle orbital. For instance in the case of axial symmetry, each nucleon has to be aligned parallel or antiparallel to the symmetry axis, and the statistical fluctuations are inhibited. In other words, a fixed wall does not heat up the system, and to get the full amount of one-body dissipation we have to break all possible symmetries.

If a continuous symmetry is broken in a solution $\rho(t)$ we have, as in the static case by applying the symmetry operation alone, an infinite set of other solutions. An example is translations of the coordinate system.

12.2.2.6. Time Reversal Invariance. A density distribution $\rho(t)$ which is a dynamical solution of the TDHF equation (12.9) is not time reversal invariant, in the sense that the time reversal operator [Me 61, Chap. XV]

$$T = K_0 e^{-i\alpha}, \quad (12.26)$$

where K_0 is the complex conjugation, changes ρ ,

$$\rho_T(t) := T\rho(t)T^+ \neq \rho(t), \quad (12.27)$$

because $\rho_T = \rho$ would require $\dot{\rho} = 0$. On the other hand, we have microscopic reversibility, which means that $\rho_T(-t)$ is also a solution to the TDHF equations. In fact, this property is often used to check the accuracy of computer programs that solve Eq. (12.9). However, this is only a microscopic reversibility and does not mean that the system can not be heated up (within this theory).

12.2.3 Quasi-static Solutions

12.2.3.1. Translations. As we saw in the last section, dynamical solutions of the TDHF equations cannot be entirely time-even. In special cases we can already find dynamical solutions of this equation from a solution of the static HF equations by a suitable transformation that breaks the time reversal symmetry.

A simple example of such a case is the Galilei transformation to a system moving with constant velocity \mathbf{v} . It is realized by the operator G (see [Me 61, Chap. XV])

$$G(\mathbf{v}, t) = \exp\left(-\frac{i}{\hbar} \mathbf{v} \cdot (m\mathbf{A} \cdot \mathbf{R} - \mathbf{P} \cdot t)\right), \quad (12.28)$$

where $\mathbf{R} = (1/A) \sum \mathbf{r}_i$ is the center of mass and $\mathbf{P} = \sum \mathbf{p}_i$ is the total momentum. To this transformation corresponds a matrix in the single-particle space: $g(\mathbf{v}, t) = \exp[-(i/\hbar)\mathbf{v}(m\mathbf{r} - \mathbf{p}t)]$ which transforms the density

$$\rho(t) \rightarrow \bar{\rho} = g\rho(t)g^+. \quad (12.29)$$

$\bar{\rho}$ obeys the equation of motion

$$0 = i\hbar \dot{\bar{\rho}} = g[\mathbf{h}, \rho]g^+ - g[\mathbf{v}\mathbf{p}, \rho]g^+ = g[\mathbf{h}(\rho) - \mathbf{v}\mathbf{p}, \rho]g^+. \quad (12.30)$$

Using Eq. (12.28) and the symmetry property $g\Gamma(\rho)g^+ = \Gamma(\bar{\rho})$, which holds for velocity-independent and translational-invariant interactions, we again find the TDHF equations in the moving frame

$$0 = i\hbar \dot{\bar{\rho}} = \left[\frac{1}{2m} (\mathbf{p} + m\mathbf{v})^2 + \Gamma(\bar{\rho}) - \mathbf{v}(\mathbf{p} + m\mathbf{v}), \bar{\rho} \right] = [\mathbf{h}(\bar{\rho}), \bar{\rho}]. \quad (12.31)$$

We thus see that the static solution $[\mathbf{h}(\bar{\rho}), \bar{\rho}] = 0$ in the moving frame transforms into a nontrivial dynamic solution of the TDHF equation in the laboratory frame. It takes the form

$$\rho(t) = e^{(i/\hbar)m\mathbf{v}t} (e^{-(i/\hbar)\mathbf{v}\mathbf{p}} \bar{\rho} e^{(i/\hbar)\mathbf{v}\mathbf{p}}) e^{-(i/\hbar)m\mathbf{v}t}, \quad (12.32)$$

which shows that the stationary solution $\bar{\rho}$ undergoes first a time-even translation of the coordinates by the amount $-\mathbf{v}t$ and then acquires a velocity by a time-odd transformation of the momenta. In the coordinate space we get

$$\rho(\mathbf{r}, \mathbf{r}', t) = e^{(i/\hbar)m\mathbf{v}(\mathbf{r}-\mathbf{r}')} \cdot e^{-\mathbf{v}t(\nabla_{\mathbf{r}} + \nabla_{\mathbf{r}'})} \bar{\rho}(\mathbf{r}, \mathbf{r}'). \quad (12.33)$$

At time $t=0$ the diagonal density $\rho(\mathbf{r}, \mathbf{r}, 0)$ is identical to the stationary value $\bar{\rho}$. The collective velocity shows up only by \mathbf{r} -dependent phase factors in the non-diagonal part.

In practical applications of the TDHF theory to heavy ion reactions, one often uses as initial condition a sum of two densities of the form (12.33) with velocities \mathbf{v}_1 and \mathbf{v}_2 at a distance such that they do not overlap. To a good approximation they represent two moving ions in their ground state before a reaction takes place.

12.2.3.2. Rotations. In the rotational case we would also like to transform to a rotating system in which the motion can be described by a static solution. However, unlike translations, rotational collective motion is non-trivial. There is no “center of mass angle” and no Galilean invariance in this case (see Sec. 11.3.3). Nevertheless, we can carry out the first part of the transformation (12.28), namely a transformation of the coordinate to a frame rotating with the angular velocity ω

$$\tilde{\rho} = e^{i\omega J t} \rho(t) e^{-i\omega J t}. \quad (12.34)$$

In analogy to Eq. (12.30), we get

$$i\hbar\dot{\tilde{\rho}} = e^{i\omega J t} [i + \Gamma(\rho) - \omega J, \rho] e^{-i\omega J t} = [h(\tilde{\rho}) - \omega J, \tilde{\rho}]. \quad (12.35)$$

We now have the stationary HF problem of the self-consistent cranking model (see Sec. 7.7 and 11.4.6.3)

$$[h(\tilde{\rho}) - \omega J, \tilde{\rho}] = 0. \quad (12.36)$$

It gives us a density $\tilde{\rho}$ with no time dependence but which contains time-odd components. In this sense it is no static density. Again,

$$\rho(t) = e^{-i\omega J t} \tilde{\rho} e^{i\omega J t} \quad (12.37)$$

is a nontrivial solution of the TDHF equations (12.9).

Equation (12.36) can also be derived more fundamentally from a projected TDHF theory in the following manner [EMR 80b]. In analogy to Eq. (12.14), we start with the Lagrangian

$$\mathcal{E} = \langle \Phi(t) | \hat{P}' (i\hbar \partial / \partial t - H) \hat{P}' | \Phi(t) \rangle,$$

where \hat{P}' is a projector onto good angular momentum (see Sec. 11.4.6). The variation of the action (12.15) with respect to the time-dependent Slater determinant $|\Phi(t)\rangle$ yields projected TDHF equations. In the limit of large deformations we can use the Kamlah expansion (11.80) up to first order and obtain Eq. (12.35). Its simplest solution is given by the static problem (12.36).

If one believes in the Cranking model, one sees in this way that the projection is a very important feature in the time-dependent HF case. This also becomes evident in other problems as, for instance, in the calculation of cross sections, where we have to project on individual reaction channels (see Sec. 12.2.4).

12.2.4 General Discussion of the TDHF Method

At a first look, the TDHF method seems to have appealing *advantages*. It provides a unified description of all kinds of *collective motions* in the nucleus, beginning with the static solution for the ground state and going on over rotational and vibrational excitations to large amplitude collective motion, such as fission, fusion, compound nucleus formations, and deep-

inelastic reactions. The system determines for itself, its path on the multi-dimensional energy surface, which includes all configurations representable by product states. In particular, we are not forced to choose *a priori* some collective coordinates, nor to force the system to a motion within unphysical external fields. We need not know anything about the flow pattern in the system, or the inertial parameters and their coordinate dependence.

On the other hand, the concept does not only describe collective phenomena: The wave function is a Slater determinant at all times. It takes care of all *single-particle structure* aspects and includes the full interplay between collective and single-particle motion.

Finally, a solution of the TDHF equation also includes friction and *damping* effects insofar as they are produced by the interaction of the particles with the wall of a time-dependent mean field, the so-called *one-body friction* ([BBN 78] and references given there).

To see where this damping comes from in the case of giant resonances we use Thouless' theorem (E.26) and express $\Phi(t)$ in the basis of the HF ground state Φ_0 :

$$\begin{aligned} |\Phi(t)\rangle &= \exp\left(\sum_{mi} z_{mi}(t) a_m^+ a_i\right) |\Phi_0\rangle \\ &= |\Phi_0\rangle + \sum_{mi} z_{mi}(t) a_m^+ a_i |\Phi_0\rangle + \sum_{mim'i'} z_{mi}(t) z_{m'i'}(t) a_m^+ a_{m'}^+ a_{i'} a_i |\Phi_0\rangle + \dots . \end{aligned} \quad (12.38)$$

We see that besides the *ph* admixtures (which are already treated in the TDA or RPA in Chap. 8) the TDHF wave functions also contain *2p2h*, *3p3h* components and so on. To obtain the strength of these admixtures as a function of their energy, we must carry out a Fourier transformation of $|\Phi(t)\rangle$.

Up to now it is unclear how much of the spreading width* of giant resonances comes from the *2p2h* admixtures of this kind (one-body friction) and how much comes from another kind of *2p2h* admixtures due to genuine two-body correlations contained in $g^{(2)}$ of Eq. (12.7) (two-body friction). The approximation that the $g^{(2)}$ terms of Eq. (12.7) can be neglected is in turn based on the belief [KK 68] that the mean free path, due to the Pauli exclusion principle, is of the order of the nuclear dimensions. The validity of this assumption certainly breaks down at energies per particle of the order of the Fermi energy, but there is a wide range of phenomena which we should be able to describe by the TDHF method.

In particular, the theory is not necessarily restricted by the adiabatic assumptions—namely, that the wave function is at each time very close to the ground state of the corresponding self-consistent well $h(t)$. For dy-

* We should be aware of the fact, however, that TDHF theory contains the escape width as it is discussed in Section 8.5.4, which means that particles are actually leaving the nucleus.

namic solutions, the TDHF single-particle functions $\varphi_i(t)$, Eq. (12.12), are different from the eigenfunctions in this well:

$$h(t)|\psi_i(t)\rangle = \epsilon_i(t)|\psi_i(t)\rangle. \quad (12.39)$$

This means that we do *not* gain the TDHF Slater determinant $|\Phi(t)\rangle$ by filling the lowest A levels in the potential $h(t)$. The density $\rho(t)$ does not commute with $h(t)$, that is, $\rho(t)$ is not diagonal in the basis of the eigenfunctions $|\psi_i(t)\rangle$ and the occupation probabilities p_j , which are the diagonal elements of ρ in this basis,

$$p_j(t) = \langle \psi_j(t) | \rho(t) | \psi_j(t) \rangle \quad (12.40)$$

are spread over many levels, that is, we obtain a *smeared out Fermi surface* in this basis. On the other hand the distribution of the occupation probabilities should not deviate from a Fermi step function too much, either, that is, it should not become completely fragmentated, otherwise the exclusion principle will no longer suppress two-body collisions. However, no detailed studies on this problem presently exist.

Besides all the great advantages of the TDHF method, however, there are some important *restrictions* which we should be aware of:

(i) The theory provides a fully microscopic description, which follows each single-particle wave function as it changes with time and requires a tremendous amount of *numerical effort*. In particular, we should keep in mind that its full beauty and power can only develop if as many symmetries as possible are broken. Realistic calculations of this type not only go to the limits of modern computer facilities, they also very often make it difficult to extract basic physical features of the system and to understand them in terms of simple models.

(ii) The theory, in a sense, shows a classical *deterministic behavior*: We start with an initial density $\rho(t)$ and follow it and its velocity $\dot{\rho}(t)$ through time in a multidimensional energy surface like a classical trajectory. This fact alone does not say that the theory is a classical one; the exact quantum mechanical statistical operator $\hat{\rho}$ obeys the von Neumann equation, which has a structure very similar to Eq. (12.9). The essential difference from a full quantum mechanical theory is that we restrict our wave function to Slater determinants at all times and end up with a nonlinear equation. We have therefore given up the *superposition principle*, that is, a linear combination of two Slater determinants is (in general) no longer a product wave function. As a consequence of the nonlinearity of our theory we get solutions of a *soliton character* (see Sec. 12.2.5), that is, density distributions which propagate without changing their shape [see, e.g., Eq. (12.32)], whereas the exact quantum-mechanical density $\rho(t) = \langle \Psi(t) | \hat{\rho} | \Psi(t) \rangle$ would certainly show the usual quantum-mechanical dispersion. The fact that the example (12.32) of the static density moving with constant velocity does not show dispersion can also be expressed by the fact that we have destroyed translational invariance in TDHF theory, that is, we are in the intrinsic system of the nucleus and consider its center of mass coordinate and its momentum as two simultaneous measurable

(classical) quantities. This, of course, is linked to considering Slater determinants as an approximation to the exact wave function.

(iii) Another quantum-mechanical effect is *tunneling* through a potential barrier. If we have two separated local minima in the energy surface, and we start with an energy smaller than the lowest saddle between these minima in one valley, we will never reach the other valley because of the conservation of energy [Eq. (12.24)]. It is a consequence of the nonlinearity that there can exist two different valleys. A linear theory always has only one minimum, namely the ground state (see Sec. 5.2). The impossibility of tunneling becomes particularly evident in cases where the set of general Slater determinants is restricted to a product wave function $|\Phi(q)\rangle$ with a few collective degrees of freedom (see Sec. 12.3.3) as in the description of the fission process. In such cases we must either quantize or introduce linear superpositions of product states. This brings us back to the method of generator coordinates (Chap. 10).

Barriers in the space of Slater determinants, which eventually go over into barriers in a collective coordinate, should not be mixed up with barriers in an external field $V(x)$ in coordinate space. For instance, let us study a static solution which moves with a certain velocity towards such a barrier. The wave function $|\Phi\rangle$ of this system consists of a product of single-particle wave functions $\varphi_i(x)$. Each of them has a tail reaching through the barrier. In general, therefore, $|\Phi\rangle$ is split into two parts at this barrier, a transmitted part and a reflected part. Separately, the two parts are no longer Slater determinants, and the single-particle wave functions φ_i belong to both parts. Depending on the incident energy, the transmitted and reflected parts have very different sizes. Figure 12.1a shows the results of a one-dimensional calculation, where a slab of nuclear matter is moving towards a barrier of Gaussian shape with an energy per particle equal to the height of the barrier. We see that the whole slab is transmitted. Without the interaction of the particles through their mean field, we would have expected a transmission probability of 0.5 for each single-particle wave function. The self-consistent field, together with the external barrier, however, gives a drastically reduced effective barrier for the particles. Figure 12.1b shows the same process at a higher barrier. Now the initial slab is split into two parts. We observe again that the collective penetrability is much higher than the penetrability for one particle.

(iv) There exist fundamental questions in the *physical interpretation* of the results contained in the wave function $|\Phi(t)\rangle$. This is already seen in the example of the slab moving towards an external barrier: Does all of the slab penetrate with a certain probability, or does the slab at each collision break into two separate parts with masses corresponding to the integrated density $|\Phi|^2$ on the left and right sides of the barrier? In the latter case we would get non-integer particle numbers in each part, because the scattered fragments, as we said, are no longer Slater determinants by themselves; thus the single-particle wave functions simultaneously belong to all of the fragments. We could also imagine a complicated mixture of these two possibilities. Physically, we are interested in the probability of the transmission of A_1 particles and the reflection of $A_2 = A - A_1$ ones, that is, the probability that there are A_2 particles to the left and A_1 particles to the

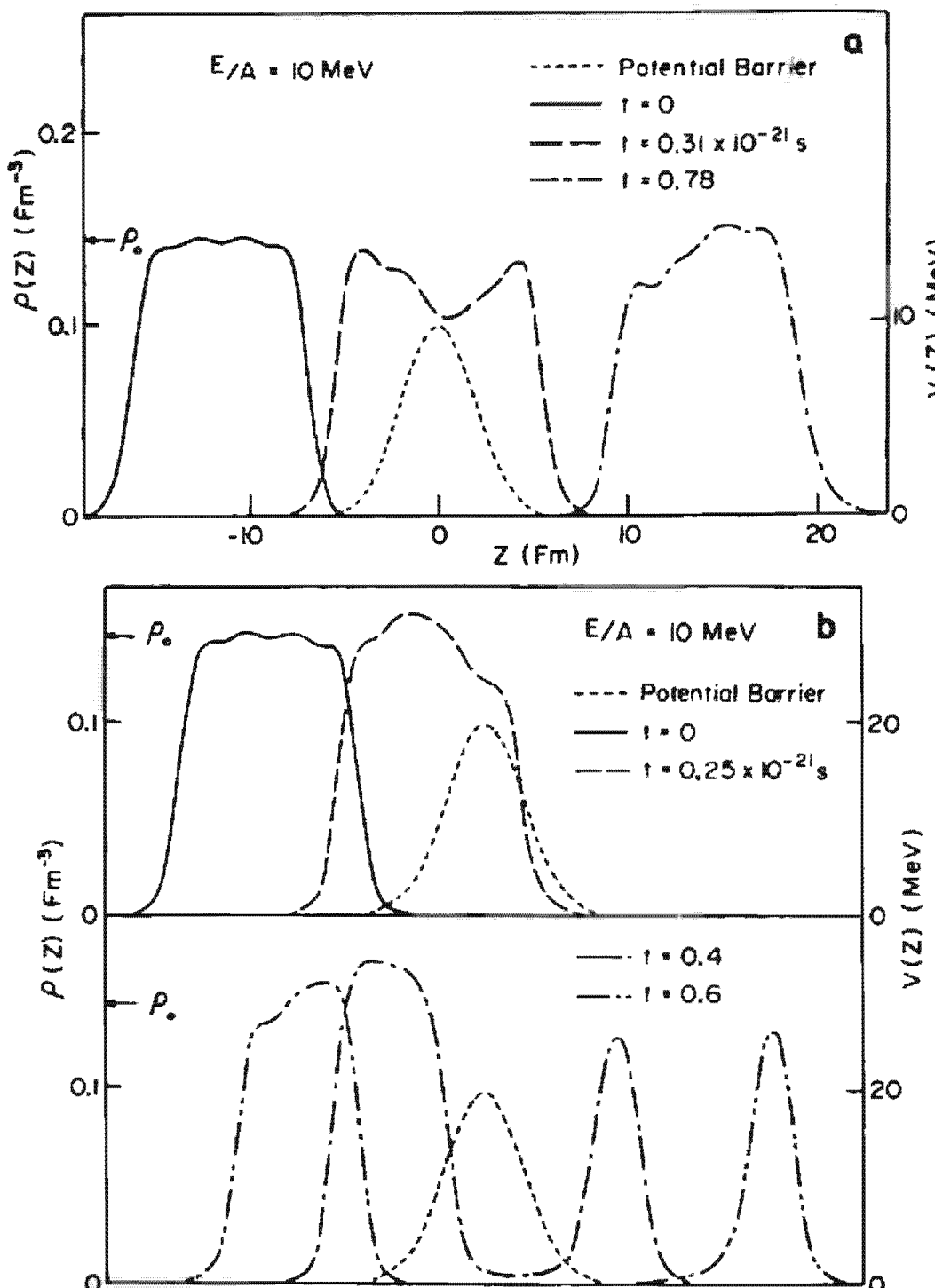


Figure 12.1. Interaction of a slab of nuclear matter with a Gaussian barrier at a height of 10 MeV (a) and 20 MeV (b). (From [BKN 76].)

right of the barrier in the limit of $t \rightarrow \infty$:

$$P_{A_1 A_2} = \frac{(A_1 + A_2)!}{A_1! A_2!} \int_0^\infty dx_1 \dots dx_{A_1} \int_{-\infty}^0 dx_{A_1+1} \dots dx_A |\Phi(x_1 \dots x_A, t \rightarrow \infty)|^2. \quad (12.41)$$

This is a practical prescription to calculate mass distributions, which has also been applied to calculations for heavy-ion collisions [Ke 76].

In the general case, however, we would like to know the S -matrix elements for the different channels in such a reaction. It is an open question whether we can get such information from a TDHF calculation. In principle, we can consider the wave packet $|\Phi(t)\rangle$ of the TDHF equation to be a valuable approximation to the exact wave packet $|\Psi(t)\rangle$ and so get the S -matrix elements from $|\Phi(t)\rangle$ in quite the same way as we would if we had $|\Psi(t)\rangle$; we could, for example, project $|\Phi\rangle$ onto a model scattering state. However, this would imply calculating the overlap of two different many-body wave functions, which can lead to very erroneous results, as can be seen from the following considerations: Let us assume that we calculate the overlap of two only very slightly different product wave functions, where all the single-particle wave functions in one determinant are different from all those in the other by an amount ϵ :

$$(1 - \epsilon)^A \sim e^{-\epsilon A} \quad (12.42)$$

that is, the overlap is exponentially small for large particle numbers. The same would be true if we wanted to calculate, for example, the overlap of a static HF wave function with the exact one, where we can assume that each single-particle orbit is depleted because of correlations due to the probability ϵ [Ne 77]. Though the HF wave function has only very small overlap with the exact wave function, we nevertheless get good results, for example, for binding energies. This is due to the fact that there we need only calculate the expectation value of one- and two-body operators, which involves at most only two single-particle wave functions. The same considerations are true in the time-dependent case: Calculating S -matrix elements from $|\Phi(t)\rangle$ (see above) means that we calculate expectation values of an A -body operator in the case of heavy-ion reactions (the configuration of all A nucleons is changed), and thus it probably gives rather doubtful results. Therefore, in the time-dependent case we must also restrict ourselves to the evaluation of few-body operators such as particle number dispersion or mean excitation energies.

Closely related to the above problems is the question of whether, starting from a Slater determinant as an initial condition, the exact wave function $|\Psi(t)\rangle$ stays close to a Slater determinant in the course of time. To this end, Lichtner and Griffin [LG 76a] investigated the time dependence of the function

$$D(t) = \frac{1}{A} \text{Tr}(\rho(t) - \rho^2(t)). \quad (12.43)$$

Starting with a Slater determinant $|\Phi_0\rangle$ at $t=0$, we find for short times,

$$D(t) = \left(\frac{t}{\tau} \right)^2 + \dots \quad (12.44)$$

with a limit on the lifetime

$$\frac{1}{\tau} > \frac{2}{\hbar} \sqrt{\frac{1}{A} \{ \langle \Phi_0 | H^2 | \Phi_0 \rangle - \langle \Phi_0 | H | \Phi_0 \rangle^2 \}} , \quad (12.45)$$

which is proportional to the energy spread per particle in the function $|\Phi_0\rangle$. For realistic nuclei, we find τ values between 10^{-22} and 10^{-21} seconds. This means that the wave function $|\Psi(t)\rangle$ already looks quite different to a Slater determinant after very short times. This again shows the fact that the overlap $\langle\Psi(t)|\Phi(t)\rangle$ becomes very small as soon as $|\Psi(t)\rangle$ is only slightly different from $|\Phi(t)\rangle$, but this does not mean that $|\Phi(t)\rangle$ cannot be used for the evaluation of few-body operators.

(v) Perhaps the most serious problem in the TDHF theory is the *spurious final state interaction*. In an exact calculation we would have many different outgoing channels, which do not interact for $t \rightarrow \infty$. In our example of a slab moving towards a barrier, we could consider, for instance, the penetration of one, two, or three particles, whereas the rest is reflected. In general, the transmitted systems would have different velocities. Within the TDHF theory, however, all the channels are trapped into one common mean potential on the right-hand side of the barrier. To stay within this potential, all the channels have to exchange momentum permanently. Therefore, for large times we also get an unphysical spurious interaction between the different channels. Even if we do not calculate S -matrix elements, we cannot exclude that this final state interaction does not also give spurious contributions to mean values of few-body operators. In analogy to the symmetry violation in the static HF problem, we should therefore do some kind of *variation after projection* (see Chap. 11) onto the different channels. The TDHF function $|\Phi(t)\rangle$ has to be understood as an "internal" wave function.

In fact, one can derive the TDHF equations from a saddle point approximation in the Feynman path integral representation [FH 65] of the exact quantum mechanical propagator [KI 77, ER 78, NLP 79, Re 79] where the above questions seem to be treated more properly.

12.2.5 An Exactly Soluble Model

In order to study some of the problems discussed above, Yoon and Negele [YN 77] investigated an exactly soluble model of N bosons interacting through a δ -force in one dimension.* The Hamiltonian is given by

$$H = -\frac{1}{2} \sum_{i=1}^N \frac{\partial^2}{\partial x_i^2} - v \sum_{i < j=1}^N \delta(x_i - x_j). \quad (12.46)$$

This model has been solved exactly for bound states [Be 31, Mc 65] and for scattering states [Ya 67]. To get the time-dependent Hartree equation for a product state where all the bosons occupy the lowest level with the wave function $\varphi(x, t)$, in a self-consistent field, we use the variation principle (12.16) with

$$\langle \Phi | i \frac{\partial}{\partial t} - H | \Phi \rangle = N \int dx \left(\varphi^* i \frac{\partial}{\partial t} \varphi + \frac{1}{2} \varphi^* \frac{\partial^2}{\partial x^2} \varphi + \frac{v}{2} (N-1) \varphi^* \varphi^* \varphi \varphi \right) \quad (12.47)$$

* A similar, but more complicated, model has been proposed for fermions [NW 76a + 78].

and find

$$i \frac{\partial}{\partial t} \varphi + \frac{1}{2} \frac{\partial^2}{\partial x^2} \varphi + \sigma(N-1) \varphi^* \varphi \varphi = 0. \quad (12.48)$$

The static solution is

$$\varphi_s(x) = \frac{\sqrt{(N-1) \cdot \sigma}}{2 \cosh((N-1)\sigma x/2)} \quad (12.49)$$

with the energy

$$E_H = - \frac{N(N-1)^2 \sigma^2}{24} \quad (12.50)$$

and the density

$$\rho_s(x) = \frac{N(N-1)\sigma}{4 \cosh^2((N-1)\sigma x/2)}. \quad (12.51)$$

In the dynamical case for $2N$ particles Eq. (12.48) has a two-soliton solution [ZS 72, Do 76] (for the definition and properties of solitons, see the review articles [SCM 73, Ra 75]):

$$\begin{aligned} \varphi(x, t) = & \frac{\sqrt{(2N-1)\sigma}}{2} e^{-(t/2)(K^2 - a^2)t} \\ & \times \frac{\left(e^{iKx} \cdot \left(e^{-a(x-Kt)} + \left[K^2/(K-ia)^2 \right] e^{-a(3x+Kt)} \right) \right) + (K \leftrightarrow -K)}{1 + 2e^{-2ax} \coth(2aKt) - 2a^2 e^{-2ax} \operatorname{Re}(e^{2iKx}/(K+ia)^2) + (K^4/(K^2+a^2)^2)e^{-4ax}}, \end{aligned} \quad (12.52)$$

with $4a = (2N-1) \cdot \sigma$ and K an arbitrary real number. It describes the transmission of two solitary waves through one another with relative momentum $2K$. The wave function is given in the center of mass system. To find the density in the system of one part of the wave, we write $y = x - Kt$ and get

$$\rho(y, t) = 2N \cdot |\varphi(y, t)|^2 \underset{t \rightarrow \infty}{=} \frac{N \cdot (N-\frac{1}{2})\sigma}{4 \cosh^2((N-\frac{1}{2})\sigma y/2)}, \quad (12.53)$$

which, for large N -values, agrees with the static density (12.51). We also can show that the time delay resulting from the interpenetration of the two waves agrees with the exact time delay for large values of N [Do 76]. On the other hand the lifetime of the determinant (12.45) goes to zero for large N . This model therefore gives us an example that results from a mean field theory and may be exact in the limit of large systems, even if the wave function has no overlap with the exact wave function.

12.2.6 Applications of the TDHF Theory

The oldest application of TDHF theory is the description of vibrations around a static solution ρ_0 in the limit of small amplitudes. In Chap. 8 we saw that by linearizing Eq. (12.9) with respect to $\delta\rho = \rho - \rho_0$ we gain the *random phase approximation*.

In the limit of small velocities \dot{p} but large amplitudes, we get the *adiabatic-TDHF theory*. This will be discussed with its applications in Section 12.3. We shall therefore restrict ourselves here to exact numerical solutions of the TDHF equations (12.9).

TDHF theory has been applied to *exactly soluble models*. We gave such an example in the last section. Another case is that of the Lipkin model [Kr 77, KLD 80]. In Fig. 5.3 the energy surface of this model is shown. The solutions of the TDHF equations are contour lines of constant energy [KLD 80].

In all the more *realistic calculations* [BKN 76, KDM 77, CMM 78, BGK 78, FKW 78], Skyrme like forces were used. The effective range corrections ($\sim p^2$) were neglected or in some cases replaced by a Yukawa force with finite range and a special exchange part which restricts it to contribute only to the direct term of the self-consistent potential. The exchange term in the Coulomb force is neglected, too. Thus Eq. (12.12) is only a differential equation and not an integrodifferential equation, as it would be in the general case.

In a further simplification we restrict our discussion to *slabs of nuclear matter* which have also been investigated [BKN 76]. This is a one-dimensional problem in the coordinate z :

$$i\hbar\dot{\varphi}_l(z, t) = \left(-\frac{\hbar^2}{2m} \frac{\partial^2}{\partial z^2} + \Gamma(z, t) \right) \varphi_l(z, t) = h(z, t) \varphi_l(z, t). \quad (12.54)$$

Discretization in the coordinate z yields a matrix equation

$$i\hbar\dot{\varphi}(t) = h(t)\varphi(t). \quad (12.55)$$

Finally, the time t is also discretized. The obvious way to proceed would be

$$i\hbar \frac{1}{\Delta t} (\varphi^{(n+1)} - \varphi^{(n)}) = h^{(n)} \varphi^{(n)} \quad (12.56)$$

or

$$\varphi^{(n+1)} = \left(1 - \frac{i}{\hbar} \Delta t \cdot h^{(n)} \right) \varphi^{(n)}. \quad (12.57)$$

Since $(1 - (i/\hbar)\Delta t \cdot h^{(n)})$ is not unitary, this yields numerical instabilities. A way to avoid this is to replace Eq. (12.56) by

$$i\hbar \frac{1}{\Delta t} (\varphi^{(n+1)} - \varphi^{(n)}) = \frac{1}{2} h^{(n)} (\varphi^{(n+1)} + \varphi^{(n)}) \quad (12.58)$$

or

$$\varphi^{(n+1)} = \frac{1 - \frac{i}{2\hbar} \Delta t \cdot h^{(n)}}{1 + \frac{i}{2\hbar} \Delta t \cdot h^{(n)}} \varphi^{(n)}, \quad (12.59)$$

with a unitary approximation to the evolution operator (the so-called Crank-Nicholson operator [CN 47]). This equation, however, involves a matrix inversion, and recently a truncation of the Taylor series of the evolution operator to the first few terms has proved to be satisfactorily accurate [FKW 78].

The force constants were adjusted so as to reproduce the properties of nuclear matter in the static case. In order to investigate the oscillations of an individual

slab, the initial conditions were chosen as

$$\varphi_i(\mathbf{r}, t=0) = e^{iS(\mathbf{r})} \varphi_i^0(\mathbf{r}), \quad (12.60)$$

where φ_i^0 are the static single-particle wave functions. The function $S(\mathbf{r})$ determines the velocity distribution for $t=0$, which is defined by the distribution of the current $j(\mathbf{r}, t)$,

$$\mathbf{v}(\mathbf{r}, t) = \frac{\mathbf{j}(\mathbf{r}, t)}{\rho(\mathbf{r}, t)} = \frac{1}{\rho(\mathbf{r}, t)} \sum_{i=1}^A \frac{\hbar}{2mi} (\varphi_i^* \nabla \varphi_i - \varphi_i \nabla \varphi_i^*) \quad (12.61)$$

or

$$\mathbf{v}(\mathbf{r}, t=0) = \frac{\hbar}{m} \nabla S(\mathbf{r}). \quad (12.62)$$

For $S(\mathbf{r}) = \alpha z^2$, we get $v(z) = (2\hbar/m)\alpha z$. With this initial condition the slab starts to oscillate. Figure 12.2 shows such vibrations, which correspond to breathing modes for different values of α . Even for small α these oscillations are not harmonic and they do not seem to be associated with a single frequency. For large α -values the oscillations show drastic fluctuations. Finally, the excitation is too strong and the slab splits into pieces (not shown).

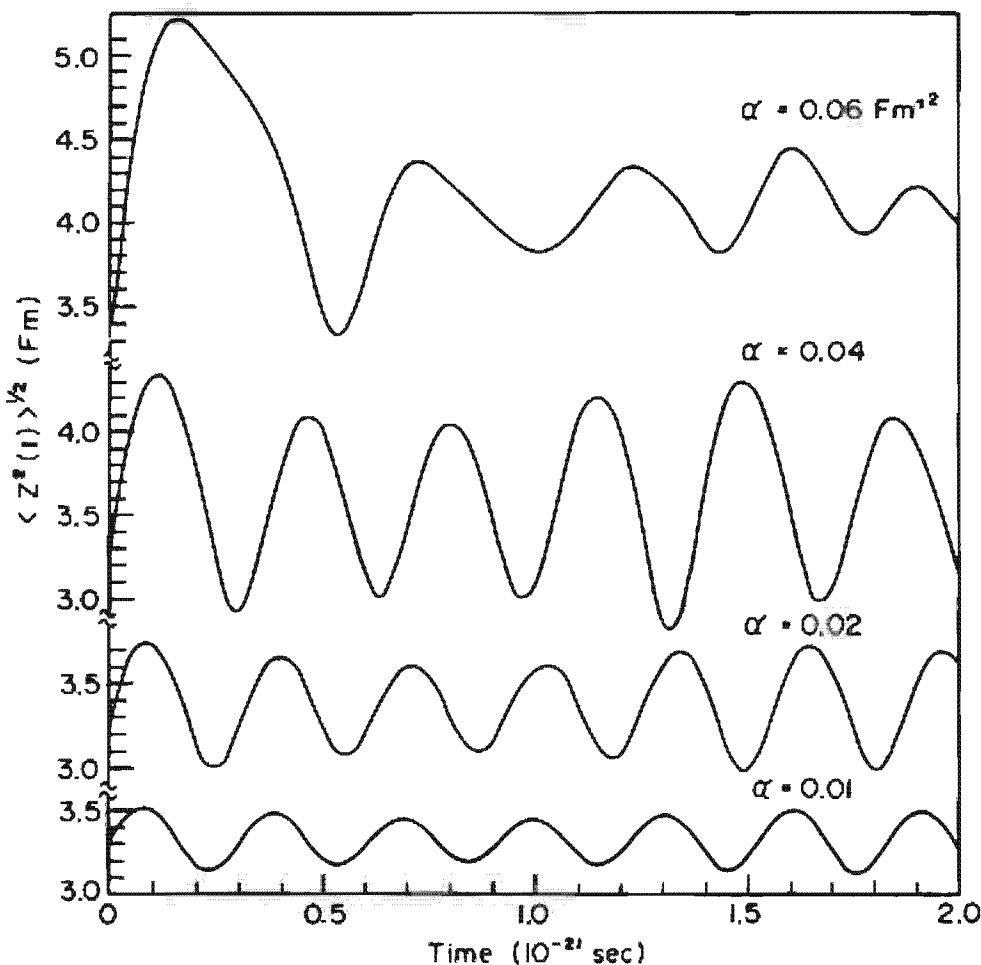


Figure 12.2. Root mean square length of an oscillating slab as a function of time in TDHF approximation for different values of the initial velocity α . (From [BKN 76].)

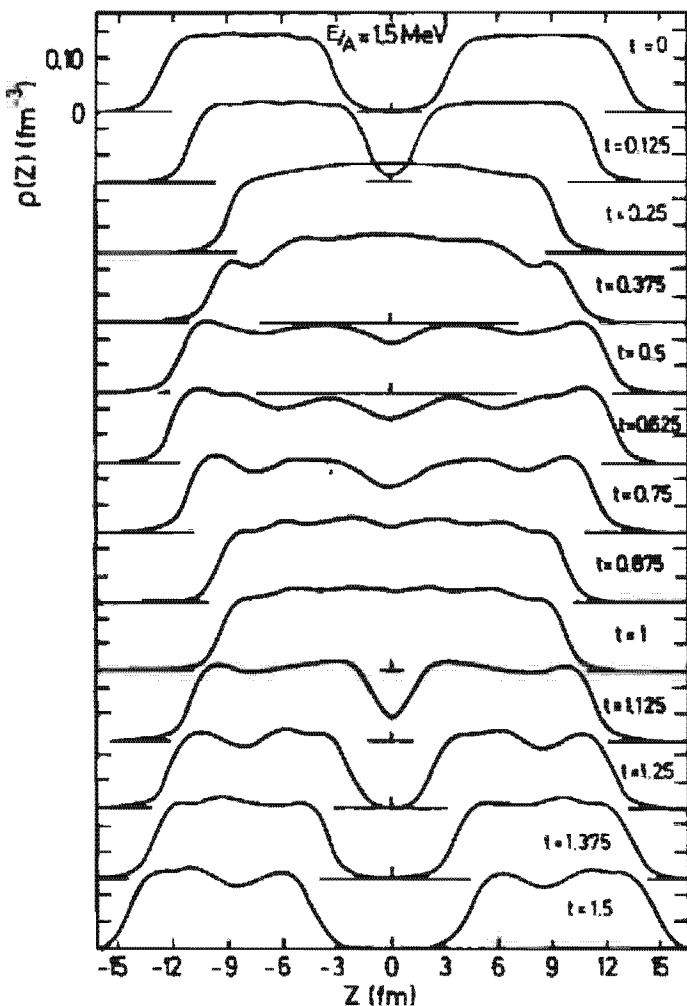


Figure 12.3. Density profiles $\rho(z, t)$ at various times for the scattering of two identical slabs at an intermediate energy. (From [BKN 76].)

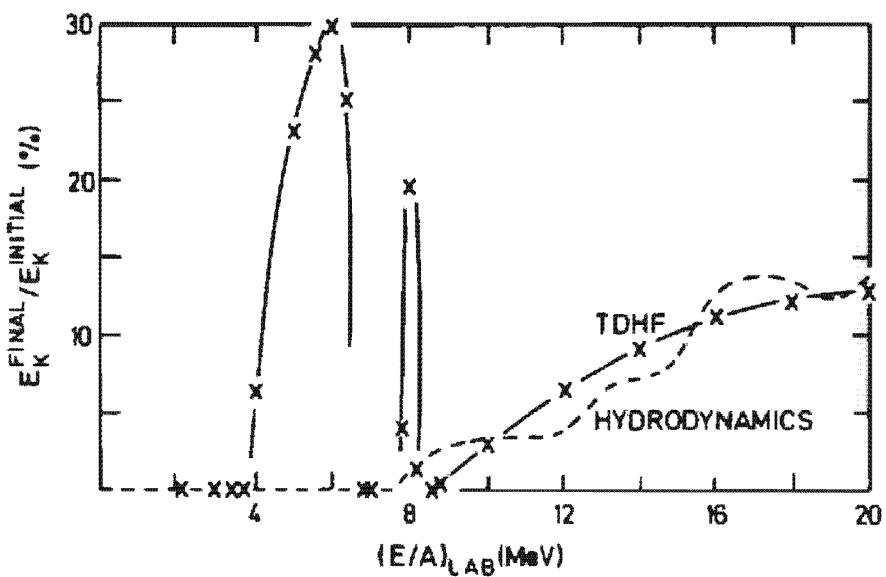


Figure 12.4. The ratio of final translational kinetic energy to initial translational kinetic energy as a function of E/A for a collision of two slabs of nuclear matter. A value of zero denotes fusion. (From [BKN 76].) The dashed line corresponds to a hydrodynamical calculation, discussed in Sec. 13.3.3. (From [WMW 77].)

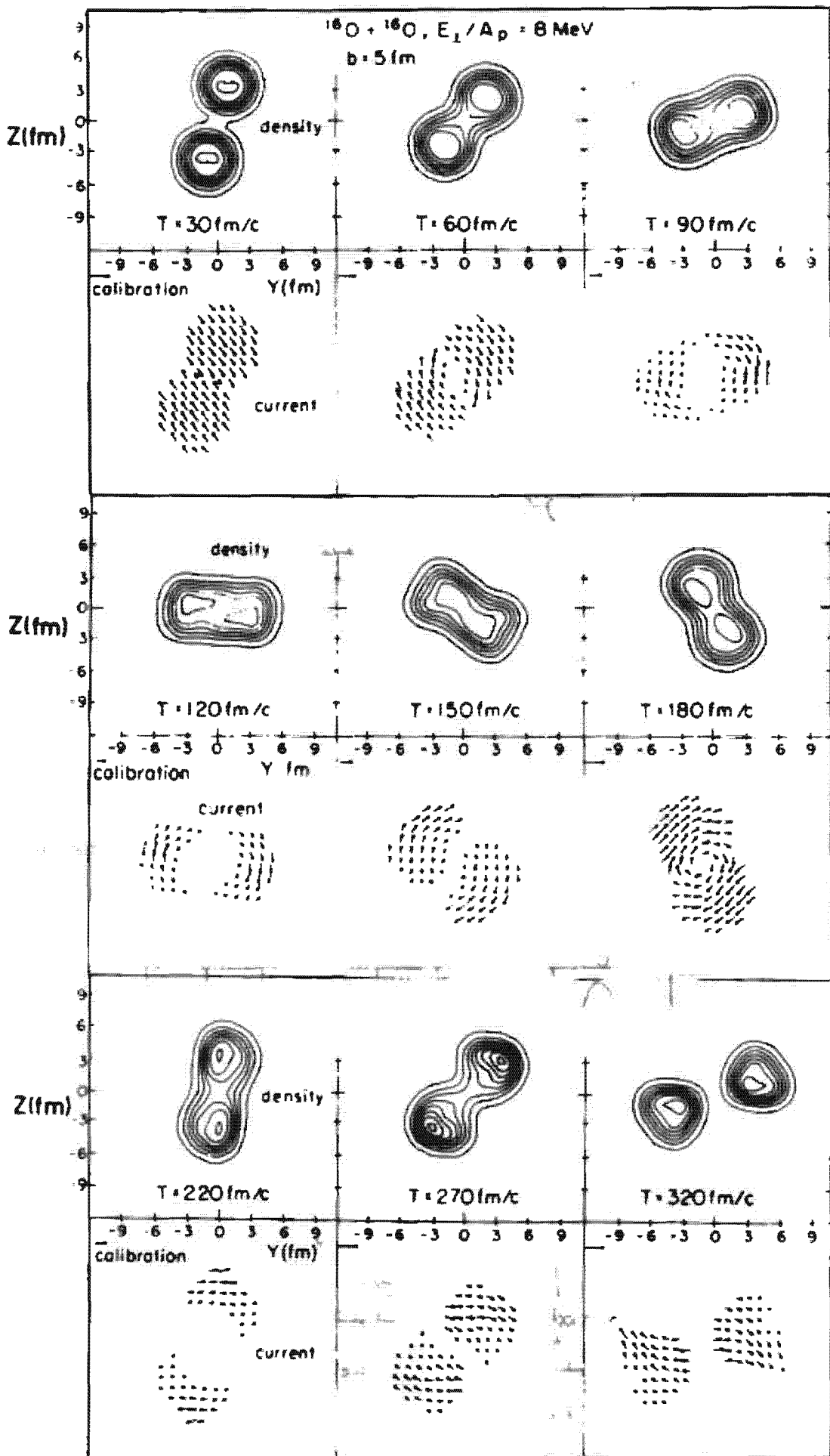


Figure 12.5. Density and velocity distributions in the laboratory system of $^{16}\text{O} + ^{16}\text{O}$ at impact parameter $b = 5 \text{ fm}$ at different times T . (From [CMM 78].)

Starting with two self-consistent slabs traveling in opposite directions, we can investigate the collision process. We find a great variety of phenomena. Depending on the bombarding energy, inelastic scattering, compound nucleus formation, resonance behavior, strongly damped collisions, transfer processes, and fragmentations have been observed. Figure 12.3 shows $\rho(z, t)$ at different times for an intermediate energy. After an initial fusion the central density is increased. The compound system begins to oscillate and undergoes fission after one period.

For other energies fusion occurs. As we see in Figure 12.4, we always get fusion for low energies and always a breakup of the compound system for high energies; in between, there is a resonance region. In detail, this depends very much on single-particle motion in the neck region at the scission point. If single-particle effects generate a depletion of this region at the relevant moment of time, scission occurs, otherwise the system oscillates back. One cycle later, much energy has perhaps dissipated in other degrees of freedom and the system stays together. Such resonance structure has actually been observed in the total fusion cross section of heavy-ion reactions [SVE 76].

The slab geometry is not very realistic, since the translational invariance in the x and y directions prevent nuclear matter splashing aside during the bombarding process, and the high degree of symmetry reduces the damping mechanism. Therefore, two-dimensional [Ko 76, CM 76, MC 76], quasi-three-dimensional [KDM 77, MDK 77] and fully three-dimensional [CSM 76, CMM 78, BGK 78, FW 78] calculations have been carried out. They require a great deal of numerical effort and give nice pictures of the density and current distributions in such heavy-ion scattering processes* (see Fig. 12.5).

A TDHF calculation has also been used to describe the fission process [NKM 78]. Starting very close to the saddle point, the system has been followed until scission into two separated fragments has occurred. However, here we do not wish to go into further details of the numerous numerical calculations using TDHF theory.

12.3 Adiabatic Time-Dependent Hartree-Fock Theory (ATDHF)

12.3.1 The ATDHF Equations

As we saw in the last section, nowadays complete numerical solution of the full TDHF equations is possible in some cases. The interpretation of the results, however, is difficult. In this section we will therefore study a theory which makes a further simplifying approximation: Besides the assumption that the wave function stays a Slater determinant for all times (which characterizes the TDHF approach), we investigate only slow processes and

* For an introduction to heavy-ion collisions see [NW 76b].

expand the velocity to second order. However, the aim of this theory is not to solve the TDHF equations (12.9) in some approximation, but to derive in a fully microscopic way a *collective Hamiltonian* for the description of collective processes which involve only small velocities. Thus it provides a connection between a microscopic theory of the nucleus and the phenomenological models discussed in Chapter 1. In particular, in this way we are able to derive microscopic expressions for the parameters of the collective model, such as moments of inertia and energy surfaces. We have already seen in Chapter 10 that the GCM method is able to give such a collective Hamiltonian. The ATDHF theory presents a somewhat different approach.

Since the collective model is quadratic in the velocities, we are restricted to the *adiabatic limit*. This requires that the collective motion is slow compared to the single-particle motion of the nucleus, so that we can neglect all terms of higher than second order in the velocities. As we shall discuss in Section 12.3.5.2, this assumption is justified for a large variety of problems in nuclear physics, such as collective excitations of small amplitude, low-lying anharmonic spectra in transitional nuclei, nuclear fission, and heavy-ion collisions at lower energies. The name "adiabatic" in this context means that the collective *velocity* is small. We often compare the corresponding frequencies, that is, the corresponding Fourier components of the time dependence. For the case of a *large amplitude* motion (for instance, fission) these frequencies have to be small to get a small velocity. For the case of *small amplitudes*, however, the frequencies need not be restricted. We can also have adiabatic motion with rather high frequencies, such as those for giant resonances. In both cases for the kinetic energy, it is sufficient to go only to second order in the velocities and both cases are treatable by the adiabatic approximation. For small amplitudes we can, in addition, stop after second order in the potential energy and obtain the harmonic limit (RPA, see Chap. 8). For large amplitudes this is no longer possible. The ATDHF approach is therefore a theory of collective motions of *arbitrary amplitude* but *small velocity*.

In the last few years there have been numerous attempts to develop approximations along these lines, and the field is still very much under investigation. To be complete within this context goes beyond the scope of this book. Therefore, in the following we shall present the version of *Baranger and Veneroni* [Ba 72a, BGV 76, BV 78] in some detail and show the connection with the work of Villars [Vi 71, 75, 77]. Other important papers in this context are given in the references [Be 65, Be 68, Ba 67, WSR 71, FC 72, He 73b, Ho 73, HY 74, RB 74, Pa 75b, EBG 75, KK 76, Go 76b, RB 76, Ma 77b]. For pedagogic reasons we shall also restrict ourselves to pure Slater determinants ($\rho^2 = \rho$), although it is possible and necessary in many practical cases to include pairing correlations.

The theory involves two approximations: (i) the *TDHF assumption*, where the wave functions stay a Slater determinant at all times; and (ii) the *adiabatic approach*, where we must include the velocities only to second order. Within the ATDHF theory the *classical aspect* of the theory is

studied in more detail. It will turn out that we can define classical coordinates and canonically conjugate momenta, which obey classical equations of motion.

The first problem, therefore, consists in defining these *coordinates* and *momenta*. In TDHF theory everything is determined by the single-particle density $\rho(t)$, which is not time-reversal invariant. Since we want to have time-reversal invariant coordinates, Baranger and Veneroni proposed the following decomposition of the density $\rho(t)$.

$$\rho(t) = e^{(i/\hbar)x(t)} \rho_0(t) e^{-(i/\hbar)x(t)}, \quad (12.63)$$

where ρ_0 and x are both Hermitian, time-even matrices, that is,

$$\rho_T(t) := T\rho(t)T^+ = e^{-(i/\hbar)x(t)} \rho_0(t) e^{(i/\hbar)x(t)}. \quad (12.64)$$

Again, ρ_0 satisfies $\rho_0^2 = \rho_0$, $\text{Tr } \rho_0 = N$, that is, it corresponds to an N -dimensional Slater determinant $|\Phi_0\rangle$. In the following the ρ_0 shall be the coordinate and as we shall see, x shall be the momentum.

We are much more familiar with a time-even determinant ρ_0 as coordinate than with the TDHF density ρ , which mixes time-even and time-odd components. In Chapter 2, for instance, we have used Nilsson functions with certain deformation coordinates q_i which correspond to time-even densities. The same is true for CHF calculations (see Sec. 7.6.) with a time-even constraint.

From the property that $\rho_0(t)$ is time-even, it follows that the total current associated with the density $\rho_0(t)$ vanishes for all times:

$$J = \frac{1}{m} \text{Tr}(\rho \rho_0(t)) = 0, \quad (12.65)$$

because the trace of the product of a time-even and a time-odd operator vanishes unless it is purely imaginary.

In the following we therefore call $\rho_0(t)$ a *static* density. It should not be confused with a time-independent density nor with the stationary density, which is a solution of the static HF equation $[h(\rho), \rho] = 0$. However, it will turn out that ρ_0 is the solution of a static HF equation with a suitable (time-dependent) time reversal invariant constraint [see Eq. (12.120b)]. Analogously, we can represent $\rho_0(t)$ by

$$\rho_0(t) = e^{-(i/\hbar)\varphi(t)} \bar{\rho} e^{(i/\hbar)\varphi(t)}, \quad (12.66)$$

where $\varphi(t)$ is a Hermitian, time-odd single-particle operator [Eq. (E.40)] and $\bar{\rho}$ is a time-independent single-particle density (for instance, the solution of the static HF problem $[h(\bar{\rho}), \bar{\rho}] = 0$).

We have already had an example of such decompositions of the density $\rho(t)$ in the case of translations [Eq. (12.32)], where x is the time-even operator $m\mathbf{v}\mathbf{r}$ and φ is the time-odd operator $m\mathbf{p}$. In the case of rotations (12.37), $i\omega\mathbf{J}$ is time-odd, that is, it corresponds to the operator φ . The density $\bar{\rho}$ itself contains time-odd components (see Sec. 7.7) and is time independent. Since there is no center of mass "angle," in this case we are unable to give an explicit expression* for the operator x .

* It has been calculated, for instance, in RPA order as the solution Q of the Thouless-Valatin equation (8.106).

In the following we will only work with the decomposition (12.63). It can be shown (see Sec. D.2) that it is unique under the following conditions.

(i) χ has only eigenvalues χ_μ with

$$-\frac{\pi\hbar}{4} < \chi_\mu < \frac{\pi\hbar}{4}. \quad (12.67a)$$

(ii) The pp and hh matrix elements of χ vanish in the basis in which ρ_0 is diagonal, that is,

$$\chi^{kk} = \rho_0 \chi \rho_0 = 0; \quad \chi^{pp} = \sigma_0 \chi \sigma_0 = 0. \quad (12.67b)$$

Here we have used the fact that ρ_0 is the projector onto hole states and $\sigma_0 = 1 - \rho_0$ is the projector onto particle states in the basis in which ρ_0 is diagonal. In the following, we will always work in this basis. It should be noticed, however, that the basis depends on the time since $\rho_0(t)$ is a function of time.

We might ask whether the conditions (12.67) are necessary. In fact, this is not the case—it is only a quite natural choice,* because the pp and hh matrix elements play a rather important role. Baranger and Veneroni [BV 78] have shown that any other decomposition with non-vanishing matrix elements χ^{pp} and χ^{hh} gives results which deviate from the ones we will derive in the following only to orders in χ that are neglected in the ATDHF approach, anyway. It is therefore consistent with this approximation to use the conditions (12.67), and we shall adopt them in the following.

The *adiabatic approximation* now consists in assuming that the density $\rho(t)$ of the system is at all times close to the density $\rho_0(t)$, that is, we have at all times a nearly static density. In other words, it means that the matrix χ which introduces time-odd components is small. This is certainly not true for all solutions $\rho(t)$ of the TDHF equations, but we are only interested in the ones for which this holds. We can thus expand $\rho(t)$ up to second order in χ and get

$$\rho = e^{(i/\hbar)\chi} \rho_0 e^{-(i/\hbar)\chi} \approx \rho_0 + \rho_1 + \rho_2 \quad (12.68)$$

with

$$\rho_1 = \frac{i}{\hbar} [\chi, \rho_0], \quad \chi = -i\hbar [\rho_1, \rho_0], \quad (12.69)$$

$$\rho_2 = \frac{-1}{2\hbar^2} [\chi, [\chi, \rho_0]] = \frac{1}{\hbar^2} \left(\chi \rho_0 \chi - \frac{1}{2} (\chi^2 \rho_0 + \rho_0 \chi^2) \right). \quad (12.70)$$

Equation (D.32) shows that ρ_1 has only ph - and hp - and that ρ_2 has only pp - and hh -matrix elements:

$$\rho_1 = \frac{i}{\hbar} (\sigma_0 \chi \rho_0 - \rho_0 \chi \sigma_0), \quad (12.71)$$

$$\rho_2 = \sigma_0 \rho_1^2 \sigma_0 - \rho_0 \rho_1^2 \rho_0. \quad (12.72)$$

* It has been shown, however, that this choice is incompatible with the assumption that χ is local in coordinate space [BQ 78] and sometimes a local χ seems to be the natural choice, as we see in the case of translations (12.32).

In the same way we can expand*

$$h(\rho) = t + \text{Tr}_1(\bar{\nu}\rho) = h_0 + \Gamma_1 + \Gamma_2 \quad (12.73)$$

with

$$h_0 = t + \text{Tr}_1(\bar{\nu}\rho_0), \quad \Gamma_1 = \text{Tr}_1(\bar{\nu}\rho_1), \quad \Gamma_2 = \text{Tr}_1(\bar{\nu}\rho_2). \quad (12.74)$$

In the expansions of ρ and of h the even terms are always even under time reversal and the odd are always odd.

If we insert the expansions (12.68) and (12.73) into the TDHF Eq. (12.9) we can decompose it according to its behavior under time reversal and get the two *ATDHF equations*:

$$(I) \quad i\hbar\dot{\rho}_0 = [h_0, \rho_1] + [\Gamma_1, \rho_0] \quad (12.75a)$$

$$(II) \quad i\hbar\dot{\rho}_1 = [h_0, \rho_0] + [\Gamma_1, \rho_1] + [\Gamma_2, \rho_0]. \quad (12.75b)$$

As we shall see later, only the $p\chi$ and $\hbar p$ parts of both equations are important. In deriving these equations we have neglected higher-order terms in χ . To be able to do that, we have to know the order in χ of the time derivatives $\dot{\rho}_0, \dot{\rho}_1, \dot{\rho}_2 \dots$. In a Fourier analysis they carry a factor ω , where ω is the corresponding frequency. Now we have to distinguish between large amplitude motion and small amplitude oscillations. In the large amplitude case, ω has to be of the order of χ and small; as we have seen, that means $\dot{\rho}_i$ is an order higher in χ than in ρ_i . In the small amplitude case ω does not necessarily have to be of the same order as χ , that is, $\dot{\rho}_i$ is of the same order in χ as ρ_i .

In Eq. (I) above we have therefore neglected all terms that are equal to or of higher order than second and in Eq. (II) all terms that are equal to or higher than third order in χ . In addition, the term $[h_0, \rho_2]$ has been neglected in Eq. (II) for reasons which we shall discuss later.

In zeroth order in χ we gain the static case

$$\dot{\rho}_0 = 0, \quad [h_0, \rho_0] = 0. \quad (12.76)$$

Equations (I) and (II) therefore always take into account the first nontrivial order in χ . In particular, this shows that in the large amplitude case, where $\dot{\rho}_i$ is of second order in χ , the term $[h_0, \rho_0]$ in (12.75b) is also at least of second order, in spite of the fact that h_0 and ρ_0 separately are large. This means that the static HF equation (12.76) is *almost* satisfied. The nucleus is almost in static equilibrium at all times and the motion is slow.

As we shall see in detail in Section 12.2.2, we can give a *classical interpretation* to the ATDHF equations, in which ρ_0 and χ are canonical conjugate coordinate and momentum. Equation (I) gives a linear connection between velocity and momentum, which depends on ρ_0 , that is, the corresponding mass is coordinate dependent. Equation (II) has the time derivative of the momentum on the l.h.s. The r.h.s. therefore represents a force. It depends on the term $[h_0, \rho_0]$ and on further terms quadratic in the momentum χ . Starting from some initial value ρ_0 at zero velocity, $[h_0, \rho_0]$ is therefore the force which accelerates the system at the beginning. Since the momenta stay small for all times, the smallness of $[h_0, \rho_0]$ for all times is

* The abbreviation Tr_1 is defined in Eq. (E.19).

therefore a necessary and sufficient condition for the existence of an adiabatic motion. If there is a whole region in the space of time-even densities ρ_0 in which $[\hbar_0, \rho_0]$ is small, then we can find a trajectory $\rho(t)$ in this region which corresponds to adiabatic motion.

We still have to show that Eqs. (I) and (II) should only be used in the ph and hp space: The pp - and hh matrix elements of Eq. (I) are at least of second order in χ . For instance, from Eq. (D.32) $\dot{\rho}_0$ has only ph and hp matrix elements, and from Eq. (12.71) the same holds for ρ_1 . The only non-vanishing hh matrix elements of the r.h.s. of Eq. (I) are therefore

$$\rho_0[\hbar_0, \rho_1]\rho_0 = -\rho_0([\hbar_0, \rho_0]\rho_1 + \rho_1[\hbar_0, \rho_0])\rho_0, \quad (12.77)$$

which is at least of second order, since $[\hbar_0, \rho_0]$ is of second order in the large amplitude case and of first order in the small amplitude case. The same holds true for the pp matrix elements of Eq. (I).

In Eq. (II) we have left out the term $[\hbar_0, \rho_2]$. From Eq. (12.72) we see that ρ_2 only has hh and pp matrix elements. The ph matrix elements of $[\hbar_0, \rho_2]$ therefore contain only ph and hp matrix elements of \hbar_0 , which are of at least first order in χ . Therefore, $[\hbar_0, \rho_2]$ can be neglected in the hp and ph part of Eq. (II). In the hh and pp parts of Eq. (II) we can no longer neglect this term, since the pp and hh matrix elements of \hbar_0 are large. We can show, however, that the pp and hh matrix elements of Eq. (II) with inclusion of the term $[\hbar_0, \rho_2]$ vanish identically. This requires a longer calculation [BV 78]; here we give only the most important steps. First we express ρ_2 by Eq. (12.72); then we use Eq. (12.71) and get for the hh matrix element of $\dot{\rho}_1$

$$\rho_0\dot{\rho}_1\rho_0 = -\rho_0(\rho_1\dot{\rho}_0 + \dot{\rho}_0\rho_1)\rho_0. \quad (12.78)$$

Finally, we insert Eq. (I) for $\dot{\rho}_0$ and find that the pp and hh parts of Eq. (II) vanish.

The set of ATDHF equations (12.75) allow us to calculate $\rho_0(t)$ and $\rho_1(t)$ at all times if we start with some initial values $\rho_0(0)$, $\rho_1(0)$ or $\rho_0(0)$ and $\dot{\rho}_0(0)$. This is, however, a problem, which is at least as difficult as the exact TDHF equations, and nobody will do that in practice. The main advantage of the adiabatic theory lies in the fact that it allows us to derive a classical Hamiltonian for the description of the collective motion.

12.3.2 The Collective Hamiltonian

We are now able to express the total energy E of the system by the variables ρ_0 and ρ_1 or ρ_0 and χ . From Eq. (5.28), we find

$$\begin{aligned} E &= \text{Tr}(i\rho) + \frac{1}{2}\text{Tr}_1\text{Tr}_1(\rho\bar{v}\rho) \\ &= K + V, \end{aligned} \quad (12.79)$$

where we collect into the kinetic energy K all terms which depend on the velocity in second order and in the potential energy V all terms which contain only the static density ρ_0 . Linear terms in ρ_1 vanish because of the time-reversal invariance of the Hamiltonian. We get for V the static HF

energy of the density distribution ρ_0 :

$$V = \text{Tr}(\imath\rho_0) + \frac{1}{2}\text{Tr}_1\text{Tr}_1(\rho_0\bar{v}\rho_0). \quad (12.80)$$

The kinetic energy assumes the form

$$K = \text{Tr}(h_0\rho_2) + \frac{1}{2}\text{Tr}_1\text{Tr}_1\rho_1\bar{v}\rho_1. \quad (12.81)$$

It depends quadratically on ρ_1 (or χ), and because of Eq. (12.75a) also quadratically on the velocity $\dot{\rho}_0$. We can write it in several ways. First we use a basis in which the pp part as well as the hh part of h_0 is diagonal. This is always possible, since ρ_0 is not changed by such a transformation. We call the eigenvalues ϵ_m (particles) and ϵ_i (holes). Using Eqs. (12.69) and (D.35) and the matrices

$$A_{minj} = (\epsilon_m - \epsilon_i)\delta_{nm}\delta_{ij} + \bar{v}_{mijn}, \quad B_{minj} = \bar{v}_{mijn}, \quad (12.82)$$

we find with $\chi_{im} = \chi_{mi}^*$

$$K = \frac{1}{2\hbar^2}(\chi^*\chi)\begin{pmatrix} A & -B \\ -B^* & A \end{pmatrix}\begin{pmatrix} \chi \\ \chi^* \end{pmatrix}, \quad (12.83)$$

where the index of the matrices runs over all ph pairs (mi) in $(\chi_{mi}^*\chi_{mi})$. It looks very similar to the RPA notation in Chapter 8. It is, however, more general, since the single-particle energies and χ depend on time.

We can also write the ATDHF equation (l) in this notation:

$$\begin{pmatrix} \dot{\rho}_0 \\ \dot{\rho}_0^* \end{pmatrix} = \frac{1}{\hbar^2}\begin{pmatrix} A & -B \\ -B^* & A^* \end{pmatrix}\begin{pmatrix} \chi \\ \chi^* \end{pmatrix}, \quad (12.84)$$

which connects velocities and momenta and shows that the matrix

$$\mathcal{M} := \hbar^2 \begin{pmatrix} A & -B \\ -B^* & A^* \end{pmatrix}^{-1} \quad (12.85)$$

represents a *mass tensor* which depends on the coordinate ρ_0 . As is easy to see, it corresponds to the Thouless-Valatin value of the moment of inertia (8.142) in the rotational case. The kinetic energy (12.83) assumes the form

$$K = \frac{1}{2}(\dot{\rho}_0^*\dot{\rho}_0)\mathcal{M}\begin{pmatrix} \dot{\rho}_0 \\ \dot{\rho}_0^* \end{pmatrix} = \frac{1}{2}\text{Tr}(\dot{\rho}_0\chi). \quad (12.86)$$

We have thus derived a *classical Hamilton function*, depending on the coordinate ρ_0 and quadratically on the momentum χ

$$E = H(\chi, \rho_0) = \frac{1}{2}(\chi^*\chi)\mathcal{M}^{-1}\begin{pmatrix} \chi \\ \chi^* \end{pmatrix} + V(\rho_0). \quad (12.87)$$

$V(\rho_0) = \langle \Phi_0 | H | \Phi_0 \rangle$ is the expectation value of the full Hamiltonian in the static wave function $|\Phi_0\rangle$. The kinetic energy has its origin completely in the time-odd parts of the wave function. As we see from Eq. (12.81), it is made up of two contributions. The first contains the static potential h_0 and the second the time-odd potential Γ_1 . Neglecting this time-odd part would mean that we forget about the residual interaction \bar{v} in the mass tensor (12.85), and we would obtain the Inglis formula (see Sec. 8.4.7).

To complete the formalism, we have to show that we can get the ATDHF equation (I) and (II) (12.75) as *Hamilton equations* from the function (12.87). The independent variables are ρ_0 and χ . Infinitesimal changes $\delta\rho_0$ and $\delta\chi$, which have, of course, only ph and hp matrix elements, produce changes in the energy (12.87). The first part is very simple. For fixed ρ_0 we get

$$\frac{\partial H}{\partial \chi^*} = \mathcal{R}^{-1} \begin{pmatrix} \chi \\ \chi^* \end{pmatrix} = \dot{\rho}_0, \quad (12.88)$$

which shows the first ATDHF equation [which corresponds to Eq. (12.84)] to be identical to the Hamilton equation $\dot{q} = \partial H / \partial p$. The derivation of the second ATDHF equation is more complicated. We first calculate the changes of ρ_1 and ρ_2 by a change $\delta\rho_0$. For fixed χ we get from Eqs. (12.69) and (12.70),

$$\delta\rho_1 = \frac{i}{\hbar} [\chi, \delta\rho_0] \quad \text{and} \quad \delta\rho_2 = -\frac{1}{2\hbar^2} [\chi, [\chi, \delta\rho_0]]. \quad (12.89)$$

The change in the energy (12.79) is therefore

$$\begin{aligned} \delta E &= \text{Tr}(\Gamma_2 \delta\rho_0 + \Gamma_1 \delta\rho_1 + h_0 \delta\rho_2) + \delta V \\ &= \text{Tr}\left(\left(\Gamma_2 + \frac{i}{\hbar} [\Gamma_1, \chi] - \frac{1}{2\hbar^2} [[h_0, \chi], \chi]\right) \delta\rho_0\right) + \delta V. \end{aligned} \quad (12.90)$$

Since χ and $\delta\rho_0$ have only ph and hp matrix elements, the only matrix elements of h_0 which contribute to these traces are ph and hp matrix elements. These are, as discussed in the last section, of at least first order in χ . To be consistent we therefore have to neglect the last term in Eq. (12.90) and find as a second Hamilton equation

$$-\dot{\chi} = \frac{\partial H}{\partial \rho_0^*} = \frac{\partial V}{\partial \rho_0^*} + \Gamma_2 + \frac{i}{\hbar} [\Gamma_1, \chi]. \quad (12.91)$$

Of course, we have to use only the ph and hp elements of these equations. With

$$\sigma_0 \dot{\rho}_1 \rho_0 = \frac{i}{\hbar} \sigma_0 \dot{\chi} \rho_0, \quad \rho_0 \dot{\rho}_1 \sigma_0 = -\frac{i}{\hbar} \rho_0 \dot{\chi} \sigma_0, \quad (12.92)$$

and the fact that the derivative of the static energy $\partial V / \partial \rho_0^*$ with respect to the density ρ_0 gives the ph matrix elements of h_0 [see Eq. (5.32)], we see that Eq. (12.91) corresponds exactly to the second ATDHF equation (12.75b).

The second ATDHF equation thus describes the *acceleration of the system*. Besides the static force ($\partial V / \partial \rho_0^*$), there are additional terms that have their origin in the coordinate dependence of the mass tensor (12.85).

We have now established the complete analogy to a classical system using the Hamilton formalism. We could also have done this using the Lagrangian formalism [BV 78].

In the *limit of small amplitudes*, we can derive the RPA in a way different than the usual one (see Sec. 8.4.). We assume that $\rho_0(t)$ stays close to the stationary

solution $\bar{\rho}$ of the static HF problem [$h(\bar{\rho}), \bar{\rho}\rangle = 0$,

$$\rho_0(t) = \bar{\rho} + \xi(t), \quad (12.93)$$

and expand the potential $V(\rho_0)$ at the point $\bar{\rho}$ up to second order [see Eq. (7.34)]:

$$V(\rho_0) = V(\bar{\rho}) + \frac{1}{2} (\xi^* \xi) \begin{pmatrix} A & B \\ B^* & A^* \end{pmatrix} \begin{pmatrix} \xi \\ \xi^* \end{pmatrix}. \quad (12.94)$$

With the *stability matrix* S [Eq. (7.37)] (curvature tensor) we get the energy

$$E(x, \xi) = E_{\text{HF}} + \frac{1}{2} (x^* x) \mathcal{M}^{-1} \begin{pmatrix} x \\ x^* \end{pmatrix} + \frac{1}{2} (\xi^* \xi) S \begin{pmatrix} \xi \\ \xi^* \end{pmatrix}. \quad (12.95)$$

This is a Hamilton function for coupled oscillators. The corresponding equations of motion are solved by harmonic oscillators of the frequency Ω , and we end up with the eigenvalue problem [Go 59]

$$\Omega^2 \mathcal{M} X = S X. \quad (12.96)$$

The frequencies $(\lambda\Omega)^2$ are the eigenvalues of the matrix

$$\mathcal{M}^{-1} S = \mathcal{M} S \mathcal{M}, \quad \text{with} \quad \mathcal{M} = \begin{pmatrix} 1 & 0 \\ 0 & -1 \end{pmatrix}. \quad (12.97)$$

They can be found by diagonalizing $\mathcal{M} S$ only, which is exactly the RPA matrix. This is only possible because the inverse of the mass tensor \mathcal{M} has a structure similar to the curvature tensor S .

12.3.3 Reduction to a Few Collective Coordinates

We come back to the problem of large amplitudes. The system of ATDHF equations (12.75) still contains all degrees of freedom and is much too general for a practical application. In particular, it is not easier than the full TDHF equation (12.9); the adiabatic approximation, however, is also valid for only few trajectories. It may therefore be possible to drastically reduce the number of degrees of freedom.

The selection of the proper collective variables is certainly a great problem. Before we discuss this in more detail, we shall first assume that we have achieved such a reduction and have a family of time-even Slater determinants

$$|\mathbf{q}\rangle = |\Phi_0(\mathbf{q})\rangle \hat{=} \Phi_0(\mathbf{r}_1, \dots, \mathbf{r}_A, q_1, \dots, q_J) \quad (12.98)$$

with corresponding densities $\rho_0(\mathbf{q})$ which have the property that the solution of the ATDHF problem will always stay within this subset of Slater determinants characterized by the real parameters \mathbf{q} ; that is, there exists a path $\mathbf{q}(t)$ with

$$\rho_0(t) = \rho_0(\mathbf{q}(t)), \quad (12.99)$$

from which we gain for the velocity

$$\dot{\rho}_0(t) = \dot{\mathbf{q}} \frac{\partial \rho_0}{\partial \mathbf{q}} := -\frac{i}{\hbar} \dot{\mathbf{q}} [\mathbf{P}, \rho_0]. \quad (12.100)$$

Since $(\partial/\partial \mathbf{q})\rho_0$ has only ph and hp matrix elements, this equation defines the corresponding elements* \mathbf{P} of the Hermitian single-particle operators $\hat{\mathbf{P}} = (\hat{P}_1, \dots, \hat{P}_f)$. The single-particle matrices \mathbf{P} have the elements [see Eq. (D.36ff)]

$$\mathbf{P}_{mi} = \mathbf{P}_{im}^* = -\langle m | \frac{\hbar}{i} \frac{\partial}{\partial \mathbf{q}} | i \rangle; \quad \mathbf{P}_{mm'} = \mathbf{P}_{ii'} = 0 \quad (12.101)$$

in the basis in which ρ_0 is diagonal.

Since we now have an explicit expression for the velocity $\dot{\rho}_0$ in terms of \mathbf{q} for the kinetic energy from Eqs. (12.86) and (12.100) we get

$$K = \frac{1}{2} \sum_{\mu, \mu'=1}^f M_{\mu\mu'}(\mathbf{q}) \dot{q}_\mu \dot{q}_{\mu'} \quad (12.102)$$

and the real collective mass tensor

$$M_{\mu\mu'}(\mathbf{q}) = \frac{1}{\hbar^2} (P^* - P)_{\mu} \Re \left(-\frac{P}{P^*} \right)_{\mu'}. \quad (12.103)$$

We also can define collective momenta p_μ and find, from Eqs. (12.84) and (12.100),

$$p_\mu := \sum_{\mu'} M_{\mu\mu'}(\mathbf{q}) \dot{q}_{\mu'} = \text{Tr}(\rho_0 P_\mu) = \text{Tr} \left(\chi \frac{\partial}{\partial q_\mu} \rho_0 \right) \quad (12.104)$$

and gain for the Hamilton function in the collective variables

$$E = H(\mathbf{p}, \mathbf{q}) = \frac{1}{2} \sum_{\mu\mu'} M_{\mu\mu'}^{-1} p_\mu p_{\mu'} + V(\mathbf{q}) \quad (12.105)$$

with

$$V(\mathbf{q}) = V(\rho_0(\mathbf{q})) = \langle \mathbf{q} | H | \mathbf{q} \rangle.$$

It remains to be shown that the collective coordinates \mathbf{q} and momenta \mathbf{p} defined in this way obey equations of motion, which correspond to Hamilton's equations derived from the function (12.105). The first equation is trivial:

$$\frac{\partial H}{\partial p_\mu} = \sum_{\mu'} M_{\mu\mu'}^{-1} p_{\mu'} = \frac{d}{dt} q_\mu. \quad (12.106)$$

In the second case we get, with Eqs. (12.87), (12.90), and (12.104), in an

* These matrices correspond to the matrix p in Eq. (12.32). We now use capital letters for them so that they are not mixed up with the collective coordinates q and p .

obvious shorthand notation [BGV 76],

$$\begin{aligned}
 \frac{\partial X}{\partial q_\mu} &= \frac{\partial E}{\partial \rho_0^*} \frac{\partial \rho_0}{\partial q_\mu} + \frac{\partial E}{\partial X^*} \frac{\partial X}{\partial q_\mu} = -\dot{X} \frac{\partial \rho_0}{\partial q_\mu} + \dot{\rho}_0 \frac{\partial X}{\partial q_\mu} \\
 &= -\dot{X} \frac{\partial \rho_0}{\partial q_\mu} - X \frac{d}{dt} \frac{\partial \rho_0}{\partial q_\mu} + \sum_{\mu'} \dot{q}_{\mu'} \frac{\partial}{\partial q_\mu} \left(X \frac{\partial}{\partial q_{\mu'}} \rho_0 \right) \\
 &= -\frac{d}{dt} \left(X \frac{\partial \rho_0}{\partial q_\mu} \right) + \sum_{\mu'} \dot{q}_{\mu'} \frac{\partial}{\partial q_\mu} p_{\mu'} \\
 &= -\frac{d}{dt} p_\mu,
 \end{aligned} \tag{12.107}$$

because p_μ and q_μ are independent variables $[(\partial/\partial q_\mu)p_{\mu'} = 0]$.

One also often introduces a set of Hermitian operators \hat{Q} which have only ph and hp elements defined by

$$\left(\begin{array}{c} Q \\ Q^* \end{array} \right)_\mu = \frac{\hbar}{i} \sum_{\mu'} M_{\mu\mu'}^{-1} \left(\begin{array}{cc} A & -B \\ -B^* & A^* \end{array} \right)^{-1} \left(\begin{array}{c} P \\ P^* \end{array} \right)_{\mu'}. \tag{12.108}$$

They are closely connected to the operator

$$X = \sum_{\mu\mu'} \dot{q}_\mu M_{\mu\mu'} Q_{\mu'} \tag{12.109}$$

and allow a simple representation of the mass tensor M :

$$M_{\mu\mu'}^{-1} = (Q^* Q)_\mu \mathcal{M}^{-1} \left(\begin{array}{c} Q \\ Q^* \end{array} \right)_{\mu'} = \frac{1}{\hbar^2} \langle \mathbf{q} | [\hat{Q}_\mu, [H, \hat{Q}_{\mu'}]] | \mathbf{q} \rangle. \tag{12.110}$$

They obey the relation

$$\langle \mathbf{q} | [\hat{P}_\mu, \hat{Q}_{\mu'}] | \mathbf{q} \rangle = (P^* - P)_\mu \left(\begin{array}{c} Q \\ Q^* \end{array} \right)_{\mu'} = \frac{\hbar}{i} \delta_{\mu\mu'}, \tag{12.111}$$

which says that \hat{P}_μ and \hat{Q}_μ are "weakly" canonical variables.

The operators \hat{P} and \hat{Q} allow us to give a representation of the wave function $|\Phi\rangle$ in the vicinity of an arbitrary point \mathbf{q}_0 . This "local" representation shows a close analogy to the case of pure translation (see Sec. 12.2.3.) and will be used in the following sections. The operators \hat{P} and \hat{Q} act like infinitesimal generators for the wave function $|\Phi\rangle$ in the vicinity of a point \mathbf{q}_0 . If we know the "momenta" \mathbf{p} (12.104) and the "coordinates" \mathbf{q} we get for the ATDHF function $|\Phi\rangle$ at a point $\mathbf{q}_0 + \mathbf{q}$

$$|\Phi(\mathbf{q}_0 + \mathbf{q})\rangle = e^{(i/\hbar)\mathbf{p}\hat{Q}} e^{-(i/\hbar)\mathbf{q}\hat{P}} |\Phi_0(\mathbf{q}_0)\rangle \tag{12.112}$$

and

$$\rho(t) = e^{(i/\hbar)\hat{P}(t)\hat{Q}} e^{-(i/\hbar)\hat{Q}(t)\hat{P}} \rho_0(q_0) e^{(i/\hbar)\hat{Q}(t)\hat{P}} e^{-(i/\hbar)\hat{P}(t)\hat{Q}}, \quad (12.113)$$

that is, we can obtain the wave function in the vicinity of q_0 (i.e., locally) by a shift in coordinate generated by the operators \hat{P} and a shift in the momentum generated by the operators \hat{Q} . These operators depend in general on the position q_0 . An example, where the \hat{P} 's and \hat{Q} 's are constant operators, is given by a Galilei transformation [see Eq. (12.32)].

In this case, we see that \hat{Q} is the center of mass coordinate and \hat{P} the total linear momentum. The tensor of inertia is a multiple of the unity and its value is just the total mass $A \cdot m$ of the nucleus. Unlike in GCM with one real generator coordinate q (see Sec. 10.7), we now get in the ATDHF approach the proper inertial parameters. The reason for that is that the ATDHF method is a dynamical theory which allows for time-odd components in the wave function (see also Sec. 11.4.5).

Starting from an arbitrary set of time-even determinants $|q\rangle$, which depend on a set of parameters q , we developed a theory which uses these parameters as collective coordinates. We also defined corresponding momenta such that the p 's and q 's fulfill the classical equations of motion derived from a Hamilton function in these variables.

It is certainly a major disadvantage of this theory that we end up with a *classical Hamiltonian*. As in the case of the collective model in Chapter 1, we have to requantize this theory to get a collective Hamilton operator, which allows us to calculate wave functions. The requantization always involves some arbitrariness. There are several methods. One possibility is the Pauli quantization [Eq. (1.53)]. Goeke and Reinhard [GR 78] proposed a different method, which has the advantage that it reproduces the same zero-point corrections $\epsilon_0(q)$ of the energy surface as the GCM theory [see Eq. (10.136)]. However, before we discuss why such a quantization is necessary, we want to present a method that determines the optimal family $\rho_0(q)$ from which we should start.

12.3.4 The Choice of the Collective Coordinates

In deriving the Hamiltonian (12.105) we have assumed that we could restrict ourselves to a few collective coordinates q_1, \dots, q_f . The question arises of how to determine these coordinates (i.e., the corresponding wave functions) and how many of them are needed. Of course, we would like to have as few as possible. Since we have seen that the solution of the ATDHF Eqs. (12.75) with certain initial conditions corresponds to a one-dimensional path in the multidimensional energy surface, it seems that one coordinate q would be sufficient if it is properly chosen. The whole concept of deriving a collective Hamiltonian in this coordinate, however, is only meaningful, if the path determined in such a way does not

depend on the initial velocity $\dot{\mathbf{q}}$, that is, we should find more or less the same path $|\Phi_0(\mathbf{q})\rangle$, if we start from different initial velocities. In general, this will not be the case for a one-dimensional path. We could then try using a two-dimensional surface and so on. The number of the necessary collective coordinates q_1, \dots, q_j therefore depends on the dynamical behavior of the system. The restriction to a few of them is only possible, if there exists a subset $|\Phi(q_1, \dots, q_j)\rangle$ of Slater determinants such that the solution of the ATDHF problem (12.75) stays within this subset for many different initial conditions. This requirement is very similar to the condition (10.24) in the GCM method, in which we had to ask for generating wave functions with the property that the corresponding collective subspace contains eigensolutions of the full Hamiltonian (see also [RG 78]).

In many physical problems it is not clear whether such a set of coordinates exists that describes a collective motion decoupled from all the other degrees of freedom. If this is not the case, we can try to include the other degrees of freedom in an averaged way. This leads to the concept of friction (see, for instance, [BBN 78]). Within this book we do not wish to go into these problems. We shall assume in the following that there is a fixed number of collective coordinates.

Under this condition we are faced with the question of how to determine the optimal set of wave functions $|\Phi_0(q_1, \dots, q_j)\rangle$. There are several ways. The first, which has been used in most of the realistic applications, is *physical intuition*. For instance, we know that for the fission processes we need at least three coordinates, describing the elongation, the neck, and the asymmetry (see Sec. 1.6), and so we choose Slater determinants in a deformed single-particle potential with these parameters. The second way is more sophisticated. We use *constrained Hartree Fock (CHF) theory* (see Sec. 7.6) with several constraining operators. The physical intuition is then restricted to the optimal choice of these operators. The third way is given by the *ATDHF method* itself and will be discussed in the following. In this way we will find a close connection to the formulation of ATDHF theory as given by Villars [Vi 75, 77].

In deriving the collective Hamiltonian (12.105) we assumed that we knew the set of static wave functions and used the first of the ATDHF equations (12.75a) to calculate the corresponding momenta and inertial parameters. The second equation (12.75b) was only used to derive the equations of motion in the few variables \mathbf{p} and \mathbf{q} . This is only a very small part of the information contained in this second equation. Additional information will be used to determine the optimal set of wave functions [GR 78].

In Sec. 7.6 we saw that any Slater determinant $|\Phi_0\rangle$ (with density ρ_0) can be found as a solution of a CHF equation with a suitable constraining operator F , which has only ph and hp matrix elements in the basis, in which ρ_0 is diagonal:

$$[h_0 - F, \rho_0] = 0. \quad (12.114)$$

In fact, the second ATDHF equation is already of the form of a CHF equation. To make this evident, we shall rewrite it somewhat: As discussed in Section 12.3.1, only the ph and hp part of this equation is interesting. With (12.69) it can be written as

$$\left[h_0 + \dot{\chi} + \Gamma_2 + \frac{i}{\hbar} [\Gamma_1, \chi], \rho_0 \right] = 0, \quad (12.115)$$

which shows that the ph matrix elements of F are given by

$$F^{ph} = \sigma_0 \left(-\dot{\chi} - \Gamma_2 - \frac{i}{\hbar} [\Gamma_1, \chi] \right) \rho_0. \quad (12.116)$$

We assume that we know χ from the solution of the first ATDHF equation and use Eq. (12.109). The time derivative of χ is then given by*

$$\dot{\chi} = MQ\ddot{q} + \dot{q}^2 \frac{d}{dq}(MQ). \quad (12.117)$$

With the equations of motion (12.106) and (12.107) we find

$$\ddot{q} = \frac{d}{dt} \frac{p}{M} = -\frac{1}{M} \frac{dV}{dq} - \frac{\dot{q}^2}{2} \frac{1}{M} \frac{dM}{dq}. \quad (12.118)$$

Since Γ_2 and $[\Gamma_1, \chi]$ are quadratic in \dot{q} , using Eq. (12.116) we gain for the constraining operator F

$$F = \frac{dV}{dq} \cdot Q + O(\dot{q}^2). \quad (12.119)$$

To get a consistent description, the terms $\propto \dot{q}^2$ have to be small and will be neglected. We therefore end up with the possibility of determining the path $\rho_0(q)$ from a constrained HF equation, where the constraint Q is given by Eq. (12.108). The mass parameter $M(q)$ in this equation is determined, for instance, by the condition (12.111). The following set of equations (Villars [Vi 75, Vi 77]) is therefore up to order \dot{q}^2 equivalent to the ATDHF equations (12.75)

$$\begin{pmatrix} A & -B \\ -B^* & A^* \end{pmatrix} \begin{pmatrix} Q \\ Q^* \end{pmatrix} = \frac{\hbar}{iM} \begin{pmatrix} P \\ -P^* \end{pmatrix}, \quad (12.120a)$$

$$\left[h_0 - \frac{dV}{dq} Q, \rho_0 \right] = 0, \quad (12.120b)$$

$$\langle \Phi_0 | [\hat{P}, \hat{Q}] | \Phi_0 \rangle = \frac{\hbar}{i}. \quad (12.120c)$$

This system is very similar to that which we get by a self-consistent determination of the path in the generator coordinate method (Sec. 10.8). For a practical application we have to start with an initial guess for the constraining operator in Eq. (12.120b) and calculate the corresponding $\rho_0(q)$. From Eq. (12.100), we can at each point q determine the correspond-

* We restrict ourselves in the following to one collective coordinate q .

ing operator P and from (12.120a) a new constraining operator Q . This procedure has to be continued until convergence is achieved.

Somewhat related is the *local harmonic approach* [HY 74, RB 76, Ma 77b, ABC 77b, MV 77], where P is determined from Eq. (12.120b) in a linear response approximation [see Eq. (8.137)] neglecting curvature corrections [RG 77].

$$\begin{pmatrix} A & -B \\ -B^* & A^* \end{pmatrix} \begin{pmatrix} P \\ P^* \end{pmatrix} = i\hbar C \begin{pmatrix} Q \\ -Q^* \end{pmatrix}, \quad (12.121)$$

where $C = (d^2V/dq^2)$, that is the curvature of our potential. We can then define a collective frequency $\Omega(q)$ [RB 76] by*

$$\Omega(q) = \sqrt{\frac{C(q)}{M(q)}} \quad (12.122)$$

and a boson operator

$$A^*(q) = \sqrt{\frac{M\Omega}{2\hbar}} \left(\hat{Q} - i \frac{1}{M\Omega} \hat{P} \right). \quad (12.123)$$

Since the Eqs. (12.120a) and (12.121) correspond exactly to the RPA equations in the form (8.99), the operator A^+ can be found as the solution of a RPA calculation at each point q (local RPA).

We do not want to go into further details of these and similar methods, which are still under investigation. Summarizing the results of this section, we can say that there are methods to determine an optimal path or an optimal hypersurface (in cases where we need more than one collective coordinate) in the large set of all Slater determinants. We thus obtain the potential and the inertia parameters as a function of the coordinates q , that is, the classical Hamiltonian function (12.105).

However, for a full description of the system, we still need its dynamical behavior. In the classical picture it is given by the functions $q(t)$. They are obtained from the solution of the classical equations of motion (12.106) and (12.107). In the quantum mechanical case we first have to requantize the Hamiltonian before solving the corresponding Schrödinger equation in collective coordinates.

12.3.5 General Discussion of the ATDHF Method

12.3.5.1 Why Is a Requantization Necessary? The ATDHF method ends up with classical equations of motion of a collective Hamilton function in a few collective variables. In particular, there is no possibility of tunnelling through potential barriers, therefore we cannot for instance describe spon-

* In cases where M or C is negative, the RPA has purely imaginary solutions. Nevertheless, P and Q are well determined and bosons can be defined (for details, see [RB 76] and Sec. 8.4.5).

taneous fission. This only becomes possible if we requantize the collective Hamiltonian. This prescription is not as ad hoc as it might seem since it can be shown [MH 72, BM 78] that the full TDHF theory can be obtained from the exact boson expansion (see Chap. 9) by replacing the boson operators or the corresponding operators for momentum and coordinate by c -numbers. In this sense, TDHF as well as ATDHF is a classical theory and it therefore seems natural to requantize. This does not mean, however, that the theory is completely classical; after all, a Slater determinant is a quantum mechanical wave function.

We have already seen in Section 12.2.4 that the restriction to Slater determinants includes some classical features, such as soliton solutions without dispersion. These features are still more pronounced if we restrict ourselves to a few collective variables q . The overlap between two wave functions $|\Phi(q)\rangle$ and $|\Phi(q')\rangle$ is sharply peaked at $q=q'$ if q is a collective variable (see Sec. 10.7.4), that is, we can write to a good approximation

$$\langle \Phi(q)|\Phi(q')\rangle \approx \delta(q-q'), \quad (12.124)$$

which says that the functions $|\Phi(q)\rangle$ are wave packets localized in q -space. At the same time, we calculate q , which violates the uncertainty relation and is therefore a classical approximation. In a quantum mechanical theory we should use a superposition of many different shapes $|\Phi(q)\rangle$, as we do, for instance, in the GCM method (see Chap. 10).

12.3.5.2 The Validity of the Adiabatic Approximation. We are now able to give a rough criterion for cases of the adiabatic approximation to be valid [BV 78]. We therefore restrict our considerations to one collective variable q (which is, in fact, no restriction, since q could be the exact solution of the ATDHF equations).

The adiabatic approach is equivalent to the fact that the time-odd component in any single-particle wave function

$$e^{i\hat{x}}|i\rangle = |i\rangle + i\hat{x}|i\rangle \quad (12.125)$$

should have a small norm:

$$|\hat{x}|i\rangle|^2 = \sum_m |\langle m|\hat{x}|i\rangle|^2 \ll 1 \quad \text{for all } i.$$

If, as a rough estimate, in Eq. (12.83) we neglect the residual interaction—that is, if we use the Inglis formula for the collective mass—we find for the kinetic energy involved in this motion

$$\mathcal{K} = \sum_{mi} \chi_{mi}^*(\epsilon_m - \epsilon_i) \chi_{mi} \approx \Delta\epsilon \sum_{mi} |\chi_{mi}|^2, \quad (12.126)$$

where $\Delta\epsilon$ is a typical ph energy. If we furthermore assume that the admixtures of odd components is equally distributed over N occupied states, from (12.126) we get the condition for adiabaticity:

$$\mathcal{K} \approx \Delta\epsilon \cdot N \sum_m |\chi_{mi}|^2 \ll \Delta\epsilon \cdot N. \quad (12.127)$$

This means that the adiabatic approximation is good as long as the collective kinetic energy is small compared to a typical single-particle excitation energy times the number of single-particle states involved in the collective motion. We should note that it is not the quotient of collective energy to single-particle energy which should be small, but that an additional factor N comes into play which measures the collectivity.

This is the reason why we can also use the adiabatic assumption for high-lying collective states in the RPA. As long as there are many particles involved, the collective energy can be much higher than the single-particle excitations. On the other hand, we see that the adiabatic assumption does not work in situations in which only one particle is involved ($N=1$). At isolated level crossings, for instance, the kinetic energy can become of the same order of magnitude as $\Delta\epsilon$ and the adiabatic approximation breaks down. This feature is similar to that already encountered in the momentum expansion of the GCM theory. In cases where many level crossings occur, one should therefore use these methods with extreme care [St 77].

12.3.6 Applications of the ATDHF Method

12.3.6.1. Quadrupole Vibrations for a $Q \cdot Q$ -Force. An early version of the ATDHF theory was given in the pairing-plus-quadrupole model (see Sec. 7.4) of Baranger and Kumar for the description of transitional nuclei [BK 68, Ku 74a]. In this case, the theory becomes extremely simple because of the separability of the force. Since the model includes pairing correlations, Baranger and Kumar solved the adiabatic time-dependent Hartree-Fock-Bogoliubov problem. In this chapter we will restrict ourselves to the pure HF case and in the following, therefore, present a version which neglects pairing. We also consider only pure axially symmetric deformations ($Y = r^2 Y_{20}$) and neglect exchange terms as discussed in Section 7.4.

The matrix element \bar{v} in this case is given by

$$\bar{v}(1, 2) = -k Y(1) \cdot Y(2), \quad (12.128)$$

where k is a force constant.

We start according to Section 12.3.3 with a family of static densities $\rho_0(q)$ that are obtained, for instance, from the solution of the CHF problem

$$[h_0(\rho_0) - q Y, \rho_0] = 0. \quad (12.129)$$

$|m\rangle, |i\rangle$ will be a set of simultaneous eigenvectors of ρ_0 and of the pp and hh parts of h_0 . We furthermore find that Γ_1 of Eq. (12.74) vanishes.

$$\Gamma_1 = -k \cdot Y \cdot \text{Tr}(Y \rho_1) = 0 \quad (12.130)$$

because Y is time-even and ρ_1 is time-odd and the trace is real. This produces a tremendous simplification, because in this case the matrix B of Eq. (12.82) vanishes and A becomes diagonal.

From Eqs. (12.84), (12.100), and (12.101) we can calculate the time-odd part:

$$X_{\alpha i} = \hbar^2 \frac{\langle m | \dot{\rho}_0 | i \rangle}{\epsilon_m - \epsilon_i} = q \hbar^2 \frac{\langle m | \partial / \partial q | i \rangle}{\epsilon_m - \epsilon_i}. \quad (12.131)$$

The matrix elements of $\partial/\partial q$ are obtained from the perturbation theory of Eq. (12.129), which in this case is equivalent to a linear response approach:

$$\langle m | \partial / \partial q | i \rangle = \frac{\langle m | Y | i \rangle}{\epsilon_m - \epsilon_i}. \quad (12.132)$$

This, together with Eq. (12.103), gives the Inglis formula for the mass:

$$M(q) = 2\hbar^2 \sum_{mi} \frac{|\langle m | \partial / \partial q | i \rangle|^2}{\epsilon_m - \epsilon_i} = 2\hbar^2 \sum_m \frac{|\langle m | Y | i \rangle|^2}{(\epsilon_m - \epsilon_i)^3}. \quad (12.133)$$

From the collective Hamiltonian, therefore, we obtain:

$$\mathcal{K} = \frac{1}{2} M \dot{q}^2 + V(q), \quad (12.134)$$

where

$$V(q) = \text{Tr}(\epsilon_0 \rho_0(q)) - \frac{1}{2} k \text{Tr}(Y \rho_0(q)) \cdot \text{Tr}(Y \rho_0(q)). \quad (12.135)$$

Baranger and Kumar [BK 68] obtained the same collective Hamiltonian with minor differences. They took the pairing-plus-quadrupole model Hamiltonian and in this way derived a collective Hamiltonian depending on the five quadrupole deformation parameters $\alpha_{2\mu}$ and the pairing gap Δ . Since they are not interested in pairing vibrations, they restricted Δ to be the solution of the static BCS equations for each value of the five other coordinates.

After a transformation to intrinsic coordinates (as discussed in Sec. 1.5) they ended up with a classical Bohr Hamiltonian (1.47)

$$\mathcal{K} = \frac{1}{2} \left(\sum_i \mathfrak{g}_i \omega_i^2 + B_{\beta\beta} \dot{\beta}^2 + B_{\beta\gamma} \dot{\beta} \dot{\gamma} + B_{\gamma\gamma} \dot{\gamma}^2 \right) + V, \quad (12.136)$$

where the seven functions $\mathfrak{g}_1, \mathfrak{g}_2, \mathfrak{g}_3, B_{\beta\beta}, B_{\beta\gamma}, B_{\gamma\gamma}$, and V depend on the variables β and γ . They are calculated microscopically. The inertial parameters correspond to the Belyaev formula (3.93). This Hamiltonian has been requantized as discussed in Sec. 1.5. Energy levels and wave functions were then calculated numerically [BK 67b, 68].

In this method the coupling between rotations and vibrations and the mixing between different phonon states is fully taken into account. In this way Baranger and Kumar investigated the transition region around the osmium and the samarium isotopes [KB 68, Ku 74a] and found good agreement with experimental data. In particular, they obtained strong deviations from the rotational picture at the low- A end of the W-Os-Pt-transition region and large deviations from the phonon model at the upper end. Their collective wave functions are often smeared out over all possible shapes.

So far, only quadrupole shapes have been used. From Eqs. (12.120) and (12.132) we see that the constraint used in the next step of the procedure, as discussed in Section 12.3.4, would be

$$Q_{mi} = \frac{\hbar^2}{M} \frac{\langle m | Y | i \rangle}{(\epsilon_m - \epsilon_i)^2}. \quad (12.137)$$

Only in cases where the ph energies are almost degenerate, this corresponds to the original constraining operator Y .

12.3.6.2. Further Applications. The ATDHF theory has also been applied to *exactly soluble models* such as the Lipkin model of Sec. 6.2 [KG 74] and a three-level

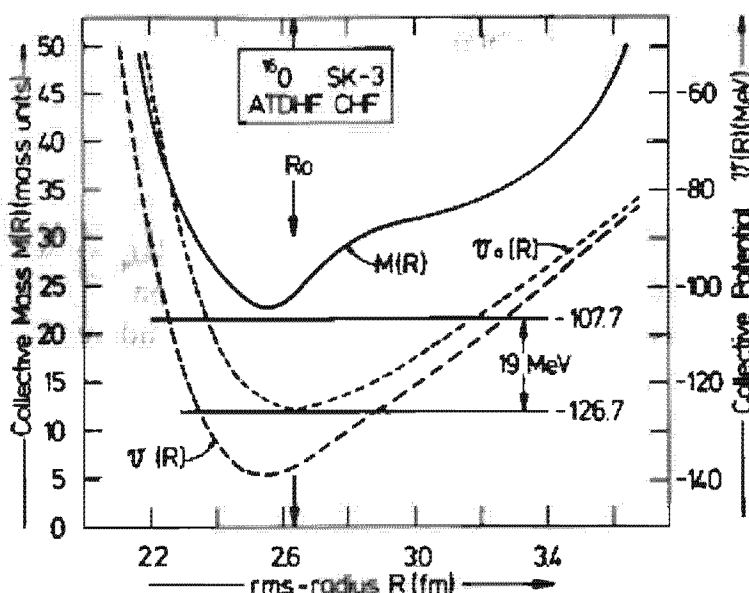


Figure 12.6. Potential energy surface and mass parameter of the isoscalar monopole mode in ^{16}O within ATDHF theory. (From [Go 77].)

Lipkin model [MV 78], which was introduced in [YKD 70]. In general, for cases of large particle numbers—that is, collective situations—the agreement with the exact result is very good.

More realistic calculations have been carried out with the Skyrme force [EBG 75, Va 75, Go 77]. In this case, it is convenient to formulate the ATDHF theory in coordinate space. Since time reversal symmetry is broken in the time-dependent theories, in addition to the densities ρ, τ and J of Eqs. (5.84f.) we need further densities and currents. In this form the theory has been applied to isoscalar monopole vibrations in ^{16}O and ^{40}Ca using the mass rms radius R as collective coordinate. Figure 12.6 shows the collective mass $M(R)$, the collective potential $v_0(R) = V(R)$, the CHF energy, and the potential $v(R)$, which is obtained by subtracting the zero-point corrections ϵ_0 of Eq. (10.136). The positions of collective eigenstates are indicated.

Giannoni et al. [GMQ 76, GQ 80] have calculated mass parameters for the isoscalar quadrupole modes in light nuclei. They find that the ATDHF mass (12.110) is very close to the simple cranking mass [see Eq. (12.146)] for Skyrme forces with an effective mass $m^*/m \approx 1$. In fact, it can be shown that the term Γ_1 in Eq. (12.75a), which produces the difference between the ATDHF mass (Thouless-Valatin mass), and the cranking mass (Inglis formula) is proportional to $1 - m^*/m$.

12.3.7 Adiabatic Perturbation Theory and the Cranking Formula

The oldest method of deriving the inertia parameters for a collective motion microscopically is the so-called *cranking formula*. It was introduced by Inglis [In 54, 56] in the case of rotations, and we have discussed it in great detail in Section 5.4. Kerman [Ke 61] has derived a similar expression for the mass parameters of more general collective motions. We have seen

in Section 12.3.2 that we obtain this formula again if we neglect the time-odd part Γ_1 of the self-consistent potential (12.74) in the kinetic energy (12.81).

This formula has been used very often in the past. We therefore want to give here the usual derivation in the context of adiabatic perturbation theory (see, for instance, [Sch 68, Di 71]). In particular, we will discuss the validity of the basic assumption of this approximation.

We consider a system of particles in a time dependent, but time even, Hamiltonian $H(t)$. The time dependence is determined by one (or several) collective shape parameter(s) $q(t)$. An example would be a single-particle Nilsson Hamiltonian (eventually with a residual two-body interaction) depending on a deformation parameter q , which in turn is a given function of t . In principle, we should determine self-consistently both the shape of the potential and the dynamical behavior of the system, namely the function $q(t)$. This is not done, however, and we will not need the explicit form of this time dependence for the derivation of a collective Hamiltonian. We will only assume that the motion is slow.

At each time t , that is, for each deformation q , we assume the eigenstates $|k\rangle$ of the Hamiltonian, the so-called *adiabatic basis* [No 77]:

$$H|k\rangle = E_k|k\rangle. \quad (12.138)$$

The eigenfunctions $|k\rangle$, as well as the energies, depend on the parameter q and therefore on the time t .

The exact solution $|\Psi(t)\rangle$ of the Schrödinger equation

$$H(t)|\Psi(t)\rangle = i\hbar \frac{\partial}{\partial t} |\Psi(t)\rangle \quad (12.139)$$

is now expanded in this basis:

$$|\Psi(t)\rangle = \sum_k a_k(t) e^{i\varphi_k(t)} |k(t)\rangle. \quad (12.140)$$

For convenience we use time-dependent phase factors

$$\varphi_k(t) = -\frac{1}{\hbar} \int' E_k(t') dt' \quad (12.141)$$

in this expansion, which essentially takes care of the trivial oscillating phase of the adiabatic states $|k\rangle$. Inserting the ansatz (12.140) in the Schrödinger equation (12.139) and multiplying with the vectors $\langle l|$ we obtain a coupled set of differential equations for the coefficients a_k ,

$$\begin{aligned} \dot{a}_l &= - \sum_k \langle l | \frac{\partial}{\partial t} |k\rangle e^{i\varphi_k} a_k \\ &= -\dot{q} \sum_k \langle l | \frac{\partial}{\partial q} |k\rangle e^{i\varphi_k} a_k, \end{aligned} \quad (12.142)$$

with $\varphi_{kl} = \varphi_k - \varphi_l$.

This equation is still exact. It is now investigated in the *adiabatic limit*, that is, for small velocities \dot{q} . We assume that the system for $t=0$ in the state $|0\rangle$ (for instance a Slater determinant, where all the levels below the

fermi surface are filled) is:

$$a_k(t=0) = \delta_{k0}. \quad (12.143)$$

Since the time derivative of a_k is proportional to \dot{q} , we expect for all times $a_k(t)$ to be small for $k \neq 0$ and a_0 to be close to unity, that is, the system always stays close to the adiabatic ground state. There are only virtual excitations to higher states, which are proportional to the velocity and produce an inertia.

In this approximation, for $I \neq 0$ we obtain

$$\dot{a}_I = -\dot{q} \langle I | \frac{\partial}{\partial q} | 0 \rangle e^{i\varphi_{0I}}. \quad (12.144)$$

Under the *additional assumption* that \dot{q} and the matrix element $\langle I | \partial/\partial q | 0 \rangle$ have only a relatively small time dependence compared to the oscillation phases φ_{0I} , we can integrate (12.144) and for $I \neq 0$ obtain

$$a_I = \frac{i\hbar\dot{q}}{(E_I - E_0)} \langle I | \frac{\partial}{\partial q} | 0 \rangle e^{i\varphi_{0I}}. \quad (12.145)$$

We have thus calculated the velocity-dependent terms in the wave function (12.140) in first-order perturbation theory and are now able to express the total energy as a function of the "collective coordinate" q and the corresponding velocity \dot{q}

$$\begin{aligned} E(q, \dot{q}) &= \langle \Psi(t) | H | \Psi(t) \rangle = E_0 + \sum_{k \neq 0} (E_k - E_0) |a_k|^2 \\ &= \frac{1}{2} M(q) \dot{q}^2 + V(q), \end{aligned} \quad (12.146)$$

with the potential energy

$$V(q) = E_0(q) = \langle 0 | H | 0 \rangle_q$$

and the inertia parameter, the well known *cranking formula*,

$$M(q) = 2\hbar^2 \sum_{k \neq 0} \frac{|\langle k | \partial/\partial q | 0 \rangle|^2}{E_k - E_0}. \quad (12.147)$$

Using the fact that the many-body functions $|k\rangle$ are eigenfunctions of the Hamiltonian $H(q)$, we can write this formula in a slightly different way:

$$M(q) = 2\hbar^2 \sum_{k \neq 0} \frac{|\langle k | [H, (\partial/\partial q)] | 0 \rangle|^2}{(E_k - E_0)^3} = 2\hbar^2 \sum_{k \neq 0} \frac{|\langle k | \partial H / \partial q | 0 \rangle|^2}{(E_k - E_0)^3}. \quad (12.148)$$

For a simple Nilsson Hamiltonian $H = H_0 - q \cdot Q$ we thus obtain

$$M(q) = 2\hbar^2 \sum_{k \neq 0} \frac{|\langle k | Q | 0 \rangle|^2}{(E_k - E_0)^3}. \quad (12.149)$$

In this form, the cranking formula has been widely used in the literature, mainly in connection with Nilsson-Strutinsky-type calculations (see Sec. 2.9) of the energy surfaces for the fission process [SSW 69, Pa 75b, Po 76, RLM 76, Ba 78, Po 78].

In the derivation of this formula we made the assumption that the matrix elements $\langle k|\partial/\partial q|0\rangle$ change very slowly in time. This is certainly not true in the region of *level crossings* [St 77] or pseudo-crossings, as in Fig. 2.22. In Section 2.8.4 we discussed the fact that in such regions the characteristic properties of the wave functions are exchanged. If this exchange takes place in a small q -region, we expect large values for the matrix elements $\langle k|\partial/\partial q|0\rangle$ and the derivation of the cranking formula may no longer be justified.

In fact, it can happen that the system does not stay in its adiabatic ground state when it moves over such a crossing. This can be most easily investigated at an *isolated crossing* of two levels ϵ_1 and ϵ_2 with an interaction matrix element V_{12} (the distance of closest approach between the levels is then $2V_{12}$). In this case, Eq. (12.142) reduces to a system of two coupled differential equations. For a constant velocity \dot{q} and a linear dependence of the levels $\epsilon_{1,2}$ on q , this can be solved analytically. For the probability $P = |a_2(\infty)|^2$, that the system jumps at the pseudo-crossing into the upper level, we obtain the *Landau-Zener formula* [La 32, Ze 32],

$$P = \exp\left(-\frac{2\pi V_{12}^2}{\hbar|\dot{q}||(d/dq)(\epsilon_1 - \epsilon_2)|}\right). \quad (12.150)$$

This probability becomes large for increasing velocities, but also for an increasing difference in the slope of the two levels, because in such cases the interaction region where the properties of the two levels are exchanged is rather short. In the formula (12.150), which is an exact formula for this model, we recognize that the function P shows a nonanalytic behavior for small velocities \dot{q} [Sch 77a]. A solution of Eq. (12.142) by an expansion in \dot{q} , which gives the cranking formula (12.147) in lowest order, therefore probably corresponds to an asymptotic expansion.

Up to now it is a somewhat open question as to in which situations the adiabatic assumption is justified. Numerical calculations for a fixed path starting at the saddle point of the fission process have shown that a very large part of the wave function is excited due to pseudo-level crossings [SW 75a+b, LPP 75, LPF 77, SW 78]. It could be, however, that in a self-consistent calculation as discussed in Section 12.3.4 this picture is changed very much. The conclusion will certainly depend on the excitation energy of the system.

CHAPTER 13

Semiclassical Methods in Nuclear Physics

13.1 Introduction

The many methods and formalisms used to deal with the nuclear many-body problem are, as we have seen, powerful, and allow us to explain an enormous number of experimental facts. In actual numerical calculations, where we want to treat realistic situations, the implementation of formalisms such as Hartree–Fock, RPA, or time-dependent Hartree–Fock lead to an enormous amount of work. It is therefore desirable to have qualitatively correct but quick estimates of such quantities as the nuclear ground state energy, density, and giant resonance frequencies.

A method which is able to provide such estimates is very well known from atomic physics, where the self-consistent Thomas–Fermi theory yields surprisingly good results [Go 48]. For a long time in nuclear physics, Thomas–Fermi theory [SB 63, Be 71, MS 69] was not exploited very much because, as we will see, it is not very well suited to handle many-body systems with very short-ranged two body forces in its primitive form. However, recently there have been some further developments of the Thomas–Fermi theory [Ki 67, BR 71b, Gr 72, BB 72, 74, BZ 73, BJC 76, BCK 76, GS 77, CJB 77, DBS 78] which make its application to nuclear physics possible, and it has become known as extended Thomas–Fermi (ETF) theory. It turns out that the corresponding semiclassical expressions represent the different quantities on the average, that is, quantum fluctuations have been averaged out. There exists, therefore, a close analogy to the Strutinsky smoothing. It is well known that if one applies a Strutinsky

smoothing to modern Hartree-Fock calculations [BQ 75a, b], the corresponding liquid drop part agrees very well with the empirical Bethe-Weizsäcker mass formula. It is the intention of the semiclassical theory explained in this chapter to set up a self-consistent procedure for the averaged quantities (density, etc.), which allows us to calculate the liquid drop part contained in Hartree-Fock calculations *without* having to know the full quantum mechanical solution.

Once a semiclassical method is established for static quantities, it is natural to generalize it to the dynamic case [WMW 75, HE 78 and references therein]. In the limit $\hbar \rightarrow 0$, the TDHF equation goes over into the collisionless Boltzmann equation. Using an appropriate generalization for the dynamic case of the semiclassical expansion of the density and kinetic energy density, we arrive at a fluid dynamic description of the giant resonances which is equivalent to the sum rule results we presented in Section 8.7. In this respect, it will be important to note that the giant resonances can be described by a fluid dynamical description of zero sound rather than by that of ordinary sound [KB 62, No 64a, Th 61b]. However, the fluid dynamic description of arbitrary nuclear collective motion is at present still the subject of intensive studies.

Naturally, many features of this chapter are related to the liquid drop picture of the nucleus (Chap. 1).

13.2 The Static Case

13.2.1 The Thomas-Fermi Theory

The Thomas-Fermi theory [Th 27, Fe 28], together with its extensions, is the semiclassical treatment of nuclear physics in its independent particle or Hartree-Fock approximation. We must therefore consider a single-particle Hamiltonian

$$H = -\frac{\hbar^2}{2m} \Delta + V, \quad H\varphi_n = \epsilon_n \varphi_n, \quad (13.1)$$

in which the potential V is, in principle, the self-consistent Hartree-Fock potential (5.34). In what follows, however, we shall often assume for the purpose of demonstration that the particles are simply moving independently in a given potential well, like, for example, the Woods-Saxon potential.

Before we go ahead, it is useful to give the definitions of quantities whose semiclassical development we want to study:

- (i) The single-particle *propagator*

$$C' = e^{-iHt/\hbar}, \quad (13.2)$$

which is the solution of the time-dependent Schrödinger equation,

$$\int d^3r'' \left[i\hbar \frac{\partial}{\partial t} \delta(\mathbf{r} - \mathbf{r}'') - H(\mathbf{r}, \mathbf{r}'') \right] C'(\mathbf{r}'', \mathbf{r}') = 0 \quad (13.3)$$

with the initial condition

$$C'^{=0}(\mathbf{r}, \mathbf{r}') = \delta(\mathbf{r} - \mathbf{r}'). \quad (13.4)$$

With (13.1) the propagator can also be written in the form,*

$$C^\beta(\mathbf{r}, \mathbf{r}') = \sum_n \varphi_n(\mathbf{r}) \varphi_n^*(\mathbf{r}') e^{-\beta \epsilon_n}, \quad (13.5)$$

where for convenience we set $\beta = it/\hbar$.†

- (ii) The trace of the propagator (*partition function*†; the factor of two takes here and henceforth care of the spin):

$$Z(\beta) = \text{Tr } C^\beta = 2 \int d^3r C^\beta(\mathbf{r}, \mathbf{r}). \quad (13.6)$$

- (iii) The *spectral density* matrix

$$g^\epsilon(\mathbf{r}, \mathbf{r}') = \langle \mathbf{r} | \delta(\epsilon - H) | \mathbf{r}' \rangle = \sum_n \varphi_n(\mathbf{r}) \varphi_n^*(\mathbf{r}') \delta(\epsilon - \epsilon_n), \quad (13.7)$$

in terms of which the propagator (13.2) is given by its Laplace transform

$$C^\beta(\mathbf{r}, \mathbf{r}') = \int_0^\infty d\epsilon e^{-\beta \epsilon} g^\epsilon(\mathbf{r}, \mathbf{r}') \equiv \mathcal{L}_{\epsilon \rightarrow \beta}[g^\epsilon(\mathbf{r}, \mathbf{r}')], \quad (13.8)$$

where we have assumed that the energy origin is at the bottom of the well. The spectral density matrix is therefore given as the inverse Laplace transform of the propagator (for properties of the Laplace transforms, see [PB 55, AS 65]):

$$\begin{aligned} g^\epsilon(\mathbf{r}, \mathbf{r}') &= 2 \mathcal{L}_{\beta \rightarrow \epsilon}^{-1}[C^\beta(\mathbf{r}, \mathbf{r}')] \\ &= \frac{2}{2\pi i} \int_{c-i\infty}^{c+i\infty} d\beta e^{\beta \epsilon} C^\beta(\mathbf{r}, \mathbf{r}') \quad (c > 0). \end{aligned} \quad (13.9)$$

- (iv) The *density of states*

$$g(\epsilon) = \text{Tr } \delta(\epsilon - H) = \mathcal{L}_{\beta \rightarrow \epsilon}^{-1} Z(\beta). \quad (13.10)$$

- (v) The *density matrix*

$$\rho(\mathbf{r}, \mathbf{r}'; \lambda) = \sum_{n=1}^{\infty} \varphi_n(\mathbf{r}) \varphi_n^*(\mathbf{r}') \Theta(\lambda - \epsilon_n) = 2 \cdot \mathcal{L}_{\beta \rightarrow \lambda}^{-1} \frac{C^\beta(\mathbf{r}, \mathbf{r}')}{\beta}, \quad (13.11)$$

* In principle, we also should have spin indices s, s' . For simplicity, we treat here only spin saturated systems (cf. Sec. 5.6.2) and will take into account the spin only by a statistical factor of two.

† The choice of β reminds one of an inverse temperature, and indeed if we had $\beta = 1/k_B T$, where k_B is Boltzmann's constant and T the temperature, (13.6) would represent the partition function of statistical mechanics. However, we have to stress the point that here we always deal with a system at $T = 0$.

where Θ is the unit step function, λ is the Fermi energy, and we have used a simple property of Laplace transforms (see [AS 65, Chap. 29]). The *density* is simply the local part of the density matrix (we will see in the following that one of the main purposes of the semiclassical approximation will be to express essential physical quantities by functionals of this local part):

$$\rho(\mathbf{r}) = \rho(\mathbf{r}, \mathbf{r}). \quad (13.12)$$

(vi) The *kinetic energy density* (5.85)

$$\tau(\mathbf{r}) = \sum_{i=1}^3 \left[\frac{\partial^2}{\partial x_i \partial x'_i} \rho(\mathbf{r}, \mathbf{r}') \right]_{\mathbf{r}'=\mathbf{r}}. \quad (13.13)$$

(vii) The *particle number*

$$N = \int_0^\lambda d\epsilon g(\epsilon) = E_{\beta \rightarrow \lambda}^{-1} \left[\frac{Z(\beta)}{\beta} \right]. \quad (13.14)$$

(viii) The *ground state energy*

$$\begin{aligned} E &= \sum_{n=1}^A \epsilon_n = \int_0^\lambda d\epsilon \epsilon g(\epsilon) = \mu N - \int_0^\lambda d\epsilon \int_0^\epsilon d\epsilon' g(\epsilon') \\ &= \lambda N - E_{\beta \rightarrow \lambda}^{-1} \left[\frac{Z(\beta)}{\beta^2} \right]. \end{aligned} \quad (13.15)$$

In Eq. (13.15) we have again assumed that the particles are in a given potential; in the HF case the ground state energy has to be modified somewhat, as shown in Eq. (5.40).

The *Thomas–Fermi theory* (see, e.g., [Th 61b]) can be explained from quite different points of view. Here we introduce it more or less in the usual way, that is the particles at each point in space feel the potential as if it were locally equal to a constant. We will see that this is also a short time (or a high-temperature; cf. footnote page 529) argument [Gr 72]. In order to actually derive the Thomas–Fermi approximation we shall immediately place our consideration in a somewhat broader context. This will permit us later to go beyond the Thomas–Fermi approximation in a natural way.

To this purpose we develop the potential $V(\mathbf{r})$ entering (13.1) around an arbitrary point \mathbf{r}_0 in a Taylor series:

$$\begin{aligned} V(\mathbf{r}) &= V(\mathbf{r}_0) + \sum_{i=1}^3 \left. \frac{\partial V}{\partial x_i} \right|_{\mathbf{r}=\mathbf{r}_0} (x_i - x_{0i}) \\ &\quad + \frac{1}{2} \sum_{i,j=1}^3 \left. \frac{\partial^2 V}{\partial x_i \partial x_j} \right|_{\mathbf{r}=\mathbf{r}_0} (x_i - x_{0i})(x_j - x_{0j}) + \dots \end{aligned} \quad (13.16)$$

If this development is convergent, the solution of (13.3) with (13.1) and (13.16) will give the exact propagator independent of \mathbf{r}_0 . If we break the development (13.16) off at the n th step the corresponding propagator will

depend on the point r_0 around which we develop the potential, and the corresponding solution

$$C_{r_0}^{(n)}(\mathbf{r}, \mathbf{r}')$$

will only be good for values of \mathbf{r}, \mathbf{r}' close to \mathbf{r}_0 . The best choice will therefore be to take the limit $\mathbf{r}, \mathbf{r}' \rightarrow \mathbf{r}_0$. Since the point \mathbf{r}_0 is arbitrary we will get a propagator $C_{r_0}^{(n)}(\mathbf{r}_0, \mathbf{r}_0)$ which is valid everywhere, that is, we can now identify \mathbf{r}_0 with our original variable \mathbf{r} . This procedure only gives us the local part of the propagator; if we want to keep the nonlocal structure of the propagator, the best we can do is not to let \mathbf{r} and \mathbf{r}' individually go to \mathbf{r}_0 but to suppose that we developed the potential locally around the center of mass of \mathbf{r} and \mathbf{r}' ; that is, we define the appropriate solution of (13.3) with (13.16) to be [DBS 78]

$$C^{(n)}(\mathbf{r}, \mathbf{r}') = \lim_{r_0 \rightarrow \frac{1}{2}(\mathbf{r}+\mathbf{r}')} C_{r_0}^{(n)}(\mathbf{r}, \mathbf{r}'). \quad (13.17)$$

For $n \rightarrow \infty$, (13.17) will eventually converge to the exact result if (13.16) is convergent. For n finite, we get a hierarchy of approximations:

$$C^{(0)}, C^{(1)}, C^{(2)}, \dots,$$

which are given in terms of the potential and its n first derivatives.

As we said at the beginning of this section, the Thomas-Fermi approximation consists in considering the potential locally as a constant. This obviously corresponds to a break-off in the expansion (13.16) at the lowest order:

$$\left\{ \frac{\partial}{\partial \beta} - \frac{\hbar^2}{2m} \Delta_r + V(r_0) \right\} C_{r_0}^{(0)}(\mathbf{r}, \mathbf{r}') = 0. \quad (13.18)$$

It can be easily verified that the solution of (13.18) is given by

$$C_{r_0}^{(0)}(\mathbf{r}, \mathbf{r}') = \left(\frac{m}{2\pi\hbar^2} \right)^{3/2} \frac{1}{\beta^{3/2}} e^{-(m/2\pi^2\hbar^2)(\mathbf{r}-\mathbf{r}')^2/\beta} e^{-\beta V(r_0)}, \quad (13.19)$$

which has the right boundary condition (13.4). With (13.19) and (13.11) we obtain the Thomas-Fermi approximation for the density matrix [AS 65, Chap. 29]:

$$\rho^{(0)}(\mathbf{r}, \mathbf{r}') \equiv \rho^{TF}(\mathbf{r}, \mathbf{r}') = \rho^{TF}(\mathbf{q}) \frac{3}{k_F(\mathbf{q})s} j_1(k_F(\mathbf{q})s) \quad (13.20)$$

with

$$\mathbf{q} = \frac{1}{2}(\mathbf{r} + \mathbf{r}'), \quad s = \mathbf{r} - \mathbf{r}', \quad (13.21)$$

and j_1 a spherical Bessel function. The local limit of the TF density matrix is given by

$$\rho^{TF}(\mathbf{r}) = \frac{1}{3\pi^2} k_F^3(\mathbf{r}) \Theta(\lambda - V(\mathbf{r})), \quad (13.22)$$

and the local momentum is defined by:

$$k_F(r) = \left[\frac{2m}{\hbar^2} (\lambda - V(r)) \right]^{1/2}. \quad (13.23)$$

It has to be emphasized that the Fermi energy λ is fixed by the condition

$$N = \int d^3r \rho^{TF}(r) \quad (13.24)$$

and that the approximate density matrix (13.20) has lost some features inherent to the exact one like $\rho^2 = \rho$:

$$\int d^3r_1 \rho^{TF}(r, r_1) \rho^{TF}(r_1, r') \neq \rho^{TF}(r, r') \quad (13.25)$$

and as a consequence ($|D\rangle$ being a Slater determinant and using Wick's theorem but not $\rho^2 = \rho$):

$$\langle D | \hat{N} | D \rangle_{TF}^2 - \langle D | \hat{N}^2 | D \rangle_{TF} = (\text{Tr}(\rho^{TF}))^2 - \text{Tr}((\rho^{TF})^2) \neq 0. \quad (13.26)$$

Thus whenever we make a variational calculation with semiclassical densities (see below) we have to fix the number of particles, as in BCS theory (Chap. 6), by adding condition (13.24) with a Lagrange multiplier.

In order to compare the Thomas-Fermi density with an exact density, in Fig. 13.1 we show a graphical representation of both densities for a Woods-Saxon potential. We see that in the interior of the nucleus the density is well represented on the "average" but in the surface region it drops off too rapidly, going to zero with zero slope at the "classical turning

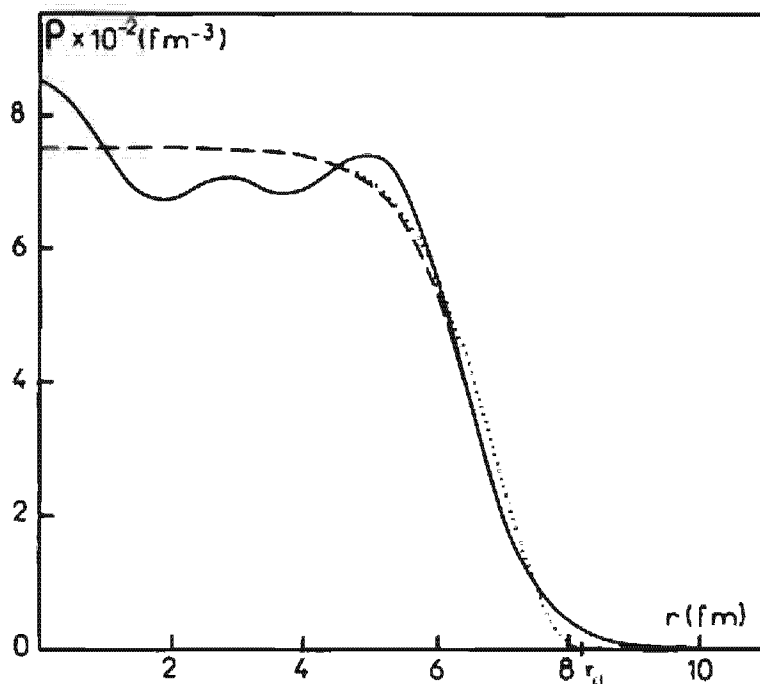


Figure 13.1. Thomas-Fermi approximation (dotted line) to the exact density (full line) in a Woods-Saxon potential for $A = 2N = 184$ particles. The parameters of the well are: $V_0 = -44$ MeV, $a = 0.67$ fm, and $R_0 = 1.27$ fm $A^{1/3}$. The broken line represents the local harmonic approximation of Section 13.2.3. (From [DBS 78].)

"point" r_{cl} given by

$$\lambda - V(r_{\text{cl}}) = 0. \quad (13.27)$$

Generally speaking, however, the exact single-particle density is surprisingly well represented by such a simple formula like (13.22). This is even more drastically demonstrated if we calculate the ground state energy in Thomas-Fermi approximation using (13.15) with (13.19) and (13.6). Taking the same parameters as those of Fig. 13.1, we obtain from a numerical integration:

$$E_0^{\text{TF}} = -3785.8 \text{ MeV}; \quad E_0^{\text{exact}} = -3696.2 \text{ MeV}.$$

The total energy calculated in Thomas-Fermi approximation is only off by $\approx 3\%$ for heavy nuclei. This means that globally, that is, over the whole space integrated quantities, the Thomas-Fermi approximation is even better than could have been guessed by simply looking at Fig. 13.1.

A comparison of Eqs. (13.11) and (13.9) yields the relation

$$g(\epsilon)(r, r') = \frac{\partial}{\partial \epsilon} \rho(r, r'; \epsilon), \quad (13.28)$$

and consequently we obtain for the density of states in Thomas-Fermi approximation:

$$g^{\text{TF}}(\epsilon) = \frac{1}{2\pi^2} \left(\frac{2m}{\hbar^2} \right)^{3/2} \int d^3r (\epsilon - V(r))^{1/2} \Theta(\epsilon - V). \quad (13.29)$$

For the harmonic oscillator potential $V = \frac{1}{2}m\omega^2 r^2$, which we will use quite often for demonstration in the following, the integral (13.29) can be evaluated analytically, and we obtain:

$$g_{\text{ho}}^{\text{TF}}(\epsilon) = \frac{\epsilon^2}{(\hbar\omega)^3}. \quad (13.30)$$

In Fig. 13.2 we compare the integral of this expression, which represents the number of particles with the exact $N(\lambda)$.

We see that again the Thomas-Fermi functions represent roughly the exact ones on the average*; below we will give a more precise discussion on how the average of quantities such as $g(\epsilon)$ shall be defined.

In order to calculate the kinetic energy density (13.13) in Thomas-Fermi approximation we use (13.19) and (13.11) to obtain:

$$\tau^{\text{TF}}(r, \lambda) = \frac{3}{5} \frac{1}{3\pi^2} \left(\frac{2m}{\hbar^2} \right)^{5/2} (\lambda - V)^{5/2} \Theta(\lambda - V) = \frac{1}{5\pi^2} k_F^5 \Theta(\lambda - V). \quad (13.31)$$

Elimination of $\lambda - V$ in (13.31) and (13.22) gives the following relation

* From the observation that $g^{\text{TF}}(\epsilon)$ represents the exact density of states in the mean, we can immediately get the usual WKB quantization rule [Ar 65] without using the rather complicated "matching conditions." We do not want to go into more detail of how WKB and TF theory are connected [Vo 77].

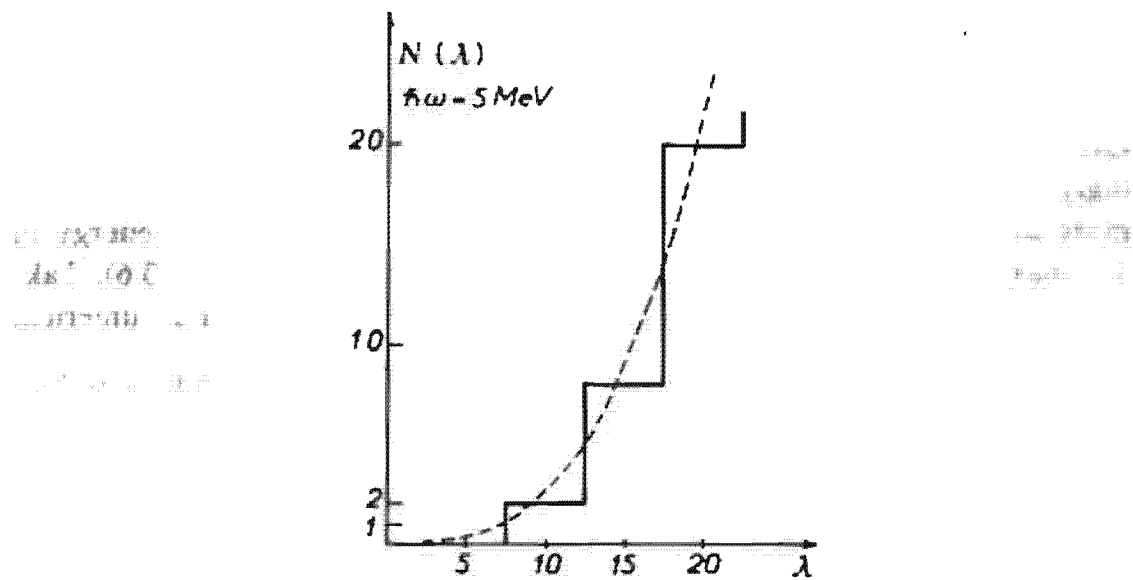


Figure 13.2. Comparison of the exact number of particles as a function of the Fermi energy with the corresponding Thomas-Fermi approximation for the harmonic oscillator.

between the kinetic energy density and the density. [The corresponding relation (5.92) takes into account the isospin.]

$$\tau^{\text{TF}} = \frac{1}{5\pi^2} (3\pi^2 \rho^{\text{TF}})^{5/3}. \quad (13.32)$$

The pure Thomas-Fermi approximation is of little use for the self-consistency problem in nuclear physics because of the short-range two-nucleon interaction, as we stated in the introduction. This can be seen from the fact that for the local part of the Skyrme mean field potential $V[\rho] = a\rho + b\rho^2$ [see Eq. (5.99)], to which the nonlocal parts give only minor changes (a consequence of the short range of the two-body force), the solution for ρ of Eq. (13.22) gives no spatial dependence of ρ whatsoever. For that to happen we will have to extend the pure Thomas-Fermi theory, as will be discussed in the following subsections.

13.2.2 Wigner-Kirkwood \hbar Expansion

13.2.2.1 The Formalism. We now want to show how the Thomas-Fermi results of Section 13.2.1 turn out to be the lowest-order contribution to different quantities, for instance, the single-particle propagator (13.2), in a systematic expansion in powers of \hbar . For this purpose it is convenient to go over to the so-called *Wigner transform*. The Wigner transform of a single-particle operator A is defined by [Ar 65]

$$A_w \equiv A(\mathbf{q}, \mathbf{p}) = \int d^3s e^{-is\mathbf{p}/\hbar} \langle \mathbf{q} + \mathbf{s}/2 | A | \mathbf{q} - \mathbf{s}/2 \rangle, \quad (13.33)$$

with \mathbf{q} and \mathbf{s} given by (13.21). The reason why the Wigner representation is

convenient is due to the fact that, for example, the Hamiltonian (13.1) is equal to its classical counterpart in this representation:

$$H(\mathbf{q}, \mathbf{p}) = \frac{\mathbf{p}^2}{2m} + V(\mathbf{q}). \quad (13.34)$$

In order to find the completely classical part of the propagator (13.2) we first develop its Wigner transform in powers of β :

$$C^\beta(\mathbf{q}, \mathbf{p}) = \left(\sum_{n=0}^{\infty} \frac{1}{n!} (-\beta H)^n \right)_w. \quad (13.35)$$

This means that we have to find the Wigner transform of products of single-particle operators. In Appendix D we derive the following formula:

$$(AB)_w = A(\mathbf{q}, \mathbf{p}) e^{(i\hbar/2)\tilde{\Lambda}} B(\mathbf{q}, \mathbf{p}) \quad (13.36)$$

with (the arrows shall indicate in which direction the gradients act):

$$\tilde{\Lambda} = \vec{\nabla}_{\mathbf{q}} \vec{\nabla}_{\mathbf{p}} - \vec{\nabla}_{\mathbf{p}} \vec{\nabla}_{\mathbf{q}}. \quad (13.37)$$

The very useful Eq. (13.36) allows us to easily verify, for example, the well-known result that the classical counterpart of a commutator is proportional to the classical Poisson bracket [Go 59]. With (13.36) we can also calculate successively the terms appearing in the development (13.35). To second order we have, for example:

$$(H^2)_w = H^2(\mathbf{q}, \mathbf{p}) - \frac{1}{4} \frac{\hbar^2}{2m} \Delta V. \quad (13.38)$$

The \hbar^2 correction in (13.38) comes from the fact that the momentum operator does not commute with the potential. It is this \hbar dependence of the single-particle propagator (13.2) which comes from the non-commutativity of the kinetic and potential energy parts of the Hamiltonian in which we are interested and which we intend to expand into a power series in \hbar ; thus we do not have to worry about the hidden \hbar^{-1} dependence in β (or some other \hbar dependences which may arise in passing from the Wigner to some other representation). It is clear from what we have said that the \hbar expansion we are talking about is perfectly manageable with the expansion (13.35) and the product rule (13.36); the powers of \hbar will always be even and equal to the sum of all derivatives in a specific term. The \hbar expansion is therefore simultaneously a *gradient expansion*. The expression to lowest order in \hbar is easily calculated from (13.35), (13.36), and (13.38) to give

$$C^{(0)}(\mathbf{q}, \mathbf{p}) = e^{-\beta H(\mathbf{q}, \mathbf{p})}. \quad (13.39)$$

Calculating the inverse Wigner transform, that is, taking the Fourier transform with respect to \mathbf{p} of (13.39), we find that it is the same as the Thomas-Fermi approximation of the propagator (13.19). It is in this sense that we say that the Thomas-Fermi results of Section 13.2.1 are the expression to lowest order in \hbar . At this point it is perhaps useful to reinterpret β as an inverse *temperature* (see footnote page 529) and (13.39)

as the classical statistical operator. Since (13.35) is a simultaneous expansion in \hbar^2 and β it is natural that we find for high temperatures—that is, small β —the classical result. It must be emphasized again that in our context β will never play the role of an inverse temperature; on the contrary, we are dealing with a Fermi system at $T=0$. On the other hand, it is important to note that the Thomas–Fermi approximation as well as its extensions, which we will derive in this section, respect the Pauli principle. This can most easily be seen in calculating the density (13.22) from its Wigner transform using (13.39) and (13.11):

$$\rho^{TF}(\mathbf{q}) = \frac{2}{(2\pi\hbar)^3} \int d^3p f^{TF}(\mathbf{q}, \mathbf{p}) = 2 \int \frac{d^3p}{(2\pi\hbar)^3} \Theta\left(\lambda - \frac{p^2}{2m} - V(\mathbf{q})\right), \quad (13.40)$$

$$f^{TF}(\mathbf{q}, \mathbf{p}) = (\rho^{TF})_w, \quad (13.41)$$

which is nothing but the sum over all quantum numbers (effective momenta) $p \leq (2m(\lambda - V))^{1/2}$ from zero up to the Fermi level, each level being occupied twice (spin up, spin down).

The powers of β in (13.35) do not go along with the powers of \hbar and in order to be correct up to \hbar^2 we have to develop (13.35) up to β^3 . The result is [Wi 32, 34; Ki 33; Ki 57, JB 75]:

$$C^\beta(\mathbf{q}, \mathbf{p}) = \exp(-\beta(p^2/2m + V(\mathbf{q}))) \left\{ 1 + \frac{\hbar^2 \beta^2}{8m} \left[-\nabla^2 V + \frac{\beta}{3} (\nabla V)^2 \right. \right. \\ \left. \left. + \frac{\beta}{3m} (\mathbf{p} \cdot \nabla)^2 V \right] + O(\hbar^4) + \dots \right\}. \quad (13.42)$$

Expression (13.42) allows us to get semiclassical corrections to all the quantities we considered in Section 13.2.1. With (13.11), we obtain, for example, for the Wigner transform f of the semiclassical density matrix (for a generalization to include a spin orbit term, see [JBB 75]):

$$f_{sc}(\mathbf{q}, \mathbf{p}; \lambda) = \Theta\left(\lambda_{sc} - \frac{p^2}{2m} - V\right) + \frac{\hbar^2}{8m} \left\{ -\nabla^2 V \delta' \left(\lambda_{sc} - \frac{p^2}{2m} - V(\mathbf{q}) \right) \right. \\ \left. - \left[\frac{(\nabla V)^2}{3} + \frac{(\mathbf{p} \cdot \nabla)^2 V}{3m} \right] \delta'' \left(\lambda_{sc} - \frac{p^2}{2m} - V \right) \right\} + O(\hbar^4), \quad (13.43)$$

where λ_{sc} is determined by (13.14) or (13.24). In (13.43) we ignored the fact that the Laplace inversion of positive powers of β does not exist in the strict sense. In formally creating the different powers of β in (13.42) by differentiation of (13.11) with respect to λ , we obtain the derivatives of the δ function in (13.43). Expression (13.43) can clearly only be used in the sense of a distribution, but we have to study in greater detail in which way the semiclassical expansion (13.42) of the propagator can be useful. From

(13.43) we obtain for the density integrating over \mathbf{p} :

$$\rho_{sc}(\mathbf{r}) = \left[\frac{1}{3\pi^2} \left(\frac{2m}{\hbar^2} \right)^{3/2} (\lambda_{sc} - V(\mathbf{r}))^{3/2} \right. \\ \left. - \frac{1}{24\pi^2} \left(\frac{2m}{\hbar^2} \right)^{1/2} \left[\frac{(\nabla V)^2}{4(\lambda_{sc} - V)^{3/2}} + \frac{\Delta V}{(\lambda_{sc} - V)^{1/2}} \right] + \dots \right] \Theta(\lambda_{sc} - V). \quad (13.44)$$

The semiclassical density does not contain any δ functions, but diverges at the classical turning point, and we again have the problem of the meaning of such an expansion.

13.2.2.2 Applicability and Interpretation of the \hbar Expansion. In order to study the validity of the expansion (13.42) and (13.43) it is very useful to investigate some examples for which the propagator is known analytically:

(i) For a one-dimensional linear potential $V_1 = ax$ it can be checked that the following form of the propagator

$$C^{(1)}(x, x') = \left(\frac{m}{2\pi\hbar^2} \right)^{1/2} \frac{1}{\beta^{1/2}} e^{-(m/2\hbar^2\beta)x^2} e^{-\beta V_1(q) + (\hbar^2/24m)\beta^3|V'_1|^2} \\ = C^{(0)}(x, x') e^{(\hbar^2/24m)\beta^3 V'_1^2} \quad (13.45)$$

fulfills the Schrödinger equation (13.3), where V'_1 means the derivative of V_1 and $C^{(0)}(x, x')$ is the one-dimensional analogue to the Thomas-Fermi approximation (13.39) of the single-particle propagator. The Wigner transform of (13.45) affects only $C^{(0)}(x, x')$ and the semiclassical expansion of the remaining factor has to agree with the expression within brackets of (13.42); this can readily be verified. It is also clear that the expansion (13.42)—for this example—is completely valid and it converges in the whole β and \hbar plane. For the calculation of physical quantities [see Eqs. (13.7–13.15)], however, we have to take the inverse Laplace transform of expansions like (13.42) and the problem which was discussed in connection with (13.43) arises. This can be studied in more detail for our example (13.45). Using (13.40) and the folding theorem for Laplace transforms [PB 55, AS 65] in the case of the linear potential we obtain for the density:

$$\rho^{(1)}(q, p; \lambda) = 2^{2/3}\sigma \int_{-\infty}^{\lambda} dE \Theta\left(\lambda - E - \frac{p^2}{2m} - V_1(q)\right) \text{Ai}(-2^{2/3}\sigma E) \quad (13.46)$$

with

$$\sigma = (2m)^{1/3} \frac{1}{[\lambda V'_1]^{2/3}}$$

and the integral representation of the Airy function [AS 65]:

$$\text{Ai}(-z) = \frac{1}{2\pi i} \int_{c-i\infty}^{c+i\infty} d\beta e^{\beta z + (1/3)\beta^3}. \quad (13.47)$$

Changing the variable in (13.47) to $y = 2^{2/3}\alpha\beta$ we see that σA_1 is proportional to $\delta(E)$ for $\hbar \rightarrow 0$ and we recover, together with (13.46), the first terms of (13.43). The higher terms are also obtained in expanding (13.45) up to \hbar^2 , which can easily be performed again using the variable y in (13.47). From there we can see that all the troubles come from the fact that (13.46) is nonanalytic in \hbar and therefore an \hbar expansion is not really possible [this is analogous to the case that a Fourier transform of e^{-ax^2} is nonanalytic in a , but we can still get a formal power series in a by using δ -functions and derivatives of δ -functions by a term-by-term transformation of the Taylor expansion of e^{-ax^2} (see also Sec. 10.5 on this point)].

(ii) As a second definite example we will treat the three-dimensional *isotropic harmonic oscillator* potential $V_2 = \frac{1}{2}m\omega^2 r^2$. It can be checked that the corresponding Schrödinger equation (13.3) is fulfilled by the following expression for the propagator (the derivation can be found in [Kr 64]):

$$\begin{aligned} C^{(2)}(\mathbf{q}, s) &= \left(\frac{m}{2\pi\hbar^2} \right)^{3/2} \left[\frac{\hbar\omega}{\sinh(\beta\hbar\omega)} \right]^{3/2} \\ &\times \exp \left\{ -\frac{m\omega}{\hbar} \left[\mathbf{q}^2 \tanh \left(\beta \frac{\hbar\omega}{2} \right) + \frac{\pi^2}{4} \coth \left(\beta \frac{\hbar\omega}{2} \right) \right] \right\}. \end{aligned} \quad (13.48)$$

In Eq. (13.15) we need the trace of this propagator, which can be easily calculated to be:

$$Z^{(2)}(\beta) = \frac{1}{4} \left[\frac{1}{\sinh \left(\beta \frac{\hbar\omega}{2} \right)} \right]^3. \quad (13.49)$$

In order to calculate $E - \lambda N$ we have to evaluate the inverse Laplace transform of $\beta^{-2}Z(\beta)$. This may be done for $Z^{(2)}$ of (13.49) by a contour integration and closing the contour to the left ($\lambda > 0$). We thus get contributions from each pole of the partition function $Z^{(2)}$ along the imaginary β axis. We have, therefore, $E - \lambda N$ given by the sum of the residues of the function $\exp(\beta\lambda)Z^{(2)}(\beta)\beta^{-2}$. The pole at $\beta = 0$ is of fifth order, whereas the other poles are of only third order. In order to evaluate the residue at the origin, we have to know the Laurent expansion of $Z^{(2)}(\beta)\beta^{-2}$ up to the term $\propto \beta^{-1}$, which is given by:

$$\frac{Z^{(2)}(\beta)}{\beta^2} = \frac{1}{\beta^2} \left[\frac{2}{(\hbar\omega\beta)^3} - \frac{1}{4(\hbar\omega\beta)} + \frac{17}{960} \hbar\omega\beta - \dots \right]. \quad (13.50)$$

Also calculating the residue to the other poles, we obtain for the energy:

$$\begin{aligned} E - \lambda N &= -\frac{\lambda^4}{12(\hbar\omega)^3} + \frac{\lambda^2}{8\hbar\omega} - \frac{17}{960} \hbar\omega \\ &- \sum_{n=1}^{\infty} \frac{2}{(\hbar\omega)^3} (-)^n \left\{ \cos \frac{2\pi n\lambda}{\hbar\omega} \left[\left(\frac{\hbar\omega}{2} \right)^2 \frac{1}{n^2\pi^2} \left(\left(\frac{\hbar\omega}{2} \right)^2 - \lambda^2 \right) \right. \right. \\ &\quad \left. \left. + 6 \left(\frac{\hbar\omega}{2} \right)^2 \frac{1}{n^4\pi^4} \right] + 4\lambda \left(\frac{\hbar\omega}{2} \right)^3 \frac{1}{n^3\pi^3} \sin \frac{2\pi n\lambda}{\hbar\omega} \right\}. \end{aligned} \quad (13.51)$$

From Eq. (13.51) we see that the contribution of the pole at the origin produces, as a function of λ , a monotonically increasing part, whereas the other poles produce oscillating contributions. These oscillations come from the poles of (13.48) and (13.49) off the real β axis. They are apparently due to the shell structure of the

harmonic oscillator potential since, for the case of the linear potential (13.45), such poles are missing.

Although the harmonic oscillator potential is certainly a very special case, we are tempted to generalize the result to any potential in the sense that the contribution of the singularity of $e^{\beta\lambda}Z(\beta)/\beta^2$ at the origin gives the smooth contribution to the ground state energy, whereas the contribution of other singularities gives the oscillating part.

In spite of the fact that we know very little about the analytical structure of $Z(\beta)$ for an arbitrary potential, these considerations can be substantiated somewhat if we investigate the connection of the Strutinski smoothed energy studied in Sec. 2.9 with the one given just above. For this we consider the *Strutinski smoothed density of states* (2.109):

$$\begin{aligned} g_{\text{st}}(\epsilon) &= \frac{1}{\gamma} \int_0^\infty d\epsilon' g(\epsilon') f_M\left(\frac{\epsilon - \epsilon'}{\gamma}\right) \\ &= \frac{1}{\gamma} \int_0^\infty d\epsilon' g(\epsilon') \mathcal{L}_{\epsilon-\epsilon'}^{-1}[f_M(\beta\gamma)]. \end{aligned} \quad (13.52)$$

With the definitions (13.6) and (13.8) and the folding theorem for Laplace transforms [PB 55, AS 65] we obtain for the partition function corresponding to (13.52)

$$Z_{\text{st}}(\beta) = Z(\beta) f_M(\beta\gamma), \quad (13.53)$$

where $f_M(\beta\gamma)$ is the Laplace transform of the curvature corrected smoothing factor [(2.111), (2.115)]:

$$f_M(\beta\gamma) = w(\beta\gamma) \sum_{n=0}^M \frac{(\beta\gamma)^{2n}}{(2n)!} \left[\frac{\partial^{2n}}{\partial(\beta\gamma)^{2n}} \frac{1}{w(\beta\gamma)} \right]_{\beta=0} \quad (13.54)$$

with

$$w(\beta\gamma) = \frac{1}{\sqrt{\pi}} e^{\beta^2\gamma^2/4}. \quad (13.55)$$

We should recognize that the polynomial in (13.54) represents just the first M terms of the development of $1/w(\beta\gamma)$. In Section 2.9 we showed that the width γ of the Strutinski smoothing must be of the order of $\hbar\omega$ or larger. This causes $f_M(\beta\gamma)$ in (13.54) to be down by five orders of magnitude at the first singularity of (13.49). In other words, Strutinski smoothing simply means cutting out a piece of the partition function (or the propagator) between the first singularities on the positive and negative imaginary β axis, which stays equal to the exact partition function as long as possible and around the poles drops to zero with a width γ . Again we generalize and assume that it is true that for any potential with a sequence of bound states to give rise in $Z(\beta)$ to singularities at roughly the mean shell spacing apart. We therefore see that the Strutinski smoothing procedure is essentially equivalent to our definition above of the smooth energy, namely to be that contribution which in (13.15) comes from the singularity of $Z(\beta)$ at the origin, that is, of the behavior of $Z(\beta)$ for small β [Je 73, 76]; this is also confirmed by the numerical examples given below.

The usefulness of the semiclassical expansions such as given by Eq. (13.42) now lies in the fact that they provide simultaneously a Laurent series in \hbar and β of the partition function $Z(\hbar, \beta)$; this is actually all we used to

calculate the contribution to the ground state energy which comes from the singularity of $Z(\beta)$ at $\beta=0$. As a matter of fact, we verify easily that for the harmonic oscillator potential $V(r) = \frac{1}{2}m\omega^2r^2$ we get exactly the expansion (13.50) using (13.42) with $Z = 2/(2\pi\hbar)^3 \int d^3q d^3p C(q, p)$ [see Eqs. (13.33) and (13.6)].*

Of course, for an arbitrary potential, the order of the singularity at the origin of $Z(\beta)$ may be very high, forcing us also to push its semiclassical development to high order. There, however, the fact that (13.42) is also an expansion in \hbar helps greatly in the sense that the series is very rapidly convergent. This is clearly demonstrated in Table 13.1, where we show the convergence of the smooth part of the ground state energy for a Woods-Saxon potential. We also give the Strutinski smoothed values and we see the remarkable fact that including fourth order in \hbar gives a convergent value which agrees very well with the Strutinski value. Compared to the exact energies, the contribution from the singularity of $Z(\beta)$ at $\beta=0$ exhausts an enormous amount of the exact total energy, the missing part lying in the parts-per-thousand region. This small amount, however, is not at all negligible, since it contains all the information about the shell structure or quantum oscillations of such quantities as the nuclear density or the total binding energy [see Eq. (13.5)]. For example, it is well known that the smooth part of the total (Strutinski or semiclassical) energy for a continuously deformed nucleus (e.g., quadrupole constraint; see Sec. 7.6) gives only the liquid drop potential curve (Fig. 2.31), whereas quantum oscillations are responsible for such details as double hump barriers, etc., governing the nuclear fission process.

We now have a quick, clear interpretation of our semiclassical or extended Thomas-Fermi method. It allows us to pick up the contribution to the binding energy, which in (13.15) comes from the singularity of $Z(\beta)$ at the origin. If we believe in the generalization of the harmonic oscillator

* It should be noted that the poles of $Z(\beta)$ could be reconstructed from its semiclassical expansion (13.50) in building out of its Laurent series the corresponding Padé approximations, thus also including some of the oscillating contributions to the binding energy. This aspect, however, has not been investigated very much [GS 77].

Table 13.1 Smooth energies in a spherical Woods-Saxon well with the same parameters as those used in Fig. 13.1. All energies are in MeV. The first column gives the nucleon number $A = 2N = 2Z$. The second, third, and fourth columns give $E_{sc}^{(0)}$, $E_{sc}^{(1)}$, and $E_{sc}^{(2)}$, which correspond to the contributions of the TF term, the $O(\hbar^2)$, and $O(\hbar^4)$ term of Eq. (13.42), respectively. The fifth column gives the total semiclassical energy E_{sc} , while the last column gives the Strutinski energy (from [Je 76]).

A	$E_{sc}^{(0)}$	$E_{sc}^{(1)}$	$E_{sc}^{(2)}$	E_{sc}	E_M
164	-3344.7	88.8	1.0	-3254.9	-3256.0 (1.2)
260	-5484.8	119.7	1.1	-5364.0	-5364.4 (0.8)
416	-9049.1	162.5	1.1	-8881.5	-8882.8 (1.2)

result, this contribution corresponds to the smooth part of the energy—and the numerical study for the Woods-Saxon potential supports that—we then have a method which does not need the quantum mechanical result for the calculation of the Strutinski smoothed energy. We should note that it is completely equivalent to use, instead of the semiclassical expansion for $Z(\beta)$ in Eq. (13.15), the ETF result for the density [(13.43) and (13.44)] and calculate $E_{sc} = \text{Tr}(H\rho_{sc})$. It becomes clear from this that the extended Thomas-Fermi method, as it stands, is not suitable to be used as a self-consistent theory; that is, given a $V[\rho]$, Eqs. (13.43) and (13.44) cannot be used to calculate ρ_{sc} self-consistently by iteration because of the divergences at the classical turning point. In the following sections we will see how this drawback of the ETF method can be circumvented.

13.2.2.3 The Functional of the Kinetic Energy Density.* One possibility of disposing of the difficulty that we cannot perform a self-consistent semiclassical calculation is the following: in order to calculate the ground state energy, we need the kinetic energy density $\tau(r)$ of Eq. (13.13). If we could express this kinetic energy density as a functional of the local density, that is, $\tau = \tau[\rho(r)]$, the binding energy would be a functional of $\rho(r)$ alone, since, for example, the Skyrme potential energy (5.87) is given in terms of ρ and τ . A variation of the binding energy with respect to ρ would then give us an equation for $\rho(r)$ alone. Though there exists the theorem by Hohenberg and Kohn [HK 64, MT 77] that the binding energy and thus also the kinetic energy density of a fermion system is a unique functional of $\rho(r)$, it seems to be quite difficult to derive this functional in practice. In our semiclassical framework, however, we are able to construct such a functional which will be valid in the sense that our semiclassical approach is valid, that is, it will ultimately give us the smooth part of (e.g.) the binding energy.

From Eqs. (13.11), (13.13), and (13.42), we are able to construct the semiclassical expansion of τ up to the second order term, which yields [Ki 67, Je 76]:

$$\begin{aligned}\tau_{sc}(r, \lambda) = & \frac{1}{3\pi^2} \left(\frac{2m}{\hbar^2} \right)^{3/2} \left\{ \frac{3}{5} (\lambda - V)^{5/2} \right. \\ & \left. - \frac{1}{8} \frac{\hbar^2}{2m} \left[5\nabla^2 V (\lambda - V)^{1/2} - \frac{9}{4} \frac{(\nabla V)^2}{(\lambda - V)^{1/2}} \right] + O(\hbar^4) \right\} \Theta(\lambda - V).\end{aligned}\quad (13.56)$$

The expression for the density (13.44) is a function of $\tilde{V} = \lambda - V$, $\nabla \tilde{V}$, and $\Delta \tilde{V}$. Calculating from (13.44) $\nabla \rho$ and $\Delta \rho$ and consistently neglecting higher than second derivatives of the potential, we have three equations: $\rho = \rho(\tilde{V})$,

* In this section, we follow to some extent the presentation given in [Br 77].

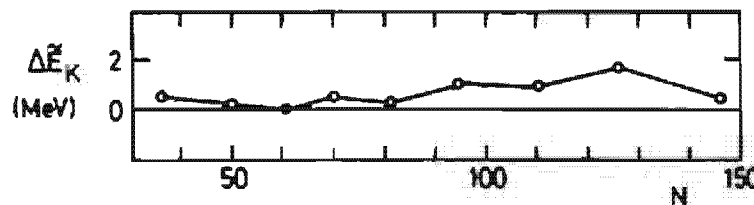


Figure 13.3. The difference $\Delta \bar{E}_K = \bar{E}_K - \bar{T}_K$, where \bar{E}_K is the Strutinsky smoothed kinetic energy and \bar{T}_K is calculated as explained in the text. The values are for a spherical Woods-Saxon potential as a function of neutron number N . (From [Br 77].)

$\nabla \tilde{V}, \Delta \tilde{V}$), $\nabla \rho = \nabla \rho(\cdots)$, and $\Delta \rho = \Delta \rho(\cdots)$, which can be solved for $\tilde{V}, \nabla \tilde{V}$, and $\Delta \tilde{V}$; inserting this into (13.56) yields [Ki 67]*:

$$\begin{aligned} \tau_{sc}[\rho_{sc}] &= \frac{3}{5} (3\pi^2)^{2/3} \rho_{sc}^{5/3} + \frac{(\nabla \rho_{sc})^2}{36\rho_{sc}} + \frac{\Delta \rho}{3} \\ &= \tau^{TF} + \tau^{(2)}. \end{aligned} \quad (13.57)$$

[To verify Eq. (13.57) it is easier to calculate the three terms in (13.57) from (13.44) and compare the corresponding result with (13.56).] The first term on the r.h.s. of (13.57) is, of course, the Thomas-Fermi term, which we have already discussed in Section 13.2.1 and is the only one surviving for infinite matter. The following terms take account of the inhomogeneity of the system. The second term is called the Weizsäcker term. The last term in Eq. (13.57) is the divergence of a vector field which vanishes at infinity; from Gauss' theorem this term will not contribute to the kinetic energy, which is the integral over $\tau(r)$. The functional (13.57) is consistent with the semiclassical expansion of ρ [Eq. (13.44)] and τ [Eq. (13.56)] up to order \hbar^2 . The whole scheme has also been carried out up to order \hbar^4 [Je 76, BJ 76b, GV 79]. We do not want to give the quite lengthy expressions here.

According to the derivation, the functional (13.57) is strictly only valid for classically allowed values of r , but it is tempting to assume that the analytical continuation of (13.57) to the region beyond the classical turning point is the correct one for averaged quantities, and in any case we can use (13.57) as a variational ansatz. As a matter of fact, if we put into the functional $\tau_{sc}[\rho_{sc}]$, which is consistent up to order \hbar^4 , instead of ρ_{sc} , a Strutinsky smoothed density of a spherical Woods-Saxon potential, we see from Fig. 13.3 that the corresponding kinetic energy \bar{T}_K differs only very little from the Strutinsky smoothed one, clearly showing that it is sensible to continue (13.57) to all values of r [BJC 76].

13.2.2.4 Variational Calculations. Having thus gained some confidence in the functional (13.57), we can adopt the following procedure for the self-consistent determination of a semiclassical density. Using (13.57) we can calculate the smooth

*Sometimes, instead of $1/36$, different factors are used in order to correctly reproduce surface energies [Ba 72b].

part of the binding energy $\bar{E}[\rho_{sc}] = \int d^3r \tau_{sc} + \int d^3r v[\rho_{sc}]$ and vary, with respect to ρ_{sc} , *

$$\frac{\delta}{\delta \rho_{sc}} \left\{ \bar{E}[\rho_{sc}] - \lambda \int d^3r \rho_{sc}(r) \right\} = 0, \quad (13.58)$$

where we assure the normalization condition (13.24) with a Lagrange multiplier, as discussed in Section 13.2.1. We should, of course, generalize the theory for Hamiltonians like the one derived from the Skyrme force (5.87) with effective mass and spin orbit terms. This will obviously modify the functional $\tau[\rho]$, which is given in [BJC 76, GV 79]. In order to demonstrate the principle, however, it will be sufficient to neglect effective mass and spin orbit terms and take from the Skyrme potential (5.99) only the local part: $V[\rho] \approx \frac{1}{8} t_0 \rho + \frac{1}{16} t_3 \rho^2$. With (13.57) we therefore get the following expression for the smooth part of the binding energy (in the following we replace ρ_{sc} by ρ):

$$\begin{aligned} \bar{E}[\rho] &= \int d^3r \epsilon[\rho], \\ \epsilon[\rho] &= \epsilon_\infty(\rho) + \frac{\hbar^2}{2m} \frac{(\nabla \rho)^2}{36\rho}, \\ \epsilon_\infty(\rho) &= \frac{\hbar^2}{2m} \frac{3}{5} (3\pi^2)^{2/3} \rho^{5/3} + \frac{3}{8} t_0 \rho^2 + \frac{1}{16} t_3 \rho^3, \end{aligned} \quad (13.59)$$

where ϵ_∞ is the energy density for infinite nuclear matter, which at saturation ($\rho = \rho_0$) has the value

$$\frac{1}{\rho_0} \epsilon_\infty(\rho_0) = E_0 = -16 \text{ MeV} \quad \text{with } \rho_0 = 0.14 \text{ fm}^{-3}. \quad (13.60)$$

To obtain a relatively simple equation, we may try to parametrize $\epsilon_\infty(\rho)$ around its saturating value for infinite nuclear matter in the following way.

$$\frac{1}{\rho} \epsilon_\infty(\rho) \approx E_0 + \frac{K}{18\rho_0^2} (\rho - \rho_0)^2. \quad (13.61)$$

where K , the nuclear incompressibility (5.95), has roughly the value $K \approx 200$ MeV. The variational procedure (13.58), together with (13.59) and (13.61), leads to the following differential equation for ρ in units of ρ_0 [$\delta(\nabla \rho)^2 = 2\nabla \rho \delta(\nabla \rho)$ and partial integration, $\lambda \approx E_0$]:

$$2 \frac{\Delta \rho}{\rho} - \frac{(\nabla \rho)^2}{\rho^2} = \frac{1}{a^2} (3\rho^2 - 4\rho + 1), \quad (13.62)$$

with

$$a = \left(\frac{\hbar^2}{2m} \frac{1}{2K} \right)^{1/2}.$$

Equation (13.62) can be solved analytically in one dimension for half-infinite nuclear matter [Br 77]: $\rho(x) = \rho_0 [1 + \exp(x/a)]^{-1}$. It is easy to get the asymptotic solution of (13.62) requiring that ρ and its derivatives vanish at infinity (no approximation for ϵ_∞ would actually be necessary for this consideration). We then

* This variational principle, in connection with a general energy functional $E[\rho]$, does not correspond to a Ritz variation as discussed in Section 5.6.1.2.

obtain an equation already discussed by Berg and Wilets [BW 56]:

$$r \rightarrow \infty: \quad 2 \frac{\Delta \rho}{\rho} - \left(\frac{\nabla \rho}{\rho} \right)^2 = a^{-2}, \quad (13.63)$$

which gives for the spherical case

$$\rho(r) \underset{r \rightarrow \infty}{\propto} \frac{1}{r^2} e^{-r/a}. \quad (13.64)$$

We see that qualitatively we get the correct behavior for the density, that is, an exponential decay; quantitatively, however, the decay is much too rapid compared to realistic densities, and a numerical solution of (13.62) shows that the exponentially decaying behavior is assumed only quite far out in the tail of the density. In Fig. 13.4, we show density profiles as well as corresponding kinetic energy densities (13.57) that have been calculated by Bohigas et al. [BCK 76], incorporating in the theory a spin-orbit term and the fact that we have different neutron and proton densities. We see that the densities still have a Thomas-Fermi-like behavior, that is, the decay is too steep compared to the real densities. Practically the same results have been obtained by Holzwarth et al. [EH 77]. It is not very astonishing that the densities in Fig. 13.4 still very much resemble Thomas-Fermi densities, since the function (13.57) has been constructed from the extended Thomas-Fermi theory, which yields densities with too steep a surface. The binding energies calculated with the densities of [BCK 76] reproduce the binding energy of the corresponding Hartree-Fock calculation only within 0.4–0.5 MeV per nucleon, indicating that higher-order terms in the functional $\tau[\rho]$ have been neglected (in this respect, see [CJB 77]).

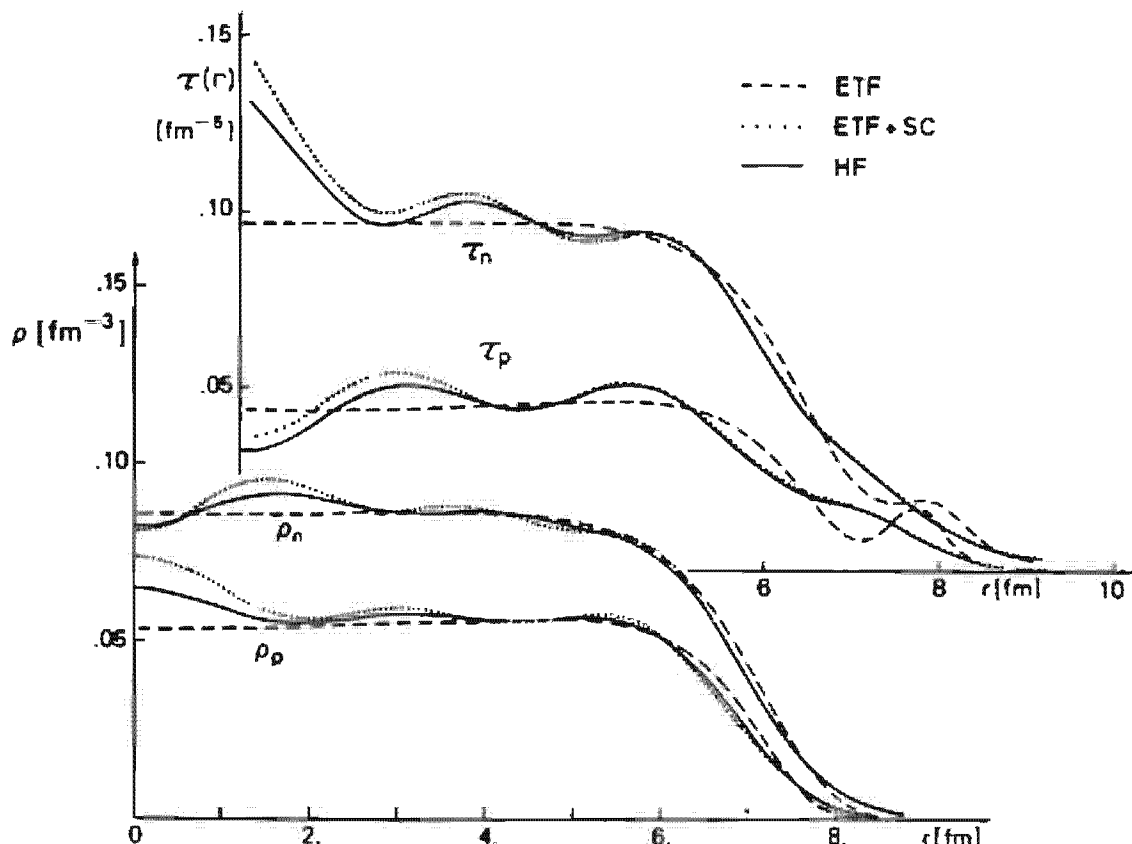


Figure 13.4. Self-consistent semiclassical densities and kinetic energy densities compared to exact results of a Skyrme Hartree-Fock calculation [BCK 76].

In concluding this section, we can say that the semiclassical functional $\tau[\rho]$, together with the Skyrme potential and the variational principle (13.58), establishes a semiclassical theory for the self-consistent calculation of the average nuclear density and the corresponding liquid drop energy. The densities, however, are still too steep in the surface compared to the exact ones, which is a serious drawback if we want to calculate quantities that are sensitive to the tail of the density, for example, the form factors for electron scattering or—in the dynamical generalization—excitation energies of surface oscillations. We will see in the next section how this shortcoming can be remedied.

It is also satisfying that it could be shown (cf. Fig. 13.4) [CJB 77, BCK 76] that starting from these densities (dashed lines) as input to a Hartree-Fock calculation only one iteration that is one quantum mechanical calculation (dotted lines) was necessary to reproduce the HF results. It might be of interest that the procedure described in this section is also quite frequently applied in other fields of physics [JM 73, Sec. 8.11.1].

13.2.3 Partial Resummation of the \hbar -Expansion

In the last section we saw that the extended Thomas-Fermi approximation is very capable of giving the smooth part of the binding energy. It became clear, however, that the density (13.44) we were implicitly using in this concept is not well defined at or beyond the classical turning point, and that even the density we got out of the density functional formalism has still more or less the Thomas-Fermi-like behavior, that is, compared to the exact density, a surface which is too steep.

In this section, we will show how we can improve on this deficiency. In order to do that, we return to the development (13.16). We had seen that keeping only the first term yields the Thomas-Fermi approximation [(13.19), (13.20)]. It turns out that the propagators $C^{(1)}(\mathbf{r}, \mathbf{r}')$, and $C^{(2)}(\mathbf{r}, \mathbf{r}')$ can still be given analytically keeping the second and third term, respectively, in (13.16).

The solution keeping only first derivatives in (13.16), which we will call the *linearized case*, can easily be obtained using (13.45) (for simplicity we will only present the solution for the one-dimensional case, but all the results below can straightforwardly be generalized to the three-dimensional case). Using (13.17) and (13.21), we obtain for the propagator [Sw 55, Ba 72b, Gr 72, Bh 77, DBS 78]

$$C^{(1)}(q, s) = \left(\frac{m}{2\pi\hbar^2} \right)^{1/2} \frac{1}{\beta^{1/2}} \exp \left\{ - \frac{m}{2\hbar^2\beta} s^2 - \beta V(q) + \frac{\hbar^2}{24m} \beta^3 \left(\frac{\partial V}{\partial q} \right)^2 \right\}. \quad (13.65)$$

It is clear that the approximation (13.65) corresponds to locally replacing the potential by a straight line, and we recover the Thomas-Fermi approximation with $\partial V/\partial q = 0$. One can also find the density corresponding to (13.65), which gives an expression analogous to (13.46). We do not want to go into the details of the linearized case, and before we discuss its

relationship to the semiclassical treatment, we want to present the solution of the so-called *locally harmonic case*, where we keep up to second derivatives of the potential in (13.16). Using the result (13.48) as a guide for the harmonic oscillator, we find for the propagator in the one-dimensional case [Gr 72, DBS 78]:

$$C^{(2)}(q, s) = \left(\frac{m}{2\pi\hbar^2} \right)^{1/2} \left[\frac{\hbar\omega(q)}{\sinh(\beta\hbar\omega(q))} \right]^{1/2} \times \exp \left\{ -\beta\tilde{V}(q) - \frac{m\omega(q)}{\hbar} \left[(\eta(q))^2 \tanh \left(\beta \frac{\hbar\omega(q)}{2} \right) + \frac{s^2}{4} \coth \left(\beta \frac{\hbar\omega(q)}{2} \right) \right] \right\}, \quad (13.66)$$

with

$$\omega(q) = \left(\frac{V''(q)}{m} \right)^{1/2}, \quad \eta(q) = \frac{V'(q)}{V''(q)}, \quad \tilde{V}(q) = V(q) - \frac{V'(q)^2}{2V''(q)},$$

where the primes mean derivatives with respect to q . We easily check that for a harmonic oscillator potential (13.66) goes over into the corresponding correct result (13.48). For $V'' \rightarrow 0$, we also see that (13.16) goes over into (13.65).

In the three-dimensional case, the locally harmonic approximation gets somewhat more complicated, because we have to replace the potential locally by a second-order surface. In order to obtain the solution, we have to find the normal coordinates according to those surfaces in which the Hamiltonian becomes just a sum of three harmonic oscillators. The corresponding propagator is then essentially a product of three propagators of the form (13.66) [DBS 78].

The connection of the linearized (13.65) and the locally harmonic case (13.66) to the extended Thomas–Fermi theory is quite straightforward. In Eq. (13.42) we saw that for the Wigner transform of the propagator, the Wigner–Kirkwood expansion is a simultaneous expansion in powers of \hbar and β for the nonclassical part. It is easy to find the Wigner transforms of (13.65) and (13.66), since they only have a Gaussian dependence in the nonlocality s . Developing, apart from the classical part, the Wigner transform of (13.66) in powers of β , we get back exactly the same series as (13.42), if we put all derivatives higher than the second equal to zero. The same is obviously true for (13.65), where we have to put all derivatives higher than the first equal to zero. The successive approximation scheme [(13.39), (13.65), (13.66)] can therefore also be interpreted in the following way. The TF approximation (13.39) consists of re-summing the series (13.35) for all terms containing no derivatives of the potential; the linearized approximation consists of re-summing all terms containing the potential and its first derivatives, and the locally harmonic approximation in re-summing all the terms containing the potential, its first and second derivatives. It is clear that higher-order derivatives cannot be completely

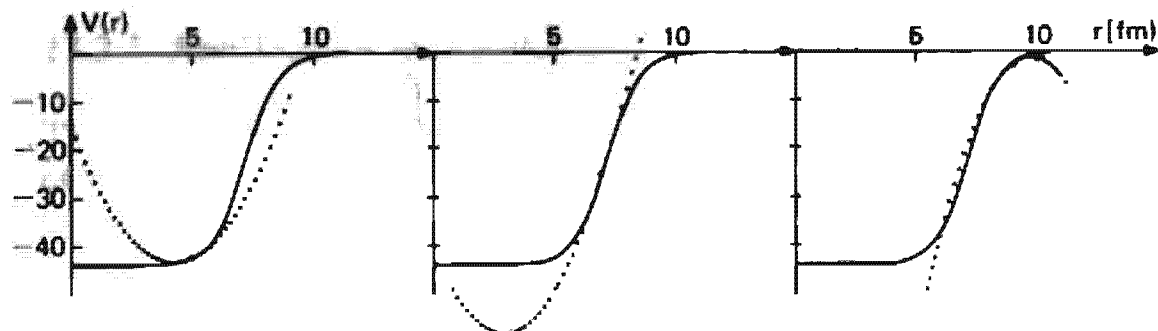


Figure 13.5. Parabolic approximation of the linear Woods-Saxon potential at three different points.

re-summed any more because cubic or higher-order potentials cannot be solved analytically. It is obvious that in terms of powers of \hbar this is only a partial resummation—not all the terms of a given order in \hbar are taken into account. These partial re-summations obviously have desirable features: As discussed above, the expansion (13.42) cannot be Laplace inverted term by term, whereas the expressions (13.65) and (13.66) can be Laplace inverted even analytically [Bh 77, DBS 78]. The partial summation of infinitely many terms can account for important effects, for instance, tunneling into the classically forbidden region, as will be shown below in a numerical example.

Let us study the *geometrical interpretation* of the locally harmonic approximation and study the implications it has for the calculation of the corresponding density. In Fig. 13.5 we show a one-dimensional Woods-Saxon potential and its locally harmonic approximation at three different points. The curves are parabolas with different curvatures in the interior of the inflection point; outside the inflection point the curves are inverted parabolas. In the outside region, we easily imagine that we have penetration into the local barrier, eventually giving rise to quite a good representation of the exponential decay of the density. In the interior the situation is more complicated: The oscillations of the true density (see Fig. 13.1) are global effects, that is, they are due to standing waves in the potential and their wave length is therefore determined by the precise position of the edges of the potential. Since we are only locally representing the potential well, the edges are badly determined and are, as a matter of fact, strongly fluctuating, as can be seen from Fig. 13.5a, b. In the interior, we are therefore introducing spurious shell fluctuations, and all we can hope for is that the density in the interior is well represented on the average, that is, we have to average out the spurious shell fluctuations.

13.2.4 The Saddle Point Method

This average can be done effectively if we perform the necessary Laplace inversions for the density (13.11) and the total energy (13.15) with the help of the saddle point method (SPM) [PB 75, Bh 77]. This consists of

writing

$$G(\lambda) \equiv \frac{1}{2\pi i} \int_{c-i\infty}^{c+i\infty} d\beta e^{\beta\lambda} F(\beta) = \frac{1}{2\pi i} \int_{c-i\infty}^{c+i\infty} d\beta e^{S(\beta)}$$

and expanding $S(\beta)$ around the stationary point β_0 determined by $\partial S/\partial\beta \equiv \dot{S}_0 = 0$ to second order: $S(\beta) \approx S_0 + \frac{1}{2}\ddot{S}_0(\beta - \beta_0)^2$. Usually this is not sufficient, and we have to introduce corrections to this simple method in expanding S to higher terms in $\beta - \beta_0$. Usually these higher terms are not kept in the exponent but expanded into a Taylor series. Putting together the terms whose order in the derivatives is the same, and including the first correction, we obtain:

$$G(\lambda) = \left(\frac{1}{2\pi\ddot{S}_0} \right)^{1/2} e^{S_0} \left[1 + \frac{1}{8\ddot{S}_0^3} \left(\ddot{S}_0 \ddot{S}_0 - \frac{5}{3} \ddot{S}_0^2 \right) + \dots \right].$$

From this it becomes clear how to construct the second-order correction, which is somewhat tedious but straightforward. However, its inclusion is necessary in most cases in order to gain a convergent result.

For a demonstration of this method we use the exact propagator of the three-dimensional harmonic oscillator (13.48) and calculate with the stationary phase method densities (Fig. 13.6) and total energies. We see that the densities are well-defined average densities in the sense that they pass in a smooth way through the quantum mechanical oscillations. Calculating in the same way the total energy (13.15), we obtain for all deformations the Strutinsky averaged value [BP 73] to within a fraction per thousand, that is, for ground state energies of several thousand MeV the deviation from the Strutinski value is never greater than 1 MeV.

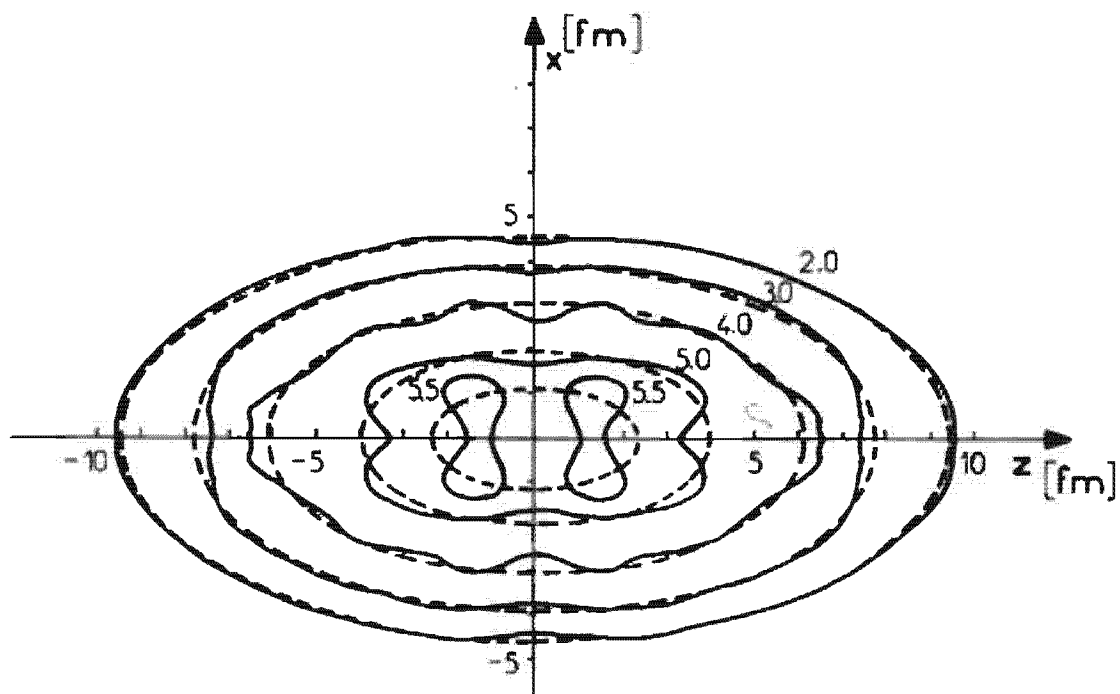


Figure 13.6. Exact densities compared to those obtained by the stationary phase method for a strongly deformed harmonic oscillator. (We are grateful to J. Bartel for the preparation of this figure.)

13.2.5 Application to a Spherical Woods-Saxon Potential

The locally harmonic form (13.66) of the propagator together with the saddle-point method of Section 13.2.4 are the main ingredients of the present theory. In Fig. 13.1 we show a density obtained with the locally harmonic approximation (13.66) for a spherical Woods-Saxon potential by using the stationary phase method for the Laplace inversion. We see the very good agreement of this density with the exact one in the tail region which should be contrasted with the steep surface of the density functional method (Fig. 13.4). Contrary to the ETF theory, the locally harmonic solution allows tunnelling into the classically forbidden region. In the interior this approximation bends over into the TF result, representing there only the average density. The density profile obtained therefore corresponds exactly to the one which we would imagine for a liquid drop. A very stringent test of the validity of the approximation is not only the quality of the density itself, but also, as we have seen, the reproduction of the average of the sum of single-particle energies. With the locally harmonic solution, the average sum of single-particle energies agrees with those of a Strutinski calculation to within 5–10 MeV, depending on the mass number of the nucleus. The theory therefore simultaneously yields very satisfying average energies *and* densities.

The missing 5–10 MeV are most likely due to the neglect of third and fourth derivatives of the potential, since they are known to be important in reproducing the Strutinski value within the Wigner-Kirkwood expansion (see Sec. 13.2.2.2 and Table 13.1). Higher derivatives can be included perturbatively, but we do not want to go into these details here.

The locally harmonic case is also suitable for a self-consistent determination of the *liquid drop parameters* since, taking $V = V[\rho]$ as an input to (13.66), we can set up with (13.11) and (13.13) an iteration procedure for the average density and kinetic energy density. It has been shown by Brack and Quentin [BQ 75a] that Strutinski smoothed Hartree-Fock calculations with the Skyrme force perfectly reproduce the liquid drop parameters of the Bethe-Weizsäcker formula. Since the results of the locally harmonic case discussed above are very close to the Strutinski results, it is quite likely that a self-consistent semiclassical treatment using the harmonized theory should give the liquid drop parameters without making the detour over a full Hartree-Fock calculation [BQ 75a]. The feasibility of the method has been shown for a one-dimensional case [EVB 79].

For a complete semiclassical treatment of the self-consistent single-particle problem we must also be able to treat, for instance, the *nonlocal parts* (effective mass) of the Skyrme potential (5.87). This can also be achieved by slightly generalizing the present formalism. However, in order to do this it is preferable to work with Wigner transforms from the beginning and we obtain for the Schrödinger equation (13.3) with (13.36), for example,

$$\left[\frac{\partial}{\partial \beta} + H(\mathbf{q}, \mathbf{p}) e^{(i\hbar/2)\tilde{\Lambda}} \right] C^\beta(\mathbf{q}, \mathbf{p}) = 0,$$

where $H(\mathbf{q}, \mathbf{p})$ is the Wigner transform of the nonlocal Hamiltonian:

$$H(\mathbf{q}, \mathbf{p}) = \frac{\mathbf{p}^2}{2m} + V(\mathbf{q}, \mathbf{p}).$$

The nonlocal Hamiltonian function can be locally approximated in the phase space \mathbf{q}, \mathbf{p} by a second-order surface, analogous to the way this was done for the local case. The corresponding propagator can again be found analytically, and the corresponding densities and energies are of the same quality as in the purely local case [DSB 80].

13.2.6 Semiclassical Treatment of Pairing Properties

Having set up a semiclassical treatment of the self-consistent single-particle density, it seems natural to try a generalization that includes pair correlation (see Chaps. 6 and 7). Since this aspect is far less investigated we will content ourselves here with the solution of the BCS equations (6.54) to lowest order in \hbar .

In Chapter 7 we saw that the BCS equation can be written in the form $[\mathcal{K}, \mathcal{R}] = 0$ [Eq. (7.43)]. To lowest order in \hbar , the commutator becomes the classical Poisson bracket, as already discussed in the context of Eq. (13.36). Together with the $\hbar \rightarrow 0$ limit of $\mathcal{R}^2 = \mathcal{R}$ [Eq. (7.28)], we obtain a set of two algebraic equations for the Wigner transforms of the normal density $\rho(\mathbf{q}, \mathbf{p})$ and the anomalous density $\kappa(\mathbf{q}, \mathbf{p})$ [Eq. (7.22)]. The solution leads to the very natural result [cf. (7.61)]

$$\rho(\mathbf{q}, \mathbf{p}) = \frac{1}{2} \left\{ 1 - \frac{\hbar(\mathbf{q}, \mathbf{p})}{E(\mathbf{q}, \mathbf{p})} \right\},$$

$$\kappa(\mathbf{q}, \mathbf{p}) = \frac{1}{2} \frac{\Delta(\mathbf{q}, \mathbf{p})}{E(\mathbf{q}, \mathbf{p})},$$

$$E(\mathbf{q}, \mathbf{p}) = \sqrt{\hbar^2(\mathbf{q}, \mathbf{p}) + \Delta^2(\mathbf{q}, \mathbf{p})},$$

with $\hbar = \mathbf{p}^2/2m + V(\mathbf{q}) - \lambda$; the Wigner transform of the pair potential $\Delta(\mathbf{q}, \mathbf{p})$ is related to the anomalous density by

$$\Delta(\mathbf{q}, \mathbf{p}) = \frac{1}{(2\pi\hbar)^3} \int d^3k v(|\mathbf{p} - \mathbf{k}|) \kappa(\mathbf{q}, \mathbf{k}).$$

$v(p)$ is a Fourier transform of the two-body interaction. Thus for the gap equation to lowest order in \hbar we obtain:

$$\Delta(\mathbf{q}, \mathbf{p}) = \frac{1}{2} \frac{1}{(2\pi\hbar)^3} \int d^3k v(|\mathbf{p} - \mathbf{k}|) \frac{\Delta(\mathbf{q}, \mathbf{k})}{E(\mathbf{q}, \mathbf{p})}. \quad (13.67)$$

In infinite nuclear matter, where there is no q -dependence, this is an exact equation [FW 71]. By solving Eq. (13.67) independently for each value of \mathbf{q} we treat the nucleus as if locally it were a piece of nuclear matter. This, of course, is the usual Thomas-Fermi assumption [notice the

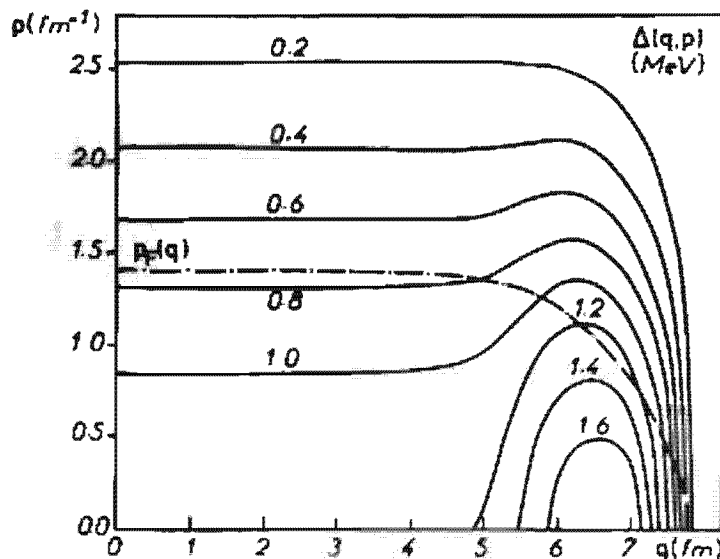


Figure 13.7. The neutron pairing gap in Wigner space, calculated with a Woods-Saxon potential ($V = -49$ MeV, $R_0 = 6.81$ fm, $a = 0.66$ fm) for neutron number 96. The parameters of the two-body force are $V_0 = -28$ MeV and $r_0 = 1.6$ fm.

close analogy to the spirit of the local density approximation for the G -matrix (Sec. 4.3.1)]. For a spherical nucleus, Eq. (13.67) was solved by iteration, taking for the interaction a Gaussian of strength V_0 and range r_0 [BS 80]. In momentum space this reads: $v(p) = -|V_0|(r_0\hbar\sqrt{\pi})^3 \exp(-p^2 r_0^2/4)$. In Fig. 13.7 we display the solution of $\Delta(q, p)$ for $V_0 = -28$ MeV and $r_0 = 1.6$ fm, and in Fig. 13.8 the solution for κ is shown. We should notice that Δ is peaked around the nucleus surface and that it is exactly zero beyond the classical turning point. The abnormal density as a function of p is very sharply peaked around the local Fermi momentum p_F (13.23). However, the width is largest in the nuclear surface. Since the abnormal energy entering the ground state energy (7.80) is the trace of the product of Δ and κ , the effective values of Δ relevant for the energy are those along the local Fermi momentum $p_F(q)$, indicated by the broken line in Fig. 13.7. In Fig. 13.9, we show a cut of Δ along this line for two values of the force parameters, giving the same pairing energy $E' \approx 2$ MeV. From this figure it becomes clear that the pairing phenomenon is essentially a

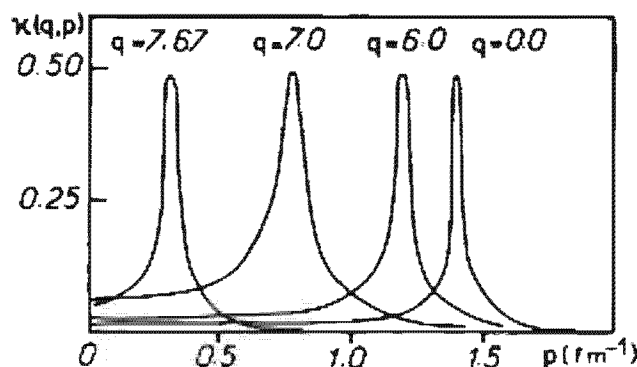


Figure 13.8. The pairing tensor at different positions, q , in the nucleus for the same parameters as in Fig. 13.7.

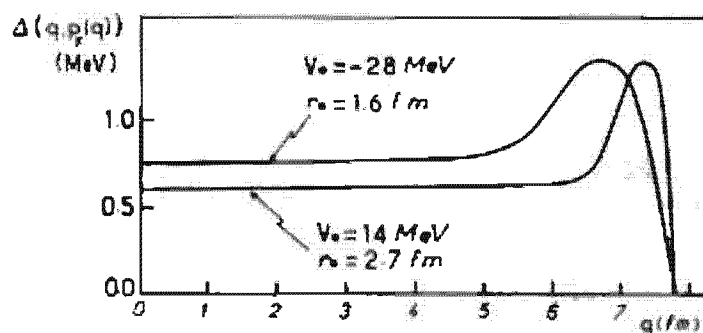


Figure 13.9. The pairing gap along the local Fermi surface [$p_F(q)$ in Fig. 13.7] for two different sets of force parameters.

surface effect for the force used here, a feature which might be important for the transfer of pairs of nucleons.

The interpretation of our results is of course the same as the Thomas-Fermi approach to the normal density: the different quantities are represented on the average, that is, shell corrections in the Strutinsky sense are missing. For example, the exact solution of the pairing gap in Fig. 13.9 should show wiggles superposed to the semiclassical curve, very much like the case for the normal density in Fig. 13.1. With the semiclassical theory, we should be able to reproduce general trends as, for example, the A -dependence of the pairing gap (Fig. 6.6). The fact that the Thomas-Fermi solution of the gap goes to zero at the classical turning point might, in this case, be a more severe shortcoming than in the case of the normal density, because of the pronounced surface character of the effect. Gradient terms (higher orders in \hbar) should therefore be included. However, no studies in this direction have been performed so far.

This concludes the semiclassical treatment of the static properties of nuclei, and we will turn next to the question of how we can use semiclassical considerations for the description of dynamic properties of the nucleus.

13.3 The Dynamic Case

Until now we have treated static properties of the nucleus, like the nuclear density and the nuclear binding energy, by semiclassical methods. It is natural to extend these theories to the dynamic case such as RPA and time-dependent Hartree-Fock theory. We will therefore have to find the limit of such theories as \hbar goes to zero. Several new features and problems arise in the dynamic case that are just at the initial stage of intensive study; thus we cannot be at all exhaustive nor can we give a rounded picture of the theory in this last section.

One of the basic equations in the dynamic case will be the classical limit of the time-dependent Hartree-Fock equations (12.9), which will lead us to nuclear fluid dynamic equations. A slightly different approach will be the derivation of such equations by a variational principle. In order to do that,

however, we need the functional $\tau[\rho]$ [see Eq. (13.57)] in the dynamic case. We will give an example of this, but this would appear rather difficult to find in general. Finally, we will discuss connections between the semiclassical results and those we obtained by sum rule considerations in Chapter 8.

13.3.1 The Boltzmann Equation

In order to take the classical limit of the TDHF equation (12.9), we have to take its Wigner transform, which we can do using the product rule (D.55). The result is [Gr 46, KK 76]

$$\frac{\partial f(\mathbf{q}, \mathbf{p}, t)}{\partial t} + \frac{2}{\hbar} f(\mathbf{q}, \mathbf{p}, t) \sin \left[\frac{\hbar}{2} (\tilde{\nabla}_q \tilde{\nabla}_p - \tilde{\nabla}_p \tilde{\nabla}_q) \right] H(\mathbf{q}, \mathbf{p}) = 0, \quad (13.68)$$

with $f(\mathbf{q}, \mathbf{p}, t)$ being the Wigner transform of ρ [cf. (13.41)], and $H(\mathbf{q}, \mathbf{p})$ the Wigner transform of the Hartree-Fock Hamiltonian. For simplicity, we will assume that the potential is local, but all formulae below can easily be generalized to nonlocal potentials, for example, of the Skyrme type (5.99), using Eq. (13.36). From (13.68) we easily get the classical limit:

$$\left[\frac{\partial}{\partial t} + \frac{\mathbf{p}}{m} \nabla_q - \frac{\partial V}{\partial q} \nabla_p \right] f^{(0)}(\mathbf{q}, \mathbf{p}, t) = 0. \quad (13.69)$$

This equation is most commonly known under the name *The Collisionless Boltzmann Equation* [UF 74, Hu 63] and $(1/(2\pi\hbar)^3) f^{(0)}(\mathbf{q}, \mathbf{p}, t)$ is therefore the classical distribution function. The physical content of (13.69) is nothing but the balance of what enters and leaves a classical phase space cell: the first term is the explicit change in time of the classical distribution function, the second one gives the change due to the velocity of the particles in the cell, and the third one represents the change of their momenta due to acceleration by a force. The Boltzmann equation is therefore nothing but the fact that the total time derivation of the classical distribution function which measures the number of particles in a given volume element of the phase space moving with time, must be zero: $df^{(0)}/dt = 0$. This, of course, is only true if we have a gas of independent particles interacting with the walls of the mean field $V[\rho]$ but having no genuine two-body collisions. This is evidently inherent to TDHF theory, from which we started. If the particles interact, we have to consider that particles can be scattered into and out of the cell, leading to the so-called Boltzmann equation with collision term: $df^{(0)}/dt = I(f^{(0)})$, where $I(f^{(0)})$ is a nonlinear integral operator in $f^{(0)}$. This collision term can be obtained again in the limit $\hbar \rightarrow 0$ from an analogous quantum mechanical term, which is contained in the two-body correlation function (12.6) we neglected in deriving the TDHF equation [cf. Eq. (12.7) and the discussion thereafter]. How this is done in detail is explained in the book *Quantum Statistical Mechanics* by Kadanoff and Baym [KB 62, Sch 72a]. We will not be more explicit here since, as we have already discussed in the context

of TDHF theory, we will only be interested in slow—that is, energetically weakly excited—phenomena. Here we should, however, be able to neglect the collision term in a first approximation [KK 68], since as we discussed in Chapter 4, the mean free path for nucleons in a ground state nucleus is of the order of the nuclear dimensions.

Note that for the time-independent case, taking the classical limit of the TDHF equation consistent with the Thomas–Fermi approximation to the distribution function, $f^{(0)}(\mathbf{q}, \mathbf{p}) = \Theta(\lambda - \mathbf{p}^2/2m - V(\mathbf{q}))$ [cf. Eq. (13.40)], since $f^{(0)}$ is solution to (13.69) for static $V(\mathbf{q})$.

It is straightforward to write down the classical analogue to the RPA equation starting from (13.69), since we know (see Sec. 8.5) that we get the RPA by linearizing the TDHF equation. Taking the simplest ansatz for $V[\rho] = a\rho(\mathbf{q}) + b\rho^2(\mathbf{q})$ [see Eq. (5.99)], we get after linearization of Eq. (13.69) with

$$\begin{aligned} f(\mathbf{q}, \mathbf{p}, t) &= f^{(0)}(\mathbf{q}, \mathbf{p}) + \delta f(\mathbf{q}, \mathbf{p}, t), \\ \rho(\mathbf{q}, t) &= \rho^{(0)}(\mathbf{q}) + \delta\rho(\mathbf{q}, t), \\ \delta\rho(\mathbf{q}, t) &= \frac{1}{(2\pi\hbar)^3} \int d^3p \delta f(\mathbf{q}, \mathbf{p}, t) \end{aligned} \quad (13.70)$$

the following equations.

$$\frac{\partial \delta f}{\partial t} + \frac{\mathbf{p}}{m} \frac{\partial \delta f}{\partial \mathbf{q}} - \frac{\partial V[\rho^{(0)}]}{\partial \mathbf{q}} \frac{\partial \delta f}{\partial \mathbf{p}} - \frac{\partial f^{(0)}}{\partial \mathbf{p}} \frac{\partial}{\partial \mathbf{q}} [(a + 2b\rho^{(0)})\delta\rho] = 0. \quad (13.71)$$

In infinite nuclear matter the third term of (13.71) vanishes and Eq. (13.71) has a special solution which can be given analytically [KB 62, No 64a]. Although this equation corresponds to the linearized Boltzmann equation, which is, in principle, a classical equation ($\hbar=0$), we can still keep the quantum mechanics correct with respect to the statistics. Thus in Eq. (13.71) for a Fermi (Bose) system, $f^{(0)}$ will be a Fermi (Bose) distribution function, and for a classical system a Boltzmann factor which completely changes the character of this equation. The analytical solution of (13.71) in the infinite matter case yields a $\delta f(\mathbf{q}, \mathbf{p}, t)$, showing that it adds to the isotropic static momentum distribution a non-isotropic distribution that is roughly egg-shaped and oscillating about its spherically symmetric equilibrium shape. This kind of vibration is called *zero sound*, in contrast to *ordinary sound* where the fermi sphere is just an oscillating translation and oscillating expansion, but its shape remains spherical (see, e.g., [KB 62, Chap. 7.4]).

In general, Eq. (13.71) cannot be solved analytically even for the infinite matter case, and for a finite system it is a rather complicated partial differential equation in seven variables which has not yet been solved for problems in nuclear physics.

13.3.2 Fluid Dynamic Equations from the Boltzmann Equation

In order to reduce the complexity of equations (13.69) and (13.71), one tries to transform them into coupled equations for the moments of $f(\mathbf{q}, \mathbf{p}, t)$ with respect to \mathbf{p} in multiplying (13.69) and (13.71) by different powers of \mathbf{p} and integrating over \mathbf{p} . This yields an infinite system of coupled partial differential equations in only four variables which are equivalent to the original equation. The simplification will consist of an appropriate decoupling of the hierarchy of coupled equations. This is a program which leads to the equations of *ordinary hydrodynamics* [UF 74, Hu 63], and we will see how in principle we have to modify the method in order to arrive at fluid dynamic equations which describe the propagation of *zero sound*.

For this purpose, we integrate Eq. (13.69) over \mathbf{p} , then multiply by p_i ($i = 1, 2, 3$) and by \mathbf{p}^2 and integrate again. After a few transformations the resulting five equations can be written in the form:

$$\frac{\partial \rho}{\partial t} + \frac{\partial}{\partial \mathbf{q}} (\rho \mathbf{u}) = 0, \quad (13.72)$$

$$m\rho \frac{D u_i}{Dt} = m\rho \left(\frac{\partial u_i}{\partial t} + \mathbf{u} \cdot \frac{\partial \mathbf{u}_i}{\partial \mathbf{q}} \right) = -\rho \frac{\partial V}{\partial q_i} - \sum_{j=1}^3 \frac{\partial P_{ij}}{\partial q_j}. \quad (13.73)$$

$$\rho \frac{D}{Dt} \left(\frac{Q}{\rho} \right) + \frac{\partial}{\partial \mathbf{q}} \mathbf{w} = - \sum_{i,j=1}^3 P_{ij} D_{ij}, \quad (13.74)$$

where we have introduced the following notation:

$u_i(\mathbf{q}, t) = \bar{p}_i/m$	the average velocity,
$U_i(\mathbf{q}, \mathbf{p}, t) = p_i/m - u_i$	deviation from the average velocity,
$Q(\mathbf{q}, t) = \frac{1}{2} m \rho \overline{U^2}$	the thermal energy density,
$P_{ij}(\mathbf{q}, t) = m \rho \overline{U_i U_j}$	the pressure tensor,
$w_i(\mathbf{q}, t) = \frac{1}{2} m \rho \overline{U_i U^2}$	the heat current density, and
$D_{ij}(\mathbf{q}, t) = \frac{1}{2} (\partial u_i / \partial q_j + \partial u_j / \partial q_i)$	the rate of strain tensor,

where the average for an arbitrary quantity A is given by (neglecting the spin):

$$\bar{A}(\mathbf{q}, t) = \frac{\int d^3 p A(\mathbf{p}, \mathbf{q}, t) \cdot f(\mathbf{p}, \mathbf{q}, t)}{\int d^3 p f(\mathbf{q}, \mathbf{p}, t)} = \frac{1}{\rho} \frac{1}{(2\pi\hbar)^3} \int d^3 p A \cdot f.$$

Equations (13.72–13.74) express nothing but the conservation laws for mass, momentum, and energy. However, these equations are, as they stand, useless, since they are not a closed system of equations. Only if we

could, for example, express the pressure tensor and the heat current density by the density ρ and velocity \mathbf{u} , respectively, would we get a closed system for unknown functions; this is exactly how we derive ordinary hydrodynamics. Here, however, we want to derive a fluid dynamical description of zero sound which is physically something completely different, as we have already briefly discussed (see also [Th 61b, KB 62, No 64a]).

In order to demonstrate the differences as clearly as possible, we first want to indicate very briefly what the physical argument is, so that we arrive at a closed system of equations coming from (13.72–13.74) for the case of ordinary hydrodynamics, and then discuss the different procedure we have to adopt to get the fluid dynamic description of zero sound and other low-energy collective nuclear phenomena.

(i) In ordinary hydrodynamics [UF 74, Hu 63] we assume that we are in a regime in which the characteristic time of typical collective motions we are interested in is very large compared to the time between successive collisions of the particles. As a consequence of these frequent collisions, the system will always be in *local equilibrium*. To understand the notion of local equilibrium, we have to realize that it was Boltzmann's achievement to show that his equation with a collision term has, for *any* initial distribution, a solution which approaches in the course of time the Maxwell–Boltzmann distribution [UF 74],

$$f_B^{(0)}(\mathbf{q}, \mathbf{p}) \propto e^{-(1/k_B T)(\mathbf{p}^2/2m + V(\mathbf{q}))}. \quad (13.75)$$

This is a function with an isotropic momentum distribution [solution to the static part of (13.69)], which characterizes equilibrium. Accordingly, under local equilibrium we shall understand that in a given volume element, the velocity distribution of the particles is such as to reproduce the average velocity $\mathbf{u}(\mathbf{q}, t)$ of the element and to be of the Maxwellian form:

$$f_B^{(0)}(\mathbf{q}, \mathbf{p}, t) = \rho(\mathbf{q}, t) \left(\frac{2\pi\hbar^2}{mk_B T(\mathbf{q}, t)} \right)^{3/2} \exp[-(1/2mk_B T(\mathbf{q}, t))(\mathbf{p} - m\mathbf{u})^2]. \quad (13.76)$$

Here all quantities are only locally defined, that is, temperature $T(\mathbf{q}, t)$ and velocity $\mathbf{u}(\mathbf{q}, t)$ depend on position and time. With the assumption of local equilibrium (13.76), we can now decouple equations (13.72–13.74) in noting that

$$\begin{aligned} P_{ij} &= P\delta_{ij}, & P &= \rho k_B T, \\ w_i &= 0, & Q &= \frac{1}{2}P, \end{aligned} \quad (13.77)$$

whence it becomes obvious why we used the name pressure tensor. Equations (13.72–13.74) therefore reduce to five coupled equations for five unknown functions: these are the ideal or Euler hydrodynamical equations

[UF 74, Hu 63, LL 59, Vol. 6]*:

$$\begin{aligned} \frac{\partial \rho}{\partial t} + \operatorname{div}(\rho \mathbf{u}) &= 0, \\ m\rho \frac{D}{Dt} \mathbf{u} &= -\rho \frac{\partial V}{\partial \mathbf{q}} + \frac{\partial}{\partial \mathbf{q}} P, \\ \frac{D}{Dt} (\rho P^{-5/3}) &= 0. \end{aligned} \quad (13.78)$$

The assumption of local equilibrium and equations (13.78) constitute the first step of a systematic improvement (*Chapman Enskog development*), where we consider small deviations from local equilibrium: $f = f_B^0 \cdot (1 + \eta)$; together with the Boltzmann equation with collision term this leads in the next step to the *Navier-Stokes equations* [UF 74].

(ii) In low-energy nuclear physics, the situation is quite different: the mean free path of the nucleons is of the order of the nuclear dimensions [KK 68] and we can therefore ignore the collisions to a first approximation (in a certain sense, a classical analogue would be a *Knudsen gas* [Kn 50]). This is the same assumption which led us to the time-dependent Hartree-Fock equation in the first place, that is, two-body correlations might be negligible to a good approximation. As a consequence, we can *not* use, at least for low-energy phenomena, the concept of local equilibrium to close the system of Eqs. (13.72–13.74). In principle, we would need the solution of (13.69) to be able to calculate the pressure tensor and the energy current density. Because of our inability to solve Eq. (13.69), however, we have to find some approximative solution. One obvious assumption is to imagine the change in time of the potential, that is, the density in (13.69), to be so slow that the potential locally in time can be considered a constant. Under the condition

$$\left| \frac{\frac{\partial V}{\partial t}}{V(t)} \right| \ll \omega, \quad (13.79)$$

where ω is a characteristic single-particle frequency, we can make the following ansatz for a solution of (13.69):

$$f^{(0)}(\mathbf{q}, \mathbf{p}, t) \approx \Theta \left(\lambda - \frac{(\mathbf{p} - m\mathbf{u})^2}{2m} - V(\mathbf{q}, t) \right). \quad (13.80)$$

This, of course, is just the usual Thomas-Fermi result (13.40), where we however replaced the static potential $V(\mathbf{q})$ by the corresponding time-

* The introduction of a temperature and a Boltzmann distribution is actually not necessary for the derivation of Eqs. (13.78). It is sufficient to assume an isotropic velocity distribution, that is f depends only on \mathbf{q} , $(\mathbf{p} - m\mathbf{u})^2$, and t . We then have, in particular

$$P = \frac{3}{2} \left(\frac{k^*}{2m} \tau - \frac{m}{2} \rho \mathbf{u}^2 \right).$$

dependent one. With the ansatz (13.80), we are again able to close the system (13.72–13.74). For example, for the pressure tensor we obtain (including the spin)

$$P_y = \frac{1}{5} \frac{\hbar^2}{m} (3\pi^2)^{2/3} [\rho(\mathbf{q}, t)]^{5/3} \delta_{ij} - \frac{m}{3} \rho \mathbf{u}^2 \quad (13.81)$$

which yields a decoupling of Eqs. (13.72) and (13.73). We therefore want to describe some applications within this framework.

13.3.3 Application of Ordinary Fluid Dynamics to Nuclei

In Chapter 1 we studied in considerable detail the application of the *liquid drop* model to nuclei. The hydrodynamical equations were very much simplified by the assumptions of a homogeneous drop with a sharp surface, incompressibility, and irrotational flow. With (1.19), (1.30), and (1.34), we gave formulae for the excitation energies of multipolarity $\lambda > 2$. They did not agree very well with experiment and we will learn why below.

Steinwedel and Jensen [SJ 50] relaxed the assumption of incompressibility somewhat, supposing that only the total density is incompressible whereas proton and neutron densities individually are not. This idea was first used to describe the giant dipole (see Fig. 13.10) resonance, but can be generalized to polarization of all multipolarities ($T=1$ polarization modes); these modes have to be contrasted with the ones prescribed by the liquid drop model of Bohr, where also the individual densities are incompressible. For the giant dipole resonance this leads to the model proposed by Goldhaber and Teller [GT 48] (see Fig. 13.10), where the proton sphere vibrates against the neutron sphere. For the other multipolarities these are $T=1$ surface vibrations, where the proton surface deforms out of phase from the neutron surface. There also exist $T=0$ surface vibrations, where the whole nucleus deforms in a coherent way around its spherical equilibrium position. This is obviously only possible incompressibly for $L \neq 0$.

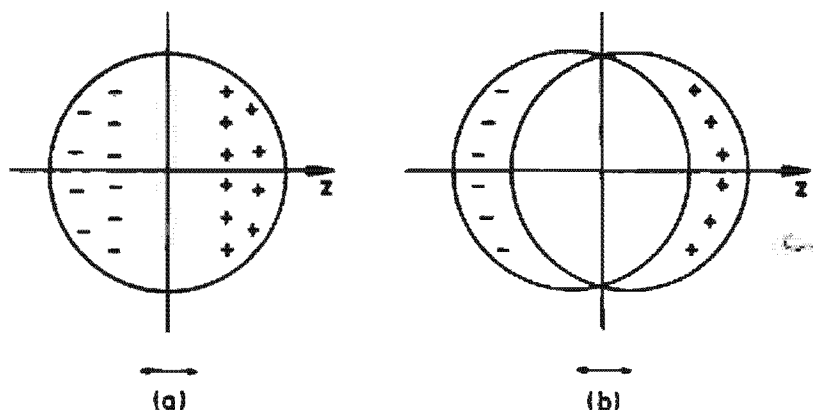


Figure 13.10. Dipole polarization of a spherical nucleus. Minus signs stand for proton defect, plus signs for neutron defect. (a) corresponds to the model of Steinwedel and Jensen, and (b) to the model of Goldhaber and Teller.

modes. For the $L=0$, $T=0$ breathing mode we have to give up the principle of incompressibility [EG 70].

From the above classification for the different possibilities of a liquid drop arises the question—for instance, for the $T=1$ modes—whether the Goldhaber-Teller model or the Steinwedel-Jensen model is physically realized. We want to present and contrast both models very briefly for the dipole case.

In the *Steinwedel-Jensen model* we assume that the total density has a sharp surface and stays constant in time:

$$\rho_0 = \rho_p(\mathbf{r}, t) + \rho_n(\mathbf{r}, t), \quad (13.82)$$

where the proton density ρ_p and neutron density ρ_n vibrate around their equilibrium values $(Z/A)\rho_0$ and $(N/A)\rho_0$. We can therefore describe the process by the difference of the deviations of both densities:

$$\rho^{(1)}(\mathbf{r}, t) = \delta\rho_p(\mathbf{r}, t) - \delta\rho_n(\mathbf{r}, t). \quad (13.83)$$

In the following, we assume that this is small compared to ρ_0 and derive equations in linear order of $\rho^{(1)}$. We can therefore linearize Eqs. (13.78), which yields for the equation of continuity,

$$\frac{\partial \rho^{(1)}}{\partial t} + \rho_0 \nabla \cdot \mathbf{u} = 0, \quad (13.84)$$

where \mathbf{u} is the velocity field which corresponds to $\rho^{(1)}$; for the Euler equation we obtain

$$\frac{\partial \mathbf{u}}{\partial t} = -\frac{1}{m} \nabla \frac{\delta^2 e[\rho]}{\delta \rho^2} \rho^{(1)}, \quad (13.85)$$

where we used the fact that $\rho^{-1} m (\partial/\partial \mathbf{r}) P = (\hbar^2/2m)(\partial/\partial \mathbf{r})(\delta/\delta \rho) \tau[\rho]$, taking for P expression (13.81) and for $\tau[\rho]$ the Thomas-Fermi expression (13.32); that is, we have assumed an isotropic momentum distribution (13.76). Together with the force term in (13.78), we can combine this to the total energy density $e[\rho] = \tau + v$. The energy density can in this case be obtained from the Bethe-Weizsäcker formula (1.4); the only term therein depending on $\rho^{(1)}$ is the symmetry energy.

$$a_I \int_V \frac{(\rho_n - \rho_p)^2}{\rho_0} d^3 r = a_I \frac{(N-Z)^2}{A} + \frac{a_I}{\rho_0} \int_V (\rho^{(1)})^2 d^3 r, \quad (13.86)$$

where we used $\int \rho^{(1)} d^3 r = 0$.

With (13.84), (13.85), and (13.86) we therefore get the following hydrodynamical wave equation for the dipole state.

$$\left(\Delta - \frac{1}{c^2} \frac{\partial^2}{\partial t^2} \right) \rho^{(1)} = 0; \quad c^2 = \frac{2a_I}{m}. \quad (13.87)$$

We have to solve this equation with the proper spherical boundary condition, namely that there is no outgoing current at the nuclear surface. We therefore decompose $\rho^{(1)}(\mathbf{r}, t)$ into its Fourier components $\rho^{(1)}(\mathbf{r}, k)$ with

respect to time ($\omega = kc$). The angular dependence of $\rho^{(1)}$ is represented by spherical harmonics $Y_{\lambda\mu}$. We find that the lowest eigenvalues are realized for dipole vibrations ($\lambda = 1$). The corresponding radial equation has spherical Bessel functions as solutions. For the transition density we get

$$\rho^{(1)}(r, k) \propto j_1(kr) Y_{1\mu}(\vartheta, \varphi). \quad (13.88)$$

The boundary condition that there is no radial current at the nuclear surface,

$$\frac{\partial \rho^{(1)}}{\partial r} \Big|_{r=R_0} \propto \frac{\partial}{\partial r} j_1(kr) \Big|_{r=R_0} = 0, \quad (13.89)$$

can only be satisfied for discrete k values. The lowest solution of this equation is

$$k_0 R_0 = 2.08,$$

yielding the frequency

$$\omega_0 = \frac{2.08c}{R_0}. \quad (13.90)$$

With $R_0 = r_0 A^{-1/3}$, (1.2), and (1.87), we obtain

$$\omega_0 = \frac{2.08}{r_0} \left(\frac{2a_1}{m} \right)^{1/2} A^{-1/3} \approx 70 A^{-1/3} [\text{MeV}], \quad (13.91)$$

that is, the model gives roughly the right A dependence and almost the correct magnitude of ω_0 (see below).

The Goldhaber-Teller model can be best treated within the Tassie model [Ta 56a] for an inhomogeneous irrotational and incompressible fluid. The nucleus is supposed to vibrate around its spherical equilibrium position $\rho_0(r)$ and from (1.24–1.26), using the equation of continuity in linearized form, we get

$$\begin{aligned} \delta\rho &= -\nabla(\rho_0(r)\mathbf{u}(r)) \\ &= -\frac{\partial\rho_0}{\partial r}\mathbf{u}_r = -\frac{\partial\rho_0}{\partial r}\frac{\partial\Phi}{\partial r}. \end{aligned} \quad (13.92)$$

Taking the Fourier transform with respect to time, together with the expansion (1.27), we obtain the following expression for the transition density of multipole order λ .

$$\delta\rho_\lambda \propto \lambda r^{\lambda-1} Y_{\lambda 0} \frac{\partial\rho_0}{\partial r}, \quad \lambda \neq 0. \quad (13.93)$$

The term $\lambda = 0$ is excluded because we obviously cannot treat the monopole vibration with the assumption of incompressibility. A similar expression (8.175), however, is obtained for the $\lambda = 0$ case in the Wernitz-Überall model [WU 66].

For the $\lambda = 1$ (dipole) case, the Tassie model corresponds to the Goldhaber-Teller model because of the assumption of incompressibility.

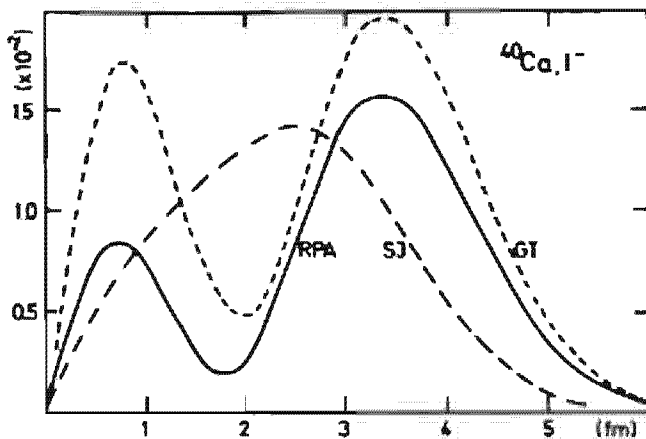


Figure 13.11. Transition densities for the dipole state of ^{40}Ca . The full curve stands for the transition density for the most collective dipole state of ^{40}Ca in the RPA. The dotted and dashed curves show those of the Goldhaber-Teller and Steinwedel-Jensen model, respectively. (From [SR 77].)

Then the only possible dipole motion is that shown in Fig. 13.10b. The A dependence of the excitation energy of the Goldhaber-Teller model is predicted [GT 48] to be $A^{-1/6}$. Experimentally we find that for light nuclei the dependence can be fitted by an $A^{-1/6}$ law, whereas for heavy nuclei it is a mixture of the Goldhaber-Teller and Steinwedel-Jensen types of motion. A more detailed investigation has been given by Myers et al. [MSK 77]. From sum rule considerations (Sec. 8.7.4), we know that the excitation operators for the Bohr-Tassie (Goldhaber-Teller) models are given by $F_\lambda = \sum r_i^\lambda Y_{\lambda 0}$, whereas in the Steinwedel-Jensen model they are given by $F_\lambda = \sum j_\lambda(kr_i) Y_{\lambda 0}$ [SR 77]. In Fig. 13.11 we compare the transition densities of the different models for the dipole state in ^{40}Ca with a microscopic RPA calculation. (For the relation of quantum mechanical densities with the $\rho^{(1)}$ defined here, compare Sec. 8.3.1.) We see that in this relatively light nucleus the vibration is mostly of the *GT* type. Similar comparisons in heavy nuclei [MSK 77] show that there the *SJ*-mode plays an increasingly important role.

From the above considerations, we see that ordinary hydrodynamics [isotropic momentum distribution (13.80, 13.81)] seems to work quite well for the explanation of the giant dipole resonances. We will see, however, in Section 13.3.6 that this, together with the breathing mode, is quite a special result, and that hydrodynamics have to be changed considerably in order to describe the giant resonances for all the other multipolarities.

The concept of isotropic momentum distribution has also been adopted by Holzwarth [Ho 77] and by Wong et al. [WMW 75, Wo 76, MWW 76, WWM 77, WM 77, WMW 77] to calculate the fluid dynamic counterpart of the TDHF slab collision discussed in Chapter 12. In Fig. 12.4 we show a comparison of both calculations for the final kinetic energy of relative motion of the outgoing slabs; zero kinetic energy means fusion. We see that below 7.6 MeV per projectile nucleon in the laboratory system, hydrodynamics always gives fusion, whereas TDHF gives resonant-like

scattering between 3.6 and 6.8 MeV and between 7.6 and 9 MeV. These "resonances" in the cross section are probably a typical quantum mechanical effect as discussed in Chapter 12, and can therefore not be reproduced by a semiclassical calculation. On the other hand, the semiclassical and quantum mechanical calculations are quite close to one another outside the resonance regions, as much in the final kinetic energies as in their density profiles. This, however, is essentially a one-dimensional calculation which cannot test what seems to be the main assumption of the ansatz (13.80), namely to give an *isotropic* momentum distribution.

We have discussed that the solution of (13.71) in the infinite matter case [KB 62, No 64a] gives an *anisotropic* momentum distribution. It seems difficult to obtain even approximately an analytic solution of (13.71) in the finite matter case, where first- and probably higher-order time derivatives of the potential are important. However, this we would need in order to close the system of equations (13.72–13.74).

Because of these difficulties, ordinary hydrodynamics has also been applied to more realistic situations. In any case, it is an interesting question whether for higher energies—for instance, in a heavy ion collision—the assumption of an isotropic momentum distribution, that is, local equilibrium, is not again a good approximation. Maruhn [Ma 77c] has performed a three-dimensional hydrodynamical calculation for the scattering of ^{16}O on ^{16}O with 18.8 MeV per nucleon in the laboratory system. He has also made a study of the Wigner distribution function of a full TDHF calculation for colliding slabs, which showed that at lower energies local equilibrium is not established. In view of this, and of what we have said about anisotropic momentum distribution above, the interpretation of low-energy ordinary hydrodynamics results should be done with great care.

Before we discuss more about this, let us first give a somewhat different derivation of fluid dynamical equations, which has some interesting aspects.

13.3.4 Variational Derivation of Fluid Dynamics

As we discussed in Chapter 12, quantum mechanics can be derived from a time-dependent variation principle [KK 76],

$$\delta I = 0,$$

where I is the action integral over the following time dependent Lagrangian.

$$I = \int_{t_1}^{t_2} dt \mathcal{L}[\Psi, \Psi^*]; \quad \mathcal{L} = \langle \Psi | i\hbar \frac{\partial}{\partial t} - H | \Psi \rangle.$$

We will now make a special variational ansatz for $|\Psi\rangle$, which will lead us to fluid dynamic equations. The exact wave function can always be decomposed into real and imaginary parts in the following way (Φ_0, S real).

$$\Psi(1\dots A, t) = \Phi_0(1\dots A, t) e^{(im/\hbar)S(1\dots A, t)}. \quad (13.94)$$

Let us suppose that the phase is of the single-particle form

$$S(\mathbf{r}_1, \dots, \mathbf{r}_A, t) = \sum_{i=1}^A s(\mathbf{r}_i, t) = \int s(\mathbf{r}, t) \hat{\rho} d^3 r, \quad (13.95)$$

with (D.1),

$$\hat{\rho} = \sum_{i=1}^A \delta(\mathbf{r}_i - \mathbf{r}),$$

which means, for instance, that if $|\Psi\rangle$ is a Slater determinant, the phases of all single-particle states are the same:

$$\rho(\mathbf{r}, \mathbf{r}', t) = e^{i(m/\hbar)s(\mathbf{r}, t)} \rho_0(\mathbf{r}, \mathbf{r}', t) e^{-i(m/\hbar)s(\mathbf{r}', t)}, \quad (13.96)$$

$$\rho_0(\mathbf{r}, \mathbf{r}', t) = \sum_{i=1}^A |\varphi_i(\mathbf{r}, t)| |\varphi_i(\mathbf{r}', t)|.$$

Comparing (13.96) with Eq. (12.63), we see that the assumption (13.95) is equivalent to (Stringari [St 79] also treated nonlocal fields)

$$\langle \mathbf{r} | \chi | \mathbf{r}' \rangle = ms(\mathbf{r}, t) \delta(\mathbf{r} - \mathbf{r}'), \quad (13.97)$$

that is, (13.96) is justified if we achieve a decomposition of the density matrix (12.82) in such a way that χ is approximately local [we recall in this context that the decomposition (12.63) is not unique].

With (13.95) we obtain for the action integral:

$$\begin{aligned} I &= \int_{t_1}^{t_2} dt \left\{ \langle \Phi_0 | -ms | \Phi_0 \rangle + i\hbar \langle \Phi_0 | \dot{\Phi}_0 \rangle - \langle \Psi | H | \Psi \rangle \right\} \\ &= \int_{t_1}^{t_2} dt \left\{ -m \int d^3 r s(\mathbf{r}, t) \rho_0(\mathbf{r}, t) - \langle \Psi | H | \Psi \rangle \right\}, \end{aligned} \quad (13.98)$$

where because of (13.97) only the local ρ_0 enters. The term $\langle \Phi_0 | \dot{\Phi}_0 \rangle$ in (13.98) vanishes because $|\Phi_0\rangle$ corresponding to ρ_0 is time even. With (13.95), the expectation value of the Hamiltonian assumes the form:

$$\mathcal{H} = \langle \Psi | H | \Psi \rangle = \frac{m}{2} \int d^3 r \rho_0(\mathbf{r}, t) \mathbf{u}^2(\mathbf{r}, t) + E_{\text{intr}}, \quad (13.99)$$

with

$$\mathbf{u} = \nabla s \quad \text{and} \quad E_{\text{intr}} = \langle \Phi_0 | H | \Phi_0 \rangle = \int d^3 r e[\rho_0]. \quad (13.100)$$

In (13.99) we assumed the potential energy of H to be velocity independent (expression (13.99), however, is also correct for the Skyrme force in spite of its velocity dependence; see [GVV 76]). Integrating the first term of (13.98) by parts, we obtain

$$I = \int_{t_1}^{t_2} dt \left\{ m \int d^3 r s \dot{\rho}_0 - \int d^3 r \left(\frac{m}{2} \rho_0 \mathbf{u}^2 + e[\rho_0] \right) \right\} + C, \quad (13.101)$$

where I has taken on the form of a classical action integral [Go 59], with ρ_0 playing the role of the coordinate conjugate to the momentum. In (13.101)

we supposed that E_{intr} exists as a functional of the local density $\rho_0(r)$ [HK 64, MT 77].

Hamilton's equations, according to (13.101), are then

$$m\dot{\rho}_0 = \frac{\delta}{\delta s} \mathcal{K}, \quad (13.102a)$$

$$-m\dot{s} = \frac{\delta}{\delta \rho_0} \mathcal{K}. \quad (13.102b)$$

The first equation gives the equation of continuity ($\delta(\nabla s)^2 = 2\nabla s \delta \nabla s$; partial integration):

$$\dot{\rho}_0 = -\nabla(\rho_0 \nabla s) = -\nabla(\rho_0 u), \quad (13.103)$$

and the gradient of the second equation yields a Euler-like equation (13.78)

$$\frac{\partial u}{\partial t} + (u \nabla) u = -\frac{1}{m} \nabla \frac{\delta e[\rho_0]}{\delta \rho_0}. \quad (13.104)$$

Since u is a gradient of the potentials, the flow associated with (13.96) and (13.97) is irrotational, a direct consequence of our assumption (13.95). We consequently should only accept solutions of (13.104) with $\nabla \times u = 0$. The relation between variational formulation of fluid dynamics [GVV 76] and the one obtained from the Boltzmann equation is not obvious though certainly intimate. In any case, there remains the problem of how to close the system of equations—that is, in (13.73)—to find an appropriate $f^{(0)}$ to calculate the pressure tensor, and in (13.104) to construct the functional $e[\rho_0]$ for the dynamic case (we will see that knowing $f^{(0)}(t)$ also enables us to find the functional, so both problems are closely related).

13.3.5 Momentum Distribution of the Density ρ_0

In the preceding sections we conjectured several times that the assumption of a spherically symmetric momentum distribution for the fluid dynamic description of collective motion may not be valid for all cases. In Section 13.3.4 we saw that this concerns the calculation of the intrinsic energy E_{intr} (13.100) of the system, which enters as the potential energy in the fluid dynamic Hamiltonian of Eq. (13.99) very much in the same way as the constrained ground state enters as a potential of the Hamiltonian of the ATDHF theory (12.80). We consider, therefore, the density ρ_0 with which we have to calculate E_{intr} from the time-even part of the dynamic density $\rho(t)$. As in the ATDHF case, therefore, we should be able to calculate ρ_0 from a static *time-even** single-particle potential, and for the moment, in order to fix our ideas, we wish to think of a quadrupole constraint.

* By static we mean here that the time enters only in a trivial way in the sense that the constraint is different at different times, but at each moment we can solve a time-independent (static) Schrödinger equation for the calculation of ρ_0 [it need not necessarily correspond to the ground state density in this potential (cf. Chap. 12)].

Suppose we start from the ground state of A nucleons in a spherical (harmonic oscillator*) potential and start to deform it. As long as the deformations are so small (see the Nilsson diagram—Fig. 2.21) that there are *no level crossings* and all particles remain in their original orbits. However, because the wave functions are squeezed in one direction the momenta of the nucleons in this direction will be higher than along the long axis of the deformation. Therefore, if we stay in the same levels for all deformations and calculate the corresponding momentum distribution we will find that it depends strongly on the deformation. However, if we want the system to stay in its ground state, at each level crossing we must redistribute the particles in such a way that only the lowest levels are occupied. The reason the levels come down in the deformed potential is the fact that the corresponding wave functions are better adapted to the actual shape of the potential. However, this means that the wave functions, after redistributing the particles among the lowest levels, are less squeezed, consequently the momentum distribution becomes almost spherical again. Since the level crossings are quite frequent, we understand that the momentum distribution stays quite isotropic over the whole range of deformations *if* the system stays in the ground state of the deformed potential.

This fact can be analytically checked using the harmonic oscillator or semiclassically by using the three-dimensional locally harmonic form of the propagator (13.66) in Wigner space, for example, for a deformed Woods-Saxon potential, and calculating the corresponding momentum distribution using (13.11) and the saddle point method (13.2.4). We will find that, even for quite large deformations, the momentum distribution stays almost spherical, and that in any case it is a small effect.

The essential question now is whether in a (adiabatic) dynamic process the particles always stay in the ground state of the Hamiltonian $h(\rho_0)$ to at least a good approximation. This question is of course very much related to the adiabaticity of the process, and in ATDHF-theory (Sec. 12.3.1) we have seen that in the large amplitude case $[h(\rho_0), \rho_0] \propto \chi^2$ —that is, if we start at $t = 0$ with the system in its ground state $\rho_0(t = 0)$ —the system will in the course of time stay almost in the ground state if χ (the momentum) is small. We may therefore also say that the deviation from sphericity of the momentum distribution is a measure of the non-adiabaticity of the process. Whether adiabaticity is fulfilled for even the slowest imaginable process, spontaneous fission, is presently an open question. On the other hand, it is clear that the faster the process, the more particles will stay in the up-going (nonadapted) levels, as a quick glance at the Landau-Zener formula (12.149) shows. Therefore, the faster the process the greater the deformation of the momentum distribution.[†] In this sense we say that a deformed

* We like to think of a harmonic oscillator, because for this potential all the statements we are going to make may be verified analytically.

[†] Only for very high energies of the system, where the mean free path of the nucleons becomes much smaller than the nuclear dimensions, may the momentum distribution again equilibrate due to the frequent two-body collisions.

momentum distribution corresponding to ρ_0 is a dynamic effect. For which processes this is an important effect is presently the subject of intensive study.

There is, however, one kind of collective motion where the deformation of the momentum sphere is known [SH 78, HE 78] to play an essential role: the giant resonances, because their deformations are so small that there will be no level crossings. Since a deformed momentum distribution yields a higher kinetic energy than a spherical one, this effect will influence the spring constant of these harmonic vibrations (Chap. 8). In the deformation of the momentum sphere all particles are participating, therefore this is a volume effect leading to the characteristic $A^{-1/3}$ -dependence of, for instance, the giant quadrupole resonance, which is in contrast to the original estimate of the liquid drop model (Sec. 1.4).

A deformed momentum sphere can, of course, also be simulated semiclassically in taking, for example, instead of the Thomas-Fermi expression (13.80) one which has *locally*—that is, at a certain place q in the nucleus—a deformed momentum distribution:

$$f^0 = \Theta\left(\lambda(q) - \frac{1}{2m}(ap_x^2 + bp_y^2 + cp_z^2)\right); \quad \lambda(q) = \lambda - V(q).$$

How such an expression can be derived mathematically will be shown in the following.

The time-even part ρ_0 of the density matrix (see above and Chap. 12) can always be expressed by the equilibrium density matrix $\bar{\rho}$ in the following form (12.66).

$$\rho_0(t) = e^{-(i/\hbar)\varphi(t)} \bar{\rho} e^{(i/\hbar)\varphi(t)}, \quad (13.105)$$

where φ is a Hermitian and time-odd operator. As an explicit example, we can consider a ρ_0 corresponding to a time-even Slater determinant; then (13.105) is simply a consequence of the Thouless theorem (E.26). The Wigner transform $\varphi = \varphi(q, p, t)$ is real and (cf. Sec. D.4) odd in p . If we suppose, as we did in the case of χ (13.97), that the nonlocality of φ is weak, then we can expand in powers of p and stop after the first term:

$$\varphi(q, p, t) \approx Q(q, t)p + \dots \quad (13.106)$$

With this approximation, we get for the equation of continuity:

$$\begin{aligned} \dot{\rho}_0(q, t) &= \frac{-i/\hbar}{(2\pi\hbar)^3} \int d^3p [\dot{\varphi}, \rho_0]_W \\ &= -\rho_0(q, t) \frac{\partial Q}{\partial q} - Q \frac{\partial \rho_0(q, t)}{\partial q} + O(\hbar^2), \end{aligned} \quad (13.107)$$

where we used the expression (D.59) for the Wigner transform of a commutator. Comparison with (13.103) shows that with (13.106) we have, to lowest order, the following relation between Q and s .

$$\dot{Q}(q, t) = \nabla s(q, t) = u. \quad (13.108)$$

The Wigner transform of (13.105) is given by the product rule (13.36) as:

$$f_0(\mathbf{q}, \mathbf{p}, t) = \left[(e^{-i\mathbf{p}/\hbar})_{\mathbf{w}} e^{i\mathbf{A}\hbar/\hbar} \bar{f}(\mathbf{q}, \mathbf{p}) \right] e^{i\mathbf{A}\hbar/\hbar} (e^{i\mathbf{p}/\hbar})_{\mathbf{w}}. \quad (13.109)$$

The evaluation of this expression with (13.106) is somewhat facilitated if we go over to the \mathbf{r} representation:

$$\rho_0(\mathbf{r}, \mathbf{r}', t) = \exp \left[-\frac{1}{2} (\nabla_r \mathbf{Q}(\mathbf{r}) + \mathbf{Q}(\mathbf{r}) \nabla_r + \nabla_{r'} \mathbf{Q}(\mathbf{r}') + \mathbf{Q}(\mathbf{r}') \nabla_{r'}) \right] \bar{\rho}(\mathbf{r}, \mathbf{r}'), \quad (13.110)$$

where ∇_r acts on every function to its right. From (13.110) we see that the approximation (13.106), means for a position independent \mathbf{Q} nothing but a scaling of the coordinates of the static density with a time-dependent velocity field $\mathbf{Q} : \mathbf{r} \rightarrow \mathbf{r}(t) = \mathbf{r} - \mathbf{Q}(t)$. The form (13.110) for ρ_0 is exactly what has been proposed by Holzwarth and Eckart [HE 78, 79]. Transforming (13.110) to relative and center of mass coordinates (\mathbf{s}, \mathbf{q}) , we obtain for the operator in the exponent up to second order in s :

$$\begin{aligned} \frac{1}{2} (\nabla \mathbf{Q} + \mathbf{Q} \nabla)_{\mathbf{q}+(s/2)} + \frac{1}{2} (\nabla \mathbf{Q} + \mathbf{Q} \nabla)_{\mathbf{q}-(s/2)} &= \nabla_{\mathbf{q}} Q_i(\mathbf{q}) + s_k Q_{ik}(\mathbf{q}) \nabla_{s_k} \\ &\quad + \frac{1}{2} \nabla_{\mathbf{q}} Q_{ijk}(\mathbf{q}) s_j s_k, \end{aligned} \quad (13.111)$$

where we adopted the notation that we have to sum over indices, figuring twice ($i = 1, 2, 3$), and

$$Q_{ijk\dots} = \dots \nabla_{q_i} \nabla_{q_j} Q_i(\mathbf{q}). \quad (13.112)$$

Using the expression (13.111) up to first order in s only, the density (13.110) can be brought into the general form (see footnote page 412):

$$\rho_0\left(\mathbf{q} + \frac{\mathbf{s}}{2}, \mathbf{q} - \frac{\mathbf{s}}{2}\right) \equiv \rho_0(\mathbf{q}, \mathbf{s}) = \exp(\nabla_{\mathbf{q}} Q_i) \exp(s_k A_{ik} \nabla_{s_k}) \bar{\rho}(\mathbf{q}, \mathbf{s}), \quad (13.113)$$

where the matrix A is given by:

$$A_{ik} = Q_{ik}(\mathbf{q}, t) - \frac{1}{2} Q_j Q_{ikj} + \dots \quad (13.114)$$

The Wigner transform (13.33) of the density

$$f_0(\mathbf{q}, \mathbf{p}, t) = \int d^3 s \rho_0(\mathbf{q}, \mathbf{s}) e^{-i\mathbf{p}\mathbf{s}/\hbar}$$

can now be calculated from (13.113) by partial integration to yield for (13.109):

$$\begin{aligned} f_0(\mathbf{q}, \mathbf{p}, t) &= \exp(\nabla_{\mathbf{q}} Q_i) \exp(-A_{ii}) \int d^3 s \bar{\rho}(\mathbf{q}, \mathbf{s}) e^{i s_k A_{kk} \nabla_{s_k}} e^{-i \mathbf{p} \mathbf{s} / \hbar} e^{-s_k A_{kk} \nabla_{s_k}} \cdot 1 \\ &= \exp(\nabla_{\mathbf{q}} Q_i) \exp(-A_{ii}) \int d^3 s \bar{\rho}(\mathbf{q}, \mathbf{s}) \exp \left[\frac{i}{\hbar} \mathbf{p} e^{i s_k A_{kk} \nabla_{s_k}} \mathbf{s} e^{-i s_k A_{kk} \nabla_{s_k}} \right] \cdot 1 \\ &= \exp(\nabla_{\mathbf{q}} Q_i) \exp(-A_{ii}) \int d^3 s \bar{\rho}(\mathbf{q}, \mathbf{s}) \exp \left[-\frac{i}{\hbar} p_k (e^{-A})_{kl} s_l \right] \\ &= \exp(\nabla_{\mathbf{q}} Q_i) \exp(-A_{ii}) \bar{f}(\mathbf{q}, \bar{\mathbf{p}}) \end{aligned} \quad (13.115)$$

where $f(\mathbf{q}, \bar{\mathbf{p}})$ is the Wigner transform of the density matrix $\bar{\rho}$ with the

momentum p replaced by

$$\tilde{p}_i = p_k (e^{-A})_{ki}. \quad (13.116)$$

From (13.115) and (13.116) we see that, to lowest order in the momentum expansion of φ (13.106), the Wigner transform of the time-even density ρ_0 can essentially be generally described by a deformation of the originally spherical momentum sphere of $\bar{\rho}$. This is exactly what we discussed at the beginning of this section. The treatment presented here is only valid for very small amplitude vibrations, because otherwise a scaling of the coordinates or the first-order expansion (13.106) is not valid. We thus have a semiclassical theory which should allow us to correctly calculate the features of the giant resonances. This will be shown in the next section.

In order to do this we first have to close the system of hydrodynamical equations. Using in (13.115) the Thomas-Fermi expression

$$\tilde{f}_{TF} = \Theta\left(\lambda - \frac{\tilde{p}^2}{2m} - \frac{\delta v[\rho_0]}{\delta \rho_0}\right), \quad (13.117)$$

we can calculate the pressure tensor (13.73), and together with (13.108) we obtain a closed system. For the case of the variational fluid dynamic equations (13.104), we have to calculate the functional $v[\rho_0]$, for instance, the functional $\tau[\rho_0]$. We will see that this is also possible using expression (13.115) and find that it will be different from the functional (13.57), which was derived under the assumption of a (almost) spherical momentum distribution.

13.3.6 Imposed Fluid Dynamic Motion

The velocity field \mathbf{u} should, of course, be given by the solution of the fluid dynamic equations [EH 79, EHS 80]; in order to get an idea of what is going on, several authors [Be 74, 75, BS 76, SH 78, KTB 80, SBB 80, JL 80] studied the much less complicated problem of fluid motion, where one assumes certain types of \mathbf{Q} fields; that is, the motion is imposed on the system [HE 78]. In Sec. 8.7 we have discussed that fields of the dipole or quadrupole type should come quite close to reality anyway because of some rule arguments. In order to keep things as simple as possible, we additionally assume that $\mathbf{Q}(\mathbf{r}, t)$ approximately factorizes in the case of small amplitude motion:

$$\mathbf{Q}(\mathbf{r}, t) = \alpha(t) \mathbf{v}(\mathbf{r}). \quad (13.118)$$

The velocity field \mathbf{v} can now be chosen to be of the monopole, dipole, quadrupole, etc. form* (the fact that the dimensions are not the ones of a

* A further very interesting example of a velocity field is the so-called twist mode (cf. Chap. 8) with $\mathbf{v} = (yz, -xz, 0)$ [HE 77, 79]. It turns out that the local density stays unchanged, and only the momentum distribution becomes distorted (twisted).

velocity is only for convenience):

$$\begin{aligned} L=0: \quad \mathbf{v}_0 &= \mathbf{r} = \nabla \frac{r^2}{2}; \\ L=1: \quad \mathbf{v}_1 &= (0, 0, 1) = \nabla z; \\ L=2: \quad \mathbf{v}_2 &= (-x, -y, 2z) = \frac{1}{2} \nabla (2z^2 - x^2 - y^2). \end{aligned} \quad (13.119)$$

As in (13.108) we see that the velocity fields can be expressed as the gradient of a potential and the motion will therefore be irrotational.

With (13.118) and (13.119) it is easy to calculate the distorted momenta (13.116) for the constrained motion:

$$\tilde{\mathbf{p}}_{L=0} = \begin{pmatrix} e^{-\alpha} & 0 & 0 \\ 0 & e^{-\alpha} & 0 \\ 0 & 0 & e^{-\alpha} \end{pmatrix} \cdot \mathbf{p}; \quad \tilde{\mathbf{p}}_{L=1} = \mathbf{p}; \quad \tilde{\mathbf{p}}_{L=2} = \begin{pmatrix} e^\alpha & 0 & 0 \\ 0 & e^\alpha & 0 \\ 0 & 0 & e^{-2\alpha} \end{pmatrix} \quad (13.120)$$

Thus we see that the momentum sphere stays spherical in the monopole case because of symmetry arguments; it also stays spherical in the dipole case because \mathbf{v}_1 does not depend on \mathbf{r} ; in the quadrupole case, however, we get a highly non-isotropic momentum distribution. From (13.117) we obtain:

$$\tilde{p}^2 < 2m(\lambda - V) \equiv p_F^2(\mathbf{q}, t). \quad (13.121)$$

Introducing polar coordinates for the momentum in the quadrupole case yields

$$p^2(e^{2\alpha} \sin^2 \theta_p + e^{-4\alpha} \cos^2 \theta_p) < p_F^2$$

or

$$p^2 < \frac{p_F^2}{e^{2\alpha} \sin^2 \theta_p + e^{-4\alpha} \cos^2 \theta_p} \approx p_F^2 \left(1 + \alpha(t) \sqrt{\frac{16\pi}{5}} Y_{20}(\theta_p) \right)^2, \quad (13.122)$$

that is, we obtain to lowest order in $\alpha(t)$ a time-dependent quadrupole deformation of the Fermi sphere. We should note, however, that this quadrupole deformation of the local momentum sphere is, to lowest order, characteristic for all kinds (apart from $L=0, 1$) of surface oscillations, and not just for the quadrupole vibration alone. This can be seen from the general expression (13.116) [HE 78] and understood by the general argument that ρ_0 must be even in \mathbf{p} , that is, the momentum distribution must be symmetric with respect to an inflection of \mathbf{p} at the origin; the distribution is thus mainly of ellipsoidal shape. It should also be noted that the ellipse of the momenta is perpendicular to the one of the density for the $L=2$ case (see (13.135)). In a more heuristic way this can immediately be understood from the uncertainty principle.

The ansatz [(13.118) and (13.119)] imposes the form of the velocity field but leaves the time dependence $\alpha(t)$ open. We can use the fluid dynamic equations (13.102) for its determination. For this purpose we have to determine the functional $\tau[\rho_0]$ in the dynamic case; we present it here for the special case of the imposed fields (13.119), but the derivation can be easily generalized to arbitrary velocity fields. The kinetic energy density is given by (D.58):

$$\hbar^2 \tau_0(\mathbf{q}, t) = \frac{\hbar^2}{(2\pi\hbar)^3} \int d^3p \tau_0(\mathbf{q}, \mathbf{p}, t) \equiv \frac{2}{(2\pi\hbar)^3} \int d^3p p^2 f_0(\mathbf{q}, \mathbf{p}, t).$$

With the volume element in momentum space

$$d^3p = d^3\tilde{p} \det(\partial p_i / \partial \tilde{p}_k) = d^3\tilde{p} e^{4\alpha}, \quad (13.123)$$

and using (13.115) together with (13.116) and (13.119), we obtain

$$\tau_0 \equiv \tau_{0\alpha} = \frac{2}{(2\pi)^3} \frac{1}{\hbar^5} e^{\alpha v_L(q)} \nabla_r \int d^3\tilde{p} p^2 \bar{f}(q, \tilde{p}) e^{4\alpha}. \quad (13.124)$$

In order to calculate the integral in (13.124) we have to express p^2 by \tilde{p}^2 , which can be achieved by inverting the relations (13.120):

$$p_{L=0}^2 = e^{2\alpha} \tilde{p}^2, \quad p_{L=1}^2 = \tilde{p}^2, \quad (13.125)$$

$$p_{L=2}^2 = \tilde{p}^2 \left[\frac{2}{3} e^{-2\alpha} + \frac{1}{3} e^{4\alpha} + (e^{4\alpha} - e^{-2\alpha}) \frac{1}{3} \sqrt{\frac{16\pi}{5}} Y_{20}(\theta_{\tilde{p}}) \right].$$

With the Thomas-Fermi approximation (13.117) for \bar{f} in (13.124), we get the dynamic kinetic energy density expressed in terms of the kinetic energy density $\bar{\tau}$ corresponding to the density matrix $\bar{\rho}$ (13.105)

$$\tau_{0\alpha}(r, t) = e^{4\alpha} W_L(\alpha) e^{\alpha v_L} \nabla_r \bar{\tau}(r), \quad (13.126)$$

with

$$W_{L=0} = e^{2\alpha}, \quad W_{L=1} = 1, \quad W_{L=2} = \frac{1}{3}(2e^{-2\alpha} + e^{4\alpha}). \quad (13.127)$$

Integrating (13.126) over r and integrating by parts, we obtain:

$$\int d^3r \tau_{0\alpha} = W_L(\alpha) \int d^3r \bar{\tau}(r). \quad (13.128)$$

In the expressions (13.126) and (13.128), all the deformation dependence has been separated out and for $\bar{\tau}$ we can now use the functional derived under the assumption of a spherical momentum distribution (13.57). (Actually, we derived (13.126) only for the pure Thomas-Fermi case, but if we neglect the angle dependence of the potential energy we can show that (13.126) also holds in the case of the extended Thomas-Fermi theory [HE 78].)

From (13.108) and (13.118) we have

$$\nabla s = \dot{\alpha} v_L \quad (13.129)$$

and the Hamiltonian (13.99) is therefore quadratic in the velocities $\dot{\alpha}$. Expanding E_{int} (13.100) up to α^2 (small amplitude motion), Eq. (13.99) takes the form of a harmonic oscillator, and we can calculate the frequency Ω with which the nucleus vibrates if the motion (13.119) is imposed:

$$\Omega^2 = \frac{C}{B}, \quad (13.130)$$

with

$$B = m \int d^3r \bar{\rho}(r) v_L^2(r), \quad (13.131)$$

$$C = \left. \frac{\partial^2}{\partial \alpha^2} E_{\text{int}} \right|_{\alpha=0}. \quad (13.132)$$

We immediately see that the coefficient B corresponds to the one we derived in Chapter 1.4, Eq. (1.30), for irrotational flow. The restoring force

C has two contributions: one which comes from the kinetic energy ($E_{kin} = \int \tau + \int v$) and one from the potential energy, $C = C_r + C_s$. The part C_r , which comes from the kinetic energy can be calculated from (13.127) and (13.128):

$$C_r = \frac{\hbar^2}{2m} \frac{\partial^2}{\partial \alpha^2} \int d^3r \tau_{0\alpha} \Big|_{\alpha=0} = \frac{\hbar^2}{2m} \begin{cases} 4 \int d^3r \bar{\tau} & L=0, \\ 0 & L=1, \\ 8 \int d^3r \bar{\tau} & L=2. \end{cases} \quad (13.133)$$

In the case of the quadrupole vibration we obtain $B = m \int d^3r \bar{\rho}(r) r^2 (2 - Y_{20}) = 2mA \langle r^2 \rangle$ and therefore, for the collective frequency,

$$\Omega_{L=2}^2 = \frac{4\langle T \rangle}{mA \langle r^2 \rangle} + \frac{C_e}{mA \langle r^2 \rangle}. \quad (13.134)$$

The first term agrees with the sum rule result (8.166) and gives the correct A dependence, $\hbar\Omega_{L=2} \approx 60A^{-1/3}$ [MeV] (8.167); to the second term are contributing only surface terms. This can be shown in the following manner. With (13.115) and (13.123) we have

$$\begin{aligned} \rho_0(\mathbf{q}, t) &= \frac{2}{(2\pi\hbar)^3} \int d^3p f_0(\mathbf{q}, \mathbf{p}, t) = \exp(\nabla_{\mathbf{q}} Q_i) \frac{2}{(2\pi\hbar)^3} \int d^3\tilde{p} \tilde{f}(\mathbf{q}, \tilde{\mathbf{p}}) \\ &= \exp(\nabla_{\mathbf{q}} Q_i) \bar{\rho}(\mathbf{q}). \end{aligned} \quad (13.135)$$

For incompressible fluids ($\nabla \cdot \mathbf{v} = 0$) we obtain for arbitrary exponents σ

$$\rho^\sigma(\mathbf{r}, t) = (e^{\alpha \nabla \cdot \mathbf{v}} \bar{\rho}(\mathbf{r}))^\sigma = \bar{\rho}^\sigma(\mathbf{r} + \alpha \mathbf{v}) = e^{\alpha \nabla \cdot \mathbf{v}} \bar{\rho}^\sigma(\mathbf{r}), \quad (13.136)$$

and therefore:

$$\int d^3r \rho_0^\sigma(\mathbf{r}, t) = \int d^3r \bar{\rho}^\sigma(\mathbf{r}), \quad (13.137)$$

because from the exponential in (13.136) only the first term of its Taylor series contributes, the others being divergences of a vector field. The volume terms are thus α independent and do not contribute to the frequency. For the Skyrme force, only the terms of $v[\rho]$ containing derivatives of ρ —that is, surface terms—are different from zero in C_s ; these yield a small $A^{-1/2}$ contribution to the collective energy, which is therefore negligible in first approximation compared to the kinetic energy terms of (13.134).

We now have the gratifying result that for the quadrupole mode, taking into account the deformation of the momentum sphere, yields the same result as that from the energy weighted sum, where we also impose the motion (8.166) to be of the quadrupole form. Imposing the form of the mode in both cases means that this state is an eigenstate of the system, and consequently the sum rule is automatically exhausted by this state because all others are orthogonal to it.

The reason we do not get the correct excitation energy in the pure liquid

drop model (1.34) can therefore be traced back to the fact that there we did not take into account the influence of the deforming walls of the mean field on the velocity distribution of the particles. The latter gives rise to the volume dependence (13.134) of the excitation energy also in the case of surface vibrations, and thus we obtain the correct A dependence.

On the other hand, we saw in Section 13.2.3 that the ordinary hydrodynamics of the liquid drop model work well for the dipole case. This is confirmed in the present model. Because of the coordinate independence of the velocity field (13.119) for $L = 1$, no deformation of the momentum sphere occurs and the kinetic energy is the same in the static and dynamic case (13.128).

There is no contribution from the kinetic energy to the dipole excitation energy (13.133), and the fact that it nevertheless has a $A^{-1/3}$ dependence in the Steinwedel-Jensen model (Sec. 13.3.3) is only due to the fact that the restoring force comes from the symmetry energy (13.86). On the other hand, we should keep in mind that the dipole resonance is mostly of the Goldhaber-Teller type. The question of whether ordinary hydrodynamics is sufficient for the breathing mode can be decided by explicitly comparing the result we get with the functional $\tau[\rho]$ (13.57) to the one we obtained in (13.128). With (13.135), we obtain for this functional:

$$\tau_a = C_1 (e^{\alpha \nabla \cdot \mathbf{v}} \rho(\mathbf{r}))^{5/3} + C_2 \frac{(\nabla e^{\alpha \nabla \cdot \mathbf{v}} \rho(\mathbf{r}))^2}{e^{\alpha \nabla \cdot \mathbf{v}} \rho(\mathbf{r})} + \dots \quad (13.138)$$

Integrating over \mathbf{r} and integrating by parts gives the relation (13.128) for the first term in (13.138), so ordinary hydrodynamics can be used in the monopole case. We thus can conclude that $L = 0, 1$ modes can be treated in the usual liquid drop model, but for all $L \geq 2$ modes important modifications have to be included, due to the fact that a nucleus is a Fermi liquid rather than an ordinary fluid.

In a further step one should not, of course, impose the velocity field on the system, but rather this should come out as a solution of the fluid dynamic equations. A closed system of such equations can be obtained by either calculating the pressure tensor with (13.115) or in slightly generalizing the derivation of the functional $\tau[\rho]$ as it is given in Section 13.2.6, but without using the special ansatz (13.118) for the velocity field \mathbf{Q} [HE 78]. It will be very interesting to see how close these solutions will come to the one we imposed on the system by (13.119) [HE 79].

Other interesting questions in this context are whether or not the approximation of irrotational flow is justified, whether the theory developed so far can be applied not only to small amplitude vibrations but also, for example, to heavy ion collisions. In this context it is important to establish the relation of this fluid dynamic description with ATDHF because of the many points in common.

13.3.7 An Illustrative Example

In order to investigate the validity of the assumptions that go into the derivation of nuclear fluid dynamics, it is very instructive to consider the following exactly soluble example. Suppose we have an initial nuclear density which corresponds to the ground state of A nucleons of a *deformed* harmonic oscillator. We let this density start to move at $t=0$ in the corresponding *spherical* harmonic oscillator which is given by the condition $\omega_0^3 = \omega_x \omega_y \omega_z$. Since the wave functions of the deformed oscillator are not, of course, eigenfunctions of the spherical one, the solution of the corresponding Schrödinger equation will be time-dependent wave functions whose solutions are given by (10.89). Since the initial density as well as the time-dependent one will always be centered at the origin, the time dependence will only be a time-dependent scaling of the coordinates, that is, essentially a breathing of the width of the individual wave functions. Using the wave functions (10.89) we can write for the time dependent density [BS 79, SB 79]

$$\rho(\mathbf{r}, \mathbf{r}', t) = e^{(i/\hbar)\chi(\mathbf{r}, t)} \rho_0(\mathbf{r}, \mathbf{r}', t) e^{-(i/\hbar)\chi(\mathbf{r}', t)}, \quad (13.139)$$

with

$$\chi(\mathbf{r}, t) = \frac{m}{2} \frac{d}{dt} (\ln \xi_x x^2 + \ln \xi_y y^2 + \ln \xi_z z^2) \quad (13.140)$$

and

$$\xi_j^2 = (\sigma_j + \tau_j \cos \omega_0 t) \quad (j = x, y, z),$$

where σ and τ are defined in (10.89c). The density ρ_0 is of course the *time-even* part of ρ . Since ρ_0 can be written as (\bar{b}_j are measured in units of $b_0 = \sqrt{\hbar/m\omega_0}$)

$$\rho_0(\mathbf{r}, \mathbf{r}', t) = \rho_0 \left(\frac{x}{\bar{b}_x(t)}, \frac{y}{\bar{b}_y(t)}, \frac{z}{\bar{b}_z(t)}, \frac{x'}{\bar{b}_x(t)}, \frac{y'}{\bar{b}_y(t)}, \frac{z'}{\bar{b}_z(t)} \right), \quad (13.141)$$

we can express ρ_0 in the following way.

$$\rho_0(\mathbf{r}, \mathbf{r}', t) = e^{\frac{i}{\hbar}[\mathbf{Q}(\mathbf{r}, t) \nabla_{\mathbf{r}} + \nabla_{\mathbf{r}'} \mathbf{Q}]} \rho_{\text{stat}}(\mathbf{r}, \mathbf{r}') e^{-\frac{i}{\hbar}[\mathbf{Q} \tilde{\nabla}_{\mathbf{r}'} + \tilde{\nabla}_{\mathbf{r}} \mathbf{Q}]}, \quad (13.142)$$

where the arrows on the three-dimensional gradient operators indicate the direction in which they are acting and ρ_{stat} is the density matrix of the ground state of the A nucleons in the *spherical* harmonic oscillator. As we see from the relation $\exp(\alpha x \partial/\partial x) f(x) = f(e^\alpha x)$, the velocity field in this example is given by

$$Q_j = \alpha_j(t) \cdot \mathbf{v}(\mathbf{r}), \quad (j = x, y, z), \quad (13.143)$$

$$\alpha_j(t) = -\ln \bar{b}_j(t), \quad \mathbf{v}(\mathbf{r}) = \mathbf{r}. \quad (13.144)$$

From this example we see that the main assumptions for the derivation of fluid dynamic equations, namely that the operators χ (12.63) and φ (12.66)

are local and only slightly nonlocal, respectively, are exactly fulfilled in this model. Since, after all, a harmonic oscillator is not such a bad approximation, we should expect that also for more realistic cases, operators χ and φ can be found which are almost local. We should stress the point, however, that the χ as it is given in (13.140) is not equivalent to the definition of χ^{BV} of Baranger and Vénérond [BV 78]. On the contrary, χ^{BV} is rather nonlocal, even in this model. To give an estimate we calculate the Wigner transform of χ^{BV} to lowest order in \hbar which should, as usual, give the right order of magnitude for the nonlocality [see Eq. (D.24)]. For small χ 's and using (D.24) and the Hermiticity of X we obtain [SB 79]

$$\chi^{BV}(q, p) = \frac{\hbar^2}{2} \rho(q, p) \tilde{\Lambda} \rho(q, -p). \quad (13.145)$$

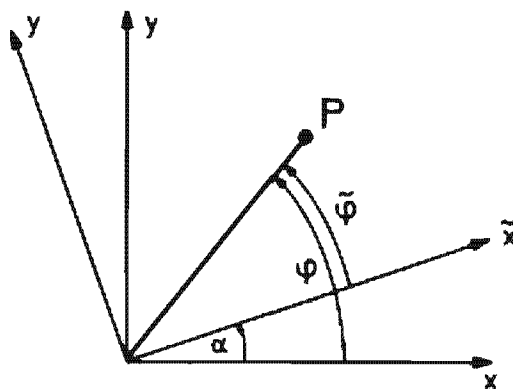
This means that the range of the nonlocality of χ^{BV} is of the same order as that for the density, which is usually quite large [~ 2 fm]. We conclude that the definition of χ as given by Baranger and Vénérond is not optimal for a fluid dynamic treatment, but it is an open question as to how to define the most local χ in general.

APPENDIX A

Angular Momentum Algebra in the Laboratory and the Body-Fixed System

Throughout the book we use the conventions and phases of Edmonds for angular momentum coupling [Ed 57]. The only place where we have to enter a little into details is the case of the transformation of angular momenta into the body-fixed system. We shall carry out this transformation in the sense of Edmonds [Ed 57, Chap. IV].

To study the transformation properties of wave functions in Hilbert space under a rotation of the coordinate system, we shall first investigate a simple one-dimensional example.



Let $f(\varphi)$ be a function, which only depends on the azimuth angle with respect to the z -axis of the system. For a rotation of this system through the angle α the azimuth of a fixed point P in space transforms into $\tilde{\varphi} = \varphi - \alpha$. Since the value of the function f at the fixed point P is not changed by a transformation of the coordinate system, the function f in the

old system transforms into a new function \tilde{f} in the new system with the property

$$\tilde{f}(\tilde{\varphi}) = f(\varphi) = f(\tilde{\varphi} + \alpha) = e^{i\omega J_z} f(\tilde{\varphi}) \quad (\text{A.1})$$

or, if we change the nomenclature and use φ instead of $\tilde{\varphi}$,

$$\tilde{f}(\varphi) = e^{i\omega J_z} f(\varphi) \quad \text{with } J_z = \frac{1}{i} \frac{\partial}{\partial \varphi}. \quad (\text{A.2})$$

In the general case of a three-dimensional rotation we use the *Euler angles* $\Omega = (\alpha, \beta, \gamma)$ as defined in [Ed 57, Chap. I]: Under a rotation of the coordinate frame around the angles Ω the wave function $|\Psi\rangle$ is transformed to

$$|\tilde{\Psi}\rangle = R(\Omega)|\Psi\rangle \quad (\text{A.3})$$

with the unitary *rotational operator*

$$R(\Omega) = e^{i\alpha J_x} e^{i\beta J_y} e^{i\gamma J_z}, \quad (\text{A.4})$$

where J_x, J_y, J_z act on the coordinates x_1, \dots, x_A . As discussed in [Ed 57], we can also include spin coordinates. J is then the sum of orbital angular momentum and spin.

Corresponding to the transformation (A.3) of vectors in the Hilbert space, we get a *transformation* for operators T :

$$T \rightarrow \tilde{T} = R T R^+ \quad (\text{A.5})$$

By definition, for a *spherical tensor operator* $T_{\lambda\mu}$ [Ed 57, Eq. (5.2.1)] we find

$$\tilde{T}_{\lambda\mu} = R(\Omega) T_{\lambda\mu} R^+(\Omega) = \sum_{\mu'} D_{\mu'\mu}^{\lambda}(\Omega) T_{\lambda\mu'}, \quad (\text{A.6})$$

where the *Wigner functions* $D_{\mu'\mu}^{\lambda}(\Omega)$ are given by

$$D_{\mu'\mu}^{\lambda}(\Omega) = \langle \lambda\mu' | R(\Omega) | \lambda\mu \rangle. \quad (\text{A.7})$$

We now wish to investigate a rotation Ω from the laboratory system (axis x, y, z) to a body-fixed system (axis 1, 2, 3) at some fixed time t . Keeping in mind that the angular momentum operators J_x, J_y, J_z are generators for the infinitesimal rotations around the axis x, y, z , we can represent these operators as differential operators in the Euler angles α, β, γ . For instance, we can achieve a rotation around the z -axis by an amount $\delta\varphi$ by diminishing the Euler angle α by $\delta\varphi$ without changing the body-fixed axis, that is,^{*}

$$L_z = -\frac{1}{i} \frac{\partial}{\partial \alpha} \hat{=} J_z. \quad (\text{A.8})$$

* In the following we shall denote the angular momentum operators expressed in terms of Euler angles by L_k ($k = x, y, z$). However, this does not mean that these operators only represent orbital angular momenta. The minus sign in Eq. (A.8) deviates from the usual representation of angular momenta in Euler angles [Ed 57, Eq. (2.2.2)]. The same change of sign occurs in the definition of the collective momentum operator $P = -(k/l)(\partial/\partial q)$ in Eq. (10.92).

In the same way, from the definition of the Euler angles [Ed 57] we get:

$$-\frac{1}{i} \frac{\partial}{\partial \beta} \hat{=} J_y = e^{i\alpha J_z} J_y e^{-i\alpha J_z} = \cos \alpha J_y + \sin \alpha J_x \quad (\text{A.9})$$

and

$$\begin{aligned} -\frac{1}{i} \frac{\partial}{\partial \gamma} \hat{=} J_z &= e^{i\alpha J_z} e^{i\beta J_z} J_z e^{-i\beta J_z} e^{-i\alpha J_z} \\ &= \cos \beta J_z - \sin \beta (\cos \alpha J_x - \sin \alpha J_y). \end{aligned} \quad (\text{A.10})$$

The inversion of (A.8)–(A.10) gives

$$\begin{aligned} L_x &:= \frac{1}{i} \left(-\cos \alpha \operatorname{ctg} \beta \frac{\partial}{\partial \alpha} - \sin \alpha \frac{\partial}{\partial \beta} + \frac{\cos \alpha}{\sin \beta} \frac{\partial}{\partial \gamma} \right) \hat{=} J_x, \\ L_y &:= \frac{1}{i} \left(\sin \alpha \operatorname{ctg} \beta \frac{\partial}{\partial \alpha} - \cos \alpha \frac{\partial}{\partial \beta} - \frac{\sin \alpha}{\sin \beta} \frac{\partial}{\partial \gamma} \right) \hat{=} J_y, \\ L_z &:= \frac{1}{i} \left(-\frac{\partial}{\partial \alpha} \right) \hat{=} J_z. \end{aligned} \quad (\text{A.11})$$

These are components of the angular momentum \mathbf{J} with respect to the axis x, y, z in the laboratory system. In the same way we can calculate the components of \mathbf{J} with respect to the body-fixed axis 1, 2, 3. To do this we use the fact that the spherical components L_μ , defined by

$$(L_\mu) = (L_{-1}, L_0, L_{+1}) := \left(\frac{1}{\sqrt{2}} (L_x - iL_y), L_z, \frac{-1}{\sqrt{2}} (L_x + iL_y) \right), \quad (\text{A.12})$$

form a spherical tensor of rank one. The spherical components of the angular momentum with respect to the body-fixed axis are therefore

$$I_\mu = \sum_{\mu'} D_{\mu' \mu}^1(\Omega) L_{\mu'} = \sum_{\mu'} L_{\mu'} D_{\mu' \mu}^1(\Omega). \quad (\text{A.13})$$

With the explicit form of $D_{\mu' \mu}^1(\Omega)$ [Ed 57, Eq. 4.1.15], after transforming back to cartesian components we gain

$$\begin{aligned} I_1 &= \frac{1}{i} \left(-\frac{\cos \gamma}{\sin \beta} \frac{\partial}{\partial \alpha} + \sin \gamma \frac{\partial}{\partial \beta} + \cos \gamma \operatorname{ctg} \beta \frac{\partial}{\partial \gamma} \right), \\ I_2 &= \frac{1}{i} \left(-\frac{\sin \gamma}{\sin \beta} \frac{\partial}{\partial \alpha} - \cos \gamma \frac{\partial}{\partial \beta} + \sin \gamma \operatorname{ctg} \beta \frac{\partial}{\partial \gamma} \right), \\ I_3 &= \frac{1}{i} \left(-\frac{\partial}{\partial \gamma} \right). \end{aligned} \quad (\text{A.14})$$

The components of \mathbf{J} in the body-fixed system have the following properties.

- (i) They commute with the components L_k in the laboratory system

$$[I_i, L_k] = 0 \quad \text{for } i = 1, 2, 3, \quad k = x, y, z. \quad (\text{A.15})$$

This means that the components $I_i = \mathbf{J} \cdot \mathbf{e}_i$ (where \mathbf{e}_i are unit vectors along the body-fixed axis) are scalars with respect to rotations in the laboratory frame.

(ii) They obey the commutation relations

$$[I_i, I_k] = -i \cdot I_l \quad \text{with } (i, k, l) \text{ cyclic } (1, 2, 3). \quad (\text{A.16})$$

They differ from the normal commutation relations for angular momenta by a minus sign.

The commutators of the operators L_k and I_i with the rotation operator $R(\Omega)$ (A.4) are given by

$$\begin{aligned} [L_x, R] &= -J_x \cdot R, & [I_1, R] &= -R \cdot J_x; \\ [L_y, R] &= -J_y \cdot R & [I_2, R] &= -R \cdot J_y; \\ [L_z, R] &= -J_z \cdot R & [I_3, R] &= -R \cdot J_z. \end{aligned} \quad (\text{A.17})$$

Now we are able to determine the tensor properties of the Wigner functions D_{MK}^{I*} under rotations around the axis in the laboratory and in the body-fixed frame. For the spherical components (A.12), we get

$$[L_\mu, D_{MK}^{I*}] = \sum_{M'} D_{M'K}^{I*} \langle IM' | J_\mu | IM \rangle \quad (\text{A.18})$$

and

$$[I_\mu, D_{MK}^{I*}] = \sum_{K'} D_{MK}^{I*} \langle IK | J_\mu | IK' \rangle. \quad (\text{A.19})$$

The functions D_{MK}^{I*} therefore behave like spherical tensors of rank I with the magnetic quantum number M under rotations of the laboratory frame. In particular, we get

$$\begin{aligned} [L_z, D_{MK}^{I*}] &= MD_{MK}^{I*} \\ [L_x \pm iL_y, D_{MK}^{I*}] &= \sqrt{I(I+1) - M(M \pm 1)} D_{M \pm 1 K}^{I*} \\ [I_3, D_{MK}^{I*}] &= KD_{MK}^{I*} \\ [I_1 \pm iI_2, D_{MK}^{I*}] &= \sqrt{I(I+1) - K(K \mp 1)} D_{MK \mp 1}^{I*}. \end{aligned} \quad (\text{A.20})$$

The normalized wave functions

$$|IMK\rangle = \sqrt{\frac{2I+1}{8\pi^2}} D_{MK}^{I*}(\Omega) \quad (\text{A.21})$$

are therefore eigenfunctions of J^2 , L_z ($\equiv J_z$), and I_3 ,

$$\begin{aligned} J^2|IMK\rangle &= I \cdot (I+1)|IMK\rangle, \\ L_z|IMK\rangle &= M|IMK\rangle, \\ I_3|IMK\rangle &= K|IMK\rangle, \end{aligned} \quad (\text{A.22})$$

and form a complete and orthogonal set in the space of the functions of the Euler angles [Ed 57, Chap. IV]:

$$\sum_{IMK} |IMK\rangle\langle IMK| = \delta(\Omega - \Omega'); \quad \langle IMK|I'M'K'\rangle = \delta_{II'} \cdot \delta_{MM'} \cdot \delta_{KK'}. \quad (\text{A.23})$$

From Eq. (A.17), for a rotation of 180° around the 1-axis we obtain

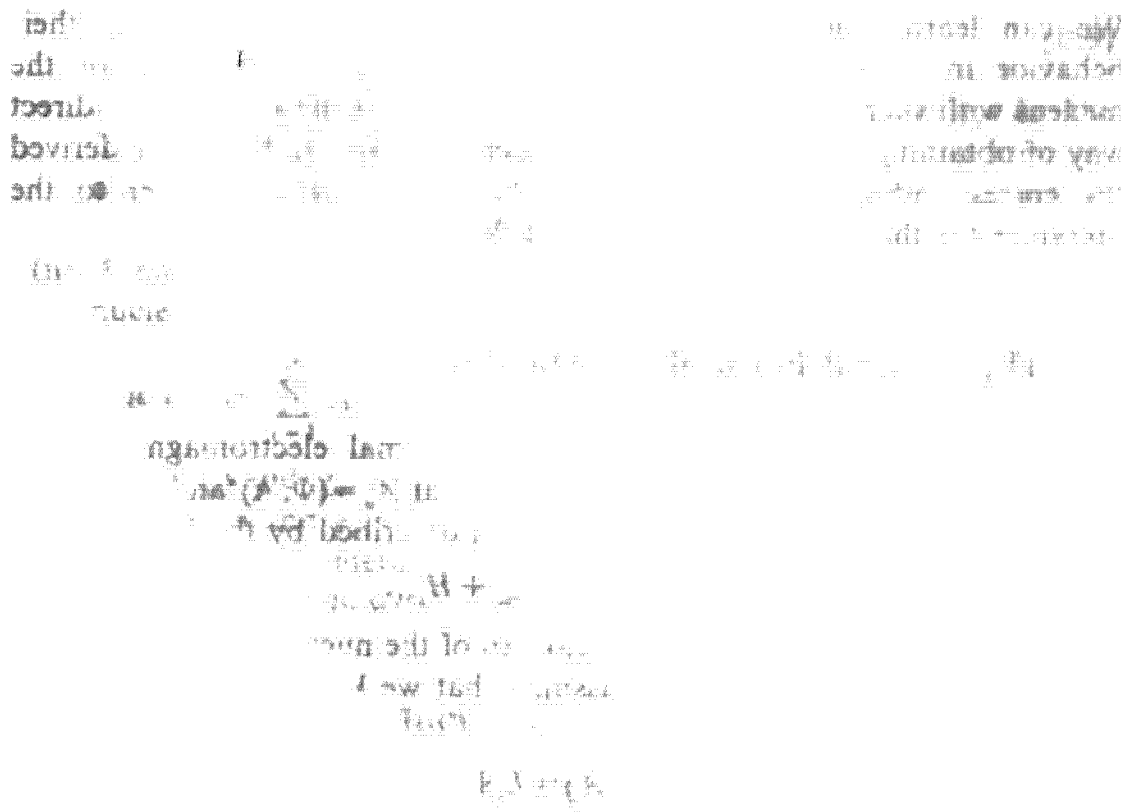
$$e^{i\pi I_1} D_{MK}^{I'}(\Omega) = \langle IM|R(\Omega)e^{-i\pi J_1}|IK\rangle^* = (-)^I \langle IM|R(\Omega)|I-K\rangle^*$$

or

$$e^{i\pi I_1}|IMK\rangle = (-)^I|IM-K\rangle, \quad (\text{A.24})$$

and similarly,

$$e^{i\pi J_2}|IMK\rangle = (-)^{I-K}|IM-K\rangle. \quad (\text{A.25})$$



APPENDIX B

Electromagnetic Moments and Transitions

We can learn much about the structure of nuclei by studying their behavior in an external electromagnetic field. The interaction of the nucleus with such a field is very well known, and is therefore a very direct way of obtaining information about a nucleus. Many authors have derived the corresponding formulae and we therefore refer the reader to the literature for the details (for example, [BW 52, Da 65a, SF 74]).

B.1 The General Form of the Hamiltonian

The system of a nucleus moving in an external electromagnetic field characterized by its four-dimensional potential $A_\mu = (\Phi, \mathbf{A})$ and the corresponding electromagnetic fields \mathbf{E} and \mathbf{B} is described by the Hamiltonian

$$H = H_{\text{nuc}} + H_{\text{field}} + H_{\text{int}}. \quad (\text{B.1})$$

It has three parts: H_{nuc} is the Hamiltonian of the nucleus, or at least some nuclear model Hamiltonian. We assume that we know its eigenfunctions $\Psi_i(1\dots A)$

$$H_{\text{nuc}}\Psi_i(1\dots A) = E_i\Psi_i(1\dots A). \quad (\text{B.2})$$

H_{field} is given by [Ja 62]

$$H_{\text{field}} = \frac{1}{8\pi} \int (\mathbf{E}^2(\mathbf{r}, t) + \mathbf{B}^2(\mathbf{r}, t)) d^3r. \quad (\text{B.3})$$

The interaction between the external field and the nucleus is

$$H_{\text{int}} = -\frac{1}{c} \int j_\mu A^\mu d^3r = \int \left(\rho(r, t) \Phi(r, t) - \frac{1}{c} \mathbf{j}(r, t) \cdot \mathbf{A}(r, t) \right) d^3r. \quad (\text{B.4})$$

$\rho(r, t)$ is the nuclear charge density:

$$\rho(r, t) = \sum_{i=1}^A e \left(\frac{1}{2} - \iota_3^{(i)} \right) \delta(r - r_i(t)). \quad (\text{B.5})$$

Here we have considered the nucleons as point particles. Actually, they have a finite extension which is given by a form factor. This could easily be introduced here [BM 69, App. 3C], but for reasons of simplicity we will disregard it in the following.

The current density $\mathbf{j}(r, t)$ in the nucleus is connected to the density $\mu(r, t)$ of the magnetic moment [Ja 62, Eq. 5.81] by

$$\mathbf{j}(r, t) = c \nabla \times \mu(r, t). \quad (\text{B.6})$$

It has two parts:

(i) An *orbit part*, which comes from the moving charges of the protons

$$j^o(r, t) = \sum_{i=1}^A e \left(\frac{1}{2} - \iota_3^{(i)} \right) \frac{1}{2} (\mathbf{v}_i \delta(r - r_i(t)) + \text{h.c.}) \quad (\text{B.7})$$

\mathbf{v}_i is given by

$$\mathbf{v}_i = \frac{i}{\hbar} [H, \mathbf{r}_i]. \quad (\text{B.8})$$

For velocity independent potentials, we get $\mathbf{v}_i = (1/m)\mathbf{p}_i$. In the following we will only consider this case. Again, (B.7) is an approximation that does not take into account the exchange current of pions; for a discussion of this point, see [SF 74].

(ii) A *spin part*, which has its origins in the spin distribution of the nucleus and is given by (B.6) and

$$\mu^s(r, t) = \sum_{i=1}^A \delta(r - r_i(t)) \frac{e\hbar}{2mc} \left\{ \left(\frac{1}{2} - \iota_3^{(i)} \right) g_p + \left(\frac{1}{2} + \iota_3^{(i)} \right) g_n \right\} \mathbf{s}_i, \quad (\text{B.9})$$

where g_p and g_n are the g -factors for free protons and neutrons ($g_p = 5.586$ and $g_n = -3.826$). Corrections for the exchange currents of pions are sometimes taken into account by using effective g -values. In the following, we use the nuclear magneton $\mu_N = e\hbar/2mc$.

B.2 Static Multipole Moments

The interaction with a static electromagnetic field causes a change of the nuclear energy in a state i , which is given in first-order perturbation theory by

$$\Delta E_i = \langle \Psi_i | H_{\text{int}} | \Psi_i \rangle. \quad (\text{B.10})$$

We introduce the density of the magnetic flux $\mathbf{B} = \nabla \times \mathbf{A}$ and we get from (B.4) and (B.6)

$$H_{\text{int}} = \int \rho(\mathbf{r}) \Phi(\mathbf{r}) d^3r - \int \mu(\mathbf{r}) \cdot \mathbf{B}(\mathbf{r}) d^3r. \quad (\text{B.11})$$

Since the sources of the external field are far from the nucleus, the quantities $\Phi(r)$ and $\mathbf{B}(r)$ fulfill the homogeneous Maxwell equations in the nuclear region.

$$\begin{aligned} \Delta \Phi(\mathbf{r}) &= 0, \\ \nabla \times \mathbf{B}(\mathbf{r}) &= 0, \\ \nabla \cdot \mathbf{B}(\mathbf{r}) &= 0. \end{aligned} \quad (\text{B.12})$$

This means that \mathbf{B} can be written as a gradient,

$$\mathbf{B}(\mathbf{r}) = -\nabla \Xi(\mathbf{r}), \quad (\text{B.13})$$

with

$$\Delta \Xi(\mathbf{r}) = 0. \quad (\text{B.14})$$

In spherical coordinates, the most general solution of the Laplace equation (B.12) and (B.14) which is not singular at the origin is given by

$$\Phi(\mathbf{r}) = \sum_{\lambda\mu} a_{\lambda\mu} r^\lambda Y_{\lambda\mu}(\theta, \varphi), \quad (\text{B.15})$$

$$\Xi(\mathbf{r}) = \sum_{\lambda\mu} b_{\lambda\mu} r^\lambda Y_{\lambda\mu}(\theta, \varphi), \quad (\text{B.16})$$

where $Y_{\lambda\mu}$ are spherical harmonics [Ed 57].

We find

$$H_{\text{int}} = \sum_{\lambda\mu} a_{\lambda\mu} \hat{Q}_{\lambda\mu} + b_{\lambda\mu} \hat{M}_{\lambda\mu} \quad (\text{B.17})$$

with the electric and magnetic multipole operators

$$\hat{Q}_{\lambda\mu} = \int \rho(\mathbf{r}) r^\lambda Y_{\lambda\mu}(\theta, \varphi) d^3r, \quad (\text{B.18})$$

$$\hat{M}_{\lambda\mu} = \int \mu(\mathbf{r}) \cdot \nabla (r^\lambda Y_{\lambda\mu}(\theta, \varphi)) d^3r. \quad (\text{B.19})$$

Before inserting the expressions (B.6) and (B.9) for the density and the current, we have to rewrite the operator $\hat{M}_{\lambda\mu}$ a little.

We use the relation

$$(\nabla \times (\nabla \times \mathbf{r})) r^\lambda Y_{\lambda\mu}(\theta, \varphi) = (\lambda + 1) \nabla (r^\lambda Y_{\lambda\mu}(\theta, \varphi)) \quad (\text{B.20})$$

and obtain, after integrating (B.19) by parts [the surface terms vanish because $\mu(\mathbf{r})$ is localized in the nucleus]:

$$\hat{M}_{\lambda\mu} = \frac{1}{\lambda + 1} \int (\mathbf{r} \times [\nabla \times \mu(\mathbf{r})]) \cdot [\nabla r^\lambda Y_{\lambda\mu}] d^3r \quad (\text{B.21})$$

$$= \frac{1}{c(\lambda + 1)} \int (\mathbf{r} \times \mathbf{j}(\mathbf{r})) \cdot [\nabla r^\lambda Y_{\lambda\mu}] d^3r. \quad (\text{B.22})$$

We now insert (B.5) into (B.18), (B.7) into (B.22), and (B.9) into (B.19), and find with $\mathbf{l}_i = (1/i)(\mathbf{r}_i \times \nabla_i)$,

$$\hat{Q}_{\lambda\mu} = e \sum_{i=1}^A \left(\frac{1}{2} - t_3^{(0)} \right) r_i^\lambda Y_{\lambda\mu}(\theta_i, \varphi_i), \quad (\text{B.23})$$

$$\hat{M}_{\lambda\mu} = \mu_N \sum_{i=1}^A \left\{ g_s^{(0)} \mathbf{s}_i + \frac{2}{\lambda+1} \cdot g_i^{(0)} \mathbf{l}_i \right\} \cdot (\nabla r^\lambda Y_{\lambda\mu}(\theta, \varphi))_{r=r_i}, \quad (\text{B.24})$$

with

$$\left. \begin{array}{ll} g_s^{(0)} = g_p \\ g_i^{(0)} = 1 \end{array} \right\} \quad \text{for protons,} \quad \left. \begin{array}{ll} g_s^{(0)} = g_n \\ g_i^{(0)} = 0 \end{array} \right\} \quad \text{for neutrons.}$$

In (B.24), the operator \mathbf{l}_i acts only on the coordinate \mathbf{r}_i in the wave function. It commutes with $\nabla r^\lambda Y_{\lambda\mu}$ because

$$\mathbf{l} \cdot (\nabla r^\lambda Y_{\lambda\mu}) \propto (\mathbf{r} \times \nabla) \cdot \nabla r^\lambda Y_{\lambda\mu} = \mathbf{r} \cdot (\nabla \times \nabla) r^\lambda Y_{\lambda\mu} = 0. \quad (\text{B.25})$$

The expectation values of these operators in a nuclear state $|\Psi\rangle$ are the electric and the magnetic moments of this state:

$$Q_{\lambda\mu} = \langle \Psi | \hat{Q}_{\lambda\mu} | \Psi \rangle, \quad (\text{B.26})$$

$$M_{\lambda\mu} = \langle \Psi | \hat{M}_{\lambda\mu} | \Psi \rangle. \quad (\text{B.27})$$

We discuss first the *selection rules* for $Q_{\lambda\mu}$ and $M_{\lambda\mu}$, because they do not depend on the special form of $|\Psi\rangle$. Since the strong and electromagnetic interactions conserve parity, it is possible to choose $|\Psi\rangle$ as an eigenstate of the parity operator. On the other side, the multipole operators $\hat{Q}_{\lambda\mu}$ and $\hat{M}_{\lambda\mu}$ have parity $(-)^{\lambda}$ and $(-)^{\lambda+1}$, respectively. This means that

$$\begin{aligned} Q_{\lambda\mu} &= 0 \quad \text{for } \lambda = 1, 3, 5, \dots, \\ M_{\lambda\mu} &= 0 \quad \text{for } \lambda = 0, 2, 4, \dots. \end{aligned} \quad (\text{B.28})$$

Using the fact that the operators $\hat{Q}_{\lambda\mu}$ and $\hat{M}_{\lambda\mu}$ are spherical tensor operators in the sense of [Ed 57, Eq. (5.2.1.)], we can apply the Wigner-Eckart theorem [Ed 57, Eq. (5.4.1)] for eigenstates of angular momentum $|I, M\rangle$,

$$Q_{\lambda\mu} = \langle IM | \hat{Q}_{\lambda\mu} | IM \rangle = (-)^{I-M} \begin{pmatrix} I & \lambda & I \\ -M & \mu & M \end{pmatrix} \langle I \| \hat{Q}_\lambda \| I \rangle, \quad (\text{B.29})$$

$$M_{\lambda\mu} = \langle IM | \hat{M}_{\lambda\mu} | IM \rangle = (-)^{I-M} \begin{pmatrix} I & \lambda & I \\ -M & \mu & M \end{pmatrix} \langle I \| \hat{M}_{\lambda\mu} \| I \rangle,$$

and get

$$\left. \begin{array}{l} Q_{\lambda\mu} \\ M_{\lambda\mu} \end{array} \right\} \neq 0 \quad \text{only for } \mu = 0 \text{ and } 0 < \lambda < 2I. \quad (\text{B.30})$$

Since the dependence of $Q_{\lambda\mu}$ and $M_{\lambda\mu}$ on the magnetic quantum number is trivial [(B.29), (B.30)], we usually only give the values for $M = I$.

The *magnetic dipole moment* is defined by

$$\mu = \sqrt{\frac{4\pi}{3}} \langle II | \hat{M}_{10} | II \rangle \quad (\text{B.31})$$

and the *electric quadrupole moment* is given by

$$Q = \sqrt{\frac{16\pi}{5}} \langle II | \hat{Q}_{20} | II \rangle. \quad (\text{B.32})$$

These values are defined in the laboratory systems and are measurable by experiment. For the internal quadrupole moment, see Eq. (1.70).

B.3 The Multipole Expansion of the Radiation Field

In the case of electromagnetic radiation, it is convenient to work in the transverse or Coulomb gauge [Ja 62, Chap. 6.5] with the conditions

$$\Phi = 0; \quad \nabla \cdot \mathbf{A} = 0. \quad (\text{B.33})$$

The Hamiltonian of the free field is then given by

$$H_{\text{field}} = \frac{1}{8\pi} \int \left(\frac{1}{c^2} \dot{\mathbf{A}}^2 + (\nabla \times \mathbf{A})^2 \right) d^3r, \quad (\text{B.34})$$

which yields the wave equation

$$\Delta \mathbf{A} - \frac{1}{c^2} \frac{\partial^2}{\partial t^2} \mathbf{A} = 0. \quad (\text{B.35})$$

To represent the most general vector potential \mathbf{A} , which obeys (B.33) and (B.35), we look for a complete orthogonal set that fulfills this requirement. At this point, one usually makes a Fourier transformation in space and time and keeps only the components perpendicular to the wave vector \mathbf{k} in order to fulfill (B.33). Because of the spherical symmetry, we only apply the *Fourier transformation in time*, that is, we assume for our basis functions a time-dependence $\exp(-ikct)$, and obtain the Helmholtz equation

$$(\Delta + k^2) \mathbf{A} = 0. \quad (\text{B.36})$$

According to the spherical symmetry of our problem, we look for solutions that are eigenfunctions of the orbital angular momentum operators \mathbf{L}^2 and L_z . A complete set of solutions that fulfill this condition and are regular at the origin, are given by $j_L(kr) \cdot Y_{LM_L}(\theta, \varphi)$, where $j_L(kr)$ are spherical Bessel functions (see [AS 65]) and Y_{LM} are the spherical harmonics [Ed 57]. Besides the orbital angular momentum \mathbf{L} , the photon has a spin \mathbf{S} with $S=1$ according to the vector character of the potential \mathbf{A} . The eigenfunctions of \mathbf{S}^2 and S_z are the vectors $e_{Ms}(M_S = +1, 0, -1)$ [Ed 57, Eq. (5.9.4)]. The total angular momentum of the photon is given by $\mathbf{I} = \mathbf{L} + \mathbf{S}$. With the rules of angular momentum coupling, we find as eigenfunctions of $\mathbf{L}^2, \mathbf{S}^2$

I^2, I_s [Ed 57, Eq. (5.9.10)] the *vector spherical harmonics*:

$$\mathbf{Y}_{ILm} = \sum_{M_L M_s} C_{M_L M_s m}^L Y_{LM_L}(\theta, \varphi) \mathbf{e}_{M_s}. \quad (\text{B.37})$$

They form a complete orthogonal set

$$\int_{4\pi} d\cos\theta d\varphi \mathbf{Y}_{ILm}^*(\theta, \varphi) \cdot \mathbf{Y}_{I'L'm'}(\theta, \varphi) = \delta_{II'} \delta_{LL'} \delta_{mm'}. \quad (\text{B.38})$$

For fixed I , the orbital angular momentum can be $I-1, I, I+1$. That means there are three independent solutions of (B.36) for each k, I, m . However we have to fulfill the transversality condition (B.33).

From [Ed. 57, Eq. (5.9.14)],

$$\mathbf{Y}_{II-}(\theta, \varphi) = \frac{1}{\sqrt{I(I+1)}} \mathbf{L} Y_{Im}(\theta, \varphi) \quad (\text{B.38})$$

we see that Eq. (B.33) is fulfilled for $j_I(kr) Y_{IIm}(\theta, \varphi)$. The orthogonal wave functions to (B.38) are linear combinations of \mathbf{Y}_{II+1m} and \mathbf{Y}_{II-1m} . There is only one such combination that has the property (B.33) (see [Ed 57, Eq. (5.9.18)ff] and [AS 65, Eq. (10.1.21)ff]):

$$\frac{i}{k} \nabla \times j_I(kr) \mathbf{Y}_{IIm} = \sqrt{\frac{I}{2I+1}} j_{I+1}(kr) \mathbf{Y}_{II+1m} - \sqrt{\frac{I+1}{2I+1}} j_{I-1}(kr) \mathbf{Y}_{II-1m}. \quad (\text{B.39})$$

We therefore have for each I and m two independent solutions of the wave equation (B.36) which fulfill the transversality condition (B.33). We characterize them by the index λ and call them electric ($\lambda = E$) and magnetic ($\lambda = M$) radiation.

$$\begin{aligned} \mathbf{A}_{Mklm}(\mathbf{r}) &= \mathcal{N} j_I(kr) \mathbf{Y}_{IIm}(\theta, \varphi) \\ &= \frac{\mathcal{N}}{\sqrt{I(I+1)}} \frac{1}{i} (\mathbf{r} \times \nabla) j_I(kr) \mathbf{Y}_{Im}(\theta, \varphi) \end{aligned} \quad (\text{B.40})$$

and

$$\begin{aligned} \mathbf{A}_{Eklm}(\mathbf{r}) &= \frac{i}{k} (\nabla \times \mathbf{A}_{Mklm}(\mathbf{r})) \\ &= \frac{-\mathcal{N}}{\sqrt{I(I+1)}} \frac{1}{k} \left\{ \nabla \left(Y_{Im}(\theta, \varphi) \frac{\partial}{\partial r} (r j_I(kr)) \right) \right. \\ &\quad \left. + k^2 r j_I(kr) Y_{Im}(\theta, \varphi) \right\}. \end{aligned} \quad (\text{B.41})$$

Equation (B.41) is obtained from (B.40) by evaluating $\nabla \times (\nabla \times \mathbf{r}) j_I Y_{Im}$ and using the fact that $j_I Y_{Im}$ satisfies Eq. (B.36). \mathcal{N} is a normalization constant. The quantum number k is discretized by requiring the proper boundary conditions at a perfectly conducting sphere with radius R . This sphere is

introduced only to define spherical boundary conditions, and at the end, R approaches large values compared to the nuclear radius R_0 . According to the laws of classical electrodynamics, the boundary conditions at the surface are [Ja 62] $E_\perp = 0$ and $B_\perp = 0$. These conditions are fulfilled only by a discrete number of k -values, k_n . In the magnetic case they are given as the zeros of the spherical Bessel function,

$$j_n(k_n R) = 0. \quad (\text{B.42})$$

In the electric case, we find the condition

$$\frac{\partial}{\partial r} (r j_n(k_n r)) \Big|_{r=R} = 0. \quad (\text{B.43})$$

In the following we use k as a discrete index, which runs over the solutions k_n of Eq. (B.42) or (B.43), respectively.

The normalization constant \mathcal{N} is chosen in such a way that the following orthogonality relation holds [AS 65 Eq. (11.4.5)].

$$\int_0^R r^2 dr \int_{4\pi} d\cos\theta d\varphi \mathbf{A}_{\lambda' k' l' m'}^*(\mathbf{r}) \cdot \mathbf{A}_{\lambda k l m}(\mathbf{r}) = \frac{2\pi\hbar c}{k} \delta_{\lambda\lambda'} \delta_{kk'} \delta_{ll'} \delta_{mm'}. \quad (\text{B.44})$$

In the limit of large R -values, \mathcal{N} turns out to be [AS 65]

$$\mathcal{N} = \sqrt{\frac{4\pi\hbar ck}{R}} \quad (\text{B.45})$$

for both λ -values.

The properties of magnetic and electric radiation under the parity transformation Π can be seen from (B.38). Since \mathbf{L} preserves the parity and the curl operation changes parity, we find that

$$\Pi \mathbf{A}_{Eklm} = (-)^{l+1} \cdot \mathbf{A}_{Eklm}; \quad \Pi \mathbf{A}_{Mklm} = (-)^l \cdot \mathbf{A}_{Mklm}. \quad (\text{B.46})$$

The most general solution of our problem is therefore given by

$$\mathbf{A}(\mathbf{r}, t) = \sum_{\lambda k} \sum_{lm} \{ a_{\lambda k l m}^* \mathbf{A}_{\lambda k l m}(\mathbf{r}) e^{-ikct} + \text{c.c.} \}. \quad (\text{B.47})$$

The coefficients $a_{\lambda k l m}$ are independent variables for the description of the electromagnetic field \mathbf{A} . The form (B.47) of $\mathbf{A}(\mathbf{r}, t)$ guarantees that (B.33) and (B.36) are fulfilled for each choice of $a_{\lambda k l m}$.

Using Eq. (B.44), we can express the Hamiltonian (B.34) of the free field by

$$H_{\text{field}} = \sum_{\lambda k} \sum_{lm} (\hbar ck)^{\frac{1}{2}} (a_{\lambda k l m}^* a_{\lambda k l m} + \text{c.c.}) \quad (\text{B.48})$$

This is the Hamiltonian of harmonic oscillators $H_{ho} = \hbar\omega a^* a$, and the rules of *canonical quantization* can be applied: The variables a_λ^* and a_λ are replaced by creation and annihilation operators \hat{a}_λ^+ and \hat{a}_λ which obey the boson commutation relations

$$\begin{aligned} [\hat{a}_{\lambda k l m}, \hat{a}_{\lambda' k' l' m'}] &= 0, \\ [\hat{a}_{\lambda k l m}, \hat{a}_{\lambda' k' l' m'}^+] &= \delta_{\lambda\lambda'} \delta_{kk'} \delta_{ll'} \delta_{mm'}. \end{aligned} \quad (\text{B.49})$$

The operator $\hat{a}_{\lambda k l m}^+$ creates a photon of the type λ (magnetic or electric radiation) with the energy $\hbar c k$ and the angular momentum quantum numbers I, m . Applying the rules of second quantization (Appendix C), we find for the Hamiltonian

$$H_{\text{field}} = \sum_{k\lambda} \sum_{lm} (\hbar c k) \left(\hat{a}_{\lambda k l m}^+ \hat{a}_{\lambda k l m} + \frac{1}{2} \right). \quad (\text{B.50})$$

The eigenstates can be represented in the occupation number representation $| \dots n_{\lambda k l m} \dots \rangle$, and the potential \mathbf{A} (B.47) goes over into the operator

$$\hat{\mathbf{A}}(\mathbf{r}, t) = \sum_{\lambda k l m} \left\{ \mathbf{A}_{\lambda k l m}(\mathbf{r}) e^{-ikrt} \hat{a}_{\lambda k l m}^+ + \mathbf{A}_{\lambda k l m}^*(\mathbf{r}) e^{ikrt} \hat{a}_{\lambda k l m} \right\}. \quad (\text{B.51})$$

B.4 Multipole Transitions

Together with the eigenstates $|\Psi_i\rangle$ of the nuclear Hamiltonian H_{nuc} , we now have a complete system of eigenstates of the unperturbed Hamiltonian

$$H_0 = H_{\text{nuc}} + H_{\text{field}}. \quad (\text{B.52})$$

The time-dependent interaction (B.4)

$$H_{\text{int}} = -\frac{1}{c} \sum_{\lambda k l m} \left\{ \hat{a}_{\lambda k l m}^+ \int \mathbf{J} \cdot \mathbf{A}_{\lambda k l m} d^3 r e^{-ikrt} + \text{h.c.} \right\} \quad (\text{B.53})$$

does not commute with the photon number. It causes transitions between nuclear states $|\Psi_i\rangle$ and $|\Psi_f\rangle$ and the corresponding absorption and emission of photons

$$|i\rangle = |\Psi_i\rangle | \dots n_{\lambda} \dots \rangle \xrightarrow{\substack{\text{absorption} \\ \text{emission}}} |\Psi_f\rangle | \dots n_{\lambda} - 1 \dots \rangle = |f\rangle,$$

$$|\Psi_f\rangle | \dots n_{\lambda} + 1 \dots \rangle = |f\rangle.$$

We calculate the transition probability in first-order Dirac perturbation theory [Me 61]:

$$T_f = \frac{2\pi}{\hbar} |\langle f | H_{\text{int}} | i \rangle|^2 g(E_f), \quad (\text{B.54})$$

where $g(E_f)$ is the number of final states per energy unit. We have to calculate T_f at the energy $c\hbar k = E_f - E_i$ of the absorbed or emitted photon.

The relations (C.12)

$$|\langle \dots n_{\lambda} - 1 \dots | \hat{a}_{\lambda} | \dots n_{\lambda} \dots \rangle|^2 = n_{\lambda} \quad (\text{B.55})$$

and

$$|\langle \dots n_{\lambda} + 1 \dots | \hat{a}_{\lambda}^+ | \dots n_{\lambda} \dots \rangle|^2 = n_{\lambda} + 1 \quad (\text{B.56})$$

show that the probability of an absorption of a photon is proportional to n_{λ} , and the probability of emission of a photon is proportional to $n_{\lambda} + 1$. Even for a vanishing field ($n_{\lambda} = 0$) we therefore have a probability for the

emission of a photon (spontaneous emission). In the following, we will only consider this case. It is identical to the absorption of a photon in a field with $n_\lambda = 1$.

The density of states $g(k)$ can be calculated from the condition (B.42) in the magnetic case (the condition (B.43) in the electric case will give the same result). In the limit of large R -values, we find

$$0 = j_I(k_n R) \approx \frac{1}{k_n R} \sin\left(k_n R - \frac{\pi}{2} I\right) \quad (\text{B.57})$$

that is,

$$k_n R = n \cdot \pi + \frac{\pi}{2} \cdot I, \quad n = 0, \pm 1, \pm 2, \dots, \quad (\text{B.58})$$

and

$$g(k) = \frac{1}{\Delta E(k)} = \frac{1}{\hbar c} \frac{1}{\Delta k} = \frac{1}{\hbar c} \frac{R}{\pi}. \quad (\text{B.59})$$

Using (B.54), (B.40), and (B.45), we get for the probability of the emission of a single photon with the quantum numbers (λ, k, I, m) ,

$$T_f(E, kIm) = \frac{8\pi k}{\hbar} \left| \langle f | \frac{1}{ck} \int \mathbf{j} \cdot \nabla \times \mathbf{j}_I(kr) Y_{Im} d^3r | i \rangle \right|^2, \quad (\text{B.60})$$

$$T_f(M, kIm) = \frac{8\pi k}{\hbar} \left| \langle f | \frac{1}{c} \int \mathbf{j} \cdot \mathbf{j}_I(kr) Y_{Im} d^3r | i \rangle \right|^2, \quad (\text{B.61})$$

which can be written as

$$T_f(\lambda, kIm) = \frac{8\pi(I+1)}{\hbar \cdot I((2I+1)!!)^2} \left(\frac{E_\gamma}{\hbar c} \right)^{2I+1} \left| \langle f | \hat{\mathcal{R}}(\lambda kIm) | i \rangle \right|^2, \quad (\text{B.62})$$

where the general multipole transition operator $\hat{\mathcal{R}}(\lambda, kIm)$ in the electric case is given by (B.60) and (B.41)

$$\hat{\mathcal{R}}(E, kIm) = \frac{i(2I+1)!!}{ck^{I+1}(I+1)} \int \mathbf{j} \cdot \nabla \times (\nabla \times \mathbf{r})(j_I(kr) Y_{Im}(\theta, \varphi)) d^3r. \quad (\text{B.63})$$

Evaluating the $\nabla \times (\nabla \times \mathbf{r})$ operator as in (B.41), we get two terms. In the first part, we can use the continuity equation after integration by parts,

$$\nabla \mathbf{j} = -\frac{\partial}{\partial t} \rho = ikc\rho, \quad (\text{B.64})$$

which results from (B.8). Finally, we obtain:

$$\hat{\mathcal{R}}(E, kIm) = \frac{(2I+1)!!}{k^I(I+1)} \int \left\{ \rho Y_{Im} \frac{\partial}{\partial r} r j_I(kr) + i \frac{k}{c} \mathbf{j} \cdot \mathbf{r} Y_{Im} j_I(kr) \right\} d^3r. \quad (\text{B.65})$$

In the magnetic case, we have

$$\hat{\mathcal{R}}(M, kIm) = \frac{-(2I+1)!!}{ck^I(I+1)} \int \mathbf{j} \cdot (\mathbf{r} \times \nabla) \cdot (j_I(kr) \cdot Y_{Im}) d^3r. \quad (\text{B.66})$$

In nuclear physics we usually work in the limit of *long wavelengths*, that is, the wavelength of the radiation is large compared to the nuclear radius ($k \cdot R_0 \ll 1$), or

$$E_\gamma \ll \frac{\hbar c}{r_0} A^{-1/3} = 197 \cdot A^{-1/3} [\text{MeV}]. \quad (\text{B.67})$$

In this case we can use the small-argument limit for the spherical Bessel function,

$$j_I(kr) \approx \frac{(kr)^I}{(2I+1)!!} \left(1 - \frac{1}{2} \frac{(kr)^2}{2I+3} + \dots \right) \quad (\text{B.68})$$

and get to first order in kr

$$\hat{\mathcal{R}}(E, kIm) = \int \rho r' Y_{Im} d^3r + \frac{ik}{I+1} \int (\mathbf{r} \times \boldsymbol{\mu}) \nabla r' Y_{Im} d^3r. \quad (\text{B.69})$$

The first part does not depend on k and corresponds to the static *electric multipole operators* \hat{Q}_{Im} (B.18). The second term, of first order in kR_0 , is usually neglected.

For the *magnetic operators* in this limit, we obtain exactly the operator (B.19) and (B.22)

$$\hat{\mathcal{R}}(M, kIm) = \frac{1}{c(I+1)} \int (\mathbf{r} \times \mathbf{j}) \cdot \nabla (r' Y_{Im}) d^3r = \hat{M}_{Im}. \quad (\text{B.70})$$

Usually we do not distinguish between the different orientations of the angular momenta (the exception being polarization measurements). We therefore assume a statistical distribution in the initial state and calculate the arithmetical average of the initial m -values. All the final m -values have to be summed up and we finally get the total probability for a certain multipole transition,

$$T_f(\lambda, I) = \frac{1}{2I_i+1} \sum_{m_i, m_f, m} T_f(\lambda, kIm). \quad (\text{B.71})$$

Using the Wigner-Eckart theorem (B.29) and the orthogonality relations of the $3j$ -symbols [Ed 57, Eq. (3.7.8)], we can carry out the sum over m_i, m_f and get for the transition probability (B.71)

$$T_f(\lambda, I) = \frac{8\pi(I+1)}{\hbar I((2I+1)!!)^2} \left(\frac{E_\gamma}{\hbar c} \right)^{2I+1} B(\lambda I, I_i \rightarrow I_f). \quad (\text{B.72})$$

The $B(\lambda)$ values are called *reduced transition probabilities* and are given by the reduced matrix elements

$$B(EI, I_i \rightarrow I_f) = \frac{1}{2I_f+1} |\langle f || \hat{Q}_f || i \rangle|^2, \quad (\text{B.73})$$

$$B(MI, I_i \rightarrow I_f) = \frac{1}{2I_f+1} |\langle f || \hat{M}_f || i \rangle|^2, \quad (\text{B.74})$$

where the multipole operators \hat{Q}_{Im} and \hat{M}_{Im} are defined in Eqs. (B.23) and (B.24). The $B(EI)$ and $B(MI)$ values contain the information about the

Table B.1 Transition probabilities T (sec^{-1}) expressed by $B(EI)$ ($e^2(\text{fm})^{2I}$) and $B(MI)$ ($\mu_N^2(\text{fm})^{2I-2}$), and the Weisskopf units B_{sp} expressed in ($e^2(\text{fm})^{2I}$) and ($\mu_N^2(\text{fm})^{2I-2}$). The energies E are measured in MeV.

$T(E1) = 1.587 \cdot 10^{15} \cdot E^3 \cdot B(E1)$	$B_{sp}(E1) = 6.446 \cdot 10^{-2} \cdot A^{2/3}$
$T(E2) = 1.223 \cdot 10^9 \cdot E^5 \cdot B(E2)$	$B_{sp}(E2) = 5.940 \cdot 10^{-2} \cdot A^{4/3}$
$T(E3) = 5.698 \cdot 10^2 \cdot E^7 \cdot B(E3)$	$B_{sp}(E3) = 5.940 \cdot 10^{-2} \cdot A^2$
$T(E4) = 1.694 \cdot 10^{-4} \cdot E^9 \cdot B(E4)$	$B_{sp}(E4) = 6.285 \cdot 10^{-2} \cdot A^{8/3}$
$T(E5) = 3.451 \cdot 10^{-11} \cdot E^{11} \cdot B(E5)$	$B_{sp}(E5) = 6.928 \cdot 10^{-2} \cdot A^{10/3}$
$T(M1) = 1.779 \cdot 10^{13} \cdot E^3 \cdot B(M1)$	$B_{sp}(M1) = 1.790$
$T(M2) = 1.371 \cdot 10^7 \cdot E^5 \cdot B(M2)$	$B_{sp}(M2) = 1.650 \cdot A^{2/3}$
$T(M3) = 6.387 \cdot 10^0 \cdot E^7 \cdot B(M3)$	$B_{sp}(M3) = 1.650 \cdot A^{4/3}$
$T(M4) = 1.899 \cdot 10^{-6} \cdot E^9 \cdot B(M4)$	$B_{sp}(M4) = 1.746 \cdot A^2$
$T(M5) = 3.868 \cdot 10^{-13} \cdot E^{11} \cdot B(M5)$	$B_{sp}(M5) = 1.924 \cdot A^{8/3}$

nuclear wave functions. They are often measured in Weisskopf units [see Eq. (B.85)]. The rest are kinematical factors. Table (B.1) gives the transition probabilities T_f and the Weisskopf units for the $B(\lambda)$ values in the most important cases.

From the structure of the matrix elements

$$\langle I_f M_f | \hat{Q}_{Im} | I_i M_i \rangle \quad \text{and} \quad \langle I_f M_f | \hat{M}_{Im} | I_i M_i \rangle \quad (\text{B.75})$$

we find the following *selection rules* for a transition from an initial state $|i\rangle = |I_i M_i\rangle$ to a final state $|f\rangle = |I_f M_f\rangle$:

$$|I_i - I_f| \leq I \leq I_i + I_f, \quad (\text{B.76})$$

$$M_f - M_i = m, \quad (\text{B.77})$$

$$\pi_i \pi_{\lambda Im} \pi_f = 1. \quad (\text{B.78})$$

The parity of the multipole radiation (λJ) $\pi_{\lambda Im}$ is given by the parity of the interaction $\propto A_\lambda \cdot \mathbf{j}$. Since \mathbf{j} changes sign under the parity transformation, we get from (B.46)

$$\pi_{EIm} = (-)^I, \quad \pi_{MIm} = (-)^{I+1}. \quad (\text{B.79})$$

From (B.72) and Table B.1 we find that the radiation with higher I -values is strongly suppressed. As long as selection rules or special effects in the nuclear structure part [$B(\lambda)$ -values] do not forbid a transition, we usually have to take into account only the lowest possible I -value. Magnetic radiation is weaker than the electric radiation. Therefore, we often have a competition between M1 and E2 radiation.

From (B.72) it also becomes clear that the transition probability T increases rapidly with the transition energy. This is the reason why transitions with small energy differences are sometimes harder to observe. Other processes (like internal conversion) become important in such cases.

B.5 Single-Particle Matrix Elements in a Spherical Basis

In all microscopic calculations of electromagnetic moments and transition probabilities, we need the matrix elements of the multipole operators. We restrict ourselves to a spherical basis, that is, the single-particle states are given by the quantum numbers $|jm\rangle = |nsljm\rangle$. Since $s = \frac{1}{2}$, it is usually omitted, but the order in slj is important.

Using the phases of Edmonds [Ed 57], we obtain for the reduced single-particle matrix elements of the *electric multipole operators* (B.23) [RBS 73]

$$\langle f || \hat{Q}_I || i \rangle = \langle f || e \sigma^I Y_I(\theta, \varphi) || i \rangle \quad (\text{B.80})$$

$$\begin{aligned} &= e \frac{(1 - (-)^{I+j+l+1})}{2} \langle f | r^I | i \rangle \sqrt{\frac{(2I+1)(2j_l+1)(2j_f+1)}{4\pi}} \\ &\times (-)^{j_f - \frac{1}{2}} \left(\begin{array}{ccc} j_f & I & j_l \\ -\frac{1}{2} & 0 & \frac{1}{2} \end{array} \right). \end{aligned} \quad (\text{B.81})$$

In the *magnetic* case we have the spin part and the orbital part:

$$\begin{aligned} \langle f || \hat{M}_I || i \rangle &= \langle f || \mu_N \left(g_s \mathbf{s} + \frac{2}{I+1} \mathbf{g}_I \mathbf{I} \right) \cdot (\nabla r^I Y_I) || i \rangle \\ &= \mu_N \frac{(1 - (-)^{I+j+l+1})}{2} \langle f | r^{I-1} | i \rangle \sqrt{\frac{(2I+1)(2j_l+1)(2j_f+1)}{4\pi}} \\ &\times (-)^{j_f - \frac{1}{2}} \left(\begin{array}{ccc} j_f & I & j_l \\ -\frac{1}{2} & 0 & +\frac{1}{2} \end{array} \right) (I-k) \left[\frac{1}{2} g_s - g_l (1 + k/(I+1)) \right] \end{aligned} \quad (\text{B.82})$$

with

$$k = (j_l + \frac{1}{2})(-)^{I+j+l+\frac{1}{2}} + (j_f + \frac{1}{2})(-)^{I+j_f+\frac{1}{2}}.$$

The radial integrals are defined as

$$\langle f | r^I | i \rangle = \int_0^\infty R_f(r) r^I R_i(r) r^2 dr \quad (\text{B.83})$$

and the g -factors are given in (B.24).

Weisskopf has used a rough estimate for the corresponding $B(\lambda)$ -values [We 51]. In the radial integration (B.83), he replaces the wave function $R_f \approx R_0$ in the nuclear interior ($r < R_0$) by a constant and gets

$$\langle r^I \rangle \approx \frac{3}{I+3} R_0^I. \quad (\text{B.84})$$

Furthermore, he uses $j_f = I + \frac{1}{2}$ and $j_l = \frac{1}{2}$. From Eqs. (B.81) and (B.73), in

the electric case we find

$$B(EI) \approx \frac{e^2}{4\pi} \left(\frac{3}{I+3} \right)^2 R_0^{2I} = \frac{(1.2)^{2I}}{4\pi} \left(\frac{3}{I+3} \right)^2 A^{2I/3} [e^2 (\text{fm})^{2I}]. \quad (\text{B.85})$$

In the magnetic case, Weisskopf estimates that the magnet $B(MI)$ -value [We 51] is

$$\begin{aligned} B(MI) &\approx \frac{10}{\pi} \left(\frac{3}{I+3} \right)^2 R_0^{2I-2} \mu_N^2 \\ &= \frac{10}{\pi} (1.2)^{2I-2} \left(\frac{3}{I+3} \right)^2 A^{(2I-2)/3} [\mu_N^2 \cdot (\text{fm})^{2I-2}]. \end{aligned} \quad (\text{B.86})$$

Equations (B.85) and (B.86) give a very rough estimate for the single-particle transitions. They are often used as units (Weisskopf or single-particle units) for the actual $B(EI)$ - and $B(MI)$ -values.

B.6 Translational Invariance and Electromagnetic Transitions

Until now we have assumed that we have the exact wave functions of the nuclear system. Such wave functions are eigenfunctions of the linear momentum, and in all the electromagnetic transitions the linear momentum is conserved. For instance, the absorption of $E1$ -radiation, which is given by the operator (B.23)

$$E1 = \sqrt{\frac{3}{4\pi}} e \sum_{i=1}^Z \mathbf{r}_i = \sqrt{\frac{3}{4\pi}} e \sum_{i=1}^A (\frac{1}{2} - t_3^{(i)}) \mathbf{r}_i, \quad (\text{B.87})$$

excites only protons. In the center of mass system the total linear momentum vanishes; that is, in that system the neutrons will have the opposite momentum. The effective elongation of the protons is therefore only $\mathbf{r}_i - \mathbf{R}$, where \mathbf{R} is the center of mass. Instead of (B.87), we get

$$\sqrt{\frac{4\pi}{3}} E1 = :eD: = e \sum_{i=1}^Z (\mathbf{r}_i - \mathbf{R}) = -e \sum_{i=1}^A t_3^{(i)} (\mathbf{r}_i - \mathbf{R}) = e \frac{NZ}{A} (\mathbf{R}_p - \mathbf{R}_n), \quad (\text{B.88})$$

where \mathbf{R}_p and \mathbf{R}_n are the centers of mass for protons and neutrons, respectively.

As long as we have wave functions $|\Psi_i\rangle$ and $|\Psi_f\rangle$, which are eigenstates of the linear momentum, the replacement $\mathbf{r} = \mathbf{r}_i - \mathbf{R}$ has no influence on the matrix elements $\langle \Psi_f | E1 | \Psi_i \rangle$, since $\langle \Psi_f | \mathbf{R} | \Psi_i \rangle$ vanishes in this case. In most applications, however, we use wave functions which violate translational symmetry. In this case $\langle \Psi_f | \mathbf{R} | \Psi_i \rangle$ gives spurious contributions and we have to use the operator D of Eq. (B.88) where this spurious contribution is subtracted on the average. It is equivalent to use the $E1$ -operator with an effective charge of $(N/A)e$ for protons and $-(Z/A)e$ for neutrons. Corresponding effective charges have been calculated for transitions with

higher multipolarity [SF 74], and it was found that they give contributions of the order of $1/A$ to the normal transition operators, which can be neglected for heavy nuclei [see, for instance, Eq. (11.49)].

B.7 The Cross Section for the Absorption of Dipole Radiation

In Section B.4 we calculated the probability for the emission of a photon with quantum numbers $(\lambda k l m)$. We are now interested in the absorption cross section for electric dipole radiation. We assume that the incoming photon is polarized in the z -direction. We use the occupation number representation of the electromagnetic field in plane waves [SF 74]:

$$\mathbf{A}(\mathbf{r}) = \frac{\hbar c}{2\pi} \sum_{\mu=1}^2 \int d^3q \frac{\mathbf{e}_{q\mu}}{\sqrt{\hbar\omega_q}} [e^{i\varphi} a_{q\mu} + h.c.]. \quad (\text{B.89})$$

$\mathbf{e}_{q\mu}$ are the two polarization vectors of the photon. The initial wave function has the form

$$|i\rangle = a_{kz}^+ |\Psi_0\rangle. \quad (\text{B.90})$$

Using Eq. (B.54), we obtain the excitation probability of the excited state with the energy E_f . Since there is now only one such final state, the density of final states $\rho_f(E)$ is a δ -function $\delta(E - E_f + E_0)$. The cross section is defined as the quotient of this excitation probability divided by the current density of incoming photons with this energy.

The photon operators $a_{q\mu}, a_{q\mu}^+$ obey the commutation relations

$$[a_{q\mu}, a_{q'\mu'}^+] = \delta(\mathbf{q} - \mathbf{q}') \delta_{\mu\mu'}, \quad (\text{B.91})$$

that is, the corresponding plane waves are normalized as $(1/\sqrt{2\pi})^3 e^{i\varphi}$, that is, to a box of volume $(2\pi)^3$. The current density of incoming photons is therefore $c/(2\pi)^3$. For the cross section of an excitation of the final state we get

$$\begin{aligned} \sigma_f(E) &= \frac{2\pi}{\hbar} \frac{(2\pi)^3}{c} \left| \langle f | -\frac{1}{c} \int \mathbf{J} \cdot \mathbf{A} d^3r | i \rangle \right|^2 \delta(E - E_f + E_0) \\ &= \frac{(2\pi)^4}{\hbar c} \left(\frac{\hbar}{2\pi} \right)^2 \frac{1}{\hbar\omega_k} \left| \langle \Psi_f | \int \mathbf{J} \cdot \mathbf{e}_{kz} e^{i\varphi} d^3r | \Psi_0 \rangle \right|^2 \cdot \delta(E - E_f + E_0). \end{aligned} \quad (\text{B.92})$$

In the long wavelength limit we can replace $\mathbf{e}_{kz} e^{i\varphi}$ by $\nabla(\mathbf{e}_{kz} \cdot \mathbf{r} e^{i\varphi})$ and use the continuity equation, which gives, in analogy to (B.64),

$$\begin{aligned} \sigma_f(E) &= \frac{(2\pi)^2}{c^2} \frac{1}{k} \left| \langle \Psi_f | \frac{i}{\hbar} \int [\mathbf{H}, \rho(\mathbf{r})] z e^{i\varphi} d^3r | \Psi_0 \rangle \right|^2 \cdot \delta(E - E_f + E_0) \\ &= \frac{(2\pi)^2}{c^2} \frac{(E_f - E_0)^2}{\hbar^2 k} \left| \langle \Psi_f | e \sum_{i=1}^Z z_i e^{i\varphi} | \Psi_0 \rangle \right|^2 \cdot \delta(E - E_f + E_0). \end{aligned} \quad (\text{B.93})$$

As in Section B.6, we have to replace \mathbf{r}_i by $\mathbf{r}_i - \mathbf{R}$ for the dipole radiation, where only the first term in an expansion of $\exp(i\mathbf{k}(\mathbf{r}_i - \mathbf{R}))$ is kept, and get

$$\sigma_f(E) = \frac{4\pi^2 e^2}{\hbar c} (E_f - E_0) |\langle \Psi_f | D_z | \Psi_0 \rangle|^2 \delta(E - E_f + E_0). \quad (\text{B.94})$$

To get similar cross sections for higher multipolarity, we have to transform the representation (B.89) of the electromagnetic potential into the representation (B.51). This is shown in great detail in [SF 74].

APPENDIX C

Second Quantization

C.1 Creation and Annihilation Operators

The name "second quantization" is misleading. This formalism has nothing to do with the further quantizing of quantum mechanics. It is just an alternative formulation of the usual quantum mechanics, which has turned out to be very useful for handling the many-body problem. It can be used for bosons and fermions, and we will give a short introduction and some important formulae.

We start with a complete orthogonal set of single-particle states $|\nu\rangle$, where ν stands for a set of quantum numbers, for example,

- (i) space coordinate r , spin $s \equiv s_z$ $|r, s\rangle$;
- (ii) the quantum numbers of an oscillator basis $|nljm\rangle$.

Orthogonality and completeness are expressed as

$$\langle \nu | \nu' \rangle = \delta_{\nu\nu'}, \quad \sum_{\nu} |\nu\rangle \langle \nu| = 1. \quad (\text{C.1})$$

(For continuous quantum numbers such as r , the $\delta_{\nu\nu'}$ will mean $\delta(r - r')$ and the sum \sum_{ν} is to be replaced by $\int d^3r$.)

The coordinate representation of the state $|\nu\rangle$ is given by

$$\varphi_{\nu}(l) = \varphi_{\nu}(r_1, s_1) = \langle r_1, s_1 | \nu \rangle. \quad (\text{C.2})$$

Starting with this set of single-particle states, we can construct a complete orthogonal set of totally symmetric N -body wave functions

$$\Phi_{s_1 \dots s_N}(1, \dots, N) = \mathcal{N} \sum_P P \{ \varphi_{s_1}(1) \cdots \varphi_{s_N}(N) \}, \quad (\text{C.3})$$

where the sum runs over all permutations $(\nu_1 \dots \nu_N)$ of the numbers $(1 \dots N)$ and \mathcal{N} is a normalization constant.

Any arbitrary, totally *symmetric* N -body wave function can be represented in this basis:

$$\Psi(1, \dots, N) = \sum_{\nu_1, \dots, \nu_N} c_{\nu_1, \dots, \nu_N} \Phi_{\nu_1, \dots, \nu_N}(1, \dots, N). \quad (\text{C.4})$$

We can also give to each of the single-particle states a number ($\nu = 1, 2, \dots$) (in the case of continuous quantum numbers, we must first introduce a finite box) and characterize the wave function $\Phi_{\nu_1, \dots, \nu_N}$ by the "occupation numbers" $\{n_\nu\}$, which tell how often a particular number ν is contained in the N numbers (ν_1, \dots, ν_N) . Obviously, we have

$$\sum_\nu n_\nu = N \quad (\text{C.5})$$

and

$$\begin{aligned} \Phi_{\{n_\nu\}}(1, \dots, N) &= \Phi_{\nu_1, \dots, \nu_N}(1, \dots, N) \\ &= \frac{1}{\sqrt{N!}} \frac{1}{\sqrt{n_1! n_2! \dots}} \sum_P P \{ \varphi_{\nu_1}(1) \dots \varphi_{\nu_N}(N) \}. \end{aligned} \quad (\text{C.6})$$

Such a state describes a boson system. In complete analogy, we can construct totally antisymmetric-basis wave functions

$$\Phi_{\{n_\nu\}}(1, \dots, N) = \frac{1}{\sqrt{N!}} \sum_P \text{sign}(P) P \{ \varphi_{\nu_1}(1) \dots \varphi_{\nu_N}(N) \}. \quad (\text{C.7})$$

They are called *Slater determinants* and describe fermion systems. In this case the numbers n_ν only take the values 0 or 1, otherwise (C.7) would vanish identically.

We can now construct a Hilbert space which contains a vacuum (no particle) $|-\rangle$, all the one-particle states, all the symmetrized (or antisymmetrized) two-particle states, and so on...

$$\mathcal{K} = \{\mathcal{K}_0, \mathcal{K}_1, \mathcal{K}_2, \dots\}. \quad (\text{C.8})$$

The wave functions $\Phi_{\{n_\nu\}}$ correspond to basis states $|n_1, n_2, \dots\rangle$ in this Hilbert space, which are characterized by the occupation numbers (occupation number representation), such that

$$\Phi_{\{n_\nu\}}(1, \dots, N) = \langle 1, \dots, N | n_1, n_2, \dots \rangle. \quad (\text{C.9})$$

These states are orthonormalized

$$\langle n'_1, n'_2, \dots, n'_N | n_1, n_2, \dots, n_N \rangle = \delta_{n'_1, n_1} \cdot \delta_{n'_2, n_2} \cdots \delta_{n'_N, n_N}. \quad (\text{C.10})$$

First we shall study boson systems and define an "annihilation operator" B_ν by

$$B_\nu |n_1, n_2, \dots, n_\nu, \dots\rangle = \sqrt{n_\nu} |n_1, n_2, \dots, n_\nu - 1, \dots\rangle. \quad (\text{C.11})$$

The operator B_ν lowers the occupation number in the state with the number ν by one. An N -body state goes over into an $(N-1)$ -body state.

The matrix elements of B_ν are

$$\langle n'_1, n'_2, \dots, n_\nu, \dots | B_\nu | n_1, n_2, \dots, n_\nu, \dots \rangle = \sqrt{n_\nu} \delta_{n_1 n'_1} \dots \delta_{n_\nu n'_\nu} \dots \quad (\text{C.12})$$

or

$$\langle n_1, n_2, \dots, n_\nu, \dots | B_\nu^+ | n'_1, n'_2, \dots, n'_\nu, \dots \rangle = \sqrt{n_\nu + 1} \delta_{n_1 n'_1} \dots \delta_{n_\nu n'_\nu} \dots \quad (\text{C.13})$$

This is valid for all basis states $\langle n_1, n_2, \dots |$. We therefore find

$$B_\nu^+ | n_1, n_2, \dots, n_\nu, \dots \rangle = \sqrt{n_\nu + 1} | n_1, n_2, \dots, n_\nu + 1, \dots \rangle. \quad (\text{C.14})$$

B_ν^+ "creates" a particle in the state with the number ν . Therefore, it is called a "*creation operator* in the state ν ." It is the Hermitian conjugate operator to B_ν .

From this definition we gain the fact that

$$(B_\mu B_\nu^+ - B_\nu^+ B_\mu) | n_1, n_2, \dots, n_\nu, \dots, n_\mu, \dots \rangle = \begin{cases} \left(\sqrt{n_\nu + 1} \sqrt{n_\mu} - \sqrt{n_\mu} \sqrt{n_\nu + 1} \right) | n_1, \dots, n_\nu + 1, \dots, n_\mu - 1, \dots \rangle = 0 & \text{for } \nu \neq \mu, \\ \left(\sqrt{n_\nu + 1} \sqrt{n_\nu + 1} - \sqrt{n_\nu} \sqrt{n_\nu} \right) | n_1, \dots, n_\nu, \dots \rangle & \text{for } \nu = \mu, \end{cases} \quad (\text{C.15})$$

and hence get the commutation relations.

$$[B_\mu, B_\nu^+] = B_\mu B_\nu^+ - B_\nu^+ B_\mu = \delta_{\mu\nu}. \quad (\text{C.16})$$

In the same way, we may show that

$$[B_\mu, B_\nu] = [B_\nu^+, B_\mu^+] = 0. \quad (\text{C.17})$$

The state with the occupation numbers $|0, 0, 0, \dots\rangle = |- \rangle$ is the *vacuum*. We thus have

$$B_\nu | - \rangle = 0 \quad \text{for all } \nu \quad (\text{C.18})$$

and

$$| n_1, n_2, \dots, n_\nu, \dots \rangle = \frac{1}{\sqrt{n_1! n_2! \dots n_\nu! \dots}} \prod_\mu (B_\mu^+)^{n_\mu} | - \rangle. \quad (\text{C.19})$$

The relation (C.11) follows from (C.16) to (C.19), which was our definition of the operators B_ν . We can therefore also go in the opposite direction and start with a set of operators B_ν, B_ν^+ which obey boson commutation relations and construct the many-body Hilbert space from (C.17) and (C.18).

The operator $B_\nu^+ B_\nu$ is called the particle-number operator for the state ν :

$$B_\nu^+ B_\nu | n_1, \dots, n_\nu, \dots \rangle = n_\nu | n_1, \dots, n_\nu, \dots \rangle. \quad (\text{C.20})$$

We now address ourselves to a fermion system. We shall use small Latin letters a_ν^+, a_ν for the creation and annihilation operators of fermions. Since n_ν can only have the values 0 and 1, we may define the action of the

operators as

$$a_\nu |n_1, \dots, n_\nu = 1, \dots \rangle = |n_1, \dots, n_\nu = 0, \dots \rangle, \quad a_\nu |n_1, \dots, n_\nu = 0, \dots \rangle = 0, \quad (\text{C.21})$$

from which we get

$$a_\nu^+ |n_1, \dots, n_\nu = 0, \dots \rangle = |n_1, \dots, n_\nu = 1, \dots \rangle, \quad a_\nu^+ |n_1, \dots, n_\nu = 1, \dots \rangle = 0, \quad (\text{C.22})$$

and

$$\begin{aligned} [a_\mu, a_\nu^+]_+ &:= (a_\mu, a_\nu^+) := a_\mu a_\nu^+ + a_\nu^+ a_\mu = \delta_{\mu\nu}, \\ [a_\mu, a_\nu]_+ &= [a_\mu^+, a_\nu^+]_+ = 0. \end{aligned} \quad (\text{C.23})$$

The vacuum is again given by $|-\rangle = |0, 0, \dots\rangle$ and we have

$$a_\nu |-\rangle = 0 \quad \text{for all } \nu, \quad (\text{C.24})$$

hence

$$|n_1, \dots, n_\nu, \dots\rangle = \prod_\mu (a_\mu^*)^{n_\mu} |-\rangle = a_{\nu_1}^+ \dots a_{\nu_N}^+ |-\rangle. \quad (\text{C.25})$$

C.2 Field Operators in the Coordinate Space*

Using the single-particle wave functions $\varphi_\nu(\mathbf{r}, s)$ in Eq. (C.2) we can define creation and annihilation operators $a^+(\mathbf{r}, s), a(\mathbf{r}, s)$, which depend on the coordinates \mathbf{r} and s^\dagger :

$$a(\mathbf{r}, s) = \sum_\nu \varphi_\nu(\mathbf{r}, s) a_\nu; \quad a^+(\mathbf{r}, s) = \sum_\nu \varphi_\nu^*(\mathbf{r}, s) a_\nu^+. \quad (\text{C.26})$$

With Eq. (C.1) we can invert this relation,

$$a_\nu = \sum_s \int d^3r \varphi_\nu^*(\mathbf{r}, s) a(\mathbf{r}, s), \quad a_\nu^+ = \sum_s \int d^3r \varphi_\nu(\mathbf{r}, s) a^+(\mathbf{r}, s). \quad (\text{C.27})$$

and gain the commutators

$$[a(\mathbf{r}, s), a^+(\mathbf{r}', s')]_+ = \sum_{\nu\nu'} \varphi_\nu(\mathbf{r}, s) \varphi_{\nu'}^*(\mathbf{r}', s') [a_\nu, a_{\nu'}^+]_+ = \delta_{ss'} \delta(\mathbf{r} - \mathbf{r}') \quad (\text{C.28})$$

and

$$[a(\mathbf{r}, s), a(\mathbf{r}', s')]_+ = [a^+(\mathbf{r}, s), a^+(\mathbf{r}', s')]_+ = 0. \quad (\text{C.29})$$

We can express the many-body wave function (C.7) by

$$\Phi_{(\pi)}(1, \dots, N) = \frac{1}{\sqrt{N!}} \langle - | a(N) \dots a(1) | n_1, n_2, \dots, n_\nu, \dots \rangle \quad (\text{C.30})$$

* In the following we investigate only the case of fermions. Analogous considerations apply for bosons.

[†]This definition agrees with the convention $\varphi_\nu(\mathbf{r}) = \langle \mathbf{r} | \nu \rangle$, and according to the definition (5.18) for a unitary transformation of the operators $a_\nu^+, \varphi_\nu(\mathbf{r})$ corresponds to D_ν^* .

and

$$|\nu_1, \nu_2, \dots, \nu_N, \dots\rangle = \int d1 \dots dN \frac{1}{\sqrt{N!}} \Phi_{(N)}(1, \dots, N) a^+(1) \dots a^+(N) |-\rangle. \quad (\text{C.31})$$

C.3 Representation of Operators

Starting from a vacuum $|-\rangle$, we have expressed all states in the many-body Hilbert space \mathcal{K} by creation and annihilation operators a_ν^+, a_ν . The same will be done for operators in the following. We have to distinguish between one- and two-body operators.

A *one-body operator* as, for example, the kinetic energy or the total momentum of an N -particle system, is given as the sum of N operators \hat{f}_i which always act on the coordinate of the particle i :

$$\hat{F} = \sum_{i=1}^N \hat{f}_i. \quad (\text{C.32})$$

Its matrix elements in the $|\nu\rangle$ representation are

$$f_{\nu\nu'} = \langle \nu | \hat{f} | \nu' \rangle, \quad (\text{C.33})$$

that is,

$$\hat{f}_i \varphi_\nu(i) = \sum_{\nu'} f_{\nu\nu'} \varphi_{\nu'}(i). \quad (\text{C.34})$$

The representation of \hat{F} in the operators a_ν^+, a_ν is given by

$$\hat{F} = \sum_{\nu\nu'} f_{\nu\nu'} a_\nu^+ a_{\nu'}. \quad (\text{C.35})$$

To show this, we have to prove

$$\sum_i \hat{f}_i \Phi(1, \dots, N) = \langle 1, \dots, N | \sum_{\nu\nu'} f_{\nu\nu'} a_\nu^+ a_{\nu'} | \Phi \rangle. \quad (\text{C.36})$$

On the l.h.s., from Eqs. (C.30), (C.26) and (C.34) up to a factor $1/\sqrt{N!}$ we gain

$$\begin{aligned} & \sum_i \hat{f}_i \langle - | a(N) \dots a(i) \dots a(1) | \Phi \rangle \\ &= \sum_i \sum_{\nu_1 \dots \nu_N} \hat{f}_i \varphi_{\nu_N}(N) \dots \varphi_{\nu_1}(i) \dots \varphi_{\nu_1}(1) \langle - | a_{\nu_N} \dots a_{\nu_1} | \Phi \rangle \\ &= \sum_i \sum_{\nu} \sum_{\nu_1 \dots \nu_N} f_{\nu\nu} \varphi_{\nu_N}(N) \dots \varphi_{\nu_1}(i) \dots \varphi_{\nu_1}(1) \langle - | a_{\nu_N} \dots a_{\nu_1} | \Phi \rangle. \end{aligned}$$

This is identical to the r.h.s.:

$$\begin{aligned} & \sum_{\nu\nu'} \sum_{\nu_1 \dots \nu_N} f_{\nu\nu'} \varphi_{\nu_N}(N) \dots \varphi_{\nu_1}(1) \langle - | a_{\nu_N} \dots a_{\nu_1} a_\nu^+ a_{\nu'} | \Phi \rangle \\ &= \sum_i \sum_{\nu} \sum_{\nu_1 \dots \nu_N} f_{\nu\nu} \varphi_{\nu_N}(N) \dots \varphi_{\nu_1}(1) \langle - | a_{\nu_N} \dots a_{\nu_1} a_\nu^+ a_\nu | \Phi \rangle. \end{aligned}$$

We give next a few examples:

The kinetic energy

$$\hat{T} = \sum_i \hat{t}_i = \sum_i \frac{-\hbar^2}{2m} \Delta_i, \quad (\text{C.37})$$

$$\begin{aligned} \hat{T} &= \sum_{\nu\nu'} \sum_s \int d^3r \varphi_\nu^*(\mathbf{r}, s) \frac{-\hbar^2}{2m} \Delta \varphi_\nu(\mathbf{r}, s) a_\nu^+ a_\nu \\ &= \sum_s \int d^3r a^+(\mathbf{r}, s) \frac{-\hbar^2}{2m} \Delta a(\mathbf{r}, s). \end{aligned} \quad (\text{C.38})$$

The single-particle density (see Appendix D)

$$\hat{\rho}(\mathbf{r}) = \sum_{i=1}^N \delta(\mathbf{r} - \hat{\mathbf{r}}_i). \quad (\text{C.39})$$

$\hat{\mathbf{r}}_i$ is the coordinate operator of the i th particle; \mathbf{r} is a number.

$$\hat{\rho}(\mathbf{r}) = \sum_{\nu\nu'} \sum_s \int d^3r' \varphi_\nu^*(\mathbf{r}', s) \delta(\mathbf{r} - \mathbf{r}') \varphi_\nu(\mathbf{r}', s) a_\nu^+ a_\nu = \sum_s a^+(\mathbf{r}, s) a(\mathbf{r}, s). \quad (\text{C.40})$$

The particle number

$$\begin{aligned} \hat{N} &= \sum_\nu a_\nu^+ a_\nu = \sum_\nu \sum_{ss'} \int d^3r d^3r' \varphi_\nu(\mathbf{r}, s) \varphi_\nu^*(\mathbf{r}', s') a^+(\mathbf{r}, s) a(\mathbf{r}', s') \\ &= \int \hat{\rho}(\mathbf{r}) d^3r. \end{aligned} \quad (\text{C.41})$$

In the most general case, \hat{f} will be an integral operator (a “nonlocal” one-particle operator):

$$\hat{f} \varphi(\mathbf{r}, s) = \sum_{s'} \int d^3r' f_{ss'}(\mathbf{r}, \mathbf{r}') \varphi(\mathbf{r}', s'). \quad (\text{C.42})$$

A *two-particle operator* as, for example, a two-body interaction, is given by a sum of operators v_{ij} which act on the coordinates of the particles i and j .

$$V = \sum_{i < j = 1}^N v_{ij}. \quad (\text{C.43})$$

In the most general case, v_{ij} will be an integral operator in two variables, with matrix elements

$$v_{\mu\nu\mu'\nu'} = \langle \mu\nu | v | \mu'\nu' \rangle = \int d1 d2 d3 d4 \varphi_\mu^*(1) \varphi_\nu^*(2) v(1, 2, 3, 4) \varphi_\mu(3) \varphi_\nu(4). \quad (\text{C.44})$$

In complete analogy to Eq. (C.35), we can show that V can be written as

$$V = \frac{1}{2} \sum_{\mu\nu\mu'\nu'} v_{\mu\nu\mu'\nu'} a_\mu^+ a_\nu^+ a_\nu a_\mu = \frac{1}{4} \sum_{\mu\nu\mu'\nu'} \bar{v}_{\mu\nu\mu'\nu'} a_\mu^+ a_\nu^+ a_\nu a_\mu, \quad (\text{C.45})$$

with the antisymmetrized matrix element

$$\bar{v}_{\mu\nu\mu'\nu'} = \langle \mu\nu | v | \mu'\nu' \rangle - \langle \mu\nu | v | \nu'\mu' \rangle. \quad (\text{C.46})$$

Very often we use local two-body interactions of the form (we neglect spin)

$$v_{ij} = v(\mathbf{r}_i, \mathbf{r}_j). \quad (\text{C.47})$$

In this case, we can verify Eq. (C.45) immediately with Eq. (C.40):

$$\begin{aligned} \frac{1}{2} \sum_{\mu\nu\mu'\nu'} v_{\mu\nu\mu'\nu'} a_\mu^+ a_\nu^+ a_\nu a_{\mu'} &= -\frac{1}{2} \int d^3 r d^3 r' a^+(\mathbf{r}) a^+(\mathbf{r}') v(\mathbf{r}, \mathbf{r}') a(\mathbf{r}) a(\mathbf{r}') \\ &= \frac{1}{2} \left(\int d^3 r d^3 r' v(\mathbf{r}, \mathbf{r}') \hat{\rho}(\mathbf{r}) \hat{\rho}(\mathbf{r}') - \int d^3 r v(\mathbf{r}, \mathbf{r}) \hat{\rho}(\mathbf{r}) \right) \\ &= \frac{1}{2} \left(\sum_{i \neq j} v(\mathbf{r}_i, \mathbf{r}_j) - \sum_i v(\mathbf{r}_i, \mathbf{r}_i) \right) = \sum_{i < j=1}^N v(\mathbf{r}_i, \mathbf{r}_j). \end{aligned} \quad (\text{C.48})$$

C.4 Wick's Theorem

In practical applications of the second quantization, Wick's theorem has turned out to be very useful. It is a rule which allows a very simple reordering of a set of N -operators a or a^+ , which have the property that the commutator (in the case of bosons) or the anticommutator (in the case of fermions) of two arbitrarily chosen operators of this set is a number.

We first define the T -product (time ordered product) of a product of operators $a(t_2), a(t_3), a^+(t_1), \dots$ to be the one where the field operators have been reordered in such a way that the time arguments are increasing from right to left (an odd permutation gives a minus sign):

$$T \{ a(t_1) a^+(t_3) a(t_2) a^+(t_4) \} = -a(t_1) a(t_2) a^+(t_3) a^+(t_4) \quad t_1 > t_2 > t_3 > t_4. \quad (\text{C.49})$$

In a *normal ordered* product, the field operators are ordered in such a way that all creation operators are to the left of all annihilation operators* (again, an odd permutation gives a minus sign):

$$N \{ a_\nu a_\mu a_\rho a_\sigma^+ \} =: a_\nu a_\mu a_\rho a_\sigma^+ := -a_\sigma^+ a_\nu a_\mu a_\rho. \quad (\text{C.50})$$

The *contraction* \widehat{UV} of two field operators U and V is defined as

$$\widehat{UV} = T \{ UV \} - N \{ UV \}. \quad (\text{C.51})$$

With these definitions, *Wick's Theorem* [Wi 50] can be stated as:

$$\begin{aligned} T \{ UVW \dots XYZ \} &= N \{ UVW \dots XYZ \} + N \{ \widehat{UVW} \dots XYZ \} \\ &\quad + \dots + N \{ \widehat{UVW} \dots \widehat{XYZ} \} + N \{ \widehat{UVW} \dots \widehat{XYZ} \} \\ &\quad + \dots + N \{ \widehat{UVW} \widehat{\dots XYZ} \} + \dots \end{aligned} \quad (\text{C.52})$$

The time ordered product of field operators is therefore equal to their normal ordered product plus the normal ordered products with one contraction (in all possible ways), plus the normal ordered product with two

* Instead of $N \{ \dots \}$ we also often use double dots $\dots \dots$.

contractions, and so on. Care has to be taken in the removal of a contraction out of a normal ordered product, as this can give a minus sign:

$$N(\widehat{UVXY}) = \widehat{UV}N(XY); N(\widehat{UVXY}) = -\widehat{UX}N(VY). \quad (\text{C.53})$$

(For the proof of Wick's theorem see, e.g., Thouless [Th 61b].)

Wick's theorem is especially useful for the calculation of ground state expectation values of time ordered products of field operators (e.g., the expectation value of particle operators with respect to the quasi-particle vacuum in Chap. 6). The result is equal to the r.h.s. of (C.52), where all operators have been contracted in all possible ways.

If there are time-independent field operators, as in (C.45), then the given order is to be defined as time ordered. The contraction of time-independent operators is especially simple; for example, we get:

$$\widehat{a_\mu a_\nu^+} = a_\mu a_\nu^+ - N(a_\mu a_\nu^+) = \delta_{\mu\nu}. \quad (\text{C.54})$$

APPENDIX D

Density Matrices

D.1 Normal Densities

For the description of the dynamics of a many-body system, we often use *density matrices*. We distinguish between one-particle density matrices, two-body density matrices, and so on. In this book we use mostly one-particle densities. For higher densities the reader is referred to the work of [Th 61b]. We shall also restrict ourselves to the fermion case.

First we define a single-particle operator $\hat{\rho}(\mathbf{r})$ in an N -body Hilbert space:

$$\hat{\rho}(\mathbf{r}) = \sum_{i=1}^N \delta(\mathbf{r} - \hat{\mathbf{r}}_i), \quad (\text{D.1})$$

where $\hat{\mathbf{r}}_i$ is the space operator of particle i and \mathbf{r} is a parameter. $\hat{\rho}(\mathbf{r})$ may be expressed in the framework of second quantization (see Appendix C):

$$\hat{\rho}(\mathbf{r}) = \sum_{pq} d_{pq} a_p^\dagger a_q, \quad (\text{D.2})$$

$$d_{pq} = \langle p | \delta(\mathbf{r} - \hat{\mathbf{r}}) | q \rangle = \sum_s \varphi_p^*(\mathbf{r}, s) \varphi_q(\mathbf{r}, s), \quad (\text{D.3})$$

$$\hat{\rho}(\mathbf{r}) = \sum_s a^\dagger(\mathbf{r}, s) a(\mathbf{r}, s). \quad (\text{D.4})$$

The expectation value of this operator in an N -body state $|\Psi\rangle$ is (see

Appendix C)

$$\langle \Psi | \hat{\rho}(\mathbf{r}) | \Psi \rangle = \sum_s \langle \Psi | a^\dagger(\mathbf{r}, s) a(\mathbf{r}, s) | \Psi \rangle \quad (\text{D.5})$$

$$= N \sum_{ss_2 \dots s_N} \int d^3 r_2 \dots d^3 r_N |\Psi(\mathbf{r}, s, \mathbf{r}_2, s_2, \dots, \mathbf{r}_N, s_N)|^2 = \rho(\mathbf{r}), \quad (\text{D.6})$$

which expresses the fact that the expectation value of $\hat{\rho}(\mathbf{r})$ is just the average particle density $\rho(\mathbf{r})$ at the point \mathbf{r} in this state. Integrating (D.6) over the whole space gives the particle number N of the system.

Equation (D.6) can also be interpreted as the diagonal element of an operator $\hat{\rho}_\Psi$ in the coordinate space representation, which is called the *density matrix*. In general, it is defined as

$$\langle \mathbf{r}, s | \hat{\rho}_\Psi | \mathbf{r}', s' \rangle := \rho(\mathbf{r}, s; \mathbf{r}', s') = \langle \Psi | a^\dagger(\mathbf{r}', s') a(\mathbf{r}, s) | \Psi \rangle. \quad (\text{D.7})$$

From Eq. (C.26) we get

$$\begin{aligned} \rho(\mathbf{r}, s; \mathbf{r}', s') &= \sum_{pq} \varphi_p(\mathbf{r}, s) \rho_{pq} \varphi_q^*(\mathbf{r}', s') \\ &= \sum_{pq} \langle \mathbf{r}, s | p \rangle \rho_{pq} \langle q | \mathbf{r}', s' \rangle, \end{aligned} \quad (\text{D.8})$$

where

$$\rho_{pq} = \langle \Psi | c_q^\dagger c_p | \Psi \rangle \quad (\text{D.9})$$

is the matrix element of the density operator $\hat{\rho}_\Psi$ in an arbitrary basis and $\hat{\rho}_\Psi$ has the form

$$\hat{\rho}_\Psi = \sum_{pq} |p\rangle \rho_{pq} \langle q|. \quad (\text{D.10})$$

It is a Hermitian single-particle operator. The matrix ρ can be diagonalized by a unitary transformation of the single-particle basis

$$(D^\dagger \rho D)_{ll'} = \rho_l \delta_{ll'}, \quad a_l^\dagger = \sum_{l'} D_{ll'} c_{l'}^\dagger, \quad (\text{D.11})$$

where

$$\rho_l = \langle \Psi | a_l^\dagger a_l | \Psi \rangle, \quad 0 \leq \rho_l \leq 1, \quad (\text{D.12})$$

is the probability that the level l is occupied in the wave function Ψ . Here we wrote ρ down in occupation number representation (see Appendix C) in the basis where ρ is diagonal. For the particle number we get

$$N = \sum_l \rho_l = \text{Tr } \rho = \sum_s \int \rho(\mathbf{r}, s; \mathbf{r}, s) d^3 r = \int \rho(\mathbf{r}) d^3 r \quad (\text{D.13})$$

and for any other single particle operator of the form (C.32) we get

$$\langle \Psi | \hat{F} | \Psi \rangle = \sum_{ll'} f_{ll'} \langle \Psi | a_l^\dagger a_{l'} | \Psi \rangle = \text{Tr}(f \cdot \rho). \quad (\text{D.14})$$

There are two important examples of single-particle densities, which we will treat in some detail.

D.2 Densities of Slater Determinants

In the case of product wave functions we have the following *theorem*.

A wave function $\Psi(1\dots N)$ is a Slater determinant if and only if the corresponding density matrix ρ_Ψ (D.10) is a projector in the single-particle Hilbert space, that is,

$$\hat{\rho}_\Psi^2 = \hat{\rho}_\Psi. \quad (\text{D.15})$$

There is a one-to-one correspondence between $\hat{\rho}_\Psi$ and $|\Psi\rangle$ in this case (of course, only up to a phase factor in $|\Psi\rangle$).

To prove this theorem we start with a Slater determinant

$$|\Psi\rangle = a_1^+ \dots a_N^+ |-\rangle \quad (\text{D.16})$$

in some single-particle basis characterized by the operators a_i^+, a_i . From (D.9) we see that ρ is diagonal in this basis, with

$$\rho_{ii} = \begin{cases} 0 & \text{for } i > N \quad (\text{empty levels, particles}), \\ 1 & \text{for } i < N \quad (\text{occupied levels, holes}). \end{cases} \quad (\text{D.17})$$

$\hat{\rho}_\Psi$ (D.10) has the form

$$\hat{\rho}_\Psi = \sum_{i=1}^N |i\rangle\langle i|. \quad (\text{D.18})$$

This is a projector onto the space of occupied states with the property (D.15).

On the other hand, we can start with a density matrix ρ with the property (D.15). It can be diagonalized [see Eq. (D.11)] and the eigenvalues ρ_i have the property

$$\rho_i^2 = \rho_i, \quad (\text{D.19})$$

that is, they are either 0 or 1. Constructing a Slater determinant from the single-particle wave functions with $\rho_i = 1$ gives us the corresponding wave function Ψ . These single-particle wave functions φ_i are not uniquely determined by the diagonalization of ρ . Any unitary transformation among the occupied levels leaves ρ invariant. As we see from (D.16), however, such a unitary transformation multiplies the wave function $|\Psi\rangle$ only by the determinant of this transformation, which is a phase.

This shows that there is a one-to-one correspondence between ρ and $|\Psi\rangle$ in the case of Slater determinants. In particular, we can use Wick's theorem (C.52) and express the expectation value $\langle\Psi|\hat{O}|\Psi\rangle$ of an arbitrary operator \hat{O} by the single-particle density ρ .

We next prove a *theorem due to Baranger and Veneroni* [BV 78, RS 77b], which states that any single-particle density matrix ρ that belongs to a Slater determinant ($\rho^2 = \rho$) can be decomposed in the following way.

$$\rho = e^{ix}\rho_0e^{-ix}, \quad (\text{D.20})$$

where χ and ρ_0 are Hermitian matrices that are even under time reversal. This decomposition is unique if we require

- (i) that χ has only ph and hp matrix elements in the basis in which ρ_0 is diagonal:

$$\rho_0 \chi \rho_0 = \sigma_0 \chi \sigma_0 = 0 \quad (\text{D.21})$$

($\sigma_0 = 1 - \rho_0$ projects onto particle states);

- (ii) that the eigenvalues χ_μ of the matrix χ have the property

$$-\frac{\pi}{4} < \chi_\mu < \frac{\pi}{4}. \quad (\text{D.22})$$

To prove this and to establish the uniqueness of the decomposition (D.20) we use the operator

$$\tau = 2\rho - 1 \quad \text{with} \quad \tau^2 = 1. \quad (\text{D.23})$$

The product, with its time reserved operator $\tau_T = T\tau T^+$, is unitary and is therefore of the form

$$\tau\tau_T = e^{4i\chi}, \quad (\text{D.24})$$

where the Hermitian operator χ is uniquely defined by the condition (D.22). By inversion, time reversal, and Hermitian conjugation,

$$\tau_T \tau = e^{-4i\chi} = e^{-4i\chi_T} = e^{-4i\chi^+}, \quad (\text{D.25})$$

we see that χ is time-reversal invariant and Hermitian.

Let $|\mu\rangle$ be a set of eigenstates of $\tau\tau_T$ with eigenvalue $\mu = e^{4i\chi_\mu}$, then $T|\mu\rangle$ is another eigenvector with the same eigenvalue μ and $\tau|T|\mu\rangle$ is an eigenvector with eigenvalue μ^* . This implies

$$(\chi\tau + \tau\chi)|\mu\rangle = (-\chi_\mu + \chi_\mu)\tau|\mu\rangle = 0, \quad (\text{D.26})$$

and thus

$$\chi\tau + \tau\chi = 0. \quad (\text{D.27})$$

This means, in particular, that for an arbitrary real number α ,

$$e^{i\alpha\chi}\tau = \tau e^{-i\alpha\chi} \quad (\text{D.28})$$

and

$$\tau_0 := e^{-2i\chi_T} = \tau e^{2i\chi} = \tau e^{-2i\chi}\tau\tau_T = e^{2i\chi}\tau_T = \tau_T e^{-2i\chi}.$$

τ_0 is therefore Hermitian and time even. The same holds for

$$\rho_0 := \frac{1}{2}(\tau_0 + 1). \quad (\text{D.29})$$

Using Eq. (D.28) again gives

$$\chi\rho_0 + \rho_0\chi = \chi, \quad (\text{D.30})$$

which is equivalent to Eq. (D.21). Q.E.D.

In the following, we give *some rules* for calculating with single-particle densities ρ of Slater determinants ($\rho^2 = \rho$, $\sigma = 1 - \rho$). An arbitrary matrix A

has the following pp , ph , hp , and hh parts in a basis in which ρ is diagonal:

$$A^{pp} := \sigma A \sigma; \quad A^{hh} = \rho A \rho; \quad A^{ph} = \sigma A \rho; \quad A^{hp} = \rho A \sigma. \quad (\text{D.31})$$

The three statements

$$A = A\rho + \rho A \Leftrightarrow A = \sigma A + A\sigma \Leftrightarrow A^{pp} = A^{hh} = 0 \quad (\text{D.32})$$

are equivalent. If two matrices A and B obey the relation $B = [A, \rho]$ it follows:

$$B^{pp} = B^{hh} = 0; \quad B^{ph} = A^{ph}; \quad B^{hp} = -A^{hp}. \quad (\text{D.32})$$

If, in addition,

$$A^{pp} = A^{hh} = 0$$

we can write

$$A = [B, \rho]. \quad (\text{D.33})$$

For Hermitian matrices A, B with vanishing pp and hh matrix elements, we often define vectors

$$\begin{pmatrix} A \\ A^* \end{pmatrix} = \begin{pmatrix} A_{mi} \\ A_{mi}^* \end{pmatrix}, \quad (\text{D.34})$$

and find the relations

$$\begin{aligned} (A^* A) \begin{pmatrix} B \\ B^* \end{pmatrix} &= \sum_{mi} A_{mi}^* B_{mi} + A_{mi} B_{mi}^* = \text{Tr}(A \cdot B) \\ (A^* A) \begin{pmatrix} B \\ -B^* \end{pmatrix} &= \text{Tr}(A \cdot [B, \rho]). \end{aligned} \quad (\text{D.35})$$

Next we investigate some properties of a family of Slater determinants $|\Phi(q)\rangle$ depending on some parameter q (e.g. the deformation) with the densities $\rho(q)$. Starting from one wave function in this family, $|\Phi(q_0)\rangle$, we can represent the other wave functions by a Hermitian single-particle operator \hat{P} , which has only ph and hp matrix elements with respect to $|\Phi(q_0)\rangle$, as follows [see Eq. (E.40)].

$$|\Phi(q+q_0)\rangle = e^{-(i/\hbar)q\hat{P}} |\Phi(q_0)\rangle, \quad (\text{D.36})$$

$$\hat{P} = P^0 + \sum_{mi} P_{mi} a_m^+ a_i + P_{mi}^* a_i^+ a_m. \quad (\text{D.37})$$

The constant P^0 eventually determines a phase. The operator \hat{P} generally depends on q and q_0 , and only in the limit $q \rightarrow 0$ does it become independent of q and we then gain

$$\hat{P} |\Phi(q)\rangle = i\hbar \frac{\partial}{\partial q} |\Phi(q)\rangle. \quad (\text{D.38})$$

For the density we have

$$\rho(q_0 + q) = e^{-(i/\hbar)q\hat{P}} \rho(q_0) e^{(i/\hbar)q\hat{P}} \quad (\text{D.39})$$

and

$$\frac{\partial}{\partial q} \rho(q) = \frac{-i}{\hbar} [P, \rho]. \quad (\text{D.40})$$

From the representation (D.18) we have

$$\frac{\partial}{\partial q} \hat{\rho}_* = \frac{\partial}{\partial q} \sum_i |i\rangle\langle i|. \quad (\text{D.41})$$

The ph -elements of \hat{P} therefore take the form

$$P_{mi} = i\hbar \langle m | \frac{\partial}{\partial q} |i\rangle = i\hbar \int d\mathbf{r} \varphi_m^*(\mathbf{r}, q) \frac{\partial}{\partial q} \varphi_i(\mathbf{r}, q). \quad (\text{D.42})$$

Very often the $|\Phi(q)\rangle$ are determined as HF solutions (see Sec. 7.6) of a Hamiltonian $H(q)$, which depends on a parameter q . From the variational principle (5.5) we get the Feynman theorem [Fe 39]:

$$\frac{d}{dq} \langle \Phi(q) | H(q) | \Phi(q) \rangle = \langle \Phi(q) | \frac{\partial H}{\partial q} | \Phi(q) \rangle. \quad (\text{D.43})$$

In cases in which $\partial H / \partial q$ is a single-particle operator, we can calculate the matrix elements P_{mi} in linear response theory (see Sec. 8.5.3). If we neglect the residual interaction, a simple perturbation theory gives (see, for instance, Sec. 3.4.2)

$$\langle m | \frac{\partial}{\partial q} |i\rangle = \frac{\langle m | \partial H / \partial q | i \rangle}{\epsilon_m - \epsilon_i}, \quad (\text{D.44})$$

where ϵ_m, ϵ_i are the single-particle energies corresponding to the operator $H(q)$.

D.3 Densities of BCS and HFB States

In the case of generalized product wave functions $|\Phi\rangle$ (see Sec. 7.2.3), we had defined the generalized density matrix

$$\mathcal{R} = \begin{pmatrix} \langle \Phi | c_l^\dagger c_l | \Phi \rangle & \langle \Phi | c_l c_l^\dagger | \Phi \rangle \\ \langle \Phi | c_l^\dagger c_l^\dagger | \Phi \rangle & \langle \Phi | c_l c_l^\dagger | \Phi \rangle \end{pmatrix} = \begin{pmatrix} \rho_H & \kappa_H \\ -\kappa_H^* & 1 - \rho_H^* \end{pmatrix}. \quad (\text{D.45})$$

Besides the normal density ρ (D.9), it contains the anomalous density κ (which is also called the pairing tensor). Under a unitary transformation D of the basis [for instance, Eq. (D.11)], the matrices ρ and κ transform in the following way.

$$\rho \rightarrow D^\dagger \rho D, \quad \kappa \rightarrow D^\dagger \kappa D^*. \quad (\text{D.46})$$

We can therefore represent κ in coordinate space [see Eq. (C.26)]:

$$\kappa(\mathbf{r}, s; \mathbf{r}', s') = \langle \Phi | a(\mathbf{r}', s') a^\dagger(\mathbf{r}, s) | \Phi \rangle = \sum_{pq} \varphi_p(\mathbf{r}, s) \kappa_{pq} \varphi_q(\mathbf{r}', s'). \quad (\text{D.47})$$

In the canonical basis $|k\rangle$ (see Sec. 7.2.1) or in the pure BCS case, κ_{pq} has

canonical form (7.25) and we get

$$\kappa(\mathbf{r}, s; \mathbf{r}', s') = \sum_{k>0} (\varphi_k(\mathbf{r}, s)\varphi_k(\mathbf{r}', s') - \varphi_k(\mathbf{r}, s)\varphi_k(\mathbf{r}', s')) u_k v_k. \quad (\text{D.48})$$

Working with the generalized density \mathfrak{R} , we can show that all the results we have obtained for Slater determinants also apply to this case.

D.4 The Wigner Transformation of the Density Matrix

The Wigner transformation of the density matrix is defined by*:

$$f_{\sigma\sigma'}(\mathbf{q}, \mathbf{p}) = \int d^3s e^{-(i/\hbar)\mathbf{p}\cdot\mathbf{s}} \rho_{\sigma\sigma'}\left(\mathbf{q} + \frac{\mathbf{s}}{2}, \mathbf{q} - \frac{\mathbf{s}}{2}\right). \quad (\text{D.49})$$

Since ρ is a Hermitian operator, (D.49) must stay the same if we replace ρ by ρ^+ . If, in addition, we take the complex conjugate, we see that $f_{\sigma\sigma'}(\mathbf{q}, \mathbf{p})$ is a Hermitian matrix in the spin indices. The diagonal elements $f_{\sigma\sigma} = f_\sigma$ are therefore real functions of \mathbf{q} and \mathbf{p} . If we neglect the spin orbit force, the Hamiltonian is invariant with respect to spin reversal, therefore $f_\sigma = f_{-\sigma}$. Under this condition the time-reversal properties of $f_\sigma(\mathbf{q}, \mathbf{p}, t)$ are very simple: f_σ is even (odd) in \mathbf{p} according to whether f_σ is time even (odd).

The inverse transformation to (D.49) is given by

$$\rho_{\sigma\sigma'}(\mathbf{r}, \mathbf{r}') = \frac{1}{(2\pi\hbar)^3} \int d^3p e^{(i/\hbar)\mathbf{p}(\mathbf{r}-\mathbf{r}')} f_{\sigma\sigma'}\left(\frac{\mathbf{r}+\mathbf{r}'}{2}, \mathbf{p}\right). \quad (\text{D.50})$$

Often, we wish to know the Wigner transform of products of operators like $\rho_W = (\exp(i\chi)\rho_0\exp(-i\chi))_W$. For this purpose we write the Wigner transform of the product of two general single-particle operators A and B in the following form.

$$(AB)_W = \int d^3r d^3r' d^3r'' e^{-(i/\hbar)\mathbf{p}(\mathbf{r}-\mathbf{r}')} \delta\left(\mathbf{q} - \frac{\mathbf{r}+\mathbf{r}'}{2}\right) \langle \mathbf{r}|A|\mathbf{r}''\rangle \langle \mathbf{r}''|B|\mathbf{r}'\rangle. \quad (\text{D.51})$$

The inverse Wigner transform (D.50) can also be written as

$$\langle \mathbf{r}|A|\mathbf{r}'\rangle = \frac{1}{(2\pi\hbar)^3} \int d^3p d^3q A(\mathbf{q}, \mathbf{p}) e^{(i/\hbar)\mathbf{p}(\mathbf{r}-\mathbf{r}')} \delta\left(\mathbf{q} - \frac{\mathbf{r}+\mathbf{r}'}{2}\right). \quad (\text{D.52})$$

Inserting (D.52) into (D.51) and performing the \mathbf{r} , \mathbf{r}' , and \mathbf{r}'' integrations gives:

$$(AB)_W = \frac{1}{(\pi\hbar)^6} \int d^3p' d^3p'' d^3q' d^3q'' e^{2i(\mathbf{p}'\mathbf{q}' - \mathbf{p}''\mathbf{q}'')/\hbar} \\ \times A(\mathbf{q} + \mathbf{q}', \mathbf{p} + \mathbf{p}') B(\mathbf{q} + \mathbf{q}'', \mathbf{p} + \mathbf{p}''). \quad (\text{D.53})$$

* In the following we use $\rho_{\sigma\sigma'}(\mathbf{q} + \mathbf{s}/2, \mathbf{q} - \mathbf{s}/2) = \rho(\mathbf{r}, \sigma; \mathbf{r}', \sigma')$ with the spin indices σ, σ' and the center of mass coordinates $\mathbf{q} = (\mathbf{r} + \mathbf{r}')/2$, $\mathbf{s} = \mathbf{r} - \mathbf{r}'$.

Replacing $A(\mathbf{q} + \mathbf{q}', \mathbf{p} + \mathbf{p}')$ and $B(\mathbf{q} + \mathbf{q}', \mathbf{p} + \mathbf{p}')$ in (D.53) by

$$\begin{pmatrix} A \\ B \end{pmatrix}(\mathbf{q} + \mathbf{q}', \mathbf{p} + \mathbf{p}') = e^{q'^2/2\hbar + p'^2/2m} \begin{pmatrix} A \\ B \end{pmatrix}(\mathbf{q}, \mathbf{p}) \quad (\text{D.54})$$

allows us to perform the \mathbf{p}' and \mathbf{q}' integrations, and the δ -functions allow us to do the \mathbf{p}' and \mathbf{q}' integration. After careful book-keeping of which derivatives act on which variables, we obtain [Gr 46, KK 76, Vo 77, BP 77b]:

$$(AB)_W = A(\mathbf{q}, \mathbf{p}) e^{(i\hbar/2)\overset{\leftrightarrow}{\Lambda}} B(\mathbf{q}, \mathbf{p}) \quad (\text{D.55})$$

with

$$\overset{\leftrightarrow}{\Lambda} = \overset{\leftarrow}{\nabla}_q \overset{\rightarrow}{\nabla}_p - \overset{\leftarrow}{\nabla}_p \overset{\rightarrow}{\nabla}_q, \quad (\text{D.56})$$

where the direction of the arrows indicates whether the gradient acts to the left or to the right.

As a small example, let us calculate the Wigner transform of the kinetic energy density matrix (13.13):

$$\begin{aligned} \tau(\mathbf{q}, \mathbf{p}) &= \left(\frac{\overset{\leftarrow}{\partial}}{\partial \mathbf{r}} \rho(\mathbf{r}) \frac{\overset{\rightarrow}{\partial}}{\partial \mathbf{r}'} \right)_W \\ &= -\frac{i}{\hbar} \mathbf{p} e^{(i\hbar/2)\overset{\leftrightarrow}{\Lambda}} f(\mathbf{q}, \mathbf{p}) e^{(i\hbar/2)\overset{\leftrightarrow}{\Lambda}} \frac{i}{\hbar} \mathbf{p} \\ &= \frac{p^2}{\hbar^2} \cdot f(\mathbf{q}, \mathbf{p}) + \frac{1}{4} \frac{\partial^2}{\partial \mathbf{q}^2} f(\mathbf{q}, \mathbf{p}). \end{aligned} \quad (\text{D.57})$$

Integration over \mathbf{p} gives the local part of the density matrix [see (D.50)]:

$$\frac{\hbar^2}{2m} \tau(\mathbf{q}) = \frac{1}{(2\pi\hbar)^3} \int d^3p \frac{p^2}{2m} f(\mathbf{q}, \mathbf{p}) + \frac{1}{4} \frac{\hbar^2}{2m} \Delta\rho(\mathbf{q}). \quad (\text{D.58})$$

In an actual calculation of the kinetic energy, the second term in (D.58) does not contribute because it is a divergence of a vector field. With formula (D.55) it is also very easy to calculate the Wigner transform of a commutator:

$$\frac{1}{\hbar} [A, B]_W = \frac{2i}{\hbar} A(\mathbf{q}, \mathbf{p}) \cdot \sin\left(\frac{\hbar}{2}\overset{\leftrightarrow}{\Lambda}\right) \cdot B(\mathbf{q}, \mathbf{p}). \quad (\text{D.59})$$

To lowest order in \hbar , the commutator just gives the classical Poisson bracket.

Theorems Concerning Product Wave Functions

In this appendix we shall derive some theorems and formulae used in connection with the general single-particle model (Chap. 7) and in more extended theories that are based on it (Chap. 10).

E.1 The Bloch–Messiah Theorem [BM 62]

The Bloch–Messiah theorem states that:

A unitary matrix \mathfrak{U} of the following special form can be decomposed into three matrices:

$$\mathfrak{U} = \begin{pmatrix} U & V^* \\ V & U^* \end{pmatrix} = \begin{pmatrix} D & 0 \\ 0 & D^* \end{pmatrix} \begin{pmatrix} \bar{U} & \bar{V} \\ \bar{V} & \bar{U} \end{pmatrix} \begin{pmatrix} C & 0 \\ 0 & C^* \end{pmatrix}, \quad (\text{E.1})$$

where the real matrices \bar{U} and \bar{V} are diagonal and of “quasi-canonical” form, as given in Eq. (7.9).

The proof is based on the property that an Hermitian matrix ρ can be diagonalized by a unitary transformation D such that

$$\bar{\rho} = D^+ \rho D \quad \text{is diagonal with real eigenvalues } \rho_k, \quad (\text{E.2})$$

and that a skew symmetric matrix κ can be brought into canonical form by (generally different) unitary matrix D :

$$\bar{\kappa} = D^+ \kappa D^* \quad \text{decomposes into } (2 \times 2) \text{ boxes of the form } \begin{pmatrix} 0 & \alpha \\ -\alpha & 0 \end{pmatrix} \quad (\text{E.3})$$

with real numbers κ_k , along the diagonal line [Zu 62]. In the next step, we show that if we have the relation

$$\rho\kappa = \kappa\rho^* \quad (\text{E.4})$$

we can find *one* matrix D which diagonalizes ρ and brings κ into canonical form. For this purpose we first diagonalize ρ and from (E.4) obtain in this basis

$$(\rho_i - \rho_k)\kappa_{ik} = 0. \quad (\text{E.5})$$

This means κ_{ik} vanishes in this basis for all values i and k with $\rho_i \neq \rho_k$, that is, we can restrict ourselves to subspaces of degenerate eigenvalues ρ_i . The κ does not mix them. In these subspaces ρ is a multiple of the unity. We can therefore bring κ into canonical form in each subspace without changing the diagonal character of ρ .

We now apply these general considerations to the transformation (E.1). First we suppose that U is Hermitian and positive semi-definite, otherwise this can be achieved by a suitable C -transformation, for instance,

$$C = (\sqrt{UU^*})^{-1} U^*. \quad (\text{E.6})$$

From Eq. (7.5) we see that the matrices

$$\rho = V^* V^T = I - UU^* \quad (\text{E.7})$$

and

$$\kappa = V^* U^T = -\kappa^T \quad (\text{E.8})$$

fulfill the condition (E.4). Therefore, we can find a basis (given by the transformation D) in which κ is in canonical form and ρ as well as U are diagonal with real eigenvalues v_k^2 and $u_k > 0$. From (E.7) we get the normalization

$$u_k^2 + v_k^2 = 1. \quad (\text{E.9})$$

We now have to distinguish between eigenspaces of U with eigenvalues $u_k \neq 0$ and those with eigenvalue 0. In the first case we can divide κ_{ik} by u_k and find from Eq. (E.8) that V is in canonical form with elements v_k . In the second case we see from Eq. (E.7) that V is unitary in these subspaces and we can shift it either to the matrix D or to the matrix C . The rest is a unity matrix.

In particular, we see from this derivation that the numbers u_k and v_k are real. Any complex phases can be shifted to the transformations C and D . As long as we restrict ourselves to real coefficients D , however, it may be interesting to use relative phases between u_k and v_k . The corresponding BCS wave functions will then depend on them.

E.2 Operators in the Quasi-particle Space

Using the inverse transformation to (7.1) we can transform all operators expressed by c^+ , c in the quasi-particle space. We now give a few examples:

For a Hermitian one-particle operator

$$\hat{F} = \sum_H f_H c_i^+ c_i + \frac{1}{2} (g_H c_i^+ c_i^+ + \text{h.c.}) \quad (\text{E.10})$$

we get

$$\hat{F} = F^0 + \sum_{kk'} F_{kk'}^{11} \beta_k^+ \beta_{k'} + \frac{1}{2} \sum_{kk'} (F_{kk'}^{20} \beta_k^+ \beta_{k'}^+ + \text{h.c.}) \quad (\text{E.11})$$

with

$$F^0 = \text{Tr}(f\rho) - \frac{1}{2} \text{Tr}(g\kappa^* + g^*\kappa), \quad (\text{E.12})$$

$$F_{kk'}^{11} = (U^+ f U - V^+ f^T V + U^+ g V - V^+ g^* U)_{kk'}, \quad (\text{E.13})$$

$$F_{kk'}^{20} = (U^+ f V^* - V^+ f^T U^* + U^+ g U^* - V^+ g^* V^*)_{kk'}, \quad (\text{E.14})$$

In the case of time-reversal invariance $T\hat{F}T^+ = \tau\hat{F}$ with $\tau = \pm 1$ this means in the canonical basis (see Sec. 7.2.1)

$$F_{kk'}^{11} = f_{kk} \xi_{kk'}^\tau - g_{kk} \eta_{kk'}^\tau, \quad (\text{E.15})$$

$$F_{kk'}^{20} = -f_{kk} \eta_{kk'}^\tau + g_{kk} \xi_{kk'}^\tau, \quad (\text{E.16})$$

where ξ^\pm and η^\pm are defined in Eq. (8.202).

An example of a Hermitian two-particle operator is the Hamiltonian

$$\hat{H} = \sum_{l_1 l_2} \epsilon_{l_1 l_2} c_{l_1}^+ c_{l_1} + \frac{1}{4} \sum_{l_1 l_2 l_3 l_4} \bar{v}_{l_1 l_2 l_3 l_4} c_{l_1}^+ c_{l_1}^+ c_{l_3} c_{l_4}. \quad (\text{E.17})$$

We get

$$\begin{aligned} \hat{H} = H^0 &+ \sum_{k_1 k_2} H_{k_1 k_2}^{11} \beta_{k_1}^+ \beta_{k_2} + \frac{1}{2} \sum_{k_1 k_2} (H_{k_1 k_2}^{20} \beta_{k_1}^+ \beta_{k_2} + \text{h.c.}) \\ &+ \sum_{k_1 k_2 k_3 k_4} (H_{k_1 k_2 k_3 k_4}^{40} \beta_{k_1}^+ \beta_{k_2}^+ \beta_{k_3}^+ \beta_{k_4} + \text{h.c.}) \\ &+ \sum_{k_1 k_2 k_3 k_4} (H_{k_1 k_2 k_3 k_4}^{31} \beta_{k_1}^+ \beta_{k_2}^+ \beta_{k_3}^+ \beta_{k_4} + \text{h.c.}) \\ &+ \frac{1}{4} \sum_{k_1 k_2 k_3 k_4} H_{k_1 k_2 k_3 k_4}^{22} \beta_{k_1}^+ \beta_{k_2}^+ \beta_{k_3} \beta_{k_4}. \end{aligned} \quad (\text{E.18})$$

With the definitions

$$h = \epsilon + \Gamma, \quad (\text{E.19a})$$

$$\Gamma_{lm} = \sum_{pq} \bar{v}_{lqmp} \rho_{pq} := \text{Tr}_1(\bar{v}\rho), \quad (\text{E.19b})$$

$$\Delta_{lm} = \frac{1}{2} \sum_{pq} \bar{v}_{lmnpq} K_{pq} := -\frac{1}{2} \text{Tr}_2(\bar{v}\kappa), \quad (\text{E.19c})$$

we can write:

$$\begin{aligned} H^0 &= \text{Tr}(\epsilon\rho + \frac{1}{2}\Gamma\rho - \frac{1}{2}\Delta\kappa^*) \\ &= \text{Tr}(\epsilon\rho) + \frac{1}{2}\text{Tr}_1\text{Tr}_1(\rho\bar{v}\rho) + \frac{1}{4}\text{Tr}_2\text{Tr}_2(\kappa^*\bar{v}\kappa), \end{aligned} \quad (\text{E.20})$$

$$H^{11} = U^+hU - V^+h^TV + U^+\Delta V - V^+\Delta^*U, \quad (\text{E.21})$$

$$H^{20} = U^+hV^* - V^+h^TU^* + U^+\Delta U^* - V^+\Delta^*V^*, \quad (\text{E.22})$$

and

$$H_{k_1 k_2 k_3 k_4}^{40} = \frac{1}{4} \sum_{l_1 l_2 l_3 l_4} \bar{v}_{l_1 l_2 l_3 l_4} U_{l_1 k_1}^* U_{l_2 k_2}^* V_{l_3 k_3}^* V_{l_4 k_4}^*, \quad (\text{E.23a})$$

$$H_{k_1 k_2 k_3 k_4}^{31} = \frac{1}{2} \sum_{l_1 l_2 l_3 l_4} \bar{v}_{l_1 l_2 l_3 l_4} (U_{l_1 k_1}^* V_{l_2 k_2}^* V_{l_3 k_3}^* V_{l_4 k_4} + V_{l_1 k_1}^* U_{l_2 k_2}^* U_{l_3 k_3}^* U_{l_4 k_4}), \quad (\text{E.23b})$$

$$\begin{aligned} H_{k_1 k_2 k_3 k_4}^{22} &= \sum_{l_1 l_2 l_3 l_4} \bar{v}_{l_1 l_2 l_3 l_4} ((U_{l_1 k_1}^* V_{l_2 k_2}^* V_{l_3 k_3} U_{l_4 k_4} - (k_1 \leftrightarrow k_2)) - (k_3 \leftrightarrow k_4) \\ &\quad + U_{l_1 k_1}^* U_{l_2 k_2}^* U_{l_3 k_3} U_{l_4 k_4} + V_{l_1 k_1}^* V_{l_2 k_2}^* V_{l_3 k_3} V_{l_4 k_4}), \end{aligned} \quad (\text{E.23c})$$

Representations of these matrix elements in the canonical basis are given in Eqs. (8.201) and (9.133).

In the case of vanishing pairing correlations, the quasi-particles are either particles or holes:

$$\beta_m^+ = a_m^+ \quad \text{for } \epsilon_m > \epsilon_F; \quad \beta_i^+ = a_i \quad \text{for } \epsilon_i < \epsilon_F.$$

In this representation, the Hamiltonian (E.18) has the form:

$$H^0 = \sum_i \left(\epsilon_i + \frac{1}{2} \sum_j \bar{v}_{ijj} \right), \quad (\text{E.24a})$$

$$H^{11} = \sum_{mm'} \left(\epsilon_{mm'} + \sum_j \bar{v}_{mj'm'j} \right) \beta_m^+ \beta_{m'}^- - \sum_{ii'} \left(\epsilon_{ii'} + \sum_j \bar{v}_{ijj} \right) \beta_i^+ \beta_{i'}^-, \quad (\text{E.24b})$$

$$H^{20} = \sum_{mi} \left(\epsilon_{mi} + \sum_j \bar{v}_{mjij} \right) \beta_m^+ \beta_i^+ + \text{h.c.}, \quad (\text{E.24c})$$

$$H^{40} = \frac{1}{4} \sum_{\substack{mn \\ ij}} \bar{v}_{mnij} \beta_m^+ \beta_i^+ \beta_n^+ \beta_j^+ + \text{h.c.}, \quad (\text{E.25a})$$

$$H^{31} = \frac{1}{2} \sum_{mi} \beta_m^+ \beta_i^+ \left(\sum_{nn'} \bar{v}_{mnin'} \beta_n^+ \beta_{n'}^- - \sum_{jj'} \bar{v}_{mj'ij} \beta_j^+ \beta_{j'}^- \right) + \text{h.c.}, \quad (\text{E.25b})$$

$$\begin{aligned} H^{22} &= \frac{1}{4} \sum_{\substack{mm' \\ nn'}} \bar{v}_{mm'nn'} \beta_m^+ \beta_n^+ \beta_{n'}^- \beta_{m'}^- + \frac{1}{4} \sum_{\substack{ij \\ ij'}} \bar{v}_{ijij'} \beta_i^+ \beta_{i'}^+ \beta_j^- \beta_{j'}^- \\ &\quad + \sum_{minj} \bar{v}_{mnyin} \beta_m^+ \beta_i^+ \beta_j^- \beta_n^-. \end{aligned} \quad (\text{E.25c})$$

E.3 Thouless' Theorem

Thouless' theorem [Th 60] states that:

Starting with a general product wave function $|\Phi_0\rangle$ which is the vacuum to quasi-particle operators β , any other general product wave function $|\Phi_1\rangle$ which is not orthogonal to $|\Phi_0\rangle$ may be expressed in the form

$$|\Phi_1\rangle = \mathcal{R} \cdot \exp \left(\sum_{k < k'} Z_{kk'} \beta_k^+ \beta_{k'}^+ \right) |\Phi_0\rangle, \quad (\text{E.26})$$

where $\mathcal{R} = \langle \Phi_0 | \Phi_1 \rangle$ is a normalization constant and Z a skew symmetric matrix. Thouless has given this theorem for pure Slater determinants Φ_0, Φ_1 . Two-quasi-particle states in this case are ph states:

$$|\Phi_1\rangle = \mathcal{R} \cdot \exp \left(\sum_{mi} Z_{mi} a_m^+ a_i \right) |\Phi_0\rangle. \quad (\text{E.27})$$

To prove this theorem we start with two sets of quasi-particle operators β, β^+ and γ, γ^+ belonging to the function $|\Phi_0\rangle$ and $|\Phi_1\rangle$:

$$\begin{aligned} \beta_k^+ &= \sum_i U_{0ik} c_i^+ + V_{0ik} c_i, \\ \gamma_k^+ &= \sum_i U_{1ik} c_i^+ + V_{1ik} c_i, \end{aligned} \quad (\text{E.28})$$

and express the operators γ^+ together with (7.6) by the operators β, β^+ :

$$\gamma_k^+ = \sum_{k'} U_{k'k} \beta_{k'}^+ + V_{k'k} \beta_k, \quad (\text{E.29})$$

with

$$\begin{aligned} U &= U_0^+ U_1 + V_0^+ V_1, \\ V &= V_0^T U_1 + U_0^T V_1. \end{aligned} \quad (\text{E.30})$$

As we shall see in Section E.4, the overlap $|\langle \Phi_1 | \Phi_0 \rangle|^2$ is given by $|\det(U)|$. Nonorthogonality of $|\Phi_1\rangle$ and $|\Phi_0\rangle$ therefore means that we can invert U and define the operators

$$\tilde{\gamma}_k^+ = \sum_{k'} U_{k'k}^{-1} \gamma_{k'}^+ = \beta_k^+ + \sum_{k'} Z_{k'k}^* \beta_{k'}, \quad (\text{E.31})$$

with the skew symmetric matrix Z [see Eq. (7.5)]:

$$Z := (VU^{-1})^* = -U^{+^{-1}}V^+ = -Z^T. \quad (\text{E.32})$$

Since (E.31) is only a transformation among the creation operators γ^+ , $|\Phi_1\rangle$ is also vacuum to the operators $\tilde{\gamma}$. This condition determines $|\Phi_1\rangle$ up to a normalization constant. We therefore have only to show that $\tilde{\gamma}_k$ annihilates the r.h.s. of Eq. (E.26):

$$\tilde{\gamma}_k \exp \left(\sum_{k < k'} Z_{kk'} \beta_k^+ \beta_{k'}^+ \right) |\Phi_0\rangle = e^{\hat{Z}} \left\{ e^{-\hat{Z}} \beta_k e^{\hat{Z}} + \sum_{k'} Z_{k'k} \beta_{k'}^+ \right\} |\Phi_0\rangle \quad (\text{E.33})$$

with

$$\hat{Z} = \sum_{k < k'} Z_{kk'} \beta_k^+ \beta_{k'}^+. \quad (\text{E.34})$$

Using

$$e^{-\hat{Z}} \beta_k e^{\hat{Z}} = \beta_k - [\hat{Z}, \beta_k] = \beta_k - \sum_{k'} Z_{k'k} \beta_{k'}^+, \quad (\text{E.35})$$

we see that the r.h.s. of Eq. (E.33) vanishes. This completes the proof of Thouless' theorem and shows that Z is uniquely defined by $|\Phi_1\rangle$. In particular, it does not depend on a C -transformation among the quasi-particles γ^+ .

We might ask whether we can represent wave functions $|\tilde{\Phi}_1\rangle$ which are orthogonal to $|\Phi_0\rangle$ in a similar way. The answer is a *generalization of Thouless' theorem*, which states that a wave function $|\tilde{\Phi}_1\rangle$ which is orthogonal to $|\Phi_0\rangle$ can be represented as a multi-quasi-particle state on a function $|\Phi_1\rangle$ which is not orthogonal to $|\Phi_0\rangle$,

$$|\tilde{\Phi}_1\rangle = \tilde{\beta}_{b_1}^+ \cdots \tilde{\beta}_{b_n}^+ |\Phi_1\rangle, \quad (\text{E.36})$$

with quasi-particle operators $\tilde{\beta}_{b_i}$ that annihilate $|\Phi_0\rangle$.

To prove this generalization and to give an explicit form for the function $|\Phi_1\rangle$, we use the fact that the transformation (E.29) from $(\beta, \beta^+) \rightarrow (\gamma, \gamma^+)$ is a general Bogoliubov transformation. We can therefore apply the Bloch-Messiah theorem again and find that it can be decomposed into a transformation among the operators β^+ :

$$\tilde{\beta}_k^+ = \sum_{k'} D_{k'k} \beta_{k'}^+, \quad (\text{E.37})$$

a special Bogoliubov transformation [(7.12) and (7.13)] to "quasi-particle" operators $\tilde{\gamma}, \tilde{\gamma}^+$ which have the vacuum $|\Phi_1\rangle$ and a C -transformation $\tilde{\gamma}^+ \rightarrow \gamma^+$.

In analogy to Eq. (7.18), $|\tilde{\Phi}_1\rangle$ can therefore be written as

$$|\tilde{\Phi}_1\rangle = \prod_{i=1}^n \tilde{\beta}_{b_i}^+ \cdot \prod_{p>0} (u_p + v_p \tilde{\beta}_p^+ \tilde{\beta}_{\bar{p}}^+) |\Phi_0\rangle, \quad (\text{E.38})$$

where $b_1 \dots b_n$ are the blocked levels and $u_p > 0$ does not vanish by definition. We therefore get for $|\Phi_1\rangle$,

$$|\Phi_1\rangle = \prod_{p>0} (u_p + v_p \tilde{\beta}_p^+ \tilde{\beta}_{\bar{p}}^+) |\Phi_0\rangle = \left(\prod_{p>0} u_p \right) \exp \left(\sum_{p>0} \frac{v_p}{u_p} \tilde{\beta}_p^+ \tilde{\beta}_{\bar{p}}^+ \right) |\Phi_0\rangle \quad (\text{E.39})$$

which finishes the proof of (E.36).

The transformation $e^{\hat{Z}} |\Phi_0\rangle$ is not unitary, because it changes the norm of the state. We might ask whether there is also a unitary transformation [RS 77b]

$$|\Phi_1\rangle = e^{i\hat{T}} |\Phi_0\rangle \quad (\text{E.40})$$

with a Hermitian single-particle operator \hat{T} which accomplishes the same. The answer is yes. This can even be accomplished for cases where $|\Phi_1\rangle$ is orthogonal to $|\Phi_0\rangle$.

To find one possible choice, we again start with the transformation (E.27) and decompose the matrices U and V according to the Bloch-Messiah theorem [Eq. (7.8)]. Since $|\Phi_1\rangle$ does not depend on the special choice of the matrix C , we use $C = D^+$ and get

$$U = D\bar{U}D^+, \quad V = D^*\bar{V}D^+. \quad (\text{E.41})$$

\bar{U} is diagonal with the diagonal elements u_k , and \bar{V} can be written as the product of a diagonal matrix \bar{V} with the elements v_k and a matrix \bar{S} , which has only diagonal elements 0 and 1 and 2×2 blocks of the form $(\begin{smallmatrix} 0 & 1 \\ -1 & 0 \end{smallmatrix})$ along the diagonal line [see (7.9)]

$$\bar{V} = \bar{V} \cdot \bar{S}. \quad (\text{E.42})$$

If we now define a diagonal matrix \bar{R} with the elements $0 < r_k < \pi/2$ and $u_k = \cos r_k$, $v_k = \sin r_k$, we get

$$U = \cos R, \quad V = S \cdot \sin R = (\sin R)^* \cdot S, \quad (\text{E.43})$$

with

$$R = D\bar{R}D^+ \quad \text{and} \quad S = D^*\bar{S}D^+ := e^{-iF}, \quad (\text{E.44})$$

where S is unitary and R and F are Hermitian.

We can now define a Hermitian operator \hat{T} ,

$$\hat{T} = \sum_{k < k'} T_{kk'} \beta_k^+ \beta_{k'}^+ + \text{h.c.}, \quad (\text{E.45})$$

which has only a two-quasi-particle part and where the matrix T is given by its "polar decomposition" [Ga 72] as

$$T = iRe^{iF} = ie^{iF} \cdot R^*. \quad (\text{E.46})$$

With the formula $e^A B e^{-A} = B + [A, B] + (1/2!)[A, [A, B]] + \dots$, it is easy to show that the transformation of the quasi-particles

$$e^{i\hat{T}} \beta_k^+ e^{-i\hat{T}} = \sum_{k'} U_{k'k} \beta_{k'}^+ + V_{k'k} \beta_{k'}^- \quad (\text{E.47})$$

has the matrices U and V in Eq. (E.43). Equation (E.32) gives a connection to the matrix Z of Thouless' theorem

$$Z = -(\tan R) \cdot e^{iF}, \quad (\text{E.48})$$

which shows that Z diverges if R has eigenvalues $r_k = \pi/2$, that is, $u_k = 0$. The advantage of the transformation $e^{\hat{T}}$ is that it is uniquely defined by the wave functions $|\Phi_1\rangle$ and $|\Phi_0\rangle$. The matrix T is only unique if we restrict ourselves to eigenvalues r_k of R in the interval $0 < r_k < \pi/2$.

Those considerations are a special case of a general formula given by Balian and Brézin [BB 69, HI 79], which holds for any Hermitian single-

particle operator \hat{S} bilinear in the operators β_k, β_k^+

$$\hat{S} = \sum_{kk'} S_{kk'}^{11} \beta_k^+ \beta_{k'} + \sum_{k < k'} (S_{kk'}^{20} \beta_k^+ \beta_{k'} + \text{h.c.}).$$

The unitary operator $e^{i\hat{S}}$ can be written as

$$e^{i\hat{S}} = \langle e^{i\hat{S}} \rangle \cdot e^{\hat{X}} e^{i\hat{Y}} e^{\hat{Z}},$$

with $\beta | \rangle = 0$ and

$$\hat{X} = \sum_{k < k'} X_{kk'} \beta_{k'} \beta_k, \quad \hat{Y} = \sum_{kk'} Y_{kk'} \beta_k^+ \beta_{k'}, \quad \hat{Z} = \sum_{k < k'} Z_{kk'} \beta_k^+ \beta_{k'}^+,$$

The matrices X, Y , and Z can be derived from the matrices U and V obtained from the unitary transformation of the operators β_k^+ [in analogy to Eq. (E.47)]:

$$e^{i\hat{S}} \beta_k^+ e^{-i\hat{S}} = \sum_{k'} U_{k'k} \beta_{k'}^+ + V_{k'k} \beta_{k'},$$

namely:

$$X = V^T U^{+-1}; \quad Z = V^* U^{*-1}; \quad e^{iY} = (U^+)^{-1}.$$

The matrices U and V can be expressed by the matrices S^{11} and S^{20} in the following way.

$$\begin{pmatrix} U & V^* \\ V & U^* \end{pmatrix} = \exp \left\{ i \begin{pmatrix} S^{11} & S^{20} \\ -S^{20} & -S^{11*} \end{pmatrix} \right\}.$$

E.4 The Onishi Formula

In the context of many problems (for instance, in the GCM method), we need the overlap integrals $\langle \Phi_1 | \Phi_0 \rangle$ of the norm and of other operators $\langle \Phi_1 | \hat{O} | \Phi_0 \rangle$ for general product wave functions $|\Phi_0\rangle$ and $|\Phi_1\rangle$. In the case of pure Slater determinants such formulas have been given by Löwdin [Lö 55]. They have been generalized for HFB wave functions by Onishi and Yoshida [OY 66]. A very elegant derivation, which can also be applied to the boson case, has been given by Balian and Brézin [BB 69].

These formulas can only be used if the overlap $\langle \Phi_1 | \Phi_0 \rangle$ does not vanish. In cases where it vanishes we can use the representation (E.36) for $|\Phi_1\rangle$.

With the definitions (E.30), (E.32), and (E.43) the overlap integral for the norm is given by*

$$\langle \Phi_1 | \Phi_0 \rangle = \sqrt{\det U} = \sqrt{\det(U_0^+ U_1 + V_0^+ V_1)} = \sqrt{\det(\cos R)}. \quad (\text{E.49})$$

Before we give the proof of this formula we rewrite it in different ways. In the basis where U is diagonal, it is easy to show that

$$\det(U) = \exp(\text{Tr} \ln U). \quad (\text{E.50})$$

* Since the wave functions $|\Phi_0\rangle$ and $|\Phi_1\rangle$ from the definition (7.15) are only given to a phase, there is also a phase open in the following formulas. We assume U to be Hermitian and positive definite (see Eq. E.6).

Using the transformations (E.28), we express the wave functions $|\Phi_i\rangle$ ($i=0, 1$) by the operators c_i^\dagger and the bare vacuum $|-\rangle$ (which is only possible if $\langle\Phi_1|-\rangle \neq 0$), and get from (E.49) with $Z_i = (V_i U_i^{-1})^*$

$$\langle -|e^{\hat{Z}_1} e^{\hat{Z}_0}|-\rangle = \exp\left\{\frac{1}{2}\text{Tr}(\ln(1 - Z_1^* Z_0))\right\}. \quad (\text{E.51})$$

Next we give the formula for the Hamilton overlap:

$$\langle\Phi_1|H|\Phi_0\rangle = \langle\Phi_1|\Phi_0\rangle \cdot \left\{ \text{Tr}(\rho^{10}) + \frac{1}{2}\text{Tr}_1\text{Tr}_1(\rho^{10}\bar{\nu}\rho^{10}) + \frac{1}{4}\text{Tr}_2\text{Tr}_2(\kappa^{01*}\bar{\nu}\kappa^{10}) \right\}. \quad (\text{E.52})$$

Where the notation of Eq. (E.19) is used, the transition densities ρ^{10}, κ^{10} and κ^{01} are defined by

$$\rho_{H^*}^{10} = \frac{\langle\Phi_1|c_i^\dagger c_i|\Phi_0\rangle}{\langle\Phi_1|\Phi_0\rangle}, \quad (\text{E.53a})$$

$$\kappa_{H^*}^{10} = \frac{\langle\Phi_1|c_i c_i^\dagger|\Phi_0\rangle}{\langle\Phi_1|\Phi_0\rangle}, \quad (\text{E.53b})$$

$$\kappa_{H^*}^{01*} = \frac{\langle\Phi_1|c_i^\dagger c_{i'}^\dagger|\Phi_0\rangle}{\langle\Phi_1|\Phi_0\rangle}. \quad (\text{E.53c})$$

These matrices can be expressed by the densities ρ_0, κ_0 , the HFB coefficients U_0, V_0 , which belong to $|\Phi_0\rangle$, and by the Thouless matrix Z [Eq. (E.32)], or after some calculations with the orthogonality relations for U_0, V_0, U_1, V_1 in a more symmetric way by Z_0 and Z_1 [see Eq. (E.51)]:

$$\rho^{10} = \rho_0 = V_0^* Z^* U_0^+ = -Z_0(1 - Z_1^* Z_0)^{-1} Z_1^* = V_0^* U^{T-1} V_1^T. \quad (\text{E.54a})$$

$$\kappa^{10} = \kappa_0 = V_0^* Z^* V_0^+ = -Z_0(1 - Z_1^* Z_0)^{-1} = V_0^* U^{T-1} U_1^T, \quad (\text{E.54b})$$

$$\kappa^{01*} = \kappa_0^* + U_0^* Z^* U_0^+ = -(1 - Z_1^* Z_0)^{-1} Z_1^* = -U_0^* U^{T-1} V_1^T. \quad (\text{E.54c})$$

We see that for $|\Phi_1\rangle \rightarrow |\Phi_0\rangle$, these densities go over into the usual densities ρ, κ, κ^* . In the same way we can calculate the overlap integral for arbitrary operators expressed by c_i^\dagger and c_i . We must first derive the expectation value with respect to a HFB wave function. According to Wick's theorem (C.4), we can express such expectation values by the contractions $\rho \sim c^\dagger c, \kappa \sim \bar{c}c; \kappa^* \sim c^\dagger c^+$. To get the overlap integral, we only have to replace ρ by ρ^{10} , κ by κ^{10} , and κ^* by κ^{01*} , and multiply by $\langle\Phi_1|\Phi_0\rangle$. Obviously, these conclusions are also valid if we replace the bare vacuum by an arbitrary HFB function $|\Phi\rangle$ and the operators c^\dagger, c by the corresponding quasi-particle operators.

In the following we present a derivation of the formulae (E.49) and (E.54):

To get $\langle\Phi_1|\Phi_0\rangle$ we present $|\Phi_1\rangle$ in the canonical basis of the transformation (E.29). This is done in Eq. (E.38). Since $\langle\Phi_1|\Phi_0\rangle$ does not vanish, there are no blocked levels and we get $\langle\Phi_1|\Phi_0\rangle$ as a product of all the real positive numbers u_p . These are the two-fold degenerate eigenvalues of the

matrix U [Eq. (E.41)]:

$$\langle \Phi_1 | \Phi_0 \rangle = \prod_{p>0} (u_p) = \left(\prod_{p \geq 0} u_p \right)^{1/2} = (\det U)^{1/2}. \quad (\text{E.55})$$

Next we derive the overlap integral for an arbitrary operator expressed by the basis operators c, c^+ . From Thouless's theorem, with (E.34), we get

$$|\Phi_1\rangle = e^{\hat{z}} |\Phi_0\rangle \langle \Phi_0 | \Phi_1 \rangle, \quad e^{-\hat{z}^+} |\Phi_0\rangle = |\Phi_0\rangle, \quad (\text{E.56})$$

and

$$\langle \Phi_1 | c_{l_1}^+ \cdots c_{l_p}^+ c_{k_1} \cdots c_{k_q} | \Phi_0 \rangle = \langle \Phi_1 | \Phi_0 \rangle \langle \Phi_0 | \bar{d}_{l_1} \cdots \bar{d}_{l_p} d_{k_1} \cdots d_{k_q} | \Phi_0 \rangle, \quad (\text{E.57})$$

where we have introduced the operators

$$\bar{d}_l = e^{\hat{z}^+} c_l^+ e^{-\hat{z}^+} \quad \text{and} \quad d_l = e^{\hat{z}^+} c_l e^{-\hat{z}^+}. \quad (\text{E.58})$$

These operators obey Fermi commutation relations. We can therefore apply Wick's theorem (C.4) to evaluate the matrix element (E.53), which shows that we need only the contractions $\bar{d}\bar{d}$, dd , and $\bar{d}d$. They are given by ρ^{10} , κ^{10} , and κ^{01} , respectively, in Eqs. (E.53) and can be calculated by expressing the operators d, \bar{d} in terms of the operators β, β^+ :

$$\begin{aligned} \bar{d}_l &= \sum_k U_{0lk}^* \beta_k^+ + \sum_k (V_0 + U_0^* Z^*)_{lk} \beta_k, \\ d_l &= \sum_k (U_0 + V_0^* Z^*)_{lk} \beta_k + \sum_k V_{0lk}^* \beta_k^+. \end{aligned} \quad (\text{E.59})$$

E.5 Bogoliubov Transformations for Bosons

As in the case of fermions, starting from a basis set of boson operators B_μ, B_μ^+ with the "bare" vacuum $|-\rangle$, we can make a Bogoliubov transformation to other bosons O_ν, O_ν^+ as

$$\begin{pmatrix} B \\ B^+ \end{pmatrix} = \begin{pmatrix} X & Y^* \\ Y & X^* \end{pmatrix} \begin{pmatrix} O \\ O^+ \end{pmatrix} = \mathcal{X} \begin{pmatrix} O \\ O^+ \end{pmatrix}, \quad (\text{E.60})$$

in which the matrix \mathcal{X} is unitary with respect to the metric

$$\mathcal{X} = \begin{pmatrix} 1 & 0 \\ 0 & -1 \end{pmatrix}, \quad \mathcal{X} \mathcal{X}^* = \mathcal{X}, \quad \mathcal{X}^* \mathcal{X} = \mathcal{X}. \quad (\text{E.61})$$

Corresponding to the Bloch-Messiah theorem (E.1), we can show that each matrix \mathcal{X} of this kind can be decomposed in the following way.

$$\mathcal{X} = \begin{pmatrix} D & 0 \\ 0 & D^* \end{pmatrix} \begin{pmatrix} \bar{X} & \bar{Y} \\ \bar{Y} & \bar{X} \end{pmatrix} \begin{pmatrix} C & 0 \\ 0 & C^* \end{pmatrix}, \quad (\text{E.62})$$

where D and C are unitary and \bar{X} and \bar{Y} are diagonal with real nonnegative diagonal elements x_k, y_k with the relation $x_k^2 - y_k^2 = 1$ (Bloch-Messiah theorem for bosons).

An operator quadratic in bosons

$$\hat{F} = \sum_{\mu\nu} f_{\mu\nu} B_{\mu}^{+} B_{\nu} + \frac{1}{2} \sum_{\mu\nu} (g_{\mu\nu} B_{\mu}^{+} B_{\nu}^{+} + \text{h.c.}) \quad (\text{E.63})$$

may be expressed by the new bosons O, O^{+} in the following way.

$$\hat{F} = \frac{1}{2} \text{Tr}(F^{11} - f) + \sum_{\mu\nu} F_{\mu\nu}^{11} O_{\mu}^{+} O_{\nu} + \frac{1}{2} \sum_{\mu\nu} (F_{\mu\nu}^{20} O_{\mu}^{+} O_{\nu}^{+} + \text{h.c.}), \quad (\text{E.64})$$

with

$$F^{11} = X^{+} f X + Y^{+} f^{*} Y + X^{+} g Y + Y^{+} g^{*} X, \quad (\text{E.65})$$

$$F^{20} = X^{+} f Y^{*} + Y^{+} f^{*} X^{*} + X^{+} g X^{*} + Y^{+} g^{*} Y^{*}. \quad (\text{E.66})$$

The vacuum $|\Phi\rangle$ belonging to the bosons O is uniquely defined by

$$O_{\mu} |\Phi\rangle = 0 \quad \text{for all } \mu. \quad (\text{E.67})$$

If we have two such vacua $|\Phi_0\rangle$ and $|\Phi_1\rangle$ with the operators $O^{(0)}$ and $O^{(1)}$, and if we define

$$X = X_0^{+} X_1 - Y_0^{+} Y_1; \quad Y = X_0^T Y_1 - Y_0^T X_1, \quad (\text{E.68})$$

we can prove a *Thouless' Theorem for bosons*^{*}:

$$|\Phi_1\rangle = (\Phi_0|\Phi_1\rangle) \cdot \exp\left(\frac{i}{2} \sum_{\mu\nu} Z_{\mu\nu} O_{\mu}^{(0)+} O_{\nu}^{(0)+}\right) |\Phi_0\rangle \quad (\text{E.69})$$

with

$$Z = (YX^{-1})^{*} = (X^{+})^{-1} Y^{+} = Z^T. \quad (\text{E.70})$$

This representation is always possible, because vacua that are connected by a finite Bogoliubov transformation are never orthogonal. In contrast to the fermion case, it is impossible to represent a multi-boson state $O_1^{+} \dots O_n^{+} |\Phi_0\rangle$ as a new vacuum for new bosons. In analogy to (E.40), we can also write

$$|\Phi_1\rangle = e^{i\hat{T}} |\Phi_0\rangle, \quad (\text{E.71})$$

where

$$\hat{T} = \frac{1}{2} \sum_{\mu\nu} T_{\mu\nu} O_{\mu}^{(0)+} O_{\nu}^{(0)+} + \text{h.c.} \quad (\text{E.72})$$

and the matrix T can be found in analogy Eq. (E.46) as

$$T = -iD\bar{R}D^T, \quad (\text{E.73})$$

where the matrix \bar{R} is a diagonal matrix with $\sinh r_k = y_k$ and D and y_k are given by the decomposition (E.62) of the transformation (E.68). With $R = D\bar{R}D^+$, and $S = D^* D^+ = e^{-iF}$ we obtain

$$T = -iRe^{iF}, \quad Z = \tgh(R)e^{iF}. \quad (\text{E.74})$$

* In the boson case simple shift operations are also possible. They give a linear term in the exponent of (E.69). In order not to complicate the formulae, we treat them later [Eq. (E.77)].

For the overlap integral $(\Phi_1|\Phi_0)$ we get, in analogy to the Onishi formulas (E.49ff.),

$$(\Phi_1|\Phi_0) = (\det X)^{-1/2} = (\det(X_0^+ X_1 - Y_0^+ Y_1))^{-1/2} = \exp(-\frac{1}{2} \text{Tr} \ln X). \quad (\text{E.75})$$

Overlap integrals of general operators are calculated again by using Wick's theorem and the transition densities

$$\begin{aligned} \rho_{\mu\mu'}^{10} &= \frac{(\Phi_1|B_\mu^+ B_\mu^+|\Phi_0)}{(\Phi_1|\Phi_0)} = (\rho_0 + Y_0^* Z^* X_0^+)_{\mu\mu'} = Z_0(1 - Z_1^* Z_0)^{-1} Z_1^*, \\ \kappa_{\mu\mu'}^{10} &= \frac{(\Phi_1|B_\mu^- B_\mu^-|\Phi_0)}{(\Phi_1|\Phi_0)} = (\kappa_0 + Y_0^* Z^* Y_0^+)_{\mu\mu'} = Z_0(1 - Z_1^* Z_0)^{-1}, \quad (\text{E.76}) \\ \kappa_{\mu\mu'}^{01*} &= \frac{(\Phi_1|B_\mu^+ B_{\mu'}^+|\Phi_0)}{(\Phi_1|\Phi_0)} = (\kappa_0^* + X_0^* Z^* X_0^+)_{\mu\mu'} = (1 - Z_1^* Z_0)^{-1} Z_1^*, \end{aligned}$$

where

$$\rho_0 = Y_0^* Y_0^T; \quad \kappa_0 = Y_0^* X_0^T; \quad Z_0 = Y_0^* X_0^{*-1}; \quad Z_1 = Y_1^* X_1^{*-1}.$$

In the boson case there exists still a further type of linear transformation to a new set of boson operators, namely *translations* or shift operations

$$O_\mu^\pm = B_\mu^\pm + c_\mu^* \quad (\text{E.77})$$

with complex numbers c_μ . The vacuum, which belongs to O_μ , has the form of a *coherent state*

$$|\Phi_0\rangle = \mathcal{N} \exp\left(-\sum_\mu c_\mu B_\mu^+\right)|-\rangle, \quad (\text{E.78})$$

and the overlap between two boson vacua is

$$(\Phi_1|\Phi_0) = \exp\left(-\frac{1}{2} \sum_\mu |c_\mu^1 - c_\mu^0|^2\right). \quad (\text{E.79})$$

In such cases there also exist non-vanishing expectation values of single bosons:

$$(\Phi_1|B_\mu|\Phi_0) = -(\Phi_1|\Phi_0)c_\mu^0. \quad (\text{E.80})$$

APPENDIX F

Many-Body Green's Functions

In this appendix we want to give a brief outline of the theory of many-body Green's functions (GF). These techniques are usually not applied very much to nuclear theory, whereas they are widely used in many other many-body areas of work. The advantages of the GF method are that it is very flexible in constructing many-body approximations, and that the GFs have a direct physical interpretation, representing the propagation of particles or holes in the many-body medium. Also, the question of effective interactions can be systematically investigated in this formalism. Because of the brevity of this outline we urge the reader to consult the current literature and text books for standard formulations [Mi 67, AGD 65, No 64a, Ma 67b, FW 71] and we will thus only go into the details where we feel that our representation deviates from the usual one.

F.1 Single-Particle Green's Function and Dyson's Equation

We want to establish the so-called Dyson equation for the single-particle GF, which is defined by:

$$\begin{aligned} G(1, 1') &= (-i) \langle 0 | T \{ a(1) a^\dagger(1') \} | 0 \rangle \\ &= -i \Theta(t_1 - t_{1'}) \langle 0 | a_1(t_1) a_{1'}^\dagger(t_{1'}) | 0 \rangle \\ &\quad + i \Theta(t_{1'} - t_1) \langle 0 | a_{1'}^\dagger(t_{1'}) a_1(t_1) | 0 \rangle. \end{aligned} \quad (\text{F.1})$$

Here and henceforth we use the convention that numbers in brackets comprise all quantum numbers (p) to characterize the single-particle state,

such as momentum, spin, isospin, plus time, that is, $(1, 2) \hat{=} (p_1 t_1; p_2 t_2)$. Repeated arguments shall be summed or integrated (time) over unless otherwise stated. A number as an index comprises everything besides the time. In (F.1), $|0\rangle$ stands for the exact ground state of the A particle system and T is the time ordering operator (C.49). The single-particle operators

$$a^+(1) \equiv a_1^+(t_1) = e^{iHt_1/\hbar} a_1^+(0) e^{-iHt_1/\hbar} \quad (\text{F.2})$$

develop in time along with the full two-body Hamiltonian

$$H = \sum_i \epsilon_i a_i^+ a_i + \frac{1}{4} \sum_{1234} \bar{v}_{1234} a_1^+ a_2^+ a_3 a_4; \quad \epsilon_i = \frac{p_i^2}{2m}. \quad (\text{F.3})$$

The usefulness of the single-particle GF of (F.1) comes from the fact that it concisely contains many directly measurable quantities, such as:

(i) The *single particle density*

$$\rho_{11'} = \langle 0 | a_{1'}^+ a_1 | 0 \rangle = -i \lim_{t_1' - t_1 \rightarrow +0} G(1, 1') = \frac{1}{2\pi i} \oint d\omega G_{11'}(\omega), \quad (\text{F.4})$$

where $G_{11'}(\omega)$ is the Fourier transform of $G(1, 1')$:

$$G_{11'}(\omega) = \int_{-\infty}^{+\infty} d(t_1 - t_1') e^{i\omega(t_1 - t_1')} G(1, 1'). \quad (\text{F.5})$$

(ii) The *excitation energies of the $A \pm 1$ particle system*: This can be made explicit in using a complete set of states in (F.1):

$$\begin{aligned} G_{11}(t_1 - t_1') &= -i \sum_{\nu(A+1)} \Theta(t_1 - t_1') \langle 0 | a_1 | \nu \rangle \langle \nu | a_{1'}^+ | 0 \rangle e^{-(i/\hbar)(E_\nu^{A+1} - E_0^A)(t_1 - t_1')} \\ &\quad + i \sum_{\nu(A-1)} \Theta(t_1' - t_1) \langle 0 | a_{1'}^+ | \nu \rangle \langle \nu | a_1 | 0 \rangle e^{-(i/\hbar)(E_0^A - E_\nu^{A-1})(t_1 - t_1')} \end{aligned} \quad (\text{F.6a})$$

or

$$G_{11'}(\omega) = \hbar \sum_{\nu(A+1)} \frac{\langle 0 | a_1 | \nu \rangle \langle \nu | a_{1'}^+ | 0 \rangle}{\hbar\omega - (E_\nu^{A+1} - E_0^A) + i\eta} + \hbar \sum_{\nu(A-1)} \frac{\langle 0 | a_{1'}^+ | \nu \rangle \langle \nu | a_1 | 0 \rangle}{\hbar\omega - (E_0^A - E_\nu^{A-1}) - i\eta}, \quad (\text{F.6b})$$

where the $|\nu\rangle$ are exact eigenstates of the Hamiltonian (F.3):

$$H |\nu, A \pm 1\rangle = E_\nu^{A \pm 1} |\nu, A \pm 1\rangle.$$

(iii) The *ground state energy*

$$\begin{aligned} E_0 &= \langle 0 | H | 0 \rangle = -\frac{i}{2} \lim_{t_1' - t_1 \rightarrow +0} \sum_i \left(\epsilon_i + i\hbar \frac{\partial}{\partial t_1} \right) G_{11}(t_1 - t_1') \\ &= \frac{1}{2} \oint \frac{d\omega}{2\pi i} \sum_i (\epsilon_i + \hbar\omega) G_{11}(\omega), \end{aligned} \quad (\text{F.7})$$

where we have used the equation of motion for the operators a, a^+ :

$$i\hbar \frac{\partial}{\partial t_1} a(1) = \epsilon_1 a(1) + j(1), \quad (\text{F.8a})$$

$$-i\hbar \frac{\partial}{\partial t_1} a^+(1) = \epsilon_1 a^+(1) + j^+(1), \quad (\text{F.8b})$$

with

$$j(1) = \frac{1}{2} \bar{v}_{1234} a_2^+(t_1) a_4(t_1) a_3(t_1). \quad (\text{F.9})$$

We now proceed to derive Dyson's equation. With the help of Eqs. (F.8) we can establish the equation of motion for the GF:

$$G^{00^{-1}}(1, 2) G(2, 1') = \delta(1, 1') + G(j(1), 1') \quad (\text{F.10})$$

with

$$\delta(1, 1') = \delta_{11'} \delta(t_1 - t_{1'}) \hbar,$$

$$G^{00^{-1}}(1, 1') \equiv [G^{00}]_{11'}(t_1, t_{1'}) = \delta(1, 1') \left(i\hbar \frac{\partial}{\partial t_{1'}} - \epsilon_{1'} \right), \quad (\text{F.11})$$

and

$$G(j(1), 1') = -i \langle 0 | T \{ j(1) a^+(1') \} | 0 \rangle. \quad (\text{F.12})$$

Applying the equation of motion again, we obtain

$$G(j(1), 2) G^{00^{-1}}(2, 1') = \bar{v}_{1234} \langle 0 | a_2^+ a_4 | 0 \rangle \hbar \delta(t_1 - t_{1'}) + G(j(1), j(1')), \quad (\text{F.13})$$

where we used the form equivalent to (F.11)

$$G^{00^{-1}}(1, 1') = \left(-i\hbar \frac{\partial}{\partial t_1} - \epsilon_1 \right) \delta(1, 1') \quad (\text{F.14})$$

and $G(j(1), j(1'))$ is given by

$$G(j(1), j(1')) = -i \langle 0 | T \{ j(1) j^+(1') \} | 0 \rangle. \quad (\text{F.15})$$

The inverse of $G(1, 1')$ is defined by

$$G^{-1}(1, 2) \cdot G(2, 1') = \delta(1, 1') \quad (\text{F.16})$$

and we can therefore write

$$G^{00^{-1}}(1, 2) G(2, 1') = G^{-1}(1, 2) \cdot G(2, 3) G^{00^{-1}}(3, 4) G(4, 1'), \quad (\text{F.17})$$

which yields, together with the adjoint of Eq. (F.10),

$$G(1, 2) G^{00^{-1}}(2, 1') = \delta(1, 1') + G(1, j(1')). \quad (\text{F.18})$$

the relation

$$G^{00^{-1}}(1, 2) G(2, 1') = \delta(1, 1') + G^{-1}(1, 2) G(2, j(3)) G(3, 1'). \quad (\text{F.19a})$$

In the same manner we can derive

$$G(1, 2)G^{00-1}(2, 1) = \delta(1, 1') + G(1, 2)G(j(2), 3)G^{-1}(3, 1'). \quad (\text{F.19b})$$

Multiplying (F.13) from the right with a single-particle GF and using (F.19a), we obtain:

$$G(j(1), 1') = \bar{v}_{1234} \langle 0 | a_2^+ a_4 | 0 \rangle G_{31'}(\iota_1, \iota_1') + R(j(1), j(2))G(2, 1') \quad (\text{F.20})$$

with [ES 69]:

$$R(j(1), j(1')) = G(j(1), j(1')) - G(j(1), 2)G^{-1}(2, 2')G(2', j(1')). \quad (\text{F.21})$$

Inserting the result (F.20) into (F.10) yields, after Fourier transforming,

$$(\hbar\omega - \epsilon_1)G_{11'}(\omega) = \delta_{11'} + M_{12}(\omega)G_{21'}(\omega) \quad (\text{F.22a})$$

or

$$G(1, 1') = G^{00}(1, 1') + G^{00}(1, 2)M(2, 2')G(2', 1') \quad (\text{F.22b})$$

with

$$M_{11'}(\omega) = M_{11'}^0 + M'_{11'}(\omega), \quad (\text{F.23})$$

$$M_{11'}^0 = \bar{v}_{121'4}\rho_{42}, \quad (\text{F.24})$$

$$M'_{11'}(\omega) = R_{j(1) j(1')}(\omega). \quad (\text{F.25})$$

Equation (F.22) is the well-known *Dyson equation* and $M(1, 1')$ is the corresponding so-called *mass operator*, which has a static (frequency-independent) part M^0 and a dynamic (frequency-dependent) part M' . The latter is expressed somewhat unusually, and we shall come to its significance later.

It will be the approximation of $M(1, 1')$ which will determine the approximation for $G(1, 1')$. Let us first make the most simple approximation and drop M' completely; this yields

$$(\hbar\omega - \epsilon_1)g_{11'}(\omega) = \delta_{11'} + \Gamma_{12}g_{21'}(\omega), \quad (\text{F.26})$$

$$\Gamma_{11'} = \bar{v}_{121'4} \oint \frac{d\omega}{2\pi i} g_{42}(\omega). \quad (\text{F.27})$$

This constitutes a closed set of nonlinear equations that are equivalent to the Hartree-Fock equation of Chapter 5. This can be seen most easily by inserting $\omega \cdot g_{11'}$ of (F.26) into (F.7) and observing that the resulting expression for the ground state energy is exactly of the Hartree-Fock form (5.40). Also, in moving towards one of the poles of $g_{11'}$ in (F.26) we recover exactly the Hartree-Fock equation (5.44). In analogy to (F.6a, b), the formal solution of (F.26) is then given by

$$g_{11'}(\omega) = \hbar \left(\frac{1 - \rho}{\hbar\omega - h + i\eta} \right)_{11'} + \hbar \left(\frac{\rho}{\omega - h - i\eta} \right)_{11'}, \quad (\text{F.28})$$

where ρ is the HF density operator and h the HF Hamiltonian (5.37).

Analogously, in time-space we have:

$$g(1, 1') = -i(\Theta(t_1 - t_{1'})(1 - \rho) - \Theta(t_{1'} - t_1)\rho)_{12}(e^{-(i/\hbar)h(t_1 - t_{1'})})_{21}. \quad (\text{F.29})$$

In order to better understand the significance of the dynamic part of the mass operator (F.25) we will first show that the complete mass operator corresponds to the most general energy-dependent *optical model potential* for elastic nucleon-nucleus scattering. To show this we work in the momentum representation and write for the elastic scattering *S*-matrix in the usual way [ES 69]:

$$S_{p_1 p_1'} = -\langle p_1 | p_1' \rangle^+ \quad (\text{F.30})$$

with

$$\begin{aligned} |p\rangle^\pm &= \lim_{t \rightarrow \mp\infty} e^{-i(p^2/2m)t/\hbar} a_p^\pm(t)|0\rangle \\ &= \lim_{t \rightarrow \mp\infty} e^{-i(E_p - H)t/\hbar} a_p^\pm|0\rangle; \end{aligned} \quad (\text{F.31})$$

$$E_p = \frac{p^2}{2m} + E_0^A.$$

We can therefore express the *S*-matrix in terms of the single-particle GF of (F.1):

$$S_{p_1 p_1'} = i \lim_{\substack{t \rightarrow +\infty \\ t' \rightarrow -\infty}} e^{i(p_1^2/2m)t/\hbar} G_{p_1 p_1'}(t - t') e^{-i(p_1'^2/2m)t'/\hbar}. \quad (\text{F.32})$$

We now rewrite Eq. (F.22) in the following form.

$$\begin{aligned} G(1, 1') &= G^{00}(1, 1') + G^{00}(1, 2)T(2, 2')G^{00}(2', 1'), \\ T(1, 1') &= M(1, 1') + M(1, 2)G^{00}(2, 2')T(2', 1'), \end{aligned} \quad (\text{F.33})$$

where G^{00} is the inverse of (F.11), viz:

$$\begin{aligned} G_{p_1 p_1'}^{00}(t_1 - t_{1'}) &= -i\delta_{p_1 p_1'} \exp\left[-\frac{i}{\hbar} \frac{p_1^2}{2m}(t_1 - t_{1'})\right] \cdot (\Theta(t_1 - t_{1'}) \cdot \Theta(p_1^2/2m - \lambda) \\ &\quad - \Theta(t_{1'} - t_1) \cdot \Theta(\lambda - p_1'^2/2m)), \end{aligned} \quad (\text{F.34})$$

and λ is the Fermi energy, that is, G^{00} is the single-particle GF for a completely free many-body system. The equivalence of (F.33) and (F.22) can be established by simple iteration. Using (F.34) and (F.33) in performing the time limit we find for (F.32):

$$S_{p_1 p_1'} = \delta_{p_1 p_1'} - 2\pi i T_{p_1 p_1'}(\omega = p_1^2/2m) \delta((p_1^2 - p_1'^2)/2m). \quad (\text{F.35})$$

We see, therefore, that the matrix $T(1, 1')$ defined by Eq. (F.33) corresponds to the scattering *T*-matrix of elastic nucleon-nucleus scattering. The second of Eqs. (F.33) then also tells us that $M(1, 1')$ corresponds to the

optical model potential, which is generally, of course, energy dependent and nonlocal. Usually the optical potential is derived with the help of Feshbach's projection operator formalism (cf. Sec. 4.3.2) using the complete set of shell model states $1p, 2p - 1h, 3p - 2h, \dots$ and projecting out the $2p - 1h, 3p - 2h, \dots$ components. Therefore, we see that the meaning of the mass operator is that of an "effective" single-particle potential where, within the dynamic part, all couplings to the higher configurations are hidden.* As for all effective potentials, we can also "unfold" the energy dependence for the mass operator and instead write a matrix equation in a larger space (examples will be given later). The mass operator is generally a complex and non-Hermitian quantity and, as usual, special rules have to be observed for the calculation of eigenvectors and eigenvalues of such operators. We do not want to go into these details, and refer the reader to the literature [BD 71, Appendix C].

As we have seen, the calculation of the one-particle GF depends on the knowledge of the mass operator. In order to be able to obtain some approximation for it we first have to learn how to construct a perturbation series for M .

F.2 Perturbation Theory

Before we go into the details of the perturbation theory, we would like to give a very brief outline of how to represent graphically the different expressions we are going to derive with the GF theory. These graphical representations are very useful for grasping at a glance the physical content of an eventually rather complicated equation. We wish to stress the point, however, that we are going to avoid as far as possible deriving relations using purely graphical arguments. Instead, we shall try to derive formulae analytically, especially in the case of perturbation theory.

The single-particle GF (F.1) is a function of two times t_1, t_1' , consisting of two parts, one with $t_1 > t_1'$, and the other with $t_1 < t_1'$. We will represent this function on a horizontal time scale by a straight line going from t_1' to t_1 :

$$G(1, 1') \Rightarrow \xrightarrow{t_1'} \quad \text{or} \quad \xleftarrow{t_1} \quad . \quad (\text{F.36})$$

The arrow gives the line a direction going from t_1' to t_1 . Defining the time as increasing from left to right, we can then say that "the *particle* propagates from t_1' to t_1 " if $t_1 > t_1'$, and "the *hole* propagates from t_1 to t_1' " if $t_1 > t_1'$. In this context we should recognize that the first part of (F.1) just represents the overlap of wave functions with a particle added to the ground state at time t_1 , and $t_1 > t_1'$. In the second part, a hole has been created at time t_1 and $t_1 > t_1'$. In the pure HF approximation (F.28), only the first part survives if it is a particle (above the Fermi level) and only the

* The equivalence of the optical potential defined by the Feshbach projection operator formalism and the one given here in a perturbative treatment is a somewhat tricky point which we will not treat here.

second one if it is a hole (below the Fermi level). In general, however, both parts contribute to the perturbation series (see below) of a given order.

The antisymmetrized matrix elements of the two-body interaction will be represented by a dot:

$$\bar{v}_{1234} \Rightarrow \bullet \quad (\text{F.37})$$

where the dot must always be joined by four lines (one particle GF's) two of them going into the point at 12 and two leaving it at 34.

More particle GF's (see below) will always be represented by as many lines as there are particles (or holes) connected by a bubble.

The Dyson equation (F.22) can now be represented in the following way

$$\text{---} = \text{---} + \text{---} + \text{---} \quad (\text{F.38})$$

with

$$\text{M}' \equiv \text{R} \quad (\text{F.39})$$

where R stands for the special combination of GF's figuring in (F.25, 21). The broken line in (F.38) represents the completely free GF G^{00} of Eq. (F.34).

In order to derive perturbation theory analytically (which has the virtue that factors and signs of specific terms can be obtained straightforwardly), we start out from the definition of the so-called multi-time n -body GF:

$$\begin{aligned} G(1, 2, \dots, n; 1', 2', \dots, n') &= (-i)^n \langle 0 | T \{ a(1)a(2)\dots a(n)a^+(n')\dots a^+(2')a^+(1') \} | 0 \rangle \\ &= (-i)^n \sum_{\text{all permutations}} (-)^P P \{ \Theta(t_1 - t_2) \cdot \Theta(t_2 - t_3) \cdots \\ &\quad \cdot \Theta(t_{n-1} - t_n) \Theta(t_n - t_{n'}) \Theta(t_{n'} - t_{n'-1}) \cdots \Theta(t_2 - t_1) \\ &\quad \cdot \langle 0 | a(1)a(2)\dots a(n)a^+(n')\dots a^+(1') | 0 \rangle \}. \end{aligned} \quad (\text{F.40})$$

The definition (F.40) implies that the operators are always ordered in such a way that their time arguments increase from right to left. It can also easily be seen that expression (F.40) is completely antisymmetric with respect to the interchange of any two of the indices. We want to write down the equation of motion for the GF, (F.40), which can be easily proved for the one- and two-body case; it is, however, tedious to prove it

in general and we refer the interested reader to the standard literature [Mi 67, AGD 65]:

$$\begin{aligned}
 G^{00-1}(1, 1'') \cdot G(1'', 2 \dots n; 1' \dots n') \\
 = \sum_{l=1}^n (-)^{l+1} \delta(1, l') \cdot G(2 \dots n; 1' \dots l'-1, l'+1, \dots, n') \\
 - \frac{i}{2} \bar{v}(1, n'+1; 1'', n+1) \cdot G(1'', 2 \dots n, (n+1)^+; 1' \dots n', (n'+1)^{++}). \tag{F.41}
 \end{aligned}$$

A plus sign on an argument means that the corresponding time argument has to be displaced by a positive infinitesimal amount, that is, $1^+ = p_1, t_1 + 0$ and $1^{++} = p_1, t_1 + 0 + 0$. The matrix element of the two-body interaction is given by

$$\bar{v}(1, 2; 3, 4) = \delta(t_1 - t_2) \delta(t_3 - t_4) \delta(t_1 - t_3) \bar{v}_{1234}. \tag{F.42}$$

It is useful to invert the equation of motion (F.41):

$$\begin{aligned}
 G(1 \dots n; 1' \dots n') = & \sum_{l=1}^n (-)^{l+1} G^{00}(1, l') G(2 \dots n; 1' \dots l'-1, l'+1 \dots n') \\
 & - \frac{i}{2} G^{00}(1, 1'') \bar{v}(1''', n'+1; 1'', n+1) \\
 & \cdot G(1'', 2 \dots n, (n+1)^+; 1' \dots n', (n'+1)^{++}). \tag{F.43a}
 \end{aligned}$$

The adjoint equation has the form:

$$\begin{aligned}
 G(1 \dots n; 1' \dots n') = & \sum_{l=1}^n (-)^{l+1} G(1 \dots l-1, l+1 \dots n; 2' \dots n') G^{00}(l, 1') \\
 & - \frac{i}{2} G(1 \dots n, (n+1)^{++}; 1'', 2' \dots n', (n'+1)^+) \\
 & \bar{v}(n'+1, 1''; n+1, 1''') G^{00}(1''', 1'). \tag{F.43b}
 \end{aligned}$$

We see that the equation of motion relates the n -body GF with the $(n \pm 1)$ -body GF's. From Eqs. (F.43) we quite easily derive the expression $G^{00}(1 \dots n; 1' \dots n')$ of the n -body GF in the approximation where we neglect the two-body interaction completely:

$$G^{00}(1 \dots n; 1' \dots n') = \det |G^{00}(i, j)|. \tag{F.44}$$

It is then clear how the first order expression of an n -body GF has to be calculated: we first calculate the first-order contribution of the one-body GF using (F.44) for the two-body GF. The two-body GF couples to the one-body and three-body GF. The first order of the one-body GF is known from the preceding step, and the three-body GF can be calculated to zeroth order by (F.44); this yields the first order of the two-body GF. We can go on with this scheme to calculate the first order of an n -body GF. To calculate the second order we need the first-order expressions and

we can then set up an analogous scheme. This can then be repeated to any order.

F.3 Skeleton Expansion

For many problems, we are not so much interested in the representation of the expansion terms by $G^{00}(l, l')$'s, but we want to have an expansion in powers of exact $G(l, l')$'s (skeleton expansion). That such a partial resummation of the perturbation series is possible can be shown by an investigation of the series involving the $G^{00}(l, l')$'s only. We can derive the skeleton expansion by multiplying (F.43a) from the left with (F.19b) and using Eqs. (F.9, 12):

$$\begin{aligned} G(1 \dots n; 1' \dots n') = & \sum_{l=1}^n (-)^{l+1} G(1, l') \cdot G(2 \dots n; 1' \dots l'-1, l'+1 \dots n') \\ & - \frac{i}{2} G(1, l'') \bar{v}(l'', n'+1; 1'', n+1) \\ & \cdot R(1'', 2 \dots n, (n+1)^+; 1' \dots n', (n'+1)^{++}), \end{aligned} \quad (\text{F.45})$$

with

$$\begin{aligned} R(1 \dots n, n+1; 1' \dots n', n'+1) = & G(1 \dots n, n+1; 1' \dots n', n'+1) \\ & - G(1, n+1; 1'', n'+1) G^{-1}(1'', 2'') G(2'', 2 \dots n; 1' \dots n'). \end{aligned} \quad (\text{F.46})$$

As in the case of the expansion in powers of $G^{00}(l, l')$, we see from (F.45) that for the skeleton expansion the zeroth order skeleton contribution is given by

$$G^{\text{skeleton}}(1 \dots n; 1' \dots n') \equiv G^0(1 \dots n; 1' \dots n') = \det |G(i, j)|, \quad (\text{F.47})$$

that is, to lowest-order skeleton the n -body GF is just the antisymmetrized product of corresponding one-body GFs. Proceeding now in essentially the same way as in the completely free case, we obtain from (F.45, 46, 47) the successive order of the skeleton expansion. We should note thereby that the lowest order of (F.46) is *not* the antisymmetrized product anymore, but the second term on the rhs of (F.46) takes out of the first term just what has already been resumed in the lowest order of the first term on the rhs of (F.45). The reader is invited to convince himself of this fact in taking a definite example.

The above prescription to derive the skeleton expansion is straightforward, yielding the right signs and prefactors of a given order term automatically. Depending on the example and the order, the derivation might be quite tedious. Practice is unavoidable to perform these calculations economically, which is a common feature of all perturbation expansion techniques. In order to become more familiarized with the procedures we propose to verify the following fact: Expression (F.25) for the dynamic

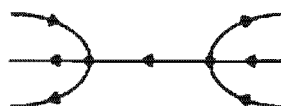


Figure F.1. Second-order contribution to both terms of (F.48).

part of the mass operator contains a generalized three-body GF [ES 69]:

$$\begin{aligned} R(1, 2, 3; 1', 2', 3') &= G(1, 2, 3; 1', 2', 3') \\ &\quad - G(1, 2; 1'', 2'')G^{-1}(1'', 1''')G(1''', 3; 1', 3'). \end{aligned} \quad (\text{F.48})$$

Verify that both the first and second terms on the rhs of (F.48) contain (to second order) a term with the structure shown in Fig. F.1 and that they exactly cancel one another. One says that the dynamic part of the mass operator is *one-line irreducible*, that is, it contains no graphs which can be cut into two parts by just cutting one fermion line. A closer investigation shows that *all* graphs of the second term of (F.48) are one-line reducible and these terms cancel equal terms contained in the first term of (F.48). What remains is irreducible.

The second-order skeleton expansion of the mass operator can be easily calculated from (F.48), with (F.47), to give

$$M^{(2)}(1, 1') = \frac{1}{2}\bar{v}(1, 2'; 1''', 2)G(1''', 1'')G(2, 3')\bar{v}(3', 1''; 3, 1'), \quad (\text{F.49})$$

which is represented graphically in Fig. F.2. In Fig. F.3 we present very schematically some higher-order terms contained in (F.48). In the drawing we do not present the exchange graphs.



Figure F.2. Graphical representation of the second-order skeleton contribution to the mass operator.

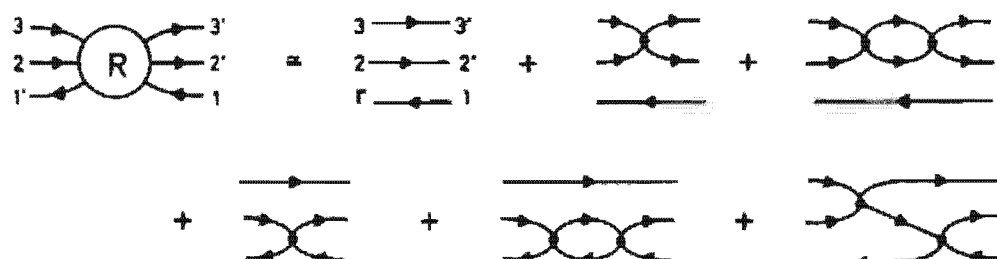


Figure F.3. Higher-order terms contributing to the GF contained in the mass operator.

F.4 Factorization and Brückner-Hartree-Fock

An important feature of n -body GF's is the fact that they approximately factorize into antisymmetric products of lower GF's. This can be verified by an extensive study of the corresponding perturbation series. In Fig. F.3

we see, for example, that the five first terms are just the beginning of the following factorization.

$$\begin{aligned} R(1, 2, 3; 1', 2', 3') \simeq & G(1, 1') \cdot G(2, 3; 2', 3') \\ & + \{ [G(2, 2') \cdot R(1, 3; 1'3') - (3 \leftrightarrow 2)] - [3' \leftrightarrow 2'] \} \\ & + \{ [G(2, 2') \cdot G(1, 1') \cdot G(3, 3') - (3 \leftrightarrow 2)] - [3' \leftrightarrow 2'] \}, \end{aligned} \quad (\text{F.50})$$

with

$$R(1, 3; 1', 3') = G(1, 3; 1'3') + G(1, 3') \cdot G(3, 1'). \quad (\text{F.51})$$

The function (F.51) is essentially identical with the linear response function defined in (8.130)*; the fact that we have to add the second term in (F.51) can be verified in comparing (F.51) with (8.131).

A confusing feature for the beginner is the fact that the factorization (F.50)—that is, all terms apart from the triple products of one-body GF's—does not give the correct lowest-order skeleton term of (F.48), that is, it does not reproduce expression (F.49). The factorization is only valid for the correlated parts, that is, for the second-, third-, fourth-, fifth-, and all corresponding higher-order diagrams (Fig. F.3) contained in (F.48). In order to adjust the correct lowest-order contribution, we have to add to the factorization the triple product of $G(i, j)$'s in (F.50). On the other hand, the correlated parts sum up the infinite sub-series contained in the exact two-body correlation functions figuring in (F.50), therefore factorization may be a powerful approximation.

We recognize that the first term on the rhs of (F.50) sums up the particle-particle (pp) correlations (see Fig. F.3) and these are the important ones for the treatment of short-range correlations introduced by the hard core of the bare nucleon-nucleon force, as we discussed in Section 4.3. Therefore, if we want to treat only those correlations, we can drop the other terms in (F.50) and write for the mass operator:

$$M(1, 1') = T(1, 2; 1', 4)G(4, 2) \quad (\text{F.52})$$

with the T -matrix

$$T(1, 2; 1', 4) = \bar{v}(1, 2; 1', 4) + \frac{1}{4}\bar{v}(1, 2; 3'4')G(3', 4'; 5, 6)\bar{v}(5, 6; 1'4). \quad (\text{F.53})$$

There exists a well-known integral equation for the two-body GF figuring in (F.53) (see below) [Mi 67]:

$$\begin{aligned} G(1, 2; 1', 2') = & G^0(1, 2; 1', 2') \\ & - \frac{1}{4}G^0(1, 2; 3, 4)K^{pp}(3, 4; 3', 4')G(3', 4'; 1', 2'), \end{aligned} \quad (\text{F.54})$$

* The response function defined in (8.130) is in time space for $t_1 = t'_1$ and $t_3 = t'_3$ given by $\tilde{R}(1, 3; 1'3') = -i\Theta(t_1 - t'_1)\langle 0 | [a^*(1)a(1), a^*(3')a(3)] | 0 \rangle$. This definition differs from (F.51) by the sign of $i\eta$ in the second term of (8.130), by an additional factor $(-i)$ and by the order of the fermion operators. Since the physical content of both definitions is the same, we can work with both functions.

where K^{pp} is an effective pp -force and to lowest order is given by

$$K^{pp}(3, 4; 3', 4') \simeq \bar{v}(3, 4; 3', 4'). \quad (\text{F.55})$$

If we furthermore replace the one-body GF's in (F.54) by their HF expression using (F.28, 29) and neglect in (F.28, 29) the second part (hole contribution); it can be shown that the hole lines are of higher order in the density and are therefore supposed to be smaller than the particle contribution; see, e.g., [Ma 67b]), we obtain with (F.52–55) the structure of the Brückner–Hartree–Fock equation (5.72). We now have to recognize that the T -matrix (F.53) depends effectively only on one time difference, giving rise to an energy dependence after Fourier transformation. If this energy dependence is replaced by the prescription (5.75), we can identify Eqs. (F.52) and (F.53) exactly with the Brückner HF equations (5.72).

F.5 Hartree–Fock–Bogoliubov Equations

It is very instructive to derive not only Brückner Hartree–Fock theory but also Hartree–Fock–Bogoliubov theory using GF techniques. For this purpose we again retain only the first term on the rhs of (F.50), because we already know that pairing correlations are pp -correlations. The hole-GF $G(1, 1')$ in the first term of (F.50) is calculated using only the static part of the mass operator. For the two-body GF we need to give the spectral representation:

$$\begin{aligned} G_{12,1'2'}(t-t') &= (-i)^2 \langle 0 | T \{ a_1(t) a_2(t) a_2^+(t') a_1^+(t') \} | 0 \rangle \\ &= (-i)^2 \left\{ \Theta(t-t') \sum_{\rho^+} \langle 0 | a_1 a_2 | \rho^+ \rangle \langle \rho^+ | a_2^+ a_1^+ | 0 \rangle e^{-(i/\hbar)(E_\rho^{A+2} - E_0^A)(t-t')} \right. \\ &\quad \left. + \Theta(t'-t) \sum_{\rho^-} \langle 0 | a_2^+ a_1^+ | \rho^- \rangle \langle \rho^- | a_1 a_2 | 0 \rangle e^{-(i/\hbar)(E_0^A - E_\rho^{A-2})(t-t')} \right\} \end{aligned} \quad (\text{F.56})$$

or, after Fourier transformation,

$$G_{12,1'2'}^{(\omega)} = (-i) \left\{ \sum_{\rho^+} \frac{\langle 0 | a_1 a_2 | \rho^+ \rangle \langle \rho^+ | a_2^+ a_1^+ | 0 \rangle}{\omega - \Omega_\rho^{pp} + i\eta} - \sum_{\rho^-} \frac{\langle 0 | a_2^+ a_1^+ | \rho^- \rangle \langle \rho^- | a_1 a_2 | 0 \rangle}{\omega - \Omega_\rho^{hh} - i\eta} \right\},$$

$$\hbar\Omega_\rho^{pp} = E_\rho^{A+2} - E_0^A, \quad \hbar\Omega_\rho^{hh} = E_0^A - E_\rho^{A-2}, \quad (\text{F.57})$$

where the $E_\rho^{A\pm 2}, E_0^A$ are exact eigenenergies.

The HFB theory implicitly assumes that in the ρ -sum of (F.57) only the ground states are relevant, that is, they are supposed to be so collective that in the sum of the residues of (F.57) (which is a constant) the residue of the ground state gathers almost all the strength. As we explained in Chapter 11, the notion of the collectivity of a specific mode is an essential feature of a phase transition—here, the transition to a superfluid state. Remembering that the single-particle GF of the first term in (F.50) becomes a hole line in the mass operator, we get [using (F.21), (F.22), and

(F.50)] the following approximate Dyson equation, in which we have isolated the so-called Cooper poles [Pi 61] in the dynamic part of the mass operator* [for the derivation, one should work entirely in time-space using (F.29) and Fourier transform only at the end]:

$$\begin{aligned} (\hbar\omega - \epsilon_1)G_{11'}(\omega) &= \delta_{11'} + \bar{v}_{1234}p_{42}G_{31}(\omega) + M_{12}^{\text{Cooper}} \cdot G_{21'}(\omega), \\ M_{11'}^{\text{Cooper}}(\omega) &= \Delta_{12}^{(+)} \cdot \left(\frac{\rho}{\hbar\omega - \hbar\Omega_0^P + h^*} \right)_{22'} \cdot \Delta_{21'}^{(+)*} + \Delta_{12}^{(-)} \cdot \left(\frac{1-\rho}{\hbar\omega - \hbar\Omega_0^M + h^*} \right)_{22'} \cdot \Delta_{21'}^{(-)*}, \end{aligned} \quad (\text{F.58})$$

with

$$\begin{aligned} \Delta_{12}^{(+)} &= -\frac{1}{2}\bar{v}_{1234}\langle 0|a_3a_4|A+2,0\rangle, \\ \Delta_{12}^{(-)} &= -\frac{1}{2}\bar{v}_{1234}\langle A-2,0|a_3a_4|0\rangle. \end{aligned} \quad (\text{F.59})$$

We can forget about the infinitesimal $\pm i\eta$ in the denominators of (F.58) because we shall only consider bound state problems. The next approximation we can make for the case of a phase transition to a superfluid state is:

$$\begin{aligned} \hbar\Omega_0^P &\simeq 2(E_0^{A+1} - E_0^A) = 2\lambda^{(+)}, \\ \hbar\Omega_0^M &\simeq 2(E_0^A - E_0^{A-1}) = 2\lambda^{(-)}. \end{aligned} \quad (\text{F.60})$$

This approximation implies that the correlation energy of the two particles forming the Cooper pair is zero. This, of course, is another assumption we can make in treating a phase transition: the specific mode becomes so soft that its excitation energy goes to zero. We finally make a further (number nonconserving) approximation in assuming that for large systems (this approximation can also be avoided [Mi 67, Sec. 1.4.6]):

$$\Delta^{(+)} \simeq \Delta^{(-)} = \Delta; \quad \lambda^{(+)} \simeq \lambda^{(-)} = \lambda. \quad (\text{F.61})$$

Thus we arrive at the so-called *Gorkov equations* [Go 58]:

$$\begin{aligned} (\hbar\omega' - h')_{12}G_{21'} &= \hbar\delta_{11'} - \Delta_{12}F_{21'}^*, \\ (\hbar\omega' + h'^*)_{12}F_{21'}^* &= \Delta_{12}^*G_{21'}, \end{aligned}$$

or

$$\begin{pmatrix} \hbar\omega' & 0 \\ 0 & \hbar\omega' \end{pmatrix}_{12} \begin{pmatrix} G \\ -F^* \end{pmatrix}_{21'} = \begin{pmatrix} \hbar\delta_{11'} \\ 0 \end{pmatrix} + \begin{pmatrix} h' & \Delta \\ -\Delta^* & -h'^* \end{pmatrix}_{12} \begin{pmatrix} G \\ -F^* \end{pmatrix}_{21'}, \quad (\text{F.62})$$

where we have made the identification $\hbar\omega' = \hbar\omega - \lambda$, $h' = h - \lambda$, and

$$F_{11'}^* = -\left(\frac{1}{\hbar\omega' + h'^*} \right)_{12} \Delta_{22'}^* G_{21'}. \quad (\text{F.63})$$

* We should notice that for a hole line the direction of the Dyson equation is inverted and, therefore, the complex conjugate of the single-particle potential is figuring in (F.58). It can also be verified perturbatively for the *R*-function in (F.39). This, however, becomes important only for time-reversal non-invariant single-particle Hamiltonians.

On the rhs of (F.62) we recognize the familiar HFB matrix \mathcal{K} of Eq. (7.39). As usual, we can write down a spectral representation for $G(1, 1)$ (F.6a, b) and from (F.63) we see that this is also possible for $F^*(1, 1)$:

$$\begin{aligned} G_{11'}(\omega) &= \hbar \sum_k \frac{V_{1k}^* V_{1'k}}{\hbar\omega + E_k - i\eta} + \frac{U_{1k} U_{1'k}^*}{\hbar\omega - E_k + i\eta}, \\ -F_{11'}^*(\omega) &= \hbar \sum_k \frac{U_{1k}^* V_{1'k}}{\hbar\omega + E_k - i\eta} + \frac{V_{1k} U_{1'k}^*}{\hbar\omega - E_k + i\eta}. \end{aligned} \quad (\text{F.64})$$

From (F.64) we find that at the poles Eqs. (F.62) are identical to the HFB equations (7.42).

In order to close the system of equations we have to show how Δ is obtained from the solutions $G_{11'}, F_{11'}^*$. For this purpose we write for the amplitudes appearing in (F.59):

$$\begin{aligned} \langle 0 | a_3 a_4 | A+2, 0 \rangle &= \\ &= \lim_{\substack{t_1 = t_2 = t_1 + 0 \rightarrow -\infty \\ t_3 = t_4 + 0 \rightarrow 0}} \exp(-i\Omega^{pp} t) \frac{\langle 0 | T \{ a(3) a(4) a^+(2) a^+(1) \} | 0 \rangle}{\langle A+2, 0 | a_2^+ a_1^+ | 0 \rangle}. \end{aligned} \quad (\text{F.65})$$

This relation [WE 70] can be shown to be true in passing from the time limit to the Abelian limit:

$$\begin{aligned} |A+2, 0\rangle &= \lim_{\eta \rightarrow 0} \eta \int_{-\infty}^0 dt e^{i\eta t} \frac{e^{-i\Omega^{pp} t}}{\langle A+2, 0 | a_2^+ a_1^+ | 0 \rangle} a_2^+(t) a_1^+(t) | 0 \rangle \\ &= \lim_{\eta \rightarrow 0} \frac{\eta}{\langle A+2, 0 | a_2^+ a_1^+ | 0 \rangle} \sum_{\tau} \frac{\langle A+2, \tau | a_2^+ a_1^+ | 0 \rangle}{-i(E_0^{A+2} - E_{\tau}^{A+2} + i\eta)} |A+2, \tau\rangle \\ &= |A+2, 0\rangle. \quad \text{Q.E.D.} \end{aligned} \quad (\text{F.66})$$

For the two-body GF appearing in (F.65), we can make use of the integral equation (F.54); replacing one of the one-body GF's in front of K^{pp} by its lowest-order expression (F.26) and inserting (F.54) with (F.55) into (F.65), we obtain, with (F.61) and (F.63), the "gap equation":

$$\Delta_{12} = \frac{1}{2} \bar{v}_{1234} \frac{1}{2\pi i} \oint d\omega F_{34}(\omega). \quad (\text{F.67})$$

Therefore, together with (F.62) we have a closed system of equations. The fact that we have replaced one of the one-body GF's in (F.54) by its lowest-order expression (F.26) may seem a somewhat asymmetric treatment of the two one-body GF's in (F.54); it is, however, consistent with the approximation (F.58) of the mass operator, as the derivation of the Gorkov equations (F.62) has shown.

We would like to make a graphical and physical interpretation of the set

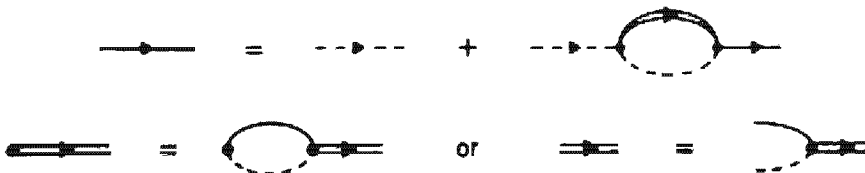


Figure F.4 (a) Graphical representation of (F.58), where the broken lines represent the lowest-order approximation (F.26) and \Rightarrow stands for the pairing mode. (b) Graphical representation of the gap equation (F.67).

of coupled equations we have just derived. Equation (F.58) is graphically represented in Fig. F.4a and Eq. (F.67) in Fig. F.4b.

From Fig. F.4 we see that the content of the HFB equations in the language of GF's is that the pairing mode is calculated with single-particle propagators which themselves are renormalized by the coupling of a particle to the pairing mode and a hole. The solution of these coupled equations implicitly sums up an important part of the perturbation series, thus allowing the description of a phase transition.

The fact that for the derivation of Brückner HF theory and HFB theory we initially used the same approximation for the mass operator [first term on the rhs of (F.50)] may be perplexing. It should be recognized, however, that Brückner HF theory never isolates the Cooper pole contained in the two-body GF of (F.50). The fact that we treat this pole explicitly in the HFB theory is therefore not in conflict with Brückner HF, and we can thus also combine both theories within the Brückner HFB theory.

Until now we have treated phase transitions from a normal to a superfluid state, and we have shown how the fact that one particular $p\!p$ -mode takes up almost all collectivity, and as a consequence becomes very soft, allows us to derive the HFB equations. From our earlier considerations (see Chap. 7), we know that the HFB equations allow for spherical (rotational symmetry conserving) and deformed (rotational symmetry breaking) solutions. In our treatment of the pairing phenomenon, however, we have nowhere assumed that a breaking of rotational symmetry can take place—we have always supposed that $\rho_{11} = \langle 0 | a_1^\dagger a_1 | 0 \rangle$ is a density corresponding to a ground state having good angular momentum (i.e., $I = 0$ for the even-even nuclei to fix ideas). From what was stated in Chapters 7 and 11 about the phase transition from a spherical to a deformed nucleus, we know that this is just associated with another soft mode—the quadrupole vibration. We will show in more detail how this can be described in the GF formalism.

It is obvious that in order to deal with the transition from a spherical to a deformed state we have to isolate the coupling of a particle to the quadrupole phonon in the mass operator (F.25). This can be most easily achieved by retaining from the factorization (F.50) only those terms in which the response functions (F.51) appear. The spectral decomposition then yields the excitation energies of the A system (8.130) (see footnote

page 633):

$$R_{13,1'3'}(\omega) = i \sum_{\mu > 0} \frac{\langle 0 | a_1^+ a_3 | \mu \rangle \langle \mu | a_3^+ a_1 | 0 \rangle}{\omega - \Omega_{\mu}^{ph} + i\eta} - \frac{\langle 0 | a_3^+ a_1 | \mu \rangle \langle \mu | a_1^+ a_3 | 0 \rangle}{\omega + \Omega_{\mu}^{ph} - i\eta}. \quad (\text{F.68})$$

As in the case of the pairing mode, we now assume that the lowest of the excitations in (F.68) practically exhausts all the strength, and that its excitation energy goes to zero ($\Omega_{\mu}^{ph} \rightarrow 0$). Here we assume that this is usually the case for the quadrupole mode (indeed, its excitation energy becomes very low for rotational nuclei), however, it is sometimes possible (^{208}Pb) for other modes to become lowest in excitation. For the single-particle GF's figuring in (F.50) we take again the lowest-order approximation (F.26). The Dyson equation thus takes the following form.

$$(\hbar\omega - \epsilon_1) G_{11'}(\omega) = \delta_{11'} + \bar{v}_{1234} \rho_{42} G_{31'}(\omega) + M_{12}^{\text{phonon}} G_{21'}(\omega), \quad (\text{F.69})$$

with

$$M_{11'}^{\text{phonon}}(\omega) = Q_1^{\frac{1}{2}+2} \left(\frac{1}{\hbar\omega - h} \right)_{12} Q_1^{\frac{1}{2}+2*}. \quad (\text{F.70})$$

and

$$Q_1^{\frac{1}{2}+2} = \bar{v}_{1(324)} \langle 0 | [a_3^+ a_4]_{2+} | 2^+ \rangle. \quad (\text{F.71})$$

It should be noted that until now we have not made any symmetry-violating approximation, since—as has been indicated—everything is coupled to good angular momentum (we couple the particle 2 or 2' to the quadrupole phonon to give the angular momentum j_1 of the external particle). We should also recognize that the Q -field of (F.71) corresponds to the γ -vertices of particle vibration coupling theory in Section 9.3.3 (with no factor $\frac{1}{2}$; see discussion footnote page 386). We can again write (F.69, 70) in the form of two coupled equations by introducing

$$P_{11'} = - \left(\frac{1}{\hbar\omega - h} \right)_{12} Q_2^{\frac{1}{2}+2*} G_{21'}, \quad (\text{F.72})$$

and therefore obtain

$$\begin{aligned} (\hbar\omega - h)_{12} G_{21'}(\omega) &= \delta_{11'} + Q_1^{\frac{1}{2}+2} P_{21'}^*(\omega), \\ (\hbar\omega - h)_{12} P_{21'}^*(\omega) &= - Q_2^{\frac{1}{2}+2*} G_{21'}(\omega). \end{aligned} \quad (\text{F.73})$$

As in the pairing case, we have to close the system of equations. This can be done analogously here by using instead of (F.50) the Bethe-Salpeter equation for the response function (8.131). The result is

$$\langle 0 | [a_3^+ a_4]_{2+} | 2^+ \rangle = \delta\rho_{12}^{(2+)} = \frac{1}{2\pi i} \oint d\omega P_{43}(\omega). \quad (\text{F.74})$$

Insertion of (F.74) into (F.71) constitutes, together with (F.73), the “gap equation” for the “order parameter” Q of the deformation field.

Two single-particle fields enter into Eqs. (F.76), one involving the ordinary density $\rho_{12} = \langle 0 | a_2^+ a_1 | 0 \rangle$ and the other the transition density

$$\delta\rho_{12}^{(2+)} = \langle 0 | [a_2^+ a_1]_{2+} | 2^+ \rangle.$$

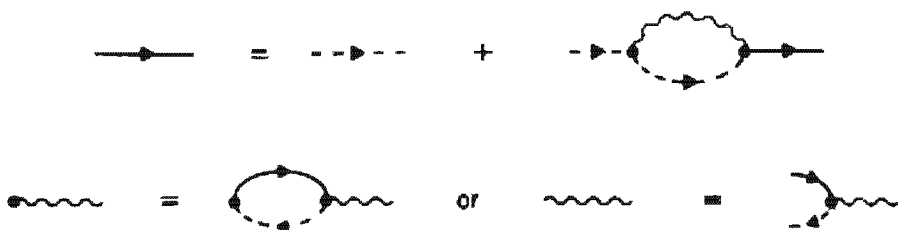


Figure F.5 (a) Graphical representation of Eq. (F.69). The wavy line represents the soft quadrupole phonon. (b) Graphical representation of the "gap equation" for the deformation field Q .

The transition density, of course, projects out the quadrupole part of the $p\hbar$ force in (F.71) and the ordinary density projects out the monopole part of the force in (F.69). We again wish to stress the point that no symmetry-violating approximation has been made so far, as we have coupled everything to good angular momentum. The symmetry breaking of deformed HF theory can be introduced by saying that the 2^+ becomes identical with the ground state of the internal system. At this moment, having angular momentum coupling no longer makes sense and Eqs. (F.73) just reduce to the usual deformed HF equations. We explicitly find two potentials V_0 and Γ_2 , introduced in Sec. 11.2, which now constitute an angular momentum nonconserving single-particle Hamiltonian of the internal system.

As we have already stated, the "gap equation" for the deformation field (F.71, 74) can again be derived from the Bethe-Salpeter equation for the response function (8.131). From (F.74) and (F.72) we see, however, that it can be represented graphically as shown in Fig. F.5b. Eq. (F.69) is represented in Fig. F.5a. Again, the typical nonlinear coupling of single-particle motion and collective vibration becomes evident from Fig. F.5a, b.

In general, we should, of course, separate the Cooper pole and the phonon poles of all multipolarities in the mass operator simultaneously and thus generate the general single-particle theory we treated in Chapter 7.

From (F.71) and (F.59), we see that the transition densities enter the deformation and pair fields. As we have seen that these are peaked at the nuclear surface (Chaps. 8 and 13), it may be a good approximation to replace the forces entering (F.71) and (F.59) by separable ones. This leads naturally to the *pairing-plus-quadrupole model* discussed in Chapter 7, and thus we again see the meaning of this model within the context of nuclear phase transitions.

From the GF treatment of this theory, it also becomes clear how a possible generalization might work: the essential feature would be to solve the RPA modes *self consistently* with the single-particle states, that is, where the single states are coupled back to the RPA modes in the way shown in Fig. F.5a, b. Also, the symmetry-conserving formulation (F.62) of HFB should be an interesting variant of the theory; in fact a much more elaborate theory of this kind has been proposed by Janssen [Ja 79].

F.6 The Bethe-Salpeter Equation and Effective Forces

In the course of the derivation of the HFB equations we have made reference to Bethe-Salpeter equations (BSE) for two-body GF's on several occasions. Since these equations are derived in many textbooks [Mi 67, AGD 65, FW 71], we shall be very brief here. The BSE for the response function (F.51) is given by:

$$R(1, 3; 1', 3') = G(1, 1')G(3, 3') - G(3, 5)G(6, 1')K^{\text{ph}}(5, 7; 6, 8)R(1, 8; 7, 3'). \quad (\text{F.75})$$

Equation (F.75) is an exact equation, where K^{ph} is called an effective particle-hole force; it sums up skeleton graphs of the response function, which cannot be cut into two parts by cutting only two lines. The BSE (F.75) is graphically represented in Fig. F.6, together with a typical second-order contribution to K^{ph} . We see that these contributions to K^{ph} can be cut into two halves only by cutting four lines. Equation (F.75) can be verified to any order skeleton perturbation. Repeated indices in (F.75) indicate, as usual, summation over quantum numbers and integration over times. It should be mentioned that (F.75) is sometimes convenient in deriving formal relations. Going beyond the RPA treatment (F.75), however, is extremely complicated, because the kernel generally depends on three times (after taking into account translational invariance with respect to time) or three energies. For practical purposes we sometimes, therefore, use an integral equation for the response function with a kernel depending only on one energy [Sch 71c, Sch 76]. In this way, we arrive at a Dyson equation for bosons (RPA) with a boson mass operator which is quite analogous to the Dyson equation (F.22) for fermions [SE 73, Sch 76]. This treatment of correlation functions is similar in spirit to what has now become known as Mori theory [Mo 65] in the field of condensed matter. To nuclear physics this has been applied by Werner [We 76, 78].

Everything we have said about the BSE for the response function also holds good for the analogous BSE of the two-body GF (F.54):

$$G(1, 2; 1' 2') = G^0(1, 2; 1', 2') - \frac{1}{4}G^0(1, 2; 3, 4)K^{\text{pp}}(3, 4; 3', 4')G(3', 4'; 1', 2').$$

Here K^{pp} again sums up all graphs contributing to $G(1, 2; 1', 2')$ which cannot be cut in two by just cutting two skeleton lines. In Fig. F.7 we give a graphical representation of (F.54) together with a second-order skeleton

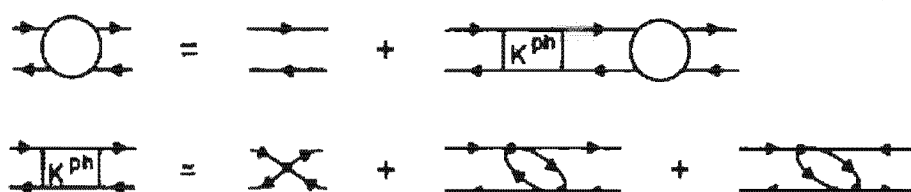


Figure F.6. Bethe-Salpeter equation for the response function (F.50) and schematic representation of lowest-order contributions to K^{ph} .

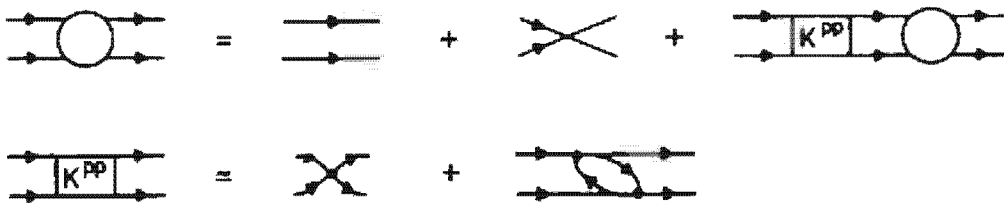


Figure F.7. Bethe-Salpeter equation for the pp GF of (F.76) and schematic representation of the lowest order contribution to K''' .

contribution to K''' ; the lowest order being, of course, the bare interaction itself.

As we have shown above, the gap equations for the pair field Δ (F.67) and for the deformation field Q (F.71) can be derived from the corresponding BS equations (F.54) and (F.75). It is therefore obvious that these order parameters have to be calculated with the corresponding effective pp and ph forces K''' and K'' , respectively. To show this explicitly is somewhat tricky, and presenting details would be very clumsy, so we will only sketch the main features here.

We have already shown that in the gap equations for Δ and Q we have to use K''' and K'' , respectively. It is more difficult to show how K''' and K'' come into play in the first of equations (F.62) and (F.73), respectively. Let us denote the R -function appearing in the mass operator (F.25) by R_6 ; then for the mass operator we can write in an obvious shorthand notation

$$M'(\omega) = \bar{v} R_6 R_6^{-1} R_6 \bar{v}. \quad (\text{F.76})$$

We have seen that HFB theory corresponds to approximating R_6 by the first term on the rhs of (F.50), which we will denote by GG_4 . In this approximation we also have, of course,

$$R_6^{-1} = [GG_4]^{-1}. \quad (\text{F.77})$$

We now observe that from (F.45) and (F.46) we have

$$\begin{aligned} G(1, 2; 1', 2') &= G^0(1, 2; 1', 2') \\ &\quad - \frac{i}{2} R(1, 2, 3^{++}; 1'', 2', 3'^+) \bar{v}(3', 1''; 3, 1''') \cdot G(1'', 1'). \end{aligned} \quad (\text{F.78})$$

Together with (F.54), we deduce the identity:

$$\begin{aligned} R(1, 2, 3^{++}; 1'', 2', 3'^+) \bar{v}(3', 1''; 3, 1''') &= G(2, 3^{++}; 2', 3'^+) \\ &\quad \cdot G(1, 1'') K'''(3', 1''; 3, 1'''). \end{aligned} \quad (\text{F.79})$$

Replacing the parts $R_6 \bar{v}$ and $\bar{v} R_6$ in (F.76) by (F.79) and its adjoint, respectively, and using (F.77), we see that in (F.58) and (F.62) we have to use K''' everywhere. Analogously, we can, of course, show that we have to

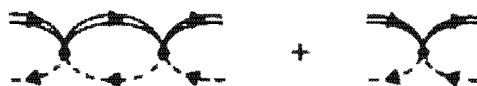


Figure F.8. Hole-pairing mode scattering process omitted in (F.77).

use K^{ph} in (F.69) and (F.73). It can be shown [ES 69] that the terms we have neglected by the approximation (F.77) are of the type shown in Fig. F.8, where the hole scatters from the pairing mode.

This shall conclude our brief outline of GF theory, and for more details of the standard techniques we again refer the reader to the literature cited in this appendix.

Bibliography

Italic numbers following each reference refer to the page(s) of this volume on which the reference is cited.

- [AAZ 77] V. C. Aguilera, S. G. Andrade, A. H. Zimerman, L. Doehnert, M. De Llano, and A. Plastino. Phys. Rev. C16 (1977) 2081. 441
- [AB 59] R. D. Amado and K. A. Brueckner. Phys. Rev. 115 (1959) 778. 131
- [Ab 78] S. Åberg. Nucl. Phys. A306 (1978) 89. 145
- [ABC 63] D. W. Anderson, A. J. Bureau, B. C. Cook, J. E. Griffin, J. R. McConnell, and K. H. Nybo. Phys. Rev. Lett. 10 (1963) 250. 294
- [ABC 69] Y. Abgrall, G. Baron, E. Caurier, and G. Monsonego. Nucl. Phys. A131 (1969) 609. 481
- [ABC 77a] A. Alves, L. P. De Brito, M. H. Caldeira, J. M. Domingos, P. Martins, H. Pascoal, J. Da Providencia, M. C. Ruivo, E. M. Silva, C. A. De Sousa, and J. N. Urbano. Progr. Theor. Phys. 58 (1977) 223. 475
- [ABC 77b] A. Alves, L. P. De Brito, M. H. Caldeira, J. M. Domingos, P. Martins, J. Da Providencia, M. C. Ruivo, E. M. Silva, C. A. De Sousa, and J. N. Urbano. Nucl. Phys. A284 (1977) 420. 432, 519
- [ABH 56] K. Alder, A. Bohr, T. Huus, B. R. Mottelson, and A. Winter. Rev. Mod. Phys. 28 (1956) 432. 112
- [ABP 68] S. M. Abecasis, H. E. Bosch, and A. Plastino. Nuovo Cim. 54B (1968) 245. 25
- [ABH 78] O. Andersen, R. Bauer, G. B. Hagemann, M. L. Halbert, B. Herskind, M. Neiman, H. Oeschler, and H. Ryde. Nucl. Phys. A295 (1978) 163. 98
- [ABR 75] S. André, J. Boutet, J. Rivier, J. Tréherne, J. Jastrzebski, J. Lukasiak, Z. Sujkowski, and C. Sébille-Schück. Nucl. Phys. A243 (1975) 229. 123

- [ABV 63] R. Arvieu, E. Baranger, M. Véneroni, M. Baranger, and V. Gillet. *Phys. Lett.* **4** (1963) 119. 345
- [AC 75] Y. Abgrall and E. Caurier. *Phys. Lett.* **56B** (1975) 229. 433
- [ADD 70] B. L. Andersen, F. Dickmann, and K. Dietrich. *Nucl. Phys.* **A159** (1970) 337. 81, 95
- [ADW 78] H. Arenhövel, D. Drechsler, and H. J. Weber. *Nucl. Phys.* **A305** (1978) 485. 294
- [AEE 78] V. L. Alexeev, B. A. Emelianov, A. I. Egorov, L. P. Kabina, D. M. Kaminker, Y. L. Khazov, I. A. Kondurov, E. K. Leushkin, Y. E. Loginov, V. V. Martynov, V. L. Rumiantsev, S. L. Sakharov, P. A. Sushkov, H. G. Börner, W. F. Davidson, J. A. Pinston, and K. Schreckenbach. *Nucl. Phys.* **A297** (1978) 373. 187
- [AG 61] A. A. Abrikosov and L. P. Gorkov. *Sov. Phys. JETP* **12** (1961) 1243. 277
- [AG 74] K. Allaart and W. F. Van Gunsteren. *Nucl. Phys.* **A234** (1974) 53. 482
- [AGD 63] A. A. Abrikosov, L. P. Gorkov and I. E. Dzyaloshinski. *Methods of Quantum Theory in Statistical Physics*. Prentice Hall, Englewood Cliffs, NJ, 1963. 260, 284
- [AGD 65] A. A. Abrikosov, L. P. Gorkov, and I. E. Dzyaloshinski. *Quantum Field Theoretical Methods in Statistical Physics*. Pergamon, Oxford, 1965. 623, 630, 640
- [AGM 74] K. Allaart, K. Goeke, H. Müther, and A. Faessler. *Phys. Rev.* **C9** (1974) 988. 435
- [AH 71a] K. Arima and H. Horie. *Nucl. Phys.* **A173** (1971) 97. 394, 395
- [AH 71b] A. Arima and I. Hamamoto. *Ann. Rev. Nucl. Sci.* **21** (1971) 55. 389
- [AHL 78] C. G. Andersson, G. Hellström, G. Leander, I. Ragnarsson, S. Åberg, J. Krumlinde, S. G. Nilsson, and Z. Szymanski. *Nucl. Phys.* **A309** (1978) 141. 145
- [AHK 72] N. Auerbach, J. Hüfner, A. K. Kerman, and C. M. Shakin. *Rev. Mod. Phys.* **44** (1972) 207, 209
- [AI 75a] A. Arima and F. Iachello. *Phys. Lett.* **57B** (1975) 39. 373, 377
- [AI 75b] A. Arima and F. Iachello. *Phys. Rev. Lett.* **35** (1975) 1069. 373, 377
- [AI 76] A. Arima and F. Iachello. *Ann. Phys. (New York)* **99** (1976) 253. 379
- [AI 78a] A. Arima and F. Iachello. *Ann. Phys. (New York)* **111** (1978) 201. 379
- [AI 78b] A. Arima and F. Iachello. *Phys. Rev. Lett.* **40** (1978) 385. 379
- [AK 77] C. G. Andersson and J. Krumlinde. *Nucl. Phys.* **A291** (1977) 21. 145
- [Al 67] G. Alaga. *Varenna Lectures* **40** (1967) 28. 385
- [ALL 76] C. G. Andersson, S. E. Larsson, G. Leander, P. Möller, S. G. Nilsson, I. Ragnarsson, S. Åberg, R. Bengtsson, J. Dudek, B. Nerlo-Pomorska, K. Pomorski, and Z. Szymanski. *Nucl. Phys.* **A268** (1976) 205. 27, 34, 134, 137, 139, 140, 141, 145
- [ALP 77] V. C. Aguilera, M. De Llano, S. Peltier, and A. Plastino. *Phys. Rev.* **C16** (1977) 1642. 441
- [Am 67] J. P. Amiel. *Z. Phys.* **202** (1967) 150. 367
- [AMK 69] V. C. Aguilera, M. Moshinsky, and P. Kramer. *Ann. Phys. (New York)* **54** (1969) 379. 456
- [An 58] P. W. Anderson. *Phys. Rev.* **112** (1958) 1900. 201
- [AN 71] A. Ansari and S. C. K. Nair. *Nucl. Phys.* **A163** (1971) 56. 482
- [AOI 77] A. Arima, T. Otsuka, F. Iachello, and I. Talmi. *Phys. Lett.* **66B** (1977) 205. 373
- [AOI 78] A. Arima, T. Otsuka, F. Iachello, O. Scholten, and I. Talmi. *Proc. Int. Conf. on Nuclear Structure*, Tokyo, 1977, *J. Phys. Soc. Japan* **44 Suppl.** (1978) 509. 379
- [AP 76] G. Alaga and V. Paar. *Phys. Lett.* **61B** (1976) 129. 122, 385

- [APS 75] G. Alaga, V. Paar, and L. Sips (Eds.). Proceedings of the Topical Conference on Problems of Vibrational Nuclei, Zagreb 1975. North Holland, Amsterdam, 1975. 385, 389
- [Ar 63] R. Arvieu. Ann. Phys. (Paris) **8** (1963) 407. 345
- [Ar 65] P. Argyres. Physics **2** (1965) 131. 533, 534
- [AS 65] M. Abramowitz and I. A. Stegun. Handbook of Mathematical Functions. Dover, New York, 1965. 87, 88, 529, 530, 531, 537, 539, 584, 585, 586
- [AS 71] N. Anantaraman and J. P. Schiffer. Phys. Lett. **37B** (1971) 229. 173, 186
- [ASS 69] D. A. Arseniev, A. Sobiczewski, and V. G. Soloviev. Nucl. Phys. **A126** (1969) 15. 27
- [ASV 64] R. Arvieu, E. Salusti, and M. Vénéroni. Phys. Lett. **8** (1964) 334. 345
- [Au 70] N. Austern. Direct Nuclear Reaction Theories. Wiley-Interscience, New York, 1970. 59
- [AV 63] R. Arvieu and M. Vénéroni. Phys. Lett. **5** (1963) 142. 345
- [AW 61] J. D. Anderson and C. Wong. Phys. Rev. Lett. **7** (1961) 250. 299
- [AW 66] K. Alder and A. Winter. Coulomb Excitation. Academic, New York, 1966. 97
- [AW 74] K. Alder and A. Winter. Theory of Coulomb Excitation with Heavy Ions. North Holland, Amsterdam, 1974. 97
- [AY 59] A. Arima and S. Yoshida. Nucl. Phys. **12** (1959) 139. 482
- [AY 78] S. Adachi and S. Yoshida. Nucl. Phys. **A306** (1978) 53. 323
- [Ba 60a] M. Baranger. Phys. Rev. **120** (1960) 957. 343
- [Ba 60b] B. F. Bayman. Nucl. Phys. **15** (1960) 33. 463
- [Ba 61] M. Baranger. Phys. Rev. **122** (1961) 992. 254
- [Ba 62] V. Bargmann. Rev. Mod. Phys. **34** (1962) 829. 411, 412
- [Ba 63a] M. Baranger. Phys. Rev. **130** (1963) 1244. 254
- [Ba 63b] M. Baranger. Cargese Lectures in Theoretical Physics. M. Levi, Ed. Benjamin, New York, 1963. 254
- [Ba 67] J. Bar-Touv. Phys. Rev. **164** (1967) 1241. 506
- [Ba 69a] M. Baranger. Varenna Lectures **40** (1969) 511. 204, 205
- [Ba 69b] G. Baumgartner. Z. Phys. **218** (1969) 266. 473
- [Ba 72a] M. Baranger. J. Phys. (Paris) **33** (1972) C5-61. 506
- [Ba 72b] R. Baltin. Z. Naturforschung **27A** (1972) 1176. 542, 565
- [Ba 78] A. Baran. Phys. Lett. **76B** (1978) 8. 526
- [BB 36] H. A. Bethe and R. F. Bacher. Rev. Mod. Phys. **8** (1936) 82. 4
- [BB 59] G. E. Brown and M. Bolsterli. Phys. Rev. Lett. **3** (1959) 472. 285, 286
- [BB 66] D. R. Bes and R. A. Broglia. Nucl. Phys. **80** (1966) 289. 300
- [BB 67] D. M. Brink and E. Boeker. Nucl. Phys. **91** (1967) 1. 177, 209, 433
- [BB 69] R. Balian and E. Brézin. Nuovo Cim. **64B** (1969) 37. 617, 618
- [BB 71] D. R. Bes and R. A. Broglia. Phys. Rev. **C3** (1971) 2349. 183
- [BB 72] R. Balian and C. Bloch. Ann. Phys. (New York) **69** (1972) 76. 527
- [BB 73] B. Banerjee and D. M. Brink. Z. Phys. **258** (1973) 46. 419, 421
- [BB 74] R. Balian and C. Bloch. Ann. Phys. (New York) **85** (1974) 514. 527
- [BB 76] D. R. Bes and R. A. Broglia. Varenna Lectures **69** (1976) 55. 445, 448
- [BBB 75] R. Beck, J. Borysowicz, D. M. Brink, and M. V. Mihailović. Nucl. Phys. **A244** (1975) 45. 58. 399
- [BBB 77] P. F. Bortignon, R. A. Broglia, D. R. Bes, and R. J. Liotta. Phys. Rep. **30C** (1977) 305. 386, 391, 394, 395

- [BBB 79a] F. A. Beck, E. Bozek, T. Byrski, C. Gehringer, J. C. Merdinger, Y. Schutz, J. Styczen, and J. P. Vivien. *Phys. Rev. Lett.* **42** (1979) 493. 107
- [BBB 79b] G. F. Bertsch, P. F. Bortignon, R. A. Broglia, and C. H. Dasso. *Phys. Lett.* **80B** (1979) 161. 323
- [BBC 71] H. Beil, R. Bergere, P. Carlos, A. Lepretre, A. Veyssiére, and A. Parlag. *Nucl. Phys.* **A172** (1971) 426. 294
- [BBC 72] M. Bouten, M. C. Bouten, and E. Caurier. *Nucl. Phys.* **A193** (1972) 49. 481
- [BBH 77] J. Blomqvist, I. Bergström, C. J. Herlander, C. G. Linden, and K. Wikström. *Phys. Rev. Lett.* **38** (1977) 543. 145
- [BBL 80] M. Buenerd, C. Bonhomme, D. Lebrun, P. Martin, J. Chauvin, G. Duhamel, G. Perrin, and P. de Saintignon. *Phys. Lett.* **84B** (1980) 305. 296
- [BBN 74a] D. R. Bès, R. A. Broglia, and B. S. Nilsson. *Phys. Rep.* **16C** (1974) 1. 397
- [BBN 74b] R. A. Broglia, D. R. Bès, and B. S. Nilsson. *Phys. Lett.* **50B** (1974) 213. 185
- [BBN 78] J. Blocki, Y. Boneh, J. R. Nix, J. Randrup, M. Robel, A. J. Sierk, and W. J. Swiatecki. *Ann. Phys. (New York)* **113** (1978) 330. 494, 517
- [BBP 63] H. A. Bethe, B. H. Brandow, and A. G. Petschek. *Phys. Rev.* **129** (1963) 225. 163
- [BC 73] D. M. Brink and J. J. Castro. *Nucl. Phys.* **A216** (1973) 109. 441
- [BCD 75] G. Baym, D. Campbell, R. Dashen, and J. Manassah. *Phys. Lett.* **58B** (1975) 304. 441
- [BCH 64] R. L. Bramblett, J. T. Caldwell, R. R. Harvey, and S. C. Fultz. *Phys. Rev.* **I33** (1964) B869. 281
- [BCK 76] O. Bohigas, X. Campi, H. Krivine, and J. Treiner. *Phys. Lett.* **64B** (1976) 381. 527, 544
- [BCS 57] J. Bardeen, L. N. Cooper, and J. R. Schrieffer. *Phys. Rev.* **108** (1957) 1175. 221, 228
- [BD 71] R. Balian and C. De Dominicis. *Ann. Phys. (New York)* **62** (1971) 229. 628
- [BDJ 72] M. Brack, J. Damgaard, A. S. Jensen, H. C. Pauli, V. M. Strutinski, and C. Y. Wong. *Rev. Mod. Phys.* **44** (1972) 320. 29, 30, 67, 81, 91, 93, 95
- [BDL 75] H. Beuscher, W. F. Davidson, R. M. Lieder, A. Neskakis, and C. Mayer-Böricke. *Nucl. Phys.* **A249** (1975) 379. 119
- [Be 31] H. A. Bethe. *Z. Phys.* **71** (1931) 205. 499
- [Be 59] S. T. Belyaev. *Mat. Fys. Medd. Dan. Vid. Selsk.* **31** (No. 11) (1959). 131, 221, 240, 253
- [Be 61] S. T. Belyaev. *Nucl. Phys.* **24** (1961) 322. 131
- [Be 63] D. R. Bès. *Nucl. Phys.* **49** (1963) 544. 345
- [Be 65] S. T. Belyaev. *Nucl. Phys.* **64** (1965) 17. 506
- [Be 66] S. T. Belyaev. *Sov. J. Nucl. Phys.* **4** (1966) 936. 486
- [Be 68] S. T. Belyaev. *Collective Excitations in Nuclei*. Gordon and Breach, New York, 1968. 26, 506
- [Be 71] H. A. Bethe. *Ann. Rev. Nucl. Sci.* **21** (1971) 93. 163, 164, 206, 527
- [Be 73] G. F. Bertsch. *Phys. Rev. Lett.* **31** (1973) 121. 323
- [Be 74] G. F. Bertsch. *Ann. Phys. (New York)* **86** (1974) 138. 568
- [Be 75] G. F. Bertsch. *Nucl. Phys.* **A249** (1975) 253. 368
- [Be 76] F. E. Bertrand. *Ann. Rev. Nucl. Sci.* **26** (1976) 457. 295
- [BE 68] J. De Boer and J. Eichler. *Adv. Nucl. Phys.* **1** (1968) 1. 26
- [BEL 70] B. L. Birbrair, K. I. Erokhina, and I. K. Lemberg. *Nucl. Phys.* **A145** (1970) 129. 345
- [BER 75] R. Bauer, K. Ebert, P. Ring, W. Theis, E. Werner, and W. Wild. *Z. Phys.* **A274** (1975) 41. 179, 327

- [BES 76] H. C. Britt, B. H. Erkkila, R. H. Stokes, H. H. Gutbrod, F. Plasil, R. L. Ferguson, and M. Blann. *Phys. Rev.* **C13** (1976) 1483. 35
- [BET 61] G. E. Brown, J. A. Evans, and D. J. Thouless. *Nucl. Phys.* **24** (1961) 1. 285, 303
- [BF 74] G. Baym and E. Flowers. *Nucl. Phys.* **A222** (1974) 29. 441
- [BF 76] J. Blocki and H. Flocard. *Nucl. Phys.* **A273** (1976) 45. 486
- [BFG 75] M. Beiner, H. Flocard, N. Van Giai, and P. Quentin. *Nucl. Phys.* **A238** (1975) 29. 175, 213, 215, 329
- [BFN 72] M. Bolsterli, E. O. Fiset, J. R. Nix, and J. L. Norton. *Phys. Rev.* **C3** (1972) 1050. 81, 95
- [BFV 74] M. Beiner, H. Flocard, M. Vénéroni, and P. Quentin. *Physica Scripta* **10A** (1974) 84. 268
- [BG 49] M. Born and H. S. Greene. *A General Kinetic Theory of Liquids*. Cambridge Univ. Press, 1949. 487
- [BG 57] H. A. Bethe and J. Goldstone. *Proc. Roy. Soc. (London)* **A238** (1957) 551. 157
- [BG 65] C. Bloch and V. Gillet. *Phys. Lett.* **16** (1965) 62; **18** (1965) 58. 323
- [BG 77] J. P. Blaizot and D. Gogny. *Nucl. Phys.* **A284** (1977) 429. 203, 317, 328, 332
- [BGG 69] J. Bar-Touv, A. Goswami, A. L. Goodman, and G. L. Struble. *Phys. Rev.* **178** (1969) 1670. 263
- [BGG 76] J. P. Blaizot, D. Gogny, and B. Grammaticos. *Nucl. Phys.* **A265** (1976) 315. 296, 322, 328
- [BGK 78] P. Bonche, B. Grammaticos, and S. E. Koonin. *Phys. Rev.* **C17** (1978) 1700. 501, 505
- [BGR 65] W. H. Bassichis, B. Giraud, and G. Ripka. *Phys. Rev. Lett.* **15** (1965) 980. 481
- [BGV 76] D. M. Brink, M. J. Giannoni, and M. Vénéroni. *Nucl. Phys.* **A258** (1976) 237. 506, 515
- [BGW 58] K. A. Brueckner, J. L. Gammel, and H. Weitzner. *Phys. Rev.* **110** (1958) 431. 163, 207
- [Bh 77] R. K. Bhaduri. *Phys. Rev. Lett.* **39** (1977) 329. 545, 546, 547
- [BH 67] B. Buck and A. D. Hill. *Nucl. Phys.* **A95** (1967) 271. 323
- [BHM 78] R. Bengtsson, I. Hamamoto, and B. R. Mottelson. *Phys. Lett.* **73B** (1978) 259. 122
- [BHR 73] R. A. Broglia, O. Hansen, and C. Riedel. *Adv. Nucl. Phys.* **6** (1973) 287. 300, 449
- [Bi 68] B. L. Birbrair. *Nucl. Phys.* **A108** (1968) 449. 345
- [Bi 72] J. Birkholz. *Nucl. Phys.* **A189** (1972) 385. 323
- [Bi 76] B. L. Birbrair. *Nucl. Phys.* **A257** (1976) 445. 440
- [BJ 76a] G. E. Brown and A. D. Jackson. *The Nucleon-Nucleon Interaction*. North Holland, Amsterdam, 1976. 148, 155, 187
- [BJ 76b] M. Brack and B. K. Jennings. *Nucl. Phys.* **A258** (1976) 264. 131, 139, 542
- [BJC 76] M. Brack, B. K. Jennings, and Y. H. Chu. *Phys. Lett.* **65B** (1976) 1. 527, 542, 543
- [BJS 75] S. O. Bäckmann, A. D. Jackson, and J. Speth. *Phys. Lett.* **56B** (1975) 209. 176, 209, 329
- [BK 61] R. Beringer and W. J. Knox. *Phys. Rev.* **121** (1961) 1195. 34
- [BK 65] M. Baranger and K. Kumar. *Nucl. Phys.* **62** (1965) 113. 260
- [BK 67a] G. E. Brown and T. T. S. Kuo. *Nucl. Phys.* **A92** (1967) 481. 169
- [BK 67b] M. Baranger and K. Kumar. *Nucl. Phys.* **A92** (1967) 608; **A100** (1967) 490. 181
- [BK 68] M. Baranger and K. Kumar. *Nucl. Phys.* **A110** (1968) 529; **A122** (1968) 241, 273. 182, 185, 260, 261, 285, 521, 522
- [BK 69] J. Blomqvist and T. T. S. Kuo. *Phys. Lett.* **29B** (1969) 544. 170, 172, 326

- [BK 73] B. R. Barrett and M. W. Kirson. *Adv. Nucl. Phys.* **6** (1973) 219, 166, 169
- [BKD 73] B. Banerjee, S. B. Khadkikar, and K. R. S. Devi. *Phys. Rev. C7* (1973) 1010, 262
- [BKN 76] P. Bonche, S. E. Koonin, and J. W. Negele. *Phys. Rev. C13* (1976) 1226, 497, 501, 502, 503
- [BKS 67] W. H. Bassichis, A. K. Kerman, and J. P. Svenne. *Phys. Rev. 160* (1967) 746, 268
- [BKS 72] G. G. Bunayan, V. M. Kolomietz, and V. M. Strutinski. *Nucl. Phys. A128* (1972) 225, 93
- [Bl 60] J. M. Blatt. *J. Austr. Math. Soc.* **1** (1960) 465.
- [Bl 62] C. Bloch. *Lectures on the Manybody Problem*. Tata Institute, Bombay, 1962. Reprinted in C. Bloch, *Scientific Works Vol. 2*. North Holland, Amsterdam, 1975, 255
- [Bl 76] J. P. Blaizot. *Phys. Lett.* **60B** (1976) 435, 333
- [BL 76] D. M. Brink and R. Leonardi. *Nucl. Phys. A258* (1976) 285, 332
- [BLD 67] M. Bouten, P. Van Leuven, and H. Depuydt. *Nucl. Phys. A94* (1967) 687, 481
- [BLL 75] R. Bengtsson, S. E. Larsson, G. Leander, P. Möller, S. G. Nilsson, S. Åberg, and Z. Szymański. *Phys. Lett.* **57B** (1975) 301, 139
- [BLM 79] O. Bohigas, A. M. Lane, and J. Martorell. *Phys. Rep.* **51C** (1979) 267, 330, 331
- [BLP 74] M. Brack, T. Lederman, H. C. Pauli, and A. S. Jensen. *Nucl. Phys. A234* (1974) 185, 81
- [BLR 61] K. A. Brueckner, A. M. Lockett, and A. M. Rotenberg. *Phys. Rev. 121* (1961) 255, 163
- [BM 53] A. Bohr and B. R. Mottelson. *Mat. Fys. Medd. Dan. Vid. Selsk.* **27** (No. 16) (1953), 12, 97, 107
- [BM 55] A. Bohr and B. R. Mottelson. *Mat. Fys. Medd. Dan. Vid. Selsk.* **30** (No. 1) (1955), 131
- [BM 58] A. Bohr and B. R. Mottelson. *Kon. Norske Vidensk. Selskab Forhandlinger* **31** (No. 12) (1958), 453, 458
- [BM 62] C. Bloch and A. Messiah. *Nucl. Phys.* **39** (1962) 95, 246, 611
- [BM 69] A. Bohr and B. R. Mottelson. *Nuclear Structure*, Vol. I. Benjamin, New York, 1969, 2, 36, 37, 63, 236, 581
- [BM 74] A. Bohr and B. R. Mottelson. *Physica Scripta* **10A** (1974) 13, 100, 102, 143
- [BM 75] A. Bohr and B. R. Mottelson. *Nuclear Structure*, Vol. II. Benjamin, New York, 1975, 1, 23, 28, 66, 67, 82, 97, 125, 134, 135, 300, 334, 351, 382, 383, 386, 388
- [BM 78] J. P. Blaizot and E. R. Marshalek. *Nucl. Phys. A309* (1978) 422, 453, 350, 373, 374, 382, 520
- [BML 76] O. Bohigas, J. Martorell, and A. M. Lane. *Phys. Lett.* **64B** (1976) 1, 330
- [BMP 58] A. Bohr, B. R. Mottelson, and D. Pines. *Phys. Rev. 110* (1958) 936, 221
- [BMR 70] R. Beck, H. J. Mang, and P. Ring. *Z. Phys.* **231** (1970) 26, 126, 462, 468, 470, 478, 479, 481
- [BMR 73] B. Banerjee, H. J. Mang, and P. Ring. *Nucl. Phys. A215* (1973) 366, 250, 258, 278
- [BN 77] C. E. Bemis and J. R. Nix. *Comments on Nucl. Part. Phys.* **7** (1977) 65, 95
- [Bo 51] A. Bohr. *Phys. Rev. 81* (1951) 134, 66
- [Bo 52] A. Bohr. *Mat. Fys. Medd. Dan. Vid. Selsk.* **26** (1952) No. 14, 9, 18, 21, 97, 336
- [Bo 54] A. Bohr. *Rotational States of Atomic Nuclei*. Ejnar Munksgaards Forlag, Copenhagen, 1954.
- [Bo 58] N. N. Bogoliubov. *Sov. Phys. JETP* **7** (1958) 41, 245

- [Bo 59a] N. N. Bogoliubov. Sov. Phys. Usp. 2 (1959) 236. 245
- [Bo 59b] N. N. Bogoliubov. Usp. Fiz. Nauk. 67 (1959) 549. 245, 343
- [Bo 64] A. Bohr. Congrès Int. De Physique Nucléaire. P. Guggenberger, Ed. Centre de la Recherche Scientifique, Paris, 1964, p. 487. 300
- [Bo 76a] A. Bohr. Rev. Mod. Phys. 48 (1976) 365. 137
- [Bo 76b] A. Bohr. Varenna Lectures 69 (1976) I. 21, 137, 142, 143, 476
- [Bö 76] M. Böhning. Zulassungsarbeit, T.U. Munich, 1976. 417
- [BP 53] D. Bohm and D. Pines. Phys. Rev. 92 (1953) 609. 301, 454
- [BP 71] J. P. Boisson and R. Piepenbring. Nucl. Phys. A168 (1971) 385. 72
- [BP 73] M. Brack and H. C. Pauli. Nucl. Phys. A207 (1973) 401. 88, 89, 90, 91, 548
- [BP 77a] N. L. Balazs and H. C. Pauli. Z. Phys. A281 (1977) 395. 37
- [BP 77b] N. L. Balazs and H. C. Pauli. Z. Phys. A282 (1977) 221. 610
- [BPC 72] M. I. Baznat, N. I. Pyatov, and M. I. Chernej. Physica Scripta 6 (1972) 227. 120
- [BPO 76] J. P. Boisson, R. Piepenbring, and W. Ogle. Phys. Rep. 26C (1976) 99. 185
- [BQ 75a] M. Brack and P. Quentin. Proc. Int. Conf. on Nuclear Selfconsistent Fields, Trieste, 1975. G. Ripka and M. Porneuf, Eds. North Holland, Amsterdam, 1975. 92, 93, 270, 528, 549
- [BQ 75b] M. Brack and P. Quentin. Phys. Lett. 56B (1975) 421. 92, 528
- [BQ 78] P. Bonche and P. Quentin. Phys. Rev. C18 (1978) 1891. 508
- [Br 55] K. A. Brueckner. Phys. Rev. 97 (1955) 1353. 156
- [Br 64] G. E. Brown. Unified Theory of Nuclear Models. North Holland, Amsterdam, 1964. 128, 163, 299, 303
- [Br 65a] D. M. Brink. Nuclear Forces. Pergamon Press, New York, 1965. 2, 154
- [Br 65b] W. Brenig. Advances Theor. Phys. 1 (1965) 59. 294
- [Br 67a] B. H. Brandow. Rev. Mod. Phys. 39 (1967) 771. 766
- [Br 67b] R. A. Bryan. Proc. Int. Conf. on Nuclear Physics, Gatlinburg, 1967, R. L. Becker, Ed. Academic Press, New York, 1967. 155
- [Br 71] G. E. Brown. Rev. Mod. Phys. 43 (1971) I. 178
- [Br 77] M. Brack. Habilitationsschrift, Institut Laue Langevin, Grenoble, 1977. 541, 542, 543
- [Br 78] R. Brockmann. Phys. Rev. C18 (1978) 1510. 44
- [BR 37] H. A. Bethe and M. E. Rose. Phys. Rev. 51 (1937) 283. 456
- [BR 71a] M. E. Bunker and C. W. Reich. Rev. Mod. Phys. 43 (1971) 348. 79
- [BR 71b] R. K. Bhaduri and C. K. Ross. Phys. Rev. Lett. 27 (1971) 606. 139, 527
- [BR 76] G. Bertin and L. A. Radicati. Astrophys. J. 206 (1976) 815. 33
- [BRS 68] R. A. Broglia, C. Riedel, and B. Sørensen. Nucl. Phys. A107 (1968) I. 342
- [BS 56] J. S. Bell and T. H. R. Skyrme. Phil. Mag. 1 (1956) 1055. 175
- [BS 59] N. N. Bogoliubov and V. G. Soloviev. Sov. Phys. Doklady 4 (1959) 143. 245, 254
- [BS 61] D. R. Bès and Z. Szymański. Nucl. Phys. 28 (1961) 42. 80
- [BS 64] W. Brenig and P. Schuck. Congrès Int. de Physique Nucléaire. P. Guggenberger, Ed. Centre de la Recherche Scientifique, Paris 1964, Vol. II. 294
- [BS 68a] G. Baumgärtner and P. Schuck. Kernmodelle. Bibliographisches Institut, Mannheim, 1968. 217, 225
- [BS 68b] R. A. Broglia and B. Sørensen. Nucl. Phys. A110 (1968) 241. 350
- [BS 69] D. R. Bès and R. A. Sørensen. Adv. Nucl. Phys. 2 (1969) 129. 260
- [BS 71] P. K. Banerjee and D. W. L. Sprung. Nucl. Phys. A168 (1971) 273.

- [BS 76] G. F. Bertsch and K. Stricker. Phys. Rev. C13 (1976) 1312. 568
- [BS 79] J. P. Blaizot and H. Schulz. Proceedings of the Workshop on the Time Dependent HF Method. Orsay, Saclay, 1979. P. Bonche, B. Giraud and P. Quentin, Eds. Editions de Physique, Paris 1979. 573
- [BS 80] R. Bengtsson and P. Schuck. Phys. Lett. 89B (1980) 321. 551
- [BSB 69] W. Burk, D. Schütte, and K. Bleuler. Nucl. Phys. A133 (1969) 581. 440
- [BSC 75] M. V. Banaschik, R. S. Simon, P. Colombani, D. P. Soroka, F. S. Stephens, and R. M. Diamond. Phys. Rev. Lett. 34 (1975) 892. 98, 276
- [BSK 73] R. Bauer, J. Speth, V. Klemt, P. Ring, E. Werner, and T. Yamazaki. Nucl. Phys. A209 (1973) 535. 63, 179, 326
- [BSL 79] J. P. Boisson, B. Silvestre-Brac, and R. J. Liotta. Nucl. Phys. A330 (1979) 307. 392
- [BSV 76] W. H. Bassichis, M. R. Strayer, and M. T. Vaughn. Nucl. Phys. A263 (1976) 379. 270
- [BT 71] J. Boutet and J. P. Torres. Nucl. Phys. A175 (1971) 167. 119
- [BT 75] G. F. Bertsch and S. F. Tsai. Phys. Rep. 18C (1975) 125. 337, 328, 325, 324
- [BTK 65] D. M. Brink, A. F. R. De Toledo Piza, and A. K. Kerman. Phys. Lett. 19 (1965) 413. 376, 379
- [BTR 77] A. Bonaccorso, M. Di Toro, and G. Russo. Phys. Lett. 72B (1977) 27. 258
- [BV 71] A. Bouyssy and N. Vinh Mau. Phys. Lett. 35B (1971) 269. 341
- [BV 78] M. Baranger and M. Vénéroni. Ann. Phys. (New York) 114 (1978) 123. 506, 508, 510, 512, 520, 574, 605
- [BW 39] N. Bohr and J. A. Wheeler. Phys. Rev. 56 (1939) 426. 28
- [BW 52] J. M. Blatt and V. F. Weisskopf. Theoretical Nuclear Physics. Wiley, New York, 1952. 580
- [BW 56] R. A. Berg and L. Willets. Phys. Rev. 101 (1956) 201. 544
- [BW 60] J. Blomqvist and S. Wahlborn. Arkiv Fysik 16 (1960) 545. 59
- [BW 68] D. M. Brink and A. Weiguny. Nucl. Phys. A120 (1968) 59. 399, 408
- [BW 71] W. H. Bassichis and L. Willets. Phys. Rev. Lett. 27 (1971) 1451. 268
- [BW 76] G. E. Brown and W. Weise. Phys. Rep. 27C (1976) 1. 441
- [BZ 62] S. T. Belyaev and V. G. Zelevinskii. Nucl. Phys. 39 (1962) 582. 352, 358
- [BZ 73] N. L. Balazs and G. G. Zipfel. Ann. Phys. (New York) 77 (1973) 139. 527

- [Ca 61] B. C. Carlson. J. Math. Phys. 2 (1961) 441. 35
- [CAF 77] R. R. Chasman, L. Ahmad, A. M. Friedman, and J. R. Erskine. Rev. Mod. Phys. 49 (1977) 833. 79
- [CBA 73] E. Caenier, B. Bourrotte-Bilwes, and Y. Abgrall. Phys. Lett. 44B (1973) 411. 433
- [CBP 78] R. F. Casten, H. G. Börner, J. A. Pinston, and W. F. Davidson. Nucl. Phys. A309 (1978) 206. 379
- [CC 78] R. F. Casten and J. A. Cizewski. Nucl. Phys. A309 (1978) 477. 263, 379
- [CCF 79] O. Castaños, E. Chacón, A. Frank, and M. Moshinsky. J. Math. Phys. 20 (1979) 35. 378
- [CCJ 65] P. Camiz, A. Covello, and M. Jean. Nuovo Cim. 36 (1965) 663. 263
- [CCJ 66] P. Camiz, A. Covello, and M. Jean. Nuovo Cim. 42B (1966) 199. 263
- [CDS 77] M. Cerkaski, J. Dudek, Z. Szymański, C. G. Andersson, G. Leander, S. Åberg, S. G. Nilsson, and I. Ragnarsson. Phys. Lett. 79B (1977) 9; 72B (1977) 149. 145
- [CDS 78] S. Cwiok, J. Dudek, and Z. Szymański. Acta Physica Polonica B9 (1978) 725.

- [CE 65] J. M. Clark and J. P. Elliott. *Phys. Lett.* **19** (1965) 294. 175
- [CG 67] H. T. Chen and A. Goswami. *Phys. Lett.* **24B** (1967) 257. 263
- [Ch 66] B. E. Chi. *Nucl. Phys.* **83** (1966) 97. 79
- [Ch 69] S. Chandrasekhar. *Ellipsoidal Figures of Equilibrium*. Yale Univ. Press, New Haven, CT, 1969. 33
- [Ch 70] B. E. Chi. *Nucl. Phys.* **A146** (1970) 449. 306
- [Ch 75] B. D. Chang. *Phys. Lett.* **56B** (1975) 205.
- [CJB 77] Y. H. Chu, B. K. Jennings, and M. Brack. *Phys. Lett.* **68B** (1977) 407. 527, 544
- [CL 73] R. Y. Cusson and H. C. Lee. *Nucl. Phys.* **A211** (1973) 429. 482
- [CLF 73] M. Cailliau, J. Letessier, H. Flocard, and P. Quentin. *Phys. Lett.* **46B** (1973) 11. 268
- [CLL 73] W. N. Cottingham, M. Lacombe, B. Loiseau, J. M. Richard, and R. Vinh Mau. *Phys. Rev. D8* (1973) 800. 148, 155
- [CM 63] B. C. Carlson and G. L. Morley. *Am. J. Phys.* **31** (1963) 209. 35
- [CM 76] R. Y. Cusson and J. A. Maruhn. *Phys. Lett.* **62B** (1976) 134. 505
- [CMM 78] R. Y. Cusson, J. A. Maruhn, and H. W. Meldner. *Phys. Rev. C18* (1978) 2589. 501, 504, 505
- [CMR 75] S. Y. Chu, E. R. Marshalek, P. Ring, J. Krumlinde, and J. O. Rasmussen. *Phys. Rev. C12* (1975) 1017. 272, 277, 279
- [CN 47] J. Crank and P. Nicholson. *Proc. Camb. Phil. Soc.* **43** (1947) 50. 501
- [Co 55] F. Coester. *Phys. Rev.* **99** (1955) 170. 454
- [Co 56] F. Coester. *Nuovo Cim.* **4** (1956) 1307. 453, 458
- [Co 71] J. O. Corbett. *Nucl. Phys.* **A169** (1971) 426. 474
- [Co 72] J. O. Corbett. *Nucl. Phys.* **A193** (1972) 401. 462
- [CP 70] B. Castell and J. C. Parikh. *Phys. Rev. C1* (1970) 990. 481
- [CPS 74] S. Cohen, F. Piasil, and W. J. Swiatecki. *Ann. Phys. (New York)* **82** (1974) 557. 33, 34, 35, 99
- [CS 62] S. Cohen and W. J. Swiatecki. *Ann. Phys. (New York)* **19** (1962) 67. 28, 30
- [CS 63] S. Cohen and W. J. Swiatecki. *Ann. Phys. (New York)* **22** (1963) 406. 28, 30, 31
- [CS 72] X. Campi and D. W. L. Sprung. *Nucl. Phys.* **A194** (1972) 401. 176, 207, 213
- [CS 73] P. D. Curry and D. W. L. Sprung. *Nucl. Phys.* **A216** (1973) 125. 268
- [CSM 76] R. Y. Cusson, R. K. Smith, and J. A. Maruhn. *Phys. Rev. Lett.* **36** (1976) 1166. 505
- [CV 66] K. Y. Chan and J. G. Valatin. *Nucl. Phys.* **82** (1966) 222. 276
- [Da 58] M. Danos. *Nucl. Phys.* **5** (1958) 23. 294
- [Da 59] A. S. Davydov. *Sov. Phys. JETP* **9** (1959) 1103. 26
- [Da 65a] A. S. Davydov. *Quantum Mechanics*. Pergamon, Oxford, 1965. 80, 580
- [Da 65b] J. P. Davidson. *Rev. Mod. Phys.* **37** (1965) 105. 26
- [Da 67] B. D. Day. *Rev. Mod. Phys.* **39** (1967) 719. 156, 159
- [Da 68] J. P. Davidson. *Collective Models of the Nucleus*. Academic, New York, 1968. 13, 21, 97
- [Da 70] G. Do Dang. *Nucl. Phys.* **A157** (1970) 231. 481
- [Da 75] J. Dabrowski. *Phys. Lett.* **59B** (1975) 132. 131
- [DB 70] G. G. Dussel and D. R. Bes. *Nucl. Phys.* **A143** (1970) 623. 377
- [DB 73] T. K. Das and B. Banerjee. *Phys. Rev. C7* (1973) 2590. 104
- [DBM 73] H. R. Dalafi, B. Banerjee, H. J. Mang, and P. Ring. *Phys. Lett.* **44B** (1973) 327. 278, 462

- [DBS 78] M. Durand, M. Brack, and P. Schuck. *Z. Phys. A286* (1978) 381, 527, 531, 532, 545, 546
- [DC 60] A. S. Davydov and A. A. Chaban. *Nucl. Phys.* **20** (1960) 499, 27
- [DDK 70] T. K. Das, R. M. Dreizler, and A. Klein. *Phys. Rev. C2* (1970) 632, 376, 377, 379
- [DDK 71] G. J. Dreiss, R. M. Dreizler, A. Klein, and G. Do Dang. *Phys. Rev. C3* (1971) 2412, 311
- [De 78] C. DeTar. *Phys. Rev. D17* (1978) 302, 323, 148
- [DF 58] A. S. Davydov and B. F. Filippov. *Nucl. Phys.* **8** (1958) 237, 26, 132
- [DF 73] T. J. Deal and S. Fallieros. *Phys. Rev. C7* (1973) 1709, 335
- [DF 77] F. Dönau and S. Frauendorf. *Phys. Lett. 71B* (1977) 263, 122
- [DFG 68] R. M. Dreizler, P. Federman, B. Giraud, and E. Osnes. *Nucl. Phys. A113* (1968) 145, 481
- [DG 80] J. Decharge and D. Gogny. *Phys. Rev. C21* (1980) 1568, 265
- [DGG 75] J. Decharge, M. Girod, and D. Gogny. *Phys. Lett. 55B* (1975) 361, 265
- [DH 68] K. Dietrich and K. Hara. *Nucl. Phys. A111* (1968) 392, 323
- [Di 30] P. A. M. Dirac. *Proc. Camb. Phil. Soc.* **26** (1930) 376, 488
- [Di 71] K. Dietrich. *Lectures on Nuclear Fission*. Int. Center for Theor. Phys., Trieste, Italy, 1971, 90, 524
- [Di 76] R. M. Diamond. *Nukleonika* **21** (1976) 29, 98
- [DJ 73] F. Dönau and D. Janssen. *Nucl. Phys. A209* (1973) 109, 382, 391, 395
- [DK 66] G. Do Dang and A. Klein. *Phys. Rev. C6* (1966) 735, 463
- [DKS 77] J. S. Dehesa, S. Krewald, J. Speth, and A. Faessler. *Phys. Rev. C15* (1977) 1858, 323
- [DMG 76] M. Didong, H. Müther, K. Goeke, and A. Faessler. *Phys. Rev. C14* (1976) 1189, 437
- [DMP 64] K. Dietrich, H. J. Mang, and J. H. Pradal. *Phys. Rev. 135* (1964) B22, 463, 464
- [DMP 66] K. Dietrich, H. J. Mang, and J. H. Pradal. *Z. Phys. 190* (1966) 357, 263, 264
- [DMR 75] H. R. Dalafi, H. J. Mang, and P. Ring. *Z. Phys. A273* (1975) 47, 463, 466
- [DMS 72] K. T. R. Davies, R. J. McCarthy, and P. U. Sauer. *Phys. Rev. C6* (1972) 1461.
- [DMS 73] K. T. R. Davies, R. J. McCarthy, and P. U. Sauer. *Phys. Rev. C7* (1973) 943, 205
- [DNM 77] T. Dassing, K. Neergård, K. Matsuyanagi, and H. C. Chang. *Phys. Rev. Lett.* **39** (1977) 1395, 145
- [Do 76] L. Dolan. *Phys. Rev. D13* (1976) 528, 500
- [DPP 69] J. Damgaard, H. C. Pauli, V. V. Pashkevich, and V. M. Strutinski. *Nucl. Phys. A135* (1969) 432, 67, 81
- [DR 59] A. S. Davydov and V. S. Rostovsky. *Nucl. Phys.* **12** (1959) 58, 26
- [DR 66] M. Demeur and F. Reidemeister. *Ann. Phys. (Paris)* **1** (1966) 181, 81
- [DSB 77] J. W. Durso, M. Saarela, G. E. Brown, and A. D. Jackson. *Nucl. Phys. A278* (1977) 445, 148, 155
- [DSB 80] M. Durand, P. Schuck, and M. Brack. *Z. Phys. A296* (1980) 87, 550
- [Dy 56] J. F. Dyson. *Phys. Rev. 102* (1956) 1217, 1230, 350
- [EAD 75] P. Ebersold, B. Aas, W. Dey, R. Eichler, H. J. Leisi, W. W. Sapp, and H. K. Walter. *Phys. Lett. 58B* (1975) 428, 97
- [EBG 75] Y. M. Engel, D. M. Brink, K. Goeke, S. J. Krieger, and D. Vautherin. *Nucl. Phys. A249* (1975) 215, 506, 523

- [Ed 57] A. R. Edmonds. *Angular Momentum in Quantum Mechanics*. Princeton Univ. Press, Princeton, 1957. 7, 10, 11, 13, 18, 25, 52, 60, 61, 116, 180, 184, 226, 227, 325, 332, 575, 577, 578, 582, 583, 584, 585, 589, 591
- [EF 57] J. P. Elliott and B. H. Flowers. Proc. Roy. Soc. (London) **A242** (1957) 57. 174, 293, 325, 326
- [EG 70] J. M. Eisenberg and W. Greiner. *Nuclear Models*. North Holland, Amsterdam, 1970. 1, 6, 9, 12, 17, 18, 22, 23, 43, 97, 217, 559
- [EH 77] G. Eckart and G. Holzwarth. Z. Phys. **A281** (1977) 385. 544
- [EH 79] G. Eckart and G. Holzwarth. Phys. Lett. **87B** (1979) 147. 568
- [EHS 80] G. Eckart, G. Holzwarth, and B. Schwesinger. Phys. Lett. **94B** (1980) 453. 568
- [EJM 68] J. P. Elliott, A. D. Jackson, H. A. Mavromatis, E. A. Sanderson, and B. Singh. Nucl. Phys. **A121** (1968) 241. 185
- [EKV 69] C. Ellegaard, J. Kantele, and P. Vedelsby. Nucl. Phys. **A129** (1969) 113. 58
- [El 58] J. P. Elliott. Proc. Roy. Soc. (London) **A245** (1958) 128. 562. 182, 379
- [El 70] P. J. Ellis. Nucl. Phys. **A155** (1970) 625. 386
- [EL 57] J. P. Elliott and A. M. Lane. *Handbuch der Physik*. Vol. XXXIX, p. 241. Springer-Verlag, Berlin, 1957. 63
- [EM 72] J. W. Ehlers and S. A. Moszkowski. Phys. Rev. **C6** (1972) 217. 209
- [EMR 80a] J. L. Egido, H. J. Mang, and P. Ring. Nucl. Phys. **A334** (1980) I. 257, 258, 273, 278
- [EMR 80b] J. L. Egido, H. J. Mang, and P. Ring. Nucl. Phys. **A339** (1980) 390. 273, 279, 345, 493
- [EO 77] P. J. Ellis and E. Osnes. Rev. Mod. Phys. **49** (1977) 777. 166
- [ER 78] D. Ebert and H. Reinhardt. Nucl. Phys. **A298** (1978) 60. 499
- [ER 80] J. L. Egido and P. Ring. Phys. Lett. **B** (1980). 470
- [ERM 78] J. L. Egido, P. Ring, and H. J. Mang. Phys. Lett. **77B** (1978) 123. 279
- [ERW 78] K. Ebert, P. Ring, W. Wild, V. Klemt, and J. Speth. Nucl. Phys. **A298** (1978) 285. 327
- [ES 55] J. P. Elliott and T. H. R. Skyrme. Proc. Roy. Soc. (London) **A232** (1955) 561. 456
- [ES 69] S. Ethofer and P. Schuck. Z. Phys. **228** (1969) 264. 626, 627, 632, 642
- [EVB 79] I. Easson, M. Vallieres, and R. K. Bhaduri. Phys. Rev. **C19** (1979) 1089. 549
- [EW 72] C. A. Engelbrecht and H. A. Weidenmüller. Nucl. Phys. **A184** (1972) 385. 59
- [Fa 68] A. Faessler. Fortschr. Phys. **16** (1968) 309. 180
- [FC 72] L. S. Ferreira and M. H. Caldeira. Nucl. Phys. **A189** (1972) 250. 419, 506
- [FDB 77] A. Faessler, K. R. S. Devi, and A. Barroso. Nucl. Phys. **A286** (1977) 101. 278
- [FDG 76] A. Faessler, K. R. S. Devi, F. Grümmer, K. W. Schmid, and R. R. Hilton. Nucl. Phys. **A256** (1976) 106. 139, 278, 462
- [Fe 28] E. Fermi. Z. Phys. **48** (1928) 73. 528
- [Fe 39] R. P. Feynman. Phys. Rev. **56** (1939) 340. 331, 608
- [Fe 57] R. A. Ferrell. Phys. Rev. **107** (1957) 1631. 488
- [Fe 58] H. Feshbach. Ann. Phys. (New York) **5** (1958) 357. 331
- [Fe 62] H. Feshbach. Ann. Phys. (New York) **19** (1962) 287. 165, 171, 381
- [FG 62] A. Faessler and W. Greiner. Z. Phys. **168** (1962) 425; **170** (1962) 105. 25
- [FG 64] A. Faessler and W. Greiner. Z. Phys. **177** (1964) 190. 25
- [FGE 72] A. Faessler, J. E. Galonska, J. W. Ehlers and S. A. Moszkowski. Nuovo Cim. **11A** (1972) 63.

- [FGP 73] A. Faessler, F. Gruemmer, and A. Plastino. *Z. Phys.* **260** (1973) 305. 435
- [FGS 65] A. Faessler, W. Greiner, and R. K. Sheline. *Nucl. Phys.* **70** (1965) 33. 25
- [FGS 66] A. Faessler, W. Greiner, and R. K. Sheline. *Nucl. Phys.* **80** (1966) 417. 25
- [FH 62a] E. G. Fuller and E. Hayward. *Nucl. Phys.* **30** (1962) 613. 294
- [FH 62b] E. G. Fuller and E. Hayward. *Nuclear Reactions*, Vol. I. P. M. Endt and P. B. Smith, Eds. North Holland, Amsterdam, 1962. 294
- [FH 65] R. P. Feynman and A. R. Hibbs. *Quantum Mechanics and Path Integrals*. McGraw-Hill, New York, 1965. 499
- [FHM 69] J. B. French, E. C. Halbert, J. B. McGrory, and S. S. M. Wong. *Adv. Nucl. Phys.* **3** (1969) 193. 50
- [FHM 73] M. Fellah, T. F. Hamman, and D. E. Medjadi. *Phys. Rev.* **C8** (1973) 1585. 463
- [FWH 74] H. Friedrich, H. Hüskens, and A. Weiguny. *Nucl. Phys.* **A220** (1974) 125. 399
- [FIS 64] N. Fukuda, F. Iwamoto, and K. Sawada. *Phys. Rev.* **135** (1964) A932. 340
- [FJM 71] S. Frauendorf, D. Janssen, and L. Münchow. *Sov. J. Nucl. Phys.* **12** (1971) 512; **13** (1971) 33. 476
- [FKS 72] B. Fink, D. Kolb, W. Scheid, and W. Greiner. *Ann. Phys. (New York)* **69** (1972) 375. 452, 456
- [FKW 78] H. Flocard, S. E. Koonin, and M. S. Weiss. *Phys. Rev.* **C17** (1978) 1682. 501
- [Fl 71] S. Flügge. *Practical Quantum Mechanics*. Springer-Verlag, Berlin, 1971. 69
- [Fl 72] T. Fliessbach. *Nucl. Phys.* **A194** (1972) 625. 399
- [FLW 73] A. Faessler, L. Lin, and F. Wittmann. *Phys. Lett.* **44B** (1973) 127. 462
- [FLW 75] W. Fritsch, R. Lipperheide, and U. Wille. *Nucl. Phys.* **A241** (1975) 79. 59
- [FMR 79] J. Fleckner, U. Mosel, P. Ring, and H. J. Mang. *Nucl. Phys.* **A331** (1979) 288. 278
- [FN 76] J. L. Friar and J. W. Negele. *Adv. Nucl. Phys.* **8** (1976) 219. 3
- [Fo 28] V. A. Fock. *Z. Phys.* **49** (1928) 339. 411
- [Fo 30] V. A. Fock. *Z. Phys.* **61** (1930) 126. 193
- [Fo 70] V. N. Fomenko. *J. Phys. (G. B.) A3* (1970) 8. 463, 465
- [FP 67] A. Faessler and A. Plastino. *Nucl. Phys.* **A94** (1967) 580. 180
- [FP 78] A. Faessler and M. Ploszajczak. *Phys. Lett.* **76B** (1978) 1. 107
- [FPD 76] A. Faessler, M. Ploszajczak, and K. R. S. Devi. *Phys. Rev. Lett.* **36** (1976) 1028. 145
- [FPM 67] A. Faessler, A. Plastino, and S. A. Moszkowski. *Phys. Rev.* **156** (1967) 1064. 1072. 345
- [FPS 80] A. Faessler, M. Ploszajczak, and K. W. Schmid. *Progr. in Part. and Nucl. Phys.*, vol. 5, D. H. Wilkinson Ed., Pergamon Press, Oxford, 1980.
- [FQK 73] H. Flocard, P. Quentin, A. K. Kerman, and D. Vautherin. *Nucl. Phys.* **A203** (1973) 433. 268, 269
- [FQV 73] H. Flocard, P. Quentin, and D. Vautherin. *Phys. Lett.* **46B** (1973) 304. 265, 266
- [FQV 74] H. Flocard, P. Quentin, D. Vautherin, M. Véroni, and A. K. Kerman. *Nucl. Phys.* **A231** (1974) 176. 268, 270, 271
- [Fr 39] J. Frenkel. *Phys. Rev.* **53** (1939) 987. 28
- [Fr 76] S. Frauendorf. *Nucl. Phys.* **A263** (1976) 150. 276
- [FR 75] S. Fantoni and S. Rosati. *Nuovo Cim.* **25A** (1975) 593. 205
- [FR 76a] S. Fantoni and S. Rosati. *Lett. Nuovo Cim.* **16** (1976) 531. 205
- [FR 76b] B. U. Felderhof and S. P. Raval. *Physica* **82A** (1976) 151. 137
- [FRS 78] R. Frey, A. Richter, A. Schwierczinski, E. Spamer, O. Titze, and W. Knuepfer. *Phys. Lett.* **74B** (1978) 45. 297

- [FS 66] A. Faessler and R. K. Sheline. *Phys. Rev.* **148** (1966) 1003. 67
- [FS 76] G. Fonte and G. Schiffrer. *Nucl. Phys.* **A259** (1976) 20. 270
- [FT 72] S. Fukuda and Y. Torizuka. *Phys. Rev. Lett.* **29** (1972) 1108. 295
- [FT 75] A. Faessler and H. Toki. *Phys. Lett.* **59B** (1975) 211. 122
- [Fu 77] H. Fukutome. *Progr. Theor. Phys.* **58** (1977) 1692. 375
- [FV 56] R. A. Ferrell and W. M. Visscher. *Phys. Rev.* **102** (1956) 450. 433
- [FV 74] H. Flocard and D. Vautherin. *Phys. Lett.* **52B** (1974) 399. 423
- [FV 75] H. Flocard and D. Vautherin. *Phys. Lett.* **55B** (1975) 259. 434
- [FV 76] H. Flocard and D. Vautherin. *Nucl. Phys.* **A264** (1976) 197. 434
- [FW 70] W. A. Friedman and L. Wilets. *Phys. Rev. C2* (1970) 892. 472
- [FW 71] A. L. Fetter and J. D. Walecka. *Quantum Theory of Many Particle Systems.* McGraw-Hill, New York, 1971. 156, 162, 550, 623, 640
- [FW 78] H. Flocard and M. S. Weiss. *Phys. Rev. C18* (1978) 573. 505
- [FYN 77] H. Fukutome, M. Yamamura, and S. Nishiyama. *Progr. Theor. Phys.* **57** (1977) 1554. 375
-
- [Ga 72] F. R. Gantmacher. *The Theory of Matrices, Vol. 2 Ch. XI.* Chelsea, New York, 1972. 617
- [Ga 78] P. Garbaczewski. *Phys. Rep.* **36C** (1978) 65. 348
- [GB 57] M. Gell-Mann and K. A. Brueckner. *Phys. Rev.* **106** (1957) 364. 301
- [GB 65] V. N. Guman and B. L. Birbrair. *Nucl. Phys.* **70** (1965) 545. 178
- [GED 71] P. W. M. Glaudemans, P. M. Endt, and A. E. L. Dieperink. *Ann. Phys. (New York)* **63** (1971) 134. 50
- [GFW 72] K. Goeke, A. Faessler, and H. H. Wolter. *Nucl. Phys.* **A183** (1972) 352. 481
- [GG 67] J. R. Grover and J. Gilat. *Phys. Rev.* **157** (1967) 802. 98
- [GG 71] G. Gneuss and W. Greiner. *Nucl. Phys.* **A171** (1971) 449. 376, 377
- [GG 74a] B. Giraud and B. Grammaticos. *Nucl. Phys.* **A233** (1974) 373. 424
- [GG 74b] A. L. Goodman and A. Goswami. *Phys. Rev. C9* (1974) 1948. 106
- [GG 75] B. Giraud and B. Grammaticos. *Nucl. Phys.* **A255** (1975) 141. 419, 424, 425, 433
- [GG 78] M. Girod and B. Grammaticos. *Phys. Rev. Lett.* **40** (1978) 361. 27, 268
- [GG 79] M. Girod and B. Grammaticos. *Nucl. Phys.* **A330** (1979) 40. 428
- [GGA 74] F. Grümmer, K. Goeke, K. Allaart, and A. Faessler. *Nucl. Phys.* **A225** (1974) 443. 262, 481
- [GGF 73] K. Goeke, J. Garcia, and A. Faessler. *Nucl. Phys.* **A208** (1973) 477. 262, 463, 481
- [GGS 66] V. Gillet, A. M. Green, and E. A. Sanderson. *Nucl. Phys.* **88** (1966) 321. 174, 326
- [Gi 64] V. Gillet. *Nucl. Phys.* **51** (1964) 410. 326
- [GIS 73] F. A. Gareev, S. P. Ivanova, V. G. Soloviev, and S. I. Fedotov. *Sov. J. Part. and Nucl.* **4** (1973) 148. 67, 79
- [GK 65] A. Goswami and L. S. Kisslinger. *Phys. Rev.* **140** (1965) B26. 263
- [GI 63] R. J. Glauber. *Phys. Rev.* **130** (1963) 2529; **131** (1963) 2766. 412
- [GI 65] N. K. Glendenning. *Phys. Rev.* **137** (1965) B102. 300
- [GL 70] D. H. E. Gross and R. Lipperheide. *Nucl. Phys.* **A150** (1970) 449. 59
- [GL 77] B. G. Giraud and J. LeTourneau. *Phys. Rev. C16* (1977) 906. 271
- [GLM 78] K. Goeke, A. M. Lane, and J. Martorell. *Nucl. Phys.* **A296** (1978) 109. 332, 335

- [GLN 67] C. Gustafson, I. L. Lamm, B. Nilsson, and S. G. Nilsson. *Arkiv Fysik* **36** (1967) 613. 76, 80
- [GLS 67] A. Goswami, L. Lin, and G. L. Struble. *Phys. Lett.* **25B** (1967) 451. 277
- [GLW 70] B. Giraud, J. LeTourneau, and S. K. M. Wong. *Phys. Lett.* **32B** (1970) 23. 268
- [GM 65] I. M. Green and S. A. Moeskowski. *Phys. Rev.* **139** (1965) B790. 179
- [GM 71] J. A. Glen and N. MacDonald. *Nucl. Phys.* **A165** (1971) 524. 482
- [GMA 75] K. Goeke, M. V. Mihailović, K. Allaart, and A. Faessler. *Nucl. Phys.* **A243** (1975) 440. 435
- [GMG 69] G. Gneuss, U. Mosel, and W. Greiner. *Phys. Lett.* **30B** (1969) 397. 377
- [GMG 70] G. Gneuss, U. Mosel, and W. Greiner. *Phys. Lett.* **31B** (1970) 269. 377
- [GMO 71] J. Grumann, T. Morović, and W. Greiner. *Z. Naturforschung* **26A** (1971) 643. 81
- [GMQ 76] M. J. Giannoni, F. Moreau, P. Quentin, D. Vautherin, M. Véroni, and D. M. Brink. *Phys. Lett.* **65B** (1976) 305. 523
- [GMZ 78] D. Glas, U. Mosel, and P. G. Zint. *Z. Phys.* **A285** (1978) 83. 133
- [GNS 70] A. Goswami, O. Nalcioglu, and A. I. Sherwood. *Nucl. Phys.* **A153** (1970) 433. 445. 311
- [Go 48] P. Gombas. *Die Statistische Theorie des Atoms und ihre Anwendungen*. Springer-Verlag, Vienna, 1948. 527
- [Go 52] P. Gombas. *Ann. Phys. (Leipzig)* **10** (1952) 253. 209
- [Go 58] L. P. Gorkov. *Sov. Phys. JETP* **7** (1958) 505. 260, 635
- [Go 59] H. Goldstein. *Classical Mechanics*. Addison-Wesley, London, 1959. 489, 513, 535, 563
- [Go 64] A. Goswami. *Nucl. Phys.* **60** (1964) 228. 262
- [Go 72] A. L. Goodman. *Nucl. Phys.* **A186** (1972) 475. 263
- [Go 73] D. Gogny. Proc. Int. Conf. on Nuclear Physics, Munich 1973. J. De Boer and H. J. Mang, Eds. North Holland, Amsterdam, 1973. 265
- [Go 74] A. L. Goodman. *Nucl. Phys.* **A230** (1974) 466. 261
- [Go 75a] D. Gogny. *Nucl. Phys.* **A237** (1975) 399. 265
- [Go 75b] D. Gogny. Proceedings of the International Conference on Nuclear Selfconsistent Fields, Trieste, 1975. G. Ripka and M. Porneuf, Eds. North Holland, Amsterdam, 1975. 176, 209, 265, 266
- [Go 76a] A. L. Goodman. *Nucl. Phys.* **A256** (1976) 113. 278
- [Go 76b] K. Goeke. *Nucl. Phys.* **A265** (1976) 301. 506
- [Go 77] K. Goeke. *Phys. Rev. Lett.* **38** (1977) 212. 428, 523
- [Go 79] A. L. Goodman. *Adv. Nucl. Phys.* **11** (1979) 263. 255, 256, 262
- [GP 63] A. Goswami and M. K. Pal. *Nucl. Phys.* **44** (1963) 294. 311
- [GPA 71] U. Götz, H. C. Pauli, and K. Alder. *Nucl. Phys.* **A175** (1971) 481. 67
- [GPA 72] U. Götz, H. C. Pauli, K. Alder, and K. Junker. *Nucl. Phys.* **A192** (1972) 1. 27
- [GQ 80] M. J. Giannoni and P. Quentin. *Phys. Rev.* **C21** (1980) 2060, 2076. 523
- [Gr 46] H. J. Gronewald. *Physica* **12** (1946) 405. 553, 610
- [Gr 60] E. P. Gross. *Nucl. Phys.* **14** (1960) 389. 132, 471
- [Gr 62] L. Grodzins. *Phys. Lett.* **2** (1962) 88. 14
- [Gr 67] J. R. Grover. *Phys. Rev.* **157** (1967) 832. 98
- [Gr 71] J. J. Griffin. *Nucl. Phys.* **A170** (1971) 395. 32
- [Gr 72] D. H. E. Gross. *Phys. Lett.* **42B** (1972) 41. 527, 530, 545
- [Gr 74] Y. T. Grin. *Phys. Lett.* **52B** (1974) 135. 277
- [GR 60] J. J. Griffin and M. Rich. *Phys. Rev.* **118** (1960) 850. 132

- [GR 78] K. Goeke and P. G. Reinhard. *Ann. Phys. (New York)* **112** (1978) 328. 516, 517
- [GS 57] S. Gartenhaus and C. Schwartz. *Phys. Rev.* **108** (1957) 482. 455
- [GS 64] V. Gillet and E. A. Sanderson. *Nucl. Phys.* **54** (1964) 472. 326
- [GS 69] B. Giraud and P. U. Sauer. *Phys. Lett.* **30B** (1969) 218. 482
- [GS 77] G. Gumpertsberger and P. Schuck. *Phys. Lett.* **66B** (1977) 219. 527, 540
- [GSB 70] A. L. Goodman, G. L. Struble, J. Bar-Touv, and A. Goswami. *Phys. Rev. C2* (1970) 380. 263
- [GSD 73] E. Grosse, F. S. Stephens, and R. M. Diamond. *Phys. Rev. Lett.* **31** (1973) 840. 107
- [GSF 75] F. Grümmer, K. W. Schmid, and A. Faessler. *Z. Phys. A275* (1975) 391. 436
- [GSF 78a] F. Grümmer, K. W. Schmid, and A. Faessler. *Nucl. Phys. A306* (1978) 134. 482
- [GSF 78b] F. Grümmer, K. W. Schmid, and A. Faessler. *Nucl. Phys. A308* (1978) 77. 274
- [GSG 68] A. L. Goodman, G. L. Struble, and A. Goswami. *Phys. Lett.* **26B** (1968) 260. 263
- [GSK 75] K. Y. Gromov, H. U. Siebert, V. G. Kalinnikov, G. Musiol, and H. Strusny. *Sov. J. Part. and Nucl.* **6** (1975) 393. 79
- [GSZ 74] M. Golin, R. W. Sharp, and L. Zamick. *Nucl. Phys. A221* (1974) 546. 187
- [GT 48] M. Goldhaber and E. Teller. *Phys. Rev.* **74** (1948) 1046. 295, 558, 561
- [GV 64] V. Gillet and N. Vinh Mau. *Nucl. Phys.* **54** (1964) 321. 326
- [GV 79] B. Grammaticos and A. Voros. *Ann. Phys. (New York)* **123** (1979) 359. 542, 543
- [GVL 73] R. E. Griffin, A. B. Volkov, and K. R. Lasssey. *Can. J. Phys.* **51** (1973) 2054. 209
- [GVS 76] A. L. Goodman, J. P. Vary, and R. A. Sorensen. *Phys. Rev. C13* (1976) 1674. 278
- [GVV 76] M. J. Giannoni, D. Vautherin, M. Vénéroni, and D. M. Brink. *Phys. Lett.* **63B** (1976) 8. 563, 564
- [GW 57] J. J. Griffin and J. A. Wheeler. *Phys. Rev.* **108** (1957) 311. 409
- [GW 68] J. N. Ginocchio and J. Wenner. *Phys. Rev.* **170** (1968) 859. 440, 441
- [GWW 58] L. C. Gomes, J. D. Walecka, and V. F. Weisskopf. *Ann. Phys. (New York)* **3** (1958) 241. 156
- [GY 70] D. H. E. Gross and M. Yamamura. *Nucl. Phys. A140* (1970) 625.
-
- [Ha 28] D. R. Hartree. *Proc. Camb. Phil. Soc.* **24** (1928) 89. 193
- [Ha 65a] S. M. Harris. *Phys. Rev.* **138** (1965) B509. 103
- [Ha 65b] E. Hayward. *Photonuclear Reactions, Nuclear Structure and Electromagnetic Transitions*. N. MacDonald, Ed. Plenum, New York, 1965. 294
- [Ha 67] J. C. Hafele. *Phys. Rev.* **159** (1967) 996. 387
- [Ha 68] M. Harvey. *Adv. Nucl. Phys.* **1** (1968) 67. 379
- [Ha 72] I. Hamamoto. *Physica Scripta* **6** (1972) 266. 296
- [Ha 74a] I. Hamamoto. *Phys. Rep.* **10C** (1974) 63. 388, 389
- [Ha 74b] S. S. Hanna. *Proceedings of the International Conference on Nuclear Structure and Spectroscopy*, Vol. II. Amsterdam, 1974.
- [Ha 76] I. Hamamoto. *Nucl. Phys. A271* (1976) 15. 274
- [Ha 77] I. Hamamoto. *Phys. Lett.* **66B** (1977) 222. 274
- [HA 76] T. Hoshino and A. Arima. *Phys. Rev. Lett.* **37** (1976) 266. 323
- [HBI 77] M. N. Harakeh, K. Van der Borg, R. Ishimatsu, H. P. Morsch, A. Van der Woude, and F. E. Bertrand. *Phys. Rev. Lett.* **38** (1977) 676. 296
- [HD 71] H. Hofmann and K. Dietrich. *Nucl. Phys. A165* (1971) 1. 32

- [He 32] W. Heisenberg. *Z. Phys.* **77** (1932) 1. 54
- [He 61] G. Hertz. *Lehrbuch der Kernphysik, Vol. II, Physik der Atomkerne.* Dansien, Leipzig, 1961. 78, 79
- [He 71] K. T. Hecht. *Nucl. Phys.* **A170** (1971) 34. 456
- [He 73a] K. T. Hecht. *Ann. Rev. Nucl. Sci.* **23** (1973) 123. 50
- [He 73b] J. H. Hetherington. *Nucl. Phys.* **A204** (1973) 110. 506
- [HE 77] G. Holzwarth and G. Eckart. *Z. Phys.* **A283** (1977) 219. 291, 568
- [HE 78] G. Holzwarth and G. Eckart. *Z. Phys.* **A284** (1978) 291. 528, 566, 567, 568, 570, 572
- [HE 79] G. Holzwarth and G. Eckart. *Nucl. Phys.* **A325** (1979) 1. 567, 568, 572
- [HGA 74] S. S. Hanna, H. F. Glavish, R. Avida, J. R. Calareo, E. Kuhlmann, and R. Lacanna. *Phys. Rev. Lett.* **32** (1974) 114. 295
- [HGH 68] D. L. Hendrie, N. K. Glendenning, B. G. Harvey, O. N. Jarvis, H. H. Duhm, J. Saudinos, and J. Mahoney. *Phys. Lett.* **26B** (1968) 127. 67, 81
- [HI 79] K. Hara and S. Iwasaki. *Nucl. Phys.* **A332** (1979) 61. 617
- [HIT 79] K. Hara, S. Iwasaki, and K. Tanabe. *Nucl. Phys.* **A332** (1979) 69. 482
- [HNL 70] P. Haapakoski, T. Honkaranta, and P. O. Lipas. *Phys. Lett.* **31B** (1970) 493. 377
- [HJ 62] T. Hamada and I. D. Johnston. *Nucl. Phys.* **34** (1962) 382. 155
- [HJE 78] P. Hubert, N. R. Johnson, and E. Eichler. *Phys. Rev.* **C17** (1978) 622. 26
- [HJJ 76] G. Holzwarth, D. Janssen, and R. V. Jolos. *Nucl. Phys.* **A261** (1976) 1. 364, 365, 367
- [HJS 49] O. Haxel, J. H. D. Jensen, and H. E. Suess. *Phys. Rev.* **75** (1949) 1766. 43
- [HK 64] P. Hohenberg and W. Kohn. *Phys. Rev.* **136** (1964) B864. 541, 564
- [HK 72] G. H. Herling and T. T. S. Kuo. *Nucl. Phys.* **A181** (1972) 113. 167, 168, 289
- [HK 75] K. Hara and S. Kusuno. *Nucl. Phys.* **A245** (1975) 147. 120
- [HK 77] S. A. Hjorth and W. Klamra. *Z. Phys.* **A283** (1977) 287. 120
- [HL 72a] G. Holzwarth and S. G. Lie. *Z. Phys.* **249** (1972) 332. 376, 380
- [HL 72b] M. Hage-Hassan and M. Lambert. *Nucl. Phys.* **A188** (1972) 545. 352
- [HLM 78] H. P. Hellmeister, K. P. Lieb, and W. Müller. *Nucl. Phys.* **A307** (1978) 515. 98
- [HLR 74] H. M. Hofmann, S. Y. Lee, J. Richert, H. A. Weidenmüller, and T. H. Schucan. *Ann. Phys. (New York)* **85** (1974) 410. 170
- [HM 57] S. Hayakawa and T. Marumori. *Progr. Theor. Phys.* **18** (1957) 396. 454, 458
- [HMG 69] P. Holzer, U. Mosel, and W. Greiner. *Nucl. Phys.* **A138** (1969) 241. 81
- [HMS 75] E. C. Halbert, J. B. McGrory, G. R. Satchler, and J. Speth. *Nucl. Phys.* **A245** (1975) 189. 295
- [HMW 71] E. C. Halbert, J. B. McGrory, B. H. Wildenthal, and S. P. Pandya. *Adv. Nucl. Phys.* **4** (1971) 315. 50, 288
- [HN 77] P. Hoodbhoy and J. W. Negele. *Nucl. Phys.* **A288** (1977) 23. 265
- [Ho 68] G. Holzwarth. *Nucl. Phys.* **A113** (1968) 448. 279
- [Ho 70] G. Holzwarth. *Nucl. Phys.* **156** (1970) 511. 377
- [Ho 71a] G. Holzwarth. *Nucl. Phys.* **A174** (1971) 97. 376, 377
- [Ho 71b] P. E. Hodgson. *Nuclear Reactions and Nuclear Structure.* Clarendon, Oxford, 1971. 59
- [Ho 72] G. Holzwarth. *Nucl. Phys.* **A185** (1972) 268. 352, 408
- [Ho 73] G. Holzwarth. *Nucl. Phys.* **A207** (1973) 545. 200, 419, 421, 422, 429, 506
- [Ho 75] W. F. Hornyak. *Nuclear Structure.* Academic, New York, 1975. 4, 45
- [Ho 77] G. Holzwarth. *Phys. Lett.* **66B** (1977) 29. 561
- [Ho 80] K. Holinde. *Phys. Rep. C* (1980). 148, 155

- [Hö 61] J. Högaasen-Feldman. *Nucl. Phys.* **28** (1961) 258. 342
- [HP 40] T. Holstein and H. Primakoff. *Phys. Rev.* **58** (1940) 1098. 348
- [HR 68] R. G. Helmer and C. W. Reich. *Nucl. Phys.* **A114** (1968) 649. 145
- [HR 74] J. Hadermann and A. C. Rester. *Nucl. Phys.* **A231** (1974) 120. 376
- [HRH 70] S. A. Hjorth, H. Ryde, K. A. Hagemann, G. Levhoiden, and J. C. Waddington. *Nucl. Phys.* **A144** (1970) 513. 120
- [HS 57] L. Hulten and M. Sugawara. *Handbuch der Physik*, Vol. XXXIX p. I. Springer-Verlag, Berlin, 1957. 174
- [HS 62] K. T. Hecht and G. R. Satchler. *Nucl. Phys.* **32** (1962) 286. 122
- [Hu 57] J. Hubbard. *Proc. Roy. Soc. (London)* **A240** (1957) 539; **A243** (1957) 336. 301
- [Hu 63] K. Huang. *Statistical Mechanics*. Wiley, New York, 1963. 553, 555, 556, 557
- [HV 68] F. Herbut and M. Vujčić. *Phys. Rev.* **172** (1968) 1031. 251
- [HW 53] D. L. Hill and J. A. Wheeler. *Phys. Rev.* **89** (1953) 1102. 7, 28, 34, 76, 400, 424
- [HW 72] P. K. Haff and L. Wilets. *Phys. Rev. C7* (1972) 951. 419, 428
- [HW 74] P. K. Haff and L. Wilets. *Phys. Rev. C10* (1974) 353. 420, 428
- [HY 74] G. Holzwarth and T. Yukawa. *Nucl. Phys.* **A219** (1974) 125. 431, 432, 506, 519
- [HZ 53] T. Huus and C. Zupancic. *Mat. Fys. Medd. Dan. Vid. Selsk.* **28** (1953) No. 1. 97
- [Ia 77] F. Iachello. *Nukleonika* **22** (1977) 107. 379
- [Ia 78] F. Iachello, Ed. *Proceedings of the first Symposium on Interacting Bosons in Nuclear Physics*. Erice, Sicily, 1978. Plenum, New York 1978. 379
- [IA 74] F. Iachello and A. Arima. *Phys. Lett.* **53B** (1974) 309. 376, 379
- [IMR 79] S. Islam, H. J. Mang, and P. Ring. *Nucl. Phys.* **A326** (1979) 161. 481, 482, 483
- [IMS 76] S. Iwasaki, T. Marumori, F. Sakata, and K. Takada. *Progr. Theor. Phys.* **56** (1976) 1140. 397
- [In 54] D. R. Inglis. *Phys. Rev.* **96** (1954) 1059. 126, 130, 523
- [In 56] D. R. Inglis. *Phys. Rev.* **103** (1956) 1786. 126, 131, 523
- [IO 67] F. Iwamoto and N. Onishi. *Progr. Theor. Phys.* **37** (1967) 682. 463
- [Ir 72] J. M. Irvine. *Nuclear Structure Theory*. Pergamon, Oxford, 1972. 38
- [IRS 79] S. Iwasaki, P. Ring, and P. Schuck. *Nucl. Phys.* **A331** (1979) 81. 391
- [IRS 80] S. Iwasaki, P. Ring, and P. Schuck. *Nucl. Phys.* **A339** (1980) 365. 367, 391, 392, 394, 395
- [IST 77] S. Iwasaki, F. Sakata, and K. Takada. *Progr. Theor. Phys.* **57** (1977) 1289. 364
- [ISY 73] A. Ikeda, R. K. Sheline, and S. Yoshida. *Phys. Rev. C8* (1973) 2101. 435
- [IUY 65] K. Ikeda, T. Udagawa, and H. Yamaura. *Progr. Theor. Phys.* **33** (1965) 22. 311
- [IY 78] H. Ichihashi and M. Yamamura. *Progr. Theor. Phys.* **60** (1978) 753. 351
- [Ja 62] J. D. Jackson. *Classical Electrodynamics*. Wiley, New York, 1962. 581, 584, 586
- [Ja 79] D. Janssen. *Nucl. Phys.* **A331** (1979) 311. 639
- [JB 71] M. B. Johnson and M. Baranger. *Ann. Phys. (New York)* **62** (1971) 172. 166
- [JB 75] B. K. Jennings and R. K. Bhaduri. *Nucl. Phys.* **A237** (1975) 149. 536
- [JBB 75] B. K. Jennings, R. K. Bhaduri, and M. Brack. *Nucl. Phys.* **A253** (1975) 29. 536
- [JDF 71] D. Janssen, F. Dönau, S. Frauendorf, and R. V. Jolos. *Nucl. Phys.* **A172** (1971) 145. 352, 369, 406, 408
- [JDJ 75] R. V. Jolos, F. Dönau, and D. Janssen. *Sov. J. Nucl. Phys.* **22** (1975) 503. 379
- [JDK 69] E. R. Johnson, R. M. Dreizler, and A. Klein. *Phys. Rev.* **186** (1969) 1289. 386

- [Je 73] B. K. Jennings. *Nucl. Phys.* **A207** (1973) 538. 139, 339
- [Je 76] B. K. Jennings. Ph. D. Thesis, McMaster University, Hamilton, Ontario, 1976. 539, 540, 541, 542
- [JH 77] K. Junker and J. Hadermann. *Z. Phys.* **A282** (1977) 391. 81
- [JJD 74] D. Janssen, R. V. Jolos, and F. Dönau. *Nucl. Phys.* **A224** (1974) 93. 375, 377, 378
- [JL 80] A. S. Jensen and S. M. Larsen. *Phys. Lett.* **94B** (1980) 280. 568
- [JLM 76] J. P. Jeukenne, A. Lejeune, and C. Mahaux. *Phys. Rep.* **25C** (1976) 83. 206
- [JM 73] W. Jones and N. H. March. *Theoretical Solid State Physics*, Vol. II. Wiley-Interscience, New York, 1973. 545
- [JMR 69] D. Justin, M. V. Mihailović, and M. Rosina. *Phys. Lett.* **29B** (1969) 458. 435
- [JMR 72] D. Justin, M. V. Mihailović, and M. Rosina. *Nucl. Phys.* **A182** (1972) 54. 435
- [JNS 70] T. Johansson, S. G. Nilsson, and Z. Szymański. *Ann. Phys. (Paris)* **5** (1970) 377. 95
- [JRH 72] A. Johnson, H. Ryde, and S. A. Hjorth. *Nucl. Phys.* **A179** (1972) 753. 101, 105
- [JRS 71] A. Johnson, H. Ryde, and J. Szarkier. *Phys. Lett.* **34B** (1971) 605. 101
- [JS 64] B. Jancovici and D. H. Schiff. *Nucl. Phys.* **58** (1964) 678. 308, 352, 408, 424
- [JS 73] A. Johnson and Z. Szymański. *Phys. Rep.* **7C** (1973) 181. 97, 103

- [Ka 68] A. Kamila. *Z. Phys.* **216** (1968) 52. 424, 462, 466, 478
- [Ka 69] S. P. Kamerdzhev. *Sov. J. Nucl. Phys.* **9** (1969) 190. 345
- [Ka 73] A. Kamila. *Proceedings of the International Conference on Nuclear Physics*, Munich, 1973. J. De Boer and H. J. Mang, Eds. North Holland, Amsterdam, 1973. 425, 430
- [KB 62] L. P. Kadanoff and G. Baym. *Quantum Statistical Mechanics*. Benjamin, New York, 1962. 528, 553, 554, 556, 562
- [KB 66] T. T. S. Kuo and G. E. Brown. *Nucl. Phys.* **85** (1966) 40. 167, 326
- [KB 68] K. Kumar and M. Baranger. *Nucl. Phys.* **110** (1968) 529; **A122** (1968) 273. 27, 522
- [KBB 70] T. T. S. Kuo, J. Blomqvist, and G. E. Brown. *Phys. Lett.* **31B** (1970) 93. 170, 172, 326
- [KBF 74] S. Krewald, J. Birkholz, A. Faessler, and J. Speth. *Phys. Rev. Lett.* **33** (1974) 1386. 328
- [KCS 74] D. Kolb, R. Y. Cusson, and H. W. Schmitt. *Phys. Rev.* **C10** (1974) 1529. 268
- [KD 75] A. Keleman and R. M. Dreizler. *Z. Phys.* **A275** (1975) 23. 482
- [KD 76] A. Keleman and R. M. Dreizler. *Z. Phys.* **A278** (1976) 269. 482
- [KDM 77] S. E. Koonin, K. T. R. Davies, V. Maruhn-Rezwani, H. Feldmeier, S. J. Krieger, and J. W. Negele. *Phys. Rev.* **C15** (1977) 1359. 501, 505
- [Ke 56] A. K. Kerman. *Mat. Fys. Medd. Dan. Vid. Selsk.* **30** (1956) No. 15. 111
- [Ke 61] A. K. Kerman. *Ann. Phys. (New York)* **12** (1961) 300. 222, 523
- [Ke 63] I. Kelson. *Phys. Rev.* **132** (1963) 2189. 215
- [Ke 66] I. Kelson. *Nucl. Phys.* **89** (1966) 387. 474, 482
- [Ke 76] A. K. Kerman. *Varenna Lectures* **69** (1976) 135. 497
- [KF 70] E. I. Kao and S. Fallieros. *Phys. Rev. Lett.* **25** (1970) 827. 335
- [KG 74] S. J. Krieger and K. Goeke. *Nucl. Phys.* **A234** (1974) 269. 522
- [KG 78] K. K. Kan and J. J. Griffin. *Nucl. Phys.* **A301** (1978) 258. 131
- [KH 76] W. Knüpfel and M. G. Huber. *Phys. Rev.* **C14** (1976) 2254. 328

- [Ki 33] J. G. Kirkwood. *Phys. Rev.* **44** (1933) 31. 536
- [Ki 57] D. A. Kirzhnits. *Sov. Phys. JETP* **5** (1957) 64. 536
- [Ki 67] D. A. Kirzhnits. *Field Theoretical Methods in Many Body Systems*. Pergamon, Oxford, 1967. 527, 541, 542
- [Ki 78] M. W. Kirson. *Nucl. Phys.* **A301** (1978) 93. 332
- [KK 64] A. Kallio and K. Koliuveit. *Nucl. Phys.* **53** (1964) 87. 175
- [KK 68] K. Kikuchi and M. Kawai. *Nuclear Matter and Nuclear Reactions*. North Holland, Amsterdam, 1968. 37, 494, 554, 557
- [KK 74] S. B. Khadkikar and D. R. Kulkarni. *Phys. Rev.* **C10** (1974) 1189. 435
- [KK 76] A. K. Kerman and S. E. Koonin. *Ann. Phys. (New York)* **100** (1976) 332. 489, 506, 553, 562, 610
- [KKS 77] S. Krewald, V. Klemt, J. Speth, and A. Faessler. *Nucl. Phys.* **A281** (1977) 166. 209, 323, 328, 330
- [KI 52] P. F. A. Klinkenberg. *Rev. Mod. Phys.* **24** (1952) 63. 71
- [KI 69] M. Kleber. *Phys. Lett.* **30B** (1969) 588. 350, 362
- [KI 70] M. Kleber. *Z. Phys.* **231** (1970) 421. 436, 482
- [KI 77] H. Kleinert. *Phys. Lett.* **69B** (1977) 9. 499
- [KL 64] I. Kelson and C. A. Levinson. *Phys. Rev.* **I34** (1964) B269. 474, 481
- [KL 77] T. L. Khoo and G. Løvhøiden. *Phys. Lett.* **67B** (1977) 271. 145
- [KLD 80] K. K. Kan, P. C. Lichtner, M. Dworzecka, and J. J. Griffin. *Phys. Rev.* **C21** (1980) 1098. 490, 501
- [KLM 61] A. K. Kerman, R. D. Lawson, and M. H. Macfarlane. *Phys. Rev.* **124** (1961) 162. 449, 463
- [KLZ 75] H. Kümmel, K. H. Lührmann, and J. G. Zabolitzky. *Proceedings of the International Conference on Nuclear Selfconsistent Fields*, Trieste, 1975. G. Ripka and M. Porneuf, Eds. North Holland, Amsterdam, 1975. 206
- [KLZ 78] H. Kümmel, K. H. Lührmann, and J. G. Zabolitzky. *Phys. Rep.* **36C** (1978) 1. 187, 206
- [KM 66] P. Kramer and M. Moshinsky. *Nucl. Phys.* **82** (1966) 241. 456
- [KMM 72] A. Kuriyama, T. Marumori, and K. Matsuyanagi. *Progr. Theor. Phys.* **47** (1972) 498. 395
- [KMM 75a] A. Kuriyama, T. Marumori, and K. Matsuyanagi. *Suppl. Progr. Theor. Phys.* **58** (1975) 53. 395, 396
- [KMM 75b] A. Kuriyama, T. Marumori, K. Matsuyanagi, and R. Okamoto. *Progr. Theor. Phys.* **53** (1975) 489. 395
- [KMS 76] V. Klemt, S. A. Moszkowski, and J. Speth. *Phys. Rev.* **C14** (1976) 302. 179
- [KMY 75] T. Kishimoto, J. M. Moss, D. H. Youngblood, J. D. Bronson, C. M. Rozsa, D. R. Brown, and A. D. Bacher. *Phys. Rev. Lett.* **35** (1975) 552. 296, 345
- [Kn 50] M. H. C. Knudsen. *The Kinetic Theory of Gases*. Wiley, New York, 1950. 557
- [Ko 76] S. E. Koonin. *Phys. Lett.* **161B** (1976) 227. 505
- [Kö 65] H. S. Köhler. *Phys. Rev.* **137** (1965) B1145; **138** (1965) B831. 207
- [Kö 71] H. S. Köhler. *Nucl. Phys.* **A170** (1971) 88.
- [Kö 75] H. S. Köhler. *Phys. Rep.* **18C** (1975) 217. 204
- [Kö 76] H. S. Köhler. *Nucl. Phys.* **A258** (1976) 301. 209
- [KO 77] A. K. Kerman and N. Onishi. *Nucl. Phys.* **A281** (1977) 373. 473
- [KP 59] D. Kurath and L. Picman. *Nucl. Phys.* **10** (1959) 313. 481
- [KPW 68] N. Kemmer, D. L. Pursey, and S. A. Williams. *J. Math. Phys.* **9** (1968) 1224. 375
- [Kr 60] M. Kretzschmar. *Z. Phys.* **158** (1960) 284. 456

- [Kr 64] G. Krivchenkov. *Collected Problems in Quantum Mechanics*. D. Ter Haar, Ed. Infosearch, London, 1964. 538
- [Kr 70] S. J. Krieger. *Phys. Rev. C1* (1970) 76. 176, 209
- [Kr 77] S. J. Krieger. *Nucl. Phys. A276* (1977) 12. 501
- [Kr 79] A. J. Kreiner. *Phys. Rev. Lett.* 42 (1979) 829. 120
- [KRG 76] S. Krewald, R. Rosenfelder, J. E. Galonska, and A. Faessler. *Nucl. Phys. A269* (1976) 112. 433, 434
- [KS 60] L. S. Kisslinger and R. A. Sorensen. *Mat. Fys. Medd. Dan. Vid. Seisk.* 32 (1960) No. 9. 260
- [KS 62] A. K. Kerman and C. M. Shakin. *Phys. Lett. I* (1962) 151. 376
- [KS 63] L. S. Kisslinger and R. A. Sorensen. *Rev. Mod. Phys.* 35 (1963) 853. 180, 182, 185, 387, 395
- [KS 72] D. Kolb and R. Y. Cusson. *Z. Phys.* 253 (1972) 282. 209
- [KS 73] J. Krumlinde and Z. Szymański. *Ann. Phys. (New York)* 79 (1973) 201. 276
- [KS 74] S. Krewald and J. Speth. *Phys. Lett.* 52B (1974) 295. 327
- [KS 76] V. Klemt and J. Speth. *Z. Phys. A278* (1976) 59. 341
- [KSM 78] O. C. Kistner, A. W. Sunyar, and E. der Mateosian. *Phys. Rev. C17* (1978) 1417. 106, 273, 274
- [KT 71] T. Kishimoto and T. Tamura. *Nucl. Phys. A163* (1971) 100. 375
- [KT 72] T. Kishimoto and T. Tamura. *Nucl. Phys. A192* (1972) 246. 362, 381
- [KT 76] T. Kishimoto and T. Tamura. *Nucl. Phys. A270* (1976) 317. 362, 380, 381
- [KTB 80] H. Krivine, J. Treiner, and O. Bohigas. *Nucl. Phys. A336* (1980) 155. 568
- [Ku 25] W. Kuhn. *Z. Phys.* 33 (1925) 408. 294
- [Ku 56] D. Kurath. *Phys. Rev.* 101 (1956) 216. 174
- [Ku 62] K. Kumar. *Perturbation Theory and the Nuclear Many Body Problem*. North Holland, Amsterdam, 1962. 628
- [Ku 72] K. Kumar. *Physica Scripta* 6 (1972) 270. 276
- [Ku 74a] K. Kumar. *Nucl. Phys. A231* (1974) 189. 521, 522
- [Ku 74b] T. T. S. Kuo. *Ann. Rev. Nucl. Sci.* 24 (1974) 101. 164
- [Ku 72] O. Kübler. *Nucl. Phys. A196* (1972) 113. 466
- [KW 69] S. B. Khadkikar and C. S. Warke. *Nucl. Phys. A130* (1969) 577. 56
- [KWB 75] K. T. Knöpfle, G. J. Wagner, H. Breuer, M. Rogge, and C. Mayer-Böricke. *Phys. Rev. Lett.* 35 (1975) 779. 295
- [KZ 70] M. W. Kirson and L. Zamick. *Ann. Phys. (New York)* 60 (1970) 188. 169
- [La 32] L. D. Landau. *Phys. Z. Sov.* 2 (1932) 46. 526
- [La 59] L. D. Landau. *Sov. Phys. JETP* 8 (1959) 70. 177, 245
- [La 64] A. M. Lane. *Nuclear Theory*. Benjamin, New York, 1964. 181
- [La 65] A. Lande. *Ann. Phys. (New York)* 31 (1965) 525. 463
- [La 72] K. R. Lasssey. *Nucl. Phys. A192* (1972) 177. 209
- [La 74] L. F. F. Lathouwers. *Nucl. Phys. A228* (1974) 125. 400
- [La 75] A. M. Lane. *Proceedings of the International Symposium on Highly Excited States in Nuclei*, Juelich, 1975. A. Faessler, C. Mayer-Böricke, and P. Turek, Eds. Jülich Report. 331, 333
- [La 76] L. F. F. Lathouwers. *Ann. Phys. (New York)* 102 (1976) 347. 400, 401
- [LA 74] B. Lorazo and R. Arvieu. *Phys. Lett.* 49B (1974) 231. 228
- [LAD 77] I. Y. Lee, M. M. Alleonard, M. A. Deleplanque, Y. El Masri, J. O. Newton, R.

- S. Simon, R. M. Diamond, and F. S. Stephens.** Phys. Rev. Lett. **38** (1977) 1454. 107
- [LB 68] **H. A. Lamme and E. Boeker.** Nucl. Phys. **A111** (1968) 492. 474, 481
- [LB 69] **H. A. Lamme and E. Boeker.** Nucl. Phys. **A136** (1969) 609. 481
- [LB 72] **M. B. Lewis and F. E. Bertrand.** Nucl. Phys. **A196** (1972) 337. 295
- [LB 76] **K. F. Liu and G. E. Brown.** Nucl. Phys. **A265** (1976) 385. 209, 328, 330
- [LCS 76] **J. Y. Lee, D. Cline, R. S. Simon, P. A. Butler, P. Colombani, H. W. Guidry, F. S. Stephens, R. M. Diamond, N. R. Johnson, and E. Eichler.** Phys. Rev. Lett. **37** (1976) 420. 274
- [Le 76] **G. Leander.** Nucl. Phys. **A273** (1976) 286. 122
- [LG 76a] **P. C. Lichtner and J. J. Griffin.** Phys. Rev. Lett. **37** (1976) 1521. 498
- [LG 76b] **K. F. Liu and N. Van Giai.** Phys. Lett. **65B** (1976) 23. 324, 329
- [LH 75] **S. G. Lie and G. Holzwarth.** Phys. Rev. **C12** (1975) 1035. 362, 376, 380
- [LHR 62] **K. E. Lassila, M. H. Hull, H. M. Ruppel, F. A. McDonald, and G. Breit.** Phys. Rev. **126** (1962) 881. 135
- [Li 55] **H. J. Lipkin.** Suppl. Nuovo Cim. **4** (1955) 1147. 453
- [Li 58] **H. J. Lipkin.** Phys. Rev. **110** (1958) 1395. 453
- [Li 60a] **H. J. Lipkin.** Ann. Phys. (New York) **9** (1960) 272. 439, 472
- [Li 60b] **H. J. Lipkin.** Ann. Phys. (New York) **12** (1960) 425. 463
- [LL 59] **L. D. Landau and E. M. Lifshitz.** Course of Theoretical Physics. Pergamon, Oxford, 1959. 76, 430, 557
- [LL 77] **L. F. F. Lathouwers and R. L. Lozes.** J. Phys. (G. B.) **A10** (1977) 1465. 405
- [LLR 75] **M. Lacombe, B. Loiseau, J. M. Richard, R. Vinh Mau, P. Pires, and R. De Tourreil.** Phys. Rev. **D12** (1975) 1495. 148, 155
- [LLR 78] **S. E. Larsson, G. Leander, and I. Ragnarsson.** Nucl. Phys. **A307** (1978) 189. 122
- [LM 66] **K. E. G. Löbner and S. G. Malmkog.** Nucl. Phys. **80** (1966) 505. 126
- [LM 74] **A. M. Lane and A. Z. Mekjian.** Adv. Nucl. Phys. **7** (1974) 97. 56
- [LMG 65] **H. J. Lipkin, N. Mechkov, and A. J. Glick.** Nucl. Phys. **62** (1965) 188, 199, 211. 197
- [LMV 73] **K. R. Lassey, M. R. P. Manning, and A. B. Volkov.** Can. J. Phys. **51** (1973) 2522. 176, 209
- [Lo 75] **B. Lorazo.** Ann. Phys. (New York) **92** (1975) 95. 228
- [Lo 55] **P. O. Löwdin.** Phys. Rev. **97** (1955) 1474. 48, 618
- [Lo 64] **P. O. Löwdin.** Rev. Mod. Phys. **36** (1964) 966. 474
- [LOL 76] **E. Lipparini, G. Orlandini and R. Leonardi.** Phys. Rev. Lett. **36** (1976) 660. 333
- [LP 73] **T. Lederman and H. C. Pauli.** Nucl. Phys. **A207** (1973) 1. 95
- [LPF 77] **T. Lederman, Z. Paltiel, Z. Fraenkel, and H. C. Pauli.** Nucl. Phys. **A275** (1977) 280. 526
- [LPP 75] **T. Lederman, Z. Paltiel, H. C. Pauli, G. Schutte, Y. Yaniv, and Z. Fraenkel.** Phys. Lett. **56B** (1975) 417. 526
- [LR 69] **H. R. Lewis and W. B. Riesenfeld.** J. Math. Phys. **10** (1969) 1458. 417
- [LR 76] **G. Levheden, and J. Rekstad.** Phys. Lett. **60B** (1976) 335. 114
- [LR 77] **K. F. Liu and G. Ripka.** Nucl. Phys. **A293** (1977) 333. 135
- [LR 78] **R. M. Lieder and H. Ryde.** Adv. Nucl. Phys. **10** (1978) 1. 97, 103, 104, 105, 106
- [LRB 72] **T. Lindblad, H. Ryde, and D. Barnéoud.** Nucl. Phys. **A193** (1972) 155. 120
- [LS 62] **A. M. Lane and J. M. Soper.** Nucl. Phys. **37** (1962) 663. 56
- [LS 77] **L. J. Lantto and P. J. Siemens.** Phys. Lett. **68B** (1977) 308. 205

- [LST 55] H. J. Lipkin, A. De Shalit, and I. Talmi. *Nuovo Cim.* **2** (1955) 773. 453, 457
- [Lü 60] G. Lüders. *Z. Naturforschung* **15A** (1960) 371. 131
- [LV 68] R. H. Lemmer and M. Vénéroni. *Phys. Rev.* **170** (1968) 883. 323
- [LV 71] K. R. Lassay and A. B. Volkov. *Phys. Lett.* **36B** (1971) 4. 209
- [Ly 58] R. A. Lyttleton. *The Stability of Rotating Liquid Masses*. Cambridge University, Cambridge, 1958. 33
- [Ma 49] M. G. Mayer. *Phys. Rev.* **75** (1949) 1969. 43
- [Ma 50] M. G. Mayer. *Phys. Rev.* **78** (1950) 22. 219
- [Ma 65] E. R. Marshalek. *Phys. Rev.* **139** (1965) B770. 133
- [Ma 67a] E. R. Marshalek. *Phys. Rev.* **158** (1967) 993. 133
- [Ma 67b] R. D. Mattuck. *A Guide to Feynman Diagramms in the Manybody Problem*. McGraw-Hill, New York, 1967. 284, 345, 623, 634
- [Ma 69] M. H. Macfarlane. *Varenna Lectures* **40** (1969) 457. 166, 167, 170
- [Ma 70] N. MacDonald. *Adv. Phys.* **19** (1970) 371. 459, 481
- [Ma 71] E. R. Marshalek. *Nucl. Phys.* **A161** (1971) 401. 358
- [Ma 73] E. R. Marshalek. *Phys. Lett.* **44B** (1973) 5. 382
- [Ma 74] E. R. Marshalek. *Nucl. Phys.* **A224** (1974) 221, 245. 182, 286, 358, 360, 382
- [Ma 75a] H. J. Mang. *Phys. Rep.* **18C** (1975) 325. 250, 253, 466, 478
- [Ma 75b] E. R. Marshalek. *Phys. Rev.* **C11** (1975) 1426. 351
- [Ma 76a] E. R. Marshalek. *Phys. Lett.* **62B** (1976) 5. 311, 361
- [Ma 76b] E. R. Marshalek. *Nucl. Phys.* **A266** (1976) 317. 205
- [Ma 77a] E. R. Marshalek. *Nucl. Phys.* **A275** (1977) 416. 279, 440
- [Ma 77b] T. Marumori. *Progr. Theor. Phys.* **57** (1977) 112. 506, 519
- [Ma 77c] J. A. Maruhn. *Proceedings of the Topical Conference on Heavy Ion Collisions*, Fall Creek Falls, Tennessee, 1977. E. C. Halbert, Ed. U. S. Govt. Printing Office, Springfield, 1977. 362
- [Ma 79] E. R. Marshalek. *Nucl. Phys.* **A331** (1979) 429. 351
- [MAG 75] H. Müther, K. Allaart, K. Goeke, and A. Faessler. *Nucl. Phys.* **A248** (1975) 451. 437
- [MB 65] R. Muthukrishnan and M. Baranger. *Phys. Lett.* **18** (1965) 160. 209
- [MB 69] H. J. Mikeska and W. Brenig. *Z. Phys.* **220** (1969) 321. 179
- [MBF 76] J. Martorell, O. Bohigas, S. Fallieros, and A. M. Lane. *Phys. Lett.* **60B** (1976) 313. 330, 333
- [MBZ 64] J. D. McCullen, B. F. Bayman and L. Zamick. *Phys. Rev.* **134** (1964) B515. 185
- [Mc 56] R. McWeeny. *Proc. Roy. Soc. (London)* **A235** (1956) 496. 258
- [Mc 60] R. McWeeny. *Rev. Mod. Phys.* **32** (1960) 335. 258
- [Mc 65] J. McGuire. *J. Math. Phys.* **6** (1965) 432. 499
- [MC 76] J. A. Maruhn and R. Y. Cusson. *Nucl. Phys.* **A270** (1976) 471. 505
- [MD 73] I. W. Mayes and J. S. Dowker. *J. Math. Phys.* **14** (1973) 434. 19
- [MDK 77] V. Maruhn-Rezwani, K. T. R. Davies, and S. E. Koonin. *Phys. Lett.* **67B** (1977) 134. 505
- [MDN 78] K. Matsuyanagi, T. Dössing, and K. Neergård. *Nucl. Phys.* **A307** (1978) 253. 145
- [Me 61] A. Messiah. *Quantum Mechanics*. North Holland, Amsterdam, 1961. 9, 19, 52, 151, 157, 158, 160, 202, 228, 324, 491, 492, 587
- [Me 75] J. Meyer-ter-Vehn. *Nucl. Phys.* **A249** (1975) 111, 141. 27, 122, 123, 124

- [Me 78] J. Meyer-ter-Vehn. Proceedings of the first Symposium on Interacting Bosons in Nuclear Physics. Erice, Sicily, 1978. F. Iachello, Ed. Plenum, New York 1978. 379
- [Me 79] J. Meyer-ter-Vehn. Z. Phys. A259 (1979) 319. 372
- [MEL 76] M. A. Morrison, T. L. Estle, and N. F. Lane. Quantum States of Atoms, Molecules and Solids. Prentice-Hall, Englewood Cliffs, NJ, 1976. 398
- [MF 39] L. Meitner and O. R. Frisch. Nature 143 (1939) 239. 28
- [MG 63] H. Morinaga and P. C. Gugelot. Nucl. Phys. 46 (1963) 210. 97
- [MG 72] J. A. Maruhn and W. Greiner. Z. Phys. 251 (1972) 431. 81
- [MG 78] E. R. Marshalek and A. L. Goodman. Nucl. Phys. A294 (1978) 92. 274
- [MGA 77] H. Müther, K. Goeke, K. Allaart, and A. Faessler. Phys. Rev. C15 (1977) 1467. 437
- [MH 72] E. R. Marshalek and G. Holzwarth. Nucl. Phys. A191 (1972) 438. 358, 520
- [MHT 58] T. A. J. Maris, P. Hillman, and H. Tyren. Nucl. Phys. 7 (1958) 1. 57
- [Mi 59] A. B. Migdal. Nucl. Phys. 13 (1959) 655. 132, 345
- [Mi 60] A. B. Migdal. Sov. Phys. JETP 10 (1960) 176. 132, 345
- [Mi 67] A. B. Migdal. Theory of Finite Fermi Systems and Applications to Atomic Nuclei. Wiley Interscience, New York, 1967. 177, 245, 260, 326, 345, 390, 623, 630, 633, 635, 640
- [MJ 55] M. G. Mayer and J. H. D. Jensen. Elementary Theory of Nuclear Shell Structure. Wiley, New York, 1955. 38, 42, 43, 44, 53, 62
- [MJ 78] I. N. Mikhailov and D. Janssen. Phys. Lett. 72B (1978) 303. 345
- [MJB 75] A. Molinari, M. B. Johnson, H. A. Bethe, and W. M. Alberico. Nucl. Phys. A239 (1975) 45. 184, 186
- [MKL 71] M. V. Mihailović, E. Kujawski, and J. Lesjak. Nucl. Phys. A161 (1971) 252. 474, 481
- [MKS 74] A. B. Migdal, N. A. Kirichenko, and G. A. Sorokin. Phys. Lett. 50B (1974) 411. 441
- [ML 64] A. B. Migdal and A. I. Larkin. Nucl. Phys. 51 (1964) 561. 345
- [MLE 67] W. J. Mulhall, R. J. Liotta, J. A. Evans, and R. P. J. Perazzo. Nucl. Phys. A93 (1967) 261. 340
- [MM 76] N. Mankoc-Borštnik and M. V. Mihailović. J. Comp. Phys. 22 (1976) 271. 474
- [MMG 67] H. A. Mavromatis, W. Markiewicz, and A. M. Green. Nucl. Phys. A90 (1967) 101. 326
- [MMR 75] N. Mankoc-Borštnik, M. V. Mihailović, and M. Rosina. Nucl. Phys. A239 (1975) 321. 435
- [MMS 73] M. G. Mustafa, U. Mosel, and H. W. Schmitt. Phys. Rev. C7 (1973) 1519. 81
- [MMW 73] N. MacDonald, I. Morrison, and A. Watt. Nucl. Phys. A217 (1973) 429. 463, 481
- [MMW 75] N. Marty, M. Morlet, A. Willis, V. Camparat, and R. Frascaria. Proceedings of the International Symposium on Highly Excited States in Nuclei, Juelich, 1975. A. Faessler, C. Mayer-Börnke, and P. Turek, Eds. Jülich Report. 296
- [MN 55] B. R. Mottelson and S. G. Nilsson. Phys. Rev. 99 (1955) 1615. 80
- [MN 59] B. R. Mottelson and S. G. Nilsson. Mat. Fys. Skr. Dan. Vid. Selsk. 1 (1959) No. 8. 78, 125, 132
- [MN 73] P. Möller and J. R. Nix. Proceedings of the International Symposium on Physics and Chemistry of Fission, Vienna, 1973. IAEA-Sm-174/202, Vienna, 1969, p. 103. 81, 82, 95
- [MN 76] P. Möller and J. R. Nix. Nucl. Phys. A272 (1976) 502. 31

- [MNS 76] L. A. Malov, V. O. Nesterenko and V. G. Soloviev. Phys. Lett. **64B** (1976) 247. 292, 345
- [MNY 77] Y. Mizobuchi, S. Nishiyama, and M. Yamamura. Progr. Theor. Phys. **57** (1977) 96. 375
- [Mo 56] S. A. Moszkowski. Phys. Rev. **103** (1956) 1328. 131
- [Mo 57] S. A. Moszkowski. Handbuch der Physik, Vol. XXXIX, p. 411. Springer-Verlag, Berlin, 1957. 41
- [Mo 65] H. Mori. Progr. Theor. Phys. **34** (1965) 399. 640
- [Mo 67] B. R. Mottelson. Proceedings of the International Conference on Nuclear Structure. Tokyo, 1967, Suppl. to the J. OF THE Phys. Soc. Japan, vol. **24**. 386, 387
- [Mo 69] M. Moshinsky. The Harmonic Oscillator in Modern Physics. Gordon and Breach, New York, 1969. 456
- [Mo 70] S. A. Moszkowski. Phys. Rev. **C2** (1970) 402. 176, 209
- [Mo 76a] B. R. Mottelson. Rev. Mod. Phys. **48** (1976) 375. 290
- [Mo 76b] B. R. Mottelson. Varenna Lectures **69** (1976) 31. 290
- [Mo 76c] S. A. Moszkowski. Nukleonika **21** (1976) 655. 187
- [Mo 72] P. Möller. Nucl. Phys. **A192** (1972) 529. 81
- [MP 73] E. R. Marshalek and J. Da Providencia. Phys. Rev. **C7** (1973) 2281. 322
- [MPR 65] H. J. Mang, J. K. Poggenburg, and J. O. Rasmussen. Nucl. Phys. **64** (1965) 353. 240, 463, 464
- [MR 70] C. W. Ma and J. O. Rasmussen. Phys. Rev. **C2** (1970) 798. 133
- [MR 72] A. Molinari and T. Regge. Phys. Lett. **41B** (1972) 93. 106
- [MR 77] C. W. Ma and J. O. Rasmussen. Phys. Rev. **C16** (1977) 1179. 463
- [MRR 66] H. J. Mang, J. O. Rasmussen, and M. Rho. Phys. Rev. **141** (1966) 941. 463
- [MS 60] S. A. Moszkowski and B. L. Scott. Ann. Phys. (New York) **11** (1960) 65; **14** (1961) 107. 163
- [MS 66] W. D. Myers and W. J. Swiatecki. Nucl. Phys. **81** (1966) 1. 4, 39, 83
- [MS 69] W. D. Myers and W. J. Swiatecki. Ann. Phys. (New York) **55** (1969) 186. 4, 5. 527
- [MS 73] W. D. Myers and W. J. Swiatecki. Ann. Phys. (New York) **84** (1969) 395. 5
- [MSB 69] M. A. J. Mariscotti, G. Scharff-Goldhaber, and B. Buck. Phys. Rev. **178** (1969) 1864. 104
- [MSD 74] J. Meyer-ter-Vehn, F. S. Stephens, and R. M. Diamond. Phys. Rev. Lett. **32** (1974) 1383. 27, 122, 123
- [MSK 77] W. D. Myers, W. J. Swiatecki, T. Kodama, L. J. El Jaick, and E. R. Hilf. Phys. Rev. **C15** (1977) 2032. 487, 561
- [MSR 76] H. J. Mang, B. Samadi, and P. Ring. Z. Phys. **A279** (1976) 325. 257, 258, 273, 274, 275
- [MSU 67] O. Mikishiba, R. K. Sheline, T. Udagawa, and S. Yoshida. Nucl. Phys. **A101** (1967) 202. 345
- [MSV 72] J. Meyer-ter-Vehn, J. Speth, and J. H. Vogeler. Nucl. Phys. **A193** (1972) 60. 132, 133
- [MT 56] T. Miyazima and T. Tamura. Progr. Theor. Phys. **15** (1956) 255. 454
- [MT 73] C. W. Ma and W. W. True. Phys. Rev. **C8** (1973) 2313. 289
- [MT 75] C. W. Ma and C. F. Tsang. Phys. Rev. **C11** (1975) 213. 132
- [MT 77] V. Mikolas and M. Tomasek. Phys. Lett. **64A** (1977) 109. 541, 564
- [MV 60] B. R. Mottelson and J. G. Valatin. Phys. Rev. Lett. **5** (1960) 511. 101, 107, 276

- [MV 77] E. Moya de Guerra and F. Villars. Nucl. Phys. A285 (1977) 297. 519
 [MV 78] E. Moya de Guerra and F. Villars. Nucl. Phys. A298 (1978) 109.
 [MW 68] H. J. Mang and H. A. Weidenmüller. Ann. Rev. Nucl. Sci. 18 (1968) 1. 253
 [MW 69a] C. Mahaux and H. A. Weidenmüller. Shell-Model Approach to Nuclear Reactions. North Holland, Amsterdam, 1969. 323
 [MW 69b] E. R. Marshalek and J. Wenner. Ann. Phys. (New York) 53 (1969) 569. 309, 312, 440
 [MW 70] E. R. Marshalek and J. Wenner. Phys. Rev. C2 (1970) 1682. 312, 314, 440
 [MWW 74] I. Morrison, A. Watt, and R. R. Whitehead. J. Phys. (G. B.) A7 (1974) L75. 482
 [MWW 76] J. A. Maruhn, T. A. Welton, and C. Y. Wong. J. Comp. Phys. 20 (1976) 320. 361
 [My 69] W. D. Myers. Nucl. Phys. A145 (1969) 387. 4
 [MY 55] T. Marumori and E. Yamada. Progr. Theor. Phys. 13 (1955) 557. 454
 [MYM 68] T. Marumori, M. Yamamura, Y. Miyanishi, and S. Nishiyama. Progr. Theor. Phys. Suppl. (1968) 179. 311
 [MYT 55] T. Marumori, J. Yukawa, and R. Tanaka. Progr. Theor. Phys. 13 (1955) 442. 454
 [MYT 64a] T. Marumori, M. Yamamura, and A. Tokunaga. Progr. Theor. Phys. 31 (1964) 1009. 352, 362, 369
 [MYT 64b] T. Marumori, M. Yamamura, A. Tokunaga, and A. Takada. Progr. Theor. Phys. 32 (1964) 726. 352, 362

- [Na 57] R. S. Nataf. Nucl. Phys. 2 (1957) 497. 453, 457
 [NA 62] P. E. Nemirovski and Y. V. Adamchuk. Nucl. Phys. 39 (1962) 551. 236
 [NDK 68] C. W. Nestor, K. T. R. Davies, S. J. Krieger, and M. Baranger. Nucl. Phys. A113 (1968) 14. 209
 [Ne 70] J. W. Negele. Phys. Rev. C1 (1970) 1260. 163, 205, 207, 208, 213
 [Ne 75] J. W. Negele. Lecture Notes in Physics 40. B. R. Barret, Ed. Springer-Verlag, Berlin, 1975. 163, 164, 207, 208
 [Ne 77] J. W. Negele. Topical Conference on Heavy Ion Collisions, Fall Creek State Park, Tennessee, 1977. E. C. Halbert, Ed. U. S. Govt. Printing Office, Springfield, 1977. 498
 [Ni 55] S. G. Nilsson. Mat. Fys. Medd. Dan. Vid. Selsk. 29 (1955) No. 16. 68, 70, 71, 72, 76
 [Ni 69] J. R. Nix. Nucl. Phys. A130 (1969) 241. 31, 81
 [Ni 72] J. R. Nix. Ann. Rev. Nucl. Sci. 22 (1972) 65. 5, 28, 81, 95
 [NKM 78] J. W. Negele, S. E. Koonin, P. Möller, J. R. Nix, and A. J. Sierk. Phys. Rev. C17 (1978) 1098. 505
 [NLM 76] A. Nesnakpis, R. M. Lieder, M. Müller-Veggian, H. Beuscher, W. F. Davidson, and C. Mayer-Böricken. Nucl. Phys. A261 (1976) 189. 107
 [NLP 79] J. W. Negele, S. Levit, and Z. Paltiel. Proceedings of the Workshop on the Time Dependent HF Method. Orsay, Saclay, 1979. P. Bonche, B. Giraud and P. Quentin, Eds. Editions de Physique, Paris, 1979. 499
 [NMH 73] J. Nemeth, R. Machleidt, and K. Holinde. Proceedings of the International Conference on Nuclear Physics, Munich, 1973. J. De Boer and H. J. Mang, Eds. North Holland, Amsterdam, 1973. 213
 [NN 65] P. Nathan and S. G. Nilsson. Alpha-, Beta- and Gamma-Ray Spectroscopy. K. Siegbahn, Ed. North Holland, Amsterdam, 1965. 15, 125

- [NN 74] S. G. Nilsson and N. R. Nilson, Eds. Superheavy Elements, Proceedings of the 27th Nobel Symposium, Ronneby, Sweden, 1974. *Physica Scripta* **10A** (1974) 1–187. 95
- [No 64a] P. Nozieres. Theory of Interacting Fermi Systems. Benjamin, New York, 1964. 318, 528, 554, 556, 562, 623
- [No 64b] Y. Nogami. *Phys. Rev.* **134** (1964) B313. 463
- [No 71] J. V. Noble. *Ann. Phys. (New York)* **67** (1971) 98. 335
- [No 78] J. V. Noble. *Phys. Rep.* **40C** (1978) 241. 330
- [NP 61] S. G. Nilsson and O. Prior. *Mat. Fys. Medd. Dan. Vid. Selsk.* **32** (1961) No. 16. 132, 133, 238, 242
- [NP 75] K. Neergård and V. V. Pashkevich. *Phys. Lett.* **59B** (1975) 218. 139
- [NPF 76] K. Neergård, V. V. Pashkevich, and S. Frauendorf. *Nucl. Phys.* **A262** (1976) 61. 139
- [NR 71] C. Ngo-Trong and D. J. Rowe. *Phys. Lett.* **36B** (1971) 553. 302
- [NR 72] J. Nemeth and G. Ripka. *Nucl. Phys.* **A194** (1972) 329. 207
- [NR 77] J. W. Negele and G. Rinker. *Phys. Rev.* **C15** (1977) 1499. 264
- [NS 65] J. R. Nix and W. J. Swiatecki. *Nucl. Phys.* **71** (1965) 1. 28, 31
- [NS 78] K. Nichols and R. A. Sorensen. *Nucl. Phys.* **A309** (1978) 45. 277
- [NTP 77] K. Neergård, H. Toki, M. Ploszajczak, and A. Faessler. *Nucl. Phys.* **A287** (1977) 48. 139, 140
- [NTS 69] S. G. Nilsson, C. F. Tsang, A. Sobiczewski, Z. Szymański, S. Wycech, C. Gustafson, I. L. Lamm, P. Möller, and B. Nilsson. *Nucl. Phys.* **A131** (1969) 1. 81
- [NTT 69] S. G. Nilsson, S. G. Thompson, and C. F. Tsang. *Phys. Lett.* **28B** (1969) 458. 94, 95
- [NV 70] J. Nemeth and D. Vautherin. *Phys. Lett.* **32B** (1970) 561. 207
- [NV 72] J. W. Negele and D. Vautherin. *Phys. Rev.* **C5** (1972) 1472. 176
- [NV 75] J. W. Negele and D. Vautherin. *Phys. Rev.* **C11** (1975) 1031. 208
- [NVR 75] K. Neergård, P. Vogel and M. Radomski. *Nucl. Phys.* **A238** (1975) 199. 103
- [NW 29] J. V. Neumann and E. P. Wigner. *Phys. Z.* **30** (1929) 427. 76
- [NW 72] H. Nopre and E. Werner. *Z. Phys.* **254** (1972) 345; **257** (1972) 410. 179
- [NW 74] H. Nopre and E. Werner. *Z. Phys.* **267** (1974) 165. 179, 327
- [NW 76] Y. Nogami and C. S. Warke. *Phys. Lett.* **59A** (1976) 251. 499
- [NW 78] Y. Nogami and C. S. Warke. *Phys. Rev.* **C17** (1978) 1905. 499
- [NZ 64] Y. Nogami and I. J. Zucker. *Nucl. Phys.* **60** (1964) 203. 463
- [OAI 78] T. Otsuka, A. Arima, and F. Iachello. *Nucl. Phys.* **A309** (1978) 1. 379
- [Ok 58] K. Okamoto. *Phys. Rev.* **110** (1958) 143. 294
- [Ok 74] S. Okubo. *Phys. Rev.* **C10** (1974) 2048. 372, 382
- [OM 58] S. Okubo and R. E. Marshak. *Ann. Phys. (New York)* **4** (1958) 166. 151
- [On 68] N. Onishi. *Progr. Theor. Phys.* **40** (1968) 84. 462
- [ON 78] N. Onishi and J. W. Negele. *Nucl. Phys.* **A301** (1978) 336. 176
- [ORG 75] E. Osnes, J. Rekstad and O. K. Gjotterud. *Nucl. Phys.* **A253** (1975) 45. 120
- [OS 69] P. L. Ottaviani and M. Savoia. *Phys. Rev.* **187** (1969) 1306. 482
- [OSY 70] N. Onishi, R. K. Sheline, and S. Yoshida. *Phys. Rev.* **C2** (1970) 1304. 482
- [OU 75] N. Onishi and T. Ume. *Progr. Theor. Phys.* **53** (1975) 504. 425, 430
- [Ov 60] A. W. Overhauser. *Phys. Rev. Lett.* **4** (1960) 415. 441

- [OWP 71] W. Ogle, S. Wahlborn, R. Piepenbring, and S. Fredriksson. *Rev. Mod. Phys.* **43** (1971) 424. 79
- [OY 66] N. Onishi and S. Yoshida. *Nucl. Phys.* **80** (1966) 367. 618
- [Pa 33] W. Pauli. *Handbuch der Physik*, Vol. XXIV. Springer-Verlag, Berlin, 1933, p. 120. 19
- [Pa 61] V. V. Pashkevich. *Izv. Akad. Nauk. USSR (Ser. Fiz.)* **25** (1961) 782. 122
- [Pa 67] F. Palumbo. *Nucl. Phys.* **99** (1967) 100. 456
- [Pa 73] H. C. Pauli. *Phys. Rep.* **7C** (1973) 35. 81, 95
- [Pa 75a] P. Paul. *International Symposium on Highly Excited States*, Juelich, 1975. A. Faessler, C. Mayer-Boericke, and P. Turek, Eds. Jülich Report. 297
- [Pa 75b] H. C. Pauli. *Nukleonika* **20** (1975) 601. 506, 526
- [Pa 76] K. H. Passler. *Nucl. Phys.* **A257** (1976) 253. 209
- [PAG 62] I. Perlman, F. Asaro, A. Ghiorso, A. Larsh, and R. Latimer. *Phys. Rev.* **127** (1962) 917. 145
- [PAM 66] A. Plastino, R. Arvieu, and S. A. Moszkowski. *Phys. Rev.* **145** (1966) 837. 180
- [PB 55] B. Van der Pol and H. Bremmer. *Operational Calculus*. Cambridge Univ. Press, Cambridge, 1955. 529, 537, 539
- [PB 73] V. R. Pandharipande and H. A. Bethe. *Phys. Rev. C7* (1973) 1312. 205
- [PB 75] M. A. Preston and R. K. Bhaduri. *Structure of the Nucleus*. Addison-Wesley, Reading, MA, 1975. 547
- [PBB 77] J. Pedersen, B. B. Back, F. M. Bernthal, S. Bjørnholm, J. Borggreen, O. Christensen, F. Folkmann, B. Herskind, T. L. Khoo, M. Neiman, F. Pühlhofer, and G. Sletten. *Phys. Rev. Lett.* **39** (1977) 990. 145
- [PBD 74] R. Pitthan, F. R. Buskirk, E. B. Dally, J. N. Dyer, and X. K. Maruyama. *Phys. Rev. Lett.* **33** (1974) 849. 297
- [PDK 62] S. M. Polikanov, V. A. Druin, V. A. Karnaukhov, V. L. Mikheev, A. A. Pleve, N. K. Skobelev, V. G. Subbotin, G. M. Ter-Akopjan, and V. A. Fomichev. *Sov. Phys. JETP* **15** (1962) 1016. 67
- [Pe 77] A. M. Perelomow. *Sov. Phys. Usp.* **20** (1977) 703. 412
- [PFL 78] M. Płoszajczak, A. Faessler, G. Leander, and S. G. Nilsson. *Nucl. Phys.* **A301** (1978) 477. 145
- [Pi 61] D. Pines. *The Manybody Problem*. Benjamin, New York, 1961. 635
- [PKD 68] S. C. Pang, A. Klein, and R. M. Dreizler. *Ann. Phys. (New York)* **49** (1968) 477. 350, 362, 366
- [PL 77] J. Pelet and J. LeTourneau. *Nucl. Phys.* **A281** (1977) 277. 432, 435
- [PM 76] K. H. Passler and U. Mosel. *Nucl. Phys.* **A257** (1976) 242. 277
- [Po 76] K. Pomorski. *Acta Physica Polonica B7* (1976) 595. 526
- [Po 78] K. Pomorski. *Nukleonika* **23** (1978) 125. 526
- [PO 78] T. Pedersen and E. Osnæs. *Nucl. Phys.* **A303** (1978) 345. 115
- [Pr 66] J. Da Providencia. *Phys. Lett.* **21** (1966) 668. 311
- [Pr 74] J. Da Providencia. *Nucl. Phys.* **A224** (1974) 262. 382
- [PR 62] L. W. Person and J. O. Rasmussen. *Nucl. Phys.* **36** (1962) 666. 122
- [PR 68] J. C. Parikh and D. J. Rowe. *Phys. Rev.* **175** (1968) 1293. 311
- [PS 65] V. V. Pashkevich and R. A. Sardaryan. *Nucl. Phys.* **65** (1965) 401. 122
- [PS 68] J. M. Pearson and G. Saunier. *Phys. Rev.* **173** (1968) 991. 209
- [PS 77] N. I. Pyatov and D. I. Salamov. *Nukleonika* **22** (1977) 127. 312
- [PT 62] R. E. Peierls and D. J. Thouless. *Nucl. Phys.* **38** (1962) 154. 418, 428, 473

- [PTF 78] M. Ploszajczak, H. Toki, and A. Faessler. *Z. Phys.* **A287** (1978) 103. 145
- [PUF 71] J. Da Providencia, J. N. Urbano, and L. S. Ferreira. *Nucl. Phys.* **A170** (1971) 129. 406
- [PVD 77] V. Paar, Ch. Vieu, and J. S. Dioniso. *Nucl. Phys.* **A284** (1977) 199. 122, 385
- [PW 71] R. Pittau and T. Walcher. *Phys. Lett.* **36B** (1971) 563. 295
- [PW 72] B. M. Freedman and B. H. Wildenthal. *Phys. Rev.* **C6** (1972) 1633. 435
- [PY 57] R. E. Peierls and J. Yoccoz. *Proc. Phys. Soc. (London)* **A70** (1957) 381. 460, 469, 474
- [QF 78] P. Quentin and H. Flocard. *Ann. Rev. Nucl. Sci.* **28** (1978) 523. 197, 208
- [Qu 72] P. Quentin. *J. Phys. (Paris)* **33** (1972) 457. 209
- [Ra 43] G. Racah. *Phys. Rev.* **63** (1943) 367. 223
- [Ra 50] J. Rainwater. *Phys. Rev.* **79** (1950) 432. 66
- [Ra 70] J. Raynal. *J. Phys. (Paris)* **31** (1970) 3. 482
- [Ra 75] R. Rajaraman. *Phys. Rep.* **21C** (1975) 227. 500
- [Ra 76] J. Rainwater. *Rev. Mod. Phys.* **48** (1976) 385. 66
- [RB 74] D. J. Rowe and R. Bassermann. *Nucl. Phys.* **A220** (1974) 404. 506
- [RB 76] D. J. Rowe and R. Bassermann. *Can. J. Phys.* **54** (1976) 1941. 310, 506, 519
- [RBK 75] G. Ripka, J. P. Blaizot, and N. Kassis. Extended Seminar on Nuclear Physics, 1975. Int. Center for Theor. Phys. Trieste, Paper IAEA-Smr-14/19. 133, 135, 136
- [RBM 70] P. Ring, R. Beck, and H. J. Mang. *Z. Phys.* **231** (1970) 10. 256, 261, 272, 276
- [RBP 77] B. Rouben, F. Brut J. M. Pearson, and G. Saunier. *Phys. Lett.* **70B** (1977) 6. 176, 209
- [RBS 73] P. Ring, R. Bauer, and J. Speth. *Nucl. Phys.* **A206** (1973) 97. 179, 326, 390, 591
- [RD 76] A. A. Raduta and R. M. Dreizler. *Nucl. Phys.* **A258** (1976) 109. 377
- [Re 58] M. G. Redlich. *Phys. Rev.* **110** (1958) 468. 481
- [Re 68] P. V. Reid. *Ann. Phys. (New York)* **50** (1968) 411. 155
- [Re 75a] J. Rekstad. *Nucl. Phys.* **A247** (1975) 7. 114
- [Re 75b] H. Reinhardt. *Nucl. Phys.* **A251** (1975) 317. 391
- [Re 75c] P. G. Reinhard. *Nucl. Phys.* **A252** (1975) 120, 133. 427
- [Re 76a] P. G. Reinhard. *Nucl. Phys.* **A261** (1976) 291. 419, 424
- [Re 76b] P. G. Reinhard. *Habilitationsschrift*, University of Mainz, 1976. 419, 422, 423, 424
- [Re 77] P. G. Reinhard. *Nucl. Phys.* **A281** (1977) 221. 420
- [Re 78] P. G. Reinhard. *Nucl. Phys.* **306** (1978) 19. 427
- [Re 79] H. Reinhardt. *Nucl. Phys.* **A331** (1979) 353. 499
- [RFM 74] H. Rothbaas, J. Friedrich, K. Merle, and B. Dreher. *Phys. Lett.* **51B** (1974) 23. 339
- [RG 77] P. G. Reinhard and K. Goeke. *Phys. Lett.* **69B** (1977) 17. 519
- [RG 78] P. G. Reinhard and K. Goeke. *Nucl. Phys.* **A312** (1978) 121. 517
- [RGB 77] A. A. Raduta, A. Gheorghe, and M. Badea. *Z. Phys.* **A283** (1977) 79. 377
- [Ri 66] R. W. Richardson. *Phys. Rev.* **141** (1966) 949. 449, 463
- [Ri 68] G. Ripka. *Adv. Nucl. Phys.* **1** (1968) 183. 202, 481
- [Ri 77] P. Ring. Proceedings of the International Workshop of Gross Properties in Nuclei V, Hirschegg, 1977. F. Beck, Ed. T. H. Darmstadt. 119, 121, 278

- [Ri 79] G. Ripka. Phys. Rep. **56C** (1979) 1. 205
- [RL 76] G. Lovheden and J. Rekstad. Nucl. Phys. **A267** (1976) 40. 76
- [RLM 76] J. Randrup, S. E. Larsson, P. Möller, S. G. Nilsson, K. Pomorski, and A. Sobczewski. Phys. Rev. **C13** (1976) 229. 526
- [RM 74] P. Ring and H. J. Mang. Phys. Rev. Lett. **33** (1974) 1174. 121, 278, 479
- [RMB 74] P. Ring, H. J. Mang, and B. Banerjee. Nucl. Phys. **A225** (1974) 141. 121, 256, 278, 479
- [RMS 67] J. Raynal, M. A. Melkanoff, and T. Sawada. Nucl. Phys. **A101** (1967) 369. 323
- [RN 75] D. J. Rowe and C. Ngo-Trong. Rev. Mod. Phys. **47** (1975) 471. 302
- [RNS 78] I. Ragnarsson, S. G. Nilsson, and R. K. Sheline. Phys. Rep. **45C** (1978) 1. 81, 95, 137
- [Ro 59] R. M. Rockmore. Phys. Rev. **116** (1959) 469. 131
- [Ro 67] C. E. Rosenkilde. J. Math. Phys. **8** (1967) 84, 88, 98. 33
- [Ro 68a] D. J. Rowe. Rev. Mod. Phys. **40** (1968) 153. 301, 311, 360
- [Ro 68b] D. J. Rowe. Phys. Rev. **175** (1968) 1283. 340
- [Ro 70] D. J. Rowe. Nuclear Collective Motion. Methuen, London, 1970. 97, 301, 311
- [RP 69] G. Ripka and R. Padjen. Nucl. Phys. **A132** (1969) 489. 340
- [RPS 72] B. Rouben, J. M. Pearson, and G. Saunier. Phys. Lett. **42B** (1972) 385. 176, 209
- [RS 64] R. W. Richardson and N. Sherman. Nucl. Phys. **52** (1964) 221. 449
- [RS 72] M. Reed and B. Simon. Methods of Modern Mathematical Physics. Academic, New York, 1972. 401
- [RS 73] P. Ring and J. Speth. Phys. Lett. **44B** (1973) 477. 327
- [RS 74a] P. Ring and J. Speth. Nucl. Phys. **A235** (1974) 315. 179, 296, 297, 326, 327, 328, 433
- [RS 74b] P. Ring and P. Schuck. Z. Phys. **269** (1974) 323. 368, 391
- [RS 77a] P. Ring and P. Schuck. Phys. Rev. **C16** (1977) 801. 367, 368, 382
- [RS 77b] P. Ring and P. Schuck. Nucl. Phys. **A292** (1977) 20. 605, 616
- [RSS 74] L. L. Riedinger, G. J. Smith, P. H. Stelson, E. Eichler, G. B. Hagemann, D. C. Hensley, N. R. Johnson, R. L. Robinson, and R. O. Sayer. Phys. Rev. Lett. **33** (1974) 1346. 107
- [RT 25] F. Reiche and W. Thomas. Z. Phys. **34** (1925) 510. 294
- [Ru 73] H. Ruder. Z. Naturforschung **28A** (1973) 206. 1500. 453, 458
- [RV 69] H. Ruder and H. Volz. Z. Naturforschung **24A** (1969) 1171. 453
- [RW 54] M. G. Redlich and E. P. Wigner. Phys. Rev. **95** (1954) 122. 474
- [RW 69] D. J. Rowe and S. S. M. Wong. Phys. Lett. **30B** (1969) 147. 302
- [RW 70] D. J. Rowe and S. S. M. Wong. Nucl. Phys. **A153** (1970) 561. 302
- [RW 73] P. Ring and E. Werner. Nucl. Phys. **A211** (1973) 198. 39, 215
- [RY 66] H. Rouhaninejad and J. Yoccoz. Nucl. Phys. **78** (1966) 353. 461, 470
-
- [Sa 57] K. Sawada. Phys. Rev. **106** (1957) 372. 301
- [Sa 62] J. Sawicki. Phys. Rev. **126** (1962) 2231. 311
- [Sa 65] E. A. Sanderson. Phys. Lett. **19** (1965) 141. 311
- [Sa 68] P. U. Sauer. Nuovo Cim. **57B** (1968) 62. 255
- [Sa 72a] G. R. Satchler. Comments on Nucl. Part. Phys. **5** (1972) 145. 295
- [Sa 72b] G. R. Satchler. Nucl. Phys. **A195** (1972) 1. 295
- [Sa 74] G. R. Satchler. Phys. Rep. **14C** (1974) 97. 295
- [Sa 76] G. R. Satchler. Varenna Lectures **69** (1976) 211. 295

- [SB 63] R. G. Seyler and C. H. Blanchard. Phys. Rev. **131** (1963) 355. 527
- [SB 64] J. L. Schwartz and S. Borowitz. Phys. Rev. **133** (1964) A122. 131
- [SB 75] S. Shlomo and G. F. Bertsch. Nucl. Phys. **A243** (1975) 507. 324
- [SB 79] P. Schuck and J. Bartel. Proceedings of the Workshop on the Time Dependent HF Method. Orsay, Saclay, 1979. P. Bonche, B. Giraud and P. Quentin, Eds. Editions de Physique, Paris 1979. 573, 574
- [SBB 80] F. E. Serr, G. F. Bertsch, and J. Borysowicz. Phys. Lett. **92B** (1980) 241. 568
- [SBC 76] R. S. Simon, M. V. Banaschik, P. Colombani, D. P. Soroka, F. S. Stephens, and R. M. Diamond. Phys. Rev. Lett. **36** (1976) 359. 98, 139
- [SBD 77] R. S. Simon, M. V. Banaschik, R. M. Diamond, J. O. Newton, and F. S. Stephens. Nucl. Phys. **A290** (1977) 253. 98, 99
- [SBP 67] G. G. Seaman, E. M. Bernstein, and J. M. Palms. Phys. Rev. **161** (1967) 1223. 125
- [Sch 61] H. Schmidt. Diploma Thesis, University of Frankfurt am Main (1961) (unpublished). 129, 252
- [Sch 64a] H. Schmidt. Congrès Internationale de Physique Nucléaire, Centre de la Recherche Scientifique, Paris, 1964. P. Guggenberger, Ed. Paris, 1964. 300, 340
- [Sch 64b] H. Schmidt. Z. Phys. **181** (1964) 532. 300, 340
- [Sch 65] J. Schwinger. Quantum Theory of Angular Momentum. L. Biedenharn and H. Van Dam, Eds. Academic, New York 1965. 350
- [Sch 68] L. I. Schiff. Quantum Mechanics. McGraw-Hill, New York, 1968. 524
- [Sch 71a] H. Schmidt. Varenna Lectures **53** (1971) 144. 445, 449
- [Sch 71b] J. P. Schiffer. Ann. Phys. (New York) **66** (1971) 798. 186
- [Sch 71c] P. Schuck. Z. Phys. **241** (1971) 395. 640
- [Sch 72a] P. Schuck. J. Low Temp. Phys. **7** (1972) 459. 553
- [Sch 72b] J. P. Schiffer. Proceedings of the International Symposium on the Two Body Force in Nuclei, Gall Lake, Michigan, 1972. S. M. Austin and G. M. Crawley, Eds. Plenum, New York, 1972. 173, 186, 187
- [Sch 75] T. H. Schulcan. Lecture Notes in Physics **40**. B. R. Barret, Ed. Springer-Verlag, Berlin, 1975. 170
- [Sch 76] P. Schuck. Z. Phys. **A279** (1976) 31. 368, 397, 640
- [Sch 77a] G. Schütte. Z. Phys. **A283** (1977) 183. 526
- [Sch 77b] B. Schwesinger. Z. Phys. **A282** (1977) 173; **A287** (1978) 373. 456
- [SCM 73] A. Scott, F. Chu, and D. McLaughlin. Proc. IEEE **61** (1973) 1443. 500
- [SDG 76] G. Scharff-Goldhaber, C. B. Dover, and A. L. Goodman. Ann. Rev. Nucl. Sci. **26** (1976) 239. 24, 104
- [SDL 72] F. S. Stephens, R. M. Diamond, J. R. Leigh, T. Kammuri, and K. Nakai. Phys. Rev. Lett. **29** (1972) 438. 117
- [SDN 73] F. S. Stephens, R. M. Diamond, and S. G. Nilsson. Phys. Lett. **44B** (1973) 429. 115
- [Se 64] E. Segré. Nuclei and Particles. Benjamin, New York, 1964. 64
- [SE 73] P. Schuck and S. Ehofer. Nucl. Phys. **A212** (1973) 269. 311, 361, 640
- [SEB 74] K. A. Snover, K. Ebisawa, D. R. Brown, and P. Paul. Phys. Rev. Lett. **32** (1974) 317. 297
- [SF 74] A. De Shalit and H. Feshbach. Theoretical Nuclear Physics, Vol. I, Nuclear Structure. Wiley, New York, 1974. 1, 5, 97, 163, 167, 333, 580, 581, 593, 594
- [SFW 69] P. U. Sauer, A. Faessler, H. H. Wolter, and M. M. Stingl. Nucl. Phys. **A125** (1969) 257. 209
- [SG 68] W. Scheid and W. Greiner. Ann. Phys. (New York) **48** (1968) 493. 452, 456

- [SG 79] K. W. Schmid and F. Grümmer. *Z. Phys.* **A292** (1979) 15. 462
- [SGM 71] D. Scharnweber, W. Greiner, and U. Mosel. *Nucl. Phys.* **A164** (1971) 257. 81
- [Sh 65] J. Shapiro. *J. Math. Phys.* **6** (1965) 1680. 482
- [SH 78] H. Sagawa and G. Holzwarth. *Progr. Theor. Phys.* **59** (1978) 1213. 566, 568
- [SHJ 73] Ø. Saethre, S. A. Hjorth, A. Johnson, S. Jägare, H. Ryde, and Z. Szymanski. *Nucl. Phys.* **A207** (1973) 486. 103
- [Si 37] A. J. F. Siegert. *Phys. Rev.* **52** (1937) 787. 63
- [SI 75] V. M. Strutinski and F. A. Ivanjuk. *Nucl. Phys.* **A255** (1975) 405. 86, 89
- [SJ 50] H. Steinwedel and J. H. D. Jensen. *Z. Naturforschung* **5A** (1950) 413. 558
- [Sk 56] T. H. R. Skyrme. *Phil. Mag.* **1** (1956) 1043. 175
- [Sk 57] T. H. R. Skyrme. *Proc. Phys. Soc. (London)* **A70** (1957) 433. 472
- [Sk 59] T. H. R. Skyrme. *Nucl. Phys.* **9** (1959) 615. 175
- [SK 65] L. A. Sliv and Y. I. Kharitonov. *Phys. Lett.* **16** (1965) 176. 56
- [SKS 74] F. S. Stephens, P. Kleinheinz, R. K. Sheline, and R. S. Simon. *Nucl. Phys.* **A222** (1974) 235. 119
- [Sl 51] J. C. Slater. *Phys. Rev.* **81** (1951) 385. 209
- [SLD 65] F. S. Stephens, N. L. Lark, and R. M. Diamond. *Nucl. Phys.* **63** (1965) 82. 97
- [SLO 78] S. Stringari, E. Lipparini, G. Orlandini, M. Traini, and R. Leonardi. *Nucl. Phys.* **A309** (1978) 177. 322, 333
- [SLR 73] G. Saunier, J. LeTourneau, B. Rouben, and R. Padjen. *Can. J. Phys.* **51** (1973) 629. 329
- [SM 72] H. W. Schmitt and U. Mosel. *Nucl. Phys.* **A186** (1972) 1.
- [SM 76] V. M. Strutinski and A. G. Magner. *Sov. J. Part. Nucl.* **7** (1976) 138. 82
- [SM 78] B. Sinha and S. A. Motszkowski. *Nucl. Phys.* **A302** (1978) 237. 209
- [SMO 77] V. M. Strutinski, A. G. Magner, S. R. Ofengenden, and T. Delsing. *Z. Phys.* **A283** (1977) 269. 82
- [So 61] V. G. Soloviev. *Kgl. Dan. Vid. Selsk. Mat. Fys. Skr.* **1** (No. 11) (1961). 238
- [So 57] J. M. Soper. *Phil. Mag.* **2** (1957) 1219. 174
- [So 65] V. G. Soloviev. *Nucl. Phys.* **69** (1965) 1. 345
- [So 67] A. Sobiczewski. *Nucl. Phys.* **A93** (1967) 353. 80
- [So 69] J. M. Soper. Isospin Purity of Lowlying Nuclear States. In D. H. Wilkinson, Ed. *Isospin in Nuclear Physics*. North Holland, Amsterdam, 1969. 36
- [So 71] V. G. Soloviev. *Theory of Complex Nuclei*. Nauka, Moscow, 1971. 343
- [So 72] R. A. Sorensen. *Phys. Lett.* **38B** (1972) 376. 463, 465
- [So 73] R. A. Sorensen. *Rev. Mod. Phys.* **45** (1973) 353. 103, 127
- [So 77] R. A. Sorensen. *Nucl. Phys.* **A281** (1977) 475. 478
- [So 67] B. Sørensen. *Nucl. Phys.* **A97** (1967) 1. 362, 380
- [So 68a] B. Sørensen. *Nucl. Phys.* **A119** (1968) 65. 362, 380
- [So 68b] B. Sørensen. *Progr. Theor. Phys.* **39** (1968) 1468. 362, 380
- [So 69] B. Sørensen. *Nucl. Phys.* **A134** (1969) 1. 362, 380
- [So 70] B. Sørensen. *Nucl. Phys.* **A142** (1970) 392, 411. 346, 362, 380
- [So 71] B. Sørensen. *Nucl. Phys.* **A177** (1971) 465. 343, 362
- [So 73] B. Sørensen. *Nucl. Phys.* **A217** (1973) 505. 362
- [Sp 68] B. M. Spicer. *Adv. Nucl. Phys.* **2** (1969) 1. 293
- [Sp 72] D. W. L. Sprung. *Adv. Nucl. Phys.* **5** (1972) 225. 206
- [Sp 74] H. J. Specht. *Rev. Mod. Phys.* **46** (1974) 773. 67
- [SP 70] G. Saunier and J. M. Pearson. *Phys. Rev. C1* (1970) 1353. 209

- [SP 77a] D. Schütte and J. Da Providencia. *Nucl. Phys.* **A282** (1977) 518. 446
- [SP 77b] B. Silvestre-Brac and R. Piepenbring. *Nucl. Phys.* **A288** (1977) 408. 362
- [SP 77c] B. Silvestre-Brac and R. Piepenbring. *Phys. Rev. C16* (1977) 1638. 365
- [SP 78] B. Silvestre-Brac and R. Piepenbring. *Phys. Rev. C17* (1978) 364. 364
- [SR 76] T. Suzuki and D. J. Rowe. *Phys. Lett.* **61B** (1976) 417. 336
- [SR 77] T. Suzuki and D. J. Rowe. *Nucl. Phys.* **A286** (1977) 307. 336, 561
- [SR 78] T. S. Sandhu and M. L. Rustgi. *Phys. Rev. C17* (1978) 796. 463
- [SS 72a] F. S. Stephens and R. S. Simon. *Nucl. Phys.* **A183** (1972) 257. 101, 107, 121, 276
- [SS 72b] C. D. Siegal and R. A. Sorensen. *Nucl. Phys.* **A184** (1972) 81. 435, 436
- [SS 76] M. K. Srivastava and D. W. L. Sprung. *Adv. Nucl. Phys.* **8** (1976) 121. 187
- [SSM 75] R. O. Sayer, J. S. Smith, and W. T. Milner. *Atomic Data and Nuclear Data Tables* **15** (1975) 85. 103
- [SSV 77] V. G. Soloviev, C. Stoyanov, and A. I. Vdovin. *Nucl. Phys.* **A288** (1977) 376. 323
- [SSW 69] A. Sobczewski, Z. Szymański, S. Wycech, S. G. Nilsson, J. R. Nix, C. F. Tsang, C. Gustafson, P. Möller, and B. Nilsson. *Nucl. Phys.* **A131** (1969) 67. 526
- [St 66] V. M. Strutinski. *Yad. Fiz.* **3** (1966) 614. 67
- [St 67] V. M. Strutinski. *Nucl. Phys.* **A95** (1967) 420. 83
- [St 68] V. M. Strutinski. *Nucl. Phys.* **A122** (1968) 1. 83, 93
- [St 74] V. M. Strutinski. *Nucl. Phys.* **A218** (1974) 169. 93
- [St 75a] F. S. Stephens. *Rev. Mod. Phys.* **47** (1975) 43. 110, 114, 118
- [St 75b] V. M. Strutinski. *Nukleonika* **20** (1975) 679. 82
- [St 76] F. S. Stephens. *Varenna Lectures* **69** (1976) 172. 97, 107, 185
- [St 77] V. M. Strutinski. *Z. Phys.* **A280** (1977) 99. 521, 526
- [St 78] A. P. Stamp. *Z. Phys.* **A284** (1978) 305. 136
- [St 79] S. Stringari. *Nucl. Phys.* **A325** (1979) 199. 292, 337, 339, 563
- [ST 63] A. De Shalit and I. Talmi. *Nuclear Shell Structure*. Academic, New York, 1963. 51, 288
- [ST 76] J. P. Schiffer and W. W. True. *Rev. Mod. Phys.* **48** (1976) 191. 185
- [ST 77] M. Sasao and Y. Torizuka. *Phys. Rev. C15* (1977) 217. 296
- [Su 73] T. Suzuki. *Nucl. Phys.* **A217** (1973) 182. 334
- [Sü 54] G. Süssmann. *Z. Phys.* **139** (1954) 543. 454
- [SV 63] V. G. Soloviev and P. Vogel. *Phys. Lett.* **6** (1963) 126. 345
- [SV 73] B. C. Smith and A. B. Volkov. *Phys. Lett.* **47B** (1973) 193. 107
- [SVE 76] P. Sperr, S. Vigdor, Y. Eisen, W. Henning, D. G. Kovar, T. R. Ophel, and B. Zeidman. *Phys. Rev. Lett.* **36** (1976) 405. 505
- [Sw 55] W. J. Swiatecki. *Proc. Phys. Soc. (London)* **A65** (1955) 285. 545
- [SW 66] A. De Shalit and J. D. Walecka. *Phys. Rev.* **147** (1966) 763. 174
- [SW 72] T. H. Schucan and H. A. Weidenmüller. *Ann. Phys. (New York)* **73** (1972) 108. 170
- [SW 73] T. H. Schucan and H. A. Weidenmüller. *Ann. Phys. (New York)* **76** (1973) 483. 170
- [SW 75a] G. Schütte and L. Willets. *Nucl. Phys.* **A252** (1975) 21. 526
- [SW 75b] G. Schütte and L. Willets. *Phys. Rev. C12* (1975) 2100. 526
- [SW 78] G. Schütte and L. Willets. *Z. Phys.* **A286** (1978) 313. 526
- [SWK 72] H. J. Specht, J. Weber, E. Konecny, and D. Heunemann. *Phys. Lett.* **41B** (1972) 43. 67

- [SWK 76] J. Speth, J. Wambach, V. Klemi, and S. Krewald. Phys. Lett. **63B** (1976) 257. 297
- [SWR 76] P. Schuck, R. Wittmann, and P. Ring. Lett. Nuovo Cim. **17** (1976) 107. 368, 391
- [SWW 77] J. Speth, E. Werner, and W. Wild. Phys. Rep. **33C** (1977) 127. 327
- [Sz 61] Z. Szymański. Nucl. Phys. **28** (1961) 63. 80
- [SZ 72] M. Soyeur and A. P. Zuker. Phys. Lett. **41B** (1972) 135. 50, 435
- [SZ 73] R. W. Sharp and L. Zamick. Nucl. Phys. **A208** (1973) 130. 329
- [SZR 74] J. Speth, L. Zamick, and P. Ring. Nucl. Phys. **A232** (1974) 1. 296
- [Ta 56a] L. J. Tassie. Austr. J. Phys. **9** (1956) 407. 336, 360
- [Ta 56b] T. Tamura. Nuovo Cim. **4** (1956) 713. 453
- [Ta 62] I. Talmi. Rev. Mod. Phys. **34** (1962) 704. 185
- [Ta 64] F. Tabakin. Ann. Phys. (New York) **30** (1964) 51. 155
- [Ta 71] I. Talmi. Nucl. Phys. **A172** (1971) 1. 228
- [Ta 76] I. Talmi. Varenna Lectures **69** (1976) 352. 228
- [TA 79] T. Troudet and R. Arvieu. Phys. Lett. **82B** (1979) 308. 136
- [TBK 70] D. R. Tuerpe, W. H. Bassichis, and A. K. Kerman. Nucl. Phys. **A142** (1970) 49.
- [TF 75] H. Toki and A. Faessler. Nucl. Phys. **A253** (1975) 231. 27, 122
- [TG 69] S. N. Tewari and D. Grillot. Phys. Rev. **177** (1969) 1717. 481
- [Th 27] L. H. Thomas. Proc. Camb. Phil. Soc. **23** (1927) 542. 528
- [Th 60] D. J. Thouless. Nucl. Phys. **21** (1960) 225. 310, 615
- [Th 61a] D. J. Thouless. Nucl. Phys. **22** (1961) 78. 305, 331
- [Th 61b] D. J. Thouless. The Quantum Mechanics of Many Body Systems. Academic, New York, 1961. 528, 530, 556, 602, 603
- [Th 73] P. Thieberger. Phys. Lett. **45B** (1973) 417. 107
- [TIS 75] Y. Torizuka, K. Itoh, Y. M. Shin, Y. Kawazoe, H. Matsuzaki, and G. Takeda. Phys. Rev. **C11** (1975) 1174. 297
- [TK 73] T. Tamura and T. Kishimoto. J. Phys. Soc. Japan **34** Suppl. (1973) 393. 391
- [TK 76] J. Treiner and H. Krivine. J. Phys. (G. B.) **G2** (1976) 285. 209
- [TNV 77] H. Toki, K. Neergård, P. Vogel, and A. Faessler. Nucl. Phys. **A279** (1977) 1. 122
- [To 55] S. Tomonaga. Progr. Theor. Phys. **13** (1955) 467, 482. 454
- [TP 78] A. F. R. De Toledo Piza and E. J. V. De Passos. Nuovo Cim. **45B** (1978) 1. 400, 401
- [TPG 77] A. F. R. De Toledo Piza, E. J. V. De Passos, D. Galetti, M. C. Nemes, and M. M. Watanabe. Phys. Rev. **C15** (1977) 1477. 400
- [TQ 74] C. Titin-Schnaider and P. Quentin. Phys. Lett. **49B** (1974) 397. 209
- [TRG 73] The Resonating Group. Generator Coordinate Method for Nuclear Bound States and Reactions. Fizika **5** Suppl. (1973). 399
- [Ts 78] S. F. Tsai. Phys. Rev. **C17** (1978) 1862. 324
- [TU 64] T. Tamura and T. Udagawa. Nucl. Phys. **53** (1964) 33. 311
- [TV 62] D. J. Thouless and J. G. Valatin. Nucl. Phys. **31** (1962) 211. 312, 322
- [TW 73] W. Theis and E. Werner. Phys. Lett. **44B** (1973) 481. 339
- [TW 78] W. Theis and E. Werner. Z. Phys. **A287** (1978) 323. 328
- [Ty 70] A. S. Tyapin. Yad. Fiz. **11** (1970) 98. 139
- [Ty 71] A. S. Tyapin. Yad. Fiz. **14** (1971) 88. 139

- [TYF 77] H. Toki, H. L. Yadav, and A. Faessler. Phys. Lett. **66B** (1977) 310; **71B** (1977) I. 122
- [UB 68] H. Uti and L. C. Biedenharn. Phys. Lett. **27B** (1968) 608. 413
- [Ue 71] H. Ueberall. Electron Scattering from Complex Nuclei. Academic, New York, 1971. 295
- [UF 74] G. Uhlenbeck and G. Ford. Lectures in Statistical Mechanics. American Mathematical Society, Providence, RI, 1974. 553, 555, 556, 557
- [UIO 76] T. Ueda, A. Ikeda and N. Onishi. Progr. Theor. Phys. **55** (1976) 498. 475
- [Ul 71] N. Ullah. Phys. Rev. Lett. **27** (1971) 439. 474
- [Ul 72] N. Ullah. Phys. Rev. **C5** (1972) 285. 474
- [Un 63] I. Unna. Phys. Rev. **132** (1963) 2225. 482
- [UR 69] N. Ullah and D. J. Rowe. Phys. Rev. **188** (1969) 1640. 311
- [UR 71] N. Ullah and D. J. Rowe. Nucl. Phys. **A163** (1971) 257. 307
- [Us 60] T. Usui. Progr. Theor. Phys. **23** (1960) 787. 370
- [UT 58] I. Unna and I. Talmi. Phys. Rev. **112** (1958) 452. 456
- [UW 65] I. Unna and J. Weneser. Phys. Rev. **137** (1965) B1455. 440
- [Va 56] J. G. Valatin. Proc. Roy. Soc. (London) **A238** (1956) 132. 128, 133, 135
- [Va 61] J. G. Valatin. Phys. Rev. **122** (1961) 1012. 245, 252
- [Va 73] D. Vautherin. Phys. Rev. **C7** (1973) 296. 264
- [Va 75] D. Vautherin. Phys. Lett. **57B** (1975) 425. 523
- [Va 77] R. Vandenberghe. Ann. Rev. Nucl. Sci. **27** (1977) I. 67
- [VB 72] D. Vautherin and D. M. Brink. Phys. Rev. **C5** (1972) 626. 176, 209, 210, 212, 214
- [VC 70] F. Villars and G. Cooper. Ann. Phys. (New York) **56** (1970) 224. 109, 453, 457, 458
- [Ve 60] B. J. Verhaar. Nucl. Phys. **21** (1960) 508. 456
- [Ve 63] B. J. Verhaar. Nucl. Phys. **45** (1963) 129. 469
- [Ve 64] B. J. Verhaar. Nucl. Phys. **54** (1964) 641. 469
- [Ve 68] J. D. Vergados. Nucl. Phys. **A111** (1968) 681. 379
- [VF 57] W. M. Visscher and R. A. Ferrell. Phys. Rev. **107** (1957) 781. 174
- [VG 71] J. P. Vary and J. N. Ginocchio. Nucl. Phys. **A166** (1971) 479. 341
- [VGB 72] M. J. A. De Voigt, P. W. M. Glaudemans, J. De Boer, and B. H. Wildenthal. Nucl. Phys. **A186** (1972) 365. 50
- [VH 70] M. Vujičić and F. Herbut. Nuovo Cim. **65B** (1970) 221. 251
- [Vi 57a] F. Villars. Nucl. Phys. **3** (1957) 240. 452, 457
- [Vi 57b] F. Villars. Ann. Rev. Nucl. Sci. **7** (1957) 185. 127, 452, 454, 457
- [Vi 58] F. Villars. Ann. Phys. (New York) **5** (1958) 224. 452
- [Vi 63] F. Villars. Varenna Lectures **23** (1963) I. 472
- [Vi 66] F. Villars. Varenna Lectures **36** (1966) I. 14. 470, 474, 480
- [Vi 71] F. Villars. Proceedings of the International Conference on Dynamic Structures of Nuclear States, Mont Tremblant, 1971. D. J. Rowe, L. E. Trainor, S. S. M. Wong, T. W. Donnelly, Eds., Toronto, University Press, 1972. 506
- [Vi 75] F. Villars. Proceedings of the International Conference on Nuclear Selfconsistent Fields, Trieste, 1975. G. Ripka and M. Porneuf, Eds. North Holland, Amsterdam, 1975. 424, 425, 428, 431, 506, 517, 518
- [Vi 77] F. Villars. Nucl. Phys. **A285** (1977) 269. 432, 506, 517, 518

- [Vi 78] R. Vinh Mau. The Paris Nucleon-Nucleon Potential. In M. Rho and D. Wilkinson, Eds., Mesons in Nuclei. 36, 148, 155
- [VLS 79] M. Vallieres, S. G. Lie, and D. W. L. Sprung. Can. J. Phys. 56 (1978) 1190; 57 (1979) 601, 470
- [VNR 75] V. Vanagas, E. Nadjakov, and P. Raychev. Bulg. J. Phys. 2 (1975) 558, 377
- [VPK 69] H. Vučetić, A. Plastino, and F. Krmpotić. Z. Phys. 220 (1969) 218, 180
- [Vo 65] A. B. Volkov. Nucl. Phys. 74 (1965) 33, 209
- [Vo 70] P. Vogel. Phys. Lett. 33B (1970) 400, 113
- [Vo 77] A. Voros. Ph. D. Thesis, Université De Paris-Sud, Centre D'Orsay, 1977. 533, 610
- [VS 71] F. Villars and N. Schmeing-Rogerson. Ann. Phys. (New York) 63 (1971) 443, 427, 462, 481
- [Wa 56] Y. Watanabe. Progr. Theor. Phys. 16 (1956) 1, 453
- [Wa 62a] J. D. Walecka. Phys. Rev. 126 (1962) 653, 246
- [Wa 62b] S. Wahlborn. Nucl. Phys. 37 (1962) 554, 238
- [Wa 70a] M. Wakai. Nucl. Phys. A141 (1970) 423, 276
- [Wa 70b] A. Watt. Nucl. Phys. A159 (1970) 202, 481
- [Wa 71] A. Watt. Nucl. Phys. A172 (1971) 260, 481
- [Wa 73] T. Walcher. Proceedings of the International Conference on Nuclear Physics, Munich, 1973. J. De Boer and H. J. Mang, Eds. North Holland, Amsterdam, 1973, 16
- [Wa 74] C. S. Warke. Phys. Rev. C10 (1974) 418, 482
- [WB 69] S. Wahlborn and J. Blomqvist. Nucl. Phys. A133 (1969) 50, 63
- [WBB 75] D. Ward, H. Bertschat, P. A. Butler, P. Colombani, R. M. Diamond, and F. S. Stephens. Phys. Lett. 56B (1975) 139, 107
- [WCL 76] D. Ward, P. Colombani, I. Y. Lee, P. A. Butler, R. S. Simon, R. M. Diamond, and F. S. Stephens. Nucl. Phys. A266 (1976) 194, 26, 97
- [We 35] C. F. von Weizsäcker. Z. Phys. 96 (1935) 431, 4
- [We 50] V. F. Weisskopf. Helv. Phys. Acta 23 (1950) 187; Science 113 (1951) 101, 163
- [We 51] V. F. Weisskopf. Phys. Rev. 83 (1951) 1073, 591, 592
- [We 67] H. A. Weidenmüller. Nucl. Phys. A99 (1967) 269, 323
- [We 76] E. Werner. Z. Phys. A276 (1976) 265, 275, 640
- [We 78] E. Werner. Z. Phys. A284 (1978) 105, 640
- [WE 70] E. Werner and K. Emrich. Z. Phys. 236 (1970) 464, 636
- [WF 78a] M. Wakai and A. Faessler. Nucl. Phys. A295 (1978) 86, 278
- [WF 78b] M. Wakai and A. Faessler. Nucl. Phys. A307 (1978) 349, 98
- [WFS 70] H. H. Wolter, A. Faessler, and P. U. Sauer. Phys. Lett. 31B (1970) 516, 263
- [WFS 71] H. H. Wolter, A. Faessler, and P. U. Sauer. Nucl. Phys. A167 (1971) 108, 262, 263
- [WG 67a] J. D. Walecka and L. C. Gomes. Am. da Acad. Brasileira de Ciencias 39 (1967) 361, 163
- [WG 67b] C. S. Warke and M. R. Gunye. Phys. Rev. 155 (1967) 1084; 156 (1967) 1087, 481
- [Wh 72] R. R. Whitehead. Nucl. Phys. A182 (1972) 290, 50, 288, 435
- [WHG 66] H. J. Weber, M. G. Huber, and W. Greiner. Z. Phys. 190 (1966) 25, 375
- [Wi 32] E. P. Wigner. Phys. Rev. 40 (1932) 749, 536
- [Wi 33] N. Wiener. The Fourier Integral and Certain of its Applications. Cambridge Univ. Press, Cambridge, 1933. 410

- [Wi 34] E. P. Wigner. Phys. Rev. **46** (1934) 1002. 336
- [Wi 37] E. P. Wigner. Phys. Rev. **51** (1937) 106. 54
- [Wi 48] G. C. Wick. Phys. Rev. **73** (1948) 51. 130
- [Wi 50] G. C. Wick. Phys. Rev. **80** (1950) 268. 601
- [Wi 64] L. Wilets. **Theories of Nuclear Fission**. Clarendon, Oxford, 1964. 12, 30, 32
- [Wi 65] J. H. Wilkinson. **The Algebraic Eigenvalue Problem**. Clarendon, Oxford, 1965. 306
- [Wi 67] R. M. Wilcox. J. Math. Phys. **8** (1967) 962. 412
- [Wi 76] B. H. Wildenthal. Varenna Lectures **69** (1976) 383. 50
- [Wi 77] W. Wild. Physikalische Blaetter **33** (1977) 298, 356 (Physik Verlag, Weinheim, Germany). 204, 206
- [WJ 56] L. Wilets and M. Jean. Phys. Rev. **102** (1956) 788. 27, 379
- [WKB 73] W. T. Weng, T. T. S. Kuo, and G. E. Brown. Phys. Lett. **46B** (1973) 329. 294
- [WKS 78] J. Wambach, V. Klemt, and J. Speth. Phys. Lett. **77B** (1978) 245. 296
- [WM 66] K. Wildermuth and W. McClure. Springer Tracts in Modern Physics **41**. G. Höhler, Ed. Springer-Verlag, Berlin, 1966. 399
- [WM 77] C. Y. Wong and J. A. McDonald. Phys. Rev. **C16** (1977) 1196. 561
- [WMH 71] B. H. Wildenthal, J. B. McGrory, E. C. Halbert, and H. D. Gruber. Phys. Rev. **C4** (1971) 1708. 50
- [WMR 77] J. Wambach, V. A. Madsen, G. A. Rinker, and J. Speth. Phys. Rev. Lett. **39** (1977) 1443. 296
- [WMW 75] C. Y. Wong, J. A. Maruhn, and T. A. Welton. Nucl. Phys. **A253** (1975) 469. 527, 561
- [WMW 77] C. Y. Wong, J. A. Maruhn, and T. A. Welton. Phys. Lett. **66B** (1977) 19. 503, 561
- [Wo 70] C. W. Wong. Nucl. Phys. **A147** (1970) 545. 403
- [Wo 75] C. W. Wong. Phys. Rep. **15C** (1975) 283. 399, 459, 472, 481
- [Wo 76] C. Y. Wong. J. Math. Phys. **17** (1976) 1008. 561
- [WP 68] S. A. Williams and D. L. Pursey. J. Math. Phys. **9** (1968) 1230. 375
- [WS 54] R. D. Woods and D. S. Saxon. Phys. Rev. **95** (1954) 577. 40
- [WS 72] W. L. Wang and C. M. Shakin. Phys. Rev. **C5** (1972) 1898. 323, 330
- [WSR 71] S. K. M. Wong, G. Saunier, and B. Rouben. Nucl. Phys. **A169** (1971) 294. 506
- [WU 66] C. Werntz and H. Ueberrall. Phys. Rev. **149** (1966) 762. 336, 560
- [WWC 77] R. R. Whitehead, A. Watt, B. I. Cole, and I. Morrison. Adv. Nucl. Phys. **9** (1977) 123. 50
- [WWM 77] C. Y. Wong, T. A. Welton, and J. A. Maruhn. Phys. Rev. **C15** (1977) 1558. 561

- [Ya 65] M. Yamamura. Progr. Theor. Phys. **33** (1965) 199. 382
- [Ya 67] C. N. Yang. Phys. Rev. Lett. **19** (1967) 1312. 409
- [Ya 74] M. Yamamura. Progr. Theor. Phys. **52** (1974) 538. 349, 352
- [YKD 70] S. Yung-Li, A. Klein, and R. M. Dreizler. J. Math. Phys. **11** (1970) 975. 523
- [YMR 76] D. H. Youngblood, J. M. Moes, C. M. Rozsa, J. D. Bronson, A. D. Bacher, and D. R. Brown. Phys. Rev. **C13** (1976) 994. 295
- [YN 76] M. Yamamura and S. Nishiyama. Progr. Theor. Phys. **56** (1976) 124. 375
- [YN 77] B. Yoon and J. W. Negele. Phys. Rev. **A16** (1977) 1451. 499
- [YNN 76] T. Yamazaki, H. Nakayama, T. Numao, and T. A. Shibata. J. Phys. Soc. Japan **44** (1978) 1421. 122

- [Yo 57] J. Yoccoz. Proc. Phys. Soc. (London) A70 (1957) 388. 469
 [Yo 66] J. Yoccoz. Varenna Lectures 36 (1966) 474. 461
 [YRM 77] D. H. Youngblood, C. M. Rozsa, J. M. Moss, D. R. Brown, and J. D. Bronson. Phys. Rev. Lett. 39 (1977) 1188. 296
 [YSI 78] M. Yamamura, T. Suzuki, and H. Ichihashi. Progr. Theor. Phys. 60 (1978) 197. 351
 [YTF 77] H. L. Yadav, H. Toki, and A. Faessler. Phys. Rev. Lett. 39 (1977) 1128. 122
 [YTF 78] H. L. Yadav, H. Toki, and A. Faessler. Phys. Lett. 76B (1978) 144. 122
 [Yu 35] H. Yukawa. Proc. Phys. Math. Soc. Japan 17 (1935) 48. 155
 [YZ 72] S. Yoshida and L. Zamick. Ann. Rev. Nucl. Sci. 22 (1972) 121.
- [Za 73] L. Zamick. Phys. Lett. 45B (1973) 313; 47B (1973) 119. 334
 [Za 74a] L. Zamick. Nucl. Phys. A232 (1974) 13. 334
 [Za 74b] D. Zawischa. Z. Phys. 266 (1974) 117. 394, 395
 [Ze 32] C. Zener. Proc. Roy. Soc. (London) A137 (1932) 696. 526
 [Ze 65] H. D. Zeh. Z. Phys. 188 (1965) 361. 461, 462, 470
 [Ze 67] H. D. Zeh. Z. Phys. 202 (1967) 38. 459, 476, 477, 480
 [Ze 75] V. G. Zelevinskii. Sov. J. Nucl. Phys. 22 (1975) 565. 133
 [ZGS 67] N. Zeldes, A. Grill, and A. Simicer. Mat. Fys. Skr. Dan. Vid. Selsk. 3 (No. 5) (1967). 236
 [Zi 78] P. G. Zint. Z. Phys. A286 (1978) 281. 277
 [ZN 77] A. Zaringhalam and J. W. Negele. Nucl. Phys. A288 (1977) 417. 470
 [ZR 71] J. Zofka and G. Ripka. Nucl. Phys. A168 (1971) 65. 176, 209
 [ZS 72] V. E. Zakharov and A. B. Shabat. Sov. Phys. JETP 34 (1972) 62. 500
 [ZS 75] D. Zawischa and J. Speth. Phys. Lett. 56B (1975) 225. 345
 [ZS 76] D. Zawischa and J. Speth. Phys. Rev. Lett. 36 (1976) 843. 345
 [ZSP 78] D. Zawischa, J. Speth, and D. Pal. Nucl. Phys. A311 (1978) 445. 345
 [Zu 62] B. Zumino. J. Math. Phys. 3 (1962) 1055. 246, 612

Author Index

To find a given author in the text: Find the author's name in this index. Beside the name is (are) the abbreviation(s) of the reference(s) in which that author appears in the Bibliography. The italic numbers following the Bibliography reference are the page numbers on which that author is mentioned.

- Aas, B. [EAD 75]
Abecasis, S. M. [ABP 68]
Åberg, S. [BLL 75], [ALL 76], [CDS 77], [Ab 78], [AHL 78]
Abgrall, Y. [ABC 69], [CBA 73], [AC 75]
Abramowitz, M. [AS 65]
Abrikosov, A. A. [AG 61], [AGD 63], [AGD 65]
Adachi, S. [AY 78]
Adamchuck, Y. V. [NA 62]
Aguilera, V. C. [AMK 69], [AAZ 77], [ALP 77]
Ahmad, L. [CAF 77]
Alaga, G. [AI 67], [APS 75], [AP 76]
Alberico, W. M. [MJB 75]
Alder, K. [ABH 56], [AW 66], [GPA 71], [GPA 72], [AW 74]
Leonard, M. M. [LAD 77]
Alexeev, V. L. [AEE 78]
Allaart, K. [AGM 74], [AG 74], [GGA 74], [GMA 75], [MAG 75], [MGA 77]
Alves, A. [ABC 77a], [ABC 77b]
Amado, R. D. [AB 59]
Amiet, J. P. [Am 67]
Anantaraman, N. [AS 71]
Andersen, B. L. [ADD 70]
Andersen, O. [ABH 78]
Anderson, D. W. [ABC 63]
Anderson, J. D. [AW 61]
Anderson, P. W. [An 58]
Andersson, C. G. [ALL 76], [AK 77], [CDS 77], [AHL 78]
Andrade, S. G. [AAZ 77]
André, S. [ABR 75]

- Ansari, A. [AN 71]
 Archenhövel, H. [ADW 78]
 Argyres, P. [Ar 65]
 Arima, A. [AY 59], [AH 71b], [IA 74],
 [AI 75a], [AI 75b], [AI 76], [HA
 76], [AOI 77], [AI 78a], [AI 78b],
 [AOI 78], [OAI 78]
 Arita, K. [AH 71a]
 Arseniev, D. A. [ASS 69]
 Arvieu, R. [ABV 63], [Ar 63], [AV 63],
 [ASV 64], [PAM 66], [LA 74], [TA
 79]
 Asaro, F. [PAG 62]
 Auerbach, N. [AHK 72]
 Austern, N. [Au 70]
 Avida, R. [HGA 74]
- Bacher, A. D. [KMY 75], [YMR 76]
 Bacher, R. F. [BB 36]
 Back, B. B. [PBB 77]
 Bäckmann, S. O. [BJS 75]
 Bădea, M. [RGB 77]
 Balazs, N. L. [BZ 73], [BP 77a], [BP
 77b]
 Balian, R. [BB 69], [BD 71], [BB 72],
 [BB 74]
 Baltin, R. [Ba 72b]
 Banaschik, M. V. [BSC 75], [SBC 76],
 [SBD 77]
 Banerjee, B. [BB 73], [BKD 73], [BMR
 73], [DBM 73], [DB 73], [RMB 74]
 Banerjee, P. K. [BS 71]
 Baran, A. [Ba 78]
 Baranger, E. [ABV 63]
 Baranger, M. [Ba 60a], [Ba 61], [ABV
 63], [Ba 63a], [Ba 63b], [BK 65],
 [MB 65], [BK 67b], [BK 68], [KB
 68], [NDK 68], [Ba 69a], [JB 71],
 [Ba 72a], [BV 78]
 Bardeen, J. [BCS 57]
 Bargmann, V. [Ba 62]
 Barnéoud, D. [LRB 72]
 Baron, G. [ABC 69]
 Barrett, B. R. [BK 73]
 Barroso, A. [FDB 77]
 Bartel, J. [SB 79]
 Bar-touv, J. [Ba 67], [BGG 69], [GSB
 70]
 Bassermann, R. [RB 74], [RB 76]
- Bassichis, W. H. [BGR 65], [BKS 67],
 [TBK 70], [BW 71], [BSV 76]
 Bauer, R. [BSK 73], [RBS 73], [BER
 75], [ABH 78]
 Baumgärtner, G. [BS 68a], [Ba 69b]
 Baym, G. [KB 62], [BF 74], [BCD 75]
 Bayman, B. F. [Ba 60b], [MBZ 64]
 Baznat, M. I. [BPC 72]
 Beck, F. A. [BBB 79a]
 Beck, R. [BMR 70], [RBM 70], [BBB
 75]
 Beil, H. [BBL 71]
 Beiner, M. [BFV 74], [BFG 75]
 Bell, J. S. [BS 56]
 Belyaev, S. T. [Be 59], [Be 61], [BZ 62],
 [Be 65], [Be 66], [Be 68]
 Bemis, C. E. [BN 77]
 Bengtsson, R. [BLL 75], [ALL 76],
 [BHM 78], [BS 80]
 Berg, R. A. [BW 56]
 Bergere, R. [BBL 71]
 Bergström, I. [BBH 77]
 Beringer, R. [BK 61]
 Bernstein, E. M. [SBP 67]
 Bernthal, F. M. [PBB 77]
 Bertin, G. [BR 76]
 Bertrand, F. E. [LB 72], [Be 76], [HBI
 77]
 Bertsch, G. F. [Be 73], [Be 74], [Be 75],
 [BT 75], [SB 75], [Be 76a], [BBB
 79b], [SBB 80]
 Berischat, H. [WBB 75]
 Bès, D. R. [BS 61], [Be 63], [BB 66],
 [BS 69], [DB 70], [BB 71], [BBN
 74a], [BBN 74b], [BB 76], [BBB 77]
 Bethe, H. A. [Be 31], [BB 36], [BR 37],
 [BG 57], [BBP 63], [Be 71], [PB 73],
 [MJB 75]
 Beuscher, H. [BDL 75], [NLM 76]
 Bhaduri, R. K. [BR 71b], [JBB 75], [JB
 75], [PB 75], [Bh 77], [EBV 79]
 Biedenharn, L. C. [UB 68]
 Birbrair, B. L. [GB 65], [Bi 68], [BEL
 70], [Bi 76]
 Birkholz, J. [Bi 72], [KBF 74]
 Bjørnholm, S. [PBB 77]
 Blaizot, J. P. [RBK 75], [BGG 76], [Bi
 76], [BG 77], [BM 78], [BS 79]
 Blanchard, C. H. [SB 63]
 Blann, M. [BES 76]

- Blatt, J. M. [BW 52], [BI 60]
 Bleuler, K. [BSB 69]
 Bloch, C. [BI 62], [BM 62], [BG 65],
 [BB 72], [BB 74]
 Blocki, J. [BF 76], [BBN 78]
 Blomqvist, J. [BW 60], [BK 69], [WB
 69], [KBB 70], [BBH 77]
 Böhning, M. [Boe 76]
 Boeker, E. [BB 67], [LB 68], [LB 69]
 Boer, J. De [BE 68]
 Börner, H. G. [AEE 78]
 Bogoliubov, N. N. [Bo 58], [Bo 59a],
 [Bo 59b], [BS 59]
 Bohigas, O. [BCK 76], [BML 76],
 [MBF 76], [BLM 79], [KTB 80]
 Bohm, D. [BP 53]
 Bohr, A. [Bo 51], [Bo 52], [BM 53],
 [Bo 54], [BM 55], [ABH 56], [BMP
 58], [BM 58], [Bo 64], [BM 69],
 [BM 74], [BM 75], [Bo 76a], [Bo
 76b]
 Bohr, N. [BW 39]
 Boisson, J. P. [BP 71], [BPO 76], [BSL
 79]
 Bolsterli, M. [BB 59], [BFN 72]
 Bonaccorso, A. [BTR 77]
 Bonche, P. [BKN 76], [BGK 78], [BQ
 78]
 Boneh, Y. [BBN 78]
 Bonhomme, C. [BBL 80]
 Borg, K. Van der [HBI 77]
 Borggreen, J. [PBB 77]
 Born, M. [BG 49]
 Borowitz, S. [SB 64]
 Bortignon, P. F. [BBB 77], [BBB 79b]
 Borysowicz, J. [BBB 75], [SBB 80]
 Bosch, H. E. [ABP 68]
 Bourotte-Bilwes, B. [CBA 73]
 Bouter, M. [BLD 67], [BBC 72]
 Bouter, M. C. [BBC 72]
 Boutet, J. [BT 71], [ABR 75]
 Bouyssy, A. [BV 71]
 Bozek, E. [BBB 79a]
 Brack, M. [BDJ 72], [BP 73], [BLP 74],
 [BQ 75a], [BQ 75b], [JBB 75], [BJC
 76], [BJ 76b], [Br 77], [CJB 77],
 [DBS 78], [DSB 80]
 Bramblett, R. L. [BCH 64]
 Brandow, B. H. [BBP 63], [Br 67a]
 Breit, G. [LHR 62]
 Bremmer, H. [PB 55]
 Brenig, W. [BS 64], [Br 65b], [MB 69]
 Breuer, H. [KWB 75]
 Brézin, E. [BB 69]
 Brink, D. M. [Br 65a], [BTK 65], [BB
 67], [BW 68], [VB 72], [BB 73], [BC
 73], [BBB 75], [EBG 75], [BGV 76],
 [BL 76], [GMQ 76], [GVV 76]
 Brito, L. P. De [ABC 77a], [ABC 77b]
 Britt, H. C. [BES 76]
 Brockmann, R. [Br 78]
 Broglia, R. A. [BB 66], [BRS 68], [BS
 68b], [BB 71], [BHR 73], [BBN
 74a], [BBN 74b], [BB 76], [BBB 77],
 [BBB 79b]
 Bronson, J. D. [KMY 75], [YMR 76],
 [YRM 77]
 Brown, D. R. [SEB 74], [KMY 75],
 [YMR 76], [YRM 77]
 Brown, G. E. [BB 59], [BET 61], [Br
 64], [KB 66], [BK 67a], [KBB 70],
 [Br 71], [WKB 73], [BJ 76a], [BW
 76], [LB 76], [DSB 77]
 Brueckner, K. A. [Br 55], [GB 57],
 [BGW 58], [AB 59], [BLR 61]
 Brut, F. [RBP 77]
 Bryan, R. A. [Br 67b]
 Buck, B. [BH 67], [MSB 69]
 Buenerd, M. [BBL 80]
 Bunessian, G. G. [BKS 72]
 Bunker, M. E. [BR 71a]
 Bureau, A. J. [ABC 63]
 Burr, W. [BSB 69]
 Buskirk, F. R. [PBD 74]
 Butler, P. A. [WBB 75], [LCS 76],
 [WCL 76]
 Byrski, T. [BBB 79a]
 Cailliau, M. [CLF 73]
 Calarco, J. R. [HGA 74]
 Caldeira, M. H. [FC 72], [ABC 77a],
 [ABC 77b]
 Caldwell, J. T. [BCH 64]
 Camiz, P. [CCJ 65], [CCJ 66]
 Camparat, V. [MMW 75]
 Campbell, D. [BCD 75]
 Campi, X. [CS 72], [BCK 76]
 Carlos, P. [BBL 71]
 Carlson, B. C. [Ca 61], [CM 63]
 Castaños, O. [CCF 79]

- Castell, B. [CP 70]
 Casten, R. F. [CBP 78], [CC 78]
 Castro, J. J. [BC 73]
 Caurier, E. [ABC 69], [BBC 72], [CBA 73], [AC 75]
 Cerkaski, M. [CDS 77]
 Chaban, A. A. [DC 60]
 Chacón, E. [CCF 79]
 Chan, K. Y. [CV 66]
 Chandrasekhar, S. [Ch 69]
 Chang, B. D. [Ch 75]
 Chang, H. C. [DNM 77]
 Chasman, R. R. [CAF 77]
 Chauvin, J. [BBL 80]
 Chen, H. T. [CG 67]
 Chernej, M. I. [BPC 72]
 Chi, B. E. [Ch 66], [Ch 70]
 Christensen, O. [PBB 77]
 Chu, F. [SCM 73]
 Chu, S. Y. [CMR 75]
 Chu, Y. H. [BJC 76], [CJB 77]
 Cizewski, J. A. [CC 78]
 Clark, J. M. [CE 65]
 Cline, D. [LCS 76]
 Coester, F. [Co 55], [Co 56]
 Cohen, S. [CS 62], [CS 63], [CPS 74]
 Cole, B. I. [WWC 77]
 Colombani, P. [BSC 75], [WBB 75], [LCS 76], [SBC 76], [WCL 76]
 Cook, B. C. [ABC 63]
 Cooper, G. [VC 70]
 Cooper, L. N. [BCS 57]
 Corbett, J. O. [Co 71], [Co 72]
 Cottingham, W. N. [CLL 73]
 Covello, A. [CCJ 65], [CCJ 66]
 Crank, J. [CN 47]
 Curry, P. D. [CS 73]
 Cusson, R. Y. [KS 72], [CL 73], [KCS 74], [CM 76], [CSM 76], [MC 76], [CMM 78]
 Cwiok, S. [CDS 78]
 Dabrowski, J. [Da 75]
 Dalafi, H. R. [DBM 73], [DMR 75]
 Dally, E. B. [PBD 74]
 Damgaard, J. [DPP 69], [BDJ 72]
 Dang, G. Do [DK 66], [Da 70], [DDK 71]
 Danos, M. [Da 58]
 Dashen, R. [BCD 75]
 Dasso, C. H. [BBB 79b]
 Das, T. K. [DDK 70], [DB 73]
 Davidson, J. P. [Da 65b], [Da 68]
 Davidson, W. F. [BDL 75], [NLM 76], [AEE 78]
 Davies, K. T. R. [NDK 68], [DMS 72], [DMS 73], [KDM 77], [MDK 77]
 Davydov, A. S. [DF 58], [Da 59], [DR 59], [DC 60], [DA 65a]
 Day, B. D. [Da 67]
 Deal, T. J. [DF 73]
 Decharge, J. [DGG 75], [DG 80]
 Dehesa, J. S. [DKS 77]
 Deleplanque, M. A. [LAD 77]
 Demeur, M. [DR 66]
 Depuydt, H. [BLD 67]
 Detar, C. [De 78]
 Devi, K. R. S. [BKD 73], [FDG 76], [FPD 76], [FDB 77]
 Dey, W. [EAD 75]
 Diamond, R. M. [SLD 65], [SDL 72], [GSD 73], [SDN 73], [MSD 74], [BSC 75], [WBB 75], [Di 76], [LCS 76], [SBC 76], [WCL 76], [LAD 77], [SBD 77]
 Dickmann, F. [ADD 70]
 Didong, M. [DMG 76]
 Dieperink, A. E. L. [GED 71]
 Dietrich, K. [DMP 64], [DMP 66], [DH 68], [ADD 70], [Di 71], [HD 71]
 Dioniso, J. S. [PVD 77]
 Dirac, P. A. M. [Di 30]
 Doechnert, L. [AAZ 77]
 Dönnau, F. [JDF 71], [DJ 73], [JJD 74], [JDJ 75], [DF 77]
 Dolan, L. [Do 76]
 Domingos, J. M. [ABC 77a], [ABC 77b]
 Dominicis, C. De [BD 71]
 Døssing, T. [DNM 77], [SMO 77], [MDN 78]
 Dover, C. B. [SDG 76]
 Dowker, J. S. [MD 73]
 Drechsel, D. [ADW 78]
 Dreher, B. [RFM 74]
 Dreiss, G. J. [DDK 71]
 Dreizler, R. M. [DFG 68], [PKD 68], [JDK 69], [DDK 70], [YKD 70], [DDK 71], [KD 75], [KD 76], [RD 76]

- Druin, V. A. [PDK 62]
 Dudek, J. [ALL 76], [CDS 77], [CDS 78]
 Duhamel, G. [BBL 80]
 Duhm, H. H. [HGH 68]
 Durand, M. [DBS 78], [DSB 80]
 Durso, J. W. [DSB 77]
 Dussel, G. G. [DB 70]
 Dworzecka, M. [KLD 80]
 Dyer, J. N. [PBD 74]
 Dyson, J. F. [Dy 56]
 Dzyaloshinski, I. E. [AGD 63], [AGD 65]
- Easson, I. [EVB 79]
 Ebersold, P. [EAD 75]
 Ebert, D. [ER 78]
 Ebert, K. [BER 75], [ERW 78]
 Ebisawa, K. [SEB 74]
 Eckart, G. [EH 77], [HE 77], [HE 78], [HE 79], [EH 79], [EHS 80]
 Edmonds, A. R. [Ed 57]
 Egido, J. L. [ERM 78], [EMR 80a], [EMR 80b], [ER 80]
 Egorov, A. I. [AEE 78]
 Ehlers, J. W. [EM 72], [FGE 72]
 Eichler, E. [RSS 74], [LCS 76], [HJE 78]
 Eichler, J. [BE 68]
 Eichler, R. [EAD 75]
 Eisen, Y. [SVE 76]
 Eisenberg, J. M. [EG 70]
 El-Jaick, L. J. [MSK 77]
 Ellegaard, C. [EKV 69]
 Elliott, J. P. [ES 55], [EF 57], [EL 57], [El 58], [CE 65], [EJM 68]
 Ellis, P. J. [El 70], [EO 77]
 El-Masri, Y. [LAD 77]
 Emelianov, B. A. [AEE 78]
 Emrich, K. [WE 70]
 Endt, P. M. [GED 71]
 Engelbrecht, C. A. [EW 72]
 Engel, Y. M. [EBG 75]
 Erkkila, B. H. [BES 76]
 Erokhina, K. I. [BEL 70]
 Erskine, J. R. [CAF 77]
 Estle, T. L. [MEL 76]
 Ethofer, S. [ES 69], [SE 73]
 Evans, J. A. [BET 61], [MLE 67]
- Faessler, A. [FG 62], [FG 64], [FGS 65], [FGS 66], [FS 66], [FPM 67], [FP 67], [Fae 68], [SFW 69], [WFS 70], [WFS 71], [FGE 72], [GFW 72], [FGP 73], [FLW 73], [GGF 73], [AGM 74], [GGA 74], [KBF 74], [FT 75], [GMA 75], [GSF 75], [MAG 75], [TF 75], [DMG 76], [FDG 76], [FPD 76], [KRG 76], [DKS 77], [FDB 77], [KKS 77], [MGA 77], [NTP 77], [TNV 77], [TYF 77], [YTF 77], [FP 78], [GSF 78a], [GSF 78b], [PFL 78], [PTF 78], [WF 78a], [WF 78b], [YTF 78], [FPS 80]
- Fallieros, S. [KF 70], [DF 73], [MBF 76]
 Fantoni, S. [FR 75], [FR 76a]
 Federman, P. [DFG 68]
 Fedotov, S. I. [GIS 73]
 Felderhof, B. U. [FR 76b]
 Feldmeier, H. [KDM 77]
 Fellah, M. [FHM 73]
 Ferguson, R. L. [BES 76]
 Fermi, E. [Fe 28]
 Ferreira, L. S. [PUF 71], [FC 72]
 Ferrell, R. A. [FV 56], [Fe 57], [VF 57]
 Feshbach, H. [Fe 58], [Fe 62], [SF 74]
 Fetter, A. L. [FW 71]
 Feynman, R. P. [Fe 39], [FH 65]
 Filippov, B. F. [DF 58]
 Fink, B. [FKS 72]
 Fiset, E. O. [BFN 72]
 Fleckner, J. [FMR 79]
 Fliessbach, T. [Fl 72]
 Flocard, H. [CLF 73], [FQK 73], [FQV 73], [BFV 74], [FQV 74], [FV 74], [BFG 75], [FV 75], [BF 76], [FV 76], [FKW 78], [FW 78], [QF 78]
 Flowers, B. H. [EF 57]
 Flowers, E. [BF 74]
 Flügge, S. [Fl 71]
 Fock, V. A. [Fo 28], [Fo 30]
 Folkmann, F. [PBB 77]
 Fomenko, V. N. [Fo 70]
 Fomichev, V. A. [PDK 62]
 Fonte, G. [FS 76]
 Ford, G. [UF 74]
 Fraenkel, Z. [LPP 75], [LPF 77]
 Frank, A. [CCF 79]

- Frascaria, R. [MMW 75]
 Frauendorf, S. [FJM 71], [JDF 71],
 [Fr 76], [NPF 76], [DF 77]
 Fredriksson, S. [OWP 71]
 French, J. B. [FHM 69]
 Freinkel, J. [Fr 39]
 Frey, R. [FRS 78]
 Friar, J. L. [FN 76]
 Friedman, A. M. [CAF 77]
 Friedman, W. A. [FW 70]
 Friedrich, H. [FHW 74]
 Friedrich, J. [RFM 74]
 Frisch, O. R. [MF 39]
 Fritsch, W. [FLW 75]
 Fukuda, N. [FIS 64]
 Fukuda, S. [FT 72]
 Fukutome, H. [Fu 77], [FYN 77]
 Fuller, E. G. [FH 62a], [FH 62b]
 Fultz, S. C. [BCH 64]
- Galetti, D. [TPG 77]
 Galonska, J. E. [FGE 72], [KRG 76]
 Gammel, J. L. [BGW 58]
 Gantmacher, F. R. [Ga 72]
 Garbaczewski, P. [Ga 78]
 Garcia, J. [GGF 73]
 Gareev, F. A. [GIS 73]
 Gartenhaus, S. [GS 57]
 Gehring, C. [BBB 79a]
 Gell-Mann, M. [GB 57]
 Gheorghe, A. [RGB 77]
 Ghiorso, A. [PAG 62]
 Giai, N. Van [BFG 75], [LG 76b]
 Giannoni, M. J. [BGV 76], [GMQ 76],
 [GVV 76], [GQ 80]
 Gilat, J. [GG 67]
 Gillet, V. [ABV 63], [Gi 64], [GS 64],
 [GV 64], [BG 65], [GGS 66]
 Ginocchio, J. N. [GW 68], [VG 71]
 Giraud, B. G. [GL 77]
 Giraud, B. [BGR 65], [DFG 68], [GS
 69], [GLW 70], [GG 74a], [GG 75]
 Girod, M. [DGG 75], [GG 78], [GG
 79]
 Gjotterud, O. K. [ORG 75]
 Glas, D. [GMZ 78]
 Glauber, R. J. [GI 63]
 Glaudemans, P. W. M. [GED 71],
 [VGB 72]
 Glavish, H. F. [HGA 74]
 Glen, J. A. [GM 71]
- Glendenning, N. K. [GI 65], [HGH
 68]
 Glick, A. J. [LMG 65]
 Gneuss, G. [GMG 69], [GMG 70],
 [GG 71]
 Goeke, K. [GFW 72], [GGF 73],
 [AGM 74], [GGA 74], [KG 74],
 [EBG 75], [GMA 75], [MAG 75],
 [DMG 76], [Go 76b], [Go 77],
 [MGA 77], [RG 77], [GLM 78],
 [GR 78], [RG 78]
 Götz, U. [GPA 71], [GPA 72]
 Gogny, D. [Go 73], [DGG 75], [Go
 75a], [Go 75b], [BGG 76], [BG 77],
 [DG 80]
 Goldhaber, M. [GT 48]
 Goldstein, H. [Go 59]
 Goldstone, J. [BG 57]
 Golin, M. [GSZ 74]
 Gombas, P. [Go 48], [Go 52]
 Gomes, L. C. [GWW 58], [WG 67a]
 Goodman, A. L. [GSG 68], [BGG 69],
 [GSB 70], [Go 72], [GG 74b], [Go
 74], [Go 76a], [GVS 76], [SDG 76],
 [MG 78], [Go 79]
 Gorkov, L. P. [Go 58], [AG 61], [AGD
 63], [AGD 65]
 Goswami, A. [GP 63], [Go 64], [GK
 65], [CG 67], [GLS 67], [GSG 68],
 [BGG 69], [GNS 70], [GSB 70],
 [GG 74b]
 Graber, H. D. [WMH 71]
 Grammaticos, B. [GG 74a], [GG 75],
 [BGG 76], [BGK 78], [GG 78],
 [GG 79], [GV 79]
 Green, A. M. [GGS 66], [MMG 67]
 Green, I. M. [GM 65]
 Greene, H. S. [BG 49]
 Greiner, W. [FG 62], [FG 64], [FGS
 65], [FGS 66], [WHG 66], [SG 68],
 [GMG 69], [HMG 69], [EG 70],
 [GMG 70], [GG 71], [GMG 71],
 [SGM 71], [FKS 72], [MG 72]
 Griffin, J. E. [ABC 63]
 Griffin, J. J. [GW 57], [GR 60], [Gr
 71], [LG 76a], [KG 78], [KLD 80]
 Griffin, R. E. [GVL 73]
 Grill, A. [ZGS 67]
 Grillot, D. [TG 69]
 Grin, Y. T. [Gr 74]
 Grodzins, L. [Gr 62]

- Gromov, K. Y. [GSK 75]
 Gronewald, H. J. [Gr 46]
 Gross, D. H. E. [GL 70], [GY 70], [Gr 72]
 Gross, E. P. [Gr 60]
 Grosse, E. [GSD 73]
 Grover, J. R. [GG 67], [Gr 67]
 Grüninger, F. [FGP 73], [GGA 74], [GSF 75], [FDG 76], [GSF 78a], [GSF 78b], [SG 79]
 Grumann, J. [GMG 71]
 Gugelot, P. C. [MG 63]
 Guidry, H. W. [LCS 76]
 Guman, V. N. [GB 65]
 Gumpertsberger, G. [GS 77]
 Gunsteren, W. F. Van [AG 74]
 Gunye, M. R. [WG 67b]
 Gustafson, C. [GLN 67], [NTS 69], [SSW 69]
 Gutbrod, H. H. [BES 76]

 Haapakoski, P. [HNL 70]
 Hadermann, J. [HR 74], [JH 77]
 Hafele, J. C. [Ha 67]
 Haff, P. K. [HW 72], [HW 74]
 Hage-Hassan, M. [HL 72b]
 Hagemann, G. B. [RSS 74], [ABH 78]
 Hagemann, K. A. [HRH 70]
 Halbert, E. C. [FHM 69], [HMW 71], [WMH 71], [HMS 75]
 Halbert, M. L. [ABH 78]
 Hamada, T. [HJ 62]
 Hamamoto, I. [AH 71b], [Ha 72], [Ha 74a], [Ha 76], [Ha 77], [BHM 78]
 Hamman, T. F. [FHM 73]
 Hanna, S. S. [Ha 74b], [HGA 74]
 Hansen, O. [BHR 73]
 Hara, K. [DH 68], [HK 75], [HI 79], [HIT 79]
 Harakeh, M. N. [HBI 77]
 Harris, S. M. [Ha 65a]
 Hartree, D. R. [Ha 28]
 Harvey, B. G. [HGH 68]
 Harvey, M. [Ha 68]
 Harvey, R. R. [BCH 64]
 Haxel, O. [HJS 49]
 Hayakawa, S. [HM 57]
 Hayward, E. [FH 62a], [FH 62b], [Ha 65b]
 Hecht, K. T. [HS 62], [He 71], [He 73a]
 Heisenberg, W. [He 32]
 Hellmeister, H. P. [HLM 78]
 Hellström, G. [AHL 78]
 Helmer, R. G. [HR 68]
 Hendrie, D. L. [HGH 68]
 Henning, W. [SVE 76]
 Hensley, D. C. [RSS 74]
 Herbut, F. [HV 68], [VH 70]
 Herlander, C. J. [BBH 77]
 Herling, G. H. [HK 72]
 Herskind, B. [PBB 77], [ABH 78]
 Hertz, G. [He 61]
 Hetherington, J. H. [He 73b]
 Heunemann, D. [SWK 72]
 Hibbs, A. R. [FH 65]
 Hilf, E. R. [MSK 77]
 Hill, A. D. [BH 67]
 Hill, D. L. [HW 53]
 Hillman, P. [MHT 58]
 Hilton, R. R. [FDG 76]
 Hjorth, S. A. [HRH 70], [JRH 72], [SHJ 73], [HK 77]
 Hodgson, P. E. [Ho 71b]
 Hofmann, H. [HD 71]
 Hofmann, H. M. [HLR 74]
 Högaasen-Feldman, J. [Ho 61]
 Hohenberg, P. [HK 64]
 Holinde, K. [NMH 73], [Ho 80]
 Holstein, T. [HP 40]
 Holzer, P. [HMG 69]
 Holzwarth, G. [Ho 68], [Ho 70], [Ho 71a], [HL 72a], [Ho 72], [MH 72], [Ho 73], [HY 74], [LH 75], [HJJ 76], [EH 77], [HE 77], [Ho 77], [HE 78], [SH 78], [HE 79], [EH 79], [EHS 80]
 Honkarana, T. [HNL 70]
 Hoodbhoy, P. [HN 77]
 Horie, H. [AH 71a]
 Hornyak, W. F. [Ho 75]
 Hoshino, T. [HA 76]
 Huang, K. [Hu 63]
 Hubbard, J. [Hu 57]
 Huber, M.G. [WHG 66], [KH 76]
 Hubert, P. [HJE 78]
 Hüfner, J. [AHK 72]
 Hull, M. H. [LHR 62]
 Hulten, L. [HS 57]
 Hüsker, H. [FWH 74]
 Huus, T. [HZ 53], [ABH 56]

- Iachello, F. [IA 74], [AI 75a], [AI 75b], [AI 76], [AOI 77], [Ia 77], [AI 78a], [AI 78b], [AOI 78], [Ia 78], [OAI 78]
- Ichihashi, H. [YSI 78], [IY 78]
- Ikeda, A. [ISY 73], [UIO 76]
- Ikeda, K. [IUY 65]
- Inglis, D. R. [In 54], [In 56]
- Irvine, J. M. [Ir 72]
- Ishimatsu, R. [HBI 77]
- Islam, S. [JMR 79]
- Itoh, K. [TIS 75]
- Ivanjuk, F. A. [SI 75]
- Ivanova, S. P. [GIS 73]
- Iwamoto, F. [FIS 64], [IO 67]
- Iwasaki, S. [IMS 76], [IST 77], [Hi 79], [HIT 79], [IRS 79], [IRS 80]
- Jackson, A. D. [EJM 68], [BJS 75], [BJ 76a], [DSB 77]
- Jackson, J. D. [Ja 62]
- Jägare, S. [SHJ 73]
- Jancovici, B. [JS 64]
- Janssen, D. [FJM 71], [JDF 71], [DJ 73], [JJD 74], [JDJ 75], [HJJ 76], [MJ 78], [Ja 79]
- Jarvis, O. N. [HGH 68]
- Jastrzebski, J. [ABR 75]
- Jean, M. [WJ 56], [CCJ 65], [CCJ 66]
- Jennings, B. K. [Je 73], [JBB 75], [JB 75], [BJC 76], [BJ 76b], [Je 76], [CJB 77]
- Jensen, A. S. [BDJ 72], [BLP 74], [JL 80]
- Jensen, J. H. D. [HJS 49], [SJ 50], [MJ 55]
- Jeukenne, J. P. [JLM 76]
- Johansson, T. [JNS 70]
- Johnson, A. [JRS 71], [JRH 72], [JS 73], [SHJ 73]
- Johnson, E. R. [JDK 69]
- Johnson, M. B. [JB 71], [MJB 75]
- Johnson, N. R. [RSS 74], [LCS 76], [HJE 78]
- Johnston, I. D. [HJ 62]
- Jolos, R. V. [JDF 71], [JJD 74], [JDJ 75], [HJJ 76]
- Jones, W. [JM 73]
- Junker, K. [GPA 72], [JH 77]
- Justin, D. [JMR 69], [JMR 72]
- Kabina, L. P. [AEE 78]
- Kadanoff, L. P. [KB 62]
- Kalinnikov, V. G. [GSK 75]
- Kallio, A. [KK 64]
- Kamerdzhiev, S. P. [Ka 69]
- Kaminker, D. M. [AEE 78]
- Kamlah, A. [Ka 68], [Ka 73]
- Kammuri, T. [SDL 72]
- Kantele, J. [EKV 69]
- Kan, K. K. [KG 78], [KLD 80]
- Kao, E. I. [KF 70]
- Karnaughov, V. A. [PDK 62]
- Kassis, N. [RBK 75]
- Kawai, M. [KK 68]
- Kawazoe, Y. [TIS 75]
- Keleman, A. [KD 75], [KD 76]
- Kelson, I. [Ke 63], [KL 64], [Ke 66]
- Kemmer, N. [KPW 68]
- Kerman, A. K. [Ke 56], [Ke 61], [KLM 61], [KS 62], [BTK 65], [BKS 67], [TBK 70], [AHK 72], [FQK 73], [FQV 74], [Ke 76], [KK 76], [KO 77]
- Khadkikar, S. B. [KW 69], [BKD 73], [KK 74]
- Kharitonov, Y. I. [SK 65]
- Khazov, Y. L. [AEE 78]
- Khoo, T. L. [KL 77], [PBB 77]
- Kikuchi, K. [KK 68]
- Kirichenko, N. A. [MKS 74]
- Kirkwood, J. G. [Ki 33]
- Kirson, M. W. [KZ 70], [BK 73], [Ki 78]
- Kirzhnits, D. A. [Ki 57], [Ki 67]
- Kishimoto, T. [KT 71], [KT 72], [TK 73], [KMY 75], [KT 76]
- Kisslinger, L. S. [KS 60], [KS 63], [GK 65]
- Kistner, O. C. [KSM 78]
- Klamra, W. [HK 77]
- Kleber, M. [KI 69], [KI 70]
- Kleinert, H. [KI 77]
- Kleinheinz, P. [SKS 74]
- Klein, A. [DK 66], [PKD 68], [JDK 69], [DDK 70], [YKD 70], [DDK 71]
- Klemt, V. [BSK 73], [KMS 76], [KS 76], [SWK 76], [KKS 77], [ERW 78], [WKS 78]
- Klinkenberg, P. F. A. [KI 52]

- Knöpfle, K. T. [KWB 75]
 Knox, W. J. [BK 61]
 Knudsen, M. H. C. [Kn 50]
 Knuepfer, W. [KH 76], [FRS 78]
 Kodama, T. [MSK 77]
 Köhler, H. S. [Ko 65], [Ko 71], [Ko 75], [Ko 76]
 Kohn, W. [HK 64]
 Kolb, D. [FKS 72], [KS 72], [KCS 74]
 Kolltveit, K. [KK 64]
 Kolomietz, V. M. [BKS 72]
 Kondurov, I. A. [AEE 78]
 Konecny, E. [SWK 72]
 Koonin, S. E. [BKN 76], [KK 76], [Ko 76], [KDM 77], [MDK 77], [BGK 78], [FKW 78], [NKM 78]
 Kovar, D. G. [SVE 76]
 Kramer, P. [KM 66], [AMK 69]
 Kreiner, A. J. [Kr 79]
 Kretzschmar, M. [Kr 60]
 Krewald, S. [KBF 74], [KS 74], [KRG 76], [SWK 76], [DKS 77], [KKS 77]
 Krieger, S. J. [NDK 68], [Kr 70], [KG 74], [EBG 75], [KDM 77], [Kr 77]
 Krivchenkov, G. [Kr 64]
 Krivine, H. [BCK 76], [TK 76], [KTB 80]
 Krmpotic, F. [VPK 69]
 Krumlinde, J. [KS 73], [CMR 75], [AK 77], [AHL 78]
 Kübler, O. [Ku 72]
 Kuhlmann, E. [HGA 74]
 Kuhn, W. [Ku 25]
 Kujawski, E. [MKL 71]
 Kulkarni, D. R. [KK 74]
 Kumar, K. [Ku 62], [BK 65], [BK 67b], [BK 68], [KB 68], [Ku 72], [Ku 74a]
 Kümmel, H. [KLZ 75], [KLZ 78]
 Kuo, T. T. S. [KB 66], [BK 67a], [BK 69], [KBB 70], [HK 72], [WKB 73], [Ku 74b]
 Kurath, D. [Ku 56], [KP 59]
 Kuriyama, A. [KMM 72], [KMM 75a], [KMM 75b]
 Kusuno, S. [HK 75]
 Lacanna, R. [HGA 74]
 Lacombe, M. [CLL 73], [LLR 75]
 Lambert, M. [HL 72b]
 Lamme, H. A. [LB 68], [LB 69]
 Lamm, I. L. [GLN 67], [NTS 69]
 Landau, L. D. [La 32], [La 59], [LL 59]
 Lande, A. [La 65]
 Lane, A. M. [EL 57], [LS 62], [La 64], [LM 74], [La 75], [BML 76], [MBF 76], [GLM 78], [BLM 79]
 Lane, N. F. [MEL 76]
 Lantto, L. J. [LS 77]
 Lark, N. L. [SLD 65]
 Larkin, A. I. [ML 64]
 Larsen, S. M. [JM 80]
 Larsh, A. [PAG 62]
 Larsson, S. E. [BLL 75], [ALL 76], [RLM 76], [LLR 78]
 Lassey, K. R. [LV 71], [La 72], [GVL 73], [LMV 73]
 Lassila, K. E. [LHR 62]
 Lathouwers, L. F. F. [La 74], [La 76], [LL 77]
 Latimer, R. [PAG 62]
 Lawson, R. D. [KLM 61]
 Leander, G. [BLL 75], [ALL 76], [Le 76], [CDS 77], [AHL 78], [LLR 78], [PFL 78]
 Lebrun, D. [BBL 80]
 Ledergerber, T. [LP 73], [BLP 74], [LPP 75], [LPF 77]
 Lee, H. C. [CL 73]
 Lee, I. Y. [LCS 76], [WCL 76], [LAD 77]
 Lee, S. Y. [HLR 74]
 Leigh, J. R. [SDL 72]
 Leisi, H. J. [EAD 75]
 Lejeune, A. [JLM 76]
 Lemberg, I. K. [BEL 70]
 Lemmer, R. H. [LV 68]
 Leonard, R. [BL 76], [LOL 76], [SLO 78]
 Lepretre, A. [BBL 71]
 Lesjak, J. [MKL 71]
 Letessier, J. [CLF 73]
 Letourneau, J. [GLW 70], [SLR 73], [GL 77], [PL 77]
 Leushkin, E. K. [AEE 78]
 Leuven, P. Van [BLD 67]
 Levinson, C. A. [KL 64]
 Levit, S. [NLP 79]
 Lewis, H. R. [LR 69]

- Lewis, M. B. [LB 72]
 Lichtner, P. C. [LG 76a], [KLD 80]
 Lie, S. G. [HL 72a], [LH 75], [VLS 79]
 Lieb, K. P. [HLM 78]
 Lieder, R. M. [BDL 75], [NLM 76],
 [LR 78]
 Lifshitz, E. M. [LL 59]
 Lin, L. [GLS 67], [FLW 73]
 Lindblad, T. [LRB 72]
 Linden, C. G. [BBH 77]
 Liotta, R. J. [MLE 67], [BBB 77],
 [BSL 79]
 Lipas, P. O. [HNL 70]
 Lipkin, H. J. [Li 55], [LST 55], [Li 58],
 [Li 60a], [Li 60b], [LMG 65]
 Lipparini, E. [LOL 76], [SLO 78]
 Lipperheide, R. [GL 70], [FLW 75]
 Liu, K. F. [LB 76], [LG 76b], [LR 77]
 Llano, M. De [AAZ 77], [ALP 77]
 Löbner, K. E. G. [LM 66]
 Lockett, A. M. [BLR 61]
 Loginov, Y. E. [AEE 78]
 Loiseau, B. [CLL 73], [LLR 75]
 Løvhøiden, G. [HRH 70], [LR 76],
 [RL 76], [KL 77]
 Löwdin, P. O. [Loe 55], [Loe 64]
 Lozaro, B. [LA 74], [Lo 75]
 Lozes, R. L. [LL 77]
 Lüders, G. [Lu 60]
 Lührmann, K. H. [KLZ 75], [KLZ 78]
 Lukasiak, J. [ABR 75]
 Lyttleton, R. A. [Ly 58]
- Ma, C. W. [MR 70], [MT 73], [MT
 75], [MR 77]
 MacDonald, N. [Ma 70], [GM 71],
 [MMW 73]
 MacFarlane, M. H. [KLM 61], [Ma
 69]
 Machleidt, R. [NMH 73]
 Madsen, V. A. [WMR 77]
 Magner, A. G. [SM 76], [SMO 77]
 Mahaux, C. [MW 69a], [JLM 76]
 Mahoney, J. [HGH 68]
 Malmeskog, S. G. [LM 66]
 Malov, L. A. [MNS 76]
 Manassah, J. [BCD 75]
 Mang, H. J. [DMP 64], [MPR 65],
 [DMP 66], [MRR 66], [MW 68],
 [BMR 70], [RBM 70], [BMR 73],
 [DBM 73], [RMB 74], [RM 74],
 [DMR 75], [Ma 75a], [MSR 76],
 [ERM 78], [FMR 79], [IMR 79],
 [EMR 80a], [EMR 80b]
 Mankoc-Borstnik, N. [NMR 75],
 [MM 76]
 Manning, M. R. P. [LMV 73]
 March, N. H. [JM 73]
 Mariscotti, M. A. J. [MSB 69]
 Maris, T. A. J. [MHT 58]
 Markiewicz, W. [MMG 67]
 Marshak, R. E. [OM 58]
 Marshalek, E. R. [Ma 65], [Ma 67a],
 [MW 69b], [MW 70], [Ma 71], [MH
 72], [Ma 73], [MP 73], [Ma 74],
 [CMR 75], [Ma 75b], [Ma 76a],
 [Ma 76b], [Ma 77a], [BM 78], [MG
 78], [Ma 79]
 Martin, P. [BBL 80]
 Martins, P. [ABC 77a], [ABC 77b]
 Martorell, J. [BML 76], [MBF 76],
 [GLM 78], [BLM 79]
 Martynov, V. V. [AEE 78]
 Marty, N. [MMW 75]
 Maruhn-Rezwani, V. [KDM 77],
 [MDK 77]
 Maruhn, J. A. [MG 72], [WMW 75],
 [CM 76], [CSM 76], [MC 76],
 [MMW 76], [Ma 77c], [WMW 77],
 [WWM 77], [CMM 78]
 Marumori, T. [MYT 55], [MY 55],
 [HM 57], [MYT 64a], [MYT 64b],
 [MYM 68], [KMM 72], [KMM
 75a], [KMM 75b], [IMS 76], [MA
 77b]
 Maruyama, X. K. [PBD 74]
 Mateosian, E. [KSM 78]
 Matsuyanagi, K. [KMM 72], [KMM
 75a], [KMM 75b], [DNM 77],
 [MDN 78]
 Matsuzaki, H. [TIS 75]
 Mattuck, R. D. [Ma 67b]
 Mavromatis, H. A. [MMG 67], [EJM
 68]
 Mayer-Börcke, C. [BDL 75], [KWB
 75], [NLM 76]
 Mayer, M. G. [Ma 49], [Ma 50], [MJ
 55]
 Mayes, I. W. [MD 73]
 McCarthy, R. J. [DMS 72], [DMS 73]
 McClure, W. [WM 66]
 McConnell, J. R. [ABC 63]

- McCullen, J. D. [MBZ 64]
 McDonald, F. A. [LHR 62]
 McDonald, J. A. [WM 77]
 McGrory, J. B. [FHM 69], [HMW 71],
 [WMH 71], [HMS 75]
 McGuire, J. [Mc 65]
 McLaughlin, D. [SCM 73]
 McWeeny, R. [Mc 56], [Mc 60]
 Mechkov, N. [LMG 65]
 Medjadi, D. E. [FHM 73]
 Meitner, L. [MF 39]
 Mekjian, A. Z. [LM 74]
 Meldner, H. W. [CMM 78]
 Melkanoff, M. A. [RMS 67]
 Merdinger, J. C. [BBB 79a]
 Merle, K. [RFM 74]
 Messiah, A. [Me 61], [BM 62]
 Meyer-Ter-Vehn, J. [MSV 72], [MSD
 74], [Me 75], [Me 78], [Me 79]
 Migdal, A. B. [Mi 59], [Mi 60], [ML
 64], [Mi 67], [MKS 74]
 Mihailovic, M. V. [JMR 69], [MKL
 71], [JMR 72], [BBB 75], [GMA
 75], [MMR 75], [MM 76]
 Mikeska, H. J. [MB 69]
 Mikhailov, I. N. [MJ 78]
 Mikheev, V. L. [PDK 62]
 Mikishiba, O. [MSU 67]
 Mikolas, V. [MT 77]
 Milner, W. T. [SSM 75]
 Miyanishi, Y. [MYM 68]
 Miyazima, T. [MT 56]
 Mizobuchi, Y. [MNY 77]
 Möller, P. [NTS 69], [SSW 69], [Moe
 72], [MN 73], [BLL 75], [ALL 76],
 [MN 76], [RLM 76], [NKM 78]
 Molinari, A. [MR 72], [MJB 75]
 Monsonego, G. [ABC 69]
 Moos, J. M. [YMR 76]
 Moreau, F. [GMQ 76]
 Mori, H. [Mo 65]
 Morinaga, H. [MG 63]
 Morlet, M. [MMW 75]
 Morley, G. L. [CM 63]
 Morovič, T. [GMG 71]
 Morrison, I. [MMW 73], [MWW 74],
 [WWC 77]
 Morrison, M. A. [MEL 76]
 Morsch, H. P. [HBI 77]
 Mosel, U. [GMG 69], [HMG 69],
 [GMG 70], [SGM 71], [SM 72],
 [MMS 73], [PM 76], [GMZ 78],
 [FMR 79]
 Moshinsky, M. [KM 66], [AMK 69],
 [Mo 69], [CCF 79]
 Moss, J. M. [KMY 75], [YRM 77]
 Moszkowski, S. A. [Mo 56], [Mo 57],
 [MS 60], [GM 65], [PAM 66],
 [FPM 67], [Mo 70], [EM 72], [FGE
 72], [KMS 76], [Mo 76c], [SM 78]
 Mottelson, B. R. [BM 53], [BM 55],
 [MN 55], [ABH 56], [BMP 58],
 [BM 58], [MN 59], [MV 60], [Mo
 67], [BM 69], [BM 74], [BM 75],
 [Mo 76a], [Mo 76b], [BHM 78]
 Moya-de-Guerra, E. [MV 77], [MV
 78]
 Müller-Veggian, M. [NLM 76]
 Müller, W. [HLM 78]
 Münchow, L. [FJM 71]
 Müther, H. [AGM 74], [MAG 75],
 [DMG 76], [MGA 77]
 Mulhall, W. J. [MLE 67]
 Musiol, G. [GSK 75]
 Mustafa, M. G. [MMS 73]
 Muthukrishnan, R. [MB 65]
 Myers, W. D. [MS 66], [MS 69], [My
 69], [MS 73], [MSK 77]
 Nadjakov, E. [VNR 75]
 Nair, S. C. K. [An 71]
 Nakai, K. [SDL 72]
 Nakayama, H. [YNN 76]
 Nalcioğlu, O. [GNS 70]
 Nataf, R. S. [Na 57]
 Nathan, P. [NN 65]
 Neergård, K. [NP 75], [NVR 75],
 [NPF 76], [DNM 77], [NTP 77],
 [TNV 77], [MDN 78]
 Negele, J. W. [Ne 70], [NV 72], [Ne
 75], [NV 75], [BKN 76], [FN 76],
 [HN 77], [KDM 77], [Ne 77], [NR
 77], [YN 77], [ZN 77], [NKM 78],
 [ON 78], [NLP 79]
 Neiman, M. [PBB 77], [ABH 78]
 Nemes, M. C. [TPG 77]
 Nemeth, J. [NV 70], [NR 72], [NMH
 73]
 Nemirovski, P. E. [NA 62]
 Nerlo-Pomorska, B. [ALL 76]
 Neskakis, A. [BDL 75], [NLM 76]
 Nesterenko, V. O. [MNS 76]

- Nestor, C. W. [NDK 68]
 Neumann, J. von [NW 29]
 Newton, J. O. [LAD 77], [SBD 77]
 Ngo-Trong, C. [NR 71], [RN 75]
 Nichols, K. [NS 78]
 Nicholson, P. [CN 47]
 Nilsson, N. R. [NN 74]
 Nilsson, B. [GLN 67], [NTS 69], [SSW 69]
 Nilsson, B. S. [BBN 74a], [BBN 74b]
 Nilsson, S. G. [MN 55], [Ni 55], [MN 59], [NP 61], [NN 65], [GLN 67], [NTS 69], [NTT 69], [SSW 69], [JNS 70], [SDN 73], [NN 74], [BLL 75], [ALL 76], [RLM 76], [CDS 77], [AHL 78], [PFL 78], [RNS 78]
 Nishiyama, S. [MYM 68], [YN 76], [FYN 77], [MNY 77]
 Nix, J. R. [NS 65], [Ni 69], [SSW 69], [BFN 72], [Ni 72], [MN 73], [MN 76], [BN 77], [BBN 78], [NKM 78]
 Noble, J. V. [No 71], [No 78]
 Nogami, Y. [No 64b], [NZ 64], [NW 76], [NW 78]
 Nopre, H. [NW 72], [NW 74]
 Norton, J. L. [BFN 72]
 Nozières, P. [No 64a]
 Numao, T. [YNN 76]
 Nybo, K. H. [ABC 63]
 Oeschler, H. [ABH 78]
 Ofengenden, S. R. [SMO 77]
 Ogle, W. [OWP 71], [BPO 76]
 Okamoto, K. [Ok 58]
 Okamoto, R. [KMM 75b]
 Okubo, S. [OM 58], [Ok 74]
 Onishi, N. [OY 66], [IO 67], [On 68], [OSY 70], [OU 75], [UIO 76], [KO 77], [ON 78]
 Ophel, T. R. [SVE 76]
 Orlandini, G. [LOL 76], [SLO 78]
 Osnes, E. [DFG 68], [ORG 75], [EO 77], [PO 78]
 Otsuka, T. [AOI 77], [AOI 78], [OAI 78]
 Ottaviani, P. L. [OS 69]
 Overhauser, A. W. [Ov 60]
 Paar, V. [APS 75], [AP 76], [PVD 77]
 Padjen, R. [RP 69], [SLR 73]
 Pal, D. [ZSP 78]
 Pal, M. K. [GP 63]
 Palms, J. M. [SBP 67]
 Paltiel, Z. [LPP 75], [LPF 77], [NLP 79]
 Palumbo, F. [Pa 67]
 Pandharipande, V. R. [PB 73]
 Pandya, S. P. [HMW 71]
 Pang, S. C. [PKD 68]
 Parikh, J. C. [PR 68], [CP 70]
 Parlag, A. [BBL 71]
 Pascoal, H. [ABC 77a]
 Pashkevich, V. V. [Pa 61], [PS 65], [DPP 69], [NP 75], [NPF 76]
 Passler, K. H. [Pa 76], [PM 76]
 Passos, E. J. V. De [TPG 77], [TP 78]
 Paul, P. [SEB 74], [Pa 75a]
 Pauli, H. C. [DPP 69], [GPA 71], [BDJ 72], [GPA 72], [BP 73], [LP 73], [Pa 73], [BLP 74], [LPP 75], [Pa 75b], [BP 77a], [BP 77b], [LPF 77]
 Pauli, W. [Pa 33]
 Pearson, J. M. [PS 68], [SP 70], [RPS 72], [RBP 77]
 Pedersen, J. [PBB 77]
 Pedersen, T. [PO 78]
 Peierls, R. E. [PY 57], [PT 62]
 Pelet, J. [PL 77]
 Peltier, S. [ALP 77]
 Perazzo, R. P. J. [MLE 67]
 Perelomow, A. M. [Pe 77]
 Perlman, I. [PAG 62]
 Perrin, G. [BBL 80]
 Person, L. W. [PR 62]
 Petschek, A. G. [BBP 63]
 Picman, L. [KP 59]
 Piepenbring, R. [BP 71], [OWP 71], [BPO 76], [SP 77b], [SP 77c], [SP 78]
 Pines, D. [BP 53], [BMP 58], [Pi 61]
 Pinston, J. A. [AEE 78]
 Pires, P. [LLR 75]
 Pittan, R. [PW 71]
 Pittian, R. [PBD 74]
 Plasil, F. [CPS 74], [BES 76]
 Plastino, A. [PAM 66], [FPM 67], [FP 67], [ABP 68], [VPK 69], [FGP 73], [AAZ 77], [ALP 77]
 Pleve, A. A. [PDJK 62]
 Ploszajczak, M. [FPD 76], [NTP 77], [FP 78], [PFL 78], [PTF 78], [FPS 80]
 Poggenburg, J. K. [MPR 65]
 Pol, B. Van-Der [PB 55]

- Polikanov, S. M. [PDK 62]
 Pomorski, K. [ALL 76], [Po 76],
 [RLM 76], [Po 78]
 Pradal, J. H. [DMP 64], [DMP 66]
 Preedom, B. M. [PW 72]
 Preston, M. A. [PB 75]
 Primakoff, H. [HP 40]
 Prior, O. [NP 61]
 Providencia, J. Da [Pr 66], [PUF 71],
 [MP 73], [Pr 74], [ABC 77a], [ABC
 77b], [SP 77a]
 Pühlhofer, F. [PBB 77]
 Pursey, D. L. [KPW 68], [WP 68]
 Pyatov, N. I. [BPC 72], [PS 77]
- Quentin, P. [Qu 72], [CLF 73], [FQK
 73], [FQV 73], [BFV 74], [FQV 74],
 [TQ 74], [BFG 75], [BQ 75a], [BQ
 75b], [GMQ 76], [BQ 78], [QF 78],
 [GQ 80]
- Racah, G. [Ra 43]
 Radicati, L. A. [BR 76]
 Radomski, M. [NVR 75]
 Raduta, A. A. [RD 76], [RGB 77]
 Ragnarsson, I. [ALL 76], [CDS 77],
 [AHL 78], [LLR 78], [RNS 78]
 Rainwater, J. [Ra 50], [Ra 76]
 Rajaraman, R. [Ra 75]
 Randrup, J. [RLM 76], [BBN 78]
 Rasmussen, J. O. [PR 62], [MPR 65],
 [MRR 66], [MR 70], [CMR 75],
 [MR 77]
 Raval, S. P. [FR 76B]
 Raychev, P. [VNR 75]
 Raynal, J. [RMS 67], [Ra 70]
 Redlich, M. G. [RW 54], [Re 58]
 Reed, M. [RS 72]
 Regge, T. [MR 72]
 Reich, C. W. [HR 68], [BR 71A]
 Reiche, F. [RT 25]
 Reid, P. V. [Re 68]
 Reidemeister, F. [DR 66]
 Reinhard, P. G. [Re 75c], [Re 76a],
 [Re 76b], [Re 77], [RG 77], [GR
 78], [Re 78], [RG 78]
 Reinhardt, H. [Re 75b], [ER 78], [Re
 79]
 Rekstad, J. [ORG 75], [Re 75a], [LR
 76], [RL 76]
 Rester, A. C. [HR 74]
 Rho, M. [MRR 66]
- Rich, M. [GR 60]
 Richardson, R. W. [RS 64], [Ri 66]
 Richard, J. M. [CLL 73], [LLR 75]
 Richert, J. [HLR 74]
 Richter, A. [FRS 78]
 Riedel, C. [BRS 68], [BHR 73]
 Riedinger, L. L. [RSS 74]
 Riesenfeld, W. B. [LR 69]
 Ring, P. [BMR 70], [RBM 70], [BMR
 73], [BSK 73], [DBM 73], [RBS 73],
 [RS 73], [RW 73], [RMB 74], [RM
 74], [RS 74a], [RS 74b], [SZR 74],
 [BER 75], [CMR 75], [DMR 75],
 [MSR 76], [SWR 76], [Ri 77], [RS
 77a], [RS 77b], [ERM 78], [ERW
 78], [FMR 79], [IMR 79], [IRS 79],
 [EMR 80a], [EMR 80b], [ER 80],
 [IRS 80]
- Rinker, G. A. [WMR 77]
 Rinker, G. [NR 77]
 Ripka, G. [BGR 65], [Ri 68], [RP 69],
 [ZR 71], [NR 72], [RBK 75], [LR
 77], [Ri 79]
 Rivier, J. [ABR 75]
 Robel, M. [BBN 78]
 Robinson, R. L. [RSS 74]
 Rockmore, R. M. [Ro 59]
 Rogge, M. [KWB 75]
 Rosati, S. [FR 75], [FR 76a]
 Rose, M. E. [BR 37]
 Rosenfelder, R. [KRG 76]
 Rosenkilde, C. E. [Ro 67]
 Rosina, M. [JMR 69], [JMR 72],
 [MMR 75]
 Ross, C. K. [BR 71b]
 Rostovsky, V. S. [DR 59]
 Rotenberg, A. M. [BLR 61]
 Rothhaas, H. [RFM 74]
 Rouben, B. [WSR 71], [RPS 72], [SLR
 73], [RBP 77]
 Rouhaninejad, H. [RY 66]
 Rowe, D. J. [PR 68], [Ro 68a], [Ro
 68b], [RW 69], [UR 69], [Ro 70],
 [RW 70], [NR 71], [UR 71], [RB
 74], [RN 75], [RB 76], [SR 76], [SR
 77]
 Rozsa, C. M. [KMY 75], [YMR 76],
 [YRM 77]
 Ruder, H. [RV 69], [Ru 73]
 Ruivo, M. C. [ABC 77a], [ABC 77b]
 Rumiantsev, V. L. [AEE 78]
 Ruppel, H. M. [LHR 62]

- Russo, G. [BTR 77]
 Rustgi, M. L. [SR 78]
 Ryde, H. [HRH 70], [JRS 71], [JRH 72], [LRB 72], [SHJ 73], [ABH 78], [LR 78]
- Saarela, M. [DSB 77]
 Saethre, O. [SHJ 73]
 Sagawa, H. [SH 78]
 Saintignon, P. de [BBL 80]
 Sakata, F. [IMS 76], [IST 77]
 Sakharov, S. L. [AEE 78]
 Salamov, D. I. [PS 77]
 Salusti, E. [ASV 64]
 Samadi, B. [MSR 76]
 Sanderson, E. A. [GS 64], [Sa 65], [GGS 66], [EJM 68]
 Sandhu, T. S. [SR 78]
 Sapp, W. W. [EAD 75]
 Sardaryan, R. A. [PS 65]
 Sasao, M. [ST 77]
 Satchler, G. R. [HS 62], [Sa 72a], [Sa 72b], [Sa 74], [HMS 75], [Sa 76]
 Saudinos, J. [HGH 68]
 Sauer, P. U. [Sa 68], [GS 69], [SFW 69], [WFS 70], [WFS 71], [DMS 72], [DMS 73]
 Saunier, G. [PS 68], [SP 70], [WSR 71], [RPS 72], [SLR 73], [RBP 77]
 Savoia, M. [OS 69]
 Sawada, K. [Sa 57], [FIS 64]
 Sawada, T. [RMS 67]
 Sawicki, J. [Sa 62]
 Saxon, D. S. [WS 54]
 Sayer, R. O. [RSS 74], [SSM 75]
 Scharff-Goldhaber, G. [MSB 69], [SDB 76]
 Scharnweber, D. [SGM 71]
 Scheid, W. [SG 68], [FKS 72]
 Schiff, D. H. [JS 64]
 Schiff, L. I. [Sch 68]
 Schiffer, J. P. [AS 71], [Sch 71b], [Sch 72b], [ST 76]
 Schiffrer, G. [FS 76]
 Schmeing-Rogerson, N. [VS 71]
 Schmidt, H. [Sch 61], [Sch 64a], [Sch 64b], [Sch 71a]
 Schmid, K. W. [GSF 75], [FGD 76], [GSF 78a], [GSF 78b], [SG 79], [FPS 80]
 Schmitt, H. W. [SM 72], [MMS 73], [KCS 74]
 Scholten, O. [AOI 78]
 Schreckenbach, K. [AEE 78]
 Schrieffler, J. R. [BCS 57]
 Schucan, T. H. [SW 72], [SW 73], [HLR 74], [SCH 75]
 Schuck, P. [BS 64], [BS 68a], [ES 69], [Sch 71c], [Sch 72a], [SE 73], [RS 74b], [Sch 76], [SWR 76], [GS 77], [RS 77a], [RS 77b], [DBS 78], [IRS 79], [SB 79], [BS 80], [DSB 80], [IRS 80]
 Schütte, D. [BSB 69], [SP 77a]
 Schütte, G. [LPP 75], [SW 75a], [SW 75b], [Sch 77a], [SW 78]
 Schulz, H. [BS 79]
 Schutz, Y. [BBB 79a]
 Schwartz, C. [GS 57]
 Schwartz, J. L. [SB 64]
 Schwesinger, B. [Sch 77b], [EHS 80]
 Schwierczinski, A. [FRS 78]
 Schwinger, J. [Sch 65]
 Scott, A. [SCM 73]
 Scott, B. L. [MS 60]
 Seaman, G. G. [SBP 67]
 Sebille-Schueck, C. [ABR 75]
 Segre, E. [Se 64]
 Serr, F. E. [SBB 80]
 Seyler, P. G. [SB 63]
 Shabat, A. B. [ZS 72]
 Shakin, C. M. [KS 62], [AHK 72], [WS 72]
 Shalit, A. D. [LST 55], [ST 63], [SW 66], [SF 74]
 Shapiro, J. [Sm 65]
 Sharp, R. W. [SZ 73], [GSZ 74]
 Sheline, R. K. [FGS 65], [FGS 66], [FS 66], [MSU 67], [OSY 70], [ISY 73], [SKS 74], [RNS 78]
 Sherman, N. [RS 64]
 Sherwood, A. I. [GNS 70]
 Shibata, T. A. [YNN 76]
 Shin, Y.M. [TIS 75]
 Shlomo, S. [SB 75]
 Siebert, H. U. [GSK 75]
 Siegal, C. D. [SS 72B]
 Siegert, A. J. F. [Si 37]
 Siemens, P. J. [LS 77]
 Sierk, A. J. [BBN 78], [NKM 78]
 Silva, E. M. [ABC 77a], [ABC 77b]
 Silvestre-Brac, B. [SP 77b], [SP 77c], [SP 78], [BSL 79]
 Simeric, A. [ZGS 67]

- Simon, B. [RS 72]
 Simon, R. S. [SS 72a], [SKS 74], [BSC 75], [LCS 76], [SBC 76], [WCL 76], [LAD 77], [SBD 77]
 Singh, B. [EJM 68]
 Sinha, B. [SM 78]
 Sips, L. [APS 75]
 Skobelev, N. K. [PDK 62]
 Skyrme, T. H. R. [ES 55], [BS 56], [Sk 56], [Sk 57], [Sk 59]
 Slater, J. C. [SI 51]
 Sletten, G. [PBB 77]
 Sliv, L. A. [SK 65]
 Smith, B. C. [SV 73]
 Smith, G. J. [RSS 74]
 Smith, J. S. [SSM 75]
 Smith, R. K. [CSM 76]
 Snover, K. A. [SEB 74]
 Sobczewski, A. [So 67], [ASS 69], [NTS 69], [SSW 69], [RLM 76]
 Soloviev, V. G. [BS 59], [So 61], [SV 63], [So 65], [ASS 69], [So 71], [GIS 73], [MNS 76], [SSV 77]
 Soper, J. M. [So 57], [LS 62], [So 69]
 Sorensen, B. [So 67], [BRS 68], [BS 68b], [So 68a], [So 68b], [So 69], [So 70], [So 71], [So 73]
 Sorensen, R. A. [KS 60], [KS 63], [BS 69], [So 72], [SS 72b], [So 73], [GVS 76], [So 77], [NS 78]
 Soroka, D. P. [BSC 75], [SBC 76]
 Sorokin, G. A. [MKS 74]
 Sousa, C. A. De [ABC 77a], [ABC 77b]
 Soyeur, M. [SZ 72]
 Spamer, E. [FRS 78]
 Specht, H. J. [SWK 72], [Sp 74]
 Sperr, P. [SVE 76]
 Speth, J. [MSV 72], [BSK 73], [RBS 73], [RS 73], [KBF 74], [KS 74], [RS 74a], [SZR 74], [BJS 75], [HMS 75], [ZS 75], [KMS 76], [KS 76], [SWK 76], [ZS 76], [DKS 77], [KKS 77], [SWW 77], [WMR 77], [ERW 78], [WKS 78], [ZSP 78]
 Spicer, B. M. [Sp 68]
 Sprung, D. W. L. [BS 71], [CS 72], [Sp 72], [CS 73], [SS 76], [VLS 79]
 Srivastava, M. K. [SS 76]
 Stamp, A. P. [St 78]
 Stegun, I. A. [AS 65]
 Steinwedel, H. [SJ 50]
 Stelson, P. H. [RSS 74]
 Stephens, F. S. [SLD 65], [SDL 72], [SS 72a], [GSD 73], [SDN 73], [MSD 74], [SKS 74], [BSC 75], [St 75a], [WBB 75], [LCS 76], [SBC 76], [St 76], [WCL 76], [LAD 77], [SBD 77]
 Stingl, M. M. [SFW 69]
 Stokes, R. H. [BES 76]
 Stoyanov, C. [SSV 77]
 Strayer, M. R. [BSV 76]
 Stricker, K. [BS 76]
 Stringari, S. [SLO 78], [St 79]
 Struble, G. L. [GLS 67], [GSG 68], [BGG 69], [GSB 70]
 Strusny, H. [GSK 75]
 Strutinski, V. M. [ST 66], [St 67], [St 68], [DPP 69], [BDJ 72], [BKS 72], [St 74], [SI 75], [ST 75b], [SM 76], [SMO 77], [St 77]
 Styczen, J. [BBB 79a]
 Subbotin, V. G. [PDK 62]
 Suess, H. E. [HJS 49]
 Süssmann, G. [Sue 54]
 Sugawara, M. [HS 57]
 Sujkowski, Z. [ABR 75]
 Sunyar, A. W. [KSM 78]
 Sushkov, P. A. [AEE 78]
 Suzuki, T. [Su 73], [SR 76], [SR 77], [YSI 78]
 Svenne, J. P. [BKS 67]
 Swiatecki, W. J. [Sw 55], [CS 62], [CS 63], [NS 65], [MS 66], [MS 69], [MS 73], [CPS 74], [MSK 77], [BBN 78]
 Sztarkier, J. [JRS 71]
 Szymański, Z. [BS 61], [Sz 61], [NTS 69], [SSW 69], [JNS 70], [JS 73], [KS 73], [SHJ 73], [BLL 75], [ALL 76], [CDS 77], [AHL 78], [CDS 78]
 Tabakin, F. [Ta 64]
 Takada, A. [MYT 64b]
 Takada, K. [IMS 76], [IST 77]
 Takeda, G. [TIS 75]
 Talmi, I. [LST 55], [UT 58], [Ta 62], [ST 63], [Ta 71], [Ta 76], [AOI 77], [AOI 78]
 Tamura, T. [MT 56], [Ta 56b], [TU 64], [KT 71], [KT 72], [TK 73], [KT 76]
 Tanabe, K. [HIT 79]
 Tanaka, R. [MYT 55]

- Tassie, L. J. [Ta 56a]
 Teller, E. [GT 48]
 Ter-Akopjan, G. M. [PDK 62]
 Tewari, S. N. [TG 69]
 Theis, W. [TW 73], [BER 75], [TW 78]
 Thieberger, P. [Th 73]
 Thomas, L. H. [Th 27]
 Thomas, W. [RT 25]
 Thompson, S. G. [NTT 69]
 Thouless, D. J. [Th 60], [BET 61], [Th 61a], [Th 61b], [PT 62], [TB 62]
 Titin-Schnaider, C. [TQ 74]
 Titze, O. [FRS 78]
 Toki, H. [Ft 75], [TF 75], [NTP 77], [TNV 77], [TYF 77], [YTF 77], [PTF 78], [YTF 78]
 Tokunaga, A. [MYT 64a], [MYT 64b]
 Toledo-Piza, A. F. R. De [BTK 65], [TPG 77], [TP 78]
 Tomasek, M. [MT 77]
 Tomonaga, S. [To 55]
 Torizuka, Y. [FT 72], [TIS 75], [ST 77]
 Toro, M. Di [BTR 77]
 Torres, J. P. [BT 71]
 Tourteil, R. De [LLR 75]
 Traini, M. [SLO 78]
 Tréherne, J. [ABR 75]
 Treiner, J. [BCK 76], [TK 76], [KTB 80]
 Troudet, T. [TA 79]
 True, W. W. [MT 73], [ST 76]
 Tsai, S. F. [BT 75], [Ts 78]
 Tsang, C. F. [NTS 69], [NTT 69], [SSW 69], [MT 75]
 Tuerpe, D. R. [TBK 70]
 Tyapin, A. S. [Ty 70], [Ty 71]
 Tyren, H. [MHT 58]
 Udagawa, T. [TU 64], [IUY 65], [MSU 67]
 Ueberall, H. [WU 66], [Ue 71]
 Uhlenbeck, G. [UF 74]
 Ui, H. [UB 68]
 Ullah, N. [UR 69], [Ul 71], [UR 71], [Ul 72]
 Une, T. [OU 75], [UIO 76]
 Unna, I. [UT 58], [UW 65]
 Urbano, J. N. [PUF 71], [ABC 77a], [ABC 77b]
 Usui, T. [Us 60]
 Valatin, J. G. [Va 56], [MV 60], [Va 61], [TV 62], [CV 66]
 Vallieres, M. [EVB 79], [VLS 79]
 Vanagas, V. [VNR 75]
 Vandenbosch, R. [Va 77]
 Vary, J. P. [VG 71], [GVS 76]
 Vaughn, M. T. [BSV 76]
 Vautherin, D. [NV 70], [NV 72], [VB 72], [FQK 73], [FQV 73], [Va 73], [FGV 74], [FV 74], [EBG 75], [FV 75], [NV 75], [Va 75], [FV 76], [GMQ 76], [GVV 76]
 Vdovin, A. I. [SSV 77]
 Vedelsby, P. [EKV 69]
 Vénéroni, M. [ABV 63], [AV 63], [ASV 64], [LV 68], [BFV 74], [FQV 74], [BGV 76], [GMQ 76], [GVV 76], [BV 78]
 Vergados, J. D. [Ve 68]
 Verhaar, B. J. [Ve 60], [Ve 63], [Ve 64]
 Veyssiére, A. [BBL 71]
 Vieu, Ch. [PVD 77]
 Vigdor, S. [SVE 76]
 Villars, F. [Vi 57a], [Vi 57b], [Vi 58], [Vi 63], [Vi 66], [VC 70], [Vi 71], [VS 71], [Vi 75], [MV 77], [Vi 77], [MV 78]
 Vinh-Mau, N. [GV 64], [BV 71]
 Vinh-Mau, R. [CLL 73], [LLR 75], [Vi 78]
 Visscher, W. M. [FV 56], [VF 57]
 Vivien, J. P. [BBB 79a]
 Vogel, P. [SV 63], [Vo 70], [NVR 75], [TNV 77]
 Vogeler, J. H. [MSV 72]
 Voigt, M. J. A. De [VGB 72]
 Volkov, A. B. [Vo 65], [LV 71], [GVL 73], [LMV 73], [SV 73]
 Volz, H. [RV 69]
 Voros, A. [Vo 77], [GV 79]
 Vucetich, H. [VPK 69]
 Vujičić, M. [HV 68], [VH 70]
 Waddington, J. C. [HRH 70]
 Wagner, G. J. [KWB 75]
 Wahlborn, S. [BW 60], [Wa 62b], [WB 69], [OWP 71]
 Wakai, M. [Wa 70a], [WF 78a], [WF 78b]
 Walcher, T. [RW 71], [Wa 73]

- Walecka, J. D. [GWW 58], [Wa 62a],
 [SW 66], [WG 67a], [FW 71]
 Walter, H. K. [EAD 75]
 Wambach, J. [SWK 76], [WMR 77],
 [WKS 78]
 Wang, W. L. [WS 72]
 Ward, D. [WBB 75], [WCL 76]
 Warke, C. S. [WG 67b], [KW 69], [Wa
 74], [NW 76], [NW 78]
 Watanabe, M. M. [TPG 77]
 Watanabe, Y. [Wa 56]
 Watt, A. [Wa 70b], [Wa 71], [MMW
 73], [MWW 74], [WWC 77]
 Weber, H. J. [WHG 66], [ADW 78]
 Weber, J. [SWK 72]
 Weidenmüller, H. A. [We 67], [MW
 68], [MW 69a], [EW 72], [SW 72],
 [SW 73], [HLR 74]
 Weiguny, A. [BW 68], [FWH 74]
 Weise, W. [BW 76]
 Weiss, M. S. [FKW 78], [FW 78]
 Weisskopf, V. F. [We 50], [We 51],
 [BW 52], [GWW 58]
 Weitzner, H. [BGW 58]
 Weizsäcker, C. F. Von [We 35]
 Welton, T. A. [WMW 75], [MWW
 76], [MW 77], [WWM 77]
 Weneser, J. [UW 65], [GW 68], [MW
 69b], [MW 70]
 Weng, W. T. [WKB 73]
 Werner E. [WE 70], [NW 72], [BSK
 73], [RW 73], [TW 73], [NW 74],
 [BER 75], [We 76], [SWW 77], [We
 78], [TW 78]
 Werntz, C. [WU 66]
 Wheeler, J. A. [BW 39], [HW 53],
 [GW 57]
 Whitehead, R. R. [Wh 72], [MWW
 74], [WWC 77]
 Wick, G. C. [Wi 48], [Wi 50]
 Wiener, N. [Wi 33]
 Wigner, E. P. [NW 29], [Wi 32], [Wi
 34], [Wi 37], [RW 54]
 Wikstroem, K. [BBH 77]
 Wilcox, R. M. [Wi 67]
 Wild, W. [BER 75], [SWW 77], [Wi
 77], [ERW 78]
 Wildenthal, B. H. [HMW 71], [WMH
 71], [PW 72], [VGB 72], [Wi 76]
 Wildermuth, K. [WM 66]
 Wilets, L. [BW 56], [WJ 56], [Wi 64],
 [FW 70], [BW 71], [HW 72], [HW
 74], [SW 75a], [SW 75b], [SW 78]
 Wilkinson, J. H. [Wi 65]
 Wille, U. [FLW 75]
 Williams, S. A. [KPW 68], [WP 68]
 Willis, A. [MMW 75]
 Winter, A. [ABH 56], [AW 66], [AW
 74]
 Wittmann, F. [FLW 73]
 Wittmann, R. [SWR 76]
 Wolter, H. H. [SFW 69], [WFS 70],
 [WFS 71], [GFW 72]
 Wong, C. [AW 61]
 Wong, C. W. [Wo 70], [Wo 75]
 Wong, C. Y. [BDJ 72], [MMW 75],
 [MWW 76], [Wo 76], [MMW 77],
 [WM 77], [WWM 77]
 Wong, S. K. M. [GLW 70], [WSR 71]
 Wong, S. S. M. [FHM 69], [RW 69],
 [RW 70]
 Woods, R. D. [WS 54]
 Woude, A. Van-der [HBI 77]
 Wycech, S. [NTS 69], [SSW 69]
 Yadav, H. L. [TYF 77], [YTF 77],
 [YTF 78]
 Yamada, E. [MY 55]
 Yamamura, M. [MYT 64a], [MYT
 64b], [Ya 65], [MYM 68], [GY 70],
 [Ya 74], [YN 76], [FYN 77], [IMNY
 77], [YSI 78], [IY 78]
 Yamaura, H. [IUY 65]
 Yamazaki, T. [BSK 73], [YNN 76]
 Yang, C. N. [Ya 67]
 Yaniv, Y. [LPP 75]
 Yoccoz, J. [PY 57], [Yo 57], [RY 66],
 [Yo 66]
 Yoon, B. [YN 77]
 Yoshida, S. [AY 59], [OY 66], [MSU
 67], [OSY 70], [YZ 72], [ISY 73],
 [AY 78]
 Youngblood, D. H. [KMY 75], [YMR
 76], [YRM 77]
 Yukawa, H. [Yu 35]
 Yukawa, J. [MYT 55]
 Yukawa, T. [HY 74]
 Yung-Li, S. [YKD 70]
 Zabolitzky, J. G. [KLZ 75], [KLZ 78]
 Zakharov, V. E. [ZS 72]
 Zamick, L. [MBZ 64], [KZ 70], [YZ

- 72], [SZ 73], [Za 73], [GSZ 74],
[SZR 74], [Za 74a]
Zaringhalam, A. [ZN 77]
Zawischa, D. [Za 74b], [ZS 75], [ZS
76], [ZSP 78]
Zeh, H. D. [Ze 65], [Ze 67]
Zeidman, B. [SVE 76]
Zeldes, N. [ZGS 67]
Zelevinskii, V. G. [BZ 62], [Ze 75]
Zener, C. [Ze 32]
Zimerman, A. H. [AAZ 77]
Zint, P. G. [GMZ 78], [Zi 78]
Zipfel, G. G. [BZ 73]
Zofka, J. [ZR 71]
Zucker, I. J. [NZ 64]
Zuker, A. P. [SZ 72]
Zumino, B. [Zu 62]
Zupancic, C. [HZ 53]

Subject Index

Abelian symmetry groups 459
Abnormal coupling states 396
Abnormal density 251, 551, 608
Absorption probability 587
Acceleration of system 512
Action integral 489, 563
A-dependence
– *B* (*E*2)-values 14
– binding energy 4
– giant resonance energy 15, 16, 293, 295,
 334, 360, 571
– gyromagnetic ratio 13
– moment of inertia 19
– radius 3
Adiabatic approximation 508, 520
Adiabatic basis 495, 524
Adiabaticity 520, 565
Adiabatic limit 506, 524
Adiabatic motion 510
Adiabatic perturbation theory 523ff.
Adiabatic time-dependent Hartree–Fock
 (ATDHF) 501–525
– applications 521–523
– approximation 507
– equations 509, 511, 518
– Hamiltonian 511, 514
– local representation 515
– mass 511, 515
Airy function 537

Alignment (rotational) 101, 111, 115–118,
 123, 276, 385
Analog (isobaric)
– resonance 291, 297
– state 299
Angular momentum
– algebra 348, 575–579
– boson representation 348
– collective 108
– commutation relation 348
– constraint 272, 278
– coupling 10, 52, 226, 325
– intrinsic components 20, 457, 577
– maximal stable 35
– projection 473–484
– representation by Euler angles 577
– selection rules 583, 590
– total 490
Angular velocity 103, 127, 130, 272
Anharmonicities 17, 347, 375, 397
Annihilation operator 596
Anti-commutator 598, 601
Anti-linear operators 251
Anti-pairing effect (*see* Coriolis anti-pairing
effect)
Asymmetric rotor 26, 123
Asymptotic quantum number 72
ATDHF (*see* Adiabatic time-dependent
Hartree–Fock)

- Attenuation factor 120, 278
- Attractive interaction 286
- Average field 39, 210
- Average level density 86
- Average potential 38, 210
- Averaging procedure 86–90
- Axial symmetry 22, 109, 477, 478

- β -band 348
- β -vibration 22
- B -coefficient 103, 133
- $B(E0)$ -values 327, 434
- $B(E2)$ -values
 - enhanced 450
 - experimental 14
 - liquid drop 13
 - particle-plus-rotor model 125
 - rotor model 25
 - RPA 327, 328
 - seniority model 227
- $B(E1)$ - and $B(M1)$ -values
 - definition 13, 589
 - projected 480
 - RPA-calculation 327
- $B(MI)$ -values
 - particle-plus-rotor model 125
 - RPA 328
- Back bending 101, 104–107, 121, 272, 274
 - giant 140
 - plot 104, 106, 140, 274
 - second 107
- Baker–Campbell–Hausdorff formula 412
- Balian–Brézin formula 617–618
- Band crossing 106, 274, 277
- Band head 78, 112
- Baranger–Vénéroni decomposition 507, 605–606
- Bargmann
 - δ -function 413
 - measure 412
 - representation 408, 412–414
 - space 411
- Bartlett force 154
- Basic operators 352
- BCS (Bardeen, Cooper, Schrieffer)
 - and coherent states 449
 - and gauge symmetry 448
 - decomposition of the wave function 483
 - equations 230, 262, 550
 - phase convention 184
 - state 343
 - theory 228–243
 - wave function 228
- Belyaev formula 131
- Belyaev–Zelevinskii boson
 - representation 352, 354–362, 383
- Beringer–Knox shapes 34, 99
- Bethe–Goldstone equation 156, 204, 207
- Bethe–Salpeter equation 319, 324, 640–642
- Bethe–Weizsäcker formula 4, 84
- Binding energy
 - per nucleon 2, 3
- Biorthogonal basis 403, 475
- Bloch–Messiah theorem 246, 251, 261, 272, 611–612, 616
 - for bosons 620
- Blocked levels 248
- Blocking 101, 234, 237, 248, 249, 257, 258
- Body-fixed system 18, 21, 457, 576
- Bogoliubov quasi-particles 234
- Bogoliubov transformation
 - for bosons 620–622
 - general 245–251, 308, 361
 - special 234, 248
- Bohr Hamiltonian
 - rotation-vibration 18, 20, 522
 - vibration-particle-coupling 383
- Bohr–Tassie model 336, 561
- Boltzmann equation 553
 - collisionless 553
 - linearized 554
- Bombarding energy 505
- Bose–Einstein condensation 229, 446
- Boson–boson interaction 367, 373, 378
- Boson commutation relation (*see* Commutation rules)
- Boson condensate 301, 446, 450
- Boson operator 9, 307, 341, 597
- Boson representation 346–397
 - and GCM 406–408, 414
 - and phase transitions 445
 - applications 375–381
 - Belyaev–Zelevinskii 352–362
 - Dyson 350, 367, 370, 390
 - for even systems 348–381
 - for odd mass systems 382–397
 - Holstein–Primakoff 348, 350, 360, 374, 378
 - Marumori 352, 362–366
 - mathematical background 368–372
 - microscopic 380
 - of angular momenta 348–351
 - perturbative 358–361
 - phenomenological 375
 - Schwinger 350, 354, 373
- Boson vacuum 348, 352, 363, 620
- Breathing mode 291, 296, 327, 333, 334, 337, 433, 523, 572
- Brink–Booker force 177, 433

- Broken symmetry (*see* Symmetry violation)
- Brueckner G-matrix 156, 203
- Brueckner–Hartree–Fock 203, 633, 635
- BSE (*see* Bethe–Salpeter equation)
- Bulk properties 83

- Canonical**
 - basis 248, 251, 256, 272, 344
 - coordinate 309, 312, 338, 509, 515
 - form 247, 251, 609, 611
 - momentum 312, 509, 515
 - quantization 9, 586
 - variables (weakly) 515
- CAP-effect 100, 275
- Casimir operator 349, 352
- C-coefficient 103, 133
- Center of mass
 - angle 313, 457, 493, 507
 - coordinate 313, 452, 490
 - motion 6, 456, 492
 - system 454, 592
- Central force 152, 174
- Centrifugal forces 128, 137
- Chapman–Enskog development 557
- Charge distribution 214, 581
- Chemical potential λ
 - and gauge transformations 448
 - as frequency of pairing rotations 447
 - as generator coordinate 435, 473
 - in the BCS model 230, 236
 - in the HFB theory 254, 259
 - in the Strutinski method 85, 89
 - in the Thomas–Fermi theory 532
- CHF (*see* Constraint Hartree–Fock)
- Classical
 - approximation 520
 - aspects of coherent states 415
 - aspects of the mean field approach 446
 - aspects of the TDHF method 496, 509
 - Bohr Hamiltonian 522
 - case for giant resonances 336
 - deterministic behavior 495
 - equation of motion 490, 507, 512, 515, 564
 - Hamilton function 511, 516
 - limit of TDHF 522
 - path 417
 - TDHF 520
 - trajectory 495
 - turning point 532
- Closed shell nuclei 434
- Closure relations 289, 303, 306, 341, 355, 412
- Cluster representation 399
- Coester line 206

- Coherent states**
 - and phase transitions 446, 449, 450
 - definition 412
 - properties 415, 622
- Coherent superposition 281, 286, 288, 299
- Collective 3⁻-state (*see* Octupole vibration)
- Collective coordinates 430–432, 452, 513, 516
- Collective effect of transition 227
- Collective energy 287, 320, 521
- Collective excitations 281, 287, 290–301
- Collective fermion pairs 346, 353, 355, 364, 446
- Collective Hamiltonian
 - ATDHF 506, 510, 514, 522
 - coordinate transformation 452
 - GCM 402, 419–432
 - liquid drop model 9, 20
 - particle-plus-rotor model 107
- Collective mode 290–301, 450
- Collective model 9, 20, 107
- Collective path 425, 430–432, 517
- Collective *p*_h vibration 290
- Collective states 287
 - low lying 293
 - classification 292
- Collective strength 281, 288, 321
- Collective subspace
 - boson representation 347, 359, 364
 - generator coordinates 402, 406, 409, 410
 - projection methods 451, 458
- Collective velocity 492
- Collective vibration 290–301, 450
- Collisions 487
- Commutation rules
 - angular momenta 222, 348
 - bosons 307, 352, 369, 586, 597
 - canonical 309, 312
 - fermion pairs 355, 382
 - fermions 234, 246, 598
- Completeness relations (*see* Closure relations)
- Compressibility (*see* Incompressibility)
- Compressible 336
- Compression modulus 321
- Condensate of bosons 229, 301, 446, 450
- Condon–Shortley phases 184
- Conjugate states (canonically) 228, 248, 272
- Conservation
 - laws 555
 - of energy 490
 - of orthogonality 489
 - of symmetries 490
- Constrained Hartree–Fock (CHF)
 - theory 266–271
 - and ATDHF 517, 521

- Constrained Hartree-Fock (CHF) [*cont.*]
- and linear response 321
 - and sum rules 333
 - applications 270, 272, 433
 - (*see also* Constraint)
- Constrained motion 569
- Constraint
- linear 267
 - optimal 268, 432, 518
 - quadratic 267
 - second 271, 463
 - self-consistent 432
 - unbounded 270
- Constraint of
- angular momentum 272, 278
 - deformation 269
 - fluctuations 271, 463
 - orthogonality 257, 278
 - particle number 230, 259, 268, 449
- Contact force 174
- Continuity equation 588
- Continuous symmetry 203, 311, 317
- Continuum RPA 322–325
- Contraction 601, 619
- Convergence of boson expansions
- Belyaev-Zelevinskii 359
 - Dyson 367
 - horizontal 368
 - Marumori 365
 - vertical 368
- Cooper pairs 99, 219, 260, 275, 354, 372
- Cooper pole 635
- Coordinate, generalized 309, 338, 515
- Coordinate space representation
- ATDHF 523
 - Bethe-Salpeter equation 324
 - density matrix 604, 608
 - field operators 598
 - HF equations 196
 - TDHF equations 488
- Core polarization 169, 216, 390
- Coriolis anti-pairing (CAP) effect 100, 275
- Coriolis force 128
- Coriolis term 100
- attenuation of 120
 - effect of 100, 123, 274–277
 - in TDHF 493
 - in the cranking model 128, 275
 - in the Nilsson model 137
 - in the particle-plus-rotor model 108, 110, 116
- Correlation
- energy 445, 448
 - function 487
- Correlations 439, 491, 633
- *ph-* 302
- *2p-2h-* 283
 - ground state 303, 342, 343
 - long range 185
 - of valence nucleons 288
 - short range 185
- Coulomb gauge 584
- Coulomb potential
- and analog resonances 297
 - in HF calculations 209
 - in TDHF calculations 501
 - in the Nilsson model 80
 - in the shell model 47
- Coulomb term 5
- Coupling
- intermediate 390–397
 - minimal 453
 - strong 110–112
 - weak 112–115, 385–389, 397
- Cranking formula
- for general collective motion 525
 - for rotations 130, 131, 314, 322
- Cranking frequency 103, 127, 130, 272, 468, 479
- Cranking model for general collective motions 523–525
- Cranking model for rotations
- and the harmonic oscillator 133–137
 - and phase transitions 449
 - as approximate projection 468, 478
 - as TDHF-solution 493
 - pure single-particle case 126–145
 - self-consistent (SCC) case 271–279, 478–480
 - semiclassical derivation 127
- Crank–Nicholson operator 501
- Creation operator 597
- Critical coupling constant
- and phase transitions 443, 444
 - in the BCS model 343, 465
 - in the GCM 435
 - in the Lipkin model 200, 361
 - in the RPA 320, 342, 361
- Critical level density 443, 465
- Cross section of dipole absorption 294
- Current density 581
- Current distributions 504
- Curvature corrections
- to the collective path 519
 - to the Strutinski method 87
- Curvature of the energy surface 12, 191, 199, 211, 321, 329
- Curvature tensor 253, 513
- d*-boson 373, 377
- δ -force 173, 174, 197, 499

- D*-functions 576
- D*₂-group 21, 476
- Damped collisions (strongly) 505
- Damping 494
- Daughter nucleus 297, 298
- DBE (*see* Dyson boson expansion)
- Decay width 323
- Decoupled bands 102, 117
- Decoupling factor 112, 125
- Decoupling limit 110, 115–118
- Deformations
 - and BCS 219
 - and level crossings 565
 - and phase transitions 443–450
 - changes in 106, 140, 274
 - equilibrium 80
 - hexadecupole 6, 66, 81, 265
 - in the liquid drop model 5–9
 - in the shell model 65–83
 - octupole 6, 442
 - of the Fermi sphere 566–571
 - prolate–oblate 118, 142
 - quadrupole 6–9, 66, 260, 441–451
 - triaxial 27, 101, 122, 140, 385
- Deformation alignment 110–112
- Deformation energies
 - liquid drop 12
 - shell model 79
- Deformation energy surface
 - constrained HF 270
 - liquid drop model 12, 28, 30, 32
 - rotating 33, 139–141
 - shell model 83
 - Strutinski 92, 95
- Deformation equation 261, 442, 450
- Deformation parameter
 - $\alpha_{\lambda\mu}$ 5
 - β_λ 5
 - β 5, 34, 69, 275
 - γ 5, 34, 275
 - δ 68
 - ϵ_1 72
 - q 261
- Deformed harmonic oscillator 68, 548
- Density 209, 289, 530
 - and sum rules 335
 - distributions 214, 271, 532, 544, 548
 - Hartree–Fock 209, 214
 - oscillations 532, 548
 - semiclassical 537
 - Strutinski smoothed 90, 93
 - TDHF profiles 503, 504
 - Thomas–Fermi 531, 544
- Density dependent forces 174, 176–178
 - Hartree–Fock (DDHF) 203–215
 - HFB 264–265
- linear response 316, 317
- RPA 317
- sum rules 332
- Density matrix 529, 603–610
 - abnormal 251, 550, 608
 - generalized 252, 608
 - normal 251, 608
 - one-particle 603
 - two-body 487
- Density of states (*see* Level density)
- Dipole
 - moment (*see* Magnetic moment)
 - operator 294, 592
 - radiation 593
 - sum rule 294
 - transition density 561
 - vibrations 434, 569
- Dirac perturbation theory 587
- Direct term 285
- Discretization
 - continuum RPA 323, 325
 - GCM 401, 403, 404, 433
 - TDHF 501
- Dispersion relation 320, 342
- Distorted rotational bands 119
- Double projection 418, 473
- Double variational method 431, 477
- Droplet model 5
- Dynamic kinetic energy density 570
- Dynamic part of the mass operator 635
- Dynamic polarizability 322
- Dynamic properties
 - of boson representation 347, 359, 365
 - of the GCM 403
- Dynamic semiclassical theory 550–574
- Dynamic solution of TDHF 492
- Dyson boson expansion 350, 367, 370, 390, 408
- Dyson equation 635, 638
 - for bosons 640
- Dyson operator 369
- Effective charge 65, 389–390
- Effective fermion space 365
- Effective *g*-factors 581
- Effective interaction
 - and Green's functions 640–642
 - and VPC-theory 385
 - between valence particles (*pp*) 164–170, 641
 - between particles and holes (*ph*) 170–172, 640
 - between quasi-particles 178, 640ff.
 - experimental 185–187
 - *G*-matrix 156–164

- Effective interaction [cont.]**
- microscopic 156–172
 - momentum dependence 173
 - phenomenological 172–185
 - renormalized 177, 326
- Effective mass** 139, 212, 214, 523
- Effective matrix element** 389
- Effective single-particle potential** 628
- Electromagnetic moments** 581–584
- liquid drop 13
 - particle-plus-rotor model 125
 - projected theory 480
 - rotor model 25, 26
 - shell model 60
- Electromagnetic multipole operators** 12, 582
- Electromagnetic transitions** 587–590
- liquid drop 13
 - particle-plus-rotor model 125
 - projected theory 480
 - rotor model 25, 26
 - shell model 60
- Elliott–Clark force** 175
- Elliott model** 379
- Elongation coordinate** 29
- Emission probability** 587
- Energy curve** 32, 83, 92, 270, 523
- Energy density** 209, 555
- Energy functional** 194
- Energy gap** 218, 236
- Energy overlap** (*see* Overlap functions)
- Energy of resonance** 331
- Energy in the rotating frame** 129, 142
- Energy spin traps** 144
- Energy spread** 499
- Energy surface**
- and collective motion 431, 451
 - and phase transition 443
 - ATDHF 523
 - boson model 376
 - constraint HF 269–270
 - curvature 191, 199, 211, 321, 329
 - Hartree–Fock 253
 - HPB 258, 264
 - in the rotating frame 139–141
 - Lipkin model 200
 - liquid drop model 28, 30, 32
 - multidimensional (TDHF) 494
 - projected 462
 - RPA 317
 - shell model 83
 - Strutinski method 92, 95
- Energy of surface vibration** 334
- Energy weighted moments** 330
- Energy weighted sum rule** 294, 331
- Enhanced transition** 321
- Equation of continuity** 559, 564, 588
- Equation of motion** 301, 340, 487, 625
- classical 490, 507, 512, 515, 564
- Equilibrium deformation** 80
- Equipotential line** 490
- Equipotential surfaces** 388
- Escape width** 494
- ETF theory** (*see* Extended Thomas–Fermi theory)
- Euler angles** 18, 443, 453, 457, 473, 576
- Euler equation** 557, 559, 564
- Evolution operator** 485, 501
- Exchange mixtures** 174
- Exchange operator** 150, 153
- Exchange potential** 196, 488 (*see also* Fock potential)
- Exchange term** 285, 387
- Excitation**
- $p\hbar$ 48, 283, 292
 - $2p\cdot 2h$ 300, 304, 323, 435
 - probability 319, 326, 589
 - strength 323
- Extended Thomas–Fermi theory** 527, 534–550
- External field**
- static 267
 - time dependent 314
- Factorization** 225, 487, 633
- Fallieros sum rules** 335
- Favored states** 114, 116
- FBCS-theory** 462, 464
- Fermi commutation relations** 234, 246, 598
- Fermi momentum** 210, 532, 569
- Fermi sphere, deformed** 566–571
- Fermi surface, smeared out** 495
- Fermion operators** 597
- Fermion pair operators** 307, 351, 354
- collective 346, 353, 355
 - non-collective 354
- Ferrel–Vischer force** 174
- Feshbach projection formalism** 165, 171, 628
- Feynman graphs** 285
- Feynman theorem** 321, 608
- Field operators** 598
- Final state interaction (spurious)** 499
- Finite range** 173, 176, 187, 501
- Fissibility parameter** 29, 31
- Fission** 28–32, 95, 270, 505
- barrier 31, 83, 270
 - isomers 66, 83, 95
 - path 31, 95, 269–271
 - process 266, 270
 - valley, 31, 269

- Flow pattern** 11, 504
- Fluctuations**
 - and phase transitions 445
 - and projection techniques 467, 479, 483
 - as constraint 271
 - in the angular momentum 479, 483
 - in the momentum 425, 428
 - in the order parameter 445
 - in particle number 230, 233, 242, 483
 - of the symmetry operator 470
- Fluid dynamics** 555, 562, 568, 573
- Fock potential** 197, 261, 488
- Fock space** 347
- Folded diagrams** 166
- Folded Yukawa potential** 81
- Fomenko method** 463
- Form factor** 325, 388
- Fragmentation coordinate** 29
- Friction** 517
- Fusion** 505, 561

- Galilean invariance** 128, 151, 313, 452, 454, 470, 473
- γ -band** 273, 278, 345
- γ -cascade** 98
- γ -continuum** 98
- γ -soft oscillator** 379
- γ -vibration** 22
- Γ -coefficients** 356, 363
- Gap equation** 199, 232, 233, 238, 343, 441, 450, 636, 638
 - analytic solution 240
- Gap parameter Δ** 213–233, 236, 242
 - and phase transition 449
 - as generator coordinate 435
 - semiclassical 552
- Gapless superconductivity** 277
- Gauge**
 - angle 447, 452
 - Coulomb- 584
 - symmetry 457, 459
 - transformations 447
- Gaussian barrier** 497
- Gaussian force** 174, 176, 551
- Gaussian overlap** 409, 414, 420, 425, 467, 475
 - approximation (GOA) 424–428
 - multidimensional 430
- Gaussian wave packets** 414–417
- GCM** (*see* Generator coordinate method)
- Generalized coordinate** 309, 338, 515
- Generalized momentum** 309, 338, 515
- Generating function** 399, 410

- Generator coordinate method**
 - (GCM) 398–437
 - and boson representations 352, 406
 - and projection methods 458
 - and RPA 308
 - applications 433–437
 - numerical solution 404
 - wavefunction 399
- Generator coordinates** 399, 476
 - complex 400, 410, 411–414
 - redundant 418
- Geodesic distance** 430
- GF** (*see* Green's functions)
- g -factor** 63, 581
- Giant dipole resonance** 15, 16, 281, 293–295
 - fluid dynamics 568–572
 - hydrodynamical models 558–561
 - RPA 325–329
 - splitting 294
- Giant quadrupole resonance** 16, 295, 327, 334, 445
- Giant resonances**
 - classification 290–297
 - deformed nuclei 294, 296, 345
 - fine structure 281, 289, 294
 - fluid dynamics 568–572
 - GCM 433–435
 - hydrodynamical models 558–561
 - RPA 325–330
 - sum rules 333–339
 - width 323
- Gillet force** 174, 326
- Global approximation** 423
- Global properties** 330
- G-matrix** 157, 203–207
- Gogny force** 176, 265
- Goldhaber–Teller model** 295, 558, 560
- Gorkov equations** 635
- Gradient expansion** 535
- Gradient method** 200, 255, 258–259, 268
- Gram–Schmidt method** 306, 401
- Graph** 284, 304, 628
- Graphical solution** 287, 320
- Green's functions** 623–642
- Grodzin's rule** 14
- Ground state**
 - correlations 301, 320, 341, 433, 436
 - deformations 80
 - deformed 262
 - energy 79, 194, 209, 300, 530, 533, 624
 - rotational band 100, 273, 278, 433, 478
 - spins 78, 219
- Gyromagnetic ratio**
 - cranking model 132
 - particle-plus-rotor model 125

- Gyromagnetic ratio [cont.]
 - rotor model 13
 - shell model 63

- \hbar -correction 535
- \hbar -expansion 535, 545
- Hamada-Johnston potential 155, 167
- Hamilton equations 512, 515, 564
- Hamilton function in collective variables 514
- Hamilton overlap (*see* Overlap functions)
- Hard core 155, 159–163, 185, 203
- Harmonic approximation
 - locally 519, 545–547
 - RPA 308, 513
- Harmonic interaction 455
- Harmonic oscillator
 - and center of mass motion 456
 - and coherent states 412–417
 - and GCM 409–411
 - and RPA 309, 513
 - anisotropic 68–70
 - deformed 68–70, 548
 - propagator 538–545
 - quantization 9, 586
 - rotating 133–139
 - spectrum 41
 - shifted 415
 - spherical 40–42
 - surface vibrations 9, 10
 - time dependent 416–417, 573
 - wave packets 414–417
- Harmonic spectrum 10, 41, 224, 300
- Harris model 103
- Hartree-Fock (HF) 189–216
 - and shell corrections 92, 93
 - and symmetries 201–203
 - applications 205, 213–215
 - basis 193, 315, 614
 - constrained 266–271
 - density 193, 209, 214, 316
 - density dependent-(DDHF) 203–215
 - energy 194, 209
 - equations 195, 196, 212, 626
 - Hamiltonian 196
 - numerical solution 197, 258
 - potential 196, 487
 - wave functions 192, 201
- Hartree-Fock-Bogoliubov (HFB) 244–279
 - basis 246, 253, 613–614
 - calculations 262–266, 271–279
 - constrained 266–271
 - densities 251–252, 551
 - density dependent 264–266
 - energy 254, 265, 613
 - equations 254, 266, 272, 635
 - Hamiltonian 254
 - in the rotating frame 271–279
 - matrix 254, 265, 636
 - numerical solution 258
 - potentials 254, 265
 - wave functions 249, 250
- Healing distance, 163, 205
- Heat current density 555
- Heavy ion scattering 497, 504
- Heisenberg force 154
- Helmholtz equation 584
- Hermite wave packets 417
- Hexadecupole deformations 6, 66, 81, 265
- HF (*see* Hartree-Fock)
- HFB (*see* Hartree-Fock-Bogoliubov)
- Higher RPA 311
- High spin states 96–145, 271–279
- Hilbert-Schmidt type 401, 409
- Hill-Wheeler coordinates 7, 34, 141
- Hill-Wheeler equation 400, 404, 413
- Hiskes shape 34, 99
- Hohenberg-Kohn theorem 541
- Holstein-Primakoff boson
 - representation 348, 350, 360, 374, 378
- Hulthen force 174
- HW equation (*see* Hill-Wheeler equation)
- Hydrodynamical models 11, 336, 558–562
- Hypernetted chain formalism 205

- IBA (*see* Interacting boson model)
- $I=0$ pairs 219
- Incompressibility
 - and breathing mode 296, 433
 - and force parameters 211
 - and linear response 321
 - and velocity distribution 336, 337
 - definition 211
 - Goldhaber-Teller model 560
 - liquid drop model 11
 - semiclassical theory 543
 - Steinwedel-Jensen model 560
- Inelastic scattering 295
- Inertial parameter 470–472 (*see also* Mass parameter; Moment of inertia)
- Inertia tensor 430, 457, 511, 514, 522
- Infinitesimal generators 515
- Inglis formula 131, 134, 322, 471, 472, 522
- Interacting boson model 373, 377–379
 - γ -soft limit 379
 - rotational limit 379
 - vibrational limit 379

- Interaction (*see* Nuclear forces)
- Intermediate coupling 390–397
- Internal (*see* Intrinsic)
- Intrinsic
 - components of the angular momentum 20, 457, 577
 - coordinates 443, 451–458
 - degrees of freedom 452
 - Hamiltonian 452, 455
 - quadrupole moment 25, 66, 123, 439, 480
 - wave function 127, 272, 474, 475, 478, 482, 499
- Intruder state 113, 170
- Invariance 311
 - of nucleon–nucleon force 150–152
- Inverse energy weighted sum rule 333
- Irreducible graphs 632
- Irrational
 - flow 11, 336, 337, 560, 564, 569, 570
 - moment of inertia 19, 20, 122, 135
- Island of isomers 65, 145
- Isomers
 - high spin 65, 102, 143–146
 - K - 145
 - shape 67, 83, 95
- Isolated crossing (of levels) 526
- Isoscalar excitations ($\Delta T=0$) 291, 295, 333, 334, 523
- Isoscalar monopole mode (*see* Breathing mode)
- Isospin 53–56
 - and analog resonances 297–299
 - and the giant dipole resonance 925
 - dependence of the residual interaction 286
 - flip 291
 - impurity 56
 - invariance 151
 - modes 291
- Isotopic spin (*see* Isospin)
- Isovector excitations ($\Delta T=1$) 291, 295, 559
 - (*see also* Giant dipole resonance)
- Iterative diagonalization 200, 255, 257

- $j-j$ coupling scheme 43
- Jacobi coordinates 452
- Jacobi shapes 33, 140

- Kallio–Koltveit force 175
- Kamalah expansion 467, 478, 480
- $K=0$ bands 22

- $K \neq 0$ bands 23
- K -forbidden transitions 126, 145
- Kinematic properties
 - of boson representations 347, 359, 365
 - of the GCM 403
- Kinetic energy 16, 511, 520, 514, 600
 - density 209, 530, 533, 544, 610
 - density functional 541
 - of surface vibrations 11
- K -isomers 145
- Knudsen gas 557
- Kuo-Brown force 167ff., 326
- Kurath force 174

- LACM (*see* Large amplitude collective motion)
- Lagrange multiplier 123, 230, 252, 259, 267, 532
- Lagrangian 489, 562
- Laguerre polynomials 88
- Λ -shell 239
- Landau–Zener formula 526, 565
- Laplace equation 582
- Laplace transformation 529
- Large amplitude collective motion (LACM) 398, 422, 506, 513
- Large deformations 67, 466
- LCAO-method 398
- Level
 - blocked 248
 - paired 248
- Level bunching 82, 84
- Level crossing 76
 - and ATDHF 521
 - and deformation 565
 - and GCM 420
 - and reoccupation 565
 - in the Nilsson diagram 76
 - time dependent 526
- Level density
 - and deformation 81, 82
 - and pairing correlations 242
 - and shell effects 84
 - average 86, 529
 - even–odd effect in 218, 225
 - model with uniform 240
 - shell model 85
 - Strutinski smoothed 86, 529
- l -forbidden M1-transitions 63, 145
- l^2 -term 70, 72, 139
- Life time of Slater determinants 498
- Linear constraint 267
- Linear momentum (total) 460, 490

- Linear potential 537, 545
- Linear response theory 132, 314–325
- Linked matrix elements 427
- Lipkin model 197–198
 - and ATDHF 522
 - and boson representations 350, 352, 357, 366
 - and Gaussian overlap approximation 428–429
 - and GCM 405–406
 - and gradient method 200
 - and Hartree–Pock 198–201
 - and SCRPA 361
 - and TDHF 490, 501
 - energy surface 200
 - exact solution 405–406
 - overlap functions 405
 - with three levels 432
- Lippmann–Schwinger equation 156
- Liquid drop 1–35
 - and shell corrections 83–95
 - energy surface 28, 30, 32
 - model 1–35
 - parameters 4, 549
 - rotating 32–35, 99
- Local approximation (LA) 423
- Local density approximation (LDA) 163, 206, 551
- Local equilibrium 556
- Local force 149
- Local harmonic approach 519
- Locally harmonic 545, 546
- Local momentum 532
- Local potential 196ff.
- Local redundancy 419
- Local representation of ATDHF 515
- Local response function 324
- Local RPA 519
- Löwdin projector 474
- Long range order 441
- Long wavelength limit 589

- Maclaurin shape 33
- Magic number 37, 38, 83
- Magnetic moment (dipole) 584
 - and center of mass motion 456
 - density 581
 - in the cranking model 132
 - in the liquid drop model 13
 - in the particle-plus-rotator model 125
 - in the shell model 61–63
 - tensor component 63
- Magnetic multipole operators 13, 583, 589
- Magnetic resonance 297, 327

- Majorana force 154
- Many-body Green's functions 629
- Many-body Schrödinger equation 45
- Many-quasi-particle state 49, 251
- Marumori boson representation 352, 362–366, 371–372
- Marumori operator 363, 371
- Mass distribution 497
- Mass operator 626
- Mass parameters 470–473
 - ATDHF 511, 515
 - boson model 376
 - cranking formula 525
 - GCM 422, 427, 429
 - liquid drop model 11
 - (*see also* Moment of inertia)
- Mass tensor 430, 511, 513, 515
- Maximal overlap, principle of 76, 115, 123, 144, 145, 220
- Maxwell–Boltzmann distribution 556
- MBZ-interaction 185
- MDI-interaction (*see* Modified δ -interaction)
- Mean field 316, 317, 439, 441, 444, 491
- Mean free path 37, 494, 557
- Mean square deviation (*see* Fluctuation)
- Mean square radius (*see* Root mean square radius)
- Mesonic degrees of freedom 147, 155
- Metric
 - GCM 425, 430
 - RPA 304
- Metric tensor 19, 430
- Migdal force 177–179, 326–328, 433
- Minimal coupling, principle of 453
- Mode coupling 397, 436
- Modified δ -interaction (MDI) 176, 433
- Moment expansion (*see* Symmetric moment expansion)
- Moment of inertia 458, 470–473
 - ATDHF 511, 516, 523
 - average (single particle rotation) 143
 - Belyaev 131
 - cranking model 129–132, 274
 - experimental 19, 103, 104, 219
 - harmonic oscillator 136, 457
 - hydrodynamical 18, 135, 457
 - Inglis 130, 134, 471, 522
 - irrotational flow 19, 20, 122, 135
 - linear response 133, 322
 - rigid body 19, 33, 131, 135, 137, 139
 - self-consistent 271, 313, 322, 469
 - Skyrme 472
 - Thouless–Valatin 313, 322, 458, 469, 471, 472, 511
 - variable (VMI) 104

- Yoccoz (OCM) 428, 469, 472, 475
- Moment of the strength function 330ff.
- Momentum
 - generalized 312, 416, 509, 515
 - total linear 490
- Momentum dependence 173
- Momentum distribution 562, 564, 569 (*see also* Velocity distribution)
- MONA-effect 145
- M*1-transitions 63, 125
- Monopole
 - mode, (*see* Breathing mode)
 - pairing force 184
 - part of the mean field 441
 - sum rule 333
 - transition density 337
- Mori theory 640
- Mother nucleus 298
- Mottelson-Suzuki model 334
- Mottelson-Valatin effect 101, 107, 276, 465
- Moving frame 492
- Multidimensional energy surface (*see* Energy surface)
- Multidimensional Gaussian overlap 430
- Multipole expansion 582, 584ff.
- Multipole-multipole forces 182
- Multipole operators 582, 588ff.
- Multipole pairing forces 185
- Multipole radiation 587-590
- Multipole strength 14, 327
- Multipole transitions 587ff.

- Narrow overlap approximation 467, 479
- Natural states 402, 403, 404
- Navier-Stokes equations 557
- Neck coordinate 29
- Negative parity band 273
- Negative quasi-particle energy 257, 275
- Neumann-Wigner no-crossing rule 76, 526
- NFT (*see* Nuclear field theory)
- Nilsson
 - diagram 72-77, 138
 - energies 79
 - Hamiltonian 70
 - levels (slope) 77
 - model 70-80, 262
 - parameters 70, 76
 - potential 70, 261
 - quantum numbers 69
 - rotating model 137-139
 - wave function 77
- No-alignment limit 113
- No-crossing rule 76, 106
- Non-Abelian symmetry groups 460

- Non-collective bosons 369-372, 373, 383
- Nonlocal behavior of the density ρ 207, 291
- Nonlocal operator 600
- Nonlocal potential
 - Hartree-Fock 197
 - semiclassical treatment 549
- Nonlocality of χ -BV 574
- Non-orthogonal basis 368, 392, 401, 475
- Normal ordered product 150, 255, 414, 421, 601
- Norm matrix
 - bosons 363-368, 371
 - GCM 401, 404
 - projection 475
- Norm overlap (*see* Overlap functions)
- Nuclear field theory (NFT) 386, 391
- Nuclear forces 147-188
 - bare 156-159
 - effective 156-172 (*see also* Effective interaction)
 - experimental 185-187
 - invariances of 150-152
 - phenomenological 172-185
- Nuclear magneton 61
- Nuclear matter 159, 206, 210, 543, 550
 - slab of 497
- Nuclear Meissner effect 276
- Nuclear twist 291
- Nucleon-nucleon force 149, 153
 - invariances of 150-152
- Number parity 250, 256
- Numerical solution
 - HF 197, 258
 - HFB 258
 - GCM 404
 - RPA 306, 325
 - shell model 50
 - TDHF 501

- Oblate deformations 101, 118, 142, 263
- Occupation number representation 587, 596
- Occupation numbers 604
 - BCS 228, 232
 - generalized (Strutinski) 89
 - HF 193
 - HFB 251, 256, 264
 - quasi-particle (Landau) 177
 - self-consistent cranking 273
 - second quantization 596
 - shell model 90
 - TDHF 495
 - with projection 463
- Octupole
 - deformations 6, 442

- Octupole [*cont.*]
 - transition density 339
 - vibration 10, 206, 287, 292, 326, 339
- Odd-even effect 218, 236
- Odd I-values 477
- Odd-mass nuclei
 - BCS 235, 237
 - GCM 437
 - HF 215
 - HFB 257, 278
 - particle-plus-rotor model 107–126
 - particle-plus-vibrator model 381–396
 - seniority model 225
 - shell model 51, 60, 61, 78
- Off-shell behavior of the NN-force 187
- One-body
 - density 603
 - dissipation 491
 - friction 487, 494
 - operator 599
- One-pion exchange potential (OPEP) 155
- One quasi-particle state 237, 250
- Onishi formula 407, 424, 618–620
 - for bosons 622
- Open shell Hartree–Fock 215
- Open shell nuclei 288
- Open shell RPA 302
- Optical model potential 627
- Optimal constraint 268, 432, 518
- Order parameter 279, 443, 450, 638
- Orthogonality relations 289, 305, 341, 355
- Orthogonalization 259, 306, 363, 371, 392, 401, 475
 - Gram–Schmidt 306, 401
 - symmetric 401
- Oscillating charge 291
- Oscillating slabs 502
- Oscillator (*see* Harmonic oscillator)
- Oscillator frequency 41
- Oscillator length 41
 - as generator coordinate 433
 - deformation dependent 68
 - time dependent 416, 573
- O(6) model 379
- Overcomplete basis 392
- Overhauser states 441
- Overlap angle 186
- Overlap functions
 - for boson vacua 622
 - for the Lipkin model 405
 - for oscillator functions 433
 - for projections 466, 481
 - for Slater determinants 498
 - Gaussian form 409, 424, 467
 - in GCM 401, 406, 407, 409, 420, 428, 434
 - multidimensional 430, 481
 - Onishi formula 618–620
 - with Skyrme forces 433
- Overlap integrals (*see* Overlap functions)
- Pair condensate 225
- Pair creation operator 229
- Pair transfer 450
- Pair wave function 220
- Paired levels 248
- Pairing correlations 80, 91, 122, 217, 270, 343, 436, 446, 465
- Pairing energy 91, 242, 551
- Pairing field Δ 221, 254, 260, 261, 266, 279, 449, 550 (*see also* Gap parameter)
- Pairing force 184, 221, 232–234, 239, 260, 264, 342, 435, 449
- Pairing gap (*see* Gap parameter)
- Pairing rotations 445, 448, 451
- Pairing, semiclassical 550
- Pairing tensor 251, 551, 608
- Pairing vibrations 299–301
 - and phase transition 341–343, 450
 - boson representation 380
 - GCM 435
 - pp -TDA 289
 - pp -RPA 339–341
 - seniority model 224
 - weak coupling 397
- Pairing-plus-quadrupole force 185, 260, 345, 373, 380, 381
- Pairing-plus-quadrupole model 259–262, 263, 639
- Parent nucleus 297
- Parity operation 7, 151
- Parity violation 440
- Partial resummation of \hbar -expansion 545
- Particle-hole (ph)
 - calculations 325–328
 - in self-consistent basis 328–330
 - correlations 244, 260, 279, 302, 342, 640
 - coupling 52, 113
 - creation operator 283
 - excitations 48, 107, 283, 292
 - interaction 133, 170–172, 177, 640
 - matrix element 344
- Particle number 231, 490, 530, 604
 - conservation 341
 - on the average 230, 252, 462
 - non-integer values 496
 - operator 597, 600
 - projected HFB 465
 - projection 463–466
 - symmetry 447–451

- uncertainty 230, 231, 233, 242
- violation 229, 252, 260, 396, 450, 532
- Particle-particle (*pp*)**
 - bosons 372–375, 377
 - correlations 217–221, 244, 260, 279, 288, 300, 342, 633
 - interaction 133, 164–170, 177, 344
 - matrix element 344
 - *pp*-RPA 339–341
 - *pp*-TDA 288–289
- Particle-plus-rotor model (PRM)** 97, 107–126
 - axially symmetric 109–122
 - electromagnetic properties 125
 - triaxial 122–124
- Partition function** 529, 538ff.
- Path on the energy surface** 31, 200, 259, 269, 431–432, 494, 513, 517–519
- Pauli exclusion principle** 1, 36, 46, 59, 150, 153, 157, 187, 197, 220, 237, 356, 365, 369, 378, 387, 494
 - violation of 303, 341, 371
- Pauli projector** 158
- PBCS-theory** 462, 464
- Peierls–Thouless method** 473
- Peierls–Yoccoz projection** 459, 469
- Perturbation theory** 112, 130, 131, 134, 166–172, 385–387, 405, 587, 628–630
 - adiabatic 523ff.
- Perturbative boson expansion** 358–361
- ph (see Particle-hole)**
- Phase space** 491
- Phase transition**
 - and boson condensation 229, 445
 - and GCM 398, 435
 - and Green's functions 634, 637
 - and projection methods 465
 - and symmetry violations 439, 443
 - spherical-deformed 201, 377, 380, 637
 - to superfluidity 101, 107, 229, 300, 341, 634
- Phonon pole** 639
- Photo**
 - absorption 294, 593
 - cross section 329
- Physical subspace**
 - boson representation 349, 352, 369
 - redundant variables 453
- Pion condensation** 440, 451
- Plateau condition** 88, 89
- Poisson bracket** 535, 610
- Polar decomposition** 617
- Polarizability** 321, 335
- Polarization**
 - and effective charges 63, 65, 390
 - charge 390
 - core 169, 216, 390
- of the mean field 216, 257
- waves 291
- Potential barrier** 496
- pp (see Particle-particle)**
- Pressure tensor** 555, 556, 558, 564
- Product rule for Wigner transforms** 535, 567, 610
- Product wave functions** 46, 192, 201, 234, 438, 611–622
 - generalized 250
 - (see also Slater determinants)
- Projected**
 - BCS 462, 464
 - HF 481
 - TDA 483
 - TDHF 493
- Projected energy** 466, 469, 475, 479
 - surface 462
- Projection**
 - methods 451, 458–484
 - onto good angular momentum 466, 473–484
 - onto good linear momentum 460
 - onto good particle number 435, 459, 463–466
 - operators 459, 460, 466, 474
- Projection theorem for vector operators** 61, 125
- Projector-like operators** 473
- Prolate deformations** 99, 118, 142, 263
- Propagator**
 - free 535
 - harmonic oscillator 537, 545
 - linear potential 538, 545
- Proton gap** 236, 275
- Proton–neutron pairing** 239, 262
- Pushing model** 471, 480

- $Q|Q$ -force (see Quadrupole–quadrupole force)**
- Quadratic constraint** 267
- Quadrupole**
 - bosons 352, 372, 373, 375–381
 - correlations 442–446, 450, 638
 - deformations 6–9, 66, 260, 441–451
 - moment 63, 64, 66, 265, 439, 584
 - operator 227, 377, 583
 - pairing force 185, 381, 442
 - part of the mean field 441
 - sum rule 15, 295
 - transition density 337
 - transitions (electric) (see $B(E2)$ -values)
 - vibrations 14, 221, 334, 380, 433–435, 521, 523, 571
- Quadrupole–quadrupole force** 182, 185

- Quantization**
- ATDHF 516
 - canonical 9, 586
 - Pauli 19
 - second 595–602
 - WKB 533
- Quasi-boson approximation** 303, 304, 307, 311
- Quasi-particle**
- band 278
 - energy 131, 235, 254, 256, 275
 - excitations 251, 254, 278
 - interaction 177, 614
 - operators 49, 234, 245–248, 450
 - phonon-coupling 395
 - representation 253, 343, 354, 613–614
 - RPA equation 343, 344
 - states 49, 235, 249, 251
 - vacuum 249–250
- Quasi-particles**
- BCS 234
 - HF 614
 - HFB 245–248
 - Landau 177, 245
 - shell model 49
- Quasi-spin** 198, 222, 446
- Quasi-static** 492
- Radial shapes** 291
- Radiation field** 584–587
- Random phase approximation** (*see* RPA)
- Rate of strain tensor** 555
- Rearrangement potential** 208
- Recoil term**
- rotational 108, 110, 115, 120
 - translational 455
- Recursion relation**
- fermion norm 364ff.
 - residue integrals 463
- Reduced transition probabilities** (*see* $B(EI)$ – and $B(MI)$ – values)
- Redundant generator coordinates** 418
- Redundant variables** 109, 399, 453
- Reference spectrum method** 163
- Reid soft core potential** 155, 205, 278
- Relative coordinate** 452
- Renormalized effective interaction**
- (quasi-particle interaction) 177, 326
- Repulsive interaction** 286
- Requantization** 516, 519 (*see also* Quantization)
- Residual interaction** 49, 131, 132, 165, 281, 286, 314, 316
- Residues method** 463
- Resonance** 322
- Response function** 316, 323, 633
- Restoring force** 570 (*see also* Stiffness coefficient)
- Re-summation** 546
- Rigid body** 19, 33, 131, 135, 137, 139
- Ritz variation principle** 129, 190, 252, 543
- $\mathfrak{A}_{1,2}$ = symmetry 22, 111, 113, 116, 137, 261, 272, 476, 579
- Root mean square (rms) radii** 41, 213, 333, 433
- Rosenfeld force** 174, 326
- Rotating**
- frame 127ff., 271ff.
 - harmonic oscillator 133–139
 - liquid drop 32–35
 - quasi-particle RPA 345
- Rotation**
- and TDHF 493
 - and RPA 313
 - collective 17, 101
 - around symmetry axis 142ff.
 - single-particle 102, 142ff.
- Rotational**
- alignment 101, 111, 115ff., 123, 276, 385
 - bands 24, 103, 119, 273, 278, 448, 451, 461
 - invariances 51, 72, 151, 260, 443ff., 476
 - motion 451, 457–458
 - operator 576ff.
 - spectrum (*see* Rotational band)
- Rotation–vibration coupling** 25
- Rotor model** 17–28, 107, 118
- and projection 475
 - boson representation 351
- RPA (random phase approximation)** 301ff., 444, 500, 511, 512
- amplitudes 307
 - and boson-representation 360ff.
 - and phase transitions 441, 442
 - calculation 328
 - derivation 301–304, 308, 317, 408, 513
 - equation 135, 303, 317
 - excitation probability 326
 - for density dependent forces 315
 - ground state 302, 309, 310
 - Hamiltonian 313
 - higher 311
 - in the continuum 322
 - matrix 305, 513
 - metric 304, 620
 - numerical solution 306, 325
 - open shell 302
 - spurious states 311ff.

- sum rules 332
- symmetry restoration 440

- Saddle point 31
- Saddle point method 547
- Saturation 2, 211
- Saturation potential 208
- s*-boson 377ff.
- Scale transformation 425
- Scaling of coordinates 333, 433, 567
- Scattering matrix (*see S*-matrix)
- Scattering of slabs 503
- SCC (*see Cranking model*)
- Schematic model 285, 319, 342
- Schiffer interaction 186
- Schmidt lines 61, 62
- Schwarz inequalities 331
- Schwinger boson representation 350, 354, 373
- Scott-Moszkowski method 163
- Screening term 326
- Second band 106, 278
- Second constraint 271, 463
- Second minimum 83, 95, 270
- Second quantization 595–602
- Secularly unstable 33
- Selection rules
 - for multipole moments 583
 - for multipole transitions 590
- Self-consistency 197, 256, 272
 - condition 132, 134, 136, 199, 253
- Self-consistent
 - basis 195, 328
 - calculation 212, 265, 544
 - constraint 432
 - cranking model 271–279
 - field 195, 254, 260, 274, 279, 487
 - path 518
 - RPA 361
 - symmetry 202, 256, 261, 491
- Semiclassical
 - derivation of cranking 127
 - energy 540
 - pairing 550
 - theory 527, 536, 540
- Semidecoupled bands 103
- Semi-empirical mass formula 4
- Seniority
 - model 221, 350, 378, 446
 - quantum number 223, 446
- Separable forces 180, 285, 345
- Separation energy 37ff.
- Separation method 163
- Serber force 174
- Shape vibrations 435 (*see also Vibrations*)

- Shell corrections 83–95, 139–143, 522
- Shell effects 37ff., 81, 99, 538
- Shell model 36–95
 - deformed 63–95
 - spherical 36–63
- Shell model calculations 50, 145, 481
- Shell model configuration mixing 288
- Shift operations
 - for bosons 415, 622
 - for collective motion 415, 421, 424, . . . , 514ff., 607ff.
- Short-range interaction 183, 219
- Side feeding 98
- Siegert theorem 63
- Signautre 137, 476, 478
- Single *j*-shell
 - BCS 233
 - configurations 53
 - quasi-particle states 235
 - IBA 373, 379
 - seniority 221ff., 446
- Single-particle
 - density 193, 530, 600, 624
 - Green's function 324, 623ff.
 - levels 59
 - matrix elements of multipole operators 63, 591
 - states 49, 56ff.
 - units 592
- Skeleton expansion 631
- Skyrme force 175, 203, 208, 264, 270, 278, 323, 328, 332, 334, 433, 434, 523, 534
 - generalization 330, 501
- Skyrme inertia 472
- Slab
 - collision 561
 - of nuclear matter 501
 - oscillating 502
- Slater determinant 46, 192, 315, 486, 596, 605
 - stability of 498
- Small amplitude motion 506, 570
- Small amplitudes 314, 317, 506–512
- Small velocities 507
- S*-matrix 498, 627
- Smooth energy 92, 540
- SO*(2*M*)-algebra 355
- Soft core 155
- Soft mode 443, 635
- Solitary wave 500
- Soliton 495, 500
- Super force 174
- Sound
 - ordinary 544
 - zero 544

- Spectral density matrix 529
- Spectral representation 318, 624, 634, 636
- Spectroscopic factor 59, 392
- Spectroscopic quadrupole moment 66
- Spherical tensor operator 576
- Spin
 - degree of freedom 292
 - distribution 581
 - saturation 176
 - waves 292
- Spin-orbit
 - coupling 42–45, 70
 - density 210
 - interaction 153
 - potential 212
 - term
 - deformed 67
 - spherical 43
- Spontaneous emission 588
- Spreading width 323, 330, 494
- Spring constant 322
- Spurious
 - components in HF wave function 483
 - excitation 293, 314
 - motion 314
 - rotational energy 469, 479
 - solution 311, 318
 - state and symmetry violation 51
 - state and boson representation 371, 374, 392
 - state and redundant variables 453, 455
 - translational energy 313, 455
- Square well potential 40
- Stability matrix 253, 305, 317, 513
- Stability of rotating liquid drops 33
- Staggering 119
- Static
 - deformation 338
 - density 507
 - HF energy 510
 - polarizability 321, 333
 - Thomas–Fermi 528
- Steepest descent 258
- Steinwedel–Jensen model 559, 572
- Stephens–Simon
 - band 273
 - effect 101, 107, 276
- Stiffness coefficient 12 (*see also* Curvature of the energy surface)
- Stretching effect 274
- Strength function 325, 329, 330, 334
- Strong coupling scheme 110–112, 117
- Structure spin traps 145
- Strutinsky
 - energy theorem 93
 - method 83ff., 539
 - – and rotation 139ff.
 - – applications 95, 141
- SU(2)*–group 348
- SU(3)*–model 379
- SU(5)*–model 375, 379
- SU(6)*–model 373, 375, 377ff.
- Subspace
 - collective 347, 359, 364
 - physical 349, 352, 369
- Sum rule 15, 288, 294, 322, 326, 330–336, 445
- Superconductor 228
- Superheavy nuclei 95
- Superfluid
 - behavior 100, 449, 450
 - nuclei 217ff.
 - state 300
- Superposition principle 495
- Surface
 - energy 12
 - oscillations (*see also* Vibrations) 9–17
 - tension 5
 - term 4
 - thickness 40, 67
 - vibration 291, 558
 - vibration of liquid drop 336
- Surface δ -interaction 179, 380, 345
- Sussex force 185
- Symmetric moment expansion (SME) 420–423
- Symmetric ordering 421
- Symmetric orthogonalization 401
- Symmetry 290, 314, 438ff.
 - axis 142
 - conservation 462, 463, 490
 - continuous 203, 311, 317
 - energy 5, 47, 299, 559
 - operator 438
 - properties 50
 - transformation on a density-dependent force 203
- Symmetry violations
 - and correlations 201, 637, 639
 - and density dependent forces 203, 317
 - and phase transitions 441–451
 - and the mean field approach 441–451
 - and the RPA 312, 317, 361
 - and zero-frequency modes 311–313
 - in the BCS model 446
 - in the HF method 201
 - in the Nilsson model 67, 77
 - in the shell model 51
 - projection methods 458–484
 - restauration 438–484

- Tabakin potential 155
 Tamm-Dancoff
 - and symmetry violation 293
 - equation 164, 170
 - method 282, 284, 301
 - projected 482
 - sum rules 332
 Tassie model 336, 560
 Tauberian theorem 410
 TDHF (time-dependent Hartree-Fock)
 - derivation 486-489
 - equations 488
 - exactly soluble model 522
 - numerical solution 501
 - properties 489-491
 - symmetries 489
 - wave functions 496ff.
 Temperature 529, 535, 556, 557
 Tensor component of the magnetic dipole 63
 Tensor force 152
T-0 pairing 263
 Thomas-Fermi theory 89, 143, 206, 527,
 528, 530, 531, 568
 - extended (ETF) 540, 570
 Thomas-Reiche-Kuhn sum rule 294
 Thouless theorem 253, 258, 400, 424, 494,
 566, 615-616
 - for bosons 621
 - generalized 616
 Thouless-Valatin equations 312, 322
 Thouless-Valatin inertia 313, 322, 458, 469,
 471, 472, 511
 Three-body correlations 206
 Three-body interaction 175, 176, 210
 Time-dependent
 - density 487, 573
 - description 289, 314
 - harmonic oscillator 416ff., 573
 - Hartree-Fock (see TDHF)
 - mean field 317
 - one-body density 315
 - perturbation theory 318
 - phase factor 524
 - variational principle 489, 562
 - wave function 485
 Time-even 338
 - density 566, 573
 - matrices 507
 Time-odd 338, 507, 521
 - component 516, 520
 Time ordered product 601, 624
 Time-reversal invariance 151, 256, 261, 272,
 421, 424, 426, 491, 510, 609
 Time-reversal operator 7, 184, 228, 248, 491
 matrix 156, 627, 633
 Total mass of the nucleus 313
 Trajectory 489, 495
 Transition
 - current 335, 338
 - density 290, 291, 303, 325, 335, 336,
 338, 561, 638
 - matrix element 13, 25, 60, 321, 587
 - operator 60, 336, 587
 - probability (see Electromagnetic
 transitions) 13, 287, 304, 319
 Transitional nuclei 24, 118, 122, 216
 - and boson model 375ff.
 - and ATDHF 522
 Translation 293, 313, 492
 Translational excitations 445
 Translational invariance 50, 151, 260, 439,
 460, 592
 Translational kinetic energy of slabs 503
 Translational motion 454-456
 Triaxial
 - deformations 27, 101, 122, 140, 385
 - particle-plus-rotor model 122
 - projection 481
 - rotor 21, 26, 122ff.
 Tunneling 496, 549
 Turning point, classical 532
 Twist mode 291, 568
 Two-body
 - density 487
 - friction 487, 494
 - operator 600
 Two center model 81
 Two-particle-two-hole (2p-2h)
 admixtures 494
 Two-particle wave function 150
 Two-phonon multiplet 397, 346, 376
 Two-phonon norm 363
 Two-quasi-particle state 235, 257

 Unbounded constraint 270
 Uncertainty relation 2, 415
 Unfavored states 114, 117
 Unfilled shells 50
 Unified model 97
 Unitary approximation to evolution
 operator 501
 Unpaired particle 237
 Usui operator 370

 Vacuum
 - bare 372, 374, 596
 - boson 310, 348, 352, 374
 - quasi-particle 249ff.

- Vacuum projector 363, 382
- Valence particles 107, 164, 167, 393
- Valley of β -stability 35
- VAP method (*see* Variation after projection)
- Variable moment of inertia (VMI) model 104
- Variation
 - after projection (VAP) 461, 468, 470, 499
 - before projection (VBP) 460, 469, 472
 - with constraints 230, 267
- Variational calculations 542
- Variational principle 129, 190, 252, 400, 431, 543
 - and energy density functional 206ff., 543
 - in fluid dynamics 562
 - of Hamilton 469
 - of Ritz 190–192, 252, 400, 431
 - time-dependent 489, 562
- VBP method (*see* Variation before projection)
- Vector spherical harmonics 585
- Velocity 11, 337, 506, 568
 - distribution 131, 136, 291, 504, 556ff., 565
 - field 136, 337, 568, 573
- Vertex (vibration particle coupling) 384, 387ff., 638
- Vibration particle coupling (VPC) 381ff.
 - Hamiltonian 383
 - perturbation theory 385
 - vertex 384, 387ff.
- Vibrations
 - liquid drop 9–17
 - particle-hole 280–345
 - particle-particle 288, 339–343
 - quasi-particle 343–345
 - TDHF 501
- Villars equations 518
- Virial theorem 80
- Virtual bosons 342
- Virtual phonon excitation 390
- Volume conservation 6, 34, 68, 136
- Volume term 4
- VPC (*see* Vibration particle coupling)

- Wave packet 289, 315, 338, 416, 485
- Weak coupling scheme
 - and rotations 110, 112ff., 117
- and vibrations 385ff., 397
- Weakly canonical variables 515
- Weight function 399ff., 434
- Weisskopf units 590, 592
- Weizsäcker term 542
- Wernitz–Überall mode 560
- Wick's theorem 194, 254, 255, 601–602, 605, 619, 620
- Width
 - of giant resonance 323, 330
 - of norm overlap 410, 425
 - of resonance 331
- Wigner–Eckart theorem 227, 583
- Wigner force 153, 154, 174, 294
- Wigner functions 7, 576
- Wigner–Kirkwood expansion 534ff., 546
- Wigner transformation 535, 609–610
- Wigner transform of pair potential 550
- Wilet–Jean model 379
- WKB quantization rule 533
- Wobbling 28, 101, 351
- Woods–Saxon potential 40, 59, 214, 540, 547
 - deformed 67
 - generalized 81
 - rotating 139

- Yale potential 155
- Yoccoz-inertia 428, 469, 472, 475
- Yrare levels 98
- Yrast line 28, 98ff., 104ff., 274, 278
- Yrast traps 102, 140, 143ff.
- Yukawa force 155, 326, 501

- Zero eigenvalues 312, 402
- Zero-frequency mode 450
- Zero plus (0^+) ground state 299
- Zero plus (0^+) pair 220, 342
- Zero-point energy 427ff., 523
- Zero-point fluctuations 140
- Zero range forces 323, 334
- Zero sound 554

Texts and Monographs in Physics

Edited by W. Beiglböck, M. Goldhaber, E. Lieb, and W. Thirring

Texts and Monographs in Physics includes books from any field of physics that might be used as basic texts for advanced training and higher education in physics, especially for lectures and seminars at the graduate level.

Polarized Electrons

by J. Kessler

1976. ix, 223p. 104 illus. cloth

The Theory of Photons and Electrons

The Relativistic Quantum Field

Theory of Charged Particles with Spin

One-Half

Second Expanded Edition

By J. Jauch and F. Rohrlich

1976. xix, 553p. 55 illus. cloth

Essential Relativity

Special, General, and Cosmological

Revised Second Edition

By W. Rindler

1980. xvii, 284p. 44 illus. paper

Inverse Problems in Quantum Scattering

Theory

By K. Chadan and P. Sabatier

1977. xxii, 344p. 23 illus. cloth

Quantum Mechanics

By A. Böhm

1979. xvii, 521p. 105 illus. cloth

Relativistic Particle Physics

By H. Pilkuhn

1979. xii, 427p. 89 illus. cloth

The Concepts and Logic of Classical Thermodynamics as a Theory of Heat Engines

Rigourously Constructed upon the Foundation Laid by S. Carnot and F. Reech

By C. Truesdell and S. Bharatha

1977. xxii, 154p. 15 illus. cloth

Principles of Advanced Mathematical Physics

By R.D. Richtmyer

Volume I

1978. xv, 400p. 45 illus. cloth

Volume II

In preparation

Foundations of Theoretical Mechanics

By R.M. Santilli

Part I: The Inverse Problem in Newtonian Mechanics

1978. 288p. cloth

Part II: Generalizations of the Inverse Problem in Newtonian Mechanics

In preparation

Advanced Quantum Theory and Its Applications Through Feynman Diagrams

By M.D. Scadron

1979. xiv, 386p. 78 illus. cloth

Operator Algebras and Quantum Statistical Mechanics

By O. Bratteli and D.W. Robinson

Vol. I: C* and W* Algebras. Symmetry Groups. Decomposition of States

1979. 500p. cloth

Vol. II: Equilibrium States. Models in Quantum Statistical Mechanics

1981. 469p. approx. cloth

The Nuclear Many-Body Problem

By P. Ring and P. Schuck

1980. 624p. approx. 171 illus. cloth

Nuclear Reactions with Heavy Ions

By R. Bass

1980. 410p. 176 illus. 31 tables. cloth